NASA SP-365

Part II

NATIONAL GEODETIC SATELLITE PROGRAM

A REPORT COMPILED AND EDITED FOR NASA BY THE AMERICAN GEOPHYSICAL UNION

PARTICIPATING ORGANIZATIONS

Applied Physics Laboratory/The Johns Hopkins University
Department of Commerce/National Ocean Survey
Department of Defense
Air Force Cambridge Research Laboratories
Engineer Topographic Laboratories
Defense Mapping Agency/Aerospace Center
Defense Mapping Agency/Topographic Command
Naval Surface Weapons Center/Dahlgren Laboratory
National Aeronautics and Space Administration
Goddard Space Flight Center
Jet Propulsion Laboratory/California Institute of Technology
Wallops Flight Center
Ohio State University
Smithsonian Astrophysical Observatory
University of California, Los Angeles

Scientific and Technical Information Office 1977
NATIONAL AERONAUTICS AND SPACE ADMINISTRATION
Washington, D.C.

Contents

7

NATIONAL GEODETIC SURVEY

H. Schmid

7.1 INTRODUCTION: FOUNDATIONS OF SATELLITE GEODESY AND THE CREATION OF WORLDWIDE GEODETIC REFERENCE SYSTEMS

7.1.1 Geometric and Geophysical Aspects in Satellite Geodesy

Artificial satellites in close-to-Earth orbits have contributed to the field of geodesy a new technique which, theoretically speaking, is capable of completely reorienting the methods and procedures of the geodetic discipline. Application of newly developed methods of precision measurements in satellite triangulation confirm early predictions of a reformation in the domain of classical geodetic field operations (Schmid, 1966a).

Without entering here into questions concerning the dividing line between geodesy and geophysics, it can be stated that the fundamental problem of geodesy is the mathematical description of the Earth's gravity field together with the determination of the geometry of the physical surface of the Earth, with unambiguous correspondence between the Earth-fixed coordinate systems or datums and the spherical coordinate system for a given epoch that serves as reference frame for metric astronomy. With satellite geodesy it is possible to find a solution to the fundamental problem on a synoptical basis, i.e., with reference to the whole Earth. Furthermore, triangulation with satellites, in conjunction with position and time determinations of satellite orbits, eventually provides the necessary link between the geometric and geophysical measuring concepts of geodesy.

Thus, with the aid of satellite geodesy it becomes possible to undertake the geometric description of the surface and the analytical description of the gravity field of the earth by means of worldwide measuring systems and to derive results in the form of three-dimensional models based on a minimum of a priori hypotheses.

These mathematical models then represent the frame of reference into which one can fit the existing geodetic results from the various local datums, as well as all geodetic measurements to be executed in the future. The relevant necessary adjustment should not confine itself to the limited, in practice, classical concept of the treatment of accidental errors, but must, with the aid of a generalization of the Gaussian algorithm, take advantage of the increasing knowledge derived from interdisciplinary research sources concerning the various geophysical parameters involved, with a meaningful inclusion of the corresponding covariance matrices.

From a formalistic mathematical point of view, the significance of artificial satellites for geodesy consists of the ability to express the time-position curve of the orbit of a close-to-Earth satellite in terms of functions of certain parameters, which give in turn information concerning geometric and geophysical properties of the earth and its surrounding space. In this development, the quantities describing the gravitational field are of prime importance to gravimetry; the remainder of the geophysical forces affecting the orbit or arising from the satellite itself are treated as perturbation sources.

The quantitative determination of the parameters appearing in the mathematical simulation of the satellite orbits is accomplished by setting up observation equations which functionally relate the measurements made for the orbit determination with the parameters describing the orbit. It is then apparent that, in addition to these orbital parameters, these equations will involve the position coordinates of the Earth-fixed observation stations which, in the geophysical content of the problem, represent the position of these stations relative to the Earth's mass center. If there is a sufficiently large number of observations, optimally distributed, it is possible to determine from the corresponding

adjustment not only the geophysical parameters affecting the orbit, but also the geocentric parameters of the observing stations. Thus presents itself the opportunity of a simultaneous solution of the geometric and gravimetric problems of geodesy in a worldwide frame.

This, from a purely theoretical standpoint, attractive train of thought has found great appeal, among astronomers and geophysicists in particular, and has already led to impressive results and new insights (Kozai, 1966a). Being more intimately connected with triangulation measurements proper, however, the measurement engineer and, in particular, the practicing geodesist will have certain reservations, based on the fact that the relatively large number of parameters appearing in the complex system of equations of such an adjustment are all more or less strongly correlated. In direct consequence of the simultaneous solution there exists, first of all, correlation among the various parameters of the same type, e.g., the coefficients of the harmonic functions describing the gravity field. In addition, statistical dependence exists between the gravimetric quantities and the geophysical parameters introduced to describe certain orbital perturbations. And, of course, the coordinates of the observing stations introduced into the solution and adjusted together with the other parameters are not only correlated among themselves but also with these nongeometric quantities. In practice, the number of observations, as well as their distribution in time and space, leaves much to be desired, which only serves to amplify these correlations.

Even when—as a consequence of using a larger capacity electronic computer—it is possible to unite a very large number of observations in a single solution, it may be that the geometry of the observing stations obtained from such a solution does not necessarily represent the actual spatial relations. Although the computed parameters in their entirety are well suited to describe, within the limits of accuracy of the original observations, the geometry of the satellite orbits, the possibility nevertheless exists that an isolated group of such parameters (for example, the station coordinates) may have only limited accuracy. Their significance must be judged in the light of the underlying geophysical and astronomical hypotheses. In short, the geometry of the observation stations is prejudiced by the specific properties of the mathematical model chosen to simulate the geophysical-dynamic nature of the satellite orbit.

This in no way lessens the significance of the geophysical solution. On the contrary, dynamic satellite geodesy gains thereby. Once the three-dimensional geometry of a sufficiently large number of points of the Earth's surface has been established with a purely geometric solution, based only on Euclidean (flat space) geometry and the right ascension-declination system of metric astronomy, orbital observations from these stations can be used for the exclusive purpose of determining geophysical parameters. Such a system will be relieved of the problem of computing station coordinates in the adjustment.

Thus, the number of unknowns to be determined from a given available set of observations is reduced—in itself a desirable objective—and, in addition, correlation is eliminated between the geometry and the geophysics, at least with respect to the station coordinates and the orbital elements.

Given the results of the geometric solution, the opportunity presents itself, by way of a purely geometric orbit determination, to ascertain the geometrical shape of the surface of the oceans by applying laser and radar techniques to measure the distances between the satellite and the ocean surface. The influence of weather and tides on the measured profiles can be eliminated with measurements over a sufficiently long period of time. This would not only help to complete the presentation of the geometry of the physical surface of the Earth, but would also give a purely geometric, hence unconstrained by hypothesis, representation of a large portion of a surface which, though not quite rigorously, is a very good approximation to the geoid. The objection that with the preceding com-

ments concerning a purely geometric solution the information content of the dynamic solution is not completely exhausted, can be countered by seeing the eventual solution of the problem of satellite geodesy as a combination of the separate, individual geometric and dynamic solutions. In such a solution the station coordinates will no longer be treated as free variables for the dynamic solution, but will be introduced from the geometric adjustment together with their associated covariances.

This will be the real contribution of satellite geodesy to the principal geodetic mission. The problems of describing the Earth's gravity field and determining the geometry of the physical surface are solved in a consistent formulation; optimal results from a geophysical hypothetical as well as a metrological standpoint are yielded, the geometric and geophysical concepts mutually supporting each other. The amalgamation of the outputs of geometric and dynamic satellite geodesy must in the end be consummated, from the theoretical as well as the practical standpoint, by the inclusion of geodetic data measured on the surface of the Earth. This requirement seems necessary because, although the significant contribution of satellite geodesy to physical geodesy has been to open up the third dimension in the investigation of the Earth's gravity field, the fact still remains that the essential tasks of geodesy are the determination of the geometry of the physical surface of the Earth and the representation of the gravity field in detail and relatively close to the crust (Kaula, 1967a).

7.1.2 Development and Organization of a Geodetic Satellite Program for Creating a Worldwide Geodetic Reference System

The history of satellite geodesy and its theoretical development began with the implementation of an idea that had been for decades an intermediary goal for scientists concerned with rocket development: to increase the cutoff velocity of the rocket to the point where it goes into orbit around the Earth.

The realization of this technical goal with the launch of the first Russian and, shortly thereafter, of the first American artificial satellite created renewed interest among experts in the fields of astronomy and aeronomy in the theoretical problems concerned with the description of the track of a body of small weight orbiting around an oblate mass, specifically around the Earth. The classical theories and procedures of physical geodesy being inadequate to the solution of all these problems, it has become the practice to apply almost exclusively the classical principles of celestial mechanics together with theories and results from the fields of aeronomy and related geosciences, which with the aid of rocket experiments have already made considerable advances in their studies on the subject.

This development explains the dominating influence of dynamic satellite geodesy to this day, reflected also in the planning and execution of the first American geodetic satellite program. The basic requirement for the satellite launched in the first American geodetic experiment, known as ANNA, and for the subsequent GEOS satellite program was compact construction and rotation-symmetric form to the highest possible degree. The resulting mass to cross-section ratio was designed to minimize the perturbing influence of the atmosphere and other geophysical forces, such as solar radiation pressure, in order not to complicate unnecessarily the adjustment of the orbit relative to the gravitational field.

In order to be able to sense the essential components of the Earth's gravitational field while keeping perturbing influences within bounds, a problem intimately connected with that of assuring the satellite a sufficiently long lifetime, the necessary experiments were executed at heights of 1000 to 1600 km above the Earth, and the nearly circular orbits were distributed over as wide a band of inclination as possible. The equipment for this type of satellite was characteristic of its purpose, the instruments on the satellite allowing, when operated together with instruments on the Earth's surface, measurements of the satel-

lite distance and direction, and the difference in distance to the satellite at two points in its orbit (or equivalently, the frequency of radio waves received from the satellite; see chs. 2 and 5 and sec. 7.2 of this chapter).

It is apparent that, viewed in the light of the present state of development, dynamic satellite geodesy in general faces two complexes of questions requiring further study in the planning for future geodetic satellite projects. From the theoretical side, for one, the question arises: To what extent are the concepts derived from classical celestial mechanics and applicable to spherical fields valid in the immediate vicinity of an oblate spheroidal mass? Of perhaps even greater significance are the questions regarding the validity of our concepts with respect to the various geophysical forces other than gravity that influence the orbit of an Earth satellite. So far as practical measuring techniques are concerned (assuming proper professional use of the equipment), there is little left to be desired with respect to data density and precision (internal accuracy) of data obtained by means of Doppler shift in radio frequency. However, even when care in the necessary time and spatial distribution of the measurements is exercised, there remains sufficient reason to suspect that even today occasional systematic errors creep in, not so much as the result of lack of reliability in the equipment but as of uncertainties in the corrections that are necessary to transform the velocity of light in vacuo into the wave propagation velocity existing at the time of observation. The frequencies in use at the present are particularly affected by periodic changes in the ionosphere.

The possibility of calibrating frequency-measuring equipment by comparison with data from laser-type DME, by way of position and time determination, offers little hope in a long-term program, if only for sighting reasons. Particularly ineffective in this connection have been the unsuccessful attempts to initiate an efficient and sufficiently extensive calibration program in which all the measuring methods to be used are systematically examined under typical observation conditions by simultaneous orbit observations from previously and precisely surveyed observation sites. The method followed at present of judging the metric accuracy of the various procedures from the internal accuracy of, at times, very arbitrarily selected series of observations, or at any rate of deriving absolute accuracy from the differences between end results of measuring systems quite different in the techniques used in measuring and adjusting, is unsatisfactory for the metrological engineer in general and the geodesist in particular (see ch. 1).

In addition to the previously mentioned GEOS satellites, serving primarily the purposes of dynamic satellite geodesy, a balloon-type satellite (PAGEOS) was used exclusively for the purpose of geometric satellite triangulation within the framework of the NGSP (see ch. 5). The balloon, with a 30-meter diameter, is similar in material and construction to the balloon satellite ECHO–1 and has a casing 0.013 mm thick that specularly reflects sunlight, unlike the ECHO–2 satellite, whose somewhat thicker casing has a more diffusely reflecting surface. PAGEOS (passive geodetic satellite) was launched 23 June 1966, in a nearly circular, nearly polar orbit at a height of about 4200 km above the earth. With the launching was established an elevated target suitable for worldwide satellite triangulation. The U. S. Coast and Geodetic Survey (later the National Ocean Survey within the National Oceanic and Atmospheric Administration), together with National Aeronautics and Space Administration and the Department of Defense, set up a worldwide network of tracking stations to take advantage of PAGEOS. The coordinates of the stations are given in table 1.28; the network is shown graphically in figure 1.2 of chapter 1.

The compromise in the distribution of the stations necessitated by logistic and political considerations represents a good approximation to an optimal solution. The open mesh in the South Pacific Ocean is due to a lack of any kind of island, whereas the open space over central Asia obviously results from a political situation.

The triangulation method based on photogrammetric principles will be described in detail in section 7.4.

7.2 INSTRUMENTATION

7.2.1 Photogrammetric Camera

7.2.1.1 General

The techniques used in the measurement of rocket trajectories, particularly because of their high accuracy requirements, had an early influence on the development of photogrammetric data acquisition and evaluation instrumentation. Characteristic in this field of application is the necessity to combine a great number of observations in a single photogram in which each individual observation is generally registered very accurately against a time or frequency standard. Consequently, there is a requirement on the photogrammetric instrumentation for great stability over extended periods of observation. This requirement led to the development of the so-called ballistic camera, which, on the whole, is based on the phototheodolite of terrestrial photogrammetry. In order to adapt the instruments to the unorthodox requirements of the geometry encountered in tracking rocket trajectories and at the same time increase the accuracy of the direction determination, cameras were developed that could be arbitrarily oriented and that had objectives with long focal lengths. A corresponding decrease in viewing angle is inevitable because of practical limitations on the size of the plate. Exact elements of exterior orientation are obtained with the use of elements from the classical geodetic angle-measuring instruments, such as precision spindles, circles, and hypersensitive levels.

The development of instrumentation reflecting these concepts reached a high point in the 1940's with the Askania phototheodolite (Lacman, 1950). This camera had a 370–mm focal length, f/5.5, 13– by 18–cm plate format, and a synchronous drive for the rotary shutters, producing 1.5, 3, 6, and 12 exposures per second with a synchronization accuracy of 10^{-3} sec. In addition, a louver shutter was available to block out certain exposures in the sequence or to generate time-related star trails. The horizontal and vertical circles could be set to within 3^{cc}.

These instruments were used in Peenemünde for measuring the V–2 trajectory up to the point of engine cutoff. On the resumption of similar projects in the United States after 1945, interest in photogrammetric precision metrology faded because of, as it turned out, too-optimistic expectations from electronic approaches to the problem of trajectory measurements. When it became apparent that neither these electronic approaches nor the capability of the cinetheodolite could do justice to the developing rocket technique, the author had the opportunity, in connection with his assigned duties at the Ballistic Research Laboratories of the Aberdeen Proving Ground, Maryland, to initiate plans for improved precision theodolites, resulting, with the active and sympathetic cooperation of the Swiss firm Wild-Heerbrugg, in today's well-known BC–4 phototheodolite system. At the time, the experience gained in the various fields of experimentation created a demand for the development of a series of cameras with different angles of view, to be used interchangeably to a great extent on the same mount. In addition to the necessary variation in picture sequence over a wide range, the requirement for maximum accuracy in exposure synchronization was considered of utmost importance. The development of the complete system stretched out over a period of 10 years, and the general concept is described in Schmid (1962). The technical details of the BC–4 phototheodolite are explained in the literature of Wild-Heerbrugg.

In the early 1960's the idea of applying the photogrammetric technique for geometric satellite triangulation to the establishment of a continental net began to be seriously considered (U.S. Department of Commerce, 1965). The technical requirements for such a project differ from those of conventional trajectory mensuration in that first, the exterior orientation of the camera is not deter-

mined with graduated circles, but is determined from the photogram itself on the basis of the photographed control points (star images), and second, the unusually high accuracy demands require that the parameters needed for the reconstruction of the photogrammetric bundle (the generalized model of interior orientation) be recomputed for each individual plate. This makes it necessary to effect a compromise between focal length (increase of intrinsic accuracy) and a field of view large enough to enable the observer to record a sufficient number of available catalogued stars in any portion of the sky. Absolute synchronization between the widely separated stations is complicated, actually impossible in theory, in view of the unknown light travel time at the instant of observation. Hence, in satellite triangulation it is merely necessary to record the instants of satellite observation very accurately (to at least 10^{-4} sec) against the frequency standard at each station. However, the station clocks (frequency standards) must be calibrated with respect to a basically arbitrary but uniquely defined time sequence. Synchronization of the clocks to within about 10^{-5} sec is attained by periodic comparison at all stations with a traveling calibration clock, which in turn is compared at regular intervals with an atomic standard (e.g., that of the U.S. Naval Observatory). Stations with limited accessibility are additionally equipped with a cesium standard. The transmission, via satellites, of time signals for clock comparisons has proved quite satisfactory, with accuracies of from ± 2 to ± 10 μsec, depending on the electronic equipment available at the receiving station. These procedures assure the elimination of the error source due to uncertainties in the propagation of light and reduce all other timing errors below the overall error level of the system. All other residual errors can therefore be neglected in the adjustment.

E. A. Taylor describes the BC–4 installation as modified to the specifications of the U.S. Coast and Geodetic Survey from the original missile trajectory instrumentation. The present BC-4 phototheodolite differs from the installation described by E. A. Taylor mainly in the optic now in use, a special objective designed by Dr. Bertele and constructed by the Wild-Heerbrugg Co., which, taking all theoretical and practical considerations into account, represents an optimal solution for satellite triangulation. The Cosmotar objective has a focal length of 450 mm with a relative opening of 1:3.4, its chief advantage lying in the fact that it has minimal change of radial distortion within the visible spectrum. This practically eliminates differences in radial distortion for the centroids of images of stars of various colors and of the sun's image reflected from the satellite. Figure 7.1 shows a camera with the Cosmotar objective and the Henson capping shutter mentioned in the next section. Figure 7.2 shows a typical BC–4 station.

7.2.1.2 Camera Shutters and Their Mechanical Drives

When continuously illuminated satellites are used for the triangulation, the tracks of

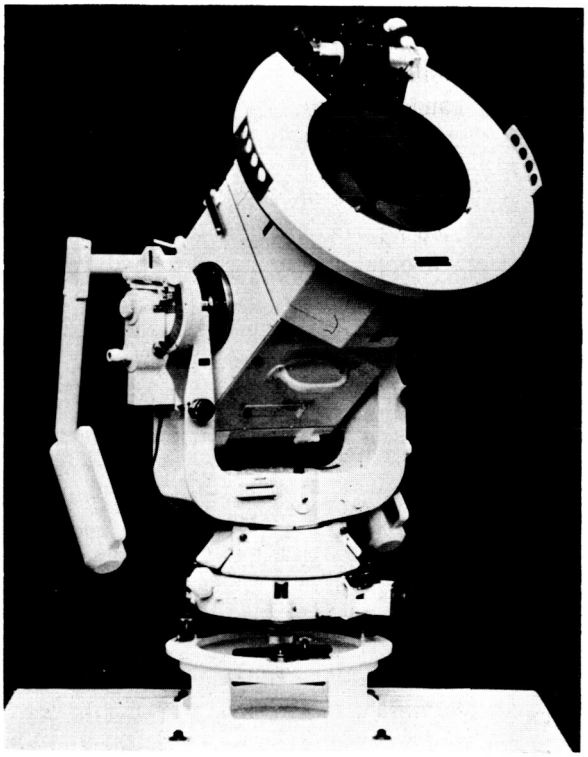

FIGURE 7.1.—Camera fitted with Cosmotar objective and Henson capping shutter.

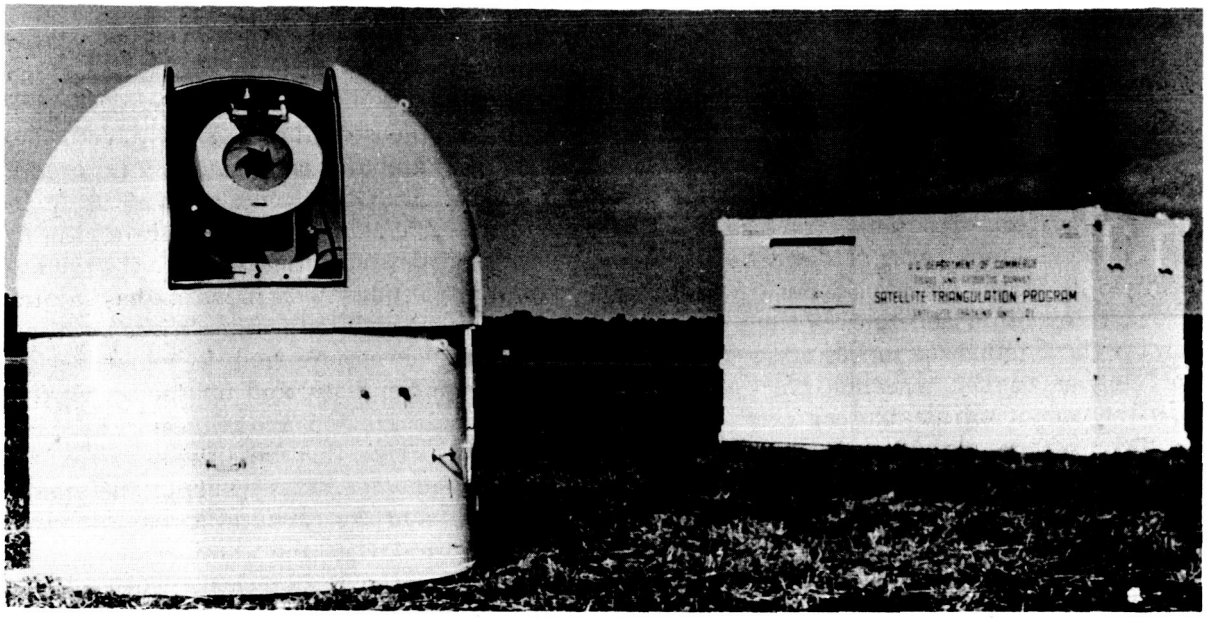

FIGURE 7.2.—Typical BC–4 installation.

the stars and of the satellites on the photogram must be chopped into a sequence of individual time-related images. The star trails are the result of the earth's rotation, shared by the Earth-fixed camera, whereas the track of the satellite is largely due to its own motion, although of course the Earth's rotation during the satellite pass contributes a component to the track. The track interruptions on the plate are effected in the BC–4 camera by three rotating disk shutters inserted between the lens elements, approximately in the principal plane of the lens system. Two of the disks rotate at equal rates in opposite directions to achieve maximum symmetry in the exposure and a high degree of efficiency (about 70%) of the shutter. The third disk subdivides the primary image sequence generated by the rotation velocity of the first two disks, which in addition fixes the exposure interval of the individual images. The most useful combinations of primary image sequence or exposure interval and actual exposure sequence in satellite triangulation, within the technical limitations of the BC–4, are given in table 7.1.

The shutter is activated by a synchronous motor specially developed for a frequency of 500 Hz. Registration of the image centroid is initiated by an adjustable magnetic pickup. Further technical details of the shutter drive, developed and manufactured by Fred C. Henson Co., Pasadena, California, are given in the literature of that company.

Corresponding to the combination selected from table 7.1, the rotating disk shutter generates a chronologically regular sequence of images. In order to create arbitrary groupings in this sequence for the purpose of identification or to further subdivide the primary image sequence, an additional iris-type shutter is installed in front of the exchangeable filter element of the BC–4 (also made by the Henson Co. and known in the trade as a capping shutter). This shutter is activated through solenoids, and thus it is possible to open or close the shutter between two successive exposures generated by the rotating shutters. Technical details of the shutter operation are given in the manufacturer's literature.

Although it would be desirable from the photogrammetric standpoint to register the stars, as well as the satellite, by means of a shutter located in the principal plane of the lens system—i.e., by means of, say, the rotating disks—a compromise is imposed by the limitations of the f-stop. Although it is

possible, even necessary (cf. sec. 7.3.1), to record stars during the period of the satellite passage, only low-magnitude stars will register adequately, and their number is insufficient for the adjustment. It is necessary, therefore, to expose stars with the aid of the capping shutter before and after the activation of the disk shutters; in other words, before and after the satellite exposure proper. In order to obtain the correct time correlation for these images, signals for the opening and closing of this shutter are generated with the aid of adjustable contacts, so that the mean of the corresponding two instants of time is associated with the midpoint of the segment of the so-called star trail, which is of finite length even for relatively short intervals of exposure.

7.2.1.3 Electronic Control Instrumentation

The electronic control performs the following principal functions:

(1) Drives the 500–Hz synchronous motor of the rotary disk shutter from the built-in station frequency standard.

(2) Controls the station clock with the same frequency standard.

(3) Synchronizes the signal from the magnetic pickup of the rotating disk shutter with the station clock.

(4) Controls both shutter systems.

(5) Illuminates the fiducial marks and the display of auxiliary data for later identification evaluation.

(6) Drives the nine-channel registration equipment that records the course of the observation program.

(7) Compares the station clock with an external time standard or signal and monitors the accuracy of the rate of the frequency standard of the station by means of a received calibration frequency (VLF).

In order to synchronize the rotating disk shutter with the station clock, the exposure sequence for a satellite pass is set mechanically by a suitable selection of gear ratio in the camera control (see table 7.1) with a similar electronic program in the synchronization system. This results in a display on the oscilloscope of a pulse sequence for the time code generator corresponding to the selected program (for example, two exposures per second). Simultaneously, the pulses from the magnetic pickup, indicating the mid-open position of the shutters, are fed to the oscillograph. By a phase comparison the two, in time initially different, signals are brought into coincidence, effecting synchronization between station clock and exposure. Owing to practical limitations in the mechanical precision of the drive, there are slight irregularities in the shutter rates, causing the signal returning from the cameras to vary irregularly in time with the comparison signal originating in the station clock. These deviations are of the order of from ± 20 to ± 40 μsec. The actual synchronization process is, therefore, to give the signal from the station clock an adjustable bandwidth to each side of, for example, 100 μsec. If the signal from the BC–4 falls within this gate, it is registered as synchronous on the oscillograph tape; otherwise, it is not. The rate of the frequency standard is monitored with a received frequency (VLF), and absolute time is assigned by the method described at the end of section 7.2.1.1.

When the auxiliary capping shutter is in operation for star exposure, with the rotating disk shutters at rest, its opening and closing

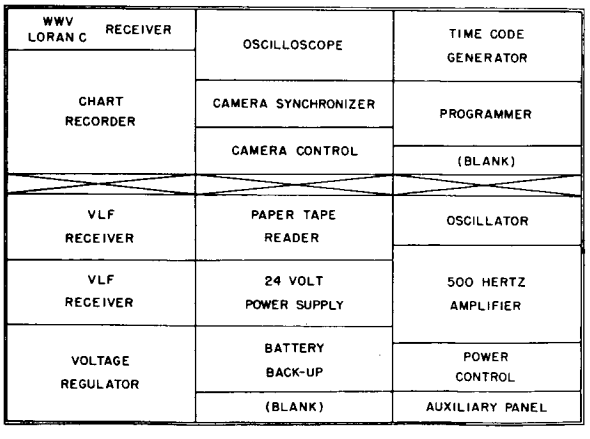

FIGURE 7.3.—BC–4 electronics console schematic.

are recorded by the oscillograph tape together with the station clock signals. This record determines time for the star exposures. The arrangement of the console, which at this time is part of all the BC–4 systems, is shown in figure 7.3

7.3 DATA

The survey coordinates of the stations whose observations were used are given in table 7.2. The distribution of the stations is shown in figures 7.4 and 7.5 through 7.10.

The set of interstation directions derived from the observations was associated with a scalar by including eight interstation distances computed from ground survey (fig. 7.11). These distances are given in table 7.3; the sources for the distances are listed in table 7.4.

Table 7.5 gives the number of photograms taken and processed for each station. The geographic distribution of the observations (location and direction of subsatellite points) is shown in figures 7.5 through 7.10.

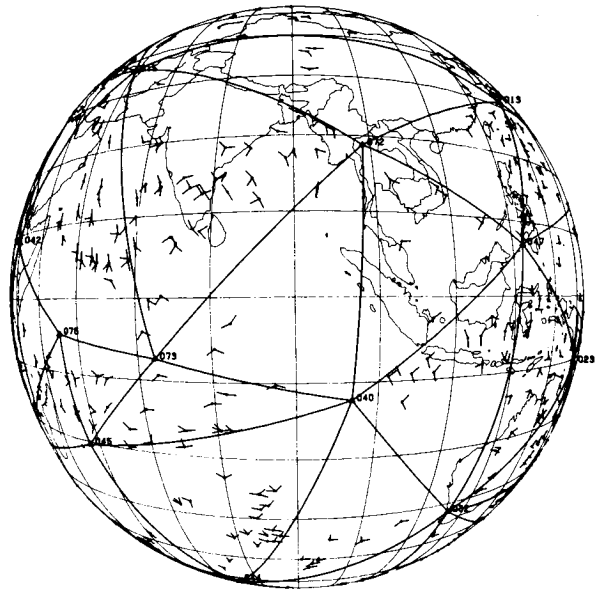

FIGURE 7.5.—Geographic distribution of stations and observations. Center of view: latitude 0°, longitude, 90° east.

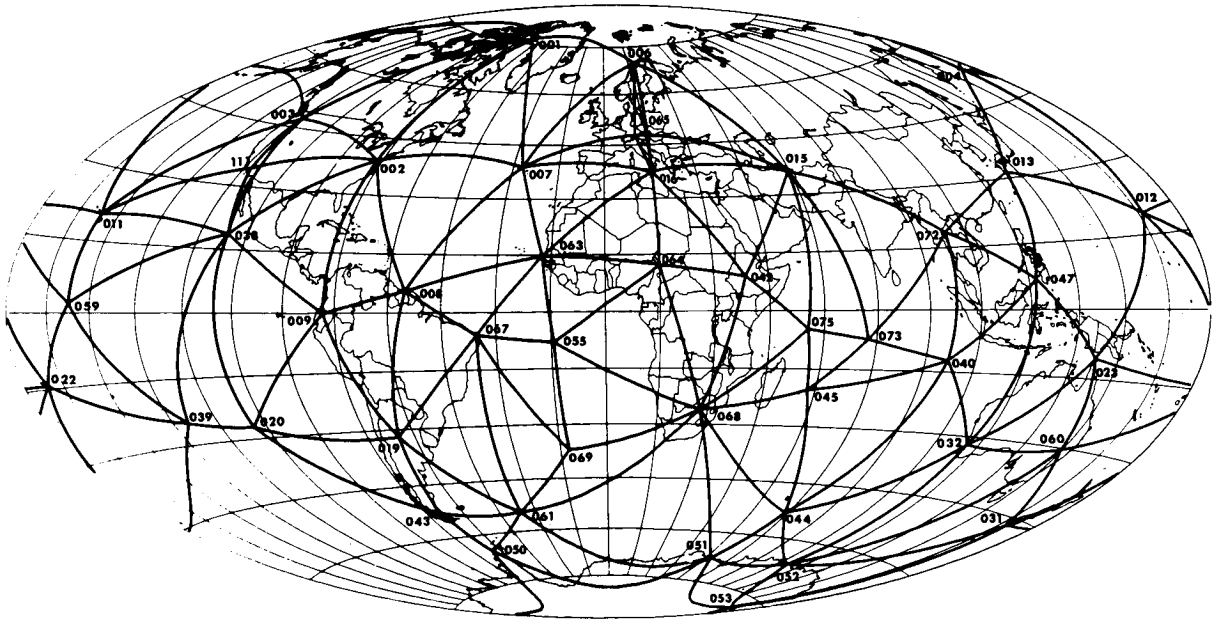

FIGURE 7.4.—Forty-five-station, worldwide, BC–4 photogrammetric satellite triangulation network. (Aitoff-Hammer equal area projection.)

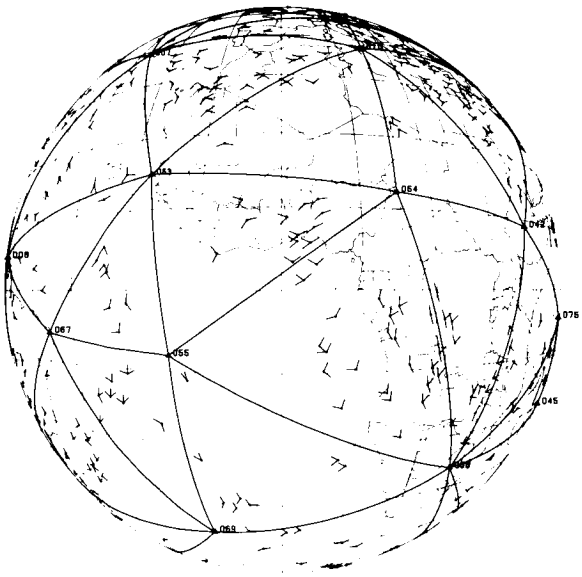

FIGURE 7.6.—Geographic distribution of stations and observations. Center of view: latitude 0°, longitude 0°.

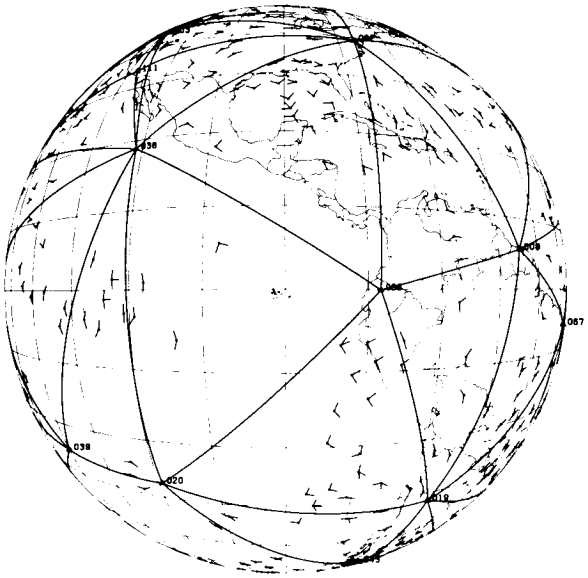

FIGURE 7.8.—Geographic distribution of stations and observations. Center of view: latitude 0°, longitude 90° west.

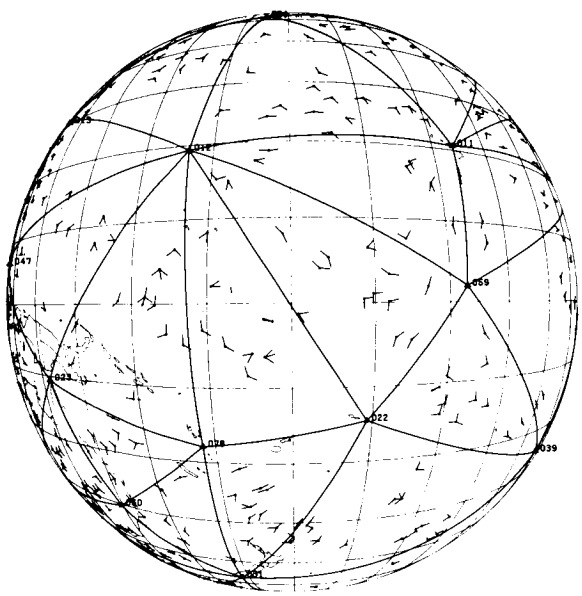

FIGURE 7.7.—Geographic distribution of stations and observations. Center of view: latitude 0°, longitude 180°.

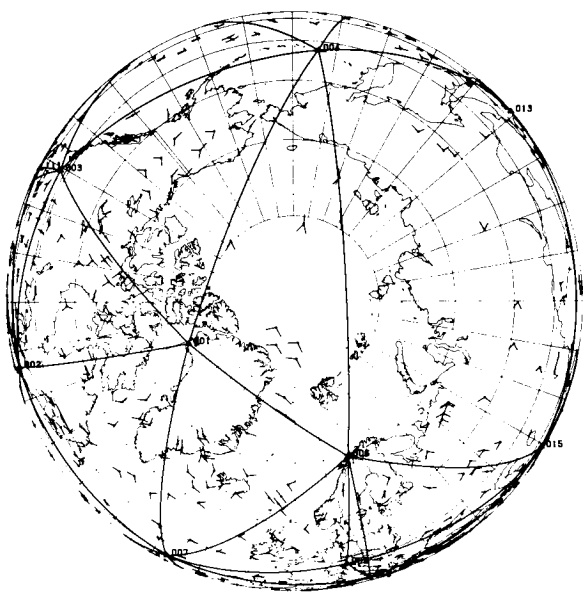

FIGURE 7.9.—Geographic distribution of stations and observations. Center of view: North Pole.

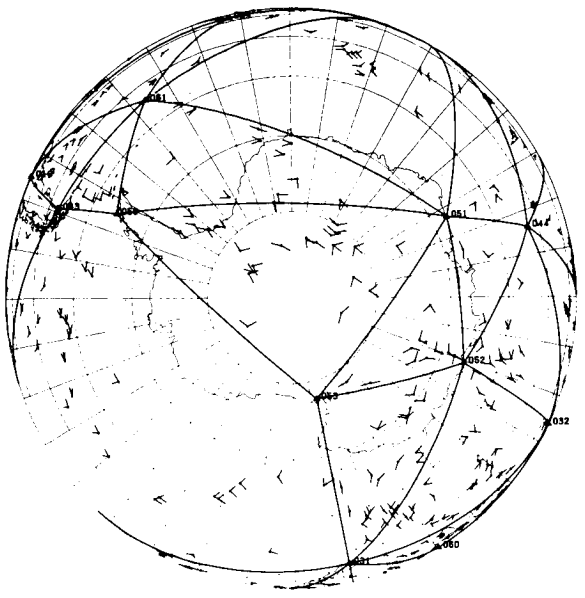

FIGURE 7.10.—Geographic distribution of stations and observations. Center of view: South Pole.

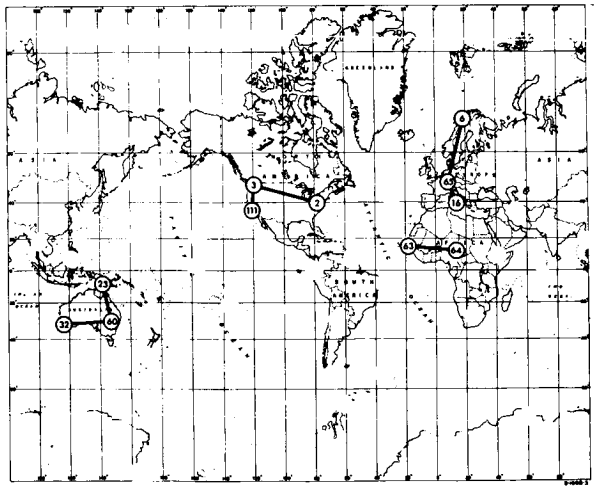

FIGURE 7.11.—Base lines used in adjustment.

7.3.1 Photogrammetric Registration

The size of the effective photographic area of the BC–4 plates is 18×18 cm. The plates are either 6 or 10 mm thick, and those of best quality have a flatness of 3 μm. A good compromise between sensitivity and grain size is found in the Eastman Kodak emulsion 103–F. After accurately controlled developing of the plate, particular care must be exercised in the drying process: the plate must be turned continuously. The essential information content of an individual photogram consists of the point-shaped star images and the satellite trail. For star registration a sequence of five successive individual images is necessary, for statistical reasons. In order to obtain uniform star images independent of star magnitude, it is necessary to expose several such sequences with various shutter speeds. The selection of optimal exposure time is, in addition, dependent on the range in declination of the stars. Star photography, using the capping shutter, is executed before as well as after the satellite pass. During the satellite pass, additional images of the brighter stars in the field of view are generated by appropriate programing of the rotating disk shutters. These stellar images are of particular importance for the exterior orientation, since they are recorded simultaneously with the satellite trail. With suitable choice of exposure interval it is possible to obtain a presentation of both stars and the satellite in a series of similar point-shaped images.

In measuring the negative itself, one is presented with the problem of centering a black measuring mark within a dark point-shaped image. (To date—1973—ring-shaped measuring marks with a diameter of 20 to 30 μm are not available.) A series of experiments has shown that the plate measurement process is faster and more reliable if a diapositive is first produced, so that the black measuring mark can be set within a white round image.

The negatives are copied in almost monochromatic blue light under vacuum onto a 6-mm-thick glass plate covered with an exceedingly fine-grained emulsion. Statistical tests have shown that the copying process introduces no marked deterioration in accuracy. Figure 7.12 shows the star and satellite images schematically. The sequences *A*, *B*, *C*, and *D*, *E*, *F* represent five star images, each taken with the capping shutter and various

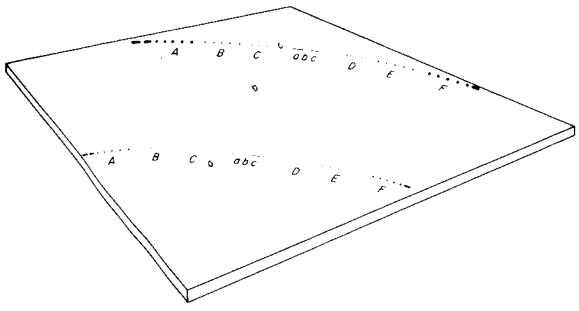

FIGURE 7.12.—Schematic presentation of star and satellite images.

shutter speeds, before and after the satellite pass, the upper star trails representing a brighter star. The sequences *a, b, c* symbolize images of the satellite and of stars recorded simultaneously by means of the rotating disk shutter. Because of the limited resolution of the objective and emulsion, only a single approximately point-shaped star image *b* corresponds to the three satellite images designated *b*, whereas the star imagery corresponding to the satellite exposure intervals *a* and *c* appear as star trails, unresolved into individual images. Stars that are insufficiently bright produce no measurable image *b*, and those of higher magnitude are not recorded at all through the rotating disk shutter. Figure 7.13 is a magnified portion of a plate, showing trails of the balloon satellites ECHO–1 and ECHO–2 generated by the rotating disk shutter.

7.3.2 Coordinate Measurements on the Comparator and Their Reduction

Measurement of the photograms, either of the original negative or of a diapositive copy, produces rectangular coordinates in the plate plane with a basically arbitrary origin. The comparator used does not have to operate necessarily on this principle, but can, for example, measure polar coordinates instead (D. C. Brown, unpublished). These must, however, be transformed to the x, y coordinates needed later in the adjustment, and the corresponding weight matrix, correlated in this case, must be computed. Since the measurement of photograms is one of the most essential phases of analytical photogrammetry and as such has been discussed in detail in the literature, and since, furthermore, the specific measuring method used depends not only on the type of comparator used but also on the organizational and environmental conditions, only those phases that are typical for the problem in question but do not necessarily have applicability for other more or less conventional working procedures will be discussed.

If a high degree of accuracy in the end results of geometric satellite triangulation is to be achieved, it is necessary to bear in mind from the outset the fact that a large number of points (600 to 750 star images and up to 600 satellite images) must be measured on each photogram, and consequently that 5 to 8 hours are required for the measurement. Special care must therefore be exercised in the selection of the type of comparator, the environmental conditions, and the arrangement of working procedures, so that systematic error influences can be held to a minimum or can be corrected computationally. A description of the current procedures at the U. S. National Ocean Survey (NOS) follows.

The measurements are made on comparators equipped with independent x and y screws with a working length of about 225 mm each. The instruments, manufactured by the firm of David Mann, Lincoln, Massachusetts, are equipped with a direct binocular microscope, magnification adjustable in steps up to 40×, and a circular measuring mark (dot) with a diameter of about 30 μm. The comparators are operated in a controlled environment (temperature 22° C$\pm$0.5°, humidity 50%$\pm$5%) and tested about every 2 months for linear and periodic scale errors in the x and y screws as well as for orthogonality of the motions. Calibrated grid plates in each of four positions are measured for this purpose by each of three observers. The measured coordinates to the nearest micron are registered electronically on a typewriter, punched tape, or card. The initial operations revealed the fact that the operator's body heat generated an unacceptably

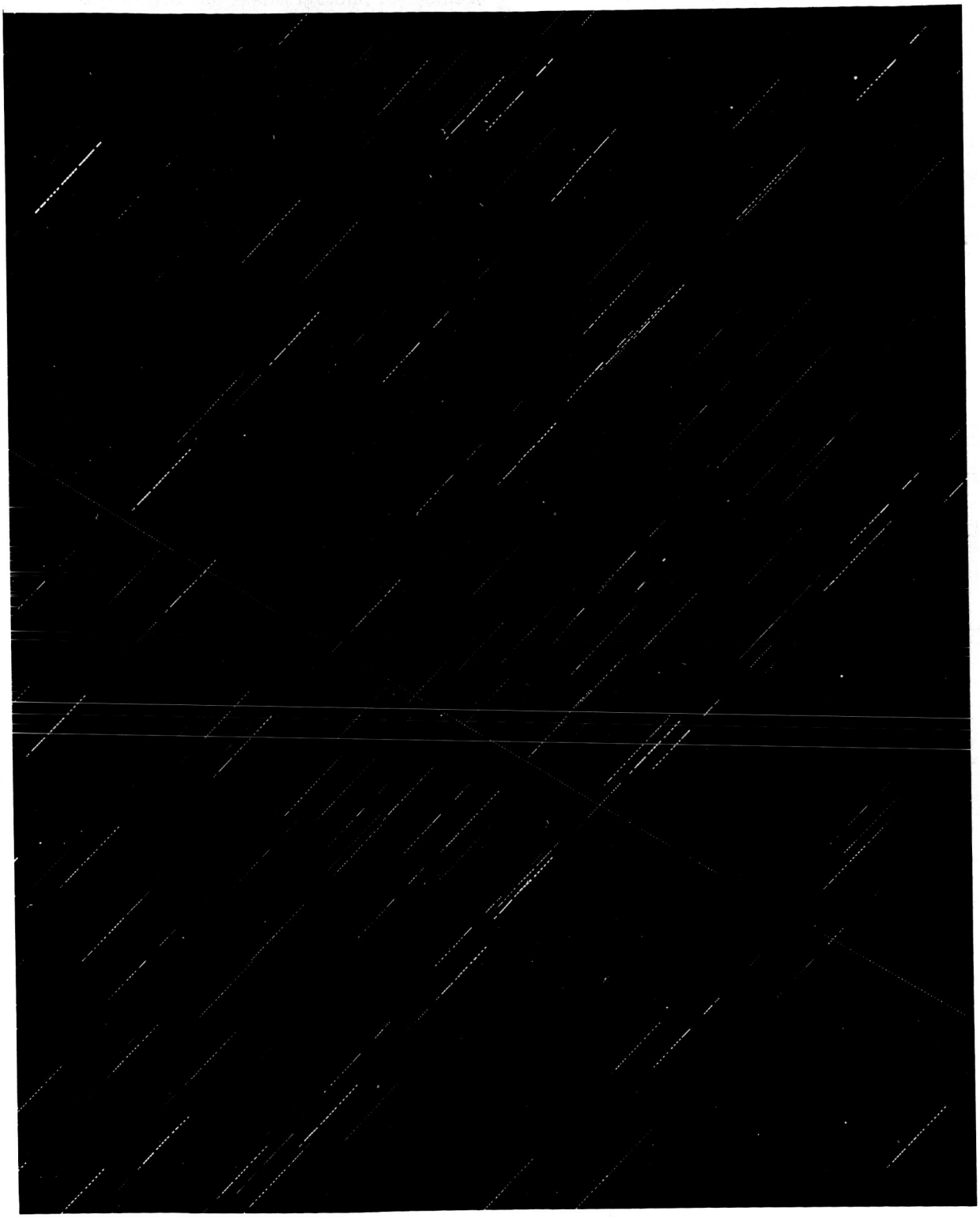

FIGURE 7.13.—Star plate.

large systematic error in the measurements, because the optics of the comparator was not constructed in accordance with the Abbe principle. It was necessary, therefore, to modify the construction to project the measuring mark into the plane of measurement. Extensive tests have shown that the comparators now are stable for operating periods of from 2 to 3 hours. However, it is still necessary to subdivide the measurement of a plate into several such periods.

The first step is to drill eight circular holes into the emulsion, approximately 40 to 50 μm in diameter. These are located at the four corners, the extremities of the legs of the conventional fiducial marks pointing toward the center, and at the approximate center of each edge. These drill holes are measured at the beginning and end of each measuring session, and the differences are used to check the stability of the instrument during that period. Before continuing with the description of the measuring procedure, some essentials on the preparation for plate measurement must be mentioned.

The readings on the circles in the field give an orientation of the camera in azimuth and elevation to within 10 to 20′. With the time of observation and approximate station coordinates, a range in right ascension and declination on the celestial sphere can be computed. The computer searches the star catalog tape for all stars in this portion of the sky, and their coordinates together with the nominal camera constants and the approximated orientation data are used to compute plate coordinates for these stars. These points are projected on a cathode-ray tube associated with the electronic computer and are photographed to the scale of the photogram to produce a star chart. The stars are subdivided into three groups of magnitudes and labeled accordingly. Another symbol designates a group of at least eight stars as bright as possible and located in a circular ring 3 cm wide near the edges of the plate. Since the registration on the original photogram or diapositive varies according to magnitude, it is easy to bring the photogram and the "computed star chart" into coincidence on a light table. At the same time, a grid template is superimposed, dividing the plate format into 100 equal squares. The photogram is now examined under the binocular magnification of the comparator. In each of the squares a star of the series, before and after the satellite pass, that coincides with an image on the star chart is selected and marked. In addition, all stars recorded during the satellite pass (cf. fig. 7.12) and the specially selected bright stars near the edge of the plate are marked with an identification symbol.

After this preparation, the plate is placed in the comparator. In order to eliminate as far as possible the influence of unknown systematic errors, a subgroup of stars and satellite images covering the whole extent of the plate is measured at each of the two or three sessions required. At the completion of the measurements all premarked stars and satellite images will have been measured. In connection with the satellite trail it should be added that it crosses the plate within at most a few millimeters of the center and its images are measured to a maximum distance of 6 cm from the center, in order to avoid edge effects in the emulsion. To combine in a consistent system the reading obtained from the two or three necessary comparator sittings, the individual sets are translated, rotated, and stretched with two scale corrections in adjustment, in accordance with the coordinates of the relevant drill holes to best fit the configuration of drill holes, showing the smallest mean error. The residuals of the reference points after these transformations are typically 0.3 μm. The entire measuring process is then repeated with the plate turned through approximately 180 degrees. Both results are then meaned by fitting the latter result to the first, again by means of an adjustment (determination of two components of translation, a rotation, and two scale factors). From the residual differences between corresponding double measurements in this adjustment, a characteristic mean error of 1.6 μm results as a measure of precision of the measured coordinates.

In addition, the plate coordinates of all premarked star and satellite images are referred

to the plate center as determined by the fiducial marks. The coordinates of the above-mentioned bright stars near the edges of the plate that are easily identifiable in the catalog are now used to compute an approximate orientation. With this result, right ascensions and declinations are computed from the image coordinates of all measured stars (cf. sec. 7.4.6). The same program compares these values with the tape containing the star catalog, identifies the stars, and updates them to the observation epoch and true equinox (cf. sec. 7.4.3, eqs. 7.1–7.15).

The step in the overall adjustment procedure of satellite triangulation under discussion represents a mutually interacting combination of human effort and electronic computing. The contributions from the human element, such as the execution of the measurements and evaluation of the statistical intermediate results, are the critical operations; the computing system prepares star charts, presents catalogued data, and makes the necessary computations.

After completion of this operation, measured coordinates for all selected stars and satellite images are available, as well as the star coordinates reduced up to a certain point. These data are now further reduced in a numerical adjustment to be discussed in section 7.4.6.

7.4 THEORY

7.4.1 Introductory Considerations

In the classical treatment of geometric geodesy, i.e., the part of geodesy that concerns itself with the derivation of rigorous geometric results, difficulties arise from the fact that the measured quantities cannot be rigorously related to the geometric model that is to be established. Physical influences are responsible for this dilemma. The so-called measurements of horizontal and vertical angles are vitiated to an unknown extent by systematic influences such as anomalies in the gravity field and refraction. The reduction of baseline measurements is in principle similarly affected.

In addition, the classical method of triangulation is forced to adopt a number of complex postulates whose geometric content is based on certain hypotheses. Typical examples are the present-day correction methods generally known as "isostatic reduction procedures." The physical principle underlying these procedures is the assumption of homogeneity and hydrostatic equilibrium of the masses within the Earth's crust. The resulting corrections to all geodetic observations will prejudice the end result in favor of Clairaut's theory. Aside from the physical assumptions, an unavoidable characteristic of classical geodetic triangulation consists of the practical limitation of sight length between points on or near the surface of the Earth. Not only are such geodetic triangulations incapable of making intercontinental connections, but the first-order nets must be pieced together with an excessive number of individual arcs. The disadvantage of this method arises not so much from the relatively large number of stations involved as from the fact that accuracy is impaired, especially in extensive nets, by error propagation.

As a consequence, geodetic theory has developed complex methods of adjustment designed to eliminate the contradictions in the data by iteration, permitting the results of partly geometric and partly geophysical adjustment operations to interact until all results become internally consistent. Although they are attractive from a theoretical standpoint, such methods have practical limitations. For this reason a purely geometrically defined, three-dimensional worldwide geodetic reference system is desired in order to transcend the shortcomings of the classical geodetic triangulation method. Moreover, such a worldwide geometric solution is superior to a mere connection of the various geodetic datums, which has at times been called the purpose of satellite geodesy.

The significance of a three-dimensional triangulation method, emphasized repeatedly in the recent history of geodesy, becomes especially apparent in connection with the field of satellite geodesy, which because of its geometric and geophysical aspects demands a three-

dimensional solution. Perhaps the greatest significance of geometric satellite triangulation, however, lies in the fact that with this method there exists, for the first time in the history of geodesy, the possibility for the creation of a worldwide three-dimensional reference system that is supported by a minimum of a priori hypotheses, in particular without reference to either the magnitude or the direction of the force of gravity.

Establishing geometric correspondence among a number of selected nonintervisible points of the physical surface of the Earth can be accomplished with spatial triangulation by means of auxiliary targets elevated sufficiently above the Earth's surface.

The generation of light signals visible over large distances is possible by means of artificial satellites. Because of the high velocity of such targets, observation of directions to them can at present be made only with photogrammetric precision cameras. Owing to the physical and chemical properties of the photogrammetric measurement components, the absolute accuracy as well as the reproducibility of the observation conditions in this method is limited. To obtain observational results with maximum absolute accuracy, the adjustment of the photogrammetric measurements must be based on a method of interpolation.

A suitable reference system into which an elevated target can be intercalated is obviously the right ascension-declination system of metric astronomy. This system is all the more attractive from the geodetic point of view because one of its axes is parallel to the Earth's axis of rotation. A large number of fixed stars are available whose coordinates are tabulated in catalogs. These control points being practically at an infinite distance, it follows that their direction coordinates are insensitive to a parallel displacement of the observer and hence cannot be used for scale determination. It is therefore necessary to determine the scale of the satellite triangulation independently: for example, by measuring the distance between two adjacent stations. As will be shown later (sec. 7.4.3), it is necessary to carry out such scale determinations in several portions of the worldwide triangulation net.

7.4.2 Geometric Foundations

We turn our attention now to a three-dimensional method of triangulation that is based on direction measurement and designed to determine the coordinates of nonintervisible triangulation stations.

The relevant geometric solution is not new. In fact, there is little room for originality in the field of the application of photogrammetry to ballistic and related problems. The use of star photography for the calibration of photogrammetric cameras is a proven method, especially with astronomers. The use of star images to orient photogrammetric cameras and the corresponding triangulation of additionally photographed target points was used successfully in the 1930's by Hopmann and Lohmann (1943) in the tracking of missiles before the method was applied in the development of the V–2 rocket at Peenemünde, Germany, and subsequently in various other countries.

There are several ways to present the geometric principles of this triangulation method. Väisälä's proposal contains a lucid geometric explanation. Two rays issuing from the end-points of a given baseline and directed at a common point define a plane in space whose orientation can be determined from the direction cosines of the rays. When two such planes have been fixed, the direction in space of the baseline can be computed as the intersection of the two planes. The principle involved is shown in figures 7.14 and 7.15.

After two directions AB and AC issuing from station A have been determined in this fashion, the shape and spatial orientation of the station triangle ABC is fixed by intersecting AB and AC with a plane whose orientation is known from observing the satellite position S_5 from B and C. Thus, five planes are necessary and sufficient to fix the shape and orientation of a station triangle. Each of these planes contains two stations and one point of the satellite orbit; therefore, there

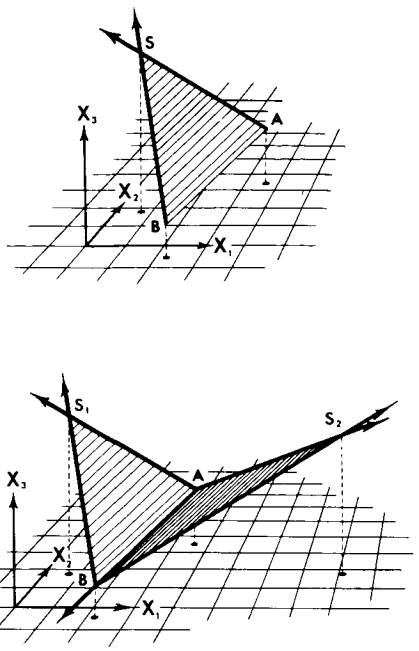

FIGURE 7.14

are five positions of the orbit, together with the positions of the three stations *A*, *B*, *C*, or $(5+3)\times 3=24$ unknowns to be determined.

Since each pair of simultaneous observations of a satellite position—or, in other words, the determination in space of two intersecting lines—gives rise to four equations, there are, in all, $5\times 4=20$ equations available. Hence, $24-20=4$ additional independently determined geometric quantities are required for a complete solution of the triangle. The most obvious of the many theoretically available choices are the three coordinates of one of the stations, which, in principle, can be assumed arbitrarily, for example, as the origin of the coordinate system. It is equally logical to choose as the fourth assumption the length of one of the sides of the triangle, which fixes the scale for the whole triangulation. For purposes of explaining the principle of satellite triangulation it is sufficient to introduce this side-length as the unit of length.

It is interesting to note that three of the five necessary planes can be determined with a single pass of the satellite, if the satellite subpoint lies near the middle of the triangle

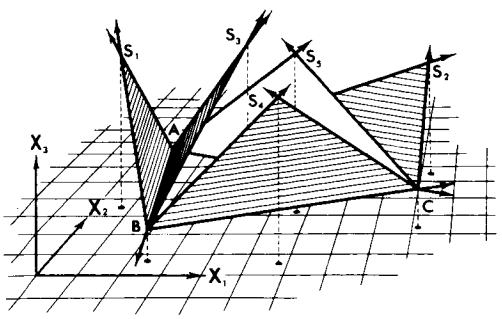

FIGURE 7.15

of stations (see fig. 7.16). For this case, a unique solution can be obtained with the determination of $(3+3)\times 3=18$ unknowns from $7\times 2=14$ available condition equations. Again, four additional independently determined parameters must be introduced.

From the viewpoint of analytical photogrammetry, the geometric principle of satellite triangulation can be explained by identifying the unknown positions of the triangulation stations and the unknown orientations of the observing cameras with the corresponding conditions in classical aerial photogrammetry. The unknown orbital positions of the satellite correspond to the relative control points, with the restriction that they cannot furnish scale, since they lie at an infinite distance.

The geometric concept of photogrammetric satellite triangulation must, however, be interpreted in the light of the fact that at each station the stars (absolute control points) are used for the determination of the elements of the interior orientation necessary for the reconstruction of the photogrammetric bundle,

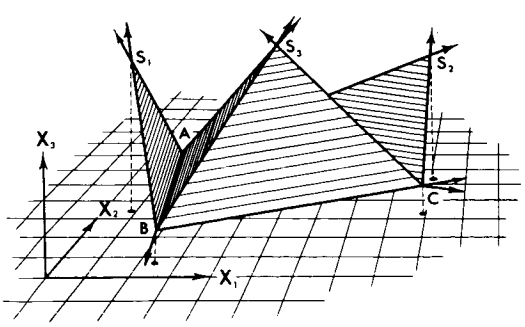

FIGURE 7.16

together with the determination of the three rotation elements of the exterior orientation. The condition of intersection of the rays resulting for each satellite image observed from more than one station is used exclusively to determine the three elements of translation of the exterior orientation. This circumvents the unfavorable correlation between the elements of rotation and translation that is typical in aerial triangulation, an advantage that is reflected in the favorable error propagation characteristics of satellite triangulation (see sec. 7.3.3).

The geometric content of satellite triangulation, in complete agreement with the corresponding concepts in the general field of analytical photogrammetry, is thus based on a multitude of individual rays whose directions must be determined from the relevant photograms. Hence, the idealized conditions must be satisfied: that the three points— objective (satellite), center of projection (triangulation station), and image (photographed satellite image)—lie on one straight line. This condition is the geometric basis for satellite triangulation, just as it is the necessary and sufficient criterion for any photogrammetric triangulation (Schmid, 1958, 1959).

It is obvious that after fixing the first station triangle in space nothing prevents the addition of further stations as vertices of triangles adjacent to the first. Postulating the possibility of scale determination, either by direct measurement of a side of one of the space triangles or, for example, by simultaneous distance measurement from at least four stations to a satellite position, the positions of a number of points on the physical surface of the Earth can be determined in a homogeneous three-dimensional reference system. In practice, the arrangement of the stations, and hence the shape of the configuration, is to a great extent dictated by the geographical distribution of islands over the oceans.

Aside from using the method to determine a worldwide geodetic reference system, the same technique can be applied to establish the frames for continental triangulations. On the basis of accuracies in the determination of directions attained even today and of the basically favorable error propagation characteristic of satellite triangulation, these frames are equivalent or superior to classical first-order nets, particularly where such nets cover extensive areas (see fig. 7.17).

Judging by present technical standards, it seems unlikely that, because of their limited life span, satellites with a height above the earth of under 1000 km will be used. Therefore, as a consequence of the nearly linear decrease in accuracy of the triangulation results with increased height (see sec. 7.4.3), the practically acceptable shortest average distance between points of a continental satellite triangulation net should be 500 to 1000 km. Without changing in any way the geometric principle—although the influence of the physical parameters is different and not necessarily more favorable from the standpoint of measuring technique—the described method of satellite triangulation becomes a type of three-dimensional triangulation with elevated targets, taking into account present-day capabilities to generate a large number of light flashes or to burn pyrotechnic signals on airplanes, which may in the near future be

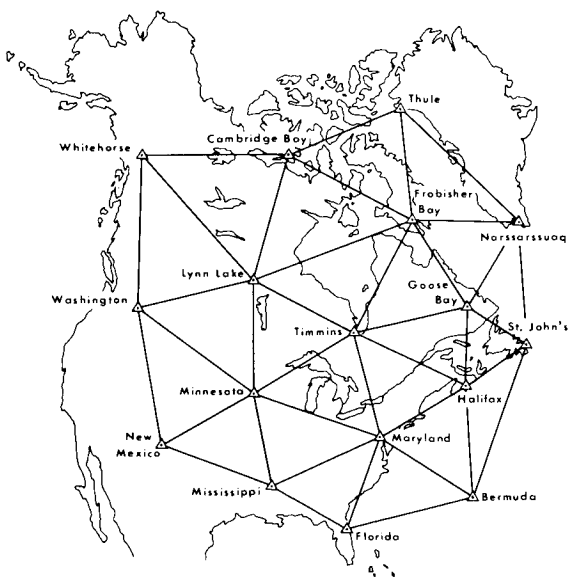

FIGURE 7.17.—Satellite-triangulation network in North America.

expected to fly at heights of 20 to 25 km. In addition to the theoretically desirable three-dimensional character of the triangulation method, it will be a question of economic feasibility whether the development of such a technique will, in part, replace classical first-order triangulation in certain areas of the Earth.

Quite independently of the measurements of the individual spatial triangulation figures, the basic geometrical concept underlying the method of satellite triangulation requires, at least in principle, simultaneously executed observations of directions to the target (in our case the satellite) from at least two stations. Clearly, the requirement to measure directions rather than merely angles implies the necessity of orienting the observed bundle in each case relative to a uniquely defined system of reference. This is otherwise self-evident in view of the fact that our end result is to represent a consistent spatial reference system.

A spatial coordinate system to which a direction to a target sufficiently elevated above the horizon can be referred is the right ascension-declination system. This reference system, surrounding the whole Earth, is qualitatively as well as quantitatively suitable, a great number of precisely measured reference points being readily available. Of especial significance to the photogrammetric mensuration principle is the abundance of such absolute control points, since because of the physical and chemical nature of its numerous components and procedures the photogrammetric method can satisfy the requirements for highest accuracy only if the corresponding observational and adjustment procedures are executed in a close-interval interpolation process.

We emphasize here, therefore, that the claim of satellite triangulation, that it produces results without the aid of physical hypotheses and practically free of systematic errors, derives chiefly from the fact that photogrammetric direction determination in satellite triangulation not only operates with the aid of geometric interpolation within the reconstructed photogrammetric bundle but represents equally an interpolation into the physical process of astronomic refraction (see sec. 7.4.5). This also means that the absolute accuracy of photogrammetric satellite triangulation depends primarily on the quality of the right ascension-declination system, particularly on its freedom from systematic errors. On account of the importance of the astronomic reference system to satellite triangulation, some relevant remarks will be made in the next section, specifically as they apply to the data processing in satellite triangulation.

7.4.3 Astronomical Reference System [1, 2]

In satellite triangulation, photographing the fixed stars serves to reconstruct and to uniquely orient in space the photogrammetric bundle. The problem of reconstructing the bundle is fundamentally identical with the problem of calibrating a photogrammetric camera. The geometric interpretation of the relevant parameters is independent of the orientation of the camera. It would therefore suffice to have given the relative geometric arrangement of the images of the stars on a particular plate in an arbitrary coordinate

[1] For the proper interpretation of the computations in this section it is recommended that the reader first study sections 7.4.6 and 7.4.8.

[2] The symbolism used in this chapter is common in photogrammetric practice, and the author did not wish it changed. Some of the symbols are used with different meanings outside of photogrammetry (in particular in geodesy and astronomy) and even occur in this chapter with two or more meanings. Therefore, care should be exercised in interpreting the equations in this chapter. For this reason, the following ambiguities are indicated by footnotes: (1) α is used in this chapter to denote one of the angles defining the orientation of a camera and to denote right ascension; the latter sense is that used in the rest of the volume. (2) The symbol c is used to denote one or (with subscripts) more of the characteristics of a camera and to denote the velocity of light; only the latter convention is used in the rest of this volume. Where used in this chapter in the former sense and where confusion may occur, the exceptions are noted by (1) a dagger (†) for α denoting one of the angles defining the orientation of the camera, and (2) a double dagger (‡) for c denoting a characteristic of the camera. Editor.

system. However, the determination of an unambiguous orientation for all the bundles of rays serving the triangulation is predicated on the fact that all given control points (the totality of fixed stars used) are given in a uniquely defined reference system, which furthermore can be uniquely transformed to an Earth-fixed coordinate frame. The right ascension-declination system of metric astronomy, as was previously mentioned, furnishes the metric basis for geometric satellite triangulation. The point of departure is the apparent position coordinates of stars tabulated for a given epoch in star catalogs such as *Apparent Places of 1535 Fundamental Stars,* published by the Astronomisches Rechen-Institut, Heidelberg; the *General Catalogue* (Boss, 1936), with approximately 33 000 apparent star positions; or in probably the most complete catalog to date, issued by the Smithsonian Astrophysical Laboratory, in which over 250 000 stars with their apparent places are tabulated (see chs. 1 and 9).

The choice of stars selected for the purpose of satellite triangulation depends primarily on the accuracy of their coordinates. Stars with large proper motions should be avoided and double stars should not be used at all.

To counteract the influence of spectral differences of the stars, a special lens was used (see sec. 7.2). Finally, the selection was limited by the magnitude registered by the specific optical system and emulsion used. With the BC–4 system and the Eastman-Kodak emulsion 103–F in use today, stars of the seventh and eighth magnitude still produced good, measurable images over the entire plate. Using very bright stars at the same time raised the question concerning the influence of relative systematic errors in locating the centroid of the image. With the focal lengths in use at present for satellite triangulation purposes, the existence of a magnitude effect, which is not negligible in astronomical measurements, has not as yet been quantitatively demonstrated.

In Bossler (1966), the distribution over the celestial sphere with respect to right ascension and declination of the Smithsonian catalog stars is described from the standpoint used in the selection.

Geometric satellite triangulation can at best, therefore, attain the accuracy of the astronomical reference system (see sec. 7.3.1). Hence, for a critical study of the theoretical accuracy of satellite triangulation, the observation and adjustment procedures used in metric astronomy to establish star catalogs are of fundamental importance. Within the frame of this presentation it must suffice to refer to the literature on these highly specialized and complex procedures: Clemence, 1963; Scott, 1957, 1963; Vasilevskis, 1963; Dieckvoss, 1963; Woolard and Clemence, 1966.

To understand geometric satellite triangulation, it is necessary to interpret correctly the qualitative (geometric) and quantitative (statistical) data listed in the star catalogs in order to grasp the reductions necessary to transform the time- and space-dependent geometry of the individual photogrammetric exposures into a homogeneous geometric system. The problems arising in this connection are basically the same as those faced in the reduction of astronomic geodetic field observations.

The star catalogs list for apparent places a pair of spherical coordinates for a specified epoch, right ascension α and declination δ (see ch. 1). The specification that the cataloged values refer to a given epoch (generally the beginning of the tropical year 1950.0 in the newer catalogs) means that time-dependent corrections must be added to the star coordinates before they represent the actual position at the instant of observation, in our case the time of exposure.

The reason for these corrections is chiefly to be found in the dynamics of the universe, although purely physically based corrections must also be taken into consideration. Theoretical explanations are described in detail in standard works on geodetic astronomy (e.g., König, 1962; Clemence, 1966; Wayman, 1966; Fricke and Kopff, 1963; Morgan, 1952; Gliese, 1963; Kopff *et al.*, 1964). Nevertheless, it seems useful to outline here, in terms of formulas, the sequence of corrections used.

For one thing, such a presentation will present a computerized method designed to reduce a large number of star places, including circumpolars, that are needed in geometric satellite triangulation. For another, it helps to clarify the contribution of the individual corrections to the overall adjustment procedure of satellite triangulation and to judge the technical and economical aspects involved.

The following computations are made for the purpose of deriving, from the star catalog data for a specific epoch, that unit vector which designates the apparent geocentric direction of a star with reference to the true equinox at the instant T of observation. The solution shown here is based on the method now in use at the U. S. Naval Observatory. The lower indices to the right of the matrices designate first, the equinox to which the coordinates are referred, and second, the epoch. To begin with, the heliocentric unit vector $\mathbf{x}_{00}$, referred to the epoch and equinox of the catalog used, is computed with the catalog entries α and δ.

$$\mathbf{x}_{00}\begin{bmatrix} x_1 \\ x_2 \\ x_3 \end{bmatrix}_{00} = \begin{bmatrix} \cos\delta\sin\alpha \\ \cos\delta\sin\alpha \\ \sin\delta \end{bmatrix}_{00} \qquad (7.1)$$

Then the star coordinates are corrected for the proper motion of the star. The corresponding correction vector $\mathbf{\mu}_x$ is computed by using the proper motion components in right ascension μ_α and in declination μ_δ listed in the catalog and by differentiating the vector in equation 7.1), since $\mathbf{\mu}_x = d\mathbf{x}/dt$ by definition,

$$\mathbf{\mu}_x = \begin{bmatrix} -\cos\delta\sin\alpha & -\sin\delta\cos\alpha \\ \cos\delta\sin\alpha & -\sin\delta\cos\alpha \\ 0 & \cos\delta \end{bmatrix}_{00} \begin{bmatrix} \mu_\alpha \\ \mu_\delta \end{bmatrix}_{00}$$
$$= \begin{bmatrix} -x_2 & -x_3x_1(1-x_3^2)^{-1/2} \\ x_1 & -x_3x_2(1-x_3^2)^{-1/2} \\ 0 & (1-x_3^2)^{1/2} \end{bmatrix}_{00} \begin{bmatrix} \mu_\alpha \\ \mu_\delta \end{bmatrix}_{00} \qquad (7.2)$$

with μ_α and μ_δ in radians.

A second differentiation yields the components of the secular variations. The corresponding vector $\mathbf{\mu}_x$ is then

$$\dot{\mathbf{\mu}}_x = -\mu^2\mathbf{x}_{00} \text{ with } \mu^2 = \mu_{x_1}^2 + \mu_{x_2}^2 + \mu_{x_3}^2 \qquad (7.3)$$

If the radial velocity of the stars is to be applied, equation (7.3) is augmented to

$$\dot{\mathbf{\mu}} = -\mu^2\mathbf{x}_{00} - 0.000205\pi V\,\mathbf{\mu}_x \qquad (7.4)$$

in which π is the parallax of the stars in seconds of arc and V is the radial velocity of the star in kilometers per second. The second term in (7.4) is quite small and needs to be considered for only a few stars.

With (7.1), (7.2), and (7.3) or (7.4) the unit vector $\mathbf{x}_{0T}$ referred to epoch T and the catalog equinox is

$$\mathbf{x}_{0T} = \mathbf{x}_{00} + \begin{bmatrix} \mu x_1 & \dot{\mu}x_1 \\ \mu_{x_2} & \dot{\mu}_{x_2} \\ \mu_{x_3} & \dot{\mu}_{x_3} \end{bmatrix} \begin{bmatrix} T \\ \frac{1}{2}T^2 \end{bmatrix} \qquad (7.5)$$

Expression (7.5) is obviously the Taylor-Maclaurin expression of vector $\mathbf{x}$ in time to second order. The time interval T is in tropical years or centuries, depending on the interval for which μ_α, μ_δ are listed in the particular catalog used; T includes the fraction τ of the year in which the observation is made. Values for τ are taken from the volume of the *American Ephemeris and Nautical Almanac* in question. The result (7.5) can be transformed for convenience in programming to

$$\mathbf{x}_{0T} = \left(1 - \frac{\mu^2T^2}{2}\right)\mathbf{x}_{00} + (T - 0.0001025\pi VT)\,\mathbf{\mu}_x \qquad (7.6)$$

The next step rotates the vector $\mathbf{x}_{0T}$ from (7.5) or (7.6) in accordance with precession, so that the transformed rectangular coordinates will be referred to the mean equinox for the beginning of the Besselian year T' nearest the date of observation. The transformation is

$$\mathbf{x}_{T'T} = \underset{3}{R}\,(-\zeta, \underset{2}{0}, -z)\,\mathbf{x}_{0T} \qquad (7.7)$$

in which the rotation matrix has the following meaning:

$$\underset{3\,2\,3}{R}(-\zeta,\theta,-z)=\underset{3}{R}(-z)\underset{2}{R}(\theta)\underset{3}{R}(-\zeta)$$
$$=\begin{bmatrix}\cos z & -\sin z & 0\\ \sin z & \cos z & 0\\ 0 & 0 & 1\end{bmatrix}\begin{bmatrix}\cos\theta & 0 & -\sin\theta\\ 0 & 1 & 0\\ \sin\theta & 0 & \cos\theta\end{bmatrix}\begin{bmatrix}\cos\zeta & -\sin\zeta & 0\\ \sin\zeta & \cos\zeta & 0\\ 0 & 0 & 1\end{bmatrix} \tag{7.8}$$

The indices under the angles in the rotation matrices designate the axis around which the rotation takes place (for direction of rotation see sec. 7.4.6.2.2). When Newcomb's constants are used, the rotation angles are

$$\begin{aligned}\zeta&=(2304''.250+1''.396T_0)+0''.302T^2\\&\quad+0''.018T^3\\ z&=\zeta+0''.791T^2\\ \theta&=(2004''.682-0''.853T_0)T-0''.426T^2\\&\quad-0''.042T^3\end{aligned} \tag{7.9}$$

The geometric meaning of the angles is given in *Explanatory Supplement to the Astronomical Ephemeris and the American Ephemeris and Nautical Almanac*. T_0 (in tropical centuries) is the interval between 1900.0 and the epoch of the catalog used; T, also in tropical centuries, is the difference between the Besselian year T' nearest the date of observation and the epoch of the catalog.

The vector of (7.7) is next corrected for annual aberration, for which daily values are listed in the *American Ephemeris and Nautical Almanac*. Since these tabulated values are computed from the true motion of the Earth with reference to the mean equinox at the beginning of the Besselian year nearest the date for which they are published, they can be applied directly to this vector. The annual aberration corrections must be interpolated with first and second differences to the date of observation. The resulting constants $-D$, C, and $C\tan\epsilon$ in radian measure may be regarded as displacements of the rectangular coordinates. Thus, the position vector of a star for the epoch T, referred to the mean equinox of T' and including the aberration, is

$$\mathbf{x}_{(T'T)}=\mathbf{x}_{T'T}+\begin{bmatrix}-D\\ +C\\ C\tan\epsilon\end{bmatrix} \tag{7.10}$$

with the mean inclination of the ecliptic

$$23^\circ 26'44''.840-46''.850T-0''.003T^2+0''.002T^3 \tag{7.11}$$

with T as above.

The transformation (7.7) accounts for precession up to the beginning of the Besselian year nearest the date of observation. An additional rotation is necessary to transform the position coordinates from the corresponding mean equinox to the true equinox at the time T of observation.

With allowable neglect of terms of second and higher order that do not contain the factor $\tan\delta$ one obtains

$$\mathbf{x}_{(TT)}=\underset{1\,2\,3}{R}(B,A,-f)\,\mathbf{x}_{(T'T)} \tag{7.12}$$

where A, f, and B in radians are taken from the *American Ephemeris and Nautical Almanac* and interpolated to second differences. The rotation matrix (7.12) has the meaning

$$\underset{1\,2\,3}{R}(B,A,-f)=\underset{3}{R}(-f)\underset{2}{R}(A)\underset{1}{R}(B)$$
$$=\begin{bmatrix}\cos f & -\sin f & 0\\ \sin f & \cos f & 0\\ 0 & 0 & 1\end{bmatrix}\begin{bmatrix}\cos A & 0 & -\sin A\\ 0 & 1 & 0\\ \sin A & 0 & \cos A\end{bmatrix}\begin{bmatrix}1 & 0 & 0\\ 0 & \cos B & \sin B\\ 0 & -\sin B & \cos B\end{bmatrix} \tag{7.13}$$

or, with sufficient accuracy,

$$\underset{1\,2\,3}{R}(B,A,-f)=\begin{bmatrix}1 & -f & -(A+Bf)\\ f & 1 & (B-Af)\\ A & -B & 1\end{bmatrix} \tag{7.14}$$

The rectangular coordinates used up to this point are heliocentric, and it is necessary to transform them to geocentric coordinates whenever the absolute parallax π appearing in the *General Catalogue of Trigonometric Stellar Parallaxes* (Jenkins, 1952) exceeds 0".010. This last correction is obtained with

$$\mathbf{x}_{TT}=\mathbf{x}_{(TT)}+\begin{bmatrix}-C\sec\epsilon\\-D\cos\epsilon\\-D\sin\epsilon\end{bmatrix}\frac{\pi}{k} \qquad (7.15)$$

with C, D, and ϵ as in (7.10). The aberration constant $k=20''.496$. The $\mathbf{x}_{TT}$ vector indicates the apparent geometric direction to a star for the observation epoch and the corresponding true equinox. The corresponding apparent right ascension and declination are obtained with the inversion of (7.1) from (7.15) as

$$\begin{aligned}\alpha&=\arctan x_2/x_1\\ \delta&=\arctan x_3/(x_1^2+x_2^2)^{1/2}\end{aligned} \qquad (7.16)$$

For a computer program a convenient sequence of operations is obtained by combining the individual steps chosen in (7.6), (7.7), (7.10), (7.12), and (7.15). In connection with (7.1), (7.2), (7.3), (7.8), (7.9), (7.11), and (7.13) or (7.14), auxiliary computations are required based on tabulated or, where necessary, interpolated values. The geocentric directions computed with the rectangular coordinates (7.15) or the orthogonal spherical coordinates (7.16) can be adopted without change as topocentric directions, since the stars are sufficiently remote; i.e., no additional parallax correction is needed. The situation is shown in figure 7.18a, where the basically geometric astronomic reference system $x_{1,2,3}$ is shown in parallel displacement to an arbitrary point of the earth's surface on a unit sphere surrounding this point.

The orientation of this assumed spatially stationary astronomic system differs, therefore, from the orientation of a geocentric coordinate system $y_{1,2,3}$ that rotates with the Earth by an angle θ_{Gr} that corresponds to this rotation and is formed by the plane of the Earth-fixed null meridian of longitude ($\lambda'=0$) and the plane of the astronomic null meridian ($\alpha=0$). The geometrical meaning of the angle θ_{Gr} is apparent from figure 7.19. It is the sidereal time of the null meridian and is computed from Universal Time (UT) (mean Greenwich time) by converting mean to Sidereal Time (i.e., by multiplication with the ratio 366.2427/365.2427 or 1.002 737 91) and adding to θ_{0Gr}. The angle θ_{0Gr} is listed in the *American Ephemeris and Nautical Almanac* for 0^h UT of each day. The introduction of Universal Time for the instant of observation makes it necessary to raise certain questions in connection with the measurement of time. This train of thought is presented in section 7.4.4.

By studying the further steps in the reduction it will become apparent that it is advantageous to change the spatial orientation of the astronomical reference system $x_{1,2,3}$ in a way to simplify the form of certain corrections.

The first is diurnal aberration. In consequence of the daily rotation of the earth-fixed observation stations with respect to the right ascension-declination system, assumed stationary, we must, in addition to the annual aberration caused by the Earth's movement around the Sun, consider a so-called diurnal aberration. This is a function of the true position (ϕ', λ') of the observation site on the Earth and the angle θ_{Gr} (see fig. 7.18a), as well as of the direction of observation, i.e., of the α and δ of the star. After the x system of figure 7.18a is turned through the angle θ about the x_3 axis (see fig. 7.19), the resulting x_1' direction lies in the meridian plane of the observation site and x_2' points to the east, i.e., in the direction of the linear velocity vector $\mathbf{v}_{\phi'}$ of the Earth's rotation.

Figure 7.20a shows a unit circle in the plane that contains the unit vector $\mathbf{x}_0'$ (direction to the star) and its x_2 component, and hence also the $\mathbf{v}_{\phi'}$ vector.

From this the length of the aberration vector $\boldsymbol{\Delta}$ is

$$|\boldsymbol{\Delta}|=\frac{v_{\phi'}}{c}\cos\gamma \qquad (7.17)$$

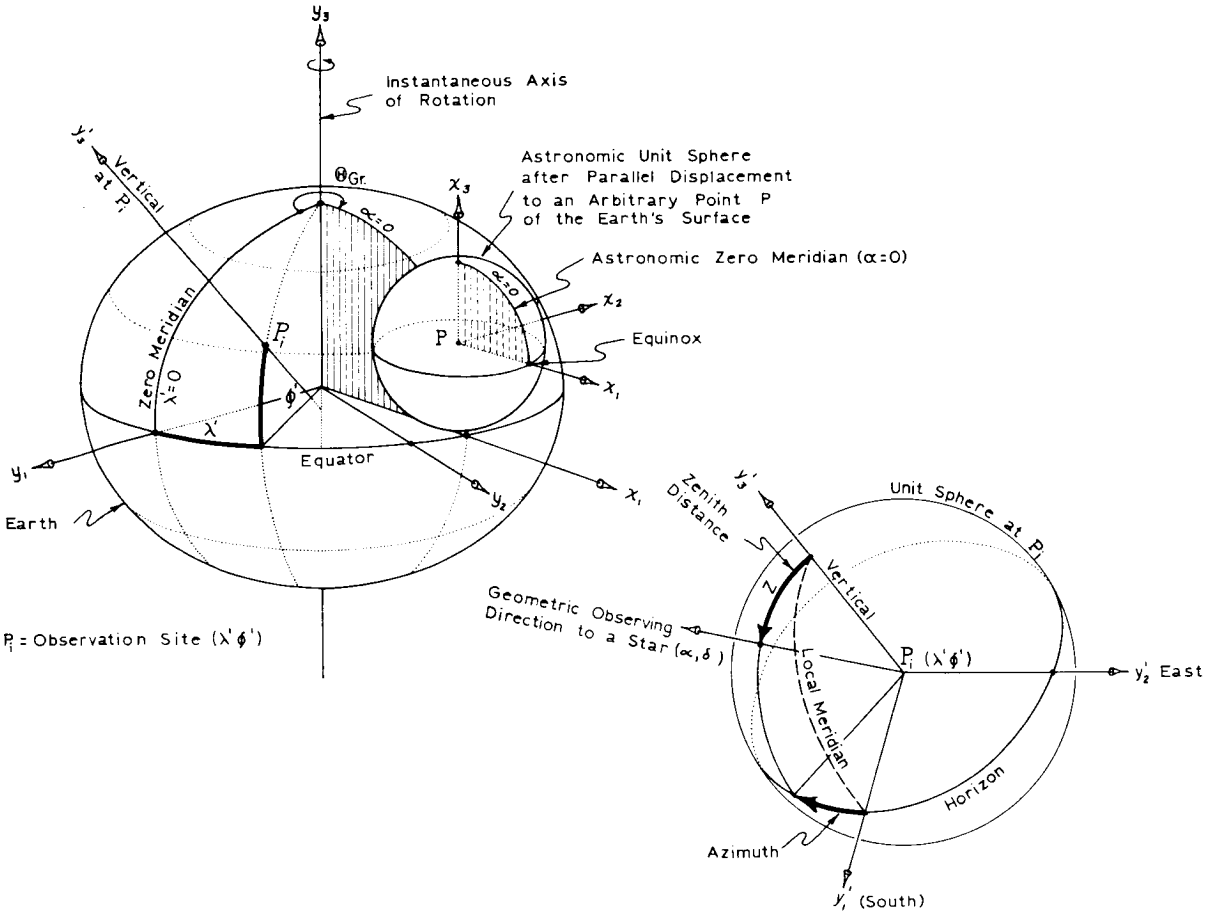

FIGURE 7.18.—Coordinate systems.

in which $v_{\phi'}$ is the linear velocity of the Earth's rotation in latitude ϕ' and c is the velocity of light.

The components of $\boldsymbol{\Delta}$ in the $x'_{1,2,3}$ directions (see fig. 7.20 and eq. 7.73) are

$$\boldsymbol{\Delta}=\begin{bmatrix} -x'_1x'_2 \\ (1-x'^2_2) \\ -x'_3x'_2 \end{bmatrix}\cdot k' \qquad (7.18)$$

with $k'=v_{\phi'}/c$, or sufficiently close for the purpose,

$$k'=0''.319\cos\phi' \qquad (7.19)$$

To compute (7.18), we must rotate the x system to which the $\mathbf{x}_{TT}$ vector (7.15) is referred through the angle θ. This results in

$$\mathbf{x}'_{TT}=\underset{3}{R}(\theta)\,\mathbf{x}_{TT} \qquad (7.20)$$

where

$$\underset{3}{R}(\theta)=\begin{bmatrix} \cos\theta & \sin\theta & 0 \\ -\sin\theta & \cos\theta & 0 \\ 0 & 0 & 1 \end{bmatrix} \qquad (7.21)$$

The unit vector $\mathbf{x}'_{TT}$ corrected for diurnal aberration is, with (7.18) and (7.19),

$$\mathbf{x}'_{(TT)}=\mathbf{x}'_{TT}+\begin{bmatrix} -x'_1\cdot x'_2 \\ (1-x'^2_2) \\ -x'_3\cdot x'_2 \end{bmatrix} k' \qquad (7.22)$$

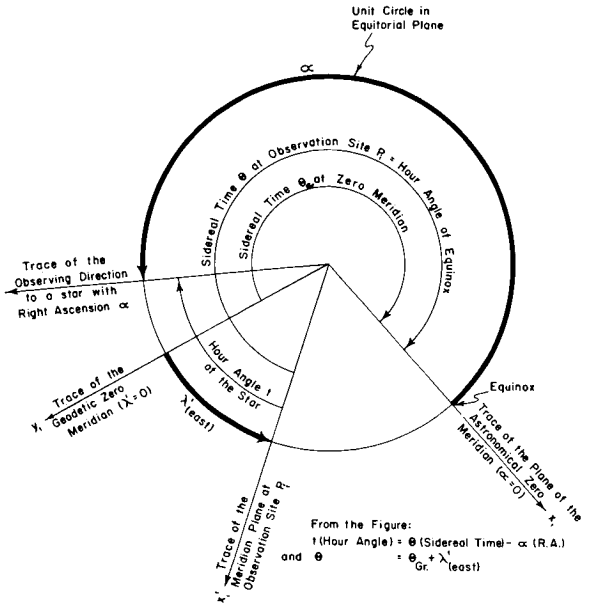

FIGURE 7.19.—Relation of local times to other times.

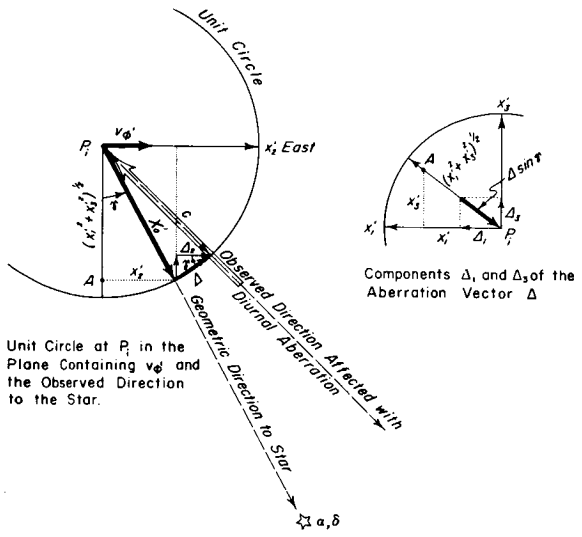

FIGURE 7.20

To account for astronomic refraction, a further correction is necessary. Since astronomic refraction is most conveniently computed as a function of the geometric zenith distance ζ of the observed direction, the x'_{TT} system (7.20) is rotated through $(90°-\phi')$ about its x'_2 axis into the local rectangular y' system (see fig. 7.20b). The resulting unit vector from (7.22) is

$$\mathbf{y}' = \underset{2}{\underline{R}}(90°-\phi')\,\mathbf{x}'_{(TT)} \qquad (7.23)$$

with

$$\underset{2}{\underline{R}}(90°-\phi') = \begin{bmatrix} \sin\phi' & 0 & -\cos\phi' \\ 0 & 1 & 0 \\ \cos\phi' & 0 & \sin\phi' \end{bmatrix} \qquad (7.24)$$

and, correspondingly, with (7.16) from (7.23) the azimuth A (from south over west) and zenith distance ζ are

$$A = \arctan\frac{y'_2}{y'_1}$$
$$\zeta = \arctan\frac{(y'^2_1+y'^2_2)}{y'_3} \qquad (7.25)$$

The astronomic refraction r_∞ is next computed, on the basis of the mathematical model described in section 7.4.5, as functions of the weather data obtained during the observation (air temperature, pressure, relative humidity, etc.). The vector $\mathbf{y}'$ of (7.23) is corrected for this refraction in accordance with (7.74) of section 7.4.6.2 (cf. also eq. (7.42)), giving

$$\mathbf{y}'_r = \mathbf{y}' + \begin{bmatrix} -\cos\left(\zeta - \frac{r_\infty}{2}\cos A\right) \\ \cos\left(\zeta - \frac{r_\infty}{2}\sin A\right) \\ \sin\left(\zeta - \frac{r_\infty}{2}\right) \end{bmatrix} 2\sin\frac{r_\infty}{2} \qquad (7.26)$$

When r_∞ is small in a differential sense in relation to the expected limit of accuracy, (7.26) simplifies in accordance with (7.73) to:

$$\mathbf{y}'_r = \mathbf{y}' + \begin{bmatrix} -y'_1\,y'_3 \\ -y'_2\,y'_3 \\ (1-y'^2_3) \end{bmatrix} r_\infty (1-y'^2_3)^{-1/2} \qquad (7.27)$$

where r_∞ is in radians.

Corresponding spherical coordinates can be obtained from (7.26) or (7.27) with (7.25).

More suitable for further development of our problem are the rectangular coordinates ξ and η in the plane tangent at the zenith of the observer to a unit sphere, as shown in figure 7.27 of section 7.4.6.2. These coordinates are commonly designated as standard coordinates in astronomy and are computed with the expressions on the left of (7.26) or (7.27) in accordance with (7.66) and (7.67) of section 7.4.2.6:

$$\begin{aligned} \xi_r &= y'_1/y'_3 \\ \eta_r &= y'_2/y'_3 \end{aligned} \qquad (7.28)$$

Hence (cf. eq. (7.64) and (7.65) of sec. 7.4.6.2):

$$\begin{aligned} A &= \arctan \eta_r/\xi_r \\ \zeta_r &= \arctan (\xi_r^2+\eta_r^2)^{1/2} \end{aligned} \qquad (7.29)$$

The correction steps of the preceding paragraphs can again be combined in a sequence of steps convenient for programed computation. From (7.20), (7.22), (7.23), and (7.26) or (7.27) results the direction vector $\mathbf{y}'_r$ in the local coordinate system as derived from the $\mathbf{x}_{TT}$ vector (7.15) in the astronomic x system. These directions represent a stationary oriented bundle of rays at the point of observation for the instant T, expressed in UT, of the observation. The rays forming this bundle pierce the tangent plane of the unit sphere at the zenith of the observing station in points whose locations are defined by their coordinates ξ_r, η_r. The $\xi\eta$ system corresponds in its orientation to the y' system. By obtaining the coordinates ξ_r, η_r, therefore, we have transformed the spherical coordinates, originally tabulated in a star catalog for a specified epoch, into three-dimensional rectangular coordinates such that all the reference points lie in a plane tangent to the unit sphere. The coordinates assigned to these points with reference to the center of the sphere as origin and axes parallel to the directions $y'_{1,2,3}$ are therefore ξ_r, η_r, $+1$.

The images of the stars corresponding to these control points lie in the plane of the photographic plate on which their position is determined with reference to an arbitrarily oriented plane rectangular coordinate system (x, y) introduced into the plate plane (see fig. 7.32 of sec. 7.4.6.2). There remains the problem of establishing the projective correspondence between the two sets of points on the two planes, one set defined by coordinates (ξ_r, η_r), the other by corresponding image coordinates (x, y). This principal problem of the photogrammetric measuring technique is solved by the application of the principles of generalized central perspective. The mathematical model for this solution is described in detail in section 7.4.6.3. For the present, it is necessary only to accept the fact that this step establishes, either directly or indirectly, the orientation of the photogram with respect to the coordinate system in which the control points are given, in our case with reference to the local y' system. Similarly, all the derived rays from this oriented bundle, such as the directions to the additionally photographed individual satellite positions (see sec. 7.4.6.5.1), are obtained in this coordinate system. Since in the subsequent triangulation (see sec. 7.4.7.2) all directions from the various stations must be referred to a common coordinate system, one can rotate the locally introduced coordinate systems so as to make their axes parallel to those of the common system chosen for the spatial triangulation before the photogrammetric reduction of the individual single cameras. This rotation can also be effected after the reduction of the single camera. The rotation matrices which determine the orientation of the photogrammetric exposure, and which, as was mentioned, refer to the local y' systems, are transformed for this purpose so that they refer with their elements of orientation to the common coordinate system chosen for the triangulation. Hence, the next step in the computation is the transformation of either the local y' system established at the point of observation P (ϕ', λ') or the local orientation matrix $\underline{R}'_y$ (α,ω,κ) † obtained in the photogrammetric reduction to z system selected for the subsequent triangulation (see sec. 7.4.6.2.6). First, the local y'

system is transformed to the corresponding geocentric y system. The necessary rotations are through the angle $(270°+\phi)$ about the z axis, and then through the angle $(-\lambda_{east})$ about the turned 3 axis. This gives

$$\mathbf{y} = \underset{3}{R}(-\lambda'_{east})\, \underset{2}{R}(270°+\phi')\mathbf{y}'_r = \begin{bmatrix} \cos\lambda' & -\sin\lambda' & 0 \\ \sin\lambda' & \cos\lambda' & 0 \\ 0 & 0 & 1 \end{bmatrix} \begin{bmatrix} \sin\phi' & 0 & \cos\phi' \\ 0 & 1 & 0 \\ -\cos\phi' & 0 & \sin\phi' \end{bmatrix} \mathbf{y}'_r \tag{7.30}$$

or analogously,

$$\underline{R}_y(\alpha, \omega, \kappa) = \underset{3}{\underline{R}}-\lambda'_{east})\, \underset{2}{\underline{R}}(270°+\phi') \underline{R}'_y(\alpha, \omega, \kappa) \tag{7.31}\dagger$$

where $\underline{R}_y(\alpha, \omega, \kappa)\dagger$ corresponds in the y system to the photogrammetric orientation matrix.

Basically, the aim of the reductions so far discussed is to refer all the photographically registered directions to stars—observed from different stations and, in general, at different times—to a consistent stationary coordinate system. The computations would produce a rigorous geometric solution only if we could assume that the direction of the Earth's axis of rotation, i.e., the y_3 direction of figure 7.18a labeled instantaneous axis of rotation, remains invariant in space. We know, however, that the poles describe more or less irregular loops in a period of approximately 430 days about a mean position which itself possibly has a secular displacement. From a geometrical point of view it is immaterial whether this so-called polar motion is treated as an additional motion relative to the astronomic reference system (a sort of additional precession and nutation) or whether one accepts the direction of the rotation axis as invariant and ascribes the phenomenon to a displacement of the crust. However, in addition to this purely geometric and computable effect, the influence of polar motion is coupled with the problem of time determination at the observation site. For this reason the discussion of these corrections will be combined with the questions of time determination in the following section.

7.4.4 Meaning and Measurement of Time

The significance of time determination for the problem of geometric satellite triangulation is twofold. First, because of the dynamic characteristics of the universe, i.e., because of the Earth's motion in space, we must determine the instant of the photographic exposure of the star image within an interval based on astronomic observations. In addition, because of the motion of the satellite itself, the instants of observation of the satellite at all stations observing the pass must be correlated with respect to an otherwise arbitrary measuring frequency, which amounts to a relative time determination.

With this, one interpolates points along the satellite track whose images, from a geometric standpoint, represent basically arbitrary but uniquely defined points on the orbit. In registering the pass of a satellite whose track is marked by short-duration light flashes this requirement is not necessary. Because of the finite speed of light, part of the photons emitted in the flash will, in general, not arrive at the different observation sites simultaneously, but for that very reason they will produce images whose positions on the various photograms correspond to a single point in space, the origin of the flash, and thus fulfill automatically the "geometric condition of simultaneity." Following is a discussion of those problems concerned with the impact on satellite triangulation of the time of observation needed for star imagery. We emphasize again the fact that the requirement for time correlation in star observations is, in principle, of a purely geometric nature. This conclusion follows from the fact that the spatial position of the Earth with its observation stations changes with time, relative to the astronomic reference system. The measurement of time, therefore, serves to refer the spatial orientation of the Earth at the instant of observation back to an orientation assumed as a normal position and corresponding at a specified epoch.

For the motion of the Earth around the Sun it is necessary to refer the Julian day and fraction of a day, as represented by UT for the instant of observation, to the beginning of the corresponding tropical year, the latter representing a point of time independent of all calendar reckoning and the same for all meridians (cf. Jordan/Eggert, 1939). The interval T so determined is needed for all the reductions described in section 7.4.3. The interval derived from the time of day serves as the basis for determining local sidereal time in accordance with the steps given in the previous section. There now arises in satellite triangulation the problem of the geometrical meaning of the measure of time known as Universal Time (UT).

As is well known, the time of day is transmitted by radio signals broadcast from numerous stations distributed all over the world. Abstracting the delays due to physical causes in the transmitters and receivers and their antennas and to variations in the propagation velocity of light caused by atmospheric influences, these time signals represent a sequence of extremely regular intervals. They are monitored by atomic clocks with great and long-term stability ($\pm 10^{-10}$ sec over a period of months with daily variations of $<10^{-11}$ sec).

In principle, these transmitted signals do not represent a time referred to the Earth's rotation, but to a definite signal sequence. For most daily and public purposes, however, it can be considered directly as the "time of day." By means of stellar observations at a group of observatories linked in an international service, the relation between these time signals and time referred to the Earth's rotation is established. In addition, this international working group concerns itself with the determination of the instantaneous position of the pole. These figures are published in the form of preliminary and later definitive values. One set lists the position of the instantaneous pole with respect to a selected null position; other tables give time corrections for converting the transmitted signals to Universal Time 1 (UT1) and Universal Time 2 (UT2). The results from the various observations (58 are participating at this time) are combined at the Bureau International de l'Heure (BIH) into a "mean observatory" value. This eliminates neglected influences such as refraction anomalies, secular polar motions, and irregular changes in the Earth's rotation statistically, at least to some extent. It also smooths out the errors in the determination of time due to systematic biases caused by the assumed nominal longitudes of the various observations and long-term refraction influences. Universal Time 2 in this system refers to a fictitious Earth that is practically independent of periodic, chiefly seasonally dependent, changes in the rate of the Earth's rotation.

UT1 is characterized by the fact that it, like the original observation, contains the periodic, seasonal variations of the Earth's rotation and therefore represents a measure of the instantaneous rate of rotation. Hence, it is a more suitable time for the present purpose, even though it is not uniform, and the time interval so determined can, as was indicated above, be converted into the corresponding sidereal interval by multiplication with 1.002 737 91. Since 24 hours of sidereal time represents exactly one revolution of the earth relative to the right ascension-declination system, the so-computed sidereal time is proportional to an angle of rotation, the geometric equivalent of our time coordinate, and is represented in figure 7.19 in a form convenient to the purpose, as sidereal time of the null meridian (see also fig. 7-18a). By introducing two great circles to include this angle, one obtains a definition valid for all instantaneous positions of the pole. One great circle is the meridional trace of the plane containing the instantaneous axis and pole of the Earth's rotation and the point of the celestial equator that represents the equinox of the observational period. The other great circle is the null meridian, which is the trace of a plane again containing the instantaneous axis of rotation plus an arbitrary but uniquely defined point of the Earth's surface. This point, by international convention, has the coordinates longitude $\lambda_0 = 0$ and latitude $\phi_0 = 0$ referred to the mean position of the pole for

the period 1900–1905. Unfortunately, this point lies in the Atlantic Ocean, and no direct obervations are possible from it. This situation is regrettable from a geodetic standpoint, but conceivably reveals the foresight of the specialists involved in the extraordinarily complex and difficult problem of reducing astronomical observations made for the purpose of time determination.

The ultimate refinements in time determination are not of decisive importance in the method of geometric satellite triangulation treated here, since the accuracy required in timing the instant of star exposures is at most ± 3 msec. Consequently, UT1 furnishes geometric satellite triangulation with a time coordinate whose geometric equivalent, when it is transformed into a sidereal interval, is compatible with the coordinate transformation (7.20) of the previous section.

In the past the situation described above was complicated by the fact that UT1 and UT2 were not referred to the conventional 1900–1905 pole, but were until 1958 referred to a pole which dropped periodically, and thereafter these times had as a reference pole a periodically displaced pole with a so-called secular motion. Since for all these various positions of the pole the corresponding null meridian passed through Greenwich, its intersection with the conventional equator was correspondingly displaced. As a consequence, for the period from 1958 to 31 December 1967, UT1 cannot be used as a rigorous measure for rotation. After 1 January 1968 the time pole is stationary and identical with the 1900–1905 conventional pole (CIO) as recommended by the International Astronomical Union 1967.

It should be noted, however, that the classical null meridian of Greenwich should be replaced by either a correspondingly rotated geodetic meridian or an equivalent discontinuity introduced into universal time on 1 January 1968 (see sec. 1.4). After that, the situation is clarified, our basic considerations have validity, and UT1 can be accepted as a measure of the Earth's rotation. Under these assumptions, the y system obtained with (7.30) represents a reference system corresponding to an instantaneous position of the Earth to which, therefore, the photogrammetric rotation matrix $\underset{y}{R}(\alpha,\omega,\kappa)$† computed with (7.31) is referred as well. From the geometric considerations above, it follows readily that for the eventual geometric normalization of the observation results, i.e., for the transformation of these data into the system chosen for the triangulation of the station coordinates, it will be necessary to rotate the y system referred to the observation period into the z system of the epoch selected for the spatial triangulation.

From figure 7.20 it is apparent that only two rotational components are needed. First the y system must be turned about its 2 axis through the angle $-a$, and then this turned system must be turned about its 1 axis through the angle $-b$. The 3 axis thus obtained will then define the direction of the rotation axis for the epoch chosen; the intersection of the 1 axis with the sphere will represent the origin of the system of time measurement adopted by international agreement, its meridian corresponding to the classical Greenwich meridian. From figure 7.21, this transformation is

$$\mathbf{z}=\underset{2}{\underset{}{R}}(-a,\ -b)\underset{1}{}\mathbf{y} \tag{7.32}$$

with

$$\begin{aligned}\underset{2}{\underset{}{R}}(-\mathrm{a},\ -\mathrm{b})\underset{1}{} &= \underset{1}{\underset{}{R}}(-b)\underset{2}{\underset{}{R}}(-a)\\ &= \begin{bmatrix} 1 & 0 & 0 \\ 0 & \cos b & -\sin b \\ 0 & \sin b & \cos b \end{bmatrix} \begin{bmatrix} \cos a & 0 & \sin a \\ 0 & 0 & 0 \\ -\sin a & 0 & \cos a \end{bmatrix}\end{aligned} \tag{7.33}$$

The rotation angles a and b are small and equal to the differential displacements x and y published by the BIH for defining the instantaneous pole with respect to the conventional origin (the 1900–1905 pole in our case). The rotation (7.33) becomes

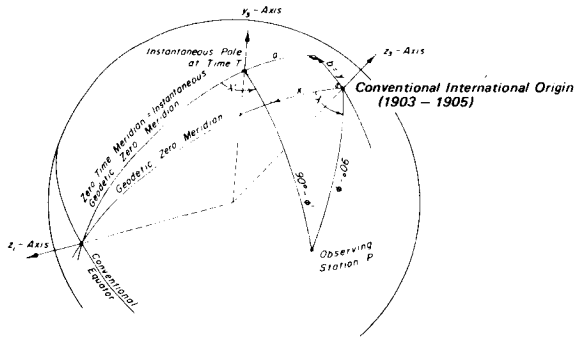

FIGURE 7.21.—Relations between instantaneous pole and conventional pole (1903–1905).

$$\underset{2}{\underset{1}{\underline{R}}}(-x,\ -y) = \begin{bmatrix} 1 & 0 & x \\ 0 & 1 & -y \\ -x, & y & 1 \end{bmatrix} \qquad (7.34)$$

$\underline{R}_y$ of (7.31) transforms into the corresponding photogrammetric rotation matrix

$$\underline{R}_z(\alpha,\omega,\kappa) = \underset{2}{\underset{1}{\underline{R}}}(-x,\ -y)\,\underline{R}_y(\alpha,\omega,\kappa) \qquad (7.35)\dagger$$

When the satellite triangulation is adjusted within a local rectangular coordinate system, a process which could be entirely practical within a given geodetic datum, expression (7.35) must be further rotated. If, for example, the rectangular Cartesian coordinate system to be used in the final triangulation is to be erected at the point $P(\lambda_{east},\ \phi,\ h=0)$, we will have, analogous to the preceding transformations,

$$\mathbf{z}' = \underset{3}{\underset{2}{\underline{R}}}[\lambda_{east},\ (90^\circ-\phi)]\,\mathbf{z} \qquad (7.36)$$

with

$$\underset{3}{\underset{2}{\underline{R}}}[\lambda_{east},\ (90^\circ-\phi)] = \underset{2}{\underline{R}}(90^\circ-\phi)\,\underset{3}{\underline{R}}(\lambda_{east})$$

$$= \begin{bmatrix} \sin\phi & 0 & -\cos\phi \\ 0 & 1 & 0 \\ \cos\phi & 0 & \sin\phi \end{bmatrix} \begin{bmatrix} \cos\lambda & \sin\lambda & 0 \\ -\sin\lambda & \cos\lambda & 0 \\ 0 & 0 & 1 \end{bmatrix} \qquad (7.37)$$

and similarly for the transformation of the photogrammetric orientation matrix

$$\underline{R}'_z(\alpha,\omega,\kappa) = \underline{R}[\lambda_{east},\ (90^\circ-\phi)]\,\underline{R}_z(\alpha,\omega,\kappa) \qquad (7.38)\dagger$$

7.4.5 Additional Geometric and Physical Influences

The preceding section has treated all the coordinate transformations needed (based on the given star catalog data) to reconstruct analytically the photogrammetric bundle of rays and orient it in space. The analytical reconstruction is determined by means of those parameters which simulate interior orientation and distortion, whereas the elements of exterior orientation express the orientation in space of the bundle with respect to a uniquely defined Earth-fixed coordinate system. To reproduce the oriented bundle, a mathematical model is used (see secs. 7.4.6.4 and 7.4.7 for a more detailed description).

For the present, it will be assumed that this problem has been solved, and we will pass on to an explanation of the corrections necessary to derive, from the image coordinates of the satellite points together with the parameters from bundle reconstruction, those directions needed later in the triangulation of the station coordinates. It will be assumed further that the measured images of the satellite trail have, by means of the parameters obtained in the bundle reconstruction, been made to conform to the mapping principle of a rigorous central perspective. Then, the direction in space corresponding to any point image computed with the corresponding elements of interior and exterior orientation will be tangent at the center of projection to the ray of light representing the physical light bundle. The center of projection in the present case is the center of the unit sphere. The unit vector $\mathbf{y}'_{0_r}$ in this direction is derived, as will be shown in section 7.4.6.2 with (7.81), from the photogrammetric bundle vector $\mathbf{p}$. In section 7.4.3 it

was explained that this direction refers to the same coordinate system as the photogrammetric rotation matrix in use. Hence, by use of the $\underline{R}_y\ (\alpha,\omega,\kappa)$† matrix mentioned there, one obtains the unit vector $\mathbf{y}'_{0_r}$ corresponding to an arbitrary image, where in accordance with (7.61),

$$\mathbf{y}_{0_r}=\begin{bmatrix} y'_1 \\ y'_2 \\ y'_3 \end{bmatrix}_r \equiv \mathbf{y}'_r \qquad (7.39)$$

(The subscript 0 used to designate a unit vector will be omitted in what follows, unless its use is necessary for better understanding.)

This observed direction must first be corrected for refraction. The problem of refraction is pictured schematically in figure 7.22 for both star and satellite images. Astronomical refraction r_∞ for zenith distances up to 85 degrees can be computed to sufficient accuracy with, for example, Garfinkel's (1944, 1967) formula:

$$r_\infty=\underline{T}^{1/2}W\left(\tau_1 \tan\frac{\beta}{2}+\tau_2\tan^3\frac{\beta}{2}+\tau_3\tan^5\frac{\beta}{2}+\tau_4\tan^7\frac{\beta}{2}\right) \qquad (7.40)$$

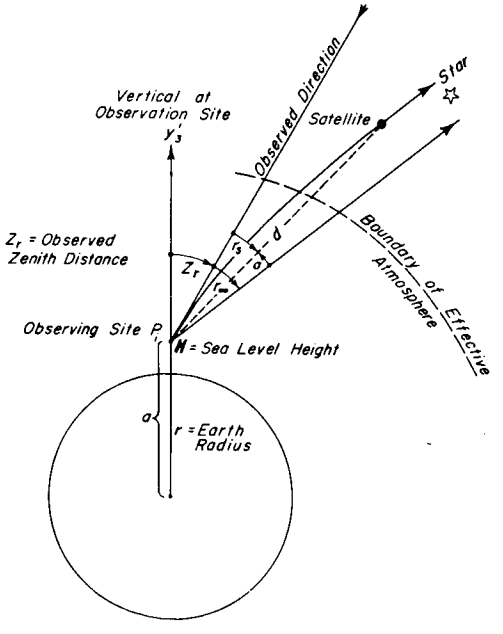

FIGURE 7.22.—Schematic presentation of star and satellite refraction.

in which

$\underline{T}=T/T_0$, where $T_0=273.16°\mathrm{K}$

$W=P/T_0$, where $P=p/p_0$ and $p_0=760$ mm Hg

$\tan\beta=(\underline{T}^{1/2}/\gamma)\tan z_r$, where $\gamma=8.7137$ and z_r is the observed zenith distance.

If the coefficients τ_1 to τ_4 are referred to geometric zenith distances, then an iteration loop must be provided for the computation of refraction from observed zenith distances.

Refraction for a satellite observation r_s is

$$r''_s=r''_\infty\left(1-\frac{a\cdot s}{d\cos z_r}\right) \qquad (7.41)$$

where

$a=r+H$, i.e., the Earth radius plus the height above sea level of the observing site

$s=RT_0/r$, where $R=29.2745$, the pressure height of a homogeneous atmosphere, and hence $s=0.001255$

d=distance between satellite and station in meters

The unit vector corrected for refraction is obtained from (7.39) by using (7.25), (7.26), or (7.27) as

$$\mathbf{y}'=\mathbf{y}'_r-\begin{bmatrix} -\cos\left(z_r+\frac{r_s}{2}\right)\cos A \\ \cos\left(z_r+\frac{r_s}{2}\right)\sin A \\ \sin\left(z_r+\frac{r_s}{2}\right)\end{bmatrix}2\sin\frac{r_s}{2} \qquad (7.42)$$

or, with (7.73) in section 7.4.6,

$$\mathbf{y}'=\mathbf{y}'_r+\begin{bmatrix} y'_1\,y'_3 \\ y'_2\,y'_3 \\ -(1-y'^2_3)\end{bmatrix}r_s(1-y'^2_3)^{-1/2} \qquad (7.43)$$

where r_s is expressed in radians.

To compute the refraction r_s for the direction to the satellite in (7.41), the distance d between the station and satellite is needed. This quantity is also necessary for the computation of subsequent corrections. However, only a good approximation for the distance is

needed, and it will also be sufficient in computing y' from (7.42) or (7.43) to replace r_s with r_∞.

With (7.79), (7.85), and (7.86) from section 7.4.6.2, the relevant coordinates of the images can be computed; these, in conjunction with the $\underline{R}(\alpha,\omega,\kappa)$ † matrix from (7.35) or (7.38) and the approximated station coordinates, can be used to make a preliminary triangulation of the satellite positions and hence to compute the distance d needed. For the adjustment procedure in practice, see section 7.4.6.5.

A further correction is necessary to account for the fact that the satellite images are not rigorously common target points. The flashes emitted by the so-called active satellites (e.g., ANNA, GEOS–1, GEOS–2) can be treated as uniquely defined target points in space, but the present-day "passive" geodetic satellites ECHO–1 and ECHO–2,[3] PAGEOS) are balloons which merely reflect sunlight. They must be sufficiently large to reflect an adequate amount of light. Those in use to date have diameters of 30 m. The surface of the balloon, active as a mirror, reflects the image of the Sun, the position of this image on the balloon sphere being a function of the geometric arrangement in space of the sun, satellite, and observing site at the instant of exposure. The necessary correction is analogous to an eccentric reduction in surveying. This correction varies not only for every station observing the target, but also for each direction at a given station. The purpose of the correction is to reduce each observed direction to the center of the balloon; this correction is called phase correction, because the position of the Sun's image depends on the illumination phase of the satellite. It is assumed that the satellite retains the spherical shape it had when it was launched into orbit. Figure 7.23 shows schematically the geometry involved.

It can be assumed that the Sun is at a great enough distance so that the direction to the Sun, indicated by the unit vector $\boldsymbol{l}$ at the

[3] ECHO–1 terminated its orbit on 23 May 1968, and ECHO–2 on 7 June 1969.

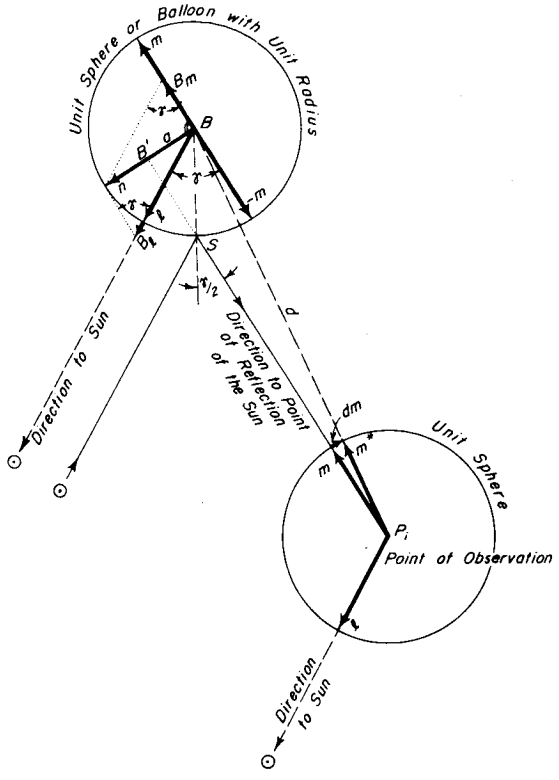

FIGURE 7.23.—Phase correction.

satellite, is the same at the point of observation. In accordance with Snell's law of reflection, the points B (balloon center), the center of the Sun, the image S of the Sun on the balloon, and the point of observation P_i all lie in one plane, so that the unit vectors $\mathbf{l}$, $\mathbf{m}$, $\mathbf{m}^*$, $\mathbf{n}$ and the vector $B'B$ are coplanar.

From figure 7.23 it follows directly that

$$\mathbf{n}=\mathbf{BB}_l+\mathbf{BB}_m \tag{7.44}$$

or

$$\mathbf{n}=\frac{1}{\sin\gamma}\boldsymbol{l}+\cot\gamma\,\mathbf{m}=\frac{1}{\sin\gamma}(\mathbf{l}+\cos\gamma\,\mathbf{m}) \tag{7.45}$$

The scalar product of the unit vectors $\boldsymbol{l}$ and $-\mathbf{m}$ is

$$\cos\gamma=\boldsymbol{l}\cdot(-\mathbf{m}) \tag{7.46}$$

Again, from figure 7.23,

$$\mathbf{B'B}=-a\mathbf{n} \tag{7.47}$$

The distance between the observer and the satellite d is large in relation to the balloon radius, and hence in relation to a, so that to a sufficient degree of approximation

$$\mathbf{dm} = -(a/d)\mathbf{n} \qquad (7.48)$$

or, with (7.45),

$$\mathbf{dm} = -\frac{a}{d \sin \gamma}(\boldsymbol{l} + \cos \gamma \, \mathbf{m}) \qquad (7.49)$$

The displacement a from the center for a reflecting satellite with radius ξ_b is, from figure 7.23,

$$a = \xi_b \sin (\gamma/2) \qquad (7.50)$$

For a balloon with a diffusively reflecting surface it can be argued that the centroid of the satellite image corresponds to the centroid of the illuminated portion of the balloon surface as seen from the observation site. In this case, we have

$$\mathrm{a} = \frac{\xi_b}{2}(1 - \cos \gamma) \qquad (7.51)$$

Finally, with (7.50) or (7.51), as the case may be,

$$\mathbf{m}^* = \mathbf{m} + d\mathbf{m} \qquad (7.52)$$

To compute (7.49), the unit vectors $\boldsymbol{l}$ and $\mathbf{m}$ are needed. Up to this point we have assumed only that they are referred to an arbitrary but consistent coordinate system. We set, therefore, with (7.43),

$$\mathbf{m} = \mathbf{y}' \qquad (7.53)$$

With the right ascension and declination values of the Sun $\alpha_\odot$ and $\delta_\odot$ interpolated for the time of observations, the $\mathbf{x}_\odot$ vector is computed with (7.1), neglecting refraction and other corrections, and then the $\mathbf{x}'_\odot$ vector is computed by using local sidereal time $\theta =$ 1.002 739 91 (UTI) $+\lambda'_{east}$ and (7.20), (7.21). Finally the $\mathbf{y}'_\odot$ vector is derived with (7.23) and (7.24). Then,

$$\mathbf{y}'_\odot = \boldsymbol{l} \qquad (7.54)$$

Similarly, with equation (7.52) the unit vector $\mathbf{y}'$ in the direction of the balloon center is

$$\mathbf{y}' = \mathbf{m}^* \qquad (7.55)$$

A detailed explanation of the phase correction is given in Schmid (1971).

In order to interpret the direction of (7.55) correctly in a geometric sense, it is necessary to bear in mind that the satellite serving as a target and the station site are subject to independent motions. The satellite, in orbiting the Earth, shares the motion of the Earth around the Sun, so that the annual aberration effect is canceled. However, because of the Earth's rotation, the linear velocity component of the observation stations creates a displacement of the observed directions corresponding to diurnal aberration. In addition, the relative spatial relation between the satellite and the observing station changes in the time required for the light to travel from the satellite to the station. This situation is shown schematically in figure 7.24 for a flash emitted from the satellite. The position of the observing station (ϕ', λ') and its Earth-

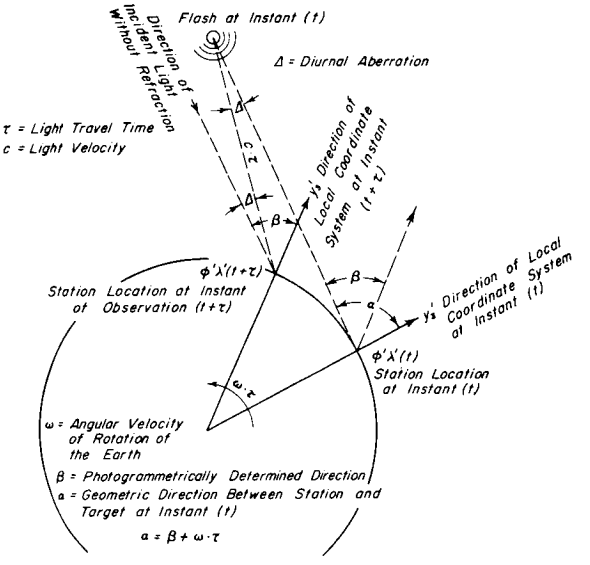

FIGURE 7.24.—Influence of diurnal aberration and earth rotation when recording light flashes originating at satellite.

fixed y' reference system (symbolized by the y_3 direction) is shown at the instant t of the emission. Let the geometric direction at time t from the station to the flash be indicated by the direction angle α. Owing to its finite propagation velocity c, the light requires an interval τ to reach the station by traversing the distance d:

$$\tau = d/c \tag{7.56}$$

During the interval τ, however, the station has reached a position differing from the initial position by the angle $\omega\tau$, where $\omega = 15''/$sec is the Earth's angular velocity. From the aberration theory (cf. Schaub, 1950), it follows that the apparent direction of observation differs from the corresponding geometrical direction by the aberration angle Δ. The latter direction is parallel to the geometrical direction existing between the station and the satellite at the instant t. This statement is rigorous to the order to which the Earth's rotational velocity may be considered linear and constant. It follows that the flash is observed at the directional angle β relative to the local coordinate frame. The angle α needed in the subsequent treatment of the problem is therefore obtained from

$$\alpha = \beta + \omega \cdot \tau \tag{7.57}$$

The situation is complicated somewhat for the case in which satellite triangulation is carried out not by means of flashes but by means of a continuously illuminated satellite. The shutter mechanism of the observing camera permits the chopping of the satellite trail into a series of separate images. Thus, the individual images are formed at times t_1, t_2, . . ., t_n, to which appertain corresponding light travel durations τ_1, τ_2, . . ., τ_n. The images corresponding to instants $t_1+\tau_1$, $t_2+\tau_2$, . . ., $t_n+\tau_n$ must now be interpolated into the image sequence. Strictly speaking, acording to figure 7.25, the interpolation should be for the instants $t_1+\tau_1^*$, $t_2+\tau_2^*$, . . ., $t_n+\tau_n^*$, where

$$\tau_1^* = \tau_1 + \frac{\tau_2 - \tau_1}{t_2 - t_1}\tau_1, \text{ etc.}$$

The difference $\tau_1^* - \tau_1$ is, however, negligible. To effect the interpolation, a time-related function of position is set up, expressing the photographic image sequence.

Figure 7.25 shows the relations existing between the recorded time, the satellite position, and the observation station, the symbols used having the same meaning as in figure 7.24. The principle of interpolation is shown, in considerably simplified form, for only two observations occurring at instants t and $t+\Delta t$. As before, the needed direction angle α is obtained from the interpolated observed direction β by means of (7.57).

The direction α thus obtained reproduces the geometry between station and satellite existing at the instant t. From a similar treatment of the observations at other stations observing the same pass, directions to the satellite position at the instant t can be computed. These, then, are geometrically coherent directions with which the eventual

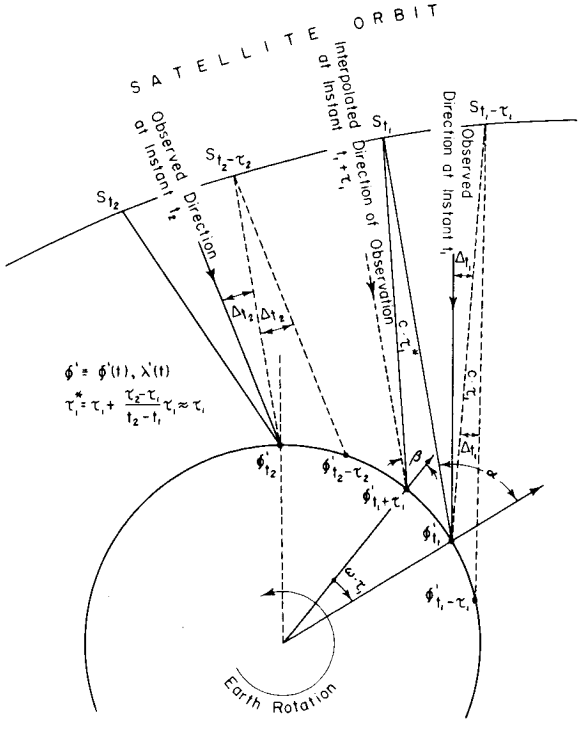

FIGURE 7.25.—Influence of diurnal aberration and earth rotation when recording a continuously illuminated satellite.

space triangulation of the observing stations will be carried out. The interpolation of fictitious satellite images referred to above also serves the purpose of taking into account the time differences between the station clocks at the various sites (see sec. 7.3). The time differences can be considered as shifts in the origins of the time bases at the several observation stations at the same time.

In order to execute the various reductions just described, it is necessary to derive the corresponding image coordinates $\bar{x}$, $\bar{y}$ with (7.85) and (7.86) referred to the vector $\mathbf{y}'$ of (7.55). On the assumption that the exposure sequence has been carefully monitored (the practice with the BC–4 system is to monitor to within better than 50 μsec), the following polynomials can be set up as interpolation functions:

$$\begin{aligned}\bar{x} &= a_0 + a_1 t + a_2 t^2 + a_3 t^3 + a_4 t^4 + a_5 t^5 + \ldots \\ \bar{y} &= b_0 + b_1 t + b_2 t^2 + b_3 t^3 + b_4 t^4 + b_5 t^5 + \ldots\end{aligned} \tag{7.58}$$

The coefficients a_0, a_1, . . . , a_n and b_0, b_1, . . . , b_n are obtained from an adjustment (see section 7.4.6.2.1). The degree assumed for the polynomial depends chiefly on the length of the recorded satellite trail, i.e., more or less on the aperture of the camera used. With the BC–4 system a polynomial of the fifth degree, at least for the component in the direction of the trail, is necessary (see sec. 7.4.1). Several hundred satellite images are used to compute the polynomial. The adjustment effects a smoothing that is of decisive importance for the accuracy of satellite triangulation, since it eliminates the influence of scintillation. Regardless of its amplitude, which, depending on local meteorological conditions, can attain several seconds of arc, scintillation is always characterized by a nearly ideal normal distribution and hence can be eliminated practically completely with a Gaussian adjustment, provided a sufficiently large number of satellite images is available. This condition is not met by the use of present-day light flashes.

The polynomials (7.58) are now used to interpolate fictitious satellite images. Image coordinates $\bar{x}$, $\bar{y}$ are computed for the instant (in station time) that corresponds to the satellite position at time T. Since, as was indicated above, the times assigned to the various observing stations are not necessarily referred to the same null point, the local $t_i + \tau_i$ values must be reduced to a consistent clock time by the addition of ΔT_i (represented schematically in fig. 7.26).

To repeat, the station times $t_i + \tau_i$, $t_j + \tau_j$, $t_k + \tau_k$, . . . used for interpolation at station i, j, k, . . . do not represent the same instant T at the clock, but fix image coordinates which are geometrically consistent; i.e., they satisfy the "geometric condition of simultaneity" mentioned in section 7.4.4.

With the image coordinates $\bar{x}$, $\bar{y}$ thus obtained, the corresponding $\mathbf{y}'$ vector is recomputed from the corresponding bundle vector $\mathbf{p}$ of (7.81). The last correction modifies the orientation of this vector to account for the Earth's rotation during the light travel time τ. Theoretically, this is accomplished by rotating the local y' system about its 2 axis through an angle $-(90° - \phi')$, which brings the 3 axis into coincidence with the Earth's rotation axis. Next, the system is rotated about this latter axis through the angle $-\omega\tau$. This rotation cancels the effect of the Earth's rotation. Finally, the twice-rotated 2 axis is turned through the angle $(90° - \phi)$, resulting in a system with the unit vector $\mathbf{y}_s$. The necessary computations are, therefore,

$$\begin{aligned}\mathbf{y}' &= \underset{2}{\underline{R}}(90° - \phi')\,\underset{3}{\underline{R}}(-\omega\tau)\,\underset{2}{\underline{R}} - (90° - \phi')\,\mathbf{y} \\ &= \begin{bmatrix} \sin\phi' & 0 & -\cos\phi' \\ 0 & 1 & 0 \\ \cos\phi' & 0 & \sin\phi' \end{bmatrix} \\ &\quad \begin{bmatrix} \cos\omega\tau & -\sin\omega\tau & 0 \\ \sin\omega\tau & \cos\omega\tau & 0 \\ 0 & 0 & 1 \end{bmatrix} \begin{bmatrix} \sin\phi' & 0 & \cos\phi' \\ 0 & 1 & 0 \\ -\cos\phi' & 0 & \sin\phi' \end{bmatrix} \mathbf{y}'\end{aligned} \tag{7.59}$$

Since $\omega\tau$ is small, (7.59) simplifies to

$$\mathbf{y}_s' = \mathbf{y}' + \begin{bmatrix} -y_2' \sin\phi' \\ y_1' \sin\phi' + y_3' \cos\phi' \\ -y_2' \cos\phi' \end{bmatrix} \cdot \omega\tau \tag{7.60}$$

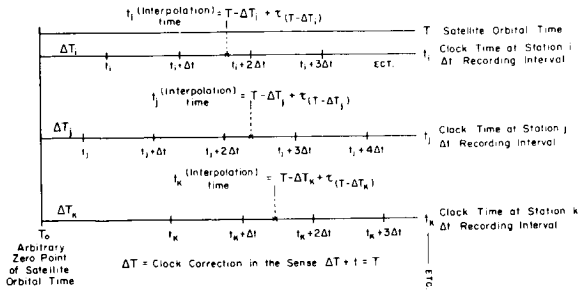

FIGURE 7.26.—Principle of time interpolation for the "geometrical condition of simultaneity."

The transformation of the direction of the unit vector $\mathbf{y}'_s$ into the chosen z or z' system can now be effected in accordance with (7.30) and (7.32) or (7.36), as the case may be.

This completes the discussion of all the steps needed in preparing for the satellite triangulation proper.

7.4.6 Numerical Adjustment

7.4.6.1 Introductory Remarks

In this section the attempt will be made to present the mathematical concept of the method of geometric satellite triangulation, considering the problem, so far as possible, from the standpoint of analytical photogrammetry. The principle of the photogrammetric measuring method is most conveniently identified with the concept of a direction fixed within a certain coordinate system. It is therefore reasonable to expect a clear and computationally economical solution with a vectorial presentation. In this connection it should be borne in mind that the mathematical expression for a direction in space can be changed either by rotating the coordinate system to which the direction is referred or by making a change in direction within the fixed reference frame. The latter can be accomplished either by rotating the given vector or by adding a correction vector. From a mathematical standpoint, rotating the coordinate system and changing the direction are equivalent. However, in associating this generally valid geometric concept with a specific measuring process by forming a mental picture of the direction and the related coordinate system in object space, definite advantages can be derived from such a specific interpretation, at any rate, to explain the measuring process geometrically. One difference between the two cited operations is that a rotation of the coordinate system does not affect the geometry existing between the object points. The concept of a linear coordinate transformation, including, if necessary, translations, therefore seems meaningful. A change in direction within a given coordinate system, on the other hand, effects a change of the spatial position of this direction in object space. The designation "change in direction" will therefore be reserved for this operation.

Finally, as simple a representation as possible will be given of the photogrammetric measuring method, whose concept rests on the principles of a central perspective. For this purpose it is necessary merely to get a mental picture of a unit vector $\mathbf{x}_0$ assigned to a specified direction in object space, with reference to an arbitrary but uniquely defined coordinate system. With the assumption that the starting point of this vector coincides with the center of projection of the central perspective (e.g., at the center of the unit sphere), the photogrammetric bundle vector $\mathbf{p}$ in object space, reduced to unit length, is, geometrically speaking, identical with the vector $\mathbf{x}_0$, mentioned above. The photogrammetric bundle vector $\mathbf{p}$ being referred to the coordinate system $\overline{x}$, $\overline{y}$, c of the camera, merely a rotation of the coordinate system is required to transform the vector $\mathbf{x}_0$ into vector $\mathbf{p}$ or vice versa. This step, described above as a coordinate transformation, represents the fundamental analytical operation of the photogrammetric measuring method (see sec. 7.4.6.2.1). It remains now only to consider those displacements of the image from the central perspective concept that are the result of the physical photographic process. Before an adjustment algorithm is developed from this line of thought, the more important mathematical aids needed in this discussion will be listed in logical order.

7.4.6.2 Mathematical Aids

7.4.6.2.1 VARIOUS MATHEMATICAL EXPRESSIONS FOR THE UNIT VECTOR

From figure 7.27 directly,

$$\mathbf{x}_0=\begin{bmatrix}x_1\\x_2\\x_3\end{bmatrix}=\frac{\mathbf{x}}{|\mathbf{x}|}$$

$$=\begin{bmatrix}X-X_0\\Y-Y_0\\Z-Z_0\end{bmatrix}\times[(X-X_0)^2+(Y-Y_0)^2+(Z-Z_0)^2]^{-1/2}$$

$$=\begin{bmatrix}\xi\\\eta\\1\end{bmatrix}(\xi^2+\eta^2+1^2)^{-1/2} \tag{7.61}$$

where either

$$\mathbf{x}=\begin{bmatrix}(X-X_0)\\(Y-Y_0)\\(Z-Z_0)\end{bmatrix} \quad \text{or} \quad \mathbf{x}=\begin{bmatrix}\xi\\\eta\\1\end{bmatrix} \tag{7.62}$$

Furthermore,

$$\mathbf{x}_0=\begin{bmatrix}\cos\beta\cos\alpha\\\cos\beta\sin\alpha\\\sin\beta\end{bmatrix} \tag{7.63}$$

where from figure 7.27

$$\tan\alpha=\frac{x_2}{x_1}=\frac{\eta}{\xi} \tag{7.64}$$

$$\tan\beta=\frac{x_3}{(x_1+x_2)^{1/2}}(\xi^2+\eta^2)^{-1/2} \tag{7.65}$$

$$\xi=\frac{(X-X_0)}{(Z-Z_0)}=\frac{x_1}{x_3} \tag{7.66}$$

$$\eta=\frac{(Y-Y_0)}{(Z-Z_0)}=\frac{x_2}{x_3} \tag{7.67}$$

7.4.6.2.2 COORDINATE TRANSFORMATION

$$\mathbf{x}'=\underset{1\,2\,3}{\underline{R}}(\gamma_1\gamma_2\gamma_3)\,(\mathbf{x}+\Delta\mathbf{x}) \tag{7.68}$$

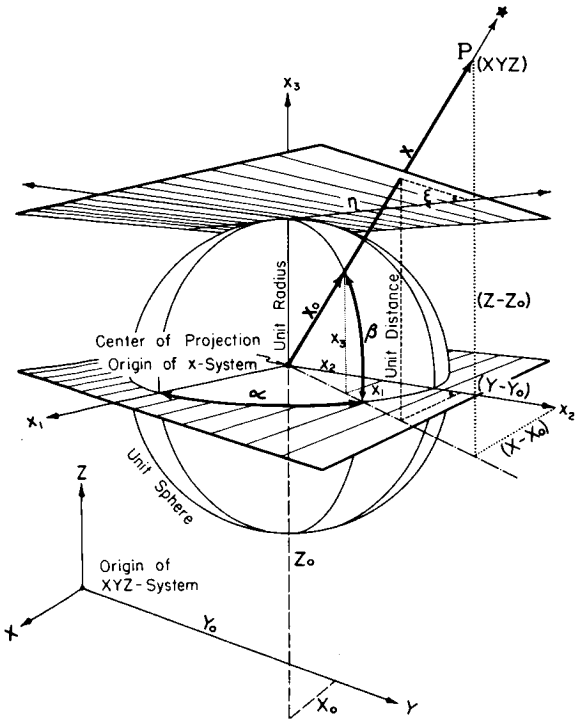

FIGURE 7.27

where the rotation matrix has the following meaning:

$$\underset{1\,2\,3}{\underline{R}}(\gamma_1\gamma_2\gamma_3)=\underset{3}{\underline{R}}(\gamma_3)\underset{2}{\underline{R}}(\gamma_2)\underset{1}{\underline{R}}(\gamma_1) \tag{7.69}$$

The γ designates the angles through which rotation takes place in the indicated order, the indices under the angle showing the axis around which rotation takes place. Counterclockwise rotation (as seen from above) is positive.

7.4.6.2.3 CHANGE OF DIRECTION

From figure 7.28

$$\mathbf{x}_0'=\mathbf{x}_0+\Delta\mathbf{x} \tag{7.70}$$

The differential $d\mathbf{x}_0$ of a unit vector $\mathbf{x}_0$ is a vector of infinitesimal length with a direction perpendicular to $\mathbf{x}_0$, since the length of the unit vector is constant by definition. The vector $\mathbf{x}_0$ can therefore turn only through an

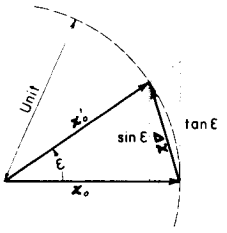

FIGURE 7.28

infinitesimal angle ϵ, whose measure in radians is equal to the length of the linear displacement $d\mathbf{x}_0$. For small displacements the following equalities follow, therefore, from figure 7.28:

$$|\Delta\mathbf{x}| = |d\mathbf{x}_0| = \epsilon = \sin\epsilon = \tan\epsilon \qquad (7.71)$$

and hence

$$\mathbf{x}_0' = \mathbf{x}_0 + d\mathbf{x}_0 \qquad (7.72)$$

For the special case where $d\mathbf{x}_0$ is coplanar with one of the coordinate axes, e.g., with x_3, it follows from figure 7.29 that

$$d\mathbf{x}_0 = \begin{bmatrix} -x_1 \cdot x_3 \\ -x_2 \cdot x_3 \\ +(1-x_3^2) \end{bmatrix} \epsilon (1-x_3^2)^{-1/2} \qquad (7.73)$$

in radians. Then $\mathbf{x}_0$ follows from (7.72).

Similar expressions for the other axes are obtained by cyclic permutation of the subscripts and the vector components in (7.73) in the order $(1)\rightarrow(2)\rightarrow(3)\rightarrow(1)$

For larger values of ϵ, one obtains from (7.63)

$$\mathbf{x}_0' = \begin{bmatrix} \cos(\beta+\epsilon)\cos\bar{\alpha} \\ \cos(\beta+\epsilon)\sin\bar{\alpha} \\ \sin(\beta+\epsilon) \end{bmatrix} \qquad (7.74)$$

7.4.6.2.4 CENTRAL PERSPECTIVE

From figure 7.30 the photogrammetric bundle vector $\mathbf{p}$ is

$$\mathbf{p} = \bar{x}\cdot\mathbf{i} + \bar{y}\cdot\mathbf{j} + c\cdot\mathbf{k} = \begin{bmatrix} \bar{x} \\ \bar{y} \\ c \end{bmatrix} \qquad (7.75)\ddagger$$

and, with (7.61),

$$\mathbf{p}_0 = \frac{\mathbf{p}}{|\mathbf{p}|} \qquad |\mathbf{p}| = (\bar{x}^2 + \bar{y}^2 + c^2)^{1/2} \qquad (7.76)$$

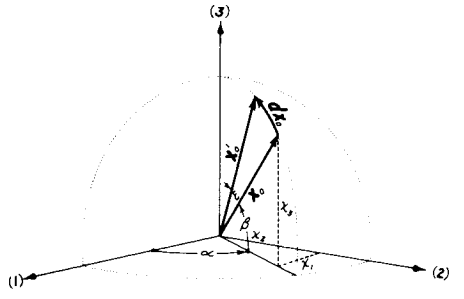

FIGURE 7.29

From (7.68), with $\Delta\mathbf{x}=0$, follows the fundamental equation of analytical photogrammetry

$$\mathbf{p}_0 = \underset{213}{R}(\alpha,\omega,\kappa)\,\mathbf{x}_0 \qquad (7.77)\dagger$$

where

$$\underset{213}{R}(\alpha,\omega,\kappa) = \underset{3}{R}(\kappa)\,\underset{1}{R}(\omega)\,\underset{2}{R}(\alpha) = \begin{bmatrix} r_{11} & r_{12} & r_{13} \\ r_{21} & r_{22} & r_{23} \\ r_{31} & r_{32} & r_{33} \end{bmatrix} \qquad (7.78)$$

The r_{ij} in the orthogonal matrix (7.78) are actually the direction cosines—in other words, the components of the corresponding unit vectors—in the x coordinate system of the corresponding axes after the indicated rotations through angles α, ω, and κ shown in figure 7.31. They are found to be

$$r_{11} = \cos\alpha\cos\kappa + \sin\alpha\sin\omega\sin\kappa$$
$$r_{12} = \cos\omega\sin\kappa$$
$$r_{13} = -\sin\alpha\cos\kappa + \cos\alpha\sin\omega\sin\kappa$$
$$r_{21} = -\cos\alpha\sin\kappa + \sin\alpha\sin\omega\cos\kappa$$

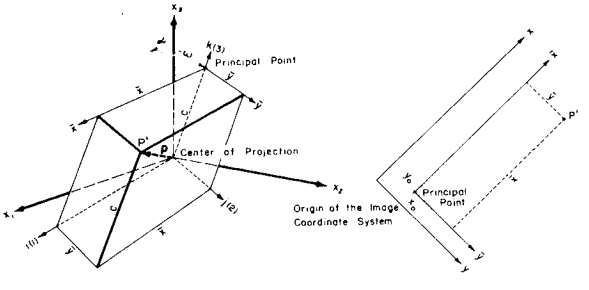

FIGURE 7.30.—(Left) The photogrammetric bundle vector $\mathbf{p}$. (Right) Diapositive as seen from center of projection.

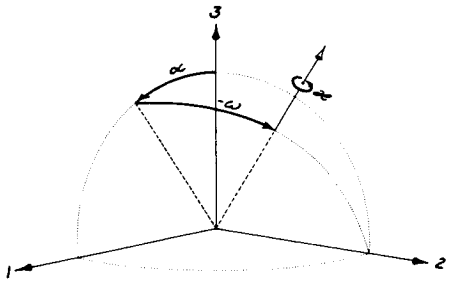

FIGURE 7.31.—Sense of direction of exterior elements of orientation.

$$
\begin{aligned}
r_{22} &= \cos\omega\cos\kappa \\
r_{23} &= \sin\alpha\sin\kappa + \cos\alpha\sin\omega\cos\kappa \\
r_{31} &= \sin\alpha\cos\omega \\
r_{32} &= -\sin\omega \\
r_{33} &= \cos\alpha\cos\omega
\end{aligned}
\tag{7.79}
$$

For the orthogonal matrix $R(\alpha,\omega,\kappa)$

$$
\underset{2\,1\,3}{R}^{-1}(\alpha,\omega,\kappa) = \underset{2\,1\,3}{R}^{*}(\alpha,\omega,\kappa) \tag{7.80}
$$

so that with (7.77), (7.78), and (7.79),

$$
\mathbf{x}_0 = \frac{\mathbf{x}}{|\mathbf{x}|} = \underset{2\,1\,3}{R}^{*}(\alpha,\omega,\kappa)\frac{\mathbf{p}}{|\mathbf{p}|} \tag{7.81}
$$

Furthermore, from (7.77) with (7.78), (7.61) and (7.65),

$$
\begin{bmatrix} \overline{x} \\ \overline{y} \\ c \end{bmatrix} = \begin{bmatrix} r_{11} & r_{12} & r_{13} \\ r_{21} & r_{22} & r_{23} \\ r_{31} & r_{32} & r_{33} \end{bmatrix} \begin{bmatrix} (X-X_0) \\ (Y-Y_0) \\ (Z-Z_0) \end{bmatrix} \frac{|\mathbf{p}|}{|\mathbf{x}|} \tag{7.82}
$$

so that

$$
\frac{\overline{x}}{c} = \frac{r_{11}(X-X_0)+r_{12}(Y-Y_0)+r_{13}(Z-Z_0)}{r_{31}(X-X_0)+r_{32}(Y-Y_0)+r_{33}(Z-Z_0)} = \frac{m}{q} \tag{7.83}
$$

$$
\frac{\overline{y}}{c} = \frac{r_{21}(X-X_0)+r_{22}(Y-Y_0)+r_{23}(Z-Z_0)}{r_{31}(X-X_0)+r_{32}(Y-Y_0)+r_{33}(Z-Z_0)} = \frac{n}{q} \tag{7.84}
$$

Finally, for (7.83) and (7.84),

$$
\overline{x} = cm/q \tag{7.85}
$$

$$
\overline{y} = cn/q \tag{7.86}
$$

7.4.6.2.5 DEVIATIONS FROM THE CENTRAL PERSPECTIVE BUNDLE

Refraction effects a displacement in direction which with equation (7.73) (see eqs. 7.26 and 7.27) can be applied to the unit vector in the direction in question, or which with (7.74) leads directly to the unit vector corrected for refraction.

We consider next those influences which displace the image from its central perspective position and which are due to the constructive properties of the camera. It is known from experience that the image of the object point P is formed not at P' but at P^*, which is displaced relative to P' by a vector Δ lying in the plane of the photogram.

From figure 7.32 we have

$$
\overline{x} = x - x_0 - \Delta x \tag{7.87}
$$

$$
\overline{y} = y - y_0 - \Delta y \tag{7.88}
$$

in which Δx and Δy are the components of Δ.

The coordinates x and y are obtained from the corresponding comparator coordinates, corrected for the nonorthogonality ϵ of the comparator spindles as shown in figure 7.32, from

$$
x = x_{meas} + y\,\epsilon \tag{7.89}
$$

$$
y = y_{meas} \tag{7.90}
$$

Since the vector Δ is always small, a sufficiently accurate linear scale correction re-

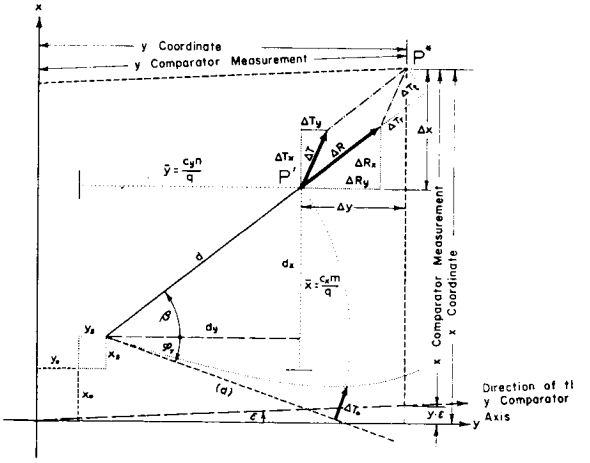

FIGURE 7.32.—Diapositive as seen from projection center.

sults from replacing the scale factor c in (7.85) and (786) by c_x and c_y. Thus,

$$\bar{x}=c_x m/q \tag{7.91}$$

$$\bar{y}=c_y m/q \tag{7.92}$$

The required expressions for Δx and Δy are, from figure 7.32,

$$\Delta x=\Delta R_x+\Delta T_x \tag{7.93}$$

$$\Delta y=\Delta R_y+\Delta T_y \tag{7.94}$$

The symmetric radial distortion ΔR is, as usual, expressed as a polynomial in odd powers of the distance d. Omitting the first power, which is equivalent to a scale correction, one obtains

$$\Delta R=K_1 d^3+K_2 d^5+K_3 d^7 \tag{7.95}$$

where

$$d=[(\bar{x}-x_s)^2+(\bar{y}-y_s)^2]^{1/2} \tag{7.96}$$

$$\Delta R_x=\frac{\Delta R(\bar{x}-x_s)}{d}(\bar{x}-x_s)(K_1 d^2+K_2 d^4+K_3 d^6) \tag{7.97}$$

$$\Delta R_y=\frac{\Delta R(\bar{y}-y_s)}{d}=(\bar{y}-y_s)(K_1 d^2+K_2 d^4+K_3 d^6) \tag{7.98}$$

A model for the distortion due to the unavoidable residual errors in entering the individual elements of the lens system was given by Conrady, 1919 (see also Brown, 1966). In figure 7.32 the minimal component of this distortion is purely tangential and is designated ΔT_0. For high-quality objectives, ΔT_0 can be expressed sufficiently accurately with two terms of an even polynomial in d:

$$\Delta T_0=K_4 d^2+K_5 d^4 \tag{7.99}$$

According to Conrady, the components of this nonsymmetric distortion are, using the designations in figure 7.32, in the tangential direction

$$\Delta T_t=\Delta T_0 \cos(\phi_T+\beta) \tag{7.100}$$

and in radial direction

$$\Delta T_r=3\Delta T_0 \sin(\phi_T+\beta) \tag{7.101}$$

Hence,

$$\Delta\mathbf{T}=\begin{bmatrix}\Delta T_x\\ \Delta T_y\end{bmatrix}=\begin{bmatrix}\cos\beta & \sin\beta\\ -\sin\beta & \cos\beta\end{bmatrix}\begin{bmatrix}\Delta T_t\\ \Delta T_r\end{bmatrix} \tag{7.102}$$

Finally, with (7.99), (7.100), and (7.101) one obtains from (7.102)

$$\Delta\mathbf{T}=\begin{bmatrix}\Delta T_x\\ \Delta T_y\end{bmatrix}=(K_4+K_5 d^2)\begin{bmatrix}2(\bar{x}-x_s)(\bar{y}-y_s) & 3(\bar{x}-x_s)^2+(\bar{y}-y_s)^2\\ 3(\bar{y}-y_s)^2+(\bar{x}-x_s)^2 & 2(\bar{x}-x_s)(\bar{y}-y_s)\end{bmatrix}\begin{bmatrix}\sin\phi_T\\ \cos\phi_T\end{bmatrix} \tag{7.103}$$

Figure 7.33 shows schematically the components for radial and decentering distortion for a certain distance d.

Finally, one obtains with (7.89), (7.90), (7.97), (7.98), and (7.103), in accordance with (7.87), (7.88), and (7.93), (7.94) and Figure 7.32

$$\bar{x}=x+y\cdot\epsilon-(\bar{x}-x_s)(K_1 d^2+K_2 d^4+K_3 d^6)-(K_4+K_5 d^2)\{2(\bar{x}-x_s)(\bar{y}-y_s)\sin\phi_T+[3(\bar{x}-x_s)^2+(\bar{y}-y_s)^2]\cos\phi_T\}-x_0 \tag{7.104}$$

$$\bar{y}=y-(\bar{y}-y_s)(K_1 d^2+K_2 d^4+K_3 d^6)-(K_4+K_5 d^2)\{[3(\bar{y}-y_s)^2+(\bar{x}-x_s)^2]\sin\phi_T+2(\bar{x}-x_s)(\bar{y}-y_s)\cos\phi_T\}-y_0 \tag{7.105}$$

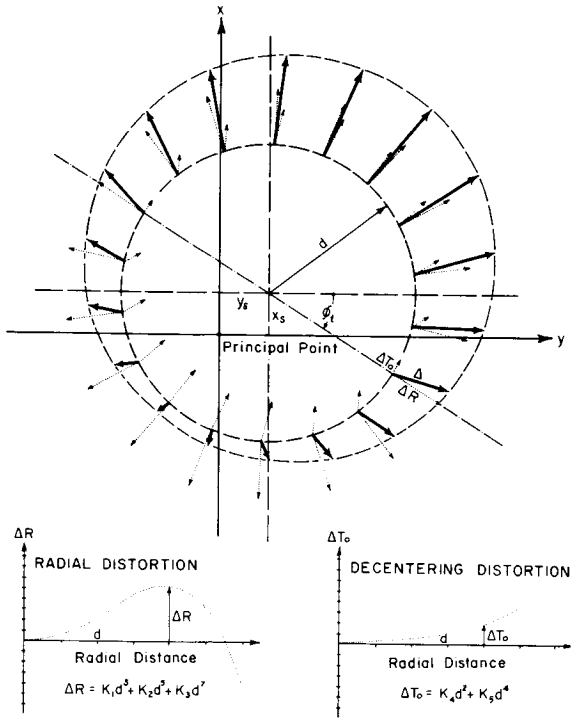

FIGURE 7.33.—Components of distortion.

where the meaning of d is defined by (7.96) and x and y are the comparator coordinates measured on the photogram.

7.4.6.2.6 DESCRIPTION OF THE RECTANGULAR COORDINATE SYSTEMS

In order to make the computations for the adjustment of geometric satellite triangulation as clear and synoptic as possible, three rectangular coordinate systems are used. Each of the three systems has a subgroup. The three principal systems are designated x, y, and z systems, and the corresponding subsystems are x', y', and z'. The x system corresponds to the astronomic reference system, in that the x_3 axis points to the celestial north pole and the x_1 axis intersects the equator at the vernal equinox. The origin of this system is the center of the unit sphere which circumscribes the Earth's center (origin of the rectangular geometric coordinates) or any arbitrary point of observation.

Turning the x system about its x_3 axis through the hour angle θ of the equinox (local sidereal time at observation site P) results in the x' system

$$\mathbf{x}'=\underset{3}{R}(\theta)\mathbf{x} \qquad (7.106)$$

(See also (7.20) and (7.21).)

The y system (see fig. 7.18a) designates the rectangular geocentric coordinate system, which corresponds to the orientation of the earth for a specific epoch and in which the y_3 axis points to the instantaneous north pole. The intersection of the instantaneous null meridian with the instantaneous equator determines the direction of the y_1 axis. The instantaneous null meridian is defined on the reference ellipsoid as the trace of the plane containing the instantaneous axis of rotation of the Earth and that point whose coordinates in the reference system (1900–1905 pole) are $\phi=0$, $\lambda=0$ (see sec. 7.4.4). At an arbitrary point of observation in the y system, the corresponding instantaneous coordinates are ϕ' and λ'_{east}. If the y system is rotated first through the angle λ'_{east} about its y_3 axis, the local y' system is obtained. In this system the y_3' axis points to the station zenith, while the y_1' axis lies in the plane of the meridian as well as of the horizon, and hence points south. Therefore:

$$\mathbf{y}'=\underset{2}{R}(90^\circ-\phi')\underset{3}{R}(\lambda'_{east})\mathbf{y}=\underset{2}{R}(90^\circ-\phi')\mathbf{x}' \qquad (7.107)$$

See also (7.23) and (7.30), the latter being the inverse transformation.

Finally, we have the z and z' systems, which coincide essentially with the y and y' systems, except that the z systems are referred to the conventional (1900–1905) pole (CIO). If the displacement of the instantaneous pole relative to the conventional pole is given, as is the practice, by the components x and y (see sec. 7.4.4 and fig. 7.21), the transformation is effected by

$$\mathbf{z}=\underset{1}{R}(-y)\underset{2}{R}(-x)\mathbf{y} \qquad (7.108)$$

and

$$\mathbf{z}' = \underset{2}{R}(90^\circ - \phi)\,\underset{3}{R}(\lambda_{east})\,\mathbf{z} \qquad (7.109)$$

(see also (7.32), (7.34), (7.36), and (7.37)).

Coordinates corresponding to the z system are designated ϕ and λ.

7.4.6.2.7 TRANSFORMATION OF GEODETIC COORDINATES ϕ, λ, h INTO RECTANGULAR COORDINATES AND CONVERSELY

The astronomical systems x and x' introduced in the previous section are, with respect to their informational content, essentially two-dimensional, defining merely directions in three space. On the other hand, the y, y', z, z' systems are used in the three-dimensional positioning of points on the Earth's surface (station coordinates) (e.g., see figs. 7.18a and 7.18b). In the course of reducing the satellite triangulation it is therefore necessary to transform coordinates into three-dimensional rectangular coordinates and vice versa. It is also necessary to make provisions for the introduction of given coordinates with their weights into the adjustment of the spatial triangulation. This brings up the problem of a purely geometric solution for transformations. Finally, the problem of determining ellipsoid constants arises when one desires to refer the rectangular station coordinates resulting from an extended satellite triangulation to a best-fitting ellipsoid for this area. In consequence of our assumption that electronic computers are being used, such computations are rigorously performed with closed formulas rather than the differential transformation of classical geodesy.

The designations for the constants of the reference ellipsoid are taken from figure 7.34:

$$\begin{aligned} a &= \text{semimajor axis} \\ b &= \text{semiminor axis} \\ e &= \text{eccentricity} = \left(\frac{a^2-b^2}{a^2}\right)^{1/2} \end{aligned} \qquad (7.110)$$

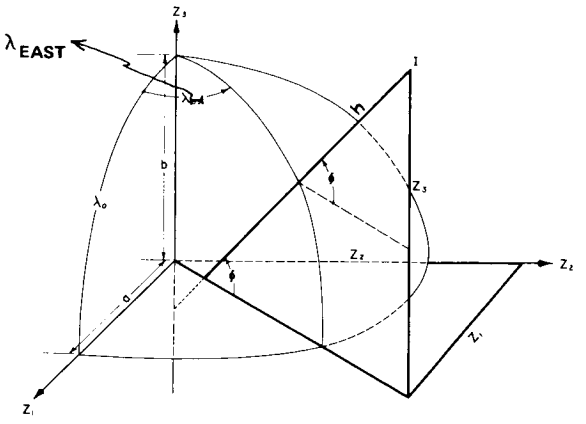

FIGURE 7.34

Figure 7.35 represents the plane of the meridian λ.

To transform the ϕ, λ, h into geocentric rectangular coordinates z_1, z_2, z_3 (see sec. 7.4.6.2.6 and fig. 7.34), the following formulas are used:

$$z_1 = [a^2(a^2 + b^2\tan^2\phi)^{-1/2} + h\cos\phi]\cos\lambda \qquad (7.111)$$

$$z_2 = [a^2(a^2 + b^2\tan^2\phi)^{-1/2} + h\cos\phi]\sin\lambda \qquad (7.112)$$

$$z_3 = (a^2 + b^2\tan^2\phi)^{-1/2} b^2\tan\phi + h\sin\phi \qquad (7.113)$$

For the inverse transformation,

$$\tan\lambda = z_2/z_1 \qquad (7.114)$$

$$\tan\beta_0 = z_3(z_1^2+z_2^2)^{-1/2}\, a\cdot b^{-1} \qquad (7.115)$$

$$\Delta\beta = \frac{\tan\beta_0 - ae^2(z_1^2+z_2^2)^{-1/2}\sin\beta_0 - a^{-1}bz_3(z_1^2+z_2^2)^{-1/2}}{1+\tan^2\beta_0 - ae^2(z_1^2+z_2^2)^{-1/2}\cos\beta_0} \qquad (7.116)$$

$$\beta = \beta_0 + \Delta\beta \qquad (7.117)$$

$$\tan\phi = ab^{-1}\tan\beta \qquad (7.118)$$

$$h = [(z_1^2+z_2^2)^{1/2} - a\cos\beta]\sec\phi \qquad (7.119)$$

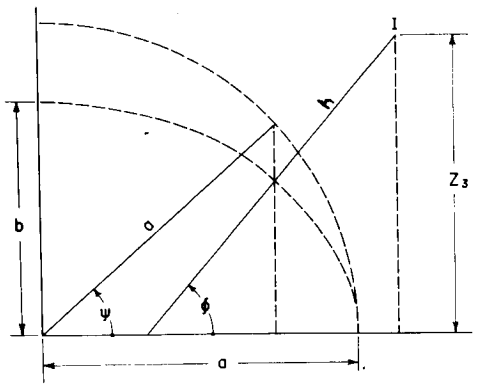

FIGURE 7.35

Equations 7.116 and 7.117 are introduced to avoid the alternative of solving the fourth-degree equation.

$$\tan\beta - ae^2(z_1^2+z_2^2)^{-1/2}\sin\beta - a^{-1}bz_3(z_1^2+z_2^2)^{-1/2}=0$$

Their use requires an iteration loop. Transforming ϕ to reduced latitude β accelerates the convergence of the process.

To transform, if necessary, the geocentric rectangular coordinates into local rectangular or vice versa, use (7.68) in appropriate connection with (7.30) or (7.36). Such a transformation represents the link between the y and y' or z and z' systems of section 7.4.6.2.6. For example, with the z systems

$$\mathbf{z}' = \underset{3}{\underline{R}}[\lambda_0, \underset{2}{(90^\circ-\phi_0)}](\mathbf{z}-\mathbf{z}_0) \tag{7.120}$$

where the $\mathbf{z}_0$ vector is computed from (7.111), (7.112), and (7.113) with ϕ_0, λ_0, h_0, the coordinates of the selected origin of the z' system.

In introducing certain coordinates

$$\boldsymbol{\phi} = \begin{bmatrix} \phi \\ \lambda \\ h \end{bmatrix} \tag{7.121}$$

with their given weights

$$\mathbf{P}_\phi = \begin{bmatrix} P_\phi & P_{\phi,\lambda} & P_{\phi,h} \\ P_{\phi,\lambda} & P_\lambda & P_{\lambda,h} \\ P_{\phi,h} & P_{\lambda,h} & P_h \end{bmatrix} \tag{7.122}$$

into the adjustment of the spatial satellite triangulation as additional conditions, it should be noted that

$$\mathbf{z}' = \begin{bmatrix} z_1' \\ z_2' \\ z_3' \end{bmatrix} \tag{7.123}$$

can be represented as a vector function of ϕ. Hence we can compute

$$\frac{d\mathbf{z}'}{d\boldsymbol{\phi}} = \underline{T}_\phi = \begin{bmatrix} \frac{\partial z_1'}{\partial\phi} & \frac{\partial z_1'}{\partial\lambda} & \frac{\partial z_1'}{\partial h} \\ \frac{\partial z_2'}{\partial\phi} & \frac{\partial z_2'}{\partial\lambda} & \frac{\partial z_2'}{\partial h} \\ \frac{\partial z_3'}{\partial\phi} & \frac{\partial z_3'}{\partial\lambda} & \frac{\partial z_3'}{\partial h} \end{bmatrix} \tag{7.124}$$

and

$$\Delta\mathbf{z}' = \underline{T}_\phi \Delta\boldsymbol{\phi} \tag{7.125}$$

Since, furthermore,

$$\frac{d\boldsymbol{\phi}}{d\mathbf{z}'} = \underline{T}_\phi^{-1} \tag{7.126}$$

we have

$$\Delta\boldsymbol{\phi} = \underline{T}_\phi^{-1}\Delta\mathbf{z}' \tag{7.127}$$

From similar considerations we have, in addition,

$$\underline{P}_{z'} = (\underline{T}_\phi^{-1})^* \underline{P}_\phi \underline{T}_\phi^{-1} \tag{7.128}$$

The partial derivatives in the $\underline{T}_\phi$ matrix (7.124) are computed with the coordinates ϕ_0, λ_0 of the origin of the local system:

$$\underline{T}_\phi = \underset{3}{\underline{R}}[\lambda_0, \underset{2}{(90^\circ-\phi_0)}]\frac{d\mathbf{z}}{d\boldsymbol{\phi}} \tag{7.129}$$

where $d\mathbf{z}/d\boldsymbol{\phi}$ is computed by differentiation of the expressions (7.111), (7.112), and (7.113) as follows

$$\frac{d\mathbf{z}}{d\boldsymbol{\phi}} \begin{bmatrix} -\mathrm{I}\cos\lambda & -\mathrm{II}\sin\lambda & \cos\phi\cos\lambda \\ -\mathrm{I}\sin\lambda & \mathrm{II}\cos\lambda & \cos\phi\sin\lambda \\ \mathrm{I}\cot\phi & 0 & \sin\phi \end{bmatrix} \tag{7.130}$$

where

$$\mathrm{I} = \{a^2 b^2 \tan\phi [\cos^2\phi (a^2 + b^2 \tan^2\phi)^{1/2}]^{-1} + h \sin\phi\} \rho^{-1} \quad (7.131)$$

$$\mathrm{II} = [a^2 (a^2 + b^2 \tan^2\phi)^{-1/2} + h \cos\phi] \rho^{-1} \quad (7.132)$$

with $\rho = 206\ 264''.8$.

The $\Delta\phi$ ($\Delta\phi$, $\Delta\lambda$, Δh) vector computed with (7.127) is in seconds of arc for $\Delta\phi$ and $\Delta\lambda$ and in meters for Δh; corresponding values are substituted in (7.125).

The classical coordinates of the triangulation stations, referred at times—especially in the world net—to different datums, are most conveniently recomputed on a common reference ellipsoid before they are introduced into the spatial triangulation as initial approximations, as is described later on. These purely geometric ellipsoid transformations can be accomplished with the formulas above by (1) computing from the given coordinates ϕ, λ, h with (7.111), (7.112), (7.113), geocentric coordinates pertaining to a specific ellipsoid; (2) translating, if necessary, the origin—the ellipsoid center—of these rectangular coordinates; and (3) transforming these rectangular coordinates into coordinates ϕ, λ, h, using (7.114) to (7.119), taking into account the parameters of the new reference ellipsoid.

This type of transformation is common, especially in connection with comparison of the final results of satellite triangulation with classical geodetic surveys.

The determination of the constants of a reference ellipsoid which best fits the results of an extended satellite triangulation is discussed in the sections immediately following. Such solutions must include the results of dynamic satellite geodesy, and the formulas so far developed serve as the basis for such a solution, since with (7.110) and (7.119) the geoid undulation N can be written, after suitable transformation, as

$$N = (h - H) = -H - (z_1^2 + z_2^2)^{1/2} \sec\phi - a(1 - e^2 \sin^2\phi)^{-1/2} \quad (7.133)$$

If the leveling height H is assumed to be free of error, the other partial derivatives are

$$\frac{\partial N}{\partial z_1} = \cos\phi \cos\lambda$$

$$\frac{\partial N}{\partial z_2} = \cos\phi \sin\lambda$$

$$\frac{\partial N}{\partial z_3} = \sin\phi \quad (7.134)$$

$$\frac{\partial N}{\partial a} = -W$$

$$\frac{\partial N}{\partial f} = b \sin^2\phi\, W^{-1}$$

with

$$W^2 = (1 - e^2 \sin^2\phi) \quad (7.135)$$

By means of an adjustment, three translation components Δz_1, Δz_2, Δz_3 and new ellipsoid parameters a and $f = 1 - (b/a)$ can be computed, subject to the condition $\Sigma v_N^2 = \min$. The fundamental concepts for such a solution are treated in Schmid and Schmid (1971).

7.4.6.3 Setting Up the General Photogrammetric Observation Equations

The general photogrammetric observation equations are obtained through combination of the expressions given in (7.91), (7.92), (7.104), and (7.105), with reference to the relations (7.79), (7.83), (7.84), and (7.96).

The mathematical model is

$$F = \overline{x} - y_\epsilon + (\overline{x} - x_s)(K_1 d^2 + K_2 d^4 + K_3 d^6) + \{2(\overline{x} - x_s)(\overline{y} - y_s)\sin\phi_T + [3(\overline{x} - x_s)^2 + (\overline{y} - y_s)^2]\cos\phi_T\}(K_4 + K_5 d^2) + x_0 - l_x = 0 \quad (7.136)$$

$$G = \overline{y} + (\overline{y} - y_s)(K_1 d^2 + K_2 d^4 + K_3 d^6) + \{[3(\overline{y} - y_s)^2 + (\overline{x} - x_s)^2]\sin\phi_T + 2(\overline{x} - x_s)(\overline{y} - y_s)\cos\phi_T\}(K_4 + K_5 d^2) + y_0 - l_y = 0 \quad (7.137)$$

where, according to figure 7.32 and (7.91), (7.92), and (7.96),

$$\overline{x} = \frac{c_y m}{q} \quad (7.138)$$

$$\overline{y}=\frac{c_y n}{q} \tag{7.139}$$

$$d^2=\left(\frac{c_x m}{q}-x_s\right)^2+\left(\frac{c_y n}{q}-y_s\right)^2 \tag{7.140}$$

and l_x, l_y are the measured values of x and y.

The meaning of m, n, and q is apparent from (7.83), (7.84), the direction cosines r_{ij} being obtained from (7.79).

Substituting (7.138), (7.139), and (7.140) in (7.136) and (7.137), taking into account (7.83), (7.84), and (7.79), results in expressions for the equations F and G which represent the mathematical model for the generalized central perspective.

Since, however, especially at the beginning of the adjustment, the approximation values for the exterior orientation parameters are not necessarily good ones, it is better to adopt the following computational procedure, which, in general, converges more rapidly and leads to a simpler solution with sufficiently close approximation. It should be noted that the radial distortion (7.95), and particularly the decentering distortion ΔT_0 (7.99), as functions of d, are small and vary relatively little with a change in d.

At the beginning of each iteration step of the adjustment, $\overline{x}$ and $\overline{y}$ are computed by using the comparator coordinates x and y, neglecting the influence of their measuring error, in accordance with figure 7.32 and (7.87), (7.88), (7.89), (7.90), (7.93), and (7.94). Since the coordinates x and y are replaced by the actual measurements l_x and l_y, the designations $l_{\bar{x}}$ and $l_{\bar{y}}$ will now be introduced for $\overline{x}$ and $\overline{y}$.

$$l_{\bar{x}}=l_x+l_y\cdot\epsilon-x_0-\Delta R_x-\Delta T_x \tag{7.141}$$

$$l_{\bar{y}}=l_y-y_0-\Delta R_y-\Delta T_y \tag{7.142}$$

With this,

$$(\overline{x}-x_s)=(l_{\bar{x}}-x_s)=d_x \tag{7.143}$$

$$(\overline{y}-y_s)=(l_{\bar{y}}-y_s)=d_y \tag{7.144}$$

$$d^2=d_x^2+d_y^2 \tag{7.145}$$

The radial and Conrady components of distortion, ΔR_x, ΔR_y, ΔT_x, and ΔT_y in (7.141) and (7.142) are computed with (7.97), (7.98), and (7.103). Since the mathematical models of the distortion, and hence also the distance d with its components d_x and d_y, refer to the geometry of the central perspective (see fig. 7.32), an iteration loop must be designed for computing all the distortion components used in (7.141) and (7.142). In (7.97), (7.98), and (7.103), $\overline{x}$ and $\overline{y}$ are first replaced by

$$\overline{x}=l_{\bar{x}}\approx l_x+l_y\cdot\epsilon-x_0 \tag{7.146}$$

$$\overline{y}=l_{\bar{y}}\approx l_y-y_0 \tag{7.147}$$

The ΔR_x, ΔR_y, ΔT_x, and ΔT_y so computed are substituted in (7.141) and (7.142) to give new $l_{\bar{x}}$, $l_{\bar{y}}$ values, with which distortion components are again computed, followed by new $l_{\bar{x}}$ and $l_{\bar{y}}$ values. This iteration is continued until the difference between successive $l_{\bar{x}}$ and $l_{\bar{y}}$ becomes less than a prescribed tolerance.

Introduction of l_x and l_y and substitution for m, n, and q in accordance with (7.83) and (7.84) changes (7.136) and 7.137) to

$$\begin{aligned}F=&-l_y\cdot\epsilon\\&+\frac{c_x[r_{11}(x-x_0)+r_{12}(y-y_0)+r_{13}(z-z_0)]}{r_{31}(x-x_0)+r_{32}(y-y_0)+r_{33}(z-z_0)}\\&+x_0+(l_{\bar{x}}-x_s)(K_1d^2+K_2d^4+K_3d^6)\\&+\{2(l_{\bar{x}}-x_s)(l_{\bar{y}}-y_s)\sin\phi_T+[3(l_{\bar{x}}-x_s)^2\\&+(l_{\bar{y}}-y_s)^2]\cos\phi_T\}(K_4+K_5d^2)-l_x=0\end{aligned} \tag{7.148}$$

$$\begin{aligned}G=&\frac{c_y[r_{21}(x-x_0)+r_{22}(y-y_0)+r_{23}(z-z_0)]}{r_{31}(x-x_0)+r_{32}(y-y_0)+r_{33}(z-z_0)}\\&+y_0+(l_{\bar{y}}-y_s)(K_1d^2+K_2d^4+K_3d^6)\\&+\{[3(l_{\bar{y}}-y_s)^2+(l_{\bar{x}}-x_s)^2]\sin\phi_T\\&+2(l_{\bar{x}}-x_s)(l_{\bar{y}}-y_s)\cos\phi_T\}(K_4+K_5d^2)\\&-l_y=0\end{aligned} \tag{7.149}$$

with

$$d^2=(l_{\bar{x}}-x_s)^2+(l_{\bar{y}}-y_s)^2 \tag{7.150}$$

The meaning of the r_{ij} is apparent from (7.78) and (7.79), and the $l_{\bar{x}}$, $l_{\bar{y}}$ are computed iteratively with (7.141) and (7.142).

Equations 7.148 and 7.149 are analytical expressions for the generalized central perspective principle. The influences requiring generalization are:

(1) Skewness ϵ of the comparator carriage; its effect is simulated by the term ϵl_y in (7.148).

(2) Linear scale error, in the measuring screws of the comparator; their influence is adequately accounted for with the scale factors c_x and c_y in (7.148) and (7.149), respectively.

(3) Distortion; the two last terms in each of (7.148) and (7.149) simulate the components of the distortion vector Δ as the sum of radial and decentering distortion. In addition, the actual conditions are more closely approximated by displacing the origin (x_s, y_s) of the distortion from the principal point (x_0, y_0). These relations are shown schematically in figures 7.32 and 7.33.

For the further treatment of expressions 7.148 and 7.149, it is necessary only to note that the direction cosines (see (7.62), (7.83), and (7.84)) in the third term of (7.148) and in the second term of (7.149) refer to refracted corrections.

The next step is to set up the observation equations. In the adjustment, a generalized adjustment algorithm described in Schmid (1965b) and Schmid and Schmid (1965) is used. The mathematical model is given with the two functions F and G of (7.148) and (7.149), and the general observation equations are obtained by expanding these functions in Taylor series and neglecting terms of the second and higher order as

$$\frac{\partial F}{\partial \mathbf{u}}\Delta\mathbf{u}+F_0=0 \qquad (7.151)$$

$$\frac{\partial G}{\partial \mathbf{u}}\Delta\mathbf{u}+G_0=0 \qquad (7.152)$$

in which $\mathbf{u}$ is the vector of all parameters in the mathematical model, including the measured quantities. Table 7.6 lists the symbols designating the various partial derivatives of F and G, where

$$\begin{aligned} J_x &= D_x & K_x &= -E_x & L_x &= -F_x \\ J_y &= -D_y & K_y &= -E_y & L_y &= -F_y \end{aligned} \qquad (7.153)$$

The corresponding analytical expressions, including the necessary auxiliary quantities, are

$$\begin{aligned} ① &= (\bar{x}-x_0)/c_x & ⑤ &= ① F - r_{13} \\ ② &= (\bar{y}-y_0)/c_y & ⑥ &= ② D - r_{21} \\ ③ &= ① D - r_{11} & ⑦ &= ② E - r_{22} \\ ④ &= ① E - r_{12} & ⑧ &= ② F - r_{23} \\ & & ⑨ &= ② r_{12} - ① r_{22} \end{aligned} \qquad (7.154)$$

$$\begin{aligned} A_x &= c_x(①\cdot⑨+⑦) & A_y &= +c_y\,②\cdot⑨ \\ B_x &= +c_x[(1+①^2)\sin\kappa+①\cdot②\cos\kappa] & B_y &= +c_y[(1+②^2)\cos\kappa+①\cdot②\sin\kappa] \\ C_x &= +c_x② & C_y &= -c_y① \\ D_x &= \frac{c_x}{q}③ & D_y &= \frac{c_y}{q}⑥ \\ E_x &= \frac{c_x}{q}④ & E_y &= \frac{c_y}{q}⑦ \\ F_x &= \frac{c_x}{q}⑤ & F_y &= \frac{c_y}{q}⑧ \\ G_x &= ① & G_y &= ② \\ H_x &= 1+P_x & H_y &= P_y \\ I_x &= Q_x & I_y &= 1+Q_y \\ M_x &= d_x d^2 & M_y &= d_y d^2 \\ N_x &= d_x d^4 & N_y &= d_y d^4 \\ O_x &= d_x d^6 & O_y &= d_y d^6 \end{aligned}$$

$$\begin{aligned} P_x &= -\frac{\Delta R}{d}-d_x^2 D_r - d_x D_w\cos\phi_T \\ &\quad -4d_x[K_4+(2d_x^2+d_y^2)K_5]\cos\phi_T \\ &\quad -2d_y[K_4+(d_x^2+3d_y^2)K_5]\sin\phi_T \\ P_y &= -d_x d_y D_r - d_x D_w\sin\phi_T - 2d_y\{[K_4 \\ &\quad +(3d_x^2+d_y^2)K_5]\cos\phi_T + 2d_y K_5\sin\phi_T\} \\ Q_x &= -d_x d_y D_r - d_y D_w\cos\phi_T - 2d_x\{[K_4 \\ &\quad +(d_x^2+3d_y^2)K_5]\sin\phi_T \\ Q_y &= -\frac{\Delta R}{d}-d_y D_r - d_y D_w\sin\phi_T - 2d_x[K_4 \\ &\quad +(d_x^2+2d_y^2)K_5]\cos\phi_T - 4d_y[K_4 \\ &\quad +(d_x^2+2d_y^2)K_5]\sin\phi_T \end{aligned} \qquad (7.155)$$

where

$$d_x = (l_{\bar{x}} - x_s) \qquad d_y = (l_{\bar{y}} - y_s)$$

$$D_r = [2K_1 + 4K_2 d^2 + 6K_3 d^4]$$

$$D_w = [2K_4 + 4K_5 d^2]$$

$$d^2 = d_x^2 + d_y^2$$

$$R_x = d^2 \cos \phi_T + 2(d_x^2 \cos \phi_T + d_x d_y \sin \phi_T)$$

$$R_y = d^2 \sin \phi_T + 2(d_y^2 \sin \phi_T + d_x d_y \cos \phi_T)$$

$$S_x = d^4 \cos \phi_T + 2d^2(d_x^2 \cos \phi_T + d_x d_y \sin \phi_T)$$

$$S_y = d^4 \sin \phi_T + 2d^2(d_y^2 \sin \phi_T + d_x d_y \cos \phi_T)$$

$$T_x = -\sin \phi_T (K_4 d^2 + K_5 d^4) + 2(K_4 + K_5 d^2)(d_x d_y \cos \phi_T - d_x^2 \sin \phi_T)$$

$$T_y = \cos \phi_T (K_4 d^2 + K_5 d^4) + 2(K_4 + K_5 d^2)(d_y^2 \cos \phi_T - d_x d_y \sin \phi_T)$$

$$U_z = l_y \qquad U_y = 0$$

$$Z_x = -1 \qquad Z_y = -1 \tag{7.155a}$$

With an arbitrarily selected mean error of unit weight m_0 before adjustment the weight matrix (see (7.196)) assigned to the observation equations (7.151) and (7.152) is computed. The adjustment then determines the $\Delta\mathbf{u}$ vector subject to the condition

$$\Delta\mathbf{u}^* \underline{P} \Delta\mathbf{u} = \min \tag{7.156}$$

The required parameters are then

$$\mathbf{u} = \mathbf{u}_0 + \Delta\mathbf{u} \tag{7.157}$$

where $\mathbf{u}_0$ are the approximations for the parameters (see (7.208) to (7.210)).

7.4.6.4 Mathematical Model for the Photogrammetric Camera

Each of the various different applications of the photogrammetric measurement method requires the development of an appropriate analytical expression from the general formulation. A special application will now be shown as the first step in satellite triangulation. As was outlined initially in section 7.4.3, the parameters needed for the reconstruction of the bundle from the star images (in this case, ϵ, c_x, c_y, x_0, y_0, x_s, y_s, K_1, K_2, K_3, K_4, K_5, ϕ_T) and of the exterior orientation (α,ω,κ) are to be computed.

Since the directions to the fixed stars refer to the center of the unit sphere at the center of projection, the coordinates X_0, Y_0, Z_0 of (7.148) and (7.149) are set equal to zero. Furthermore, it was shown toward the end of section 7.4.3 that the coordinates expressing the direction to a star can be transformed to standard coordinates ξ_r, η_r, $+1$ (see fig. 7.27 and eqs. (7.66), (7.67) with (7.61)). This changes (7.148) and (7.14) into

$$F = -l_x - l_y \cdot \epsilon + \frac{c_x(r_{11}\xi_r + r_{12}\eta_r + r_{13})}{r_{31}\xi_r + r_{32}\eta_r + r_{33}} + x_0 + (l_{\bar{x}} - x_s)(K_1 d^2 + K_2 d^4 + K_3 d^6) + \{2(l_{\bar{x}} - x_s)(l_{\bar{y}} - y_s) \sin \phi_T + [3(l_{\bar{x}} - x_s)^2 + (l_{\bar{y}} - y_s)^2] \cos \phi_T\}(K_4 + K_5 d^2) = 0 \tag{7.158}$$

$$G = -l_y + \frac{c_y(r_{21}\xi_r + r_{22}\eta_r + r_{23})}{r_{31}\xi_r + r_{32}\eta_r + r_{33}} + y_0 + (l_{\bar{x}} - y_s)(K_1 d^2 + K_2 d^4 + K_3 d^6) + \{[3(l_{\bar{y}} - y_s)^2 + (l_{\bar{x}} - x_s)^2] \sin \phi_T + 2(l_{\bar{x}} - x_s)(l_{\bar{y}} - y_s) \cos \phi^T\}(K_4 + K_5 d^2) = 0 \tag{7.159}$$

We note, first of all, that right ascension α and declination δ, together with their mean errors, are given quantities. Consequently, it is necessary to minimize the sum of the $(v_\alpha v_\alpha + v_\delta v_\delta)$, weighted in accordance with the weight matrix $\underline{P}_{\alpha,\delta}$ given for the stars, not the sum of squares of the v_ξ and v_η residuals. To accomplish this, the ξ_r and η_r are differentiated with respect to α and δ, and the coefficients in the observation equations used to compute the $\Delta\xi$ and $\Delta\eta$ are multiplied accordingly. After appropriate arrangement, coefficients are obtained in the observation equations which do not refer to the corrections $\Delta\xi$ and $\Delta\eta$, but to v_α and v_δ. Using (7.66) and (7.67), one obtains in the y' system

$$\xi_r = y_1'/y_3' \tag{7.160}$$

$$\eta_r = y_2'/y_3' \tag{7.161}$$

from which, when the index r is omitted,

$$d\xi = \frac{y_3' dy_1' - y_1' dy_3'}{y_3'^2} \tag{7.162}$$

$$d\eta = \frac{y_3' dy_2' - y_2' dy_3'}{y_3'^2} \tag{7.163}$$

From (7.1) with (7.20), (7.23) and figure 7.19, it follows that

$$\mathbf{x}' = \begin{bmatrix} x_1' \\ x_2' \\ x_3' \end{bmatrix} = \begin{bmatrix} \cos\delta & \cos t \\ -\cos\delta & \sin t \\ & \sin\delta \end{bmatrix} = \begin{bmatrix} \sin\phi' & 0 & \cos\phi' \\ 0 & 1 & 0 \\ -\cos\phi' & 0 & \sin\phi' \end{bmatrix} \begin{bmatrix} y_1' \\ y_2' \\ y_3' \end{bmatrix} \tag{7.164}$$

Differentiating (7.164), noting that $dt = -d\alpha$, gives

$$\mathbf{dx}' = \begin{bmatrix} -x_2' & -\sin\delta\cos t \\ x_1' & \sin\delta\sin t \\ 0 & \cos\delta \end{bmatrix} \begin{bmatrix} d\alpha \\ d\delta \end{bmatrix} \tag{7.165}$$

From (7.23),

$$\mathbf{dy}' = \underset{2}{\underline{R}}(90^\circ - \phi')\,\mathbf{dx}' \tag{7.166}$$

which with (7.165) gives

$$\mathbf{dy}' = \begin{bmatrix} -x_2'\sin\phi' - (x_3'\cos t\sin\phi' + \cos\delta\cos\phi') \\ x_1' \qquad\qquad x_3'\sin t \\ -x_2'\cos\phi'\,(-x_3'\cos t\cos\phi' + \cos\delta\sin\phi') \end{bmatrix} \begin{bmatrix} d\alpha \\ d\delta \end{bmatrix} \tag{7.167}$$

With the relations found in (7.160), (7.161), and (7.164), the application of (7.167) with (7.162) and (7.163) yields

$$\frac{d\xi}{d\alpha} = \frac{-y_2'\sin\phi'}{y_3'} + \xi_r \frac{y_2'\cos\phi'}{y_3'} = \eta_r(\xi_r\cos\phi' - \sin\phi') \tag{7.168}$$

$$\frac{d\eta}{d\alpha} = \frac{y_1'}{y_3'} + \eta_r^2\cos\phi' = \xi_r\sin\phi' + (1+\eta_r^2)\cos\phi' \tag{7.169}$$

and, similarly, the intermediate steps having been omitted,

$$\frac{d\xi}{d\phi} = -\cos t\,(1+\xi_r^2+\eta_r^2) \tag{7.170}$$

$$\frac{d\eta}{d\delta} = \sin t\sin\phi'\,(1+\xi_r^2+\eta_r^2) \tag{7.171}$$

Other quantities needed are

$$\frac{\partial F}{\partial\alpha} = J_x^* = J_x\cdot\frac{d\xi}{d\alpha} + K_x\cdot\frac{d\eta}{d\alpha} \tag{7.172}$$

$$\frac{\partial F}{\partial\delta} = K_x^* = J_x\cdot\frac{d\xi}{d\delta} + K_x\cdot\frac{d\eta}{d\delta} \tag{7.173}$$

$$\frac{\partial G}{\partial\alpha} = J_y^* = J_y\cdot\frac{d\xi}{d\alpha} + K_y\cdot\frac{d\eta}{d\alpha} \tag{7.174}$$

$$\frac{\partial G}{\partial\delta} = K_y^* = J_y\cdot\frac{d\xi}{d\delta} + K_y\cdot\frac{d\eta}{d\delta} \tag{7.175}$$

in which $d\xi/d\alpha$, $d\xi/d\delta$, $d\eta/d\alpha$, and $d\eta/d\delta$ are given with (7.168) through (7.171) and J_x, J_y, K_x, and K_y are computed from (7.153) through (7.155).

If one accepts the coordinates corrected for refraction ξ_r and η_r, the corresponding linearized observation equations can be set up directly with (7.158), (7.159) and the introduction of (7.172) to (7.175). Just as the central perspective bundle was altered by additional physical influences, the direction given with the coordinates ξ_r, η_r can be subjected to a further refraction correction by further improving the τ constants used for the original refraction correction.

In consonance with (7.40) one can therefore write

$$\Delta r_\varkappa = \underset{\frac{1}{2}}{\underline{T}} W\left(\tan\frac{\beta}{2}\Delta\tau_1 + \tan^3\frac{\beta}{2}\Delta\tau_2 + \tan^5\frac{\beta}{2}\Delta\tau_3 + \tan^7\frac{\beta}{2}\Delta\tau_4\right) \tag{7.176}$$

Assuming further that refraction does not affect azimuth, we have $\xi_r/\eta_r = \text{constant}$, and therefore

$$\Delta\xi/\Delta\eta = \xi_r/\eta_r \tag{7.177}$$

and, in analogy with (7.66) and (7.67),

$$\xi_r^2+\eta_r^2=\tan^2 z_r=\frac{y_1'^2+y_2'^2}{y_3'^2} \qquad (7.178)$$

Differentiating (7.178) gives

$$\xi_r\Delta\xi+\eta_r\Delta\eta=\tan z_r\ (1+\tan^2 z_r)\,\Delta z \qquad (7.179)$$

Substituting (7.171) in (7.179) gives

$$\Delta z=\Delta r_\infty \qquad (7.180)$$

$$\begin{aligned}\Delta\xi&=\xi_r\frac{(1+\tan^2 z_r)}{\tan z_r}\Delta r_\infty\\&=\frac{2\xi_r}{\sin 2z_r}\Delta r_\infty\\&=\frac{y_1'}{y_3'^2}\,(y_1'^2+y_2'^2)^{-1/2}\,\Delta r_\infty\end{aligned} \qquad (7.181)$$

$$\begin{aligned}\Delta\eta&=\eta_r\frac{(1+\tan^2 z_r)}{\tan z_r}\Delta r_\infty\\&=\frac{2\eta_r}{\sin 2z_r}\Delta r_\infty\\&=\frac{y_2'}{y_3'^2}\,(y_1'^2+y_2'^2)^{-1/2}\,\Delta r_\infty\end{aligned} \qquad (7.182)$$

in which Δr_∞ is given with (7.176).

When (7.176), (7.181), and (7.182) are taken into consideration and the designations of table 7.6 are used, the partial derivatives of the functions F and G needed in the refraction correction are now introduced, giving

$$\frac{\partial F}{\partial\tau}=\begin{bmatrix}V_x\\W_x\\X_x\\Y_x\end{bmatrix}=\begin{bmatrix}\tan\beta/2\\\tan^3\beta/2\\\tan^5\beta/2\\\tan^7\beta/2\end{bmatrix}\cdot\tau_x \qquad (7.183)$$

$$\frac{\partial G}{\partial\tau}=\begin{bmatrix}V_y\\W_y\\X_y\\Y_y\end{bmatrix}=\begin{bmatrix}\tan\beta/2\\\tan^3\beta/2\\\tan^5\beta/2\\\tan^7\beta/2\end{bmatrix}\cdot\tau_y \qquad (7.184)$$

where

$$\tau_x=\underline{T}^{1/2}\,W\frac{(J_x y_1')+(K_x y_2')}{y_3'^2\,(y_1'^2+y_2'^2)^{1/2}}=\underline{T}^{1/2}\,W\frac{2\,(J_x\xi_r+K_x\eta_r)}{\sin 2z_r} \qquad (7.185)$$

$$\tau_y=\underline{T}^{1/2}\,W\frac{(J_y y_1')+(K_y y_2')}{y_3'^2\,(y_1'^2+y_2'^2)^{1/2}}=\underline{T}^{1/2}\,W\frac{2\,(J_y\xi_r+K_y\eta_r)}{\sin 2z_r} \qquad (7.186)$$

with $\underline{T}$ and W as in (7.40).

The observation equations (7.151), (7.152) for the single camera are therefore set up in accordance with (7.158), (7.159), table 7.3, (7.153) to (7.155), and with (7.172) to (7.175), (7.183), and (7.184). Since the skewness ϵ of the comparator axes is always small, the term $v_{l_y\epsilon}$ is negligible. We thus have the system of observation equations

$$\boldsymbol{A}\boldsymbol{v}_u+\boldsymbol{l}=0 \qquad (7.187)$$

with the weight matrix, $P_u=m_o^2\sigma_u^{-1}$, where, in general, we have for each pair of observation equations

$\underline{A}=$

$\mathbf{v}_u^*$																							
$\boldsymbol{\Delta}^*$																							
$\mathbf{v}_{l_{x,y}}^*$		$\mathbf{v}_{\alpha,\delta}^*$		$\boldsymbol{\Delta}_o^*$																			
l_x	l_y	α^1	δ	ν	ω	x	c_x	c_y	x_0	y_0	K_1	K_2	K_3	x_s	y_s	K_4	K_5	$\gamma\tau$	ϵ	τ_1	τ_2	τ_3	τ_4
-1	$-$	J_x^*	K_x^*	A_x	B_x	C_x	G_x	—	H_x	I_x	M_x	N_x	O_x	P_x	Q_x	R_x	S_x	T_x	U_x	V_x	W_x	X_x	Y_x
$-$	-1	J_y^*	K_y^*	A_y	B_y	C_y	—	G_y	H_y	I_y	M_y	N_y	O_y	P_y	Q_y	R_y	S_y	T_y	—	V_y	W_y	X_y	Y_y
$-\underline{A}_1$		$\underline{B}_{\alpha,\delta}$		$\underline{B}_0$																			
$\underline{B}$																							

(7.188)

α^1 being right ascension.

$\boldsymbol{l}$ is computed (see (7.151), (7.152)) from the approximation and measured values as

$$\boldsymbol{l}=\begin{bmatrix} F_0 \\ G_0 \end{bmatrix}_i \tag{7.189}$$

$$\underline{P}_u=\left[\begin{array}{c|c|c|c} \underline{P}_{l_x,\,l_y} & 0 & 0 & 0 \\ \hline 0 & \underline{P}_{\alpha,\,\delta} & 0 & 0 \\ \hline 0 & 0 & \underline{P}_0 & 0 \\ \hline 0 & 0 & 0 & \underline{P}_\tau \end{array}\right] \tag{7.190}$$

The $\underline{P}_u$ matrix (7.190) theoretically could be completely filled, but it is necessary to normalize all weights with respect to a selected value for m_0, and, in addition, the mean errors of the rotation parameters must be in radians. Thus, it becomes possible to account for all existing correlations. In practice, however, as is indicated in (7.190), there are uncorrelated groups, since no correlation exists between the σ_l matrix specifying the accuracy of comparator measurements, the $\underline{\sigma}_{\alpha,\delta}$ matrix specifying the accuracy of the star coordinates, the $\underline{\sigma}_0$ matrix specifying the accuracy of the other, chiefly photogrammetric, parameters, and the $\underline{\sigma}_\tau$ matrix specifying the accuracy of the refraction determination.

Since in what follows it will be repeatedly necessary to compute accuracy criteria, the meaning of the various designations used will now be explained.

Measures of Accuracy Before Adjustment. —The mean error of unit weight arbitrarily fixed before the adjustment is m_0. The mean error of a measurement i is designated m_i. Hence

$$p_i=m_0^2/m_i^2 \tag{7.191}$$

The corresponding weight matrix, e.g., for the comparator measurements l_x, l_y, is

$$\underline{P}l_i=\begin{bmatrix} pl_x & pl_{x,y} \\ pl_{x,y} & pl_y \end{bmatrix}=m_0^2\begin{bmatrix} \sigma l_x^2 & \sigma l_{x,y} \\ \sigma l_{x,y} & \sigma l_y^2 \end{bmatrix}^{-1}=m_0^2\underline{\sigma}_{l_i}^{-1} \tag{7.192}$$

with $\sigma_{l_{x,y}}=\rho_{x,y}\sigma_{l_x}\sigma_{l_y}$; $\rho_{x,y}$ denotes the correlation coefficient which equals 0 for comparator measurements when the comparator has independent mechanisms for measuring x and y.

Measures of Accuracy After Adjustment. —The mean error of unit weight after the adjustment is

$$s_0=\left(\frac{\mathbf{v}^*\underline{P}\mathbf{v}}{n-u}\right)^{1/2} \tag{7.193}$$

and the mean error of an observation after the adjustment is

$$s_i=\frac{s_0}{m_0}m_i \tag{7.194}$$

With respect to the unknowns u computed in the adjustment there exists the relation

$$s_0^2\underline{N}_u^{-1}=\mathfrak{s}_u^2=\mathfrak{d}_u=\underbrace{\begin{bmatrix} \underline{s_{u_1u_1}} & s_{u_1u_2} & \cdot & \cdot & s_{u_1u_n} \\ & \underline{s_{u_2u_2}} & \cdot & \cdot & s_{u_2u_n} \\ & & \cdot & & \cdot \\ & & & \cdot & \cdot \\ & & & & \cdot \\ & & & & \underline{s_{u_nu_n}} \end{bmatrix}}_{\text{Covariance matrix}} \tag{7.195}$$

in which $s_{u_iu_j}=\rho_{ij}s_{u_i}s_{u_j}$. With (7.193) and (7.195) we obtain

$$\underline{P}_u=m_0^2\mathfrak{d}_u^{-1}=\frac{m_0^2}{s_0^2}\underline{N}_u \tag{7.196}$$

Omitting the index u in order to simplify the notation, we have $s_{ij}=\rho_{ij}s_is_j$, and the dimensionless correlation matrix that corresponds to (7.195) is then

$$\varrho = \begin{bmatrix} s_i^{-1} & & & & & \\ & s_j^{-1} & & & & \\ & & \cdot & & & \\ & & & \cdot & & \\ & & & & \cdot & \\ & & & & & s_n^{-1} \end{bmatrix} s^2 \begin{bmatrix} s_i^{-1} & & & & & \\ & s_j^{-1} & & & & \\ & & \cdot & & & \\ & & & \cdot & & \\ & & & & \cdot & \\ & & & & & s_n^{-1} \end{bmatrix}$$

$$= \begin{bmatrix} 1 & \rho_{ij} & \cdot & \cdot & \cdot & \rho_{i_n} \\ \rho_{ij} & 1 & & & & \cdot \\ \cdot & & \cdot & & & \cdot \\ \cdot & & & \cdot & & \cdot \\ \cdot & & & & \cdot & \cdot \\ \rho_{ij} & \cdot & \cdot & \cdot & \cdot & 1 \end{bmatrix} \tag{7.197}$$

in which all $\rho_{ii}=1$ and the numerical values of the correlation coefficients ρ_{ij}, as well as the numerical value of the determinant $|\rho|$, lie between 0 and 1.

Finally, it is desirable to compute the axes and orientation of error ellipses and of the error ellipsoids arising in connection with the spatial triangulation to be discussed later. In a solution designed for electronic computation it is convenient to treat the relatively simple two-dimensional case as a special case of the three-dimensional solution given here.

The characteristic equation

$$\begin{bmatrix} s_x^2-\lambda & s_{x,y} & s_{x,y} \\ s_{x,y} & s_y^2-\lambda & s_{y,z} \\ s_{x,z} & s_{y,z} & s_z^2-\lambda \end{bmatrix} = 0 \tag{7.198}$$

becomes, on development of the determinant, a polynomial equation in λ, the eigenvalues of the covariance matrix:

$$\lambda^3 - r\lambda^2 + s\lambda - t = 0 \tag{7.199}$$

The lengths of the semiaxes of the error ellipsoid are square roots of the roots λ_1, λ_2, λ_3 of this equation. To obtain the direction cosines of the axes, the eigenvectors $\mathbf{x}_1$, $\mathbf{x}_2$, and $\mathbf{x}_3$ are computed in those separate steps by substituting in turn each of the $\lambda_{1,2,3}$ values in (7.198) and solving the three sets of simultaneous linear homogeneous equations:

$$\begin{bmatrix} s_x^2-\lambda & s_{x,y} & s_{x,z} \\ s_{x,y} & s_y^2-\lambda & s_{y,z} \\ s_{x,z} & s_{y,z} & s_z^2-\lambda \end{bmatrix} \begin{bmatrix} x_{i_1} \\ x_{i_2} \\ x_{i_3} \end{bmatrix} = 0 \tag{7.200}$$

Each of the three solutions $(x_{i_1}, x_{i_2}, x_{i_3})$ contains a free variable with which the vector $\mathbf{x}_i$ can be expressed in length λ_i or as a unit vector, thus defining the direction of the axis. The procedure is described in Zurmühl (1965).

For the two-dimensional case the 2×2 covariance matrix is extended to a 3×3 matrix by introducing the number 1, or any other number, as the three-dimensional diagonal term and zeros for the other additional entries to account for the fictitious third dimenson. The capacity of the larger electronic computers makes it attractive to design a program which can compute eigenvalues and vectors for the n-dimensional case. However, the computational effort increases with the third power of n.

If it is desired to do justice to maximal accuracy requirements in satellite triangulation, it is necessary to recalibrate the camera for each event. Hence $\underline{P}_0$ is in general a null matrix. The need for an additional refraction correction is questionable because of the existing correlation between the τ values and the elements of exterior orientation, especially when the cameras used are equipped with objectives requiring relatively small viewing angles. When the $\Delta\tau_i$ corrections are not computed, the $\underline{P}_u$ matrix consists of only the $\underline{P}_l$ and $\underline{P}_{\alpha,\delta}$ portions. As is shown in

(7.188), $\underline{A}_l$ is always a unit matrix. If we introduce, for the moment, $\underline{P}_{\alpha,\delta}$ as a null matrix with $\underline{P}_l$ from (7.192), the normal equations system corresponding to the observation equations (7.187) is

$$\sum_{i=1}^{m} [\underline{B}^* \underline{P}_l \underline{B}]_i \boldsymbol{\Delta} + \sum_{i=1}^{m} [\underline{B}^* P_l \boldsymbol{l}]_i = 0 \tag{7.201}$$

where m is the number of star images.

Each pair of observation equations for an individual star image i contributes to the normal equations system (7.201) in the following manner:

$$\underline{B}_i^* \underline{P}_{li} \underline{B}_i \boldsymbol{\Delta} + \underline{B}^* \underline{P}_{li} \boldsymbol{l}_i = 0 \tag{7.202}$$

Subdividing the $\underline{B}$ matrix further by using the notations introduced in (7.188) results in the following scheme for (7.202):

$$\begin{matrix} \mathbf{v}_{\alpha,\delta} & \boldsymbol{\Delta}_0 \end{matrix}$$

$$\left[\begin{array}{c|c} (\underline{B}^*_{\alpha,\delta} \underline{P}_l \underline{B}_{\alpha,\delta})_i & (\underline{B}^*_{\alpha,\delta} \underline{P}_l \underline{B}_0)_i \\ \hline (\underline{B}^*_0 \underline{P}_l \underline{B}_{\alpha,\delta})_i & (\underline{B}^*_0 \underline{P}_l \underline{B}_0)_i \end{array}\right] + \left[\begin{array}{c} (\underline{B}^*_{\alpha,\delta} \underline{P}_l \boldsymbol{l})_i \\ \hline (\underline{B}^*_0 \underline{P}_l \boldsymbol{l})_i \end{array}\right] = 0 \tag{7.203}$$

The accuracy of the given α, δ values expressed with the $\underline{P}_{\alpha,\delta}$ matrix is, in accordance with the concepts developed in Schmid (1965b), taken into consideration by replacing the term $(\underline{B}^*_{\alpha,\delta} \underline{P}_l \underline{B}_{\alpha,\delta})_i$ in (7.203) with

$$(\underline{B}^*_{\alpha,\delta} \underline{P}_l \underline{B}_{\alpha,\delta} + \underline{P}_{\alpha,\delta})_i \tag{7.204}$$

Elimination of the $\mathbf{v}_{\alpha,\delta}$ vector reduces the normal equation system to

$$\overbrace{\sum_i [\underline{B}^*_0 \underline{P}_l \underline{B}_0 - \underline{B}^*_0 \underline{P}_l \underline{B}_{\alpha,\delta} (\underline{B}^*_{\alpha,\delta} \underline{P}_l \underline{B}^*_{\alpha,\delta} + \underline{P}_{\alpha,\delta})^{-1} \underline{B}_{\alpha,\delta} \underline{P}_l \underline{B}_0]_i}^{\underline{N}} \boldsymbol{\Delta}_0 + \underbrace{\sum_i^i [\underline{B}^*_0 \underline{P}_l \boldsymbol{l} - \underline{B}^*_0 \underline{P}_l \underline{B}_{\alpha,\delta} (\underline{B}^*_{\alpha,\delta} \underline{P}_l \underline{B}_{\alpha,\delta} + \underline{P}_{\alpha,\delta})^{-1} \underline{B}^*_{\alpha,\delta} \underline{P}_l \boldsymbol{l}]_i}_{-\Delta l} = 0 \tag{7.205}$$

From (7.205), finally, the vector $\boldsymbol{\Delta}_0$ of parameter corrections is obtained as

$$\boldsymbol{\Delta}\ (7.206)_0 = \underline{N}^{-1}\, \Delta \boldsymbol{l}$$

and

$$\underline{0} = \underline{0}_0 + \boldsymbol{\Delta}_0 \tag{7.207}$$

In consequence of the fact that in linearizing the original functions F and G, terms of the second and higher order were neglected, the result of an adjustment must be iterated until the change in $\mathbf{v}^* \underline{P} \mathbf{v}$ in successive iterations becomes equal to or less than a prescribed tolerance.

The treatment of given right ascension and declination values in the above manner allows the determination of unknown stellar coordinates by simply introducing the $\underline{P}_{\alpha,\delta}$ matrix as a null matrix. It is, of course, necessary to find in this case adequate approximation values (α_0, δ_0) to replace the normally given α, δ values.

Although the determination of unknown stellar coordinates is merely incidental to the problem at hand, it should be stated here that the use of uncataloged stars contributes to the calibration of the camera whenever the uncataloged star is photographed at sufficiently large intervals of time, but at least twice. By means of the associated instants of time the corresponding angle of the Earth's rotation can be introduced into the adjustment to help fix the geometry. Thus, the images of such stars furnish additional data and contribute in a small way to the determination of the parameters of interior orientation. In satellite triangulation it is scarcely possible to gain any advantage from this, because the total period of observation of an event, i.e., the elapsed interval between the

pre- and post-satellite pass star recordings, is deliberately held to a minimum in order to minimize the chance of changes in environmental conditions. Experience has shown that elimination of these changes is not always possible, especially when the requirements for accuracy are high.

For that reason an observation technique was developed, designed to detect small variations in camera orientation occurring during the normal 20– to 30–min period of observation. The method provides for stellar observations during the actual period of transit of the satellite, as well as before and after. Since it is reasonable to assume (actually there is no other choice) that the elements of interior orientation do not vary significantly within the period of observation, a mathematically closer simulation of the actual situation is obtained by computing three separate and independent exterior orientations, one for each of the three periods—before, after, and during the transit of the satellite across the field of view of the camera. The single camera observation equations (7.187) are therefore augmented to include three sets of corrections to the exterior orientation $\Delta\alpha$, $\Delta\omega$, $\Delta\kappa$, instead of just one subset. The first term in (7.205), schematically represented, will then have the form shown in figure 7.36.

In order to increase the internal accuracy of the photogrammetric measuring process,

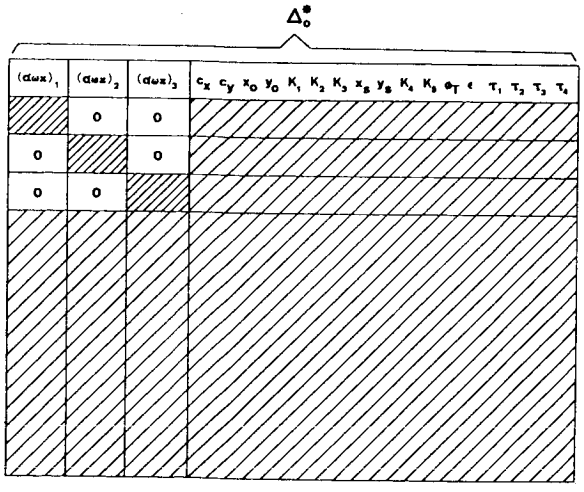

FIGURE 7.36

particularly to minimize the influence of the emulsion and shimmer, it is the practice to measure, for each star, sequences of generally five consecutive single images. This means that each of these l_x, l_y coordinate measurements has its individual residuals, but only one pair of corrections to the right ascension and declination values of the star may be postulated. Hence, for a star recorded n times it is necessary first to construct the partial normal equations system (7.203) as the sum of the corresponding n subsystems, followed by the addition, in accordance with (7.204), of $\underline{P}_{\alpha,\delta}$ just once before continuing the computations with the elimination of the v_α and v_δ to set up the final normal equations (7.205). If $\Delta\tau$ corrections are to be computed, it is advisable to first carry out a solution without the $\Delta\tau$ to avoid the unfavorable influence of existing correlations on the numerical adjustment. In a final iteration step the $\Delta\tau$ will then be included as additional unknowns to produce the end result. If measurements of unknown stars are included in the system, it is best not to set up coefficients for refraction corrections in the relevant observation equations, because of the limited geometrical content of such equations.

For example, whenever values for certain photogrammetric parameters, as determined from an independently executed camera calibration e, are to be introduced together with their measures of accuracy into the adjustment, the corresponding weight matrix $\underline{P}_{0_e}$ (cf. eq. 7.196).

$$\underline{P}_{0_e}=\frac{m_0^2}{s_{0e}^2}\underline{N}_{0_e} \qquad (7.208)$$

must be added to the normal equations system (7.205). It must be borne in mind that this $\underline{P}_{0_e}$ matrix has reference to the given values which are appropriately used as approximation values in the first iteration. Since in the course of the iteration, however, the approximation for the 0_0 vector undergoes changes, a modification of the vector of absolute terms in the normal equations system is necessary at each iteration step, in that a vector

$$\underline{P}_{0_c}\Delta l_{0_c} \tag{7.209}$$

is added to the Δl vector for that iteration, where

$$\Delta l_{0_c} = \underline{0}_{0_c} - \underline{0}_c \tag{7.210}$$

The purpose and effect of this operation is to initialize the $\underline{0}_c$ components of the $\underline{0}_0$ vector to their given values before proceeding with the next iteration step. For parameters that are not given, the Δl_{0_c} vector has zero components.

It can be argued that the determination of three different sets of orientation parameters does not lead to an optimum solution in cases where the exterior orientation of the camera does not change at all during the entire observation, so that only one or two sets of α, ω, κ are justified. For this reason, we first compute directions in space for a number of fictitious images along the plate diagonal, using the results of the present solution. For each of the fictitious point images whose coordinates x,y are assumed free of error, three unit vectors corresponding to the three orientations are computed by use of (7.81) in the y' system:

$$\mathbf{y}'_{j=1,2,3} = \underline{R}'_{y_{j=1,2,3}}(\alpha,\omega,\kappa)\frac{\mathbf{p}}{|\mathbf{p}|} \tag{7.211}$$

where

$$\mathbf{p} = \begin{bmatrix} \overline{x} \\ \overline{y} \\ c \end{bmatrix} \frac{c_x}{c_y} \tag{7.212}$$

$$|\mathbf{p}| = \left[\overline{x}^2 + \left(\overline{y}\frac{c_x}{c_x}\right)^2 + c_x^2\right]^{1/2} \tag{7.213}$$

Premultiplication of the $\mathbf{y}'_{j=1,2,3}$ vectors with $\underline{R}(270^\circ+\phi')$ yields, in accordance with (7.107), the corresponding $\mathbf{x}'_{j=1,2,3}$ vectors. With $\mathbf{y}'$ or $\mathbf{x}'$ vectors, as the case may be, one computes with (7.28) the corresponding ξ and η values, and with (7.29) the azimuths and zenith distances or hour angles and declinations.

Next, one computes for each pair from the $\mathbf{y}'_{j=1,2,3}$ or $\mathbf{x}'_{j=1,2,3}$ the small angle ϵ_{jk} between the computed directions. For the combination 1, 2 in an x' system, one obtains, for example,

$$\epsilon_{1,2} = |\mathbf{x}'_2 - \mathbf{x}'_1| \tag{7.214}$$

or, in radians,

$$\epsilon_{1,2} = [(x'_{21}-x'_{11})^2 + (x'_{22}-x'_{12})^2 + (x'_{23}-x'_{13})^2]^{1/2} \tag{7.215}$$

If the differences between corresponding right ascensions and declinations or azimuths and zenith distances, so computed from the three orientations, exceed their confidence limits, a timing error or camera motion may be the cause. Before one can decide whether these computed differences in direction are significant, one must find the mean errors either of the direction components (α, δ) and (A, z), or at least of the angles ϵ_{jk}, which can be looked upon as combinations in pairs of the computed (α, δ) or (A, z).

Since α and δ are parameters of the mathematical model on which the adjustment is based, the following solution offers itself. Using (7.204) and taking into account the considerations leading to (7.202) and (7.203), we can schematically represent the first term of the normal equations system (7.201) as

$$\begin{bmatrix} (\underline{B}^*_{\alpha,\delta}\underline{P}_l\underline{B}_{\alpha,\delta}+\underline{P}_{\alpha,\delta})_1 & \underline{0} & \underline{0} & (\underline{B}^*_{\alpha,\delta}\underline{P}_l\underline{B}_0)_1 \\ \underline{0} & \ddots & \underline{0} & \vdots \\ \underline{0} & \underline{0} & (\underline{B}^*_{\alpha,\delta}\underline{P}_l\underline{B}_{\alpha,\delta}+\underline{P}_{\alpha,\delta})_m & (\underline{B}^*_{\alpha,\delta}\underline{P}_l\underline{B}_0)_m \\ (\underline{B}^*_0\underline{P}_l\underline{B}_{\alpha,\delta})_1 & \cdots & (\underline{B}^*_0\underline{P}_l\underline{B}_{\alpha,\delta})_m & \sum_{i=1}^{i=m}(\underline{B}^*_0\underline{P}_l\underline{B}_0)_i \end{bmatrix} \equiv \begin{bmatrix} \underline{A}_{11} & \underline{A}_{12} \\ \underline{A}^*_{12} & \underline{A}_{22} \end{bmatrix} \tag{7.216}$$

Designate the inverse of the matrix (7.216) as

$$\begin{bmatrix} \underline{A}_{11} & \underline{A}_{12} \\ \underline{A}_{12}^{*} & \underline{A}_{22} \end{bmatrix}^{-1} = \begin{bmatrix} \underline{Q}_{11} & \underline{Q}_{12} \\ \underline{Q}_{12}^{*} & \underline{Q}_{22} \end{bmatrix} \quad (7.217)$$

From (7.216) and (7.217) it is apparent that for the inverted normal equations system of (7.206)

$$[\underline{A}_{22} - \underline{A}_{12}^{*} \underline{A}_{11}^{-1} \underline{A}_{12}]^{-1} = \underline{N}^{-1} = \underline{Q}_{22} \quad (7.218)$$

Furthermore, since

$$\begin{bmatrix} \underline{A}_{11} & \underline{A}_{12} \\ \underline{A}_{12}^{*} & \underline{A}_{22} \end{bmatrix} \begin{bmatrix} \underline{Q}_{11} & \underline{Q}_{12} \\ \underline{Q}_{12}^{*} & \underline{Q}_{22} \end{bmatrix} = E \quad (7.219)$$

it follows from (7.217) that

$$\underline{Q}_{11} = \underline{A}_{11}^{-1} + \underline{A}_{11}^{-1} \underline{A}_{12} \underline{N}^{-1} \underline{A}_{12}^{*} \underline{A}_{11}^{-1} \quad (7.220)$$

From the schematic shown in (7.216) it follows that the computation indicated with (7.220) can be performed in independent steps for each individual pair i of values α, δ. Hence we can write

$$\begin{aligned} \mathbf{s}^2_{(\alpha,\delta)i} = s_0^2 [& (\underline{B}^{*}_{\alpha,\delta} \underline{P}_l \underline{B}_{\alpha,\delta} + \underline{P}_{\alpha,\delta})_i^{-1} \\ & + (\underline{B}^{*}_{\alpha,\delta} \underline{P}_l \underline{B}_{\alpha,\delta} + \underline{P}_{\alpha,\delta})_i^{-1} (\underline{B}^{*}_{\alpha,\delta} \underline{P}_l \underline{B}_0)_i \underline{N}^{-1} \\ & (\underline{B}^{*}_{\delta} \underline{P}_l \underline{B}_{\alpha,\delta})_i (\underline{B}^{*}_{\alpha,\delta} \underline{P}_l \underline{B}_{\alpha,\delta} + \underline{P}_{\alpha,\delta})_i^{-1}] \end{aligned} \quad (7.221)$$

With (7.221) we obtain the covariance matrix for the corrected values of α, δ for the stars originally selected for the adjustment. If the star in question was originally unknown, it is merely necessary to set the relevant $\underline{P}_{\alpha,\delta}$ equal to a null matrix and to introduce the corresponding $\underline{P}_l$ matrix, which must, of course, relate to the initially chosen m_0 value. In the present case a further simplification is present, since the $\underline{B}_{\alpha,\delta}$ matrix is quadratic and nonsingular, hence invertible. The covariance matrix for an originally unknown star is, therefore, from (7.221)

$$\mathbf{s}_{\alpha,\delta} = s_0 (\underline{B}^{-1}_{\alpha,\delta} \underline{P}_l^{-1} \underline{B}^{-1^{*}}_{\alpha,\delta} + \underline{B}^{-1}_{\alpha,\delta} \underline{B}_0 \underline{N}^{-1} \underline{B}_0^{*} \underline{B}^{-1^{*}}_{\alpha,\delta}) \quad (7.222)$$

Finally, to compute the accuracy of a direction defined by a fictitious, errorless point, the $\underline{P}^{-1}$ matrix in (7.222) becomes a null matrix, resulting in

$$\mathbf{s}^2_{\alpha,\delta} = s_0^2 (\underline{B}^{-1}_{\alpha,\delta} \underline{B}_0 \underline{N}^{-1} \underline{B}_0^{*} \underline{B}^{-1^{*}}_{\alpha,\delta}) \quad (7.223)$$

Formula (7.223) is now applied for a selected fictitious point to the three orientations obtained from the solution of the system (7.205). The resulting covariance matrix $\mathbf{s}_{\alpha,\delta}$ is of the dimension 6×6. The three 2×2 submatrices along the diagonal are the three covariances $\mathbf{s}^2(\alpha,\delta)_{j=1,2,3}$ associated with the three sets of α, δ. The analogous covariance matrices of the azimuth and elevation components are obtained with (7.107) as

$$\begin{aligned} \mathbf{s}^2(\underline{A},z)_{j=1,2,3} = & \underline{R}\left(90^\circ - \frac{\phi}{2}\right) \mathbf{s}^2(\alpha,\delta)_{j=1,2,3} \\ & \times \underline{R}^{*}\left(90^\circ - \frac{\phi}{2}\right) \end{aligned} \quad (7.224)$$

Finally, the variances s_{21}^2, s_{32}^2, s_{31}^2 of the three ϵ angles of (7.215) are the diagonal terms of the covariance matrix

$$\mathbf{s}_\epsilon^2 = \underline{F}^{*} \mathbf{s}^2_{\alpha,\delta} \underline{F} \quad (7.225)$$

where

$$\mathbf{F} = \begin{bmatrix} \frac{\partial \epsilon}{\partial \alpha_1} & 0 & \frac{\partial \epsilon}{\partial \alpha_1} \\ \frac{\partial \epsilon}{\partial \delta_1} & 0 & \frac{\partial \epsilon}{\partial \delta_1} \\ \frac{\partial \epsilon}{\partial \alpha_2} & \frac{\partial \epsilon}{\partial \alpha_2} & 0 \\ \frac{\partial \epsilon}{\partial \delta_2} & \frac{\partial \epsilon}{\partial \delta_2} & 0 \\ 0 & \frac{\partial \epsilon}{\partial \alpha_3} & \frac{\partial \epsilon}{\partial \alpha_3} \\ 0 & \frac{\partial \epsilon}{\partial \delta_3} & \frac{\partial \epsilon}{\partial \delta_3} \end{bmatrix} \quad (7.226)$$

In (7.226) for each combination j, k

$$\begin{bmatrix} \frac{\partial \epsilon}{\partial \alpha_j} \\ \frac{\partial \epsilon}{\partial \delta_j} \\ \frac{\partial \epsilon}{\partial \alpha_k} \\ \frac{\partial \epsilon}{\partial \delta_k} \end{bmatrix} = \frac{1}{\epsilon_{jk}} \begin{bmatrix} x'_{j_1}x'_{k_2} - x'_{j_2}x'_{k_2} \\ x'_{j_1}x'_{k_1}x'_{k_3}(1-x'^{2}_{k_3})^{-1/2} + x'_{j_2}x'_{k_2}x'_{k_3}(1-x'^{2}_{k_3})^{-1/2} - x'_{j_3}(1-x'^{2}_{k_3})^{1/2} \\ x'_{j_2}x'_{k_1} - x'_{j_1}x'_{k_2} \\ x'_{k_1}x'_{j_1}x'_{j_3}(1-x'^{2}_{j_3})^{-1/2} + x'_{k_2}x'_{j_2}x'_{j_3}(1-x'^{2}_{j_3})^{-1/2} - x'_{k_3}(1-x'^{2}_{j_3})^{1/2} \end{bmatrix} \tag{7.227}$$

If all $|\epsilon_{1,2,3}|$ exceed the corresponding quantity $K \cdot s_{\epsilon_{1,2,3}}$ (where K is a constant selected on the basis of personal experience), then it must be assumed that the camera orientation has changed during the three observation periods. In this case the second solution indicated in the schematic of figure 7.36 will be accepted as definitive, this being the orientation corresponding to the stars recorded during the satellite transit.

On the other hand, if certain values of ϵ are less than the corresponding $K \cdot s_\epsilon$, then these orientations can be combined. Thus, if

$$\epsilon_{12} < K s_{\epsilon_{12}} \tag{7.228a}$$

combine orientations 1 and 2; if

$$\epsilon_{23} < k s_{\epsilon_{23}} \tag{7.228b}$$

combine orientations 2 and 3; if

$$\epsilon_{13} < k s_{\epsilon_{13}} \tag{7.228c}$$

combine orientations 1 and 3.

The result is obtained as shown in Schmid and Schmid (1965) in the form

$$\begin{aligned} \Delta_0 = &[\underline{N}^{-1} - \underline{N}^{-1}\underline{C}^* (\underline{C}\underline{N}^{-1}\underline{C}^*)^{-1}\underline{C}\underline{N}^{-1}] \\ &[\Delta \boldsymbol{l} + \underline{N}^{-1}\underline{C}^* (\underline{C}\underline{N}^{-1}\underline{C}^*)^{-1}\boldsymbol{l}] \end{aligned} \tag{7.229}$$

where $\underline{N}^{-1}$ and $\Delta \boldsymbol{l}$ are from the last iteration in the solution of the original system (7.205) and

$$\underline{C} = \begin{bmatrix} 1 & 0 & 0 & -1 & 0 & 0 & 0 & 0 & 0 \\ 0 & 1 & 0 & 0 & -1 & 0 & 0 & 0 & 0 \\ 0 & 0 & 1 & 0 & 0 & -1 & 0 & 0 & 0 \\ 0 & 0 & 0 & 1 & 0 & 0 & -1 & 0 & 0 \\ 0 & 0 & 0 & 0 & 1 & 0 & 0 & -1 & 0 \\ 0 & 0 & 0 & 0 & 0 & 1 & 0 & 0 & -1 \end{bmatrix} \bigcirc \tag{7.230}$$

where $\underline{C}$ is a 6×0 matrix (0 being the number of components of the Δ_0 vector), the first nine columns being as indicated and the balance of the matrix consisting of zero entries. The form of the 6×9 portion will vary according to the results of the criteria (7.228). The form in (7.230) corresponds to the case of combining all three orientations. For such a case, furthermore,

$$\boldsymbol{l} = \begin{bmatrix} \alpha_2^0 - \alpha_1^0 \\ \omega_2^0 - \omega_1^0 \\ \kappa_2^0 - \kappa_1^0 \\ \alpha_3^0 - \alpha_2^0 \\ \omega_3^0 - \omega_2^0 \\ \kappa_3^0 - \kappa_2^0 \end{bmatrix} \tag{7.231}$$

The values with the superscript 0 are the approximation values used in the final iteration in the solution of the system shown in figure 7.36. The correction vector computed with (7.229) pertains to these approximations. The final result is then computed with (7.229) and (7.207).

The last phase of the computations covers the partial results, and a summary of these results now follows. Values for distortion at a prescribed interval, e.g., in 3–mm steps, are

computed to a maximal radial distance d_{max} dictated by the plate format. If the radial distortion for a prescribed distance d_0 is to be made equal to 0, the corresponding camera constant c^* is computed with

$$c^* = \frac{c_x + c_y}{2}(1 - K_0) \qquad (7.232)$$

in which

$$K_0 = -(K_1 d_0^2 + K_2 d_0^4 + K_3 d_0^6) \qquad (7.233)$$

The radial distortion is then computed successively for the required distance d with (7.95). The transformed radial distortion corresponding to c^* is

$$(\Delta R) = d \cdot K_0 + \Delta R \qquad (7.234)$$

Values for the decentering distortion are computed similarly with (7.99).

If it is desired to study the values of astronomic refraction within the range of the photogrammetric exposure, they can be computed from (7.40) as a function of z in suitable intervals, with either the given or the newly computed τ values.

Computing distortion and refraction values is of particular significance when star observations are evaluated for the calibration of photogrammetric cameras or used in error studies of individual photographs. In satellite triangulation the computation of such data recommends itself strongly for the purpose of gaining insight into the behavior of all cameras in use, in view of the fact that the photogrammetric registration in a continental, and especially in a worldwide, net is exposed to extreme ranges of local and seasonal environmental conditions. It is therefore required, on the one hand, to be informed as to the reliability and metric quality of the instrumentation used; it is also expected that a systematic study of these results will allow the drawing of conclusions with respect to the individual photograms.

Finally, we must compute the corrections to the given values resulting from the adjustment, the statistical measures of accuracy, such as the mean error of unit weight, the mean errors of the computed quantities as well as mean errors of values, computed as functions of those quantities.

Corrections to the measured images are computed with (7.189). With the parameters obtained in the adjustment one has

$$\begin{aligned} v_{l_{xi}} &= F_i \\ v_{l_{yi}} &= G_i \end{aligned} \qquad (7.235)$$

To get a better picture of the distribution of these residuals, it is useful to compute the radial and tangential components of these corrections. Computation of the corrections v_α and v_δ for each given star is carried out with (7.203) (7.204), where now Δ_0 is a zero vector:

$$\mathbf{v}_{(\alpha,\delta)_i} = -(\underline{B}^*_{\alpha,\delta}\underline{P}_l\underline{B}_{\alpha,\delta} + \underline{P}_{\alpha,\delta})^{-1}_i (\underline{B}^*_{\alpha,\delta}\underline{P}_l\boldsymbol{l})_i \qquad (7.236)$$

Wherever quantities introduced by means of approximations into the adjustment differ from free variables, in that corresponding entries in the $\underline{P}_u$ matrix (7.190) (cf. also eq. (7.208)) represent a priori given weights, relevant corrections are computed, by using the results from the adjustment, from

$$v_u = u - u_0 \qquad (7.237)$$

where u stands for the adjusted and u_0 for the initial value of the parameter. Next one computes

$$\Sigma\mathbf{v}^*\underline{P}_l\mathbf{v}_l + \Sigma\mathbf{v}^*_{\alpha,\delta}\underline{P}_{\alpha,\delta}\mathbf{v}_{\alpha,\delta} + \Sigma\mathbf{v}^*_u\underline{P}_u\mathbf{v}_u = \Sigma\mathbf{v}^*\underline{P}\mathbf{v} \qquad (7.238)$$

and in accordance with (7.193) the mean error of unit weight after adjustment s_0 with

$$s_0 = \left[\frac{\Sigma\mathbf{v}^*\underline{P}\mathbf{v}}{n-u}\right]^{1/2} \qquad (7.239)$$

The mean error of the computed parameters is obtained by multiplying s_0 by the square root of the corresponding diagonal term in N^{-1} of (7.206). The mean errors of the given quantities result from dividing s_0

by the square root of the weight assigned to the quantities.

The mean error of the camera constant (7.232) and the mean error of radial and decentering distortion are computed as mean errors of functions of quantities determined in the adjustment. In general, the mean error s_u of a quantity a

$$a=F(u) \tag{7.240}$$

is

$$s_a=s_0(\mathbf{f}_a^*\underline{N}^{-1}\mathbf{f}_a)^{1/2} \tag{7.241}$$

in which $\mathbf{f}_a$ is the vector whose components are the partial derivatives $\partial F(u)/\partial u$, the components corresponding to parameters not present in (7.240) being zero. For the cases in question here,

Substituted in (7.241), the components computed with (7.242) now give the mean error of the camera constant c^*, with (7.243), of the radial distortion at the selected distances d, with (7.244), of the radial distortions corresponding to camera constants c^*, with (7.245), of the decentering distortion, and, with (7.246), of astronomic refraction as function of selected zenith distances.

This concludes the computations in connection with the reduction of the single camera.

In preparation for the next series of computations the orientation matrix $\underline{R}'_y(\alpha,\omega,\kappa)$† during the satellite pass must first be transformed from the local y' system into the final z or z' system that has been selected for the eventual spatial triangulation. $\underline{R}'_y(\alpha,\omega,\kappa)$† results from (7.79), either with the second group of elements of orientation in the

$$\mathbf{f}_{c^*}^*=\begin{array}{|c|c|c|c|c|}\hline \multicolumn{5}{|c|}{\partial/}\\ \hline \partial c_x & \partial c_y & \partial K_1 & \partial K_2 & \partial K_3\\ \hline \frac{1-K_0}{2} & \frac{1-K_0}{2} & -\frac{c_x+c_y}{2}\cdot d_0^2 & -\frac{c_x+c_y}{2}\cdot d_0^4 & -\frac{c_x+c_y}{2}\cdot d_0^6\\ \hline\end{array} \tag{7.242}$$

$$\mathbf{f}_{\Delta R}^*=\begin{array}{|c|c|c|}\hline \multicolumn{3}{|c|}{\partial/}\\ \hline \partial K_1 & \partial K_2 & \partial K_3\\ \hline d^3 & d^5 & d^7\\ \hline\end{array} \tag{7.243}$$

$$\mathbf{f}_{(\Delta R)}^*=\begin{array}{|c|c|c|}\hline \multicolumn{3}{|c|}{\partial/}\\ \hline \partial K_1 & \partial K_2 & \partial K_3\\ \hline d(d^2-d_0^2) & d(d^4-d_0^4) & d(d^6-d_0^6)\\ \hline\end{array} \tag{7.244}$$

$$\mathbf{f}_{\Delta T}^*=\begin{array}{|c|c|}\hline \multicolumn{2}{|c|}{\partial/}\\ \hline \partial K_4 & \partial K_5\\ \hline d^2 & d^4\\ \hline\end{array} \tag{7.245}$$

$$\mathbf{f}_{\tau}^*=\begin{array}{|c|c|c|c|}\hline \multicolumn{4}{|c|}{\partial/}\\ \hline \partial\tau_1 & \partial\tau_2 & \partial\tau_3 & \partial\tau_4\\ \hline \underline{T}^{1/2}W\tan\frac{\beta}{2} & \underline{T}^{1/2}W\tan^3\frac{\beta}{2} & \underline{T}^{1/2}W\tan^5\frac{\beta}{2} & \underline{T}^{1/2}W\tan^7\frac{\beta}{2}\\ \hline\end{array} \tag{7.246}$$

schematic of figure 7.36, or, in accordance with the principle of combination of (7.228), from a group of orientation elements, which also includes star recordings simultaneous with the satellite transit.

The necessary transformation is accomplished with (7.30) and (7.108) or (7.109), so that we have

$$\underset{3}{\underline{R}}'_z(\alpha,\omega,\kappa) = \underset{3}{\underline{R}}(\lambda_{east}), \underset{2}{\underline{R}}(90^\circ-\phi)\underset{2}{\underline{R}}(-x,-y)\underset{1}{\underline{R}}(270^\circ+\phi)\underset{2}{\underline{R}}(-\lambda_{east})\underset{3}{\underline{R}}'_y(\alpha,\omega,\kappa) \qquad (7.247)$$

and with (7.79), for example,

$$\left.\begin{aligned}\cos\alpha_{z'} &= r_{33}/\cos\omega_{z'}\\ \sin\omega_{z'} &= -r_{23}\\ \cos\kappa_{z'} &= r_{22}/\cos\omega_{z'}\end{aligned}\right\} \qquad (7.248)$$

The reduction just described, of a single observation of stars, is on the one hand suitable for a camera calibration, and on the other represents one of the intermediate steps in the process of photogrammetric satellite triangulation.

We now list the intermediate results from the single camera program that will be needed in the next reduction step.

(1) The parameters set up to reconstruct the photogrammetric bundle and computed in the adjustment, namely, (a) the elements of exterior orientation $(\alpha\omega\kappa)_{y'}$ referring to the local y' system and (b) in the general case, the parameters ϵ, c_x, c_y, x_0, y_0, x_s, y_s, K_1, K_2, K_3, K_4, K_5, ϕ_T, τ_1, τ_2, τ_3, τ_4.

(2) The elements of exterior orientation referred to the ultimate triangulation coordinate system, i.e., either $(\alpha\omega\kappa)_z$ or $(\alpha\omega\kappa)_{z'}$.

(3) The mean error of unit weight s_0.

(4) The inverted normal equations system N^{-1}.

(5) Meteorological data at the observation site during the satellite observations.

(6) All data necessary for the identification of observation sites and instrumentation.

(7) All supplementary information needed for time determination of the satellite images.

7.4.7 Spatial Triangulation

7.4.7.1 Preliminary Computations

The principle problem of geometric satellite triangulation is the determination of three-dimensional rectangular coordinates for the observation sites, the triangulation being executed in either the z or the z' coordinate system introduced in section 7.4.6.2.6. In preparation for these computations the treatment of the single camera (as described at the end of section 7.4.6.4) includes, among other things, the transformation of the elements of exterior orientation to $(\alpha\omega\kappa)_z$ or $(\alpha\omega\kappa)_{z'}$†. Now, in order to triangulate, it is necessary to determine, at each of the stations which have recorded simultaneously a specific satellite pass, at least one direction associated with a specific satellite location in space. Just as the elements of exterior orientation of all photograms must refer to a consistent coordinate system, all the directions obtained with such an orientation must be with respect to unambiguously defined target points in space. This requirement is filled by reducing all measured image coordinates to a rigorous central perspective and then applying all the corrections explained in section 7.4.5.

Reduction of the plate coordinates l_x, l_y to a central perspective is accomplished with (7.141) and (7.142). The expressions for ΔR_x, ΔR_y, ΔT_x, ΔT_y are computed from (7.97), (7.98), and (7.103) with the use of (7.143) through (7.147) and with an iteration loop, as was indicated earlier. The coordinates $l_{\bar{x}}$ and $l_{\bar{y}}$ so obtained correspond in measuring to (7.138) and (7.139) and must still be reduced to a common scale factor. If in (7.138) we set $c_{\bar{x}}=c$, we obtain, in agreement with (7.212),

$$l_{x_c} = l_{\bar{x}} \qquad (7.249)$$

and

$$l_{\bar{y}_c} = l_{\bar{y}} \cdot \frac{c_x}{c_y} \qquad (7.250)$$

The image coordinates $l_{\bar{x}_c}$, $l_{\bar{y}}$ refer to the principal point and the scale factor c, i.e., to the idealized central perspective. Before these fictitious point images can be used in a spatial triangulation, they must be corrected for the influences cited in section 7.4.5. These corrections can be classified under the following groupings: (1) refraction, subdivided into astronomic and parallactic refraction; (2) eccentricity of the target; and (3) time corrections, subdivided into clock corrections and light propagation effects.

In the course of the reduction the influence of scintillation is largely eliminated, at the appropriate place, by smoothing the sequence of individual images of the satellite trail with the aid of polynomials.

The computation of some of these corrections requires an approximation to the distance between the camera site and the satellite. To effect these corrections, the coordinates $l_{\bar{x}_k}$, $l_{\bar{y}_k}$ (equations 7.249 and 7.250) and the $\underline{R}'_{\mathbf{y}}(\alpha,\omega,\kappa)$ † matrix from the single camera are used to produce the unit vector $\mathbf{y}_r'$ from (7.81) and the corresponding standard coordinates ξ_r, η_r with (7.23), and then the observed zenith distance z_r with (7.29). The astronomic refraction r_x follows from (7.40) by iteration. The unit vector $\mathbf{y}'$ corrected for astronomic refraction is computed with (7.42), where r_s is replaced with r_x or, alternatively, directly with

$$z = z_r + r_x \tag{7.251}$$

and (7.74), in the form

$$\mathbf{y}' = \begin{bmatrix} \cos z & \cos A \\ \cos z & \sin A \\ \sin z & \end{bmatrix} \tag{7.252}$$

In this, the azimuth A is derived from (7.29). With $\mathbf{y}'$, new values for ξ and η are derived from (7.28). With these and by using $c = c_x$, we compute image coordinates from (7.85) and (7.86), taking the direction cosines r_{jj} from $R_{y'}(\alpha,\omega,\kappa)$ and substituting, ξ, η, 1 for $x - x_0$, $y - y_0$, and $z - z_0$, respectively. After all satellite images of a given photogram have been so reduced, the coefficients for polynomials (7.48) are determined from an adjustment in accordance with (7.266) to (7.270). With these polynomials the $l_{\bar{x}_c}$ and $l_{\bar{y}_c}$ are expressed as functions of station clock time t. Omitting the subscript c, we have then, quite generally,

$$l_{\bar{x}} = f(t) \tag{7.253}$$

$$l_{\bar{y}} = g(t) \tag{7.254}$$

With the notation of figure 7.26 we obtain observation times referred to an unambiguous time designation by adding to each locally recorded time t the corresponding clock correction ΔT, which rarely exceeds 10 msec. The normalized instants of time $T_{j_{1,2,\ldots,m}}$ recorded at stations $j_{1,2,\ldots,m}$ will then be

$$T_{j_{1,2,\ldots,m}} = t_{j_{1,2,\ldots,m}} + \Delta T_{j_{1,2,\ldots,m}} \tag{7.255}$$

In order to obtain an instant of time that is as close as possible to the range of times recorded at each station, we form the arithmetic mean of the T's and convert this mean to corresponding interpolated times referred to the individual station clocks. Thus

$$t_{j_{1,2,\ldots,m}} = \frac{\Sigma T_{j_{1,2,\ldots,m}}}{m} - \Delta T_{j_{1,2,\ldots,m}} \tag{7.256}$$

On the basis of the relevant t value at each station, $l_{\bar{x}}$, $l_{\bar{y}}$ values are computed with (7.253), (7.254) for points along the satellite trail, which, since light propagation time has as yet been neglected, refer to simultaneous instants of exposure.

Next, approximate satellite positions are computed with these data. The camera-site coordinate approximations (ϕ^0, λ^0, h^0) are, with (7.111), (7.112), (7.113), transformed to rectangular coordinates in the z system, or, if necessary, by the additional transformation (7.36) are transferred to the z' system. With the $\underline{R}_x(\alpha,\omega,\kappa)$ or $\underline{R}_{z'}(\alpha,\omega,\kappa)$ orientation matrices mentioned previously and the interpolated $l_{\bar{x}}$, $l_{\bar{y}}$ coordinates, once these values are available for all stations, approxi-

mate satellite positions can be computed by using for an intersection with m rays

$$\begin{bmatrix} m & 0 & [a_x] \\ 0 & m & [a_y] \\ [a_x] & [a_y] & [a_xa_x+a_ya_y] \end{bmatrix} \begin{bmatrix} z_{s_1} \\ z_{s_2} \\ z_{s_3} \end{bmatrix} \begin{bmatrix} +[b_x] \\ +[b_y] \\ +[a_xb_x+a_yb_y] \end{bmatrix} = 0 \quad (7.257)$$

The $z_{s_{1,2,\ldots,m}}$ are the approximated coordinates of a point on the satellite orbit. As an auxiliary computation, one forms with (7.79)

$$a_x = -\frac{(r_{11}l_{\bar{x}}) + (r_{21}l_{\bar{y}}) + (r_{31}c)}{(r_{13}l_{\bar{x}}) + (r_{23}l_{\bar{y}}) + (r_{33}c)} \quad (7.258)$$

$$a_y = -\frac{(r_{12}l_{\bar{x}}) + (r_{22}l_{\bar{y}}) + (r_{32}c)}{(r_{13}l_{\bar{x}}) + (r_{23}l_{\bar{y}}) + (r_{33}c)} \quad (7.259)$$

$$b_x = -(a_xz_3^0 + z_1^0) \quad (7.260)$$

$$b_y = -(a_yz_3^0 + z_2^0) \quad (7.261)$$

where $z_{1,2,3}^0$ are approximated rectangular station coordinates.

The distances between an observation station and the satellite positions are

$$d = [(z_{s_1}^0 - z_1^0)^2 + (z_{s_2}^0 - z_2^0)^2 + (z_{s_3}^0 - z_3^0)^2]^{1/2} \quad (7.262)$$

Instead of storing the large number of distances corresponding to the 500 to 600 satellite positions, it is preferable to express d as a function of t. As with the functions (7.253), (7.254), we again use (7.58), with, of course, just one expansion for the d. This results in one polynomial for each station or, expressed generally,

$$d = h(t) \quad (7.263)$$

We now resume the reduction of the results obtained with (7.249) and (7.250), computing first the satellite refraction r_s with (7.43) and using (7.263) along with the previously computed astronomic refraction r_∞. Then follows the unit vector $\mathbf{y}'$ corrected for refraction, from the refracted vector $\mathbf{y}_r'$ by use of (7.42) or (7.252), where now

$$z = z_r + r_s \quad (7.264)$$

Reduction of the $\mathbf{y}'$ vector is continued with the elimination of the influence of eccentricity of the target point.

After the unit vector $\mathbf{y}_\odot'$ in the direction toward the Sun has been computed, in accordance with (7.54) and the Sun's right ascension and declination at the instant of observation and with the use of (7.20), (7.21), (7.23), and (7.24), one obtains the unit vector $\mathbf{y}_{BM}'$ to the center of the balloon with (7.52) and (7.49) in the form

$$\mathbf{y}_{BM}' = \mathbf{y}' - \frac{a}{d \sin \gamma}(\mathbf{y}_\odot' + \cos \gamma \, \mathbf{y}') \quad (7.265)$$

in which the needed quantities are derived from (7.263), (7.50) or (7.51), and (7.46).

With the vector (7.265), corresponding ξ, η values are again computed with (7.28), as are $l_{\bar{x}}$, $l_{\bar{y}}$ coordinates of the corresponding fictitious satellite images with the use of $\underline{R}_{y'}(\alpha,\omega,\kappa)$ matrix. With these values in (7.58) the final interpolation polynomials are set up, which, in complete analogy with the expressions (7.253) and (7.254), represent $l_{\bar{x}}$ and $l_{\bar{y}}$ as functions of t (see also sec. 7.4.8.1). Normal equations corresponding to (7.58) are set up in order to determine the polynomial coefficients, where, to simplify the numerical calculations, the t values, assumed free of error, are replaced with a sequence of integers whose increment corresponds to the greatest common divisor of the interval recorded at the various stations involved. The normal equations system for n images has the form

$$\overbrace{\sum_{i=1}^{n} [\underline{B}_l^* \underline{P}_l \underline{B}_l]_i}^{\underline{N}_c} \mathbf{c} = \overbrace{\sum_{i=1}^{n} [\underline{B}_l^* \underline{P}_l \boldsymbol{l}]_i}^{l_c} \quad (7.266)$$

in which $\underline{P}_l$ is expressed with sufficient accuracy in terms of the weight matrix assigned to the original coordinate measurements (cf. eq. 7.192). For an m^{th}-degree polynomial $\underline{B}_l$ is, from (7.58), for each of the n points

$$\underline{B}_{\bar{l}_i}=\left[\begin{array}{cccccccc|cccccccc} \cdot & \cdot & \cdot & \cdot & \cdot & \cdot & \cdot & \cdot & \cdot & \cdot & \cdot & \cdot & \cdot & \cdot & \cdot & \cdot \\ 1 & t_i & t_i^2 & t_i^3 & \cdot & \cdot & \cdot & t_i^m & & & & 0 & & & & \\ \cdot & \cdot & \cdot & \cdot & \cdot & \cdot & \cdot & \cdot & \cdot & \cdot & \cdot & \cdot & \cdot & \cdot & \cdot & \cdot \\ \hline \cdot & \cdot & \cdot & \cdot & \cdot & \cdot & \cdot & \cdot & \cdot & \cdot & \cdot & \cdot & \cdot & \cdot & \cdot & \cdot \\ & & & & 0 & & & & 1 & t_i & t_i^2 & t_i^3 & \cdot & \cdot & \cdot & t_i^m \\ \cdot & \cdot & \cdot & \cdot & \cdot & \cdot & \cdot & \cdot & \cdot & \cdot & \cdot & \cdot & \cdot & \cdot & \cdot & \cdot \end{array}\right] \tag{7.267}$$

$\mathbf{c}$ is the vector of coefficients to be determined

$$\mathbf{c}^*=[a_0a_1a_2a_3\ldots a_mb_0b_1b_2b_3\ldots b_m] \tag{7.268}$$

and $\bar{\mathbf{l}}_i$ is the vector with components $(l_{\bar{x}}, l_{\bar{y}})$, which was obtained with the $\mathbf{y}'_{BM}$ vector of (7.265)

$$\bar{\mathbf{l}}_i=\left[\begin{array}{c} l_{\bar{x}} \\ l_{\bar{y}} \end{array}\right]_i \tag{7.269}$$

The solution for the vector of coefficients $\mathbf{c}$ follows from (7.266),

$$\mathbf{c}=\underline{N}_c^{-1}\mathbf{l}_c \tag{7.270}$$

and the covariance matrix associated with the coefficients c_m is, from (7.195),

$$\mathbf{s}_c^2=s_{0_c}^2\underline{N}^{-1} \tag{7.271}$$

The mean error s_{0_c} for the fit to the satellite trail is, from (7.193),

$$s_{0_c}=\left[\frac{\sum_{i=1}^{n}(\mathbf{v}^*\underline{P}_l\mathbf{v})_i}{2n-(2m+2)}\right]^{1/2} \tag{7.272}$$

The individual v values are computed with (7.58) and, with the designations used in (7.253) and (7.254), are

$$\mathbf{v}_i=\left[\begin{array}{c} v_{l\bar{x}} \\ v_{l\bar{y}} \end{array}\right]=\left[\begin{array}{c} f(t)-l_{\bar{x}} \\ g(t)-l_{\bar{y}} \end{array}\right]_i \tag{7.273}$$

If pairs of coordinates $l_{\bar{x}}$ and $l_{\bar{y}}$ for n points are determined by interpolation in (7.58), the corresponding covariance matrix is, in accordance with (7.240), (7.241), (7.272), and with the use of the designations introduced with (7.267),

$$(\mathbf{s}_{\bar{l}_c})^2=s_{0c}^2[\underline{B}_{\bar{l}}\underline{N}_c^{-1}(\underline{B}_{\bar{l}}^*)] \tag{7.274}$$

In order to account for all existing correlations, the $\underline{B}_{\bar{l}}$ matrix must be set up for all n points and is therefore of dimension $2n \times (2m+2)$.

Interpolation for coordinates of fictitious satellite images by means of the computed polynomials is executed, in agreement with figure 7.26, by forming interpolation times t corresponding to a selected sequence of orbital times T with

$$t=T-\Delta T+\tau_{(T-\Delta T)} \tag{7.275}$$

The $\tau_{T-\Delta T}$ are computed with (7.56). The necessary distances d are computed with sufficient accuracy for the times $T-\Delta T$ from the polynomial (7.263). Finally, the fictitious image coordinates are computed by substituting the interpolated instants t in (7.58), whose coefficients have been determined from the solution of (7.270). After the pairs of coordinates for the selected orbital times T have been computed, the last reduction is made, to remove the effect of Earth rotation that took place during the light travel time. As before, a new unit vector $\mathbf{y}'$ must be computed from the coordinate pairs $l_{\bar{x}}$, $l_{\bar{y}}$ just obtained, using (7.81) and $\underline{R}_{y'}(\alpha,\omega,\kappa)$ †. Then, with (7.60) and the $\tau_{T-\Delta T}$ values from (7.56), every $\mathbf{y}'$ vector is transformed into its corresponding $\mathbf{y}_{s'}$ vector. The final image coordinates $l_{\bar{x}}$, $l_{\bar{y}}$ result from (7.60) and the use of (7.85) and (7.86), where, as before, the direction cosines r_{ij} are taken from $\underline{R}_{y'}(\alpha,\omega,\kappa)$ † and ξ replaces $X-X_0$, η replaces $Y-Y_0$, and the number 1 replaces $Z-Z_0$. The quantities ξ and η are again derived from $\mathbf{y}_{s'}$ by the application of (7.28).

For discussion of the needed number of directions so introduced, see section 7.4.8.1. In any case, the selection of orbital times T should be such that one of these instants corresponds to a point of the orbit whose image on the several photograms is as close as possible to the principal pont.

After these preliminary computations have been completed, a pair of image coordinates, representing fictitious observations, will be available for each selected point of the orbit. These image coordinates simulate images that would have been obtained had the following conditions been met:

(1) The photogrammetric camera reproduces a rigorous central perspective.

(2) The comparator has no linear scale errors and measures in two perpendicular directions.

(3) The origin of the image coordinate system coincides with the principal point.

(4) The observation was executed in vacuo, i.e., refraction and scintillation do not exist.

(5) The images correspond to the center of the balloon.

(6) Neither Earth nor satellite has a proper motion; i.e., there is no influence from aberration or time of light propagation.

(7) All station clocks run without error with respect to a reference time, and the recording times of the stars are rigorously UT1.

(8) The images at all stations observing a specific satellite pass correspond to uniquely defined positions on the satellite orbital curve.

After processing all observational data in the manner described, we have at our disposal for the execution of the spatial triangulation for each of the observing stations and for all satellite passes observed at such stations a photogram with a number of fictitious image point coordinates $l_{\bar{x}}$, $l_{\bar{y}}$, the relevant scale factor c, and either the $\underline{R}_z(\alpha,\omega,\kappa)$ or the $\underline{R}_{z'}(\alpha,\omega,\kappa)$† orientation matrix. Since orientation matrices are referred to the same coordinate system, either the z or z' system, the spatial triangulation can now, with the idealized image coordinates $l_{\bar{x}}$, $l_{\bar{y}}$ mentioned above, be carried out in accordance with the geometrical principles of a rigorous central perspective. For this last adjustment step the covariance matrix associated with the computed image coordinates will also be needed.

With (7.274) a covariance matrix was obtained relating to the smoothing process of the orbital curve. The covariance matrix relating to the single camera reduction is computed, with the designations introduced in (7.188), from (7.195) and the results obtained with (7.206) and (7.239) of the single camera solution in the form

$$(s_{l_0})^2 = s_0^2\,[\underline{B}_0\underline{N}^{-1}\underline{B}_0^*] \qquad (7.276)$$

Since the two error contributions are independent of each other, the total covariance matrix for the values $l_{\bar{x}}$, $l_{\bar{y}}$ of a specific photogram is, with (7.274) and (7.276),

$$(s_l)^2 = (s_{l_c})^2 + (s_{l_0})^2 \qquad (7.277)$$

with the proviso that all computations are with reference to a common mean error of unit weight (cf. sec. 7.4.8.1).

For each station to be triangulated and for all satellite passes observed at the station, the following information is now available:

(1) Approximate station coordinates

$$\phi^\circ,\ \lambda^\circ,\ \text{and}\ h^\circ \qquad (7.278)$$

(2) If given, the weight matrix of these coordinates

$$\underline{P}_\phi = \begin{bmatrix} p_\phi & p_{\phi,\lambda} & p_{\phi,h} \\ p_{\phi,\lambda} & p_\lambda & p_{\lambda,h} \\ p_{\phi,h} & p_{\lambda,h} & p_h \end{bmatrix} \qquad (7.279)$$

(3) Corresponding rectangular coordinates $z_{1,2,3}$ or $z'_{1,2,3}$ derived from (7.111), (7.112), (7.113), and, if necessary, transformed with (7.36).

(4) The relevant weight matrices $\underline{P}_z$ or $\underline{P}_{z'}$ from (7.128).

(5) The elements of orientation $(\alpha\omega\kappa)_z$ or $(\alpha\omega\kappa)_{z'}$ from the single camera program (cf. eq. 7.248).

(6) The scale factor c.

(7) The fictitious image point coordinates $l_{\bar{x}}$, $l_{\bar{y}}$ corresponding to the selected satellite positions and associated satellite orbit times.

(8) The covariance matrix (7.277) of these coordinates.

The information contained in points 1 to 8 above represents the input data for the spatial triangulation proper, whose solution and adjustment is treated in the next section as the final step in the evaluation.

The evaluation procedures of this section and, in addition, computations relating to alternative approaches to these problems are described in all details and with pertinent flowcharts in R. H. Hanson (unpublished papers, 1968). The treatment of the subject to this point has demonstrated that certain computer operations must be repeated frequently. For this reason the computer programs have been designed from the standpoint of optimal economic operation and the flowcharts (R. H. Hanson, unpublished paper, 1968) reflect a corresponding organization of the computations.

7.4.7.2 Adjustment

As was stated above, the spatial triangulation of the station coordinates can now proceed in accordance with the law of central perspective. The mathematical model on which the adjustment is based is given with (7.85) and (7.86), which, with the present nomenclature and in accordance with (7.148) and (7.149), are

$$F=\frac{c[(z_{s_1}-z_1)r_{11}+(z_{s_2}-z_2)r_{12}+(z_{s_3}-z_3)r_{13}]}{(z_{s_1}-z_1)r_{31}+(z_{s_2}-z_2)r_{32}+(z_{s_3}-z_3)r_{33}} - l_{\bar{x}}=0 \qquad (7.280)\ddagger$$

$$G=\frac{c[(z_{s_1}-z_1)r_{21}+(z_{s_2}-z_2)r_{22}+(z_{s_3}-z_3)r_{23}]}{(z_{s_1}-z_1)r_{31}+(z_{s_2}-z_2)r_{32}+(z_{s_3}-z_3)r_{33}} - l_{\bar{y}}=0 \qquad (7.281)\ddagger$$

The $z_{s_{1,2,3}}$ denotes the coordinates of a satellite position and the $z_{1,2,3}$ station coordinates. In case the exterior elements of orientation $(\alpha\omega\kappa)$ † are referred to the z' system, the station coordinates are designated as z' without making any other changes in the algorithm.

With the nomenclature of table 7.6, the observation equations corresponding to expressions (7.280) and (7.281) are, according to (7.151) and (7.152) given in following inset. F° and G° are computed with approximations for the station coordinates $z_{1,2,3}$ and for the satellite position coordinates $z_{s_{1,2,3}}$ (cf. eq. 7.257). The definition of the coefficients in (7.282), (7.283) is given in (7.153) to (7.155). All pairs of coordinates $l_{\bar{x}}$, $l_{\bar{y}}$ computed for a given photogram are correlated, since all directions to the satellite depend on the orientation matrix derived from the single camera solution. Furthermore, for a passive satellite all the coordinate pairs $l_{\bar{x}}$, $l_{\bar{y}}$ of fictitious satellite images are correlated, since they are derived from the smoothing polynomials that are based on an adjustment involving all coordinate measurements of the original satellite images.

According to (7.277), $(\mathbf{s}_{\bar{l}_{i,j}})^2$ is the covariance matrix associated with the n sets of $l_{\bar{x}}$, $l_{\bar{y}}$ derived from the photogram taken at station i observing the event j. The corresponding weight matrix is, from (7.196),

$$\underline{P}_{\bar{l}_{i,j}}=m_0^2[(\mathbf{s}_{\bar{l}_{i,j}})^2]^{-1} \qquad (7.284)$$

If we now set up observation equations (7.282) and (7.283) for all the directions in-

$$\overbrace{\begin{bmatrix}\Delta z_{s_1} & \Delta z_{s_2} & \Delta z_{s_3}\end{bmatrix}}^{\Delta\mathbf{z}_s{}^*}\underbrace{\begin{bmatrix}-D_x & -E_x & -F_x\\ -D_y & -E_y & -F_y\end{bmatrix}}_{\underline{B}_{z_s}}+\overbrace{\begin{bmatrix}\Delta z_1 & \Delta z_2 & \Delta z_3\end{bmatrix}}^{\Delta\mathbf{z}^*}\underbrace{\begin{bmatrix}+D_x & +E_x & +F_x\\ +D_y & +E_y & +F_y\end{bmatrix}}_{\underline{B}_z}-\overbrace{\begin{bmatrix}v_x & v_y\end{bmatrix}}^{\mathbf{v}_l{}^*}\underbrace{\begin{bmatrix}1 & 0\\ 0 & 1\end{bmatrix}}_{\underline{A}_l}+\underbrace{\begin{bmatrix}F^\circ\\ G^\circ\end{bmatrix}}_{-\boldsymbol{l}}=\begin{bmatrix}0\\ 0\end{bmatrix} \qquad (7.282)\ (7.283)$$

troduced into the satellite triangulation net, i.e., for all the coordinate pairs $l_{\bar{x}}$, $l_{\bar{y}}$ derived from measurements of the photograms, taking into account all existing correlations as expressed in the $\underline{P}_l$ matrices, we could form directly the corresponding system of normal equations. The unknowns of such a system would be the coordinates of the observing stations as well as of the orbital points. To make the solution economically more feasible, the corrections to coordinates of the orbital points are eliminated in the formulation of the normal equations, thus producing a final system of normal equations that contains only corrections to the camera station coordinates. The procedure, which is analogous to the elimination of relative pass points in numerical aerial photo triangulation, requires a formulation of partial systems of normal equations in the following manner.

As was stated above, the n pairs of coordinates $l_{\bar{x}}$, $l_{\bar{y}}$ for a particular photogram are correlated by way of the associated $\underline{P}_l$ matrix. With (7.282), (7.283) the $2n$ observation equations pertaining to station i and event j are formed. The normal equations system is then formed, which is, with appropriate use of the designations introduced in (7.282), (7.283),

$$\begin{array}{cc} \Delta\mathbf{z}_{s_j\,1,2,3,\ldots,n} & \Delta\mathbf{z}_i \\ \left[\begin{array}{c|c} \underline{B}^*_{z_{s_j}}\underline{P}_{l_{i,j}}\underline{B}^*_{z_{s_j}} & \underline{B}^*_{z_{s_j}}\underline{P}_{l_{i,j}}\underline{B}_{z_i} \\ \hline \underline{B}^*_{z_i}\underline{P}_{l_{i,j}}\underline{B}_{z_{s_j}} & \underline{B}^*_{z_i}\underline{B}_{l_{i,j}}\underline{B}_{z_i} \end{array}\right] & = \left[\begin{array}{c} \underline{B}^*_{z_{s_j}}\underline{P}_{l_{i,j}}\boldsymbol{l}_{i,j} \\ \hline \underline{B}^*_{z_i}\underline{P}_{l_{i,j}}\boldsymbol{l}_{i,j} \end{array}\right] \end{array} \tag{7.285}$$

where

$$\Delta\mathbf{z}_{1,2,3,\ldots,n} = \begin{bmatrix} \Delta\mathbf{z}_{s_1} \\ \Delta\mathbf{z}_{s_2} \\ \cdot \\ \cdot \\ \cdot \\ \Delta\mathbf{z}_{s_n} \end{bmatrix} \tag{7.286}$$

Each of the partial vectors $\Delta\mathbf{z}_{s_{1,2,\ldots,n}}$ is the vector of corrections for a specific satellite position; $\Delta\mathbf{z}_i$ is the correction vector for the coordinates of observation station i. The system of normal equations shown schematically in (7.285) must be set up as a unit for all the fictitious points computed for the photogram in question, since the associated $\underline{P}_{l_{i,j}}$ of dimension $2n \times 2n$ is an indivisible unit. If a specific satellite event j has been observed from m stations, the partial systems (7.285) are set up individually for each of the m photograms and combined into the normal equations partial system representing the event j as shown on page 592 in the schematic arrangement in the inset.

With evident simplification, (7.287) can also be written in the form

$$\begin{bmatrix} \underline{A} & \underline{C} \\ \underline{C}^* & \underline{B} \end{bmatrix} \begin{bmatrix} \Delta\mathbf{z}_{s_j\,1,2,\ldots,n} \\ \Delta\mathbf{z}_{i\,1,2,\ldots,n} \end{bmatrix} \begin{bmatrix} \Delta\boldsymbol{l}_{s_j} \\ \Delta\boldsymbol{l}_{z_{i\,1,2,\ldots,n}} \end{bmatrix} \tag{7.288}$$

Now the correction vector $\Delta\mathbf{z}_{s_{j\,1,2,\ldots,n}}$ for the satellite positions is eliminated, and a partial system of normal equations is left for corrections to coordinates of the stations that observed the satellite event j. This system is

$$(\underline{B} - \underline{C}^*\underline{A}^{-1}\underline{C})\,\Delta\mathbf{z}_{i_{1,2,\ldots,m}} = (\Delta\boldsymbol{l}_{z_{i\,1,2,\ldots,m}} - \underline{C}^*\underline{A}^{-1}\Delta\boldsymbol{l}_{s_j}) \tag{7.289}$$

or simply

$$\underline{N}_{z_{i\,1,2,\ldots,m}}\Delta\mathbf{z}_{i_{1,2,\ldots,m}} = \boldsymbol{l}_{z_{i\,1,2,\ldots,m}} \tag{7.290}$$

When the partial systems (7.290) have been formed for all events, the final, complete system of normal equations for the corrections to coordinates of all stations involved in the satellite triangulation is formed by adding the individual systems (7.290) according to the station index. The resulting system is

$$\underline{N}_z\Delta\mathbf{z} = \boldsymbol{l}_z \tag{7.291}$$

In the present form, $\underline{N}_z$ of (7.291) is singular and not invertible, since no origin of coordinates or a scale has as yet been introduced (cf. sec. 7.4.2). To satisfy the first requirement, the introduction of an origin or the equivalent, at least three possibilities worthy of consideration present themselves.

$$
\begin{array}{c|c|c|c|c}
 & & \overbrace{\qquad\qquad\qquad\qquad}^{\Delta \mathbf{z}_{i_{1,2,\ldots,m}}} & & \\
\Delta \mathbf{z}_{s_{j_{1,2,3,\ldots,m}}} & \Delta \mathbf{z}_{i=1} & \Delta \mathbf{z}_{i=2} & \cdots & \Delta \mathbf{z}_{i=m} \\
\hline
\sum_{i=1}^{m} (\underline{B}^*_{z_{s_j}} \underline{P}_{l_{i,j}} \underline{B}_{z_{s_j}})_i & (\underline{B}^*_{z_{s_j}} \underline{P}_{l_{i,j}} \underline{B}_{z_i})_{i=1} & (\underline{B}^*_{z_{s_j}} \underline{P}_{l_{i,j}} \underline{B}_{z_i})_{i=2} & \cdots & (\underline{B}^*_{z_{s_j}} \underline{P}_{l_{i,j}} \underline{B}_{z_i})_{i=m} \\
\hline
(\underline{B}^*_{z_t} \underline{P}_{l_{i,j}} \underline{B}^*_{z_{s_j}})_{i=1} & (\underline{B}^*_{z_t} \underline{P}_{l_{i,j}} \underline{B}_{z_i})_{i=1} & \underline{0} & \underline{0} & \underline{0} \\
\cdots\cdots & \cdots\cdots & \cdots\cdots & \cdots & \cdots\cdots \\
(\underline{B}^*_{z_t} \underline{P}_{l_{i,j}} \underline{B}_{z_{s_j}})_{i=2} & \underline{0} & (\underline{B}^*_{z_t} \underline{P}_{l_{i,j}} \underline{B}_{z_i})_{i=2} & \underline{0} & \underline{0} \\
\cdots\cdots & \cdots\cdots & \cdots\cdots & \cdots & \cdots\cdots \\
\vdots & \underline{0} & \underline{0} & \ddots & \underline{0} \\
\cdots\cdots & \cdots\cdots & \cdots\cdots & \cdots & \cdots\cdots \\
(\underline{B}^*_{z_t} \underline{P}_{l_{i,j}} \underline{B}_{z_{s_j}})_{i=m} & \underline{0} & \underline{0} & \underline{0} & (\underline{B}^*_{z_t} \underline{P}_{l_{i,j}} \underline{B}_{z_i})_{i=m}
\end{array}
$$

$$
= \begin{bmatrix}
\sum_{l=1}^{m} (\underline{B}^*_{z_s} \underline{P}_{l_{i,j}} \boldsymbol{l}_{i,j})_i \\
\hline
(\underline{B}^*_{z_t} \underline{P}_{l_{i,j}} \boldsymbol{l}_{i,j})_{i=1} \\
\cdots\cdots \\
(\underline{B}^*_{z_t} \underline{P}_{l_{i,j}} \boldsymbol{l}_{i,j})_{i=2} \\
\cdots\cdots \\
\vdots \\
\cdots\cdots \\
(\underline{B}^*_{z_t} \underline{P}_{l_{i,j}} \boldsymbol{l}_{i,j})_{i=m}
\end{bmatrix} \tag{7.287}
$$

The simplest is to assume that one of the stations of the net is given with its initial coordinates $\mathbf{z}^\circ{}_{(1,2,3)_i}$ free of error. This assumption imposes on the system (7.291) the condition that the corresponding $\Delta \mathbf{z}_i$ vector be a zero vector in the solution of the system. This is accomplished by assigning the approximation coordinates an infinite weight; i.e., the quantity 10^n is introduced as weight in the relevant diagonal terms of (7.291), n being as large as the capacity of the computer allows. This step causes the $\Delta \mathbf{z}_i$ vector to vanish for all practical purposes, since the corresponding entries in the $\underline{N}^{-1}$ matrix will be multiplied by 10^{-n}.

A second possibility exists, especially in connection with triangulation of a continental satellite net in which the observation stations are part of an established geodetic reference system. For such a case, weight matrices (7.279) and, after appropriate transformation, corresponding $\underline{P}_z$ or $\underline{P}_{z'}$ matrices (7.128) are available as input data. It is then necessary only to add these weight matrices to the system (7.291) where called for.

A third possibility, which is especially attractive for error studies, is to introduce as origin of coordinates the centroid of all adjusted coordinates. This means adding to the system the supplementary condition

$$\Sigma(\mathbf{z}^\circ + \Delta \mathbf{z}) = \Sigma \mathbf{z} = 0 \tag{7.292}$$

This will result, although with modifications depending on the shape of the net, in a symmetrical distribution of mean errors for the net.

In order not to endanger the accuracy of the $\underline{N}_z$ matrix inversion, it has been found advisable in practice to combine these various possibilities. Initially, one of the stations is held fixed at the origin. After the $\underline{N}_z$ matrix inversion, the coordinate system is translated. The three condition equations (7.292) are replaced by the condition valid for each station

$$\hat{\mathbf{z}}_i = \mathbf{z}_i - \frac{\sum_{i=s} \mathbf{z}_i}{s} \qquad (7.293)$$

where s is the number of stations involved in the triangulation. The matrix of weight coefficients for the $\mathbf{z}$ values are obtained, since in this case $\underline{F}^* = \underline{F}$ from

$$\hat{\underline{N}}^{-1} = \underline{F}\underline{N}_z^{-1}\underline{F} \qquad (7.294)$$

where the $\underline{F}_z$ matrix is obtained as a symmetric quadratic matrix by differentiating the right side of (7.293). The coefficients of $\underline{F}$ are $(s-1)/s$ along the diagonal and $-1/s$ in the spaces where the correlation between the individual components of the station coordinates should appear. A sequence of operations utilizing the symmetry of the $\underline{F}$ matrix is described in detail in R. H. Hanson (unpublished paper, 1968).

The introduction of scale into the triangulation by means of measured distances between two or more stations of the net is of prime importance in satellite triangulation. Such distances can be derived, for example, from long-line traverses measured with, for instance, a geodimeter (cf. Meade, 1968; Wolf, 1967). If the two stations are designated i and j and the distance between them d, then obviously

$$d_{ij} = [(z_{i_1} - z_{j_1})^2 + (z_{i_2} - z_{j_2})^2 + (z_{i_3} - z_{j_3})^2]^{1/2} \qquad (7.295)$$

the weight of the distance d_{ij} being expressed as

$$P_{d_{ij}} = \frac{m_0^2}{m_{d_{ij}}} \qquad (7.296)$$

where $m_{d_{ij}}$ is the mean error of the distance d_{ij} in meters. With the designation

$$\mathbf{f}^* d_{ij} = \frac{\partial d_{ij}}{\partial z_{ij}} = \begin{array}{|c|c|c|c|c|c|} \hline \partial z_{i_1} & \partial z_{i_2} & \partial z_{i_3} & \partial z_{j_1} & \partial z_{j_2} & \partial z_{j_3} \\ \hline z_{i_1} - z_{j_1} & z_{i_2} - z_{j_2} & z_{i_3} - z_{j_3} & z_{j_1} - z_{i_1} & z_{j_2} - z_{i_2} & z_{j_3} - z_{i_3} \\ \hline d^\circ & d^\circ & d^\circ & d^\circ & d^\circ & d^\circ \\ \hline \end{array} \qquad (7.297)$$

it is merely necessary in the system (7.291) to add, at the locations corresponding to stations i and j, including location ij, on the left side, the appropriate portion of the matrix

$$(\mathbf{f}_d P_d \mathbf{f}_d^*)_{ij} \qquad (7.298)$$

and on the right side

$$(\mathbf{f}_d P_d \Delta l_d)_{ij} \qquad (7.299)$$

where

$$\Delta l_{d_{ij}} = d_{ij} - d_{ij}^\circ \qquad (7.300)$$

and d_{ij}° is computed with the approximations for $\mathbf{z}_{ij}^\circ$ from (7.295). Any number of scalars can thus be introduced into the adjustment. With the expected development in measuring distances with lasers it should be possible in the future to measure distances between the observing stations and the satellite, which can then be similarly introduced into the system of normal equations (7.288) before the satellite positions are eliminated with (7.289).

After the system (7.291) has been amended with the two steps described above (fixing the origin of coordinates and introducing scale), the vector of coordinate corrections for all the stations in the triangulation can now be computed as

$$\Delta\mathbf{z} = \underline{N}_z^{-1}\mathbf{l}_z \qquad (7.301)$$

and the final result of the satellite triangulation is

$$\mathbf{z} = \mathbf{z}^\circ + \Delta\mathbf{z} \qquad (7.302)$$

From (7.235), using the $\mathbf{z}$ vector and expressions (7.280), (7.281) we compute corrections $\mathbf{v}_l$, followed by the determination of corrections for all additionally introduced observations. Thus, for example, for a priori given station coordinates

$$\mathbf{v}_{z_i} = \Delta \mathbf{z}_i \tag{7.303}$$

and for distances used as scale control

$$v_{d_{ji}} = \bar{d}_{ij} - d_{ij} \tag{7.304}$$

in which $\bar{d}_{ij}$ is computed with the final coordinates of (7.295) and d_{ij} is the initially given measurement.

With these v's and their weights the mean error of unit weight s_0 for the whole triangulation is computed from

$$s_0 = \left[\frac{(\mathbf{v}_l^* \underline{P}_l \mathbf{v}_l) + (\mathbf{v}_z^* \underline{P}_z \mathbf{v}_z) + (\Sigma P_d v_d v_d)}{B + Z + D - S} \right]^{1/2} \tag{7.305}$$

where B is the number of observations, Z is the number of station coordinates, given a priori with their weights, D is the number of distances, given with their weights, and S is the number of all coordinates, station locations as well as satellite points.

If in the course of the observations, stations must be moved a relatively small distance, e.g., for meteorological or logistic reasons, such dual stations must be coupled. Corresponding conditions are introduced and their number is added in the denominator of (7.305), just as all extraneous metric conditions must be appropriately taken into account. With the covariance matrix (7.195), corresponding to the system of inverted normal equations, and the s_0 of (7.305) the mean error of the individual $z_{1,2,3}$ is obtained with the square roots of the diagonal terms of this covariance matrix and, with (7.198) to (7.200), the semiaxes of the error ellipsoid and their direction cosines.

This actually completes the result of the satellite triangulation, at least from the standpoint of photogrammetry. Further processing of the results reverts to a strictly geodetic point of view, such as the conversion of the computed $\mathbf{z}$ values into an ellipsoidal system, which can be accomplished with (7.114) to (7.119).

If the approximations ϕ°, λ°, h° were given coordinates, a correction vector could be computed with (7.126) as

$$\mathbf{v}_\phi = \underline{T}_\phi^{-1} \mathbf{v}_z \tag{7.306}$$

and the corresponding station covariance in analogy with (7.128)

$$\mathbf{s}_\phi^2 = s_0^2 [\underline{T}_\phi^{-1} \underline{Q}_z (\underline{T}_\phi^{-1})^*] = \begin{bmatrix} s_\phi^2 & s_{\phi,\lambda} & s_{\phi,h} \\ s_{\phi,\lambda} & s_\lambda^2 & s_{\lambda,h} \\ s_{\phi,h} & s_{\lambda,h} & s_h^2 \end{bmatrix} \tag{7.307}$$

in which $\underline{Q}_z$ is the appropriate 3×3 matrix from $\underline{N}^{-1}$. In principle, we can say that the measures of accuracy for all quantities derived from the $\mathbf{z}$ values are to be computed as mean errors of functions of the adjusted $\mathbf{z}$'s in conformance with (7.241). In R. H. Hanson (unpublished paper, 1968) the structure of a computing program for spatial triangulation is described and the necessary flowcharts shown, and all supplementary computations and statistical controls that are needed for check and that are of significance to the computations in an extended triangulation program are explained.

7.4.8 Theoretical Considerations of Error

7.4.8.1 Error Budget of Geometric Satellite Triangulation

As is shown in section 7.1 and at the beginning of this section, the principle of the method of geometric satellite triangulation is based on combining a large number of individual directions to satellites in a three-dimensional triangulation. The satellite directions needed at the stations to be triangulated are obtained by interpolating the individual images of the chopped satellite trail into the framework of the star background present on the photograms.

Directions to the star images are first computed, basically as functions of the observing datum, the time of observation (UT1), and the instantaneous-pole coordinates. These directions are referred either to the astronomic right ascension-declination system for a specific epoch (x system) or, after appropriate rotation, to an Earth-fixed three-dimensional reference coordinate system (y

or z system) in which the observation station locations are to be triangulated (see sec. 7.4.6.2).

The satellite images are recorded in an arbitrary time sequence that is, however, common for all stations observing an event. The satellite images are then interpolated into the directions to the stars, i.e., into the background of stars, and thus fixed in the same reference system to which the star images have been reduced. The three-dimensional position of the observing stations is found by assigning to them a location such that the satellite directions emanating from the various stations lead to the determination of the three-dimensional geometry of all observed satellite transits.

It is not necessary, aside from the practical requirements of the field observer, to know in advance the orbit of the satellite. The points of the orbit serve merely as elevated triangulation targets, and only the condition for intersection of corresponding rays is needed to fix the positions of the observation sites (cf. sec. 7.4.2). As a consequent requirement, such rays must satisfy the "geometric condition of simultaneity" explained in section 7.4.4. This condition is automatically met, for example, if the satellite trail is fixed by the recording of a sequence of flashes emitted by the satellite.

Since to date in practice not a sufficient number of such flashes can be generated to reduce the influence of scintillation adequately (cf. sec. 7.4.5), we photograph the satellite in the position of its orbit illuminated by the Sun. In this method the trace of the orbit is chopped by means of a rotating disk shutter in the camera (cf. sec. 7.3.2, figs. 7.12 and 7.13) into a series of time-dependent individual images. For physical as well as technical reasons it is, however, impossible to generate satellite images at the several observing stations that satisfy initally the geometric condition of simultaneity. Basically, it therefore becomes necessary to fit the bundle of directions to the satellite for a particular event as closely as possible to the satellite orbit, which is by its nature continuous. Since only a small portion of the orbit (about 1–2%) is involved, the observed curve may be considered as part of an elliptical orbit, obeying the Keplerian laws of motion, which predicate that the satellite directions are referred to an inertial system as approximated for instance by the right ascension-declination system.

On the other hand, a solution based on satellite directions referred to an Earth-fixed coordinate system requires, because of the Earth's rotation, the assumption of a twisted space curve as a model for the satellite orbit.

In such a procedure, satellite triangulation is basically subject to five sources of error. The first source is the uncertainties associated with the star-catalog data; the second is the accidental errors in time determination for the star and satellite exposures. The third is the accidental errors in coordinate measurement of the star and satellite images; the fourth, the influence of shimmer acting as an accidental error source; and the fifth, the irregular distortion of the photographic emulsion. All these sources must be taken into consideration.

Such a presentation of the error budget assumes first, that the corresponding systematic errors are sufficiently small, and second, that the mathematical model used to reconstruct the photographic process is sufficiently close to reality. Furthermore, the photographed sections of the satellite orbit must be valid in a qualitative sense as a tool for interpolation. All these assumptions must hold within such accuracy limits that the influence of the remaining imperfections on the triangulation computations remains a magnitude smaller than the propagation of the five cited basic error sources.

Obviously, all further secondary corrections, such as pole displacement (see end of sec. 7.4.4), astronomic and parallactic refraction, satellite phase angle, and light travel time (for all these corrections see sec. 7.4.5), correspond to geometric-physical reality with such accuracy that the effect of remaining biases is negligibly small.

The rigorous theoretical treatment of errors of the satellite triangulation method leads, even from this point of view, to a

mutually correlated matrix schematic. The individual plates are essentially uncorrelated with respect to the photogrammetric reduction, so far as processing the measured star and satellite coordinates is concerned. However, for all plates introduced into a satellite triangulation system, only one set of reference stars, limited in number and distribution, is available.

Hence, not only does the same group of stars appear repeatedly on the same plate as a result of star registration before, during, and after the event, but also similar groups are recorded on a number of plates.

In the observations for the world net, stars up to eighth magnitude and with maximum mean position errors of 0".4 were selected from the SAO star catalog. Thus, there were about 20,000 stars at our disposal (sec. 7.4). With an average frequency of about 100 stars per plate and approximately 3000 plates in the world net, this means that each star appears, on the average, on 15 plates. Since, strictly speaking, there can result only one pair of corrections for each observed star in the adjustment, the mathematical reconstructions of all the photogrammetric bundles and their orientations are correlated to such a degree that they really should be adjusted as a unit, even if, for lack of knowledge of existing correlations, one accepts for the star coordinates independent weight matrices.

In the spatial triangulation of the observing stations the satellite directions are now combined to reconstruct the geometry of the recorded satellite orbit curve. The intersection condition for the rays applied in the process—either direct or indirect by way of fitting to a spatial model of the orbit—contains additional orientation information, similar to the relative orientation in the classical photogrammetric restitution process. But, since all photogrammetric bundle parameters that determine directions to the satellite and their orientation quantities are correlated, there results a correlation between all recorded satellite events; i.e., the determination of observing station positions should, together with the determination of all observed satellite orbital curves, be obtained from one common adjustment with the use of the covariance matrix involving all reconstructed photogrammetric bundles and their orientations.

Processing the approximately 3000 plates available in the world net requires the computation of nearly 60 000 interpolation parameters. For the approximately 1400 recorded events, more than 8000 orbital parameters would have to be determined. A simultaneous adjustment of such a large number of correlated unknowns is at present, even with the largest available computer, neither economically feasible nor, because of the required computational accuracy, capable of realization.

One has, therefore, to make concessions. From the error theoretical point of view probably the most serious compromise is the necessity of separately determining the photogrammetric interpolation parameters for each plate, since these parameters determine absolute directions to the interpolated satellite images and are therefore of decisive significance in fixing the spatial positions of the observation stations. In conformance with the weights given with the star data there is obtained in this procedure in each bundle reconstruction adjustment, independent of the number of images of the particular star, a pair of corrections for the star coordinates. On completion of all the bundle reconstructions under consideration there will therefore be for each star as many corrections available as the number of times such a star was recorded on the various plates. On the basis of the observation data in the world net, this averages out to 15 times. Arguing from the concept that every adjustment represents in principle a weighted arithmetic mean, the possibility presents itself of computing for each star a unique set of corrections in the form of the arithmetic mean of the individual pairs. Care need be taken only to ensure, by use of appropriate weights, that the mean error of unit weight after adjustment is the same for all the bundle reconstructions. One could then add this average of the corrections to the

original star data and repeat the bundle reconstruction computations. With an appropriate choice of weights for these corrected star data, these values could then be held correspondingly fixed in the repeated bundle reconstruction.

The justification for such an expensive iteration depends on how close the averaged star-coordinate corrections come to the solution from a rigorous adjustment. The significance of such a solution hinges, therefore, on the extent to which these "improved star coordinates" represent in their totality a reference system which is superior to the star catalog originally available. In the processing of the world net the improved star coordinates for the 20 000 stars being used were computed so that these amended right ascensions and declinations could be presented to the astronomers for critical evaluation. Repetition of the computations for bundle reconstructions was for financial reasons, not contemplated.

As was mentioned earlier, the accidental errors of time designations for the star and satellite recordings must be taken into consideration. In the adjustment for the single camera this is taken care of automatically by carrying corrections to the right ascensions. These corrections being geometrically equivalent to UT1, it is necessary only to compute weights for the introduced right ascension values, taking into account the uncertainties in time associated with the recorded instants of observation. For the instrumentation used in the world net, this accidental timing error amounts to less than a millisecond so far as the registration of the shutter action is concerned. Since the available UT1 is in itself scarcely better than $\pm$2msec (which acts as a system error in the orientation for the individual plate), the assumption of a $\pm$3–msec overall uncertainty in the determination of time for the star exposures seems reasonable. The inaccuracy of a direction corresponding to this time uncertainty is $\pm 0''.045$, a magnitude considerably less than the photogrammetric measuring accuracy with the BC–4 system and the 450–mm lens, and hence negligible.

A similar conclusion can be drawn about the influence of random errors of the synchronization procedure on the satellite images. By means of periodic control of timing (sec. 7.2.1), the instants of observation at the various stations are fixed relative to each other within at least ± 100 μsec. The most critical situation would arise for the ECHO satellite, with a speed of 8 km/sec and a minimum distance of 1000 km, for which 100 μsec corresponds to a change in direction of $\pm 0''.16$. With the PAGEOS satellite used in the world net, because of its greater distance and consequent slower speed, a timing error of ± 100 μsec results in a maximal direction uncertainty of only $\pm 0''.04$. Although this error is negligible, a calculation employed in the adjustment discussed later (a calculation designed primarily to eliminate shimmer by polynomial curve fitting) serves to adjust as well any existing random timing errors in the synchronization.

Existing correlations between the separately reconstructed bundles of directions to stars are, as detailed above, neglected. Thus, for each single-camera computation, individual parameters are determined for the interpolation model, including, of course, the covariance matrix associated with these parameters, which is of basic significance for further evaluations.

In the step of the adjustment which now follows, the locations of the observing stations are computed. Their position in space is fixed by the condition that the bundles of directions to the satellite issuing from these stations must lead to the geometry of all satellite orbital curves that have been recorded. Since each bundle of directions is obtained basically by the interpolation of the corresponding satellite images into the relevant interpolation model and since these models are now no longer correlated, it follows that the individual satellite orbit determinations are also uncorrelated. This results in an essential simplification of the data processing, since the orbit determinations can be processed sequentially and care need be taken only that their cumulative effect bears on the station determination.

The condition of intersection on which, as was mentioned previously, the determination of the geometry of the observed satellite orbits was based, either directly or indirectly by way of a fit to a spatial orbital model, basically contains additional information for determining the parameters of the relevant interpolation models. It follows that not only the coordinates of the stations and the parameters specifying the geometry of the satellite orbit, but also all parameters of all interpolation models involved together with their individual variance-covariance matrices referred to above, must appear as unknowns in the adjustment.

The resulting system of normal equations is $Bv=\Delta$ with a range in weights P from zero to infinity. If the vector of corrections to the measured satellite image coordinates is designated by $\mathbf{v}_l$, the correction vector for the previously computed bundle interpolation parameters $\overline{O}$ by $\mathbf{v}_0$, the correction vector for the approximated satellite orbital positions by $\mathbf{v}_{x_s}$, and finally the correction vector for the approximated station coordinates by $\mathbf{v}_x$, the corresponding system of normal equations can be written as indicated in figure 7.37. The Σ are supplementary conditions that may exist between the stations to be triangulated, such as, for example, measured distances for scale determination.

Figure 7.38 shows the system of normal equations after these functional relations have been introduced. The corresponding set of correlates is designated by K. The system reduced to satellite orbit and station coordinates is given in the lower part of figure 7.38.

Because the image coordinates can be expressed as functions of the interpolation

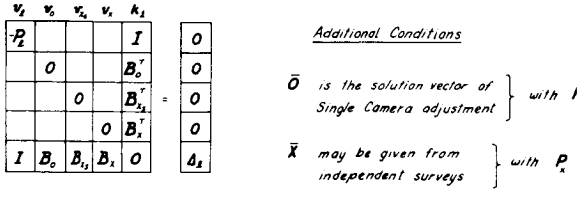

FIGURE 7.37.—Basic normal equation system for $Bv=\Delta$, $P=0\rightarrow\infty$.

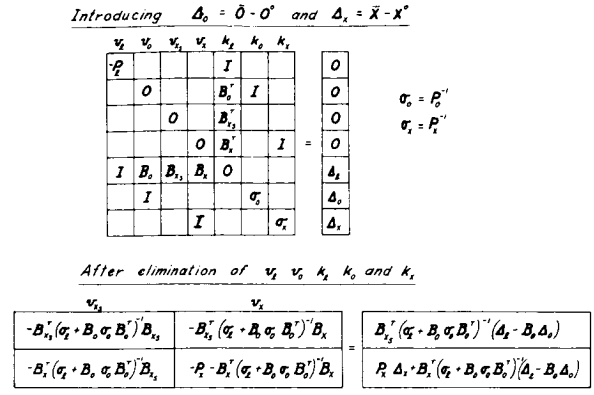

FIGURE 7.38.—System of normal equations after introduction of functional relations. (Below) System reduced to satellite orbit and station coordinates.

parameters describing the photogrammetric bundle, of the coordinates of the satellite position, and of the relevant coordinates of the observing station, it is possible, since the individual bundle reconstructions are uncorrelated, to replace the correction vector to the interpolation parameters by a corresponding correction vector to the image coordinates, thus reducing decisively the number of unknowns to be carried.

As is apparent from the lower part of figure 7.38, this computational procedure is completely rigorous only when the expression Δ_0 is carried along on the right-hand side of the system of reduced normal equations, i.e., with the vector of absolute terms; hence a rigorous elimination of the O parameters is not possible. However, since in the first iteration loop the O values as obtained from the single camera adjustment are introduced into the triangulation adjustment as approximation values, Δ_0 is initially a zero vector. This means that the elimination of the O parameters is valid to within the first order of the Δ_0 terms. Moreover, because of the large number of absolute control points (in our case about 100 stars per plate), the influence of the orientation contribution resulting from the intersection condition is quite small, so that the considerable gain in simplicity derived from the elimination of these parameters in the triangulation adjustment justifies the procedure.

This leaves the unknowns that are to be determined by means of the condition of intersection of the rays: the coordinates of the observing station and the parameters describing the geometry of the satellite orbital curves. From a conceptual point of view, this means that the bundles of directions to a satellite assigned to a particular satellite pass must fit themselves as closely as possible in the sense of an adjustment to the orbital curve, which is subject first of all to the geometric consequences of Kepler's first law, according to which the orbit can be expressed, in an inertial system, by the equation of an ellipse.

Furthermore, the fitting process must do justice to the dynamic content of Kepler's second law, according to which the true anomaly is a function of time. It seems convenient in the application to develop the true anomaly as a series in the eccentricity and the mean anomaly. Basically speaking, one can say that Kepler's first law accomplishes the fit of the bundle perpendicular to the direction of the orbital curve, and the second law accomplishes the fit along the orbit curve. Kepler's third law cannot be used, because, in the first place, the orbital period of the observed satellite is not known. Moreover, the balloon satellite with its typically unfavorable mass-ratio is exposed to disturbing influences such as residual atmospheric pressure and the Sun's radiation pressure, so that the orbital period could yield only limited information in a geometrical sense. All computational schemes must, furthermore, take into account the fact that the recorded times for satellite imagery refer to the instants of exposure, and these data must therefore be corrected for light travel time and geometrically for Earth rotation during the light travel time before they can be further processed with the application of the principles of celestial mechanics.

The practical application of orbital determination by means of bundle fitting is faced with two further obstacles. As was stated at the end of section 7.4.5, a relatively large number of satellite images is needed in the adjustment to sufficiently reduce the shimmer effect. In the world net, the number of images averages 300 per plate. Since the corresponding 300 directions are derived from one and the same group of interpolation parameters, they are correlated, which means that for each of the satellite direction bundles to be introduced into the fit a 600×600, completely filled covariance-matrix must be taken into consideration. If the event has been observed by more than two stations, undesirably large demands are very soon made on the memory capacity of the computer. Even more decisive is the fact that the shimmer effect depends on the meteorological conditions during the event, which can be quite different at the contributing stations. To prevent this "noise" from being averaged between the contributing stations to an event in the triangulation adjustment, the appropriate weight matrices for the individual direction bundles must be computed by using the mean shimmer characteristic for each station. This quantity is, however, in the evaluation method under discussion and is not as yet available.

As an alternative to the bundle-fitting concept, one could also fix the satellite orbital curve by smoothing the spatial coordinates of the triangulated satellite points with polynomials as functions of time (Wolf, 1967). Such a solution assumes that the orbital curve is designated by a series of short-duration flashes emitted from the satellite, the time sequence of the flashes being sufficiently well known. Only then will images be recorded on the individual plates, which lead to the triangulation of the corresponding orbital points. On the other hand, if, as is necessary for practical reasons at this time, the satellite images are produced on the various plates by chopping the trail of the continuously illuminated satellite with a rotating disk shutter into separate points, then one would first have to compute the necessary light travel times iteratively with approximated satellite positions. In principle, this computation would give sufficient information to interpolate on each photogram for the event image points that satisfy the geometric condition of simultaneity.

From an error-theoretical standpoint, however, such interpolation is open to question, because the position of the individual images is influenced to a different and unknown extent by shimmer. From the computational standpoints, still another disadvantage accrues to this solution, in that all the satellite directions on the selected plates are correlated, leading to variance-covariance matrices whose consideration would require an intolerable amount of computer memory space.

The theoretical and practical difficulties of the above method of solution are circumvented by modifying the approach and evaluating each plate independently to the greatest extent possible.

This concept is also valid from the standpoint of error theory and is based on the fact that the measurements at a given observing station, i.e., the photogrammetric registration of the star images and satellite orbit, together with the relevant recordings of time, are self-sufficient in the sense that the information so obtained is completely independent of and not influenced by the fact that similar operations have been carried out at other stations. Transforming these measuring data into time-correlated satellite directions requires only the additional assumption that the satellite orbital curve is by nature continuous.

If the geometric-dynamic properties of the photographed portion of the satellite orbit as described above are known, it should be possible to postulate the form of this trail on the photogram, in the direction of the trail and at right angles to it, in terms of the central perspective laws, light propagation time, and the aberration due to the Earth's rotation. The formalization would lead to an infinite-series expansion in which higher-order terms could be neglected. The orbital projection could then be adjusted to this theoretical model by fitting the satellite images to it. Another possibility, the one adopted here, is to smooth the satellite images with polynomials. Just as the triangulated spatial coordinates of discrete orbital points can be fitted to polynomial functions of time, the recorded sequence of time-related satellite images can be similarly smoothed, resulting in positions of the satellite on the photogram as a function of time. A polynomial fit is all the more justifiable from the standpoint of error theory inasmuch as the simplest conceivable projection model exists between the orbit, continuous by nature, and the corresponding satellite image sequence. The measured satellite image coordinates, by means of the bundle reconstruction parameters, as obtained from an adjustment based on reference stars and their images, are therefore first of all reduced to the concept of a rigorous central perspective, i.e., the concept of an ideal photograph. Then one applies the principle of an adjustment to compute best-fitting polynomials. To the extent that the central-perspective nature of the images of the satellite orbital points has been reproduced, this adjustment has the function of neutralizing the random errors of the comparator measurements, random emulsion shrinkage, and shimmer effects. In addition, it yields, in the form of statistical functions, an indication of the accuracy of the smoothing polynomials.

In order to verify the required degree for these polynomials, 380 satellite space coordinates for a simulated PAGEOS orbit at intervals of 0.8 sec were recorded, which corresponds to the average length of the PAGEOS arc observed with the BC–4 camera. The satellite orbit was integrated with a tenth-order Cowell-Störmer process. The Earth's gravitational field was introduced by means of an expansion in spherical functions to the fourth degree and fourth order by using the coefficients of the 1966 Smithsonian Institution Standard Earth (Lundquist and Veis, 1966). The radiation pressure of the Sun and the attraction of the Moon and Sun were also included in the integration computations. The resulting coordinates of satellite positions were then transformed into a geostationary system.

Six fictitious observing stations (fig. 7.39) were distributed relative to the computed orbit to simulate essentially the geometrical distribution of stations in practice. For each

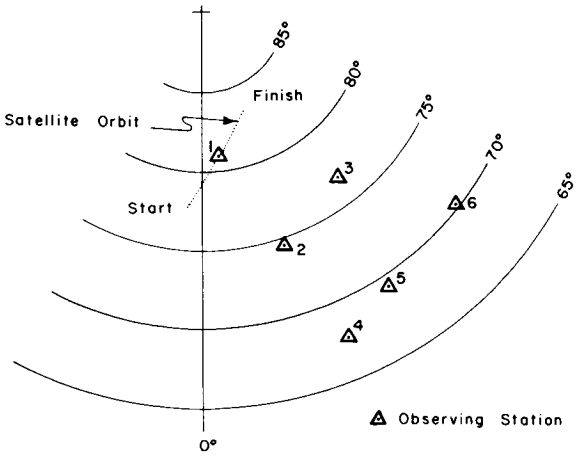

FIGURE 7.39.—Schematic representation of satellite orbit and positions of observing stations.

of the 380 fictitious points of the orbit, by applying the time of light propagation, corresponding plate coordinates were computed at each of the six stations to reproduce an exact, central-perspective mapping of the orbital geometry. These plate coordinates were then subjected to polynomial curve fits from the first to the eleventh degree in sequence. The resulting mean errors of the computed coordinates after adjustment are listed in table 7.7, σ_x referring to the coordinate component in direction of the trail and σ_y at right angles to the trail.

From table 7.7 it is seen that the required accuracy can be obtained with a polynomial of the fifth degree along the trail and of the fourth degree across the trail. At the same time no undesirable effect of oversmoothing is apparent with polynomials of higher degree, at least up to the eleventh degree. This degree is of consequence in that from an adjustment polynomial of the nth degree, only $n+1$ computed values can be used; otherwise, the corresponding covariance matrix becomes singular, while the use of fewer values does not exhaust the available information content completely.

In processing the world net, polynomials of the sixth degree are used in smoothing both x and y, so that seven fictitious directions can be used in the final triangulation, provided that the trace of the portion of the satellite orbit common with other stations extends over the whole plate. Thus, the polynomials provide the adjusted location of the satellite trace as a function of the recorded time. This relation is very useful, since it simplifies the application of the influence of time corrections, such as clock differences and light propagation. It is necessary, after a selected satellite orbital time has been transformed to a corresponding time of registration on the plate, merely to compute from the relevant polynomial with this transformed time the x and y coordinates for the corresponding fictitious plate image. By using this procedure on all photograms that have observed a common event, a fictitious image that satisfies the geometric condition of simultaneity is obtained on each photogram (see sec. 7.4.4). An approximate preliminary triangulation of the relevant orbital points will be needed to determine for each registered orbital image the variable propagation time of light. It should be noted in this connection that an error of 3 km in the approximated distance will create an error of only 10 μsec in the time. Along with the coefficients of the curve-fit polynomials, one obtains the mean dispersion of the individual images and, hence, the variance-covariance of the polynomial parameters. Since the fictitious satellite-image positions corresponding to specified times are computed as functions of the polynomial parameters (cf. eqs. 7.58 and 7.270), the corresponding error propagation computation will produce their variance-covariance matrix, which displays rigorously the correlations among the individual satellite images resulting from the polynomial smoothing. If seven such fictitious satellite images are used, as, for example, in the world net, a 14×14 covariance matrix for these points must also be computed.

At this stage the following evaluation data are available for each satellite orbit observation at a station:

(1) The bundle parameters describing the interpolation model, including the exterior elements of orientation, and the associated covariance matrix (in this case, of

dimension 20×20) scaled to an a priori introduced error of unit weight.

(2) The pairs of coordinates for the selected fictitious satellite images (in the present case, seven pairs) together with their 14×14 covariance matrix, also referred to the error of unit weight mentioned in (1) above.

The last processing step, computing the three-dimensional geometry of the observing stations, amounts basically to determining the spatial directions corresponding to the fictitious satellite images in order to triangulate the satellite orbit points and all the observation sites by means of an adjustment, subject to the condition that the sum of squares of weighted corrections to the fictitious satellite-image coordinates be a minimum. The weight matrices of the satellite direction bundles are compounded at each station by the joint influence of the covariances of the relevant interpolation parameters (statement 1 above) and the covariances of the plate coordinates of the fictitious satellite images (cf. statement 2 above).

Whenever additional a priori given information relative to the geometry of the observing sites, such as spatial distance between the sites (as for scale determination), position coupling between adjacent stations (eccentric reductions), or the like, is used as input data, such data can be introduced into the adjustment without difficulty after the necessary functional weights, referred of course to the a priori selected error of unit weight, have been computed. This is true also when additional geometric data become available through, for example, distance measurement by laser DME between satellite and station.

In the world net, such scalars are introduced in the form of measured distances of edges of the world net polygon in, primarily, the United States, Europe, Africa, and Australia, as shown in figure 7.5, section 7.3.

The basic ideas underlying the error budget of geometric satellite triangulation are presented here as explanation of the error theoretical considerations that lead to the adjustment algorithm described in section 7.4.6. Moreover, by pointing out computational possibilities that differ from the present solution and lead eventually to completely rigorous adjustment and error propagation, it is hoped that impetus will be given to perfecting the developing method of geometric satellite triangulation.

In the next section will be reported some results on the accuracies in the various evaluation phases obtained in the processing of the observational data for the world net.

7.4.8.2 Analysis of the Essential Sources of Error and the Error Propagation Into the Spatial Triangulation

In section 7.4.8.1 it was shown that, in essence, the method of geometric satellite triangulation is subject to five random error sources. The accidental errors from these sources arise in connection with:

(1) Comparator measurements of star and satellite images.

(2) Reference data from the star catalogs.

(3) Designated times of the star and satellite recordings.

(4) Atmospheric shimmer affecting the directions to the recorded star and satellite orbit points.

(5) Accidental emulsion shifts generated in the process of developing the plate.

This idealized situation will, however, exist only to the degree that, during the field observations and in the data processing, sufficient precautions are taken to either model the following systematical error sources or eliminate them by corresponding operational procedures.

Observational Phase.—

(1) Eliminating possible static instability of the camera during the average half-hour period of observation.

(2) Eliminating systematic errors in recording the instant of shutter operation that is needed to within a few milliseconds of Universal Time and, relative to all involved cameras, to within 1/10 msec.

Measurement Phase.—

(1) Adhering strictly to the Abbe comparator principle.

(2) Correcting for the lack of perpendicularity of the comparator axes.

(3) Accounting for at least linear differences in the comparator scales.

Adjustment Phase.—

(1) Determining the elements of interior orientation existing in the operational environment.

(2) Determining the comparator constants outlined necessary to correct for the lack of perpendicularity of the comparator axes and to account for the differences in comparator scales.

(3) Modeling of astronomic and parallactic refraction, the latter being needed because of the finite distance of the satellite.

(4) Modeling the phase angle of the satellite illumination as a function of size and shape of the satellite, its reflective property, and the geometric positions of the Sun, satellite, and observing station during the event.

(5) Considering influence of light travel time on station synchronization and aberration.

(6) Introducing with sufficient accuracy the spatial orientation of the instantaneous rotation axis of the Earth (pole wandering) with respect to individual camera orientations as well as with respect to the use of UT1 (true angle of Earth's rotation).

(7) Reducing star places to time of observation, involving precession, nutation, proper motion, radial velocity, annual and diurnal aberration, as well as the influence of the spectral characteristics and magnitude of the star on the photogrammetric imagery.

Quantitative results will now be given with respect to the above random errors mentioned and their propagation into the end results of the spatial satellite triangulation, errors in time determination, as was previously mentioned, being considered negligible (Schmid, 1965b, 1966b, 1967a, b, 1969).

7.4.8.2.1 ACCURACY OF THE COMPARATOR MEASUREMENTS

We discuss first the result of measuring 1210 photograms, representing practically half of the observational data from the world net.

On each photogram, on the average, 100 fixed stars were recorded before and after the satellite transit and also during the event. With repeated exposure, 500 to 800 star images in all are registered. There are, in addition, about 300 satellite images, so that on each photogram at least 800 images must be measured. In order to complete these measurements in the time alloted to the world net program, six comparators of similar design were in operation. Of significance also is the fact that a group of operators was involved in the measurements. Each photogram was measured on the comparator in two positions differing by approximately 180 degrees (cf. sec. 7.3.2). By means of a two-component translation, two scale factors, and a rotation, the two sets of measurements were brought into coincidence by an adjustment. The internal accuracy of the measuring process (precision of the comparator measurements) can then be judged on the basis of residual differences from double measurements. From the selected photograms with their 1 291 744 double measurements there resulted a mean error for the arithmetic mean of a double measurement of ± 1.63 μm. No significant differences between the precision of the x and y coordinates were detected.

It is of interest to group the measurement of plates by individual operators. The separately computed average measuring accuracy for each of the 34 comparator operators, arranged in sequence of increasing absolute amounts, is shown in figure 7.40. The number at the top of each arrow represents the number of photograms measured by the operator, and the ordinates of the arrowheads indicate the range over which the mean errors of the individual plate measurements vary for that operator.

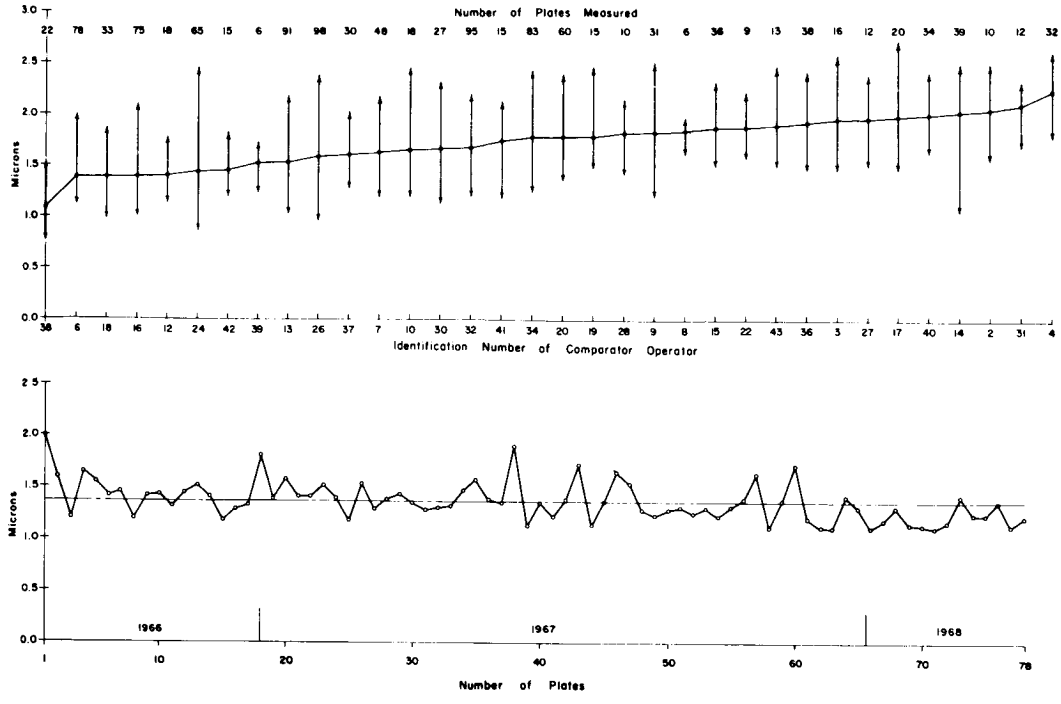

FIGURE 7.40.—Computed average measuring accuracies of 34 comparator operators. (Below) Performance of operator 6.

It can be seen that the mean measuring precision attained ranges from ± 1.1 μm (for operator 38) to 2.2 μm (for operator 4). The best single result was ± 0.76 μm by operator 38, and the worst was 2.66 μm by operator 20. As an explanation of these fairly surprising differences, one must assume not only the varying capabilities of the operators, but also the influence of environmental conditions on image quality. The lower diagram in figure 7.40 shows for operator 6 in chronological order the mean error of the 78 photograms measured by him over a period of 18 months. Although the average mean error for this operator of ± 1.37 μm is relatively low, the dispersion is typical for the behavior of all operators with respect to the quality of their individual measuring results. In addition to displaying the variation in precision from plate to plate, the diagram indicates a steady though small improvement in the measuring operation.

Figure 7.41 shows the histogram of the 1 291 744 double measurements. From the similarity of the histogram with the superimposed, theoretical, normal distribution, one can conclude a sufficiently close absence of bias errors, all the more so when the fact that the data for the histogram are composed of samples with differing mean errors is taken into consideration. On the basis of these results one can well imagine that these measurements were all made by one fictitious operator on one fictitious comparator, instead of by 34 operators on 6 comparators. Hence, for the further error theoretical studies we shall assume that the internal accuracy of image coordinates, meaned from double measurement, is sufficiently well expressed in their totality by a mean error of ± 1.63 μm.

The mean errors m_l computed separately for each photogram are plotted in figure 7.42 for 500 photograms selected for further study. The observational data selected are derived from 35 stations of the world net, plotted according to latitude. Table 7.8 shows the number of plates for each station. The location of the stations is shown in figures

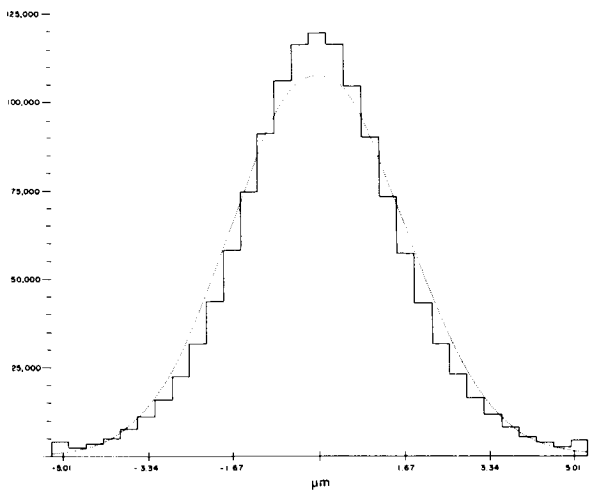

FIGURE 7.41.—Histogram of 1 291 744 double measurement differences.

7.6 through 7.11 of section 7.3. See also table 7.2 in section 7.1.2.

7.4.8.2.2 ACCURACY OF THE RECONSTRUCTIONS OF THE PHOTOGRAMMETRIC BUNDLES AND THEIR ORIENTATIONS

The parameters for reconstructing the bundle and its orientation are obtained by relating the measured star-image coordinates to the corresponding star-catalog data with an adjustment to a mathematical model. The total of these quantities, previously designated as interpolation parameters, includes, in addition to the purely photogrammetric parameters, a second scale factor and an angle for correcting for the a priori assumed

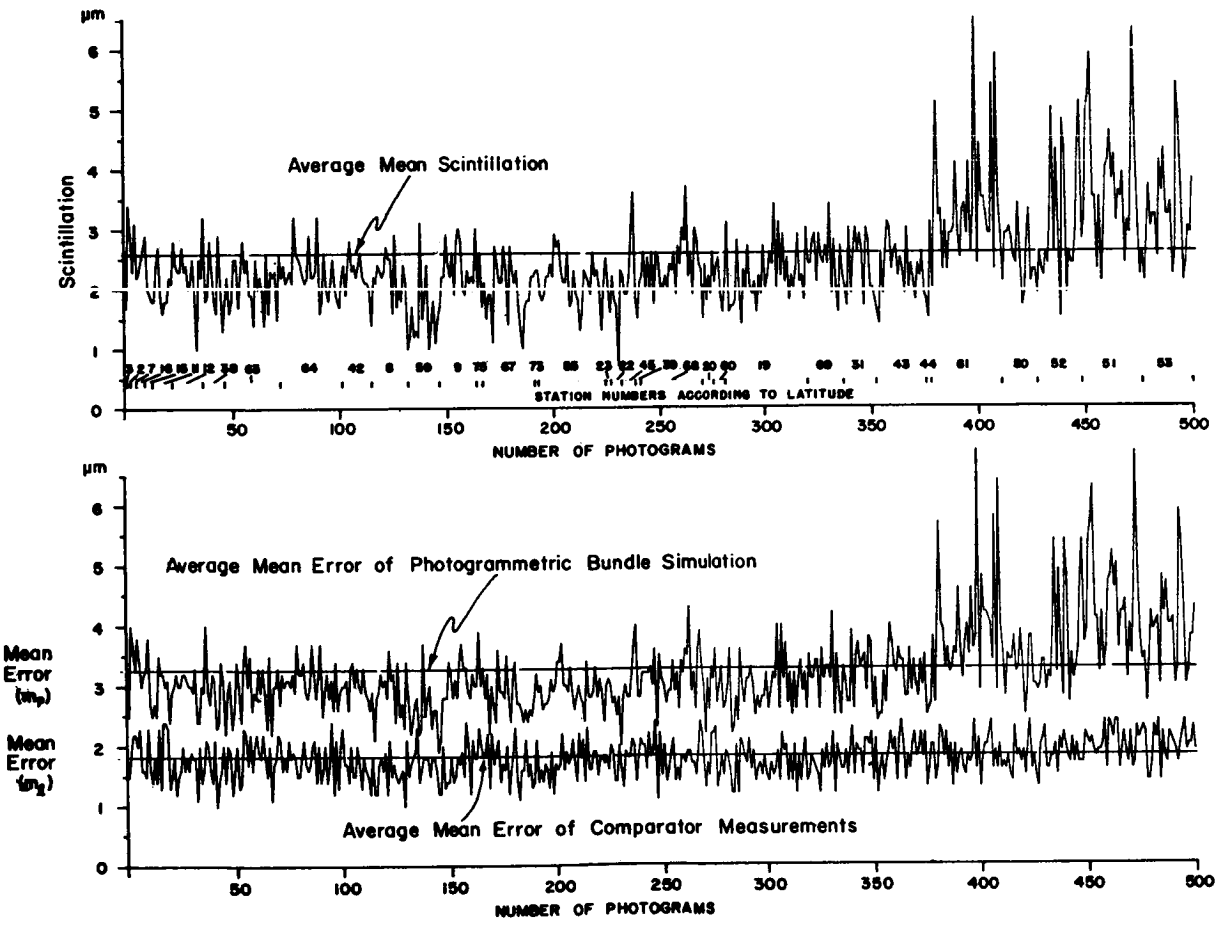

FIGURE 7.42.—Plot of mean errors for 500 photograms.

perpendicularity of the comparator spindles. The introduction of these extra parameters is justified insofar as one may assume that the homogeneity of the scale of the astronomic reference system (unit sphere) and the orthogonality of its coordinates are superior, with respect to systematic errors, to the corresponding mechanical components of the comparators. After the linear scale difference between the x and y spindles and the deviation from perpendicularity has been determined in this manner, the mean error of ± 1.63 μm, computed as a measure of precision for the image coordinates, can be considered a measure of accuracy for the subsequent treatment. (Periodic screw errors are independently tested for in comparator calibrations.) If it is assumed that the error for the astronomic coordinate α, δ of FK–4 stars, reduced to the observation datum, is $\pm 0''.3$, and for all other stars $\pm 0''.4$, and that the mathematical model for simulation of the bundle is sufficient, then, since time errors are negligible, the mean error of coordinate corrections resulting from an adjustment executed with appropriate weights will express the additive influence of the random errors produced by the comparator measurement, shimmer, and emulsion shift. Figure 7.42 shows for the 500 selected photograms the values for m_p and m_l and the rms for all the data, m_p being the mean error of the image coordinates for the photogram as obtained from the adjustment for the photogrammetric bundle reconstruction and m_l being the expression for the accuracy of the corresponding comparator measurements. A mean error of ± 1.0 m is assumed for the influence of random emulsion shift (Altman and Ball, 1961). Hence, the contribution to the total mean error

$$m_s = \pm (m_p^2 - m_l^2 - 1.0^2)^{1/2} \qquad (7.308)$$

This error component is also shown in figure 7.42. The rms values for the 500 plates are $m_p = \pm 3.31$ μm, $m_l = \pm 1.81$ μm, and $m_s = \pm 2.58$ μm.

Figure 7.43 shows the histograms of combined x and y coordinate corrections with corresponding normal distribution curves for 25 single camera adjustments. These were

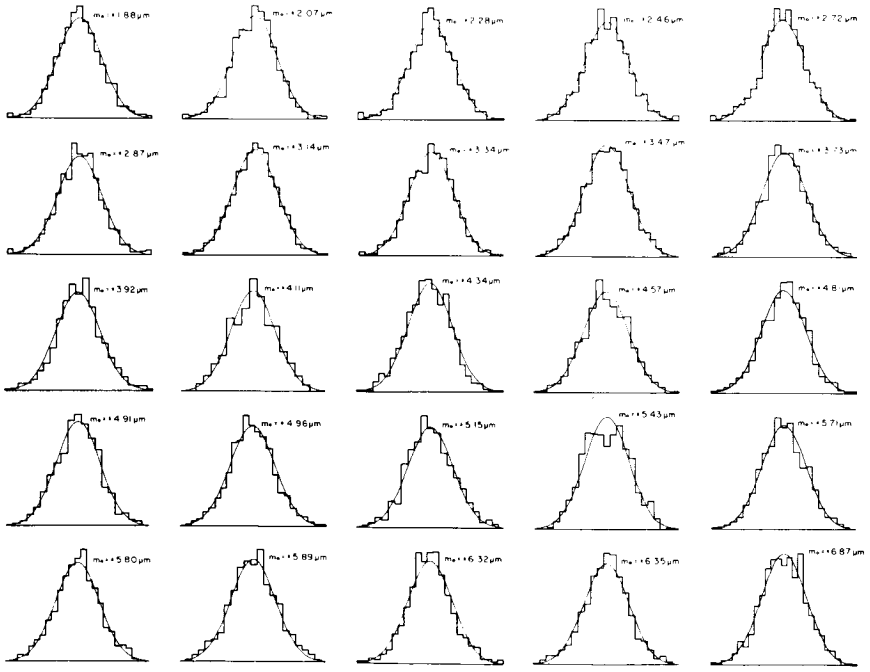

FIGURE 7.43

selected to cover uniformly the range of mean coordinate errors, after adjustment, actually obtained, i.e., the range from ± 1.88 to ± 6.87 μm. The histograms illustrate the typical behavior of the totality of evaluated observational data.

7.4.8.2.3 ACCURACY OF THE TRACE OF THE SATELLITE ORBIT AFTER THE POLYNOMIAL FIT

The mean deviation of a measured satellite point from the smoothing polynomial of degree 6 varies between ± 1.6 and ± 8.6 μm, with rms of ± 3.75 μm for the fit in direction of the satellite trail and between ± 1.3 and ± 9.3 μm with an rms of 3.28 μm perpendicular to the trail (fig. 7.44). The corresponding x, y, mean value is 3.52 μm.

The individual mean displacement is a measure of how well the satellite images on a given photogram fit the polynomial. These quantities are the sums of the superimposed random errors of the comparator measurements, the emulsion shifts, and, again, the shimmer. The mean deviation in direction of the satellite trail is, on the average, 0.47 μm larger than that at right angles to the trail. This difference is not so much due to random time errors of the recording sequence which operate in the direction of the trail, as to the fact that the comparator measurements of the trail images have a larger mean error in this direction than in the direction perpendicular to the trail, because of image blur from the satellite motion.

About 300 satellite image measurements are available per plate. From the double measurements, i.e., from their differences, the accuracy of the comparator measurements is again determined. This is on the average ± 1.79 μm for the x and y measurements, or practically the same value as that for the star image measurements. Again, with the assumption of ± 1.0 μm for the mean random emulsion shift, the opportunity is given to isolate the shimmer effect as

$$m_s = (3.52^2 - 1.79^2 - 1.0^2)^{1/2} = \pm 2.86 \ \mu\text{m} \tag{7.309}$$

The treatment of the shimmer as a random source of error is based on the fact,

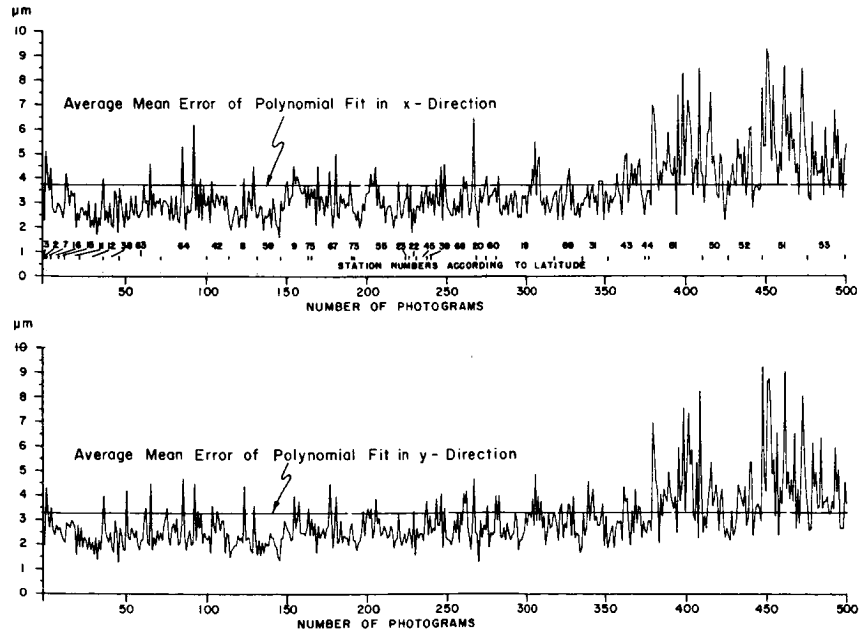

FIGURE 7.44.—Mean deviations after polynomial fit.

known from astronomical observations (Hynek, 1960), that the mean amplitude of shimmer operates as an irregular error source in all directions. When for each plate the shimmer effect on the star images is computed in accordance with (7.308) and these values are compared with the corresponding values obtained from the curve fit with (7.309), the correlation coefficient $\rho = 0.81 \pm 0.02$ is obtained with the formula

$$\rho = \frac{\sum_{i=1}^{n=500} \Delta s_1 \cdot \Delta s_2}{\left[\sum_{i=1}^{n=500} \Delta s_1^2\right]^{1/2} \left[\sum_{i=1}^{n=500} \Delta s_2^2\right]^{1/2}} \qquad (7.310)$$

where the Δ's represent deviations of the individual amounts of shimmer from their mean value, and the indices 1 and 2 refer to the shimmer computed from the bundle reconstructions and the polynomial fit, respectively.

Figure 7.45 shows the mean shimmer at each observing station, the stations arranged by latitude. From this figure it is seen that shimmer, with an overall mean for all stations of ± 2.58 μm for the star images and ± 2.86 μm for satellite images, represents a considerable error contribution to the total error budget. Also apparent is the increase in shimmer with increasing latitude, which is to be expected in consequence of the theory presented by Nettelblad (1953), according to which shimmer is least in warm ocean air masses and greatest in cold continental climates. The amplitude of the shimmer depends, in addition, on the exposure time, which may be the cause for the fact that the mean shimmer for the star exposures of between 0.2 and 3.2 sec is ± 2.58 μm and for the satellite images exposed from 1/15 to 1/30 sec is ± 2.86 μm. Obviously, the use of short-duration flashes (1/1000 sec) will increase the shimmer effect for the individual flash, thus making it all the more desirable to have a considerable number of such flashes before an adequately accurate triangulation can be performed.

7.4.8.2.4 ERROR PROPAGATION INTO THE SPATIAL TRIANGULATION

In sections 7.4.2.1 through 7.4.2.3, quantitative results were given for the significant random error contributions that must be considered in setting up an error budget for spatial triangulation. In table 7.9, average values from the processing of the selected 500 photograms are presented.

The figure in column 7 of table 7.9 indicates that an average uncertainty of 1.″57 in direction should be associated with a bundle reconstruction that is not overdetermined. Actually, this value is a function of the position of a ray within this bundle (Schmid, 1967a), and to be completely rigorous, in accordance with error theory, should be computed with the covariance matrix obtained

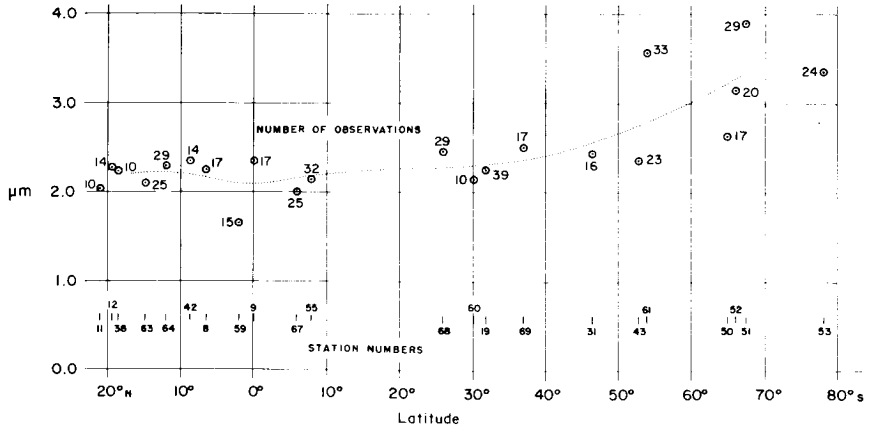

FIGURE 7.45.—Average shimmer versus latitude of observing station.

from the individual bundle reconstruction adjustment. Since the bundles under consideration here are relatively narrow, however (the angle of vision for the BC–4 camera is about 20 degrees), we can for the present ignore this fact in a general examination of the error propagation. In order to determine uniquely the 20 required interpolation parameters of an oriented bundle reconstruction, at least 10 reference stars are required, so that the use of an average of 100 stars per plate represents 10 solutions in the adjustment. Each star being, on the average, measured five times, it can be expected that the direction uncertainty for a central ray after adjustment of the bundle reconstruction will, from a combination of tabulated values in table 7.9, result as follows.

The error sources affecting the individual image coordinates add quadratically to

$$m_l = \pm (1.81^2 + 1.0^2 + 2.58^2)^{1/2} = \pm 3.31\ \mu\text{m}$$

(cf. table 7.9, columns 2, 3, 4, and 5). If it is assumed that the five images for each reference star are combined into one fictitious image, then the coordinates will have an accuracy of $3.31/\sqrt{5} = \pm 1.48\ \mu$m. Combining this with the mean star-catalog uncertainty of $\pm 0''.4 = \pm 0.87\ \mu$m (column 6), we have a mean uncertainty in direction $\pm 1.72\ \mu\text{m} = \pm 0''.79$. The combination of 10 independent solutions in one adjustment reduces this error approximately to $0''.79/\sqrt{10} = 0''.25$.

The figures of table 7.10 are results from a bundle reconstruction adjustment with a mean error of $\pm 3.31\ \mu$m for the image coordinates after adjustment involving 648 star images of 105 reference stars distributed approximately evenly over the plate. The results shown are mean accuracies of directions corresponding to various image positions on the plate, which are assumed free of error (Schmid, 1967a).

The mean error $\pm 0''.23$ from this table for the central ray ($x = y = 0$) is in good agreement with the value $0''.25$ obtined before from general considerations. When the mean satellite image error figure of $1''.61$ from table 7.9, column 8, is used, the sixth-degree polynomial fit over 300 satellite points will contribute an uncertainty in direction after adjustment of $\pm 1''.61/\sqrt{300/7} = 0''.25$. The error sources being uncorrelated, the total expected error in direction for the central ray is $(0''.25^2 + 0''.25^2)^{1/2} = \pm 0''.35$.

The use of sixth-degree polynomials makes seven directions available for satellite triangulation in each photographed bundle. However, as we know, these directions are mutually correlated. One reason is that they are all obtained with a specific group of interpolation parameters from a single camera, and another is that they all derive from a single pair of smoothing polynomials. From a study of the relevant covariance matrices in a rigorous adjustment whose reproduction here would far exceed the available space, it becomes apparent that the use of seven directions distributed evenly over the satellite trail yields a gain of 32 percent for the geometry of the bundles, as opposed to the use of a single central direction. This means that the use of all seven directions has about the same information content that would be obtained from two central rays that are not correlated.

Hence, if we conceive the total information used in the evaluation of a specific photogram as being compressed to determine a central fictitious direction, we may expect for such a direction an accuracy of $m_r = \pm 0''.35 - 32\%\ (\pm 0''.35) = 0''.24$.

According to section 7.4.7.1, the adjustment algorithm is based on the assumption that the results of bundle reconstructions at the individual stations are uncorrelated. Consequently, the directions to the satellite for a given event derived at the individual stations are also uncorrelated. To obtain a measure of the mean accuracy to be expected for the spatial triangulation of the observing sites, one can assume that the mean accuracy $0''.24$ of a direction computed above for a fictitious central direction containing all the information content is an uncorrelated function of the station. In the adjustment algorithm, this accuracy of triangulation directions associated with a specific evaluation of a photogram is expressed in the form of the

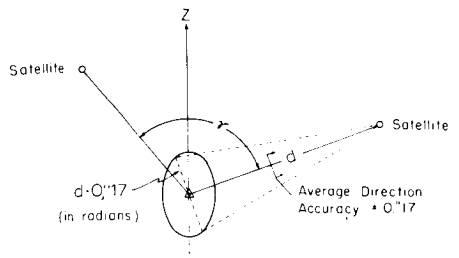

FIGURE 7.46

weight matrix associated with the coordinates of the seven fictitious satellite-images, the weight and matrix being computed from the corresponding covariance matrix derived with equation (7.277) of section 7.4.6. In section 7.4.8.1 it was mentioned that, in the mathematical formulation to be set up for the final triangulation, only the satellite and station positions were to be determined as unknowns. The basic triangulation geometry (fig. 7.14) implies that the accuracy of the triangulation in a direction perpendicular to the direction station-satellite is proportional to both the directional accuracy and the distance station-satellite. This is indicated schematically and reduced to two dimensions in figure 7.46.

The accuracy in direction of the z coordinate is obviously a function of the angle γ in which the station-satellite planes intersect. From analysis of the systems of inverted normal equations, which contain the geometry of the actual satellite observations, it follows, quite generally, that the mean error of the triangulated station in the direction of the geodetic latitude and longitude is, assuming errorless scale, proportional to the product $m_R \cdot d$, where m_R is the mean accuracy of the direction and d is the mean distance station-satellite; on the other hand, the average mean error in the direction of height is three times as large (Schmid, 1969). These relations are shown in figure 7.47, in which $\sqrt{Q}$ is the error propagation factor (sometimes called the weight reciprocal) for the position coordinate.

The same result is shown schematically in another form in figure 7.48, from which, by comparison of antipodal stations, it is apparent that the uncertainty in height determination within a world triangulation eventually has the effect of an uncertainty in scale. One can expect, therefore, that additional scale control will have a particularly

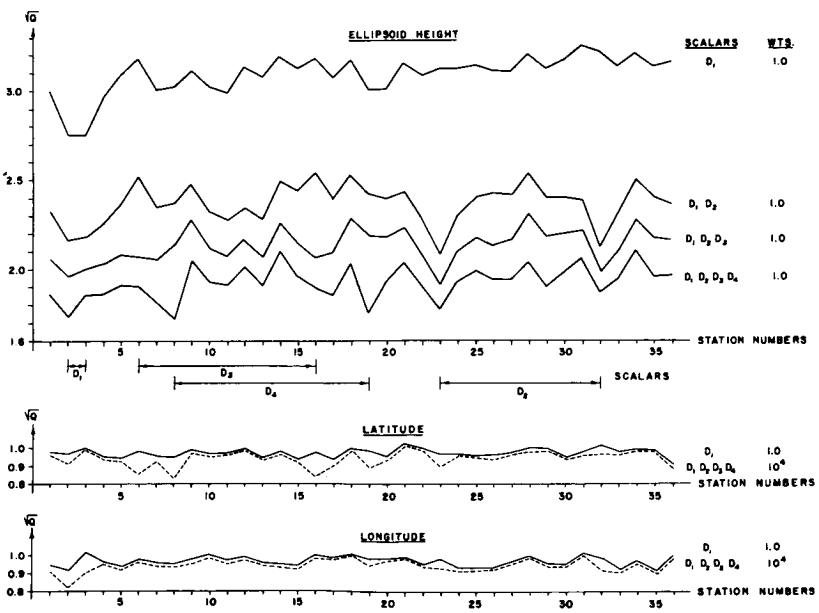

FIGURE 7.45.—Average shimmer versus latitude of observing station. using one to four scalars.

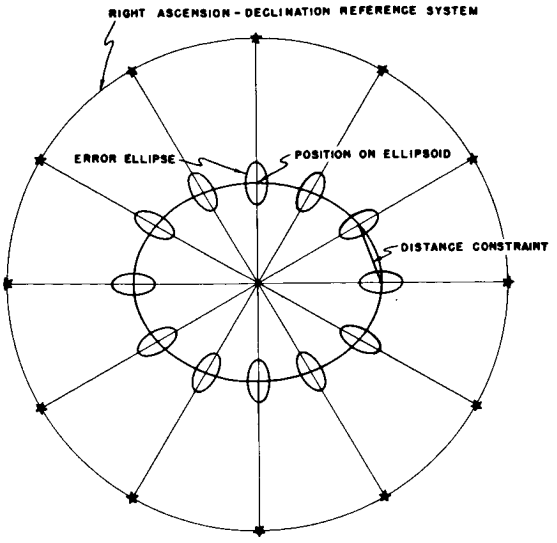

FIGURE 7.48.—Error propagation of the method of geometric satellite triangulation.

favorable influence on the accuracy of height coordinates, but will represent no real gain for the determination of the position coordinates ϕ, λ. This fact is illustrated in figure 7.47, which shows the effect of from one to four scale determinations. The lower part of figure 7.47 shows that even under the assumption of errorless scalars (weight 10^4) only the stations directly involved in the scale determination show a gain in the determination of their latitude ϕ and longitude λ. On the other hand, the error propagation coefficient for the height determination reduces from 3 to 1.8 with the use of four scalars, even when a more realistic weight of 1 is used in the scale determination (Schmid, 1969; Rinner, 1966).

In the world net, the PAGEOS satellite was observed almost exclusively. Its nominal circular orbit elevated about 4600 km above the surface of the earth resulted in an average distance station-satellite of 6000 km. With a mean direction accuracy of 0".24 and the propagation factors of figure 7.47, a triangulation solution based on two satellite transits or two events per triangle side, under the assumption of an errorless scale, produces position coordinates for the observing stations with mean errors $m_\phi = m_\lambda = \pm 7.0$ m and $m_h = \pm 21.0$ m. At this time, 2350 plates have been reduced for evaluation in the world net. The distribution of the corresponding events is shown in figures 7.6 through 7.11. These observations correspond to about five independent solutions. Therefore, adjusting all these events should yield an accuracy of $m_\phi = m_\lambda = \pm 7.0/5 = \pm 3.1$ m and $m_h = \pm 21.0/5 = \pm 9.4$ m. When the planned four scalars, measured independently with an accuracy of at least 1:1 000 000 are introduced, the expected mean error in height reduces to $m_h = \pm 3.1$ m $\times 1.8 = \pm 5.6$ m (cf. fig. 7.47) and the mean position error of a station

$$m = \pm\left(\frac{m_\phi^2 + m_\lambda^2 + m_h^2}{3}\right) = \pm 4.1 \text{ m} \qquad (7.311)$$

or m is roughly 1:1 500 000 of the mean distance station-satellite.

In the next paragraphs the result of the worldwide geometric satellite-triangulation program is presented with an associated error analysis based on the statistical information obtained during the final triangulation adjustment.

7.5 RESULTS OF THE WORLDWIDE GEOMETRIC SATELLITE TRIANGULATION [3]

7.5.1 Statement of Results

The quantitative result of the worldwide geometric satellite-triangulation program consists of the three-dimensional positions of 45 stations. Their locations can be seen from figure 7.4 and table 7.2.

The corresponding Cartesian reference coordinate system has, as was explained before, one of its axes parallel to the rotation axis of the Earth for a certain epoch (CIO). The origin of the system and the selection of

[3] NGS used a left-handed coordinate system for its x, y, z coordinates. The values in tables 7.11 and 7.15 are given in a right-handed system, to permit comparison with coordinates in other chapters. Otherwise, the system is left-handed as noted. Great care should be exercised when values from this and other sections are taken.—[Editor]

the x direction is, for reasons inherent to the method of geometric satellite triangulation, arbitrary. It was fixed by enforcing for station 2, Beltsville, Maryland, the following coordinates, which are approximate values for a geometric position:

Spatial Coordinates (m)	
1 130 761.500	x
4 830 828.597	y
3 994 704.584	z

As is discussed in the analysis of the results in the next paragraph, it was decided to enforce all eight scalars with their measured values.

Table 7.11 lists the three-dimensional Cartesian coordinates for the 45 stations and their mean errors (one-sigma level) as obtained from the final adjustment. The coordinates refer to the projective center of the BC–4 cameras. The elevation of this point above the permanent station mark is in each case +1.5 m.

7.5.2 Analysis of the Triangulation Adjustment

The input of the triangulation adjustment refers to the information obtained from the evaluation of 2350 photographic plates. Specifically, observations from 856 two-station, 194 three-station, and 14 four-station satellite events were used. The 1064 satellite events chosen for evaluation required, in addition to the determination of the spatial positions of the tracking stations, the triangulation of 6604 satellite positions. The adjustment provided for 9162 degrees of freedom. Two station-to-station couplings were introduced as additional constraints in order to tie together stations 6111–6134 (California) and 6012–6066 (Wake Island), where, for technical reasons, satellite observations were collected from neighboring observation piers. Furthermore, eight scalars were rigorously introduced. They represent the spatial distances between the stations given in table 7.3, section 7.3.0. These scalars were measured and computed by various national agencies. For references, see table 7.4.

In order to obtain a measure for the precision of the strictly photogrammetric triangulation, a first triangulation adjustment was executed with only the scalar between stations 6002–6003 enforced. This adjustment produced a sum of the squares of the weighted residuals in terms of plate coordinate corrections $[pvv] = (3.064 \pm 0.045) \times 10^{-8}\ (m^2)$.

A comparison of the measured baselines with the corresponding triangulation results provides a first insight into the internal accuracy of the geometric world net. The differences between the computed and measured distances with a complete constraint on scalar (6002–6003) are shown in table 7.12.

The sum Σd of the lengths of the measured scalars is 17 513 184 m, so that

$$\frac{\Sigma \Delta d}{\Sigma d} = 1:1\ 911\ 920$$

As can be seen from table 7.12, the difference $\Sigma \Delta d$ is only about 0.6 of the standard deviation associated with the sum of the triangulated distances.

It was therefore concluded that the scalars, at least in their totality, are probably of higher accuracy than the geometric satellite triangulation itself, a conclusion which is further evidenced when the standard errors for these scalars computed by the various computing centers are considered.

An adjustment in which all scale lines were enforced with weights corresponding to an accuracy of one part in two million of their respective lengths gave the result shown in table 7.13.

The $[pvv]$ of this adjustment was 3.068×10^{-8}, or a value which is only $0.004 + 10^{-8}$ unit larger when it is compared with the single scalar adjustment mentioned above. This difference is only $\frac{1}{10}$ of the associated sigma. It can therefore be safely concluded that the scalars do not exercise undue constraint on the triangulation system.

If all eight scalars are rigorously enforced, the $[pvv]$ sum increases to 3.071×10^{-8}, a

solution which from a statistical standpoint is equally defensible.

The numerical solution was iterated on the CDC 6600 computer (generally three times) until the maximum increments to the triangulated coordinates became <1 mm. When the normal equations matrix pertaining to the final iteration is multiplied by its corresponding inverse matrix, one obtains, as a check, the expected unit matrix to within a unit in the tenth decimal place.

The mean error of unit weight after adjustment is for all these solutions 1.830 ± 0.014, against the expectation of 1.0, indicating the presence of additional unmodeled error sources. If the increase in the overall error budget can be ascribed to additional random-error sources, then the effect is relatively harmless, resulting only in a corresponding increase in the mean errors of the triangulated station positions. But if the effect of systematic errors which are distributed in the adjustment in accordance with the least-squares principle is involved, the situation is more serious.

To gain some insight into the stability of the camera during the average half-hour period of operation, star photography taken immediately before and after the satellite transit was adjusted and sets of camera orientation parameters computed. Thus, for each plate the change in azimuth ΔA and in

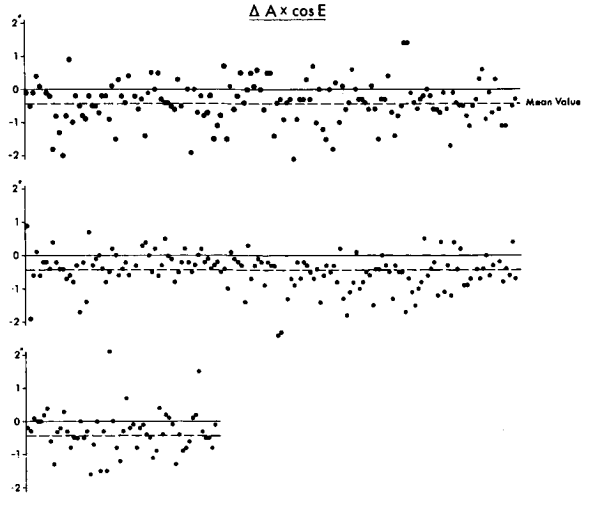

FIGURE 7.49

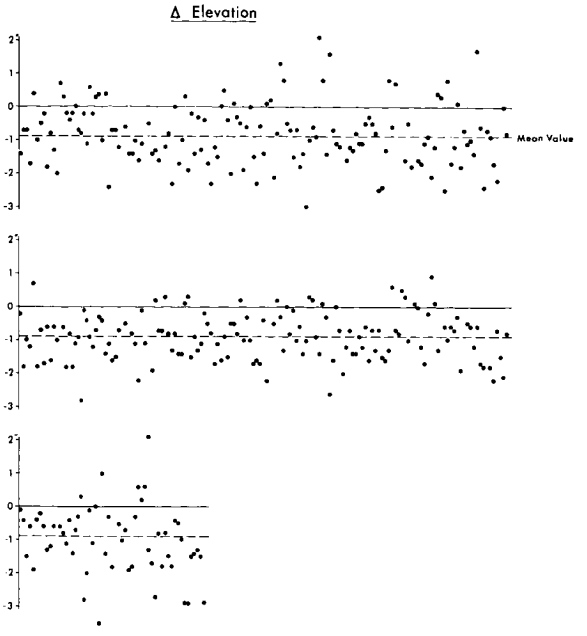

FIGURE 7.50

elevation Δh of the central ray with a corresponding rotation component Δx was computed. The Δx are random and completely within the range of their mean errors. The $\Delta A \cos h$ and, especially, the Δh component, however, indicate the influence of a systematic error, as shown in figures 7.49 and 7.50. For an evaluation of these diagrams it should be added that the individual Δ values shown have an average mean error of $\pm 0''.5$. Since star imagery is also available for the satellite transit period, it is possible to study these systematic changes in orientation over the period of observation. A roughly linear trend with time is indicated.

To eliminate this source of error, orientation parameters that were based solely on star images obtained during the period of actual satellite transit were used in the final adjustment, whenever possible. Still, we cannot entirely escape the conclusion that the instability of the camera creates an additional error which, as the diagrams show, has a systematic component and acts as a source of additional accidental errors.

For a further analysis of the results it is important to realize that, as consequence of

the interpolation of each event into the astronomic system, absolute directions are obtained. This means that it is possible to triangulate the direction of the chord joining two adjacent stations in the net independently, i.e., with only the satellite passes observed from these two stations. Such computations were made for all 170 lines of the world net. In these adjustments, as well as in the final solution, all covariance matrices resulting from the individual processing steps were included, so that all results can be considered as rigorously derived values. The line triangulations yield an average mean value for the ratio of mean error of unit weight before and after adjustment of 1:1.746, the range being from 1:0.706 to 1:2.429. The theoretical expected average value is, of course, 1:1. This means that the observational data do not completely fill the accuracy expectations computed in the partial analyses cited above, a fact which was mentioned in connection with the obtained mean error of unit weight after adjustment in the final triangulation.

However, it is gratifying to note that this value increases only slightly, from 1.746 for the average of all individual line adjustments, to 1.830 for an adjustment based on the combination of all observations. These figures indicate that the entire body of data is apparently free of perturbing systematic errors and satisfies with practically no constraint the three-dimensional geometrical closure condition of the world net.

In order to strengthen this conclusion, the directions derived from the individual line adjustments and those of the combined solution were compared. The resulting azimuth and elevation angle differences are shown in the diagrams with their three-sigma errors and combined in histograms of figures 7.51 and 7.52. Although these results do not fully meet ideal statistical expectations, it is not really possible to otherwise draw any conclusions regarding the presence of possible systematic error influences in the triangulations of the individual lines.

In order to analyze the accuracy of the shutter synchronization, the following argu-

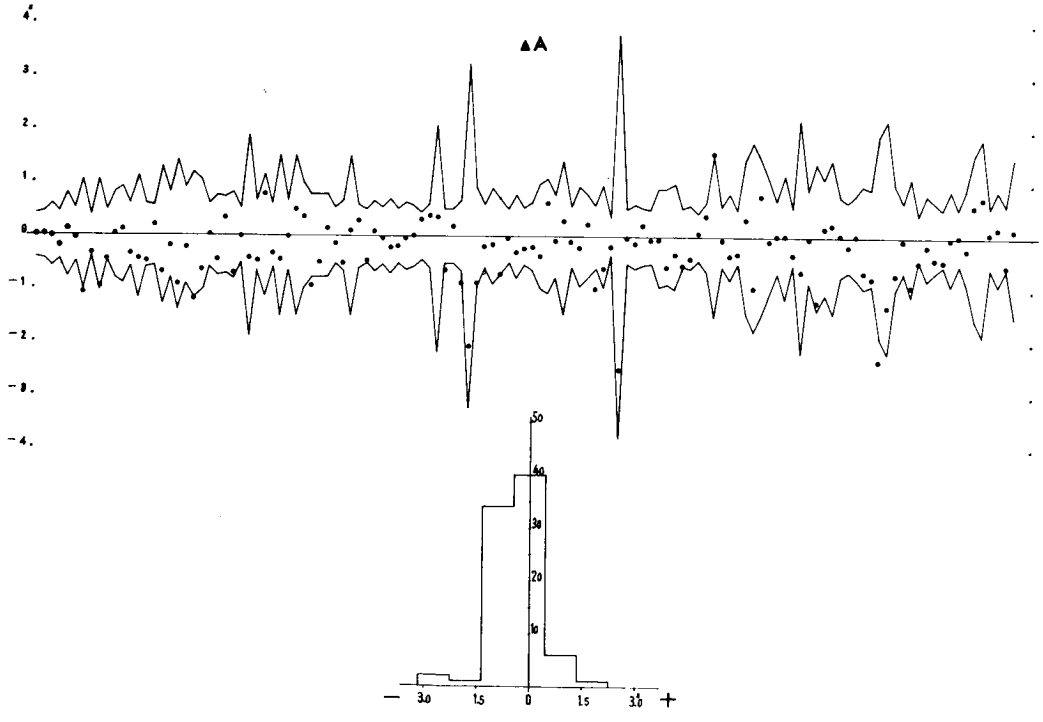

FIGURE 7.51

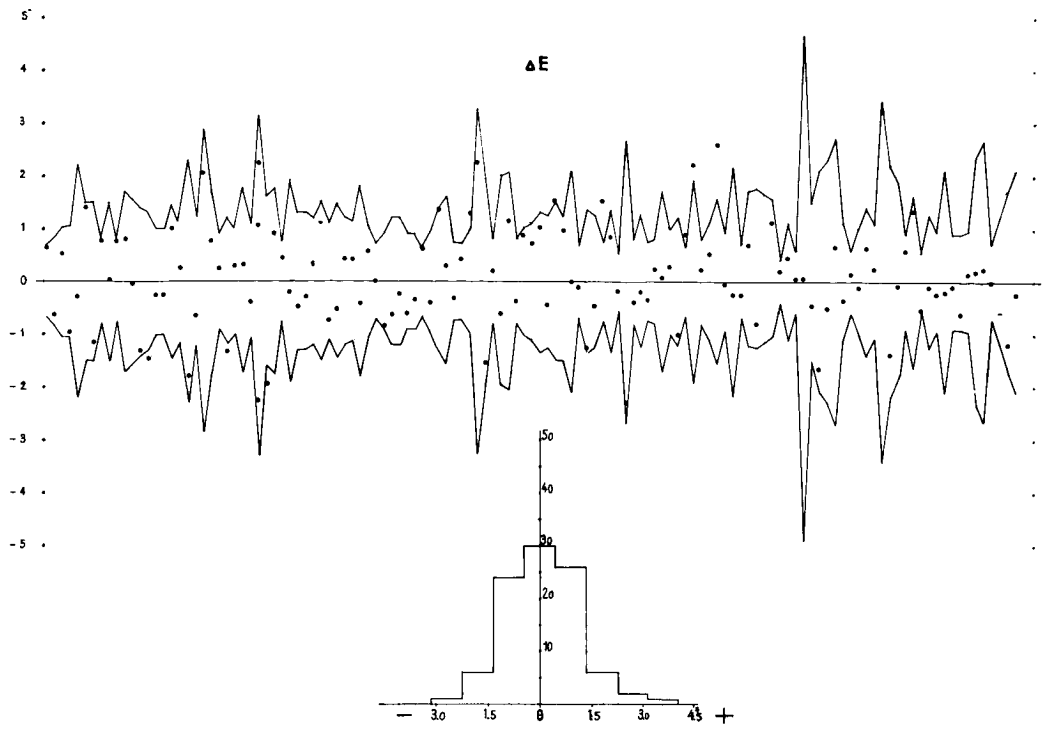

FIGURE 7.52

ment can be applied to the results of the individual line adjustments. Simple geometric considerations suggest that synchronization discrepancies will lead to larger residual errors in the spatial triangulation the larger the angle between the orbital plane of the satellite and the line to be triangulated. Because the PAGEOS satellite has an approximately polar orbit, it is sufficient to plot the mean error of unit weight after adjustment for the individual line adjustments versus the azimuth (respectively, azimuth—180 degrees) of the triangulated line. As figure 7.53 shows, the distribution of these values is circular, and no dependence on azimuth can be detected. This test at least does not indicate the influence of any synchronization errors.

An examination of the statistical distribution of the 29 104 residuals in the overall adjustment presents a further and obviously necessary opportunity to analyze the data. Figures 7.54 and 7.55 are histograms of the residuals in events that were observed from two and three stations, respectively. In order to compare these distributions with their theoretical normal-distribution curves, the residuals would have to be normalized, requiring the computation of the covariance matrix:

$$\Sigma_v = \Sigma_\epsilon - AN^{-1}A^*\sigma_0^2 \qquad (7.312)$$

This is, in the present case, a 29 104 × 29 104 completely filled, square matrix, an obvious impossibility. As a result, we are forced to neglect the geometric content of the second term of the expression (7.312) and to normalize the residuals v approximately by dividing each by the mean error of the corresponding observation before adjustment. The greater the number of observations available for the determination of the position of the satellites or, in other words, the greater the number of stations observing the satellite, the more acceptable is the proposed approximation for the normalization of the residuals. This may explain, at least in part, the fact

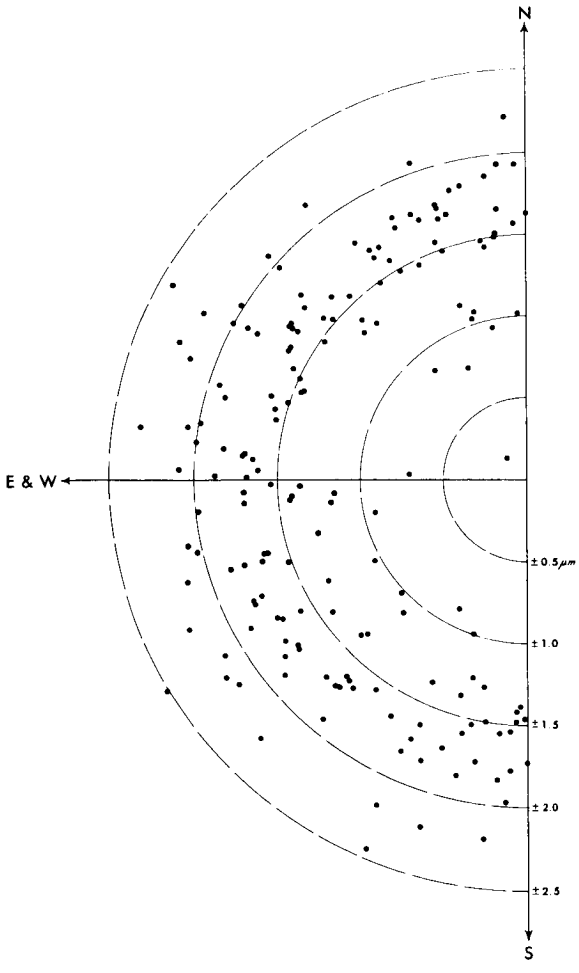

FIGURE 7.53.—Event σ's versus line azimuths.

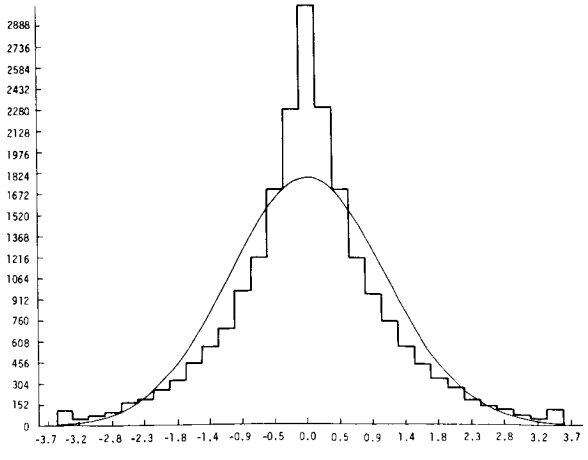

FIGURE 7.54.—Plate coordinate residuals for two-plate events. $X+Y$ values.

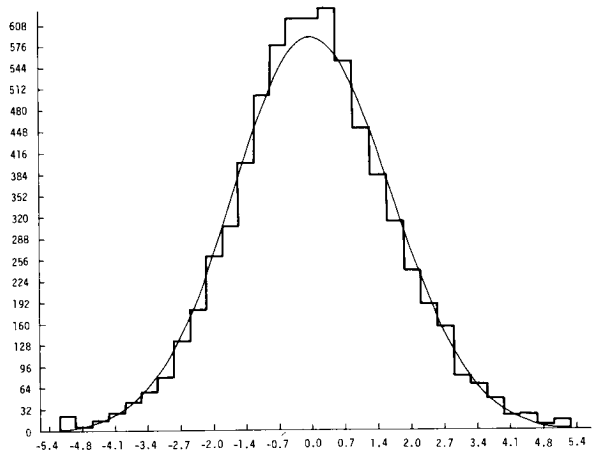

FIGURE 7.55.—Plate coordinate residuals for three-plate events. $X+Y$ values.

that the fit of the normal curve to the histogram is better for the three-station events.

If one accepts the mean error of unit weight after adjustment as a significant measure for the inherent observational accuracy, we have mean coordinate errors for the triangulated stations as shown in figure 7.56. It should be noted that although, qualitatively, the material at all stations is uniform, the quantity varies somewhat, resulting in the variations of the coordinate errors.

7.5.3 A Combination Solution

Based on the principles of celestial mechanics, the interpretation of the orbital parameters of satellites as derived from time-correlated observations permits not only the determination of the parameters of a mathematical model of the Earth's gravitational field, but also the three-dimensional positions of the satellite-observing stations within a framework of coordinates referred to the Earth's mass center.

Satellite triangulation, on the other hand, is a measuring method in which the three-dimensional positions of a number of points on the Earth's surface are established by purely geometric means.

Quite generally, satellite triangulation produces coordinates for the camera stations which should, in principle, agree, except for

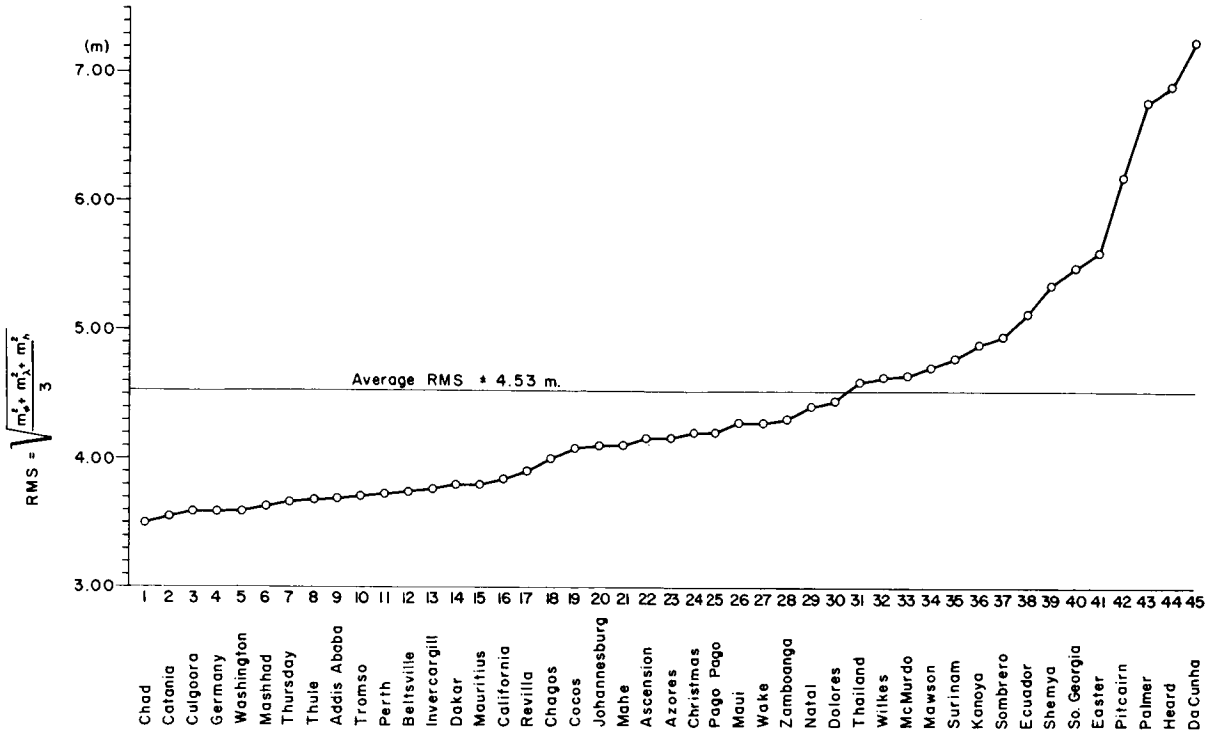

FIGURE 7.56.—Mean coordinate errors for triangulated stations.

a translation, with the corresponding results from dynamic satellite geodesy, even though the methods are completely different in conceptual approach. This difference extends as well to the determination of scale, which in geometric satellite triangulation is established by measuring the length of at least one side in the net by space traverse. In dynamic satellite geodesy the scale is determined from the physical quantity *GM* (gravitational constant × mass of the earth).

The fundamental differences of the two methods provide the logical justification for the establishment of a worldwide geodetic system using both approaches, the method of dynamic satellite geodesy and the method of geometric satellite triangulation. The basic equivalence of the results with respect to spatial coordination of the observation stations suggests a comparison and combination of such solutions.

R. J. Anderle of the Naval Weapons Laboratory, Dahlgren, kindly furnished the National Geodetic Survey a list of three-dimensional coordinates of 37 stations resulting from a dynamic solution and referred to the mass center of the Earth as origin. These stations are located in close vicinity to BC–4 stations, with the exception of five stations that are somewhat farther away. In each case, the relative positions of the two neighboring stations were determined by a local survey tie. In order to make a valid comparison of the two solutions, it is first necessary to translate the BC–4 coordinate system, which has an arbitrary origin, into the origin of the dynamic solution, the mass center, and to rotate the Doppler result about its z axis in order to make the two systems compatible with respect to longitude. However, in the comparison adjustment, two further rotations and a scale factor were modeled. These additional rotations give an indication to what extent the orientations of the conventional, pole-referenced rotation axes differ in the dynamic and the geometric solutions. Similarly, the scale factor reveals the difference in scale, which, as was pointed out

before, is derived in the one case from the product GM and in the other from the measured terrestrial baselines. The seven transformation parameters (three translations, three rotations, and a scale factor) were computed subject to a minimum condition on the sum of squares of residual coordinate differences, (in the following referred to as xyz fit).

The resulting mean-discrepancy vector is 14.4 m, a value which is influenced by discrepancies larger than 20 in five stations, as can be seen from the tabulation of the discrepancy vectors in table 7.14. Anderle gives for the precision of his positions the standard deviations $\sigma_\phi = \pm 1.5$ m, $\sigma_\lambda = \pm 1.2$ m, and $\sigma_h = \pm 1.6$ m, resulting in a station rms of $+1.44$ m. Together with the average standard deviation of the BC–4 system for these stations, neglecting for this cursory consideration the influence of the standard errors of the transformation parameters, the expectation for a mean discrepancy vector is ± 4.35 m.

The difference between the actually obtained mean discrepancy vector of ± 14.4 m and the statistically expected value of ± 4.35 m shows that the two systems are not quite compatible within the range of their standard deviations.

We cite now the transformation parameters obtained in this adjustment.

Translation of BC–4 result into mass center (BC–4 + Δ = mass centered BC–4 result):

$\Delta x = +19.590$	$\Delta y = +17.684$	$\Delta z = -14.344$
± 1.342	± 1.325	± 1.506

Rotations of Doppler data to conform to translated BC–4 results (left-handed system):

x to y	z to y	z to x
$+0''.6135$	$+0''.1478$	$+0''.0638$
$\pm 0''.0451$	$\pm 0''.0572$	$\pm 0''.0563$

Scale factor to be applied to original Doppler data to conform to BC–4 system scale:

$$s = 0.999\ 997\ 723\ 0 \pm 0.000\ 000\ 247\ 6$$

An adjustment with three scale factors, which was also executed:

$$s_x = 0.999\ 997\ 389\ 3 \pm 0.000\ 000\ 356\ 0$$
$$s_y = 0.999\ 997\ 092\ 3 \pm 0.000\ 000\ 369\ 2$$
$$s_z = 0.999\ 998\ 972\ 0 \pm 0.000\ 000\ 439\ 7$$

The translation and rotation parameters were essentially the same as those obtained before.

As can be seen, the scale parameters in x and y agree with each other within the range of their standard deviations. The z scalar shows a significant deviation, which, however, reduces the average discrepancy vector after the xyz fit by only 0.9 m. Therefore the following results were based on the solution which features only one scale factor. For this solution, table 7.14 gives the remaining coordinate differences between the BC–4 system (table 7.11) plus the translation parameters and the rotated and scaled Doppler system given above. With the coordinate differences given in table 7.14 and the translations and rotations given before, it is a straightforward matter to compute backward, from the BC–4 result (table 7.11), the Doppler station data originally given. The translated BC–4 system itself represents the strictly geometric result referred to the mass center of the dynamic solutions.

The problem for a combined solution is now to average the coordinate values as obtained for the translated BC–4 system and the rotated and scaled Doppler system. In recognition that the two transformed systems differ, as expressed by a rms discrepancy vector of 14.4 m, more than three times the amount expected from the individual solution accuracy statements, a combination solution becomes a question of the weight ratio between the two solutions. To shed light on this question, the geometric satellite triangulation system was adjusted several times, introducing as constraints the transformed Doppler position coordinates for the given 37 stations with various weights. The critical evaluation of these adjustments was made in relation to the individually obtained sum of squares of the weighted residuals for

the geometric solution, a quantity which, because of its straightforward meaning, is believed to be a quite reliable indicator. Figure 7.57 shows the sum of the *pvv*'s versus the various weight assumptions made for the Doppler results covering a range from ± 0.1 to ± 5.0 m for each of the given Doppler-derived coordinates. On the left side is given the *pvv* sum as obtained from the strictly geometric solution (without any Doppler station constraint) for the one- and eight-scalar solutions mentioned earlier. The dotted line indicates the standard deviation associated with the *pvv* sum.

From the [*pvv*] curve, one can see, as was to be expected, that an essentially rigorous enforcement of the Doppler result (standard deviation of ± 0.1 m) increases the [*pvv*] drastically; in other words, the integrity of the geometric triangulation is impaired. On the other hand, a weighting in accordance with a standard deviation of ± 5 m results in a *pvv* sum identical to the one obtained from a strictly geometric adjustment using the eight scale lines as constraints.

It is now unquestionably a decision of personal preference which weighting factor for the dynamic solution to accept as defensible for a combination result, at least in the range from ± 2.5 to ± 4.0 m. On the other hand, the resulting differences in the mean station coordinate-discrepancy vectors between these two solutions are rather small, amounting in latitude to 1.5 m, in longitude to 1.2 m, and in height to 1.6 m. In order to keep the increase in the [*pvv*] small, in comparison with the strictly geometric solution, a weighting in accordance with a standard deviation of ± 3.5 m for all Doppler coordinates was adopted. The solution was further constrained by the scalars, all weighted in accordance with a standard deviation of 1 part in 2 million. Table 7.15 gives the result of this adjustment and the associated standard deviations for the triangulated coordinates. Tables 7.16 and 7.17 show coordinate differences between the combined solution and the BC–4 and Doppler solutions, respectively.

The mean error of unit weight after adjustment is 1.830 ± 0.13 μm, the same as that for the purely geometric solution.

A comparison between the two sets of 29 104 residual errors from the purely geometric adjustment and the adjustment enforcing the Doppler results was made. These Δv values have a mean of 0.001 μm. Their distribution is shown in figure 7.58. The maximum values encountered are -0.587 μm and $+0.451$ μm.

As a byproduct, the standard deviation for each event is computed in each triangulation adjustment. A comparison of these standard deviations between the purely geometric and the combined solution shows that the range

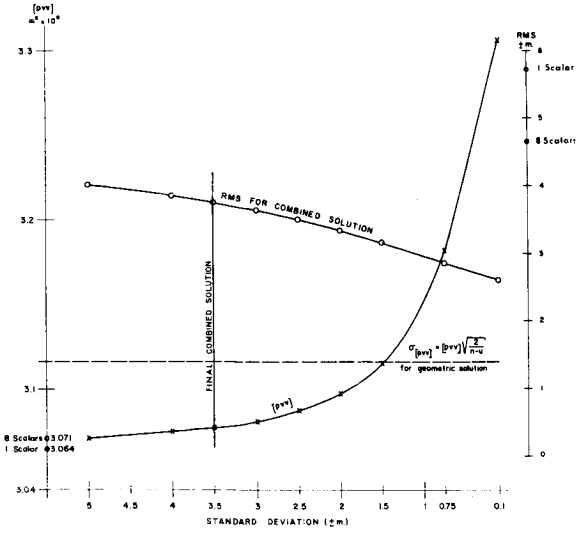

FIGURE 7.57.—Rationale for combined solution.

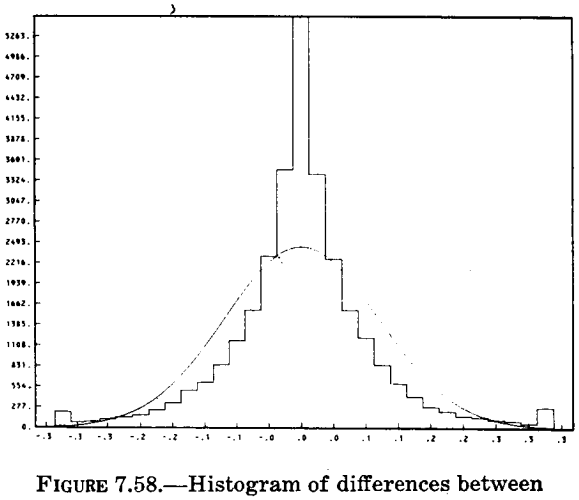

FIGURE 7.58.—Histogram of differences between two sets of residuals.

for these values in the geometric solution is from ± 0.281 μm to ± 3.462 μm and for the combined solution from ± 0.251 μm to ± 3.468 μm. The distribution of the differences of those values, which have a mean of -0.002 μm, is shown in figure 7.59.

This statistical information is presented to give evidence that in the combined solution no undue strain on the observational data of the geometric satellite triangulation is present.

7.5.4 Derived Geodetic Parameters

The semimajor axis a and the flattening f of a reference ellipsoid may be regarded as the basic parameters for a geodetic world system, its center coinciding with the Earth's center of mass. The direction of the z axis, i.e., the Earth's rotation axis, is fixed by the conventionally adopted mean pole position at a specified epoch and the direction of the x axis through the null meridian by an identifiable point on the surface of the earth. It is also possible, although hardly practical, to postulate a triaxial ellipsoid.

With the establishment of such a reference system, the xyz coordinates of the combined solution as given in table 7.15 can be transformed into latitude, longitude, and ellipsoid height. Furthermore, classical geodetic results referred to individual datum ellipsoids can be transformed to such a world system.

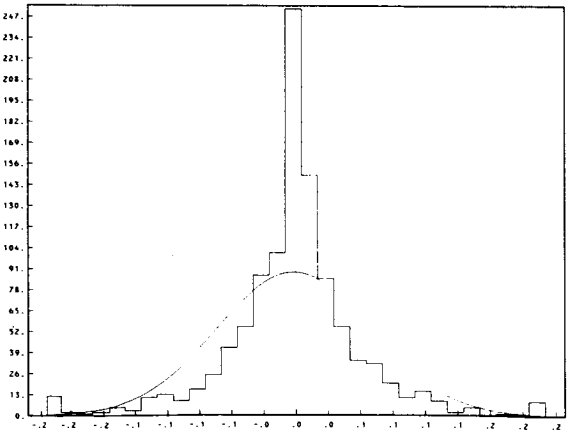

FIGURE 7.59.—Histogram of differences between two sets of event mean errors.

Using the values presented for the determination of these quantities, we arrive at the following results.

To begin with, the station coordinates obtained in the geometric satellite triangulation solution (table 7.11), reduced to sea level, were adjusted to a best-fitting ellipsoid of revolution. The significance of such a solution is somewhat dubious, in view of the fact that only 43 stations for which leveling heights were obtained are available, and that there is no a priori evidence that the mean of the corresponding geoid heights is close to zero. The result is shown in the first row of table 7.18 [left-handed coordinate system—Editor]. The resulting translations Δx, Δy, Δz on line 1, as well as those shown on lines 2, 6, 7, and 11 for other solutions, are not significant in themselves, because they depend entirely on the approximation values for the mass-centered coordinates, introduced for the origin of the geometric solution (compare beginning of sec. 7.5.1). Only their consistency in the various solutions is of interest.

The second solution is a repetition of the first, with the flattening $f=1/298.250$ held fixed, a value which is derived by dynamic satellite-geodesy methods and is now considered to be reliable. This result is on the second line. Furthermore, ellipsoid fits were executed with the results of the combined solution resembling otherwise the solutions presented on lines 1 and 2. These results are given on lines 3 and 4, respectively. Here, as on lines 8 and 9, the Δx, Δy, Δz indicate to what extent the coordinate origin of the specific solution differs from the mass center of the dynamic solution. Still another computation was performed with the combined solution holding the original position of Anderle's mass-center fixed. In this solution, only the semimajor axis a was determined. This result is shown on line 5. With the same raw material these ellipsoid-fit solutions were repeated, incorporating the geoid heights as computed from raw data from Anderle. The corresponding results are shown on lines 6 to 10. On the eleventh line the result of the station-to-station least-

squares fit is shown, based on the matching of the positions of 37 stations as determined by the geometric and the dynamic methods.

From the information presented in table 7.18 it was concluded that a reference ellipsoid with $1/f=298.250$ and a semimajor axis of 6 378 130 m would correspond best to the available information.

Table 7.19 gives the corresponding latitude, longitude (east), and ellipsoid heights with their respective standard deviations computed from the *xyz* coordinates of the combined solution (table 7.15).

In table 7.2, section 7.3, the survey data are given. A comparison of the results presented in table 7.19 with the results of astronomical position observations and the values of mean sea level observations, as given with the survey data, allows the computation of plumbline deflections and the determination of geoid heights. The corresponding results are tabulated in tables 7.20 and 7.21.

The $\Delta\lambda$ values in table 7.20 refer, in accordance with the given geographic coordinates in table 7.19, to a system of positive east longitudes, with the conventional designation: astro-geodetic $=\Delta$. The $\Delta\phi$ values represent absolute position deflections in the meridian of the station, positive to the south. The computed η values, positive to the east, however, depend quantatively on the chosen position of the null meridian of the combined solution. In order to average them out, an additional rotation in longitude would be necessary, which would have to be added as a constant to all longitudes tabulated in table 7.19.

Such a correction amounts to

$$\Delta\lambda=\frac{\sum_{i}^{i}(\lambda_A-\lambda_G)_i\cos\phi_i}{\sum_{i}^{i}\cos\phi_i}$$
$$=-0''.485 \text{ (east longitudes positive)} \qquad (7.313)$$

The significance of such a correction is, however, impaired by the relatively small number of plumbline deflections available.

Table 7.21 gives the geoid heights as computed from the combined solution (table 7.19) and the msl elevations of the survey data. For comparison, the geoid heights as obtained by Anderle from the dynamic solution are given in the second column and the corresponding differences in the third column, labeled ΔN.

With the exception of stations 6011 (Hawaii), 6012 (Wake), 6013 (Japan), and 6043 (Sombrero), these Δ values are well within the expected level of accuracy. Obviously, both sets of N values are also affected by the uncertainties in mean sea level for the various datums, to which the leveling data are referred.

A comparison between the *xyz* coordinates given in table 7.15 and the corresponding information computed from the survey data (table 7.2) results in the translations Δx, Δy, Δz. These translations transform, station by station, the survey data into a mass-centered system.

Table 7.22 shows these results, the stations grouped in terms of specific datums. Large differences in these translations for stations within a specific datum suggest distortions in such a datum.

In column N of table 7.22, the geoid height used for the computation of the station shift components is given. At stations where such information was not available from the collected survey data, the corresponding geoid heights from the combined solution (table 7.21) were used, indicated by an asterisk.

Furthermore, a set of station shift components was computed on the basis of astronomical positions of the BC–4 stations when no other survey data were available. Here again, the computations were based on geoid heights obtained from the combined solution; furthermore, an ellipsoid with $f=1:298.25$ and an equatorial radius of 6 378 130 m were used. The resulting Δx, Δy, and Δz of shifts [left-handed coordinate system—Editor] express therefore only the plumbline deflections tabulated in table 7.20.

For datums for which more than one station is available, datum shift parameters were computed, allowing for an additional scale factor and an additional rotation (in longitude) in addition to the conventional

three translations. These results are shown in table 7.23 [left-handed coordinate system —Editor]. The smaller the indicated coordinate differences, after datum shift, the more closely the survey result resembles the relative geometry as determined by satellite triangulation.

Because of the small number of stations belonging to a specific datum, it was not possible to compute meaningful datum shifts allowing an adjustment in the spatial orientation of the rotation axis of the individual datum ellipsoids, as desirable as such a test would be from the theoretical standpoint. Such a complete set of datum shift parameters will be computed for the NAD, when the results of the satellite densification program in the area of the North American continent are completed.

7.6 SUMMARY AND CONCLUSIONS

The BC–4 world net is the result of a strictly three-dimensional geometric triangulation, including a scale derived from classic geodetic surface measurements executed between several pairs of world net stations. Because the method of geometric satellite triangulation is based on absolute directions as obtained by interpolating the satellite position into the background of the surrounding field of fixed stars, the triangulation results can at best be only as accurate as the astronomical system of right ascension-declination itself. This situation holds for both the relative accuracy of the reference stars and the absolute accuracy of the astronomical reference system in its entirety. The photogrammetric triangulation, as a result of the high redundancy of data, should provide a result valid to about 1 part in 2 million in terms of the average station to satellite distance, in other words, station positions with an accuracy of ± 3 to ± 4 m in all three coordinates. The statistical information obtained as a by-product of the various data reduction steps indicates that the accuracy of the final result does not entirely fulfill the theoretical accuracy expectations. The statistically proven instability of the BC–4 camera system must be considered as a possible source of a slight systematic error, which in the adjustment algorithm is unavoidably distributed in accordance with the minimum principle for residual errors. The good agreement of the photogrammetric triangulation result with the measured baselines around the world indicates, however, that the final result is essentially free of significant bias errors. A comparison between the result of the geometric triangulation and the corresponding result obtained by dynamic satellite geodesy from Doppler data, as computed by the Navy, shows excellent agreement in an overall sense, but significant discrepancies in a few places on the globe. A combination of both results that respects fully the covariance of the photogrammetrically derived directions becomes possible by assuming a weighting of the dynamically determined coordinates in accordance with a station position mean error of ± 3.5 m. The only significant difference between the Navy-8D dynamically determined result and the geometric triangulation is in terms of scale, indicating that the dynamic solution is based on a scale larger by 2 parts in a million. The geometric solution suggests a value of 6 378 130 m for the equatorial radius a of a best-fitting ellipsoid.

APPENDIX

TABLE 7.1

Images per second	Shutter speed (100% efficiency) (sec)	Optimal subdivision with third shutter	Accuracy of timing (10^{-6} sec)
20	1/120	:2, :3, :4, :5	±20
10	1/60		±40
5	1/30		±60
2.5	1/15		±70

TABLE 7.2.—*Survey Coordinates of BC-4 Stations*

BC-4 sta. no.	Station name	Geodetic coordinates ϕ_G	Geodetic coordinates λ_G (west)	Astronomic coordinates ϕ_A	Astronomic coordinates λ_A (west)	Elev. of ref. pt. above MSL (m)	N (m)	Datum	Ellipsoid
6001	Thule	76°30′05″.3226N	68°32′33″.1709	76°30′11″.67N	68°32′48″.91	206.0	+32.0	QORNOQ	Int'l.
6002	Beltsville	39°01′39″.003N	76°49′33″.058	39°01′37″.73N	76°49′24″.65	44.3	−0.4	NAD 1927	Clarke 1866
6003	Moses Lake	47°11′07″.1324N	119°20′11″.8815	47°11′03″.24N	119°20′17″.05	368.74	−16.0	NAD 1927	Clarke 1866
6004	Shemya	52°42′54″.8940N	185°52′22″.1299	52°43′03″.48N	185°52′15″.08	36.76	−46.0	NAD 1927	Clarke 1866
6006	Tromso	69°39′44″.2901N	341°03′27″.6743	69°39′43″.24N	341°03′12″.96	106.0	+12.6	European	Int'l.
6007	Azores	38°45′36″.7250N	27°05′38″.9360	38°45′43″.28N	27°05′24″.59	53.26	----------	S. W. Base	Int'l.
6008	Surinam	05°27′04″.9824N	55°12′13″.9921	05°26′48″.96N	55°12′21″.21	18.38	+3.0	Prov. S.A. 1956	Int'l.
6009	Quito	00°05′50″.4680S	78°25′10″.7875	00°05′53″.09S	78°25′03″.09	2682.1	+24.6	S.A.D. 1969	S.A.
6011	Maui	20°42′38″.5610N	156°15′31″.4711	20°42′21″.86N	156°15′22″.95	3049.27	----------	Old Hawaiian	Clarke 1866
6012	Wake	19°17′23″.2275N	193°23′20″.2197	19°17′24″.40N	193°23′34″.82	3.46	----------	1952 Astro	Int'l.
6013	Kanoya	31°23′30″.13971N	229°07′35″.14051	31°23′38″.48N	229°07′34″.29	65.90	+27.0	Tokyo	Bessel.
6015	Mashad	36°14′29″.5269N	300°22′17″.2712	36°14′27″.82N	300°21′59″.20	991.05	−38.0	Europe 1950	Int'l.
6016	Catania	37°26′42″.3451N	344°57′12″.3041	37°26′38″.70N	344°56′56″.81	9.00	−16.6	European	Int'l.
6019	Villa Dolores	31°56′33″.9540S	65°06′18″.658	----------	----------	608.18	+13.0	S.A.D. 1969	S.A.
6020	Easter Isl.	27°10′39″.2132S	109°25′42″.5051	27°10′39″.21S	109°25′42″.51	230.8	----------	1967 Astro.	Int'l.
6022	Pago Pago	14°20′12″.216S	170°42′46″.758	14°20′08″.34S	170°42′52″.15	5.34	+22.0	Am. Samoa 1962	Clarke 1866
6023	Thursday Isl.	10°35′08″.0374S	217°47′24″.5045	10°35′06″.78S	217°47′25″.11	59.6	−4.6	AND	AND
6031	Invercargill	46°25′03″.4908S	191°40′28″.8448	46°25′01″.05S	191°40′25″.10	0.95	----------	Geodetic 1949	Int'l.
6032	Perth	31°50′28″.9922S	244°01′33″.3824	31°50′24″.57S	244°01′56″.28	26.30	+15.4	AND	AND
6038	Revilla	18°43′44″.93N	110°57′20″.72	18°43′44″.93N	110°57′20″.72	23.20	----------	Is. Soc. Astro.	Clarke 1866
6039	Pitcairn	25°04′07″.1461S	130°06′48″.1184	25°04′07″.15S	130°06′48″.12	339.39	----------	1967 Pitcairn Astro.	Int'l.
6040	Cocos	----------	----------	12°11′57″.91S	263°10′12″.92	4.41	----------	1965 Anna 1 Astro	AND
6042	Addis Ababa	08°46′08″.5013N	321°00′10″.8355	08°46′05″.74N	321°00′02″.81	1886.46	−8.0	Adindan	Clarke 1880
6043	Cerro Sombrero	52°46′52″.4683S	69°13′30″.4273	52°46′50″.74S	69°13′33″.56	80.66	----------	1963 Prov. South Chile	Int'l.
6044	Heard Isl.	----------	----------	53°01′12″.0309S	286°36′32″.5846	3.771	----------	1969 Astro	Int'l.
6045	Mauritius	20°13′41″.942S	302°34′52″.339	20°13′37″.48S	302°35′07″.20	138.2	----------	Le Ponce Astro	Clarke 1880
6047	Zamboanga	06°55′26″.132N	237°55′55″.162	06°55′18″.29N	237°55′53″.55	9.391	----------	Luzon	Clarke 1886
6050	Palmer	----------	----------	64°46′33″.98S	64°03′22″.96	16.44	----------	1969 Palmer Astro	Clarke 1880
6051	Mawson	----------	----------	67°36′03″.08S	297°07′35″.59	11.3	----------	1969 Astro	
6052	Wilkes (Casey)	----------	----------	66°16′45″.12S	249°27′55″.39	18.0	----------	1969 Astro	
6053	McMurdo	77°50′46″.2487S	193°21′52″.4155	77°50′43″.32S	193°21′46″.14	19.09	----------	Camp Area Astro 1961-62 USGS	Int'l.
6055	Ascension	07°58′16″.6342S	14°24′27″.2363	07°58′18″.27S	14°24′30″.36	70.94	----------	Ascension Is. 1958	Int'l.
6059	Christmas Isl.	----------	----------	02°00′35″.622N	157°24′38″.038	2.75	----------	Christmas Is. 1967 Astro	Int'l.
6060	Culgoora	30°18′39″.4182S	210°26′23″.1079	30°18′36″.14S	210°26′28″.89	211.1	+0.7	AND	AND
6061	So. Georgia Isl.	----------	----------	54°16′39″.5147S	36°29′17″.4690	4.180	----------	Astro	Int'l.
6063	Dakar	14°44′39″.8986N	17°28′57″.5476	14°44′44″.23N	17°29′04″.41	26.28	+20.7	Adindan	Clarke 1880
6064	Ft. Lamy	12°07′51″.7410N	344°57′53″.7659	12°07′53″.939N	344°57′51″.044	295.41	+23.6	Adindan	Clarke 1880
6065	Hohenpeissenb.	47°48′07″.009N	348°58′31″.4263	47°48′09″.54N	348°58′29″.47	943.50	−0.6	European	Int'l.
6067	Natal	05°55′37″.4136S	35°09′53″.8003	05°55′37″.74S	35°09′57″.03	40.63	+26.14	S.A. 1969	S.A.
6068	Johannesburg	25°52′56″.98S	332°17′34″.83	25°52′50″.06S	332°17′28″.82	1523.8	----------	Buffelsfont	Clarke 1880
6069	Tristan	----------	----------	37°03′26″.2572S	12°19′06″.4452	24.83	----------	1968 Astro	Int'l.
6072	Chieng Mai	18°46′06″.149N	261°01′44″.877	18°45′47″.50N	261°01′51″.62	308.4	----------	Indian	Everest
6073	Diego Garcia	07°20′58″.5270S	287°31′27″.8444	7°20′58″.53S	287°31′27″.84	3.85	----------	I.S.T.S. 1969 Astro	Int'l.
6075	Mahé	04°40′11″.614S	304°31′06″.617	4°40′10″.31S	304°31′06″.02	588.98	----------	Mahé 1971	Clarke 1880
6111	Wrightwood	34°22′54″.5368N	117°40′50″.5161	34°23′00″.80N	117°40′35″.38	2284.41	−23.0	NAD 1927	Clarke 1866

TABLE 7.3.—*Baselines Used in Adjustment*

Stations between which scalars were measured	Spatial distances (m)	σ_d (m)
6002–6003	3 485 363.232	±3.53
6003–6111	1 425 876.452	±1.59
6006–6065	2 457 765.810	±0.80
6065–6016	1 194 793.601	±1.43
[a]6006–6016	3 545 871.454	±1.64
6023–6060	2 300 209.803	±0.88
6032–6060	3 163 623.866	±0.98
6063–6064	3 485 550.755	±2.10

[a] The scalar 6006–6016 is not a truly independent scalar.

TABLE 7.4.—*Documentation*[a]

Scalar between stations[b]	Measured by:	Computed by:	Documentation
002–003 and 003–111	National Geodetic Survey (USA)	National Geodetic Survey Triangulation Branch (USA)	Office memos from NGS Triangulation Br. to Geodetic Research & Development Lab. for 002–003—B. K. Meade dated 3/29/71, for 003–111 John G. Gergen dated 8/5/73.
006–065 065–016 006–016	Geodetic Agencies of Norway Sweden Denmark Federal German Republic Austria Italy	National Geodetic Survey (USA) Triangulation Branch	Office memo from NGS Triangulation Br. to GRDL—B. K. Meade dated 4/9/70. Office memo from NGS, New Datum Br. to GRDL—John G. Gergen dated 8/5/73. Further reference literature, the results of which were not used here: Computation of the European Baseline Tromsø-Catania by R. Kube and K. Schnädelbach, Deutsches Geodätisches Forschungsinstitut, München (1973).
023–060 032–060	Dept. of National Development Div. of National Mapping, Australia	Division of National Mapping, Australia	Dept. of National Development, Div. of National Mapping, Australia Technical Report No. 11 by K. Leppert, Canberra, Australia, March 1972, entitled "Two Australian Baselines for the Pageos World Triangulation."
063–064	Dept. of Defense, Defense Mapping Agency and Institute Geographique Nationale (France)	Dept. of Army Commanding Officer US Army Engineer Topographic Production Center Code 14400 Army Topographic Stations Wash., DC 20315	Transmittal letters to Dr. H. H. Schmid, GRDL, NGS, NOAA, Rockville, Md. 20852 USA dated June 4, 1971, and July 22, 1971.

[a] The measuring and computation of these scalars were executed by various national agencies. For reference, the above information is given.

[b] Add 6000 to station numbers.

TABLE 7.5.—*Number of Successful Observations*[a]

Station-to-station line[b]	Number of successful events		Station-to-station line[b]	Number of successful events	
	L	R		L	R
1 to 2	7	16	[c]11 to 22	1	2
3	9	18	38	13	2
4	4	2	59	21	21
6	17	15	12	4	20
7	5	1	111	15	5
[c]11	0	1			
[c]15	1	0	12 to 13	1	11
[c]16	2	1	22	2	5
[c]38	1	2	23	7	9
[c]65	3	6	59	9	2
			[c]60	1	0
2 to 3	14	19			
[c]6	1	1	[c]13 to 15	2	0
7	4	5	23	0	0
8	16	8	47	8	5
9	3	3	72	4	1
38	4	10			
111	6	11	15 to 16	31	37
			[c]40	7	3
3 to 4	0	4	42	28	15
11	7	16	[c]45	9	1
38	7	13	[c]64	2	12
[c]12	0	2	65	0	5
111	24	20	72	4	10
			73	12	7
[c]4 to 6	0	2	75	11	1
11	0	3			
13	5	5	16 to 42	5	0
12	0	8	63	0	13
			64	22	9
6 to 7	2	4	65	7	12
15	9	7			
16	9	13	19 to 20	7	2
65	5	8	43	19	30
			61	4	14
7 to 8	0	0	67	6	9
16	18	11	[c]69	0	2
[c]55	0	2			
63	23	7	20 to 38	11	2
[c]64	3	1	39	1	2
65	6	0	43	4	11
[c]67	2	2			
			22 to 23	2	3
8 to 9	7	1	31	14	4
19	7	15	39	2	5
[c]61	0	1	59	9	10
63	0	1	60	15	4
67	2	3	78	0	3
9 to 19	4	12	[c]23 to 31	2	8
20	2	3	32	19	4
38	4	6	[c]40	1	1
[c]43	2	2	47	6	3

TABLE 7.5.—*(Cont'd)*

Station-to-station line[b]	Number of successful events L	R	Station-to-station line[b]	Number of successful events L	R
[c]23 to 60	20	32	44 to 45	1	1
[c]72	0	4	51	3	4
78	6	1	52	1	1
			68	1	0
[c]31 to 32	10	10			
39	3	0	[c]45 to 51	2	5
[c]51	0	1	68	13	7
52	6	4	73	13	18
53	10	12	75	22	11
[c]59	0	1			
60	31	25	[c]47 to 60	0	2
78	2	2	72	5	11
			[c]78	1	0
32 to 40	26	6			
44	4	4	50 to 51	0	1
[c]45	4	0	[c]52	2	0
47	9	4	53	4	0
[c]51	5	0	61	2	7
52	5	5			
[c]53	1	1	51 to 52	18	19
60	17	39	53	13	11
[c]72	0	1	61	5	1
			68	8	12
38 to 39	3	2			
59	1	5	52 to 53	15	13
111	3	8	60	2	6
39 to 59	6	2	[c]53 to 60	3	8
			[c]61	1	0
40 to 44	2	0			
45	26	8	55 to 63	21	8
47	4	3	64	7	8
[c]60	0	3	67	13	7
72	1	4	68	0	2
73	9	4	69	6	4
[c]75	6	2			
			61 to 67	3	0
[c]42 to 45	7	8	68	1	2
64	16	4	69	2	2
68	8	30			
[c]73	6	0	63 to 64	9	5
75	2	15	67	10	3
			[c]69	0	2
43 to 50	3	8			
61	4	9	64 to 68	3	25
			67 to 69	1	0
			68 to 69	4	0
			75	0	3

[a] For station positions compare figure 7.8.
[b] Add 6 000 to all numbers
[c] Skip lines.

TABLE 7.6.—*Partial Derivatives of F and G With Respect to* **u**

u	α ω κ X_0 Y_0 Z_0 c_x c_y x_0 y_0 X Y Z K_1 K_2 K_3 x_s y_s K_4 K_5 ϕ_T ϵ l_x l_y
$\frac{\partial F}{\partial \mathbf{u}}$	A_x B_x C_x D_x E_x F_x G_x $-H_x$ I_x J_x K_x L_x M_x N_x O_x P_x Q_x R_x S_x T_x U_x Z_x —
$\frac{\partial G}{\partial \mathbf{u}}$	A_y B_y C_y D_y E_y F_y — G_y H_y I_y J_y K_y L_y M_y N_y O_y P_y Q_y R_y S_y T_y U_y $-Z_y$

TABLE 7.7.—*Curve Fit of 380 Fictitious Satellite Images With Polynomials of Degree 1 Through 11 (x in Direction of the Trail. y Normal to It)*

	Degree of polynomial[a]	σ_x [μm]	σ_y [μm]		σ_x [μm]	σ_y [μm]
	1	404 166	215 720		494 437	57 121
Observa-	2	53 445	1 853	Observa-	53 362	0 209
tion sta.	3	1 267	0 289	tion sta.	1 571	0 039
1	4	0 090	0 006	4	0 099	0 000
	5	0 003	0 001		0 004	0 000
	6	0 000	0 000		0 000	0 000
	1	461 861	133 736		356 618	82 163
Observa-	2	54 919	0 964	Observa-	51 751	0 223
tion sta.	3	1 479	0 166	tion sta.	1 116	0 077
2	4	0 099	0 004	5	0 085	0 001
	5	0 004	0 000		0 003	0 000
	6	0 000	0 000		0 000	0 000
	1	226 233	169 385		145 585	157 387
Observa-	2	50 510	0 229	Observa-	48 951	0 476
tion sta.	3	0 709	0 204	tion sta.	0 458	0 184
3	4	0 076	0 002	6	0 070	0 000
	5	0 002	0 000		0 001	0 000
	6	0 000	0 000		0 000	0 000

[a] For polynomials of seventh to eleventh degree all entries are zero, as they are for the sixth degree.

TABLE 7.8

Seq. no.	Observ. sta. no.[a]	No. of processed plates
1	2	1
2	3	1
3	7	3
4	8	17
5	9	17
6	11	10
7	12	14
8	15	3
9	16	4
10	19	39
11	20	1
12	22	5
13	23	2
14	31	16
15	38	10
16	39	2
17	42	14
18	43	23
19	44	2
20	45	7
21	50	17
22	51	29
23	52	20
24	53	24
25	55	32
26	59	15
27	60	10
28	61	33
29	63	25
30	64	29
31	67	25
32	68	29
33	69	17
34	73	2
35	75	2
	Sum:	500

[a] Add 6000 to station numbers.

TABLE 7.9

Photogrammetric camera: Wild BC–4. lens: Cosmotar f = 450mm, aperture 132mm
Target: PAGEOS balloon satellite for 496 photograms and ECHO satellite for 4 photograms
Program: World Net
Period of observation: October 1966–September 1969
Observation material: 500 selected photograms with corresponding time recordings from 35 stations in the World Net

		(1) Type of imagery	(2) Mean errors of comparator measurements m_l (μm)	(3) Assumed mean of irregular emulsion shift (μm)	(4) Average of mean shimmer (μm)	(4) Average of mean shimmer (″)	(5) Mean coordinate error after adjustment in photogrammetric bundle simulation $[(2)^2+(3)^2+(4)^2]^{1/2}$ (m_l)(μm)	(6) Introduced mean error of reduced star catalog data (μm)	(6) Introduced mean error of reduced star catalog data (″)	(7) Total noise in photogrammetric bundle simulation adjustment $[(2)^2+(3)^2+(4)^2+(6)^2]^{1/2}$ (μm)	(7) Total noise in photogrammetric bundle simulation adjustment $[(2)^2+(3)^2+(4)^2+(6)^2]^{1/2}$ (″)	(8) Mean error of polynomial smoothing $[(2)^2+(3)^2+(4)^2]^{1/2}$ (μm)	(8) Mean error of polynomial smoothing $[(2)^2+(3)^2+(4)^2]^{1/2}$ (″)
Average values	*a*	Stars	±1.81	±1.00	±2.58	±1.18	±3.31	±0.87	±0.40	±3.42	±1.57	------	------
	b	Satellite	±1.79	±1.00	±2.86	±1.31	------	------	------	------	------	±3.52	±1.61
Minimal values	*c*	Stars	±0.97	±1.00	±1.01	±0.46	±1.88	±0.87	±0.40	±1.93	±0.88	------	------
	d	Satellite	±0.87	±1.00	±1.07	±0.47	------	------	------	------	------	±1.46	±0.67
Maximal values	*e*	Stars	±2.45	±1.00	±6.46	±2.96	±6.87	±0.87	±0.40	±7.03	±3.22	------	------
	f	Satellite	±2.68	±1.00	±6.84	±3.14	------	------	------	------	------	±8.96	±4.11

TABLE 7.10

Image coordinates x (mm)/y (mm)	0/0	10/10	20/20	30/30	40/40	50/50	60/60	70/70
Mean accuracy of direction	±0″.23	±0″.25	±0″.23	±0″.19	±0″.21	±0″.25	±0″.44	±2″.77

TABLE 7.11.—*Three-Dimensional Cartesian Coordinates*

No.	Station name	X (m)	σ_X ± (m)	Y (m)	σ_Y ± (m)	Z (m)	σ_Z ± (m)
6001	Thule	546 567.862	2.297	−1 389 990.609	3.447	6 180 239.602	3.960
6002	Beltsville	1 130 761.500	0	−4 830 828.597	0	3 994 704.584	0
6003	Moses Lake	−2 127 833.613	.790	−3 785 861.054	2.976	4 656 034.740	2.906
6004	Shemya	−3 851 782.861	4.888	+396 404.016	5.654	5 051 347.586	6.673
6006	Tromso	2 102 925.118	3.663	+721 667.562	4.772	5 958 188.868	4.748
6007	Azores	4 433 636.070	4.737	−2 268 143.467	4.362	3 971 656.223	4.945
6008	Surinam	3 623 227.823	4.563	−5 214 231.698	4.502	601 551.302	5.716
6009	Quito	1 280 815.597	4.338	−6 250 955.436	5.800	−10 793.013	5.717
6011	Maui	−5 466 020.732	5.045	−2 404 435.198	4.352	2 242 229.885	4.703
6012	Wake	−5 858 543.398	5.308	+1 394 489.166	5.281	2 093 807.584	5.391
6013	Kanoya	−3 565 865.509	5.200	+4 120 692.866	6.694	3 303 428.249	6.131
6015	Mashhad	2 604 346.389	3.988	+4 444 141.147	5.513	3 750 323.381	4.974
6016	Catania	4 896 383.234	4.080	+1 316 167.822	4.463	3 856 673.791	4.698
6019	Dolores	2 280 603.832	4.190	−4 914 545.588	4.789	−3 355 412.286	6.839
6020	Easter	−1 888 616.886	4.845	−5 354 892.780	6.246	−2 895 739.444	7.217
6022	Pago Pago	−6 099 954.446	5.392	−997 367.321	4.710	−1 568 567.088	5.883
6023	Thursday Is.	−4 955 371.694	4.671	+3 842 221.799	5.689	−1 163 828.451	5.852
6031	Invercargill	−4 313 815.856	4.687	+891 322.098	5.238	−4 597 238.676	6.398
6032	Perth	−2 375 397.874	4.579	+4 875 524.035	5.746	−3 345 372.936	6.170
6038	Revilla	−2 160 983.561	2.008	−5 642 711.612	3.653	2 035 371.417	4.062
6039	Pitcairn	−3 724 766.403	6.502	−4 421 236.249	6.480	−2 686 072.609	7.288
6040	Cocos	−741 969.205	4.859	+6 190 770.789	6.606	−1 338 530.638	5.843
6042	Addis Ababa	4 900 734.926	4.844	+3 968 226.427	5.481	966 347.675	5.103
6043	Sombrero	1 371 358.188	4.171	−3 614 760.271	4.969	−5 055 928.396	8.156
6044	Heard	1 098 896.432	6.448	+3 684 591.597	7.801	−5 071 838.356	9.919
6045	Mauritius	3 223 422.870	4.472	+5 045 312.452	6.019	−2 191 780.736	6.065
6047	Zamboanga	−3 361 946.845	4.909	+5 365 778.338	6.501	763 644.128	6.121
6050	Palmer	1 192 659.730	5.174	−2 450 995.361	7.275	−5 747 040.896	10.171
6051	Mawson	1 111 335.585	5.189	+2 169 243.189	5.456	−5 874 307.692	8.002
6052	Wilkes	−902 598.435	4.912	+2 409 507.607	5.700	−5 816 527.805	7.901
6053	McMurdo	−1 310 841.759	4.993	+311 248.105	5.500	−6 213 251.231	7.886
6055	Ascension	6 118 325.238	5.260	−1 571 746.070	4.816	−878 595.457	5.507
6059	Christmas	−5 885 331.078	5.213	−2 448 376.867	4.435	221 683.837	5.446
6060	Culgoora	−4 751 637.577	4.552	+2 792 039.266	5.653	−3 200 142.319	5.866
6061	So. Georgia	2 999 903.036	4.896	−2 219 368.228	6.055	−5 155 246.454	8.547
6063	Dakar	5 884 457.561	4.898	−1 853 492.773	4.257	1 612 863.206	5.072
6064	Chad	6 023 375.533	4.690	+1 617 924.383	4.242	1 331 742.422	4.834
6065	Hohenpeissenberg	4 213 552.554	3.730	+820 823.968	4.444	4 702 787.513	4.620
6067	Natal	5 186 398.560	5.260	−3 653 936.203	4.854	−654 277.651	5.569
6068	Johannesburg	5 084 812.984	5.229	+2 670 319.559	5.065	−2 768 065.639	6.586
6069	De Cunha	4 978 412.958	8.167	−1 086 867.619	6.918	−3 823 159.761	9.443
6072	Thailand	−941 692.348	5.593	+5 967 416.884	6.919	2 039 317.530	5.461
6073	Chagos	1 905 130.320	4.345	+6 032 252.624	6.702	−810 711.562	5.751
6075	Mahe	3 602 810.169	4.910	+5 238 217.287	6.393	−515 928.653	5.650
6111	Wrightwood	−2 448 854.721	2.088	−4 667 988.213	3.367	3 582 758.969	3.185

TABLE 7.12

Scalar[a]	Δd = meas. − comp. (m)	σ of scalar as obtained from the triang. adjust. (m)	
002–003	0	0	held fixed
003–111	−7.3	±2.8	
006–065	[b]−2.0	±4.9	
065–016	+9.3	±5.1	
023–060	+5.8	±3.9	
032–060	+8.5	±4.6	
063–064	−5.1	±5.2	
Sum	+9.2	±15.6	(σ of Σd)

[a] Add 6000 to station numbers.

[b] The German Geodetic Research Institute gives, for the baseline 006–065, a value which is 1.9 m larger than the one used here. The corresponding Δ values would then be only one decimeter.

TABLE 7.13

Scalar[a]	Assumed mean error (m)	Correction from the adjustment (m)
2–3	±1.75	−0.06
3–111	±0.72	+1.50
6–16	±1.78	−0.26
6–65	±1.23	+0.10
16–65	±0.60	+0.42
23–60	±1.15	−0.98
32–60	±1.58	−2.76
63–64	±1.75	+2.60

[a] Add 6000 to station numbers.

TABLE 7.14.—*Coordinate Differences Between Transformed Doppler Solution and Translated BC-4 Solution After XYZ Fit* ($\Delta = BC\text{-}4 - Doppler$)

No.[a]	Station name	$\Delta\phi$ (m)	$\Delta\lambda$ (m)	Δh (m)	Resultant (m)
1	Thule	10.198	−2.216	10.464	14.779
2	Beltsville	−1.254	1.201	−4.516	4.839
3	Moses Lake	−3.072	5.628	−3.670	7.388
4	Shemya	5.711	13.780	15.061	21.198
6	Tromso	−1.451	−17.014	7.566	18.677
7	Azores	−10.097	−5.716	4.377	12.401
8	Surinam	.002	1.959	−8.694	8.912
9	Quito	6.507	10.573	−7.272	14.388
11	Maui	4.162	−2.037	8.789	9.935
12	Wake	−14.550	−10.924	−24.453	30.479
13	Kanoya	6.458	.116	3.956	7.574
15	Mashhad	3.600	4.048	1.256	5.561
16	Catania	1.740	−1.638	3.341	4.107
19	Dolores	−18.425	15.163	−4.296	24.245
20	Easter	7.924	13.930	3.152	16.333
22	Pago Pago	4.227	−6.107	−5.317	9.134
23	Thursday	−1.735	−7.291	−15.435	17.159
31	Invercargill	−7.362	−9.689	−5.584	13.389
32	Perth	3.261	.162	.665	3.332
38	Revilla	−5.298	.445	3.129	6.169
40	Cocos	3.360	.864	2.135	4.073
42	Addis Ababa	14.086	−1.952	5.724	15.329
43	Sombrero	−20.140	3.173	24.247	31.680
45	Mauritius	3.838	5.642	1.044	6.903
47	Zamboanga	3.162	3.466	−9.571	10.659
50	Palmer	−19.872	−5.176	12.703	24.147
53	McMurdo	−18.103	−1.576	−4.321	18.678
55	Ascension	−7.126	−10.677	.245	12.838
59	Christmas	4.404	−4.747	−4.207	7.722
60	Culgoora	−12.420	−9.048	−2.916	15.641
63	Dakar	.998	5.593	.304	5.690
64	Chad	5.889	2.226	5.226	8.182
65	Hohenpeissenberg	5.497	−8.304	6.434	11.856
67	Natal	−10.375	−5.277	3.692	12.212
68	Johannesburg	1.352	2.525	−8.008	8.504
72	Thailand	3.350	6.659	−8.712	11.466
75	Mahe	8.413	.122	−6.102	10.394
	rms values	±8.916	±7.179	±8.697	±14.376

[a] Add 6000 to station numbers.

TABLE 7.15.—*Three-Dimensional Cartesian Coordinates From Combined Final Solution*

No.[a]	Station name	X (m)	σ_X ± (m)	Y (m)	σ_Y ± (m)	Z (m)	σ_Z ± (m)
1	Thule	546 588.043	2.524	−1 389 976.770	2.442	6 180 221.157	3.191
2	Beltsville	1 130 783.206	2.464	−4 830 812.170	2.853	3 994 691.260	2.979
3	Moses Lake	−2 127 810.402	2.337	−3 785 844.188	2.610	4 656 021.673	2.896
4	Shemya	−3 851 759.714	3.610	396 416.742	3.622	5 051 324.861	4.235
6	Tromso	2 102 943.362	2.365	721 679.260	2.697	5 958 170.871	3.090
7	Azores	4 433 652.575	3.091	−2 268 128.968	2.686	3 971 641.629	3.327
8	Surinam	3 623 251.037	3.166	−5 214 216.431	3.288	601 536.293	3.489
9	Quito	1 280 842.366	3.158	−6 250 939.190	3.947	−10 807.932	3.487
11	Maui	−5 466 002.263	3.288	−2 404 414.762	2.767	2 242 214.785	3.235
12	Wake	−5 858 531.333	3.287	1 394 513.654	2.966	2 093 798.651	3.211
13	Kanoya	−3 565 848.055	3.138	4 120 713.101	3.636	3 303 409.134	3.581
15	Mashhad	2 604 363.535	2.345	4 444 158.701	2.711	3 750 306.588	2.712
16	Catania	4 896 401.374	2.357	1 316 181.910	2.316	3 856 657.080	2.572
19	Dolores	2 280 628.090	2.674	−4 914 528.492	2.950	−3 355 416.607	3.163
20	Easter	−1 888 587.555	3.790	−5 354 875.392	3.952	−2 895 751.980	3.784
22	Pago Pago	−6 099 939.342	3.122	−997 345.983	2.730	−1 568 582.700	3.208
23	Thursday Is.	−4 955 355.561	2.613	3 842 245.988	2.427	−1 163 843.516	2.534
31	Invercargill	−4 313 799.508	2.680	891 345.724	2.588	−4 597 253.294	2.833
32	Perth	−2 375 382.732	2.505	4 875 545.638	2.621	−3 345 387.849	2.728
38	Revilla	−2 160 960.225	2.510	−5 642 694.520	3.078	2 035 358.416	3.176
39	Pitcairn	−3 724 745.647	6.280	−4 421 218.035	5.694	−2 686 087.346	5.255
40	Cocos	−741 953.040	3.161	6 190 790.099	3.069	−1 338 547.676	2.752
42	Addis Ababa	4 900 753.422	2.762	3 968 244.643	2.626	966 329.417	2.552
43	Sombrero	1 371 383.334	2.724	−3 614 745.095	3.157	−5 055 927.530	3.641
44	Heard	1 098 912.818	5.747	3 684 612.693	6.212	−5 071 853.727	7.780
45	Mauritius	3 223 440.444	2.656	5 045 332.006	2.739	−2 191 798.454	2.698
47	Zamboanga	−3 361 931.463	2.812	5 365 800.248	3.094	763 627.375	3.330
50	Palmer	1 192 684.033	3.433	−2 450 986.983	4.323	−5 747 037.701	4.672
51	Mawson	1 111 352.024	4.285	2 169 264.675	3.238	−5 874 322.862	4.844
52	Wilkes	−902 583.987	3.525	2 409 530.660	3.232	−5 816 542.503	4.730
53	McMurdo	−1 310 828.143	3.356	311 271.145	3.073	−6 213 265.956	3.958
55	Ascension	6 118 342.544	3.108	−1 571 732.245	2.883	−878 608.379	3.089
59	Christmas	−5 885 315.086	3.027	−2 448 357.151	2.732	221 669.643	3.145
60	Culgoora	−4 751 621.039	2.483	2 792 063.383	2.372	−3 200 156.628	2.442
61	So. Georgia	2 999 924.593	3.745	−2 219 357.041	4.232	−5 155 247.563	4.886
63	Dakar	5 884 475.772	2.853	−1 853 478.486	2.307	1 612 848.261	2.930
64	Chad	6 023 393.960	2.749	1 617 940.871	2.236	1 331 726.674	2.508
65	Hohenpeissenberg	4 213 570.222	2.356	820 837.313	2.346	4 702 769.262	2.758
67	Natal	5 186 415.778	3.301	−3 653 921.575	3.208	−654 288.938	3.072
68	Johannesburg	5 084 832.837	3.146	2 670 338.698	2.580	−2 768 083.655	3.248
69	Da Cunha	4 978 430.027	7.231	−1 086 856.181	5.644	−3 823 164.893	7.581
72	Thailand	−941 678.219	3.661	5 967 438.461	3.337	2 039 300.514	2.969
73	Chagos	1 905 147.827	2.911	6 032 272.479	3.482	−810 729.775	3.001
75	Mahe	3 602 828.788	3.024	5 238 237.170	3.096	−515 947.433	2.773
111	Wrightwood	−2 448 831.364	2.679	−4 667 972.160	3.052	3 582 744.578	3.162

[a] Add 6000 to station numbers.

TABLE 7.16.—*Coordinate Differences Between Translated BC-4 Solution and Combined Solution After XYZ Fit* (Δ = *BC-4 Solution − Combined Solution*)

No.[a]	Station name	$\Delta\phi$ (m)	$\Delta\lambda$ (m)	Δh (m)	Resultant (m)	
1	Thule	4.905	−0.684	3.289	5.945	
2	Beltsville	0.185	2.209	−1.853	2.889	
3	Moses Lake	−1.735	4.091	0.269	4.452	
4	Shemya	1.505	4.864	9.935	11.164	
6	Tromso	−1.757	−5.547	4.648	7.447	
7	Azores	−0.822	−4.204	1.007	4.400	
8	Surinam	0.515	2.110	−3.960	4.517	
9	Quito	0.156	7.501	−2.580	7.933	
11	Maui	0.582	−2.418	1.395	2.852	
12	Wake	−2.316	−4.665	−8.936	10.343	
13	Kanoya	5.430	−0.159	0.670	5.474	
15	Mashhad	0.712	1.603	2.850	3.347	
16	Catania	0.101	−3.388	3.223	4.677	
19	Dolores	−10.566	4.851	3.581	12.165	
20	Easter	−0.379	10.325	4.284	11.185	
22	Pago Pago	0.561	−3.868	−2.642	4.718	
23	Thursday	−0.403	−3.230	−5.313	6.231	
31	Invercargill	−2.236	−5.096	−1.787	5.845	
32	Perth	−2.256	1.600	−3.654	4.583	
38	Revilla	−1.674	4.430	0.880	4.816	
39	Pitcairn	0.968	1.486	1.936	2.625	
40	Cocos	1.943	2.522	−1.498	3.518	
42	Addis Ababa	3.113	0.599	1.303	3.427	
43	Sombrero	−13.364	5.306	10.147	17.598	
44	Heard	−1.623	3.003	−1.282	3.646	
45	Mauritius	2.317	1.935	−1.021	3.187	
47	Zamboanga	2.878	0.990	−4.290	5.260	
50	Palmer	−17.711	1.139	12.169	21.519	
51	Mawson	−1.968	3.462	−0.566	4.022	
52	Wilkes	−5.689	1.977	−1.901	6.315	
53	McMurdo	−5.707	−3.880	−0.698	6.936	
55	Ascension	−2.133	−4.243	1.390	4.948	
59	Christmas	−0.003	−2.663	−1.335	2.978	
60	Culgoora	−2.556	−4.203	−3.594	6.092	
61	So. Georgia	−13.290	−3.515	8.088	15.950	
63	Dakar	−0.078	−3.618	0.264	3.628	
64	Chad	0.396	−1.160	1.656	2.060	
65	Hohenpeissenberg	0.397	−4.163	4.660	6.261	
67	Natal	−3.810	−3.519	0.459	5.207	
68	Johannesburg	1.930	0.627	−2.082	2.908	
69	Da Cunha	−7.851	−6.563	6.722	12.243	
72	Thailand	3.621	4.358	−2.717	6.284	
73	Chagos	3.124	1.925	−1.213	3.865	
75	Mahe	3.651	1.386	−1.143	4.069	
78	Vila Efate	0.192	−4.949	−3.148	5.868	
111	Wrightwood	−0.250	4.706	0.827	4.784	
123	Point Barrow	−0.378	6.691	4.322	7.974	
	rms values	±4.817	±3.974	±4.183	±7.516	n = 47

[a] Add 6000 to station numbers.

TABLE 7.17.—*Coordinate Differences Between Transformed Doppler Solution and Combined Solution After XYZ Fit* (Δ = *Combined Solution − Doppler*)

No.[a]	Station name	$\Delta\phi$ (m)	$\Delta\lambda$ (m)	Δh (m)	Resultant (m)
1	Thule	4.948	−1.690	7.309	8.987
2	Beltsville	−2.044	−0.855	−2.602	3.418
3	Moses Lake	−1.540	1.573	−3.619	4.236
4	Shemya	4.433	8.980	5.727	11.537
6	Tromso	−0.062	−11.187	3.029	11.590
7	Azores	−10.072	−1.351	3.282	10.679
8	Surinam	−1.574	0.269	−4.707	4.970
9	Quito	5.469	3.704	−4.496	7.991
11	Maui	3.717	0.755	8.146	8.986
12	Wake	−11.845	−6.005	−14.576	19.718
13	Kanoya	1.320	0.417	4.100	4.327
15	Mashhad	2.605	2.585	−1.262	3.881
16	Catania	0.976	1.908	0.143	2.148
19	Dolores	−9.064	11.106	−7.536	16.195
20	Easter	7.860	4.731	−0.514	9.188
22	Pago Pago	4.182	−1.580	−1.630	4.758
23	Thursday	−0.665	−3.988	−8.993	9.860
31	Invercargill	−4.103	−4.126	−2.665	6.400
32	Perth	6.200	−1.870	5.400	8.432
38	Revilla	−4.009	−3.528	2.629	5.953
40	Cocos	1.678	−2.067	4.543	5.265
42	Addis Ababa	10.339	−2.729	4.697	11.679
43	Sombrero	−7.959	−1.174	14.647	16.711
45	Mauritius	1.132	3.045	2.671	4.206
47	Zamboanga	0.682	2.454	−4.308	5.004
50	Palmer	−3.410	−5.423	1.174	6.512
53	McMurdo	−11.079	2.695	−2.663	11.709
55	Ascension	−6.249	−6.384	−1.088	9.000
59	Christmas	4.643	−1.483	−1.990	5.265
60	Culgoora	−8.968	−4.719	1.850	10.302
63	Dakar	0.028	9.353	−0.024	9.354
64	Chad	4.612	3.340	3.648	6.763
65	Hohenpeissenberg	4.508	−3.934	1.788	6.244
67	Natal	−7.821	−1.469	3.266	8.602
68	Johannesburg	−1.506	1.312	−5.527	5.876
72	Thailand	−0.145	2.282	−5.246	5.723
75	Mahe	4.334	−1.677	−4.459	6.441
	rms values	±5.588	±4.436	±5.339	±8.911

[a] Add 6000 to station numbers.

TABLE 7.18

	Input	Additional data	Type of solution	a 6 378 . . . (m)	$1/f$	ΔX (m)	ΔY^a (m)	ΔZ (m)
(1)	BC–4 result, 43 stations	MSL elevations	Unconstrained ellipsoid fit	130.17	298.377	+16.20	−14.82	−16.40
(2)	BC–4 result, 43 stations	The same	Ellipsoid fit constrained to dynamically determined $1/f$	132.80	298.250	+16.29	−15.32	−16.74
(3)	Combined solution, 43 stations	The same	Unconstrained ellipsoid fit	133.98	298.246	+1.373	+2.434	−1.844
(4)	Combined solution, 43 stations	The same	Ellipsoid fit constrained to dynamically determined $1/f$	133.90	298.250	+1.370	+2.453	−1.835
(5)	Combined solution, 43 stations	The same	Ellipsoid fit constrained to dynamically determined $1/f$ and to Anderle mass center position	134.02	298.250	0	0	0
(6)	BC–4 result, 37 stations	MSL elevations and Anderle geoidal heights N	as in (1) above	126.47	298.409	+14.702	−19.482	−13.816
(7)	BC–4 result, 37 stations	The same	as in (2) above	129.45	298.250	+15.140	−20.181	−15.252
(8)	Combined solution, 37 stations	The same	as in (3) above	128.83	298.322	−1.900	−0.378	+1.183
(9)	Combined solution, 37 stations	The same	as in (4) above	130.21	298.250	−1.756	−0.764	+0.721
(10)	Combined solution, 37 stations	The same	as in (5) above	130.22	298.250	0	0	0
(11)	BC–4 result, Doppler result, for 37 stations	None	XYZ fit between Doppler and BC–4 result	130.48 ±1.58	----------	+19.590 ±1.34	−17.684 ±1.33	−14.344 ±1.51

[a] Left-handed system: reverse signs.

TABLE 7.19.—*Geographic Coordinates From Combined Solution Computed With $a = 6378130$ m and $f = 1:298.250$ m*

Station no.[a]	Station name	Latitude			σ_ϕ (m)	Longitude (east)			σ_λ (m)	Ellipsoid height (m)	σ_h (m)
		deg	min	sec		deg	min	sec			
1	Thule	N 76	30	4.8627	2.184	291	27	59.4280	2.675	219.379	3.236
2	Beltsville	N 39	01	39.3318	2.540	283	10	27.9765	2.440	−1.458	3.264
3	Moses Lake	N 47	11	6.6534	2.424	240	39	43.5760	2.308	336.069	3.069
4	Shemya	N 52	42	48.9705	3.782	174	7	26.0462	3.475	39.745	4.193
6	Tromso	N 69	39	44.4978	2.361	18	56	27.5273	2.535	133.357	3.211
7	Azores	N 38	45	36.0847	2.864	332	54	25.2813	2.652	108.829	3.546
8	Surinam	N 05	26	53.4378	3.457	304	47	40.6928	2.880	−20.115	3.585
9	Quito	S 0	5	51.7281	3.504	281	34	47.4488	3.163	2694.047	3.937
11	Maui	N 20	42	26.9218	3.045	203	44	38.3808	2.696	3075.656	3.522
12	Wake	N 19	17	28.2961	2.947	166	36	39.4948	2.896	4.297	3.589
13	Kanoya	N 31	23	42.5648	3.278	130	52	16.2716	3.390	83.416	3.694
15	Mashhad	N 36	14	25.5340	2.441	59	37	43.9207	2.459	963.436	2.860
16	Catania	N 37	26	38.5025	2.158	15	2	44.8491	2.240	45.972	2.800
19	Dolores	S 31	56	35.5287	2.992	294	53	38.5873	2.579	627.599	3.203
20	Easter	S 27	10	36.4176	3.317	250	34	22.7515	3.544	219.755	4.554
22	Pago Pago	S 14	19	54.4748	3.141	189	17	8.7112	2.701	35.347	3.223
23	Thursday Is.	S 10	35	2.9982	2.511	142	12	39.5544	2.341	119.259	2.718
31	Invercargill	S 46	24	58.1142	2.542	168	19	31.6698	2.588	−0.007	2.949
32	Perth	S 31	50	24.9112	2.482	115	58	31.8154	2.420	−8.327	2.927
38	Revilla	N 18	43	58.2071	3.020	249	2	41.4901	2.515	−14.701	3.235
39	Pitcairn	S 25	4	6.8403	3.686	229	53	12.6661	4.975	317.220	7.817
40	Cocos	S 12	11	44.0207	2.682	96	50	3.0512	3.132	−29.827	3.163
42	Addis Ababa	N 8	46	12.5193	2.574	38	59	52.1902	2.607	1872.647	2.766
43	Sombrero	S 52	46	52.5872	3.472	290	46	33.7413	2.662	95.214	3.378
44	Heard	S 53	1	9.0693	6.472	73	23	35.2173	6.032	39.662	7.314
45	Mauritius	S 20	13	53.1132	2.586	57	25	32.4106	2.634	137.814	2.869
47	Zamboanga	N 6	55	20.7741	3.324	122	4	8.8287	2.696	71.335	3.215
50	Palmer	S 64	46	26.7693	4.870	295	56	53.4936	3.289	26.028	4.184
51	Mawson	S 67	36	4.8017	3.925	62	52	23.3298	3.829	39.813	4.690
52	Wilkes	S 66	16	44.9811	3.267	110	32	7.4526	3.359	10.755	4.808
53	McMurdo	S 77	50	41.6571	3.445	166	38	30.7416	3.006	−41.095	3.907
55	Ascension	S 7	58	15.4065	3.058	345	35	34.4179	2.943	83.939	3.092
59	Christmas	N 2	0	18.3902	3.148	202	35	16.2920	2.593	24.514	3.157
60	Culgoora	S 30	18	34.2631	2.339	149	33	41.0676	2.275	235.088	2.666
61	So. Georgia	S 54	17	1.1326	3.750	323	30	20.9006	4.454	19.203	4.659
63	Dakar	N 14	44	42.1988	2.847	342	31	0.2512	2.306	55.378	2.945
64	Chad	N 12	7	54.5921	2.520	15	2	7.0547	2.223	306.766	2.756
65	Hohenpeissenberg	N 47	48	3.9953	2.184	11	1	25.0048	2.296	977.952	2.928
67	Natal	S 5	55	39.0642	3.061	324	50	4.6598	3.199	38.288	3.328
68	Johannesburg	S 25	52	59.1717	2.975	27	42	23.5867	2.587	1536.885	3.402
69	Da Cunha	S 37	3	53.6135	6.418	347	41	5.3077	5.714	45.432	8.227
72	Thailand	N 18	46	10.5737	2.770	98	58	2.9441	3.622	259.580	3.545
73	Chagos	S 7	21	6.6304	2.994	72	28	21.1236	2.969	−72.915	3.446
75	Mahe	S 4	40	14.6759	2.753	55	28	48.1258	2.830	545.382	3.298
111	Wrightwood	N 34	22	54.4315	2.628	242	19	6.1310	2.757	2252.261	3.457

[a] Add 6000 to station numbers.

TABLE 7.20.—*Components of Vertical Deflections* (Δ = *Astro* − *Geodetic*)

Station no.[a]	$\Delta\phi''$	$\Delta\lambda''$	$\eta'' = \Delta\lambda'' \cos\phi$	$\cos\phi$
001	6.81	−48.34	−11.28	0.2334
002	−1.60	7.37	5.72	0.7768
003	−3.41	−0.63	−0.43	0.6796
004	14.51	18.87	11.43	0.6058
006	−1.26	19.51	6.78	0.3475
007	7.20	10.13	7.90	0.7797
008	−4.48	−1.90	−1.89	0.9955
009	−1.36	9.46	9.46	1.0000
011	−5.06	−1.33	−1.24	0.9353
012	−3.90	−14.31	−13.51	0.9439
013	−4.08	9.44	8.06	0.8537
015	2.29	16.88	13.62	0.8066
016	0.20	18.34	14.56	0.7939
020	−2.79	−5.26	−4.68	0.8896
022	−13.87	−0.86	−0.83	0.9689
023	−3.78	−4.66	−4.58	0.9830
031	−2.94	3.23	2.23	0.6894
032	0.34	−28.10	−23.87	0.8496
038	−13.28	−2.21	−2.09	0.9470
039	−0.31	−0.79	−0.72	0.9058
040	−13.89	−15.97	−15.61	0.9774
042	−6.78	5.00	4.94	0.9883
043	1.85	−7.30	−4.42	0.6048
044	−2.96	−7.80	−4.70	0.6016
045	15.63	−39.61	−37.17	0.9383
047	−2.48	−2.38	−2.36	0.9927
050	−7.21	−16.45	−7.01	0.4260
051	1.72	1.08	0.41	0.3811
052	−0.14	−2.84	−1.14	0.4022
053	−1.66	−16.88	−3.55	0.2105
055	−2.86	−4.78	−4.73	0.9903
059	17.23	5.67	5.66	0.0994
060	−1.88	−9.96	−8.60	0.8633
061	21.62	21.63	12.63	0.5838
063	2.03	−4.66	−4.51	0.9670
064	−0.65	1.91	1.87	0.9777
065	5.54	5.53	3.71	0.6717
067	1.32	−1.69	−1.68	0.9946
068	9.11	7.59	6.83	0.8997
069	27.35	−11.75	−9.38	0.7981
072	−23.07	5.44	5.15	0.9468
073	8.10	11.04	10.95	0.9918
075	4.37	5.85	5.83	0.9967
111	6.37	18.49	15.26	0.8253

[a] Add 6000 to station numbers.

TABLE 7.21.—*Height of Geoid Above Ellipsoid* (N) = *Ellipsoid Height* (h) *Minus Mean Sea Level Elevation* (H)

Station no.[a]	(1) N Combined solution based on 6378130 (m)	(2) N Anderle solution (m)	(3) ΔN (m)
1	13.379	7.30	+6.08
2	−45.758	−43.7	−2.05
3	−32.671	−29.70	−2.97
4	2.985	−3.40	+6.38
6	27.357	24.16	+3.20
7	55.569	51.87	+3.70
8	−38.495	−34.25	−4.25
9	11.947	15.90	−3.95
11	26.386	15.81	+10.58
12	0.837	15.08	−14.24
13	17.516	27.80	−10.28
15	−27.614	−26.80	−0.81
16	36.972	36.42	0.55
19	19.419	26.44	−7.02
20	−11.045	−11.20	0.16
22	30.007	30.83	−0.82
23	59.659	67.88	−8.22
31	−0.957	0.95	−1.91
32	−34.627	−40.30	5.68
38	−37.901	−41.20	3.30
39	−22.170	------	------
40	−34.237	−39.40	5.16
42	−13.813	−18.90	5.09
43	14.554	−0.65	15.20
44	35.891	------	------
45	0.286	−3.54	3.15
47	61.944	65.56	−3.62
50	9.588	7.84	1.75
51	28.813	------	------
52	−7.245	------	------
53	−60.185	−58.20	−1.98
55	12.999	13.72	−0.72
59	21.764	22.95	−1.19
60	23.988	21.37	2.62
61	15.023	------	------
63	29.098	28.75	0.35
64	11.356	7.35	4.01
65	34.452	34.06	0.39
67	−2.342	−6.09	3.75
68	13.085	17.70	−4.62
69	20.002	------	------
72	−48.820	−44.12	−4.70
73	−76.766	------	------
75	−43.598	−39.18	−4.42
111	−32.140	------	------
			Σ = +3.33
			RMS = ±5.57

[a] Add 6000 to station numbers.

TABLE 7.22.—*Station Shifts* (Δ = *Combined Solution − Survey*)

Station[a]	Datum	ΔX (m)	ΔY[b] (m)	ΔZ (m)	N (m)	Ellipsoid
002	North American	−15.464	−175.238	+170.683	−0.4	Clarke 1866
003		−15.073	−168.389	+176.173	−16.0	
004		−14.839	−224.661	+125.460	−46.0	
111		−14.909	−156.030	+174.079	−23.0	
023	Australian	−124.696	+59.448	+145.870	−4.6	AND
032		−122.122	+61.380	+148.912	+15.4	
060		−120.584	+58.544	+140.350	+0.7	
006	European	−95.289	+87.386	−130.319	+12.6	International
015		−102.814	+116.573	−157.106	−38.0	
016		−94.780	+97.941	−128.373	−16.6	
065		−98.045	+94.773	−130.038	−0.6	
042	Adindan	−175.031	+22.702	+207.848	−8.0	Clarke 1880
063		−159.895	+18.666	+211.616	+20.7	
064		−162.790	+18.035	+201.089	+23.6	
009	S.A.D. 1969	−62.026	−30.896	−38.650	+24.6	South American
019		−84.870	−10.993	−28.779	+13.0	
067		−79.113	+2.203	−44.415	+26.14	
001	QORNOQ	+193.755	−152.336	−179.116	+32.0	International
007	S.W. Base on Int.	−146.464	−189.307	−85.530	+55.569	International[c]
008	Prov. S.A. 1956	−285.742	−124.472	−364.343	+3.0	International
011	Old Hawaiian	+89.609	+272.174	−204.940	+26.28	Clarke 1866
012	1952 Astro on Int.	+297.342	+62.206	+118.723	+0.837	International[c]
013	Tokyo	−112.208	−476.369	+643.232	+27.0	Bessel
022	Am. Samoa 1962	−75.859	−125.169	+431.583	+22.0	Clarke 1866
031	Geodetic 1949	+86.529	+29.100	+204.364	−0.957	International[c]
043	Prov. S. Chile 1963	+4.265	−209.046	+104.397	+14.554	International[c]
045	LePonce Astro on 1880	−750.581	−159.580	−507.541	−0.386	Clarke 1880[c]
047	Luzon	−72.235	+115.447	−115.971	+61.944	Clarke 1886[c]
055	Ascension Is. 1958	−231.471	−111.769	+48.248	+12.999	International[c]
068	Buffelsfont	−153.391	+130.351	−283.829	+13.085	Clarke 1880[c]
072	Indian	+230.419	−827.968	+291.150	−48.820	Everest[c]
075	Mahe 1971	+60.571	+197.879	−140.513	−43.598	Clarke 1880[c]
007	Astro	+12.302	+280.978	−173.013	+55.569	Comb. Solution[c]
012	Astro 1952	−58.951	+415.588	+113.310	+0.837	a = 6378130[c]
020	Astro 1967	+123.534	+85.205	+76.460	−11.045	f = 1:298.25[c]
038	Astro Is. Soc.	+107.336	−99.244	+386.616	−37.901	f = 1:298.25[c]
039	Astro 1967	+14.216	+17.322	+8.608	−22.170	f = 1:298.25[c]
040	Astro Anna 1 1965	−490.078	−32.066	+417.173	−34.237	f = 1:298.25[c]
044	Astro 1969	−118.468	−111.631	+55.102	+35.891	f = 1:298.25[c]
045	Astro LePonce	−1058.365	−479.038	−451.105	−0.386	f = 1:298.25[c]
050	Astro 1969	+283.896	+86.525	+95.174	+9.588	f = 1:298.25[c]
051	Astro 1969	−11.130	+49.721	−20.296	+28.813	f = 1:298.25[c]
052	Astro 1969	−34.580	+8.773	+1.786	−7.245	f = 1:298.25[c]
053	Astro Camp Area 1961/62	−74.517	+95.634	+10.908	−60.185	f = 1:298.25[c]
059	Astro Christmas Is. 1967	−84.514	−154.619	−528.955	+21.764	f = 1:298.25[c]
061	Astro	−669.022	−8.101	−390.231	+15.023	f = 1:298.25[c]
069	Astro 1968	−434.607	−392.099	−672.974	+20.602	f = 1:298.25[c]
073	ISTS Astro 1969	+313.175	+132.303	−246.794	−76.765	f = 1:298.25[c]

[a] Add 6000 to station numbers.
[b] Left-handed system; reverse signs on ΔY
[c] N obtained from combined solution (table 7.21, col. 1) because of lack of corresponding survey data.

TABLE 7.23.—*Datum Shifts*

Datum	Stations	Residual coordinate differences after datum shift			Datum shift parameters				
							Translations		
		$\Delta\phi$ [m]	$\Delta\lambda$ east [m]	Δh [m]	Scalar	$\Delta\lambda$ rotation $+\lambda$ east X to Y	ΔX (m)	ΔY (m)	ΔZ (m)
NAD	002	−1.9	−1.9	−2.4	1.000 000 065 6	−″.7680	−31.6	+171.1	+173.4
	003	+6.1	−0.5	−2.2					
	111	−2.6	+2.1	+4.6					
AUS	023	+1.2	+1.4	+1.6	0.999 999 939 9	+″.0730	−124.1	−61.0	+144.9
	032	+2.8	+0.3	−2.8					
	060	−4.8	−1.9	+1.1					
Europe	006	−0.1	−0.3	+0.2	0.999 999 172 0	+″.7563	−96.4	−78.9	−125.6
	016	−0.2	−0.3	+0.9					
	065	+0.4	+0.4	−1.1					
South American 1969	009	+5.4	+10.4	−3.4	0.999 994 906 7	+″.7101	−43.5	−1.9	−44.1
	019	−2.3	−13.5	−0.4					
	067	−3.3	+1.1	+3.7					
Adindan	042	+1.3	+0.6	−2.2	0.999 999 979 4	−″.5231	−162.6	−34.0	+206.9
	063	+5.1	−0.2	−0.6					
	064	−6.5	−0.4	+2.8					

8

OHIO STATE UNIVERSITY

I. I. Mueller

8.1 INTRODUCTION

In 1965, the Department of Geodetic Science at The Ohio State University (OSU) was requested to submit a proposal to the National Aeronautics and Space Administration for a multiyear study and analysis of data from satellites launched specifically for geodetic purposes and from other satellites useful in geodetic studies. The program of work included theoretical studies and analysis for the geometric determination of station positions derived from photographic observations of both passive and active satellites and from range observations. This chapter examines the current status of data analysis, processing, and results. Various theoretical studies have been described in the report series of the Department of Geodetic Science (Nos. 106, 110, 114, 118, 139, 147, 150, 177, 184, 185, and 191) and are not repeated here.

The ultimate goal of the data analysis was to obtain an improved global net combining all participating tracking stations in a single worldwide coordinate system. In deriving these results, OSU representatives were to work with other universities and government agencies to prepare a handbook containing the best geodetic data from satellite observations available at the time. This chapter condenses the OSU contribution to this enterprise.

The work performed during the grant period included, but was not limited to, the following:

(1) Deriving, programming, and testing the necessary mathematical formulations.

(2) Making use of the observational data as they became available to determine the relative positions of the tracking stations in an arbitrary Cartesian coordinate system.

(3) Estimating the position of this coordinate system with respect to an absolute (geocentric) system and with respect to coordinate systems used by the other agencies.

(4) Participating in working groups and other planning meetings to establish desirable operational procedures, including tracking procedures, data format, analysis procedures, etc.

(5) Providing advice to NASA on various aspects of the National Geodetic Satellite Program.

Thus, the primary objective of the OSU investigation was the geometric analysis of geodetic satellite data. The analysis was to be accomplished in three steps:

(1) A primary network was to be established in which station positions were known to an internal consistency of 10 meters or better to serve the following purposes: (a) to establish the relative relationships between the various geodetic datums in use around the world; (b) to connect isolated tracking stations, islands, navigational beacons, and other points of interest. (In fulfilling the requirement of (a), a minimum of three tracking stations were to be used on any given datum.)

(2) A densification network was to be established in which station positions were known to an internal consistency of 3 meters or better to serve the following purposes: (a) to improve the internal quality of existing geodetic networks (triangulation, etc.) by establishing "super" control points in sufficient numbers; (b) to provide control for mapping to scales as large as 1:25 000 in areas where no primary geodetic control exists.

(3) A set of scientific reference stations was to be established in which positions were known to an internal consistency of 1 meter or better for advanced (earth and ocean physics) applications.

This report contains results connected with step 1. The goals of items 2 and 3 will be fulfilled when the quality of the observational material and/or the distribution of tracking stations become better than those made available for this study. Since the National Geodetic Satellite Program is no longer funded,

it is only hoped that these goals will be incorporated into other programs.

This chapter is given in six sections. Following the brief section on instrumentation, section 8.3 contains material on observational and survey data as provided to The Ohio State University by the various data collecting agencies. After the theory is described in section 8.4, the results of the least-squares adjustment are given in section 8.5. Section 8.5 also contains the comparison of these results with various dynamic solutions and survey data. In section 8.6, conclusions are presented with some recommendations for future work. After the section captions, reference is made to the appropriate OSU Department of Geodetic Science report where more detailed information on the content of the section may be found.

Acknowledgments.—This chapter is related to the work performed by the staff of the Department of Geodetic Science, The Ohio State University, sponsored by NASA under the National Geodetic Satellite Program. Grateful acknowledgment is given for the generous support given during the past eight years, which not only made The Ohio State University's participation in this program possible but also provided a total of 34 undergraduate and graduate students with assistantships of various lengths and types during their studies. On NASA's behalf, the project was monitored by Jerome D. Rosenberg (currently Deputy Director, Communication Programs, NASA Headquarters) from 1965 to 1972, whose support and encouragement were felt and appreciated throughout. Because of a reorganization within NASA, his work was taken over with enthusiasm by Benjamin Milwitzky, Deputy Director, and James P. Murphy, Special Programs, NASA Headquarters.

Project staff, with significant contributions, are listed in table 8.1. The proportion of their individual contributions is reflected in a general way by the length of stay and/or by the issue numbers in the report series of the Department of Geodetic Science to which the individual contributed most. In a university environment, where there are important interactions between the students and the instructional staff, it is generally difficult to separate individual contributions from the team work. Thus the report numbers listed reflect, in most cases, responsibilities in a given area rather than "individual" contributions. Exceptions are the theoretical studies contained in Reports 114, 147, 150, 177, and 185, in which very little input came from students other than the authors.

Students receiving financial assistance other than direct fellowships (such as travel) are noted on table 8.1. In addition to those listed in the table, 15 students also carried short-term appointments for various generally nonprofessional responsibilities.

Graduate students on regular fellowships also received full tuition waivers from the university, which is acknowledged here. Other university contributions came from the Computer Center, which provided a significant amount of free computer time, and from the department in the form of 4.4 percent cost-sharing of the total research budget.

Last but not least, grateful acknowledgment is given to the Defense Mapping Agency (Aerospace and Topographic Centers), NASA (Goddard Space Flight Center and Wallops Flight Center), the National Geodetic Survey/NOS/NOAA, and SAO (Smithsonian Astrophysical Observatory) for supplying the observational and survey data, the basic ingredients of the work, and other information, always without reservations or delay. In this connection, the National Space Science Data Center also played an important role.

8.2 INSTRUMENTATION

The Ohio State University used data provided by other groups and did not make any observations of its own. It did not develop or use any instruments or equipment which were unique to OSU's work. The instruments

used in getting the data used by OSU are described in detail in other chapters, as indicated in table 8.2.

8.3 DATA

Details of the data used by OSU and obtained from various agencies are given in the tables of sections 8.3.1, 8.3.2.1, and 8.3.3. Before reaching OSU, the data were subjected to reductions considered necessary by the respective agencies (Gross, 1968; Hotter, 1967). Most of the data obtained needed some kind of additional treatment before they could be used for analysis; the more important details of this treatment (preprocessing) are given in section 8.3.2.2.

8.3.1 Satellites and Observation Stations
(OSU Report 71)

Data used for OSU investigations were obtained by observing the satellites listed in table 8.2. Orbital and other information on these satellites is tabulated in Girnius and Joughin (1968).

Survey information regarding the observation stations is summarized in tables 8.3 and 8.4.

8.3.2 Satellite Observational Data and Their Handling

8.3.2.1 Satellite Observational Data
(OSU Reports 187, 188, 193, 195, 196)

Data used in the four OSU partial solutions (networks) reported earlier, namely, MPS, BC, SECOR, and SA, and in the current combined solutions, designated WN (World Net), are summarized in table 8.5. These networks are shown in figures 8.1 through 8.7. Information related to the data used in the solutions is provided in tables 8.6 and 8.7 (a,b,c,d).

8.3.2.2 Data Handling

8.3.2.2.1 PREPROCESSING
(OSU Reports 70, 82, 93, 100, 106, 110, 195)

The term preprocessing covers any treatment (reductions, corrections, etc.) that must be applied to the observed data before their analysis, to remove systematic errors burdening the observations. From the point

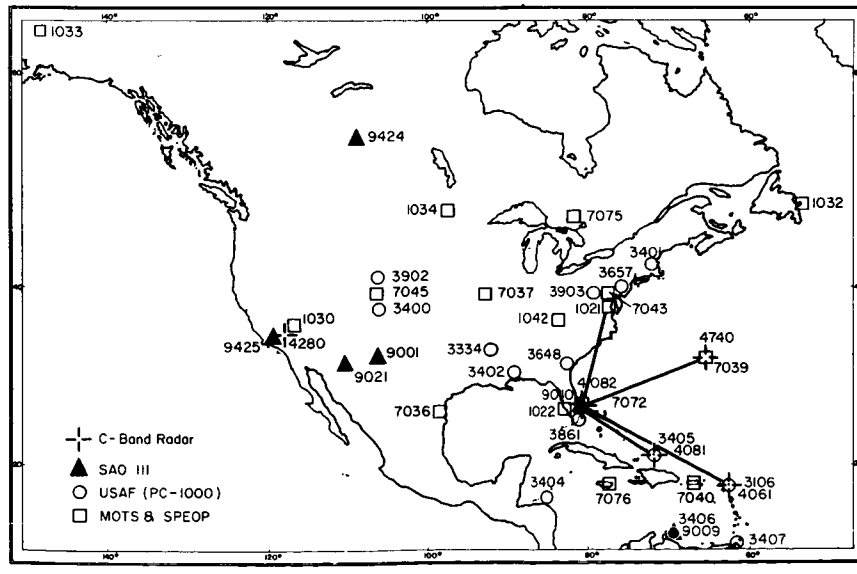

FIGURE 8.1.—MPS stations in North America.

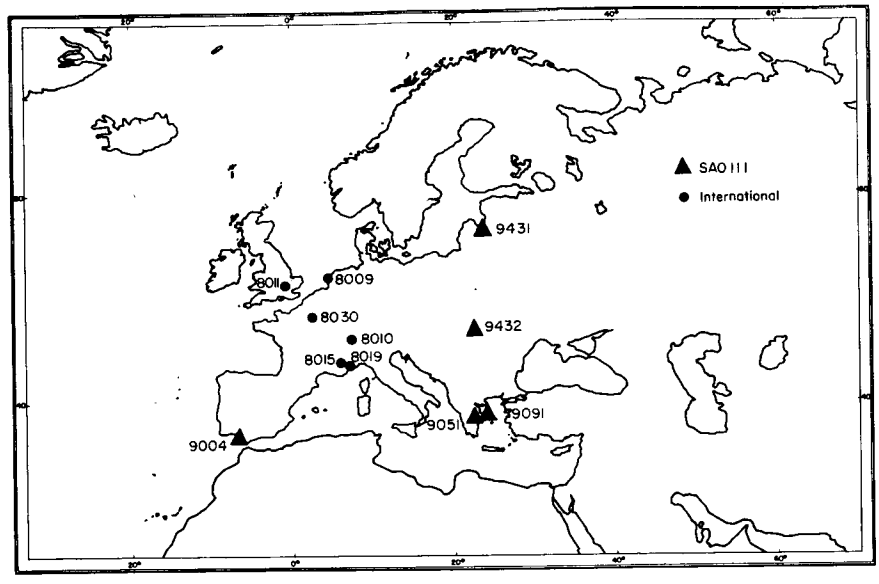

FIGURE 8.2.—MPS stations in Europe.

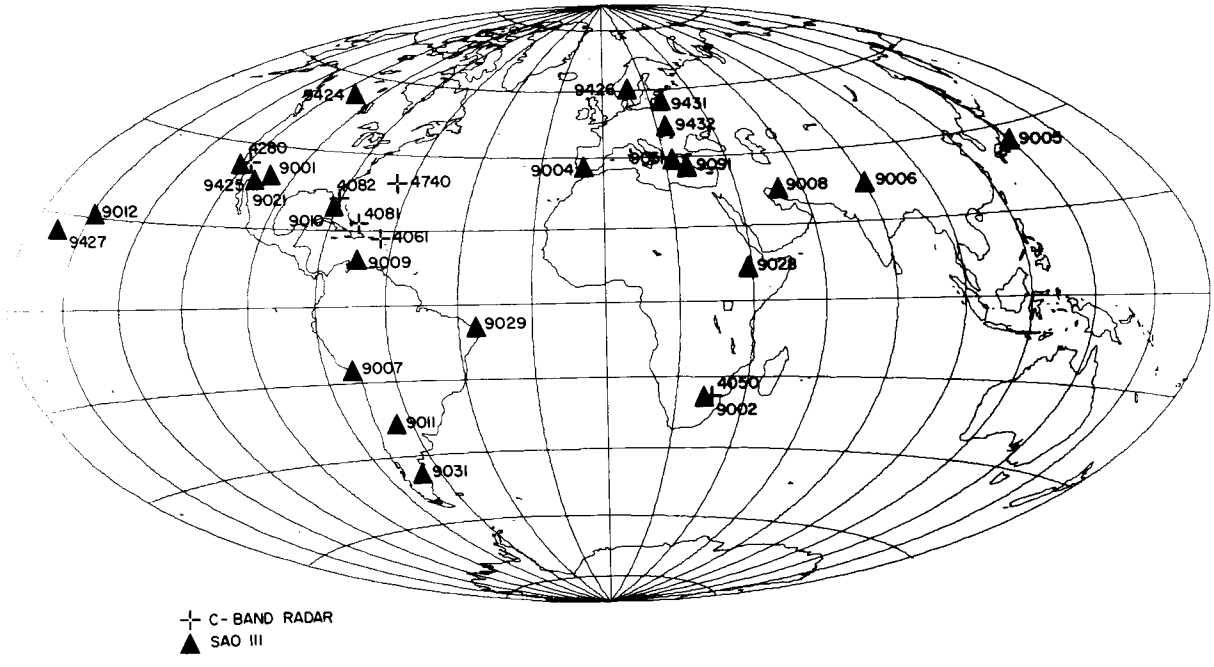

FIGURE 8.3.—SAO and C-band stations in the MPS net.

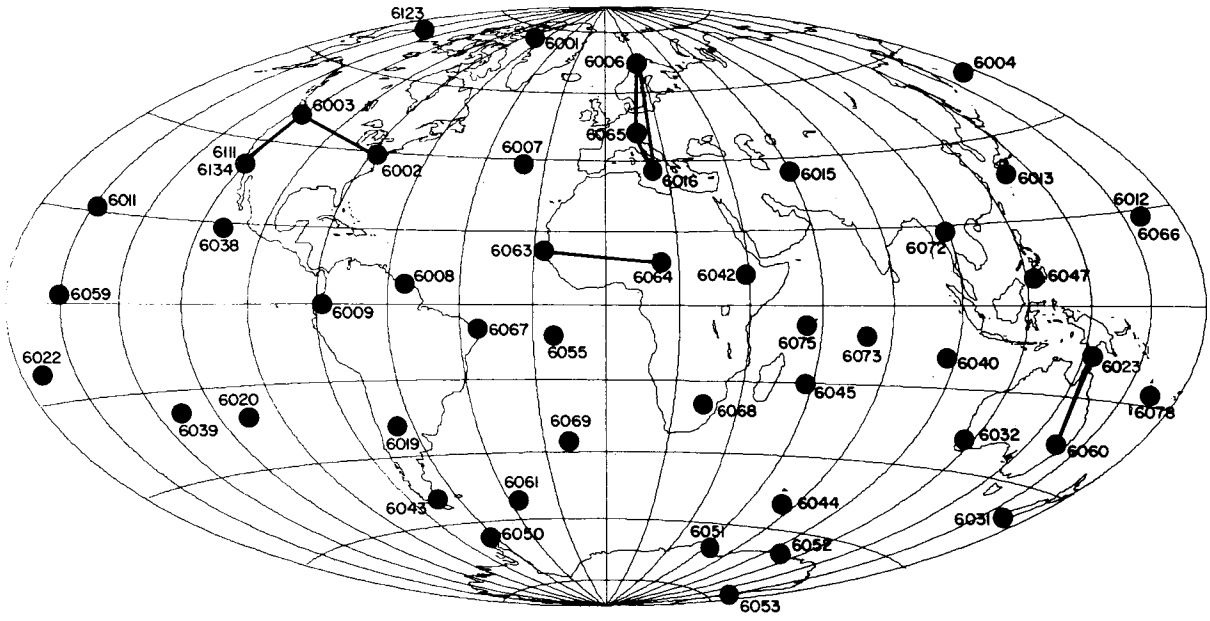

FIGURE 8.4.—BC–4 worldwide geometric satellite network.

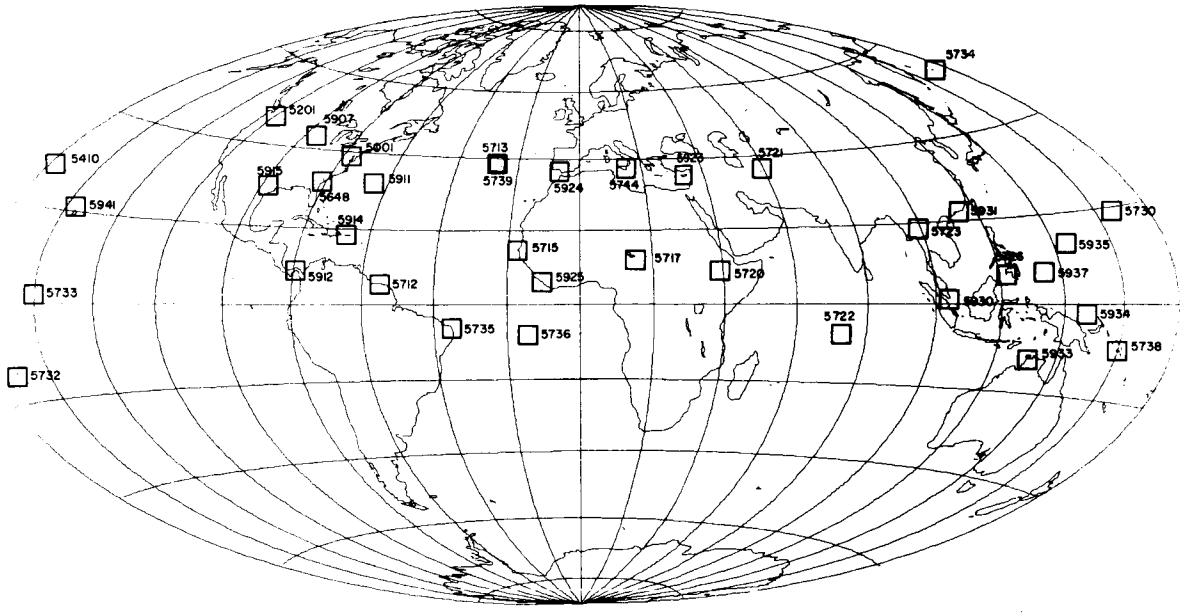

FIGURE 8.5.—SECOR equatorial network.

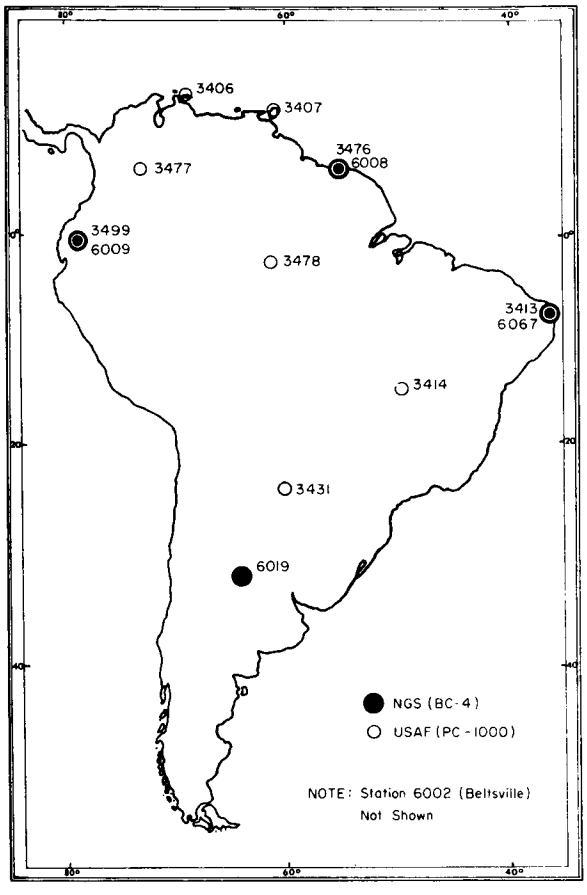

FIGURE 8.6—South American densification net.

of view of the investigator who has not participated in the actual observations, preprocessing can be considered as consisting of two parts:

(1) Reductions and corrections of observed data are made by the respective agencies responsible for the observations before the data are sent either to the National Space Science Data Center or to the individual investigator. This part of the preprocessing is dealt with by Hotter (1967) and by Gross (1968).

(2) Additional corrections to the reduced data, homogenization of the data obtained from various agencies, and screening of data for blunders and ambiguities are the parts of the preprocessing procedure to be done by the investigator.

Figure 8.8 is a self-explanatory summary of both types of preprocessing for camera observations as handled in practice. The shaded blocks represent the portion of the work performed at OSU. For more details see Hotter (1967). Figure 8.9 is a summary of preprocessing applied to the SECOR data. For more details see Gross (1968).

No preprocessing was applied to the C-band radar data (Mueller and Whiting, 1972).

8.3.2.2.2 DETECTION OF BLUNDERS AND REJECTION [1]
(OSU Report 86)

Camera Data.—Blunders in the observed declinations and right ascensions and/or observing ground station coordinates are detected during the formation of the normal equations. The procedure used is to test the variance of unit weight that would result from a preliminary least-squares adjustment of each simultaneous event. In this adjustment the ground stations are held fixed. The residuals on the ijth observed α, δ pair from such a preliminary adjustment are the first two elements of the 3×1 vector

$$V_{ij}=B_{ij}^{-1}(\mathbf{X}_i-\mathbf{X}_j^o)\,\mathbf{X}_j^o=\left\{\sum_i M_{ij}^{-1}\right\}^{-1}\left\{\sum_i M_{ij}^{-1}\mathbf{X}_i\right\}$$

(The third element is the range to the preliminary adjusted satellite position.) Thus

$$\sum_i V'_{ij}P_{ij}V_{ij}=\sum_i(\mathbf{X}_i-\mathbf{X}_j^o)'\,M_{ij}^{-1}(\mathbf{X}_i-\mathbf{X}_j^o)$$

since the third element is dispensed within the product

$$P_{ij}B_{ij}^{-1}(\mathbf{X}_i-\mathbf{X}^s)$$

(see eq. (8.34)). Therefore the variance of unit weight is computed from

$$\sigma_0^2=\frac{\sum_{\text{event}}(\mathbf{X}_i^o-\mathbf{X}_j^o)'\,M_{ij}^{-1}(\mathbf{X}_i^o-\mathbf{X}_j^o)}{2n-3} \qquad (8.1)$$

[1] To appreciate this section the reader is advised to study section 8.4 first.

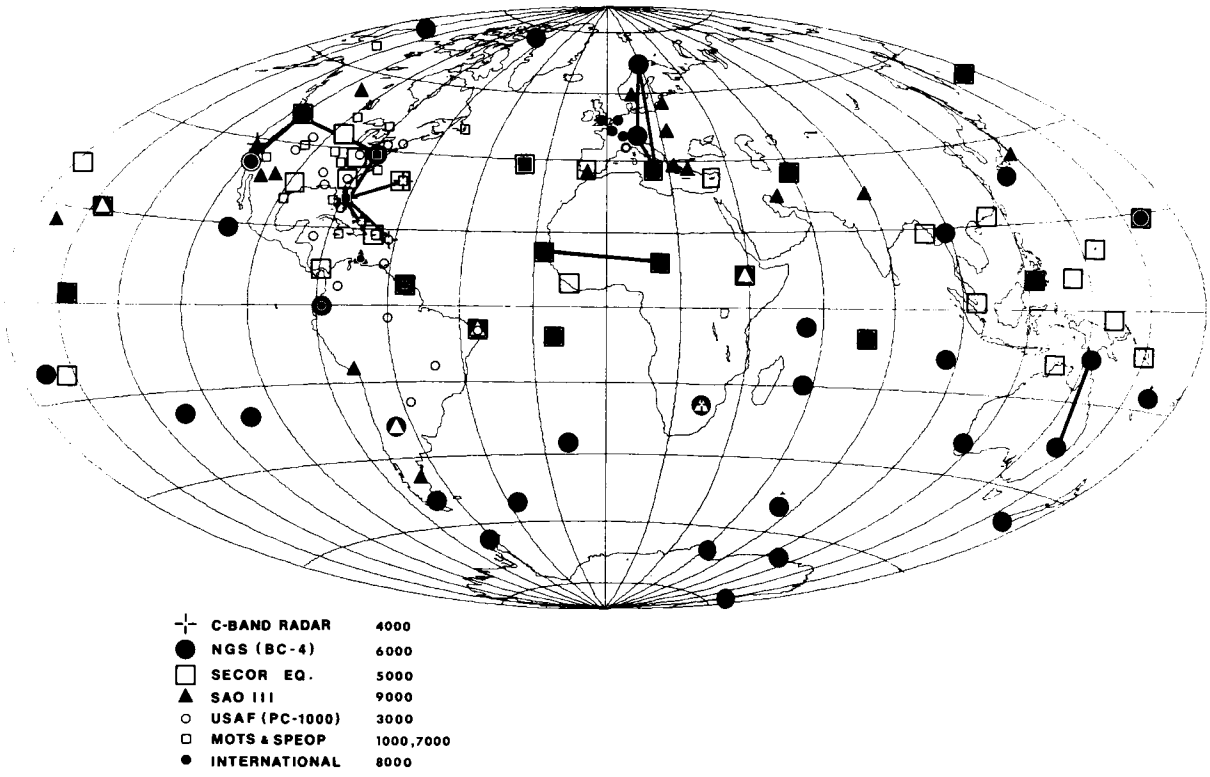

FIGURE 8.7.—OSU geometric satellite network (WN).

CAMERA NAME		DMA PC-1000			NGS BC-4 (ASTRO) BC-4 (COSMO)			NASA/GSFC MOTS 24 MOTS 40 PTH 100			SAO BAKER-NUNN K-50		
CATALOGUE		SAO			SAO			SAO			SAO		
CALIBRATION	TYPE	PHOTO			PHOTO			PHOTO			ASTRO		
	NO. OF STARS	25-30			120			40-50			B-10		
	NO. OF SAT. IMAGES (PASSIVE)	-			600						1		
	NO. OF PARAMETERS	18 (EXT. INT: 6, REFRACT: 2)			14-20 (EXT. INT: 6, DIST: 6, NON⊥: 1, DIFF. SC.: 1, AVAIL.: 6)			8 (EXT. INT: 6, REFRACT: 2)			6		
	LENS DIST. PREDETERMINED	YES			NO			YES					
TIME SYNCHRONIZATION		PORTABLE CLOCK & VLF			PORTABLE CLOCK & VLF			ACTIVE SAT. ONLY			PORTABLE CLOCK & VLF		
STAR UPDATING AND SATELLITE IMAGE CORRECTIONS		STAR	SATELLITE	TIME	STAR	SATELLITE	TIME	STAR	SATELLITE	TIME	STAR	SATELLITE	TIME
	PROPER MOTION	C			M			C			C		
	PRECESSION	C			M,C			M					
	NUTATION	C			C			C					
	ANNUAL ABERRATION	C			C			C				C	
	DIURNAL ABERRATION	C			C			C					
	ASTRO. REFRACTION (GARFINKEL)	CP	-CP WITH ADJ. COEF.		CP	-CP		CP	-CP WITH ADJ. COEF.		IMPLICIT IN PLATE REDUCTION		
	PARALL. REFRACTION								C				
	SAT. ABERRATION (LIGHT TIME)						C (P.S.O.)						C TO STA. (A.S.O.)
	UTC → UTI						C C						
	UTC → A.S.												C
	A.S. → UTI												
	PHASE (PASSIVE ONLY)					C							

M: MATRIX CORRECTION
C: CONVENTIONAL CORR.
CP: CONVENTIONAL DURING PLATE PROCESSING
P.S.O.: PASSIVE SAT. ONLY
A.S.O.: ACTIVE SAT. ONLY

: PREPROCESSING CORRECTION NEEDED

FIGURE 8.8.—Camera data preprocessing procedure summary for major U.S. agencies.

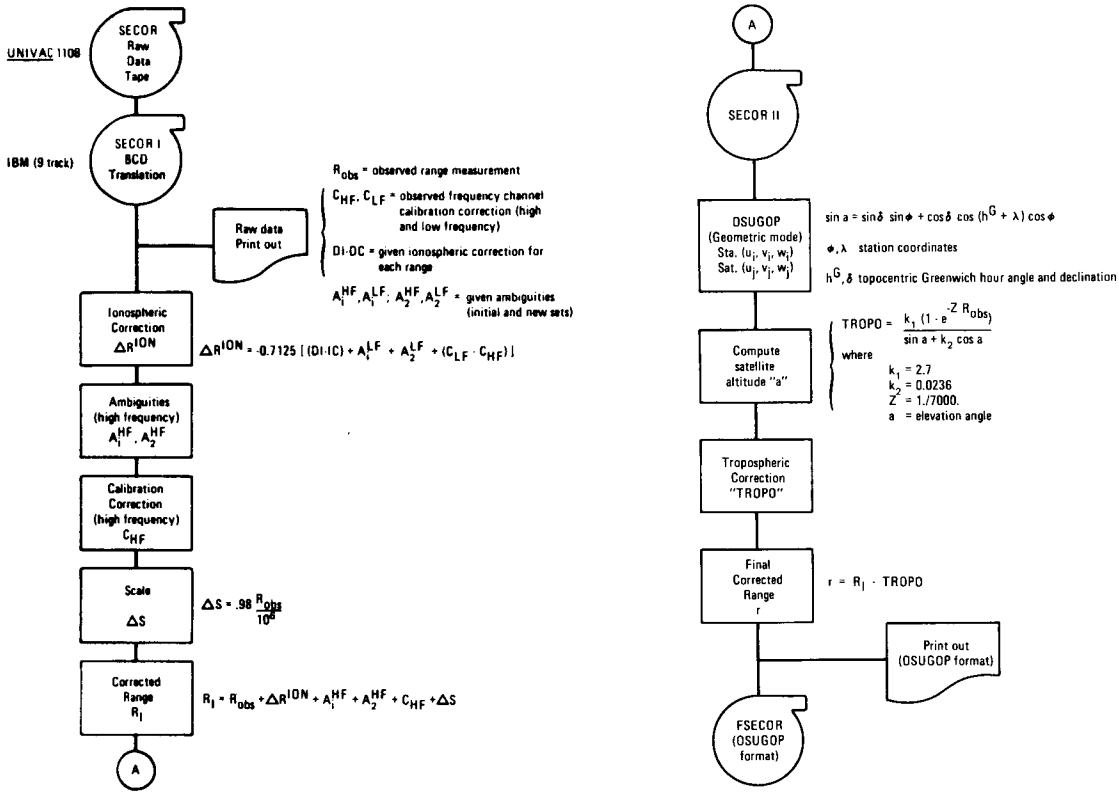

FIGURE 8.9.—Scheme of SECOR preprocessing procedure at OSU.

where the numerator can be shown to be the sum square of the weighted residuals (arc seconds squared) of all the observed declinations and right ascensions in the event and where n is the number of ground stations in the event.

If a number of rejected simultaneous events repeatedly contain a particular ground station, a blunder probably occurs in the coordinates of the particular ground station rather than in the observed quantities. In this case, the preliminary coordinates of that ground station should be verified.

Range Data.—Blunders in the observed topocentric ranges and/or ground station coordinates are detected during the formation of the normal equations. The procedure used is to test the variance of unit weight (eq. (8.10)) arising from a preliminary least-squares adjustment of each simultaneous event.

The preliminary adjustment is basically an iterative adjustment for the u_j, v_j, w_j rectangular coordinates of the satellite position by fixing the ground stations and applying the residuals of the adjustment to the observed ranges. The approximation to the parameters u_j, v_j, w_j is obtained by converting the so-called approximate geodetic coordinates of the satellite into rectangular coordinates by use of equation (8.36). The approximate geodetic coordinates of the satellite are obtained by averaging the latitudes and longitudes of the ground stations involved in the simultaneous event and estimating the ellipsoidal height of the satellite. The idea that this determination is crude is immediately rejected upon the knowledge that at most four iterations (to a tolerance of 1 cm in u_j, v_j, w_j) are required and that the electronic computers perform these iterations in less time than is necessary to solve the corresponding simultaneous exact second-order equations.

The equation giving the mathematical structure of this preliminary adjustment is identical to equation (8.75), the mathematical structure for the main range adjustment. Since only three parameters are involved, the linearized form of the mathematical structure for n ground stations in one simultaneous event becomes

$$AX-\bar{V}+W=0 \tag{8.2}$$

where the coefficient matrix

$$A=\begin{bmatrix} \frac{u_j^o-u_1^o}{r_{1j}^o} & \frac{v_j^o-v_1^o}{r_{1j}^o} & \frac{w_j^o-w_1^o}{r_{1j}^o} \\ \frac{u_j^o-u_2^o}{r_{2j}^o} & \frac{v_j^o-v_2^o}{r_{2j}^o} & \frac{w_j^o-w_2^o}{r_{2j}^o} \\ \cdot & \cdot & \cdot \\ \cdot & \cdot & \cdot \\ \cdot & \cdot & \cdot \\ \frac{u_j^o-u_k^o}{r_{kj}^o} & \frac{v_j^o-v_k^o}{r_{kj}^o} & \frac{w_j^o-w_k^o}{r_{kj}^o} \\ \cdot & \cdot & \cdot \\ \cdot & \cdot & \cdot \\ \cdot & \cdot & \cdot \\ \frac{u_j^o-u_m^o}{r_{mj}^o} & \frac{v_j^o-v_m^o}{r_{mj}^o} & \frac{w_j^o-w_m^o}{r_{mj}^o} \end{bmatrix} \tag{8.3}$$

the correction vector for the satellite coordinates

$$X=\begin{bmatrix} du_j \\ dv_j \\ dw_j \end{bmatrix} \tag{8.4}$$

the residual vector for the ranges

$$\bar{V}=\begin{bmatrix} \bar{v}_{1j} \\ \bar{v}_{2j} \\ \cdot \\ \cdot \\ \cdot \\ \bar{v}_{kj} \\ \cdot \\ \cdot \\ \cdot \\ \bar{v}_{nj} \end{bmatrix} \tag{8.5}$$

and the constant vector

$$W=\begin{bmatrix} r_{1j}^o-r_{1j}^b \\ r_{2j}^o-r_{2j}^b \\ \cdot \\ \cdot \\ \cdot \\ r_n^{oj}-r_{nj}^b \end{bmatrix} \tag{8.6}$$

where r_{1j}^o and r_{1j}^b are preliminary and observed ranges, respectively.

The normal equations

$$NX+U=0 \tag{8.7}$$

where

$$N=A'PA \tag{8.8}$$

$$U=A'PW \tag{8.9}$$

are solved for X by iteration until the elements of the vector X are less than 1 cm. At this point, X is entered into equation (8.2) and the vector of residuals $\bar{V}$ is determined; the variance of unit weight is then computed according to

$$\sigma_0^2=\frac{\bar{V}'P\bar{V}}{n-3} \tag{8.10}$$

The complete set of data for the simultaneous event is printed out for evaluation in the case that the particular σ_0^2 is greater than a chosen input value. At the same time, no contribution is made to the normal equations by the rejected event.

8.3.3 Constraints

For the explanation of the type of constraints used in the solution see section 8.4.5. Only the data used in applying the various constraints are summarized here in tables 8.8 to 8.11.

8.4 THEORY AND MATHEMATICAL MODELS

(OSU Reports 86, 150, 185, 191)

This section presents almost the complete theory used in transforming the observational data (sec. 8.3) into geodetic results. Left out of this section and given in section 8.3 instead is that part of the theory that con-

cerns the preprocessing procedure of the observed data where systematic errors in the observed data are removed, detected, and eliminated, or where generally the necessary corrections to the observed data are made before they are inserted into the method of least-squares adjustment.

8.4.1 Definitions and Coordinate Systems
(OSU Report 86)

8.4.1.1 Basic Concepts and Statement of the Problem

A theory proceeds from a set of known facts or assumptions called the data, and by manipulating these according to accepted rules, called theory, certain conclusions, called results are produced. This process is started in response to the posing of a problem. The problem in this case can be stated as follows:

Given are the approximate coordinates of a number of points (stations) on the surface of the Earth, which are assumed to be in error by unknown amounts. Also given are measured directions and/or distances from these points to other points on and also above the surface of the Earth (artificial satellites); the observations occur in sets, all observations within a given set being made at the same time. The problem is then to find the most probable values for the unknown errors in the coordinates of points (stations) on the Earth's surface.

Thus, in this "space triangulation" (or trilateration) method, satellites are observed simultaneously from groups of known and unknown ground stations. This method permits a purely geometric solution. Its main characteristic is that orbital elements are not required. If the satellite positions are needed, they can be computed from the preliminary coordinates of the ground stations and the observations themselves.

The method used to get a solution is therefore (1) to set up the equations giving the observations (angle or distance) in terms of observer and satellite coordinates, (2) to linearize these equations to give observation residuals in terms of corrections to the observer and satellite coordinates, (3) to select from the data available those which can be put into simultaneity sets, and (4) from known and assumed statistical properties of the observations to solve the equations of (2) with the use of the data of (4).

Since the method is geometric and involves coordinates of points on the Earth's surface and of points in "inertial" space, transformation between coordinate systems occurs frequently. The systems used and their interrelation are described in sections 8.4.1.2 and 8.4.1.3, respectively.

8.4.1.2 Coordinate Systems

The camera observations after preprocessing (section 8.3.2.2) are assumed to be in the true topocentric celestial system, whereas the preprocessed topocentric ranging data are independent of the coordinate systems used.

Two distinct types of coordinate systems have been used here: the terrestrial (average and instantaneous) system and the celestial (true) system.

The following summary of these systems assumes righthanded rectangular coordinates with axes numbered according to figure 8.10. Generally, the origin of the coordinate system coincides with or is near the center of gravity of the Earth.

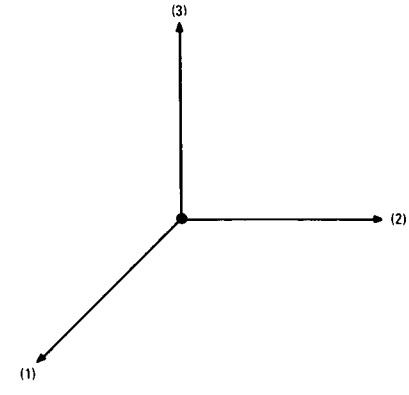

FIGURE 8.10.—Numbering of coordinate axes.

8.4.1.2.1 AVERAGE TERRESTRIAL (X)

(1) The 3 axis is directed toward the average north terrestrial pole as defined by the International Polar Motion Service (IPMS), commonly known as the Conventional International Origin (CIO) (Mueller, 1969, p. 351).

(2) The 1–3 plane is parallel to the mean Greenwich astronomic meridian as defined by the Bureau International de l'Heure (BIH) (Mueller, 1969, p. 343).

This system is the geodetic (terrestrial) coordinate system, later also referred to as the u, v, w system.

8.4.1.2.2 INSTANTANEOUS TERRESTRIAL (Y)

(1) The 3 axis is directed toward the instantaneous rotation axis of the Earth (true celestial pole), the coordinates of which are given by the IPMS or by the BIH with respect to the CIO.

(2) The 1–3 plane contains the point where the mean Greenwich astronomic meridian intersects the true equator of date.

This coordinate system is used as the intermediate connection between the terrestrial and celestrial coordinate systems.

8.4.1.2.3 TRUE CELESTIAL (Z)

(1) The 3 axis is equivalent to the 3 axis of the instantaneous terrestrial system (true celestial pole).

(2) The 1 axis is directed toward the true vernal equinox of date.

These and still other coordinate systems are discussed in detail by Veis (1963a) and Mueller (1969).

8.4.1.3 Transformations of Coordinate Systems

Transformation between terrestrial and celestial coordinate systems becomes necessary when topocentric directions to satellites are obtained by photographing the satellite against a background of stars. After corrections for the physical effects, such as differential refraction and aberration, shimmer, etc. (Mueller, 1964, pp. 309–317; Hotter, 1967), have been applied, the resulting topocentric right ascension and declination form the purely geometric ground-to-satellite direction. In terms of the corresponding direction cosines, **Z** can be expressed by the column vector

$$\mathbf{Z}=\begin{bmatrix}\cos\delta & \cos\alpha\\ \cos\delta & \sin\alpha\\ \sin\delta & \end{bmatrix}=\begin{bmatrix}Z_1\\ Z_2\\ Z_3\end{bmatrix} \qquad (8.11)$$

In order to transform **Z** from the celestial to the average terrestrial system (in which the mathematical model for the adjustment is expressed), rotations about the coordinate axes are required.

Transformation is first made into the instantaneous terrestrial system (see fig. 8.11). This transformation is a function of a single finite rotation through the Greenwich apparent sidereal time (GAST). A vector **Z** in the true celestial system is transformed into the instantaneous terrestrial system by the following equation:

$$\mathbf{Y}=R_3\,(\mathrm{GAST})\,\mathbf{Z} \qquad (8.12)$$

where **Y** is the resulting vector in the instantaneous terrestrial system and R_3 (GAST) is a 3×3 matrix that expresses a counterclock-

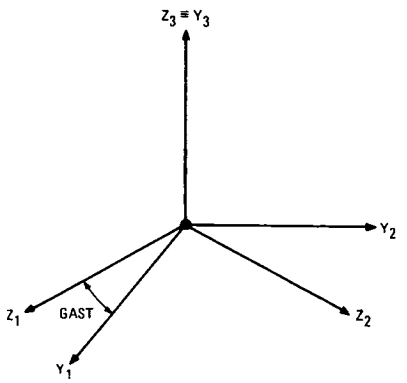

FIGURE 8.11.—True celestial and instantaneous terrestrial coordinate systems.

wise rotation, as viewed from the positive end of the 3 axis, by the amount GAST, namely,

$$R_3\,(\mathrm{GAST}) = \begin{bmatrix} \cos(\mathrm{GAST}) & \sin(\mathrm{GAST}) & 0 \\ -\sin(\mathrm{GAST}) & \cos(\mathrm{GAST}) & 0 \\ 0 & 0 & 1 \end{bmatrix} \tag{8.13}$$

Next the vector **Y** in the instantaneous terrestrial system (Y) is transformed to the average terrestrial (X) system (see fig. 8.12). This transformation is a function of two rotations through the x and y coordinates of the instantaneous terrestrial pole.

$$\mathbf{X} = R_2(-x)R_1(-y)\mathbf{Y} \tag{8.14}$$

where X is the resulting vector in the average terrestrial coordinate system; $R_1(-y)$ and $R_2(-x)$ are 1-axis and 2-axis rotations through $-y$ and $-x$. Since the x and y values are differentially small, the finite rotations may be replaced by differential rotations and equation (8.14) is reduced to

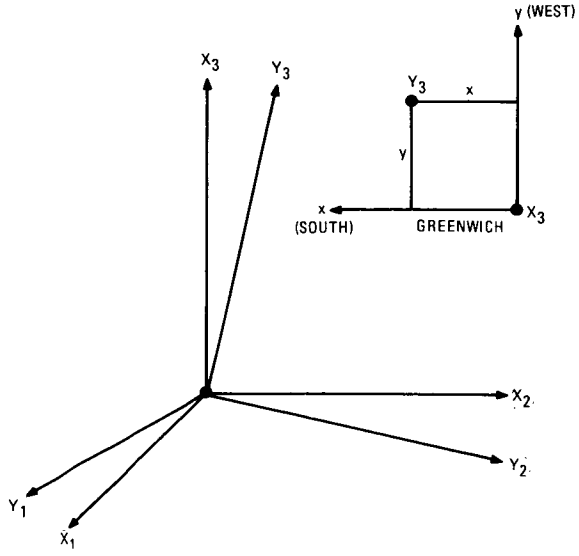

FIGURE 8.12.—Instantaneous and average terrestrial coordinate systems.

$$\mathbf{X} = \begin{bmatrix} 1 & 0 & x \\ 0 & 1 & -y \\ -x & y & 1 \end{bmatrix}\mathbf{Y} \tag{8.15}$$

by omitting the products of x and y. Thus the transformation from the true celestial to the average terrestrial coordinate system is achieved by combining the rotations expressed in equations (8.12) and (8.14), namely

$$\mathbf{X} = R_2(-x)R_1(-y)R_3(\mathrm{GAST})\ \mathbf{Z} \tag{8.16}$$

and, after equation (8.15) is considered, the matrix form is

$$\mathbf{X} = S\mathbf{Z} \tag{8.17}$$

where S is given in inset on page 659. The quantities x, y and GAST in the above equation are obtained by the method described in Mueller (1969, pp. 80, 153, 337).

8.4.2 The Direction Adjustment

8.4.2.1 Uncorrelated Events (OSU Report 86)

8.4.2.1.1 THE MATHEMATICAL MODEL

The adjustment method is by least squares, where the parameters are the three-dimensional rectangular coordinates of the ground stations and satellite positions,[2] while the observables are the topocentric range, and topocentric declination and right ascension of the satellite.

The mathematical structure relating the parameters and the observables is a function of three vectors. As depicted in figure 8.13, the three vectors are as follows: $\mathbf{X}_i$, the coordinate system origin to ground station vector; $\mathbf{X}_j$, the coordinate system origin to satellite position vector; and $\mathbf{X}_{ij}$, the ground station i to satellite position j vector. (Symbols in bold face will be reserved for vectors that

[2] These are needed in the algebraic derivation, but in the numerical computation they are either not needed or obtained to a sufficient accuracy from the observed quantities.

$$S=\begin{bmatrix} \cos\ (\text{GAST}) & \sin\ (\text{GAST}) & x \\ -\sin\ (\text{GAST}) & \cos\ (\text{GAST}) & -y \\ -x\cos\ (\text{GAST})-y\sin\ (\text{GAST}) & -x\sin\ (\text{GAST})+y\cos\ (\text{GAST}) & 1 \end{bmatrix} \tag{8.18}$$

have a finite magnitude as opposed to, say, vectors containing differential corrections.) Thus

$$\mathbf{X}_j-\mathbf{X}_i=\mathbf{X}_{ij} \tag{8.19}$$

or

$$F_{ij}=\mathbf{X}_j-\mathbf{X}_i-\mathbf{X}_{ij}=0 \tag{8.20}$$

where

$$\mathbf{X}_j=\begin{bmatrix} u_j \\ v_j \\ w_j \end{bmatrix} \tag{8.21a}$$

is a vector composed of the rectangular coordinates of an arbitrary satellite position;

$$\mathbf{X}_i=\begin{bmatrix} u_i \\ v_i \\ w_i \end{bmatrix} \tag{8.21b}$$

is a vector composed of the rectangular coordinates of an arbitrary ground station;

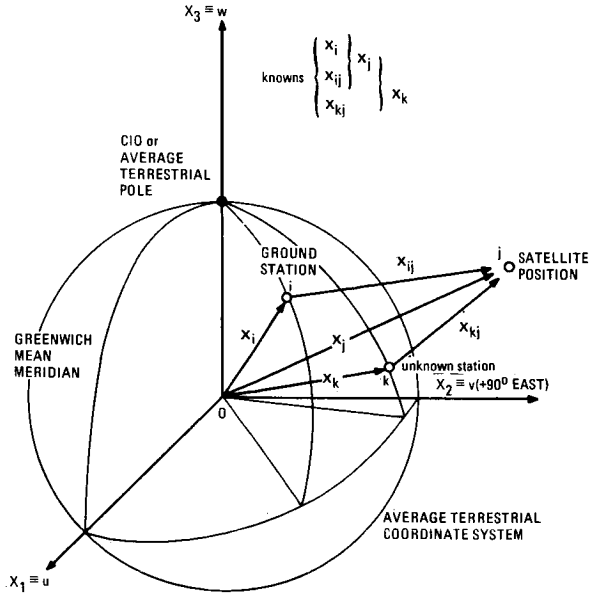

FIGURE 8.13.—The adjustment coordinate system.

$$\mathbf{X}_{ij}=S\begin{bmatrix} r_{ij}\cos\delta_{ij}\cos\alpha_{ij} \\ r_{ij}\cos\delta_{ij}\sin\alpha_{ij} \\ r_{ij}\sin\delta_{ij} \end{bmatrix} \tag{8.22}$$

r_{ij}, δ_{ij}, α_{ij} being the topocentric range, true declination, and right ascension from i to j, respectively, while S is the matrix that transforms the vector from the true celestial to the average terrestrial coordinate system (sec. 8.4.1.3).

The point-by-point buildup of the network can be visualized in the following way. Given the components of the vectors $\mathbf{X}_i$ and $\mathbf{X}_{ij}$, $\mathbf{X}_j$ is computed. Then with this position j as known, and a known vector from an unknown k station to j, the coordinates of the unknown station $\mathbf{X}_k$ are computed (see fig. 8.13). This step is extended to include many unknown and known stations, along with many redundant observations, thereby necessitating an adjustment.

Strictly speaking, pure direction or range data do not permit such a procedure to be literally followed; however, the adjustment framework (a form of collinearity) remains applicable.

The mathematical structure (eq. (8.20)) is linearized by a Taylor series expansion about the preliminary values of the ground stations and satellite positions and the observed topocentric values of the range, declination, and right ascension. The result is the following matrix equation:

$$AX+BV+W=0 \tag{8.23}$$

which represents the general linearized mathematical model.

In this equation, the design matrix A is composed of submatrices of the form

$$A_{ij}=\frac{\partial F_{ij}}{\partial \mathbf{X}_j,\,\partial \mathbf{X}_i}=\left[\begin{array}{ccc|ccc}1&0&0&-1&0&0\\0&1&0&0&-1&0\\0&0&1&0&0&-1\end{array}\right]$$
$$=[+I_3|-I_3] \qquad (8.24)$$

and the unknown X vector is composed of subvectors of the form

$$X_{ij}=\left[\begin{array}{c}X_j\\\hline X_i\end{array}\right] \qquad (8.25)$$

where

$$X_j=\begin{bmatrix}du_j\\dv_j\\dw_j\end{bmatrix} \qquad (8.26)$$

$$X_i=\begin{bmatrix}du_i\\dv_i\\dw_i\end{bmatrix} \qquad (8.27)$$

are corrections to the preliminary values of the satellite positions and ground stations, respectively. The design matrix B is composed of 3×3 submatrices of the form

$$B_{ij}=\frac{\partial F_{ij}}{\partial \delta_{ij},\,\partial \alpha_{ij},\partial r_{ij}}$$
$$=SR_3(-\alpha_{ij})R_2(-90^\circ+\delta_{ij})$$
$$\times\begin{bmatrix}1&0&0\\0&-\cos\delta_{ij}&0\\0&0&-1\end{bmatrix} \qquad (8.28)$$

where S is defined by equation (8.18); R_3 and R_2 are rotation matrices.

The matrix

$$\begin{bmatrix}r_{ij}&0&0\\0&r_{ij}&0\\0&0&1\end{bmatrix}$$

is omitted from the expression for B_{ij}, since it is multiplied into the vector of residuals V composed of the subvectors

$$V_{ij}=\begin{bmatrix}r_{ij}\delta\delta_{ij}\\(r_{ij}\cos\delta_{ij})\ \delta\alpha_{ij}\\\delta r_{ij}\end{bmatrix} \qquad (8.29)$$

These are the residuals of the adjustment in units of meters ($\delta\delta_{ij}$ and $\delta\alpha_{ij}$ are in radians). Observe that $\delta\delta_{ij}$ is measured on the circle of radius r_{ij}, while $\delta\alpha_{ij}$ is measured on the circle of radius of $r_{ij}\cos\delta_{ij}$.

Finally, the misclosure vector W is composed of the subvectors

$$W_{ij}=\mathbf{X}_j^o-\mathbf{X}_i^o-\mathbf{X}_{ij}^b \qquad (8.30)$$

where o designates "evaluated at preliminary values" and b designates "evaluated at observed values."

8.4.2.1.2 WEIGHTING OF OBSERVATIONS

The observed quantities in the case of camera observations are the topocentric declinations δ and right ascensions α. The corresponding accuracy estimates resulting from a photographic plate adjustment or some other a priori estimate are σ_δ^2 and σ_α^2, the variances, and $\sigma_{\alpha\delta}=\sigma_{\delta\alpha}$, the covariance. All units are arc seconds squared.

It is important to note that the weighting of the declinations and right ascensions is made on the basis of the estimates of variances of δ and α obtained from the plate adjustments and that it is assumed that the variances of δ and α do not vary according to the distance of the satellite from the particular observing station.

On the other hand, the weighted sum of squares of the residuals is conveniently chosen to have units of arc seconds squared; thus the weights are to have units of (arc sec)^{2}m^{-2}, since the units of the residuals have been stipulated (eq. (8.29)) to be meters. Therefore, it is necessary to transform σ_δ^2, σ_α^2, and $\sigma_{\delta\alpha}$ into linear units (meters) by the following formulas:

$$(\sigma_\delta)^2=\left|r\frac{\sigma_\delta''}{\rho''}\right|^2 \qquad (8.31)$$

$$(\sigma_\alpha)^2=\left|r\frac{\sigma_\alpha''}{\rho''}\right|^2\cos^2\delta \qquad (8.32)$$

$$\sigma_{\delta\alpha}=r^2\frac{(\sigma_{\delta\alpha}'')^2}{(\rho'')^2}\cos\delta \qquad (8.33)$$

where r is the approximate topocentric range and

$$\rho'' = \frac{1}{\sin 1''}$$

With the estimated accuracy in linear units the following variance-covariance matrix is formulated:

$$\Sigma_{\delta,\alpha,r} = \begin{bmatrix} \sigma_\delta^2 & \sigma_{\delta\alpha} & \sigma_{\delta r} \\ & \sigma_\alpha^2 & \sigma_{\alpha r} \\ \text{same} & & \\ \text{as above} & & \sigma_r^2 \\ \text{diagonal} & & \end{bmatrix}$$

where the new quantities σ_r^2, $\sigma_{\delta r}$, and $\sigma_{\alpha r}$ are the variance of the range, covariance between the declination and range, and the covariance between the right ascension and range, respectively. If the correlation coefficients

$$\rho_{\delta r} = \frac{\sigma_{\delta r}}{\sigma_\delta \sigma_r} = 0$$

$$\rho_{\alpha r} = \frac{\sigma_{\alpha r}}{\sigma_\alpha \sigma_r} = 0$$

and

$$\sigma_r \rightarrow \infty$$

the weight matrix for a single direction is

$$P_{ij} = \sigma_0^2 \begin{bmatrix} \begin{bmatrix} \sigma_\delta^2 & \sigma_{\delta\alpha} \\ \sigma_{\alpha\delta} & \sigma_\alpha^2 \end{bmatrix}^{-1} & \begin{matrix} 0 \\ 0 \end{matrix} \\ \begin{matrix} 0 & 0 \end{matrix} & 0 \end{bmatrix} \qquad (8.34)$$

where σ_0^2 is the a priori variance of unit weight.

Corresponding to P_{ij}, P denotes the weight matrix for the observed topocentric directions of the adjustment. P has the characteristic of containing nonzero 3×3 matrices only along the diagonal, since the individual directions are assumed to be independent.

The topocentric range is needed in equations (8.31) to (8.33) to convert the estimated accuracy of the directions from arc units into linear (meters) units. Four significant figures are required in the topocentric range. Equation (8.31) shows that the range need have no more significant figures than σ_δ'' or σ_α''.

The topocentric range from an arbitrary ground station i in a given simultaneous event j is computed from

$$r_{ij} = [(u_j^o - u_i^o)^2 + (v_j^o - v_i^o)^2 + (w_j^o - w_i^o)^2]^{1/2} \qquad (8.35)$$

$i = 1, 2, \ldots, n$ (number of stations in the event). u_i^o, v_i^o, w_i^o are the preliminary rectangular coordinates of the ith ground station and are computed from

$$\mathbf{X}_i^o = \begin{bmatrix} u_i^o \\ v_i^o \\ w_i^o \end{bmatrix} = \begin{bmatrix} (N+h)\cos\phi\cos\lambda \\ (N+h)\cos\phi\sin\lambda \\ [N(1-e^2)+h]\sin\phi \end{bmatrix} \qquad (8.36)$$

ϕ, λ, h, N being the geodetic latitude and longitude, the geodetic height, and radius of curvature in the prime vertical at point i, respectively, while e is the eccentricity of the reference ellipsoid. u_j^o, v_j^o, w_j^o are the preliminary rectangular coordinates of the j^{th} satellite position and are computed (note that these are needed only for the purpose of getting the approximate topocentric range) as follows:

(1) The ground vector $\mathbf{X}_{ik}$ between the first two stations listed in the particular simultaneous event

$$\mathbf{X}_{ik} = \begin{bmatrix} u_k - u_i \\ v_k - v_i \\ w_k - w_i \end{bmatrix} \qquad (8.37)$$

(2) The unit vector (direction) $\mathbf{X}_{ij}$ from the ground station i to the satellite position j is computed from

$$\mathbf{X}_{ij} = S \begin{bmatrix} \cos\delta_{ij}\cos\alpha_{ij} \\ \cos\delta_{ij}\sin\alpha_{ij} \\ \sin\delta_{ij} \end{bmatrix} \qquad (8.38)$$

where S is the transformation matrix of the true celestial to the average terrestrial coordinate systems (sec. 8.4.1.3).

(3) In the same way the direction $\mathbf{X}_{kj}$ is computed.

(4) The angle A_k at ground station k is computed from (fig. 8.14)

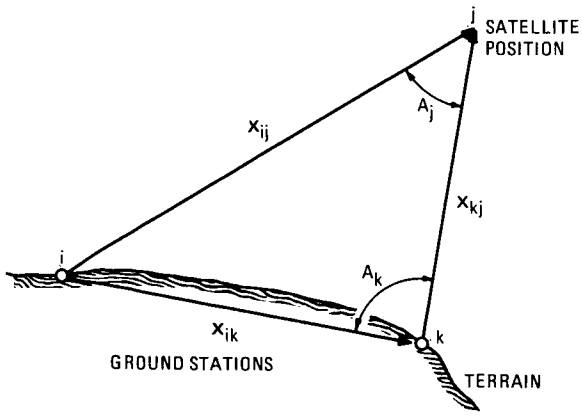

FIGURE 8.14.—The approximate satellite vector.

$$\cos A_k = \frac{\mathbf{X}_{ki} \cdot \mathbf{X}_{kj}}{|\mathbf{X}_{ki}|\,|\mathbf{X}_{kj}|} \tag{8.39}$$

(5) The angle A_j at the satellite position is computed from

$$\cos A_j = \frac{\mathbf{X}_{ji} \cdot \mathbf{X}_{jk}}{|\mathbf{X}_{ij}|\,|\mathbf{X}_{kj}|} \tag{8.40}$$

(6) Finally, the satellite position vector $\mathbf{X}_j^o$ to be used in equation (8.35) is computed from

$$\mathbf{X}_j^o = \mathbf{X}_i^o + r_{ij}\mathbf{X}_{ij} = \begin{bmatrix} u_j^o \\ v_j^o \\ w_j^o \end{bmatrix} \tag{8.41}$$

where

$$r_{ij} = |\mathbf{X}_{ik}| \frac{\sin A_k}{\sin A_j} \tag{8.42}$$

8.4.2.1.3 THE NORMAL EQUATIONS

The normal equations are derived by minimizing the quadratic form

$$V'PV + X'P_xX$$

subject to the relation (eq. (8.23))

$$AX + BV + W = 0$$

Upon introduction of Lagrange multipliers K, the variation function is

$$\Phi = V'PV + X'P_xX - 2K'(AX + BV + W) \tag{8.43}$$

where

- V is the vector of residuals corresponding to the α's and δ's
- X is the vector of corrections to the preliminary ground and satellite positions
- P is the weight matrix for the α's and δ's
- P_x is the weight matrix for the ground and satellite positions

As is described in section 8.4.2.1.1, A and B are the design matrices and W is the constant vector.

Upon the differentiation of equation (8.43) for the minimum condition (Uotila, unpublished lecture notes, 1967), the expanded form of the normal equations becomes

$$\begin{bmatrix} -P_x & 0 & A' \\ 0 & -P & B' \\ A & B & 0 \end{bmatrix} \begin{bmatrix} X \\ V \\ K \end{bmatrix} + \begin{bmatrix} 0 \\ 0 \\ W \end{bmatrix} = 0 \tag{8.44}$$

By a row and column transformation, the residual vector V is eliminated and the normal equations become

$$\begin{bmatrix} BP^{-1}B' & A \\ A' & -P_x \end{bmatrix} \begin{bmatrix} K \\ X \end{bmatrix} + \begin{bmatrix} W \\ 0 \end{bmatrix} = 0 \tag{8.45}$$

Next, the correlates are eliminated, resulting in

$$[A'(BP^{-1}B')^{-1}A + P_x]X + A'(BP^{-1}B')^{-1}W = 0 \tag{8.46}$$

The following summation form of the nonzero 3×3 submatrices of the above equation is found by replacing the A, B, and P matrices with their expanded forms in terms of 3×3 submatrices (eqs. (8.24), (8.28), and (8.34)):

$$\left[\begin{array}{c|c} \sum_i (B_{ij}P_{ij}^{-1}B_{ij}')^{-1} + P_j & -(B_{ij}P_{ij}^{-1}B_{ij}')^{-1} \\ \hline -(B_{ij}P_{ij}^{-1}B_{ij}')^{-1} & \sum_j (B_{ij}P_{ij}^{-1}B_{ij}')^{-1} + P_i \end{array}\right] \left[\begin{array}{c} X_j \\ \hline X_i \end{array}\right] + \left[\begin{array}{l} U_j = \sum_i (B_{ij}P_{ij}^{-1}B_{ij}')^{-1} W_{ij} \\ \hline U_i = -\sum_j (B_{ij}P_{ij}^{-1}B_{ij}')^{-1} W_{ij} \end{array}\right] = 0 \tag{8.47}$$

where the nonzero 3×3 submatrices occur only on the diagonal and those ij 3×3 positions corresponding to a ground-to-satellite observation; $\sum_i$ indicates a summation over all ground stations observing satellite position j; $\sum_j$ indicates a summation over all satellite positions observed from ground station i. All summations contain only 3×3 and/or 3×1 matrices.

Elimination of X_j, the corrections to the satellite positions, from the above yields the following reduced normal equations

$$N X+U=0 \tag{8.48}$$

in which the X vector will now represent the unknown corrections to the preliminary rectangular coordinates of the ground stations only; U is the constant vector; and N is the coefficient matrix.

The coefficient matrix N is made up of 3×3 matrices. By letting

$$M_{ij}^{-1}=(B_{ij}P_{ij}^{-1}B_{ij}')^{-1} \tag{8.49}$$

$$=(B_{ij}^{-1})'P_{ij}B_{ij}^{-1} \tag{8.50}$$

in equation (8.47), the expression for the 3×3 diagonal matrix corresponding to the kth ground station is given by (Krakiwsky and Pope, 1967)

$$N_{kk}=\sum_j M_{kj}^{-1}-\sum_j\left\{M_{kj}^{-1}\left(\sum_i M_{ij}^{-1}\right)^{-1}M_{kj}^{-1}\right\}+P_k \tag{8.51}$$

Note the weight, P_j, for the jth satellite position has been dropped in the second term of the above equation. The expression for the off-diagonal 3×3 matrix corresponding to the kth and the lth ground station is

$$N_{kl}=-\sum_j\left\{M_{kj}^{-1}\left(\sum_i M_{ij}^{-1}\right)^{-1}M_{lj}^{-1}\right\} \tag{8.52}$$

where the summation $\sum_j$ is performed over all satellite events observed simultaneously from both ground stations k and l.

The constant vector of the normal equations (eq. (8.48)) is made up of 3×1 vectors corresponding to each ground station. The vector U_k for the kth ground station is given by

$$U_k=-\left(\sum_j M_{kj}^{-1}W_{kj}\right)+\sum_j\left\{M_{kj}^{-1}\left(\sum_i M_{ij}^{-1}\right)^{-1}\left(\sum_i M_{ij}^{-1}W_{ij}\right)\right\} \tag{8.53}$$

where, according to equation (8.30),

$$W_{ij}=\mathbf{X}_j^o-\mathbf{X}_i^o-\mathbf{X}_{ij}^b \tag{8.54}$$

and

$$W_{kj}=\mathbf{X}_j^o-\mathbf{X}_k^o-\mathbf{X}_{kj}^b \tag{8.55}$$

At first sight it seems that the preliminary coordinates of each satellite position are required; however, substitution of equations (8.54) and (8.55) into equation (8.53) results in the cancellation or dropping out of terms containing x_j^o and the observed vector X_{ij}^b or X_{kj}^b. Specifically,

$$U_k=-\sum_j\left\{M_{kj}^{-1}\left(\mathbf{X}_j^o-\mathbf{X}_k^o-\mathbf{X}_{kj}^b\right)\right\}+\sum_j\left\{M_{kj}^{-1}\left(\sum_i M_{ij}^{-1}\right)^{-1}\left[\sum_i M_{ij}^{-1}\left(\mathbf{X}_j^o-\mathbf{X}_i^o-\mathbf{X}_{ij}^b\right)\right]\right\} \tag{8.56}$$

$$=-\sum_j\left\{M_{kj}^{-1}\mathbf{X}_j^o\right\}+\left(\sum_j M_{kj}^{-1}\right)\mathbf{X}_k^o+\sum_j\left\{M_{kj}^{-1}\mathbf{X}_{kj}^b\right\}+\sum_j\left\{M_{kj}^{-1}\left(\sum_i M_{ij}^{-1}\right)^{-1}\left(\sum_i M_{ij}^{-1}\mathbf{X}_j^o\right)\right\}-\sum_j\left\{M_{kj}^{-1}\left(\sum_i M_{ij}^{-1}\right)^{-1}\left(\sum_i M_{ij}^{-1}\mathbf{X}_i^o\right)\right\}-\sum_j\left\{M_{kj}^{-1}\left(\sum_i M_{ij}^{-1}\right)^{-1}\left(\sum_i M_{ij}^{-1}\mathbf{X}_{ij}^b\right)\right\} \tag{8.57}$$

Terms 1 and 4 in the above expression cancel (i.e., $\mathbf{X}_j^o$ satellite coordinates drop out) be-

cause $\mathbf{X}_j^o$ can be factored out of $\sum_i$ in term 4, i.e.,

$$\sum_j \left\{ M_{kj}^{-1} \left(\sum_i M_{ij}^{-1} \right)^{-1} \left(\sum_i M_{ij}^{-1} \right) \mathbf{X}_j^o \right\} = \left(\sum_j M_{kj}^{-1} \mathbf{X}_j^o \right) \tag{8.58}$$

which has an opposite sign to that of term 1. Terms 3 and 6 drop out because they are identically zero. This happens because both terms contain products like

$$B_{ij}^{-1}\mathbf{X}_{ij}^b \text{ or } B_{kj}^{-1}\mathbf{X}_{kj}^b$$

where (taking into consideration the orthogonality property of the rotation matrices and S)

$$B_{ij}^{-1} = \begin{bmatrix} 1 & 0 & 0 \\ 0 & -1/\cos\delta_{ij} & 0 \\ 0 & 0 & -1 \end{bmatrix} R_2(90^\circ - \delta_{ij})\, R_3(\alpha_{ij})\, S'$$

and after elementary matrix operations we have

$$B_{ij}^{-1}\mathbf{X}_{ij}^b = \begin{bmatrix} 0 \\ 0 \\ -1 \end{bmatrix} r_{ij}^b$$

Since in the optical adjustment, P_{ij} has the form

$$P_{ij} = \begin{bmatrix} \begin{bmatrix} * & * \\ * & * \end{bmatrix}^{-1} & \begin{matrix} 0 \\ 0 \end{matrix} \\ \begin{matrix} 0 & 0 \end{matrix} & 0 \end{bmatrix}$$

and from equation (8.50)

$$M_{ij}^{-1}\mathbf{X}_{ij}^b = 0 \tag{8.59}$$

the final expression for the constant column becomes

$$U_k = \sum M_{kj}^{-1} \left\{ \mathbf{X}_k^o - \left(\sum_i M_{ij}^{-1} \right)^{-1} \left(\sum_i M_{ij}^{-1} \mathbf{X}_i^o \right) \right\} \tag{8.60}$$

In summary, the normal equations in the adjustment of camera observations are formed by equations (8.51), (8.54), and (8.60).

8.4.2.2 Correlated Events
(OSU Report 193)

8.4.2.2.1 THE MATHEMATICAL MODEL

The theory and the mathematical model for a generalized least-squares adjustment for simultaneous directions without correlation has been described (sec. 8.4.2.1). In that case each simultaneously observed satellite image was taken as an independent event; thus the correlation between satellite directions on the same plate was not considered. The following is a description of how the mathematical model is manipulated to take care of possible correlations between directions, such as occur in the case of the NGS (National Geodetic Survey) BC–4 Type II data, where each given event consists of seven fictitious directions (Greenwich hour angle h and declination δ relative to the 1900–1905 CIO mean pole) per station and the full 14×14 variance-covariance matrix associated with the set.

The basic geometric figure to begin the mathematical development is that of a single ground station observing one satellite position, shown in figure 8.13. Using vector notation, as we know, we can write the mathematical model as

$$F_{ij_m} = \mathbf{X}_{j_m} - \mathbf{X}_i - \mathbf{X}_{ij_m} = 0 \tag{8.61}$$

where now m will identify a fictitious satellite image within the event j, *i.e.*, $m = 1,2 \ldots m_x$ (generally $4 \leq m_x \leq 7$).

The vector $\mathbf{X}_{ij_m}$ with this type of data takes the form

$$\mathbf{X}_{ij_m} = \begin{bmatrix} r_{ij_m} & \cos\delta_{ij_m} & \cos h_{ij_m} \\ -r_{ij_m} & \cos\delta_{ij_m} & \sin h_{ij_m} \\ r_{ij_m} & \sin\delta_{ij_m} & \end{bmatrix} \tag{8.62}$$

The linearized mathematical model can be written as follows

$$[A_1 \mid A_2] \begin{bmatrix} X_j \\ \hline X_i \end{bmatrix} + BV + W = 0 \tag{8.63}$$

Since all observations from one station to all fictitious satellite directions on a given plate are correlated, it is necessary to build up the model using all these satellite directions. Thus the design matrix A is divided in submatrices of the form

$$A_{ij_m} = \frac{\partial F_{ij_m}}{\partial \mathbf{X}_{j_m},\ \mathbf{X}_i} = \left[\begin{array}{c|c} A_{1_{ij}} & A_{2_{ij}} \\ {\scriptstyle m} & {\scriptstyle m} \end{array}\right] = \left[\begin{array}{c|c} & -I_3 \\ & -I_3 \\ I_{3m_x} & \cdot \\ & \cdot \\ & -I_3 \end{array}\right] \qquad (8.64)$$

$3m_x \quad 3m_x \quad 3m_x \quad 3$

and the design matrix B is of the form

$$B_{ij_m} \underset{(3m_x \times 3m_x)}{=} \left[\begin{array}{ccccc} \boxed{3\times 3} & & & & \\ & \boxed{3\times 3} & & & 0 \\ & & \boxed{3\times 3} & & \\ & & & \ddots & \\ 0 & & & & \boxed{3\times 3} \end{array}\right] \qquad (8.65)$$

After minimizing $V'PV$ under the condition (8.63), the vector of Lagrange multipliers can be expressed as

$$K = -(BP^{-1}B')^{-1}(A_1X_j + A_2X_i + W) \qquad (8.66)$$

and the normal equations will take the form

$$\left[\begin{array}{cc} A_1'(BP^{-1}B')^{-1}A_1 & A_1'(BP^{-1}B')^{-1}A_2 \\ A_2'(BP^{-1}B')^{-1}A_1 & A_2'(BP^{-1}B')^{-1}A_2 \end{array}\right]\left[\begin{array}{c} X_j \\ X_i \end{array}\right] + \left[\begin{array}{c} A_1'(BP^{-1}B')^{-1}W \\ A_2'(BP^{-1}B')^{-1}W \end{array}\right] = 0 \qquad (8.67)$$

8.4.2.2.2 THE WEIGHTING TECHNIQUE USING THE FULL VARIANCE-COVARIANCE MATRIX OF THE OBSERVED QUANTITIES

Before proceeding further, it is necessary to explain how the above equations (8.66) are actually solved. For a particular station i and event j, the B matrix has dimensions (21×21), but the original given P^{-1} matrix is (14×14). The P^{-1} matrix refers only to the actual observed quantities, which are the Greenwich hour angle h and the declinations δ, and therefore it has to be modified before it is substituted in equation (8.66). The easiest way to explain this is to look only at that part of B_{ij} that corresponds to observations on the first satellite position only:

$$B_{ij_1} \equiv B_1 = \left[\begin{array}{ccc} \frac{\partial F_1}{\partial h_1} & \frac{\partial F_1}{\partial \delta_1} & \frac{\partial F_1}{\partial r_1} \\ \frac{\partial F_2}{\partial h_1} & \frac{\partial F_2}{\partial \delta_1} & \frac{\partial F_2}{\partial r_1} \\ \frac{\partial F_3}{\partial h_1} & \frac{\partial F_3}{\partial \delta_1} & \frac{\partial F_3}{\partial r_1} \end{array}\right]_{i,j_1} \qquad (8.68)$$

The matrix P_1 (not P_1^{-1}) would have to be of the form

$$P_{ij_1} \equiv P_1 = \left[\begin{array}{ccc} \sigma^2_{h_1} & \sigma_{h_1\delta_1} & \sigma_{h_1 r_1} \\ \sigma_{h_1\delta_1} & \sigma^2_{\delta_1} & \sigma_{\delta_1 r_1} \\ \sigma_{h_1 r_1} & \sigma_{\delta_1 r_1} & \sigma^2_{r_1} \end{array}\right]^{-1}_{i,j_1} \qquad (8.69)$$

and for a single satellite image using equation (8.34) we can write

$$P_1 = \left[\begin{array}{ccc} \left[\begin{array}{cc} \sigma^2_{h_1} & \sigma_{h_1\delta_1} \\ \sigma_{h_1\delta_1} & \sigma^2_{\delta_1} \end{array}\right]^{-1} & \begin{array}{c} 0 \\ 0 \end{array} \\ \begin{array}{cc} 0 & 0 \end{array} & 0 \end{array}\right]_{i,j_1} \qquad (8.70)$$

What is really needed is $(B_1P_1^{-1}B_1')^{-1}$, but $B_1P_1^{-1}B_1'$ is singular. However, the matrix B_1 is square and nonsingular. Knowing this, we can rearrange $(B_1P_1^{-1}B_1')^{-1}$ as follows:

$$(B_1P_1^{-1}B_1')^{-1} = (B_1')^{-1}P_1B_1^{-1} = (B_1^{-1})'P_1B_1^{-1} \qquad (8.71)$$

where P_1 is defined by equation (8.70).

The preceding description applies to the case of one satellite position j_1. For the seven satellite positions the dimension of the p^{-1} matrix is (14×14). The matrix P_1 in equation (8.71) must have the dimension (21×21) and be of the form of equation (8.70). The matrix P_{ij} for the BC–4 observations can be written as follows:

$$P_{ij}_{(14\times14)} = \begin{bmatrix} \sigma^2 h_1 & \sigma h_1\delta_1 & \cdots & \cdot & \sigma h_1\delta_7 \\ \cdot & \sigma^2\delta_1 & \cdot & & \cdot \\ \cdot & & \cdot & & \cdot \\ \cdot & & & \sigma^2 h_7 & \cdot \\ \sigma h_1\delta_7 & & \cdots & & \sigma^2\delta_7 \end{bmatrix}^{-1}_{i,j} = \begin{bmatrix} W_{1,1} & W_{1,2} & \cdots & W_{1,14} \\ \cdot & & & \cdot \\ \cdot & & & \cdot \\ \cdot & & & \cdot \\ W_{14,1} & & \cdots & W_{14,14} \end{bmatrix}_{i,j} \quad (8.72)$$

Now the (21×21) version of equation (8.70) will be equation (8.73) given below. With P defined, considering equation (8.73), we can form the matrix M^{-1} using the technique shown in equation (8.71):

$$M^{-1} = (B\,P^{-1}B')^{-1} = (B^{-1})'P\,B^{-1} \quad (8.74)$$

8.4.2.2.3 THE REDUCED NORMAL EQUATIONS

Equation (8.67) can be referred to as the conventional normal equation, where the satellite position X_j is among the parameters. Since the satellite position is of no interest, it is eliminated from the solution by solving for X_j in terms of the other parameters and substituting this into the remaining equations. After elimination of X_j from equation (8.67), we will obtain the reduced normal equations. The (3×3) and (3×1) block elements of the coefficient matrix and constant vector, respectively, can be obtained by expressions similar to equations (8.51), (8.52), and (8.53). The only difference is that now the term P_k in equation (8.51) will drop out because we are only minimizing $V'PV$ (Mueller *et al.*, 1973a).

8.4.3 The Range Adjustment
(OSU Reports 86, 140)

8.4.3.1 The Mathematical Model

Figure 8.15 shows the average terrestrial coordinate system uvw (sec. 8.4.1.2) with a ground station i and a satellite position j. The observed quantity is the topocentric range r_{ij} from ground station i to satellite position j. The parameters u_i, v_i, w_i and u_j, v_j, w_j are the Cartesian coordinates of the ground station i and the satellite position j, respectively.

From figure 8.15 it can easily be seen that the mathematical model can be written as

$$r_{ij} = [(u_j-u_i)^2 + (v_j-v_i)^2 + (w_j-w_i)^2]^{1/2} \quad (8.75)$$

$$F_{ij} = [(u_j-u_i)^2 + (v_j-v_i)^2 + (w_j-w_i)^2]^{1/2} - r_{ij} = 0 \quad (8.76)$$

The basic mathematical model above is extended to include simultaneous ranges from three or more ground stations. When increasing the number of simultaneous events

$$P_{ij}_{(21\times21)} = \begin{bmatrix} W_{1,1} & W_{1,2} & 0 & W_{1,3} & W_{1,4} & 0 & \cdots & W_{1,13} & W_{1,14} & 0 \\ W_{2,1} & W_{2,2} & 0 & W_{2,3} & W_{2,4} & 0 & \cdots & W_{2,13} & W_{2,14} & 0 \\ 0 & 0 & 0 & 0 & 0 & 0 & \cdots & 0 & 0 & 0 \\ \cdot & \cdot & \cdot & \cdot & \cdot & \cdot & & \cdot & \cdot & \cdot \\ \cdot & \cdot & \cdot & \cdot & \cdot & \cdot & & \cdot & \cdot & \cdot \\ \cdot & \cdot & \cdot & \cdot & \cdot & \cdot & & \cdot & \cdot & 0 \\ W_{13,1} & W_{13,2} & 0 & W_{13,3} & W_{13,4} & 0 & \cdots & W_{13,13} & W_{13,14} & 0 \\ W_{14,1} & W_{14,2} & 0 & W_{14,3} & W_{14,4} & 0 & \cdots & W_{14,13} & W_{14,14} & 0 \\ 0 & 0 & 0 & 0 & 0 & 0 & \cdots & 0 & 0 & 0 \end{bmatrix}_{i,j} \quad (8.73)$$

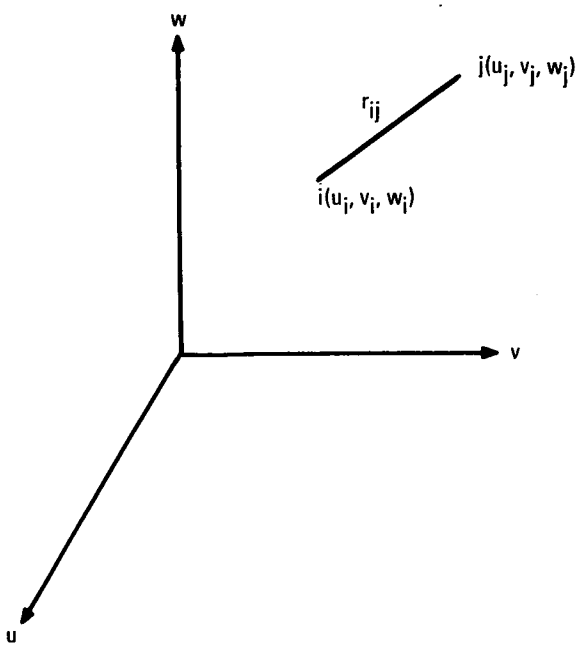

FIGURE 8.15.—The *uvw* coordinate system.

along with the number of known and unknown ground stations, an adjustment is necessary.

The mathematical model (8.76) is linearized by a Taylor series expansion about the preliminary values of the ground stations and satellite positions and the observed value of the topocentric range. The expression for the linearized mathematical model, as in the optical case, has the form

$$AX+BV+W=0 \tag{8.77}$$

where now the design matrix B is a negative unit matrix and the design matrix A is formed by submatrices of the form in the inset below.

The unknown vector **X** is made up of subvectors

$$X_{ij}=\begin{bmatrix} X_j \\ X_i \end{bmatrix} \tag{8.79}$$

where

$$X_i=\begin{bmatrix} du_i \\ dv_i \\ dw_i \end{bmatrix} \tag{8.80}$$

$$X_j=\begin{bmatrix} du_j \\ dv_j \\ dw_j \end{bmatrix} \tag{8.81}$$

The misclosure vector W is formed by the individual differences

$$W_{ij}=r^0_{ij}\,(\text{computed})-r^b_{ij}\,(\text{observed}) \tag{8.82}$$

The residual vector V is composed of the individual residuals V_{ij} (in meters) corresponding to the observed ranges r^b_{ij}.

Giving consideration to the characteristic of the design matrices, we can write the final equation for the linearized model in the range adjustment as

$$AX-V+W=0 \tag{8.83}$$

8.4.3.2 Weighting of Observed Ranges

The weighting of the observed topocentric range from ground station i to satellite position j is achieved by the following:

$$p_{ij}=\frac{\sigma_0^2}{\sigma_{ij}^2} \tag{8.84}$$

where σ_0^2 is the variance of unit weight and σ_{ij}^2 is the variance of the observed range in meters squared. P will denote the diagonal weight matrix containing all the independent weights P_{ij} to be used in the adjustment.

8.4.3.3 The Normal Equations

The variation function for the range adjustment is similar to the function for adjust-

$$A_{ij}=\frac{\partial F_{ij}}{\partial \mathbf{X}^0_j,\ \partial \mathbf{X}^0_i}=\left[\frac{u^0_j-u^0_i}{r^0_{ij}},\frac{v^0_j-v^0_i}{r^0_{ij}},\frac{w^0_j-w^0_i}{r^0_{ij}}\,\middle|\,-\frac{u^0_j-u^0_i}{r^0_{ij}},\frac{v^0_j-v^0_i}{r^0_{ij}},\frac{w^0_j-w^0_i}{r^0_{ij}}\right]=[a_{ij}\,|\,-a_{ij}] \tag{8.78}$$

where r^0_{ij} is computed from (8.75) using the initial approximate values for the stations and satellite coordinates, the latest coordinates resulting from a preliminary least-squares adjustment (for each event j) with the co-observing stations held fixed.

ment of camera observations, namely,

$$\Phi = V'PV + X'P_xX - 2K'(AX - V + W) \tag{8.85}$$

where

- V is the vector of residuals corresponding to the range observations
- X is the vector of corrections to the preliminary ground and satellite positions [3]
- P is the weight matrix for the ranges
- P_x is the weight matrix for the ground and satellite positions
- K is the vector of correlates

The differentiation of equation (8.85) for the minimum condition results in the following expanded form of the normal equations:

$$\begin{bmatrix} -P_x & 0 & A' \\ 0 & -P & -I \\ A & -I & 0 \end{bmatrix} \begin{bmatrix} X \\ V \\ K \end{bmatrix} + \begin{bmatrix} 0 \\ 0 \\ W \end{bmatrix} = 0 \tag{8.86}$$

After the elimination of the correlates and residuals and the expansion of the A and P matrices, the following expression results:

$$\left[\begin{array}{c|c} \sum_i a'_{ij}p_{ij}a_{ij} + p_j & -a'_{ij}p_{ij}a_{ij} \\ \hline -a'_{ij}p_{ij}a_{ij} & \sum_j a'_{ij}p_{ij}a_{ij} + P_j \end{array}\right] \left[\begin{array}{c} X_j \\ \hline X_i \end{array}\right] + \left[\begin{array}{c} U_j = \sum_i a'_{ij}p_{ij}W_{ij} \\ \hline U_i = -\sum_j a'_{ij}p_{ij}W_{ij} \end{array}\right] = 0 \tag{8.87}$$

Elimination of the corrections to the preliminary coordinates of the satellite position, namely X_j, from equation (8.87) results in the following three expressions: The 3×3 diagonal matrix corresponding to the kth ground station is given by

$$N_{kk} = \left(\sum_j a'_{kj}p_{kj}a_{kj}\right) - \sum_j \left\{ a'_{kj}p_{kj}a_{kj} \left(\sum_i a'_{ij}p_{ij}a_{ij}\right)^{-1} \times a'_{kj}p_{kj}a_{kj} \right\} + P_k \tag{8.88}$$

The 3×3 off-diagonal matrix corresponding to the kth and the lth ground stations is given by

$$N_{kl} = -\sum_j \left\{ a'_{kj}p_{kj}a_{kj} \left(\sum_i a'_{ij}p_{ij}a_{ij}\right)^{-1} a'_{lj}p_{lj}a_{lj} \right\} \tag{8.89}$$

where the main summation $\sum_j$ is performed over all satellite positions observed simultaneously from both ground stations k and l; the constant vector of the kth ground station is

$$U_k = -\left(\sum_j a'_{kj}p_{kj}W_{kj}\right) + \sum_j \left\{ a'_{kj}p_{kj}a_{kj} \left(\sum_i a'_{ij}p_{ij}a_{ij}\right)^{-1} \sum_i a'_{ij}p_{ij}W_{ij} \right\} \tag{8.90}$$

In the above expressions, the weight matrix P_j of each satellite position was set equal to zero as there is no independent external source from which to get a priori variance estimates which could be used to derive weights.

The equivalent expression for the constant column U_k can be shown to have the following form:

$$U_k = -\sum_j a'_{kj}p_{kj}\bar{v}_{kj} \tag{8.91}$$

where $\bar{v}_{kj}$ is the residual of the particular observed range r_{kj} arising from a least-squares adjustment of one simultaneous event with ground stations held fixed.

The quantities a_{kj} and $\bar{v}_{kj}$ needed in the formation of the reduced normal equations (eqs. (8.88), (8.89), and (8.91)) are a side product of the preliminary adjustment of each simultaneous event. Specifically, a_{kj} is contained in the A matrix given by equation (8.3) and $\bar{v}_{kj}$ is an element of the $\bar{V}$ vector of equation (8.5).

[3] As in the case of the optical adjustment, satellite positions will be considered "nuisance" parameters and therefore eliminated from the solution.

8.4.4 Addition of Normal Equations

Independent sets of normal equations formed from two or more batches of camera and/or range data can be added together. The basic idea of the combination of the normal equations is simply the algebraic addition of their corresponding terms. Letting n sets of normal equations be represented by

$$\begin{aligned} N_1X+U_1&=0\\ N_2X+U_2&=0\\ &\cdot\\ &\cdot\\ &\cdot\\ N_nX+U_n&=0 \end{aligned} \qquad (8.92)$$

and their corresponding variances of unit weight as $\sigma^2_{0_1}, \sigma^2_{0_2}, \ldots, \sigma^2_{0_n}$, we can show the addition is

$$(N_1+p_{12}N_2+\ldots+p_{1n}N_n)X+(U_1+p_{12}U_2+\ldots p_{1n}U_n)=0 \qquad (8.93)$$

In the above, the weights may be obtained as follows:

$$\begin{aligned} p_{12}&=\frac{\sigma^2_{0_1}}{\sigma^2_{0_2}}\\ &\cdot\\ &\cdot\\ &\cdot\\ p_{1n}&=\frac{\sigma^2_{0_1}}{\sigma^2_{0_n}} \end{aligned} \qquad (8.94)$$

where $\sigma^2_{0_1}, \sigma^2_{0_2}, \ldots, \sigma^2_{0_n}$ must have the same a priori variance of unit weight (see secs. 8.4.2.1.2 and 8.4.3.2).

The advantage of the above is obvious, namely batches of observed data may be adjusted separately or as a part of a combined adjustment. The same holds for the addition of two or more independent sets of range normal equations and for the addition of camera and range normal equations to each other.

The weighting of the two or more different sets of normal equations (e.g., N_{11}, U_{11}, and N_{22}, U_{22}) is a function of the goodness of the observations involved and the geometry existing between the unknown parameters and the respective observables. The first item is taken care of by proper weighting as a function of the estimated variance-covariance matrix of the observations, and this weighting is reflected in the quantities N_{11}, N_{22}, U_{11}, and U_{22}. The geometry aspect is implicit in the coefficient matrices A and B which enter into N_{11}, and so forth.

8.4.5 Contributions of Constraints to the Normal Equations

(OSU Reports 86, 140, 148)

8.4.5.1 General

Since the coefficient matrix of normal equations is singular, a unique least-squares solution is not possible. A minimal set of constraints to the normal equations provides a unique solution (Blaha, 1971).

Two alternative definitions exist for the term "constraints": the absolute constraints represent certain conditions which have to be fulfilled exactly and with no uncertainties. The relative constraints (or weighted constraints) have the same characteristics as the observations.

In general, the contribution of the functional constraint equation

$$G(X,L_C)=0$$

to the reduced normal equations $\bar{N}\bar{X}+\bar{U}=0$ can be found by bordering the normal equation matrix [4]

$$\begin{bmatrix} \bar{N} & C' \\ C & -P_C^{-1} \end{bmatrix} \begin{bmatrix} X \\ -K_C \end{bmatrix} + \begin{bmatrix} \bar{U} \\ W^c \end{bmatrix} = 0$$

where

$$C=\frac{\partial G}{\partial \mathbf{X}^0_i}$$

After elimination of K_C, where

[4] The quantities $\bar{N}$ and $\bar{U}$ represent the original reduced normal equations (without constraints).

$$K_C = -P_C(CX + W^c) \qquad (8.95a)$$

it is easy to find

$$[\bar{N} + C'P_CC]X + \bar{U} + C'P_CW^c = 0$$
$$[\bar{N} + N^c]X + U + U^c = 0 \qquad (8.95b)$$

where N^c and U^c are the contributions to the coefficient matrix and constant vector of the normal equation due to the application of constraints.

After the constraints are added, the normal equations will take the usual form

$$NX + U = 0$$

and we are in the position to obtain the contribution from a new set of constraints.

Constraints can be applied between two stations k and l or to a single station. The contribution of these constraints to the matrix $\bar{N}$ (3×3 blocks) and $\bar{U}$ (3×1 blocks) can be schematically expressed in two different ways as shown on page 671.

These blocks obtained as indicated for the corresponding case will be the only ones computed and added to the original normal equations as expressed by formula (8.95b).

8.4.5.2 Relative Position Constraints

Relative position constraints are used in order to combine the normal equations obtained from various satellite nets and to constrain "double" stations or closely situated stations of the same net. The expression for the combination of normals can be written as follows:

$$[\bar{N} + N^R]X + \bar{U} + U^R = 0$$

where N^R and U^R, computed from (8.96a) and (8.96b), are the contribution to the original combined normal equations ($\bar{N}X + \bar{U} = 0$).

If the relative position (Δu^o, Δv^o, Δw^o) of two stations is known, along with the standard deviation of these relative positions, the constraints can be formed. In this case the functional constraint equations are

$$u_k^o - u_l^o = \Delta u^o$$
$$v_k^o - v_l^o = \Delta v^o$$
$$w_k^o - w_l^o = \Delta w^o$$

Therefore

$$\underset{3\times3}{C_k^R} = I \qquad \underset{3\times3}{C_l^R} = -I$$
$$\underset{3\times1}{U_k^R} = 0 \qquad \underset{3\times1}{U_l^R} = 0$$

because $W^R = G^R(X^o, L_C^o) = 0$. Also,

$$P_R = \sigma_0^2 \begin{bmatrix} \frac{1}{\sigma^2_{\Delta u^o}} & 0 & 0 \\ 0 & \frac{1}{\sigma^2_{\Delta v^o}} & 0 \\ 0 & 0 & \frac{1}{\sigma^2_{\Delta w^o}} \end{bmatrix}$$

where $\sigma_0^2 \equiv$ a priori variance of unit weigh and

$$\underset{3\times3}{N_{kk}^R} = IP_RI = \underset{3\times3}{P_R}$$
$$\underset{3\times3}{N_{ll}^R} = IP_RI = \underset{3\times3}{P_R}$$
$$\underset{3\times3}{N_{kl}^R} = \underset{3\times3}{N_{lk}^R} = IP_R(-I) = \underset{3\times3}{-P_R}$$

Thus, the diagonal elements of P_R are added to each element of the diagonal of the blocks kk and ll of the coefficient matrix of the combined normals $\bar{N}$ and subtracted from the diagonal elements of the blocks kl and lk of $\bar{N}$. There is no contribution to the vector $\bar{U}$.

8.4.5.3 Length (Chord) Constraints

Chord constraints are introduced when scalar information is available between ground stations (e.g., distances determined through high-precision geodimeter traversing). The functional constraint equation in this case is

$$G^C(X, L_C) = 0$$

or

(1) Contribution to the normals due to the constraint applied to station k:

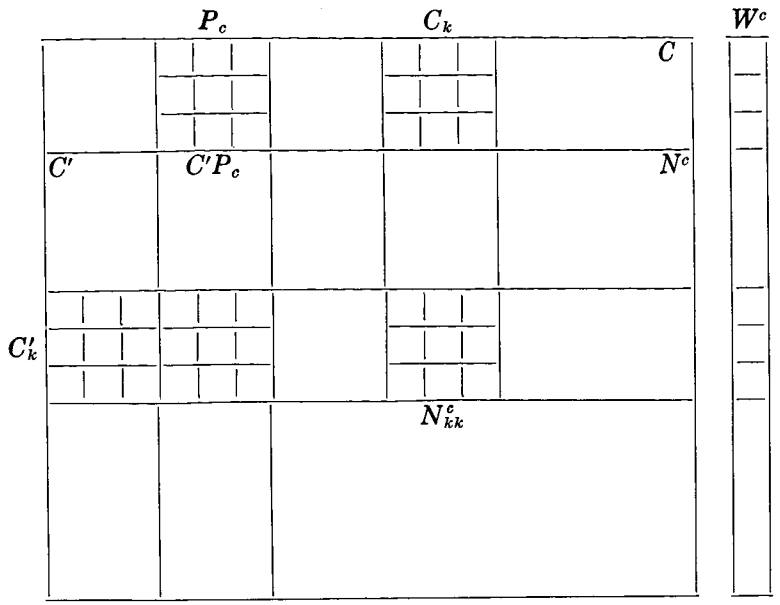

$$N_{kk}^c = C_k' P_c C_k$$
$$U_k^c = C_k' P_c W^c$$

(8.96a)

(2) Contribution to the normals due to the constraint between stations k and l:

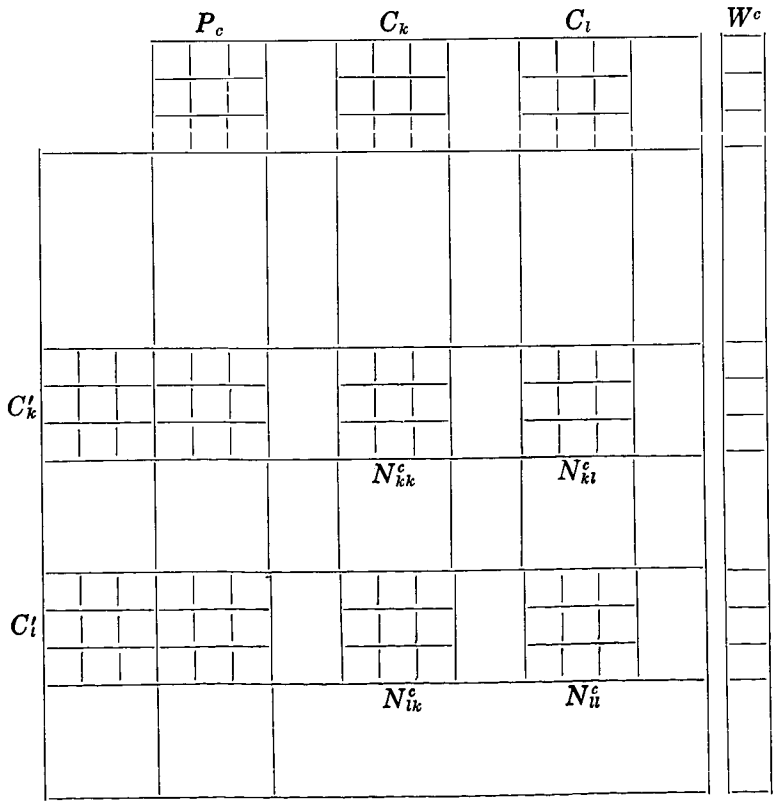

$$N_{kk}^c = C_k' P_c C_k; \quad N_{kl}^c = C_k' P_c C_l$$
$$N_{ll}^c = C_l' P_c C_l; \quad N_{lk}^c = C_l' P_c C_k$$
$$U_k^c = C_k' P_c W^c; \quad U_l^c = C_l' P_c W^c$$

(8.96b)

$$[(u_k-u_l)^2+(v_k-v_l)^2+(w_k-w_l)^2]^{1/2}=D_{kl} \tag{8.97}$$

Therefore

$$C_k^c=\left[\frac{u_k^o-u_l^o}{D_{kl}^o},\ \frac{v_k^o-v_l^o}{D_{kl}^o},\ \frac{w_k^o-w_l^o}{D_{kl}^o}\right]$$

$$C_l^c=\left[-\frac{u_k^o-u_l^o}{D_{kl}^o},-\frac{v_k^o-v_l^o}{D_{kl}^o},-\frac{w_k^o-w_l^o}{D_{kl}^o}\right]$$

$$P_C=\frac{\sigma_0^2}{\sigma_{kl}^2}=\frac{\text{a priori variance of unit weight}}{\text{variance of the chord}}$$

Then the contributions to the normals are obtained by applying equations (8.96a) and (8.96b).

$$\underset{3\times3}{N_{kk}^c}=(C_k^c)'P_CC_k^c$$

$$N_{ll}^c=(C_k^c)'P_CC_l^c$$

$$\underset{3\times3}{N_{kl}^c}=(C_l^c)'P_CC_l^c$$

$$\underset{3\times3}{U_k^c}=(C_k^c)'P_CW^c$$

$$\underset{3\times3}{U_l^c}=(C_l^c)'P_CW^c$$

The first three expressions in the above are added, respectively, to the blocks $\bar{N}_{kk}$, $\bar{N}_{ll}$ and $\bar{N}_{kl}$ of $\bar{N}$; the last two expressions are added, respectively, to the constant subvectors $\bar{U}_k$ and $\bar{U}_l$ of $\bar{U}$.

8.4.5.4 Station Position Constraint

Station position constraint is used for the purpose of defining the origin of the coordinate system. If the station coordinates (u_k^o,v_k^o,w_k^o) of station k are to be constrained and if the computed (known) variances of its approximate coordinates are $\sigma_{u_k^o}^2$, $\sigma_{v_k^o}^2$, $\sigma_{w_k^o}^2$, then the equations given in section 8.4.5.2 are valid by merely deleting the terms with index l; then $\Delta u^o=u_k^o$, $\Delta v^o=v_k^o$, $\Delta w^o=w_k^o$. Then

$$\underset{3\times3}{N_{kk}^s}=IP_SI=\underset{3\times3}{P_S}$$

where

$$P_S=\sigma_0^2\begin{bmatrix}\frac{1}{\sigma_{u_k^o}^2} & 0 & 0\\ 0 & \frac{1}{\sigma_{v_k^o}^2} & 0\\ 0 & 0 & \frac{1}{\sigma_{w_k^o}^2}\end{bmatrix}$$

8.4.5.5 Height Constraints

If the geodetic height of the station k is to be constrained, then

$$\underset{3\times3}{N_{kk}^h}=(C_k^h)'P_HC_k^h$$

where

$$C_k^h=[\cos\phi_k^o\cos\lambda_k^o,\ \cos\phi_k^o\sin\lambda_k^o,\ \sin\phi_k^o]$$

and

$$P_h=\frac{1}{\sigma_{h_k}^2}$$

where ϕ_k^o and λ_k^o are the approximate geodetic coordinates and $\sigma_{h_k}^2$ is the variance of the height for station k.

The constant vector U_k^h can be computed from

$$U_k^h=(C_k^h)'P_hW^h$$

where

$$W^h=h_k-h_k^o$$

8.4.5.6 Directional Constraints

Directional constraints are introduced when the orientation of the coordinate system is not defined through the observations (e.g., in the case of a ranging network).

The directional constraint between two stations k and l is accomplished by applying weights to two angles α^o and β^o defining the direction between them and computed from the approximate (u^o, v^o, w^o) coordinates of the two stations as follows:

$$\alpha^o=\tan^{-1}\frac{\Delta v^o}{\Delta u^o}$$

$$\beta^o=\tan^{-1}\frac{\Delta w^o}{R^o}$$

where

$$\Delta u^o = u_k^o - u_l^o$$

$$\Delta v^o = v_k^o - v_l^o$$

$$\Delta w^o = w_k^o - w_l^o$$

$$R^o = (\Delta u^{o2} + \Delta v^{o2})^{1/2}$$

The matrix C^D of partial derivatives is then formed

$$C_k^D = \begin{bmatrix} \frac{\partial \alpha^o}{\partial \Delta u^o}\frac{\partial \Delta u^o}{\partial u_k^o} & \frac{\partial \alpha^o}{\partial \Delta v^o}\frac{\partial \Delta v^o}{\partial v_k^o} & \frac{\partial \alpha^o}{\partial \Delta w^o}\frac{\partial \Delta w^o}{\partial w_k^o} \\ \frac{\partial \beta^o}{\partial \Delta u^o}\frac{\partial \Delta u^o}{\partial u_k^o} & \frac{\partial \beta^o}{\partial \Delta v^o}\frac{\partial \Delta v^o}{\partial v_k^o} & \frac{\partial \beta^o}{\partial \Delta w^o}\frac{\partial \Delta w^o}{\partial w_k^o} \end{bmatrix}$$

where

$$\frac{\partial \alpha^o}{\partial \Delta u^o} = \cos^2 \alpha^o \tan \alpha^o / \Delta u^o$$

$$\frac{\partial \alpha^o}{\partial \Delta v^o} = -\cos^2 \alpha^o / \Delta u^o$$

$$\frac{\partial \alpha^o}{\partial \Delta w^o} = 0$$

$$\frac{\partial \beta^o}{\partial \Delta u^o} = \Delta u^o \cos^2 \beta^o \tan^2 \beta^o / R^{o2}$$

$$\frac{\partial \beta^o}{\partial \Delta v^o} = \frac{\partial \beta^o}{\partial \Delta u^o} \tan \alpha^o$$

$$\frac{\partial \beta^o}{\partial \Delta w^o} = -\cos^2 \beta^o / R^o$$

and clearly $C_l^D = -C_k^D$. Then the matrix

$$N^D = (C^D)' P_D C^D \qquad (8.98)$$

is formed according to (8.96b), where P_D is the weight matrix estimated from the statistics of α^o and β^o in the customary way,

$$P_D = \sigma_0^2 \begin{bmatrix} \sigma_{\alpha^o}^2 & \sigma_{\alpha^o\beta^o} \\ \sigma_{\alpha^o\beta^o} & \sigma_{\beta^o}^2 \end{bmatrix}^{-1}$$

The matrix N^D is then added to the block elements of the reduced normal equations which correspond to each of the ground stations; i.e., its diagonal blocks will be added to $\bar{N}_{kk}$ and $\bar{N}_{ll}$ and subtracted from the off-diagonal elements $\bar{N}_{kl}$ and $\bar{N}_{lk}$.

8.4.5.7 Inner Constraints (Free Adjustment)

Even though the selection of a coordinate system is arbitrary in the case of a minimum constraint adjustment, e.g., in the case of ranging, the selection of the six coordinates (at more than two stations) to be constrained is very critical, since one set of constraints would give a different solution than another set. The "best" solution is arrived at in a coordinate system defined through the use of a set of constraint equations called "inner" constraints (Rinner *et al.*, 1967). In this sense, "best" means resulting in the smallest covariance matrix for the unknowns. Covariance matrices may be compared by means of their traces. The inner constraint equations are characterized by the property that the trace of the covariance matrix obtained with their use is a minimum among those obtained by adjusting a given set of observations augmented by a minimal set of constraint equations. This property also implies that the mean square uncertainty of the unknowns is smaller when the inner adjustment equations are used. The resulting adjustment is called a "free" adjustment. The functional inner constraints equations can be written as

$$C^I X = 0$$

where X is the set of corrections of the approximate coordinates of the unknown points and in the most general application when the "best" origin, orientation, and scale are sought.

$$C^I = \begin{bmatrix} C_1^I \\ C_2^I \\ C_3^I \end{bmatrix}$$

$$= \left[\begin{array}{ccc:ccc:c} & I & & & I & & \\ & 3\times 3 & & & 3\times 3 & & \cdots \\ \hline 0 & w_1^o & -v_1^o & 0 & w_2^o & -v_2^o & \\ -w_1^o & 0 & u_1^o & -w_2^o & 0 & u_2^o & \cdots \\ v_1^o & -u_1^o & 0 & v_2^o & -u_2^o & 0 & \\ \hline u_1^o & v_1^o & w_1^o & u_2^o & v_2^o & w_2^o & \cdots \end{array}\right]$$

The symbols (u_i^o, v_i^o, w_i^o) denote the approxi-

mate coordinates of the i^{th} unknown point where both the ground points and the satellite positions are considered.

It is also possible to design a set of constraints that will result in the "best" solution for only a subset of the points. In the adjustments reported here we were only interested in the ground station unknowns, implying that the trace of only that portion of the covariance matrix corresponding to the ground station unknowns should be minimized, while the variances of the satellite position unknowns should not be included in the minimum sum. The constraint equations that will produce such a solution have the same form as those producing the "best" solution for all the points. However, 3×3 blocks of zeros are inserted into those positions of C^I which correspond to unknowns whose variances are not to be included in the minimum sum.

The inner adjustment constraint equations can be given a geometrical interpretation that appeals to intuition. Let X_i^o denote the set of approxmate coordinates of the i^{th} unknown point, dX_i denote the corrections to these coordinates, and X_i^a denote the adjusted coordinates, i.e.,

$$X_i^a = X_i^o + dX_i$$

The first set of constraint equations, $C_1^I X = 0$, is then equivalent to the set of conditions

$$\sum_i dX_i = 0$$

The geometrical interpretation of these conditions is that the center of gravity of all the points will not change after adjustment, i.e.,

$$\sum_i X_i^a = \sum_i X_i^o$$

The second set of constraint equations, $C_2^I X = 0$, corresponds to the conditions

$$\sum_i X_i^o \times dX_i = 0$$

If the center of the system remains fixed, then the cross products $X_i^o \times dX_i$ reflect rotations of the points around the fixed center. These constraint equations ensure that the sums of the rotations around all three coordinate axes are zero. The corresponding geometrical interpretation is that the mean orientation of the system of points will not change after adjustment either.

Thus, the respective equations $C_1^I X = 0$ and $C_2^I X = 0$ effectively specify the origin and the orientation of the adjustment coordinate system. A third "inner adjustment" equation $C_3^I X = 0$ specifies the scale of the system. However, this scale equation is only used when the observations themselves do not determine the scale.

A more complete description of the inner adjustment is described in Blaha (1971).

In summary, if the normal equations with the contribution of all the constraints (except inner constraints) are represented by

$$[\bar{N} + N^R + N^C + N^S + N^H + N^D]X + \bar{U} + U^R + U^C + U^S + U^H + U^D = 0$$

or

$$NX + U = 0 \qquad (8.99)$$

then the inner adjustment can be obtained by bordering the coefficient matrix N of the normal equations as

$$\begin{bmatrix} N & (C^I)' \\ C^I & 0 \end{bmatrix}\begin{bmatrix} X \\ -K_I \end{bmatrix} = \begin{bmatrix} -U \\ 0 \end{bmatrix} \qquad (8.100)$$

Upon the addition of any kind of constraint to the normal equations, it becomes necessary to consider also its contribution to $\Sigma V'PV$. The degrees of freedom change as well. In order to compute the proper variance of unit weight, the latter must be taken into consideration.

8.4.6 Solution of Normal Equations and Formation of the Inverse Weight Matrix (OSU Report 86)

8.4.6.1 Introduction

The normal equations for the camera and range adjustments are given in the previous

section. The general form of the normal equations is

$$NX+U=0 \qquad (8.101)$$

where N is the coefficient matrix, X is the vector of unknowns, and U is the constant vector.

The adjusted values of the Cartesian coordinates of the observing ground stations are obtained by adding the corrections X to the preliminary values X^0, namely,

$$X^a=X^0+X \qquad (8.102)$$

Section 8.4.7 deals with obtaining the precision estimate of X^a through the inverse matrix N^{-1}. For this reason the method of formation of N^{-1} will be dealt with in section 8.4.6.4 along with the method of solving for X.

The procedure used to solve the normal equations is a Gauss reduction (sec. 8.4.6.2) and back solution (sec. 8.4.6.3) and computation of the inverse by the method established by Banachiewicz (sec. 8.4.6.4).

Two features which are peculiar to the specific procedure used here are: (1) the coefficient matrix N is broken down into 3×3 submatrices, and similarly the U vector is treated as being composed of 3×1 vectors; and (2) the coefficient matrix N is compacted so that 3×3 zero submatrices are neither stored nor used in the computation.

The first feature is achieved rather naturally; it occurs because of the form of the expressions given in sections 8.4.2–8.4.5, which are used to build up N and U. On the other hand, the second feature is achieved through programming logic. Specifically, a matrix L is used to tag each 3×3 nonzero submatrix of N with a row and column number. A second matrix F with a one-to-one correspondence to the first is then employed to tag the storage assigned to the particular 3×3 submatrix. The individual elements of the 3×3 submatrices are all stored in one large linear array E.

The reduced elements of N are stored in the locations previously created for elements in N. During reduction, additional 3×3 matrices arise in locations where there were none originally in N; thus "drag storage" must be assigned. In doing so, the guide matrix L and the storage tagging matrix F are updated to account for these additional matrices. Similar "drag storage" is also determined during the formation of the inverse N^{-1}.

Once the "drag storage" is determined, the reduction, back solution, and inverse determinations are guided by L, the storage located by F, and the elements to be used in the computation found in E.

8.4.6.2 Reduction

The coefficient matrix of the normal equations is written as

$$N=SR \qquad (8.103)$$

where S is a lower triangular matrix with 3×3 identity matrices along the diagonal, and R is an upper triangular matrix. All matrices and vectors discussed here are stipulated to be composed of 3×3 submatrices and 3×1 subvectors, respectively.

The reduction is accomplished by computing

$$S=I-T \qquad (8.104)$$

from

$$N=R-TR \qquad (8.105)$$

or

$$R=\mathrm{N}+TR \qquad (8.106)$$

where R and T (thus S) are built up simultaneously. The augmented matrix

$$[N,U]=\begin{bmatrix} n_{011} & n_{012} & n_{013} & \cdots & n_{01n} & u_{01} \\ n'_{012} & n_{022} & n_{023} & \cdots & n_{02n} & u_{02} \\ n'_{013} & n'_{023} & n_{033} & \cdots & n_{03n} & u_{03} \\ n'_{014} & & \cdot & & & u_{04} \\ \cdot & & & \cdot & & \cdot \\ \cdot & & & & \cdot & \cdot \\ \cdot & & & & & \cdot \\ n'_{01n} & & & & n_{0nn} & u_{0n} \end{bmatrix} \qquad (8.107)$$

is first reduced according to the algorithms

$$\begin{aligned} n_{k,i,j} &= n_{k-1,i,j} - n'_{k-1,k,i}\, n^{-1}_{k-1,k,k}\, n_{k-1,k,j} \\ k &= 1, 2, \ldots, n-1 \\ i &= k+1, k+2, \ldots, n \\ j &= i, i+1, \ldots, n \end{aligned} \tag{8.108}$$

defining

$$R = \begin{bmatrix} n_{011} & n_{012} & \cdots & \cdots & n_{01n} \\ & n_{122} & n_{123} & \cdots & n_{12n} \\ & & \cdot & & \cdot \\ \text{zeros} & & \cdot & & \cdot \\ \text{below} & & & \cdot & \cdot \\ \text{diagonal} & & & & n_{n-1,n,n} \end{bmatrix}$$

and

$$\begin{aligned} u_{k,i} &= u_{k-1,i} - n'_{k-1,k,i}\, n^{-1}_{k-1,k,k}\, u_{k-1,k} \\ k &= 1, 2, \ldots, n-1 \\ i &= k+1, \ldots, n \end{aligned}$$

defining

$$\bar{C} = \begin{bmatrix} u_{01} \\ u_{12} \\ u_{23} \\ \cdot \\ \cdot \\ \cdot \\ u_{n-1,n} \end{bmatrix} \tag{8.109}$$

A second algorithm, performed as part of equation (8.108), namely

$$\bar{n}_{k-1,k,j} = n^{-1}_{k-1,k,k}\, n_{k-1,k,j} \tag{8.110}$$

$$\bar{n}_{k-1,k,k} = I \tag{8.111}$$

$$\begin{aligned} \bar{u}_{k-1,k} &= n^{-1}_{k-1,k,k}\, u_{k-1,k} \qquad (8.112) \\ j &= k+1, k+2, \ldots, n \\ k &= 1, 2, \ldots, n-1 \end{aligned}$$

results in the following reduced matrices:

$$S' = \begin{bmatrix} I & \bar{n}_{012} & \bar{n}_{013} & \cdots & \bar{n}_{01n} \\ 0 & I & \bar{n}_{123} & & \bar{n}_{12n} \\ 0 & 0 & I & & \\ \cdot & \cdot & \cdot & \cdot & \\ \cdot & \cdot & \cdot & \cdot & \\ \cdot & \cdot & \cdot & & \cdot \\ 0 & 0 & 0 & 0 & I \end{bmatrix} \tag{8.113}$$

$$-\bar{D} = \begin{bmatrix} \bar{u}_{01} \\ \bar{u}_{12} \\ \bar{u}_{23} \\ \cdot \\ \cdot \\ \cdot \\ \bar{u}_{n-1,n} \end{bmatrix} \tag{8.114}$$

S' and $\bar{D}$ are used to obtain solution vector X (see sec. 8.4.6.3)

$$R^{-1} = \begin{bmatrix} n^{-1}_{011} & & & \text{elements} \\ & n^{-1}_{122} & & \text{above} \\ \text{zeros} & & n^{-1}_{233} & \text{diagonal} \\ \text{below} & & \cdots & \\ \text{diagonal} & & & n^{-1}_{n-1,n,n} \end{bmatrix} \tag{8.115}$$

which is used to obtain the inverse (see sec. 8.4.6.4).

8.4.6.3 Back Solution

The back solution involves the determination of the unknown vector X from elements of the reduced matrices S' and $\bar{D}$. Without derivation (Uotila, unpublished lecture notes, 1967), it can be shown that

$$X = T'X - \bar{D} \tag{8.116}$$

recalling

$$T = I - S'$$

or in summation form

$$X_i = \sum_{j=i+1}^{n} \bar{n}_{i-1,i,j}\, X_j + \bar{u}_{i-1,i} \tag{8.117}$$

8.4.6.4 Formation of Inverse

The inverse matrix N^{-1} will be computed by the method associated with the name of Banachiewicz (Uotila, unpublished lecture notes, 1967). According to equation (8.103), N^{-1} can be computed from

$$N^{-1} = R^{-1}\, S^{-1} \tag{8.118}$$

However, it turns out that N^{-1} can be formed without the aid of S^{-1}, and further only the diagonal elements of R^{-1} are needed.

The diagonal elements of R^{-1} are readily available, since the inverse of an upper triangular matrix has as its diagonal elements the reciprocal of the diagonal elements of the triangular matrix itself and the same result holds if "elements" is taken to mean 3×3. The diagonal elements of R^{-1} are computed by inverting the 3×3 diagonal matrices of R and for reasons of saving computer space are stored along the diagonal of S' (eq. (8.113)).

From equation (8.118)

$$\mathrm{R}^{-1}=N^{-1}S \tag{8.119}$$

Further, if substitution for S is made from equation (8.104),

$$R^{-1}=N^{-1}(I-T) \tag{8.120}$$
$$=N^{-1}-N^{-1}T \tag{8.121}$$

Finally,

$$N^{-1}=R^{-1}+N^{-1}T \tag{8.122}$$

The corresponding summation equation for computing any 3×3 matrix of N^{-1} is

$$n^{ij}=\sum_{k=i+1}^{n}\overline{n}_{i-1,i,k}\,n^{kj}+\delta_{ij}\,n^{-1}_{i-1,i,i} \tag{8.123}$$

where δ_{ij} is the Kronecker delta defined by

$$\delta_{ij}=\begin{cases}1 & i=j\\ 0 & i\neq j\end{cases} \tag{8.124}$$

and

$$n^{ij}=(n^{ji})' \tag{8.125}$$

8.4.7 Statistical Evaluation (Precision of Ground Stations After Adjustment)

(OSU Report 86)

8.4.7.1 Variance of Unit Weight

The variance of unit weight for the total adjustment is given by

$$\sigma_0^2=\frac{V'PV}{df} \tag{8.126}$$

where $V'PV$ is the sum of the squares of the weighted residuals of all observed quantities and df is the number of degrees of freedom in the least-squares adjustment.

8.4.7.1.1 ADJUSTMENT TO CAMERA OBSERVATIONS

Equation (8.126) will now be considered for the adjustment of camera observations. The linearized mathematical structure according to section 8.4.2 was shown to be of the form

$$AX+BV+W=0 \tag{8.127}$$

The general expression for the computation of $V'PV$ is

$$V_c'P_cV_c=-W'K-\sum^{c}(W^c)'\,K_c \tag{8.128}$$

where the first term is the contribution from equation (8.127) and the second term is the contribution from the c constraints applied. Without taking into consideration the contribution of the constraints

$$V'PV=-W'K \tag{8.129}$$

and by considering an expression for K and X from equations (8.45) and (8.46), respectively,

$$V'PV=W'(BP^{-1}B')^{-1}\,(AX+W) \tag{8.130}$$

$$X=-\{A'M^{-1}A+A+P_x\}^{-1}A'M^{-1}W \tag{8.131a}$$

Denoting

$$M=BP^{-1}B' \tag{8.131b}$$

we see that equation (8.130) with equations (8.47) and 8.131b) gives

$$V'PV = W'M^{-1}W - [U_j' U_i'] \begin{bmatrix} X_j \\ X_i \end{bmatrix} \tag{8.132}$$

Let the partitioning of equation (8.47) be denoted as

$$\begin{bmatrix} N_{11} & N_{12} \\ N_{21} & N_{22} \end{bmatrix} \begin{bmatrix} X_j \\ X_i \end{bmatrix} + \begin{bmatrix} U_j \\ U_i \end{bmatrix} = 0 \tag{8.133}$$

Then, by means of

$$\begin{bmatrix} N_{11} & N_{12} \\ N_{21} & N_{22} \end{bmatrix}^{-1} = \begin{bmatrix} Q_{11} & Q_{12} \\ Q_{21} & Q_{22} \end{bmatrix} = \begin{bmatrix} N_{11}^{-1} + N_{11}^{-1} N_{12} E\, N_{21} N_{11}^{-1} & -N_{11}^{-1} N_{12} E \\ -E\, N_{21} N_{11}^{-1} & E \end{bmatrix} \tag{8.134a}$$

where

$$E = (N_{22} - N_{21} N_{11}^{-1} N_{12})^{-1} \tag{8.134b}$$

equation (8.132) becomes

$$V'PV = W'M^{-1}W - [U_j' U_i'] \begin{bmatrix} Q_{11}U_j + Q_{12}U_i \\ Q_{21}U_j + Q_{22}U_i \end{bmatrix}$$

After substituting the values from equation (8.134a) and simplifying

$$V'PV = W'M^{-1}W - U_j' N_{11}^{-1} U_i + (U_i - N_{21} N_{11}^{-1} U_j)' E\, (U_i - N_{21} N_{11}^{-1} U_j) \tag{8.135}$$

but by elimination of X_j from equation (8.133) we get

$$X_i = -[N_{22} - N_{21} N_{11}^{-1} N_{12}]^{-1} [U_i - N_{21} N_{11}^{-1} U_j]$$

or, using the notation of equation (8.101), we have

$$X = -N^{-1} U$$

Thus we see that

$$E = N^{-1}$$

and

$$U = U_i - N_{21} N_{11}^{-1} U_j$$

and finally

$$V'PV = W'M^{-1}W - U_j' N_{11}^{-1} U_j + U'X \tag{8.136}$$

Denoting

$$Q = W'M^{-1}W - U_j' N_{11}^{-1} U_j \tag{8.137}$$

and considering equation (8.49), we find

$$Q = \sum_{ij} W_{ij}' M_{ij}^{-1} W_{ij} - \sum_j \left\{ \sum_i M_{ij}^{-1} W_{ij} \right\}' \left\{ \sum_i M_{ij}^{-1} \right\}^{-1} \left\{ \sum_i M_{ij}^{-1} W_{ij} \right\} \tag{8.138}$$

Now using equations (8.54) and (8.58) and factorization and cancellation analogous to that in equations (8.57) to (8.58), we get

$$Q = \sum_{ij} \mathbf{X}_i' M_{ij}^{-1} \mathbf{X}_i - \sum_j \left\{ \sum_i M_{ij}^{-1} \mathbf{X}_i \right\}' \left\{ \sum_i M_{ij}^{-1} \right\}^{-1} \left\{ \sum_i M_{ij}^{-1} \mathbf{X}_i \right\} \tag{8.139}$$

which is easily shown to be identically equal to

$$Q = \sum_{ij} (\mathbf{X}_i - \mathbf{X}_j^o)' M_{ij}^{-1} (\mathbf{X}_i - \mathbf{X}_j^o)$$

with

$$\mathbf{X}_j^o = \left\{ \sum_i M_{ij}^{-1} \right\}^{-1} \left\{ \sum_i M_{ij}^{-1} \mathbf{X}_i \right\}$$

so that finally, after the constraints are taken into consideration,

$$V_c' P_c V_c = \sum_{ij} (\mathbf{X}_i - \mathbf{X}_j^o)' M_{ij}^{-1} (\mathbf{X}_i - \mathbf{X}_j^o) + U'X - \sum^{c} (W^c)' K_c \tag{8.140}$$

The first term in the above is the quadratic form of all the residuals arising from all simultaneous event adjustments with ground stations held fixed and is computed and summed for each event by means of equation (8.1), for the purpose of blunder detection (sec. 8.3.2.2.2); the second term is found from

$$U'X=\bar{D}'\bar{C} \tag{8.141}$$

where the vectors $\bar{D}'$ and $\bar{C}$, a by-product in the solution of the normal equations, are defined by equations (8.114) and (8.109), respectively. K_c is obtained from equation (8.95a), where X is the solution of equation (8.100).

The total number of degrees of freedom, df, to be used in equation (8.126) is

$$\begin{aligned} df &= \text{number of equations} \\ &\quad -\text{number of unknowns} \\ df &= \left(\sum_j 2n+n_c\right)-(3s+3g) \end{aligned} \tag{8.142}$$

where $2n$ is the number of equations resulting from one simultaneous event (n=number of ground stations in a particular event j) and the summation is performed over all simultaneous events; n_c is the number of constraint equations; $3s$ is the number of unknowns due to s number of satellite positions; $3g$ is the number of unknowns due to g number of unknown ground stations. In conclusion the a posteriori variance of unit weight for the optical adjustment will be

$$\sigma_0^2=\frac{V_c'P_cV_c}{df} \tag{8.143}$$

8.4.7.1.2 RANGE ADJUSTMENT

Equations (8.126) will now be discussed in the light of the range adjustment. First, the expression for computing $V'PV$ by an analogous argument to the optical case is

$$V_c'PV=\bar{V}'P\bar{V}-X'U \tag{8.144}$$

where $\bar{V}'P\bar{V}$ is the quadratic form of the residuals arising from the adjustment of simultaneous events, the ground stations being held fixed. The second term

$$X'U=\bar{D}'\bar{C} \tag{8.145}$$

is computed according to equations (8.114) and (8.109), respectively.

The degrees of freedom, df, in the range adjustment is as usual

$$\begin{aligned} df &= \text{number of equations}-\text{number of unknowns} \\ &= \left(\sum_j n+n_r\right)-(3s+3g) \end{aligned} \tag{8.146}$$

where n is the number of ground stations (thus observed ranges) in a particular simultaneous event, and the summation is performed over all simultaneous events; n_r again is the number of constraint equations in the range adjustment; $3s$ and $3g$ are the number of unknowns due to s number of satellite positions and g number of unknown ground stations, respectively.

In summary,

$$\sigma_0^2=\frac{V_c'P_cV_c}{df} \tag{8.147}$$

8.4.7.2 Variances and Covariances of Ground Stations

8.4.7.2.1 CARTESIAN COORDINATES

The variance-covariance matrix giving the accuracy of the adjusted rectangular ground station coordinates is

$$\sum_{\substack{u\\v\\w}}=\sigma_0^2N^{-1} \tag{8.148}$$

where σ_0^2 is the variance of unit weight arising from the adjustment (sec. 8.4.7.1) and N^{-1} is the coefficient matrix discussed in section 8.4.6.4. The units for the variance-covariance matrix for the optical and range adjustments are meters squared. The square root of the diagonal elements of the variance-covariance matrix yields the corresponding standard deviations in meters.

8.4.7.2.2 GEODETIC COORDINATES

The propagation of variances and covariances from curvilinear coordinates (geodetic latitude ϕ and longitude λ and height h) in meters to three-dimensional rectangular coordinates (u,v,w) is achieved by the following matrix equation:

$$\sum_{\substack{u\\v\\w}} = G \sum_{\substack{\phi\\\lambda\\h}} G' \qquad (8.149)$$

where

$$G = \begin{bmatrix} -\sin\phi\cos\lambda & -\cos\phi\sin\lambda & \cos\phi\cos\lambda \\ -\sin\phi\sin\lambda & \cos\phi\cos\lambda & \cos\phi\sin\lambda \\ -\cos\phi & 0 & \sin\phi \end{bmatrix} \qquad (8.150)$$

When the transformation depicted by equation (8.149) is reversed, the 3×3 variance-covariance matrix corresponding to ϕ, λ, h is

$$\sum_{\substack{\phi\\\lambda\\h}} = G^{-1} \sum_{\substack{u\\v\\w}} (G')^{-1} = \begin{bmatrix} \sigma_\phi^2 & \sigma_{\phi\lambda} & \sigma_{\phi h} \\ \sigma_{\lambda\phi} & \sigma_\lambda^2 & \sigma_{\lambda h} \\ \sigma_{h\phi} & \sigma_{h\lambda} & \sigma_h^2 \end{bmatrix} \qquad (8.151)$$

all in units of (meters)^2.

In order to obtain the units

$$\begin{array}{ll} \sigma_\phi^2 & (\text{arc-sec})^2 \\ \sigma_\lambda^2 & (\text{arc-sec})^2 \\ \sigma_{\phi\lambda} \equiv \sigma_{\lambda\phi} & (\text{arc-sec})^2 \\ \sigma_h^2 & \text{meters}^2 \\ \sigma_{\phi h} \equiv \sigma_{h\phi} & \text{arc-sec} \times \text{meters} \\ \sigma_{h\lambda} \equiv \sigma_{\lambda h} & \text{arc-sec} \times \text{meters} \end{array} \qquad (8.152)$$

the elements of equation (8.151) require the following modifications:

$$\sigma_\phi''^2 = \left(\frac{\rho''}{R+h}\sigma_\phi\right)^2$$
$$\sigma_\lambda''^2 = \left(\frac{\rho''}{R+h}\sigma_\lambda\right)^2$$
$$\sigma_{\phi\lambda} \equiv \sigma_{\lambda\phi} = \left(\frac{\rho''}{R+h}\right)^2 \sigma_{\phi\lambda} \qquad (8.153)$$

$$\sigma_{h\phi} \equiv \sigma_{\phi h} = \frac{\rho''}{R+h}\sigma_{h\phi}$$
$$\sigma_{h\lambda} \equiv \sigma_{\lambda h} = \frac{\rho''}{R+h}\sigma_{h\lambda}$$

where

$$\rho'' = \frac{1}{\sin 1''}$$
$$R = 6\,370\,000 \text{ m}$$

(Note: R replaces the radius of curvature N in the prime vertical plane in the rigorous case; justification for simplification is given by the fact that only three significant figures are meaningful in propagation of variances whose magnitudes in m^2 or (arc-sec)^2 are in the units' place.)

8.4.7.3 Correlation Between Ground Stations

The amount of correlation between the adjusted ground station coordinates is described in terms of the correlation coefficient. The correlation coefficient is defined as

$$\rho_{ij} = \frac{\sigma_{ij}}{\sigma_i \sigma_j} \qquad (8.154)$$

where i and j represent any two quantities associated with a variance-covariance matrix such as that of equation (8.148); σ_{ij} is the covariance, namely, the off-diagonal term of equation (8.148); and σ_i and σ_j are the standand deviations or square root of the ith and jth variances (diagonal terms), respectively.

8.4.7.4 Error Ellipsoid Computation

Error ellipsoid computation is made for each observing ground station considered as an unknown in the adjustment. The eigenvalues and eigenvectors are computed in a topocentric three-dimensional rectangular coordinate system with its origin at the particular ground station and its axes parallel to the mean terrestrial coordinate system (sec. 8.4.1.2). For each point, one eigenvalue (λ_{ii}) corresponds to each of the three mutually perpendicular axes of the ellipsoid; the

direction of the three axes is given by their corresponding eigenvector (T^i).

The actual computation is as follows. The 3×3 on-diagonal variance-covariance matrix Σ of equation (8.148) is subjected to an orthogonal transformation

$$T'\Sigma T=\Lambda \qquad (8.155)$$

where Λ is a diagonal matrix and T is the orthogonal transformation matrix to be found which diagonalizes Σ. The transformation results in three homogeneous linear equations, namely,

$$[\Sigma-\lambda_{ii}I]T^i=0 \qquad (8.156)$$

which has a solution only if the determinant of the coefficient vanishes, i.e.,

$$|\Sigma-\lambda_{ii}I|=0$$

or

$$\begin{vmatrix} \sigma_{11}^2-\lambda_{11} & \sigma_{12} & \sigma_{13} \\ \sigma_{21} & \sigma_{22}^2-\lambda_{22} & \sigma_{23} \\ \sigma_{31} & \sigma_{32} & \sigma_{33}^2-\lambda_{33} \end{vmatrix}=0 \qquad (8.157)$$

Once the eigenvalues are obtained from equation (8.157), their corresponding eigenvectors are obtained from equation (8.156) after substitution of λ_{11}.

The length of the axes of the error ellipsoid are the square roots of the corresponding eigenvalues. The spherical coordinates (spherical latitude θ and longitude λ) which given the direction of each ellipsoidal axis are obtained from the components of the eigenvector

$$T^i=\begin{bmatrix} t_1 \\ t_2 \\ t_3 \end{bmatrix}$$

namely

$$\tan\theta=\frac{t_3}{\sqrt{t_1^2+t_2^2}} \qquad (8.158)$$

and

$$\tan\lambda=\frac{t_2}{t_1} \qquad (8.159)$$

These angles can easily be converted to altitude and azimuth if so desired.

8.4.8 Computer Programming

(OSU Reports 87, 88, 190, 193)

Computer programs related to section 8.4 may be found in Reilly *et al.* (1972) and in Mueller *et al.* (1973a).

8.5 RESULTS (SOLUTION WN14)

(OSU Reports 187, 188, 193, 195, 196, 199)

8.5.1 Reference Ellipsoid, Origin, Orientation, and Scale

The least-squares adjustment of the observations listed in tables 8.7 is performed in terms of the Cartesian coordinates of the tracking stations. The results are also converted into geodetic coordinates (latitude, longitude, height) referred to a rotational ellipsoid of the following parameters:

$$a=6\ 378\ 155.00\ \text{m}$$
$$b=6\ 356\ 769.70\ \text{m}$$

The corresponding flattening is

$$f=1/298.249\ 498\ 5=0.003\ 352\dot{8}\ 897\ 507$$

The origin of the coordinate system (or the center of the above reference ellipsoid) is free as determined through the "inner" constraints explained in section 8.4.5.7. The orientation of the system is inherent in the camera observations, through the star positions in the SAO catalog (referenced to the FK4 system) updated to their apparent positions at the epoch of the observation, and through UT1, x and y (coordinates of the true pole with respect to the CIO) as derived by the BIH. Thus the positive end of the axis u is in the direction of the Greenwich Mean Astronomical Meridian (and the zero geodetic meridian of the reference ellipsoid); the positive w axis passes through the Conventional International Origin (and coincides with the minor axis of the reference ellipsoid). The axis y completes the right-handed

coordinate system in the direction of the 90° (E) meridian and with the u axis defines the plane of the average terrestrial (geodetic) equator.

The scale in the solution is defined through the dominating nearly 30 000 SECOR range observations, through the lengths of eight EDM (Geodimeter or Tellurometer) and three C-band baselines, and also through a special procedure using constrained ellipsoidal heights.

The SECOR observations have an a posteriori standard deviation of ±4.1 m or approximately one part per million (Mueller et al., 1973b). The scale is propagated into the network through 13 camera stations whose relative positions with respect to the nearby SECOR stations are maintained in the adjustment, with their survey coordinate-differences entered as weighted constraints (see table 8.9).

The available EDM and C-band baselines are listed in table 8.11. The chord distances shown are entered in the adjustment as weighted constraints with weights computed from their estimated a priori standard deviations as listed in the table. The reasons for rejecting the east-west Australian tellurometer line (6032–6060) are explained in Mueller *et al.* (1973a). Three C-band lines were also rejected because of suspected errors in the survey coordinates of the terminal stations (Kauai (4742) in Hawaii and Pretoria (4050) in South Africa) needed to tie them to the nearest camera stations (9012 and 9002, respectively). Though these four lines were not constrained, at the end of the analysis two of them (6032–6060 and 4082–4050) compared well with the lengths computed from the adjusted coordinates (see table 8.17). Thus the only station with survey coordinates in definite error is Kauai.

The use of geodetic (ellipsoidal) heights as weighted constraints as a contribution to the scale requires a more detailed explanation (fig. 8.16). The height h above a geocentric reference ellipsoid has two main components: the orthometric (mean sea level) height MSL and the geoid undulation N. In this geocentric case, N consists of a long-wavelength

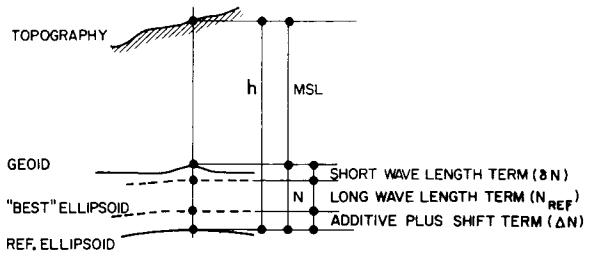

FIGURE 8.16.—Height components.

component N_{REF}, a short-wavelength term δN, and an additive part Δa. The term N_{REF} generally corresponds to regional gravitational effects and can be computed, e.g., from a truncated spherical harmonic series. The short-wavelength part δN corresponds to local gravity or mass disturbances and is generally not contained in the spherical harmonic representation. The additive part Δa is the so-called zero-degree term, which may exist because the ellipsoid may not be the same size (though it may have the same flattening) as the "best" (mean earth) level ellipsoid to which the undulations, N_{REF}, are referred. Since the N_{REF} undulations are, within reasonable limits, insensitive to the semidiameter of the level ellipsoid, it is difficult to define a correct value for Δa. If the reference ellipsoid is nongeocentric, as is the case in this solution, an additional height term dh arises because of the "shift" of the origin (ellipsoidal center) with respect to the geocenter.

Thus the geodetic height may have the following components:

$$h = MSL + N \tag{8.160}$$

$$N = N_{REF} + \delta N + \Delta N \tag{8.161}$$

where (Heiskanen and Moritz, 167, p. 207)

$$\Delta N = \Delta a + dh = \Delta a + u_0 \cos\phi \cos\lambda + v_0 \cos\phi \sin\lambda + w_0 \sin\phi \tag{8.162}$$

$\Delta a = a$ (level ellipsoid) $- a$ (reference ellipsoid)

u_0, v_0, w_0 are the coordinates of the geocenter with respect to the center of the reference

ellipsoid (origin), and ϕ, λ are the geodetic coordinates of the station to which h refers.

In practice at most satellite tracking stations, the quantity $MSL+N_{REF}$ is well known, and generally it constitutes the largest portion of the total height above the level ellipsoid. The additive+shift term ΔN can be determined empirically through an iterative interpolation procedure, as described later. Since $MSL+N_{REF}+\Delta N$ constitutes the largest portion of the total height above the reference ellipsoid, it seems reasonable not to ignore this, admittedly partial, information on the height of the station and to include it in the adjustment as a constraint ($h_{CONSTR}=MSL+N_{REF}+\Delta N$) with such a weight that the adjustment should be able to "pull out" the only remaining component, the short-wavelength term δN together with possible errors in h_{CONSTR}. In this solution the standard deviations used in computing the weights vary from ± 2.5 m to ± 8 m, depending mostly on the location of the station, from the point of view of the extent of the available surface gravity observations in the area included in the spherical harmonic expansion for N_{REF} (Rapp, 1973). Table 8.10 lists these standard deviations and the quantities h_{CONSTR} for all the stations.

In trying to determine the "best" scale for the solution or, which is the same, the "best" additive term Δa, the first step is to establish the relationship between them. This problem differently stated is the determination of the relationship between the additive term and the semidiameter of the "best" level ellipsoid to which the quantity N_{REF} refers. The meaning of the term "best" will be elaborated on later in this section. This is accomplished empirically from a set of solutions with height constraints containing different additive terms, from $\Delta a=0$ to 30 m. The shift term dh initially is estimated from comparisons with various dynamic solutions, resulting in the coordinates u_0, v_0, and w_0 needed in equation (8.162).

These solutions result in sets of geodetic heights (h_{WNi}) above the reference ellipsoid and in sets of undulations after subtracting the MSL:

$$N_{WNi}=h_{WNi}-MSL$$

These undulations thus refer to the reference ellipsoid of $a=6\,378\,155$ m, whose origin is set by the inner constraint. Disregarding the short-wave length term, the relationship between the undulations N_{WNi} and N_{REF} is given by equations (8.161) and (8.162), from which, for any station and for the solution WNi,

$$(N_{WNi}-N_{REF})-(\Delta a_i+u_{0i}\cos\phi\cos\lambda+v_{0i}\cos\phi\sin\lambda+w_{0i}\sin\phi)=0$$

Since the quantity $(N_{WNi}-N_{REF})$ is known at all stations, the parameters Δa_i, u_{0i}, v_{0i}, w_{0i} can be calculated (iterated) from least-squares adjustments for each set i. This is the same as determining the size (scale) and the origin of the level ellipsoid that best fits the geoid defined for a given set by the undulations N_{WNi}. Its size is

$$a_i=6\,378\,155+\Delta a_i$$

and its origin with respect to the origin of the reference ellipsoid is defined by the coordinates u_{0i}, v_{0i}, and w_{0i}. After some iterations these coordinates hardly change from solution (set) to solution (set), regardless of the initial selection of Δa; thus the relationship between the input additive term and the resulting semidiameter, $a=f(\Delta a)$, becomes straightforward and linear.

This empirically determined relationship is shown in figure 8.17, as the dashed line drawn from the lower left corner towards the upper right. The corresponding ordinate is on the right-hand side of the diagram. The line now allows us either to pick the correct initial additive term, which when used in the height constraints would result in an a priori defined semi-diameter (scale), or to determine which semidiameter (scale) would correspond to an a priori defined additive term. As an example, if the semidiameter of the level ellipsoid best fitting the geoid was 6 378 142 m, the WN solution would require height constraints computed with an additive term of -15 m.

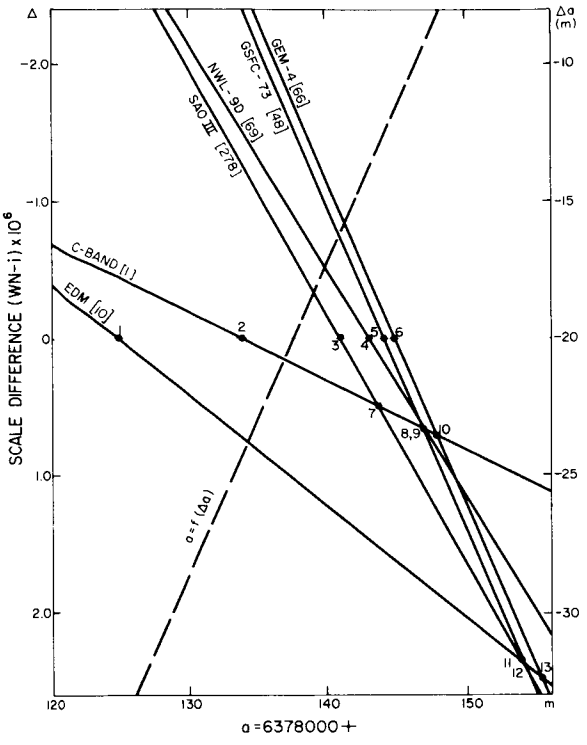

FIGURE 8.17.—Determination of scale.

The next question, of course, is just how big should this desired semidiameter be. Putting it differently, what criterion should be used to select the "best" scale? If the scale were to be determined only from the EDM and C-band baselines and/or the SECOR observations, these questions would not arise, since the scale would be inherently defined.

The use of weighted height constraints, as explained above, provides a unique tool for selecting the scale to fit some criterion. There could be several noninclusive criteria, e.g.,

(1) The lengths of the EDM baselines as computed from the adjusted coordinates of the terminal stations should be exactly the same as the lengths given in table 8.11 or their differences would be within the limit of one (average) standard deviation or within a certain limit, e.g., 1:1 000 000, etc.

(2) The lengths of the C-band baselines as computed from the adjusted coordinates of the terminal stations should be exactly the same as the lengths given in table 8.11 or their differences should be within the limit of one (average) standard deviation or within a certain limit, e.g., 1:1 000 000, etc.

(3) The scale difference as determined from the station coordinates of the WN solution, and from the same coordinates of a dynamic solution should be exactly zero, within the limit of one standard deviation of the scale difference factor, or within 1:1 000 000, etc.

(4) The scale difference as determined in (3) should be within a certain limit with respect to all of the dynamic solutions.

(5) The scale difference should be within a certain limit with respect to all of the dynamic solutions and the EDM and C-band baselines.

To be able to enforce any of these criteria, the relationship between the scale difference factor and the semidiameter has to be established. This relationship is established empirically by determining the scale differences between the different WNi solutions (used to determine the function $a=f(\Delta a)$) and the EDM and C-band baselines and the dynamic solutions NWL–9D (Anderle, 1974), SAO Standard Earth III (Gaposchkin *et al.*, 1974), GEM 4 (Lerch *et al.*, 1972a), and GSFC 73 (Marsh et al., 1973). The method of calculating the scale difference factor is described in Kumar (1972). The results are shown in figure 8.17, in which, with the ordinate on the lefthand side, the scale differences are plotted against the semidiameters corresponding to the various Δa's used in the height constraints. The numbers on the lines indicate relative weights based on the uncertainties of the scale difference determinations. It can be seen that the lines representing the geometric (EDM and C-band) scale differences are much less well determined than the dynamic ones. As an example, the scale difference factor, between the WNi solution computed with $\Delta a=-15$ m ($a=6\,378\,142$ m) and the solutions NWL–9D is -0.18×10^{-6}; the GEM 4 is -0.68×10^{-6} (the dynamic scales are larger). Also, the lengths of the EDM baselines from the adjustment differ from their directly measured values by 1.38×10^{-6} (the measured values are smaller).

The diagram is used by recognizing the importance of the various intersection points, marked by numbers. For example, point 1 illustrates the fact that if the semidiameter of the level ellipsoid was 6 378 125 m, the difference between the adjusted chord lengths and their given values would be zero; point 4 shows that with an $a=6\,378\,143$ m there would be no scale difference between WNi and NWL–9D. Fourteen similar intersection points are listed in table 8.12 with weights and interpretation.

From the table it is immediately clear that if the weighted mean of the intersection points is taken from the "geometric" scalars (points 1 and 2), the "best" semidiameter is 6 378 125.8 m, whereas if the mean is taken from the "dynamic" lines (points 3–6), it is 6 378 142.0 m. The difference of some 16 m, or about 2.5 parts in a million, seems to be real but unexplained at this time. The combined weighted mean from points 1–6 is 6 378 141.7 m, whereas from all the points (1–14) it is 6 378 142.7 m.

For the solution reported here (WN14), the criterion for the scale is (5) above, i.e., the scale should correspond well to all geometric and dynamic information available at present. On the basis of the numbers above and of previously published parameters, $a=6\,378\,142$ m was selected. This then requires an adjustment in which the scale is defined, in addition to the SECOR, EDM, and C-band observations, through height constraints with the initial additive constant $\Delta a=-15$ m. As can be seen from figure 8.17, at this semidiameter the maximum scale difference expected between WN14 and any of the dynamic solutions is about 0.8×10^{-6} and with respect to the EDM about 1.4×10^{-6} or 1:700 000 which is about the average standard deviation of the EDM baselines. From this scale the resulting geoid undulations

$$N=h_{\mathrm{WN14}}-MSL-\Delta N \qquad (8.163)$$

where

$$\Delta N\ (\text{meters})=-13-23.2\cos\phi\cos\lambda -2.9\cos\phi\sin\lambda+2.7\sin\phi$$

are consistent with dynamically computed ones when the following set of constants defining the gravity field of the level ellipsoid (Heiskanen and Moritz, 1967, p. 64) are used:

$f=1/298.25$
$\omega=0.729\,211\,514\,67\times10^{-4}$ rad sec^{-1} (rotational velocity)
$a=6.378\,142$ m
$W_0=6\,263\,688.00$ kGal m (geopotential on the geoid)

Derived from these are the following:

GM $=3.986\,009\,22\times10^{14}$ m^3 sec^{-2} (gravitational constant $\times$ earth mass)
$\gamma_e=978.032\,26$ cm sec^{-2} (equatorial normal gravity)
$C_2^0=-1\,082.686\,3\times10^{-6}$ (second-degree harmonic)

All the above constants are in good agreement with their current best estimates. The parameters in equation (8.163) ($\Delta a=-13\pm0.7$ m, $u_0=-23.2\pm0.9$ m, $v_0=-2.9\pm0.8$ m, $w_0=2.7\pm1.2$ m) are the result of fittinfi an ellipsoid to the WN14 geoid, as was explained earlier in this section. They represent the size and the position of the best fitting level ellipsoid with respect to the reference ellipsoid (of the same flattening). In case of a good global station distribution the center of this level ellipsoid is the "geometric" center of the geoid. If this point is assumed to be identical with the center of mass, then the above coordinates are its coordinates with respect to the reference-ellipsoid origin and with opposite signs they can be used to shift the WN14 coordinates to the geocenter:

$$\begin{aligned} u\ (\text{geocentric}) &= u_{\mathrm{WN14}}+23.2\ \text{m}\\ v\ (\text{geocentric}) &= v_{\mathrm{WN14}}+2.9\ \text{m}\\ w\ (\text{geocentric}) &= w_{\mathrm{WN14}}-2.7\ \text{m} \end{aligned} \qquad (8.164)$$

8.5.2 Cartesian and Geodetic Coordinates

The Cartesian and geodetic coordinates resulting from the WN14 solution are listed

in table 8.14. Standard deviations of both types of coordinates are also given together with the parameters of the error ellipsoid (see sec. 8.4.7.4.). The first section of table 8.14 explains the format and the units used. Table 8.13 is a summary of the average standard deviations. The values are also broken down to the constituent networks. The notation is explained in the first section of table 8.14, except for the average standard deviation, which is $\sigma=\sqrt{(\sigma_u^2+\sigma_v^2+\sigma_w^2)/3}$. As can be seen, the weakest portion of the network is the MPS, and the strongest is the SECOR. The average standard deviation in a Cartesian coordinate is ± 3.9 m. See table 8.18 for comparison with solutions: (1) without the weighted height constraints (WN12) and (2) without chord constraints (WN16) (see sec. 8.5.3).

The full variance-covariance matrix cannot be presented here because of lack of space; however, the correlation coefficients ρ_{ij} (see eq. (8.154)) between the u,v,w coordinates of stations i and j (the off-diagonal 3×3 matrices) are listed in table 8.15 where $\rho_{ij}>0.75$. The 3×3 correlation coefficient matrices with any element greater than 0.925 are marked by asterisks. Comparison with table 8.9 reveals that all of these station pairs have their relative positions constrained; thus such correlations are expected. Table 8.16 contains the correlation coefficients between the u,v,w coordinates of a given station, i.e., the 3×3 matrices along the diagonal of the full correlation coefficient matrix.

8.5.3 Comparisons With Geometric Information

In addition to solution WN14, two other adjustments were also performed with the same data. The only differences were that in one of them (WN12) the weighted height constraints were not applied; thus the scale is defined through the SECOR, EDM, and C-band data. In the other (WN16), the EDM and C-band lengths were not entered as weighted constraints; thus the scale is through the SECOR and the weighted height constraints. Coordinates from solution WN16 are not given; only some revealing information in a summary form, which can be compared with the WN14 results, is included.

Table 8.17 contains the differences between the adjusted and given chord lengths (table 8.11) from the three solutions. The lines originating from station 4742 (Kauai) are not listed (see sec. 8.5.1). When solutions WN14 and WN12 are compared, the effect of including the heights is not very significant. The average length discrepancy decreases to 0.48×10^{-6} for the EDM and 0.60×10^{-6} for the C-band, both numbers being within the noise level. At first glance the difference between WN14 and WN16 seems to be significant, since the average length discrepancy increases by about 4×10^{-6} or 1:250 000 for both types of observations. Close inspection, however, reveals that though the inclusion of the EDM and C-band chords in the solution improves the positions of stations 6111 (Wrightwood), 6065 (Hohenpeissenberg), and 4081 (Grand Turk), it does not otherwise contribute to the overall scale determination significantly. If the above-mentioned stations are left out of the comparison, the average length discrepancies in the WN16 solution decrease to 2.76×10^{-6} for the EDM and 1.81×10^{-6} for the C-band, both being within the noise level from WN14 (about 1×10^{-6}).

The above conclusion is also strengthened by the content of table 8.18, in which the average standard deviations of the coordinates and the heights from the three solutions are compared. It is seen that, while the inclusion of the weighted heights decreases the standard deviations significantly, the exclusion of the geometric scalars hardly changes the results.

Table 8.19 shows the results of a coordinate transformation between solutions WN14 and WN16. Inspection of the residuals given in the table shows that they are insignificant except probably at the stations already mentioned, though even there the discrepancies are within or near the noise level. That the chords 6003–6111 and 6016–6065 improve the positions of stations 6111 and 6065 (while the other chords have little effect on their

terminal stations) is not surprising, once it is recognized that these lines are too short to be determined well from observations on PAGEOS.

Table 8.20 contains the results of the transformation between WN14 and WN12. The effect of the missing height constraints is well recognizable both in the scale and in the residuals.

In the tables, the rotations, ω, ψ, and ϵ are about the w, v, and u axes, respectively. The unit in the variance-covariance matrix, for the elements corresponding to the rotations, is radian squared.

Table 8.21 shows a height analysis computed for the purpose of inspecting the height residuals from solution WN14, which, according to the explanation offered in section 8.5.1, are mostly the short-wavelength components (δN) of the geoid undulation. In the table, N_{OSUGC} denotes the quantity $h_{WN14}-MSL-dh$ where dh is computed with $u_0=-23.2$ m, $v_0=-2.9$ m, and $w_0=2.7$ m.

In case of a uniform global station distribution, the average value of N_{OSUGC}—N_{REF} should be equal to the additive term from the best fit, $\Delta a=-13$ m. As is seen at the end of table 8.21, this number is -12.94 m. The root mean square value of the residuals is ± 6.42 m. The respective numbers from the WN12 solution (no weighted height constraints) are -1.24 and ± 13.45 m. From this, it seems that the semidiameter of the level ellipsoid best fitting the geoid (defined through the N_{WN12} undulations) is 6 378 153.8 ± 13.5 m, as opposed to that of the WN14 solution, 6 378 142.1 ± 6.4 m. The proximity of these values and their noise level are only indications that the "best" semidiameter of the level ellipsoid still needs to be determined; at the present time it can only be defined to fit some criteria, as in section 8.5.1.

Table 8.22 contains the results of an independent height comparison in which undulations (N) from the WN14 solution referred to the defined level ellipsoid are compared with those (N_V) from Vincent *et al.* (1972b). The quantity

$$N=h_{WN14}-MSL-\Delta N=N_{OSUGC}-\Delta a$$

The average difference $N-N_V$ taken over the stations where N_V is available is -0.3 m, and the rms of the residuals is ± 6.1 m. Similar comparisons with the WN12 solution show an average difference of -0.2 m and the rms of the residuals of ± 16.1 m.

8.5.4 Comparisons With Dynamic Solutions

Table 8.23 is a compilation of transformation parameters between the WN_{14} (World Net) coordinates and those from the dynamic solutions NWL–9D, SAO Standard Earth III, GEM–4, and GSFC 73. The method of computing the parameters is described in Kumar (1972). In the table, the positive angles ω, ψ, and ϵ are counterclockwise rotations about the w, v, and u axes, respectively, as viewed from the end of the positive axis. The scale difference factor Δ is in units of ppm. In the transformations, the variances of both sets of the coordinates are taken into account. If the variances of the WN solution are taken as standard, the variances of the dynamic solutions are scaled by the weight factors indicated. These numbers are also indicative of the overoptimism over the quality of some of the published solutions. For example, a weight factor of 25 would indicate that the published standard deviations of a given solution need to be multiplied by $\sqrt{25}=5$.

Tables 8.24 to 8.27 contain the variance-covariance matrices, the correlation coefficients, and the residuals after transformation for the solutions mentioned above.

As is seen, there is a good agreement between the translational elements Δu's and Δv's of the main (all stations included) dynamic solutions and a discrepancy of about 8.5 ± 1.7 m with respect to the geometric values (see eq. (8.164)). The largest discrepancy occurs in the Δw components, where there seems to be a 14.2 ± 2.8 m difference between the SAO Standard Earth III and the GEM–4 solutions. When the SAO Standard Earth III value is eliminated, all Δw's, including the geometric one, are within the noise level. The weighted mean shifts from the main dynamic solutions (excluding Δw

from SAO Standard Earth III, or the coordinates of the geocenter with respect to the WN14 origin), are listed in table 8.28.

The quantity $r_0 = \sqrt{u_0^2 + v_0^2}$ is the distance of the WN14 origin from the rotation axis of the earth. Calculating the same number from the JPL-LS 37 coordinates of the Deep Space Network (stations DSN1=4711, DSN2=4712, DSN4=4714, DSN6=4742 and DSN7=4751) as given in Gaposchkin (1974), one gets $r_0 = 25.9 \pm 2.5$ m, which is nearest to the value calculated from the geometric fit.

The differences in scale between the dynamic solutions are significant (see fig. 8.17 for comparison). The largest discrepancy is between the SAO Standard Earth III and NWL–9D with $\Delta = (0.58 \pm 0.27) \times 10^{-6}$, which is larger than what one would expect from the noise. The other dynamic scales are within near noise level and, on the average, differ from the scale of the WN14 solution by $\Delta = (0.70 \pm 0.30) \times 10^{-6}$ or about one part in 1.4 million.

The largest discrepancies occur in the orientation of the various dynamic systems with respect to each other and to WN14. In the rotation about the w axis (ω), the largest difference occurs between the NWL–9D and the GSFC 73 solutions, where $\omega = 1''.1$, or about 34 m on the equator (fig. 8.18). The other differences are smaller but are significant. These rotations may be partly due to the definition of the zero meridian in the case of purely electronic systems (e.g., Doppler), partly to the various definitions of the vernal equinox in the star catalogs used, and also partly to its motion with respect to inertial space, in the case of camera observations. The latter alone requires a correction to the FK4 right ascensions amounting to $+0''.65$ at 1960.0, changing with a rate of $+1''.36$ per century (Martin and Van Flandern, 1970).

The rotations about the axes u and v are even more confusing. Figure 8.19 illustrates the situation at the pole. The weighted means of the dynamic solutions are $\psi = -0''.03 \pm 0''.50$ and $\epsilon = -0''.04 \pm 0''.02$. The discrepancy between the poles, as determined separately from the SAO Standard Earth III 6000 stations and then from the 9000 stations, is unexplained at this time. It is interesting to note that the weighted mean pole and zero meridian positions computed from the dynamic solutions hardly differ from those of the WN14 solution.

The only general conclusion that one can draw from the rotation parameters is that the coordinate systems used in the dynamic solutions need to be more carefully defined and conditions enforcing these definitions

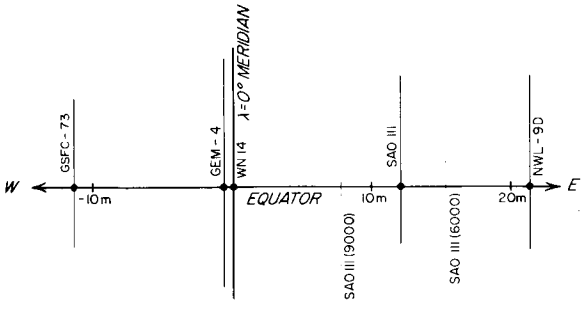

FIGURE 8.18.—Dynamic zero meridians relative to the WN14 zero meridian.

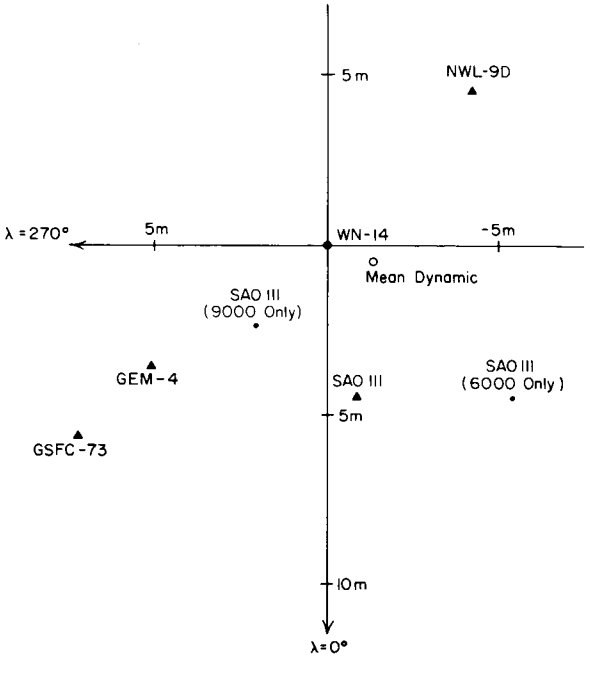

FIGURE 8.19.—Dynamic pole positions relative to the WN14 pole.

more strongly applied than is evidenced from the solutions discussed.

8.5.5 Comparisons With Geodetic Datums

In a planning document prepared in 1966, it was shown that the various countries in the world use or have used 90 different geodetic datums in their mapping activities (Mueller, 1966). Since many of these datums have been tied together with ground survey, it is possible to combine them into about 20 large and/or independent datum blocks (fig. 8.20). The original OSU goal, outlined in section 8.1, called for at least three well-distributed tracking stations on each of these datum blocks. As of the writing of this report, this goal has been accomplished only on the following datums: Australian (3 stations), European 50 (16 stations, but marginal accuracy), North American 1927 (21 stations), and South American 1969 (10 stations).

On the Tokyo datum there are also several stations, but only one of them is independently determined in the WN14 solution. In order to meet the original requirement, additional stations or observations will have to be included in future solutions in the following general areas in order of preference: Europe, the Soviet Union, India, Japan, the Philippines, the Cape (South Africa), Madagascar, New Zealand, North Africa. Observations have already been taken and will become available within reasonable time in Europe and North Africa.

Relationships between the geodetic datums and the WN14 coordinate system, as reflected from the data included, are summarized in table 8.29. Parameter values given only to the nearest meter represent estimated values, while the other parameters are the results of regular seven parameter transformations.

If the geodetic coordinates referred to in any of the datums listed are to be shifted to the "best" geocenter, subtract from the Cartesian datum coordinates the values Δu, Δv, Δw listed and add 16 m, 5 m, and -3 m (or other values from table 8.28), respectively.

The variance-covariance matrix, the coefficients of correlation, and the residuals after adjustment for those datum blocks where three or more stations are available are shown in tables 8.30 to 8.36. The datum with the poorest fit is the European 50, followed by the South American 1969.

8.6 SUMMARY AND CONCLUSIONS

The OSU WN14 solution is a geometric adjustment for the coordinates of 158 tracking stations.

The coordinate system in which the coordinates are presented is oriented towards the Greenwich Mean Astronomical Meridian (u axis) and the Conventional International Origin (w axis), both as defined by the Bureau International de l'Heure. The v axis forms a right-handed system with the u and w, and with u defines the average geodetic equator. The coordinates of the origin with respect to the geocenter are suggested to be

$$u^o_{WN14} + 16 \text{ m}, \; v^o_{WN14} = 5 \text{ m}, \; w^o_{WN14} = -3 \text{ m}$$

The scale in the solution is defined through SECOR observations and weighted height constraints. Chord distances derived from C-band radar observations and from electronic distance measurements (geodimeter and tellurometer) are also included as weighted constraints, but they seem to have little or no effect. The main reason that the SECOR observations are successfully utilized (perhaps for the first time) is that the ill-conditioning arising in quadrilateration when the four stations lie near a plane (which is always the case with SECOR) is eliminated by "pinning down" the stations to the geoid through the height constraints and the directions defined by the camera observations from the collocated stations.

The scale in the solution is such that when the coordinates are transformed to a geocentric rotational ellipsoid of $a = 6\,378\,142$ m and $1/f = 298.25$, they produce geoid undulations consistent with dynamically determined ones with $GM = 3.986\,009\,2 \times 10^{14}$ m^3 sec^{-2} and $\gamma_e = 978.032\,6$ cm sec^{-2}.

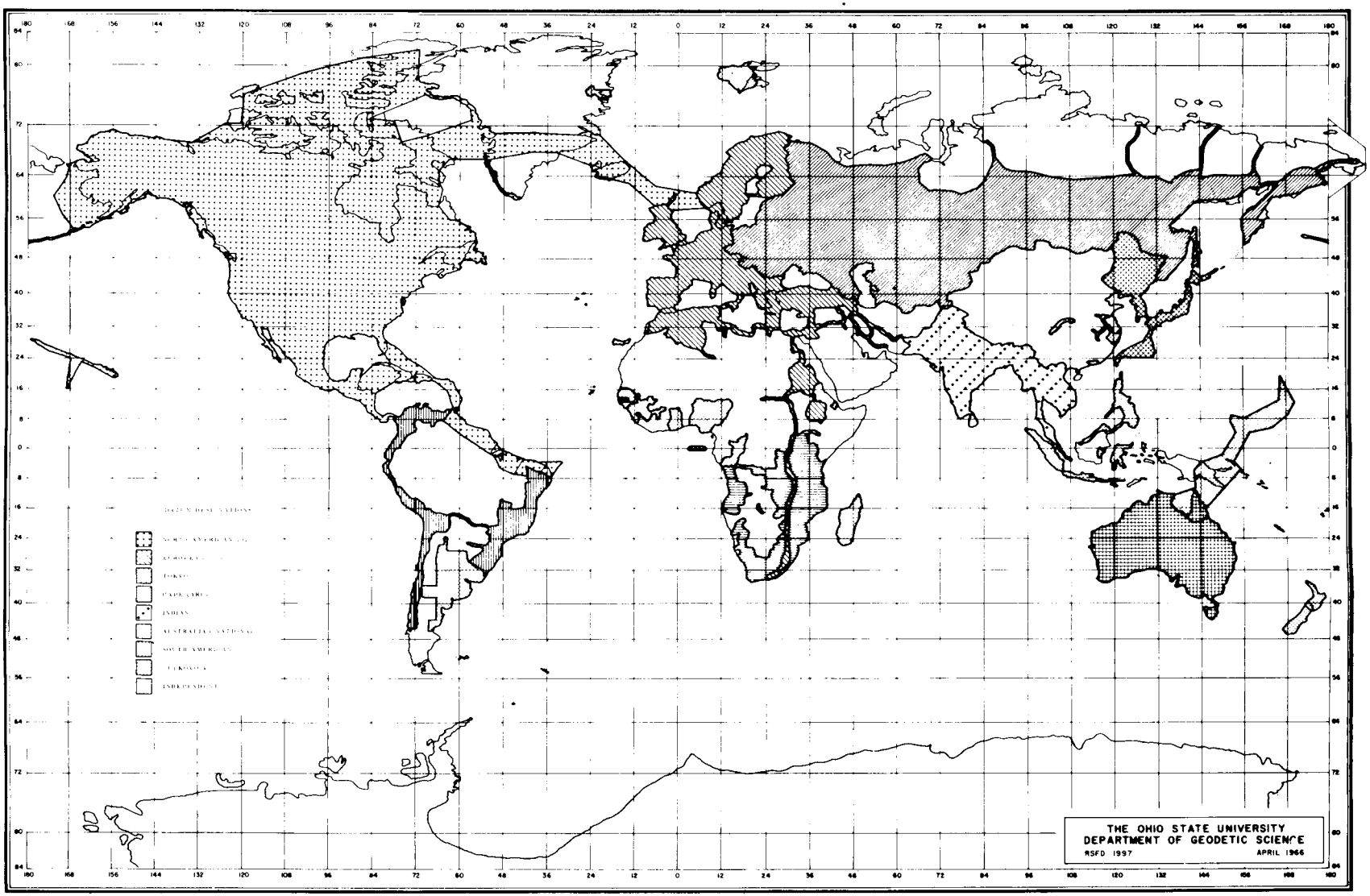

FIGURE 8.20.—Major geodetic datum blocks.

The consistency of the solution is represented by the average standard deviation in a Cartesian coordinate of ± 3.9 m and in height of ± 2.9 m. The correlations between the coordinates of a given station and those between different stations are low, except at those nearby stations where the relative positions are maintained at the surveyed values with weighted constraints.

Comparisons with the EDM chords show an average agreement of 1:575 000 with 1:2 700 000 at best and 1:330 000 at worst. The average agreement with the C-band chords is 1:1 000 000, varying between 1:2 100 000 and 1:525 000. The scale agreement with the dynamic solutions on the average is 1:3 600 000, with 1:1 000 000 at worst and 1:5 900 000 at best.

Comparisons with coordinates from dynamic satellite solutions show significant inconsistencies in the orientation of the coordinate systems, which need to be resolved. The residuals after transformation are all within the noise level.

Table 8.37 is a summary of the Cartesian coordinates from solutions WN12 and WN14. As was mentioned earlier, the WN12 solution differs from the WN14 only in that in it the heights are not constrained. The scale in WN12 is such that when the coordinates are transformed to a geocentric rotational ellipsoid of $a=6\,378\,154$ m and $1/f=298.25$, they produce geoid undulations consistent with dynamically determined ones with $GM=3.986\,008\,9\times10^{14}$ m^3 sec^{-2} and $\gamma_e=978.028\,5$ cm sec^{-2}. For various comparisons between solutions WN12 and WN14 see tables 8.17, 8.18, and 8.20.

Comparisons with geoid undulations from satellite and surface gravimetric solutions in the case of the WN14 solution show an rms residual of ± 6.1 m, with an average of only -0.3 m. Similar comparison with the WN12 solution, where the heights are not constrained, shows that the rms of the residuals is ± 16.1 m and the average -0.2 m.

Comparisons with survey coordinates result in satisfactory transformation parameters for the NAD 1927, the Australian, and the South American 1969 datums and marginal ones for the European 1950 datum. In order to fulfill the "three station per datum" general requirement for the other major datum blocks, additional observations are needed from Europe, the Soviet Union, India, Japan, the Philippines, South Africa, Madagascar, New Zealand, and North Africa, in order of preference.

APPENDIX

TABLE 8.1.—*Contributors to the NGSP Report, OSU*

	1965		1966		1967		1968		1969		1970		1971		1972		1973		Contributions to Department of Geodetic Science Reports[a]	Degrees earned		
	I	II	I	II	I	II	I	II	I	II	I	II	I	II	I	II	I	II		BS	MS	PhD
Administrative assistants Miller, J. R.		x	x	x	x	x	x	x														
Preston, J. C.		x	x	x	x	x	x	x														
Tesfai, I.						x	x	x	x	x	x											
Rist, E.												x	x	x	x	x	x					
Student assistants or associates Preuss, H. D.		x	x																70	x	x	
Krakiwsky, E. J.		x	x	x	x	x	x	x											86,87,88,114	x	x	x
Ferrier, J.			x	x															87,88			
Pope, A. J.				x															86		x	
Hotter, F. D.[b]				x	x														82		x	
Blaha, G.					x	x	x	x	x	x	x	x	x						87,140,148,150			x
Reilly, J. P.						x	x	x	x	x	x	x	x	x	x	x	x		88,125,140,187,190,193,199		x	
Schwarz, C. R.						x	x	x	x	x	x	x	x						118,125,140,147,190		x	x
Hornbarger, D. H.[b]						x	x												106		x	
Veach, J. P.[b]						x	x												110		x	
Gross, J.[b]						x	x												100		x	
Arur, M. G.[b]										x	x								139		x	
Whiting, M.												x	x	x	x				188,190,199	x	x	
Kumar, M.													x	x	x	x	x		184,193,195,196,199		x	
Soler, T.														x	x	x	x		187,195,199			
Tsimis, E.														x	x	x			185,191		x	
Joshi, C. S.[b]																x			192		x	
Research associate Saxena, N. K.										x	x	x	x	x	x	x	x		177,193,199			

[a] Index to reports of the Department of Geodetic Science produced under this project.
[b] Students receiving financial assistance other than direct fellowships.

Report No.	Author
70	Preuss (1966)
71	Mueller (1966)
82	Hotter (1967)
86	Krakiwsky and Pope (1967)
87	Krakiwsky *et al.* (1968)
88	Krakiwsky *et al.* (1967)
93	Mueller (1967)
100	Gross (1968)
106	Hornbarger (1968)
110	Veach (1968)
114	Krakiwsky (1968)
118	Schwarz (1968)
125	Mueller *et al.* (1969)
139	Arur (1970)
140	Mueller *et al.* (1970b)
147	Schwarz (1970)
148	Blaha (1971)
150	Blaha (1971)
177	Saxena (1972)
184	Kumar (1972)
185	Tsimis (1972)
187	Mueller *et al.* (1972)
188	Mueller and Whiting (1972)
190	Reilly *et al.* (1972)
191	Tsimis (1973)
193	Mueller *et al.* (1973a)
195	Mueller *et al.* (1973b)
196	Mueller and Kumar (1973)
199	Mueller *et al.* (1973c)

TABLE 8.2.—*Summary of Observed Satellites: Index to Descriptions of Instruments Used in Producing Data for OSU Work*

	Designation	Responsible group	Description given in chapter
1. Satellite instrumentation			
ANNA 1B	62 60 1	APL[a]	2
Courier 1B	60 13 1		
Dash 2	63 30 4		
Echo 1 rocket	---	NASA[b]	5
Echo 1 rocket	60 09 2		
Echo 2	---	NASA	5
Elektron 3	64 38 1		
Explorer 9	61 04 1		
Explorer 19	63 53 1		
GEOS–1	65 89 1	APL	
GEOS–2	68 02 1	APL	2
Midas 4	61 28 1		
Midas 7	63 30 1		
PAGEOS	66 56 1	NASA	5
RCS	65 34 3		
Relay 1	62 68 1		
SECOR (EGRS)	1967 65A	DOD/DMA[c]	3
Telstar 1	62 20 1		
2. Ground instrumentation			
2.1 Cameras			
2.1.1 PC–1000	---	DOD/DMA	3
2.1.2 BC–4	---	NGS[d]	7
2.1.3 MOTS	---	NASA	5
2.1.4 Baker-Nunn	---	SAO[e]	9
2.1.5 Other	---		
2.2 Radar			
2.2.1 C-band	---	NASA/DMA	6
2.2.2 SECOR	---	DOD/DMA	3

[a] Applied Physics Laboratory.
[b] National Aeronautics and Space Administration.
[c] Department of Defense/Defense Mapping Agency.
[d] National Geodetic Survey.
[e] Smithsonian Astrophysical Observatory.

TABLE 8.3.—*Survey Information of Observation Stations*

STATION NO	STATION NAME	DATUM CODE[1]	SURVEY COORDINATES[2] LATITUDE	SURVEY COORDINATES[2] LONGITUDE	ELL. H(M)	MSL[3] (M)	INSTR. HEIGHT[4] (M)	INSTR. TYPE	SOURCE CODE
1021	BLOSSOM POINT	29	38° 25' 49.628	282° 54' 48.225	7.0	5.76	1.23	MOTS 40	1
1022	FORT MYERS	29	26 32 51.891	278 8 3.926	21.0	4.81	1.23	MOTS 40	1
1030	GOLDSTONE	29	35 19 48.088	243 6 2.730	907.0	929.10	1.71	MOTS 40	1
1032	ST. JOHN'S	29	47 44 29.739	307 16 43.369	106.0	69.00	1.95	MOTS 40	1
1033	FAIRBANKS	29	64 52 19.721	212 9 47.168	165.0	162.70	2.18	MOTS 40	2
1034	E. GRAND FORKS	29	48 1 21.403	262 59 21.561	256.0	252.58	1.71	MOTS 40	1
1042	ROSMAN	29	35 12 6.926	277 7 41.008	916.0	909.40	1.69	MOTS 40	1
3106	ANTIGUA	29	17 8 52.685	298 12 37.552	8.0	1.90	*	PC-1000	1
3334	STONEVILLE	29	33 25 31.950	269 5 11.350	44.0	39.00	*	PC-1000	1
3400	COLORADO SPRINGS	29	39 0 22.440	255 7 1.010	2191.0	2184.10	*	PC-1000	1
3401	BEDFORD	29	42 27 17.530	288 43 35.033	89.0	83.00	1.32	PC-1000	1
3402	SEMMES	29	30 46 49.350	271 44 52.370	80.0	73.00	*	PC-1000	1
3404	SWAN ISLAND	*	17 24 16.570	276 3 29.870	*	40.40	*	PC-1000	1
3405	GRAND TURK	29	21 25 46.796	288 51 13.786	8.0	2.20	*	PC-1000	1
3406	CURACAO	41	12 5 26.843	291 9 45.803	-4.0	6.83	1.25	PC-1000	1
3407	TRINIDAD	41	10 44 35.844	298 23 25.652	237.0	254.80	1.25	PC-1000	1
3413	NATAL	41	- 5 54 56.253	324 49 57.605	63.0	36.90	*	PC-1000	1
3414	BRASILIA	41	-15 51 35.540	312 6 2.679	1059.0	1058.25	1.14	PC-1000	2
3431	ASUNCION	41	-25 18 56.192	302 25 15.376	162.0	149.74	1.65	PC-1000	2
3476	PARAMARIBO	41	5 26 54.645	304 47 44.226	8.6	18.27	1.25	PC-1000	1
3477	BOGOTA	41	4 49 2.379	285 55 35.482	2586.0	2557.90	1.25	PC-1000	2
3478	MANAUS	*	- 3 8 44.820	300 0 59.620	*	83.60	*	PC-1000	3
3499	QUITO	41	- 0 5 50.468	281 34 49.212	2706.4	2681.80	*	PC-1000	1
3648	HUNTER AFB	29	32 0 5.868	278 50 46.359	17.0	12.00	1.32	PC-1000	1
3657	ABERDEEN	29	39 28 18.971	283 55 44.780	6.0	5.50	1.32	PC-1000	1
3861	HOMESTEAD	29	25 30 24.690	279 36 42.690	16.0	0.20	*	PC-1000	1
3902	CHEYENNE	29	41 7 59.200	255 8 2.650	1890.0	1882.20	*	PC-1000	
3903	HERNDON	29	38 59 32.360	282 40 21.200	169.0	168.00	*	PC-1000	1
4050	PRETORIA	3	-25 56 35.340	28 21 29.950	1592.0	1584.00	*	MPS-25	2
4061	ANTIGUA	29	17 8 34.780	298 12 24.470	48.0	42.30	*	FPQ-6	2
4081	GRAND TURK	29	21 27 43.490	288 52 3.050	42.0	36.00	*	TPQ-18	2
4082	MERRITT ISLAND	29	28 25 27.930	279 20 7.380	21.0	11.25	*	TPQ-18	2
4280	VANDENBERG AFB	29	34 39 57.130	239 25 10.430	89.0	123.00	*	TPQ-18	2
4740	BERMUDA	29	32 20 52.300	295 20 44.300	11.0	19.86	*	FPS-16	2
4742	KAUAI	33	22 7 35.830	200 19 53.960	1151.0	1155.00	*	FPS-16	2
5001	HERNDON	29	38 59 37.697	282 40 16.705	129.0	127.80	9.39	SECOR	1
5201	MOSES LAKE	29	47 11 5.916	240 39 50.463	358.0	368.92	2.00	SECOR	1
5410	SAND ISLAND	27	28 12 32.061	182 37 49.531	6.0	6.10	4.13	SECOR	2
5648	FORT STEWART	29	31 55 18.405	278 26 0.260	34.0	27.80	3.90	SECOR	1
5712	PARAMARIBO	41	5 26 59.817	304 47 44.990	12.0	21.50	4.93	SECOR	1
5713	TERCEIRA	17	38 45 36.725	332 54 21.064	56.0	56.00	4.25	SECOR	1
5715	DAKAR	50	14 44 41.008	342 30 52.935	27.0	27.30	4.42	SECOR	1
5717	FORT LAMY	1	12 7 49.300	15 2 6.148	320.0	298.50	4.83	SECOR	1
5720	ADDIS ABABA	1	8 46 9.479	38 59 49.196	1881.0	1889.40	4.29	SECOR	1
5721	MASHHAD	16	36 14 30.404	59 37 40.105	962.0	994.40	4.35	SECOR	1
5722	DIEGO GARCIA	*	- 7 20 57.440	72 28 31.570	*	6.10	4.60	SECOR	2
5723	CHIANG MAI	*	18 47	99 00	*	310.80		SECOR	1
5726	ZAMBOANGA	26	6 55 26.213	122 4 3.558	14.0	13.30	4.83	SECOR	2
5730	WAKE ISLAND	49	19 17 24.100	166 36 41.206	8.0	8.10	4.29	SECOR	1

TABLE 8.3.—*(Cont'd)*

STATION NO	STATION NAME	DATUM CODE[1]	SURVEY COORDINATES[2] LATITUDE	LONGITUDE	ELL. H(M)	MSL[3] (M)	INSTR. HEIGHT[4] (M)	INSTR. TYPE	SOURCE CODE
5732	PAGO PAGO	*	*	*	*	*	*	SECOR	
5733	CHRISTMAS ISLAND	12	2 0 35.622	202 35 21.962	4.0	3.50	2.29	SECOR	1
5734	SHEMYA	29	52 42 54.894	174 7 37.870	-7.0	39.30	1.50	SECOR	1
5735	NATAL	41	- 5 54 56.253	324 49 57.605	66.0	39.40	*	SECOR	1
5736	ASCENSION ISLAND	5	- 7 58 15.220	345 35 32.385	74.0	74.00	4.32	SECOR	1
5739	TERCEIRA	17	38 45 36.311	332 54 19.686	56.0	56.10	4.25	SECOR	1
5744	CATANIA	16	37 26 40.831	15 2 44.955	-4.0	11.80	4.17	SECOR	1
5907	WORTHINGTON	*	*	*	*	*	*	SECOR	
5911	BERMUDA	*	*	*	*	*	*	SECOR	
5912	PANAMA	*	*	*	*	*	*	SECOR	
5914	PUERTO RICO	*	*	*	*	*	*	SECOR	
5915	AUSTIN	*	*	*	*	*	*	SECOR	
5923	CYPRUS	*	*	*	*	*	*	SECOR	
5924	ROTA	*	*	*	*	*	*	SECOR	
5925	ROBERTS FIELD	*	*	*	*	*	*	SECOR	
5930	SINGAPORE	*	*	*	*	*	*	SECOR	
5931	HONG KONG	*	*	*	*	*	*	SECOR	
5933	DARWIN	*	*	*	*	*	*	SECOR	
5934	MANUS	*	*	*	*	*	*	SECOR	
5935	GUAM	*	*	*	*	*	*	SECOR	
5937	PALAU	*	*	*	*	*	*	SECOR	
5938	GUADALCANAL	*	*	*	*	*	*	SECOR	
5941	MAUI	*	*	*	*	*	*	SECOR	
6001	THULE	29	76 30 3.411	291 27 51.887	238.0	206.00	1.50	BC-4	2
6002	BELTSVILLE	29	39 1 39.003	283 10 26.942	45.0	44.30	1.50	BC-4	1
6003	MOSES LAKE	29	47 11 7.132	240 39 48.118	358.0	368.74	1.50	BC-4A	1
6004	SHEMYA	29	52 42 54.890	174 7 37.870	-9.0	36.80	1.50	BC-4	1
6006	TROMSO	16	69 39 44.270	18 56 31.908	119.0	106.00	1.50	BC-4	2
6007	TERCEIRA	17	38 45 36.725	332 54 21.064	53.0	53.30	1.49	BC-4	1
6008	PARAMARIBO	41	5 26 55.325	304 47 42.832	8.7	18.38	1.49	BC-4	1
6009	QUITO	41	- 0 5 50.468	281 34 49.212	2706.7	2682.10	1.50	BC-4	1
6011	MAUI	33	20 42 38.561	203 44 28.529	3041.3	3049.27	1.50	BC-4	4
6012	WAKE ISLAND I	49	19 17 23.227	166 36 39.780	4.0	3.50	1.50	BC-4	1
6013	KANOYA	46	31 23 30.140	130 52 24.860	47.0	65.90	1.50	BC-4	1
6015	MASHHAD	16	36 14 29.527	59 37 42.729	959.0	991.00	1.50	BC-4	1
6016	CATANIA	16	37 26 42.628	15 2 47.308	-7.0	9.24	1.50	BC-4A	1
6019	VILLA DOLORES	41	-31 56 33.954	294 53 41.342	621.0	608.18	1.50	BC-4	2
6020	EASTER ISLAND	15	-27 10 39.213	250 34 17.495	231.0	230.80	1.50	BC-4	1
6022	TUTUILA	2	-14 20 12.216	189 17 13.242	5.0	5.34	1.50	BC-4A	1
6023	THURSDAY ISLAND	6	-10 35 8.037	142 12 35.495	62.0	60.50	1.50	BC-4	2
6031	INVERCARGILL	28	-46 25 3.491	168 19 31.155	1.0	0.90	1.49	BC-4	1
6032	CAVERSHAM	6	-31 50 28.992	115 58 26.618	33.0	26.30	*	BC-4	2
6038	SOCORRO ISLAND	23	18 43 44.930	249 2 39.280	23.0	23.20	1.50	BC-4	1
6039	PITCAIRN ISLAND	36	-25 4 7.146	229 53 11.882	339.0	339.40	1.50	BC-4	1
6040	COCOS ISLAND	*	-12 11 57.910	96 49 47.080	*	4.40	*	BC-4	2
6042	ADDIS ABABA	1	8 46 8.501	38 59 49.164	1878.0	1886.46	1.52	BC-4	1
6043	CERRO SOMBRERO	39	-52 46 52.468	290 46 29.573	81.0	80.70	1.48	BC-4A	1
6044	HEARD ISLAND	20	-53 1 12.030	73 23 27.420	4.0	3.80	1.50	BC-4	1
6045	MAURITIUS	*	-20 13 50	57 25 15	*	149.40	*	BC-4	1

TABLE 8.3.—*(Cont'd)*

STATION NO	STATION NAME	DATUM CODE[1]	SURVEY COORDINATES[2] LATITUDE			LONGITUDE			ELL. H(M)	MSL[3] (M)	INSTR. HEIGHT[4] (M)	INSTR. TYPE	SOURCE CODE
6047	ZAMBOANGA	26	6	55	26.132	122	4	4.838	9.0	9.39	1.50	BC-4	2
6050	PALMER STATION	51	-64	46	33.980	295	56	37.040	16.0	16.44	1.58	BC-4	2
6051	MAWSON STATION	*	-67	36	3.080	62	52	24.410	*	11.30	*	BC-4	2
6052	WILKES STATION	*	-66	16	45.120	110	32	4.610	*	*	1.50	BC-4	2
6053	MCMURDO STATION	10	-77	50	46.249	166	38	7.584	19.0	19.00	1.50	BC-4	1
6055	ASCENSION ISLAND	5	- 7	58	16.634	345	35	32.764	71.0	70.94	1.50	BC-4	1
6059	CHRISTMAS ISLAND	12	2	0	35.622	202	35	21.962	3.0	2.75	1.50	BC-4A	1
6060	CULGOORA	6	-30	18	39.418	149	33	36.892	212.0	211.08	*	BC-4	2
6061	SOUTH GEORGIA IS.	43	-54	16	39.515	323	30	42.531	4.0	4.20	1.49	BC-4A	1
6063	DAKAR	50	14	44	44.228	342	30	55.594	26.0	26.30	1.50	BC-4A	1
6064	FORT LAMY	1	12	7	51.750	15	2	6.151	316.0	295.40	1.50	BC-4A	1
6065	HOHENPEISSENBERG	16	47	48	7.011	11	1	29.378	943.0	943.20	*	BC-4A	1
6066	WAKE ISLAND II	49	19	17	24.100	166	36	41.206	5.0	5.30	1.51	BC-4	1
6067	NATAL	41	- 5	55	37.414	324	50	6.200	66.7	40.63	*	BC-4A	1
6068	JOHANNESBURG	3	-25	52	56.980	27	42	25.170	1531.8	1523.80	*	BC-4	4
6069	TRISTAN DA CUNHA	47	-37	3	26.257	347	40	53.555	25.0	24.80	*	BC-4	1
6072	CHIANG MAI	*	18	46	10	98	58	15	*	319.20	*	BC-4	1
6073	DIEGO GARCIA	*	- 7	20	58.527	72	28	32.156	*	3.90	1.50	BC-4	2
6075	MAHE	42	- 4	40	7.230	55	28	50.380	589.0	588.98	1.55	BC-4A	1
6078	PORT VILA	52	-17	41	46.956	168	17	57.921	15.0	15.20	1.50	BC-4	2
6111	WRIGHTWOOD I	29	34	22	54.537	242	19	9.484	2259.0	2284.30	1.50	BC-4	2
6123	POINT BARROW	29	71	18	49.882	203	21	20.720	-6.0	8.30	*	BC-4	2
6134	WRIGHTWOOD II	29	34	22	44.444	242	19	9.259	2173.0	2198.40	1.50	BC-4	2
7036	EDINBURG	29	26	22	45.443	261	40	9.033	66.0	59.59	1.11	MOTS 40	1
7037	COLUMBIA	29	38	53	36.068	267	47	42.120	273.0	272.68	1.11	MOTS 40	1
7039	BERMUDA	29	32	21	48.790	295	20	32.460	23.0	31.18	1.13	MOTS 40	1
7040	SAN JUAN	29	18	15	26.216	294	0	22.174	59.0	49.70	1.07	MOTS 40	1
7043	GREENBELT	29	39	1	15.014	283	10	19.934	55.0	53.46	0.64	PTH-100	1
7045	DENVER	29	39	38	48.026	255	23	41.194	1796.0	1789.63	1.11	MOTS 40	1
7072	JUPITER	29	27	1	13.168	279	53	12.485	26.0	14.19	1.10	MOTS 40	1
7075	SUDBURY	29	46	27	20.988	279	3	10.354	281.0	281.90	1.17	MOTS 40	1
7076	KINGSTON	29	18	4	31.980	283	11	26.528	486.0	445.90	1.07	MOTS 40	1
8009	WIPPOLDER	16	52	0	9.240	4	22	21.230	21.0	24.70	*	BOUWERS	2
8010	ZIMMERWALD	16	46	52	40.300	7	27	58.070	900.0	903.44	*	SCHM H	1
8011	MALVERN	16	52	8	39.130	358	1	59.470	109.0	113.20	*	SCHM A	1
8015	HAUTE PROVENCE	16	43	56	1.140	5	42	49.280	651.0	659.00	*	SCHM D	2
8019	NICE	16	43	43	36.496	7	18	3.309	369.0	377.42	*	ANTARES	1
8030	MEUDON	16	48	48	25.354	2	13	51.339	155.0	165.46	*	REFR A	1
9001	ORGAN PASS	29	32	25	24.560	253	26	51.170	1650.0	1651.33	*	B-N	1
9002	OLIFANTSFONTEIN	3	-25	57	33.850	28	14	53.910	1552.1	1544.10	*	B-N	4
9004	SAN FERNANDO	16	36	27	51.370	353	47	42.090	-9.0	25.90	*	B-N	1
9005	TOKYO	46	35	40	11.078	139	32	28.222	60.0	59.77	*	B-N	1
9006	NAINI TAL	16	29	21	38.970	79	27	25.510	1827.0	1927.00	*	B-N	1
9007	AREQUIPA	41	-16	27	55.085	288	30	26.814	2486.0	2451.86	*	B-N	1
9008	SHIRAZ	16	29	38	18.112	52	31	11.445	1553.0	1597.40	*	B-N	2
9009	CURACAO	41	12	5	25.912	291	9	46.078	-2.0	8.70	*	B-N	1
9010	JUPITER	29	27	1	12.882	279	53	13.008	27.0	15.13	*	B-N	1
9011	VILLA DOLORES	41	-31	56	33.228	294	53	38.949	621.0	608.00	*	B-N	4
9012	MAUI	33	20	42	37.500	203	44	24.080	3026.1	3034.14	*	B-N	4

TABLE 8.3.—*(Cont'd)*

STATION NO	STATION NAME	DATUM CODE[1]	SURVEY COORDINATES[2] LATITUDE			LONGITUDE			ELL. H(M)	MSL[3] (M)	INSTR. HEIGHT[4] (M)	INSTR. TYPE	SOURCE CODE
9021	MOUNT HOPKINS	29	31	41	2.670	249	7	21.350	2371.0	2382.00	*	B-N	1
9028	ADDIS ABABA	1	8	44	47.230	38	57	30.480	1895.0	1925.20	*	B-N	2
9029	NATAL	41	- 5	55	38.616	324	50	8.660	71.4	45.34	*	B-N	4
9031	COMODORO RIVADAVIA	41	-45	53	11.028	292	23	12.215	173.0	186.54	*	B-N	1
9051	ATHENS	16	37	58	40.310	23	46	42.890	180.0	187.90	*	GEO 36	1
9091	DIONYSOS	16	38	4	48.240	23	56	1.610	459.0	467.00	*	B-N	1
9424	COLD LAKE	29	54	44	33.858	249	57	26.389	702.0	704.60	*	B-N	1
9425	EDWARDS AFB	29	34	57	50.742	242	5	11.584	760.0	784.23	*	B-N	1
9426	HARESTUA	16	60	12	40.380	10	45	8.740	582.0	575.92	*	B-N	1
9427	JOHNSTON ISLAND	24	16	44	45.390	190	29	5.590	5.0	5.00	*	B-N	1
9431	RIGA	16	56	56	54.980	24	3	37.810	2.0	8.00	*	AFU 75	1
9432	UZHGOROD	*	48	38	4.560	22	17	57.880	*	189.00	*	AFU 75	1
DSN1	GOLDSTONE	29	35	23	22.346	243	9	5.262	1014.3	1036.30	11.80	85° H-D	4
DSN2	GOLDSTONE	29	35	17	59.854	243	11	43.414	966.9	988.90	11.70	85° H-D	4
DSN4	GOLDSTONE	29	35	25	33.340	243	6	40.850	1009.8	1031.80	15.50	210°A-E	4
DSN6	TIDBINBILLA	6	-35	24	8.038	148	58	48.206	664.5	656.08	15.08	85° H-D	4
DSN7	JOHANNESBURG	3	-25	53	21.150	27	41	8.530	1399.0	1391.00	13.00	85° H-D	4

* INSUFFICIENT DATA

1 REFER TO TABLE 8.4

2 GEODETIC COORDINATES OF THE INSTRUMENTAL REFERENCE POINT (OPTICAL/ELECTRONIC CENTER,ETC.) ON THE LOCAL GEODETIC DATUM

3 MEAN SEA LEVEL HEIGHT OF THE INSTRUMENTAL REFERENCE POINT

4 HEIGHT OF INSTRUMENTAL REFERENCE POINT ABOVE SURVEY MONUMENT

NOTE : ZERO IN THE LAST DIGIT MAY INDICATE THAT THE DIGIT IS UNKNOWN.

TABLE 8.4.—*Geodetic Datums*

Code	Datum	Ellipsoid	Origin	Latitude	Longitude
1	Adindan (Ethiopia)	Clarke 1880	STATION Z5 ADINDAN	22°10′07″.110	31°29′21″.608
2	American Samoa 1962	Clarke 1866	BETTY 13 ECC	−14°20′08″.341	189°17′07″.750
3	Arc-Cape (South Africa)	Clarke 1880	Buffelsfontein	−33°59′32″.000	25°30′44″.622
4	Argentine	International	Campo Inchauspe	−35°58′17″	297°49′48″
5	Ascension Island 1958	International	Mean of three stations	−07°57′	345°37′
6	Australian Geodetic	Australian National	Johnston Memorial Cairn	−25°56′54″.55	133°12′30″.08
7	Bermuda 1957	Clarke 1866	FT. GEORGE B 1937	32°22′44″.360	295°19′01″.890
8	Berne 1898	Bessel	Berne Observatory	46°57′08″.660	07°26′22″.335
9	Betio Island, 1966	International	1966 SECOR ASTRO	01°21′42″.03	172°55′47″.90
10	Camp Area Astro 1961–62 USGS	International	CAMP AREA ASTRO	−77°50′52″.521	166°40′13″.753
11	Canton Astro 1966	International	1966 CANTON SECOR ASTRO	−02°46′28″.99	188°16′43″.47
12	Christmas Island Astro 1967	International	SAT.TRI.STA. 059 RM3	02°00′35″.91	202°35′21″.82
13	Chua Astro (Brazil-Geodetic)	International	CHUA	−19°45′41″.16	311°53′52″.44
x4	Corrego Alegre (Brazil-Mapping)	International	CORREGO ALEGRE	−19°50′15″.140	311°02′17″.250
15	Easter Island 1967 Astro	International	SATRIG RM No. 1	−27°10′39″.95	250°34′16″.81
16	European	International	Helmert Tower	52°22′51″.45	13°03′58″.74
17	Graciosa Island (Azores)	International	SW BASE	39°03′54″.934	331°57′36″.118
18	Gizo, Provisional DOS	International	GUX 1	−09°27′05″.272	159°58′31″.752
19	Guam	Clarke 1866	TOGCHA LEE NO. 7	13°22′38″.49	144°45′51″.56
20	Heard Astro 1969	International	INTSATRIG 0044 ASTRO	−53°01′11″.68	73°23′22″.64
21	Iben Astro, Navy 1947 (Truk)	Clarke 1866	IBEN ASTRO	07°29′13″.05	151°49′44″.42
22	Indian	Everest	Kalianpur	24°07′11″.26	77°39′17″.57
23	Isla Socorro Astro	Clarke 1866	Station 038	18°43′44″.93	249°02′39″.28
24	Johnston Island 1961	International	JOHNSTON ISLAND 1961	16°44′49″.729	190°29′04″.781
25	Kusaie, Astro 1962, 1965	International	ALLEN SODANO LIGHT	05°21′48″.80	162°58′03″.28
26	Luzon 1911 (Philippines)	Clarke 1866	BALANCAN	13°33′41″.000	121°52′03″.000
27	Midway Astro 1961	International	MIDWAY ASTRO 1961	28°11′34″.50	182°36′24″.28
28	New Zealand 1949	International	PAPATAHI	−41°19′08″.900	175°02′51″.000

TABLE 8.4.—*(Cont'd)*

Code	Datum	Ellipsoid	Origin	Latitude	Longitude
29	North American 1927	Clarke 1866	MEADES RANCH	39°13′26″.686	261°27′29″.494
30	NAD 1927 (Cape Canaveral)[a]	Clarke 1866	CENTRAL	28°29′32″.364	279°25′21″.230
31	NAD 1927 (White Sands)[a]	Clarke 1866	KENT 1909	32°30′27″.079	253°31′01″.306
32	Old Bavarian	Bessel	Munich	48°08′20″.000	11°34′26″.483
33	Old Hawaiian	Clarke 1866	OAHU WEST BASE	21°18′13″.89	202°09′04″.20
34	Ordnance Survey G.B. 1936	Airy	Herstmonceux	50°51′55″.271	00°20′45″.882
35	Pico de las Nieves (Canaries)	International	PICO DE LAS NIEVES	27°57′41″.273	344°25′49″.476
36	Pitcairn Island Astro	International	PITCAIRN ASTRO 1967	−25°04′06″.97	229°53′12″.17
37	Potsdam	Bessel	Helmert Tower	52°22′53″.954	13°04′01″.153
38	Provisional S. American 1956	International	LA CANOA	08°34′17″.17	296°08′25″.12
39	Provisional S. Chile 1963	International	HITO XVIII	−53°57′07″.76	291°23′28″.76
40	Pulkovo 1942	Krassovski	Pulkovo Observatory	59°46′18″.55	30°19′42″.09
41	South American 1969	South American 1969	CHUA	−19°45′41″.653	311°53′55″.936
42	Southeast Island (Mahe)	Clarke 1880		−04°40′39″.460	55°32′00″.166
43	South Georgia Astro	International	ISTS 061 ASTRO POINT 1968	−54°16′38″.93	323°30′43″.97
44	Swallow Islands (Solomons)	International	1966 SECOR ASTRO	−10°18′21″.42	166°17′56″.79
45	Tananarive	International	Tananarive Observatory	−18°55′02″.10	47°33′06″.75
46	Tokyo	Bessel	Tokyo Observatory (old)	35°39′17″.51	139°44′40″.50
47	Tristan Astro 1968	International	INTSATRIG 069 RM No. 2	−37°03′26″.79	347°40′53″.21
48	Viti Levu 1916 (Fiji)	Clarke 1880	MONAVATU (latitude only) SUVA (longitude only)	−17°53′28″.285	178°25′35″.835
49	Wake Island, Astronomic 1952	International	ASTRO 1952	19°17′19″.991	166°38′46″.294
50	Yof Astro 1967 (Dakar)	Clarke 1880	YOF ASTRO 1967	14°44′41″.62	342°30′52″.98
51	Palmer Astro 1969	International	ISTS 050	64°46′35″.71	295°56′39″.53
52	Eftate	International	Belle Vue IGN	−17°44′17″.400	168°20′33″.250

[a] Local datums of special purpose, based on NAD 1927 values for the origin stations.

TABLE 8.5—*Basic Information on the OSU Solutions (Networks)*

OSU solution (network)	No. of stations	No. of observations	Number of constraints used						σ_0 (f)	Reference (g)	Figure
			Origin	Relative position	Scale (length)	Station position	Height	Directional			
MPS[a]	66	28 774	Inner	9	7	----	63	----	1.07	188	8.1,2,3
BC[b]	49	30 302	Inner	2	7	----	48	----	2.80	193	8.4
SECOR[c]	50	28 844	Inner	14	----	----	37	9	1.37	195	8.5
SA[d]	14	2 524	Inner	3	1	----	14	----	2.50	196	8.6
WN[e]	158	90 444	Inner	43	11	----	158	----	1.02	199	8.7

[a] MPS includes 14 PC–1000 stations, 15 MOTS–40 stations, 1 PTH–100 station, 7 C-band stations, 6 European stations (8000 series), and 23 SAO stations (9000 series).
[b] BC includes all 49 stations of BC–4 Worldwide Geometric Satellite Network.
[c] SECOR includes 37 SECOR stations of the Equatorial Network and 13 collocated BC–4 camera stations.
[d] SA includes 9 PC–1000 stations of South American Densification Net and 5 BC–4 stations.
[e] WN includes all the above-mentioned four networks, namely, MPS (less one C-band station: 4742), BC, SECOR, and SA.
[f] A posteriori standard deviation of unit weight.
[g] OSU Department of Geodetic Science Report Number.

TABLE 8.6.—*Summary of Observation Types*

Instrument	NASA series no.	Satellite observed	OSU network where used	Data source
MOTS	1000	GEOS–1	MPS	NSSDC[a]
PC–1000	3000	GEOS–1	MPS	NSSDC
PC–1000 So. America	3000	ECHO 1, 2 PAGEOS GEOS–2	SA	DMA/Aerospace Center[b]
C-band radar	4000	GEOS–2	MPS	NASA/Wallops Flight Center
SECOR	5000	SECOR (EGRS)	SECOR	DMA/Topographic Center
BC–4	6000	PAGEOS	BC, SA	NGS[c], NSSDC
Special optical	7000	GEOS–1	MPS	NSSDC
International optical	8000	GEOS–1, 2 PAGEOS ECHO 1, 2	MPS	SAO[d]
Smithsonian optical	9000	ANNA 1B Courier 1B Dash 2 ECHO 1 rocket Elektron 3 Explorer 9, 19 MIDAS 4, 7 RCS, Relay 1 Telstar 1	MPS	SAO

[a] National Space Science Data Center.
[b] Defense Mapping Agency.
[c] National Geodetic Survey.
[d] Smithsonian Astrophysical Observatory.

TABLE 8.7a.—*Summary of Simultaneous Observations by Line (MPS Network)*

Line station-station	No. of pairs	Line station-station	No. of pairs
1021–1022	47	1030–1042	34
1021–1030	11	1030–3401	4
1021–1032	4	1030–3402	22
1021–1034	35	1030–3404	4
1021–1042	39	1030–3657	6
1021–3106	6	1030–3861	12
1021–3401	25	1030–3903	6
1021–3402	17	1030–7036	94
1021–3405	22	1030–7037	75
1021–3406	13	1030–7043	20
1021–3407	6	1030–7045	98
1021–3648	5	1030–7072	10
1021–3657	36	1030–7075	35
1021–3861	13	1032–1042	3
1021–7036	24	1032–3401	3
1021–7037	41	1032–7043	6
1021–7039	6	1032–7072	1
1021–7040	29	1033–1034	13
1021–7043	59	1033–7045	9
1021–7045	11	1033–9425	10
1021–7072	10	1034–1042	117
1021–7075	31	1034–3334	4
1021–9001	14	1034–3400	6
1021–9010	24	1034–3401	33
1022–1030	60	1034–3402	24
1022–1034	78	1034–3404	4
1022–1042	127	1034–3648	5
1022–3106	31	1034–3657	15
1022–3400	5	1034–3861	27
1022–3401	81	1034–3902	5
1022–3402	62	1034–3903	6
1022–3404	53	1034–7036	51
1022–3405	24	1034–7037	163
1022–3406	54	1034–7039	12
1022–3407	4	1034–7040	4
1022–3648	28	1034–7043	24
1022–3657	50	1034–7045	84
1022–3861	114	1034–7072	14
1022–3903	6	1034–7075	36
1022–7036	109	1034–7076	6
1022–7037	91	1034–9001	51
1022–7039	52	1034–9010	49
1022–7040	90	1034–9424	20
1022–7043	88	1034–9425	63
1022–7045	43	1042–3106	12
1022–7072	221	1042–3400	8
1022–7075	31	1042–3401	26
1022–7076	44	1042–3402	46
1030–1033	10	1042–3404	16
1030–1034	97	1042–3406	15

TABLE 8.7a.—*(Cont'd)*

Line station-station	No. of pairs	Line station-station	No. of pairs
1042–3648	5	3401–7039	11
1042–3657	7	3401–7040	16
1042–3861	15	3401–7043	39
1042–3903	6	3401–7072	39
1042–7036	19	3401–7076	22
1042–7037	86	3402–3405	6
1042–7040	22	3402–3406	6
1042–7043	51	3402–3648	6
1042–7045	35	3402–3657	23
1042–7072	34	3402–3861	42
1042–7075	53	3402–3902	4
1042–7076	5	3402–7036	23
1042–9001	13	3402–7037	22
1042–9009	7	3402–7039	10
1042–9010	20	3402–7040	6
1042–9424	7	3402–7043	20
1042–9425	19	3402–7072	13
3106–3401	14	3402–7076	8
3106–3402	10	3404–3401	14
3106–3404	13	3404–3402	17
3106–3405	7	3404–3405	4
3106–3406	41	3404–3406	7
3106–3407	23	3404–3407	5
3106–3648	18	3404–3648	12
3106–3657	4	3404–3657	7
3106–3861	10	3404–3861	29
3106–7039	16	3404–7037	9
3106–7040	64	3404–7039	6
3106–7043	10	3404–7040	28
3106–7072	20	3404–7043	7
3106–7076	5	3404–7072	3
3334–3400	4	3404–7076	4
3334–3402	7	3405–3406	7
3334–3404	4	3405–3407	12
3334–7036	12	3405–3657	12
3334–7037	2	3405–3861	6
3334–7045	4	3405–7036	9
3400–3902	6	3405–7037	6
3400–7036	13	3405–7039	5
3400–7037	3	3405–7040	19
3400–7045	13	3405–7043	13
3401–3402	17	3405–7072	6
3401–3406	9	3406–3407	19
3401–3407	7	3406–3861	23
3401–3648	9	3406–3903	5
3401–3657	25	3406–7036	11
3401–3861	37	3406–7037	5
3401–3903	4	3406–7039	21
3401–7036	10	3406–7040	31
3401–7037	12	3406–7043	3

TABLE 8.7a.—*(Cont'd)*

Line station-station	No. of pairs	Line station-station	No. of pairs
3406–7072	25	7037–7072	24
3406–7076	19	7037–7075	48
3407–3657	6	7037–7076	29
3407–3861	14	7037–9001	27
3407–7039	4	7037–9009	6
3407–7040	31	7037–9010	57
3407–7043	7	7037–9425	38
3648–3657	10	7039–7040	10
3648–3861	28	7039–7072	5
3648–7036	6	7039–7075	21
3648–7037	20	7039–7076	17
3648–7039	6	7039–9010	18
3648–7040	7	7040–7043	18
3648–7072	16	7040–7072	9
3657–3861	24	7040–7075	7
3657–7036	19	7040–7076	10
3657–7037	15	7040–9009	7
3657–7039	4	7040–9010	22
3657–7040	6	7043–7045	33
3657–7043	31	7043–7072	24
3657–7045	6	7043–7076	6
3657–7072	28	7045–7072	9
3861–7036	33	7045–7075	11
3861–7037	34	7045–7076	4
3861–7039	5	7045–9001	6
3861–7040	8	7045–9010	11
3861–7043	8	7045–9024	11
3861–7072	73	7045–9025	54
3861–7076	13	7072–7076	29
3902–7036	12	7075–7076	7
3902–7037	12	7075–9010	22
3902–7045	6	7076–9010	21
3903–7037	6	8009–8010	4
3903–7043	6	8009–8011	10
3903–7045	6	8009–8015	10
7036–7037	124	8009–8019	11
7036–7039	14	8009–9431	8
7036–7043	6	8009–9432	4
7036–7045	56	8010–8015	58
7036–7072	44	8010–8019	48
7036–7075	31	8010–9004	74
7036–7076	43	8010–9051	6
7036–9001	66	8010–9431	27
7036–9009	6	8010–9432	11
7036–9010	49	8011–8030	7
7036–9425	17	8011–9004	4
7037–7039	27	8011–9008	5
7037–7040	5	8011–9426	1
7037–7043	33	8011–9431	7
7037–7045	63	8015–8019	112

TABLE 8.7a.—*(Cont'd)*

Line station-station	No. of pairs	Line station-station	No. of pairs
8015–9004	68	9005–9427	3
8015–9051	39	9006–9008	181
8015–9091	16	9006–9028	30
8015–9431	16	9006–9426	19
8015–9432	48	9007–9009	276
8019–8030	7	9007–9010	92
8019–9004	349	9007–9011	467
8019–9091	83	9007–9029	5
8019–9431	44	9007–9031	36
8019–9432	13	9008–9028	11
8030–9004	7	9008–9051	16
9001–9007	35	9008–9426	45
9001–9009	189	9009–9010	117
9001–9010	288	9009–9011	76
9001–9012	205	9009–9424	7
9001–9424	74	9010–9012	3
9001–9427	17	9010–9424	12
9002–9008	7	9011–9029	4
9002–9028	30	9011–9031	9
9004–9006	14	9012–9021	32
9004–9008	146	9012–9424	26
9004–9009	44	9012–9427	247
9004–9010	43	9021–9425	61
9004–9028	44	9028–9091	49
9004–9029	48	9029–9031	32
9004–9051	40	9091–9431	17
9004–9091	381	9091–9432	23
9004–9424	1	9424–9425	56
9004–9426	89	9424–9426	5
9004–9431	74	9424–9427	2
9005–9006	63	9425–9427	15
9005–9008	3	9431–9432	21
9005–9012	3		

TABLE 8.7b.—*Summary of Simultaneous Observations by Line (BC Network)*

Line station-station	No. of pairs	Line station-station	No. of pairs
6001–6002	105	6011–6012	71
6001–6003	121	6011–6022	12
6001–6004	37	6011–6038	67
6001–6006	103	6011–6059	114
6001–6007	33	6011–6111	32
6001–6011	7	6011–6134	64
6001–6015	7	6012–6013	60
6001–6016	18	6012–6022	41
6001–6038	7	6012–6023	57
6001–6065	60	6012–6059	57
6001–6123	43	6012–6060	7
6002–6003	156	6013–6015	14
6002–6006	7	6013–6040	8
6002–6007	57	6013–6047	87
6002–6008	93	6013–6072	57
6002–6009	39	6013–6078	4
6002–6038	71	6015–6016	170
6002–6111	79	6015–6040	41
6002–6134	21	6015–6042	99
6003–6004	52	6015–6045	58
6003–6011	84	6015–6064	65
6003–6012	11	6015–6065	80
6003–6038	96	6015–6072	75
6003–6111	89	6015–6073	77
6003–6123	24	6015–6075	44
6003–6134	32	6016–6042	23
6004–6006	4	6016–6063	61
6004–6011	7	6016–6064	113
6004–6012	53	6016–6065	108
6004–6013	60	6019–6020	35
6004–6123	24	6019–6043	132
6006–6007	30	6019–6061	77
6006–6015	87	6019–6067	70
6006–6016	94	6019–6069	8
6006–6065	76	6020–6038	60
6007–6016	125	6020–6039	18
6007–6055	14	6020–6043	52
6007–6063	111	6022–6023	15
6007–6064	25	6022–6031	44
6007–6065	40	6022–6039	14
6007–6067	28	6022–6059	103
6008–6009	53	6022–6060	33
6008–6019	87	6022–6078	21
6008–6061	4	6023–6031	51
6008–6063	4	6023–6032	116
6008–6067	29	6023–6040	14
6009–6019	69	6023–6047	50
6009–6020	22	6023–6060	224
6009–6038	67	6023–6066	29
6009–6043	25	6023–6072	28

TABLE 8.7b.—*(Cont'd)*

Line station-station	No. of pairs	Line station-station	No. of pairs
6023–6078	28	6045–6051	42
6031–6032	102	6045–6068	112
6031–6039	15	6045–6073	99
6031–6051	7	6045–6075	90
6031–6052	57	6047–6060	8
6031–6053	101	6047–6072	88
6031–6059	4	6047–6078	4
6031–6060	305	6050–6051	7
6031–6078	28	6050–6052	14
6032–6040	72	6050–6053	25
6032–6044	36	6050–6061	63
6032–6045	18	6051–6052	100
6032–6047	54	6051–6053	103
6032–6051	12	6051–6061	35
6032–6052	34	6051–6068	106
6032–6053	8	6052–6053	98
6032–6060	174	6052–6060	47
6032–6072	7	6053–6060	35
6038–6039	55	6053–6061	7
6038–6059	35	6055–6061	14
6038–6134	71	6055–6063	101
6039–6059	49	6055–6064	99
6040–6044	4	6055–6067	86
6040–6045	96	6055–6068	11
6040–6047	36	6055–6069	47
6040–6060	19	6061–6067	18
6040–6072	16	6061–6068	18
6040–6073	52	6061–6069	29
6040–6075	53	6063–6064	84
6042–6045	93	6063–6065	7
6042–6064	96	6063–6067	62
6042–6068	93	6063–6069	14
6042–6073	22	6064–6068	106
6042–6075	75	6067–6069	4
6043–6050	74	6068–6069	21
6043–6061	88	6068–6075	14
6044–6045	11	6072–6073	15
6044–6051	33	6072–6075	14
6044–6052	7	6073–6075	80
6044–6068	4		

TABLE 8.7c.—*Summary of Simultaneous Observations by Line (SA Network)*

Line station-station	No. of pairs	Line station-station	No. of pairs
6002–6008	23	6019–3476	19
6002–3406	14	6019–3477	6
6002–3407	11	6067–3407	3
6002–3476	7	3406–3407	9
6002–3477	7	3406–3413	25
6008–6009	10	3406–3414	41
6008–6019	36	3406–3431	53
6008–6067	14	3406–3476	20
6008–3406	26	3406–3477	13
6008–3477	3	3406–3478	14
6008–3478	6	3406–3499	4
6009–6019	7	3407–3431	16
6009–3406	14	3407–3476	19
6009–3407	6	3407–3477	23
6009–3476	6	3407–3478	9
6009–3477	5	3413–3414	29
6009–3499	9	3413–3431	2
6019–6067	35	3414–3431	22
6019–3406	19	3476–3477	15
6019–3407	38	3477–3478	2
6019–3431	4	3477–3499	5

TABLE 8.7d.—*Summary of SECOR Observations by Quadrangle*

Quad stations involved	No. of observations	Quad stations involved	No. of observations
5001–5907–5648–5911	432	5721–5720–5722–5723	296
5911–5001–5648–5914	168	5923–5721–5722–5723	36
5911–5907–5915–5912	1008	5723–5721–5722–5930	460
5911–5915–5912–5712	92	5723–5722–5930–5931	588
5911–5907–5912–5712	260	5722–5723–5930–5726	68
5911–5915–5912–5712	228	5931–5723–5930–5726	768
5911–5912–5712–5713	684	5931–5930–5726–5933	1064
5713–5911–5712–5715	1220	5723–5930–5726–5933	652
5715–5713–5712–5735	548	5726–5930–5933–5934	644
5715–5739–5712–5735	288	5726–5933–5934–5935	808
5715–5712–5735–5736	660	5931–5726–5934–5935	1144
5715–5735–5736–5717	640	5935–5726–5934–5730	2048
5715–5736–5717–5744	28	5935–5726–5934–5937	1264
5739–5715–5717–5744	384	5730–5935–5934–5938	2216
5715–5736–5717–5744	464	5730–5935–5938–5732	1380
5744–5715–5717–5923	868	5730–5938–5732–5733	756
5744–5715–5717–5924	804	5730–5732–5733–5411	752
5744–5715–5717–5925	612	5730–5733–5411–5410	648
5923–5744–5717–5720	1236	5730–5733–5411–5734	508
5923–5717–5720–5721	772	5734–5410–5411–5201	312
5744–5717–5720–5721	20	5734–5730–5411–5201	264
5721–5923–5720–5722	752		

TABLE 8.8.—*Summary of Constraint Types With the Source Information*

Code	Constraint type	Source (agency)[a]
	Relative position	
1 -----	BC–4—Baker-Nunn	SAO, NGS
2 -----	BC–4—SECOR	DMA/TC
3 -----	BC–4—BC–4	NGS
4 -----	Others	OSU
	Height	
5 -----	MSL (mean sea level heights)	CSC, NGS, NWL
6 -----	Geoidal undulations	OSU (Rapp, 1973)
	Length (chord)	
7 -----	North America	NGS
8 -----	Europe	NGS, DGFI
9 -----	Africa	NGS
10 -----	Australia	NGS, DNP
11 -----	C-band	NASA/WFC

[a] CSC Computer Sciences Corporation
DGFI Deutsche Geodätisches Forschungs Institut
DMA/TC Defense Mapping Agency/Topographic Center
DNP Division of National Mapping, Department of National Development, Australia
NGS National Geodetic Survey
NWL Naval Weapons Laboratory
SAO Smithsonian Astrophysical Observatory
WFC Wallops Flight Center

TABLE 8.9.—*Relative Position Constraints*

STATIONS	RELATIVE COORDINATES (METERS)			WEIGHTS[1]	SOURCE
	Δu	Δv	Δw	($1/\sigma^2$)	CODE[2]
1033-6123	-417481.74	-633256.41	-267774.54	0.01	4
3106-4061	245.98	359.44	514.15	0.75	4
3405-4081	-928.41	-1670.35	-3352.87	0.75	4
3406-9009	-10.62	4.41	27.55	3.00	4
3413-6067	-48.64	-289.13	1258.05	3.00	4
3476-6008	36.31	22.94	-20.80	3.00	4
3499-6009	0.0	0.0	0.0	100.00	4
3648-5648	37875.28	10510.31	7502.84	3.00	4
4050-9002	-4500.31	10094.67	1601.88	0.75	4
4082-9010	-65710.25	62288.48	137731.57	0.28	4
4280-9425	-221861.49	103220.84	-27546.08	0.12	4
4740-7039	674.06	-699.92	-1476.31	0.75	4
4742-9012	-77910.13	349731.80	145328.72	0.05	4
5201-6003	29.55	-48.21	-25.52	1.00	2
5712-6008	48.95	45.97	137.68	1.00	2
5713-5739	8.05	33.26	9.95	20.00	2
5713-6007	2.08	-1.06	1.88	1.00	2
5715-6063	1.05	-83.72	-95.45	1.00	2
5720-6042	-1.87	-0.26	30.16	1.00	2
5720-9028	-2977.60	3046.18	2495.80	1.00	4
5721-6015	49.67	-44.84	23.59	1.00	2
5726-6047	30.82	24.81	3.07	1.00	2
5730-6012	-4.69	-41.68	26.66	1.00	2
5733-6059	-0.92	-0.38	0.04	1.00	2
5734-6004	-1.20	0.12	1.59	1.00	2
5735-6067	-46.20	-290.84	1257.74	1.00	2
5736-6055	5.82	-13.48	42.60	1.00	2
5744-6016	49.84	-46.49	-42.16	1.00	2
6002-7043	56.22	499.51	568.41	3.00	4
6011-9012	49.30	-118.74	35.91	3.00	4
6012-6066	1.93	42.34	-25.67	100.00	3
6013-9005	380844.93	754432.31	-395410.11	0.01	4
6019-9011	52.02	37.19	-18.98	3.00	1
6042-9028	-2975.73	3046.44	2465.64	3.00	1
6067-9029	-44.28	-61.36	37.21	3.00	1
6068-9002	28721.97	-46167.30	7673.52	2.50	1
6111-6134	53.73	90.04	305.32	100.00	3
6111-9425	1159.34	-43554.36	-52281.82	1.62	4
6134-9021	-512117.65	409642.99	250524.73	0.02	4
7072-9010	-15.04	2.34	7.39	3.00	4
8015-8019	-1141.50	-128638.06	16776.51	0.45	4
8015-8030	372698.34	294250.47	-373345.41	0.02	4
9051-9091	11702.66	-9725.37	-9108.39	3.00	4

[1] APPLIED EQUALLY TO ALL THREE RELATIVE COORDINATES IN M^{-2} UNIT

[2] REFER TO TABLE 8.8

TABLE 8.10.—*Geoidal Undulations and Heights Used in the Constraints*

STATION NO	STATION NAME	NREF [1] (M)	HCONSTR [2] (M)	$\sigma_{HCONSTR}$ [3] (M)
1021	BLOSSOM POINT	-37.32	-45.65	2.5
1022	FORT MYERS	-31.58	-39.92	4.0
1030	GOLDSTONE	-30.00	896.45	4.0
1032	ST. JOHN'S	11.57	61.03	4.0
1033	FAIRBANKS	9.11	168.16	6.0
1034	E. GRAND FORKS	-25.47	218.56	2.5
1042	ROSMAN	-34.38	862.55	4.0
3106	ANTIGUA	-49.83	-68.70	8.0
3334	STONEVILLE	-31.54	-2.54	4.0
3400	COLORADO SPRINGS	-18.42	2159.63	2.5
3401	BEDFORD	-30.59	36.93	2.5
3402	SEMMES	-29.04	33.07	4.0
3404	SWAN ISLAND	-6.69	20.89	6.0
3405	GRAND TURK	-49.77	-64.73	6.0
3406	CURACAO	-29.19	-41.02	4.0
3407	TRINIDAD	-38.57	194.88	4.0
3413	NATAL	-12.03	-5.87	6.0
3414	BRASILIA	- 9.88	1021.23	6.0
3431	ASUNCION	11.98	137.72	6.0
3476	PARAMARIBO	-28.31	-34.02	6.0
3477	BOGOTA	10.71	2551.44	6.0
3478	MANAUS	- 7.17	53.63	6.0
3499	QUITO	16.73	2682.74	6.0
3648	HUNTER AFB	-35.70	-36.84	2.5
3657	ABERDEEN	-36.55	-45.38	2.5
3861	HOMESTEAD	-33.70	-47.20	4.0
3902	CHEYENNE	-16.53	1859.48	2.5
3903	HERNDON	-36.87	117.14	6.0
4050	PRETORIA	24.12	1573.21	6.0
4061	ANTIGUA	-49.83	-28.30	8.0
4081	GRAND TURK	-49.84	-31.01	6.0
4082	MERRITT ISLAND	-35.74	-37.91	4.0
4280	VANDERBERG AFB	-36.78	84.53	4.0
4740	BERMUDA	-43.45	-41.92	4.0
4742	KAUAI	5.61	1166.61	8.0
5001	HERNDON	-36.87	76.95	6.0

TABLE 8.10.—*(Cont'd)*

STATION NO	STATION NAME	NREF [1] (M)	HCONSTR [2] (M)	$\sigma_{HCONSTR}$ [3] (M)
5201	MOSES LAKE	-17.65	347.84	4.0
5410	MIDWAY ISLANDS	- 4.13	7.51	8.0
5648	FORT STEWART	-35.07	-20.18	2.5
5712	PARAMARIBO	-28.31	-30.79	4.0
5713	TERCEIRA	54.00	83.29	4.0
5715	DAKAR	27.20	21.50	4.0
5717	FORT LAMY	10.35	273.29	6.0
5720	ADDIS ABABA	- 5.78	1850.34	6.0
5721	MASHHAD	-20.67	949.29	4.0
5722	DIEGO GARCIA	-73.64	-92.76	8.0
5723	CHIANG MAI	-40.39	256.21	8.0
5726	ZAMBOANGA	62.16	69.14	8.0
5730	WAKE ISLAND	13.75	26.83	8.0
5732	PAGO PAGO	27.35	40.70	6.0
5733	CHRISTMAS ISLAND	16.07	25.90	8.0
5734	SHEMYA	6.22	45.72	8.0
5735	NATAL	-12.03	-3.37	6.0
5736	ASCENSION ISLAND	16.26	55.09	8.0
5739	TERCEIRA	54.00	83.39	4.0
5744	CATANIA	37.43	18.89	4.0
5907	WORTHINGTON	-28.11	445.03	2.5
5911	BERMUDA	-43.44	-39.80	8.0
5912	PANAMA	6.16	0.39	6.0
5914	PUERTO RICO	-50.08	-5.07	6.0
5915	AUSTIN	-26.32	172.03	2.5
5923	CYPRUS	24.64	158.72	8.0
5924	ROTA	54.48	36.90	6.0
5925	ROBERTS FIELD	33.75	10.31	6.0
5930	SINGAPORE	8.28	1.16	6.0
5931	HONG KONG	2.32	155.02	6.0
5933	DARWIN	50.66	61.75	8.0
5934	MANUS	74.75	81.69	8.0
5935	GUAM	48.15	86.00	8.0
5937	PALAU	69.93	137.52	8.0
5938	GUADALCANAL	59.97	74.99	8.0
5941	MAUI	2.05	40.25	8.0

TABLE 8.10.—*(Cont'd)*

STATION NO	STATION NAME	NREF [1] (M)	HCONSTR [2] (M)	$\sigma_{HCONSTR}$ [3] (M)
6001	THULE	11.66	204.62	8.0
6002	BELTSVILLE	-36.90	-6.73	2.5
6003	MOSES LAKE	-17.65	347.66	4.0
6004	SHEMYA	6.22	43.22	8.0
6006	TROMSO	27.06	113.19	4.0
6007	TERCEIRA	54.00	80.59	4.0
6008	PARAMARIBO	-28.31	-33.91	4.0
6009	QUITO	16.73	2683.04	6.0
6011	MAUI	1.75	3056.88	8.0
6012	WAKE ISLAND I	13.75	22.23	8.0
6013	KANOYA	34.27	96.47	6.0
6015	MASHHAD	-20.67	945.89	4.0
6016	CATANIA	37.43	16.33	4.0
6019	VILLA DOLORES	22.80	609.43	6.0
6020	EASTER ISLAND	- 4.75	219.02	8.0
6022	TUTUILA	27.35	38.04	8.0
6023	THURSDAY ISLAND	67.94	127.40	4.0
6031	INVERCARGILL	8.68	6.35	8.0
6032	CAVERSHAM	-30.51	-15.59	6.0
6038	SOCORRO ISLAND	-35.47	-15.81	6.0
6039	PITCAIRN ISLAND	-16.68	321.45	8.0
6040	COCOS ISLAND	-38.11	-50.26	8.0
6042	ADDIS ABABA	- 5.78	1847.40	6.0
6043	CERRO SOMBRERO	15.60	76.25	8.0
6044	HEARD ISLAND	36.61	17.16	8.0
6045	MAURITIUS	- 6.07	113.55	8.0
6047	ZAMBOANGA	62.17	65.24	8.0
6050	PALMER STATION	15.70	11.71	6.0
6051	MAWSON STATION	29.20	17.68	6.0
6053	MCMURDO STATION	-56.10	-50.90	6.0
6055	ASCENSION ISLAND	16.26	52.04	8.0
6059	CHRISTMAS ISLAND	16.07	25.15	8.0
6060	CULGOORA	27.33	236.27	6.0
6061	SOUTH GEORGIA	11.28	-10.88	8.0
6063	DAKAR	27.20	20.50	4.0
6064	FORT LAMY	10.35	270.19	6.0

TABLE 8.10.—*(Cont'd)*

STATION NO	STATION NAME	NREF [1] (M)	HCONSTR [2] (M)	$\sigma_{HCONSTR}$ [3] (M)
6065	HOHENPEISSENBERG	44.23	960.09	2.5
6066	WAKE ISLAND II	13.74	24.02	8.0
6067	NATAL	-12.03	-2.14	6.0
6068	JOHANNESBURG	24.65	1513.46	6.0
6069	TRISTAN DA CUNHA	25.52	17.30	8.0
6072	CHIANG MAI	-40.39	264.61	8.0
6073	DIEGO GARCIA	-73.64	-94.96	8.0
6075	MAHE	-44.40	514.23	8.0
6078	PORT VILA	63.10	81.72	8.0
6111	WRIGHTWOOD I	-33.18	2248.74	4.0
6123	POINT BARROW	- 1.40	1.62	6.0
6134	WRIGHTWOOD II	-33.19	2162.83	4.0
7036	EDINBURG	-19.78	32.17	4.0
7037	COLUMBIA	-33.87	229.20	2.5
7039	BERMUDA	-43.43	-30.60	4.0
7040	SAN JUAN	-50.55	-20.06	6.0
7043	GREENBELT	-36.91	2.46	2.5
7045	DENVER	-18.10	1765.36	2.5
7072	JUPITER	-36.04	-35.56	4.0
7075	SUDBURY	-39.20	230.07	2.5
7076	KINGSTON	-26.62	403.91	8.0
8009	WIPPOLDER	42.33	41.11	4.0
8010	ZIMMERWALD	44.77	920.58	2.5
8011	MALVERN	47.43	134.97	4.0
8015	HAUTE PROVENCE	46.38	676.87	4.0
8019	NICE	45.91	394.73	4.0
8030	MEUDON	44.64	183.23	2.5
9001	ORGAN PASS	-22.93	1623.14	4.0
9002	OLIFANTSFONTEIN	24.27	1533.45	6.0
9004	SAN FERNANDO	54.57	50.44	6.0
9005	TOKYO	30.20	88.17	6.0
9006	NAINI TAL	-48.12	1858.89	6.0
9007	AREQUIPA	31.82	2464.57	6.0
9008	SHIRAZ	-10.91	1559.17	6.0
9009	CURACAO	-29.19	-39.15	4.0
9010	JUPITER	-36.04	-34.63	4.0

TABLE 8.10.—*(Cont'd)*

STATION NO	STATION NAME	NREF [1] (M)	HCONSTR [2] (M)	$\sigma_{HCONSTR}$ [3] (M)
9011	VILLA DOLORES	22.80	609.25	6.0
9012	MAUI	1.76	3041.76	8.0
9021	MOUNT HOPKINS	-27.00	2351.01	4.0
9028	ADDIS ABABA	- 5.78	1886.15	6.0
9029	NATAL	-12.03	2.57	6.0
9031	COMODORO RIVADAVIA	13.43	179.36	8.0
9051	ATHENS	32.81	190.96	8.0
9091	DIONYSOS	32.84	470.13	8.0
9424	COLD LAKE	-26.21	672.13	2.5
9425	EDWARDS AFB	-32.39	749.47	4.0
9426	HARESTUA	36.39	589.17	2.5
9427	JOHNSTON ISLAND	8.83	20.59	8.0
9431	RIGA	25.67	9.76	2.5
9432	UZHGOROD	39.71	201.99	2.5

[1] FROM [RAPP,1973]

[2] HCONSTR = MSL + NREF + ΔN (SEE SECTION 8.5.1)

[3] USED IN COMPUTING THE WEIGHTS OF THE HEIGHT CONSTRAINTS

TABLE 8.11.—*Chord Constraints*

Station-station	Chord distance (meters)	$\sigma \times 10^6$ [a]	Source code[b]
6002–6003	3 485 363.232	1.00	7
6003–6111	1 425 876.452	1.11	7
6006–6065	2 457 765.810	1.43	8
6016–6065	1 194 793.601	1.18	8
6063–6064	3 485 550.755	1.18	9
6023–6060	2 300 209.803	2.00	10
6032–6060	3 163 623.866	Rejected	10
6006–6016	3 545 871.454	1.00	8
3861–7043	1 531 562.9	1.33	7
4082–4050	10 909 592	Rejected	11
4082–4742	7 362 142	Rejected	11
4082–4740	1 593 106	2.00	11
4082–4081	1 230 691	2.00	11
4082–4061	1 288 026	2.00	11
4742–4280	3 977 684	Rejected	11

[a] Used in computing the weights.
[b] Refer to table 8.8.

TABLE 8.12.—*Determination of Scale*

Point	Interpretation	Weight	a (m)	Weighted mean a (m)
1	WN = EDM	10	6 378 125.0	
				6 378 125.8
2	WN = C-band	1	6 378 133.7	(from points 1 and 2)
3	WN = SAO III	278	6 378 140.8	
				6 378 141.7
4	WN = NWL 9D	69	6 378 143.0	(from points 1–6)
				6 378 142.0
5	WN = GSFC 73	66	6 378 144.9	(from points 3–6)
6	WN = GEM 4	48	6 378 144.1	
7	C-band = SAO III	1	6 378 143.6	
				6 378 142.7
8	C-band = GSFC 73	1	6 378 146.8	(from points 1–14)
9	C-band = NWL 9D	1	6 378 147.1	
10	C-band = GEM 4	1	6 378 147.8	
11	EDM = SAO III	10	6 378 153.7	
12	EDM = GSFC 73	8	6 378 154.0	
13	EDM = GEM 4	9	6 378 155.2	
14	EDM = NWL 9D	9	6 378 160.5	

TABLE 8.13.—*Average Standard Deviations (Solution WN14)*

Average standard deviations	Constituent networks				WN14
	BC	SECOR	MPS	SA	
σ_u (m)	3.3	2.5	4.9	4.0	3.8
σ_v (m)	3.3	2.6	5.1	3.4	3.9
σ_w (m)	3.9	3.2	4.4	4.7	4.0
σ_ϕ (arc sec)	0.1	0.1	0.2	0.2	0.1
σ_λ (arc sec)	0.2	0.1	0.3	0.1	0.2
σ_h (m)	3.2	2.4	2.9	3.0	2.9
σ (m)	3.5	2.8	4.8	4.1	3.9

TABLE 8.14.—*Cartesian and Geodetic Coordinates (Solution WN 14)*

Sta. no.	u	σ_u	v	σ_v	w	σ_w
	φ	σ_φ	λ	σ_λ	h	σ_h
		a_a	A_a	r_a		
		s_b	A_b	r_b		
		a_c	A_c	r_c		

u, v, w Cartesian coordinates in meters (orientation: $u \equiv$ the Greenwich meridian as defined by the Bureau International de l'Heure; $v \equiv \lambda = 90°$ (E); $w \equiv$ Conventional International Origin).

φ, λ Geodetic latitude and longitude in angular units (degrees, minutes and seconds of arc) computed from the Cartesian coordinates and referred to a rotational ellipsoid of $a = 6\,378\,155.00$ m and $b = 6\,356\,769.70$ m.

h Geodetic (ellipsoidal) height in meters referred to the same ellipsoid.

$\sigma_u, \sigma_v, \sigma_w$ Standard deviations of the Cartesian coordinates in meters.

$\sigma_\varphi, \sigma_\lambda$ Standard deviations of the geodetic coordinates in seconds of arc.

σ_h Standard deviations of the geodetic height in meters.

a_a, A_a, r_a Altitude (elevation angle), azimuth and magnitude of the major semiaxis of the error ellipsoid, respectively. Angles in degrees, magnitude in meters. Altitude is positive above the horizon. Azimuth is positive east reckoned from the north (see sec. 8.4.7.4).

a_b, A_b, r_b Same as above for the mean axis of the error ellipsoid.

a_c, A_c, r_c Same as above for the minor axis of the error ellipsoid.

TABLE 8.14.—*(Cont'd)*

1021	1118023.12	2.84	-4876323.36	2.61	3942963.91	2.83
	38 25 49.56	0.10	282 54 48.07	0.12	-47.77	2.05
		0.08	16.31	3.25		
		-2.59	106.30	2.86		
		-87.41	-71.85	2.04		
1022	807851.91	2.25	-5651989.58	1.94	2833500.22	2.32
	26 32 52.94	0.08	278 8 3.56	0.08	-32.58	1.92
		6.37	-26.03	2.39		
		11.15	65.23	2.20		
		-77.12	34.75	1.90		
1030	-2357242.91	5.62	-4646338.51	3.30	3668306.76	3.24
	35 19 47.44	0.10	243 5 59.26	0.23	889.58	2.84
		-0.27	79.87	5.97		
		30.63	-9.97	3.16		
		-59.37	-10.59	2.71		
1032	2602688.61	39.33	-3419228.93	46.69	4697637.28	13.76
	47 44 28.60	0.65	307 16 41.12	2.84	60.96	4.05
		-0.33	73.10	61.68		
		-1.46	163.11	9.76		
		88.51	150.35	4.03		
1033	-2299282.59	6.92	-1445693.70	9.72	5751811.65	5.67
	64 52 17.50	0.24	212 9 35.93	0.74	170.23	5.15
		-1.11	-71.88	9.98		
		4.10	18.04	6.97		
		85.75	-146.80	5.14		
1034	-521704.47	3.09	-4242064.34	2.95	4718716.85	2.69
	48 1 20.63	0.11	262 59 19.55	0.15	217.55	1.97
		0.01	138.01	3.88		
		1.65	48.01	2.57		
		88.35	-131.79	1.97		

TABLE 8.14.—*(Cont'd)*

1042	647497.49	2.77	-5177935.64	2.43	3656705.89	2.84
	35 12 7.07	0.09	277 7 40.08	0.11	863.40	2.42
		8.15	-32.33	2.99		
		21.12	60.84	2.66		
		-67.22	37.74	2.37		
3106	2881838.31	3.72	-5372164.61	3.32	1868538.63	4.25
	17 8 54.85	0.13	298 12 39.03	0.13	-58.68	3.35
		18.24	-31.23	4.45		
		17.20	64.62	3.62		
		-64.49	15.09	3.17		
3334	-84963.76	13.62	-5327974.93	6.79	3493428.28	8.96
	33 25 31.00	0.34	269 5 11.03	0.53	-2.60	3.90
		-2.81	71.02	13.96		
		0.27	-18.96	10.11		
		-87.18	-103.43	3.84		
3400	-1275207.22	9.06	-4798029.30	5.11	3994208.30	5.67
	39 0 21.73	0.23	255 6 58.20	0.38	2160.40	2.50
		-3.41	77.30	9.15		
		-1.14	-12.77	7.12		
		-86.41	-121.20	2.45		
3401	1513136.10	3.18	-4463576.80	3.44	4283055.82	2.99
	42 27 17.69	0.12	288 43 35.29	0.15	34.52	2.23
		-5.50	38.05	4.08		
		-0.81	128.13	3.07		
		84.44	46.50	2.20		
3402	167259.66	3.91	-5481970.99	2.81	3245036.99	3.46
	30 46 49.95	0.11	271 44 51.37	0.15	27.89	2.78
		10.37	74.47	3.96		
		9.33	-17.25	3.48		
		-75.98	31.59	2.71		

TABLE 8.14.—*(Cont'd)*

3404	642491.44	4.70	-6053940.27	3.73	1895688.60	4.89
	17 24 19.15	0.16	276 3 28.80	0.16	-1.41	3.78
		13.00	40.70	5.32		
		12.19	133.56	4.28		
		-72.03	85.31	3.64		
3405	1919482.89	3.30	-5621088.11	3.47	2315775.25	3.95
	21 25 48.55	0.13	288 51 14.23	0.12	-67.11	3.39
		16.02	4.06	3.96		
		-37.11	81.52	3.58		
		48.44	112.95	3.17		
3406	2251800.21	2.41	-5816912.95	2.07	1327191.09	3.37
	12 5 25.86	0.11	291 9 43.37	0.08	-37.08	2.02
		8.37	-21.06	3.51		
		-5.58	68.11	2.30		
		-79.92	-55.22	1.98		
3407	2979891.14	4.67	-5513530.88	3.36	1181129.32	5.25
	10 44 34.89	0.17	298 23 23.41	0.16	186.66	3.11
		7.22	-41.79	6.26		
		23.36	51.35	3.61		
		-65.42	32.14	2.91		
3413	5186348.44	2.15	-3654222.39	2.22	-653018.86	2.67
	- 5 54 57.54	0.09	324 49 55.40	0.08	-0.16	2.02
		-10.20	5.19	2.68		
		4.99	94.29	2.35		
		78.62	-21.40	2.00		
3414	4114977.82	7.65	-4554142.51	6.11	-1732153.99	7.24
	-15 51 37.38	0.24	312 5 59.86	0.28	1016.74	5.00
		1.84	51.81	9.40		
		0.35	-38.20	5.91		
		-88.12	41.00	4.99		

TABLE 8.14.—*(Cont'd)*

3431	3093045.37	7.59	-4870081.66	6.52	-2710823.02	10.84
	-25 18 57.42	0.38	302 25 12.37	0.27	145.11	5.06
		-2.01	12.62	11.79		
		-4.59	102.79	7.31		
		84.99	78.99	5.03		
3476	3623277.34	2.20	-5214210.74	2.03	601515.27	2.97
	5 26 52.73	0.10	304 47 41.50	0.07	-36.82	1.95
		1.89	-9.70	2.99		
		4.74	80.46	2.24		
		-84.90	58.64	1.94		
3477	1744650.18	10.18	-6114286.71	6.63	532208.62	9.56
	4 49 0.25	0.31	285 55 32.03	0.35	2555.03	5.51
		-2.04	49.78	13.43		
		-51.04	142.31	5.74		
		-38.88	-41.86	5.07		
3478	3185777.03	18.72	-5514585.85	14.46	-347703.19	35.12
	- 3 8 45.73	1.15	300 0 54.12	0.74	53.58	5.97
		0.31	-32.05	41.22		
		-25.68	57.80	8.05		
		64.32	58.59	5.37		
3499	1280834.24	3.59	-6250955.94	3.43	-10800.58	4.11
	- 0 5 51.49	0.13	281 34 47.08	0.12	2683.81	3.36
		22.05	-0.15	4.24		
		-15.59	83.36	3.69		
		-62.50	-39.06	3.14		
3648	832566.24	3.56	-5349540.70	2.49	3360585.27	3.62
	32 0 6.28	0.13	278 50 46.17	0.14	-36.10	1.67
		2.59	22.92	4.07		
		-5.52	112.67	3.57		
		-83.90	-42.00	1.64		

TABLE 8.14.—*(Cont'd)*

3657	1186787.14	3.14	-4785193.13	3.05	4032882.32	2.98
	39 28 19.01	0.11	283 55 44.44	0.14	-44.57	2.22
		-4.73	33.47	3.69		
		-2.52	123.68	3.09		
		84.64	61.63	2.20		
3861	961767.93	2.97	-5679156.55	2.33	2729883.49	2.61
	25 30 26.08	0.08	279 36 42.74	0.11	-43.47	2.50
		-9.63	116.13	3.08		
		56.43	40.95	2.58		
		-31.81	20.09	2.21		
3902	-1234700.68	8.59	-4651242.77	6.25	4174758.60	6.26
	41 7 57.30	0.27	255 8 0.09	0.37	1859.36	2.53
		-1.99	105.25	8.74		
		-3.73	15.12	8.35		
		-85.78	-136.72	2.46		
3903	1088989.74	12.11	-4843005.39	8.51	3991776.62	8.91
	38 59 34.10	0.36	282 40 21.55	0.50	110.47	5.67
		0.38	120.87	12.59		
		-5.48	30.91	10.42		
		84.51	26.96	5.60		
4050	5051608.05	3.18	2726603.28	3.18	-2774166.82	4.35
	-25 56 37.88	0.14	28 21 28.57	0.12	1575.91	2.91
		-9.93	1.93	4.46		
		-13.22	94.29	3.38		
		73.36	56.07	2.82		
4061	2881592.34	3.76	-5372523.89	3.47	1868024.39	4.35
	17 8 36.95	0.14	298 12 25.95	0.13	-18.85	3.49
		20.20	-26.66	4.48		
		11.03	67.45	3.76		
		-66.75	4.42	3.31		

TABLE 8.14.—*(Cont'd)*

4081	1920410.93	3.32	-5619417.80	3.57	2319128.45	4.00
	21 27 45.25	0.13	288 52 3.48	0.12	-33.03	3.47
		10.81	17.91	4.05		
		-47.10	96.05	3.64		
		40.87	117.42	3.18		
4082	910567.21	2.64	-5539113.24	2.36	3017965.30	2.80
	28 25 28.69	0.09	279 20 7.01	0.10	-35.47	2.25
		4.20	-14.50	2.91		
		1.40	75.60	2.62		
		-85.57	4.05	2.24		
4280	-2671873.84	3.83	-4521210.51	3.32	3607490.37	3.57
	34 39 56.78	0.13	239 25 6.35	0.16	85.34	2.65
		0.76	75.54	4.06		
		2.23	-14.49	3.87		
		-87.65	4.40	2.65		
4740	2308887.30	3.35	-4874298.20	3.14	3393082.09	3.77
	32 20 52.79	0.13	295 20 46.55	0.13	-40.55	2.60
		1.12	-14.90	4.19		
		-10.00	74.90	3.32		
		79.94	81.43	2.58		
5001	1088849.37	3.64	-4842948.67	3.00	3991840.18	3.69
	38 59 37.46	0.13	282 40 16.38	0.15	83.52	2.48
		12.35	37.45	4.41		
		13.94	130.56	3.36		
		-71.21	87.39	2.26		
5201	-2127802.21	2.28	-3785911.53	2.20	4656012.10	2.44
	47 11 5.15	0.08	240 39 45.48	0.11	341.28	2.14
		18.51	20.45	2.56		
		-4.92	-67.90	2.24		
		-70.81	36.41	2.08		

TABLE 8.14.—*(Cont'd)*

5410	-5618754.08	2.29	-258237.50	2.76	2997250.19	3.62
	28 12 43.31	0.12	182 37 53.25	0.10	21.73	2.38
		17.94	-6.80	3.68		
		12.06	-100.76	2.79		
		-68.14	-42.96	2.16		
5648	794691.02	3.59	-5360051.05	2.51	3353082.41	3.65
	31 55 18.82	0.13	278 26 0.03	0.14	-19.05	1.68
		2.34	23.32	4.11		
		-6.03	113.08	3.60		
		-83.53	-45.56	1.64		
5712	3623289.81	2.06	-5214188.02	1.95	601673.22	2.91
	5 26 57.88	0.10	304 47 42.25	0.07	-33.31	1.87
		1.26	-5.25	2.92		
		1.18	84.78	2.12		
		-88.27	37.82	1.87		
5713	4433637.78	1.98	-2268153.21	2.19	3971656.80	2.46
	38 45 36.52	0.08	332 54 24.11	0.10	91.71	1.82
		17.42	-22.37	2.58		
		6.62	69.72	2.27		
		71.29	179.77	1.72		
5715	5884468.78	1.60	-1853580.06	1.96	1612760.08	2.33
	14 44 39.23	0.08	342 30 56.94	0.07	31.00	1.52
		6.24	-7.11	2.35		
		4.07	83.34	2.01		
		82.54	-153.76	1.50		
5717	6023410.73	2.00	1617946.48	2.04	1331655.76	2.68
	12 7 52.22	0.09	15 2 7.09	0.07	284.13	1.96
		-3.82	-6.72	2.74		
		14.20	82.31	2.01		
		75.28	-82.00	1.95		

TABLE 8.14.—*(Cont'd)*

5720	4900749.06	2.03	3968252.96	2.06	966354.69	2.86
	8 46 13.32	0.09	38 59 52.49	0.07	1853.32	1.94
		2.64	-0.20	2.87		
		-0.51	89.78	2.14		
		87.31	168.84	1.94		
5721	2604404.77	2.05	4444122.35	2.13	3750344.33	2.65
	36 14 26.73	0.09	59 37 41.76	0.09	952.30	1.91
		11.32	-2.43	2.79		
		12.51	90.12	2.14		
		73.01	-133.34	1.85		
5722	1905127.03	3.49	6032287.50	4.05	-810716.17	4.30
	- 7 21 6.16	0.13	72 28 21.92	0.11	-91.66	4.23
		-46.43	5.87	4.79		
		32.30	54.23	3.66		
		25.81	-53.57	3.28		
5723	-941709.38	2.54	5967444.99	2.31	2039322.91	3.46
	18 46 11.15	0.11	98 58 3.96	0.09	252.51	2.48
		20.63	9.18	3.48		
		5.06	-82.73	2.53		
		68.70	174.16	2.30		
5726	-3361946.83	2.29	5365837.02	2.20	763627.83	3.16
	6 55 20.64	0.10	122 4 8.62	0.08	85.43	2.10
		14.84	-0.73	3.18		
		5.92	-92.31	2.44		
		73.97	156.56	1.99		
5730	-5858574.55	2.06	1394467.24	2.51	2093847.41	3.14
	19 17 29.46	0.10	166 36 41.38	0.09	24.96	2.22
		17.68	1.19	3.14		
		16.86	-94.35	2.51		
		-65.17	-45.28	2.05		

TABLE 8.14.—*(Cont'd)*

5732	-6099970.46	3.56	-997355.27	3.54	-1568570.89	4.15
	-14 19 53.84	0.13	189 17 8.85	0.12	38.64	3.64
		-24.28	33.76	4.47		
		-62.75	-175.08	3.46		
		-11.61	-61.56	3.23		
5733	-5885333.94	2.75	-2448380.44	2.91	221670.69	3.86
	2 0 18.39	0.13	202 35 16.75	0.09	25.88	2.77
		8.46	17.66	3.97		
		12.89	-74.29	2.77		
		-74.50	-39.91	2.74		
5734	-3851799.01	2.72	396409.29	3.31	5051342.05	3.90
	52 42 48.32	0.11	174 7 26.66	0.17	51.71	3.45
		35.90	29.49	4.03		
		42.09	-101.36	3.35		
		-27.04	-38.82	2.47		
5735	5186350.63	2.02	-3654223.69	2.06	-653018.90	2.54
	- 5 54 57.54	0.08	324 49 55.41	0.07	2.36	1.93
		-14.68	-5.18	2.55		
		2.64	84.13	2.16		
		75.08	-15.82	1.88		
5736	6118340.28	2.30	-1571761.88	2.25	-878553.62	2.74
	- 7 58 13.62	0.09	345 35 33.46	0.08	56.48	2.26
		-14.58	3.92	2.75		
		35.15	83.37	2.41		
		-51.08	112.70	2.11		
5739	4433629.32	1.98	-2268186.23	2.20	3971646.99	2.47
	38 45 36.11	0.08	332 54 22.73	0.10	91.43	1.83
		17.59	-22.26	2.58		
		6.31	69.75	2.28		
		71.24	178.75	1.73		

TABLE 8.14.—*(Cont'd)*

5744	4896437.74	1.82	1316125.03	2.16	3856626.21	2.28
	37 26 37.31	0.08	15 2 42.23	0.09	18.41	1.65
		3.13	-20.27	2.54		
		16.86	70.68	2.04		
		72.83	-120.48	1.60		
5907	-449417.54	4.17	-4600905.48	3.18	4380288.13	4.54
	43 38 57.03	0.17	264 25 15.72	0.18	444.85	2.26
		8.60	27.67	5.61		
		-11.78	115.86	3.54		
		-75.34	-27.02	2.04		
5911	2307991.25	2.56	-4873773.25	2.34	3394463.39	2.96
	32 21 45.57	0.09	295 20 24.17	0.10	-26.09	2.40
		21.55	33.67	3.18		
		28.27	135.92	2.42		
		-53.18	91.83	2.19		
5912	1142644.48	3.06	-6196109.11	3.45	988336.58	4.06
	8 58 26.82	0.14	280 26 55.35	0.10	-5.02	3.28
		-24.25	0.41	4.45		
		37.82	69.95	3.12		
		-42.44	114.73	2.88		
5914	2349456.86	10.50	-5576027.12	7.01	2010342.57	6.44
	18 29 39.35	0.24	292 50 53.18	0.37	-9.38	5.38
		4.84	88.74	10.84		
		-27.05	1.21	8.04		
		62.45	-10.60	4.33		
5915	-744091.08	3.84	-5465238.69	3.80	3192467.45	4.73
	30 13 45.90	0.19	262 14 48.71	0.14	170.93	2.25
		-8.00	11.70	5.83		
		-5.64	102.50	3.62		
		-80.19	-132.69	2.09		

TABLE 8.14.—*(Cont'd)*

5923	4363332.16	1.88	2862254.91	2.07	3655380.73	2.44
	35 11 30.32	0.09	33 15 50.54	0.08	170.07	1.77
		5.75	-9.41	2.63		
		15.87	82.23	1.96		
		73.07	-118.73	1.74		
5924	5093556.18	1.87	-565322.26	2.61	3784268.29	2.93
	36 37 36.90	0.09	353 40 0.45	0.10	19.25	1.99
		22.12	-10.48	3.00		
		1.36	80.07	2.60		
		67.83	173.41	1.76		
5925	6237366.27	2.27	-1140241.51	2.56	687740.16	3.01
	6 13 54.17	0.10	349 38 24.92	0.08	15.82	2.21
		-17.07	-2.36	3.15		
		-14.31	92.13	2.56		
		67.43	40.01	2.07		
5930	-1542549.36	2.61	6186956.66	2.67	151833.76	3.42
	1 22 23.73	0.11	103 59 58.99	0.09	18.73	2.57
		9.95	3.46	3.44		
		33.76	-93.28	2.86		
		-54.41	-72.35	2.37		
5931	-2423914.92	2.49	5388250.32	2.52	2394869.19	3.64
	22 11 55.70	0.11	114 13 14.49	0.09	140.80	2.91
		34.18	1.63	3.69		
		54.97	167.23	2.48		
		6.78	-93.00	2.47		
5933	-4071568.36	3.16	4714253.33	3.24	-1366528.34	3.75
	-12 27 15.12	0.12	130 48 58.51	0.10	76.62	3.28
		-15.03	4.38	3.75		
		66.67	-47.11	3.25		
		-17.41	-90.45	3.14		

TABLE 8.14.—*(Cont'd)*

5934	-5367663.14	2.46	3437869.92	2.55	-225415.97	3.28
	- 2 2 20.34	0.11	147 21 40.80	0.09	82.38	2.38
		8.39	6.55	3.31		
		3.83	-84.02	2.60		
		-80.76	-18.35	2.36		
5935	-5059825.71	2.08	3591185.96	2.22	1472762.50	2.84
	13 26 22.08	0.09	144 38 5.87	0.08	97.15	2.05
		9.68	9.47	2.86		
		7.47	-81.81	2.26		
		-77.73	-28.90	2.02		
5937	-4433463.64	2.22	4512930.31	2.23	809958.73	3.17
	7 20 40.34	0.10	134 29 27.89	0.08	135.86	2.06
		11.68	4.19	3.18		
		3.10	-86.45	2.42		
		-77.90	-11.10	2.00		
5938	-5915096.47	2.96	2146860.80	2.97	-1037909.46	3.49
	- 9 25 40.94	0.11	160 3 6.61	0.10	80.95	2.97
		-1.29	5.77	3.51		
		55.71	-82.34	3.00		
		-34.26	-85.11	2.90		
5941	-5467757.28	2.52	-2381246.70	2.79	2254033.75	3.78
	20 49 54.72	0.12	203 32 0.47	0.09	59.12	2.59
		11.30	7.83	3.83		
		-28.47	-75.95	2.79		
		-58.98	78.43	2.44		
6001	546568.68	2.57	-1389993.74	2.44	6180236.66	3.40
	76 30 4.71	0.07	291 27 56.08	0.38	211.60	3.39
		76.47	40.98	3.42		
		-11.64	72.10	2.84		
		-6.80	-19.31	2.10		

TABLE 8.14.—*(Cont'd)*

6002	1130764.85	2.04	-4830831.87	1.71	3994704.05	1.92
	39 1 39.35	0.07	283 10 27.05	0.08	-6.70	1.52
		3.64	-36.38	2.13		
		3.11	53.82	1.98		
		-85.21	4.20	1.51		
6003	-2127832.13	2.11	-3785862.99	2.02	4656037.23	2.30
	47 11 6.36	0.07	240 39 43.11	0.10	340.92	2.02
		23.12	23.42	2.41		
		-1.56	-65.92	2.07		
		-66.83	27.72	1.94		
6004	-3851797.46	2.74	396409.38	3.30	5051340.48	3.91
	52 42 48.33	0.11	174 7 26.64	0.17	49.54	3.45
		34.79	28.69	4.05		
		43.25	-102.14	3.37		
		-26.91	-40.66	2.45		
6006	2102927.39	2.36	721668.52	2.92	5958180.80	2.89
	69 39 45.17	0.09	18 56 27.07	0.25	111.31	2.81
		-18.55	137.52	3.14		
		68.66	106.71	2.79		
		10.18	-135.93	2.20		
6007	4433637.30	2.04	-2268151.36	2.17	3971655.01	2.49
	38 45 36.50	0.08	332 54 24.17	0.10	89.60	1.88
		17.05	-22.41	2.62		
		7.87	70.03	2.24		
		71.11	-176.12	1.78		
6008	3623241.00	2.13	-5214233.74	1.96	601536.05	2.93
	5 26 53.40	0.10	304 47 40.10	0.07	-36.69	1.89
		1.99	-8.96	2.95		
		4.43	81.19	2.17		
		-85.14	56.94	1.88		

TABLE 8.14.—*(Cont'd)*

6009	1280834.24	3.58	-6250955.94	3.43	-10800.59	4.10
	- 0 5 51.49	0.13	281 34 47.08	0.12	2683.81	3.36
		22.07	-0.16	4.24		
		-15.60	83.34	3.69		
		-62.48	-39.07	3.14		
6011	-5466018.63	3.02	-2404431.52	2.88	2242224.36	3.34
	20 42 26.97	0.10	203 44 38.68	0.11	3074.38	2.86
		8.35	42.07	3.79		
		-62.48	115.71	2.94		
		-26.02	-43.83	2.36		
6012	-5858569.26	2.14	1394508.74	2.60	2093820.34	3.17
	19 17 28.58	0.10	166 36 39.96	0.09	20.23	2.30
		18.21	3.06	3.17		
		17.08	-92.74	2.60		
		-64.60	-43.08	2.13		
6013	-3565892.77	3.28	4120713.58	4.43	3303428.26	4.93
	31 23 42.60	0.16	130 52 17.54	0.16	93.70	3.68
		9.78	33.58	5.53		
		56.25	-71.37	3.80		
		-31.94	-50.25	3.11		
6015	2604353.27	2.06	4444166.00	2.18	3750320.52	2.64
	36 14 25.88	0.09	59 37 44.42	0.09	947.60	1.91
		10.34	-3.33	2.79		
		15.69	89.61	2.19		
		71.06	-125.44	1.84		
6016	4896388.34	1.81	1316172.12	2.19	3856668.20	2.24
	37 26 39.09	0.08	15 2 44.60	0.09	15.77	1.66
		2.05	-24.93	2.51		
		17.19	65.71	2.05		
		72.68	-121.51	1.62		

TABLE 8.14.—*(Cont'd)*

6019	2280627.09	2.37	-4914543.17	2.71	-3355402.77	3.67
	-31 56 34.93	0.12	294 53 38.32	0.09	606.26	2.55
		-11.54	-1.78	3.81		
		-54.22	104.68	2.54		
		33.33	80.51	2.34		
6020	-1888614.27	5.37	-5354894.35	4.50	-2895749.01	5.53
	-27 10 35.94	0.16	250 34 22.07	0.18	217.23	5.41
		-58.94	24.67	5.79		
		-7.72	127.67	5.42		
		-29.88	-137.86	4.10		
6022	-6099961.67	3.42	-997362.18	3.56	-1568585.49	4.66
	-14 19 54.37	0.15	189 17 9.12	0.12	34.93	3.48
		-10.68	25.44	4.93		
		-77.02	170.33	3.42		
		-7.29	-65.94	3.18		
6023	-4955386.85	3.24	3842247.82	3.04	-1163847.43	3.97
	-10 35 2.97	0.13	142 12 40.14	0.11	120.39	2.64
		6.82	21.74	4.17		
		-5.41	-67.61	3.37		
		81.28	-119.52	2.60		
6031	-4313825.29	3.41	891333.91	3.91	-4597265.83	3.84
	-46 24 57.86	0.12	168 19 32.46	0.19	-0.11	3.43
		-11.19	-106.82	4.17		
		-37.93	-7.95	3.86		
		-49.86	149.61	3.06		
6032	-2375420.64	3.29	4875546.73	3.21	-3345411.07	3.90
	-31 50 25.25	0.12	115 58 33.09	0.13	-6.10	3.13
		-21.80	-2.12	3.93		
		13.36	-86.66	3.50		
		64.06	32.57	2.94		

TABLE 8.14.—*(Cont'd)*

6038	-2160980.91	2.52	-5642710.55	2.80	2035367.82	3.83
	18 43 58.27	0.13	249 2 41.03	0.09	-15.49	2.62
		6.05	-7.29	3.89		
		-42.31	-91.76	2.79		
		-47.05	76.18	2.43		
6039	-3724765.86	6.17	-4421237.60	5.42	-2686084.74	5.55
	-25 4 6.38	0.16	229 53 12.56	0.21	316.49	6.20
		-65.27	61.40	6.38		
		-15.82	-66.56	6.01		
		-18.50	-162.00	4.63		
6040	-741981.69	4.50	6190792.95	3.69	-1338546.30	4.16
	-12 11 43.94	0.13	96 50 3.98	0.15	-49.01	3.77
		1.81	-81.59	4.54		
		-32.17	7.28	4.23		
		57.76	11.28	3.57		
6042	4900750.71	2.04	3968252.68	2.08	966325.28	2.86
	8 46 12.37	0.09	38 59 52.45	0.07	1849.93	1.94
		2.48	-0.62	2.87		
		-1.20	89.33	2.17		
		87.25	153.48	1.94		
6043	1371375.89	3.30	-3614750.34	3.84	-5055927.83	4.77
	-52 46 52.54	0.17	290 46 33.27	0.16	71.89	3.52
		-17.66	5.08	5.36		
		-68.07	-137.21	3.29		
		-12.57	99.15	2.96		
6044	1098897.91	6.82	3684606.64	6.17	-5071873.13	7.78
	-53 1 9.71	0.25	73 23 35.89	0.38	24.18	5.98
		-25.82	17.19	8.32		
		-14.04	-79.76	7.05		
		60.10	-15.53	5.12		

TABLE 8.14.—*(Cont'd)*

6045	3223432.02	3.16	5045336.27	3.15	-2191805.72	3.94
	-20 13 53.35	0.13	57 25 32.73	0.11	114.46	3.13
		-19.28	1.28	3.94		
		-10.91	-92.59	3.30		
		67.63	-30.53	3.00		
6047	-3361976.90	2.37	5365811.89	2.30	763624.74	3.23
	6 55 20.56	0.10	122 4 9.88	0.08	79.76	2.21
		14.53	-1.10	3.25		
		6.31	-92.75	2.51		
		74.10	154.41	2.11		
6050	1192678.77	4.86	-2451015.64	6.15	-5747034.19	6.09
	-64 46 26.04	0.25	295 56 52.19	0.33	7.95	4.57
		16.30	-178.22	7.90		
		-24.63	99.49	4.39		
		-59.83	-118.43	4.10		
6051	1111336.13	4.89	2169262.66	3.72	-5874334.05	4.44
	-67 36 5.21	0.14	62 52 24.45	0.39	21.81	4.09
		-16.78	-47.12	5.12		
		-45.30	60.62	4.26		
		39.90	28.28	3.62		
6052	-902608.85	4.44	2409522.13	3.95	-5816551.79	5.45
	-66 16 45.08	0.14	110 32 9.56	0.34	-5.35	5.41
		-75.06	12.80	5.49		
		-11.85	-129.08	4.52		
		8.96	-40.97	3.81		
6053	-1310852.27	4.63	311257.54	4.53	-6213276.48	4.33
	-77 50 41.09	0.15	166 38 33.62	0.69	-51.41	4.19
		22.34	157.08	4.95		
		-11.26	-117.61	4.48		
		-64.71	127.48	4.02		

TABLE 8.14.—*(Cont'd)*

6055	6118334.19	2.35	-1571748.31	2.34	-878596.53	2.82
	- 7 58 15.04	0.09	345 35 33.84	0.08	53.25	2.29
		-12.50	3.22	2.82		
		31.06	85.55	2.51		
		-55.98	112.39	2.16		
6059	-5885333.51	2.71	-2448379.00	2.86	221671.07	3.84
	2 0 18.41	0.13	202 35 16.72	0.09	24.95	2.72
		8.72	16.80	3.94		
		18.01	-76.05	2.75		
		-69.86	-48.46	2.68		
6060	-4751649.95	3.27	2792058.10	3.27	-3200163.95	3.66
	-30 18 34.11	0.12	149 33 41.79	0.13	233.02	2.79
		-4.36	32.86	3.85		
		-15.01	-58.31	3.55		
		-74.34	138.63	2.72		
6061	2999915.62	3.66	-2219369.35	5.66	-5155245.98	5.32
	-54 17 1.10	0.15	323 30 20.06	0.31	-6.94	4.39
		13.73	125.85	6.13		
		-43.95	49.47	5.02		
		42.82	22.76	3.30		
6063	5884467.41	1.73	-1853495.77	2.05	1612855.09	2.46
	14 44 42.44	0.08	342 30 59.62	0.07	29.43	1.65
		6.88	-5.34	2.47		
		5.69	85.35	2.11		
		81.06	-145.36	1.63		
6064	6023386.68	2.73	1617931.85	2.59	1331733.18	3.24
	12 7 54.86	0.11	15 2 6.83	0.09	273.97	2.73
		-2.20	-0.39	3.27		
		80.49	76.34	2.73		
		-9.25	89.97	2.55		

TABLE 8.14.—*(Cont'd)*

6065	4213564.60	2.02	820829.99	2.44	4702784.39	2.35
	47 48 4.49	0.08	11 1 24.71	0.12	959.58	1.86
		8.80	-34.04	2.69		
		14.81	58.31	2.25		
		72.67	-153.77	1.80		
6066	-5858571.20	2.14	1394466.40	2.60	2093846.01	3.17
	19 17 29.45	0.10	166 36 41.39	0.09	21.23	2.30
		18.20	3.07	3.17		
		17.08	-92.72	2.60		
		-64.61	-43.07	2.14		
6067	5186397.12	2.08	-3653933.25	2.15	-654276.92	2.61
	- 5 55 38.70	0.09	324 50 4.00	0.07	3.57	1.96
		-10.64	5.08	2.62		
		5.06	94.12	2.28		
		78.19	-20.94	1.93		
6068	5084830.42	2.99	2670341.23	2.93	-2768095.23	4.18
	-25 52 59.53	0.14	27 42 23.71	0.11	1516.09	2.77
		-11.23	1.97	4.26		
		17.98	-84.34	3.13		
		68.59	61.55	2.64		
6069	4978421.74	6.50	-1086874.04	6.44	-3823167.78	8.08
	-37 3 53.78	0.26	347 41 4.53	0.27	18.79	6.22
		-16.86	-0.53	8.33		
		25.74	81.06	6.81		
		58.51	-60.86	5.76		
6072	-941702.05	5.74	5967455.05	3.96	2039311.64	4.25
	18 46 10.71	0.13	98 58 3.66	0.19	257.21	4.26
		-0.82	-73.76	5.83		
		59.89	14.83	4.46		
		30.10	-163.28	3.57		

TABLE 8.14.—*(Cont'd)*

6073	1905134.13	3.43	6032282.45	3.72	-810732.67	4.19
	- 7 21 6.70	0.14	72 28 21.65	0.12	-92.21	3.62
		-15.47	-13.67	4.23		
		44.62	60.49	3.76		
		41.30	-89.60	3.34		
6075	3602820.62	3.75	5238240.67	3.58	-515948.29	4.02
	- 4 40 14.71	0.13	55 28 48.41	0.12	518.71	3.77
		-29.52	-18.96	4.24		
		43.81	-76.08	3.77		
		31.83	50.46	3.30		
6078	-5952303.44	9.70	1231904.93	8.02	-1925972.50	12.38
	-17 41 31.46	0.46	168 18 25.18	0.26	79.53	7.18
		18.89	-8.89	15.06		
		-12.67	-94.48	7.43		
		-66.98	27.46	5.44		
6111	-2448853.28	2.56	-4667985.83	2.11	3582754.93	2.36
	34 22 54.30	0.08	242 19 5.62	0.11	2251.54	1.73
		5.18	77.41	2.75		
		7.60	-13.29	2.47		
		-80.79	21.41	1.70		
6123	-1881799.41	4.61	-812438.96	4.39	6019590.66	4.46
	71 18 47.70	0.14	203 21 5.60	0.50	4.04	4.21
		-1.38	62.03	5.25		
		53.91	-26.08	4.55		
		-36.05	-28.97	3.49		
6134	-2448907.01	2.56	-4668075.88	2.11	3582449.61	2.36
	34 22 44.21	0.08	242 19 5.40	0.11	2165.54	1.73
		5.18	77.46	2.75		
		7.59	-13.23	2.47		
		-80.79	21.45	1.71		

TABLE 8.14.—*(Cont'd)*

7036	-828486.97	3.47	-5657471.26	2.44	2816816.00	2.95
	26 22 46.30	0.09	261 40 7.52	0.13	34.35	2.53
		7.95	67.30	3.59		
		25.78	-26.56	2.81		
		-62.84	-6.90	2.43		
7037	-191291.02	2.88	-4967293.86	2.15	3983252.57	2.42
	38 53 35.51	0.09	267 47 40.64	0.12	232.83	1.82
		0.13	124.91	3.11		
		7.61	34.89	2.42		
		-82.39	35.87	1.81		
7039	2308213.41	3.31	-4873598.28	3.07	3394558.48	3.63
	32 21 49.28	0.13	295 20 34.72	0.13	-28.44	2.54
		1.38	-15.89	4.03		
		-8.95	73.90	3.32		
		80.94	82.79	2.52		
7040	2465049.46	3.69	-5534929.97	3.20	1985513.10	4.01
	18 15 28.38	0.13	294 0 23.01	0.13	-8.68	3.20
		15.92	-44.27	4.74		
		-73.82	-54.87	3.04		
		-2.82	44.92	2.87		
7043	1130708.65	2.05	-4831331.29	1.72	3994135.53	1.91
	39 1 15.36	0.07	283 10 20.04	0.09	3.15	1.52
		-2.98	141.75	2.14		
		2.53	51.88	1.99		
		-86.09	2.07	1.52		
7045	-1240470.24	4.15	-4760242.12	2.76	4048985.26	2.88
	39 38 47.63	0.10	255 23 38.90	0.18	1767.76	2.11
		-0.61	100.02	4.32		
		4.15	10.07	3.16		
		-85.80	1.71	2.11		

TABLE 8.14.—*(Cont'd)*

7072	976261.31	2.15	-5601399.89	1.82	2880241.91	2.26
	27 1 14.12	0.07	279 53 12.13	0.08	-30.55	1.75
		7.46	-28.42	2.39		
		-0.71	61.49	2.09		
		-82.50	-33.92	1.74		
7075	692620.68	3.74	-4347076.48	3.81	4600475.43	3.45
	46 27 20.82	0.15	279 3 10.28	0.18	230.94	2.27
		-2.83	13.39	4.61		
		-1.69	103.47	3.75		
		86.71	44.29	2.26		
7076	1384158.71	4.13	-5905662.00	4.44	1966545.66	5.31
	18 4 34.63	0.17	283 11 26.83	0.14	410.95	4.55
		19.91	-26.78	5.59		
		-67.02	4.56	4.42		
		11.01	67.26	3.76		
8009	3923397.43	8.48	299869.39	10.07	5002975.49	6.86
	52 0 6.51	0.34	4 22 14.44	0.52	44.12	3.84
		-0.72	139.13	11.46		
		-5.58	49.06	8.65		
		84.37	56.47	3.76		
8010	4331306.98	5.71	567490.82	8.28	4633108.30	5.44
	46 52 36.97	0.25	7 27 51.89	0.39	920.89	2.26
		-0.12	119.88	8.51		
		0.46	-150.12	7.30		
		89.52	43.97	2.26		
8011	3920153.49	8.86	-134804.48	14.27	5012734.75	6.95
	52 8 36.27	0.34	358 1 49.85	0.76	138.88	3.84
		-0.31	115.65	15.38		
		2.38	-154.37	8.90		
		87.60	32.94	3.83		

TABLE 8.14.—*(Cont'd)*

8015	4578322.11	4.19	457936.54	8.00	4403195.29	4.38
	43 55 57.85	0.19	5 42 42.79	0.35	679.03	2.23
		-0.72	109.93	8.21		
		-1.37	19.91	5.33		
		88.46	47.83	2.23		
8019	4579463.17	4.12	586573.52	7.91	4386419.17	4.31
	43 43 33.30	0.18	7 17 56.93	0.35	394.39	2.17
		0.08	110.52	8.11		
		-1.33	20.52	5.26		
		88.67	16.92	2.17		
8030	4205626.92	6.46	163683.38	9.66	4776540.59	5.80
	48 48 22.24	0.27	2 13 43.79	0.47	182.83	2.37
		-1.15	117.70	10.06		
		1.18	-152.32	7.88		
		88.35	72.00	2.35		
9001	-1535750.66	4.17	-5167014.38	2.81	3401039.43	2.70
	32 25 24.39	0.08	253 26 48.80	0.17	1623.61	2.65
		1.24	98.65	4.42		
		59.41	6.55	2.75		
		-30.56	9.38	2.33		
9002	5056108.42	3.01	2716508.67	2.98	-2775768.77	4.21
	-25 57 36.39	0.14	28 14 52.52	0.11	1536.20	2.77
		-10.82	2.06	4.31		
		-15.92	95.19	3.18		
		70.59	59.23	2.66		
9004	5105581.46	3.42	-555271.46	9.96	3769675.97	3.97
	36 27 46.88	0.15	353 47 34.93	0.40	51.52	2.82
		-6.73	87.80	9.97		
		-0.33	-2.24	4.54		
		83.26	84.99	2.58		

TABLE 8.14.—*(Cont'd)*

9005	-3946730.47	9.20	3366286.15	8.99	3698822.94	7.51
	35 40 22.02	0.27	139 32 17.28	0.45	94.06	5.29
		-1.55	-79.69	11.28		
		3.04	10.23	8.18		
		86.58	-142.70	5.27		
9006	1018164.52	12.37	5471108.70	5.48	3109625.60	5.96
	29 21 34.71	0.19	79 27 28.60	0.47	1861.67	4.96
		-2.35	-91.67	12.60		
		14.93	-2.29	6.00		
		74.88	-172.95	4.86		
9007	1942760.95	2.50	-5804088.24	2.88	-1796900.88	4.38
	-16 27 56.11	0.15	288 30 23.66	0.09	2469.27	2.72
		-2.85	-8.78	4.50		
		-78.35	95.21	2.72		
		11.28	80.65	2.48		
9008	3376875.17	6.75	4403976.17	6.11	3136257.32	6.09
	29 38 13.87	0.20	52 31 11.20	0.29	1553.30	4.75
		5.39	-74.43	7.81		
		8.26	16.35	6.08		
		80.12	162.78	4.69		
9009	2251810.73	2.40	-5816917.57	2.07	1327163.44	3.37
	12 5 24.93	0.11	291 9 43.64	0.08	-34.94	2.02
		8.42	-21.00	3.50		
		-6.32	68.06	2.29		
		-79.44	-58.40	1.97		
9010	976276.17	2.14	-5601402.23	1.81	2880234.50	2.26
	27 1 13.84	0.07	279 53 12.65	0.08	-29.59	1.74
		7.47	-27.81	2.38		
		-0.22	62.16	2.07		
		-82.52	-29.48	1.73		

TABLE 8.14.—*(Cont'd)*

9011	2280575.30	2.37	-4914580.22	2.72	-3355383.71	3.70
	-31 56 34.20	0.12	294 53 35.94	0.09	606.19	2.56
		-11.45	-2.47	3.84		
		-54.53	104.05	2.55		
		33.04	79.96	2.34		
9012	-5466067.81	3.04	-2404312.68	2.92	2242188.45	3.35
	20 42 25.91	0.10	203 44 34.24	0.11	3059.03	2.87
		7.79	42.85	3.82		
		-62.21	117.81	2.96		
		-26.49	-43.24	2.38		
9021	-1936789.30	7.11	-5077714.74	5.34	3331922.70	5.30
	31 41 2.94	0.19	249 7 18.06	0.30	2349.90	3.25
		0.72	113.76	8.28		
		1.22	23.74	5.30		
		-88.58	54.04	3.25		
9028	4903726.56	2.06	3965206.29	2.10	963859.55	2.88
	8 44 51.11	0.09	38 57 33.76	0.07	1866.93	1.96
		2.55	-0.59	2.89		
		-0.88	89.37	2.18		
		87.31	160.38	1.95		
9029	5186441.45	2.14	-3653871.87	2.22	-654314.14	2.67
	- 5 55 39.91	0.09	324 50 6.46	0.08	8.29	2.02
		-10.14	5.92	2.68		
		4.56	95.10	2.34		
		78.86	-18.80	2.00		
9031	1693797.28	8.28	-4112353.08	8.75	-4556621.98	11.18
	-45 53 11.72	0.43	292 23 8.87	0.33	177.97	6.32
		-6.68	10.74	13.68		
		8.70	99.71	6.73		
		-79.00	137.78	6.15		

TABLE 8.14.—*(Cont'd)*

9051	4606861.50	4.19	2029692.20	10.29	3903562.20	4.42
	37 58 37.26	0.18	23 46 38.43	0.41	192.42	3.34
		6.15	108.28	10.52		
		-2.74	18.58	4.72		
		83.26	-47.49	3.15		
9091	4595158.88	4.16	2039417.60	10.27	3912670.58	4.39
	38 4 45.20	0.18	23 55 57.16	0.41	471.05	3.31
		6.26	108.39	10.51		
		-2.72	18.69	4.69		
		83.17	-47.93	3.12		
9424	-1264831.95	4.75	-3466915.40	5.54	5185450.92	4.32
	54 44 33.04	0.21	249 57 23.60	0.27	669.87	2.39
		0.79	-7.27	6.60		
		-0.26	82.73	4.76		
		89.17	154.71	2.39		
9425	-2450012.65	2.64	-4624431.57	2.17	3635036.58	2.43
	34 57 50.43	0.08	242 5 7.68	0.11	752.76	1.78
		4.51	76.25	2.83		
		7.40	-14.34	2.56		
		-81.32	17.38	1.75		
9426	3121261.30	8.63	592605.66	9.36	5512722.95	5.77
	60 12 39.83	0.34	10 45 1.00	0.58	588.48	2.46
		-0.81	151.36	11.01		
		1.29	61.38	8.25		
		88.47	-150.80	2.44		
9427	-6007428.66	8.87	-1111852.47	19.80	1825733.94	8.62
	16 44 38.39	0.30	190 29 8.26	0.71	25.36	5.10
		4.74	-111.38	22.43		
		51.86	-15.32	5.30		
		-37.74	-25.05	3.72		

TABLE 8.14.—*(Cont'd)*

9431	3183897.57	12.32	1421426.70	9.36	5322814.69	7.01
	56 56 55.73	0.39	24 3 28.83	0.69	8.09	2.38
		-0.46	-137.19	14.53		
		-0.58	132.81	8.47		
		89.27	171.15	2.38		
9432	3907419.17	7.93	1602378.59	10.36	4763922.08	5.86
	48 38 2.34	0.27	22 17 52.28	0.55	202.70	2.44
		-0.06	75.84	11.46		
		-0.05	165.84	8.19		
		89.92	116.63	2.44		

TABLE 8.15.—*Station-to-Station Correlation Coefficients $\rho_{ij} > 0.75$ (Solution WN14)*

* STA.NO.3106 WITH STA.NO.4061		
0.952	0.143	-0.121
0.141	0.942	-0.130
-0.116	-0.128	0.963
* STA.NO.3406 WITH STA.NO.9009		
0.971	0.156	-0.290
0.157	0.961	-0.057
-0.292	-0.058	0.985
* STA.NO.3413 WITH STA.NO.6067		
0.962	0.157	-0.021
0.157	0.965	0.047
-0.022	0.048	0.976
STA.NO.3476 WITH STA.NO.5712		
0.857	0.120	-0.103
0.119	0.838	-0.014
-0.088	0.008	0.923
* STA.NO.3499 WITH STA.NO.6009		
1.000	0.107	0.063
0.107	1.000	-0.184
0.063	-0.184	1.000
* STA.NO.4050 WITH STA.NO.6068		
0.910	-0.124	0.178
-0.125	0.908	0.139
0.175	0.138	0.952
STA.NO.4082 WITH STA.NO.9010		
0.741	0.022	-0.113
0.020	0.662	0.159
-0.102	0.161	0.756
STA.NO.5001 WITH STA.NO.5907		
0.844	0.307	0.313
-0.059	0.761	0.497
0.420	0.643	0.806
STA.NO.5001 WITH STA.NO.5915		
0.767	0.306	0.395
-0.225	0.565	0.477
0.273	0.657	0.777
STA.NO.5410 WITH STA.NO.5730		
0.778	0.133	0.098
-0.099	0.746	-0.064
0.129	-0.069	0.814
STA.NO.5410 WITH STA.NO.6012		
0.695	0.116	0.091
-0.079	0.699	-0.066
0.114	-0.072	0.778
STA.NO.5712 WITH STA.NO.5912		
0.686	-0.002	-0.118
-0.112	0.489	0.045
0.132	0.104	0.809
STA.NO.5713 WITH STA.NO.5715		
0.591	0.189	-0.331
0.216	0.772	0.013
-0.340	0.075	0.651

* STA.NO.3405 WITH STA.NO.4081		
0.939	0.119	0.029
0.119	0.946	0.037
0.041	0.034	0.957
STA.NO.3413 WITH STA.NO.5735		
0.853	0.145	-0.040
0.138	0.861	0.038
-0.064	0.032	0.905
* STA.NO.3413 WITH STA.NO.9029		
0.926	0.154	-0.019
0.153	0.930	0.047
-0.018	0.047	0.952
* STA.NO.3476 WITH STA.NO.6008		
0.964	0.129	-0.107
0.129	0.958	-0.021
-0.107	-0.019	0.980
* STA.NO.3648 WITH STA.NO.5648		
0.987	0.275	0.002
0.273	0.973	0.617
0.003	0.617	0.987
STA.NO.4050 WITH STA.NO.9002		
0.931	-0.126	0.180
-0.127	0.930	0.140
0.180	0.142	0.963
* STA.NO.4740 WITH STA.NO.7039		
0.940	0.060	-0.281
0.061	0.931	0.290
-0.275	0.283	0.951
STA.NO.5001 WITH STA.NO.5911		
0.809	-0.055	0.314
0.108	0.857	0.273
0.237	0.320	0.784
STA.NO.5201 WITH STA.NO.6003		
0.899	-0.019	0.156
-0.023	0.890	0.083
0.155	0.080	0.912
STA.NO.5410 WITH STA.NO.5941		
0.716	-0.259	0.136
0.052	0.755	-0.016
0.253	-0.044	0.834
STA.NO.5410 WITH STA.NO.6066		
0.695	0.116	0.091
-0.079	0.698	-0.066
0.113	-0.072	0.777
* STA.NO.5712 WITH STA.NO.6008		
0.889	0.119	-0.088
0.121	0.875	0.008
-0.103	-0.012	0.941
* STA.NO.5713 WITH STA.NO.5739		
0.994	0.206	-0.250
0.207	0.995	0.015
-0.250	0.016	0.996

*$\rho_{ij} > 0.925$

TABLE 8.15.—*(Cont'd)*

STA.NO.5713 WITH STA.NO.5924

0.797	0.126	-0.275
0.329	0.565	-0.063
-0.272	0.067	0.491

STA.NO.5715 WITH STA.NO.5736

0.412	0.240	0.121
0.145	0.765	-0.031
0.142	0.017	0.699

STA.NO.5715 WITH STA.NO.5925

0.642	0.116	-0.022
0.131	0.722	0.020
-0.036	-0.023	0.784

STA.NO.5717 WITH STA.NO.5720

0.649	-0.180	-0.032
0.019	0.751	0.015
0.029	-0.085	0.776

*STA.NO.5720 WITH STA.NO.6042

0.932	-0.096	-0.062
-0.097	0.934	-0.054
-0.060	-0.056	0.965

STA.NO.5721 WITH STA.NO.5923

0.855	0.133	-0.194
-0.128	0.814	-0.260
-0.194	-0.320	0.715

STA.NO.5723 WITH STA.NO.5726

0.821	0.057	-0.000
0.300	0.713	0.027
0.008	0.035	0.782

STA.NO.5723 WITH STA.NO.5931

0.897	-0.121	-0.057
0.186	0.863	0.018
-0.062	0.075	0.891

STA.NO.5726 WITH STA.NO.5930

0.899	0.307	-0.024
0.044	0.773	0.127
-0.119	0.083	0.831

STA.NO.5726 WITH STA.NO.5933

0.755	0.153	-0.118
0.234	0.710	0.149
-0.082	0.142	0.822

STA.NO.5726 WITH STA.NO.5935

0.865	0.108	-0.093
0.291	0.751	0.004
-0.024	-0.072	0.831

*STA.NO.5726 WITH STA.NO.6047

0.909	0.169	-0.056
0.171	0.903	0.101
-0.052	0.096	0.951

*STA.NO.5730 WITH STA.NO.6012

0.890	-0.029	0.015
-0.023	0.926	-0.018
0.008	-0.016	0.950

STA.NO.5713 WITH STA.NO.6007

0.886	0.190	-0.253
0.204	0.904	0.002
-0.244	0.014	0.921

STA.NO.5715 WITH STA.NO.5739

0.593	0.215	-0.340
0.190	0.770	0.075
-0.330	0.015	0.650

STA.NO.5715 WITH STA.NO.6063

0.838	0.194	-0.123
0.183	0.901	0.002
-0.117	-0.004	0.918

STA.NO.5717 WITH STA.NO.6042

0.610	-0.176	-0.033
0.007	0.706	0.010
0.022	-0.082	0.751

*STA.NO.5720 WITH STA.NO.9028

0.931	-0.095	-0.062
-0.095	0.934	-0.054
-0.060	-0.055	0.965

*STA.NO.5721 WITH STA.NO.6015

0.892	-0.068	-0.151
-0.074	0.899	-0.256
-0.154	-0.246	0.931

STA.NO.5723 WITH STA.NO.5930

0.817	0.191	-0.044
0.183	0.702	0.105
-0.039	-0.034	0.820

STA.NO.5723 WITH STA.NO.6047

0.750	0.057	-0.001
0.278	0.646	0.025
0.004	0.031	0.745

STA.NO.5726 WITH STA.NO.5931

0.838	0.179	0.002
0.149	0.711	-0.008
0.010	0.034	0.823

STA.NO.5726 WITH STA.NO.5934

0.792	0.109	-0.126
0.337	0.762	0.051
-0.055	0.104	0.806

*STA.NO.5726 WITH STA.NO.5937

0.962	0.132	-0.086
0.246	0.870	0.062
-0.050	0.044	0.893

STA.NO.5730 WITH STA.NO.5935

0.772	0.129	0.084
-0.030	0.905	-0.112
0.033	-0.067	0.782

*STA.NO.5730 WITH STA.NO.6066

0.889	-0.029	0.015
-0.023	0.925	-0.018
0.008	-0.017	0.950

TABLE 8.15.—*(Cont'd)*

STA.NO.5732 WITH STA.NO.5733		
0.627	−0.199	0.084
0.003	0.780	−0.301
−0.160	−0.125	0.790
STA.NO.5732 WITH STA.NO.6059		
0.582	−0.187	0.075
0.000	0.731	−0.294
−0.153	−0.129	0.764
* STA.NO.5733 WITH STA.NO.6059		
0.933	−0.018	−0.000
−0.021	0.940	−0.217
−0.001	−0.219	0.966
STA.NO.5735 WITH STA.NO.5736		
0.763	0.058	0.028
0.258	0.804	0.049
−0.029	−0.049	0.760
STA.NO.5735 WITH STA.NO.9029		
0.853	0.136	−0.064
0.142	0.861	0.033
−0.038	0.040	0.905
STA.NO.5739 WITH STA.NO.5924		
0.801	0.125	−0.274
0.329	0.564	−0.062
−0.271	0.067	0.491
STA.NO.5744 WITH STA.NO.5923		
0.926	0.015	−0.291
0.158	0.932	−0.228
−0.307	−0.199	0.812
STA.NO.5744 WITH STA.NO.6016		
0.868	0.132	−0.337
0.117	0.903	−0.167
−0.315	−0.168	0.909
STA.NO.5907 WITH STA.NO.5915		
0.902	0.387	0.458
0.120	0.859	0.717
0.203	0.793	0.894
STA.NO.5912 WITH STA.NO.6008		
0.600	−0.085	0.120
0.005	0.422	0.094
−0.127	0.019	0.762
STA.NO.5923 WITH STA.NO.6016		
0.810	0.156	−0.306
0.036	0.849	−0.197
−0.275	−0.224	0.750
STA.NO.5930 WITH STA.NO.6047		
0.816	0.044	−0.113
0.281	0.697	0.081
−0.022	0.115	0.792
STA.NO.5931 WITH STA.NO.5937		
0.794	0.119	0.065
0.237	0.562	−0.034
0.006	−0.029	0.681
STA.NO.5732 WITH STA.NO.5938		
0.750	0.043	−0.071
−0.298	0.814	−0.070
0.041	−0.276	0.760
STA.NO.5733 WITH STA.NO.5941		
0.751	−0.061	0.146
−0.041	0.765	−0.231
−0.111	−0.060	0.886
* STA.NO.5734 WITH STA.NO.6004		
0.934	−0.281	0.046
−0.287	0.954	−0.158
0.055	−0.153	0.967
* STA.NO.5735 WITH STA.NO.6067		
0.887	0.139	−0.067
0.146	0.893	0.033
−0.043	0.041	0.928
* STA.NO.5736 WITH STA.NO.6055		
0.911	0.137	−0.038
0.130	0.911	0.045
−0.037	0.038	0.938
STA.NO.5739 WITH STA.NO.6007		
0.880	0.190	−0.253
0.203	0.899	0.002
−0.243	0.013	0.917
STA.NO.5744 WITH STA.NO.5924		
0.849	0.155	−0.313
0.044	0.750	−0.074
−0.390	−0.110	0.624
STA.NO.5907 WITH STA.NO.5911		
0.763	−0.202	0.425
0.236	0.608	0.573
0.250	0.409	0.599
STA.NO.5911 WITH STA.NO.5912		
0.587	0.116	0.367
−0.329	0.273	0.150
−0.040	0.288	0.802
STA.NO.5923 WITH STA.NO.6015		
0.793	−0.117	−0.195
0.107	0.746	−0.316
−0.204	−0.250	0.689
STA.NO.5930 WITH STA.NO.5937		
0.822	0.102	−0.153
0.370	0.584	0.065
−0.015	0.075	0.708
STA.NO.5931 WITH STA.NO.5935		
0.798	0.033	0.078
0.232	0.560	−0.063
−0.005	−0.085	0.645
STA.NO.5931 WITH STA.NO.6047		
0.767	0.140	0.009
0.168	0.645	0.032
0.000	−0.005	0.782

TABLE 8.15.—*(Cont'd)*

STA.NO.5933 WITH STA.NO.5934

0.845	-0.031	-0.179
0.174	0.837	0.005
-0.093	0.066	0.853

STA.NO.5933 WITH STA.NO.5938

0.743	-0.118	-0.180
0.194	0.786	-0.048
-0.056	0.091	0.731

STA.NO.5934 WITH STA.NO.5935

0.807	0.168	-0.133
0.155	0.816	0.018
-0.072	-0.052	0.899

STA.NO.5934 WITH STA.NO.5938

0.905	-0.044	-0.149
0.107	0.925	-0.025
-0.102	0.052	0.893

STA.NO.5935 WITH STA.NO.5937

0.920	0.187	-0.025
0.097	0.884	-0.076
-0.079	-0.025	0.881

STA.NO.5935 WITH STA.NO.6012

0.682	-0.026	0.026
0.113	0.839	-0.072
0.057	-0.106	0.737

STA.NO.5935 WITH STA.NO.6066

0.682	-0.026	0.026
0.113	0.839	-0.072
0.057	-0.106	0.737

STA.NO.5941 WITH STA.NO.6059

0.709	-0.043	-0.107
-0.066	0.724	-0.065
0.135	-0.231	0.858

STA.NO.6011 WITH STA.NO.6059

0.441	-0.254	0.002
-0.133	0.756	-0.158
0.037	-0.277	0.219

★STA.NO.6012 WITH STA.NO.6066

0.999	-0.026	0.004
-0.025	0.999	-0.021
0.004	-0.021	0.999

★STA.NO.6019 WITH STA.NO.9011

0.970	-0.027	0.120
-0.024	0.977	-0.254
0.117	-0.256	0.987

STA.NO.6031 WITH STA.NO.6060

0.847	0.311	-0.166
0.385	0.605	-0.137
-0.108	0.021	0.634

STA.NO.6038 WITH STA.NO.6134

0.808	-0.179	0.211
-0.052	0.293	-0.032
0.167	-0.112	0.233

STA.NO.5933 WITH STA.NO.5937

0.754	0.141	-0.169
0.190	0.678	0.113
-0.110	0.079	0.783

STA.NO.5933 WITH STA.NO.6047

0.682	0.212	-0.077
0.139	0.639	0.137
-0.102	0.138	0.782

STA.NO.5934 WITH STA.NO.5937

0.856	0.216	-0.113
0.102	0.863	0.075
-0.124	0.015	0.857

STA.NO.5934 WITH STA.NO.6047

0.718	0.304	-0.052
0.103	0.688	0.103
-0.108	0.052	0.765

STA.NO.5935 WITH STA.NO.5938

0.583	0.099	-0.093
0.192	0.669	-0.047
-0.158	0.074	0.780

STA.NO.5935 WITH STA.NO.6047

0.792	0.266	-0.023
0.103	0.682	-0.065
-0.079	0.009	0.789

STA.NO.5937 WITH STA.NO.6047

0.876	0.225	-0.048
0.125	0.787	0.045
-0.074	0.060	0.849

★STA.NO.6002 WITH STA.NO.7043

0.959	0.030	-0.116
0.031	0.943	0.264
-0.116	0.264	0.954

★STA.NO.6011 WITH STA.NO.9012

0.981	-0.242	0.114
-0.242	0.980	-0.365
0.116	-0.365	0.985

STA.NO.6016 WITH STA.NO.6065

0.697	0.106	-0.407
0.077	0.790	-0.227
-0.436	-0.240	0.686

STA.NO.6023 WITH STA.NO.6060

0.829	0.329	-0.199
0.283	0.802	0.039
-0.267	-0.095	0.707

STA.NO.6038 WITH STA.NO.6111

0.807	-0.180	0.211
-0.052	0.292	-0.031
0.167	-0.111	0.233

STA.NO.6038 WITH STA.NO.9425

0.770	-0.177	0.208
-0.054	0.270	-0.025
0.162	-0.099	0.220

TABLE 8.15.—*(Cont'd)*

★STA.NO.6042 WITH STA.NO.9028		
0.965	-0.102	-0.060
-0.102	0.966	-0.057
-0.060	-0.055	0.982
★STA.NO.6067 WITH STA.NO.9029		
0.962	0.155	-0.022
0.154	0.965	0.049
-0.019	0.049	0.976
★STA.NO.6111 WITH STA.NO.6134		
0.999	-0.312	0.157
-0.312	0.999	0.187
0.157	0.187	0.999
STA.NO.6134 WITH STA.NO.9425		
0.953	-0.304	0.158
-0.308	0.932	0.191
0.159	0.195	0.945
STA.NO.8009 WITH STA.NO.8010		
0.619	0.149	-0.610
0.047	0.794	-0.168
-0.593	-0.217	0.602
STA.NO.8009 WITH STA.NO.8019		
0.551	0.173	-0.550
0.092	0.777	-0.242
-0.537	-0.232	0.564
STA.NO.8010 WITH STA.NO.8019		
0.726	0.085	-0.682
0.079	0.936	-0.303
-0.701	-0.261	0.768
STA.NO.8015 WITH STA.NO.8030		
0.591	0.125	-0.561
0.124	0.787	-0.186
-0.560	-0.273	0.592
STA.NO.8019 WITH STA.NO.8030		
0.578	0.123	-0.551
0.118	0.779	-0.179
-0.553	-0.274	0.581
STA.NO.9004 WITH STA.NO.9051		
0.551	0.197	-0.518
0.305	0.136	-0.224
-0.263	-0.433	0.812
STA.NO.9004 WITH STA.NO.9426		
0.322	-0.003	-0.267
0.460	0.811	-0.538
-0.264	-0.131	0.277
★STA.NO.9051 WITH STA.NO.9091		
0.990	-0.299	-0.208
-0.301	0.998	-0.383
-0.207	-0.381	0.991
STA.NO.9051 WITH STA.NO.9432		
0.598	-0.196	-0.530
-0.470	0.809	0.047
-0.151	-0.334	0.371
STA.NO.9091 WITH STA.NO.9432		
0.602	-0.196	-0.533
-0.471	0.810	0.047
-0.152	-0.335	0.374
STA.NO.6050 WITH STA.NO.6061		
0.109	-0.358	0.106
0.222	0.840	-0.153
-0.116	-0.438	0.314
★STA.NO.6068 WITH STA.NO.9002		
0.977	-0.125	0.175
-0.125	0.977	0.140
0.177	0.142	0.988
★STA.NO.6111 WITH STA.NO.9425		
0.954	-0.304	0.158
-0.308	0.933	0.191
0.159	0.195	0.946
★STA.NO.7072 WITH STA.NO.9010		
0.964	0.034	-0.140
0.035	0.949	0.156
-0.141	0.157	0.967
STA.NO.8009 WITH STA.NO.8015		
0.545	0.182	-0.545
0.095	0.778	-0.236
-0.532	-0.242	0.559
STA.NO.8010 WITH STA.NO.8015		
0.717	0.093	-0.679
0.083	0.931	-0.296
-0.695	-0.268	0.762
★STA.NO.8015 WITH STA.NO.8019		
0.950	0.095	-0.707
0.098	0.986	-0.321
-0.709	-0.310	0.954
STA.NO.8015 WITH STA.NO.9004		
0.593	0.386	-0.335
0.059	0.788	-0.313
-0.436	-0.532	0.556
STA.NO.8019 WITH STA.NO.9004		
0.615	0.391	-0.328
0.064	0.786	-0.322
-0.437	-0.540	0.581
STA.NO.9004 WITH STA.NO.9091		
0.555	0.198	-0.521
0.307	0.137	-0.225
-0.264	-0.433	0.818
STA.NO.9007 WITH STA.NO.9011		
0.752	-0.080	0.167
-0.006	0.376	-0.049
0.058	0.051	0.512
STA.NO.9051 WITH STA.NO.9431		
0.540	-0.152	-0.528
-0.523	0.826	0.283
-0.102	-0.354	0.250
STA.NO.9091 WITH STA.NO.9431		
0.543	-0.152	-0.531
-0.523	0.828	0.283
-0.103	-0.355	0.252
STA.NO.9431 WITH STA.NO.9432		
0.808	-0.451	-0.617
-0.373	0.847	-0.085
-0.750	0.180	0.721

TABLE 8.16.—*Station Correlation Coefficients $\rho_{ij} > 0.75$ (Solution WN14)*

* STA.NO.1032			STA.NO.3478		
1.000	0.967	0.779	1.000	0.875	-0.919
0.967	1.000	0.880	0.875	1.000	-0.837
0.779	0.880	1.000	-0.919	-0.837	1.000
STA.NO.3902			STA.NO.8010		
1.000	-0.155	0.087	1.000	0.027	-0.817
-0.155	1.000	0.813	0.027	1.000	-0.206
0.087	0.813	1.000	-0.817	-0.206	1.000
STA.NO.8011			STA.NO.8030		
1.000	0.408	-0.752	1.000	0.139	-0.845
0.408	1.000	-0.382	0.139	1.000	-0.241
-0.752	-0.382	1.000	-0.845	-0.241	1.000
STA.NO.9426			STA.NO.9427		
1.000	0.230	-0.857	1.000	-0.858	0.636
0.230	1.000	-0.353	-0.858	1.000	-0.813
-0.857	-0.353	1.000	0.636	-0.813	1.000
STA.NO.9431					
1.000	-0.441	-0.870			
-0.441	1.000	0.129			
-0.870	0.129	1.000			

*$\rho_{ij} > 0.925$

TABLE 8.17.—*Chord Length Comparisons (Solutions WN12, WN14, and WN16)*

		Adjusted—given length					
		WN12		WN14		WN16	
Type	Line	m	ppM	m	ppM	m	ppM
EDM	6002–6003	8.3 ± 2.5	2.38	2.7 ± 2.3	0.78	5.9 ± 3.0	1.70
	6003–6111	2.7 ± 1.4	1.90	2.3 ± 1.4	1.60	11.4 ± 3.1	8.00
	6006–6065	7.7 ± 2.1	3.13	6.1 ± 2.0	2.47	19.9 ± 3.5	8.13
	6016–6065	−2.8 ± 1.3	2.30	−2.9 ± 1.3	2.47	−18.9 ± 3.4	15.87
	6006–6016	2.7 ± 2.2	0.77	1.3 ± 2.1	0.37	1.6 ± 3.3	0.46
	6063–6064	13.7 ± 2.4	3.94	10.6 ± 2.3	3.03	15.2 ± 2.8	4.37
	6023–6060	7.9 ± 3.1	3.42	5.9 ± 3.0	2.55	9.6 ± 3.8	4.16
	[a]6032–6060	−2.4 ± 3.9	0.76	−4.5 ± 3.6	1.42	−2.9 ± 3.7	0.92
	3861–7043	2.2 ± 1.8	1.44	1.5 ± 1.8	0.99	7.6 ± 3.7	5.00
C-band	[a]4082–4050	26.5 ± 6.9	2.42	−5.2 ± 3.9	0.48	−4.2 ± 4.0	0.39
	4082–4740	2.0 ± 2.7	1.25	1.3 ± 2.7	1.90	6.6 ± 5.0	4.13
	4082–4081	3.0 ± 2.3	2.40	2.3 ± 2.3	0.79	17.9 ± 6.2	14.49
	4082–4061	−0.4 ± 3.6	0.19	−1.5 ± 3.6	0.65	2.1 ± 6.1	0.93
Average	EDM		2.22		1.74		5.40
	C-band		1.56		0.96		4.98
	All		2.02		1.50		5.27

[a] Not constrained in WN12 and WN14.

TABLE 8.18.—*Standard Deviation Comparisons (Solutions WN12, WN14, and WN16)*[a]

	Constituent Networks								WN_i	
	BC		SECOR		MPS		SA			
Solution	σ	σ_h	σ	σ_h	σ	σ_h	σ	σ_h	σ	σ_h
WN12	4.4	5.0	4.2	4.8	6.9	7.6	5.2	5.9	5.5	6.2
WN14	3.5	3.2	2.8	2.4	4.8	2.9	4.1	3.0	3.9	2.9
WN16	3.5	3.2	2.8	2.4	4.9	2.9	4.1	3.0	4.0	2.9

[a] All units in meters.

TABLE 8.19.—*Transformation: WN14 – WN16*

SCALE FACTOR AND ROTATION PARAMETERS CONSTRAINED

SOLUTION FOR 3 TRANSLATION, 1 SCALE AND 3 ROTATION PARAMETERS

(USING VARIANCES ONLY)

DU METERS	DV METERS	DW METERS	DELTA (X1.D+6)	OMEGA SECONDS	PSI SECONDS	EPSILON SECONDS
-0.08	-0.57	-0.04	-0.06	-0.00	0.00	0.01
± 0.25	± 0.25	± 0.30	± 0.00	± 0.00	± 0.00	± 0.00

VARIANCE - COVARIANCE MATRIX

σ_o^2 = 0.22

0.642D-01	0.399D-04	-0.118D-03	-0.116D-10	0.633D-10	0.186D-09	-0.356D-11
0.399D-04	0.645D-01	0.194D-03	0.159D-10	0.728D-10	-0.361D-11	-0.194D-09
-0.118D-03	0.194D-03	0.930D-01	-0.219D-10	0.682D-11	-0.102D-09	-0.147D-09
-0.116D-10	0.159D-10	-0.219D-10	0.141D-16	0.638D-20	-0.583D-20	0.272D-19
0.633D-10	0.728D-10	0.682D-11	0.638D-20	0.993D-16	-0.114D-16	0.155D-17
0.186D-09	-0.361D-11	-0.102D-09	-0.583D-20	-0.114D-16	0.140D-15	-0.343D-17
-0.356D-11	-0.194D-09	-0.147D-09	0.272D-19	0.155D-17	-0.343D-17	0.134D-15

COEFFICIENTS OF CORRELATION

0.100D+01	0.619D-03	-0.153D-02	-0.122D-01	0.251D-01	0.621D-01	-0.121D-02
0.619D-03	0.100D+01	0.250D-02	0.167D-01	0.288D-01	-0.120D-02	-0.659D-01
-0.153D-02	0.250D-02	0.100D+01	-0.191D-01	0.224D-02	-0.282D-01	-0.416D-01
-0.122D-01	0.167D-01	-0.191D-01	0.100D+01	0.170D-03	-0.131D-03	0.623D-03
0.251D-01	0.288D-01	0.224D-02	0.170D-03	0.100D+01	-0.962D-01	0.134D-01
0.621D-01	-0.120D-02	-0.282D-01	-0.131D-03	-0.962D-01	0.100D+01	-0.249D-01
-0.121D-02	-0.659D-01	-0.416D-01	0.623D-03	0.134D-01	-0.249D-01	0.100D+01

TABLE 8.19.—*(Cont'd)*

	RESIDUALS V								
	V1(WN - 16)			V2(WN - 14)			V1 - V2		
3861	0.2	-0.9	-1.6	3861	-0.2	1.0	2.6	0.4	-1.9	-4.2
4061	0.4	-0.4	-0.9	4061	-0.7	0.5	1.3	1.1	-0.9	-2.2
4081	3.2	-0.2	-3.9	4081	-6.7	0.2	7.0	9.9	-0.5	-10.9
4082	-0.9	-0.5	-0.3	4082	1.1	0.5	0.3	-1.9	-1.0	-0.5
4740	1.2	0.4	-0.5	4740	-2.1	-0.5	0.5	3.3	0.8	-1.0
6001	-0.7	0.7	-0.0	6001	0.7	-0.7	0.0	-1.5	1.4	-0.1
6002	0.5	0.4	0.5	6002	-0.6	-0.4	-0.6	1.2	0.8	1.2
6003	-0.5	1.3	1.4	6003	0.6	-1.5	-1.7	-1.0	2.8	3.1
6004	-0.2	0.4	0.5	6004	0.2	-0.4	-0.5	-0.4	0.8	1.0
6006	-1.0	0.8	0.7	6006	1.2	-0.9	-0.9	-2.1	1.7	1.5
6007	-0.1	-0.3	0.4	6007	0.1	0.3	-0.5	-0.2	-0.5	0.9
6008	0.1	-0.2	0.5	6008	-0.1	0.2	-0.5	0.1	-0.4	1.0
6009	0.1	-0.1	0.3	6009	-0.1	0.1	-0.3	0.2	-0.3	0.5
6011	-0.7	0.3	-0.5	6011	0.7	-0.3	0.5	-1.5	0.6	-1.0
6012	0.1	0.2	0.1	6012	-0.1	-0.2	-0.1	0.3	0.3	0.2
6013	0.2	-0.0	0.2	6013	-0.2	0.0	-0.2	0.4	-0.0	0.4
6015	0.2	0.2	0.4	6015	-0.2	-0.2	-0.4	0.4	0.4	0.8
6016	-0.5	0.1	1.1	6016	0.5	-0.1	-1.3	-1.1	0.1	2.4
6019	0.1	-0.5	0.5	6019	-0.1	0.5	-0.5	0.1	-1.0	1.0
6020	-0.7	-0.3	0.5	6020	0.7	0.3	-0.5	-1.4	-0.6	1.0
6022	-0.1	-0.0	0.6	6022	0.1	0.0	-0.6	-0.2	-0.0	1.1
6023	-0.1	-0.0	1.3	6023	0.1	0.0	-1.5	-0.3	-0.1	2.8
6031	-0.1	-0.4	0.0	6031	0.1	0.4	-0.0	-0.2	-0.9	0.1
6032	0.3	-0.1	0.1	6032	-0.3	0.1	-0.1	0.7	-0.2	0.1
6038	-1.0	0.1	-0.0	6038	1.1	-0.1	0.0	-2.1	0.2	-0.1
6039	-0.5	-0.0	0.6	6039	0.5	0.0	-0.6	-1.1	-0.1	1.2
6040	0.3	-0.2	0.4	6040	-0.3	0.2	-0.4	0.7	-0.4	0.9
6042	-0.2	-0.1	0.4	6042	0.2	0.1	-0.4	-0.4	-0.2	0.8
6043	-0.0	-0.5	0.3	6043	0.0	0.5	-0.3	-0.0	-0.9	0.7
6044	0.1	-0.0	0.4	6044	-0.1	0.0	-0.4	0.2	-0.1	0.8
6045	0.1	-0.2	0.7	6045	-0.1	0.2	-0.7	0.2	-0.4	1.4
6047	0.4	-0.2	0.2	6047	-0.4	0.2	-0.2	0.8	-0.4	0.4
6050	0.0	-0.5	0.3	6050	-0.0	0.5	-0.3	0.0	-1.0	0.7
6051	0.1	-0.2	0.4	6051	-0.1	0.2	-0.4	0.2	-0.4	0.8
6052	0.2	-0.3	0.2	6052	-0.2	0.3	-0.2	0.3	-0.7	0.5
6053	0.0	-0.5	0.2	6053	-0.0	0.5	-0.2	0.0	-0.9	0.5
6055	-0.3	-0.6	0.5	6055	0.3	0.6	-0.5	-0.6	-1.2	1.1
6059	-0.3	0.2	0.6	6059	0.3	-0.2	-0.6	-0.5	0.5	1.2
6060	-0.1	-0.7	-0.2	6060	0.1	0.8	0.2	-0.1	-1.5	-0.5
6061	0.1	-0.5	0.4	6061	-0.1	0.5	-0.4	0.1	-0.9	0.7
6063	-0.4	-0.7	0.7	6063	0.4	0.8	-0.7	-0.8	-1.5	1.4
6064	-0.0	1.3	0.6	6064	0.0	-1.6	-0.6	-0.0	2.9	1.2
6065	2.5	2.6	-4.3	6065	-3.3	-2.9	7.3	5.8	5.5	-11.6
6066	0.1	0.2	0.1	6066	-0.1	-0.2	-0.1	0.3	0.3	0.2
6067	-0.0	-0.5	0.7	6067	0.0	0.5	-0.7	-0.1	-1.1	1.4

TABLE 8.19.—*(Cont'd)*

RESIDUALS V

	V1(WN - 16)			V2(WN - 14)			V1 - V2		
6068	-0.1	0.3	1.1	6068	0.1	-0.3	-1.1	-0.3	0.6	2.2
6069	-0.1	-0.7	0.4	6069	0.1	0.7	-0.4	-0.1	-1.4	0.9
6072	0.3	-0.2	0.2	6072	-0.3	0.2	-0.2	0.7	-0.4	0.5
6073	0.2	-0.3	0.6	6073	-0.2	0.3	-0.6	0.4	-0.5	1.1
6075	0.0	-0.2	0.6	6075	-0.0	0.2	-0.6	0.0	-0.5	1.1
6078	-0.3	-0.3	1.1	6078	0.3	0.3	-1.1	-0.5	-0.7	2.1
6111	-0.9	-1.0	-1.8	6111	1.0	1.3	2.6	-1.9	-2.3	-4.4
6123	-0.5	0.7	0.0	6123	0.6	-0.7	-0.0	-1.1	1.3	0.1
6134	-0.9	-1.0	-1.8	6134	1.0	1.3	2.6	-1.9	-2.3	-4.4
7043	0.5	0.4	0.5	7043	-0.6	-0.5	-0.7	1.2	0.9	1.2

UNIT OF RESIDUALS (METERS)

TABLE 8.20.—*Transformation: WN14 − WN12*

SCALE FACTOR AND ROTATION PARAMETERS CONSTRAINED

SOLUTION FOR 3 TRANSLATION, 1 SCALE AND 3 ROTATION PARAMETERS

(USING VARIANCES ONLY)

DU METERS	DV METERS	DW METERS	DELTA (X1.D+6)	OMEGA SECONDS	PSI SECONDS	EPSILON SECONDS
1.02	-1.87	4.53	-1.94	-0.04	-0.05	-0.05
± 0.50	± 0.52	± 0.62	± 0.01	± 0.00	± 0.00	± 0.00

VARIANCE - COVARIANCE MATRIX

σ_o^2 = 0.68

0.246D+00	0.652D-04	-0.285D-03	-0.175D-09	0.284D-09	0.757D-09	-0.155D-10
0.652D-04	0.270D+00	0.416D-03	0.187D-09	0.255D-09	-0.139D-10	-0.705D-09
-0.285D-03	0.416D-03	0.384D+00	-0.320D-09	0.289D-10	-0.382D-09	-0.499D-09
-0.175D-09	0.187D-09	-0.320D-09	0.215D-15	0.622D-19	-0.677D-19	0.346D-18
0.284D-09	0.255D-09	0.289D-10	0.622D-19	0.378D-15	-0.472D-16	0.611D-17
0.757D-09	-0.139D-10	-0.382D-09	-0.677D-19	-0.472D-16	0.534D-15	-0.140D-16
-0.155D-10	-0.705D-09	-0.499D-09	0.346D-18	0.611D-17	-0.140D-16	0.523D-15

COEFFICIENTS OF CORRELATION

0.100D+01	0.253D-03	-0.927D-03	-0.241D-01	0.294D-01	0.661D-01	-0.137D-02
0.253D-03	0.100D+01	0.129D-02	0.246D-01	0.252D-01	-0.116D-02	-0.593D-01
-0.927D-03	0.129D-02	0.100D+01	-0.353D-01	0.240D-02	-0.267D-01	-0.352D-01
-0.241D-01	0.246D-01	-0.353D-01	0.100D+01	0.218D-03	-0.200D-03	0.103D-02
0.294D-01	0.252D-01	0.240D-02	0.218D-03	0.100D+01	-0.105D+00	0.137D-01
0.661D-01	-0.116D-02	-0.267D-01	-0.200D-03	-0.105D+00	0.100D+01	-0.265D-01
-0.137D-02	-0.593D-01	-0.352D-01	0.103D-02	0.137D-01	-0.265D-01	0.100D+01

TABLE 8.20.—*(Cont'd)*

	RESIDUALS V								
	V1(WN - 12)			V2(WN - 14)			V1 - V2		
3861	-0.2	-1.5	2.7	3861	0.3	3.8	-5.4	-0.5	-5.3	8.1
4061	-0.5	-2.7	3.9	4061	0.6	5.0	-5.1	-1.1	-7.6	9.0
4081	-1.0	0.1	1.3	4081	1.2	-0.4	-2.0	-2.2	0.5	3.3
4082	0.7	-2.4	2.4	4082	-0.9	6.2	-4.3	1.6	-8.6	6.7
4740	-0.2	-2.4	2.2	4740	0.3	7.0	-4.1	-0.5	-9.4	6.3
6001	-0.3	-0.1	-0.8	6001	0.3	0.2	1.4	-0.6	-0.3	-2.2
6002	-0.7	0.3	0.3	6002	0.8	-0.8	-0.9	-1.5	1.1	1.3
6003	-0.4	1.0	-1.4	6003	0.5	-1.8	3.3	-0.9	2.9	-4.7
6004	0.1	1.0	-1.2	6004	-0.2	-1.3	1.9	0.3	2.3	-3.1
6006	0.5	0.6	-2.0	6006	-0.6	-0.8	4.5	1.0	1.3	-6.5
6007	3.5	-1.2	3.4	6007	-6.3	1.9	-7.9	9.7	-3.1	11.3
6008	3.2	1.5	0.1	6008	-8.1	-4.2	-0.1	11.3	5.7	0.2
6009	-0.3	0.1	-0.9	6009	0.3	-0.2	1.1	-0.6	0.2	-2.0
6011	-2.6	1.5	0.5	6011	5.5	-2.0	-0.6	-8.1	3.6	1.1
6012	1.1	0.6	-0.4	6012	-2.0	-0.9	0.5	3.1	1.6	-0.9
6013	-0.3	-0.7	-0.6	6013	0.4	0.9	0.9	-0.7	-1.6	-1.5
6015	-0.7	-2.8	-0.4	6015	1.1	4.9	0.8	-1.8	-7.7	-1.2
6016	-0.6	-0.1	-0.4	6016	1.0	0.2	0.8	-1.6	-0.3	-1.2
6019	0.1	1.6	-1.9	6019	-0.2	-2.7	3.8	0.3	4.3	-5.7
6020	-1.0	1.7	-1.5	6020	1.2	-3.1	2.4	-2.2	4.8	-3.9
6022	-0.5	1.7	0.3	6022	1.0	-2.1	-0.3	-1.5	3.8	0.6
6023	1.8	-0.8	0.3	6023	-3.6	1.3	-0.4	5.4	-2.1	0.7
6031	1.1	1.5	0.9	6031	-1.9	-1.8	-1.8	3.1	3.4	2.7
6032	-0.6	-0.0	-0.3	6032	0.7	0.1	0.5	-1.3	-0.1	-0.8
6038	-0.9	0.3	-0.0	6038	1.2	-0.6	0.0	-2.1	0.9	-0.0
6039	-0.3	3.5	-0.0	6039	0.5	-6.3	0.0	-0.8	9.8	-0.0
6040	-1.6	-1.1	-0.9	6040	1.7	1.9	1.2	-3.3	-3.1	-2.1
6042	-2.7	-2.2	-1.6	6042	4.9	4.3	2.3	-7.7	-6.5	-3.9
6043	-0.7	2.8	-1.9	6043	0.8	-3.4	4.2	-1.5	6.2	-6.1
6044	-1.2	1.2	-4.0	6044	1.2	-1.4	8.1	-2.3	2.7	-12.0
6045	-1.7	-1.3	-1.3	6045	2.2	2.1	1.8	-3.9	-3.3	-3.1
6047	0.1	-1.4	0.3	6047	-0.1	2.9	-0.4	0.2	-4.3	0.7
6050	-0.8	3.3	-0.9	6050	0.9	-3.5	2.5	-1.7	6.8	-3.4
6051	-0.9	1.3	-1.4	6051	0.9	-1.7	3.7	-1.8	3.0	-5.0
6052	-0.7	1.1	-0.5	6052	0.8	-1.3	1.0	-1.5	2.4	-1.5
6053	-0.2	1.9	-0.2	6053	0.2	-2.1	0.6	-0.4	4.0	-0.9
6055	1.5	0.6	-0.1	6055	-2.9	-0.9	0.1	4.3	1.5	-0.3
6059	-1.1	2.6	-1.1	6059	2.7	-3.8	1.5	-3.8	6.4	-2.6
6060	1.4	0.1	0.8	6060	-2.6	-0.1	-1.4	4.0	0.2	2.2
6061	0.0	3.5	-2.4	6061	-0.0	-3.7	5.3	0.0	7.2	-7.7
6063	0.8	0.7	1.2	6063	-1.5	-1.1	-2.1	2.2	1.8	3.3
6064	-1.2	-0.8	-0.2	6064	1.7	1.1	0.3	-2.9	-1.9	-0.5
6065	-0.2	-0.0	-1.0	6065	0.4	0.0	2.3	-0.6	-0.0	-3.3
6066	1.1	0.6	-0.4	6066	-2.0	-0.9	0.5	3.1	1.6	-0.9
6067	2.6	1.3	0.0	6067	-6.7	-2.3	-0.0	9.3	3.6	0.0

TABLE 8.20.—*(Cont'd)*

RESIDUALS V

V1(WN - 12)				V2(WN - 14)				V1 - V2		
6068	-1.1	-0.1	-1.8	6068	2.2	0.2	2.9	-3.3	-0.3	-4.7
6069	-0.1	2.4	-3.5	6069	0.1	-2.5	5.9	-0.1	4.9	-9.4
6072	-1.7	-2.5	-0.9	6072	1.8	4.1	1.2	-3.5	-6.6	-2.1
6073	-1.7	-1.3	-1.2	6073	2.0	2.2	1.5	-3.7	-3.5	-2.6
6075	-1.4	-1.4	-1.6	6075	1.7	2.3	2.0	-3.1	-3.7	-3.6
6078	1.5	0.3	-0.5	6078	-6.2	-0.4	0.9	7.6	0.7	-1.3
6111	-0.9	-0.2	0.4	6111	1.2	0.4	-1.1	-2.1	-0.5	1.6
6123	-0.9	0.8	0.5	6123	1.0	-0.9	-1.2	-1.8	1.7	1.7
6134	-0.9	-0.2	0.4	6134	1.2	0.4	-1.1	-2.1	-0.5	1.6
7043	-0.7	0.3	0.4	7043	0.9	-0.7	-0.9	-1.6	0.9	1.3

UNIT OF RESIDUALS (METERS)

TABLE 8.21.—*Height Residuals (Solution WN14)*

STN. NO.	NOSUGC	N REF	NOSUGC-N REF	RESIDUALS
1021	-53.33	-37.32	-16.01	-3.07
1022	-38.20	-31.58	-6.62	6.33
1030	-51.74	-30.00	-21.74	-8.79
1032	-2.12	11.57	-13.69	-0.75
1033	-3.91	9.11	-13.02	-0.08
1034	-40.84	-25.47	-15.37	-2.42
1042	-47.53	-34.38	-13.15	-0.20
3106	-53.30	-49.83	-3.47	9.47
3334	-45.79	-31.54	-14.25	-1.30
3400	-32.19	-18.42	-13.77	-0.82
3401	-46.81	-30.59	-16.22	-3.28
3402	-48.34	-29.04	-19.30	-6.36
3404	-43.00	-6.69	-36.31	-23.36
3405	-65.84	-49.77	-16.07	-3.12
3406	-38.89	-29.19	-9.70	3.24
3407	-60.27	-38.57	-21.70	-8.76
3413	-19.55	-12.03	-7.52	5.43
3414	-27.84	-9.88	-17.96	-5.02
3431	5.59	11.98	-6.39	6.56
3476	-44.50	-28.31	-16.19	-3.25
3477	0.51	10.71	-10.20	2.74
3478	-20.75	-7.17	-13.58	-0.64
3499	3.87	16.73	-12.86	0.09
3648	-48.91	-35.70	-13.21	-0.26
3657	-49.62	-36.55	-13.07	-0.13
3861	-43.88	-33.70	-10.18	2.76
3902	-31.19	-16.53	-14.66	-1.72
3903	-57.45	-36.87	-20.58	-7.63
5001	-44.20	-36.87	-7.33	5.62
5201	-39.05	-17.65	-21.40	-8.46
5410	-6.20	-4.13	-2.07	10.88
5648	-47.90	-35.07	-12.83	0.12
5712	-44.22	-28.31	-15.91	-2.97
5713	49.11	54.00	-4.89	8.05
5715	23.59	27.20	-3.61	9.33

TABLE 8.21.—*(Cont'd)*

STN. NO.	NOSUGC	N REF	NOSUGC-N REF	RESIDUALS
5717	7.70	10.35	-2.65	10.30
5720	-16.89	-5.78	-11.11	1.84
5721	-32.25	-20.67	-11.58	1.37
5722	-87.78	-73.64	-14.14	-1.19
5723	-59.91	-40.39	-19.52	-6.58
5726	61.98	62.16	-0.18	12.76
5730	-4.72	13.75	-18.47	-5.53
5732	8.67	27.35	-18.68	-5.73
5733	-0.23	16.07	-16.30	-3.35
5734	-3.56	6.22	-9.78	3.17
5735	-19.53	-12.03	-7.50	5.45
5736	4.41	16.26	-11.85	1.10
5739	48.73	54.00	-5.27	7.67
5744	23.35	37.43	-14.08	-1.14
5907	-42.61	-28.11	-14.50	-1.56
5911	-43.33	-43.44	0.11	13.05
5912	-13.16	6.16	-19.32	-6.38
5914	-67.99	-50.08	-17.91	-4.97
5915	-41.79	-26.32	-15.47	-2.52
5923	22.05	24.64	-2.59	10.35
5924	23.49	54.48	-30.99	-18.04
5925	26.11	33.75	-7.64	5.31
5930	9.73	8.28	1.45	14.39
5931	-28.03	2.32	-30.35	-17.40
5933	48.80	50.66	-1.86	11.09
5934	58.59	74.75	-16.16	-3.22
5935	42.62	48.15	-5.53	7.42
5937	51.60	69.93	-18.33	-5.38
5938	49.03	59.97	-10.94	2.01
5941	4.87	2.05	2.82	15.76
6001	4.33	11.66	-7.33	5.61
6002	-50.76	-36.90	-13.86	-0.92
6003	-39.23	-17.65	-21.58	-8.64
6004	-3.23	6.22	-9.45	3.50
6006	11.02	27.06	-16.04	-3.09

TABLE 8.21.—*(Cont'd)*

STN. NO.	NOSUGC	N REF	NOSUGC-N REF	RESIDUALS
6007	49.70	54.00	-4.30	8.64
6008	-44.48	-28.31	-16.17	-3.23
6009	3.57	16.73	-13.16	-0.21
6011	3.20	1.75	1.45	14.40
6012	-4.85	13.75	-18.60	-5.66
6013	15.27	34.27	-19.00	-6.06
6015	-33.55	-20.67	-12.88	0.07
6016	23.27	37.43	-14.16	-1.22
6019	5.60	22.80	-17.20	-4.25
6020	-21.60	-4.75	-16.85	-3.90
6022	7.62	27.35	-19.73	-6.78
6023	44.08	67.94	-23.86	-10.92
6031	-14.32	8.68	-23.00	-10.05
6032	-37.42	-30.51	-6.91	6.03
6038	-49.95	-35.47	-14.48	-1.54
6039	-37.29	-16.68	-20.61	-7.66
6040	-52.86	-38.11	-14.75	-1.81
6042	-17.34	-5.78	-11.56	1.39
6043	-3.29	15.60	-18.89	-5.95
6044	28.18	36.61	-8.43	4.52
6045	-20.02	-6.07	-13.95	-1.00
6047	60.22	62.17	-1.95	10.99
6050	-2.81	15.70	-18.51	-5.56
6051	18.02	29.20	-11.18	1.76
6053	-72.38	-56.10	-16.28	-3.33
6055	4.24	16.26	-12.02	0.93
6059	-0.41	16.07	-16.48	-3.53
6060	7.28	27.33	-20.05	-7.10
6061	0.96	11.28	-10.32	2.62
6063	23.02	27.20	-4.18	8.76
6064	0.64	10.35	-9.71	3.23
6065	30.04	44.23	-14.19	-1.24
6066	-5.65	13.74	-19.39	-6.45
6067	-19.55	-12.03	-7.52	5.43
6068	13.16	24.65	-11.49	1.45

TABLE 8.21.—*(Cont'd)*

STN. NO.	NOSUGC	N REF	NOSUGC-N REF	RESIDUALS
6069	13.23	25.52	-12.29	0.66
6072	-63.61	-40.39	-23.22	-10.28
6073	-86.13	-73.64	-12.49	0.46
6075	-54.59	-44.40	-10.19	2.75
6078	44.05	63.10	-19.05	-6.10
6111	-45.28	-33.18	-12.10	0.85
6123	-14.02	-1.40	-12.62	0.33
6134	-45.38	-33.19	-12.19	0.75
7036	-31.99	-19.78	-12.21	0.73
7037	-44.47	-33.87	-10.60	2.34
7039	-54.88	-43.43	-11.45	1.49
7040	-52.74	-50.55	-2.19	10.75
7043	-50.11	-36.91	-13.20	-0.26
7045	-30.24	-18.10	-12.14	0.81
7072	-44.94	-36.04	-8.90	4.04
7075	-52.35	-39.20	-13.15	-0.21
7076	-33.40	-26.62	-6.78	6.16
8009	31.67	42.33	-10.66	2.28
8010	31.46	44.77	-13.31	-0.37
8011	37.72	47.43	-9.71	3.23
8015	34.99	46.38	-11.39	1.55
8019	32.00	45.91	-13.91	-0.97
8030	30.64	44.64	-14.00	-1.06
9001	-37.07	-22.93	-14.14	-1.19
9002	12.89	24.27	-11.38	1.56
9004	42.32	54.57	-12.25	0.69
9005	19.87	30.20	-10.33	2.62
9006	-60.51	-48.12	-12.39	0.56
9007	22.60	31.82	-9.22	3.73
9008	-31.19	-10.91	-20.28	-7.34
9009	-38.62	-29.19	-9.43	3.51
9010	-44.91	-36.04	-8.87	4.07
9011	5.71	22.80	-17.09	-4.14
9012	2.98	1.76	1.22	14.17
9021	-42.84	-27.00	-15.84	-2.89

TABLE 8.21.—*(Cont'd)*

STN. NO.	NOSUGC	N REF	NOSUGC-N REF	RESIDUALS
9028	-39.07	-5.78	-33.29	-20.34
9029	-19.54	-12.03	-7.51	5.44
9031	-2.31	13.43	-15.74	-2.80
9051	20.50	32.81	-12.31	0.64
9091	19.99	32.84	-12.85	0.10
9424	-43.09	-26.21	-16.88	-3.93
9425	-44.00	-32.39	-11.61	1.34
9426	21.80	36.39	-14.59	-1.64
9427	-2.77	8.83	-11.60	1.34
9431	10.01	25.67	-15.66	-2.71
9432	26.58	39.71	-13.13	-0.19

AVERAGE	SIGMA
-0.1294D+02	0.6420D+01

SEMI-MAJOR AXIS

6378142.06

TABLE 8.22.—*Undulation Comparison (Solution WN14)*

Sta.	N_{REF}	MSL	-dH	H_{WN14}	N	N_V	Diff.
1021	-37.32	5.76	0.20	-47.77	-40.39	-34.50	-5.89
1022	-31.58	4.81	-0.81	-32.58	-25.25	-29.50	4.25
1030	-30.00	929.10	-12.22	889.58	-38.79	-31.90	-6.89
1032	11.57	69.00	5.92	60.96	10.82	12.50	-1.68
1034	-25.47	252.58	-5.81	217.55	-27.89	-26.70	-1.19
1042	-34.38	909.40	-1.53	863.40	-34.58	-30.30	-4.28
3106	-49.83	1.90	7.28	-58.68	-40.36	-54.80	14.44
3334	-31.54	39.00	-4.19	-2.60	-32.84	-28.70	-4.14
3400	-18.42	2184.10	-8.49	2160.40	-19.24	-17.50	-1.74
3401	-30.59	83.00	1.67	34.52	-33.87	-28.40	-5.47
3402	-29.04	73.00	-3.23	27.89	-35.40	-30.40	-5.00
3405	-49.77	2.20	3.47	-67.11	-52.89	-53.30	0.41
3406	-29.19	6.83	5.02	-37.08	-25.95	-35.50	9.55
3407	-38.57	254.80	7.87	186.66	-47.33	-46.20	-1.13
3648	-35.70	12.00	-0.81	-36.10	-35.96	-31.70	-4.26
3657	-36.55	5.50	0.45	-44.57	-36.68	-33.90	-2.78
3861	-33.70	0.20	-0.21	-43.47	-30.94	-31.00	0.06
3902	-16.53	1882.20	-8.35	1859.36	-18.25	-16.40	-1.85
3903	-36.87	168.00	0.08	110.47	-44.50	-34.00	-10.50
5001	-36.87	127.80	0.08	83.52	-31.25	-34.00	2.75
5201	-17.65	368.92	-11.41	341.28	-26.11	-20.90	-5.21
5648	-35.07	27.90	-0.95	-19.05	-34.95	-30.90	-4.05
5715	27.20	27.30	19.89	31.00	36.53	25.50	11.03
5739	54.00	56.10	13.40	91.43	61.67	60.30	1.37
5744	37.43	11.80	16.74	18.41	36.29	40.80	-4.51
5907	-28.11	481.90	-5.56	444.85	-29.67	-27.90	-1.77
5911	-43.44	22.00	4.76	-26.09	-30.39	-39.20	8.81
5912	6.16	9.10	0.96	-5.02	-0.22	1.10	-1.32
5914	-50.08	63.80	5.19	-9.38	-55.05	-55.90	0.85
5915	-26.32	206.20	-6.52	170.93	-28.84	-27.10	-1.74
5924	54.48	12.40	16.64	19.25	36.44	48.60	-12.16
6002	-36.90	44.30	0.24	-6.70	-37.82	-34.00	-3.82
6003	-17.65	368.74	-11.41	340.92	-26.29	-20.90	-5.39
6006	27.06	105.70	5.41	111.31	23.97	26.00	-2.03
6007	54.00	53.30	13.40	89.60	62.64	60.30	2.34
6016	37.43	9.24	16.74	15.77	36.21	40.80	-4.59
6023	67.94	60.50	-15.81	120.39	57.02	71.30	-14.28
6032	-30.51	26.30	-5.02	-6.10	-24.48	-21.50	-2.98
6060	27.33	211.08	-14.66	233.02	20.23	31.60	-11.37
6063	27.20	26.30	19.89	29.43	35.96	25.50	10.46
6065	44.23	943.20	13.66	959.58	42.99	44.50	-1.51
6111	-33.18	2284.30	-12.52	2251.54	-32.33	-34.50	2.17
7036	-19.78	59.59	-6.75	34.35	-19.05	-24.00	4.95
7037	-33.87	272.68	-4.62	232.83	-31.53	-32.30	0.77
7040	-50.55	49.70	5.64	-8.68	-39.80	-52.30	12.50
7045	-18.10	1789.63	-8.37	1767.76	-17.29	-18.40	1.11
7072	-36.04	14.20	-0.19	-30.55	-32.00	-36.30	4.30
7075	-39.20	281.90	-1.39	230.94	-39.41	-36.90	-2.51
7076	-26.62	445.90	1.55	410.95	-20.46	-32.00	11.54
9001	-22.93	1651.33	-9.35	1623.61	-24.12	-22.80	-1.32
9004	54.57	25.90	16.70	51.52	55.26	48.40	6.86
9009	-29.19	8.70	5.02	-34.94	-25.68	-35.70	10.02
9010	-36.04	15.13	-0.19	-29.59	-31.97	-36.30	4.33
9021	-27.00	2382.00	-10.74	2349.90	-29.89	-28.10	-1.79
9051	32.81	187.90	15.98	192.42	33.45	40.60	-7.15
9091	32.84	467.00	15.94	471.05	32.94	40.60	-7.66

TABLE 8.22.—*(Cont'd)*

Sta.	N_{REF}	MSL	-dH	H_{WN14}	N	N_V	Diff.
9424	-26.21	704.60	-8.36	669.87	-30.14	-20.20	-9.94
9425	-32.39	784.23	-12.53	752.76	-31.05	-33.90	2.85
9426	36.39	575.92	9.24	588.48	34.75	36.60	-1.85
6134	-33.19	2198.40	-12.52	2165.54	-32.44	-34.50	2.06
8009	42.33	24.70	12.25	44.12	44.61	41.60	3.01
8010	44.77	903.44	14.01	920.89	44.40	46.10	-1.70
8011	47.43	113.20	12.04	138.88	50.66	47.00	3.66
8015	46.38	647.00	14.96	679.03	59.93	49.30	10.63
8019	45.91	377.42	15.03	394.39	44.94	47.30	-2.36
8030	44.64	165.50	13.31	182.83	43.58	43.60	-0.02
9431	25.67	8.00	9.92	8.09	22.96	16.80	6.16
9432	39.71	189.00	12.88	202.70	39.52	41.10	-1.58

TABLE 8.23.—*Relationships Between Various Dynamics and the WN Systems (Dynamic − WN14)*

Solution	NWL—9D			SAO III			GEM 4	GSFC 73
Sta. considered	5000	6000	All	6000	9000	All	All	All
No. stations	12	22	32	47	22	73	30	26
Weight factor[a]	1.5	7.75	~ 4	2	2	2	50	22
Δu (m)	13.8 ± 1.5	16.7 ± 1.2	16.3 ± 1.0	19.6 ± 1.2	14.1 ± 3.1	15.7 ± 1.4	15.5 ± 2.2	15.0 ± 2.2
Δv (m)	11.2 ± 1.6	9.6 ± 1.2	10.1 ± 1.0	14.2 ± 1.2	16.1 ± 3.0	15.3 ± 1.4	10.9 ± 2.2	11.3 ± 2.4
Δw (m)	−3.6 ± 1.8	−3.3 ± 1.2	−3.5 ± 1.1	−11.3 ± 1.3	−13.4 ± 3.4	−12.0 ± 1.5	2.2 ± 2.4	−1.9 ± 2.9
Δ (10^{-6})	0.69 ± 0.70	0.30 ± 0.52	0.39 ± 0.16	0.60 ± 0.18	1.09 ± 0.45	0.97 ± 0.22	0.74 ± 0.32	0.74 ± 0.34
ω (″)	0.86 ± 0.15	0.69 ± 0.05	0.72 ± 0.04	0.53 ± 0.05	0.32 ± 0.13	0.38 ± 0.05	0.02 ± 0.08	−0.34 ± 0.08
ψ (″)	0.00 ± 0.20	−0.16 ± 0.05	−0.15 ± 0.04	0.01 ± 0.06	−0.05 ± 0.14	0.02 ± 0.06	0.14 ± 0.10	0.23 ± 0.11
ϵ (″)	0.13 ± 0.29	−0.17 ± 0.06	−0.17 ± 0.05	−0.18 ± 0.06	0.00 ± 0.13	0.00 ± 0.06	0.18 ± 0.09	0.29 ± 0.11
σ_o^2	1.31	0.93	1.16	1.14	1.06	0.97	1.14	1.10

[a] Weight factor = $\sigma^2_{o,*}/\sigma^2_{o,WN14}$.

TABLE 8.24.—*Transformation: WN14 – NWL 9D*

SCALE FACTOR AND ROTATION PARAMETERS CONSTRAINED

SOLUTION FOR 3 TRANSLATION, 1 SCALE AND 3 ROTATION PARAMETERS

(USING VARIANCES ONLY)

DU METERS	DV METERS	DW METERS	DELTA (X1.D+6)	OMEGA SECONDS	PSI SECONDS	EPSILON SECONDS
15.89	10.27	-3.38	0.29	0.71	-0.15	-0.14

VARIANCE - COVARIANCE MATRIX

σ_o^2= 0.87

0.957D+00	-0.812D-03	-0.133D-02	0.958D-10	0.151D-08	0.433D-08	0.502D-09
-0.812D-03	0.955D+00	0.127D-02	0.109D-08	-0.877D-09	-0.248D-09	-0.603D-08
-0.133D-02	0.127D-02	0.112D+01	-0.293D-08	-0.205D-09	-0.708D-09	-0.196D-08
0.958D-10	0.109D-08	-0.293D-08	0.185D-14	-0.436D-18	0.277D-17	-0.530D-18
0.151D-08	-0.877D-09	-0.205D-09	-0.436D-18	0.285D-14	-0.592D-16	0.446D-15
0.433D-08	-0.248D-09	-0.708D-09	0.277D-17	-0.592D-16	0.289D-14	0.167D-15
0.502D-09	-0.603D-08	-0.196D-08	-0.530D-18	0.446D-15	0.167D-15	0.394D-14

COEFFICIENTS OF CORRELATION

0.100D+01	-0.849D-03	-0.129D-02	0.228D-02	0.289D-01	0.823D-01	0.817D-02
-0.849D-03	0.100D+01	0.123D-02	0.260D-01	-0.168D-01	-0.472D-02	-0.983D-01
-0.129D-02	0.123D-02	0.100D+01	-0.646D-01	-0.363D-02	-0.125D-01	-0.296D-01
0.228D-02	0.260D-01	-0.646D-01	0.100D+01	-0.190D-03	0.120D-02	-0.196D-03
0.289D-01	-0.168D-01	-0.363D-02	-0.190D-03	0.100D+01	-0.207D-01	0.133D+00
0.823D-01	-0.472D-02	-0.125D-01	0.120D-02	-0.207D-01	0.100D+01	0.494D-01
0.817D-02	-0.983D-01	-0.296D-01	-0.196D-03	0.133D+00	0.494D-01	0.100D+01

TABLE 8.24.—*(Cont'd)*

RESIDUALS V

	V1(NWL-9D)				V2(WN14)			V1 - V2		
5410	0.2	-0.1	-0.3	700	-13.2	3.8	10.5	13.4	-3.9	-10.9
5648	0.1	0.0	0.6	708	-1.6	-1.4	-17.7	1.7	1.5	18.3
5713	0.0	0.4	-0.0	713	-3.1	-21.4	0.0	3.1	21.8	-0.0
5733	-6.7	5.0	-4.3	733	3.0	-1.3	1.1	-9.7	6.3	-5.4
5915	2.1	0.5	4.5	709	-19.1	-2.9	-33.4	21.2	3.4	37.9
5923	-0.3	-0.4	0.1	719	11.6	8.8	-1.7	-11.9	-9.3	1.7
5924	0.1	0.6	0.0	740	-11.6	-20.3	-0.5	11.8	20.9	0.6
5933	0.3	-0.8	0.3	727	-11.8	18.7	-10.1	12.1	-19.5	10.5
5934	-0.0	-0.1	-0.3	729	0.7	1.9	12.1	-0.7	-1.9	-12.4
5935	0.3	0.0	0.2	728	-21.2	-1.5	-8.0	21.4	1.5	8.2
6001	0.8	0.1	-2.8	18	-2.0	-0.2	3.9	2.9	0.3	-6.6
6002	-0.1	0.2	1.1	742	0.5	-1.1	-4.9	-0.6	1.3	6.0
6003	0.7	-0.4	-0.1	738	-2.6	1.5	0.4	3.3	-1.8	-0.6
6004	3.7	-5.4	-5.5	739	-8.1	8.1	5.9	11.8	-13.6	-11.4
6006	0.6	-2.3	1.3	818	-1.8	4.5	-2.5	2.5	-6.8	3.7
6008	1.4	-0.8	2.9	815	-5.2	3.5	-5.4	6.7	-4.3	8.2
6011	-0.7	0.3	-4.3	811	1.3	-0.6	6.3	-2.0	0.9	-10.7
6012	0.0	0.0	-0.5	708	-0.2	-0.8	6.1	0.2	0.8	-6.6
6015	-1.1	-1.0	-1.1	817	4.4	3.5	2.6	-5.5	-4.5	-3.7
6016	0.7	1.5	0.1	812	-3.5	-5.0	-0.5	4.1	6.5	0.6
6022	-1.8	0.8	-1.9	117	2.5	-1.1	1.4	-4.2	1.9	-3.3
6023	-0.3	0.4	1.1	744	0.4	-0.8	-1.2	-0.7	1.2	2.3
6031	-0.2	2.7	3.3	809	0.3	-2.9	-3.6	-0.5	5.5	6.9
6038	-0.2	-0.1	-0.2	831	2.3	0.9	0.9	-2.5	-1.0	-1.1
6043	-1.5	-4.3	6.7	847	2.2	4.8	-4.8	-3.7	-9.1	11.4
6053	-2.0	1.7	1.0	19	1.5	-1.4	-0.8	-3.5	3.1	1.8
6055	1.4	-0.1	-0.5	722	-4.1	0.3	1.0	5.5	-0.4	-1.5
6060	-0.1	-0.4	0.8	805	1.1	4.8	-6.7	-1.2	-5.3	7.4
6064	-0.7	2.2	-1.3	822	1.4	-5.4	2.1	-2.1	7.6	-3.4
6065	-0.3	-0.7	-0.2	830	1.4	1.8	0.7	-1.7	-2.5	-1.0
6068	0.0	-0.1	1.5	115	-0.1	1.2	-9.7	0.1	-1.2	11.1
6075	-0.1	0.4	0.3	717	0.2	-0.5	-0.3	-0.3	1.0	0.5

TABLE 8.25.—*Transformation: WN14 – SAO III*

SCALE FACTOR AND ROTATION PARAMETERS CONSTRAINED

SOLUTION FOR 3 TRANSLATION, 1 SCALE AND 3 ROTATION PARAMETERS

(USING VARIANCES ONLY)

DU METERS	DV METERS	DW METERS	DELTA (X1.D+6)	OMEGA SECONDS	PSI SECONDS	EPSILON SECONDS
13.93	13.62	-10.35	-0.17	0.37	0.15	-0.03

VARIANCE - COVARIANCE MATRIX

$\sigma_o^2 =$ 1.14

0.155D+01	-0.247D-04	-0.818D-03	-0.382D-08	0.357D-08	0.355D-08	0.310D-09
-0.247D-04	0.167D+01	0.118D-02	0.288D-08	0.473D-08	-0.579D-09	-0.329D-08
-0.818D-03	0.118D-02	0.167D+01	-0.300D-08	0.342D-09	-0.584D-08	-0.491D-08
-0.382D-08	0.288D-08	-0.300D-08	0.190D-14	-0.693D-18	-0.100D-17	0.301D-17
0.357D-08	0.473D-08	0.342D-09	-0.693D-18	0.274D-14	-0.152D-15	-0.474D-16
0.355D-08	-0.579D-09	-0.584D-08	-0.100D-17	-0.152D-15	0.300D-14	0.304D-15
0.310D-09	-0.329D-08	-0.491D-08	0.301D-17	-0.474D-16	0.304D-15	0.306D-14

COEFFICIENTS OF CORRELATION

0.100D+01	-0.153D-04	-0.509D-03	-0.704D-01	0.548D-01	0.521D-01	0.450D-02
-0.153D-04	0.100D+01	0.705D-03	0.511D-01	0.699D-01	-0.819D-02	-0.459D-01
-0.509D-03	0.705D-03	0.100D+01	-0.534D-01	0.507D-02	-0.826D-01	-0.688D-01
-0.704D-01	0.511D-01	-0.534D-01	0.100D+01	-0.304D-03	-0.421D-03	0.125D-02
0.548D-01	0.699D-01	0.507D-02	-0.304D-03	0.100D+01	-0.530D-01	-0.164D-01
0.521D-01	-0.819D-02	-0.826D-01	-0.421D-03	-0.530D-01	0.100D+01	0.100D+00
0.450D-02	-0.459D-01	-0.688D-01	0.125D-02	-0.164D-01	0.100D+00	0.100D+01

TABLE 8.25—*(Cont'd)*

RESIDUALS V

	V1(SAO-III)			V2(WN14)			V1 - V2		
6002	1.7	-2.9	4.3	6002	-3.4	8.1	-9.6	5.1	-11.0	13.8
6003	0.0	0.1	0.4	6003	-0.7	-1.6	-8.2	0.7	1.7	8.6
6004	0.2	0.0	0.1	6004	-14.4	-2.4	-4.7	14.5	2.5	4.8
6006	0.0	-0.3	0.0	6006	-1.6	6.8	-0.5	1.6	-7.1	0.6
6007	-0.1	0.2	-0.3	6007	6.2	-8.7	10.0	-6.3	8.8	-10.3
6008	0.1	-0.0	0.2	6008	-6.2	2.1	-6.0	6.3	-2.2	6.1
6009	0.1	0.2	-0.3	6009	-3.5	-5.5	6.5	3.6	5.7	-6.8
6011	-0.6	1.0	0.4	6011	6.8	-12.3	-4.2	-7.4	13.3	4.7
6012	0.3	0.0	-0.4	6012	-26.6	-1.3	15.3	26.9	1.3	-15.7
6013	0.9	-0.1	0.1	6013	-24.8	1.8	-1.0	25.7	-1.9	1.0
6015	-0.1	-0.4	0.1	6015	4.2	16.0	-4.0	-4.3	-16.4	4.2
6016	-0.1	-0.3	0.2	6016	3.3	7.8	-5.4	-3.4	-8.1	5.6
6019	0.3	-0.3	-3.0	6019	-3.4	3.2	16.8	3.6	-3.5	-19.8
6020	0.3	0.4	-0.2	6020	-7.8	-14.7	4.4	8.1	15.1	-4.6
6022	0.2	0.8	0.2	6022	-4.8	-19.5	-3.0	5.0	20.2	3.2
6023	1.2	-0.0	0.2	6023	-19.7	0.8	-2.5	20.8	-0.9	2.7
6031	0.8	1.0	0.1	6031	-13.2	-12.4	-1.9	14.0	13.3	2.1
6032	1.3	0.1	1.4	6032	-29.0	-2.9	-22.3	30.3	3.1	23.7
6038	-0.1	-0.0	0.0	6038	2.2	0.1	-0.1	-2.3	-0.2	0.1
6039	0.3	0.7	-0.1	6039	-6.4	-20.1	3.6	6.7	20.8	-3.8
6040	1.0	-0.2	0.2	6040	-17.6	4.1	-4.7	18.6	-4.3	4.9
6042	-0.5	-0.7	1.2	6042	13.7	16.5	-16.0	-14.2	-17.1	17.1
6043	0.1	0.1	-1.4	6043	-4.2	-2.8	20.0	4.3	2.9	-21.4
6044	0.4	1.1	0.6	6044	-7.5	-27.4	-9.7	7.9	28.4	10.3
6045	-0.1	-0.4	1.1	6045	1.9	6.4	-12.1	-2.0	-6.8	13.1
6047	0.5	-0.1	0.2	6047	-34.2	7.4	-8.7	34.7	-7.5	9.0
6050	0.1	1.1	-1.1	6050	-4.0	-20.2	21.1	4.1	21.2	-22.2
6051	0.5	0.3	0.0	6051	-7.2	-7.1	-0.9	7.7	7.4	0.9
6052	1.1	0.6	0.1	6052	-20.0	-13.7	-1.6	21.1	14.3	1.7
6053	1.1	0.9	-0.1	6053	-17.2	-14.7	2.7	18.3	15.6	-2.8
6055	-0.3	0.2	-0.2	6055	9.8	-5.8	3.6	-10.1	6.0	-3.7
6059	-0.1	0.7	0.2	6059	2.5	-20.0	-2.9	-2.5	20.7	3.1
6060	2.2	1.2	0.3	6060	-14.7	-8.0	-1.8	16.9	9.3	2.1
6061	0.3	0.8	-0.9	6061	-10.8	-11.0	13.9	11.2	11.9	-14.8
6063	-1.3	0.5	-0.4	6063	21.0	-5.2	3.1	-22.3	5.7	-3.5
6064	-0.5	-0.2	0.4	6064	8.7	4.8	-4.6	-9.2	-5.1	5.0
6065	-0.1	-1.1	-1.4	6065	1.3	7.8	11.2	-1.5	-8.9	-12.6

TABLE 8.25—*(Cont'd)*

	RESIDUALS V								
	V1(SAO-III)			V2(WN14)			V1 - V2		
6067	0.9	0.5	-0.1	6067	-12.2	-6.3	1.3	13.1	6.8	-1.4
6068	-0.2	-0.8	-0.3	6068	0.4	1.4	0.3	-0.7	-2.2	-0.6
6069	0.1	0.3	0.3	6069	-2.1	-8.0	-5.8	2.2	8.3	6.1
6072	1.0	-0.6	0.3	6072	-10.7	13.8	-5.3	11.7	-14.4	5.5
6073	0.1	-0.6	0.7	6073	-1.3	12.5	-11.9	1.4	-13.2	12.6
6075	-0.3	-0.6	0.8	6075	4.7	11.5	-12.2	-5.0	-12.0	13.0
6078	-0.8	0.9	5.6	6078	10.0	-15.5	-40.4	-10.8	16.3	46.0
6111	-0.4	-0.0	0.7	6111	2.8	0.0	-5.5	-3.3	-0.0	6.1
6123	0.3	0.0	0.3	6123	-7.3	-0.6	-8.0	7.6	0.6	8.3
6134	-0.4	-0.0	0.7	6134	2.8	0.1	-5.5	-3.2	-0.1	6.2
8010	-9.2	13.4	0.0	8010	7.2	-5.0	-0.0	-16.4	18.3	0.0
8011	-2.1	39.2	-5.1	8011	2.1	-14.9	8.2	-4.1	54.1	-13.3
8015	-5.7	20.6	-3.5	8015	3.1	-3.1	1.7	-8.8	23.7	-5.2
8019	-1.3	14.8	-1.5	8019	5.6	-17.0	5.8	-6.9	31.8	-7.4
9001	-3.2	0.9	0.8	9001	13.5	-8.3	-7.7	-16.7	9.2	8.5
9002	-0.3	-1.1	-0.9	9002	0.3	1.1	0.4	-0.7	-2.2	-1.3
9004	-3.1	20.1	-8.7	9004	4.2	-3.2	8.7	-7.4	23.3	-17.5
9005	4.5	-1.5	2.9	9005	-16.6	5.8	-15.8	21.1	-7.3	18.6
9006	11.1	-1.8	1.9	9006	-9.9	8.2	-7.2	21.0	-10.0	9.1
9007	1.8	-4.0	-8.5	9007	-3.5	6.0	5.6	5.3	-10.1	-14.1
9008	0.9	-1.8	-1.0	9008	-3.3	7.9	4.4	4.2	-9.7	-5.4
9009	0.5	-0.2	-1.5	9009	-6.1	3.7	9.7	6.6	-3.9	-11.2
9010	0.4	0.1	0.4	9010	-6.3	-1.2	-5.5	6.7	1.3	5.8
9011	0.2	-0.3	-3.1	9011	-3.2	3.1	16.7	3.4	-3.4	-19.8
9012	-0.6	1.0	0.5	9012	7.0	-12.4	-4.2	-7.6	13.5	4.7
9021	1.0	-3.3	0.2	9021	-0.6	3.6	-0.3	1.7	-6.9	0.5
9028	0.1	-0.2	1.5	9028	-2.1	3.8	-19.2	2.1	-3.9	20.7
9029	1.0	0.5	-0.2	9029	-12.2	-6.2	1.3	13.2	6.7	-1.4
9031	-0.4	0.2	-7.0	9031	1.6	-0.7	16.8	-2.0	0.9	-23.7
9091	-1.2	15.2	-1.5	9091	12.9	-26.1	14.2	-14.1	41.3	-15.7
9424	-4.4	2.0	1.5	9424	8.2	-2.7	-3.4	-12.6	4.8	5.0
9425	-0.1	-0.0	0.2	9425	3.6	0.6	-7.0	-3.7	-0.6	7.2
9426	1.2	3.2	-2.6	9426	-5.7	-12.4	27.0	6.9	15.5	-29.6
9427	1.1	-12.9	2.9	9427	-4.8	11.0	-12.9	5.9	-23.9	15.8
9431	-11.2	6.9	-0.5	9431	28.4	-30.4	3.8	-39.6	37.3	-4.3
9432	-0.2	2.1	-0.4	9432	6.7	-51.3	32.3	-6.8	53.4	-32.7

TABLE 8.26.—*Transformation: WN14 – GEM 4*

SCALE FACTOR AND ROTATION PARAMETERS CONSTRAINED

SOLUTION FOR 3 TRANSLATION, 1 SCALE AND 3 ROTATION PARAMETERS

(USING VARIANCES ONLY)

DU METERS	DV METERS	DW METERS	DELTA (X1.D+6)	OMEGA SECONDS	PSI SECONDS	EPSILON SECONDS
14.52	11.64	1.91	0.93	-0.02	0.12	0.17

VARIANCE – COVARIANCE MATRIX

$\sigma_0^2 =$ 1.11

0.268D+01	-0.378D-01	-0.116D-01	-0.932D-08	0.235D-07	0.392D-07	0.510D-08
-0.378D-01	0.251D+01	0.761D-02	0.364D-07	0.709D-08	-0.110D-07	-0.345D-07
-0.116D-01	0.761D-02	0.291D+01	-0.305D-07	0.612D-08	-0.212D-07	-0.395D-07
-0.932D-08	0.364D-07	-0.305D-07	0.111D-13	-0.437D-16	-0.536D-17	0.402D-16
0.235D-07	0.709D-08	0.612D-08	-0.437D-16	0.999D-14	-0.204D-14	-0.166D-14
0.392D-07	-0.110D-07	-0.212D-07	-0.536D-17	-0.204D-14	0.176D-13	0.387D-14
0.510D-08	-0.345D-07	-0.395D-07	0.402D-16	-0.166D-14	0.387D-14	0.127D-13

COEFFICIENTS OF CORRELATION

0.100D+01	-0.146D-01	-0.414D-02	-0.540D-01	0.144D+00	0.180D+00	0.277D-01
-0.146D-01	0.100D+01	0.282D-02	0.218D+00	0.448D-01	-0.523D-01	-0.193D+00
-0.414D-02	0.282D-02	0.100D+01	-0.170D+00	0.359D-01	-0.939D-01	-0.205D+00
-0.540D-01	0.218D+00	-0.170D+00	0.100D+01	-0.415D-02	-0.384D-03	0.338D-02
0.144D+00	0.448D-01	0.359D-01	-0.415D-02	0.100D+01	-0.154D+00	-0.147D+00
0.180D+00	-0.523D-01	-0.939D-01	-0.384D-03	-0.154D+00	0.100D+01	0.259D+00
0.277D-01	-0.193D+00	-0.205D+00	0.338D-02	-0.147D+00	0.259D+00	0.100D+01

TABLE 8.26.—*(Cont'd)*

RESIDUALS V

	V1(GEM-4)				V2(WN14)			V1 - V2		
1021	-0.1	-0.2	0.1	1021	2.3	5.3	-2.1	-2.4	-5.5	2.2
1022	0.4	-0.1	0.4	1022	-3.2	0.4	-3.0	3.5	-0.5	3.4
1030	-4.3	-0.9	1.0	1030	4.5	1.8	-3.3	-8.8	-2.6	4.3
1032	45.0	63.5	7.1	1032	-8.7	-10.0	-10.6	53.7	73.5	17.7
1034	-1.1	0.5	0.3	1034	9.8	-5.3	-3.8	-10.9	5.8	4.0
1042	1.8	-0.6	0.1	1042	-12.2	3.7	-0.9	14.0	-4.3	1.1
7036	-1.9	1.3	-0.1	7036	8.1	-7.8	0.4	-10.0	9.1	-0.5
7037	-0.7	1.0	0.6	7037	3.7	-6.2	-4.5	-4.4	7.1	5.1
7039	-1.1	-0.7	1.7	7039	6.3	5.3	-10.2	-7.3	-6.0	11.9
7040	-0.1	0.5	1.4	7040	0.3	-2.1	-4.7	-0.4	2.7	6.1
7043	-0.2	-0.0	-0.0	7043	7.9	1.9	0.9	-8.1	-2.0	-0.9
7045	-3.7	1.0	-0.7	7045	9.0	-4.5	3.6	-12.7	5.5	-4.3
7072	0.2	0.0	-0.1	7072	-5.1	-0.9	3.1	5.4	0.9	-3.2
7075	-1.0	-0.5	0.3	7075	9.6	4.7	-2.9	-10.7	-5.2	3.2
7076	-1.0	-3.0	-0.7	7076	5.1	10.4	2.4	-6.1	-13.3	-3.1
9001	-0.9	0.8	0.8	9001	1.2	-2.0	-3.4	-2.1	2.8	4.2
9002	0.6	0.7	-1.1	9002	-1.6	-2.3	1.7	2.2	3.0	-2.8
9004	-1.7	30.2	-3.4	9004	2.3	-5.8	5.4	-4.0	35.9	-8.8
9005	13.0	-11.9	9.1	9005	-7.8	7.9	-10.0	20.8	-19.9	19.1
9006	13.0	-9.6	1.7	9006	-2.2	6.5	-1.5	15.2	-16.1	3.2
9008	-2.4	2.1	2.1	9008	2.9	-3.0	-4.4	-5.3	5.2	6.5
9009	1.3	-0.4	-0.6	9009	-12.0	6.1	3.1	13.3	-6.5	-3.7
9010	0.9	-0.9	-0.3	9010	-5.4	6.4	2.2	6.3	-7.3	-2.5
9012	1.5	0.8	-1.3	9012	-3.3	-2.0	3.1	4.8	2.8	-4.5
9021	2.6	-0.4	-1.6	9021	-5.0	1.3	6.5	7.6	-1.7	-8.2
9028	1.0	-0.2	0.3	9028	-13.7	2.4	-2.2	14.8	-2.6	2.5
9031	-5.6	1.8	-20.9	9031	5.2	-2.3	10.7	-10.9	4.1	-31.5
9091	-4.1	17.8	-2.4	9091	10.3	-7.3	7.4	-14.4	25.1	-9.8
9425	-0.1	-0.4	-0.4	9425	1.5	8.6	7.5	-1.6	-8.9	-7.9
9427	2.1	-32.0	2.2	9427	-4.6	9.9	-5.2	6.7	-41.9	7.4

TABLE 8.27.—*Transformation: WN14 – GSFC 73*

SCALE FACTOR AND ROTATION PARAMETERS CONSTRAINED

SOLUTION FOR 3 TRANSLATION, 1 SCALE AND 3 ROTATION PARAMETERS

(USING VARIANCES ONLY)

DU METERS	DV METERS	DW METERS	DELTA (X1.D+6)	OMEGA SECONDS	PSI SECONDS	EPSILON SECONDS
13.73	12.86	-1.70	0.96	-0.38	0.1"	0.24

VARIANCE - COVARIANCE MATRIX

$\sigma_o^2 =$ 1.09

0.218D+01	-0.646D-01	-0.166D-01	-0.125D-07	0.265D-07	0.500D-07	0.629D-08
-0.646D-01	0.203D+01	0.449D-01	0.508D-07	0.113D-07	-0.190D-07	-0.542D-07
-0.166D-01	0.449D-01	0.362D+01	-0.369D-07	0.132D-07	-0.343D-07	-0.648D-07
-0.125D-07	0.508D-07	-0.369D-07	0.123D-13	-0.133D-15	-0.537D-16	0.132D-15
0.265D-07	0.113D-07	0.132D-07	-0.133D-15	0.111D-13	-0.380D-14	-0.308D-14
0.500D-07	-0.190D-07	-0.343D-07	-0.537D-16	-0.380D-14	0.223D-13	0.595D-14
0.629D-08	-0.542D-07	-0.648D-07	0.132D-15	-0.308D-14	0.595D-14	0.179D-13

COEFFICIENTS OF CORRELATION

0.100D+01	-0.308D-01	-0.592D-02	-0.761D-01	0.170D+00	0.227D+00	0.318D-01
-0.308D-01	0.100D+01	0.166D-01	0.321D+00	0.753D-01	-0.894D-01	-0.284D+00
-0.592D-02	0.166D-01	0.100D+01	-0.174D+00	0.660D-01	-0.121D+00	-0.254D+00
-0.761D-01	0.321D+00	-0.174D+00	0.100D+01	-0.113D-01	-0.323D-02	0.889D-02
0.170D+00	0.753D-01	0.660D-01	-0.113D-01	0.100D+01	-0.241D+00	-0.218D+00
0.227D+00	-0.894D-01	-0.121D+00	-0.323D-02	-0.241D+00	0.100D+01	0.297D+00
0.318D-01	-0.284D+00	-0.254D+00	0.889D-02	-0.218D+00	0.297D+00	0.100D+01

TABLE 8.27.—*(Cont'd)*

	RESIDUALS V								
	V1 (GSFC-73)			V2 (WN14)			V1 - V2		
1021	0.2	-0.3	-0.3	1021	-1.3	2.7	3.5	1.5	-3.0	-3.8
1022	0.9	0.2	0.0	1022	-3.8	-0.6	-0.3	4.7	0.8	0.3
1030	-4.7	-0.6	1.1	1030	2.7	0.7	-4.5	-7.4	-1.2	5.5
1034	-1.1	1.3	0.7	1034	2.5	-2.3	-4.2	-3.6	3.6	4.9
1042	3.7	-1.0	-0.3	1042	-10.0	2.2	1.9	13.7	-3.2	-2.2
7036	-2.9	2.0	-0.1	7036	6.2	-5.4	0.9	-9.1	7.4	-1.0
7037	0.2	1.5	0.5	7037	-0.4	-4.0	-3.4	0.6	5.5	3.8
7039	0.2	-2.1	1.8	7039	-0.5	5.3	-8.1	0.7	-7.5	9.9
7040	0.6	0.7	0.3	7040	-1.2	-1.5	-1.1	1.8	2.3	1.4
7045	-3.9	0.6	-0.1	7045	4.7	-1.3	0.8	-8.7	1.9	-0.9
7072	0.7	-0.3	-0.3	7072	-7.9	4.6	4.4	8.6	-4.9	-4.7
7075	-2.0	-0.5	0.6	7075	4.5	0.9	-2.6	-6.5	-1.4	3.1
7076	-1.8	-5.7	-3.3	7076	3.5	7.4	7.8	-5.3	-13.0	-11.1
9001	-2.0	0.1	0.1	9001	3.7	-0.4	-0.7	-5.7	0.5	0.8
9002	1.1	-0.9	0.8	9002	-1.9	2.6	-1.8	3.0	-3.6	2.6
9004	-1.8	25.5	-2.1	9004	1.7	-5.0	4.7	-3.5	30.5	-6.8
9005	5.9	-4.8	3.6	9005	-11.2	23.7	-13.1	17.0	-28.4	16.7
9006	11.1	-5.4	0.2	9006	-7.7	15.3	-0.7	18.9	-20.8	0.9
9008	-2.2	-0.1	0.6	9008	14.3	0.6	-6.2	-16.5	-0.6	6.8
9009	0.6	-0.2	-0.0	9009	-17.2	9.6	1.0	17.8	-9.8	-1.1
9012	1.6	-0.2	0.3	9012	-5.7	0.8	-1.9	7.2	-0.9	2.2
9021	2.1	-3.3	-3.1	9021	-1.6	2.8	6.7	3.7	-6.2	-9.8
9028	0.6	-0.2	0.9	9028	-10.1	3.1	-9.9	10.7	-3.3	10.7
9031	-9.8	5.1	-14.7	9031	9.0	-5.3	10.4	-18.8	10.4	-25.1
9091	-3.2	24.9	-1.8	9091	4.4	-7.1	5.0	-7.6	32.0	-6.9
9425	-0.0	-0.5	-0.2	9425	0.4	5.8	2.9	-0.4	-6.3	-3.0

TABLE 8.28.—*Shifts to the Geocenter (Solution WN14)*

Source	u_o (m)	v_o (m)	w_o (m)	r_o (m)
1. Dynamic comparison	15.9 ± 0.3	11.7 ± 1.3	−5.0 ± 2.6	19.5 ± 1.1
2. Geometric fit (sec. 8.5.1)	23.2 ± 0.9	2.9 ± 0.8	−2.7 ± 1.2	23.4 ± 1.2
3. Weighted mean of 1 and 2	16.4 ± 1.9	5.4 ± 4.0	−3.1 ± 0.9	21.8 ± 1.2
4. JPL/DSN	---	---	---	25.9 ± 2.5

TABLE 8.29.—*Relationship Between Various Geodetic Datums and the WN System (Datum − WN14)*

Datum no.	Datum name[a]	No. of stations	Δu (m) [b]	Δv (m) [b]	Δw (m) [b]	ω(") [c]	ψ(") [c]	ϵ(") [c]	$\Delta(\times 10^6)$
1	Adindan (Ethiopia)	2	184 ± 19	21 ± 11	−200 ± 6	----------	----------	----------	----------
2	American Samoa 1962	1	119 ± 8	−105 ± 8	−413 ± 10	----------	----------	----------	----------
3	Arc Cape (South Africa)	1	152 ± 7	126 ± 7	298 ± 10	----------	----------	----------	----------
5	Ascension Island 1958	1	227 ± 7	−93 ± 7	−58 ± 8	----------	----------	----------	----------
6	Australian Geodetic	3	157.0 ± 3.2	59.2 ± 3.2	−131.2 ± 3.6	1.03 ± 0.49	0.97 ± 0.48	−27.0 ± 0.59	−1.14 ± 1.83
10	Camp Area Astro 1961/62 (USGS)	1	111 ± 10	148 ± 9	−238 ± 10	----------	----------	----------	----------
12	Christmas Island Astro 1967	1	−115 ± 9	−224 ± 12	529 ± 8	----------	----------	----------	----------
15	Easter Island Astro 1967	1	−182 ± 10	−138 ± 10	−128 ± 11	----------	----------	----------	----------
16	European-50 (W)[d]	11	100.0 ± 5.3	125.8 ± 5.2	115.8 ± 5.3	−1.06 ± 1.37	0.10 ± 1.03	0.11 ± 1.60	−8.43 ± 4.34
	European-50 (All stations)[e]	16	99.4 ± 5.0	132.2 ± 5.0	116.4 ± 4.8	−0.08 ± 0.67	0.03 ± 0.93	−41.0 ± 0.74	−6.06 ± 2.83
17	Graciosa Island (Azores)	1	123 ± 17	−147 ± 9	37 ± 17	----------	----------	----------	----------
20	Heard Astro 1969	1	182 ± 12	56 ± 12	−114 ± 14	----------	----------	----------	----------
22	Indian[f]	1	−165 ± 17	−711 ± 10	−228 ± 11	----------	----------	----------	----------
23	Isla Socorro Astro	1	−134 ± 12	−206 ± 7	−503 ± 9	----------	----------	----------	----------
24	Johnston Island 1961	1	−161 ± 13	51 ± 25	211 ± 13	----------	----------	----------	----------
26	Luzon 1911 (Philippines)	1	151 ± 10	51 ± 7	111 ± 8	----------	----------	----------	----------
27	Midway Astro 1961	1	−377 ± 7	84 ± 7	−279 ± 9	----------	----------	----------	----------
28	New Zealand 1949	1	−61 ± 8	41 ± 9	−192 ± 9	----------	----------	----------	----------
29	North American 1927 (W)[g]	8	20.6 ± 2.7	−139.3 ± 3.1	−179.6 ± 2.7	0.22 ± 0.44	0.49 ± 0.48	−0.30 ± 0.52	−7.60 ± 1.66
	North American 1927 (E)[h]	13	54.5 ± 19.5	−144.2 ± 11.5	−196.7 ± 11.6	0.96 ± 0.56	−0.03 ± 0.46	0.54 ± 0.40	2.26 ± 1.62
	North American (all stations)[i]	21	31.6 ± 1.7	−142.1 ± 1.6	−177.3 ± 1.5	0.89 ± 0.20	0.23 ± 0.19	0.38 ± 0.34	0.96 ± 0.98
36	Pitcairn Island Astro	1	127 ± 12	−768 ± 11	−60 ± 11	----------			
39	Provisional South Chile 1963	1	0 ± 8	−196 ± 8	−93 ± 9	----------	----------	----------	----------
41	South American 1969[j]	10	97.1 ± 4.0	13.4 ± 4.3	29.8 ± 4.1	−0.59 ± 0.43	0.25 ± 0.31	−0.11 ± 0.34	6.66 ± 1.41
42	Southeast Island (Mahe)	1	54 ± 8	186 ± 8	272 ± 9	----------	----------	----------	----------
43	South Georgia Astro	1	820 ± 8	−101 ± 11	291 ± 11	----------	----------	----------	----------
46	Tokyo	1	183 ± 10	−506 ± 9	−686 ± 9	----------	----------	----------	----------
47	Tristan Astro 1968	1	654 ± 14	−420 ± 11	622 ± 13	----------	----------	----------	----------
49	Wake Island Astronomic 1952	1	−260 ± 7	67 ± 12	−140 ± 8	----------	----------	----------	----------
50	Yof Astro 1967 (Dakar)	1	55 ± 6	−143 ± 7	−95 ± 7	----------	----------	----------	----------
51	Palmer Astro 1969	1	−218 ± 9	−8 ± 12	−226 ± 12	----------	----------	----------	----------

[a] See table 8.4 for datum description and other related information.
[b] If (datum—geocenter) is sought, add to the tabulated values of Δu, Δv, Δw the respective quantities −16 m, −5 m, 3 m (see table 8.28).
[c] ω, ψ, ϵ, when positive, represent counterclockwise rotations about the respective w, v, u axes, as viewed from the end of the positive axis.
[d] Stations included are Tromsø (6006), Catania (6016), Hohenpeissenberg (6065) Wippolder (8009) Zimmerwald (8010), Haute Provence (8015), Nice (8019), Meudon (8030), San Fernando (9004), Dionysos (9091), and Harestua (9426).
[e] Stations included are as in (d) and Mashhad (6015), Malvern (8011), Naini Tal (9006), Shiraz (9008), and Riga (9431).
[f] Based on p. 70, *Bulletin Geodesique*, 107, 1973.
[g] Stations included are Goldstone (1030), Colorado Springs (3400), Vandenberg AFB (4280), Wrightwood II (6134), Moses Lake (6003), Edinburg (7036), Denver (7045), and Organ Pass (9001).
[h] Stations included are Blossom Point (1021), Fort Myers (1022), E. Grand Forks (1034), Rosman (1042), Bedford (3401), Semmes (3402), Hunter AFB (3648), Aberdeen (3657), Homestead (3861), Beltsville (6002), Greenbelt (7043), Jupiter (7072), and Sudbury (7075).
[i] Stations included are as in (g) and (h) above.
[j] Stations included are Brasilia (3414), Asunción (3431), Bogotá (3477), Paramaribo (6008), Quito (6009), Villa Dolores (6019), Natal (6067), Arequipa (9007), Curaçao (9009), and Comodoro Rivadavia (9031).

TABLE 8.30.—*Transformation: WN14 – Australian Datum*

SCALE FACTOR AND ROTATION PARAMETERS CONSTRAINED

SOLUTION FOR 3 TRANSLATION, 1 SCALE AND 3 ROTATION PARAMETERS

(USING VARIANCES ONLY)

DU METERS	DV METERS	DW METERS	DELTA (X1.D+6)	OMEGA SECONDS	PSI SECONDS	EPSILON SECONDS
-156.97	-59.14	131.23	1.20	-1.03	-0.99	0.25
± 1.85	± 1.82	± 2.03	± 0.71	± 0.18	± 0.18	± 0.22

VARIANCE - COVARIANCE MATRIX

σ_0^2 = 0.48

0.341D+01	0.615D-02	0.258D-01	0.511D-07	0.236D-06	0.104D-06	-0.628D-07
0.615D-02	0.331D+01	0.444D-01	0.172D-06	0.125D-07	-0.775D-07	-0.224D-06
0.258D-01	0.444D-01	0.410D+01	-0.903D-07	0.135D-06	-0.560D-07	-0.384D-06
0.511D-07	0.172D-06	-0.903D-07	0.507D-12	0.335D-14	-0.155D-13	-0.457D-14
0.236D-06	0.125D-07	0.135D-06	0.335D-14	0.765D-12	-0.148D-12	-0.408D-12
0.104D-06	-0.775D-07	-0.560D-07	-0.155D-13	-0.148D-12	0.748D-12	0.379D-12
-0.628D-07	-0.224D-06	-0.384D-06	-0.457D-14	-0.408D-12	0.379D-12	0.114D-11

COEFFICIENTS OF CORRELATION

0.100D+01	0.183D-02	0.690D-02	0.389D-01	0.146D+00	0.652D-01	-0.318D-01
0.183D-02	0.100D+01	0.120D-01	0.133D+00	0.787D-02	-0.492D-01	-0.115D+00
0.690D-02	0.120D-01	0.100D+01	-0.626D-01	0.763D-01	-0.320D-01	-0.177D+00
0.389D-01	0.133D+00	-0.626D-01	0.100D+01	0.539D-02	-0.252D-01	-0.600D-02
0.146D+00	0.787D-02	0.763D-01	0.539D-02	0.100D+01	-0.196D+00	-0.436D+00
0.652D-01	-0.492D-01	-0.320D-01	-0.252D-01	-0.196D+00	0.100D+01	0.410D+00
-0.318D-01	-0.115D+00	-0.177D+00	-0.600D-02	-0.436D+00	0.410D+00	0.100D+01

TABLE 8.30.—*(Cont'd)*

RESIDUALS V

	V1(AUS.NAT.)			V2(WN- 14)			V1 - V2		
6023	0.9	-0.4	-2.9	6023	-0.8	0.4	1.8	1.7	-0.8	-4.8
6032	1.0	1.2	0.7	6032	-0.9	-1.2	-0.5	2.0	2.4	1.2
6060	-1.9	-0.8	1.9	6060	1.8	0.7	-1.4	-3.7	-1.5	3.2

UNIT OF RESIDUALS (METERS)

TABLE 8.31.—*Transformation: WN14 – European 50 Datum (W)*

SCALE FACTOR AND ROTATION PARAMETERS CONSTRAINED

SOLUTION FOR 3 TRANSLATION, 1 SCALE AND 3 ROTATION PARAMETERS

(USING VARIANCES ONLY)

DU METERS	DV METERS	DW METERS	DELTA (X1.D+6)	OMEGA SECONDS	PSI SECONDS	EPSILON SECONDS
-99.58	-124.88	-116.37	7.75	1.37	-0.04	0.13
± 4.26	± 4.42	± 4.25	± 1.39	± 0.50	± 0.38	± 0.58

VARIANCE - COVARIANCE MATRIX

σ_0^2 = 0.82

0.181D+02	-0.196D-01	0.421D+00	-0.736D-06	0.125D-05	-0.146D-05	-0.956D-06
-0.196D-01	0.195D+02	-0.165D+00	0.275D-06	0.572D-06	0.168D-07	0.159D-05
0.421D+00	-0.165D+00	0.181D+02	0.753D-06	0.974D-06	-0.140D-05	-0.162D-05
-0.736D-06	0.275D-06	0.753D-06	0.194D-11	0.377D-14	-0.622D-15	-0.703D-14
0.125D-05	0.572D-06	0.974D-06	0.377D-14	0.588D-11	-0.788D-12	-0.406D-11
-0.146D-05	0.168D-07	-0.140D-05	-0.622D-15	-0.788D-12	0.338D-11	0.785D-12
-0.956D-06	0.159D-05	-0.162D-05	-0.703D-14	-0.406D-11	0.785D-12	0.793D-11

COEFFICIENTS OF CORRELATION

0.100D+01	-0.104D-02	0.233D-01	-0.124D+00	0.121D+00	-0.186D+00	-0.797D-01
-0.104D-02	0.100D+01	-0.878D-02	0.446D-01	0.534D-01	0.207D-02	0.128D+00
0.233D-01	-0.878D-02	0.100D+01	0.127D+00	0.945D-01	-0.179D+00	-0.135D+00
-0.124D+00	0.446D-01	0.127D+00	0.100D+01	0.112D-02	-0.243D-03	-0.179D-02
0.121D+00	0.534D-01	0.945D-01	0.112D-02	0.100D+01	-0.177D+00	-0.594D+00
-0.186D+00	0.207D-02	-0.179D+00	-0.243D-03	-0.177D+00	0.100D+01	0.152D+00
-0.797D-01	0.128D+00	-0.135D+00	-0.179D-02	-0.594D+00	0.152D+00	0.100D+01

TABLE 8.31.—*(Cont'd)*

RESIDUALS V

	V1(ED-50(W))				V2(WN- 14)				V1 - V2		
6006	-0.0	-0.7	0.4	6006	0.2	19.5	-11.4		-0.2	-20.1	11.8
6016	0.4	-1.0	-0.0	6016	-16.8	31.3	1.4		17.2	-32.3	-1.4
6065	0.2	-0.7	-0.3	6065	-3.5	9.1	3.6		3.6	-9.8	-3.9
8009	-3.3	1.8	0.4	8009	11.8	-4.5	-2.1		-15.2	6.3	2.5
8010	-1.4	2.5	0.9	8010	11.0	-9.5	-7.7		-12.5	12.1	8.6
8015	-0.3	6.5	-0.1	8015	2.5	-14.6	1.1		-2.8	21.1	-1.3
8019	-0.0	2.1	-0.1	8019	1.5	-21.1	1.8		-1.5	23.2	-1.9
8030	-2.4	9.5	0.4	8030	8.3	-14.7	-1.6		-10.8	24.3	2.0
9004	0.0	2.0	-0.0	9004	-1.7	-20.8	0.3		1.8	22.8	-0.4
9091	0.0	6.8	-0.3	9091	-1.0	-28.5	6.1		1.1	35.3	-6.4
9426	0.1	3.2	-0.4	9426	-0.5	-16.2	5.0		0.5	19.4	-5.4

UNIT OF RESIDUALS (METERS)

TABLE 8.32.—*Transformation: WN14 – European 50 Datum*

SCALE FACTOR AND ROTATION PARAMETERS CONSTRAINED

SOLUTION FOR 3 TRANSLATION, 1 SCALE AND 3 ROTATION PARAMETERS

(USING VARIANCES ONLY)

DU METERS	DV METERS	DW METERS	DELTA (X1.D+6)	OMEGA SECONDS	PSI SECONDS	EPSILON SECONDS
-99.43	-132.00	-115.98	6.75	0.31	-0.14	0.48
± 4.39	± 4.54	± 4.34	± 0.84	± 0.21	± 0.32	± 0.23

VARIANCE - COVARIANCE MATRIX

$\sigma_o^2 =$ 1.03

0.193D+02	0.187D+00	0.172D+00	-0.153D-06	0.101D-06	-0.102D-05	0.306D-06
0.187D+00	0.206D+02	0.100D+00	-0.129D-06	0.228D-06	-0.406D-06	0.597D-06
0.172D+00	0.100D+00	0.188D+02	0.316D-06	0.109D-06	-0.557D-06	0.302D-06
-0.153D-06	-0.129D-06	0.316D-06	0.700D-12	-0.168D-14	-0.167D-15	-0.241D-15
0.101D-06	0.228D-06	0.109D-06	-0.168D-14	0.105D-11	-0.490D-12	0.986D-13
-0.102D-05	-0.406D-06	-0.557D-06	-0.167D-15	-0.490D-12	0.236D-11	-0.698D-12
0.306D-06	0.597D-06	0.302D-06	-0.241D-15	0.986D-13	-0.698D-12	0.126D-11

COEFFICIENTS OF CORRELATION

0.100D+01	0.936D-02	0.901D-02	-0.417D-01	0.225D-01	-0.151D+00	0.621D-01
0.936D-02	0.100D+01	0.508D-02	-0.339D-01	0.491D-01	-0.583D-01	0.117D+00
0.901D-02	0.508D-02	0.100D+01	0.870D-01	0.246D-01	-0.837D-01	0.621D-01
-0.417D-01	-0.339D-01	0.870D-01	0.100D+01	-0.196D-02	-0.130D-03	-0.256D-03
0.225D-01	0.491D-01	0.246D-01	-0.196D-02	0.100D+01	-0.312D+00	0.858D-01
-0.151D+00	-0.583D-01	-0.837D-01	-0.130D-03	-0.312D+00	0.100D+01	-0.405D+00
0.621D-01	0.117D+00	0.621D-01	-0.256D-03	0.858D-01	-0.405D+00	0.100D+01

TABLE 8.32.—*(Cont'd)*

RESIDUALS V

	V1(ED- 50)			V2(WN- 14)			V1 - V2		
6006	0.1	-1.1	0.4	6006	-2.9	33.2	-12.0	2.9	-34.3	12.4
6015	0.1	0.0	0.1	6015	-12.4	-4.3	-14.6	12.4	4.3	14.7
6016	0.3	-1.2	-0.0	6016	-13.1	35.0	1.1	13.4	-36.2	-1.1
6065	0.2	-1.1	-0.2	6065	-3.3	14.1	3.1	3.5	-15.3	-3.3
8009	-2.7	0.1	0.6	8009	9.5	-0.2	-3.3	-12.2	0.3	3.9
8010	-1.3	1.6	1.0	8010	10.1	-5.8	-8.7	-11.4	7.3	9.7
8011	-0.5	10.0	0.2	8011	3.9	-30.7	-2.1	-4.3	40.6	2.2
8015	-0.2	5.4	0.0	8015	1.4	-12.1	-0.1	-1.6	17.4	0.1
8019	-0.0	1.8	-0.0	8019	0.9	-17.6	0.7	-1.0	19.3	-0.7
8030	-1.7	7.7	0.7	8030	5.8	-11.9	-2.9	-7.4	19.5	3.6
9004	0.1	1.9	0.0	9004	-7.3	-19.8	-3.0	7.4	21.7	3.1
9006	-1.5	0.4	-0.2	9006	6.0	-8.4	3.9	-7.5	8.8	-4.1
9008	-0.5	0.9	0.7	9008	7.5	-15.7	-12.5	-8.1	16.6	13.3
9091	-0.2	5.7	-0.3	9091	5.9	-23.6	6.9	-6.1	29.3	-7.2
9426	0.4	1.6	-0.3	9426	-2.6	-8.2	4.4	3.1	9.9	-4.7
9431	-0.5	14.0	-3.6	9431	1.4	-70.5	32.4	-1.9	84.5	-36.0

UNIT OF RESIDUALS (METERS)

TABLE 8.33.—*Transformation: WN14 – NAD 1927 (W)*

SCALE FACTOR AND ROTATION PARAMETERS CONSTRAINED

SOLUTION FOR 3 TRANSLATION, 1 SCALE AND 3 ROTATION PARAMETERS

(USING VARIANCES ONLY)

DU METERS	DV METERS	DW METERS	DELTA (X1.D+6)	OMEGA SECONDS	PSI SECONDS	EPSILON SECONDS
-20.07	139.51	179.29	7.91	-0.21	-0.59	0.45
± 1.87	± 1.89	± 1.72	± 0.46	± 0.20	± 0.21	± 0.23

VARIANCE - COVARIANCE MATRIX

$\sigma_o^2 =$ 0.29

0.350D+01	0.278D+00	-0.387D+00	0.188D-06	-0.174D-06	-0.465D-06	0.261D-06
0.278D+00	0.357D+01	-0.520D+00	0.803D-08	-0.107D-05	-0.630D-06	0.893D-06
-0.387D+00	-0.520D+00	0.295D+01	0.549D-07	0.351D-06	0.996D-06	-0.421D-06
0.188D-06	0.803D-08	0.549D-07	0.207D-12	-0.639D-14	-0.580D-14	0.102D-13
-0.174D-06	-0.107D-05	0.351D-06	-0.639D-14	0.930D-12	0.395D-12	-0.382D-12
-0.465D-06	-0.630D-06	0.996D-06	-0.580D-14	0.395D-12	0.105D-11	-0.579D-12
0.261D-06	0.893D-06	-0.421D-06	0.102D-13	-0.382D-12	-0.579D-12	0.123D-11

COEFFICIENTS OF CORRELATION

0.100D+01	0.787D-01	-0.120D+00	0.220D+00	-0.966D-01	-0.242D+00	0.126D+00
0.787D-01	0.100D+01	-0.160D+00	0.933D-02	-0.586D+00	-0.325D+00	0.426D+00
-0.120D+00	-0.160D+00	0.100D+01	0.702D-01	0.212D+00	0.565D+00	-0.221D+00
0.220D+00	0.933D-02	0.702D-01	0.100D+01	-0.146D-01	-0.124D-01	0.201D-01
-0.966D-01	-0.586D+00	0.212D+00	-0.146D-01	0.100D+01	0.400D+00	-0.356D+00
-0.242D+00	-0.325D+00	0.565D+00	-0.124D-01	0.400D+00	0.100D+01	-0.508D+00
0.126D+00	0.426D+00	-0.221D+00	0.201D-01	-0.356D+00	-0.508D+00	0.100D+01

TABLE 8.33.—*(Cont'd)*

RESIDUALS V

	V1(NAD27(W))				V2(WN- 14)				V1 - V2		
1030	-0.9	0.4	1.6	1030	4.6	-1.5	-6.9		-5.5	2.0	8.5
3400	2.2	0.5	3.0	3400	-6.9	-2.9	-6.8		9.2	3.4	9.8
4280	0.1	-0.2	-0.9	4280	-0.5	0.9	3.8		0.6	-1.1	-4.7
6003	0.2	-0.1	-0.2	6003	-4.5	4.3	1.7		4.7	-4.4	-1.9
6134	0.2	-0.2	-0.6	6134	-2.5	1.8	4.9		2.7	-2.0	-5.5
7036	-0.1	-0.4	-1.0	7036	0.2	1.6	3.6		-0.4	-2.0	-4.5
7045	-1.1	0.5	0.0	7045	2.3	-2.0	-0.0		-3.4	2.5	0.0
9001	-0.2	0.1	0.5	9001	2.7	-2.0	-5.4		-2.9	2.2	5.9

UNIT OF RESIDUALS (METERS)

TABLE 8.34.—*Transformation: WN14 – NAD 1927 (E)*

SCALE FACTOR AND ROTATION PARAMETERS CONSTRAINED

SOLUTION FOR 3 TRANSLATION, 1 SCALE AND 3 ROTATION PARAMETERS

(USING VARIANCES ONLY)

DU METERS	DV METERS	DW METERS	DELTA (X1.D+6)	OMEGA SECONDS	PSI SECONDS	EPSILON SECONDS
-30.98	140.97	174.93	-2.15	-1.01	0.01	-0.54
± 1.76	± 2.01	± 1.88	± 0.62	± 0.19	± 0.16	± 0.14

VARIANCE - COVARIANCE MATRIX

σ_o^2 = 0.76

0.311D+01	-0.113D+00	0.392D-01	-0.566D-06	-0.258D-08	-0.127D-06	0.628D-08
-0.113D+00	0.404D+01	-0.871D+00	0.770D-07	0.128D-05	0.571D-06	0.210D-07
0.392D-01	-0.871D+00	0.355D+01	0.109D-06	-0.598D-06	-0.956D-06	0.505D-07
-0.566D-06	0.770D-07	0.109D-06	0.379D-12	0.130D-14	-0.194D-14	0.207D-15
-0.258D-08	0.128D-05	-0.598D-06	0.130D-14	0.866D-12	0.392D-12	-0.101D-12
-0.127D-06	0.571D-06	-0.956D-06	-0.194D-14	0.392D-12	0.618D-12	-0.676D-13
0.628D-08	0.210D-07	0.505D-07	0.207D-15	-0.101D-12	-0.676D-13	0.462D-12

COEFFICIENTS OF CORRELATION

0.100D+01	-0.320D-01	0.118D-01	-0.521D+00	-0.157D-02	-0.918D-01	0.524D-02
-0.320D-01	0.100D+01	-0.230D+00	0.622D-01	0.686D+00	0.362D+00	0.154D-01
0.118D-01	-0.230D+00	0.100D+01	0.941D-01	-0.341D+00	-0.645D+00	0.395D-01
-0.521D+00	0.622D-01	0.941D-01	0.100D+01	0.227D-02	-0.400D-02	0.495D-03
-0.157D-02	0.686D+00	-0.341D+00	0.227D-02	0.100D+01	0.535D+00	-0.159D+00
-0.918D-01	0.362D+00	-0.645D+00	-0.400D-02	0.535D+00	0.100D+01	-0.126D+00
0.524D-02	0.154D-01	0.395D-01	0.495D-03	-0.159D+00	-0.126D+00	0.100D+01

TABLE 8.34.—*(Cont'd)*

RESIDUALS V

	V1(NAD27(E))				V2(WN- 14)				V1 - V2		
1021	0.6	0.2	1.3	1021	-2.5	-1.0	-3.8		3.1	1.2	5.1
1022	0.1	0.8	0.5	1022	-0.7	-4.7	-2.5		0.8	5.5	3.0
1034	-3.2	1.1	0.6	1034	6.0	-3.2	-2.0		-9.2	4.3	2.6
1042	2.4	0.3	0.9	1042	-7.2	-1.1	-2.7		9.6	1.5	3.6
3401	1.6	-0.9	-1.0	3401	-6.7	3.5	2.9		8.3	-4.4	-3.8
3402	0.5	-0.5	0.4	3402	-0.8	1.7	-1.0		1.4	-2.2	1.4
3648	-1.2	0.4	1.4	3648	2.7	-1.7	-2.6		-3.9	2.1	4.1
3657	2.0	0.6	-0.4	3657	-7.3	-2.4	1.0		9.3	3.0	-1.4
3861	-1.3	-0.3	-0.0	3861	4.3	1.5	0.2		-5.7	-1.8	-0.2
6002	-0.1	-0.6	-0.9	6002	1.1	5.8	6.6		-1.3	-6.3	-7.5
7043	-0.2	-0.6	-0.9	7043	1.1	5.8	6.5		-1.3	-6.4	-7.4
7072	0.4	0.4	0.5	7072	-4.4	-4.4	-5.1		4.8	4.7	5.5
7075	-3.4	-1.2	-0.3	7075	7.9	3.5	0.9		-11.3	-4.8	-1.2

UNIT OF RESIDUALS (METERS)

TABLE 8.35.—*Transformation: WN14 – NAD 1927*

SCALE FACTOR AND ROTATION PARAMETERS CONSTRAINED

SOLUTION FOR 3 TRANSLATION, 1 SCALE AND 3 ROTATION PARAMETERS

(USING VARIANCES ONLY)

DU METERS	DV METERS	DW METERS	DELTA (X1.D+6)	OMEGA SECONDS	PSI SECONDS	EPSILON SECONDS
-31.71	142.34	177.32	-0.80	-0.86	-0.23	-0.33
± 1.35	± 1.26	± 1.23	± 0.27	± 0.06	± 0.05	± 0.10

VARIANCE - COVARIANCE MATRIX

$\sigma_o^2 =$ 0.76

0.182D+01	-0.258D-02	-0.280D-02	-0.724D-07	0.521D-08	-0.216D-07	0.823D-08
-0.258D-02	0.159D+01	0.154D-02	0.103D-07	0.624D-07	-0.318D-08	0.856D-07
-0.280D-02	0.154D-02	0.151D+01	0.207D-07	-0.757D-08	-0.565D-07	0.131D-07
-0.724D-07	0.103D-07	0.207D-07	0.734D-13	-0.200D-15	0.191D-16	0.262D-15
0.521D-08	0.624D-07	-0.757D-08	-0.200D-15	0.771D-13	0.959D-14	-0.100D-13
-0.216D-07	-0.318D-08	-0.565D-07	0.191D-16	0.959D-14	0.695D-13	-0.293D-13
0.823D-08	0.856D-07	0.131D-07	0.262D-15	-0.100D-13	-0.293D-13	0.242D-12

COEFFICIENTS OF CORRELATION

0.100D+01	-0.151D-02	-0.169D-02	-0.198D+00	0.139D-01	-0.607D-01	0.124D-01
-0.151D-02	0.100D+01	0.992D-03	0.302D-01	0.178D+00	-0.956D-02	0.138D+00
-0.169D-02	0.992D-03	0.100D+01	0.621D-01	-0.222D-01	-0.174D+00	0.217D-01
-0.198D+00	0.302D-01	0.621D-01	0.100D+01	-0.266D-02	0.267D-03	0.197D-02
0.139D-01	0.178D+00	-0.222D-01	-0.266D-02	0.100D+01	0.131D+00	-0.734D-01
-0.607D-01	-0.956D-02	-0.174D+00	0.267D-03	0.131D+00	0.100D+01	-0.226D+00
0.124D-01	0.138D+00	0.217D-01	0.197D-02	-0.734D-01	-0.226D+00	0.100D+01

TABLE 8.35.—*(Cont'd)*

RESIDUALS V

	V1(NAD-27)			V2(WN- 14)			V1 - V2		
1021	1.0	0.2	1.3	1021	-3.9	-0.9	-3.8	4.8	1.1	5.1
1022	0.0	0.5	0.5	1022	-0.1	-3.0	-2.3	0.2	3.5	2.8
1030	-0.5	-0.3	1.4	1030	2.7	0.9	-6.2	-3.2	-1.2	7.6
1034	-2.9	1.8	1.2	1034	5.4	-5.4	-3.9	-8.3	7.1	5.0
1042	2.5	0.2	1.1	1042	-7.6	-0.8	-3.1	10.1	1.0	4.1
3400	0.5	0.6	2.2	3400	-1.5	-3.2	-5.1	2.0	3.8	7.4
3401	2.2	-0.8	-1.1	3401	-9.1	3.1	3.1	11.3	-3.9	-4.2
3402	0.2	-0.7	0.7	3402	-0.3	2.4	-1.6	0.5	-3.1	2.3
3648	-1.1	0.2	1.5	3648	2.5	-0.8	-2.7	-3.6	1.0	4.2
3657	2.5	0.6	-0.4	3657	-8.8	-2.4	1.0	11.3	3.1	-1.4
3861	-1.5	-0.8	-0.2	3861	4.7	3.4	0.6	-6.2	-4.1	-0.8
4280	0.9	-1.0	-0.9	4280	-4.4	5.1	4.1	5.3	-6.1	-5.1
6002	0.1	-0.6	-0.9	6002	-0.5	5.8	6.5	0.5	-6.3	-7.4
6003	0.0	-0.5	-0.9	6003	-0.5	17.5	6.9	0.6	-18.1	-7.7
6134	0.5	-0.4	-0.6	6134	-5.5	4.5	5.2	6.0	-4.9	-5.8
7036	-2.2	2.2	0.2	7036	4.5	-9.6	-0.7	-6.7	11.7	0.9
7043	0.1	-0.6	-0.9	7043	-0.5	5.8	6.4	0.5	-6.4	-7.3
7045	-3.6	0.5	-0.6	7045	7.5	-1.9	2.0	-11.1	2.5	-2.6
7072	0.4	0.2	0.4	7072	-4.1	-2.5	-4.7	4.5	2.7	5.1
7075	-2.7	-0.8	-0.1	7075	6.3	2.3	0.2	-9.0	-3.1	-0.3
9001	-0.4	0.4	0.6	9001	5.2	-6.8	-6.2	-5.6	7.1	6.8

UNIT OF RESIDUALS (METERS)

TABLE 8.36.—*Transformation: WN14 – South American 1969 Datum*

SCALE FACTOR AND ROTATION PARAMETERS CONSTRAINED

SOLUTION FOR 3 TRANSLATION, 1 SCALE AND 3 ROTATION PARAMETERS

(USING VARIANCES ONLY)

DU METERS	DV METERS	DW METERS	DELTA (X1.D+6)	OMEGA SECONDS	PSI SECONDS	EPSILON SECONDS
-96.57	-13.67	-29.36	-6.67	0.63	-0.17	0.12
± 3.02	± 3.02	± 3.15	± 0.59	± 0.17	± 0.12	± 0.13

VARIANCE - COVARIANCE MATRIX

σ_0^2 = 0.97

0.915D+01	-0.172D+00	-0.202D+00	0.419D-06	0.325D-06	0.291D-06	0.674D-07
-0.172D+00	0.912D+01	0.697D-01	0.231D-06	-0.769D-06	0.579D-07	-0.409D-06
-0.202D+00	0.697D-01	0.989D+01	-0.410D-06	-0.122D-06	0.346D-06	-0.185D-06
0.419D-06	0.231D-06	-0.410D-06	0.352D-12	0.128D-14	0.159D-14	0.252D-14
0.325D-06	-0.769D-06	-0.122D-06	0.128D-14	0.657D-12	-0.103D-12	0.463D-14
0.291D-06	0.579D-07	0.346D-06	0.159D-14	-0.103D-12	0.340D-12	0.585D-13
0.674D-07	-0.409D-06	-0.185D-06	0.252D-14	0.463D-14	0.585D-13	0.373D-12

COEFFICIENTS OF CORRELATION

0.100D+01	-0.188D-01	-0.212D-01	0.234D+00	0.133D+00	0.165D+00	0.365D-01
-0.188D-01	0.100D+01	0.734D-02	0.129D+00	-0.314D+00	0.329D-01	-0.222D+00
-0.212D-01	0.734D-02	0.100D+01	-0.219D+00	-0.479D-01	0.189D+00	-0.965D-01
0.234D+00	0.129D+00	-0.219D+00	0.100D+01	0.266D-02	0.458D-02	0.696D-02
0.133D+00	-0.314D+00	-0.479D-01	0.266D-02	0.100D+01	-0.219D+00	0.934D-02
0.165D+00	0.329D-01	0.189D+00	0.458D-02	-0.219D+00	0.100D+01	0.164D+00
0.365D-01	-0.222D+00	-0.965D-01	0.696D-02	0.934D-02	0.164D+00	0.100D+01

TABLE 8.36.—*(Cont'd)*

RESIDUALS V

	V1(SAD-69)			V2(WN- 14)			V1 - V2		
3414	4.1	-1.3	6.3	3414	-1.8	0.8	-3.0	5.9	-2.1	9.2
3431	-1.0	2.5	0.1	3431	1.1	-3.7	-0.1	-2.0	6.2	0.2
3477	16.3	2.3	13.9	3477	-10.1	-3.4	-9.8	26.3	5.8	23.7
6008	0.0	0.3	2.0	6008	-0.3	-5.1	-14.6	0.4	5.4	16.6
6009	-2.0	-1.0	-1.9	6009	9.9	5.4	7.1	-11.9	-6.4	-9.0
6019	-0.1	-0.2	-0.8	6019	1.5	2.1	3.8	-1.6	-2.3	-4.6
6067	-0.2	-0.5	-0.8	6067	2.8	7.4	7.5	-3.0	-7.9	-8.3
9007	1.0	0.4	-1.2	9007	-10.7	-2.9	3.9	11.8	3.3	-5.1
9009	-0.5	0.0	-1.9	9009	5.8	-0.6	10.8	-6.3	0.6	-12.8
9031	-5.0	1.6	2.2	9031	4.6	-1.3	-1.1	-9.6	2.9	3.3

UNIT OF RESIDUALS (METERS)

TABLE 8.37.—*Summary of Cartesian Coordinates (Solutions WN12 and WN14)*

STATION		SOLUTION WN-12						SOLUTION WN-14					
NO	NAME	U	V	W	σ_u	σ_v	σ_w	U	V	W	σ_u	σ_v	σ_w
1021	BLOSSOM POINT	1118021.8	-4876331.7	3942970.9	3.1	4.0	4.2	1118023.1	-4876323.4	3942963.9	2.8	2.6	2.8
1022	FORT MYERS	807850.8	-5652004.0	2833509.0	2.6	3.3	3.3	807851.9	-5651989.6	2833500.2	2.2	1.9	2.3
1030	GOLDSTONE	-2357249.2	-4646346.4	3668312.5	6.1	4.4	4.7	-2357242.9	-4646338.5	3668306.8	5.6	3.3	3.2
1032	ST. JOHN'S	2602704.3	-3419179.7	4697621.1	49.1	89.5	29.9	2602688.6	-3419228.9	4697637.3	39.3	46.7	13.8
1033	FAIRBANKS	-2299292.3	-1445690.5	5751823.3	7.5	10.0	10.5	-2299282.6	-1445693.7	5751811.6	6.9	9.7	5.7
1034	E. GRAND FORKS	-521708.3	-4242074.9	4718726.5	3.5	4.0	4.4	-521704.5	-4242064.3	4718716.8	3.1	3.0	2.7
1042	ROSMAN	647495.9	-5177948.0	3656714.4	3.1	3.6	4.0	647497.5	-5177935.6	3656705.9	2.8	2.4	2.8
3106	ANTIGUA	2881840.5	-5372180.7	1868548.5	4.1	4.6	4.9	2881838.3	-5372164.6	1868538.6	3.7	3.3	4.3
3334	STONEVILLE	-84969.1	-5327986.3	3493434.3	15.6	14.0	10.8	-84963.8	-5327974.9	3493428.3	13.6	6.8	9.0
3400	COLORADO SPRINGS	-1275239.4	-4798062.9	3994229.5	16.3	12.4	8.6	-1275207.2	-4798029.3	3994208.3	9.1	5.1	5.7
3401	BEDFORD	1513134.8	-4463580.1	4283061.2	3.5	5.3	4.6	1513136.1	-4463576.8	4283055.8	3.2	3.4	3.0
3402	SEMMES	167256.1	-5481980.4	3245042.6	4.2	4.3	4.6	167259.7	-5481971.0	3245037.0	3.9	2.8	3.5
3404	SWAN ISLAND	642485.7	-6053942.4	1895690.5	5.0	5.3	5.5	642491.4	-6053940.3	1895688.6	4.7	3.7	4.9
3405	GRAND TURK	1919482.1	-5621096.5	2315780.1	3.6	5.6	4.9	1919482.9	-5621088.1	2315775.3	3.3	3.5	4.0
3406	CURACAO	2251802.9	-5816929.0	1327197.4	2.8	3.5	3.8	2251800.2	-5816912.9	1327191.1	2.4	2.1	3.4
3407	TRINIDAD	2979892.9	-5513532.6	1181126.8	5.2	5.1	5.9	2979891.1	-5513530.9	1181129.3	4.7	3.4	5.3
3413	NATAL	5186366.4	-3654225.1	-653022.7	3.4	2.9	3.2	5186348.4	-3654222.4	-653018.9	2.1	2.2	2.7
3414	BRASILIA	4114987.8	-4554148.5	-1732166.1	9.9	8.4	7.9	4114977.8	-4554142.5	-1732154.0	7.7	6.1	7.2
3431	ASUNCION	3093056.1	-4870100.4	-2710845.8	8.5	9.3	12.5	3093045.4	-4870081.7	-2710823.0	7.6	6.5	10.8
3476	PARAMARIBO	3623293.6	-5214213.7	601514.0	3.4	3.3	3.6	3623277.3	-5214210.7	601515.3	2.2	2.0	3.0
3477	BOGOTA	1744649.6	-6114305.6	532205.2	10.4	13.7	9.8	1744650.2	-6114286.7	532208.6	10.2	6.6	9.6
3478	MANAUS	3185785.4	-5514574.5	-347713.2	19.3	35.4	35.8	3185777.0	-5514585.9	-347703.2	18.7	14.5	35.1
3499	QUITO	1280834.0	-6250966.2	-10805.5	3.8	5.9	4.5	1280834.2	-6250955.9	-10800.6	3.6	3.4	4.1
3648	HUNTER AFB	832562.6	-5349553.4	3360596.4	4.1	5.0	5.4	832566.2	-5349540.7	3360585.3	3.6	2.5	3.6
3657	ABERDEEN	1186786.1	-4785205.1	4032892.3	3.4	5.0	4.5	1186787.1	-4785193.1	4032882.3	3.1	3.0	3.0
3861	HOMESTEAD	961766.7	-5679170.6	2729893.8	3.3	3.8	3.7	961767.9	-5679156.6	2729883.5	3.0	2.3	2.6
3902	CHEYENNE	-1234689.4	-4651235.9	4174763.4	28.6	32.1	11.3	-1234700.7	-4651242.8	4174758.6	8.6	6.3	6.3
3903	HERNDON	1088980.0	-4842973.2	3991763.9	12.3	15.5	11.4	1088989.7	-4843005.4	3991776.6	12.1	8.5	8.9
4050	PRETORIA	5051614.8	2726608.6	-2774181.0	4.4	3.8	5.5	5051608.1	2726603.3	-2774166.8	3.2	3.2	4.4
4061	ANTIGUA	2881594.5	-5372540.2	1868034.3	4.2	4.7	5.0	2881592.3	-5372523.9	1868024.4	3.8	3.5	4.3
4081	GRAND TURK	1920409.9	-5619426.1	2319133.4	3.7	5.7	5.0	1920410.9	-5619417.8	2319128.5	3.3	3.6	4.0
4082	MERRITT ISLAND	910567.9	-5539130.2	3017974.8	2.9	3.8	3.7	910567.2	-5539113.2	3017965.3	2.6	2.4	2.8
4280	VANDENBERG AFB	-2671883.7	-4521217.3	3607495.0	4.3	4.4	4.8	-2671873.8	-4521210.5	3607490.4	3.8	3.3	3.6
4740	BERMUDA	2308888.6	-4874314.8	3393092.0	3.8	5.4	5.1	2308887.3	-4874298.2	3393082.1	3.3	3.1	3.8
5001	HERNDON	1088874.4	-4842954.9	3991857.8	4.9	10.2	7.9	1088849.4	-4842948.7	3991840.2	3.6	3.0	3.7
5201	MOSES LAKE	-2127810.4	-3785912.3	4656011.9	2.7	2.8	3.7	-2127802.2	-3785911.5	4656012.1	2.3	2.2	2.4
5410	MIDWAY ISLANDS	-5618764.5	-258231.5	2997243.8	2.9	3.2	4.1	-5618754.1	-258237.5	2997250.2	2.3	2.8	3.6
5648	FORT STEWART	794687.3	-5360063.7	3353093.5	4.2	5.0	5.5	794691.0	-5360051.1	3353082.4	3.6	2.5	3.6
5712	PARAMARIBO	3623307.1	-5214190.5	601672.3	3.4	3.3	3.6	3623289.8	-5214188.0	601673.2	2.1	2.0	2.9
5713	TERCEIRA	4433654.4	-2268159.2	3971673.1	2.7	2.8	3.8	4433637.8	-2268153.2	3971656.8	2.0	2.2	2.5

TABLE 8.37—*(Cont'd)*

STATION		SOLUTION WN-12						SOLUTION WN-14					
NO	NAME	U	V	W	σ_u	σ_v	σ_w	U	V	W	σ_u	σ_v	σ_w
5715	DAKAR	5884479.9	-1853580.1	1612763.8	2.3	2.5	3.1	5884468.8	-1853580.1	1612760.1	1.6	2.0	2.3
5717	FORT LAMY	6023416.1	1617949.5	1331651.2	2.7	2.8	3.3	6023410.7	1617946.5	1331655.8	2.0	2.0	2.7
5720	ADDIS ABABA	4900750.1	3968255.1	966348.3	2.7	2.9	3.4	4900749.1	3968253.0	966354.7	2.0	2.1	2.9
5721	MASHHAD	2604406.6	4444124.9	3750345.7	2.6	2.8	3.5	2604404.8	4444122.3	3750344.3	2.1	2.1	2.7
5722	DIEGO GARCIA	1905122.3	6032294.5	-810726.4	4.2	5.5	4.8	1905127.0	6032287.5	-810716.2	3.5	4.1	4.3
5723	CHIANG MAI	-941713.7	5967448.6	2039317.5	3.1	3.3	4.1	-941709.4	5967445.0	2039322.9	2.5	2.3	3.5
5726	ZAMBOANGA	-3361953.2	5365845.5	763623.6	3.0	3.3	3.8	-3361946.8	5365837.0	763627.8	2.3	2.2	3.2
5730	WAKE ISLAND	-5858583.8	1394474.9	2093844.7	2.8	3.1	3.8	-5858574.6	1394467.2	2093847.4	2.1	2.5	3.1
5732	PAGO PAGO	-6099984.0	-997345.6	-1568577.0	5.7	4.4	4.9	-6099970.5	-997355.3	-1568570.9	3.6	3.5	4.1
5733	CHRISTMAS ISLAND	-5885350.8	-2448375.3	221663.1	4.4	3.5	4.6	-5885333.9	-2448380.4	221670.7	2.7	2.9	3.9
5734	SHEMYA	-3851808.1	396416.1	5051343.3	3.2	3.7	4.9	-3851799.0	396409.3	5051342.0	2.7	3.3	3.9
5735	NATAL	5186368.5	-3654226.0	-653022.6	3.3	2.8	3.1	5186350.6	-3654223.7	-653018.9	2.0	2.1	2.5
5736	ASCENSION ISLAND	6118355.5	-1571763.1	-878558.4	3.3	2.9	3.3	6118340.3	-1571761.9	-878553.6	2.3	2.2	2.7
5739	TERCEIRA	4433646.0	-2268192.2	3971663.3	2.7	2.8	3.8	4433629.3	-2268186.2	3971647.0	2.0	2.2	2.5
5744	CATANIA	4896444.1	1316129.4	3856628.4	2.4	2.8	3.2	4896437.7	1316125.0	3856626.2	1.8	2.2	2.3
5907	WORTHINGTON	-449391.6	-4600910.6	4380315.4	5.8	13.8	13.5	-449417.5	-4600905.5	4380288.1	4.2	3.2	4.5
5911	BERMUDA	2308010.4	-4873778.3	3394476.1	3.6	4.9	5.2	2307991.2	-4873773.2	3394463.4	2.6	2.3	3.0
5912	PANAMA	1142664.4	-6196104.1	988340.8	4.8	9.1	7.0	1142644.5	-6196109.1	988336.6	3.1	3.4	4.1
5914	PUERTO RICO	2349423.9	-5576023.2	2010340.5	13.5	21.1	9.7	2349456.9	-5576027.1	2010342.6	10.5	7.0	6.4
5915	AUSTIN	-744066.7	-5465234.3	3192485.8	5.6	15.3	12.8	-744091.1	-5465238.7	3192467.4	3.8	3.8	4.7
5923	CYPRUS	4363335.9	2862258.8	3655380.7	2.5	2.7	3.3	4363332.2	2862254.9	3655380.7	1.9	2.1	2.4
5924	ROTA	5093565.8	-565319.1	3784273.1	2.4	3.1	3.8	5093556.2	-565322.3	3784268.3	1.9	2.6	2.9
5925	ROBERTS FIELD	6237376.8	-1140241.8	687740.0	3.0	3.1	3.6	6237366.3	-1140241.5	687740.2	2.3	2.6	3.0
5930	SINGAPORE	-1542556.4	6186964.6	151827.8	3.3	3.9	4.0	-1542549.4	6186956.7	151833.8	2.6	2.7	3.4
5931	HONG KONG	-2423919.1	5388254.8	2394863.9	3.1	3.5	4.3	-2423914.9	5388250.3	2394869.2	2.5	2.5	3.6
5933	DARWIN	-4071578.3	4714267.0	-1366533.3	4.3	4.4	4.3	-4071568.4	4714253.3	-1366528.3	3.2	3.2	3.7
5934	MANUS	-5367671.7	3437881.4	-225419.4	3.6	3.5	3.8	-5367663.1	3437869.9	-225416.0	2.5	2.5	3.3
5935	GUAM	-5059832.6	3591194.2	1472759.4	2.9	3.0	3.4	-5059825.7	3591186.0	1472762.5	2.1	2.2	2.8
5937	PALAU	-4433470.5	4512939.3	809955.3	3.1	3.2	3.7	-4433463.6	4512930.3	809958.7	2.2	2.2	3.2
5938	GUADALCANAL	-5915106.0	2146873.2	-1037912.8	4.4	3.9	4.0	-5915096.5	2146860.8	-1037909.5	3.0	3.0	3.5
5941	MAUI	-5467771.9	-2381242.7	2254024.0	3.5	3.2	4.4	-5467757.3	-2381246.7	2254033.8	2.5	2.8	3.8
6001	THULE	546566.4	-1389993.6	6180242.4	2.7	2.7	4.4	546568.7	-1389993.7	6180236.7	2.6	2.4	3.4
6002	BELTSVILLE	1130762.7	-4830837.6	3994709.9	2.2	2.7	3.1	1130764.9	-4830831.9	3994704.0	2.0	1.7	1.9
6003	MOSES LAKE	-2127839.9	-3785864.2	4656037.4	2.5	2.7	3.5	-2127832.1	-3785863.0	4656037.2	2.1	2.0	2.3
6004	SHEMYA	-3851806.8	396416.1	5051341.7	3.2	3.7	5.0	-3851797.5	396409.4	5051340.5	2.7	3.3	3.9
6006	TROMSO	2102930.3	721674.1	5953181.7	2.7	3.3	4.4	2102927.4	721668.5	5958180.8	2.4	2.9	2.9
6007	TERCEIRA	4433653.3	-2268156.9	3971671.0	2.7	2.7	3.8	4433637.3	-2268151.4	3971655.0	2.0	2.2	2.5
6008	PARAMARIBO	3623257.3	-5214236.7	601534.8	3.4	3.3	3.6	3623241.0	-5214233.7	601536.1	2.1	2.0	2.9
6009	QUITO	1280834.0	-6250966.2	-10805.5	3.8	5.9	4.5	1280834.2	-6250955.9	-10800.6	3.6	3.4	4.1
6011	MAUI	-5466039.2	-2404429.3	2242224.6	4.4	3.4	3.9	-5466018.6	-2404431.5	2242224.4	3.0	2.9	3.3

TABLE 8.37—*(Cont'd)*

STATION		SOLUTION WN-12						SOLUTION WN-14					
NO	NAME	U	V	W	σ_u	σ_v	σ_w	U	V	W	σ_u	σ_v	σ_w
6012	WAKE ISLAND I	-5858578.8	1394516.4	2093817.4	2.9	3.2	3.8	-5858569.3	1394508.7	2093820.3	2.1	2.6	3.2
6013	KANOYA	-3565901.4	4120723.2	3303426.9	4.0	5.2	5.9	-3565892.8	4120713.6	3303428.3	3.3	4.4	4.9
6015	MASHHAD	2604355.4	4444169.2	3750321.7	2.6	2.9	3.5	2604353.3	4444166.0	3750320.5	2.1	2.2	2.6
6016	CATANIA	4896394.6	1316176.2	3856670.7	2.4	2.8	3.2	4896388.3	1316172.1	3856668.2	1.8	2.2	2.2
6019	VILLA DOLORES	2280630.7	-4914547.7	-3355417.9	2.7	3.6	5.2	2280627.1	-4914543.2	-3355402.8	2.4	2.7	3.7
6020	EASTER ISLAND	-1888621.5	-5354898.4	-2895762.3	6.0	6.1	6.9	-1888614.3	-5354894.4	-2895749.0	5.4	4.5	5.5
6022	TUTUILA	-6099975.9	-997357.7	-1568593.6	4.8	3.9	5.2	-6099961.7	-997362.2	-1568585.5	3.4	3.6	4.7
6023	THURSDAY ISLAND	-4955391.2	3842255.7	-1163855.5	4.5	3.9	4.7	-4955386.8	3842247.8	-1163847.4	3.2	3.0	4.0
6031	INVERCARGILL	-4313830.4	891340.6	-4597277.7	4.4	4.2	5.3	-4313825.3	891333.9	-4597265.8	3.4	3.9	3.8
6032	CAVERSHAM	-2375426.0	4875557.6	-3345424.5	3.7	4.3	5.0	-2375420.6	4875546.7	-3345411.1	3.3	3.2	3.9
6038	SOCORRO ISLAND	-2160989.6	-5642717.9	2035368.0	2.9	3.8	4.4	-2160980.9	-5642710.5	2035367.8	2.5	2.8	3.8
6039	PITCAIRN ISLAND	-3724775.0	-4421234.4	-2686094.4	7.9	7.2	7.3	-3724765.9	-4421237.6	-2686084.7	6.2	5.4	5.5
6040	COCOS ISLAND	-741986.1	6190803.6	-1338557.1	4.7	4.8	4.7	-741981.7	6190792.9	-1338546.3	4.5	3.7	4.2
6042	ADDIS ABABA	4900752.0	3968255.1	966318.9	2.7	2.9	3.4	4900750.7	3968252.7	966325.3	2.0	2.1	2.9
6043	CERRO SOMBRERO	1371376.5	-3614750.6	-5055947.1	3.5	4.2	7.0	1371375.9	-3614750.3	-5055927.8	3.3	3.8	4.8
6044	HEARD ISLAND	1098898.5	3684617.0	-5071900.1	6.9	6.7	11.1	1098897.9	3684606.6	-5071873.1	6.8	6.2	7.8
6045	MAURITIUS	3223434.7	5045343.6	-2191818.0	3.6	4.0	4.6	3223432.0	5045336.3	-2191805.7	3.2	3.1	3.9
6047	ZAMBOANGA	-3361983.5	5365820.6	763620.5	3.1	3.4	3.8	-3361976.9	5365811.9	763624.7	2.4	2.3	3.2
6050	PALMER STATION	1192679.3	-2451013.2	-5747052.4	5.0	6.3	9.8	1192678.8	-2451015.6	-5747034.2	4.9	6.1	6.1
6051	MAWSON STATION	1111337.1	2169270.2	-5874355.2	5.0	4.2	7.3	1111336.1	2169262.7	-5874334.1	4.9	3.7	4.4
6052	WILKES STATION	-902611.4	2409530.0	-5816569.9	4.6	4.4	7.4	-902608.8	2409522.1	-5816551.8	4.4	4.0	5.4
6053	MCMURDO STATION	-1310854.8	311262.9	-6213294.3	4.8	4.8	7.4	-1310852.3	311257.5	-6213276.5	4.6	4.5	4.3
6055	ASCENSION ISLAND	6118349.3	-1571749.2	-878601.3	3.3	2.9	3.4	6118334.2	-1571748.3	-878596.5	2.3	2.3	2.8
6059	CHRISTMAS ISLAND	-5885350.2	-2448374.4	221663.6	4.3	3.4	4.5	-5885333.5	-2448379.0	221671.1	2.7	2.9	3.8
6060	CULGOORA	-4751655.0	2792065.7	-3200174.2	4.5	4.0	4.7	-4751650.0	2792058.1	-3200164.0	3.3	3.3	3.7
6061	SOUTH GEORGIA IS.	2999921.2	-2219366.3	-5155267.1	3.9	5.9	7.8	2999915.6	-2219369.3	-5155246.0	3.7	5.7	5.3
6063	DAKAR	5884479.3	-1853496.4	1612858.7	2.4	2.6	3.2	5884467.4	-1853495.8	1612855.1	1.7	2.1	2.5
6064	FORT LAMY	6023394.4	1617934.2	1331731.7	3.3	3.1	3.7	6023386.7	1617931.9	1331733.2	2.7	2.6	3.2
6065	HOHENPEISSENBERG	4213570.2	820833.7	4702786.5	2.6	3.0	3.6	4213564.6	820830.0	4702784.4	2.0	2.4	2.3
6066	WAKE ISLAND II	-5858580.7	1394474.0	2093843.0	2.9	3.2	3.8	-5858571.2	1394466.4	2093846.0	2.1	2.6	3.2
6067	NATAL	5186415.0	-3653935.9	-654280.7	3.3	2.8	3.1	5186397.1	-3653933.3	-654276.9	2.1	2.2	2.6
6068	JOHANNESBURG	5084837.1	2670346.5	-2768109.3	4.2	3.5	5.3	5084830.4	2670341.2	-2768095.2	3.0	2.9	4.2
6069	TRISTAN DA CUNHA	4978430.9	-1086871.1	-3823187.7	8.3	6.6	10.4	4978421.7	-1086874.0	-3823167.8	6.5	6.4	8.1
6072	CHIANG MAI	-941707.8	5967462.5	2039307.4	5.9	5.1	4.9	-941702.1	5967455.1	2039311.6	5.7	4.0	4.3
6073	DIEGO GARCIA	1905134.3	6032292.0	-810742.3	3.7	4.8	4.7	1905134.1	6032282.4	-810732.7	3.4	3.7	4.2
6075	MAHE	3602824.5	5238248.2	-515957.7	4.2	4.6	4.5	3602820.6	5238240.7	-515948.3	3.8	3.6	4.0
6078	PORT VILA	-5952307.7	1231910.5	-1925983.7	19.9	9.4	16.6	-5952303.4	1231904.9	-1925972.5	9.7	8.0	12.4
6111	WRIGHTWOOD I	-2448862.8	-4667992.3	3582759.4	3.0	3.2	3.8	-2448853.3	-4667985.8	3582754.9	2.6	2.1	2.4
6123	POINT BARROW	-1881807.4	-812435.3	6019599.3	4.9	4.6	7.1	-1881799.4	-812439.0	6019590.7	4.6	4.4	4.5
6134	WRIGHTWOOD II	-2448916.5	-4668082.4	3582454.1	3.0	3.2	3.8	-2448907.0	-4668075.9	3582449.6	2.6	2.1	2.4

TABLE 8.37—*(Cont'd)*

STATION		SOLUTION WN-12						SOLUTION WN-14					
NO	NAME	U	V	W	σ_u	σ_v	σ_w	U	V	W	σ_u	σ_v	σ_w
7036	EDINBURG	-828491.0	-5657486.5	2816825.5	3.8	3.9	4.0	-828487.0	-5657471.3	2816816.0	3.5	2.4	2.9
7037	COLUMBIA	-191294.8	-4967308.3	3983264.5	3.2	3.5	3.9	-191291.0	-4967293.9	3983252.6	2.9	2.2	2.4
7039	BERMUDA	2308214.8	-4873614.8	3394568.4	3.7	5.3	5.0	2308213.4	-4873598.3	3394558.5	3.3	3.1	3.6
7040	SAN JUAN	2465050.9	-5534945.5	1985522.2	4.0	4.4	4.7	2465049.5	-5534930.0	1985513.1	3.7	3.2	4.0
7043	GREENBELT	1130706.5	-4831337.2	3994141.4	2.2	2.7	3.1	1130708.6	-4831331.3	3994135.5	2.0	1.7	1.9
7045	DENVER	-1240475.1	-4760256.0	4048997.8	4.6	4.2	4.7	-1240470.2	-4760242.1	4048985.3	4.2	2.8	2.9
7072	JUPITER	976261.3	-5601416.4	2880251.4	2.5	3.3	3.3	976261.3	-5601399.9	2880241.9	2.2	1.8	2.3
7075	SUDBURY	692618.7	-4347090.4	4600487.7	4.0	5.7	5.4	692620.7	-4347076.5	4600475.4	3.7	3.8	3.4
7076	KINGSTON	1384159.2	-5905680.0	1966554.4	4.3	5.8	5.9	1384158.7	-5905662.0	1966545.7	4.1	4.4	5.3
8009	WIPPOLDER	3923429.9	299866.1	5003013.3	13.3	13.1	15.2	3923397.4	299869.4	5002975.5	8.5	10.1	6.9
8010	ZIMMERWALD	4331312.7	567499.7	4633118.9	7.9	10.9	11.5	4331307.0	567490.8	4633108.3	5.7	8.3	5.4
8011	MALVERN	3920188.9	-134806.7	5012776.2	12.8	16.5	15.5	3920153.5	-134804.5	5012734.8	8.9	14.3	6.9
8015	HAUTE PROVENCE	4578328.1	457945.6	4403204.8	6.4	10.7	10.2	4578322.1	457936.5	4403195.3	4.2	8.0	4.4
8019	NICE	4579469.1	586582.7	4386428.4	6.3	10.6	10.1	4579463.2	586573.5	4386419.2	4.1	7.9	4.3
8030	MEUDON	4205629.1	163695.4	4776550.9	9.0	12.3	11.8	4205626.9	163683.4	4776540.6	6.5	9.7	5.8
9001	ORGAN PASS	-1535755.1	-5167026.6	3401047.1	4.6	3.9	3.8	-1535750.7	-5167014.4	3401039.4	4.2	2.8	2.7
9002	OLIFANTSFONTEIN	5056115.1	2716514.0	-2775782.9	4.2	3.6	5.3	5056108.4	2716508.7	-2775768.8	3.0	3.0	4.2
9004	SAN FERNANDO	5105589.8	-555269.7	3769680.6	6.3	12.9	8.5	5105581.5	-555271.5	3769676.0	3.4	10.0	4.0
9005	TOKYO	-3946751.4	3366303.2	3698830.3	11.2	10.3	9.8	-3946730.5	3366286.1	3698822.9	9.2	9.0	7.5
9006	NAINI TAL	1018153.3	5471119.3	3109622.2	14.2	10.9	9.6	1018164.5	5471108.7	3109625.6	12.4	5.5	6.0
9007	AREQUIPA	1942762.4	-5804101.6	-1796905.8	2.8	4.0	5.3	1942760.9	-5804088.2	-1796900.9	2.5	2.9	4.4
9008	SHIRAZ	3376872.6	4403980.0	3136250.1	8.1	10.3	9.5	3376875.2	4403976.2	3136257.3	6.8	6.1	6.1
9009	CURACAO	2251813.5	-5816933.6	1327169.7	2.8	3.5	3.8	2251810.7	-5816917.6	1327163.4	2.4	2.1	3.4
9010	JUPITER	976276.2	-5601418.8	2880244.0	2.5	3.3	3.3	976276.2	-5601402.2	2880234.5	2.1	1.8	2.3
9011	VILLA DOLORES	2280578.9	-4914584.8	-3355398.8	2.7	3.6	5.3	2280575.3	-4914580.2	-3355383.7	2.4	2.7	3.7
9012	MAUI	-5466088.5	-2404310.5	2242188.7	4.5	3.4	3.9	-5466067.8	-2404312.7	2242188.4	3.0	2.9	3.3
9021	MOUNT HOPKINS	-1936799.1	-5077719.4	3331926.1	7.3	6.8	6.4	-1936789.3	-5077714.7	3331922.7	7.1	5.3	5.3
9028	ADDIS ABABA	4903727.7	3965208.6	963853.2	2.8	2.9	3.4	4903726.6	3965206.3	963859.6	2.1	2.1	2.9
9029	NATAL	5186459.3	-3653874.6	-654317.9	3.4	2.9	3.2	5186441.4	-3653871.9	-654314.1	2.1	2.2	2.7
9031	COMODORO R*DAVIA	1693795.5	-4112354.3	-4556644.1	8.4	9.4	14.3	1693797.3	-4112353.1	-4556622.0	8.3	8.8	11.2
9051	ATHENS	4606866.7	2029708.0	3903567.4	6.0	12.6	8.9	4606861.5	2029692.2	3903562.2	4.2	10.3	4.4
9091	DIONYSOS	4595164.1	2039433.4	3912675.8	6.0	12.6	8.9	4595158.9	2039417.6	3912670.6	4.2	10.3	4.4
9424	COLD LAKE	-1264834.5	-3466912.6	5185449.2	5.2	6.5	7.7	-1264831.9	-3466915.4	5185450.9	4.7	5.5	4.3
9425	EDWARDS AFB	-2450022.2	-4624438.2	3635041.1	3.1	3.2	3.8	-2450012.7	-4624431.6	3635036.6	2.6	2.2	2.4
9426	HARESTUA	3121262.6	592607.0	5512720.9	9.6	11.4	15.5	3121261.3	592605.7	5512723.0	8.6	9.4	5.8
9427	JOHNSTON ISLAND	-6007458.1	-1111834.2	1825730.0	10.9	20.6	8.8	-6007428.7	-1111852.5	1825733.9	8.9	19.8	8.6
9431	RIGA	3183891.2	1421439.3	5322819.8	13.1	11.7	14.7	3183897.6	1421426.7	5322814.7	12.3	9.4	7.0
9432	UZHGOROD	3907423.8	1602394.2	4763932.7	10.2	12.6	13.7	3907419.2	1602378.6	4763922.1	7.9	10.4	5.9

9

SMITHSONIAN ASTROPHYSICAL OBSERVATORY

D. A. Arnold
E. M. Gaposchkin
Y. Kozai
J. Latimer
C. G. Lehr
C. A. Lundquist
G. Mendes
M. R. Pearlman
J. M. Thorp
C. R. H. Tsiang
G. Veis
F. L. Whipple
M. R. Williamson
J. Wohn

9.1 HISTORICAL INTRODUCTION

(C. A. Lundquist and F. L. Whipple)

9.1.1 Initial Objectives of the SAO Satellite-Tracking Program

As the principal objective of its participation in the International Geophysical Year (IGY), the Smithsonian Astrophysical Observatory (SAO) conceived of and established a systematic program to observe positions of artificial satellites and to derive geophysical information from these observations (Whipple and Hynek, 1956, 1958a,b). The fundamental concepts for this program existed in the minds and studies of SAO Director Fred L. Whipple and his colleagues (see Ryan, 1952) well before President Eisenhower announced in 1955 that the United States would launch a scientific satellite during the IGY. These plans originated with Project Orbiter, followed by Project Vanguard, which in turn was superseded by the Army program that launched Explorer–I (5800101), the first United States satellite (Hayes, 1968). When this satellite attained its orbit on January 30, 1958, the SAO observation network and analytical apparatus were ready with partial operational status.

As stated in 1957, the principal objectives of this early SAO activity were (1) "to tie together the observing stations and the center of the geoid to a precision of the order of 10 m," (2) "to add appreciably to our knowledge of the density distribution of the earth, particularly in crustal volumes," and (3) to provide "the value of the [atmospheric] density a few kilometers above the initial perigee distance, and periodic effects or predictable cyclic effects that may occur in the earth's high atmosphere" (Whipple and Hynek, 1958a). The first two objectives evolved into similar, but more demanding, ones for subsequent programs, such as the National Geodetic Satellite Program (NGSP) (Rosenberg, 1968).

9.1.2 Establishment of the Baker-Nunn Network

To establish the required satellite observation capability, SAO initially developed a photographic system (Whipple and Hynek, 1958b). The basic tracking camera, named Baker-Nunn after its optical and mechanical designers, has f/1 Schmidt optics. During the first several years of field operation, a Norrman time standard, also named for its designer, provided epoch measurements. The Baker-Nunn tracking system has accuracies in the arc-second and millisecond range. Twelve stations with this equipment went into operation as a global network during the IGY.

With the passage of time, the Baker-Nunn network continued operation with only small changes (Whipple and Lundquist, 1967). The modes of camera operation required slight modification to accommodate a variety of satellite characteristics. A few stations were moved to higher latitudes because many satellites were launched into high-inclination orbits. A new, more accurate, time standard replaced the Norrman standard.

It is a tribute to the designers of the Baker-Nunn system that for nearly a decade the accuracy of the Baker-Nunn data exceeded the accuracies of the analytical treatment of these data and of the geodetic parameters derived from them. Indeed, Baker-Nunn observations contributed appreciably to the NGSP results reported here. By about 1966, however, the accuracy of the derived geodetic parameters began to approach that of the observations, thus motivating significant moves toward deployment of new tracking systems of superior accuracy.

9.1.3 Introduction of Laser Systems

When the accuracy of photographic methods began to pose a serious limit on future

geodetic investigations, laser systems to measure Earth-to-satellite ranges offered the best prospect for substantial reduction of measurement uncertainties. Range measurements with pulsed laser systems became possible in 1964 after the BE–B satellite (6406401), which carried an array of optical retroreflectors, was launched (Plotkin, 1964). In 1965, SAO and the General Electric Company began laser ranging experiments in conjunction with the Baker-Nunn system at Organ Pass, New Mexico (Anderson *et al.*, 1966).

Experience with the equipment at Organ Pass led to the specification and development of a greatly improved instrument, and the prototype model of this ruby-laser system began operating in late 1967 at Mt. Hopkins Observatory, Arizona (Lehr *et al.*, 1968). After appropriate tests of this prototype and after identification of design modifications indicated by them, SAO procured three additional laser ranging systems. In late 1970, these three units began operating at the SAO sites in Arequipa, Peru; Natal, Brazil; and Olifantsfontein, South Africa. The prototype remained at Mt. Hopkins.

These SAO instruments, and similar laser systems deployed by other groups, contributed the major data base used in the final NGSP results presented here. It is the improved accuracy of these data, relative to earlier observations, that allows further refinements of geodetic parameters.

9.1.4 Evolution of International Cooperation

The network of Baker-Nunn satellite-tracking stations was conceived by SAO as a cooperative international enterprise during the IGY. Its implementation depended crucially on agreements between SAO and appropriate scientific organizations in the nations hosting the stations. Many of these agreements have continued to the present, with occasional renewals and modifications as needed. The viability and success of such a network stem from a recognition that little can be accomplished on global problems by a single station working in isolation, whereas a well-coordinated global network can achieve much.

The cooperative aspects of the efforts coordinated by SAO naturally extend to the analysis and interpretation of the data. First, it has been a policy that data generated by the network are available to all network participants. Also, SAO data are eventually published or otherwise made available to the general scientific community. Second, several visiting scientists from host countries have been deeply involved at SAO in geodetic investigations that employ the network data (in particular, Veis, 1960, 1961, 1963a,b, 1965c, 1966a,b; Kozai, 1960, 1962a,b, 1963a,b, 1964; Giacaglia, 1973).

In recent years, cooperative efforts have increased further through various international observing campaigns. These campaigns involve a concerted effort among the several existing networks, as well as between individual stations. Such campaigns have been responsible for some of the most valuable data used in the analyses reported here. Thus, credit for the basic support behind these results must go to many nations, organizations, and individuals.

9.1.5 Cooperative Observing Programs

The first of the inter-network cooperative observing programs occurred in the spring of 1967 (Lundquist, 1967). The timing of this campaign followed the launch of Diademe–1 (D1C, 6701101), and Diademe–2 (D1D, 6701401), which carried retroflectors for laser ranging. The major participants—Centre National d'Etudes Spatiales (CNES), Goddard Space Flight Center (GSFC), and SAO—arranged an observing schedule to be followed by the stations of these three organizations. The arrangements emphasized the need to coordinate observations taken by the small number of laser instruments in operation at that time. Lasers were located at three CNES stations, in Haute Provence,

France; Colomb-Bechir, Algeria; and Stephanion, Greece; at a GSFC station in Greenbelt, Maryland; and at the SAO station in Organ Pass. The Baker-Nunn and other camera systems also participated.

For this observation campaign, intervals of favorable satellite visibility lasting several weeks were selected for the five satellites with retroreflectors. During each selected interval, all participating stations were dedicated to obtaining maximum tracking coverage of the designated satellite. This became known as the saturation-tracking mode. Such periods of high-density data are particularly valuable in determinations of longitude-dependent coefficients in the gravity field of the Earth.

SAO took the initiative in organizing a second, international, geodetic-satellite tracking effort in 1968, following the launch of GEOS–2 (6800201). GEOS–2 was the second satellite launched under the aegis of the NGSP and equipped with retroreflectors. Again, intervals of several weeks were designated for saturation tracking of the six retroreflector satellites. By 1968, a few more laser instruments were operational, and they participated in this observation campaign. The two CNES lasers were located at Haute Provence and at the SAO station in San Fernando, Spain; two NASA lasers were at Greenbelt and at Rosmund, North Carolina; and an SAO laser was located at Organ Pass.

A two-laser collocation experiment was conducted at the SAO Mt. Hopkins Observatory in 1969. A GSFC mobile laser system and the SAO prototype obtained simultaneous observations on GEOS–2, enabling an evaluation of system performance to be made.

The next observation campaign in this series was the International Satellite Geodesy Experiment (ISAGEX), organized by CNES in conjunction with the launch of PEOLE (7010901), a new retroreflector satellite in a low-inclination orbit. This effort extended from January 5 to August 31, 1971.

9.1.6 Evolution of Results

The results presented here by SAO, corresponding to the completion of the NGSP, are but the latest in a sequence of advances in the determination of geodetic parameters. This sequence started with the early works of Izsak (1963, 1964, 1966), Kozai (1963a,b, 1964), and Veis (1965c).

A major effort in 1966 resulted in the first Smithsonian Institution Standard Earth (SE) (Lundquist and Veis, 1966), the combined work of many authors. This was the first solution for geodetic parameters based on a combination of dynamical and geometrical data and analyses. The 1969 SE II (Gaposchkin and Lambeck, 1970) was the next milestone in the SAO series. This solution for geodetic parameters not only combined dynamical and geometric data, but also incorporated surface-gravity information and results from Jet Propulsion Laboratory's (JPL) Deep Space Net (DSN). This was also the first solution to employ some laser range data, resulting from the 1967 and 1968 observation campaigns. Finally, the solution presented here is again a combination of all the varieties of data used in the 1969 solution, laser range data playing a dominant role. The available surface-gravity data are more complete then they were in 1969 and, hence, bear strongly on the final results. Survey data are also included.

9.2 INSTRUMENTATION [1]

(M. R. Pearlman, J. M. Thorp, C. R. H. Tsiang, D. A. Arnold, C. G. Lehr, and J. Wohn)

9.2.1 Baker-Nunn Camera

9.2.1.1 Description of Technique

The Baker-Nunn camera photographs satellites against a star background. It can

[1] Also included in this part is material originally prepared by G. Veis, K. Lambeck, and K. L. Haramundanis. We are grateful to them for their contributions.

photograph either passive, Sun-illuminated satellites or active-satellite flashes under night-sky conditions. The *Smithsonian Astrophysical Observatory Star Catalog* has an average standard deviation in star position of 0".5 (epoch of 1963.5) (Staff, Smithsonian Astrophysical Observatory, 1966). The SAO field timing system is kept within 100 μsec or better of Universal Time Coordinated (UTC) as maintained by and referred to the United States Naval Observatory (USNO); hereafter, we shall express such time as UTC(USNO). With the use of the catalog and the timing system, the reduction technique can provide an accuracy of 2". Observations are routinely reduced at the observing station to an accuracy of 40" to 60".

The camera was originally designed to photograph very small satellites in poorly known orbits without the aid of active systems on the satellites themselves. For this reason, it has a fast optical system and a wide field of view. Pointing predictions need an accuracy of only several degrees.

9.2.1.2 Instrument Description

The Baker-Nunn is a three-axis camera designed according to the specifications of SAO for satellite tracking. The optical system was designed by James G. Baker; the mounting and mechanical system, by Joseph Nunn. The camera is approximately 2.5 m high and 3 m wide and weighs about 9000 kg. It combines an extremely fast f/1 optical system with a sophisticated film transport, and currently uses 55.6–mm Royal X extended red film (Kodak S0–338). It is best known for its light-gathering power and can photograph stars 3×10^4 fainter than those visible to the naked eye. The camera, which operates only at night, can photograph Sun-illuminated satellites as well as satellites with flashing lights.

9.2.1.2.1 CAMERA OPERATION

The Baker-Nunn camera (see fig. 9.1) is basically a Schmidt telescope with refinements designed to improve its optical performance. The focal ratio of the system is f/1 with an aperture of 508 mm (20 inches). This focal length gives a film scale of 406" mm^{-1}.

Light enters the camera through the three-element lens assembly (two positive and one negative), which corrects for spherical and chromatic aberrations, and is reflected from the 787–mm (31-inch) diameter, spherical pyrex mirror onto the photographic film. During exposure, tension is applied to the film to force it to conform to the shape of the backup plate, which is figured to the required aspherical focal surface.

A clamshell-type focal-plane shutter begins and ends the exposure, which is preset for 0.2, 0.4, 0.8, 1.6, or 3.2 sec. A barrel-type shutter rotating in front of the focal surface chops the star trails or satellite trail (depending on the operating mode) and provides five reference breaks for measurement. The chopping shutter is coupled to a set of timing points that close at the third break and trigger a time presentation, readable to 0.1 msec, which is recorded on the film. When the exposure is completed, the film is advanced until the next frame is positioned against the backup plate. For a $15°\times5°$ field, including time presentation, one frame is 152 mm of film. The film-transport mechanism, chopper shutter, and clamshell shutter are mechanically synchronized.

The camera is supported on a massive altitude-azimuth mount (see fig. 9.2) with a third mechanized tracking axis normal to the altitude axis. Both altitude and azimuth are manually set, normally to $\pm0°.2$, and clamped into position during photography. The camera then tracks along a great circle about the tracking axis at a prescribed rate. This motion approximates the apparent satellite motion over a short arc. Movement about the azimuth axis is limited only by the length of the power and slave-clock cables, which permits approximately 400° of freedom. Altitude is limited by stops at 20° and 160°, and track angle is limited by microswitches at 27° and 153°. Continuously variable angular velocities of 0 to 7000" sec^{-1} are available.

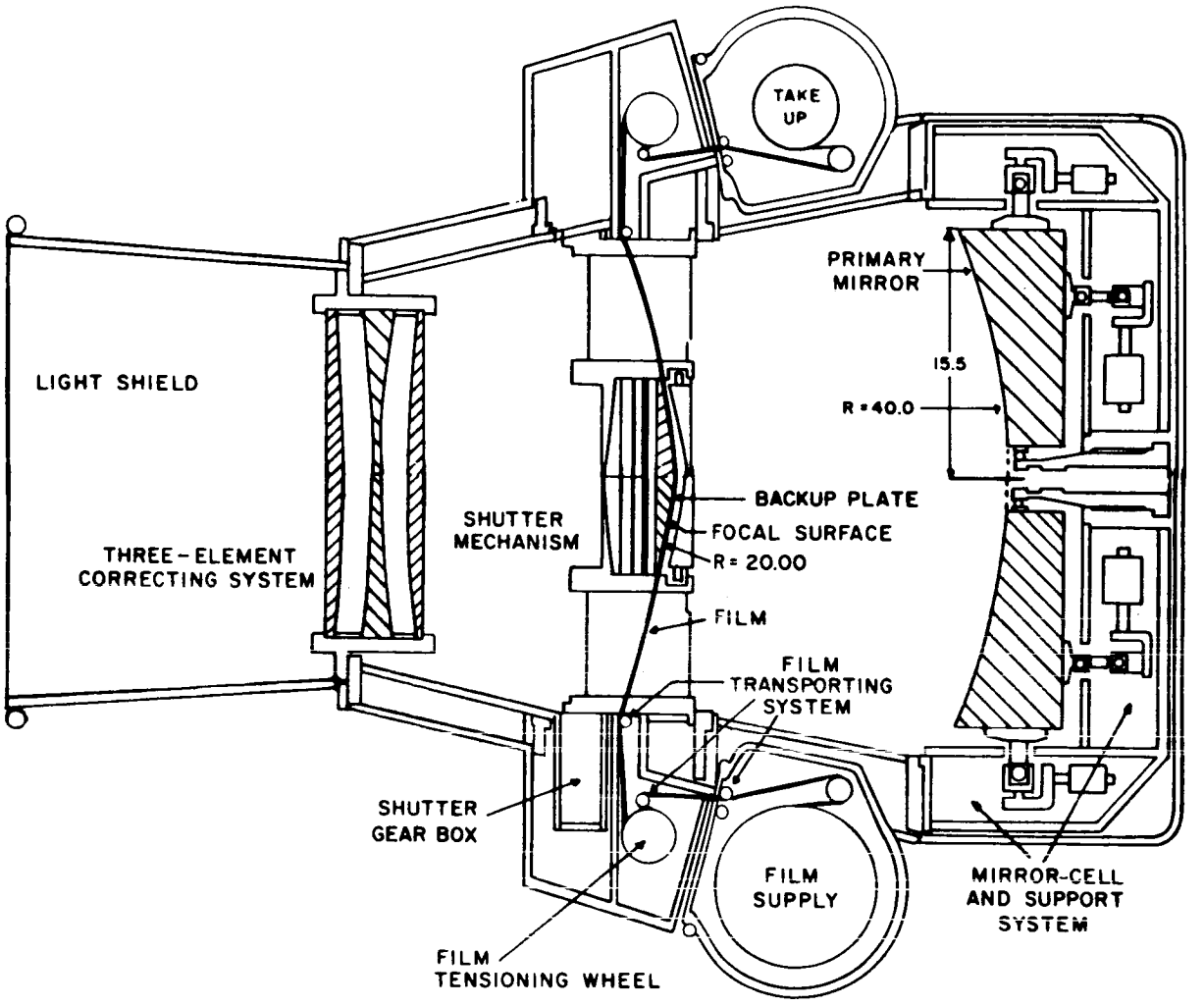

FIGURE 9.1.—Cross section of the Baker-Nunn camera.

9.2.1.2.2 OPTICS

The modified Schmidt optical system was chosen because it has a fast speed and a wide field of view and it yields good images over the entire field of view. To compensate for aberrations introduced by the spherical primary mirror, the camera has a three-element lens assembly, or corrector cell, mounted at the aperture stop. The cell has little focusing power but a strong spherical aberration approximately equal to and opposite that of the mirror. This permits a large field, fast speed, and good images. In the Baker-Nunn, no attempt has been made to flatten the focal surface: Instead, the film is made to conform to the curved focal surface. Chromatic aberration is minimized in the corrector cell by the use of two types of glass: Schott K2FS–2 glass on the two outer elements and Schott SK–14 glass on the inner element. The outer glass is subject to etching in the presence of water, and care must be taken in the field to keep the outer surface dry.

The mirror is very accurately supported by 12 counterweights and a center collimating post to position the mirror at the correct distance from the film. This supporting sys-

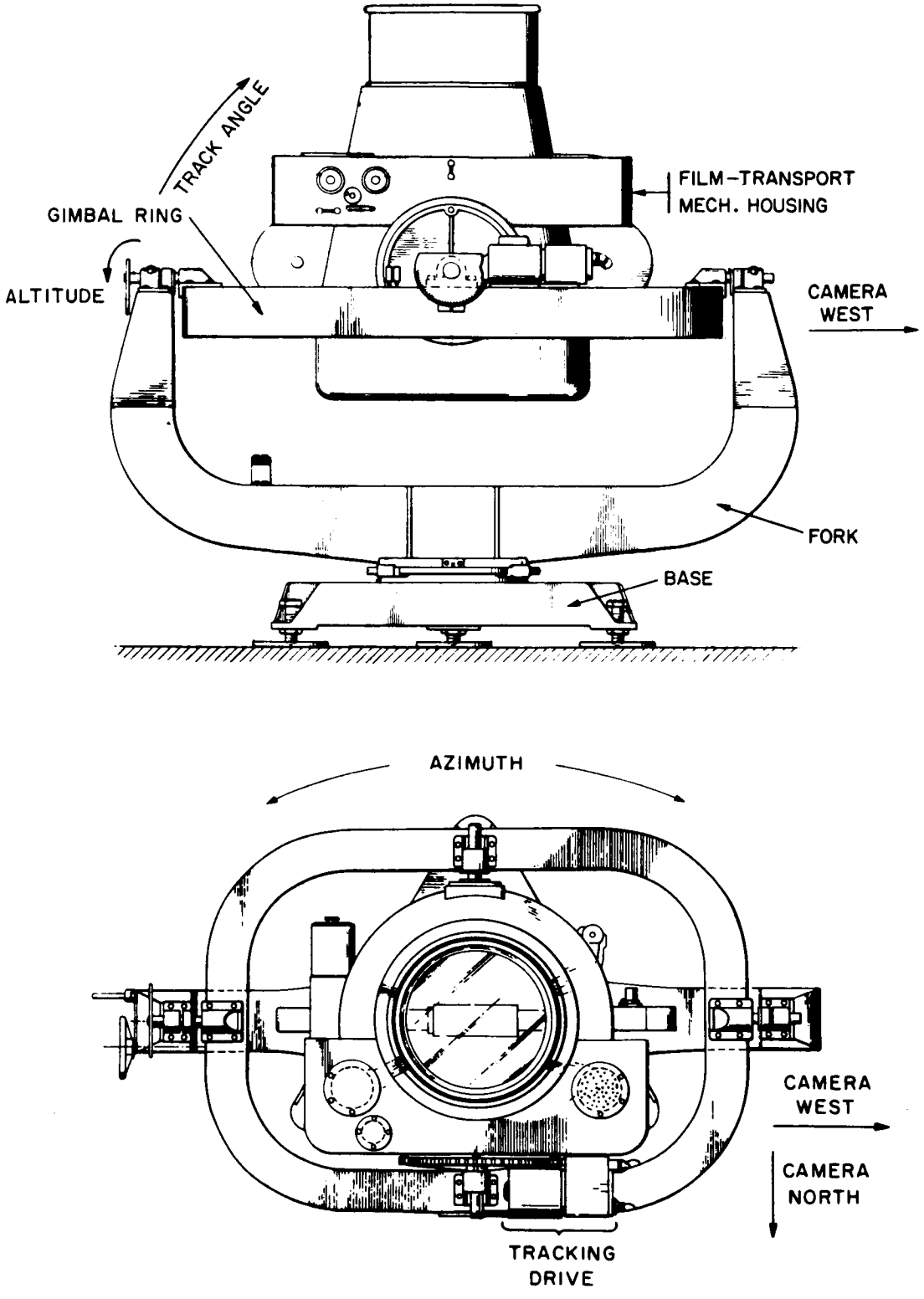

FIGURE 9.2.—Top and side views of the Baker-Nunn camera, showing three axes of rotation.

tem was designed to minimize image degradation due to temperature change and mechanical flexure.

9.2.1.2.3 MECHANICS

The operation of the camera depends on the synchronous operation of a gross (clamshell) shutter and a fast (chopping) shutter. These shutters and the film transport are mechanically linked and driven by a synchronous motor and a cycle-speed-selector transmission. Speeds of 2, 4, 8, 16, or 32 sec per cycle can be selected. There are two exposures per cycle with an effective exposure time of one-tenth the cycle. The system was originally designed to have both a tracking and a stationary exposure on each frame. However, this complicated the problems of reduction, and the camera is now operated either in the stationary mode or in the tracking mode for the entire arc photographed. The latter is used for faint satellites, and the former, for the brighter (visual) satellites.

The film is transported from a supply reel to a takeup reel by means of two drums and a system of idler rollers. The drums are powered by a system that applies tension, transports, and holds to the film during the camera's operation cycle. The drive that operates the shutters also operates the film transport in such a way that as the cycle period is decreased, the speed of transport increases. For example, for a 2-sec cycle, the film is exposed and transported at 1 frame sec^{-1}.

Timing of an event on the Baker-Nunn camera requires exact knowledge of the position of the chopping shutter at the moment the time display is triggered. The camera timing points are adjusted so that an epoch corresponding to the third passage of the shutter through the field of view is recorded on the film. The break in the image caused by the passage of the shutter is called a "chop." Figure 9.3 is a Baker-Nunn photograph in which the satellite, shown by the arrow, is being tracked by the camera and the star trails are chopped five times. During the third passage of the shutter, a strobe lamp with a collimating lens, located in the body of the camera, illuminates the chopping shutter, whose shadow is recorded on the film. The length of this shadow on the film is measured and used in the reduction process to calculate the angular position of the chopper.

The track-angle axis of the Baker-Nunn camera mount is driven by a reversible synchronous motor, a Graham variable-speed drive, and a multiplier transmission. The Graham drive allows a variation in speed from 0 to 70″ sec^{-1}. The transmission has three gearing ranges of 1, 10, and 100, allowing a total variation of 0 to 7000″ sec^{-1}. The lower the gear range, the more accurately the angular velocity can be set.

9.2.1.2.4 ELECTRONICS

For a proper sequencing of events, accurate exposure times, and accurate angular velocity, the camera must operate on precise 60–Hz power. Since this frequency is not available in many countries, the camera is operated on an amplified 60–Hz phase-shiftable reference signal from the station clock. By instantaneously increasing or decreasing the phase, the camera motors can be speeded up or slowed down. This procedure allows the center (third) chop to occur at a preset firing time and the camera to be synchronized for satellite-flash photography.

A display of the station clock is mounted on each camera at the point where film leaves the camera tube. On a demand pulse from the timing points, epoch is displayed and photographed by the camera. With the EECo clock, manufactured by the Electronic Engineering Company (EECo) of Santa Ana, California, time is displayed on the film in hours, minutes, seconds, and fractions to 0.0001 sec.

9.2.1.3 Accuracy and Error Budget

The accuracy of a satellite-position measurement with the Baker-Nunn camera is

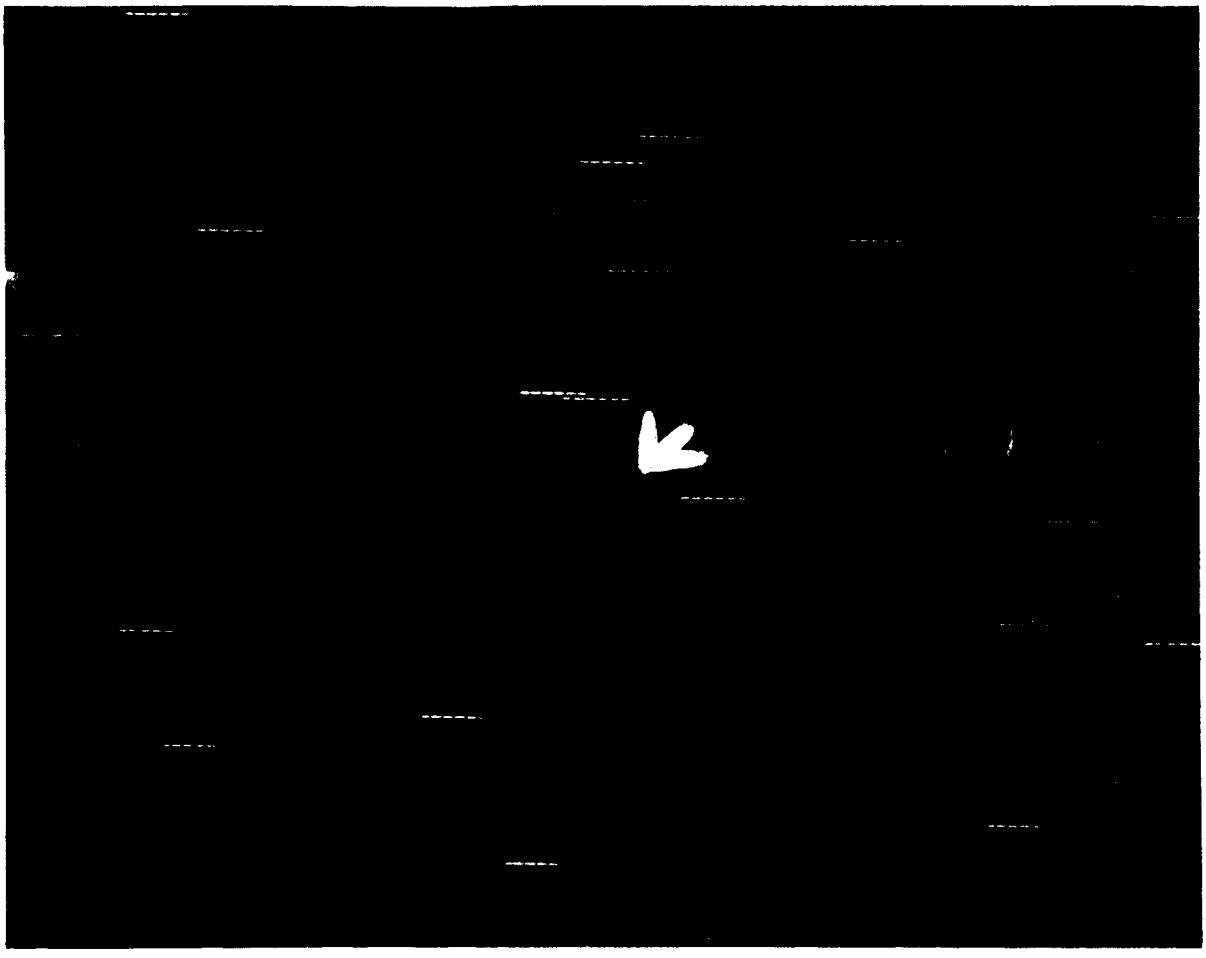

FIGURE 9.3.—Baker-Nunn photograph of satellite 6506301 (EG–RS–5). The satellite is indicated by the arrow, and the chopped star image tracks are in the background.

dictated primarily by (1) the film measurement and reduction procedure, (2) the accuracy of star positions, (3) atmospheric influences, and (4) the accuracy of timing maintained by the station clocks. In those cases where the great-circle approximation is an accurate representation of the satellite's apparent motion, the instrumentation introduces very minor errors in measurement. In those cases where the great-circle approximation may no longer be accurate, the accuracy of the observation is degraded because the satellite image may be spread. This condition may occur when long exposure times are required to obtain images of very faint satellites, or when the satellite angular velocity is very large.

9.2.2 Laser Ranging System

9.2.2.1 Description of Technique

A laser ranging system is an optical radar used to measure the distance from a ground station to a satellite. When accurate timing and appropriate corrections for range bias caused by the atmosphere are incorporated, this is one of the most accurate satellite-tracking techniques available.

The technique is made possible by the availability of Q-switched lasers that produce sharply defined pulses of nearly monochromatic high energy in a beam with a very low angle of divergence. Equally important is the availability of nanosecond-risetime elec-

tronics instrumentation to handle these optical signals. The fast-risetime, small-width pulses make time-interval measurements at nanosecond resolution possible on the basis of a single observation. The high degree of collimation enables the laser beam to hit the satellite with a significant amount of radiant energy. Finally, the technique requires optical retroreflectors on the satellite to ensure measurable return signals. The monochromatic nature of the laser output allows for efficient filtering to improve the signal-to-noise ratio.

The basic ranging system consists of a laser transmitter, a photoreceiver, a mount for the transmitter and receiver, and a time interval counter. The observed range time is the two-way time of flight of the laser pulse, measured by the time interval counter.

In operation, the laser beam is pointed to the predicted satellite position and is pulsed at specified times. During a normal satellite pass, the system makes many range measurements in order to take advantage of the satellite geometry and to permit accumulation of data for analysis.

9.2.2.2 Instrument Description

9.2.2.2.1 SMITHSONIAN ASTROPHYSICAL OBSERVATORY LASER SYSTEM

The SAO laser system (see fig. 9.4) was designed for the particular requirements and needs of the observatory's program in satellite geodesy. The system has a static-pointing mount (or pedestal) that is aimed by means of computed predictions of satellite azimuth and altitude. This method of steering permits the system to operate when the station is in daylight or the satellite is in the Earth's shadow, i.e., 24 hours per day. The static-pointing mount was selected because it is economical and operationally simple. The system operates routinely at 4 pulses min^{-1} and is capable of operating at rates as high as 10 pulses min^{-1}.

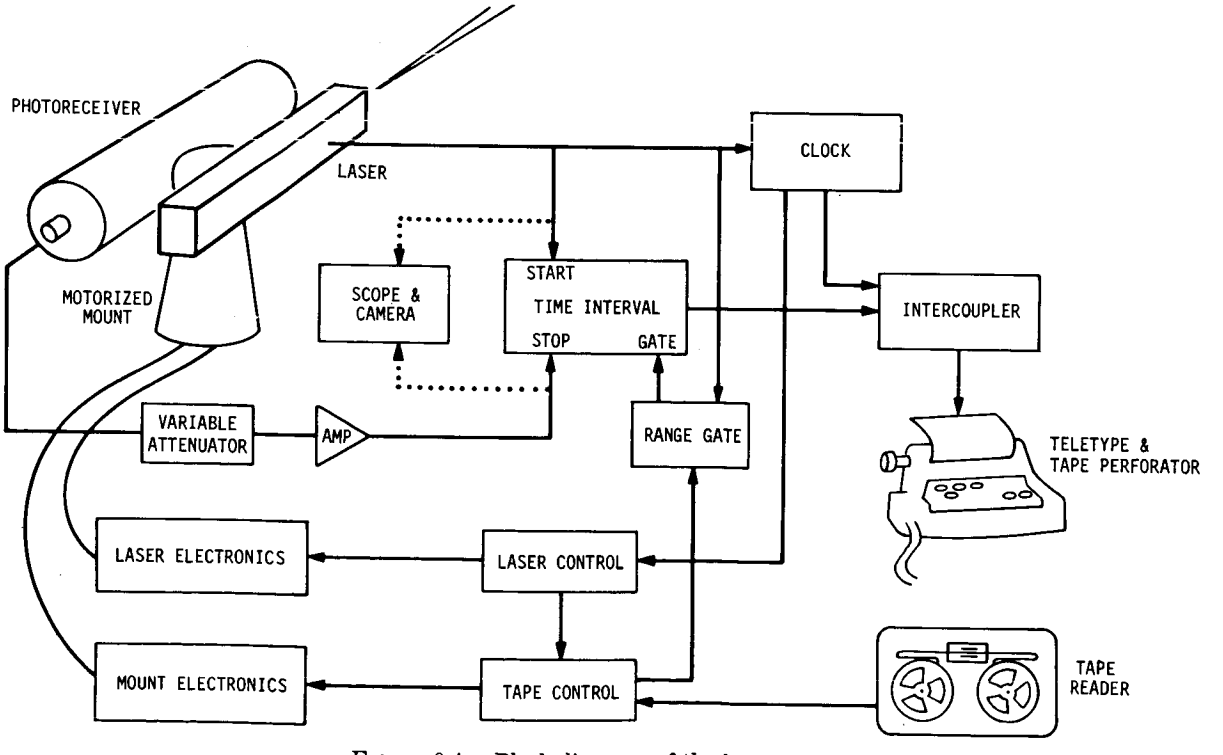

FIGURE 9.4.—Block diagram of the laser system.

The laser, built in an oscillator-amplifier configuration, generates an output of 5 to 7 joules in a 20–nsec pulse (half-power, full width). The laser transmitter system was produced by Spacerays, Inc., of Englewood, Colorado. The system uses a Pockels cell and a Brewster stack for a Q-switch and can maintain a pulse repetition rate of 10 ppm. Both the 0.85–cm (3/8-inch) diameter oscillator ruby rod and the 1.59–cm (5/8-inch) diameter amplifier rod are mounted in 15.24–cm (6-inch) double elliptical cavities, each containing two linear flashlamps. The optical cavity of the oscillator is formed by a flat rear mirror, with a reflectivity of 99.9 percent, and the uncoated front of the oscillator rod.

The oscillator output of 1 to 2 joules is coupled into the amplifier through a small beam-expanding telescope. The amplifier has a single-pass gain of about 4. Both ends of the amplifier rod are antireflective-coated.

The amplifier output is expanded to fill the 12.7–cm (5-inch) objective lens of a Galilean telescope. The telescope optics allows adjustment of the output beam divergence from a diameter of 0.5 to 5.0 mrad. Mounted at the output of the laser, ITT FW128 photodiodes pick up atmospherically scattered light from the outgoing pulse and send an electrical start signal to the time interval counter.

The optical elements of the laser are mounted on the machined upper surface of an aluminum I-beam, so that dimensional stability between the optical components will be maintained for all pointing orientations. Separate water-cooling systems are provided for the ruby rods and for the flashlamps. The coolant for the ruby rods is maintained at a temperature of $10° \pm 1°$ by thermostatically controlled cooling or heating elements. The lamp coolant is maintained within 10° C of the ambient air temperature. There is provision for applying nitrogen under pressure to the cavities, but experience has shown that this is not necessary. A cover over the I-beam is sealed, and desiccated air under slight pressure is circulated through the system.

The electronics of the laser transmitter are basically power supplies and pulse trigger circuits. The 1875–μf capacitor bank for the oscillator and amplifier lamps can be operated from 2000 to 4000 volts dc. Serial triggering of the lamps begins the discharge, which lasts slightly over 1 msec. Approximately 800 μsec after the lamp pulse begins, the system is Q-switched by quickly switching to ground the high-voltage input to the Pockels cell.

The ranging-system electronics consist of a clock, a firing control, a range gate control, and a time interval counter. The clock, synchronized to within ± 1 μsec of the station master clock, controls the firing time of the laser and provides the epoch of observation. The firing rate and the time of the laser firing are controlled by the laser control unit. The laser firing time can be shifted by a multiple of 0.001 sec, with a maximum of ± 10 sec, to account for the early or late arrival of a satellite at a predicted point in its orbit. The range gate control sends a delayed pulse of adjustable width to the counter so that the counter can be stopped only during a small interval of time about the predicted range time. The range gate provides protection against triggering by sky-background noise. The Eldorado 796 range counter is a time interval counter with 1-nsec resolution. It uses leading-edge, voltage, threshold discriminators on the start- and stop-signal lines. A start signal ranging from 5 to 20 volts is produced by the photodiode at the laser output. This signal is not processed or amplified before it reaches the start channel of the counter. The photomultiplier tube (PMT) output passes through a 0– to 50–db variable-step attenuator and a 32–db fixed-gain pulse amplifier before it reaches the stop-channel discriminator.

Stepping motors that point the mount are driven by position control electronics manufactured by Zehntel, Inc., Berkeley, California. Position information is maintained in the control units, which generate the appropriate number of drive pulses for the motors once a new azimuth or altitude position is demanded of the system.

The laser ranging system has a data subsystem that reads predicted satellite positions from punched paper tape and sends the information to the mount and laser control electronics and to the range gate. Azimuth and altitude pointing angles are given in thousandths of a degree; the range gate setting is specified in microseconds. The epoch for a predicted observation is displayed. Once the predictions start, operation continues automatically until the satellite pass is completed. Operation of the punched paper-tape reader is synchronized with the rest of the system by the laser control unit. Output data are also handled automatically by the data subsystem. The binary-coded-decimal (BCD) form of the epoch of firing and the range-time interval in nanoseconds is serialized, converted to Baudot code, and printed by an ASR32 Teletype machine. ASR32 punched tape can be fed directly into the radio communications system once a heading is put on each data pass. The input/output, clock, and control systems were designed and constructed by SAO.

The receiving telescope, made by Tinsley Laboratories, Inc., Berkeley, California, is a 50.8-cm (20-inch) Cassegrain system with additional optics designed to focus an image of the primary mirror on the photocathode of the PMT. The optics following the flat secondary mirror pass the collimated return signal through a 7-Å filter that is both tilt- and temperature-dependent. A micrometer tilt adjustment tunes the filter to compensate for effects of age and temperature. Adjustable field stops and a provision to insert combinations of neutral-density filters are available.

The photodetector, an RCA 7265, was chosen for its quantum efficiency of 4 percent or greater at 6943 Å. This PMT has a gain of 5×10^7 and a risetime of approximately 3 nsec as operated in the SAO system.

The azimuth-altitude static-pointing mount, also built by Tinsley, has a pointing accuracy of better than $\pm30''$. Verification of the mount position is made by viewing a goniometer in the mount; but under normal operations, the system is driven in an open-loop fashion from the electronic control unit. The stepping-motor drive-system gearing allows for slewing speeds of 2° sec^{-1} and positioning increments of 0°.001. The unit can be hand-cranked, but this limits the pulse repetition rate to 2 ppm, whereas the laser and the data subsystem have the capability to go to 10 ppm.

9.2.2.2.2 ATHENS LASER SYSTEM

The laser system in Athens was built as a cooperative project between the National Technical University and SAO and began operation in 1968.

The laser transmitter is a Q-switched ruby laser, manufactured by the TRG Company, now Hadron, Inc., Westbury, Long Island. The laser transmitter has a 1-joule, 24-nsec (half-power, full width) output pulse. The Q-switch is a rotating roof prism with a bleachable dye. The roof prism is driven by a synchronous motor at a speed of 30 000 rpm (500 rps). The bleachable dye is Kodak Cryptocyanine, a metal pthalocyanine, in an alcohol solution. The laser beam divergence of 5 mrad is reduced to 1 to 2 mrad with a 5-cm-diameter Galilean telescope.

The flashlamp power supply has a 900-μf capacitor bank with a maximum charging voltage of 975 volts (960 joules). A typical threshold is 560 joules when all optical components are in good condition and accurately aligned.

Photosensitive monitors are used both to start the ranging counter when the laser pulse leaves the transmitter and to monitor the output power. An RCA 931 PMT senses the light reflected from a glass plate oriented 45° to the beam. Its output is used to start the range counter. The power monitor is an EG&G SGD-100 semiconductor photodiode that senses the laser light scattered from the back of the rotating-prism Q-switch. The output of the photodiode is monitored on a high-speed oscilloscope.

The receiver of the system is a Cassegrain telescope with a 40.6-cm (16-inch) parabolic primary and a hyperbolic secondary. The system has a focal length of 6.55 m and

a focal ratio of 16. Incoming light first passes through a 10′ field stop at the focal plane and through a 20–Å interference filter and then falls directly on the PMT (RCA 7265), which is uncooled and operates at an anode voltage of 2400 volts.

The laser and photoreceiver are mounted on a modified surplus 3-inch gun mount, which is hand-cranked in altitude and azimuth by two observers. One observer tracks in azimuth and the other in altitude by observing the sun-illuminated satellite in the illuminated reticle of a 2.7–cm (5-inch) elbow telescope. Both observers sit directly on the mount and move with it as a system. This method of aiming the laser limits operations to times when the satellite is in sunlight and the station in darkness. Pulse detection is by leading-edge fixed-threshold discriminators.

The outgoing laser pulse starts a counter with 1–nsec resolution. The light pulse reflected from the satellite enters the receiving telescope and goes through the optical chain to the PMT, whose output is amplified and used to stop the counter. A range gate between the pulse amplifier and the ranging counter reduces the possibility of erroneous range measurements due to sky-background noise.

During operation, the laser fires every 30 sec—on the even minute and at 30 sec after the minute. Both the exact firing time of the laser and the range measurement are recorded with a camera system that automatically photographs the counter readings.

9.2.2.3 Accuracy and Error Budget

The accuracy of the laser systems can be discussed in terms of random and systematic error components. The former are those that are uncorrelated and appear as range scatter on a point-to-point basis, while systematic errors are correlated and vary regularly over a single pass or longer.

The random noise level of the systems has been computed from data on short-arc analyses taken during the International Satellite Geodesy Experiment (1971) and the Earth Physics Satellite Observation Campaign (1971 to 1973). This type of analysis generally detects only random errors, because systematic errors tend to be absorbed into the orbit parameters when they are adjusted in the least-squares-fitting procedures. The best-fitting curves for single transits were obtained by varying the mean anomaly, its first derivative, and the right ascension of the node. The standard deviation of the data varied from 30 to 120 cm, with a median of less than 60 cm. The dominant random-error component is due to the variation in size and shape of the return signals. The fixed-threshold, leading-edge pulse-detection system we are now using is very susceptible to such irregularities in return pulses. The return signals from the PMT may contain as few as 1 to 10 photoelectrons. They also may vary widely in size and shape during a single transit, owing primarily to scintillation from the satellite retroreflector array, irregularities in the laser beam pattern, and the statistical nature of the PMT detector. The expected random variation in the triggering times of the leading-edge threshold is a few nanoseconds (50 cm) for our transmitted pulse width of 20 nsec. Other random influences in the data, such as the least-count error in the counter and the random variability of the atmosphere, have smaller effects.

Systematic errors are considerably more difficult to grasp. However, the size of the systematic errors, per pass, has been estimated from performance and field tests. The ± 50–μsec uncertainty in epoch timing could be responsible for a systematic error of as much as 35 cm for some satellite-pass geometries. The models used by SAO and others compute the optical range correction due to tropospheric refraction from ground-based data. These models have an estimated systematic error of a few centimeters at zenith, with an approximate secant dependence for zenith angles down to about 70°. The residual error in current tropospheric-propagation-correction models is, on the average, probably about 4 cm per pass. The

geometry of the satellite and the placement of the retroreflectors relative to the satellite's center of mass are responsible for a systematic contribution of about 10 cm. This error is the result of uncertainties (1) in satellite attitude, (2) in retroreflector optical properties and placement, and (3) in the resultant return-signal shape and size from the entire satellite retroreflector array. The fixed-threshold, leading-edge detection system is probably responsible for systematic errors of about 3 nsec (50 cm) for a 20–nsec pulse width. This is in addition to the random variations and arises from systematic differences in the triggering point on the outgoing and the return pulses. Calibration on a fixed target is also an area where systematic influences are introduced through survey error and inaccuracies in the time interval measurement. It is estimated that systematic errors of about 10 cm may be introduced during calibration. If the sources of these errors are assumed to be independent, the total estimated influence, or root sum squared, is about 57 cm.

A two-laser collocation test was performed on satellite 6800201 (GEOS–2) at SAO's Mt. Hopkins Observatory, Arizona, from October 1969 to January 1970. SAO's laser there and a mobile laser system operated by National Aeronautics and Space Administration (NASA) participated. The objective was to determine the relative accuracy of two laser systems that were being used in the routine collection of satellite geodetic data. Since the two systems were built, calibrated, and operated by independent groups and since the instrumentation designs were different, the experiment gave a good estimate of the system-induced bias errors that can be expected. During the experiment, the two systems demonstrated a relative ranging accuracy of 1 to 2 m. In half the satellite passes, the difference in the range measurements of the two systems had a bias of less than 1.2 (see fig. 9.5). The sign of the bias changed several times during the 4-month experiment. At the time, it was felt that these bias components were primarily introduced into one or both of the systems during

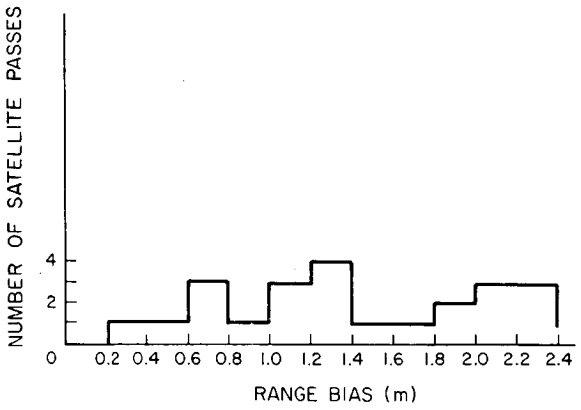

FIGURE 9.5.—Distribution of relative system biases.

the calibration procedure, which involved a determination of the system delay by ranging on a target at a known distance from each laser. Both systems have undergone significant modifications since the time of the collocation, and the systematic error in each has been substantially reduced.

9.2.3 Timing System

Each station has a timekeeping system to provide precise epoch data for each observation. The station clock is basically a crystal oscillator, a time accumulator, and a system of time and frequency monitoring aids. The clock has a dual-channel redundancy and a battery-backed power system to guard against loss of time continuity.

The clocks that were used in the Baker-Nunn network until the mid-1960's relied on a WWV-emitted time pulse and tone reference for both time and frequency settings. The active electronic components were vacuum tubes, and the time readout was in the form of rotating mechanical indicators and a rotating spot on an oscilloscope. Limitations on the stability and reading accuracy of the oscilloscope display led to the use of a fully electronic system featuring solid-state digital circuitry and a high-stability frequency standard.

The present clock has a Sulzer 5-MHz crystal oscillator stable to 1×10^{-10} day^{-1} and is generally kept within 5×10^{-10} of UTC

(USNO). It can be adjusted to 1×10^{-10}. The frequency of the oscillator is maintained through frequency and phase comparisons with stable VLF transmissions from stations such as NAA and NLF.

A locally generated 100–kHz signal is phase-locked to the VLF signal and then compared in phase to a 100–kHz reference signal from the clock. A relative phase position record is kept, which helps maintain station time to greater accuracies than is possible with the HF timing pulses.

The components of the EECo timing system are the clock's accumulator, the Sulzer oscillator, a VLF tracking receiver, a WWV receiver, a chart recorder to display the VLF/clock phase relationship, an oscilloscope (Tektronix 561A), and an ac–dc–ac battery-backed power system. Some stations have a secondary timing system, made up by duplicating most of these same elements. Other stations have a backup clock, consisting simply of an oscillator and a miniaturized digital counter.

The accumulator of the master clock system is a 100–kHz digital counter that offers a visual display of time in hours, minutes, seconds, and fractions of seconds to 10–μsec steps for precise timing control.

Timing at the stations is checked primarily by means of portable-clock trips. Although the VLF tracking receiver does not give epoch information, it does provide an accurate method of maintaining a record of time position relative to the setting obtained from the portable-clock comparison. Maintenance of accurate time between trips is facilitated in some locations by using the time tick of WWV and times sources of other agencies. The HF time signals offer the station a convenient time reference, but accuracies are limited to ±0.5 msec at best, owing to variations occurring over the long propagation paths to the stations.

At the laser stations, clocks routinely provide epoch to ±50 μsec (UTC) by means of portable-clock trips, which are conducted once a year on the average. During specific experimental periods, time has been corrected to ±25 μsec through extra care in VLF monitoring, more frequent checks by portable clocks, or other means of reference. The less stringent timing requirements at the camera stations (±100 μsec) are achieved through less frequent portable-clock trips.

9.2.4 SAO Satellite-Tracking Network

9.2.4.1 Sites

The first Baker-Nunn camera was sent to Organ Pass, New Mexico, at the observing site of the Harvard Meteor Program. The first successful observation was made November 26, 1957, just a month and a half after the launch of the first artificial earth satellite. The network had expanded by the following August to 12 operating Baker-Nunn stations. Table 9.1 shows the history of the Baker-Nunn sites to date.

After 8 years, it became apparent that higher accuracies were needed for future scientific projects. By March 1966, SAO had assembled, tested, and operated its first laser system. It consisted of a rented General Electric laser mounted on a 3-inch gun mount with a searchlight as receiver. This system operated successfully for over a year at the New Mexico site, during which time plans were formulated for a prototype laser system with components designed and built specifically for that purpose.

The prototype system was operating at Mt. Hopkins in December 1967. Three production laser systems, based on the design and experience gained with the prototype, were fielded in late 1970. In 1972, the Mt. Hopkins prototype was reworked to make it similar to the three production systems. Table 9.2 shows the history of the lasers to date. Figure 9.6 shows the present global distribution of stations, including the location of laser systems.

The present SAO sites that contain both a laser and a Baker-Nunn camera are Mt. Hopkins, South Africa, Peru, and Brazil. The last three stations are staffed and operated by SAO personnel with logistic support provided by cooperating agencies in each country: the Council for Scientific and

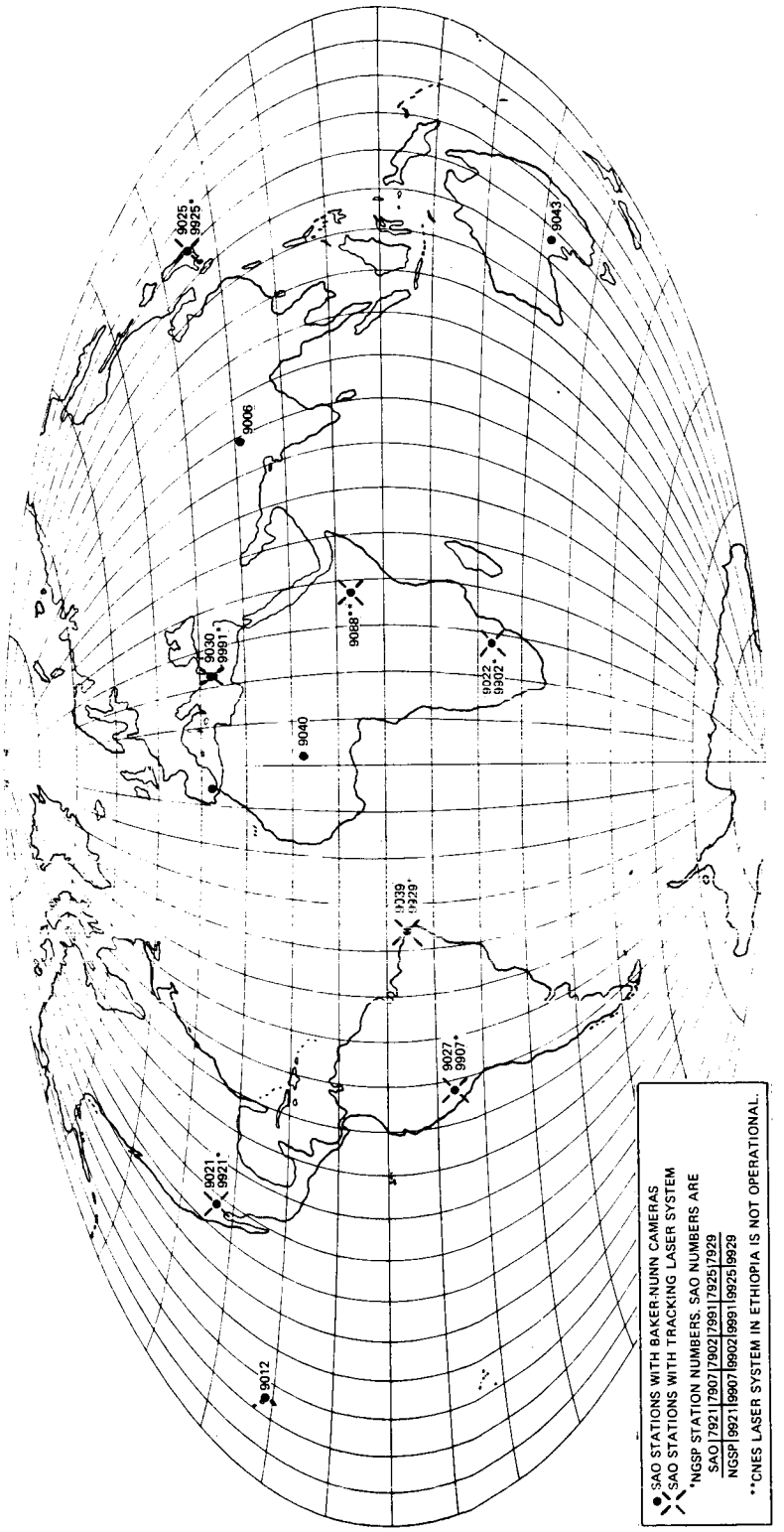

FIGURE 9.6.—SAO field stations.

Industrial Research in South Africa, the Instituto Geofisico del Peru and the Universidad Nacional de San Agustin in Peru, and the Instituto Nacional de Pesquisas Espaciais in Brazil.

The Baker-Nunn site in Maui, Hawaii, is staffed and operated by SAO personnel in conjunction with the University of Hawaii. The camera in Australia is operated by the Department of Supply of the Australian government. The stations in Spain, Ethiopia, and Greece are supported and operated jointly by the Smithsonian and cooperating agencies: the Spanish Naval Observatory in Spain, the Haile Selassie I University in Ethiopia, and the NTU in Greece. NTU also operates a laser system. A laser system belonging to the Centre National d'Etudes Spatiales (CNES) is currently located at Addis Ababa, Ethiopia.

The tracking station in Japan is operated by the Tokyo Astronomical Observatory and has, in addition to the Baker-Nunn camera, a laser system designed and built in Japan. The Baker-Nunn camera in India is operated by the Uttar Pradesh State Observatory.

A Baker-Nunn camera on loan to CNES has been used at several locations in Africa; it is currently in operation in Ouagadougou, Upper Volta.

Beginning in 1964, several Baker-Nunn cameras operated by the 7th Aerospace Squadron at ENT Air Force Base have participated in SAO satellite-tracking programs. The sites are listed in table 9.3. SAO scheduled observing times and provided predictions for simultaneous observations. These data have been included in the SAO analysis and are incorporated in the SAO data file.

9.2.4.2 Operations

The SAO Baker-Nunn cameras and laser systems receive new satellite predictions each week. The predictions are computed from up-to-date observations provided by the SAO network and by camera, MINITRACK, and laser system observations made by other agencies (see table 9.4).

The predictions for the Baker-Nunn camera consist of azimuth- and altitude-pointing angles, which need be accurate to only a few degrees, and tracking-angle rates to simulate the satellite motion (Cherniack and Gaposchkin, 1963). These predictions are generated from orbits computed with a simple model of the earth's gravity field. The short-periodic terms due to C_2 and the long-period terms due to the odd zonal harmonics are included. The secular rate of the apsidal line and the argument of perigee are determined from the data for each orbit. The orbits are generated with the Smithsonian's Differential Orbit Improvement (DOI) program (Gaposchkin, 1964) from observations covering a period of about 2 weeks.

The laser, on the other hand, requires azimuth- and altitude-predicted pointing angles accurate to within several minutes of arc and a predicted range propagation time accurate to within 20 μsec for a given epoch. Orbits for laser tracking predictions are also generated with the DOI program by using a gravity field with most of the tesseral harmonics through degree and order 16 and with a number of higher resonance terms. Lunar perturbations are also included. Again, orbits are computed from data covering a period of about 2 weeks. Predictions for satellites equipped with retroreflectors are made for passes that reach altitudes greater than 25°.

The success of the network has depended on the timely flow of data from the field, the development of pointing predictions from up-to-date data, and the use of these fresh predictions at the field stations. The rapid data-prediction cycle is most critical for the laser, which has stringent pointing requirements; however, it is also an important factor in the Baker-Nunn operation, especially for simultaneous observations between stations for geometric geodesy.

Until 1968, direct links by teletype between the field stations and Cambridge provided real-time communications. Since then, a combination of means has been used to give real-time or near real-time communications at each site. Peru and Brazil receive predic-

tions and send their camera and laser data by direct radio-teletype link operated by SAO personnel. These stations have prearranged contact times for data transmission. Atmospheric disturbances severe enough to affect the link are infrequent. The tracking sites in Hawaii, Japan, Spain, Greece, and Arizona use facilities of the United States military communications network for transmission and receipt of data. The first three stations have direct access to this network, while those in Greece and Arizona must pick up and deliver messages at local military bases. The stations in Australia and South Africa use the NASA data network (teletype). Predictions for the Ethiopia station are sent via NASA teletype link to CNES in France and are retransmitted on their lines to Ethiopia. CNES generates and sends predictions for their laser, located in Ethiopia, as well as predictions for the 12th Baker-Nunn camera, now in Upper Volta. Data are currently returned to Cambridge by Embassy mail. The site in India receives predictions from SAO via the United States Embassy in New Delhi and sends its data back by way of commercial cable.

For the Baker-Nunn camera, predictions cover a period of 1 week, with an extra day in case of transmission delays. At present, an average of 10 arcs is predicted per station per night. In the past, as many as 50 arcs were predicted for each station. Observations are reduced in the field to an accuracy of 40″ to 60″ and sent to Cambridge immediately for use in the prediction cycle. The camera film is sent by commercial mail for subsequent precise reduction (photoreduction).

Predictions for the laser system are in the form of punched paper tape, which is used directly to point the laser. Each predicted arc contains from 10 to 90 separate points (4 min^{-1}), depending on the geometry of the pass. Stations receive 40 to 100 predicted arcs per week for three satellites currently being tracked: GEOS–1, GEOS–2, and BE–C. All seven retroreflector-equipped satellites have been tracked. Satellite ranging data, system calibration data, and ground-based meteorological data are sent to SAO.

9.3 DATA AND DATA REDUCTION

(Søren W. Henriksen)

This section summarizes the data used in (1) deriving coordinates for the locations of various tracking stations (sec. 9.5.1) and in (2) determining the Earth's gravitational potential (sec. 9.5.2). Data relating to the former are summarized in section 9.3.1; those relating to the latter are summarized in section 9.3.2. The section also describes (sec. 9.3.3) the preprocessing applied to data from Baker-Nunn cameras and laser systems.

9.3.1 Data Used in Determining Coordinates

(G. M. Gaposchkin, J. Latimer, and G. Veis)

9.3.1.1 Geometric Method

The geometrical solution included two networks: 27 stations of the SAO network, including the U.S. Air Force's Baker-Nunn cameras and several European stations; and 48 stations of the National Ocean Survey (NOS) BC–4 network. Of the SAO group, 21 stations were also included in the dynamical solution. The SAO data block consisted of 5200 pairs of synthetic simultaneous observations (table 9.5), or about 50 000 individual direction observations processed at SAO. The satellites observed were 6102801 (MIDAS–4), 6303004, 6508901 (GEOS–1), 6605601 (PAGEOS), 6800201 (GEOS–2), and 6305501. The BC–4 data consisted of 2157 pairs of simultaneous events (photographs of PAGEOS). Each event generally consisted of seven directions and a covariance matrix from each of the two stations. When more than two stations observed the satellite simultaneously, we treated each station pair separately. The BC–4 data were obtained from the National Space Sciences Geodetic Satellite Data Service at the National Aeronautics and Space Administration/Goddard Space Flight Center (NASA/GSFC) (see ch. 1). The data

were acquired, reduced, and processed by the NOS. The standard deviations assigned to the directions are given in table 9.26b.

In geometric work, SAO observations refer to the equator and equinox of 1950.0. They are corrected for the effects of annual aberration, diurnal aberration, parallactic refraction, and planetary aberration and then converted to the terrestrial system of SAO, which is fundamentally defined by the mean pole of 1900–1905 of the International Polar Motion Service (IPMS) and by the meridian of the Mean Observatory and UT1 of the Bureau International de l'Heure (BIH). The BC–4 data are in the same reference system.

9.3.1.2 Data Used in Dynamic Method

The stations whose data were used in the dynamic method are listed in table 9.6; the observations used are from the satellites listed in table 9.7. The distribution of these satellites (inclination versus height) is plotted in figure 9.7. Satellite arcs were chosen from satellites whose orbits were relatively uncorrupted by errors. Specifically, we eliminated satellites with drag model errors (large area-to-mass ratio and low perigee height) particular sensitivity to gravity-field model errors (resonances), or poor orbital distribution (less than six stations observing the satellite). The data were kept in two parts. Before 1970 most of the observations were directions. A number of laser system ranges were made, and where it was possible to do so, they were included in the orbits. In 1971, the International Satellite Geodesy Experiment, ISAGEX, a cooperative tracking program with 10 laser stations, was carried out and provided for

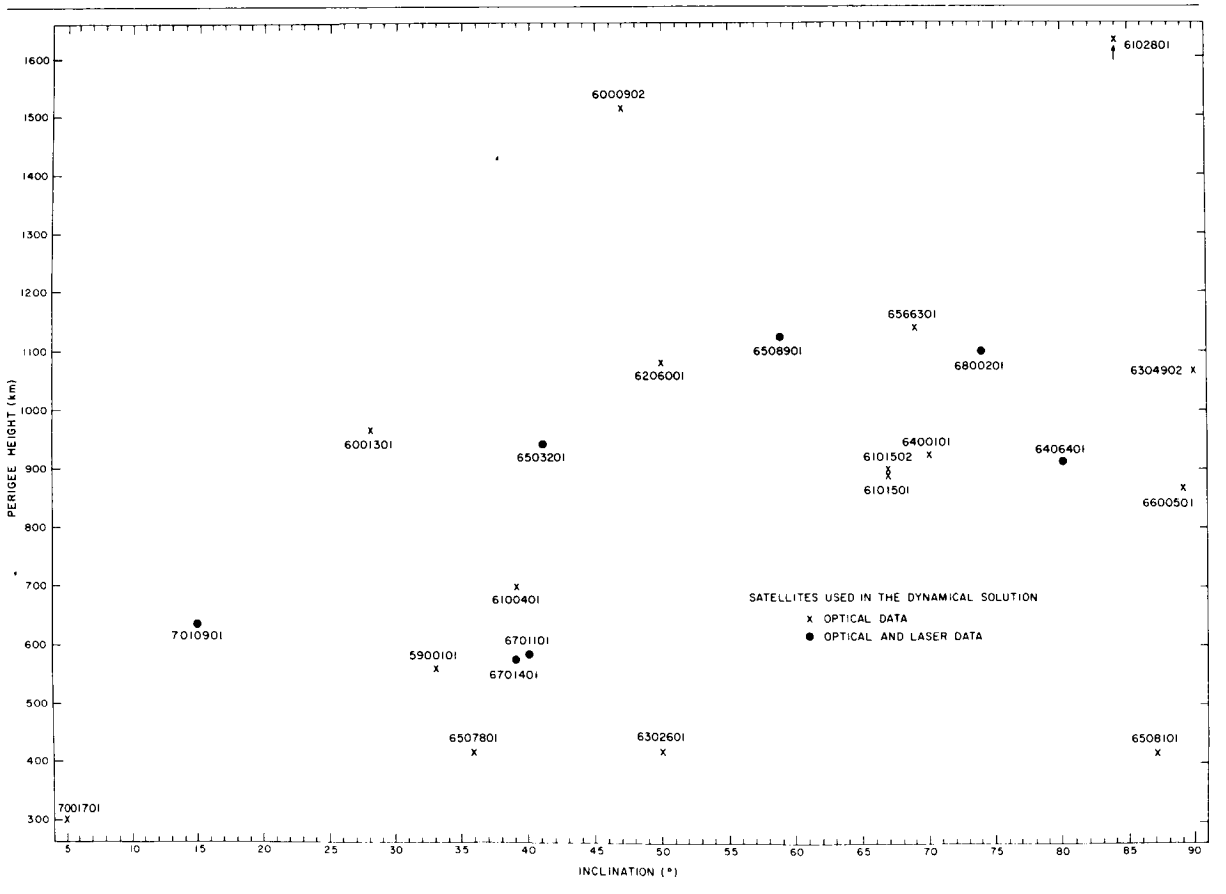

FIGURE 9.7.—Distribution of satellites used in SE III.

the first time relatively complete orbital and geographical coverage with laser data. From these ISAGEX data, 15 orbits were selected and used in the dynamical determination of station coordinates.

The assumed accuracies of the instruments are given in table 9.8. Camera data were given an assumed accuracy of 4″. When five or more observations were made within a few minutes, e.g., of GEOS flashes, a smoothed or synthetic observation was determined. The same calculation was used to generate simultaneous observations, since in general one cannot make exactly simultaneous observations. These synthetic observations were given an accuracy determined from the polynomial fit. If the computed uncertainty was less than 2″, then 2″ was used. In the reduction of camera data, annual aberration and parallactic refraction which were determined from mean nighttime temperature and pressure for each station, in addition to precession and nutation, were applied.

The distance measurement in range data used in this analysis has a precision of 1 to 2 m. The accuracy, including timing errors, will not be so good. In addition, other errors, e.g., those due to the gravitational field, are that large. Therefore, the assumed accuracy of the laser system data was taken to be 5 m. Some laser system data taken in 1967 appear to have errors in timing of a millisecond, and these data were given an assumed accuracy of 10 m. Furthermore, certain laser systems provide a larger volume of data than is useful here (e.g., more than 400 points per pass). Therefore, for passes containing more than 25 points, approximately 25 evenly distributed observations were selected. Numerical experiments indicated no improvement in the results by smoothing the points or calculating synthetic observation.

The laser system data were corrected for tropospheric refraction with the use of observed values of pressure, temperature, and relative humidity. In addition, the observations were reduced to the center of mass of the satellite by means of the formulas presented in table 9.9. These formulas relate the range correction Δ in meters to the angle ϕ in degrees between the satellite's axis of symmetry and the line of sight to the observing station. The corrections made in this manner are relatively small but systematic. The tropospheric correction is 2.1 m at zenith, and the reduction to the center of gravity is 80 cm for GEOS–1.

Table 9.8 summarizes the adopted uncertainties. Table 9.10 gives the number of observations selected from the data.

The dynamical solution used data taken between 1962 and 1969 on 140 arcs of 15 satellites and ISAGEX data taken in 1970 on 15 arcs of 3 satellites. These two sources of data were kept separate, and several solutions were made.

Since the ISAGEX data are of a new type, we examined the origin of the node and the relative weighting in order to find the best treatment. Two iterations were performed as part of the larger computation of station coordinates. The pre-ISAGEX data were in arcs from 4 to 30 days, as appropriate, and the ISAGEX data were in 10-day arcs.

The length scale in a dynamical solution is, for all practical purposes, fixed by the value of GM, which directly enters the calculations of radius vector through

$$r=\left(\frac{GM}{n^2}\right)^{1/3}(1-\cos E)\,(1+\text{perturbations})$$

With camera directions, no further information in scale is available. With range data, both scale and GM can, in principle, be determined. The unit of distance then is defined by the speed of light and becomes the "light second." In this analysis, GM was assumed to be the value given in table 9.11. Our dynamical scale is therefore defined by GM. If this value of GM is far from the true value, some deterioration of the coordinate will result. We return to this question in the discussion and evaluation of results.

Table 9.11 gives the values adopted, in this computation, for GM, c, and k_2.

9.3.1.3 Data Combined With Both Methods

9.3.1.3.1 INFORMATION FROM DEEP-SPACE PROBES

JPL operates the Deep Space Net (DSN), eight stations for tracking deep-space probes. Data from the DSN have been used to obtain, among other parameters, the longitudes (relative and absolute) of each station and the distance of its antennas to the Earth's instantaneous axis of rotation (Vegos and Trask, 1967; Trask and Vegos, 1968). The DSN data are particularly interesting because (1) they constitute a unique, complementary, and independent determination of geocentric locations, and (2) they provide a very strong determination of scale.

Comparisons of the JPL and SAO results were made by Veis (1966a) and Vegos and Trask (1967) from data from the Ranger missions and from SE I (Lundquist and Veis, 1966). More refined JPL solutions were combined with satellite-tracking data in the determination of SE II. The combination was made with Location Set (LS) 25, as determined by Mottinger (1969), by using data from the Mariner 4 and 5 missions. Continued refinement of the DSN data has provided LS 37, which is used in the present analysis.

Each DSN site is located near other stations whose coordinates were determined in the analysis presented here. Surface-triangulation data, in the form of geodetic coordinates, can be used to relate the DSN coordinates to the SAO coordinates.

The ephemeris r of a deep-space probe is assumed known. For a distant spacecraft, the observed range rate $\dot{\rho}$ can be expressed approximately as

$$\dot{\rho}=\dot{r}+\omega r_s \cos\delta \sin(\alpha_s-\alpha_0)$$

where ω is the earth's rotation rate, r_s is the spin-axis distance of the observer, δ and α_0 are the declination and right ascension of the spacecraft, and α_s is the right ascension of the observer. Each station observes a diurnal variation in $\dot{\rho}$, the amplitude and phase depending on r_s and α_s, respectively.

Generally, any data can be analyzed. However, cruise data seem less reliable than close-encounter data for determining α_s and they are used only for the determination of r_s. In any case, refraction (tropospheric and ionospheric) and orbit computation must be done with great care, and recent improvements come from refinements in the treatment of refraction. The ephemeris r, (δ, α_0) will be determined in the system of the JPL planetary ephemeris. We can expect to find a systematic difference in the definition of longitude between the planetary ephemeris and the astronomical reference system (FK4) used for analysis of close-earth satellites. The DSN data reduction used numerical values for pole position and UT1 from BIH, as was done for the close-Earth-satellite analyses.

The data for LS 37 are summarized in table 9.12. The main improvements over LS 25 are as follows: (1) better treatment of refraction, particularly ionospheric; (2) inclusion of more data because of (1); (3) inclusion of Mariner–6 encounter data; (4) revision of the planetary ephemeris; and (5) use of BIH polar motion and UT1. Realistic estimates of accuracy are 2 m for r_s, 4 m for absolute longitude, and 2 m for relative longitude (Mottinger, private communication, 1972).

Mottinger provided a solution and covariance matrix for r_s, λ, in addition to the masses of Venus, Mars, and the Moon and the oblateness of Mars. This system was transformed by SAO for corrections in coordinates X, Y of the station. These converted equations were then added to the larger system of normal equations, which included the other stations sought.

The LS 37 coordinates for the DSN stations are given in table 9.13. In LS 37, the relative coordinates of DSS 11, DSS 12, and DSS 14 and of DSS 61 and DSS 62 were constrained to agree with the survey data.

9.3.1.3.2 INFORMATION FROM SURFACE TRIANGULATION

Extensive surface-triangulation data exist that relate station positions. These data are generally given in terms of datum coordinates and occasionally in terms of interstation vectors for collocated stations. We have used this information in four ways:

(1) For stations in the same datum, the geodetic coordinates are used as observations relating the positions of the stations in the general combination adjustment.

(2) For collocated instruments, these datum coordinates are used as a constraint relating the two sites. These cases could be treated as in (1) above.

(3) The geodetic coordinates are utilized as a check on the accuracy of the final coordinates.

(4) The geodetic coordinates are employed to determine the relation of each datum to a geocentric reference system.

Evaluating geodetic coordinates is the most difficult aspect of this analysis. When reliable, they are very accurate; but problems often exist in relating the local survey at the station to the datum.

In (1), (2), and (3) above, care must be taken to ensure that datum tilts, distortions, and scale differences do not corrupt the results. For most uses, limiting the application of geodetic coordinates to lengths of 100 km or less is satisfactory. Otherwise, the datum orientation must be determined and applied before the geodetic coordinates can be used with geocentric satellite-based coordinates.

The use of datum coordinates as observations of relative station positions assumes no correlation between X, Y, and Z. If we have datum coordinates for station i, X_i^d, Y_i^d, Z_i^d, and initial values for the geocentric coordinates that are to be corrected, X_i^g, Y_i^g, Z_i^g, we can write observation equations for each component of the vector between two stations:

$$X_i^d - X_j^d = X_i^g - X_j^g + \Delta X_i - \Delta X_j$$

with similar expressions for Y and Z. If these are given weights W_{ij}, we can immediately write the normal system as

$$\begin{bmatrix} \sum_i \sigma_{ij} & \cdots & -\sigma_{ij} \\ \vdots & & \vdots \\ -\sigma_{ij} & \cdots & \sum_j \sigma_{ij} \end{bmatrix} \begin{bmatrix} \Delta X_i \\ \vdots \\ \Delta X_j \end{bmatrix} = \begin{bmatrix} \sum_i \sigma_{ij}[(X_i^d - X_j^d) - (X_i^g - X_j^g)] \\ \vdots \\ \sum_j \sigma_{ij}[(X_j^d - X_i^d) - (X_j^g - X_i^g)] \end{bmatrix}$$

where $\sigma_{ij} = (1/W_{ij})^2$. This system can augment a normal system for determining ΔX, ΔY, ΔZ.

The weight W_{ij} of the geodetic ties chosen is given in table 9.14. Table 9.15 presents the geodetic coordinates for all the stations used in the 1973 Smithsonian Standard Earth (SE III).

9.3.2 Data Used for Potential

(E. M. Gaposchkin, M. R. Williamson, Y. Kozai, and G. Mendes)

The potential was divided into two parts: one expressed by zonal harmonics and the other by tesseral (sec. 9.4.3). The data used for the two parts were different. In the determination of the zonal coefficients, secular changes in the Keplerian elements were expressed as functions of the zonal coefficients. (The "observed" quantities in secs. 9.3.2.1, 9.4.3, and 9.5.2 are not observations but values of $\dot{\omega}$, $\dot{\Omega}$, etc., computed from observations.)

9.3.2.1 Data Used in Determining Coefficients of Zonal Harmonics

Table 9.16 gives the orbital elements for the 14 satellites of this analysis. Gaps still exist in inclinations around 20° and 40°. The

values of $(O\text{-}C)$ for the secular motions and the amplitudes of $\begin{matrix}\sin\\\cos\end{matrix}\Big\}\omega$ terms based on 1964 values (Kozai, 1964) follow:

	$\dot{\omega}$ day^{-1}	$\dot{\Omega}$ day^{-1}	A_ω
DIAL	$-0^\circ.01806$	$0^\circ.01012$	$-0^\circ.070$
	± 9	± 7	± 5
PEOLE	-0.0022	0.00516	0.045
	± 8	± 10	± 30

	A_Ω	A_I	A_e
DIAL	$-0^\circ.019$	$0^\circ.0043$	-9.1×10^{-5}
	± 3	± 3	± 6
PEOLE	-0.002	-0.0017	2.8×10^{-5}
	± 5	± 30	± 2.0

The large values of $(O\text{-}C)$ for these two satellites show that the previous sets of zonal-harmonic coefficients were inadequate.

The data for DIAL were derived from orbital elements from March 18 to July 16, 1970; during that period, the argument of perigee made four revolutions. The orbital elements for PEOLE were obtained for January 9 to March 13, 1971, and for March 28 to August 30, 1971. These data are not so accurate as those for DIAL, since there were not enough observations and there was a period during which no orbital elements were available.

In this new determination, the $(O\text{-}C)$ values for satellite 6000902 are a revision by Gaposchkin for February 10, 1961, to April 21, 1963.

The other satellites included in this determination are 6001301, 5900101, 6202901, 6302601, 6206001, 6508901, 6101501, 6400101, 6406401, 6508101, and 6102801. The data for these satellites are the same as those given by Kozai (1964). The $(O\text{-}C)$ values were computed from the 1964 values of coefficients as given in table 9.17.

The following values have been used for the geocentric gravitational constant and the equatorial radius of the Earth:

$$GM = 3.986\,01\times10^{20}\ \text{cm}^2\ \text{sec}^{-2}$$

$$a_e = 6.378\,16\times10^{8}\ \text{cm} \qquad (9.1)$$

Table 9.18 lists the values of $(O\text{-}C)$, based on the coefficients from Kozai (1964), for the secular motions of the 14 satellites and their standard deviations. The latter are used to compute weights assigned to the data. The columns headed I and II represent the differences computed by 12 unknowns and 11 unknowns, respectively, and the dates refer to previous Kozai solutions. Kozai (1969) intentionally increased some of the standard deviations, since he thought that neglect of higher order terms would cause errors larger than the standard deviations of the observed values. For the same reason, we have increased the standard deviation (10^{-6} degree per day) to $3^\circ\times10^{-6}$ day^{-1} for $\dot{\omega}$ of satellite 5900101 and $\dot{\Omega}$ of satellites 5900101, 6000902, 6302601, 6206001, 6101501, and 6508101. The standard deviation assigned to the secular motions of 6508901 was erroneously given in the previous paper.

In the determination of even-order harmonic coefficients, we have used the secular motions and the amplitudes of $\begin{matrix}\cos\\\sin\end{matrix}2\omega$ terms for selected orbital elements of those satellites for which the eccentricities are small. We could not use data from the other satellites, since the orbital elements available for them were not of sufficient accuracy. The $(O\text{-}C)$ values and their standard deviations for the amplitudes of the long-periodic terms are given in tables 9.19 and 9.20. The longitude of the ascending node and the inclination have been omitted for some of the satellites in tables 9.19 and 9.20 because their amplitudes are extremely small. The differences for ω of 6508901 and 6101501 and for e of 6400101 computed after the determination were found to be much larger than their standard deviations computed from observations. Also, since the inclinations of these satellites are near the critical inclination, higher degree interaction terms neglected in the computations—such as C_3^2/C_2 and $C_2^2\,C_3/C_4$—might have affected the data reduction. For these reasons, we increased the standard deviations assigned to these data from 1.5, 2, and 1 to 4, 5, and 3, respectively; the increased values are given

in table 9.20. One misprint appeared in table 2b of Kozai (1969): $(O\text{-}C)$ for ω of 6508901 should be $(6\pm2)\times10^{-3}$ instead of $(6\pm2)\times10^{-4}$.

9.3.2.2 Data Used in Determining Coefficients of Tesseral Harmonics

9.3.2.2.1. SATELLITE TRACKING DATA

Laser data from ISAGEX provided global coverage with 2-m data for the first time. Table 9.7 lists all the satellites used in the analysis, including those from which ISAGEX and earlier observing programs obtained laser data, and figure 9.7 shows their distribution in inclination and height. Separation of the station-coordinate and the gravity-field determinations allowed a better selection of satellite data. For the former, high satellites less affected by the anomalous gravity field were emphasized, while for the latter, lower satellites, with a better distribution, were stressed. Certain satellites with unmanageable, long-period resonances (e.g., 5900701) were used only for the determination of station coordinates; they have such a rich body of data that relatively short-arc orbits (4 days) could be derived for this purpose.

Each observation was given an a priori weight (detailed in table 9.21 so that when the normal equations were combined, each type of data could be scaled. The scale factor for surface-gravity data was arrived at by experiment. The scale factors for the 550 km$\times$550 km anomalies and for the zero anomalies were chosen so that the resulting solution improved the satellite orbit, the surface-gravity residuals, and the errors in the surface-gravity comparison and did not introduce spurious short-wavelength detail where no surface-gravity data were available.

All available optical data were used for the orbital arcs chosen. For each pass of laser data containing more than 30 points, approximately 30 uniformly distributed observations were selected.

9.3.2.2.2 TERRESTRIAL GRAVITY DATA

The primary objective of the analysis of terrestrial gravity data was to obtain mean anomalies for regions 550 km $\times$ 550 km. When these data are combined with the satellite-perturbation analysis, the spherical harmonics representing the geopotential can be determined. A set of gravity data with known (and preferably simple) statistical properties is needed. Our approach is based on covariance analysis, following the ideas of Wiener (1966) and Kolmogoroff. When this technique is used in communications engineering, it is sometimes known as filtering theory. The ideas here are an extension of a one-dimensional time series to the two-dimensional surface of a sphere (Kaula, 1967d).

Estimation of gravity by covariance methods hinges on the stationarity of gravity data; that is, the statistical properties of the data are independent of location. There is some evidence that gravity data are not stationary; however, if some subsets of the total gravity population are stationary, then gravity covariance functions between sets and within each set can be defined.

The $1°\times1°$ Data Available.—A set of $1°\times1°$ mean free-air anomalies, containing 19 115 measured means, was obtained from ACIC (1971), and another set, of 1454 $1°\times1°$ means for Australia, from Mather (1970). The two sets were combined, with the Mather data being used for all areas they covered. Figure 9.8 shows the geographical coverage of all the data. The combined data set contained 19 328 means. A complete set of $1°\times1°$ mean topographic heights, used to define oceanic and continental areas, was obtained from Kaula (Kaula and Lee, 1967). The distribution of $1°\times1°$ mean gravity data is summarized below:

Depth of boundary (km)	Ocean		Continent	
	Measured	Total	Measured	Total
0	9213	42 918	10 115	21 882
−1	7015	36 199	12 313	28 601

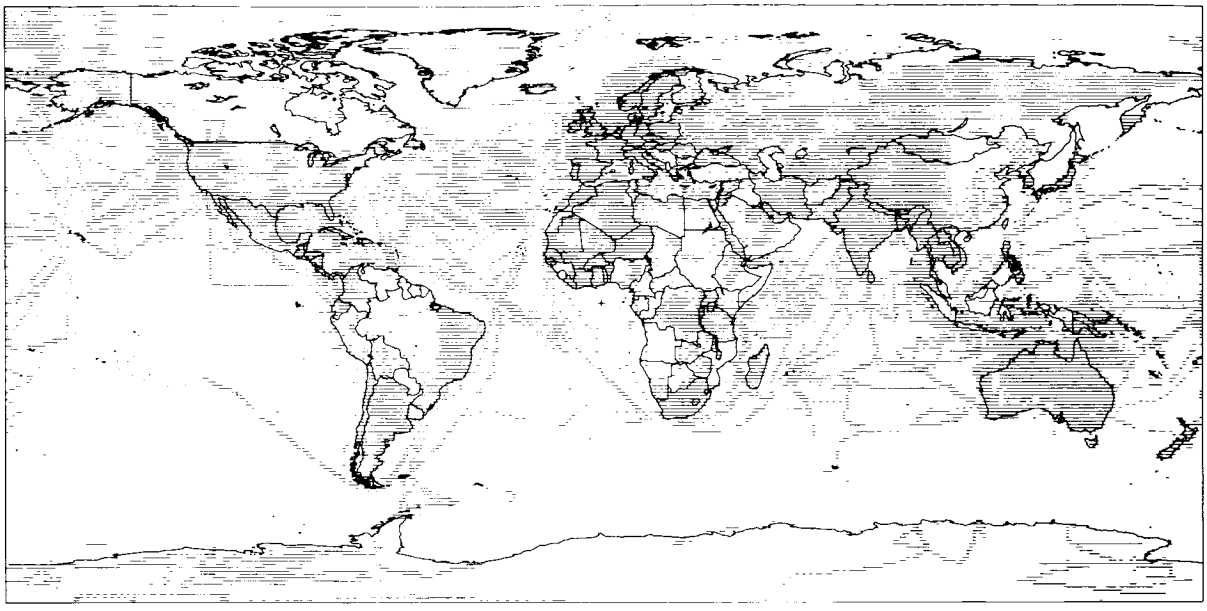

FIGURE 9.8.—Distribution of $1° \times 1°$ surface gravity data.

The estimated uncertainty given with each gravity anomaly for 99.9 percent of the data is less than 25 mGal. Comparing the Mather data with the ACIC data at the 1241 common points, we find that the average difference is 1.7 mGal and the root-mean-square difference is 20 mGal. At a number of points, the discrepancy between the two sets exceeds 100 mGal.

The Estimation Procedure.—Kaula (1967d) has developed a procedure that greatly simplifies the calculation of covariance function which is called the block covariance function, and the gravity estimates. This method has both advantages and disadvantages. The disadvantages are (1) the estimate of gravity does not make use of all the gravity information (i.e., the estimates are not as good as possible); and (2) the covariance function must be determined by using only the combinations of anomalies within blocs and therefore is not determined with all possible combinations of the data.

The advantages of Kaula's method are as follows: (1) it greatly simplifies calculation of the covariance function and the gravity estimates; (2) it produces mean anomalies 550 km $\times$ 550 km with uncorrelated errors; and (3) the statistical properties of data within a block may be closer to stationarity since the method involves primarily the short-distance covariance.

If gravity were a stationary process, then it would have the same statistical properties everywhere. Possible nonstationarity was investigated by determining the covariance function for subsets of gravity data. A separation of oceanic from continental gravity was used. A 0– and a 1–km depth were used to define the ocean-continent boundary, which was determined from topographic data. The boundary was also expanded to a width of 400 km for the 1–km depth, and the covariance functions were computed without the gravity data in that region. Finally, gravity data were divided into an equatorial set, $|\phi| < \pi/4$, and a polar set, $|\phi| > \pi/4$. The covariance functions for all the gravity data and the four sets of split data and the block covariance function are plotted in figure 9.9.

Since the differences between the covariance functions are significant, we conclude that gravity is not stationary. Any estimation procedure that makes that assumption must be carefully examined.

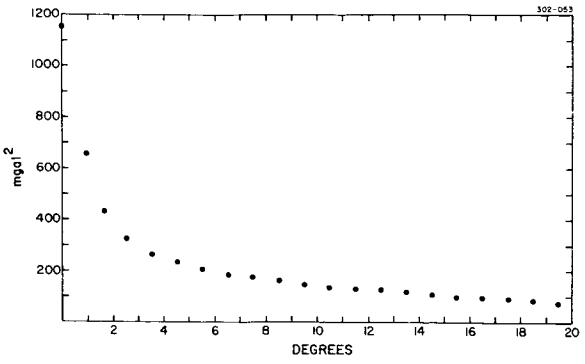

FIGURE 9.9a.—The covariance function of mean 1°×1° gravity anomalies.

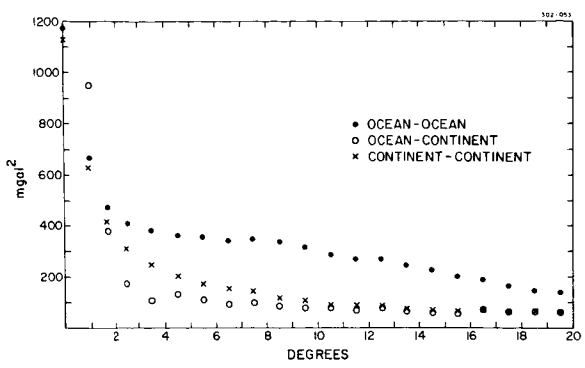

FIGURE 9.9b.—The covariance function of mean 1°×1° gravity anomalies for a 1-km ocean-continent boundary.

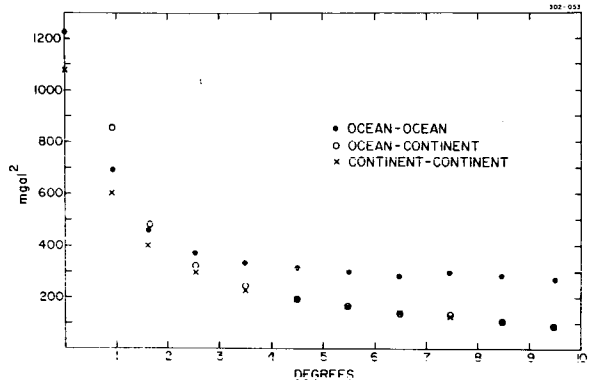

FIGURE 9.9c.—The covariance functions of mean 1°×1° gravity anomalies for a 0-km ocean-continent boundary.

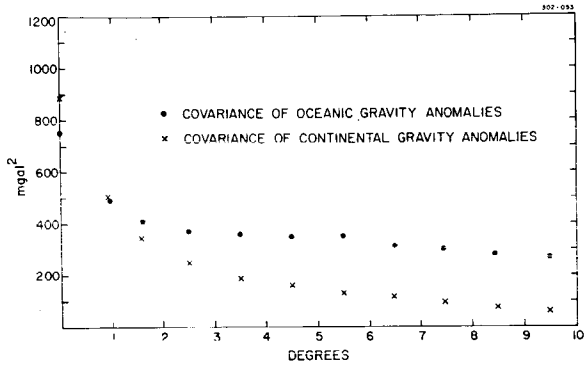

FIGURE 9.9d.—The covariance functions of mean 1°×1° gravity anomalies for a 1-km ocean-continent boundary 400 km wide.

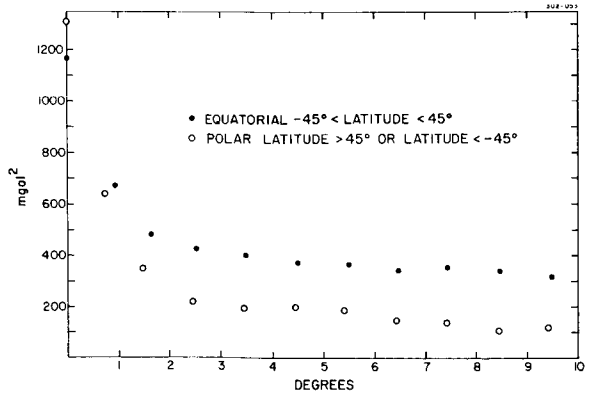

FIGURE 9.9e.—The covariance functions of mean 1°×1° oceanic gravity anomalies for polar and equatorial regions.

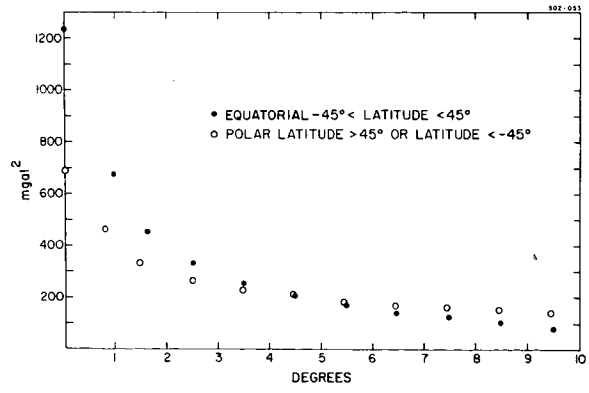

FIGURE 9.9f.—The covariance functions of mean 1°×1° continental gravity anomalies for polar and equatorial regions.

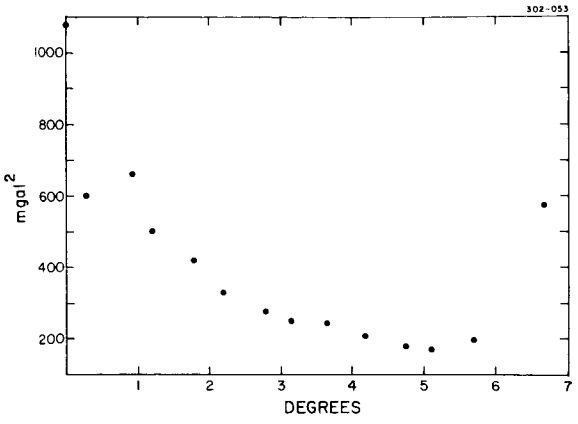

FIGURE 9.9g.—The block covariance function of unit gravity anomalies.

The different estimates of gravity from the global covariance estimator, from the split covariance estimators with a 0- and a −1-km ocean-continent boundary, and from the Kaula estimator were obtained and compared. At the equator, the Kaula-type units and the $1°\times1°$ areas coincide, so that the four estimates can be compared directly. Figure 9.10 shows a few blocks at the equator. Large differences are in blocks with few observed points. In the combination with satellite data, these points will have a small effect due to the weighting, which is proportional to the number of units contributing to the average. Therefore, by using the block covariance estimator of Kaula, we obtained a statistically independent set of 550 km × 550 km averages with no loss of accuracy. Block covariance provides the optimum set of gravity anomalies to be used in combination with satellite observations. Of course, of all the methods used here, the split covariance estimator is preferable for the prediction of $1°\times1°$ mean gravity anomalies.

The gravity anomalies are given with respect to the International Gravity Formula (Heiskanen and Moritz, 1967, p. 79) and must be corrected to refer to the best-fitting ellipsoid defined by C_2 and the adopted values of a_e, GM, and ω_e. We must also include the Potsdam correction of −14 mGal. Using the following initial values:

$$\bar{C}_2 = -484.170\times10^{-6}$$
$$a_e = 6.378\ 140\times10^{8}\ \text{cm}$$
$$GM = 3.986\ 013\times10^{20}\ \text{cm}^3\ \text{sec}^{-2}$$
$$\omega_e = 7.292\ 115\ 085\times10^{-5}\ \text{sec}^{-1}$$

we have

$$1/f = 298.256$$

and the correction

$$\delta g_{\text{SAO}} - \delta g_{\text{int}} = 1.3 - 13.8\ \sin^2\phi\ \text{mGal}$$

9.3.3 Preprocessing

(M. R. Pearlman, J. M. Thorp, C. R. H. Tsiang, D. A. Arnold, C. G. Lehr, and J. Wohn)

9.3.3.1 Baker-Nunn Camera Data

9.3.3.1.1 STAR CATALOG

The stellar reference system used for the Baker-Nunn reductions is defined by the SAO Star Catalog (Staff, Smithsonian Astrophysical Observatory, 1966) which contains approximately 260 000 stars. The average standard deviation of the positions in the SAO catalog is of the order 0″.5 for the current epoch, although individual values may range from 0 to 2″.5. The SAO catalog is in the FK4 system, which has possible systematic errors of 0″.2; further, in the compilation of the other star catalogs into this fundamental system, substantial systematic differences may have resulted for some regions of the sky. Until more observational data become available from new catalogs, there is no means of determining the magnitudes of these errors; and as these discrepancies will be systematic over large parts of the sky, they cannot be detected from the film reduction. The best safeguard against systematic errors is to observe the satellite in as many regions of the sky as possible. This means that more observations are required for a specific problem than would be indicated by a simple theory based on random errors.

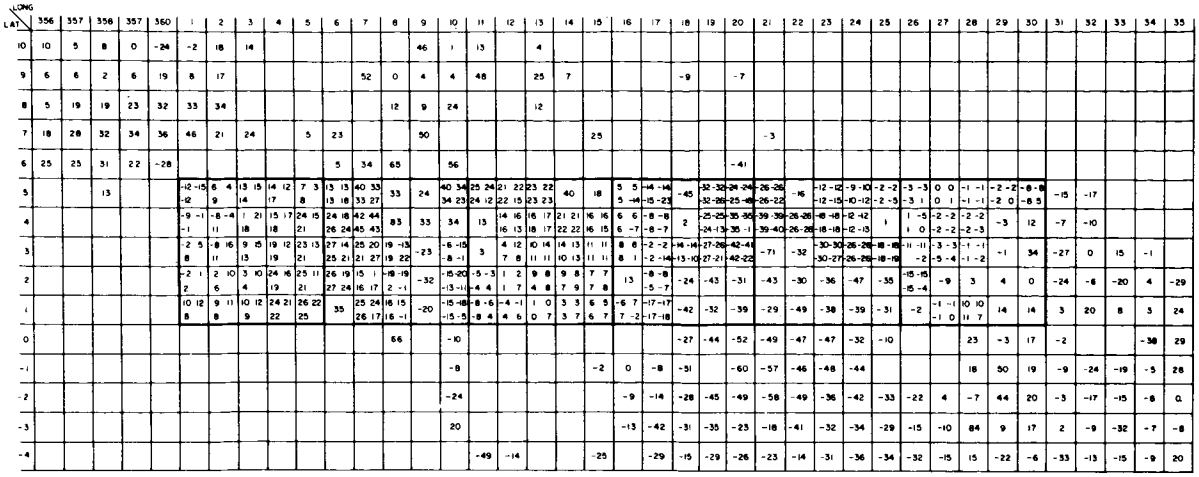

FIGURE 9.10.—Comparison of the four estimate procedures. $1° \times 1°$ squares with single numbers represent the measured mean free-air gravity anomalies. $1° \times 1°$ squares with four numbers represent estimates as follows: upper left, the split covariance estimator with a 0-km ocean-continent boundary; lower left, the global covariance estimate; upper right, the split covariance estimator with a 1-km ocean-continent boundary; lower right, the Kaula estimator.

9.3.3.1.2 PRECISE REDUCTIONS

Methods and Rationale.—The reduction procedure of SAO's Baker-Nunn observations has been discussed by Haefner (1967) and Haefner and Martin (1966); the latter presents, with some minor modifications, the standard reduction procedures now in use at SAO. Our reduction procedure is based on astrometric principles, which differ significantly from the photogrammetric methods widely used in conjunction with ballistic cameras.

Because of the differences in the data-acquisition and reduction techniques, a direct comparison of the astrometric and photogrammetric methods is not valid. A brief generalization, however, can be made: Astrometric methods are most suitable where narrow fields ($<5°$) are used; the photogrammetric methods are most applicable to wide fields (20° to 30°); and in the intervening range, a compromise between the two methods will often provide the most practical solution. The reduction procedure to be employed is the one that is most economical yet commensurate with the physical characteristics of the camera and with the external phenomena affecting the observations. This economic requirement is particularly important because a total of over 200 000 Baker-Nunn observations have been reduced during the program.

The chief advantage of the astrometric (Turner's) method is that a variety of phenomena affecting the relative positions of the satellite and the star images need not be corrected for explicitly. The method describes an affine transformation between the standard coordinates and the plate coordinates. It assumes that (1) the two coordinate planes are parallel and (2) a small field is used. This first requirement is adequately satisfied by the design of the camera, the principal ray at any point being normal to the backup plate. The second requirement is met by using only those reference stars that lie within 2° to 2°.5 of the satellite image. The reductions are valid for any small area away from the physical film center, although residual distortions at the outer parts of the field mean that the satellite image should lie within about 10° of the center.

Transformations.—The relationship between the stellar coordinates and the standard coordinates is expressed by the azimuthal equidistant projection. Let D_0 and A_0, respectively, denote the declination and right ascension of the adopted film center, and δ and α, the declination and right ascension of the satellite position. Then

$$\begin{pmatrix} v_1 \\ v_2 \\ v_3 \end{pmatrix} = \begin{pmatrix} 1 & 0 & 0 \\ 0 & \sin D_0 & \cos D_0 \\ 0 & -\cos D_0 & \sin D_0 \end{pmatrix} \begin{pmatrix} -\sin A_0 & \cos A_0 & 0 \\ -\cos A_0 & -\sin A_0 & 0 \\ 0 & 0 & 1 \end{pmatrix} \begin{pmatrix} \cos\alpha\cos\delta \\ \sin\alpha\cos\delta \\ \sin\delta \end{pmatrix}$$

and the standard coordinates (ζ, η) of a reference point become

$$\zeta = \frac{v_1}{v_2} \cdot \frac{\theta}{D} \cdot f$$

$$\eta = \frac{v_2}{v_3} \cdot \frac{\theta}{D} \cdot f$$

where f is the camera focal length and θ is the angle between the plate center and the star; that is,

$$\theta = \tan^{-1}\left(\frac{\sqrt{v_1^2 + v_2^2}}{v_3}\right)$$

$$\mathrm{D} = \tan\theta$$

Such a projection is valid for any region of the film. The adopted choice for the film "center" is the geometric center of the selected images of reference stars. With well-distributed reference points, the separation between this center and the satellite image is less than 0°.5. The projection preserves the azimuth and scale in the radial direction from the adopted film center, but distortions in other directions will occur. These distortions, however, are small, and the average distortion over the small field used is less than 0.5 μ.

Corrections.—In the process of precise reductions, a number of corrections must be applied to the data.

(1) Shutter corrections: During the exposure of the Baker-Nunn film, the satellite image and the star images trail along the film. These trails are periodically broken into six segments by the two diametrically opposite staves of a rotating barrel shutter. The third break corresponds to the satellite position to be measured, and its time is not directly recorded; the other breaks are not currently used. At some instant during the stave passage, its position and time are recorded on the film. The time of the image and the time of the stave passage are related by the shutter-sweep correction. Thus, if β is the angle of rotation of the shutter about its axis between the two events, the sweep correction Δt is given in the first instance by

$$\Delta t = \frac{\beta}{\omega}$$

ω being the angular velocity of the shutter.

The situation is somewhat complicated because the time is not necessarily displayed when the stave passes over the film center. However, if the stave displacement $\Delta\beta$ is not excessive, the camera has a device for measuring $\Delta\beta$, and the total sweep correction becomes

$$\Delta t = \frac{\beta - \Delta\beta}{\omega}$$

Zadunaisky (1960) gives the equations necessary to compute the angles β and $\Delta\beta$. These formulations are based on a number of simplifying assumptions whose effects on the accuracy of the time determination can be investigated.

(2) Aberration corrections: The film reduction is carried out for the epoch of 1950.0, and the only aberration correction applied at this stage is for annual aberration. Owing to the small field, the correction is applied to the satellite position, rather than to each star position individually. The formulas used are the closed expressions:

$$\Delta\alpha = -\frac{20''.47 \sin\alpha \sin\odot + 18''.87 \cos\alpha \cos\odot}{\cos\delta}$$

$$\Delta\delta = -[20''.47 \sin\delta \cos\alpha \sin\odot + 18''.87 (0.433\,666\,1 \cos\delta - \sin\delta \sin\alpha) \cos\odot]$$

where $\odot$ is the geocentric longitude of the sun. Though not rigorous, these expressions will always be correct to better than 0".1 (Scott, 1964).

(3) Atmospheric-refraction corrections: In the film-reduction process, atmospheric-refraction corrections are not applied to individual star positions, since it is assumed that the atmospheric-refraction correction varies linearly over the 4° to 5° field used in the reduction. This condition is nearly always satisfied since observations are seldom made at zenith distances of greater than 70°. At this zenith distance, the average departure of the differential refraction from linearity is about 1", and with eight well-distributed stars, the uncertainty in the satellite position (all other factors being ignored) will be at most 0".4.

A parallactic-refraction correction is applied to the satellite position during analysis. The value for the refractivity constant in this correction is based not on the atmospheric conditions at the time of observation, but rather on the average year-round, nighttime conditions for the station from which the observations are made. For the present Baker-Nunn camera locations, the error in the refraction correction is less than 20 percent of the value of the correction itself. As this correction is always small, the error is minimal.

Of greater importance than uncertainties in the parallactic-refraction correction is the random-image displacement caused by microturbulence in the atmosphere. When the Baker-Nunn camera is used in the stationary mode, this image motion will exist in both the along-track and the across-track directions, with the greater deviations occurring in the former because of the different time-integration effects. The satellite position will not be seriously affected when the camera is used in the tracking mode, but each star image may be displaced. The average one-dimensional deviation from the mean, σ_ψ, can be approximately formulated (Lambeck, 1968) as follows:

$$\sigma_\psi = \left\{(0.03)^2 + \left[\frac{4.5\ \sec^{1/2}\zeta}{\sqrt{D}}(1 - 0.35 \log \Delta t)\right]^2\right\}^{1/2}$$

$$\Delta t < 1000 \text{ msec}$$

where D is the aperture in centimeters and Δt, the exposure time in milliseconds.

(4) GEOS flash corrections: The star and satellite images of Baker-Nunn films of passive objects refer to the same instant of time. This is not the case for observations of flashing satellites, so a correction must be applied to the observed position to ensure that both the star images and the satellite image refer to the same time instant. For operational reasons, the star-trail exposure is offset by $\approx$0.1 sec from the flash time. The correction is computed by precessing the satellite position to the date of observation, adding the correction

$\Delta\alpha = 1.0027 \times$ (time difference between satellite and star exposure)

and precessing the corrected position back to the epoch of 1950.0. Because of the small time interval between the star exposures and the flash observation, nutation need not be considered.

9.3.3.1.3 SYNTHETIC OBSERVATIONS

The arcs formed by several successive observations can be used to create synthetic observations at some intermediate time by interpolation. Simultaneous observations used in the geometrical satellite solution rely almost entirely on such synthetic observations, and they are also used in the dynamical solution whenever four or more successive frames are available.

Since it is virtually impossible to observe a passive satellite at exactly the same

instant from two or more distant stations, the only practical way of obtaining simultaneous observations is to observe the satellite from the participating stations for approximately the same time interval and to interpolate for a fictitious simultaneous instant. In orbital analysis, use of synthetic observations reduces the amount of data to be handled without any significant loss of accuracy and resolution. But probably the most cogent reason for using synthetic observations is that a better accuracy or reliability estimate can be associated with the synthetic observation than with a single observation. Only average values can be assigned to the errors in a single observation. Some of these errors vary more or less randomly from exposure to exposure and will be reflected in the residuals resulting from a least-squares interpolation procedure for a synthetic observation.

A second-degree polynomial is adequate for the majority of observations. Since a seven-frame arc generally subtends less than 10° of arc, the object's orbit can be adequately approximated by quadratic functions. When there are more than seven or eight frames in a sequence, a third-degree polynomial may be required, but proper constraints must be placed on the coefficients to ensure that the curve approximates the orbit and does not reflect characteristics of the image-forming process for the points in the sequence. If higher degree polynomials are used without such constraints, the accuracy estimates of the interpolated positions become optimistic, although the mean position of the satellite is not seriously affected.

The interpolation procedure is based on several assumptions: (1) that the errors in successive positions in the arc are uncorrelated, (2) that the along- and across-track errors for each position are uncorrelated, (3) that the along-track uncertainties are equal for all frames, and (4) that the across-track uncertainties are equal for all frames. Since systematic errors in timing would destroy the first assumption, timing uncertainties are not included in the uncertainty of each position. Other correlations between successive Baker-Nunn images are much smaller than with ballistic cameras, where images lie on a single frame. For the Baker-Nunn, plate constants are derived independently for each frame, so that the influence of such factors as measuring uncertainties, nonlinear lens and film distortions, and short-period atmospheric effects (on each satellite position) will be random from frame to frame. Since the same reference stars may be used in two or even three successive frames, errors in stellar coordinates could introduce some correlated errors between successive frames.

Synthetic simultaneous directions are corrected for parallactic refraction, diurnal aberration, and light travel time between the station and the satellite (see Haefner and Martin (1966) for the corrections used) and refer to the terrestrial system defined by the mean pole of 1900 to 1905 and by the meridian plane at 75°03′55″.94 east of the mean meridian of the USNO. The time of the observations is expressed in Smithsonian Atomic Time as defined in table 9.22. The directions are given as direction cosines, and their standard deviations are given in the along- and across-track components. Timing uncertainties have been introduced in the former. The angle the satellite trail makes with the right-ascension axis is also computed so that the accuracy of the direction in the right-ascension and declination components can be determined.

9.3.3.1.4 ACCURACY AND ERROR BUDGET FOR DATA FROM BAKER-NUNN CAMERA

A summary of the principal error sources in the determination of star positions and an estimate of the total influence are given below (Lambeck, 1968) :

Measuring errors	1″.2 (6 measurements)
Calibration of comparator	0″.2
Film and emulsion distortion	0″.8

Atmospheric refraction	1″.1 (image motion for tracking camera)
	0″.8 (differential refraction)
	0″.3 (wandering)
Approximations in reduction method	0″.2
Star positions from SAO catalog	0″.5 (random)
	0″.2 (systematic)
Total standard deviation of each star position	1″.8 (stationary mode)
	2″.1 (tracking mode)

The principal error sources in the determination of satellite position and an estimate of the total influence are summarized below (Lambeck, 1968) :

Measuring errors	0″.8 (12 measurements)
Calibration of comparator	0″.2
Film and emulsion distortion	0″.8
Atmospheric refraction	1″.1 (image motion along track, or flash images)
	0″.5 (image motion across track)
	0″.3 (wandering)
	0″.1 (parallactic refraction)
Contribution of standard deviation of 8 stars	0″.8 (stationary)
	0″.9 (tracking)
Total standard deviation of satellite position	1″.8 (stationary, along track)
	1″.5 (stationary, across track)
	1″.6 (tracking)

Before 1965, time was maintained at the stations by the Norrman clock and by the monitoring of WWV broadcasts at HF and VHF. The root-mean-square (rms) accuracy of an observation epoch was about 1 msec, with excursions of several milliseconds in some cases.

Installation of the EECo clock system in 1964 and use of frequency broadcasts on VLF and of portable clocks improved the timing situation. All the stations had ± 100-μsec clock accuracies by 1967.

A summary of the overall accuracy of a single Baker-Nunn observation for different topocentric velocities of a satellite is given in table 9.23.

Before the installation of the EECo clocks, the average accuracy of the synthetic observations was about 1″.1 in each component. Now, with the improved timekeeping procedures, the average accuracy of the synthetic observation is about 0″.9 along track and 0″.7 across track.

9.3.3.2 Data From a Laser System

9.3.3.2.1 CALIBRATION

The laser systems are calibrated by ranging on a fixed land-based target situated at a known distance from the laser. The system delay or system-calibration constant is the difference between the raw target range time measured by the system, τ_m, and the range time to the target, τ_s, computed from the surveyed distance between the laser and the target and corrected for local atmospheric refraction. The targets, which are 8 ft $\times$ 8 ft wooden surfaces painted flat white, are 0.5 to 2.0 km distant from the laser system. The exact placement is usually dictated by local terrain.

The routine calibration of the system is performed nightly and consists of 20 measurements on the target. For these measurements, the return-pulse intensity is controlled by use of neutral-density filters to produce signal levels similar to satellite echoes.

Computation of a calibration correction factor τ_c, which must be added (algebraically) to all satellite range-time observations, is obtained from

$$\tau_c = \tau_s - \tau_m$$

where τ_m is the average of the 20 range-time measurements. The computed range time to the target is given by

$$\tau_s = \frac{d_s}{0.15}\left[1 + (N \times 10^{-6}) \div (6.917 \times 10^{-1})\right]$$

where d_s is the surveyed distance to the target and N is the local atmospheric refractivity

$$N = 80.29\frac{P}{T} - 11.9\frac{e}{T}$$

in which P is the measured barometric pressure in millibars, e is the partial pressure of water vapor, and T is the temperature in degrees Kelvin.

The effect of local variations in barometric pressure on the value of τ_s for distances of less than 1 km was found to be small enough so that a constant value of the atmospheric refractivity could be defined for each station. This value was taken from a chart prepared to give a direct conversion from station altitude in kilometers to values of N (Gaposchkin, 1972, unpublished).

During individual nightly (or daily) calibration sequences, the range scatter from one measurement to the next is seldom more than a few nanoseconds. The variation in the target-range averages is rarely more than a few tenths of a nanosecond from calibration to calibration, giving a stability of better than 10 cm. The target surveys at the stations currently have an estimated accuracy of about 10 cm.

9.3.3.2.2 ATMOSPHERIC CORRECTIONS

Ranges determined by using the vacuum velocity of light must be corrected for the fact that the laser pulse travels at a lower velocity in the earth's atmosphere. We used the following correction during this program (G. Thayer, 1967, private communication):

$$r_m = r_v - \frac{2.238 + 0.0414\,PT^{-1} - 0.238\,h_s}{\sin\alpha + 10^{-3}\cot\alpha}$$

where r_v is the uncorected range in meters, r_m is the corrected range in meters, P is the atmospheric pressure at the laser station, T is the temperature at the laser station, h_s is the laser's height above mean sea level in kilometers, and α is the elevation angle of the satellite. The formula holds for a ruby laser, which operates at 694 nm.

The formula was derived from a regression analysis based on a large sample of radiosonde balloon flights from a number of locations that were chosen to give a reasonable sampling of anticipated atmospheric conditions. The error in range correction is estimated to be about 2 to 3 cm at zenith.

9.3.3.2.3 TRANSFER FUNCTIONS OF A SATELLITE-RETROREFLECTOR ARRAY

Range erors now present in routine tracking by laser systems are actually smaller than the satellite dimensions. Since we must relate all observations to the satellite center of mass (both for dynamic and for purely geometric analyses), it is necessary to derive some means for reducing each range observation to the distance from the ground-based laser to the satellite center of mass, which, in all cases, is displaced from the reflecting elements. For this purpose, we have developed and applied in our geodetic analyses a set of retroreflector-array transfer functions for each of the United States satellites with cube corners now in orbit. These transfer functions are computed from the geometric and optical parameters of each retroreflector array and take into account the satellite geometry and position. The functions for 6508901 (GEOS–1), GEOS–2, 6406401 (BE–B), 6503201 (BE–C), 6701101 (D1C), 6701401 (D1D), and 7010901 (PEOLE) were computed.

The computer model includes both incoherent and coherent return signals for arrays of retroreflectors whose faces are cut in the form of a circle, triangle, or even-sided polygon (such as a hexagon). Diffraction, including changes in amplitude and polariza-

tion of the reflected laser beam, and influences of dihedral-angle errors can also be accounted for. The model accommodates obscuration of retroreflectors by satellite and subsystem structure, a particular problem with the two GEOS spacecraft and with PEOLE. When the position of each reflector is being computed, the model accounts for the dielectric properties of the retroreflectors in terms of ray bending and propagation velocity. Once the return signal has been constructed, the relationship of the centroid of the signal to the satellite center of mass is determined and then applied as a range correction to the laser data used in the geodetic analyses.

The major limitation on the accuracy with which transfer functions can be determined for the existing satellites with retroreflectors is the lack of precise information on the beam patterns of the retroreflectors in relation to the large size of the arrays. With the existing uncertainties in retroreflector optical characteristics, geometric placement, and satellite attitude, we estimate that the range corrections for these satellites have an accuracy of about 10 cm. It should be noted that this error is quite systematic.

9.3.3.3 Network Time Base

9.3.3.3.1 STATION-CLOCK SYNCHRONIZATION

Synchronization of the station clocks throughout the network is achieved by relating all the time and frequency references to UTC as maintained by USNO. The field stations steer their clock frequencies with VLF transmissions from stations NAA and NLK, and in some cases, WWVL or WWVB. Crude epoch checks are made at many of the stations by monitoring HF/VHF time signals. The USNO and the National Bureau of Standards (NBS) timing bulletins, which give the relative phase values of VLF stations and time intercomparisons with other timing services, are used to relate all field timing values to UTC(USNO).

Use of a portable clock is the principal method of synchronizing with a source of reliable timing. The comparison of the portable clock with the clock at the station gives a correction relating the station time to the source time, and published comparison values relate the source time to UTC (USNO). Therefore, each field-station clock is referred to a common time scale with an accuracy dependent on the reliability of the portable-clock comparison and on the accuracy of the published comparison value.

The trips to the field stations have been conducted with a Sulzer A5 portable crystal clock that carries time related to UTC (USNO). These trips have been run by SAO or, in some instances, by other agencies (such as NASA, USNO, Naval Research Laboratory, and NBS) who have either carried an SAO clock or been in the vicinity of an SAO field station with a clock of their own. Portable-clock comparisons are made with each station on a biennial basis. However, to maintain higher levels of accuracy and reliability, a portable-clock comparison is made at least once a year at the laser stations. Time corrections, determined to be necessary by portable-clock comparisons or intercomparison between station-clock and VLF-monitor readings, are documented and applied directly to the station clocks. Corrections for the difference between the VLF stations and USNO are applied in Cambridge during data preprocessing.

9.3.3.3.2 ACCURACY AND ERROR BUDGET

The accuracy of station timing depends on (1) the success of the portable-clock trips, (2) the ability to trace the relationship of the time references back to USNO, (3) the ability of the station to maintain the time setting with the aid of the VLF tracking receiver, and (4) the uncontrollable variations in propagation path of the VLF signal. The requirements for system timing originally called for the station clocks to be within ± 1 msec of WWV (rms of net devia-

tion from UTC(NBS) over a month). This requirement was tightened to ±100 μsec UTC (USNO) for the camera stations and ±50 μsec for the laser stations. This improvement was made possible by the installation of the EECo timing systems in the mid-1960's and was realized by 1967. In practice, many of the camera stations have been operating within ±50 μsec of UTC(USNO).

The synchronization accuracy by use of a portable clock depends on the amount of unpredictable time drift experienced during the period spent traveling to and from the field station. Most of the trips to the field stations use a crystal clock and provide a time set accurately to within 5 to 25 μsec of USNO. The least reliable results have been in India and South America, where the stations are fairly remote and long travel times are involved.

USNO publishes a weekly bulletin, "Daily Phase Values, Series 4," giving the emitted phase values of the major VLF transmitting stations to 1 μsec. The time differences between UTC as maintained by USNO, NBS, and the Bureau International de l'Heure (BIH) are well documented by each agency to microsecond accuracy. The relationships between the HF time broadcasts of foreign countries and UTC(USNO) are generally less precisely known.

Timing accuracy at the field station is maintained by controlling the clock drift with the aid of VLF monitoring equipment. In cases of minor clock failures, time has often been recovered with fair accuracy by referring to backup clocks and to VLF and HF monitor references. The clock-time drift is a product of oscillator frequency offset and is generally controlled to keep the station epoch within 50 μsec of the VLF reference position.

The accuracy of VLF-derived time is a function of receiver and propagation-path stability. The uncertainties of the day-to-day and seasonal path variations added to the error contribution of the receiver amount to less than 5 μsec in epoch uncertainty. The system timing accuracy is a composite figure encompassing setting accuracy, uncorrected drift of the clock, and inaccuracy of the VLF monitor.

The degree of accuracy in setting a portable clock gives the initial accuracy of the station epoch, and VLF monitoring permits the clock to maintain time. When subsequent incidents of minor clock failure that affect time and frequency increase the epoch uncertainty to ±50 μsec, another portable-clock comparison is considered. When requirements are stringent, additional efforts are made to obtain more accurate time comparisons, to reduce the oscillator drift, and to minimize the acccrual of uncertainty due to repeated clock resets. This extra effort is the key to maintaining station epochs at the ±50–μsec level with a minimum of clock trips.

9.4 THEORY

The following three sections provide the theory used for determining (1) coordinates of ground tracking systems and (2) the gravitational potential of the Earth. The coordinates were determined both by a purely geometric method (sec. 9.4.2.1) and by the dynamic method (sec. 9.4.2.2), which uses the equations of motion of satellites, together with the geometric. The gravitational potential can be determined with the help of the equations of motion alone, the gravimetric theory alone, or the two together. The zonal harmonics of the gravitational potential of Standard Earth III were determined by using the equations of motion alone (sec. 9.4.3.2); the tesseral harmonics were determined by using both the equations of motion and the gravimetric theory (sec. 9.4.3.3). Because the equations of motion have been used for determining both coordinates and the potential, their theory is discussed first.

9.4.1 Orbital Theory

(E. M. Gaposchkin)

The theory used to connect the position of a satellite to the time of observation at a single station is the dynamics of a particle

in an approximately central field of force. The theory is presented in this section. It is used to find both the coordinates of the tracking station and the constants that determine the field of force. The coordinates, the constants, or both may be determined at the same time as the six constants of integration that, together with the time, determine the orbit.

The symbolism used in this chapter differs from that used throughout the rest of this volume. The major deviations are as follows:

J_n	for	$-C_n$
$\bar{P}_{lm}, \bar{C}_{lm}, \bar{S}_{lm}$	for	P_n^m, C_n^m, S_n^m
I	for	i
μ	for	GM
ϕ	for	ψ

9.4.1.1 Transformation and Coordinate Systems

Consider the coordinate system x_1, y_1, z_1, a point

$$[P]=\begin{bmatrix} p_x \\ p_y \\ p_z \end{bmatrix}$$

and a second coordinate system rotated about the z axis by an angle Ω. The coordinates of p in the x_2, y_2, z_2 system can be expressed with the matrix operation

$$[P_2]=R_3(\Omega)\,[P_1]$$

where

$$R_3=\begin{bmatrix} \cos\Omega & \sin\Omega & 0 \\ -\sin\Omega & \cos\Omega & 0 \\ 0 & 0 & 1 \end{bmatrix} \qquad (9.2)$$

In an analogous way, we can define rotation around any axis with

$$R_1=\begin{bmatrix} 1 & 0 & 0 \\ 0 & \cos I & -\sin I \\ 0 & \sin I & \cos I \end{bmatrix} \qquad (9.3)$$

about the x axis and

$$R_2=\begin{bmatrix} \cos\phi & 0 & -\sin\phi \\ 0 & 1 & 0 \\ \sin\phi & 0 & \cos\phi \end{bmatrix} \qquad (9.4)$$

about the y axis. Here, R_1, R_2, and R_3 are matrices, and their mathematical properties are the subject of linear algebra. We need know only that these quantities have the following properties:

(1) The length of a vector is unchanged by rotation.

(2) Multiplication of matrices does not commute; that is,

$$R_i(\phi)\,R_j(\lambda)\neq R_j(\lambda)\,R_i(\phi)$$

(3) Multiplication does satisfy the associative rule; that is,

$$R_i(R_jR_k)=(R_iR_j)\,R_k$$

(4) Rotation about the same axis is additive; that is,

$$R_i(\phi)\,R_i(\lambda)=R_i(\phi+\lambda)$$

(5) For rotation matrices, the inverse and transpose are related by

$$R_i^{-1}(\phi)=R_i^T(\phi)=R_i(-\phi)$$

(6) We also have

$$(R_iR_j)^{-1}=R_j^{-1}R_i^{-1}$$

(7) Differentiation and integration are performed on each element.

Although multiplication does not commute, for small rotations around the x, y, and z axes—that is, ϵ_x, ϵ_y, ϵ_z—we can define the infinitesimal rotation matrix

$$R(\epsilon_x, \epsilon_y, \epsilon_z)=\begin{bmatrix} 1 & \epsilon_z & -\epsilon_y \\ -\epsilon_z & 1 & \epsilon_x \\ \epsilon_y & -\epsilon_x & 1 \end{bmatrix} \qquad (9.5)$$

which does commute.

In satellite geodesy, dynamical astronomy, and astrometry, we are concerned with four reference frames: (1) the terrestrial system,

(2) the inertial system, (3) the celestial (sidereal) system, and (4) the orbital system. Since a systematic account of these systems and their relationships to one another can be found in Veis (1960, 1963) and elsewhere, we confine ourselves to a descriptive summary.

The terrestrial system is fixed to the Earth. Positions on the surface can be considered invariant in time if we ignore tides and crustal motions for the moment. The representation of the terrestrial system can be in terms of geocentric coordinates or datum coordinates. The datum can be defined in a geocentric system with the following seven parameters: the three datum origin coordinates, the three orientation parameters, and a scale factor. Datum coordinates can be determined from precise knowledge of the geocentric coordinates. One of the objectives of satellite geodesy is to determine coordinates in a geocentric system. Through coordinates common to geocentric and datum systems, the relation of the datum to the geocentric system is determined.

The inertial system is fundamental to dynamics, and all orbit theory is ultimately developed in this system. We hope to materialize the inertial through the celestial system. The latter is defined by the stars and, it is hoped, with respect to the distant galaxies. The distant galaxies define an inertial reference frame.

The celestial system is represented by coordinates of stars insofar as we can treat proper motion accurately. Individual star catalogs are similar to compilations of geodetic coordinates in that the positions are relative. Positions can be combined into a uniform system by use of stars common to any two catalogs. This technique was used to compile the SAO Star Catalog (Staff, Smithsonian Astrophysical Observatory, 1966), which is in computer-accessible form, covers the whole sky, and contains about 250 000 stars with their positions and proper motions reduced to the FK4 system.

The equations of motion are most easily given in an inertial reference frame. However, in this system, the Earth is moving in an irregular manner, and the gravitational field, assumed static in an Earth-fixed system, has an irregular time dependence. This irregular temporal variation will give rise to perturbations.

For this reason, we have adopted an intermediate, quasi-inertial reference frame. This orbital system has a fixed equinox (the mean equinox of 1950.0) and a moving equator (the instantaneous equator of date), and the gravitational field is rotating about the z axis at a constant rate. This orbital system has been shown by Kozai (1960) and Kozai and Kinoshita (1973) to be optimum for our work. That is to say, short-period terms are unaffected by the change, and the effects of being noninertial and those of variations of the gravity field are minimized. We can then proceed with the theory for periodic perturbations as if we had an inertial reference frame and make some corrections (section 9.4.1.7). A further result of this choice is that the Earth is rotating uniformly in this system, thus giving a particularly simple expression for the sidereal angle.

The relation between the celestial system and the terrestrial is established in two steps. A general theory of precession and nutation deals with the secular and periodic parts, respectively, of the forced motion due to the gravitational attraction of the Sun and Moon. A general reference for these effects is chapter 2 of the *Explanatory Supplement to the Astronomical Ephemeris and the American Ephemeris and Nautical Almanac* (hereafter called ESAENA). The instantaneous orientation of the Earth is described to 2×10^{-6} rad with these formulas. The irregular fluctuations of the Earth's orientation with respect to this computed orientation are routinely measured as three angles and published by the Bureau International de l'Heure. The free nutation of the Earth is the motion of the adopted reference point of the z axis about the spin axis in the terrestrial system. The spin axis, of course, moves owing to precession and nutation, and that axis defines the astronomical equator. The rotation rate has small fluctuations, resulting in irregular fluctuations in the true

sidereal angle. The coordinates of the reference pole (x,y) and the change in the sidereal angle (ΔUT1) are observed quantities and provide the relationship between the celestial and the terrestrial systems.

The variations of pole position are not strictly periodic. There is considerable uncertainty about the actual properties of the polar motion. As a result, an arbitrary reference point was adopted by the International Union of Geodesy in 1967. This point was the mean pole for the time 1900.0 to 1905.0, and all pole coordinates are now given with respect to it. The mean pole today is about 10 m west of the adopted pole.

In summary, we now give the relations between the orbital system and the others. If X_0 is the position of a station in an Earth-fixed system, then X is the position in the orbital system:

$$X = R_3(-\theta) R(y, x, 0) X_0 \qquad (9.6)$$

where θ is the sidereal angle computed from

$$\theta = 0.277\,987\,616 + 1.002\,737\,811\,91 \\ (T - 33\,282.0) + \Delta\text{UT1}\,(\text{rev}) \qquad (9.7)$$

and x and y are the observed coordinates of the pole.

In general, camera observations provide directions in a celestial system at some epoch T_0. To express this direction in the adopted orbital system, we must apply precession κ, ω, ν from T_0 to 1950.0, and then apply κ, ω, ν to the motion of the equator, thus preserving the origin of 1950.0. If $\kappa(b,a)$ is the amount of precession in right ascension from dates a to b, and if similar expressions are given for ω and ν, then

$$[\hat{l}] = R(-\Delta\epsilon, \psi \sin \epsilon, 0) R_3[\kappa(T, 1950)] \\ R_2[\nu(T, 1950)] R_3[-\kappa(T, 1950)] \\ R_3[-\omega(1950, T_0)] R_2[-\nu(1950, T_0)] \\ R_3[-\kappa(1950, T_0)] [\hat{l}_0] \qquad (9.8)$$

expresses the direction in the orbital system. The nutation $(\Delta\epsilon, \psi \sin \epsilon)$ must also be applied to the original direction if the true coordinates are given. The reader is referred to the ESAENA for numerical values. It has been found satisfactory to use the quadratic expressions for precession and to retain all terms in nutation such that the total neglected part is less than 0.5 m.

9.4.1.2 Two-Body Motion

The first approximation for satellite motion is two-body motion, which forms the reference for all subsequent analysis. Two-body motion can be completely solved in closed form by simple methods. (See, e.g., Brouwer and Clemence, 1961.)

If the origin of coordinates is taken at the center of mass of the system, then the paths of both bodies lie in a common plane through that point and the path of each body is an ellipse with one focus at that point. When the mass of one body is immensely greater than that of the other, only the mass M of the larger body need be considered. The equation for the motion of a point with unit mass moving in the gravitational field of such a large body is

$$r = \frac{a(1 \quad e^2)}{1 + e \cos v} = a(1 - e \cos E) \qquad (9.9)$$

with

$$r \sin v = a(1-e^2)^{1/2} \sin E \\ r \cos v = a(\cos E - e)$$

The angles are defined in figure 9.11. By comparing the constants, we find that

$$e = \left(1 + 2\mathcal{H}\frac{N^2}{\mu^2}\right)^{1/2} \\ a = -\frac{\mu}{2\mathcal{H}} = \frac{N^2}{\mu(1-e^2)} \qquad (9.10)$$

where $\mathcal{H}$ is the Hamiltonian of the system, N is a constant of integration, and $\mu \equiv GM$. From these equations, it is easy to derive the relation between mean motion n and semi-major axes a:

$$n^2 a^3 = \mu \qquad (9.11)$$

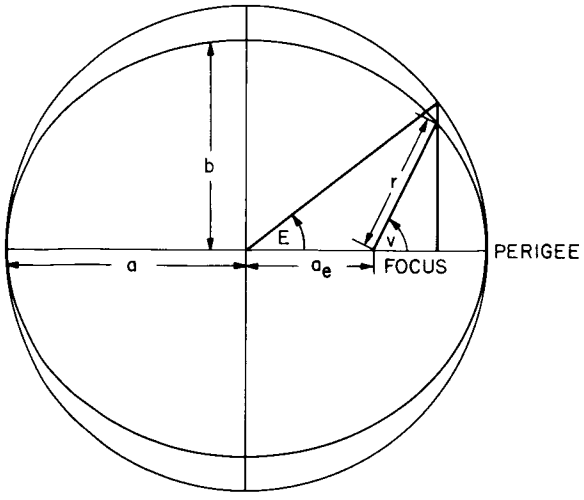

FIGURE 9.11.—Geometry of ellipse.

which is equivalent to Kepler's third law.

We proceed to find $v(t)$ by differentiating (9.9):

$$\frac{dr}{dt}=ae\sin E\frac{dE}{dt}=\frac{a(1-e^2)e\sin v}{1+e\cos v}\frac{dv}{dt} \tag{9.12}$$

This equation reduces to

$$\frac{dE}{dt}=\left(\frac{\mu}{a}\right)^{1/2}\frac{1}{r}=\frac{\mu^{1/2}}{a^{3/2}(1-e\cos E)} \tag{9.13}$$

which integrates to

$$E-e\sin E=n(t-t_0)\equiv M \tag{9.14}$$

which is Kepler's equation.

Given a time, (9.14) must be solved by iteration. Using (9.9), we obtain the true anomaly v and the radius vector r. The position is calculated from

$$\begin{bmatrix}x\\y\\z\end{bmatrix}=r\begin{bmatrix}\cos v\\\sin v\\0\end{bmatrix}=a\begin{bmatrix}\cos E-e\\(1-e^2)^{1/2}\sin E\\0\end{bmatrix} \tag{9.15}$$

The velocity is obtained directly,

$$\begin{bmatrix}\dot{x}\\\dot{y}\\\dot{z}\end{bmatrix}=\frac{na}{(1-e^2)^{1/2}}\begin{bmatrix}-\sin v\\e+\cos v\\0\end{bmatrix}=\frac{na}{1-e\cos E}\begin{bmatrix}-\sin E\\(1-e^2)^{1/2}\cos E\\0\end{bmatrix} \tag{9.16}$$

We have given the analysis of two-body Keplerian motion in a plane. To refer the position $\begin{bmatrix}x\\y\\0\end{bmatrix}$ to the orbital system, we perform the coordinate transformation

$$[X]=R_3(-\Omega)R_1(-I)R_3(-\omega)\begin{bmatrix}x\\y\\0\end{bmatrix} \tag{9.17}$$

The angle ω corresponds to v_0. The angles Ω and I specify the orientation of the orbital plane.

Given the position and velocity, we use the constancy of the angular momentum to determine the angles Ω, I, ω. The direction of the angular momentum is computed from

$$[\hat{L}]=[X]\times[\dot{X}]/|X||\dot{X}| \tag{9.18}$$

and the inclination is obtained from

$$\cos I=\left|[\hat{L}]\times\begin{bmatrix}0\\0\\1\end{bmatrix}\right| \tag{9.19}$$

If $\hat{L}_z$ is negative, the convention is to take $\pi-I$ for the inclination. The node is defined by a unit vector in the direction of the node:

$$\hat{e}_\Omega=\begin{bmatrix}\cos\Omega\\\sin\Omega\\0\end{bmatrix}=\begin{bmatrix}0\\0\\1\end{bmatrix}\times[\hat{L}] \tag{9.20}$$

To find ω, we must determine the satellite position in the orbital plane referred to the node. Using

$$[X']=R_1(I)R_3(\Omega)[X]$$

we have

$$\cos(v+\omega) = X'_x/r$$

$$\sin(v+\omega) = X'_y/r$$

which determine $v+\omega$. With v from (9.9), we immediately have ω.

We give here the equations for a hyperbolic orbit. The position is

$$x = r\cos v = -a(e-\cosh F)$$

$$y = r\sin v = -a(e^2-1)^{1/2}\sinh F$$

$$r = \frac{-a(e^2-1)}{1+e\cos v} = a(e\cosh F - 1)$$

where $a<0$. We still have

$$n^2(-a)^3 = \mu$$

Kepler's equation becomes

$$n(t-t_0) = e\sinh F - F$$

and $r^2v - N$ is still a constant of the motion.

The final question in the discussion of two-body motion concerns the development of (9.9) and its generalization in series. Kepler's equation, (9.14), is transcendental, and closed expressions are not possible. However, rapidly converging series are available. They are needed for the development of perturbations, a topic that will be treated by itself in a later section.

9.4.1.3 Equations of Motion

For conservative forces, rectangular coordinates are canonical, and the Poisson brackets have the values

$$[\dot{x}_i,\dot{x}_j] = 0$$

$$[x_i,x_j] = 0 \qquad (9.21)$$

$$[x_i,\dot{x}_j] = \delta_{ij}$$

The equations of motion can be written in any set of variables $\{\mathcal{E}_i\}$ by using Poisson brackets:

$$d\mathcal{E}_i/dt = -\sum_k [\mathcal{E}_i,\mathcal{E}_k]\,\partial\mathcal{H}/\partial\mathcal{E}_k \qquad (9.22)$$

where $\mathcal{H}$ is the Hamiltonian for the system.

In addition, if $\mathcal{H} = \mathcal{H}_0 + \mathcal{H}_1$ and if we can obtain a solution

$$x_i^0 = x_i^0(\alpha_i,t)$$

$$\dot{x}_i^0 = \dot{x}_i^0(\alpha_i,t)$$

(α_i being constant) for $\mathcal{H}_0$, then by selecting $\mathcal{E}_i$ to be α_i, we can write

$$d\mathcal{E}_i/dt = -\sum_k [\mathcal{E}_i,\mathcal{E}_k]_{x^0,\dot{x}^0}\,\partial\mathcal{H}_1/\partial\mathcal{E}_k \qquad (9.23)$$

where $[\mathcal{E}_i,\mathcal{E}_k]_{x^0,\dot{x}^0}$ are evaluated for the solvable problem. In what follows, we will use only variables that are the solution of the two-body problem (section 9.4.1.2). This choice is not unique, for one could select any combination of $\mathcal{H}$ that had a solution; e.g., there is a separable solution for a potential:

$$\mathcal{U} = -\frac{\mu}{r}\left[1 + \sum_{n=1}^{\infty}\left(\frac{a_e}{r}\right)^n (-J_2)^n P_{2n}(\sin\phi)\right] \qquad (9.24)$$

which is due to Vinti (1959) and has been explored by Izsak (1963b).

The Kepler elements a, e, I, M, ω, Ω are the most commonly used. Using (9.17) in the expression for the Lagrange brackets and employing the time independence of $\{\mathcal{E}_i, \mathcal{E}_j\}_{x^0,\dot{x}^0}$, we obtain for the Lagrange brackets

$$\{\Omega,I\} = -\{I,\Omega\} = -(\mu a)^{1/2}(1-e^2)^{1/2}\sin I$$

$$\{\Omega,a\} = -\{a,\Omega\} = (1-e^2)^{1/2}[\cos(I/2)]\,(\mu/a)^{1/2}$$

$$\{\Omega,e\} = -\{e,\Omega\} = [-(\mu a)^{1/2}\cos I]/(1-e^2)^{1/2}$$

$$\{\omega,a\} = -\{a,\omega\} = [(1-e^2)^{1/2}/2]\,(\mu/a)^{1/2}$$

$$\{\omega,e\} = -\{e,\omega\} = -(\mu a)^{1/2}e/(1-e^2)^{1/2}$$

$$\{a,M\} = -\{M,a\} = -\tfrac{1}{2}(\mu/a)^{1/2} \qquad (9.25)$$

the other combinations being zero. By inverting the matrix implied by (9.25), we obtain for the Poisson brackets

$$
\begin{aligned}
&[a,M] = -[M,a] = 2(a/\mu)^{1/2} \\
&[e,\omega] = -[\omega,e] = -(1-e^2)^{1/2}/(\mu a)^{1/2}e \\
&[I,\Omega] = -[\Omega,I] = -1/[\mu a)^{1/2}(1-e^2)^{1/2}\sin I] \\
&[e,M] = -[M,e] = (1-e^2)/(\mu a)^{1/2}e \\
&[I,\omega] = -[\omega,I] = (\cos I)/(\mu a)^{1/2} \\
&\qquad (1-e^2)^{1/2}\sin I
\end{aligned}
\tag{9.26}
$$

Equations (9.26) inserted into (9.23) can be integrated numerically. They remain a set of coupled differential equations. Analytical solutions are obtained by approximate methods. A particular difficulty arises if these equations are used in a straightforward manner.

It is customary to express the Hamiltonian

$$
\mathcal{H} = \frac{1}{2}V^2 + u = \frac{1}{2}V^2 - \frac{\mu}{r} - R \tag{9.27}
$$

where $R < \mu/a$ and is called the disturbing function. Then R is expressed in a trigonometric series of the form

$$
\sum A(a,e,I) \begin{matrix}\sin \\ \cos\end{matrix} [\alpha M + \beta\omega + \gamma\Omega + \phi(t)]
$$

with $M = M_0 + nt$, where n is the mean motion. Straightforward use of (9.26) introduces

$$
\frac{\partial}{\partial a} A(a,e,I) \begin{matrix}\sin \\ \cos\end{matrix} [\alpha M + \beta\omega + \gamma\Omega + \phi(t)]
$$

giving

$$
\frac{\partial A}{\partial a} \begin{matrix}\sin \\ \cos\end{matrix} [\alpha M + \beta\omega + \gamma\Omega + \phi(t)] + A \begin{matrix}\cos \\ \sin\end{matrix} [\alpha M + \beta\omega + \gamma\Omega + \phi(t)] \alpha \frac{\partial n}{\partial a} t
$$

since n^2a^3 is a constant. The occurrence of t outside a trigonometric argument leads to terms that are not periodic.

If we consider all occurrences of a in coefficients of trigonometric terms and all occurrences of n in the trigonometric argument, then the differential equation for M becomes

$$
M = 2\left(\frac{a}{\mu}\right)^{1/2} \left\{ \left.\frac{\partial \mathcal{H}}{\partial a}\right|_{n=\text{const}} + \frac{\partial \mathcal{H}}{\partial M}\frac{dM}{dn}\frac{dn}{da} \right\} + \frac{1-e^2}{(\mu a)^{1/2}e}\frac{\partial \mathcal{H}}{\partial e}
$$

Now

$$
\frac{da}{dt} = -2\left(\frac{a}{\mu}\right)^{1/2}\frac{\partial \mathcal{H}}{\partial M}
$$

and

$$
\frac{dM}{dn} = t
$$

giving

$$
\begin{aligned}
\frac{\partial \mathcal{H}}{\partial a} &= \frac{\mu}{2a} - \left.\frac{\partial R}{\partial a}\right|_{n=\text{const}} \\
\frac{\partial \mathcal{H}}{\partial e} &= -\frac{\partial R}{\partial e} \\
\frac{\partial \mathcal{H}}{\partial M} &= -\frac{\partial R}{\partial M}
\end{aligned}
$$

that is,

$$
M = n - t\frac{dn}{dt} - 2\left(\frac{a}{\mu}\right)^{1/2}\left.\frac{\partial R}{\partial a}\right|_{n=\text{const}} - \frac{1-e^2}{(\mu a)^{1/2}e}\frac{\partial R}{\partial e}
$$

where $n = (\mu)^{1/2}/a^{3/2}$ and is not constant.

With the previously described separation of a and n, we can write the Lagrange planetary equations (LPE) in their usual form.

$$
\frac{da}{dt} = \frac{2}{na}\frac{\partial R}{\partial M}
$$

$$
\frac{de}{dt} = \frac{1-e^2}{na^2e}\frac{\partial R}{\partial M} - \frac{(1-e^2)^{1/2}}{na^2e}\frac{\partial R}{\partial \omega}
$$

$$
\frac{d\omega}{dt} = -\frac{\cos I}{na^2(1-e^2)^{1/2}\sin I}\frac{\partial R}{\partial I} - \frac{(1-e^2)^{1/2}}{na^2e}\frac{\partial R}{\partial e}
$$

$$\frac{dI}{dt}=\frac{\cos I}{na^2(1-e^2)^{1/2}\sin I}\frac{\partial R}{\partial \omega}-\frac{1}{na^2(1-e^2)^{1/2}\sin I}\frac{\partial R}{\partial \Omega}$$

$$\frac{d\Omega}{dt}=\frac{1}{na^2(1-e^2)^{1/2}\sin I}\frac{\partial R}{\partial I}$$

$$\frac{dM}{dt}=n-\frac{(1-e^2)^{1/2}}{na^2e}\frac{\partial R}{\partial e}-\frac{2}{na}\frac{\partial R}{\partial a}$$

$$n^2a^3=\mu \tag{9.28}$$

Kepler elements are used extensively. They have the advantage over Cartesian coordinates in that five of the elements are constant for two-body motion and the sixth (M) increases linearly with time. In addition, each element has a geometrical interpretation. However, any five constants could be chosen, as long as they lead to a unique calculation of position and velocity.

As $e\to 0$, the element ω ceases to have any geometrical meaning. Since the position of the satellite depends on $v+\omega$, we can consider the new variables

$$\begin{array}{ll}\lambda=M+\tilde{\omega} & e=e\\ \tilde{\omega}=\omega+\Omega & \Omega=\Omega\\ a=a & I=I\end{array} \tag{9.29}$$

with the Poisson brackets

$$[a,\lambda]=-[\lambda,a]=\frac{2}{na}$$

$$[\lambda,e]=-[e,\lambda]=\frac{(1-e^2)^{1/2}[1-(1-e^2)^{1/2}]}{na^2e}$$

$$[\lambda,I]=-[I,\lambda]=\frac{\tan(I/2)}{na^2(1-e^2)^{1/2}}$$

$$[e,\tilde{\omega}]=-[\tilde{\omega},e]=-\frac{(1-e^2)^{1/2}}{na^2e} \tag{9.30}$$

$$[\Omega,I]=-[I,\Omega]=\frac{1}{na^2(1-e^2)^{1/2}\sin I}$$

$$[I,\tilde{\omega}]=-[\tilde{\omega},I]=[I,\lambda]$$

It has also been found useful to eliminate e and $\tilde{\omega}$ by use of the variables

$$\begin{array}{ll}h=e\sin\tilde{\omega} & a=a\\ k=e\cos\tilde{\omega} & \Omega=\Omega\\ \lambda=\lambda & I=I\end{array} \tag{9.31}$$

These variables have the following Poisson brackets, written for convenience in terms of e:

$$[h,k]=-[k,h]=\frac{(1-e^2)^{1/2}}{na^2}$$

$$[h,\lambda]=-[\lambda,h]=\frac{-h(1-e^2)^{1/2}}{na^2[1+(1-e^2)^{1/2}]}$$

$$[h,I]=-[I,h]=\frac{k\tan(I/2)}{na^2(1-e^2)^{1/2}} \tag{9.32}$$

$$[k,\lambda]=-[\lambda,k]=\frac{-k(1-e^2)^{1/2}}{na^2[1+(1-e^2)^{1/2}]}$$

$$[k,I]=-[I,k]=\frac{-h\tan(I/2)}{na^2(1-e^2)^{1/2}}$$

with $[a,\lambda]$, $[\lambda,I]$, $[\Omega,I]$ as given in (9.30). Of course, these equations hold for all eccentricities.

A further modification would be to use the variables

$$\begin{array}{ll}p=\tan I\sin\Omega & k=k\\ q=\tan I\cos\Omega & \lambda=\lambda\\ h=h & a=a\end{array} \tag{9.33}$$

These have the following Poisson brackets, written for convenience in terms of e and I:

$$[p,q]=-[q,p]=\frac{\cos I}{na^2(1-e^2)^{1/2}}$$

$$\begin{aligned}[p,\lambda]=-[\lambda,p]&=\frac{1}{k}[p,h]=-\frac{1}{k}[h,p]\\ &=-\frac{1}{h}[p,k]=\frac{1}{h}[k,p]\\ &=-\frac{p\cos I}{2na^2(1-e^2)^{1/2}\cos^2(I/2)}\end{aligned} \tag{9.34}$$

$$\begin{aligned}[q,\lambda]=-[\lambda,q]&=\frac{1}{k}[q,h]=-\frac{1}{k}[h,q]\\ &=-\frac{1}{h}[q,k]=\frac{1}{h}[k,q]\\ &=-\frac{q\cos I}{2na^2(1-e^2)^{1/2}\cos^2(I/2)}\end{aligned}$$

$$[q, p] = -\frac{\cos I}{na^2(1-e^2)^{1/2}}$$

where $[h, k]$, $[h, \lambda]$, $[k, \lambda]$ are the same as (9.32) and where we take $[a, \lambda]$ from (9.30). The variables p and q should not be confused with generalized coordinates. These expressions are valid for all e and I but are especially valuable for small e and I—for example, in the planetary theory.

It is possible to construct other combinations. For example, one could use

$$\begin{array}{ll} \chi = M + \omega & a = a \\ \xi = e \sin \omega & \Omega = \Omega \\ \eta = e \cos \omega & I = I \end{array} \tag{9.35}$$

We now turn to sets of canonical variables that have the simplest form of Poisson brackets. We have observed that Cartesian coordinates are canonical. We give two other sets, the Delaunay and the Hill.

The combination of coordinates and conjugate momenta for Delaunay variables are the following:

Coordinates	*Momenta*
$l = M$	$L = (\mu a)^{1/2}$
$g = \omega$	$G = [\mu a(1-e^2)]^{1/2}$
$h = \Omega$	$H = [\mu a(1-e^2)]^{1/2} \cos I$

(9.36)

Now, l, g, h are new labels for three familiar Kepler elements, in order to provide a symmetric notation. We see that G is the angular-momentum constant N in the two-body motion given by (9.10) and that H is the projection of the angular momentum on the z axis.

Another set of canonical variables introduced into satellite theory by Izsak (1962) and used to great advantage by Aksnes (1970) consists of the Hill variables, as follows:

Coordinates	*Momenta*
$r = a(1 - e \sin E)$	$\dot{r} = (e/r) L \sin E$
$u = v + \omega$	$G = G$
$h = \Omega$	$H = H$

(9.37)

These are natural coordinates, with the important advantage that there is no singularity for small eccentricity—in contrast to the situation with Delaunay variables, which complicates their use.

Finally, we consider the equations of LPE type, which contain the forces explicitly. Consider the forces with components S, T, and W, which are, respectively, along the radius vector, in the orbital plane normal to the radius vector (along track), and perpendicular to the orbital plane (cross track). The direction cosines of satellite position are

$$\hat{l}_S = R_3(-\Omega) R_1(-I) R_3(-u) \begin{bmatrix} 1 \\ 0 \\ 0 \end{bmatrix} \tag{9.38}$$

We can define the direction cosines along track and cross track with

$$\hat{l}_T = R_3(-\Omega) R_1(-I) \times R_3(-\Omega) \begin{bmatrix} \dot{x} \\ \dot{y} \\ 0 \end{bmatrix} \Big/ (\dot{x}^2 + \dot{y}^2)^{1/2} \tag{9.39}$$

$$\hat{l}_W = \hat{l}_T \times \hat{l}_S \tag{9.40}$$

where $\dot{x}$, $\dot{y}$ are obtained from (9.16). If we let $\mathcal{E}_i$ be any variable, then

$$\frac{\partial R}{\partial \mathcal{E}_i} = \frac{\partial R}{\partial x}\frac{\partial x}{\partial \mathcal{E}_i} + \frac{\partial R}{\partial y}\frac{\partial y}{\partial \mathcal{E}_i} + \frac{\partial R}{\partial z}\frac{\partial z}{\partial \mathcal{E}_i}$$

But $\frac{\partial R}{\partial x}, \frac{\partial R}{\partial y}, \frac{\partial R}{\partial z}$ are the components of force along x, y, z given by

$$\begin{bmatrix} \frac{\partial R}{\partial x} \\ \frac{\partial R}{\partial y} \\ \frac{\partial R}{\partial z} \end{bmatrix} = \begin{bmatrix} & & \\ \hat{e}_S & \hat{e}_T & \hat{e}_W \\ & & \end{bmatrix} \begin{bmatrix} S \\ T \\ W \end{bmatrix} \tag{9.41}$$

With expressions $\bar{x} = \bar{x}(\mathcal{E}_i)$, say, (9.17), we can form $\partial x/\partial \mathcal{E}$ and substitute the result in

(9.23). This could be done for any set of variables. We give here the results for the Kepler elements, since they are widely used. We have

$$\frac{da}{dt}=\frac{2}{n(1-e^2)^{1/2}}\left[S\,e\sin v+T\frac{p}{r}\right]$$

$$\frac{de}{dt}=\frac{(1-e^2)^{1/2}}{na}\times\left\{S\sin v+T\left[\cos v+\frac{1}{e}\left(1-\frac{r}{a}\right)\right]\right\}$$

$$\frac{dI}{dt}=\frac{1}{na(1-e^2)^{1/2}}W\frac{r}{a}\cos\,(v+\omega)$$

$$\frac{d\Omega}{dt}=\frac{1}{na(1-e^2)^{1/2}\sin I}W\frac{r}{a}\sin\,(v+\omega)$$

$$\frac{d\omega}{dt}=-\cos I\frac{d\Omega}{dt}+\frac{1}{na}\frac{(1-e^2)^{1/2}}{e}\times\left[-S\cos v+T\left(1+\frac{r}{p}\right)\sin v\right]$$

$$\frac{dM}{dt}=n-\frac{2}{na}S\frac{r}{a}-(1-e^2)^{1/2}\left(\frac{d\omega}{dt}+\cos I\frac{d\Omega}{dt}\right)$$

$$p=a(1-e^2) \qquad (9.42)$$

These expressions are known as the LPE in Gaussian form. They have been calculated by using a force derived from a potential. However, the equations would have the same form for any force, and they can be so used. These expressions are especially useful in numerical integration and with nonconservative forces such as air drag and radiation pressure.

9.4.1.4 Spherical Harmonics

Legendre functions and associated Legendre functions arise naturally in the solution of Laplace's equations in spherical coordinates. They also constitute a set of orthogonal base functions for mapping arbitrary functions in spherical coordinates. In dynamical astronomy and satellite geodesy, spherical coordinates are the natural ones. We find that much of the subsequent analysis is facilitated by use of these functions, and we give here a short summary of their properties. Hobson (1955) is an excellent reference for mathematical proofs, and texts on mathematical physics (e.g., Jeffreys and Jeffreys, 1956; Morse and Feshback, 1953) provide many useful formulas. Legendre functions are extensively used in quantum mechanics, and its literature is recommended for the transformation properties.

For numerical computation, an expansion of P_{lm} in power series in z can be used. This expression can have large roundoff errors, and direct use may require multiple-precision computation. One alternative device is to employ the recurrence relationship

$$P_{l,m+2}(z)+2(m+1)\,[z/(1-z^2)^{1/2}]\,P_{l,m+1}(z)+(l-m)\,(l+m+1)P_{lm}(z)=0 \qquad (9.43)$$

where $z=\sin\phi$, and use

$$P_{ll}(z)=[(2l)!/2^l l!]\cos^l\phi$$
$$P_{l,l-1}(z)=z\,P_{ll}(z)$$

For each degree l, we compute all the $P_{lm}(z)$ from (9.43). In general, we require all the $P_{lm}(z)$, and this device will be efficient as well as accurate. We will need to find the expression for $P_{lm}(z)\,e^{im\lambda}$ in a coordinate system rotated by the Euler angles I, Ω, ω. The results given here are taken from Jeffreys (1965). We can write

$$\bar{P}_{lm}(\sin\phi)\;e^{im\lambda}=\sum_{s=-l}^{l}(i)^{s-m}E_{lms}(I)\,\bar{P}_{ls}(\sin\phi')\,e^{i[s(\lambda'+\omega')+m\Omega]} \qquad (9.44)$$

with

$$E_{lms}(I)=N_{lms}\sum_{r=\max\left|\begin{smallmatrix}0\\-(m+s)\end{smallmatrix}\right.}^{\min\left|\begin{smallmatrix}l-s\\l-m\end{smallmatrix}\right.}(-1)^{l-m-r}\binom{l+m}{m+s+r}\binom{l+m}{r}\gamma^{2r+m+s}\sigma^{2(l-r)-m-s} \qquad (9.45)$$

where

$$\gamma = \cos\ (I/2)$$

$$\sigma = \sin\ (I/2)$$

$$N^2_{lms} = \frac{(l-s)\,!\,(l+s)\,!\,\epsilon_m}{(l-m)\,!\,(l+m)\,!\,\epsilon_s}$$

Further, if $\phi' = 0$, we can write this in a more compact form as

$$\bar{P}_{lm}(\sin\phi)\, e^{im\lambda} = \sum_{p=0}^{l} (i)^{l-m} D_{lmp}(I)\, e^{i[(l-2p)(\lambda'+\omega')+m\Omega]} \tag{9.46}$$

for $l \geq m \geq l$, where

$$D_{lmp}(I) = \frac{1}{N_{lm}} \frac{(l+m)\,!}{2^l l!} \sum_{r=\max\left|\begin{smallmatrix} 0 \\ 2p-l-m \end{smallmatrix}\right.}^{\min\left|\begin{smallmatrix} l-m \\ 2p \end{smallmatrix}\right.} (-1)^{l-m-r} \binom{l}{p} \binom{2p}{r} \binom{2l-2p}{l-m-r} \gamma^{l+m+2r-2p} \sigma^{l-m-2r+2p} \tag{9.47}$$

where

$$r = \cos\ (I/2)$$

$$\sigma = \sin\ (I/2)$$

$$N^2_{lm} = \frac{(l+m)\,!}{\epsilon_m (2l+1)\,(l-m)\,!}$$

We note that

$$\bar{P}_{l,m}(z) = (-1)^m \bar{P}_{l,|m|} z \tag{9.48}$$

If we make the association $v = \lambda$, we see that (9.46) is a natural expression of spherical harmonics in Kepler elements. The development has been carried out by Kaula (1966b) on other considerations for conventional harmonics. The $D_{lmp}(I)$ here are related to the inclination functions of Kaula by

$$D_{lmp}(I) = [(-1)^{\{(l-m)/2\}}/N_{lm}] F_{lmp}(I) \tag{9.49}$$

The two developments are equivalent. We give here the expressions for calculating $F_{lmp}(I)$ as derived by Kaula, since they are extensively used:

$$F_{lmp}(I) = \sum_{t=0}^{\min\left|\begin{smallmatrix} \{(l-m)/2\} \\ p \end{smallmatrix}\right.} \frac{(2l-2t)\,!}{t!\,(l-t)\,!\,(l-m-2t)\,!\,2^{2l-2t}} S^{l-m-2t} \times \sum_{s=0}^{m} \binom{m}{s} C^s \sum_{c} \binom{l-m-2t+s}{c} \binom{m-s}{p-t-c} (-1)^{c-k} \tag{9.50}$$

where $S = \sin I$ and $C = \cos I$. Kaula gives tables of $F_{lmp}(I)$ through 4,4,4. Since (9.50) has three summations, whereas (9.47) has only one, the latter is somewhat more economical for computing numerical values.

9.4.1.5 Elliptic Expansions

In section 9.4.1.2, we found the relation between the mean anomaly M, the eccentric anomaly E, and the true anomaly v. Whereas E and v have geometric significance and are related by

$$\tan\ (v/2) = [(1+e)/(1-e)]^{1/2} \tan\ (E/2) \tag{9.51}$$

the mean anomaly has dynamical significance, increasing proportionally with time; that is,

$$M = M_0 + nt \tag{9.52}$$

The connection between M and E and hence v is made through Kepler's equation (9.14):

$$M = n(t-t_0) = E - e \sin E \tag{9.53}$$

Equations (9.51) to (9.53) are sufficient for all computations in two-body motion. Equation (9.53) is transcendental for E in terms of M and can easily be solved numerically by iteration. The obvious iteration is

$$E_0 = M$$

$$E_{n+1} = M + e \sin E_n \tag{9.54}$$

which converges very quicky for small eccentricity. Typical geodetic satellites have $e > 0.1$, for which (9.54) is quite sufficient. There are numerical methods to speed con-

vergence, and in cases where efficiency is important, methods like Newton's have been successful.

In developing complete solutions by use of, for example, LPE, we are faced with integrals of the following forms:

$$\int f(v)\,dt \qquad \int f(E)\,dt \tag{9.55}$$

It is therefore useful to be able to express functions of v and E in terms of t or M. These expressions generally involve infinite series in powers of eccentricity.

A particularly useful device for transforming (9.55) is to use

$$dv=(a/r)^2(1-e^2)^{1/2}dM=(a/r)^2(1-e^2)^{1/2}ndt \tag{9.56}$$

$$dE=(a/r)\,dM=(a/r)\,ndt$$

(See Gaposchkin, 1973.)

By use of (9.56), integrals in t can be converted to integrals in v or E. Where necessary, a/r can be expressed in v or E by (9.9), repeated here for convenience:

$$a/r=(1+e\cos v)/a(1-e^2)=1/(1-e\cos E) \tag{9.57}$$

Transformation (9.56) is useful when M is absent from the integral. Generally, this is not the case, and we must explicitly make the conversion. More general expressions are used, complete developments being carried out on computers either numerically or algebraically. In the following, we develop some of these formulas.

If, following many authors (e.g., Plummer, 1918), we define the variable $\beta(e)$ by

$$(1+\beta)/(1-\beta)=[(1+e)/(1-e)]^{1/2} \tag{9.58}$$

we have

$$e=2\beta/(1+\beta^2) \tag{9.59}$$

$$\beta=e/[1+(1-e^2)^{1/2}] \tag{9.60}$$

We see that $\beta\approx e/2$.

By using the Bessel function $J_n(x)$, we can write

$$E-M=2\sum_{s=1}^{\infty}\frac{1}{s}J_s(se)\sin sM \tag{9.61}$$

$$v-M=2\sum_{s=1}^{\infty}\frac{1}{s}\Big\{J_s(se)+\sum_{p=1}^{\infty}\beta^p[J_{s-p}(se)+J_{s+p}(se)]\Big\}\sin sM \tag{9.62}$$

The first few terms of (9.61) and (9.62) are

$$E-M=\Big(e-\frac{1}{8}e^3+\ldots\Big)\sin M+\Big(\frac{e^2}{2}+\ldots\Big)\sin 2M+\frac{3}{8}\Big(e^3+\ldots\Big)\sin 3M \tag{9.63}$$

$$v-M=\Big(2e-\frac{1}{4}e^3+\qquad\Big)\sin M+\Big(\frac{5}{4}e^2+\ldots\Big)\sin 2M+\Big(\frac{13}{12}e^3+\ldots\Big)\sin 3M \tag{9.64}$$

Brouwer and Clemence (1961) give these expressions to seventh order in eccentricity.

We have need of similar expressions when v or E occurs in the argument of a trigonometric function. There are several methods to obtain such expressions. We give two here. The first is due to Kaula (1966b) and taken from Tisserand (1960). Kaula investigates the conversion of

$$\Big(\frac{a}{r}\Big)^{l+1}\begin{pmatrix}\cos\\ \sin\end{pmatrix}[(l-2p)v+\psi]$$

where ψ does not depend on v, and gives it in the form

$$\Big(\frac{a}{r}\Big)^{l+1}\begin{pmatrix}\cos\\ \sin\end{pmatrix}[(l-2p)v+\psi]=\sum_{q=-\infty}^{\infty}G_{lpq}(e)\begin{pmatrix}\cos\\ \sin\end{pmatrix}[(l-2p+q)m+\psi] \tag{9.65}$$

This form is natural for the computation of perturbations due to tesseral harmonics. The

formulas have two forms. The first is for "long-term" terms, i.e., those terms in (9.65) independent of M—that is, $q=2p-l$. These can be obtained by integrating (9.65) with respect to M from 0 to 2π. Using the transformation (9.56), we obtain

$$G_{lp,\,2p-l}(e)=\frac{1}{(1-e^2)^{l-(1/2)}}\sum_{d=0}^{p'-1}\binom{l-1}{2d+l-2p'}\binom{2d+l-2p'}{d}\left(\frac{e}{2}\right)^{2d+l-2p'} \tag{9.66}$$

in which

$$p'=l-p \quad \text{for } p\geq l/2$$
$$p'=p \quad \text{for } p\leq l/2$$

For the short-period terms, $l-2p+q\neq 0$, we have

$$G_{lpq}(e)=(-1)^{|q|}(1+\beta^2)^{l}\beta^{|q|}\sum_{k=0}^{\infty}P_{lpqk}Q_{lpqk}\beta^{2k} \tag{9.67}$$

where

$$\beta=e/[1+(1-e^2)^{1/2}]$$

$$P_{lpqk}=\sum_{r=0}^{h}\binom{2p'-2l}{h-r}\frac{(-1)^r}{r!}\left[\frac{(l-2p'+q')\,e}{2\beta}\right]^r \tag{9.68}$$

$$h=k+q \quad \text{for } q'>0$$
$$h=k \quad \text{for } q'<0$$

and

$$Q_{lpqk}=\sum_{r=0}^{h}\binom{-2p'}{h-r}\frac{1}{r!}\left[\frac{(l-2p'+q')\,e}{2\beta}\right]^r \tag{9.69}$$

where

$$h=k \quad \text{for } q'>0$$
$$h=k-q' \quad \text{for } q<0$$
$$\left.\begin{aligned}p'&=p\\q'&=q\end{aligned}\right\} \text{ for } p\leq l/2$$
$$\left.\begin{aligned}p'&=l-p\\q'&=-q\end{aligned}\right\} \text{ for } p>l/2$$

The transformation (9.65) is a doubly infinite sum over q. However, it is important to note that

$$G_{lpq}(e)\propto\beta^{|q|}\approx(e/2)^{|q|}$$

We can choose a desired accuracy and select a finite number of terms. For small e, the number can be very limited. This selection can be made numerically or analytically.

A second and more general method for this development, given in Plummer (1918, p. 44), involves the Hansen coefficients X_q^{nm}, defined by

$$(r/a)^n e^{imv}=\sum_{q=-\infty}^{\infty}X_q^{nm}(e)\,e^{iqM} \tag{9.70}$$

where the $X_q^{nm}(e)$ are polynomials in eccentricity. We have

$$X_q^{mn}(e)=(1+\beta^2)^{-(n+1)}\sum_p J_p(qe)\,X_{qp}^{mn} \tag{9.71}$$

and

$$\left.\begin{aligned}
X_{qp}^{nm}&=(-\beta)^{q-p-m}\binom{n+1-m}{q-p-m}F(q-p-n-1,-m-n-1,q-p-m+1,\beta^2) && \text{for } q-p-m>0\\
X_{qp}^{nm}&=(-\beta)^{-q+p+m}\binom{n+1+m}{-q+p+m}F(-q+p-n-1,m-n-1,-q+p+m+1,\beta^2) && \text{for } q-p-m<0\\
X_{qp}^{nm}&=F(m-n-1,-m-n-1,1,\beta^2) && \text{for } q-p-m=0
\end{aligned}\right\} \tag{9.72}$$

We have the Bessel function

$$J_n(z) = (z/2)^n \sum_{k=0}^{\infty} \left(-\frac{1}{4}z^2\right)^k \Big/ [k!(n+k)!] \tag{9.73}$$

and the hypergeometric function

$$F(a,b,c,z) = \sum_{n=0}^{\infty} [(a)_n (b)_n / (c)_n] (z^n/n!) \tag{9.74}$$

where Pochhammer's symbol is

$$\left.\begin{aligned} (a)_n &= a(a+1)(a+2)\cdots(a+n-1) \\ (a)_0 &= 1 \end{aligned}\right\} \tag{9.75}$$

We see by comparing coefficients that

$$G_{lpq}(e) = X^{-(l+1),l-2p}_{l-2p+q}(e) \tag{9.76}$$

However, formulas (9.67) to (9.69) are valid only for $l+1>0$, whereas (9.70) to (9.76) are valid for any $n=-(l+1)$. Both forms have been used. With recent developments in the computing of elementary functions, the latter seems more economical for numerical calculation. For use with computer algebra, one would prefer to obtain polynomials in eccentricity with rational fractions as coefficients. This has been done through a recurrence relation originated by Andoyer (1903) and introduced into satellite work by Izsak *et al.* (1964). The method starts with the observation that

$$(r/a)^{\pm n} e^{i(\pm mv)} = X^{\pm n,\pm m} = (X^{\pm 1,0})^n (X^{0,\pm 1})^m$$

We compute $X^{\pm 1,0}$, $X^{0,\pm 1}$ by any method, and all other combinations are determined by simple polynomial multiplication. Cherniack (1972) gives these polynomials to 12th order in e. Kaula (1966b) gives a table through 4,4,2. Cayley (1961) gives more extensive tables.

9.4.1.6 First-Order Perturbations Due to the Potential

We have seen that the potential can be expressed in terms of associated Legendre functions (sec. 9.4.1.4) and a set of numerical constants,

$$\mathcal{U} = \mathcal{R}e\left(\frac{GM}{r}\right) \times \left[1 + \sum_{l=2}^{\infty}\sum_{m=0}^{l} \overline{\mathcal{C}}_{lm}\left(\frac{a_e}{r}\right)^l \bar{P}_{lm}(\sin\phi)\, e^{im\lambda}\right] \tag{9.77}$$

where ϕ, λ, r are the coordinates of a point in the terrestrial or Earth-fixed system. The terms $\overline{\mathcal{C}}_{1,0}$, $\overline{\mathcal{C}}_{1,1}$, $\overline{\mathcal{C}}_{2,1}$ are missing owing to the orientation and origin of the system chosen. In fact, the elastic Earth introduces the terms $\overline{\mathcal{C}}_{2,1}$, which will be discussed along with other questions relating to the Earth's elasticity in section 9.4.1.7. Selecting Kepler elements, we now use (9.77) in (9.28) for the disturbing function r, omitting, of course, GM/r.

The conversion of $R(r,\phi,\lambda)$ to $R(a,e,I,v,\omega, \Omega-\theta)$ is accomplished as follows. We express $R(r,\phi,\lambda)$ in the orbital system by rotating by $-\theta$. This introduces $\lambda-\theta$ in place of λ in (9.77). From the formula (9.46), we have

$$R = \mathcal{R}e\left(\frac{GM}{r}\right)\sum_{l=2}^{\infty}\sum_{m=0}^{l}\overline{\mathcal{C}}_{lm}\left(\frac{a_e}{r}\right)^l (i)^{l-m} \sum_{p=0}^{l} D_{lmp}(I)\, e^{i[(l-2p)(v+\omega)+m(\Omega-\theta)]} \tag{9.78}$$

where $i=\sqrt{-1}$ and $D_{lmp}(I)$ are polynomials in $\cos(I/2)$, $\sin(I/2)$. This is further converted to the mean anomaly with (9.67) or (9.70), giving

$$R = \mathcal{R}eGM\sum_{l=2}^{\infty}\sum_{m=0}^{l}\sum_{p=0}^{l}\sum_{q=-\infty}^{\infty}\left(\frac{1}{a}\right)\left(\frac{a_e}{a}\right)^l (i)^{l-m} D_{lmp}(I)\, G_{lpq}(e)\, e^{i\psi} \tag{9.79}$$

where

$$\psi = (l-2p)\omega + (l-2p+q)M + m(\Omega-\theta)$$

Equation (9.79) can also be written in terms of Hansen coefficients with (9.76).

The first-order secular rates can be determined by selecting terms in R independent of $\omega,\Omega,M,\vartheta$. These arise for $m=0$—that is, only zonal harmonics and $l-2p=q=0$. By use of algebra, we find secular terms only in ω, Ω, M.

A corollary is that the size a of the orbit, its shape e, and its orientation can have only periodic perturbations. We have shown it to first order only, but it is true for any order (Kozai, 1959c). We obtain for the first-order secular rates

$$\dot{\omega} = n(3\sqrt{5}/4)\,[\bar{C}_{2,0}/(1-e^2)^2]\,(a_e/a)^2\,(1-5\cos^2 I)$$

$$\dot{\Omega} = n(3\sqrt{5}/2)\,[\bar{C}_{2,0}/(1-e^2)^2]\,(a_e/a)^2\cos I$$

$$M = n\{1-(3\sqrt{5}/4)\,[\bar{C}_{2,0}/(1-e^2)^{3/2}]\,(a_e/a)^2(3\cos^2 I-1)\} \tag{9.80}$$

First-order periodic perturbations are easily obtained by assuming that a, e, I are relatively constant on the right-hand side of (9.28) and that ω, Ω, M, θ have linear rates; that is,

$$\begin{aligned} \omega &= \omega_0 + \dot{\omega}t \\ \Omega &= \Omega_0 + \dot{\Omega}t \\ M &= M_0 + nt \\ \theta &= \theta_0 + \dot{\theta}t \end{aligned} \tag{9.81}$$

The equations are integrated as a linear harmonic oscillator for those terms containing any of the variables in (9.81). In actual computation, we would use the values of $\dot{\omega}$, $\dot{\Omega}$, n, $\dot{\theta}$ derived from observations.

Letting $\mathcal{E}_i$ be a generic element, we have the following:

$$\Delta\mathcal{E}_i = \sum_{l=2}^{\infty}\sum_{m=0}^{l}\sum_{p=0}^{l}\sum_{q=-\infty}^{\infty}\Delta\mathcal{E}_{lmpq}$$

$$\Delta a_{lmpq} = \mathcal{R}e\frac{GMa_e^l(i)^{l-m}}{na^{l+2}}\frac{2}{\dot{\psi}_{lmpq}}D_{lmp}(I)\,G_{lpq}(e)\,(l-2p+q)\,\bar{C}_{lm}e^{i\psi_{lmpq}}$$

$$\Delta e_{lmpq} = \mathcal{R}e\frac{GMa_e^l(i)^{l-m}}{na^{l+3}e\dot{\psi}_{lmpq}}D_{lmp}G_{lpq}(1-e^2)^{1/2}[(1-e^2)^{1/2}(l-2p+q)-(l-2p)]\,\bar{C}_{lm}e^{i\psi_{lmpq}}$$

$$\Delta I_{lmpq} = \mathcal{R}e\frac{GMa_e^l(i)^{l-m}}{na^{l+3}(1-e^2)^{1/2}\dot{\psi}_{lmpq}}D_{lmp}G_{lpq}[(l-2p)\cos I-m]\,\bar{C}_{lm}e^{i\psi_{lmpq}} \tag{9.82}$$

$$\Delta\omega_{lmpq} = \mathcal{R}e\frac{GMa_e^l(i)^{l-m-1}}{na^{l+3}(1-e^2)^{1/2}\sin I\,\dot{\psi}_{lmpq}}\left[\frac{(1-e^2)^{1/2}}{e}D_{lmp}\frac{\partial G_{lm}}{\partial e}\frac{\cos I}{\sin I}\frac{G_{lmp}}{(1-e^2)^{1/2}}\frac{\partial D_{lmp}}{\partial I}\right]\bar{C}_{lm}e^{i\psi_{lmpq}}$$

$$\Delta\Omega_{lmpq} = \mathcal{R}e\frac{GMa_e^l(i)^{l-m-1}G_{lpq}}{na^{l+3}(1-e^2)^{1/2}\sin I\,\dot{\psi}_{lmpq}}\frac{\partial D_{lmp}}{\partial I}\bar{C}_{lm}e^{i\psi_{lmpq}}$$

$$\Delta M_{lmpq} = \mathcal{R}e\frac{GMa_e^l(i)^{l-m-1}}{na^{l+3}\dot{\psi}_{lmpq}}\left[-\frac{(1-e^2)^{1/2}}{e}\frac{\partial G_{lpq}}{\partial e}+2(l+1)\,G_{lpq}\right]D_{lmp}\bar{C}_{lm}e^{i\psi_{lmpq}}$$

where

$$\dot{\psi}_{lmpq} = (l-2p)\,\dot{\omega}+(l-2p+q)\,n+m(\dot{\Omega}-\dot{\theta})$$

After the substitution of (9.44), these formulas agree with Kaula (1966b).

The final calculation necessary is to determine $\int n\,dt$ for the perturbation in M according to (9.28). We see that for $l-2p+q\neq 0$, we have a perturbation in a from the first equation of (9.82). From $n^2a^3=GM$, we have

$$\Delta n_{lmpq} = -(3/2)\,(n/a)\,\Delta a_{lmpq} \tag{9.83}$$

Therefore, to the last equation of (9.82), we must add the term

$$\begin{aligned}\Delta M_{lmpq} &= \int \Delta n_{lmpq}\,dt \\ &= \mathcal{R}e\left[\frac{-3GMa_e^l(i)^{l-m-1}}{a^{l+3}(\dot{\psi}_{lmpq})^2}\right] \\ &\quad\times D_{lmp}G_{lpq}(l-2p+q)\,\bar{C}_{lm}e^{i\psi_{lmpq}}\end{aligned} \tag{9.84}$$

We can combine both parts and obtain

$$\begin{aligned}\Delta M_{lmpq} = \mathcal{R}e\,\frac{GMa_e^lD_{lmp}}{a^{l+3}}\Bigg[&-\frac{(1-e^2)^{1/2}}{ne\dot{\psi}_{lmpq}}\frac{\partial G_{lpq}}{\partial e} \\ &+\frac{2(l+1)}{n\dot{\psi}_{lmpq}}G_{lpq}-\frac{3G_{lpq}(l-2p+q)}{(\dot{\psi}_{lmpq})^2}\Bigg] \\ &\times i^{l-m-1}\bar{C}_{lm}e^{i\psi_{lmpq}}\end{aligned}$$

This completes the first-order theory. If we take as our goal an accuracy of 10^{-7}, then it is quite satisfactory unless $|\bar{C}_{lm}|$ is larger than 10^{-4} or $\dot{\psi}_{lmpq}$ is very small. From observations, we find that $\bar{C}_{2,0} \approx 10^{-3}$ and that all the remaining $|\bar{C}_{lm}| \approx 10^{-6}$. Therefore, this theory is inadequate for the effects of $\bar{C}_{2,0} = -J_2/\sqrt{5}$, and so other methods are used, as described in section 9.4.1.8. The discussion of small ψ_{lmpq} goes by the name of resonance, which will be dealt with shortly.

If we consider the rate

$$\dot{\psi}_{lmpq} = (l-2p)\,\dot{\omega} + (l-2p+q)\,n + m(\dot{\Omega}-\dot{\theta}) \qquad (9.85)$$

and $\dot{\omega}$, $\dot{\Omega}$ from (9.80), we see that $(\dot{\omega}, \dot{\Omega}) \propto 10^{-3}\, n$. The rotation rate of the Earth, $\dot{\theta}$, is once per day, and n for geodetic satellites is 12 ± 2 revolutions per day. Therefore, the period of a perturbation is primarily determined by

$$2\pi/P = (l-2p+q)\,n - m\dot{\theta} \qquad (9.86)$$

We see that in general the largest perturbations—that is, the smallest divisors—are for $l-2p+q=0$, and we have periodic terms with frequency $m\dot{\theta}$. Resonance occurs with the near-commensurability of $(l-2p+q)n$ and $m\dot{\theta}$. That means that when the mean motion of the satellite is approximately equal to the order of the tesseral harmonics, we can have arbitrary long periods and large amplitudes. When analyzing terms with small divisors, we must include the effects of $\dot{\omega}$ and $\dot{\Omega}$ to obtain meaningful results. Resonance has yet to be treated completely. For a single resonant term, a solution in terms of elliptic functions can be obtained, and these have played an important role in the study of synchronous satellites. For close-Earth satellites, the problems are more difficult, since the satellite will be resonant with the whole set of harmonics of order m. In addition, if the drag changes n appreciably during one resonant oscillation, the theory is not even approximately correct. Fortunately, geodetic satellites have had relatively short resonant periods (≈ 10 days), and the linear theory seems to work well enough.

A second class of long-period perturbations is due to the zonal harmonics ($m=0$, $l-2p+q=0$). These have the principal period of the rotation of perigee, as given by (9.80). The period of these terms can go to zero for the so-called critical inclination—that is, when $(1-5\cos^2 I)=0$ or $I \cong 63^\circ.4$. The theory given here is not valid near that region of inclination. It has variously been viewed as a resonant phenomenon and as a physically important effect. Izsak (1963*c*), Garfinkle (1963), and others have discussed this question.

Table 9.24 gives here for a typical geodetic satellite a short table of amplitudes of the perturbations due to the Earth's field.

9.4.1.7 Third-Body Perturbations, Elasticity, and Tides

There is an extensive literature on third-body perturbations. The principal effect of the Moon is a perturbation ≈ 120 m, and that of the Sun, about 6 times that amount. Continuous analysis has been necessary because of three factors:

(1) The Moon's motion is itself complicated, making integration of the equations of motion difficult. The inclination of the Moon's orbit is not constant in the adopted orbital system. There is a rich spectrum of periodic terms in the lunar longitude.

(2) The Moon and Sun deform the elastic Earth. This variation in mass distribution has significant orbital effects. Improved geophysical information is needed in order to account for them.

(3) The Sun and Moon cause precession and nutation. These motions are the reason for our adopting a quasi-inertial reference system. We must include in the theory terms to compensate for the noninertialness. These terms can be viewed as an indirect effect of the lunisolar perturbations.

There are two avenues to be taken. The first is to eliminate periodic perturbations with periods commensurate with the length

of orbit we wish to determine—that is, periods <20 days. We take an analytical approach by assuming linear variation of the orbital elements of the disturbing body. The second avenue is for long-period analysis, in which we obtain averaged equations—that is, ones not depending on the mean anomaly of the satellite. These can be integrated numerically and are used for study of all long-period effects.

In the following, we develop the disturbing function for the Moon; that for the Sun has the same form. We assume that the semimajor axis of the satellite is small with respect to that of the Sun or the Moon. This disturbing function can be averaged and then numerically integrated with (9.28), or if a, e, I' of the Moon are assumed constant, it can be integrated approximately.

We introduce the elastic deformation of the Earth at this point, as it is most easily incorporated into the theory from the beginning. Following A. E. H. Love (Munk and MacDonald, 1960, ch. 5), the additional potential $\mathcal{U}_n$ due to the deformation from a potential of degree n is

$$\mathcal{U}_n' = k_n (a_e/r)^{2n+1} \mathcal{U}_n \tag{9.87}$$

where k_n are numerical constants depending on the elastic properties of the Earth. The total potential acting on the satellite is then

$$[1 + k_n (a_e/r)^{2n+1}] \mathcal{U}_n \tag{9.88}$$

Now the direct potential acting on the satellite due to the Moon (or Sun) can be written

$$\mathcal{U} = GM' \left[(1/\Delta) - (\bar{r} \cdot \bar{r}'/|r'|^3) \right] \tag{9.89}$$

where $\bar{r}$ and $\bar{r}'$ are the positions of the satellite and of the disturbing body, respectively, M' is the mass of the disturbing body, and Δ is the distance between r and r'. As is well known, we can write $1/\Delta$ in spherical harmonics. To calculate orbital perturbations, we use the gradient of $\mathcal{U}$ with respect to the satellite position, and we can drop the $l=0$ term in $1/\Delta$. The $l=1$ term just cancels $\bar{r} \cdot \bar{r}'/|r'|^3$. Thus, we have for the third-body potential, including the tidal deformation,

$$\mathcal{U} = GM' \mathcal{R}e \sum_{l=2}^{\infty} \sum_{m=0}^{l} \frac{1}{2l+1} \left[\frac{r^l}{r'^{l+1}} + \frac{k_l a_e^{2l+1}}{(r'r)^{l+1}} \right] \bar{P}_{lm} (\sin \phi) \, \bar{P}_{lm} (\sin \phi') \, e^{im(\lambda - \lambda')} \tag{9.90}$$

To include the effects of tidal phase lag, we introduce a fictitious Moon lagging the real Moon by Δt and separate (9.90) into two parts. In this case, the disturbing potential cannot be written in such a compact form. We proceed by assuming $\Delta t = 0$, the revision of the theory being straightforward if the effect of lag is desired.

By introducing the rotation operation (9.45) and Hansen coefficients (9.70), we can write the disturbing function as

$$R = \mathcal{R}e \sum_{l=2}^{\infty} \sum_{m=0}^{l} \sum_{p=0}^{l} \sum_{p'=0}^{l} \sum_{q=-\infty}^{\infty} \sum_{q'=-\infty}^{\infty} R_{lmpp'qq'} \tag{9.91}$$

where

$$R_{lmpp'qq'} = \frac{GM' (-l)^{l+m}}{2l+1} D_{lmp}(I) D_{l,-m,p'}(I') \times \left[\frac{a^l}{a'^{l+1}} X_q^{lm}(e) X_{q'}^{-l-1,m}(e') + \frac{k_l a_e^{2l+1}}{(a'a)^{l+1}} X^{-l-1,m}(e) X_{q'}^{-l-1,m}(e') \right] e^{i\psi} \tag{9.92}$$

in which

$$\psi = qM + q'M' + (l-2p)\omega + (l-2p')\omega' + m(\Omega - \Omega')$$

We can integrate the LPE (9.28) by utilizing the disturbing function (9.91) and the same techniques used for the tesseral harmonics. Considerable simplification is achieved by the following steps:

(1) We delete all terms containing M—that is, $q=0$. These short-period effects are about 1 m and can be ignored for some problems. A consequence is that $\Delta a = 0$.

(2) For the second-degree terms, we can use, for the Moon,

$$GM_\oplus = n_\leftmoon^2 a_\leftmoon^3 \tag{9.93a}$$

and

$$GM' = GM_\oplus (M_\leftmoon/M_\oplus) = (M_\leftmoon/M_\oplus) n_\leftmoon^2 a_\leftmoon^3 \tag{9.93b}$$

where $M_\leftmoon/M_\oplus = 1/81.53$ and, for the Sun,

$$GM' = n_\odot^2 a_\odot^3 \tag{9.93c}$$

(3) The third-degree terms from the Sun are negligible, and those from the Moon are $\approx$1 m and can be ignored for some problems. However, the third-degree terms and the short-period terms in the second-degree development must be included for future work. The interaction between J_2 and the lunar perturbations is the same size and must also be added, that is, the contributions to $\dot{\omega}$ and $\dot{\Omega}$ from

$$\begin{aligned} &\frac{d\dot{\omega}}{de}\Delta e + \frac{\partial \dot{\omega}}{\partial I}\Delta I \\ &\frac{d\dot{\Omega}}{de}\Delta e + \frac{d\dot{\Omega}}{dI}\Delta I \\ &\frac{d\dot{M}}{de}\Delta e + \frac{d\dot{M}}{dI}\Delta I \end{aligned} \tag{9.94}$$

where $\dot{\omega}$, $\dot{\Omega}$, and $\dot{M}$ are given by (9.80).

A number of formulas have been used (e.g., Kozai, 1973; Gaposchkin, 1966a). We give here just the secular rates in ω, Ω, and M and a representative periodic term. The complete expressions for lunar perturbations are developed by computer algebra and are described in section 9.4.1.11. We have

$$\begin{aligned} \dot{\omega}_{L\text{-}S} = &\frac{3}{4}\frac{n'^2}{n} m' \frac{1}{(1-e^2)^{1/2}} \\ &\times \left(2 - \frac{5}{2}\sin^2 I + \frac{1}{2}e^2\right)\left(1 - \frac{3}{2}\sin^2 I'\right) \\ &\times \left(1 + \frac{3}{2}e'^2\right)\left[1 + k_2\left(\frac{a_e}{a}\right)^2\right] \\ \dot{\Omega}_{L\text{-}S} = &-\frac{3}{4}\frac{n'^2}{n} m' \frac{\cos I}{(1-e^2)^{1/2}} \\ &\times \left(1 + \frac{3}{2}e^2\right)\left(1 - \frac{3}{2}\sin^2 I'\right) \\ &\times \left(1 + \frac{3}{2}e'^2\right)\left[1 + k_2\left(\frac{a_e}{a}\right)^2\right] \end{aligned} \tag{9.95}$$

$$\begin{aligned} \dot{M}_{L\text{-}S} = &-\frac{1}{4}\frac{n'^2}{n} m' \left(1 - \frac{3}{2}\sin^2 I'\right) \\ &\times \left(1 - \frac{3}{2}\sin^2 I\right)\left(1 + \frac{3}{2}e'^2\right) \\ &\times \left[7 + 3e^2 - 3(1+4e^2) k_2 \left(\frac{a_e}{a}\right)^2\right] \end{aligned}$$

where, for the Moon, $m' = M_\leftmoon/M_\oplus = 1/81.53$, and, for the Sun, $m' = 1$, and where

$$\begin{aligned} \sin^2 I' = &\frac{1}{2}\sin^2 J (1 + \cos^2 \epsilon) + \sin^2 \epsilon \cos^2 J \\ &+ \frac{1}{2}\sin 2\epsilon \sin 2J \cos N \\ &- \frac{1}{2}\sin^2 J \sin^2 \epsilon \cos 2N \end{aligned} \tag{9.96}$$

Here, J is the lunar inclination, N is the lunar longitude referred to the ecliptic, and ϵ is the obliquity. Although I is not constant, it is a reasonable approximation for a year or so. We note that $J = 5''.145\,396$. The other dements can be taken from the ESAENA. For the Sun, of course, $m' = J = 0$. For the periodic perturbation, we give as an example, for the second degree,

$$\begin{aligned} \Delta I_{2,m,p,q',q'} = &\frac{n'^2 (-1)^m}{\partial \psi} D_{2,m,p}(I) D_{2,-m,q'}(I') \\ &\times \left[X_q^{2,m}(e) X_{q'}^{-3,m}(e') \right. \\ &\left. + k_2 \left(\frac{a_e}{a}\right)^5 X_q^{-3,m}(e) X_{q'}^{-3,m}(e') \right] \\ &\times [2(1-p)\cos I - m] \cos \psi \end{aligned} \tag{9.97}$$

where

$$\begin{aligned} \dot{\psi} = &2(1-p)\dot{\omega} + 2(1-p')\dot{\omega}' + qn + q'n' \\ &+ m(\dot{\Omega} - \dot{\Omega}') \end{aligned}$$

We note that the secular rates depend on k_2, which corresponds to that part of the oblateness resulting from the permanent tidal deformation. Conventionally, this term is omitted from the lunar theory and is effectively included in the numerical value of J_2. A slight error will arise since, in the lunar theory, k_2 occurs multiplied by a_e/a^5, whereas J_2 is multiplied by a_e/a^3. Furthermore, the

secular term in M must be included in the definition of the semimajor axis.

The adopted reference system for orbit computation is the equinox of 1950.0 and the equator of date. The equations of motion must be modified to include the motion of the reference system. There is no need to modify the short-period perturbations in the linear theory described above. However, for the complete set of LPE with (9.92) for long-period perturbations or in terms of coordinates (Kozai and Kinoshita, 1973), we can include the following factors:

$$\left.\begin{aligned} di/dt &= \cdots \partial i/\partial t \\ d\omega/dt &= \cdots \partial \omega/\partial t \\ d\Omega/dt &= \cdots \partial \Omega/\partial t \end{aligned}\right\}$$

where

$$\left.\begin{aligned} \frac{\partial i}{\partial t} &= -\frac{d(\theta\cos\alpha)}{dt}\cos\Omega - \frac{d(\theta\sin\alpha)}{dt}\sin\Omega \\ \frac{\partial \omega}{\partial t} &= \operatorname{cosec} i\left[\frac{d(\theta\sin\alpha)}{dt}\cos\Omega - \frac{d(\theta\cos\alpha)}{dt}\sin\Omega\right] \\ \frac{\partial \Omega}{\partial t} &= -\cot i\left[\frac{d(\theta\sin\alpha)}{dt}\cos\Omega - \frac{d(\theta\cos\alpha)}{dt}\sin\Omega\right] \\ &\quad + \frac{1}{2}\left[\frac{d(\theta\sin\alpha)}{dt}\theta\cos\alpha - \frac{d(\theta\cos\alpha)}{dt}\theta\sin\alpha\right] \end{aligned}\right\} \quad (9.98)$$

$$\left.\begin{aligned} \theta\sin\alpha &= (0.3979 + \epsilon_1 - \epsilon_0)\sin\psi \\ \theta\cos\alpha &= 0.3651\ (1-\cos\psi) - \epsilon_1 + \epsilon_0 \end{aligned}\right\} \quad (9.99)$$

$$\begin{aligned} \psi = &-17''.24\sin N + 0''.21\sin 2N \\ &-1''.27\sin 2L_\odot + 0''.13\sin l_\odot \\ &-0''.20\sin 2L_\mathbb{C} + 0''.07\sin l_\mathbb{C} \\ &+0''.137\,914\,6\,t \\ \epsilon_1 - \epsilon_0 = &\ 9''.21\cos N - 0''.09\cos 2N \\ &+0''.55\cos 2L_\odot + 0''.09\cos 2L_\mathbb{C} \\ &-0''.001\,281\,t \end{aligned}$$

where $l_\odot$, $l_\mathbb{C}$, $L_\odot$, and $L_\mathbb{C}$ are the mean anomalies and mean longitudes of the Sun and the Moon, respectively; t is the number of days from 1950.0; and N is the lunar ascending node referred to the ecliptic. We have

$$\left.\begin{aligned} \frac{d(\theta\sin\alpha)}{dt} &= 0.9175\sin\psi\frac{d(\epsilon_1-\epsilon_0)}{dt} + 0.3979\cos\psi\frac{d\psi}{dt} \\ \frac{d(\theta\cos\alpha)}{dt} &= -(0.1583 + 0.8418\cos\psi)\frac{d(\epsilon_1-\epsilon_0)}{dt} + 0.3651\sin\psi\frac{d\psi}{dt} \end{aligned}\right\} \quad (9.100)$$

$$\left.\begin{aligned} \frac{d\psi}{dt} &= -17''.24\,\dot{N}\cos N + 0''.42\,\dot{N}\cos 2N - 2''.54\,n_\odot\cos 2L_\odot + 0''.13\,n_\odot\cos l_\odot \\ &\quad - 0''.40\,n_\mathbb{C}\cos 2L_\mathbb{C} + 0''.07\,n_\mathbb{C}\cos l_\mathbb{C} + 0''.137\,914\,6 \\ \frac{d(\epsilon_1-\epsilon_0)}{dt} &= -9''.21\,\dot{N}\sin N + 0''.18\,\dot{N}\sin 2N - 1''.10\,n_\odot\sin 2L_\odot \\ &\quad - 0''.18\,n_\mathbb{C}\sin 2L_\mathbb{C} - 0''.001\,281 \end{aligned}\right\} \quad (9.101)$$

where $\dot{N} = dN/dt$, $n_\odot$ is the mean motion of the Sun, and $n_\mathbb{C}$ is the mean motion of the Moon.

We have incorporated the effects of body tides on satellite motion. There remain to be included ocean and atmospheric tides. The former, expressed in spherical harmonics, is not yet very well known and so we give only a qualitative analysis. The M_2 tide has been studied by Pekeris and Accad (1969) and by Hendershott (1972) and we will examine it. If we develop the tide in an Earth-fixed system as

$$\zeta = \mathcal{R}e\sum_{lm}\bar{C}_{lm}\bar{P}_{lm}(\sin\phi)\ e^{i(m\lambda+\theta t)} \quad (9.102)$$

then the tide will appear static in the inertial reference frame of the satellite. The external potential due to this tide, including the loading effect, is

$$\mathcal{U}=\mathcal{R}e\sum_{lm}\frac{(1+k_l')\,4\pi G\rho_w a_e^{l+2}}{(2l+1)\,r^{l+1}}\bar{C}_{lm}\bar{P}_{lm}(\sin\phi)\,e^{im\lambda}) \tag{9.103}$$

where k is the loading Love number (Munk and MacDonald, 1960) and ρ_w is the density of ocean water. This can be developed in terms of orbital elements along the lines of the tesseral harmonics; we have

$$\mathcal{U}=\sum_{lmp}\mathcal{U}_{lmp}$$

in which

$$\mathcal{U}_{lmp}=\Gamma_{lm}(a_e^{l+2}/r^{l+1})\,D_{lmp}(I)\,e^{i[(l-2p)(v+\omega)+m(\Omega-v'-\omega'-\Omega')]} \tag{9.104}$$

where

$$\Gamma_{lm}=4\pi G\rho_w(1+k_l')\,\bar{C}_{lm}/(2l+1) \tag{9.105}$$

We can develop equation (9.104) into perturbations, giving, for example,

$$\Delta\omega_{lmpqq'}=\mathcal{R}e\,(i)^{l-m}\,\Gamma_{lm}(a_e^{l+2}/na^{l+2})\,[D_{lmp}(I)/\dot{\psi}]\,X_q^{-l-1}(e)^{l-2p}X_{q'}^{q,m}(e')\times[(l-2p)\cos I-m]e^{i\psi} \tag{9.106}$$

where

$$\psi=qM+q'M'+(l-2p)\,\omega+m(\Omega-\Omega'-\omega')$$
$$\psi=qn+q'n'+(l-2p)\,\dot{\omega}'+m(\dot{\Omega}-\dot{\Omega}'-\dot{\omega}')$$

It is useful to note characteristics of lunar and solar perturbations in addition to the secular terms given in (9.95). The principal periodic terms from the Moon have a 14-day period and an amplitude of about 120 m. The principal solar term is of 6-month period and about 800 m. The tidal effects are of the order of 10 percent of the direct effect, or about 15 m for the lunar tides. Therefore, it is essential to compute lunar effects when orbits are being determined for more than a few days. The solar effects can be absorbed in the orbital elements. There are also very important long-period perturbations from the Moon. Of greater difficulty in the treatment of long-period perturbations is the solar radiation pressure, which is yet to be satisfactorily computed (section 9.4.1.9).

It is instructive to determine the ocean-tide equivalent of the body tide. We can do this only approximately. The correspondence is made by comparing the potentials in (9.92) and (9.106) for a particular lmp combination. We have

$$\mathcal{U}_{lmp}^{\text{body}}=\frac{GM'(-1)^{l+m}}{2l+1}\frac{k_l a_e^{l+1}}{r'^{l+1}r^{l+1}}D_{lmp}(I)\sum_{p'=0}^{l}D_{l(-m)p'}(I')\,e^{i\phi} \tag{9.107}$$

where $\phi=(l-2p)\,(v+\omega)+(l-2p')\,(v'+\omega')+m(\Omega-\Omega')$; and

$$\mathcal{U}_{lmp}^{M_2}=\frac{4\pi G\rho_\omega(1+k_l')}{2l+1}\frac{a_e^{l+2}}{r^{l+1}}\bar{C}_{lm}(i)^{l-m}D_{lmp}(I')\,e^{i\psi} \tag{9.108}$$

where $\psi=(l-2p)\,(v+\omega)-m(v'+\omega'+\Omega'-\Omega)$. We note that the lunar inclination is $I'=23°\pm5°$ and that $D_{2,-2,0}\cong0.925$, $D_{2,-2,1}\cong0.160$, and $D_{2,-2,2}\cong0.0036$. So, for the principal semidiurnal term, we can take $l=2$, $m=2$, $l-2p=2$, $p=0$, and $p'=0$, giving

$$\frac{k_2}{1+k_2'}=\frac{4\pi G\rho_\omega\bar{C}_{2,2}}{\mu n'^2a_cD_{2,-2,0}(I')} \tag{9.109}$$

$$\bar{C}_{2,2}=\frac{k_2}{1+k_2'}\frac{\mu n'^2a_cD_{2,-2,0}(I')}{4\pi G\rho_\omega} \tag{9.110}$$

where k_2 would have a complex value. Using nominal values, we have

$$k_2=0.0114\bar{C}_{lm}/D_{2,-2,0}(I') \tag{9.111}$$

From K. Lambeck (1972, private communication), the Pekeris and Accad (1969) solution with dissipation gives (in cm)

$$\bar{C}_{2,2}=4.4e^{-i330\pi/180}=-2.19-3.81i$$

We then have $k_2^{\text{ocean}}=-0.026-0.047\text{i}$. Adding this to the body tide, we obtain the effective

Love number that a satellite would sense. Choosing $k_2^{\text{body}}=0.29$ with no dissipation, we have

$$k_2^{\text{effective}}=k_2^{\text{body}}+k_2^{\text{ocean}}=0.264-0.047\,i$$

Therefore, a satellite would sense a Love number of 0.268 with a phase lag of 10°.09 or 40 m. Conversely, by adopting a value for k_2^{body} and determining $k_2^{\text{effective}}$ from satellite observations, the height of the ocean tide could be calculated.

We have analyzed perturbations due to the $\bar{P}_{2,2}$ component of the ocean tide and note that they have the same dependence on the satellite inclination as does the body tide. Therefore, it is not possible to separate the second-degree body and ocean tide with satellite perturbation analysis. The ocean tides have a much richer spectrum in spherical harmonics than do the body tides (Hendershott, 1973). Selected terms of equation (9.102) are important, principally, $\bar{P}_{4,2}$ and $\bar{P}_{6,2}$. Although they result in orbital perturbations with the same frequency spectrum as does $\bar{P}_{2,2}$, the inclination dependence allows the determination of these coefficients by use of several satellites, in an analogous way to the geopotential.

Finally, we consider another effect of the Earth's elasticity. The orbital system we have adopted is not precisely a system of the principal axis of inertia. Rather, we use a mean pole. There is a free nutation of the Earth called polar motion, which introduces the tesseral harmonics $\bar{C}_{lm}=\bar{C}_{lm}-i\,\bar{S}_{lm}$. There are two effects that to some extent cancel each other: The first is the motion of the axis of the principal moment of inertia; the second, the deformation due to the rotation about a moving axis. If we let ξ, η be the coordinates of the principal moments with respect to the mean pole and let l_1, l_2 be the coordinates of the instantaneous rotation axis, then we can write

$$\begin{aligned}\bar{C}_{2,1}=&-\bar{C}_{2,0}\sqrt{3}\,(\xi-i\eta)\\&-k_2(\omega_e^2a_e^3/\sqrt{15}\,GM)\;(l-il_2)\end{aligned}$$

where $\omega_e=\dot{\theta}$. This harmonic is a slowly varying function of time with a 14-month period. If we assume $\xi=l_1$, $\eta=l_2$—that is, that we know where the principal axes are—then we have

$$\bar{C}_{2,1}=-\bar{C}_{2,0}\sqrt{3}-k_2(\omega_e^2a_e^3/\sqrt{15}\,GM)\,]\;(\xi-i\eta)$$

Using these values, we know

$$\bar{C}_{2,1}=(0.838-k_2x0.893)\;(\xi-i\eta)$$

the elasticity reducing the effect by about one-third. The perturbations for the seven retroreflector satellites are all about 1 m.

9.4.1.8 Higher Order Perturbations Due to Oblateness; Methods of Von Zeipel and Lie-Hori

Although a linear first-order approximation to the equations of motion proved adequate to obtain 1–m accuracy for the tesseral harmonics and the zonal harmonics excluding J_2 and J_3, we must have a more thorough treatment for the oblateness perturbations. Various solutions and formulas have been used (Brouwer, 1959; Kozai, 1959c, 1962b, 1966c; Izsak, 1963b; Aksnes, 1970), but only the last has proved completely satisfactory. Except for Kozai's (1959c), the methods depend on a canonical transformation. We sketch the basic ideas here. There are two equivalent approaches. The first, based on a device employed by Von Zeipel (1916) and known by his name, utilizes expansions in the form of Taylor series. It was introduced into the satellite problem by Brouwer (1959). The second, from a transformation due to Hori (1966), is based on expansions in Lie series and is known as the Lie-Hori method.

In both developments, we use canonical variables,

$$\left.\begin{array}{ll}l=M & L=(\mu a)^{1/2}\\ g=\omega & G=L(1-e^2)^{1/2}\\ h=\Omega & H=G\cos I\end{array}\right\}\qquad(9.112)$$

In the Aksnes theory, use is also made of the Hill variables introduced into satellite theory by Izsak (1963d):

$$r,\ v+\omega,\ h,\ \dot{r},\ G,\ H \qquad (9.113)$$

In the mathematical problem we are discussing, the Hamiltonian is

$$\mathcal{H}=\frac{\mu^2}{2L^2}-\frac{\mu^4 J_2 a_e^2}{L^6}\left\{\left[-\frac{1}{2}+\frac{3}{2}\left(\frac{H}{G}\right)^2\right]\left(\frac{a}{r}\right)^3+\left[\frac{3}{2}-\frac{3}{2}\left(\frac{H}{G}\right)^2\right]\left(\frac{a}{r}\right)^3\cos\,(2g+2v)\right\} \qquad (9.114)$$

Since t and h are both absent from $\mathcal{H}$, we therefore have immediately

$$H=G\cos I=\text{const} \qquad (9.115)$$

and $\mathcal{H}=\text{const}$. We have limited this discussion to J_2, and all the developments mentioned above have carried the analysis to higher orders.

The method of Von Zeipel (1916) was proposed by Poincaré (1893). The latter showed that a transformation was always possible, but he was not convinced that the expansion would converge; Barrar (1970) has discussed this question further. We look for a determining function $S(L',G',H',l,g,h) = F_2$ relating the new momenta and old coordinates, such that the new Hamiltonian $\mathcal{H}^*$ does not depend on l; that is,

$$\mathcal{H}(L,G,H,l,g)=\mathcal{H}^*(L,G,H,g) \qquad (9.116)$$

We then have

$$\left.\begin{array}{ll} l'=\partial S/\partial L' & L=\partial S/\partial l \\ g'=\partial S/\partial G' & G=\partial S/\partial g \\ h'=\partial S/\partial H' & H=\partial S/\partial h \end{array}\right\} \qquad (9.117)$$

Since this is a canonical transformation, we have

$$\left.\begin{array}{l} dL'/dt=\partial\mathcal{H}^*/\partial l' \\ dl'/dt=-\partial\mathcal{H}^*/\partial L' \end{array}\right\} \qquad (9.118)$$

and four similar equations. Having solved this problem, we can perform a second transformation to eliminate g' and obtain a third set of variables, L'',G'',H'',l'',g'',h'', where the Hamiltonian is

$$\mathcal{H}^{**}(L'',G'',H'')=\mathcal{H}^*(L',G',H',g)$$

We proceed by expressing $\mathcal{H}$ and S in a Taylor series in terms of a small parameter α, which will be proportional to J_2:

$$\left.\begin{array}{l} \mathcal{H}=\mathcal{H}_0+\alpha\mathcal{H}_1 \\ S=S_0+\alpha S_1+\alpha^2 S_2+\cdots \\ \mathcal{H}^*=\mathcal{H}_2^*+\alpha\mathcal{H}_1^*+\alpha^2\mathcal{H}_2^*+\cdots \end{array}\right\} \qquad (9.119)$$

We want an identity transformation for $\alpha=0$; therefore,

$$S_0=L'l+G'g+H'h \qquad (9.120)$$

We proceed by using expression (9.117) in (9.116) to give

$$\mathcal{H}_0\left(\frac{\partial S}{\partial L}\right)+\mathcal{H}_1\left(\frac{\partial S}{\partial l},\frac{\partial S}{\partial g},\frac{\partial S}{\partial h},l,g\right) \equiv \mathcal{H}_0^*+\mathcal{H}_1^*\left(L',G',H',\frac{\partial S}{\partial G'}\right) \qquad (9.121)$$

If we expand (9.121) into a Taylor series and equate equal powers of α, we have

$$\left.\begin{array}{l} \mathcal{H}_0(L')=\mathcal{H}_0^*(L')=\dfrac{\mu^2}{2L'^2} \\ \dfrac{\partial\mathcal{H}_0}{\partial L'}\dfrac{\partial S_1}{\partial l}+\mathcal{H}_1=\mathcal{H}_1^* \\ \dfrac{\partial\mathcal{H}_0}{\partial L'}\dfrac{\partial S_2}{\partial l}+\dfrac{1}{2}\dfrac{\partial^2\mathcal{H}_0}{\partial L'^2}\left(\dfrac{\partial S_1}{\partial l}\right)^2 \\ \quad+\dfrac{\partial\mathcal{H}_1}{\partial L'}\dfrac{\partial S_1}{\partial l}+\dfrac{\partial\mathcal{H}_1}{\partial G'}\dfrac{\partial S_1}{\partial g}=\mathcal{H}_2^*\dfrac{\partial\mathcal{H}_1^*}{\partial g}\dfrac{\partial S_1}{\partial G} \end{array}\right\} \qquad (9.122)$$

Kozai (1962b) correctly gives the third-order expression.

We now separate $\mathcal{H}_1$ into a part independent of l (called $\mathcal{H}_{1sec}$) and a part dependent on l (called $\mathcal{H}_{1p}$) and then make the association

$$\left.\begin{array}{l} \dfrac{\partial\mathcal{H}_0}{\partial L'}\dfrac{\partial S_1}{\partial l}+\mathcal{H}_{1p}=0 \\ \mathcal{H}_{1sec}=\mathcal{H}_1^* \end{array}\right\} \qquad (9.123)$$

The expression for S_1 obtained from (9.123) can be used in the last line of equation (9.122), again separating the parts dependent on l or not. We obtain a solution for S_2, and so on. Through equations (9.117), we obtain

$$\begin{aligned} l' &= l'(L',G',H',l,g) \\ L &= L(L',G',H',l,g) \end{aligned}$$

and four similar expressions for g',h',L,H. These expressions must be inverted to obtain

$$\left.\begin{aligned} l &= l(L',G',H',l',g') \\ L &= L(L',G',H',l',g') \end{aligned}\right\} \quad (9.124)$$

which is accomplished by Taylor expansion to the desired order and is very tedious.

The Lie-Hori method is developed along somewhat different lines. Hori (1966) considered a transformation from p,q to P,Q given by

$$\left.\begin{aligned} p_i &= P_i + \frac{\partial S}{\partial Q_i} + \frac{1}{2}\left[\frac{\partial S}{\partial Q_i}, S\right] + \cdots \\ q_i &= Q_i - \frac{\partial S}{\partial P_i} - \frac{1}{2}\left[\frac{\partial S}{\partial P_i}, S\right] + \cdots \end{aligned}\right\} \quad (9.125)$$

where $[a,b]$ are Poisson brackets. In this notation, any function can be written

$$f(p,q) = f(P,Q) + [f,S] + \frac{1}{2}\left[[f,S],S\right] + \cdots \quad (9.126)$$

The canonical equations are

$$\left.\begin{aligned} dP_i/dt &= \partial\mathcal{H}^*/\partial Q_i \\ dQ_i/dt &= -\partial\mathcal{H}^*/\partial P_i \end{aligned}\right\} \quad (9.127)$$

We further assume that S and $\mathcal{H}$ can be written in terms of a small parameter

$$\left.\begin{aligned} S &= S_1 + S_2 + \cdots \\ \mathcal{H}^* &= \mathcal{H}_1^* + \mathcal{H}_2^* + \cdots \end{aligned}\right\} \quad (9.128)$$

If a parameter τ defined by

$$\left.\begin{aligned} dP_i/d\tau &= \partial\mathcal{H}_0/\partial Q_i \\ dQ_i/d\tau &= -\partial\mathcal{H}_0/\partial P_i \end{aligned}\right\} \quad (9.129)$$

is eliminated from $\mathcal{H}^*$, we have

$$\left.\begin{aligned} \mathcal{H}_0^* &= \text{const} \\ \mathcal{H} &= \text{const} \end{aligned}\right\} \quad (9.130)$$

This development led Hori to the following formulas:

$$\left.\begin{aligned} \mathcal{H}_0^* &= \mathcal{H}_0 \\ \mathcal{H}_1^* &= \mathcal{H}_{1\text{sec}} \\ S_1 &= \int \mathcal{H}_{1p}\, d\tau \\ \mathcal{H}_2^* &= \mathcal{H}_{2\text{sec}} + \frac{1}{2}[\mathcal{H}_1 + \mathcal{H}_1^*, S_1]_{\text{sec}} \\ S_2 &= \int\left(\mathcal{H}_{2p} + \frac{1}{2}[\mathcal{H}_1 + \mathcal{H}_1^*, S_1]_p\right) d\tau \end{aligned}\right\} \quad (9.131)$$

Here we designate the subscripts sec and p to mean the parts independent of and dependent on l, respectively, as in the Von Zeipel method. These formulas are given by Aksnes (1970).

The Lie-Hori method has a number of advantages. The transformation is completely in terms of the new variables, and no inversion of series is necessary. The formulas are all canonically invariant, so they hold for any canonical variables. Aksnes could then make two fundamental advances in the treatment of oblateness perturbations. First, he chose as an intermediate orbit a precessing ellipse that incorporated all the first-order secular terms and most of the periodic terms. That is to say, in the analogous process of finding $\partial\mathcal{H}/\partial q_i$, he discovered another solution, q^0, p^0, that included a part of the disturbing function instead of a Kepler ellipse. Second, with a canonically invariant formulation, he employed appropriate variables. For long-period and secular effects, Delaunay variables were used. The results agree with the Von Zeipel method. For short-period perturbations, Hill variables were used, a procedure that eliminates the difficulty with small eccentricities.

The first-order determining functions for the Lie-Hori and the Von Zeipel methods are the same, as can be seen by comparing the defining equations or the results (Kozai, 1962b; Aksnes, 1970). In fact, this must be

so because both formulations work for Delaunay variables and have been shown to be equivalent. Therefore, the first-order perturbations are the same.

Space does not permit us to give a more detailed account of this beautiful theory or the detailed formulas, for which we refer the reader to Aksnes (1970).

We summarize the status of oblateness perturbations:

(1) Two complete second-order developments, one by the Von Zeipel method (Kozai, 1962b) and the other by the Lie-Hori method, have been compared. For short-periodic perturbations, the agreement is 10 cm. The secular rates predicted by the two theories can be reconciled to within their given accuracy (Aksnes, 1972).

(2) The second-order development of Aksnes has the advantages of compactness and efficiency of computation, and no singularity for small eccentricity. The small-eccentricity problem is avoided by the use of Hill variables.

(3) For long-period and secular perturbations to 10 cm, further work is necessary. Terms in J_2J_3, J_2J_4, etc. must be included, as well as interaction with all other forces—lunar and solar effects, tesseral harmonics, drag, and radiation pressure.

We cannot give the complete set of formulas, but we present the first-order periodic and second-order secular perturbations as developed by Aksnes (1970), although we have dropped the primes:

$$\Delta\dot{r} = (-\gamma G^3/2\mu r^2)\left[s^2 \sin 2u - \frac{1}{8} D\, s^2 e \sin (2u-v) \right]$$

$$\Delta r = (\gamma G^2/4\mu)\left[1-3c^2+s^2\cos 2u - \frac{1}{4} D\, s^2 e \cos (2u-v) \right]$$

$$\Delta G = (\gamma G/4)\left[3s^2 e \cos (2u-v) + s^2 e \cos (2u+v) - \frac{1}{4} D\, s^2 e^2 \cos (2u-2v) \right]$$

$$\Delta u = (-\gamma/4)\left\{ (2-12c^2)\, e \sin v - \frac{1}{8}(4+D\,e^2)\, s^2 \sin 2u - (2-5c^2 + \frac{1}{2} D s^2)\, e \sin (2u-v) + c^2 e \sin (2u+v) - \frac{1}{4}[D - D^{(1)} s^2]\, c^2 e^2 \sin (2u-2v) \right\}$$

$$\Delta h = (-\gamma c/4)\left\{ 6e \sin v - 3e \sin (2u-v) - e \sin (2u+v) + \frac{1}{4}[D - D^{(1)} s^2] e^2 \sin (2u-v) \right\}$$

where

$$D = (1-15c^2)/(1-5c^2)$$

$$D^{(1)} = \partial D/\partial c^2$$

$$c = \cos I$$

$$s = \sin I$$

$$\gamma = J_2/a^2\eta^4$$

$$\eta^2 = 1-e^2$$

The secular rates can be obtained from letting

$$g_{21} = -\frac{3}{4}\gamma(1-5c^2) - \frac{1}{64}\gamma^2 (41+30c^2-135c^4)$$

$$g_{32} = -\frac{3}{16} c[8\gamma + \gamma^2 (7-33c^2)]$$

with

$$\gamma_4 = J_4/J_2^2$$

$$\dot{M} = n + \frac{3}{128} n\gamma^2\eta[8(1-6c^2+5c^4) - 5(5-18c^2+5c^4)\, e^2 - 15\,\gamma_4 (3-30c^2+35c^4)\, e^2]$$

$$\dot{\omega} = \dot{g} + g_{21}(\dot{g}+\dot{M}) = -\frac{1}{128} n\gamma^2[44-300c^4 + (75-378c^2+135c^4)\, e^2 + 60\,\gamma_4 (3-36c^2+49c^4) + 135\,\gamma_4 (1-14c^2+21c^4)\, e^2]$$

$$\dot{\Omega} = \dot{h} + g_{32}(\dot{\omega}+\dot{M})$$

$$h = \frac{3}{32} nc\gamma^2[2-10c^2-(9-5c^2)\, e^2 - 5\gamma_4 (3-7c^2)\,(2+3e^2)]$$

As was discussed in section 9.4.1.5, periodic perturbations for J_2 were developed by using computer algebra. The expressions were employed in orbit computation, and the orbital fits were identical. This agreement validates both sets of formulas since they are based on quite different methods. The mean elements in the two developments are different by factors of order J_2. Aksnes (1970) has given the formulas relating the two theories and a numerical verification. If we let a subscript 0 designate the Von Zeipel element, then the elements of a, e, I are related by

$$
\begin{aligned}
1/a &= (1/a_0)\left\{1-\frac{1}{2}\eta_0\gamma_0(1-3\cos^2 I_0)\right. \\
&\quad +\frac{1}{32}\eta_0\gamma_0^2[1+6\eta_0-(6+36\eta_0)\cos^2 I_0 \\
&\quad \left.+(45+54\eta_0)\cos^4 I_0]+\cdots\right\} \\
G &= G_0\left[1+\frac{1}{4}\gamma_0(1-3\cos^2 I_0)\right]+\cdots \\
\cos I &= \cos I_0=\left[1+\frac{3}{4}\gamma_0(1-\cos^2 I_0)\right]+\cdots \\
\eta^2 &= 1-e^2 \\
G^2 &= \eta^2\,\mu a \\
\gamma &= J_2/a^2\,\eta^4
\end{aligned}
$$

9.4.1.9 Atmospheric Drag and Radiation Pressure

For several reasons, atmospheric drag and radiation pressure are treated by different methods than are gravitational perturbations. First, they are not conservative forces derivable from a potential function. Second, they involve considerably more unknowns. Whereas the geopotential may be considered unknown and require improvement, we can assume that the main field is constant in time, that tidal variations are known, and that the geopotential has a known mathematical and physical form. Similarly, for lunar and solar perturbations, we assume sufficient knowledge of the mass and position of the Moon and the Sun. With drag and radiation pressure, we are in a much less favorable position. In drag perturbations, the atmospheric density is critical; it has been studied extensively from its orbital effects. The parameters controlling density variations are becoming known, and one can probably predict a posteriori the mean-density structure to within a factor of 2. However, the satellite aspect and the drag coefficient must also be known. Radiation-pressure effects involve similar problems: What is the value of the solar constant and is it constant? How much is diffuse and how much specular reflection? How do the reflective properties change with time? How variable is the albedo radiation? How does the satellite aspect change? And how is the boundary of the Earth's shadow defined? For some satellites, this information is available, though difficult to obtain. Some of these questions are subjects of current research.

The following treatment of radiation pressure developed by Kozai (1963c) and extended by Lála (1968, 1971) and Lála and Sehnal (1969) assumes, for one revolution, the following: (1) the satellite is spherical, with constant reflective properties; (2) the solar parallax can be neglected; (3) the solar flux is constant; and (4) there is no albedo radiation.

The natural vehicle for treating forces directly is the Lagrange planetary equations in Gaussian form (9.42). The forces are expressed as

$$
\left.
\begin{aligned}
S &= n^2a^3\,F\,S(v) \\
T &= n^2a^3\,F\,T(v) \\
W &= n^2a^3\,F\,W
\end{aligned}
\right\} \qquad (9.132)
$$

where

$$F=(A/M)\,(K/GM)\approx 0.5\times 10^{-4}\,(A/M)$$

with A (area)/M (mass) in $\mathrm{cm^2\,g^{-1}}$. We have

$$
\begin{aligned}
S(v) = &-\cos^2(I/2)\cos^2(\epsilon/2)\cos(\lambda_\odot-L-\Omega) \\
&-\sin^2(I/2)\sin^2(\epsilon/2)\cos(\lambda_\odot+\Omega-L) \\
&-\frac{1}{2}\sin I\sin\epsilon\,[\cos(\lambda_\odot-L) \\
&-\cos(-\lambda_\odot-L)\,] \\
&-\sin^2(I/2)\cos^2(\epsilon/2)\cos(\Omega-\lambda_\odot-L) \\
&-\cos^2(I/2)\sin^2(\epsilon/2)\cos(-\lambda_\odot-L-\Omega)
\end{aligned}
\qquad (9.133)
$$

$$\begin{aligned}\Gamma(v) = &-\cos^2(I/2)\cos^2(\epsilon/2)\sin(\lambda_\odot - L - \Omega) - \sin^2(I/2)\cos^2(\epsilon/2)\sin(\lambda_\odot + \Omega - L)\\ &-\frac{1}{2}\sin I \sin\epsilon[\sin(\lambda_\odot - L) - \sin(-\lambda_\odot - L)]\\ &-\sin^2(I/2)\cos^2(\epsilon/2)\sin(\Omega - \lambda_\odot - L) - \cos^2(I/2)\sin^2(\epsilon/2)\sin(-\lambda_\odot - L - \Omega) \qquad (9.134)\end{aligned}$$

$$W = \sin I\cos^2(\epsilon/2)\sin(\lambda_\odot - \Omega) - \sin I\sin^2(\epsilon/2)\sin(\lambda_\odot + \Omega) - \cos I\sin\epsilon\sin\lambda_\odot \qquad (9.135)$$

where $L = v + \omega$, $\lambda_\odot$ = the longitude of the Sun, and ϵ = the obliquity. We have the LPE

$$\left.\begin{aligned}&\frac{da}{dt} = \frac{2na^3}{(1-e^2)^{1/2}}F\left[S(v)\,e\sin v + T(v)\frac{p}{r}\right] \qquad p = a(1-e^2)\\ &\sin I\frac{d\Omega}{dt} = \frac{na^2}{(1-e^2)^{1/2}}WF\frac{r}{a}\sin L \qquad \frac{dI}{dt} = \frac{na^2}{(1-e^2)^{1/2}}WF\frac{a}{r}\cos L\\ &\frac{de}{dt} = na^2(1-e^2)^{1/2}F\left\{S(v)\sin v + T(v)\left[\cos v + \frac{1}{e}\left(1 - \frac{r}{a}\right)\right]\right\}\\ &\frac{d\omega}{dt} = -\cos I\frac{d\Omega}{dt} + na^2\frac{(1-e^2)^{1/2}}{e}F\left[-S(v)\cos v + T(v)\left(1 + \frac{r}{p}\right)\sin v\right]\\ &\frac{dM}{dt} = n - 2a^2FS(v)\frac{r}{a}n - (1-e^2)^{1/2}\left(\frac{d\omega}{dt} + \cos I\frac{d\Omega}{dt}\right)\end{aligned}\right\} \qquad (9.136)$$

Since radiation pressure is a discontinuous force, it is difficult to obtain analytical solutions for it. Two approaches have been used successfully. The first, by Kozai (1963c), is to determine numerically the time of shadow exit E_1 and shadow entry E_2 in terms of the eccentric anomaly. Then, by assuming everything else constant for one revolution, Kozai obtains the following first-order perturbations after one revolution, where $S = S(0)$, $T = T(0)$ are written for their values at $L = \omega$:

$$\left.\begin{aligned}&\delta a = 2a^2F\Big|[S\cos E - T(1-e^2)^{1/2}\sin E]\Big|_{E_1}^{E_2}\\ &\delta e = a^2F(1-e^2)^{1/2}\left[\left|\frac{1}{4}S(1-e^2)^{1/2}\cos 2E + T\left(-2e\sin E + \frac{1}{4}\sin 2E\right)\right|_{E_1}^{E_2} + \frac{3}{2}\int T\,dE\right]\\ &\delta I = a^2F\frac{W}{(1-e^2)^{1/2}}\left\{\left|\left[(1+e^2)\sin E - \frac{e}{4}\sin 2E\right]\cos\omega\right.\right.\\ &\qquad\left.\left. + (1-e^2)^{1/2}\left(\cos E - \frac{e}{4}\cos 2E\right)\sin\omega\right|_{E_1}^{E_2} - \frac{3}{2}e\int\cos\omega\,dE\right\}\\ &\sin I\,\delta\Omega = a^2F\frac{W}{(1-e^2)^{1/2}}\left\{\left|\left[(1+e^2)\sin E - \frac{e}{4}\sin 2E\right]\sin\omega\right.\right.\\ &\qquad\left.\left. - (1-e^2)^{1/2}\left(\cos E - \frac{e}{4}\cos 2E\right)\cos\omega\right|_{E_1}^{E_2} - \frac{3}{2}e\int\sin\omega\,dE\right\}\\ &\delta\omega = -\cos I\,\delta\Omega + a^2F\frac{(1-e^2)^{1/2}}{e}\left[\left|S\left(e\sin E + \frac{1}{4}\sin 2E\right)\right.\right.\\ &\qquad\left.\left. + \frac{T}{(1-e^2)^{1/2}}\left(e\cos E - \frac{1}{4}\cos 2E\right)\right|_{E_1}^{E_2} - \frac{3}{2}\int S\,dE\right]\\ &\delta M = -\frac{3}{2}\int_0^{2\pi}\frac{\delta a}{a}dM - (1-e^2)^{1/2}\,\delta\omega - (1-e^2)^{1/2}\cos I\,\delta\Omega - 2a^2F\\ &\qquad\left\{\left|S\left[(1+e^2)\sin E - \frac{e}{4}\sin 2E\right]\right.\right.\\ &\qquad\left.\left. - T(1-e^2)^{1/2}\left(\cos E - \frac{e}{4}\cos 2E\right)\right|_{E_1}^{E_2} - \frac{3}{2}e\int S\,dE\right\}\end{aligned}\right\} \qquad (9.137)$$

If the satellite does not enter the shadow, then the terms evaluated at E_1 and E_2 vanish. How the perturbations after part of a revolution can be computed is obvious. These expressions provide the differential equations to be integrated for mean elements—that is, $d\bar{a}/dt = \delta a/\delta t = n\delta a$, and so on. This is the method used to calculate the long-term effects due to radiation pressure in the determination of zonal harmonics and tidal parameters. In addition, one can determine quite reasonable mean reflectivities for the satellites.

An alternative approach was taken by Lála (1968, 1971) and Lála and Sehnal (1969). They developed the shadow function in Fourier series in E and found solutions for the periodic perturbations. They required 36 terms in the development to obtain agreement with the above special perturbation formulas. These periodic perturbations were formally integrated. For further details, the reader is referred to the Lála and Sehnal papers.

The development of drag perturbations by Sterne (1959) follows the same lines. Assuming a rotating atmosphere with an oblate planet, he considers the drag force per unit mass

$$\frac{1}{2}C_D\frac{A}{M}\rho V^2 \tag{9.138}$$

where C_D is a drag coefficient, A/M is the area-to-mass ratio, ρ is the atmospheric density, and V is the satellite velocity with respect to the atmosphere. Now, C_D, A/M, and ρ are all difficult to know. Sterne adopts $C_D \approx 2.2$. If precise values of A/M are not known, then the average A is taken as one-fourth the total surface area. He then gives the forces acting on the satellite as

$$\begin{bmatrix} S \\ T \\ W \end{bmatrix} = \begin{bmatrix} \dot{r} \\ r\dot{v} - \dot{\theta} r \cos I \\ \dot{\theta} r \sin I \cos (v+\omega) \end{bmatrix} \tag{9.139}$$

and after calculation, the velocity as

$$V = \left(\frac{\mu}{a}\right)^{1/2}\left(\frac{1+e\cos E}{1-e\cos E}\right)^{1/2}\left(1 - d\frac{1-e\cos E}{1+e\cos E}\right) \tag{9.140}$$

where

$$d = \frac{\dot{\theta}}{n}(1-e^2)^{1/2}\cos I \tag{9.141}$$

and the forces per unit mass are

$$\begin{bmatrix} S \\ T \\ W \end{bmatrix} = \frac{1}{2}C_D\frac{A}{M}\rho\, aV \begin{bmatrix} e\sin E\,\dot{E} \\ -(1-e^2)^{1/2}\left[1 - d\frac{(1-e\cos E)^2}{1-e^2}\right]\dot{E} \\ -\frac{\dot{\theta}}{n}(1-e\cos E)^2 \sin I \cos (v+\omega)\dot{E} \end{bmatrix} \tag{9.142}$$

With these equations, the LPE can be integrated numerically. Alternatively, if we can specify how C_D, A/M, and ρ vary, we could attempt a formal solution. We make the analogous solution to that for radiation pressure, assuming C_D and A/M constant, and obtain formal quadrature formulas for the perturbations after one revolution. These formulas are given in the inset on page 855. We see from the last two expressions of (9.143) that the direct perturbation in $M+\omega$ is quite small, the major change in M coming from

$$\delta n = (-3n/2a)\ \delta a$$

These expressions are used with numerical quadrature to obtain the evolution of mean elements. The implementation is done by Slowey (1974) for studying drag. Alternatively, taking Jacchia's (1960, 1964) density model, Sehnal and Mills (1966) have developed ρ in harmonic functions and obtained formulas for the periodic terms. These are sometimes used in analyses of satellite orbits. However, since for geodetic satellites the short-period drag terms are always less than 1 m, we can ignore them. The secular part is more conveniently absorbed in some constants of our orbital model. Therefore, the principal use of these formulas is in the

$$
\begin{aligned}
\delta a &= -C_D \frac{A}{M} a^2 \int_0^{2\pi} \rho(E) \frac{(1+e\cos E)^{3/2}}{(1-e\cos E)^{1/2}} \left(1 - d\frac{1-e\cos E}{1+e\cos E}\right)^2 dE \\
\delta e &= -C_D \frac{A}{M} \frac{(1-e^2)^{1/2} a}{2\pi} \int_0^{2\pi} \rho(E) \left(\frac{1+e\cos E}{1-e\cos E}\right)^{1/2} \left(1 - d\frac{1-e\cos E}{1+e\cos E}\right) \\
&\quad \left[\cos E - \frac{d}{2(1-e^2)}(1-e\cos E)(2\cos E - e - e\cos^2 E)\right] dE \\
\delta I &= \frac{1}{8\pi} C_D \frac{A}{M} \frac{a}{n} \dot{\theta} \sin I \frac{1}{(1-e^2)^{1/2}} \int_0^{2\pi} \rho(E)\,(1-e\cos E)^{1/2}\,(1+e\cos E)^{1/2} \\
&\quad \times \left(1 - d\frac{1-e\cos E}{1+e\cos E}\right)\left[1 + \cos 2\omega \frac{(2-e^2)\cos^2 E - 1 + 2e^2 - 2e - 2e\cos E}{(1-e\cos E)^2}\right] dE \\
\delta\Omega &= -\frac{1}{8\pi} C_D \frac{A}{M} \frac{a}{n} \frac{\dot{\theta} \sin 2\omega}{(1-e^2)^{1/2}} \int_0^{2\pi} \rho(E)\,(\mathrm{v} - e^2\cos^2 E)^{1/2} \\
&\quad \left(1 - d\frac{1-e\cos E}{1+e\cos E}\right)[2e^2 - 1 - 2e\cos E + (2-e^2)\cos^2 E] dE \\
\delta\omega &= -\cos I\, \delta\Omega \\
\delta M &= -(1-e^2)^{1/2}\, d\omega + \int \delta n\, dt
\end{aligned}
\qquad (9.143)
$$

analysis of long-period effects by numerical integration of these mean elements, along the same lines as those used for radiation pressure. In this case, we are able to make a reliable determination of drag factors, which could be systematic errors in the density model, or an estimate of C_D or A/M. These factors are generally between 0.5 and 1.5, which is less than the uncertainty of these parameters.

9.4.1.10 Computer Algebra

A great deal of the analysis used for satellite-perturbation theory involves considerable tedious algebra. One is led to do some of this work on a computer. A major support of the development of analytical theories has been the computer program Smithsonian Package for Algebra and Symbolic Manipulation (SPASM), described by Hall and Cherniack (1969), and Cherniack (1973) has contrasted it with other algebra systems. Since the subject of computer algebra is beyond the scope of this discussion, we confine ourselves to a few remarks and the description of two problems in satellite theory.

Algebra programs perform the elementary operations of addition, multiplication, subtraction, division, differentiation, and integration of a certain class of functions. We can define functions, make substitutions, and truncate on powers of designated parameters. We can examine expressions term by term and parenthesize and expand them. Numerical coefficients are kept as rational numbers where possible. One can read expressions in, print them out, or punch them as FORTRAN cards for subsequent numerical computation. We have two forms of internal representation—expressions and Poisson series. Each has its advantages. An expression may be

$$(ETA**2 - R)/E$$

The Poisson series are of the form

$$\sum A_i \begin{pmatrix} \sin \\ \cos \end{pmatrix} B_i$$

where A_i and B_i are any expressions. All the operations described apply to both expressions and Poisson series.

Poisson series have three advantages: (1) all trigonometric identities are automatically applied; (2) because of the highly structured nature of Poisson series, multi-

plication and addition can be optimized, and further, secondary computer storage can be used for long Poisson series; and (3) the bulk of problems in celestial mechanics is solved by developing the disturbing function in Poisson series and integrating term by term.

In addition to the operations described above, we can convert from expressions to Poisson series, and then back. Great efficiency is gained by judiciously choosing the form. Consider

$$(\cos^{20}x)^{30}-(\cos^{30}x)^{20}$$

As a trigonometric polynomial, this operation is trivial; as a Poisson series, it is not. We have here two very important features of computer algebra: the noncommutativity of operations with respect to time, and intermediate swell. The above expression is obviously zero, but one has two 50-term Poisson series along the way. Neither of these problems occurs in numerical work.

SPASM is 99 percent in FORTRAN; storage management is accomplished with SLIP, which is accessible from FORTRAN programs. We are concerned with the efficiency of SPASM and with the size and speed of the FORTRAN code generated. These are part of the more general problem of expression simplification.

Although general simplification seems to be very difficult, we have had some success with the following approach. We assume that the coefficients of Poisson series can be factored as the product of polynomials. Further, we want to consider the choice of variables. In developing perturbation theories, we convert to Poisson series all angle variables except the inclination. Therefore, we have the side relations

$$\eta^2+e^2=1$$

$$SI^2+CI^2=SIP^2+CIP^2=1$$

where we have substituted SI for sin (I), CI for cos (I), SIP for sin (IP), and CIP for cos (IP). The P designates the primed variables—in this case, the elements of the disturbing body (see sec. 9.4.1.7). We try each substitution, as indicated. It would be more direct to convert each coefficient of the Poisson series to a Poisson series, using $e=\sin\phi$, $\eta=\cos\phi$, in order to obtain all simplifications, and then to convert back to an expression. However, the substitution and the test for length of expression are easily done. We retain the expression that has the fewest terms and remove all common factors. Next, we assume that the remaining expression can be written

$$f\begin{pmatrix} e & SI & eP & SIP \\ \eta & CI & \eta P & CIP \end{pmatrix} = P_e\begin{pmatrix} e \\ \eta \end{pmatrix} P_I\begin{pmatrix} SI \\ CI \end{pmatrix} P_{e'}\begin{pmatrix} eP \\ \eta P \end{pmatrix} P_{I'}\begin{pmatrix} SIP \\ CIP \end{pmatrix}$$

where P_i is just a polynomial. In turn, by setting all the variables but one equal to zero, we obtain each polynomial. The results of factorization are then verified by expanding and subtracting. We have found that in this way we obtain all the simplifications that would have been obtained by hand.

SPASM has been used for a wide variety of problems. We describe here two of particular relevance to satellite theory: development of oblateness perturbations in Delaunay variables by the method of Von Zeipel, and third-body perturbations in Kepler elements by use of LPE.

Von Zeipel's method is described in section 9.4.1.8. Two features can be pointed out. First, once the determining function S is known, the perturbations are obtained by differentiation. Second, the first- and second-order determining functions can be obtained in closed form, as was done by Kozai (1962b) by a change of variable using

$$dv=(1/\eta^3)\ (a/r)^3\,dl$$

Both these operations are within the scope of SPASM, and the problem proved tractable.

The necessity of an accurate theory for J_2 was discussed in section 9.4.1.8. The development by Kozai (1962b) had been used, but

with such a complicated development that further verification was necessary. The details of the work are recounted by Gaposchkin *et al.* (1971, unpublished). The important results are the following:

(1) The problem proved tractable with an algebra program.

(2) The determining function of Kozai (1962b) has been verified, and the problem solved to second order.

(3) The accuracy of the theory and the inversion have been verified against numerical integration. The inversion was checked by use of the numerical inverse from (9.124).

(4) The difficulty with the small eccentricity remains. The third-order periodic perturbations were developed and were shown to contain $1/e$ terms. Numerical tests indicate $1/e^2$ terms in the fourth order. We conclude that this is due to the Delaunay variables we had selected.

(5) The development of computer algebra enabled us to obtain the third-order perturbations in 3 weeks; we would probably not have attempted it by hand.

(6) The perturbation theory was used in the orbit-computation program. The theory of Aksnes (1970) (see sec. 9.4.1.8) was also used; it gave identical results for orbital position, thus verifying both developments.

The second problem attempted is the perturbation due to a third body. In this case, we start with equation (9.89) (sec. 9.4.1.7 analytically develops that expression). Using the algebra program, we now determine $1/\Delta$ by analytical inversion. The basic idea, due to Broucke (1971), allows the inversion of invertible expressions; that is,

$$(E)^{-a/b}=Z$$

An iterative scheme is developed, with each iterant

$$Z_{n+1}-Z_n=\Delta Z_n=-\frac{a}{b}(EZ_n^{b/a}-1)\,Z_n$$

This is enormously powerful. Since we can invert any expression without division, it is applicable to computers without a divide instruction. In the case of lunar perturbations, we have $a/b=\frac{1}{2}$, where

$$E=(\bar{X}-Y)\cdot(\bar{X}-\bar{Y})$$

Here, $\bar{X}$ is the position of the satellite, and Y is the position of the Moon. We have

$$\bar{X}=r\begin{bmatrix}\cos u\cos\Omega-\sin u\sin\Omega\cos I\\ \cos u\sin\Omega+\sin u\cos\Omega\cos I\\ \sin u\sin I\end{bmatrix}$$

A similar expression for Y uses r', u', Ω', I'. With this expression, we perform the analytical inversion, starting with Z_0-1/r' and truncating on r^3. We have a simple check: The r/r'^2 are all canceled by the $(X\cdot Y)/|Y|^3$ term. The effects of body tides are easily introduced at this point by the substitution

$$r^n\rightarrow r^n+k_n\frac{a_e^{2n+1}}{r^{n+1}}$$

Next, the expressions are expanded with use of Hansen coefficients as described in section 9.4.1.5. The resulting expressions are then put in the LPE and integrated on the assumption that the angular variables, except the inclinations, have a linear change with time. The resulting expressions are simplified as described above.

In conclusion, we can say that computer algebra has been a successful tool for satellite-dynamics problems. It balances efficiency and expediency. The lunar perturbations were being used in the orbit computation program a month after the work started with SPASM, and we developed the third-order perturbation due to J_2 in 3 weeks. We can develop even more efficient programs by careful analysis (cf. formulas of Kozai (1962b) and Aksnes (1970)).

9.4.1.11 Orbit Determination and Parameter Estimation

The elaboration of an orbital theory, the main objective of the preceding sections, is but one of the four aspects of using satellite-tracking data to obtain ephemerides and

other information. We also have the data reduction, the relation between the observations and the parameters sought, and the estimation procedure.

We adopt Kepler elements as the orbital parameters to be determined. However, we choose to determine n, the mean motion, rather than a, as n is the best known of the orbital parameters. In addition, we recognize that the coefficients of the gravitational field and the nongravitational forces are imperfectly known, thus introducing model errors. We can reduce these errors to some extent by determining secular rates for each of the elements. Therefore, the uncertainty in the orbital model will be limited to the short-period perturbations.

The polynomial representations of the elements account for the bulk of the nongravitational forces, including the long-period effect of gravitational perturbations. The polynomials (mean elements) can be analyzed to obtain the zonal harmonics of the gravity field, some long-term resonant terms, and the reflective and drag properties of the satellites.

The basic relation used here is

$$\left.\begin{aligned} \bar{\rho} &= \bar{r} - R \\ \dot{\bar{\rho}} &= \frac{d}{dt}\bar{\rho} = \dot{\bar{r}} - \dot{R} \end{aligned}\right\} \quad (9.144)$$

where $\bar{\rho}$ is the topocentric station-to-statellite vector, $\bar{r}$ is the satellite position, and R is the station position. It is convenient to use this equation in the orbital system; therefore, R is given by (9.7) and $\bar{r}$ by (9.17). We generally observe $A\bar{\rho}$, where A is a transformation matrix. So we have

$$\mathcal{O} = \text{observation} = A\bar{\rho} = A\bar{r} - AR \quad (9.145)$$

In principle, any parameter that enters (9.145) can be determined from the observations, but it may not be unique.

There are basically four distinct types of observation to be considered: (1) optical directions given in a celestial reference frame (e.g., Baker-Nunn data); (2) direction observations in a topocentric reference frame (e.g., MINITRACK); (3) range observations (e.g., laser); and (4) range-rate observations (e.g., TRANET Doppler). The transformations for each type are as follows:

(1) Right ascension and declination:

$$\begin{bmatrix} \Delta\delta \\ \cos\delta\,\Delta\alpha \end{bmatrix} = \begin{bmatrix} -\cos\alpha\sin\delta & -\sin\alpha\sin\delta & \cos\delta \\ -\sin\alpha & \cos\alpha & 0 \end{bmatrix} \overline{\Delta\rho}$$

(2) Altitude (a), azimuth (A_z), range (ρ) are given in the inset below with ϕ, λ as the latitude and longitude of the observer, and ρ_x, ρ_y, ρ_z as the components of $\bar{\rho}$.

(3) Range:

$$\Delta\rho = \hat{\rho}\cdot\overline{\Delta\rho} = (\bar{\rho}/|\bar{\rho}|)\,\overline{\Delta\rho}$$

(4) Range rate:

$$\Delta\dot{\rho} = \hat{\rho}\cdot\overline{\Delta\dot{\rho}}$$

The domain of parameters to be determined can be expanded to include gravitational coefficients, station coordinates, GM, a scale factor for all stations, and the position of the Earth's pole of rotation. For unique

$$\begin{bmatrix} da \\ -\cos a\; d(A_z) \\ \dfrac{d\rho}{\rho} \end{bmatrix} = \left\{ \begin{bmatrix} -\sin A_z \sin a & -\cos A_z \sin a & \cos a \\ \cos A_z & \sin A_z & 0 \\ \rho_x/\rho & \rho_y/\rho & \rho_z/\rho \end{bmatrix} \begin{bmatrix} -\sin(\lambda+0) & \cos(\lambda+0) & 0 \\ -\cos(\lambda+0)\sin\phi & -\sin(\lambda+0)\sin\phi & \cos\phi \\ \sin(\lambda+0)\cos\phi & \sin(\lambda+0)\cos\phi & \sin\phi \end{bmatrix} \right\} \overline{\Delta\rho}$$

and meaningful results to be obtained, several orbits may have to be combined. This is most conveniently done by dealing with normal equations, which will be discussed later.

If we wish to determine any parameter p_i from observations, we use our elaborated theory for $\bar{r}$ and our initial estimate for p, p_i^0 and compute

$$C = A\bar{\rho} \qquad (9.146)$$

In general, the dependence of C on p_i is nonlinear and we must linearize. We want to find a correction to p_i that will reduce the difference between O and C; that is,

$$O - C = (\partial/\partial p_i) A\bar{\rho}\Delta p_i \qquad (9.147)$$

Now if A can be determined from the observation, we need only $\partial\bar{\rho}/\partial p_i$. For range rate, A depends on p_i, and the expressions are more involved. For those parameters influencing C through the orbit, we obtain

$$\frac{\partial\bar{r}}{\partial p_i} = \frac{\partial\bar{r}}{\partial\omega}\frac{\partial\omega}{\partial p_i} + \frac{\partial\bar{r}}{\partial\Omega}\frac{\partial\Omega}{\partial p_i} + \frac{\partial\bar{r}}{\partial I}\frac{\partial I}{\partial p_i} + \frac{\partial\bar{r}}{\partial e}\frac{\partial e}{\partial p_i} + \frac{\partial\bar{r}}{\partial M}\frac{\partial M}{\partial p_i} - \frac{2}{3}\frac{a}{n}\frac{\partial\bar{r}}{\partial a}\frac{\partial n}{\partial p_i}$$

Now, from Izsak (1962) and Gaposchkin (1966*a*, p. 107), we have

$$\partial\bar{r}/\partial\omega = \hat{e}_n \times \bar{r}$$

$$\partial\bar{r}/\partial\Omega = \hat{e}_z \times \bar{r}$$

$$\partial\bar{r}/\partial I = r \sin u \hat{e}_n$$

$$\partial\bar{r}/\partial e = (\hat{e}_n \times \bar{r})\ (a/r)\ [\sin E/(1-e^2)^{1/2}] - \bar{a}$$

$$\partial\bar{r}/\partial M = 2\pi\bar{r}/n$$

$$\partial\bar{r}/\partial a = \bar{r}/a$$

where

$$u = v + \omega$$

$$\hat{e}_n = \begin{bmatrix} \sin I \sin\Omega \\ -\sin I \cos\Omega \\ \cos I \end{bmatrix}$$

$$\hat{e}_z = \begin{bmatrix} 0 \\ 0 \\ 1 \end{bmatrix}$$

expressed in the orbital system. For example, if $p_i = \omega_0$, the constant of perigee is then $\partial\omega/\partial p_i = 1$, the other being zero. If $p_i = \bar{C}_{lm}$, then with $C_{lm} = 1$

$$\partial\omega/\partial C_{lm} = \sum_p \sum_q \Delta\omega_{lmpq}$$

$$\partial\Omega/\partial C_{lm} = \sum_p \sum_q \Delta\Omega_{lmpq}$$

and so on. If $p_i = GM$, then

$$\partial\bar{r}/\partial(GM) = \frac{1}{3}\bar{r}/GM$$

If we want to determine station coordinates, we have

$$R = R_3(-\theta)\, R(y,x,0)\, X_0$$

giving

$$\left[\left[\frac{\partial\bar{\rho}}{\partial X}\right], \left[\frac{\partial\bar{\rho}}{\partial Y}\right], \left[\frac{\partial\bar{\rho}}{\partial Z}\right]\right] = -R_3(-\theta)\, R(y,x,0) \begin{bmatrix} 1 & 0 & 0 \\ 0 & 1 & 0 \\ 0 & 0 & 1 \end{bmatrix}$$

If we want a scale factor α for all stations—that is, $\overline{\Delta R} = \alpha\bar{R}_0$—we have

$$\partial\bar{\rho}/\partial\alpha = -R_3(-\theta)\, R(y,0)\, X_0$$

To determine the polar motion, we have

$$\frac{\partial\bar{\rho}}{\partial y}\begin{bmatrix} \sin\theta Z_0 \\ -\cos\theta Z_0 \\ Y_0 \end{bmatrix}$$

$$\frac{\partial\bar{\rho}}{\partial x}\begin{bmatrix} \cos\theta Z_0 \\ \sin\theta Z_0 \\ -X_0 \end{bmatrix}$$

If we have the instantaneous coordinate

$$R=\begin{bmatrix} X \\ Y \\ Z \end{bmatrix}$$

of the station, then

$$X_0 = X\cos\theta + Y\sin\theta$$

$$Y_0 = -X\sin\theta + Y\cos\theta$$

$$Z_0 \approx Z$$

The data reduction falls into two parts: those reductions necessary for all data, and those related to particular data types.

All data must be expressed in the same time system. For orbital computation, we need a uniform time system, and so we have chosen AS, an atomic time system, as a standard. The differences between AS and A3 and between AS and A1 are

$$\text{AS} - \text{A1} = 0.8983 \text{ msec}$$

$$\text{AS} - \text{A3} = 35.4 \text{ msec}$$

Although these values change slowly, the adopted constants are sufficient for data taken between 1965 and 1971. Numerical values of AS−UTC are given in the form of polynomials and are published (e.g., Gaposchkin, 1972).

We must also know the physical point to be associated with each time. For optical data, the time detected is that of receiving the light. The orbital position corresponds to an earlier time, the difference being the travel time of light. For a flashing-light satellite, the flash times are given at the satellite. Nominal values of range are sufficient for correcting the time associated with the satellite position. With ranging data, we often have the time of firing of the laser—that is, the time of transmission—and therefore the satellite time is later by the travel time. In all cases, we must know precisely what the satellite position time is.

We have a similar situation with the station position. The position of the Earth is a measured quantity given in terms of UT1. We must use the actual value of UT1 to compute the sidereal angle in (9.7). The time associated with the station is the received time for optical observations, but it is the satellite time for range observations. The satellite time corresponds to the average position of the station during the round trip of the signal.

Data from cameras must be reduced to the adopted reference system by use of (9.8). In addition, we must apply annual aberration and parallactic refraction. The first is usually applied during film reduction, and parallactic refraction is computed from

$$\Delta R = [(0.435\times 0.484813\times 10^{-5})/\rho]\,(\tan z/\cos z)\,[1-\exp(-138.5\,\rho\cos z)]$$

where ρ is the topocentric range in megameters, z is the zenith angle, and ΔR is the correction in radians. Now we have

$$\Delta\delta = -\Delta R\cos q$$

$$\Delta\alpha = -\Delta R\sin q/\cos\delta$$

where q is the parallactic angle measured in a positive (clockwise direction) from the object to the great circle through the pole (Veis, 1960, p. 119). This correction is based on standard pressure and temperature. If measured values are available, a better value can be obtained by taking mean nighttime data. A table of corrections is given in Gaposchkin (1972).

For laser range observations, we make a correction for the tropospheric refraction and for the geometry of the satellite. The refraction correction becomes (Lehr, 1972)

$$\Delta r = -\frac{2.238+0.0414\,(P/T)-0.238\,h_s}{\sin\alpha+10^{-3}\cot\alpha}$$

where P is the atmospheric pressure (mb) at the laser station, T is the temperature (K), h_s is the elevation above mean sea level (km), and α is the elevation angle of the satellite. This formula holds true for light

from a ruby laser at 694 nm when the apparent elevation angle is greater than 5°.

The accuracy of data from laser systems is connected with the physical size of the satellite equipped with corner reflectors. Arnold (1972) (unpublished) gives in tabular form a correction to reduce the observed range to the center of mass of the satellite as a function of angle of incidence. By use of these data, all observations by laser systems can be reduced to the center of mass.

Equation (9.147) will, in general, be overdetermined, and so we use the method of least squares to obtain an estimate of the unknowns. The general references are Arley and Buch (1950) and Linnik (1961). By collecting normal equations, we can merge the observations from many orbital arcs.

In the least-squares estimate, the weight or accuracy of each observation must be established a priori. For the estimation process, only the relative accuracy is important; however, one can have greater confidence if the standard error of unit weight comes to be unity.

For the weighting, we assume that the errors are uncorrelated, probably not a bad assumption with data taken over several years. We have given each observation an individual weight, as described in table 9.10.

In addition, where there were more than 30 points in a pass of laser data, 30 points were chosen, evenly distributed through the pass. Some numerical tests indicate this was no worse than if we had averaged the points.

Finally, the process of parameter estimation must be iterative, for two reasons: The model is nonlinear, and gross observation errors must be discarded. On each iteration, the computation discards data on a 3σ criterion; that is, a point is discarded if

$$(O-C)\sqrt{w}>3\sigma \quad .$$

where w is the weight, and σ is the standard deviation at the last iteration. The process is said to converge or stabilize when

$$|(\sigma_n-\sigma_{n-1})/\sigma_n|<0.01$$

9.4.2 Coordinates

(E. M. Gaposchkin, J. Latimer, and G. Veis)

A number of approaches can be used to determine the position of points on the Earth's surface. Of these, we have chosen tracking of close-Earth satellites, deep-space probes, and surface-triangulation measurements for this analysis. The data and the method of analysis have been selected to optimize the results for a global network of reference points.

The satellite methods separate nicely into two distinct types of analysis: geometrical and dynamical. The former hinges on making simultaneous observations of a satellite from two or more points on the earth's surface. When these are camera observations, the vector connecting the two stations must lie in the plane defined by the two observed directions. A number of independent simultaneous observations will define the direction between the two stations. The Smithsonian Astrophysical Observatory (SAO) has obtained a sufficient number of simultaneous observations to determine a network for its stations. The National Ocean Survey (NOS) of the National Oceanic and Atmospheric Administration (NOAA) has carried out a program of observations with the BC–4 camera to establish a global geometrical network.

Alternatively, the dynamical analysis assumes that the satellite's orbit is known, and computes the location of the observing station from individual observations. In practice, the orbit is determined from the same observations. The orbital mode has been used by SAO to analyze tracking data on close-Earth satellites and by the Jet Propulsion Laboratory (JPL) to analyze tracking data on deep-space probes.

Surface-triangulation measurements are reduced by organizations such as the U. S. Coast and Geodetic Survey (now NOS) and the Army Map Service (now DMA/TC), who publish coordinates of given points referred to a datum that, in general, has an arbitrary origin, orientation, and scale. The relative positions of stations are determined from these data.

The main objectives of this analysis were the following:

(1) To improve the accuracy of the fundamental stations. Heretofore (SE II), the accuracy was estimated as 5 to 10 m.

(2) To improve the distribution of reference points or tracking sites. In SE II, coordinates were obtained for 39 independent sites.

(3) To use the latest available data. New data included the complete BC–4 network and all the laser tracking data taken during the International Satellite Geodesy Experiment (ISAGEX) program. Surface-triangulation data were used as observations rather than as constraints.

The analysis assumes that the stations form a fixed system (i.e., there is no relative motion), that the pole position and the instantaneous position of the Earth are known without error from numerical values published by the International Polar Motion Service (IPMS) and the Bureau International de l'Heure (BIH), that the error in observing time is random, and that Atomic Time is a satisfactory system for ephemeris calculations.

9.4.2.1 Geometrical Solution

In deriving a geometrical solution, the objective was to produce a system of normal equations for use in combination with other data. The data consisted of direction observations only, and there is no scale information in the geometric net. Nor is there any information to locate the origin of a geometrical network. Hence, any purely geometrical solution with these data would require an arbitrary scale and origin. The combination of normal systems avoids this problem, as other data sets contain scale and origin information. The result of an unscaled, purely geometrical solution is a set of interstation directions, independent of the arbitrary scale and origin introduced.

The computation was divided into two stages. First, all data between pairs of stations were used to determine, by least squares, the interstation direction and its covariance matrix for each pair. The mathematical model for determining this direction uses the condition that the interstation direction (u_3) and the two directions from the stations to the satellite (u_1, u_2) must be coplanar:

$$\hat{u}_1 \cdot \hat{u}_2 \times \hat{u}_3 = 0 \qquad (9.148)$$

A system of first-order Taylor expansion approximations to equation (9.148) is solved by least squares to determine u_3 and its 2×2 covariance matrix. In order for truly simultaneous directions (u_1, u_2) to be obtained, synthetic observations were computed by interpolation from a series of observations overlapping in time from two stations (Aardoom *et al.*, 1966).

The synthetic observations (u_1, u_2) were weighted according to the quadratic fit of the individual observations used to determine the synthetic ones. The weight was modified according to SE II to account for the possibility of systematic errors, principally in station timing. Separate synthetic observations were considered to be uncorrelated. For BC–4 data, the NOS has derived seven simultaneous observations from each photographic plate (event) with the associated 14×14 covariance matrix for each set of directions. These were the data provided and used to determine u_3.

The data were then screened. When the adjustments to u_1 and u_2 (corrections to the observations) were judged to be too large with respect to the remaining data for that interstation direction, those points were deleted and the direction redetermined. For the SAO block, 68 directions were determined, and for the BC–4 group, 152.

The second stage consisted of a network adjustment for each data block. The mathematical model for stage two is that of variation of coordinates:

$$\mathbf{u}_1 - \mathbf{u}_2 - \mathbf{u}_3 = 0$$

where $\mathbf{u}_1$ is the vector from station 1 to the satellite, $\mathbf{u}_2$, is that from station 2 to the satellite, and $\mathbf{u}_3$ is the interstation vector.

Satellite positions are eliminated, and we obtain a solution for station coordinates, thus deriving adjusted interstation directions. This is equivalent to adjusting the directions directly by using the coplanarity condition for each triangle formed by observed directions between three stations. The advantage of this normal system is that it refers to coordinates, not directions, and can be readily combined with other normal systems for station coordinates. These directions are given in table 9.25.

We had available for comparison the interstation directions and their accuracy estimates σ_1^2 resulting from simultaneous-observation data and also the new directions and accuracy estimates σ_2^2 resulting from the network adjustment. Table 9.26b lists σ_1^2, σ_2^2, and the square of the difference δ^2 between the two estimates of the interstation direction.

We expected that, on the average, for the interstation direction adjustment δ,

$$\delta^2 \leq (\sigma_1^2+\sigma_2^2)/2$$

To satisfy this condition, we must multiply the variance estimates by a factor

$$k^2 = \frac{\delta^2}{(\sigma_1^2+\sigma_2^2)/2}$$

From table 9.26b the average value for k^2 is 2.65, and the accuracy estimates for the geometrical solution are scaled by this number. A similar analysis of the BC–4 network (see table 9.26a) gives an average value for k^2 of 2.60.

9.4.2.2 Dynamical Solution

An observation θ of direction, right ascension and declination, or range can be related to the satellite position $\bar{r}(t)$ and to the station position X by

$$\theta = [A]\,[\bar{r}(t) - R(\theta,x,y)\,X] \quad (9.149)$$

In general, A is an easily computed transformation matrix. Further, the orbit $\bar{r}(t)$ depends on the orbital elements, the gravitational field, the atmospheric density, solar and lunar gravitational attraction, and radiation pressure. Finally, equation (9.149) depends on UT1—i.e., the sidereal angle θ—and on the pole position x and y. None of these quantities is known without error and each, in itself, provides a number of difficult problems. For a certain class of satellites, the Earth's gravitational field presents the major source of error but is improved as part of the analysis described above.

Two types of data have been used in the dynamical solution. Observations of direction are made by photographing the satellite against a star background. The star positions then define the direction from the observing station to the satellite in the coordinates of right ascension and declination. The star positions are taken from a catalog and refer to its epoch. Precession and nutation are therefore applied to refer the observation to the reference system desired. For reasons related to the orbital theory for $\bar{r}(t)$, we have chosen to work in the quasi-inertial reference system defined by the equinox of 1950.0 and the equator of date. In addition, UT1 and pole positions are applied to bring the terrestrial reference frame, defined by the Conventional International Origin and the zero meridian of the BIH, into this system. Therefore, orbital elements and station positions are expressed in this quasi-inertial reference system when determined with direction observations. Specifically, the right ascension of the ascending node of the satellite (hereafter called the node) is unambiguously defined.

Observations of range relate the relative position of the satellite to the observer and not to the reference system; i.e., the observation is unchanged if the reference system is transformed by translation or rotation. Specifically, the node is defined only relative to the adopted value of +UT1. Therefore, when only observations of range (and velocity) are used, a correction for the longitude must be allowed for in each orbit. This is accomplished with the following device. In gen-

eral, the normal system for each orbit has the form

$$\begin{Bmatrix} N & B \\ B^T & C \end{Bmatrix} \begin{Bmatrix} \overline{\Delta X} \\ \overline{\Delta p} \end{Bmatrix} = \begin{Bmatrix} \bar{a} \\ \bar{b} \end{Bmatrix} \quad (9.150)$$

where $\overline{\Delta X}$ are the corrections to the station coordinates, and $\overline{\Delta p}$ are the corrections to the orbital elements.

It has been observed that with direction observations, $B \approx 0$, and so the interactions between orbital elements and station coordinates can be ignored. For observations of range, we form the set of reduced normal equations

$$[N - BCB^T]\overline{\Delta X} = \bar{a} - BC\bar{b} \quad (9.151)$$

These equations eliminate the correction $\overline{\Delta p}$ while preserving the interactions between $\overline{\Delta p}$ and $\overline{\Delta X}$. This set of reduced normal equations can be added to another set, and the solution for $\overline{\Delta X}$ can be used to determine $\overline{\Delta p}$ if so desired. The complete set of $\overline{\Delta p}$ was computed and found to be very small. The same device is used in processing simultaneous observations to eliminate the satellite position from each simultaneous observation. In summary, orbits determined by direction observations were processed directly by assuming $B = 0$. Those orbits based primarily on range data were reduced by means of equation (9.151).

9.4.3 Gravitational Field

9.4.3.1 Analysis of Satellite Orbital Data

(E. M. Gaposchkin, M. R. Williamson, Y. Kozai, and G. Mendes)

The external potential of the Earth is represented by a set of orthogonal functions:

$$\mathcal{U} = \mathcal{R}e \frac{GM}{r} \sum_{l=0}^{\infty} \sum_{m=0}^{l} \left(\frac{a_e}{r}\right)^l \bar{C}_{lm} \bar{P}_{lm}(\sin\phi)\, e^{im\lambda} \quad (9.152)$$

where M is the mass of the Earth, including the atmosphere; G is the universal constant of gravitation; $C_{lm} = C_{lm} - iS_{lm}$; $\bar{C}_{l0} = -J_l/\sqrt{2l+1}$; $\mathcal{R}e\ \{\ \}$ designates the real part of $\{\ \}$; $\bar{P}_{lm}(\sin\phi)$ are fully normalized associated Legendre polynomials; and r, ϕ, λ are the coordinates of the test particle. It is possible to choose a coordinate system such that

$$\bar{C}_{2,0} = \bar{C}_{1,1} = \bar{C}_{2,1} = 0 + i0$$

and we assume that the instantaneous spin axis as defined by the International Polar Motion Service and the center of gravity of the Earth are that system. This assumption is not strictly true, but the departures are small and are ignored in this analysis.

It is observed that for the Earth the amplitude of $E(|\bar{C}_{lm}|)$ decreases uniformly according to

$$E(|\bar{C}_{lm}|) = \frac{10^5}{l^2} \quad (9.153)$$

Although for theoretical reasons $E(|\bar{C}_{lm}|)$ must decrease more rapidly than equation (9.153) at some point, and individual coefficients can be arbitrarily large, this rule seems valid throughout the range of l used in this investigation.

We use two types of data on the Earth's gravity field: those derived from gravimeters and those obtained from the motion of artificial satellites. The gravity calculated from the gradient of equation (9.152) is

$$\Delta g = \gamma \mathcal{R}e \sum_{l=2}^{\infty} \sum_{m=0}^{l} (l-1)\left(\frac{a_e}{r}\right)^l \bar{C}'_{lm} \bar{P}_{lm}(\sin\phi)\, e^{im\lambda} \quad (9.154)$$

where $\gamma = GM/r^2$ and $\bar{C}'_{lm}$ are $\bar{C}_{lm}$ modified to accommodate those effects of the reference ellipsoid (or gravity formula) that change the definition of $\bar{C}_{2,0}$, $\bar{C}_{4,0}$, and $\bar{C}_{6,0}$. Comparing equations (9.152) and (9.154) makes it apparent that Δg is more influenced by $\bar{C}_{lm}$ of high degree and order than is $\mathcal{U}$ and that measurements of Δg are more useful for

determining these high-degree and high-order coefficients.

Determination of $\bar{C}_{lm}$ from analysis of satellite observations requires a theory for satellite motion. General solutions for the motion in an arbitrary potential field have not yet been found. We must therefore restrict ourselves to approximate solutions, which are quite sufficient for the following reasons. It is observed that for the Earth, the second-degree zonal harmonic $\bar{C}_{2,0}$ makes the largest contribution to the anomalous potential and is 10^{-3} of the main term. The remaining anomalous potential is 10^{-3} of $\bar{C}_{2,0}$, or 10^{-6} of the main term. Therefore, to calculate the trajectory to 10^{-6} (our objective), we require at least a second-order theory for $\bar{C}_{2,0}$ (i.e., one including $\bar{C}_{2,0}$), but only a first-order linear theory for the remaining $\bar{C}_{lm}$. Although there are notable exceptions—resonances and some zonal harmonics—these considerations provide a workable base.

The Earth's motion is complicated because of precession, nutation, polar motion, and rotation. A convenient reference frame is defined by the stars and, in practice, is defined (imperfectly) in terms of a star catalog at some epoch. On the other hand, in an inertial frame, the Earth's gravity field has a temporal variation that significantly complicates the construction of an analytical theory. For this reason, a compromise quasi-inertial reference frame referred to an equinox (epoch 1950.0) and an equator (epoch of date) has been adopted. Veis (1960a) knew, Kozai (1960) proved, and we have used the fact that this coordinate system minimizes the additional effects required to account for the temporal variations of the gravity field and the noninertial property of the coordinate system.

Accordingly, the determination of $\bar{C}_{lm}$ from analysis of satellite observations uses the elaboration of a satellite perturbation theory. This elaboration is too lengthy to detail here, so we confine ourselves to a few remarks. The perturbation theory is developed by expressing equation (9.152) in terms of satellite coordinates (a, the semimajor axis; e, the eccentricity; I, the inclination; ω, the argument of perigee; Ω, the right ascension of the ascending node; and M, the mean anomaly). If we express equation (9.152) as

$$\mathcal{U}=\sum_{l=0}^{\infty}\sum_{m=0}^{l}\mathcal{U}_{lm} \tag{9.155}$$

we can write

$$\mathcal{U}_{lm}=\mathcal{R}e\sum_{p=0}^{l}\sum_{q=-\infty}^{\infty}\bar{C}_{lm}A_{lmpq}(a,e,I)\,e^{i\psi} \tag{9.156a}$$

where

$$A_{lmpq}(a,e,I)=\frac{GM}{a}\left(\frac{a_e}{a}\right)^l D_{lmp}(I)\,G_{lpq}(e) \tag{9.156b}$$

and

$$\psi=(l-2p)\,\omega+(l-2p+q)\,M+m\,(\Omega-\theta)+(l-m)\,\frac{\pi}{2} \tag{9.156c}$$

These four equations are the exact equivalent of equation (9.152). Expressed in this way, the variables with large secular change (ω, Ω, M) are separated from those with only periodic changes (a, e, I). Therefore, the functions $A_{lmpq}(a,e,I)$ can, with sufficient accuracy, be considered constant. In addition, $G_{lpq}(e)\approx 0(e^{|q|})$. Since satellites of interest have small or modest eccentricity, only a few terms in the sum over q are necessary. The number of terms is selected automatically for each satellite by means of a numerical test; typically, $|q|<5$ is sufficient.

The differential equations relating the disturbing potential and the changes in orbital elements are known as the Lagrange planetary equations, a set of simultaneous ordinary differential equations of the form

$$\frac{d}{dt}\mathcal{E}^k=\mathcal{L}^k(a,e,I)\,\mathcal{U} \tag{9.157}$$

where $\mathcal{E}^k$ is a generic element, $\mathcal{L}^k(a,e,I)$ is a linear differential operator, and $\mathcal{U}$ is the disturbing potential. If we assume that the

interaction of perturbations can be ignored, then we can write

$$\mathcal{E}^k = \mathcal{E}_0^k + \sum_{l=2}^{\infty} \sum_{m=0}^{l} \delta\mathcal{E}_{lm}^k \qquad (9.158)$$

where $\mathcal{E}_0^k$ is the unperturbed element. This is an excellent assumption except for $\bar{C}_{2,0}$. The secular changes in ω, Ω, and M due to $\bar{C}_{2,0}$ interact significantly with all the perturbations, and so for these angles variables, we use

$$\mathcal{E}^k = \mathcal{E}_0^k + \dot{\mathcal{E}}^k t + \sum_{l=2}^{\infty} \sum_{m=0}^{l} \delta\mathcal{E}_{lm}^k \qquad (9.159)$$

Substituting (9.155), (9.156), (9.158), and (9.159) into (9.157), formally expanding the resulting equation, and discarding all interactions on the right-hand side, we obtain

$$\frac{d}{dt}\delta\mathcal{E}_{lm}^k = \mathcal{R}e\, \mathcal{L}^k(a_0,e_0,I_0) \times \sum_{p=0}^{l} \sum_{q=-\infty}^{\infty} \bar{C}_{lm} A_{lmpq}(a_0,e_0,I_0)\, e^{i\psi_0} \qquad (9.160a)$$

where

$$\psi_0 = (l-2p)(\omega_0+\dot{\omega}t) + (l-2p+q)(M_0+nt) + m(\Omega_0+\dot{\Omega}t-\theta) + (l-m)\frac{\pi}{2} \qquad (9.160b)$$

Here, $\dot{\omega}$, n, and $\dot{\Omega}$ are the secular rates of ω, M, and Ω. The rotation of the Earth is sufficiently uniform so that we can write

$$\theta = \theta_0 + \dot{\theta}t \qquad (9.161)$$

Finally, $\delta\mathcal{E}_{lm}^k$ is the perturbation in element $\mathcal{E}^k$ due to the potential coefficient $\bar{C}_{lm}$. Equations (9.160) are now uncoupled differential equations, which can be integrated immediately to

$$\delta\mathcal{E}_{lm}^k = \mathcal{R}e\, \mathcal{L}^k(a_0,e_0,I_0) \sum_{p=0}^{l} \sum_{q=-\infty}^{\infty} \bar{C}_{lm} A_{lmpq}(a_0,e_0,I_0) \frac{e^{i[\psi_0-(\pi/2)]}}{\dot{\psi}_0} \qquad (9.162a)$$

$$\dot{\psi}_0 = (l-2p)\dot{\omega} + (l-2p+q)n + m(\dot{\Omega}-\dot{\theta}) \qquad (9.162b)$$

The general properties of the solution are now apparent. We see that $\dot{\psi}$ can be exactly zero only when $m=0$. Therefore, only even zonal harmonics $\bar{C}_{l0}$ can cause secular perturbations. The period of the periodic terms is given by equation (9.162b), and we see from equation (9.162a) that the longer the period is, the larger the perturbation. Thus, when $m=0$, long-period terms with argument ω, 2ω, 3ω, . . . occur when $q=-1, -2, -3, \ldots$. For nonzonal harmonics, long-period, large-amplitude perturbations arise when $\dot{\psi} \approx 0$. Since $n(\approx 13 \text{ rev day}^{-1}) > \dot{\theta}(\approx 1 \text{ rev day}^{-1}) \gg \dot{\omega}, \dot{\Omega} \propto \bar{C}_{2,0}\, n = 10^{-3}n$, this resonance condition occurs when $n \approx m\dot{\theta}$—that is, when the mean motion n is approximately an integral number (the order m) of revolutions per day. In fact, resonant conditions always exist to some extent. Resonant terms occur in both satellite theory and planetary theory, and there is extensive literature on the subject (e.g., Kaula, 1966b; Hagihara, 1961a), but as yet there is no completely satisfactory treatment. It is true, for example, that a solution such as that employed here by using linearized equations can be invalid for some cases, since the series are not uniformly convergent; fortunately, this does not occur here. The occurrence of resonances between the field of the Earth and a satellite has been viewed as an opportunity to determine particular harmonics to high precision. In fact, some of the low-degree harmonics have been studied extensively with synchronous satellites, and many harmonics of orders 12, 13, and 14 have been determined by SAO and others. Long-period terms in ω, 2ω, 3ω, . . . from the zonal harmonics are resonant perturbations in the sense of the term as discussed here. Satellites with strong resonances interact with the field to $l=35$ and higher. Finally, we have seen that the largest perturbations result when equation (9.162b) is smallest. With $m=0$, the largest terms are for $l-2p+q=0$—that is, there is no dependence on M. Therefore,

long-period terms can be analyzed. For $m \neq 0$, the largest effects are also without M. In this case, the frequency is m oscillations per day, and the first-order term will be the largest. Terms for $m = 8$—that is, eight oscillations per day—become very difficult to determine, and reliable values for $m \geq 10$ can be obtained only by the study of resonances or from terrestrial gravimetry.

The formal theory, equation (9.162), accounts for both resonances and short-period terms. For example, the resonant perturbation in mean anomaly for satellite 5900701 is

$$\delta M = \bar{C}_{11,11}\left\{-1.387\times 10^{2}\cos\left[\frac{2\pi}{35.8}(t-t_0)\right] - 1.798\times 10^{5}\cos\left[\frac{2\pi}{1124.8}(t-t_0)\right]+\cdots\right\} \tag{9.163}$$

with similar terms for $\bar{S}_{11,11}$, $\bar{C}_{12,11}$, ... The 1124-day term is much longer than any span of data for one orbit. Because we have imperfect knowledge of the coefficient $\bar{C}_{11,11}$, the empirically determined orbit will absorb the residual 1124-day term into the mean elements. The mean elements can be analyzed for improvements to the field in the same way as is done for zonal harmonics.

Because most of the zonal harmonics give rise to short-period perturbations, the residuals of individual observations are analyzed to determine these field coefficients. Since we are dealing with instantaneous observations of position, the observation equation is of the form

$$\Delta X = \left(\frac{\partial \bar{r}}{\partial M}\frac{\partial \delta M}{\partial \bar{C}_{lm}} + \frac{\partial \bar{r}}{\partial \omega}\frac{\partial \delta \omega}{\partial \bar{C}_{lm}} + \cdots\right)\Delta \bar{C}_{lm} \tag{9.164}$$

As an example, the perturbations in M for satellite D1D are given on page 868 for only the principal terms, with $m = 1,2$; $l = 3,4,5,6,7,8$. For this satellite, $a = 7614$ km, $e = 0.0843$, and $I = 39°.455$.

Even if we assume the satellite to be a perfect filter, uncontaminated by other model errors, and the tracking data and analysis process to be perfect, we see that with one satellite, we can determine only spectral components that are linear combinations of the gravity field ($\bar{C}_{lm}$) and functions of orbital elements [$A_{lmpq}(a,e,I)$]. From each satellite, we obtain one or two linear combinations of harmonics for l odd and for l even. With additional data, we can only refine the numerical value of these linear combinations. The coefficients of the relations will depend on the orbital elements, so that other linear combinations can be determined only from additional distinct orbits. Generally, this is achieved by selecting satellites with different inclinations, but independent linear relations can also be obtained with changes in eccentricity or semimajor axis.

As the degree increases, the perturbations become negligible, and so the linear relation does not involve an infinite number of parameters. Of course, the spectrum analysis gives both amplitude and phase, or, as generally written, $\bar{C}_{lm}$.

From equation (9.166), we see that one linear combination of $\bar{C}_{3,1}$, $\bar{C}_{5,1}$, $\bar{C}_{7,1}$, . . . can be determined from the -1.001-day period term and another of equal size from the -0.971-day term. The third term is a factor of 10 smaller and will not contribute significantly as an observation equation; there are also many smaller terms. The linear combination of $\bar{C}_{3,2}$, $\bar{C}_{5,2}$, $\bar{C}_{7,2}$, . . . has only one significant spectral component for the -0.327-day period.

The linear relations are not determined with equal accuracy; for example, the resonant harmonics have a very large effect and the spectral component is strongly determined. However, the resonant period is commensurate with the arc length, which will cover only a small number of cycles. This makes it difficult to separate nearly commensurate periods.

If we consider equations (9.162) as expressing the spectral decomposition of the perturbation, we see that each harmonic $\bar{C}_{lm}$ of order m causes the same spectrum of perturbations. Further, the spectrum has several lines close together. With a short

$$
\begin{aligned}
\delta M = {} & \bar{C}_{3,1}[-7.1\sin(\omega+\Omega-\theta)+0.8\sin(\omega+2M+\Omega-\theta)-63.3\sin(-\omega+\Omega-\theta)+\cdots] \\
& +\bar{C}_{3,2}\{-42.5\cos[\omega+2(\Omega-\theta)]+10.5\cos[\omega+2M+2(\Omega-\theta)]-13.6\cos[-\omega+2(\Omega-\theta)]+\cdots\} \\
& +\bar{C}_{4,1}[7.0\cos(-M+\Omega-\theta)-8.2\cos(M+\Omega-\theta)+5.1\cos(-2\omega+\Omega-\theta)+\cdots] \\
& +\bar{C}_{4,2}\{-10.3\sin[-M+2(\Omega-\theta)]+14.2\sin[M+2(\Omega-\theta)]+\cdots\} \\
& +\bar{C}_{5,1}[-87.4\sin(\omega+\Omega-\theta)+6.9\sin(\omega+2M+\Omega-\theta)+87.9\sin(-\omega+\Omega-\theta)+\cdots] \\
& +\bar{C}_{5,2}\{8.6\cos[\omega+2(\Omega-\theta)]-1.4\cos[\omega+2M+2(\Omega-\theta)]+43.9\cos[-\omega+2(\Omega-\theta)]+\cdots\} \\
& +\bar{C}_{6,1}[5.1\cos(-M+\Omega-\theta)-6.0\cos(M+\Omega-\theta)-16.2\cos(-2\omega+\Omega-\theta)+\cdots] \\
& +\bar{C}_{6,2}\{5.4\sin[-M+2(\Omega-\theta)]-7.4\sin[M+2(\Omega-\theta)]+\cdots\} \\
& +\bar{C}_{7,1}[33.1\sin(\omega+\Omega-\theta)+0.0\sin(\omega+2M+\Omega-\theta)+1.4\sin(-\omega+\Omega-\theta)+\cdots] \\
& +\bar{C}_{7,2}\{40.0\cos[\omega+2(\Omega-\theta)]-5.5\cos[\omega+2M+2(\Omega-\theta)]-40.3\cos[-\omega+2(\Omega-\theta)]+\cdots\} \\
& +\bar{C}_{8,1}[-6.8\cos(-M+\Omega-\theta)+7.9\cos(M+\Omega-\theta)+19.1\cos(-2\omega+\Omega-\theta)+\cdots] \\
& +\bar{C}_{8,2}\{4.1\sin[-M+2(\Omega-\theta)]-5.7\sin[M+2(\Omega-\theta)]+\cdots\}
\end{aligned}
\tag{9.165}
$$

We can rearrange this expression in terms of the same frequency (with the period P of each term in days given in parentheses):

$$
\begin{aligned}
\delta M = {} & (-7.1\bar{C}_{3,1}-87.4\bar{C}_{5,1}+33.1\bar{C}_{7,1}+\cdots)\sin(\omega+\Omega-\theta) && (-1.001\text{ day}) \\
& +(0.8\bar{C}_{3,1}+6.9\bar{C}_{5,1}+0.0\bar{C}_{7,1}+\cdots)\sin(\omega+2M+\Omega-\theta) && (0.040) \\
& +(-63.3\bar{C}_{3,1}+87.9\bar{C}_{5,1}+1.4\bar{C}_{7,1}+\cdots)\sin(-\omega+\Omega-\theta) && (-0.971) \\
& +(7.0\bar{C}_{4,1}+5.1\bar{C}_{6,1}-6.8\bar{C}_{8,1}+\cdots)\cos(-M+\Omega-\theta) && (-0.071) \\
& +(-8.2\bar{C}_{4,1}-6.0\bar{C}_{6,1}+7.9\bar{C}_{8,1}+\cdots)\cos(M+\Omega-\theta) && (0.083) \\
& +(5.1\bar{C}_{4,1}-16.2\bar{C}_{6,1}+19.1\bar{C}_{8,1}+\cdots)\cos(-2\omega+\Omega-\theta) && (-0.958) \\
& +(-42.5\bar{C}_{3,2}+8.6\bar{C}_{5,2}+40.0\bar{C}_{7,2}+\cdots)\cos[\omega+2(\Omega-\theta)] && (-0.497) \\
& +(10.5\bar{C}_{3,2}-1.4\bar{C}_{5,2}-5.5\bar{C}_{7,2}+\cdots)\cos[\omega+2M+2(\Omega-\theta)] && (0.041) \\
& +(-13.6\bar{C}_{3,2}+43.9\bar{C}_{5,2}-40.3\bar{C}_{7,2}+\cdots)\cos[-\omega+2(\Omega-\theta)] && (-0.327) \\
& +(-10.3\bar{C}_{4,2}+5.4\bar{C}_{6,2}+4.1\bar{C}_{8,2}+\cdots)\sin[-M+2(\Omega-\theta)] && (-0.066) \\
& +(14.2\bar{C}_{4,2}-7.4\bar{C}_{6,2}-5.7\bar{C}_{8,2}+\cdots)\sin[M+2(\Omega-\theta)] && (0.091) \\
& +\cdots
\end{aligned}
\tag{9.166}
$$

span of data, these spectral components are difficult to separate.

The large number of harmonics affecting a satellite is related by a linear equation similar to equation (9.166). For one satellite, only a linear combination of coefficients can be determined. In those cases where an insufficient number of satellites is observed, additional assumptions are necessary in order to obtain independent equations. The usual assumption is to set some of the higher degree terms to zero, leading to lumped coefficients that are useful for orbit determination but that may be unrelated to the actual field.

In summary, the process of field determination begins with the evaluation of the secular and long-period perturbations to determine the J_n. The perturbations accumulate for weeks and months, and the effects are very large. The mean orbital elements, determined from overlapping 4-day arcs, constitute the basic data used in the analysis. Data and reference orbits of moderate accuracy are adequate for the J_n determination. The unbiased recovery of the J_n requires painstaking evaluation of the long-period and secular perturbations from other sources, principally solar radiation pressure, atmospheric drag, and lunar and solar attraction.

This phase of the analysis is accomplished first. The tesseral harmonics are determined from the short-period (1 revolution to 1 day) changes in the orbit. The detailed structure of the orbit must be observed, and each observation provides an observation equation. Data of the highest possible precision are needed. The unbiased recovery of $\bar{C}_{lm}$ requires the evaluation of the periodic terms from other sources that have periods similar to those arising from the potential coefficients. The most important are the short-period terms due to J_n and the lunar attraction. Because they are smaller than 1 m for the satellites used in this analysis, the periodic effects of air drag and radiation pressure can be ignored. The nonperiodic terms are empirically determined and hence accounted for. The short-period terms due to J_2 must be carried to second order.

9.4.3.2 Coefficients of Zonal Spherical Harmonics in the Potential

9.4.3.2.1 INTRODUCTION

Coefficients of zonal spherical harmonics in the potential determined from secular variations of angular variables and from amplitudes of long-periodic terms with the argument of perigee ω in the orbits of artificial satellites are more accurate than are coefficients derived by classical terrestrial methods. The reason is that the component of geoid height represented by the zonal harmonics is amplified by a factor of 1000 when they appear as secular and long-periodic perturbations of satellites. However, because these perturbations are averaged effects, contributions from the harmonics in each are not very different from one satellite to another unless their orbital elements are quite different. Also, few satellites with inclinations below 30° have been employed in the determination of the coefficients, since accurate observations of such satellites have been scarce. It was also found that many more terms than expected were necessary to represent the potential. Therefore, it has usually been very difficult to separate the contributions from each harmonic in the observed values of the secular motion and of the amplitudes of the long-periodic terms. In other words, different sets of coefficients could represent these observations within observed accuracies for satellites with inclinations larger than 30°.

9.4.3.2.2 EQUATIONS OF CONDITION

A computer program has been developed to calculate coefficients of $J_n (n \leq 55)$ in expressions of secular motion and of the amplitudes of $\begin{matrix}\cos \\ \sin\end{matrix} 2\omega$ and $\begin{matrix}\cos \\ \sin\end{matrix} \omega$ terms. Numerical values for $n \leq 37$ are given in tables 9.27 to 9.29 for 14 satellites. Since secondary effects due to the interaction with the J_2 secular terms were not included, the values here for the coefficients of the amplitudes of the long-periodic terms in the argument of perigee and the longitude of the ascending node are slightly different from those we gave previously.

For the two angular variables ω and Ω, the secular and long-periodic perturbations have been derived from

$$\frac{d(\omega,\Omega)}{dt} - (\dot{\omega},\dot{\Omega}) + A \sin \omega + B \cos 2\omega \qquad (9.167)$$

where $\dot{\omega}$ and $\dot{\Omega}$, the secular parts, are functions of the semimajor axis, inclination, and eccentricity, which are not constant and, except for the semimajor axis, have long-periodic terms. The inclination and the eccentricity cannot be assumed constant in expressions for $\dot{\omega}$, $\dot{\Omega}$ in equation (9.167) but must include long-period terms. The effects of these long-period terms are of the same order as A and B and produce secondary effects. Therefore, if constant values for secular motions are adopted in order to analyze the data, the secondary effects in expressions for the long-period terms must be included in equation (9.167). In earlier papers by Kozai, the secular motions were determined from observation by assuming they were constant. Corrections to the secu-

lar motions and the amplitudes of the long-periodic terms were derived in recent papers by fitting the observed orbital elements with the integrated results of equation (9.167) by using assumed values of J_n and the instantaneous observed mean values of the semimajor axis, inclination, and eccentricity. Thus, it is not necessary to incorporate the interaction terms, as they have already been included numerically and subtracted from the observed data.

As tables 9.27 to 9.29 show, the decrease of the coefficients with degree of the harmonics is slow, particularly for low-altitude and for low-inclination satellites. For DIAL and PEOLE, the coefficients of the secular motions for lower harmonics are not independent, as $\dot{\omega}$ is almost twice as large as $-\dot{\Omega}$.

For low-inclination satellites, the signs of the coefficients change continually as the degree of the harmonics is increased, while for high-inclination satellites, they change only rarely. Therefore, to reduce correlations between the coefficients in the determination of zonal spherical harmonics, it is necessary to use data for satellites with well-distributed orbital elements. However, such data are usually not available.

9.4.3.3 Determination of Tesseral Harmonics

Tesseral harmonics were computed by combining satellite perturbations and terrestrial gravimetry. In the computation of the normal system, terms with small contributions have been omitted. Therefore, the normal system determined from orbit analysis is complete through $l=m=12$. In each higher order, terms have been omitted—for example, 13,6 through 13,9 and 14,5 through 14,11. Resonance harmonics through 23,14 have been incorporated. Of course, all terms were included in the computation of the residuals. In the same way, for surface gravity all available potential coefficients have been used, but no partial derivatives for the zonal harmonics or tesseral harmonics less than ninth degree were computed, since they are negligibly small.

For each orbital arc, a set of six mean elements, $\bar{c}_i$, is determined. The linear rates are derived empirically, as is the mean anomaly. In addition, higher polynomials in the mean anomaly are employed, where appropriate, to account for the nonperiodic, yet nonsecular, effects of air drag and radiation pressure. Twelve or more orbital elements are determined for each arc, and the arcs range in length from 4 to 30 days. Therefore, with the more than 100 orbital arcs used in this solution, over 1500 additional parameters need to be determined. By use of a device described in section 9.4.2.2 for reducing the normal equations, this can be accomplished without dealing with 2000×2000 matrices. For systems of 2000 unknowns, the time required to compute reduced normal equations is much greater than that for the adopted method, which is a block Gauss-Seidel iteration. Reduced normal equations are used with more limited problems—e.g., in a solution for resonant harmonics—because they rigorously account for the interaction of the elements and unknowns.

The determination of orbital elements and of geodetic parameters (potential and station coordinates) was done separately and iterations were performed alternately; this method improves first one set and then the other. As the iterations proceed, the choice of unknowns is modified: Satellite data were either deleted or augmented, depending on whether coefficients (and station coordinates) appeared to be ill-determined or significant.

Equations (9.162) lead us to the method of selecting those coefficients that affect the orbit and that therefore can be determined from observing the orbit. We know that $\bar{C}_{lm}$, a, e, and I determine the size of $\delta\bar{C}^k_{lmpq}$, which can be computed by using an estimate of $|\bar{C}_{lm}|$ and the value of the mean elements. We estimate $|\bar{C}_{lm}|=\alpha l^{-\beta}$ to test for significance, and only terms greater than $\alpha l^{-\beta}$ are retained. All the $\delta\bar{C}^k$ are calculated and combined into a shift of position $\sqrt{d\bar{\rho}\cdot d\bar{\rho}}$; they

are given in table 9.24 for satellite 6701401 with $l=11,12,...,20$. The units are adjusted so that with $\bar{C}_{lm}$ expressed in units of 10^{-6} (e.g., $\bar{C}_{2,2}=2.4$), the perturbation in position is in meters. Conservative values for α and β are used, and more terms are carried than are perhaps necessary. For example, for $l=11$, $m=5$, and $C_{lm}=10^{-5}/l^2=0.083$, the perturbation is $0.083\times 38\approx 3$ m. From such tabulations for each satellite, we can choose the coefficients that affect the motion of the satellite and ascertain how many satellites contribute to the determination of a coefficient. In addition, the accuracy of the available data controls the size of the effect that can be detected. The choice of coefficients is made by balancing the amount and precision of the data available for a particular satellite against the sensitivity of that satellite to particular coefficients. Further, it is apparent that the surface-gravity data are stronger than the satellite information for some coefficients, and for that reason some higher coefficients have been dropped from the satellite solution.

Table 9.24 illustrates two points referred to earlier. The amplitudes for $m=13$ are quite large because of the resonance; the large size of the effects continues well into the 20th-degree terms. The $m-12$ and $m=14$ harmonics also have sizable effects because they are adjacent to a resonant harmonic.

Apart from the resonant harmonics, terms higher than $l=12$, $m=12$ are weakly determined by the satellite data, but it had been demonstrated in earlier iterations that the surface gravity could determine these higher harmonics. The satellite solution was limited to those harmonics that have an effect greater than 3 to 4 m on the orbit. The resulting terms were complete through $l=12$, $m=12$. The higher order terms selected were $C/S(l,1)$ $13\leq l\leq 16$; $C/S(l,2)$ $13\leq l\leq 15$; $C/S(14,3)$; $C/S(l,12)$ $13\leq l\leq 19$; $C/S(l,13)$ $13\leq l\leq 23$; and $C/S(l,14)$ $14\leq l\leq 24$.

The $m=9$, 12, 13, 14 terms are resonant with some satellites, which are listed in table 9.30 along with their resonant periods. Several satellites are resonant with more than one order. For example, 6701101 has a 1.6-day period with the 13th order and a 2.6-day period with the 14th, the latter being the principal effect. Other resonances have several periods, as illustrated by equation (9.163) for 5900701 (which was not used in the final solution) and in table 9.30 for 6701401. The multiple periods are due to the nonzero eccentricity, which causes the frequency splitting.

9.5 RESULTS

As was explained in section 9.4, the process used by SAO in solving for station coordinates and the gravitational potential is such that station coordinates and the potential are determined both independently and in combination. These quantities are therefore easily discussed and analyzed separately. The station coordinates are discussed in section 9.5.1. The potential, in terms of coefficients $\bar{C}_{lm}$, $\bar{S}_{lm}$, is given and discussed in section 9.5.2. The geoid derived from this potential is discussed in section 9.5.3.

The analysis was divided into two parts because of the initial high accuracy of the geodetic parameters, the good coverage of all types of observational material, and the result from Gaposchkin and Lambeck (1970) indicating that the interaction between the potential and the station coordinates is relatively small. The determinations of the potential and of station coordinates were carried out in parallel. In an iterative process, the improved coordinates were used in the next iteration for the potential, and then the improved potential was used in the subsequent iteration for the station coordinates. This process, known as the block Gauss-Seidel iteration, will rigorously converge.

9.5.1 Coordinates

(E. M. Gaposchkin, J. Latimer, and G. Veis)

Each subset of data was treated to provide a system of normal equations and residuals. These systems are combined

with their relative weights. In addition, each system *may* have a different origin, orientation, and scale, but these differences should *not* occur if each system had been referred to the defined system without error. In the combination, additional parameters as necessary were introduced into the combined normal system to account for possible systematic errors. The SAO dynamical, pre-ISAGEX data were taken as the reference. Since the geometrical networks have no scale, only translation and rotation parameters were introduced. For practical purposes, the SAO geometrical network covers only one hemisphere in an east-west orientation, so only the rotation about the z axis (ϵ_z) may be meaningful. This corresponds to a correction to UT1. The polar orientation (ϵ_x, ϵ_y) for the SAO geometrical network turned out to be smaller than the formal uncertainty. The JPL net had only a scale and ϵ_z parameter as it is not sensitive to ϵ_x, ϵ_y or to the origin. Experiments with determining corrections ($\Delta\Omega$) to the node for each arc of ISAGEX data indicated that (1) the corrections were small, generally less than 1 μrad, and (2) they were satisfactorily included through the reduced normal equations. Therefore, formally, the combination solution contained 14 additional parameters. The final values of these parameters are given in table 9.31. The translation of the two geometrical networks is the correction to the station used as the origin. Excellent agreement occurs between these translations and the coordinates determined from an a posteriori geometric adjustment. The formal uncertainty for the translation of the SAO geometrical network is not given, because the origin, station 9051, has very few observations and is not determined very well.

Two iterations were completed, the first starting with the coordinates given in Gaposchkin and Lambeck (1970). Examination of the solutions indicated problem stations; in particular, the geodetic coordinates were sometimes seriously in error.

The strategy used to determine the relative weights and the formal uncertainty was based on the geometrical solutions, and all other solutions were referred to them. Geometrical solutions are relatively uncomplicated and free from assumptions. Furthermore, the statistics are straightforward.

The accuracy of each station-to-station direction was computed. This estimate can be verified by comparison with the direction determined in the network adjustment. The adjustment essentially enforces the coplanarity condition for any three directions that connect three stations. By comparing these estimates of the direction, we can compute a scale factor that is a measure of the agreement between the formal statistics of the adjustment and the actual errors. This scale factor turned out to be $k^2=2.65$ for the SAO geometrical network and $k^2=2.60$ for the BC–4. Since the difference between these estimates of k^2 is not significant, we adopted an overall scale factor of $k^2=2.625$ for the geometrical networks. It is interesting to note that when only the 12 SAO Baker-Nunn cameras are used, the scale factor becomes $k^2=1.03$, indicating excellent control of systematic errors.

In the combination of the six types of data, the geometrical networks, the JPL network, and the geodetic survey data were used with a priori variances. The pre-ISAGEX dynamical data were given a weight of 0.25 for the combination of the normal equations, which effectively doubles the assumed accuracy. In addition, the assumed accuracy of the pre-ISAGEX laser data was further multiplied by a factor of $1/\sqrt{10}$, and thus the assumed accuracy of the laser data was multiplied by 6. The ISAGEX data were given an overall weight of 0.0625; i.e., the assumed accuracy was multiplied by 4. Thus, the reference orbits were computed by using the assumed accuracy in table 9.8, but the normal system was scaled by these factors. These adjustments were necessary in order to accommodate the enormous volume of data used for the dynamical solutions. Large volumes of well-distributed data lead to cancellation of errors, which is desirable, but give optimistic estimates of variance. The balance of weights presented here leads to an internally consistent solution, which has

acceptable agreement with independent determinations.

Table 9.32 lists the geocentric coordinates for the stations determined in SE III together with their uncertainties scaled by $k^2=2.625$. Station 8820, Dakar, Senegal, is not given, the poor agreement and paucity of data precluding reliable results.

The solution for coordinates from the combination scaled by $k^2=2.625$ gave estimates of variance of 2 m for the best stations. Since no comparison exists that can verify this accuracy for geocentric coordinates, we are limited to consistency checks. The coordinates should agree with the standard at least as well as the accuracy of the standard. A number of internal checks (e.g., between geometrical and dynamical solutions) can be performed. Comparisons can be made with surface data, but they test only the relative position and not the geocentric position of the coordinates. Nevertheless, these comparisons are instructive and indicate that the computed variances (uncertainties) are realistic estimates. Further, the general agreement internally in the satellite data—and externally with the terrestrial data—indicates that, as a rule, discrepancies are within the expected uncertainties. The large discrepancies are probably due to errors in the survey data, and further analysis is needed.

Comparisons with satellite orbits are inconclusive at best, because of the large number of error sources. In section 9.5.2.3 numerical results are given for orbit computations with laser data by using the latest potential and station coordinates. This comparison indicates that the orbit computing system (data, theory, physical parameters, and station coordinates) has an accuracy of 5 to 10 m, which is not consistent with a 2- to 5-m accuracy for the station coordinates.

The typical direction is determined with an accuracy of 5 μrad, equivalent to a relative position of 10 m. For selected sets of stations, figure 9.12 compares the determined direction (both before and after the coplanarity condition is applied), the dynamical solution, and the combination solution. In some cases, a direction from the SAO geometrical net and another from the BC–4 geometrical net are available. These comparisons are perhaps unfavorable in that the errors of both stations are reflected in the figures. The error ellipses for all the directions are scaled by the factor $k^2=2.625$. In order to express all the directions in the same coordinate system, the plotted directions are rotated by the parameters given in table 9.35.

When the origin and scale are provided, the BC–4 network of 48 stations gives a geometric solution that can be compared with the combination solution. Table 9.33 gives the results of such a comparison, with differences in X, Y, and Z and North, East, and height. The geometrical solution has an average uncertainty of 5 m for each coordinate, while the combined solution has the uncertainty given in table 9.32. The adjustment uses a weight computed from the two solutions. The root mean square of 12 m and the standard error of unit weight $\sigma_0=0.8$ indicate the excellent agreement in the coordinates and the estimated uncertainties. A number of the individual coordinates are too large. The North-South difference of -25 m for station 6068, which is tied geodetically to 7092 and 4751, is the most troublesome.

The JPL coordinates given by the LS 37 solutions, rotated and scaled by the results in table 9.31 are compared in table 9.34 with the coordinates determined in the combination solution.

Comparisons within each datum are possible. The four major datums where this was done are North American datum (NAD 1927), South American datum (SAD 1969), Australian datum (AGD), and European datum (EU50).

As described earlier, the use of datum coordinates in the combination solution has been restricted to nearby stations, primarily in order to relate different types of observations. Therefore, datum coordinates constitute a relatively independent set of data. However, each datum has an arbitrary origin, orientation, and scale, and the relation between each datum and the geocentric

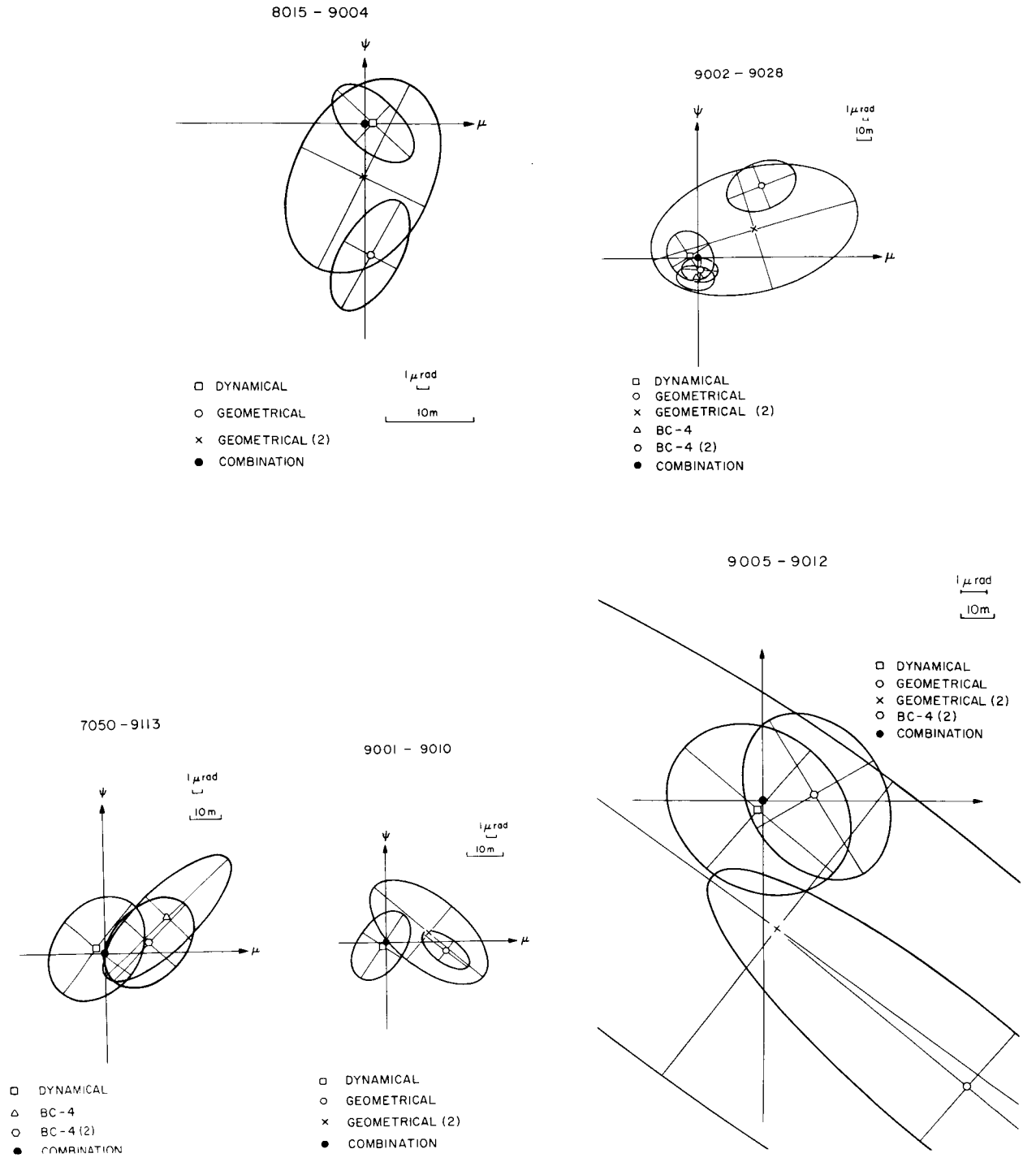

FIGURE 9.12.—Comparison of interstation directions from the combination, dynamical, and geometrical solutions. Each of the two geometrical solutions yields two directions. BC-4 (2) and geometrical (2) are the directions obtained from the network adjustment. ψ is in the direction of increasing declination, and μ is in the direction of increasing right ascension.

system must be determined. One can therefore determine up to seven parameters, but depending on the size of the datum and the distribution of stations on the datum, some of these transformation parameters may not be significant. The seven transformation parameters are three translations, three rotations, and one scale. We have elected to express the rotations as rotations of the datum origin about the normal to the ellipsoid and around two axes in the tangent plane oriented north-south and east-west. These rotations have a physical interpretation since they express an error in the azimuth of orientation of the datum and a tilt of the ellipsoid. Accordingly, the transformation will be given by

$$\bar{X}_{sat}=\bar{X}_{dat}+\bar{T}+(1+K)\bar{R}(\bar{X}_{dat}-\bar{X}_0)$$

where $\bar{X}_{sat}$ and $\bar{X}_{dat}$ are the coordinates from the satellite solution and the datum, respectively, $\bar{T}$ is the vector of the three translation parameters, K is the scale correction, $\bar{X}_0$ are the coordinates of the datum origin, and $\bar{R}$ is a rotation matrix depending on the three rotational parameters and the latitude and longitude of the datum origin.

Table 9.35 gives the translation, rotation and scale parameters for four major datums as computed from the adjustment of the datum coordinates to the satellite solution. A positive scale here means that the datum scale has to be increased in order to agree with the satellite scale. The table also gives the number of stations used in each datum. In the computation of datum shifts, each station was assigned a weight computed from the standard deviation of the satellite solution and the standard deviation of the datum coordinates, which was taken as $\sigma(m)=5\times(S\times10^{-6})^{3/4}(m)$, where S is the distance of the station from the datum origin in meters. In all cases, the standard deviation of unit weight σ_0 (given in table 9.35) after the adjustment is smaller than 1, which means that the weights are somewhat pessimistic. The rms, $\sigma(m)$, of the final differences for each datum in table 9.36 is between 5 and 16 m. It is apparent that the European and the South American datum coordinates do not agree very well with the satellite solution. The European datum is rather inhomogeneous and its extension into Africa and Asia, which we used, makes it rather weak.

Further checks with datum information can be obtained with station heights. The height above the reference ellipsoid (h_{ell}) should be equal to the mean height above sea level (H_{msl}), which is approximately the height above the geoid plus the geoid height N; i.e., the disagreement between these two estimates, Δh, is

$$\Delta h=h_{ell}-H_{msl}-N-\overline{H}_{\text{datum mean}}$$

If we use the satellite geoid to calculate N, we can make this comparison for all stations but we lose the detailed variation in geoid height. The computation does provide a value for the semimajor axis of the best-fitting ellipsoid used to calculate h_{ell}. We get

$$a_e=6\ 378\ 140.4\pm1.2\ \text{m}$$

To employ the detailed geoid-height information given for each datum in table 9.15, we must refer the coordinates to the datum origin by using the datum shifts in table 9.35. Table 9.36 lists the standard deviations of the heights calculated for each datum. The average of 3.98 must be considered excellent in view of all the uncertainties in calculating Δh. Figure 9.13 shows these heights residuals as a function of latitude.

The results by Gaposchkin and Lambeck (1970) were derived in the same manner, by combining several types of data, establishing relative weights, and verifying the accuracy by intercomparison. Their accuracy was 7 to 10 m for the fundamental stations. In table 9.37 we give the corrections derived in this analysis for selected stations. The overall agreement of $\sigma=10$ m and a standard error of unit weight $\sigma_0=0.662$ indicate excellent agreement in the derived coordinates and the accuracy estimates; if any-

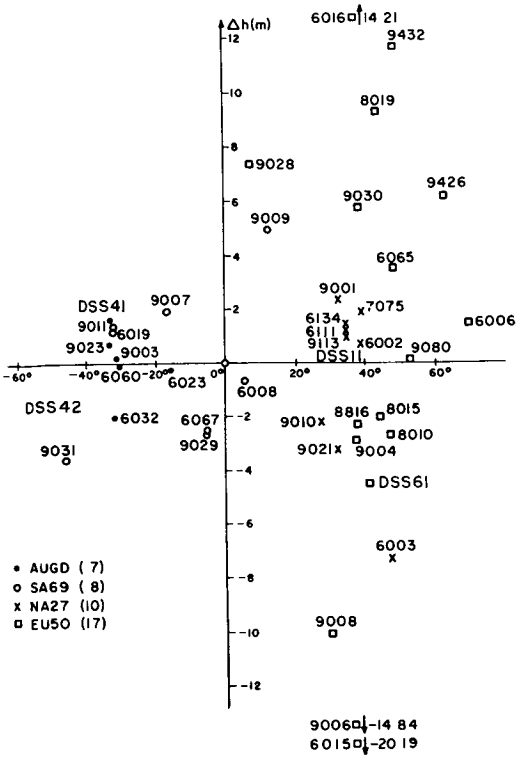

FIGURE 9.13.—Geoid height comparison as a function of latitude $\Delta h = h_{ell} - H_{msl} - N_{datum\ geoid} - h_{datum\ mean}$, where h_{ell} is transformed by the appropriate datum shift parameters $\sigma_{\Delta h} = 3.98$ m.

thing, the accuracy estimates are pessimistic. The very small shift in origin indicates that the whole reference system has not changed.

Williams *et al.* (1972) have determined the spin-axis distance of McDonald Observatory from lunar-laser observations. Table 9.38 compares this distance with that deduced by means of the coordinates of station 9001 from survey data. The agreement of -3.51 m must be considered acceptable.

The scale of the combination solution is defined by the value of GM adopted in the dynamical solution, given in table 9.11. We found a scale difference of 0.18 ± 0.55 ppm between the JPL and the SAO coordinates, the JPL ones being slightly larger. If the discrepancy with lunar laser is attributed to scale, the scale difference would be 0.7 ppm.

The scale obtained for the four major datums is given in table 9.35. It appears from the NAD 1927, EU50, and AGD datums that the datum scale is smaller than the satellite scale by approximately 2 ± 1 ppm, while from the SAD 1969 datum, it is larger by 1 ± 1 ppm. Since the survey scales are not expected to be established to better than a few ppm, the weighted mean of 1.6 ± 1 ppm is not considered to be significantly different from zero.

Each geometrical network has an arbitrary origin specified by the intial coordinates of one station, a station not explicitly determined in the combination solution. The translation parameters in table 9.33 correspond to the correction to the origin of the network, i.e., the correction to the initial coordinates of the reference station.

In principle, the orientation of the two geometrical systems and that of the dynamical system should be identical. Orientation parameters (ϵ_x, ϵ_y, ϵ_z) are determined to accommodate possible systematic differences in the actual representation of the three systems. Since the SAO geometrical network covers only one hemisphere in an east-west orientation, the orientation of its pole (ϵ_x, ϵ_y) may be poorly determined.

The polar orientation of the BC–4 system with respect to the SAO dynamical system is $1.88 = \sqrt{1.76^2 + 0.65^2} \pm 1.16$ μrad. This systematic difference is obtained by comparing the observed BC–4 directions with directions determined from eleven stations in the combination solution with characteristic interstation distances of 2 to 3 Mm. In metric terms, the orientation difference is $1.88 \times 10^{-6} \times 2 \times 10^6 \approx 4$ m. The accuracy of the mean station for the 11 stations is approximately 4 m. It is assumed that the value of 1.88 μrad results from differences in pole-position data or in processing methods.

The rotation in longitude (ϵ_z) corresponds to a correction in UT1. Figure 9.14 indicates the relative position of the zero meridian of each system. We note almost the same relation between SAO and the JPL systems that we found in SE II, which was 4.0 μrad. The difference between the SAO geometrical and the SAO dynamical systems is -0.40 ± 1.43, and that between BC–4 and the SAO dynamical is -2.20 ± 0.82. The relative rotation in

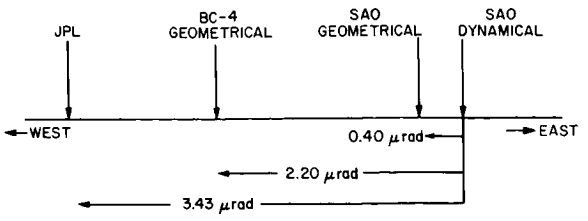

FIGURE 9.14.—The relative zero meridians of the different systems.

longitude between the JPL and the SAO systems is probably due to a difference between the JPL's planetary ephemeris and the FK4 system used by SAO, while that between the geometrical and dynamical nets most likely results from differences in the UT1 data or in the processing methods.

The results described above, the procedures, the tests and comparisons, and the experience of carrying out the work have led to the following conclusions about the use of artificial satellites for the determination of station coordinates:

(1) Observations of close-Earth satellites have been successfully combined with observations of deep-space probes and surface triangulation enabling us to determine the coordinates of 90 satellite-tracking sites in a uniform homogeneous system.

(2) The combination of these data provides a better solution than we can obtain from each set of data separately, because more complete coverage results and because the combination enables us to overcome weaknesses in each system.

(3) The methods of processing each type of data are sufficiently understood to make a rational combination.

(4) Successive solutions have resulted in improvements. When compared with the previous solution, each new one has agreed to within the estimated uncertainty, and that uncertainty has steadily decreased from 10 to 20 m in 1966, to 5 to 10 m in 1969, to 2 to 8 m in 1973.

(5) Formal statistics are generally optimistic, and therefore the uncertainty in coordinates is established by intercomparison, a method that has proved reliable.

(6) A comparison between coordinates indicates an accuracy of 2 to 4 m for fundamental stations and 5 to 10 m for most others.

(7) The body of data available from laser systems, though small, has made a significant contribution. The laser data dominate the solution through the relatively great weight assigned and thereby essentially establish the reference frame for the station's coordinates.

(8) The use of a variety of orbits spanning a considerable period of time is very important. Data from such orbits average over error sources with a slow variation such as UT1 or epoch timing and eliminate poor orbital geometry. The laser data suffered from both problems.

(9) Geometrical data require a minimum of assumptions, and geometrical solutions have relatively straightforward statistics. Geometrical data are more difficult to obtain owing to the necessity of simultaneous observations. Dynamical data are more plentiful, but their processing requires an elaborate orbit-computation program that may introduce model errors. The well-behaved statistical properties of the geometrical data allowed the use of the geometrical networks to establish the uncertainties.

(10) Small but significant systematic differences in scale and orientation are found between satellite coordinate systems. These differences may result from variations in data-processing methods or from fundamental and obscure differences in the definition of reference systems, e.g., the FK4 system and the JPL planetary ephemeris.

(11) Satellite determinations of site location are now sufficiently accurate to verify terrestrial survey data. The most troublesome part of the analysis was finding the erroneous survey coordinates. Considerable effort remains in providing global geodetic coordinates with sufficient reliability.

(12) Scale obtained for the four major datums is systematically smaller than the satellite results by 1.6 ± 1 ppm. Since survey scales are not expected to be established to better than a few ppm, this result is not significantly different from zero.

9.5.2 Potential

(E. M. Gaposchkin, M. R. Williamson, Y. Kozai, and G. Mendes)

The Smithsonian Astrophysical Observatory has published a series of Standard Earth models based on satellite-tracking and other data (Kozai, 1964, 1969; Gaposchkin, 1967, 1970a; Köhnlein, 1967; Veis, 1967a,b; Whipple, 1967; Lundquist and Veis, 1966; Lambeck, 1970; Gaposchkin and Lambeck, 1970). There has been a steady advance in the accuracy of the analytical treatment, in both the accuracy as well as the completeness of the data, and in the significance of the results.

Each Standard Earth model consists of (1) a set of geocentric coordinates for stations observing satellites and (2) a set of spherical harmonics representing the potential. These two sets of unknowns can be correlated, and both sets of parameters have been determined in the same computation. This led, for example in Gaposchkin and Lambeck (1970), to solving a system with 428 unknowns—i.e., for 39 stations and potential coefficients complete through degree and order 16. Evaluation of the Gaposchkin and Lambeck (1970) results indicated that the remaining errors in these parameters were small; that is, the corrections to the parameters would be small. Therefore, the effect of errors in the adopted station coordinates on the determination of the potential, and vice versa, would be small. Because these effects are small the two sets of parameters could be computed separately.

A general revision of the parameters for SE III was undertaken because of new and improved data for almost all types of observations. Observations by cameras have been augmented by a considerable number of data from laser DME with global coverage from ISAGEX. Two satellites with inclinations significantly lower (5° and 15°) than previously available have been launched since 1970. Available surface-gravity data have been significantly improved by the distribution of a compilation of gravity anomalies by the Aeronautical Chart and Information Center (ACIC). Determinations of station coordinates have been improved by data from the worldwide BC–4 geometrical network. Finally, among these improved data is the information on site locations from JPL's DSN which has been revised with the addition of new data and improved processing techniques.

Gaposchkin (1970a) has shown that, except for isolated harmonics, the terms beyond 18th or 20th degree have a negligible effect on a satellite. The only exceptions are some zonal harmonics that give rise to secular and long-period effects, and the resonant harmonics. Therefore, one cannot hope to obtain from analysis of satellite perturbations much more detail beyond 16th degree and order than is already available. Greater detail will have to come from other methods, such as terrestrial gravimetry. Many of the harmonics between 10th and 18th degree are not very well determined from satellite-perturbation analysis, but terrestrial gravimetry provides a good determination of the coefficients when combined with satellite data. So, our objectives are to improve the low-degree and low-order harmonics from satellite data and the higher harmonics from terrestrial data that best represent the gravity field.

Since the terms beyond 18th degree do not give rise to an observable change in satellite position, the satellite observations could be modeled with the use of a potential complete through degree and order 18, including, of course, some additional resonant and zonal harmonics. Therefore, there is no model error due to neglected higher harmonics. However, the surface-gravity data are given in area-means of 550 km $\times$ 550 km squares. This surface distribution of gravity would require a spherical harmonic development to $l=m-36$. Therefore, using a potential through degree and order 18 will have a significant model error that must be taken into account in establishing weights and making comparisons with surface-gravity data.

9.5.2.1 Coefficients of Zonal Harmonics [2]

The equations of condition were solved by least squares for both the even-degree and the odd-degree harmonics. They were solved first with 11 unknowns, $J_n (n \leqq 23)$, and then with 12, the 12th being $J_n (24 \leqq n \leqq 49)$. Eight solutions were obtained. The solutions, given in tables 9.39 and 9.40, include the sums of the squared differences from the assumed values. The values for coefficients of degrees lower than 14 express corrections to those in table 9.16.

Tables 9.39 and 9.40 show that the solutions are quite stable, especially for lower degree coefficients, and that the data can be expressed quite nicely by including J_{35} and J_{36}. The sum of the squared differences drops from 114 to 39 when J_{36} is included for the even degree and from 53.7 to 40.6 when J_{35} is incorporated for the odd degree. Although there is some uncertainty as to whether J_{35} and J_{36} can have such large values, the 12-unknown solutions that include them are regarded as the best. The sum of squared residuals cannot be reduced much further even if the number of unknowns were increased beyond 12.

In tables 9.41, 9.42, and 9.43, the differences computed for the 12 unknowns and for the 11 unknowns are given under the headings I and II, respectively. Solution I for even orders can express the secular motions of all the satellites except 7010901 and 6202901. Since only in table 9.43 is the difference between difference I and difference II much larger than the standard deviation for the data on 7001701, 6508901, and 6508101, it can be said that J_{36} is determined essentially from the data on these three satellites. If more accurate data become available for 7010901, so that the standard deviations for this satellite become smaller than the differences, a more definite conclusion regarding J_{36} can be obtained. Table 9.43 shows no essential difference between differences I and II; for odd degrees, the 12-unknown solution is not yet much better than the 11-unknown one.

[2] Note that $J_n = -C_n$.

For comparison, five previous solutions (Kozai, 1959b, 1961a, 1963a, 1964, 1969) are given in table 9.44. These solutions were derived from the following numbers of satellites with inclinations ranging from 28° to 96°:

Date	*Number of satellites*	*Inclination range (deg)*
1959	1	34
1961	3	33 to 50
1963	13	32 to 65
1964	9	33 to 96
1969	12	28 to 96

Except for some from the 1963 determination, the standard deviations in the first three determinations are more than 10 times larger than the present ones; therefore, the differences computed by these solutions are very large even for satellites within the indicated inclination ranges. The differences from the 1964 solution are listed as $(O-C)$ in tables 9.41, 9.43, and 9.44. Both the 1964 and the 1969 solutions give very large differences for PEOLE and DIAL. Table 9.44 also includes a solution by Cazenave, Forestier, Nouel, and Pieplu (1971, unpublished), who incorporated data for PEOLE, DIAL, and SAS (7010701; $I=3°$) in addition to the satellites used by Kozai (1969). Their solution agrees quite well with ours except for the odd higher degree coefficients.

9.5.2.2 Tesserals

The results of the dynamical solution must be discussed in the context of the combination solutions. A summary of the data is given in table 9.7. The selection of data and unknowns evolved through the analysis. The number of satellites used ranged from 21 to 25, and the number of arcs in the largest solution was 203. Arcs were added or rejected on the basis of their contribution to the normal equations, the number of observations for a particular station, the improvement of distribution for a resonant harmonic, and the quality of the orbital fit.

Two iterations were performed to find the potential. The first employed the potential and station coordinates determined by Gaposchkin and Lambeck (1970) as initial values; and the second used the results of the first iteration for the potential and the station coordinates determined earlier in this chapter.

For each iteration, several solutions were obtained. Orbital arcs were added or deleted to improve the satellite distribution and the variance-covariance matrix.

Several weights for the surface gravity were used. For areas without surface-gravity data, we had four choices of treatment:

(1) We could make no assumptions about unobserved areas.

(2) We could use a zero anomaly with a very large variance; that is, the expected value of gravity would be zero.

(3) We could use a reference gravity field with a very large variance; that is, only the higher harmonics would have an expected value of zero.

(4) We could use a model anomaly, for example, one determined from topography.

Adoption of method (1) would introduce very large short-wavelength features into those regions where no gravity is measured. In addition, the statistical comparisons discussed later are very poor, although the $(O-C)$ values and the satellite orbits are good. Therefore, (1) had to be discarded. Gaposchkin and Lambeck tried methods (2) and (4) and found them equivalent. Choice (3) is an improvement over (2) because the low-degree and low-order terms are well determined by means of satellite data. Therefore, (3) was adopted, with the weight given in table 9.21. Comparing the results of choices (1) and (3), we found that satellite comparisons are identical, the $(O-C)$ for the surface gravity is marginally improved, and the statistical comparisons of the surface gravity are quite acceptable.

The fully normalized spherical-harmonic coefficients of the adopted solution are given in table 9.45. Figure 9.15 shows the mean potential coefficient by degree, extended by numerical quadrature.

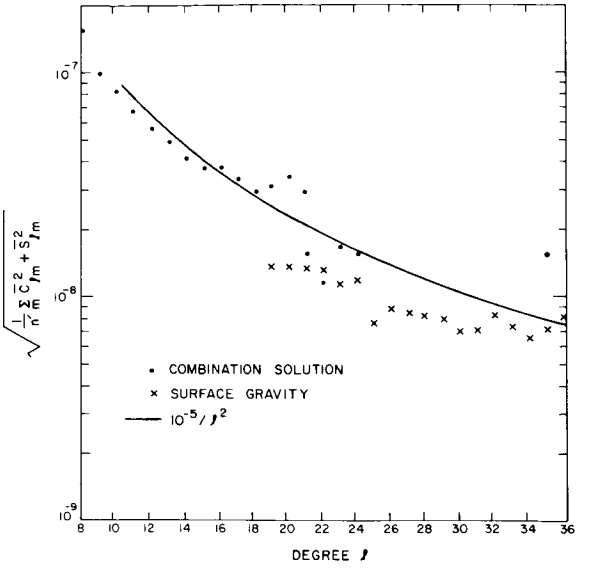

FIGURE 9.15.—Mean potential coefficient by degree.

9.5.2.3 Results of Comparison

9.5.2.3.1 ORBIT DETERMINATION BY USE OF SE III

A detailed evaluation of SE III results with satellite orbits is difficult. Although other effects—such as lunar and solar perturbations, body tides, radiation pressure, and air drag—are all included in the orbit computation, none of these is known without error, and each, in itself, provides a number of problems. Also, the coordinates of the tracking stations are not known without error. Furthermore, incomplete orbital coverage can result in overoptimistic estimates of orbital accuracy from formal statistics. Finally, the tracking data contain errors. A few comparisons are given here to indicate approximately the accuracy of the total orbit-computation system. The potential is certainly one of the larger contributors to the error budget.

From ISAGEX data, consecutive orbits were computed every 2 days, by using 4 days of data (except for 6800201, where 6 days of data were employed). This type of analysis is especially valuable for (1) detection of bad observations, since each observation is

used in two orbits, and (2) evaluation of the reliability of the orbital elements by comparison of adjacent orbits.

Results for 6508901, 6800201, and 6701401 are given in table 9.46, together with the number of observed points used in the final iteration. All calculations were performed by using the final station coordinates and the tidal parameter $k_2=0.30$; radiation-pressure perturbations were calculated with a fixed area-to-mass ratio.

We see that with good orbital coverage, we can expect to have rms residuals of between 4 and 10 m.

Satellite 6701401 has a relatively low perigee, and the poorer orbits from MJD 41072 to 41078 coincide with increased solar activity resulting in increased drag.

Of the 4– to 10–m rms residuals, 2 to 3 m come from station coordinates and 1 to 4 m could be attributed to the orbital theory. Therefore, the accuracy of the gravity field for orbit computation may actually be somewhat better than indicated by table 9.46.

9.5.2.3.2 COMPARISON WITH GRAVITY

To compare a model (g_s) with observed values of surface gravity (g_t), the following quantities defined by Kaula (1966b) can be computed:

- $\langle g_t^2 \rangle$ the mean value of g_t^2, where g_t is the mean free-air gravity anomaly based on surface gravity, indicating the amount of information contained in the surface-gravity anomalies
- $\langle g_s^2 \rangle$ the mean value of g_s^2, where g_s is the mean free-air gravity anomaly computed from the potential model, indicating the amount of information in the computed gravity anomalies
- $\langle g_t g_s \rangle$ an estimate of g_h—i.e., the true value of the contribution to the average gravity anomaly of the potential model and the amount of information common to both g_t and g_s
- $\langle (g_t-g_s)^2 \rangle$ the mean-square difference of g_t and g_s
- $E(\epsilon_s^2)$ the mean-square error in the gravity anomalies
- $E(\epsilon_t^2)$ the mean-square error of the observed gravity
- $E(\delta g^2)$ the mean square of the error of omission—that is, the difference between true gravity and g_h; this term is then the model error

If the potential model were perfect, then $\langle g_s^2 \rangle = \langle g_h^2 \rangle$, which in turn would equal $\langle g_t g_s \rangle$ if g_t were free from error and known everywhere. Then, ϵ_s^2 would be zero even though g_s would not contain all the information necessary to describe the total field. The information not contained in the model field—i.e., the error of omission, δg—then consists of the higher order coefficients. The quantity $\langle (g_t-g_s)^2 \rangle$ is a measure of the agreement between the two estimates g_t and g_s and is equal to

$$\langle (g_t-g_s)^2 \rangle = E(\epsilon_s^2) + E(\epsilon_t^2) + E(\delta g^2)$$

Another estimate of g_h can be obtained from the gravimetric estimates of degree variance σ_l^2 (Kaula, 1966b):

$$E(g_h^2) = D = \sum_l \frac{n_l}{2l+1} \sigma_l^2$$

where n_l is the number of coefficients of degree l included in g_h, and

$$\sigma_l^2 = \gamma^2 (l-1)^2 \sum_m (\bar{C}_{lm}^2 + \bar{S}_{lm}^2)$$

We also have

$$E(\epsilon_s^2) = \langle g_s^2 \rangle - \langle g_s g_t \rangle$$

and

$$E(\epsilon_t^2) = \langle g_t^2 \rangle / \langle n \rangle$$

Table 9.47 summarizes the above quantities for SE III. The improvement over SE II in the coverage of surface-gravity data is evident. The more limited gravity coverage

used for SE II resulted in accuracy estimates that were consistently optimistic. The revised set of average gravity anomalies has greater coverage and is more independent of the model used for the potential. Even so, line 2 represents an estimate of the accuracy, $E(\epsilon_s^2) = 52$ mGal^2, that is more optimistic than that based on independent gravity data for SE II, which was 99 mGal^2 (Gaposchkin and Lambeck, 1970).

We used the 306 average gravity anomalies with more than 19 observed units in each average for the comparison. There is very good agreement between $\langle g_t g_s \rangle$, $\langle g_s^2 \rangle$, and D, which would be equal for a perfect solution. In $E(\delta g^2)$, we have a measure of the information remaining in the higher harmonics. The formal statistics give an error in the combination reference field of $E(\epsilon_s^2) = 15$ mGal^2.

An alternative is to eliminate δg by use of

$$\begin{bmatrix} \Delta\bar{C}_{lm} \\ \Delta\bar{S}_{lm} \end{bmatrix} = \frac{1}{4\pi\gamma(l-1)} \int_{\text{sphere}} (g_t - g_{ref}) \left\langle \bar{P}_{lm}(\sin\phi) \begin{bmatrix} \cos m\lambda \\ \sin m\lambda \end{bmatrix}_\sigma \right\rangle d\sigma$$

where

$$\left\langle \bar{P}_{lm}(\sin\phi) \begin{bmatrix} \cos m\lambda \\ \sin m\lambda \end{bmatrix} \right\rangle$$

is the mean of

$$\bar{P}_{lm}(\sin\phi) \begin{bmatrix} \cos m\lambda \\ \sin m\lambda \end{bmatrix}$$

over the area defined for the gravity anomaly. We can compute any harmonic with respect to a reference gravity field, but care must be used in treating areas where no observed gravity is available. A gravity field defined by g_{ref} and the $\Delta\bar{C}_{lm}$, $\Delta\bar{S}_{lm}$ will have an error of

$$\langle (g_t - g)^2 \rangle = E(\epsilon_s^2) + E(\epsilon_t^2) + E(\delta g^2) + E(\epsilon_{\text{quad}}^2)$$

where $E(\epsilon_s^2)$ is the error in the composite field and $E(\epsilon_{\text{quad}}^2)$ is the error due to the inexact quadrature and imperfect distribution of the data.

Table 9.48 gives the results of this numerical quadrature with reference fields defined by the first l degrees of SE III. Computing all the potential coefficients to $l = m = 36$, i.e., the null reference field, we get $E(\epsilon_s^2) \equiv 0$, and

$$E(\epsilon_t^2) + E(\delta g^2) + E(\epsilon_{\text{quad}}^2) = 29 \text{ mGal}^2$$

Using an increasingly detailed reference field, we obtain an estimate of $E(\epsilon_s^2)$ as a function of degree. As expected, the mean-square error for the low-degree and low-order harmonics estimated from a comparison with terrestrial gravimetry is quite small. The satellite data provide accurate values, and the low harmonics have a smaller effect on gravity anomalies. The mean-square error for the 8th to 18th degrees is relatively constant, as expected, since these harmonics are determined largely by surface-gravity data. The mean-square error $E(\epsilon_s^2)$ estimated from the quadrature is in good agreement with that obtained from statistical analysis. For comparison, the values are given in table 9.49.

The estimate of $E(\epsilon_s^2)$ assumes that g_s and g_t are independent; i.e., they have uncorrelated errors. Since the terrestrial gravity (g_t) was used to determine the combination solution (g_s), this assumption is certainly incorrect, and therefore, the estimate of $E(\epsilon_s^2) = 15$ mGal^2 is definitely optimistic. A better test could be made with independent data for g_t. Since the mean gravity anomalies used in the combination solution were computed, two compilations of $1° \times 1°$ anomalies have been published: the North America and the North Atlantic (Talwani *et al.*, 1972) and for the Indian Ocean (Kahle and Talwani, 1973). These compilations were published after the set of mean anomalies used here became available, but some basic data are probably common to both. The processing methods used by Talwani and his coworkers were different from those of ACIC, and additional data were included. It is true that these two new compilations may not be completely independent of the data used in the combination solution.

Two comparisons are nevertheless instructive. A simple $5° \times 5°$ average was computed

for these data since all $1° \times 1°$ areas had values given in the region of interest. These $5° \times 5°$ averages, with the mean of the whole region subtracted, were used to compute the same statistical quantities given in table 9.49. The number n is the number of points, centered in a $1° \times 1°$ area, for which a $5° \times 5°$ mean was computed. Therefore, we have a moving $5° \times 5°$ mean calculated every 1°. Most of the gravity data in these ancillary compilations were taken at sea, and the estimate $E(\epsilon_t^2)$ of their variance may be optimistic. The weighted mean of $E(\epsilon_s^2)$ is 65 mGal^2, equivalent to 3.1 m in geoid height. The remaining gravity information in the higher harmonics, δg, equals 68 mGal^2. We notice that δg for the Indian Ocean is larger than δg for North America and the Atlantic and is probably due to the very sharp low below the Indian subcontinent, which cannot be modeled very well by the generalized geoid. Further, $\langle (g_t - g_s)^2 \rangle$, $\langle g_s^2 \rangle$, $\langle g_t^2 \rangle$, and $\langle g_t g_s \rangle$, which are all in good agreement with the global values from Table 9.47. Therefore, we feel reasonably certain that for comparison purposes, both the North America and North Atlantic region and the Indian Ocean region are typical. Thus, we conclude that the generalized geoid has an accuracy of ± 3 m in geoid height and ± 8 mGal for the whole earth. Figures 9.16 to 9.19 give north-south and east-west profiles for both North America and the Indian Ocean.

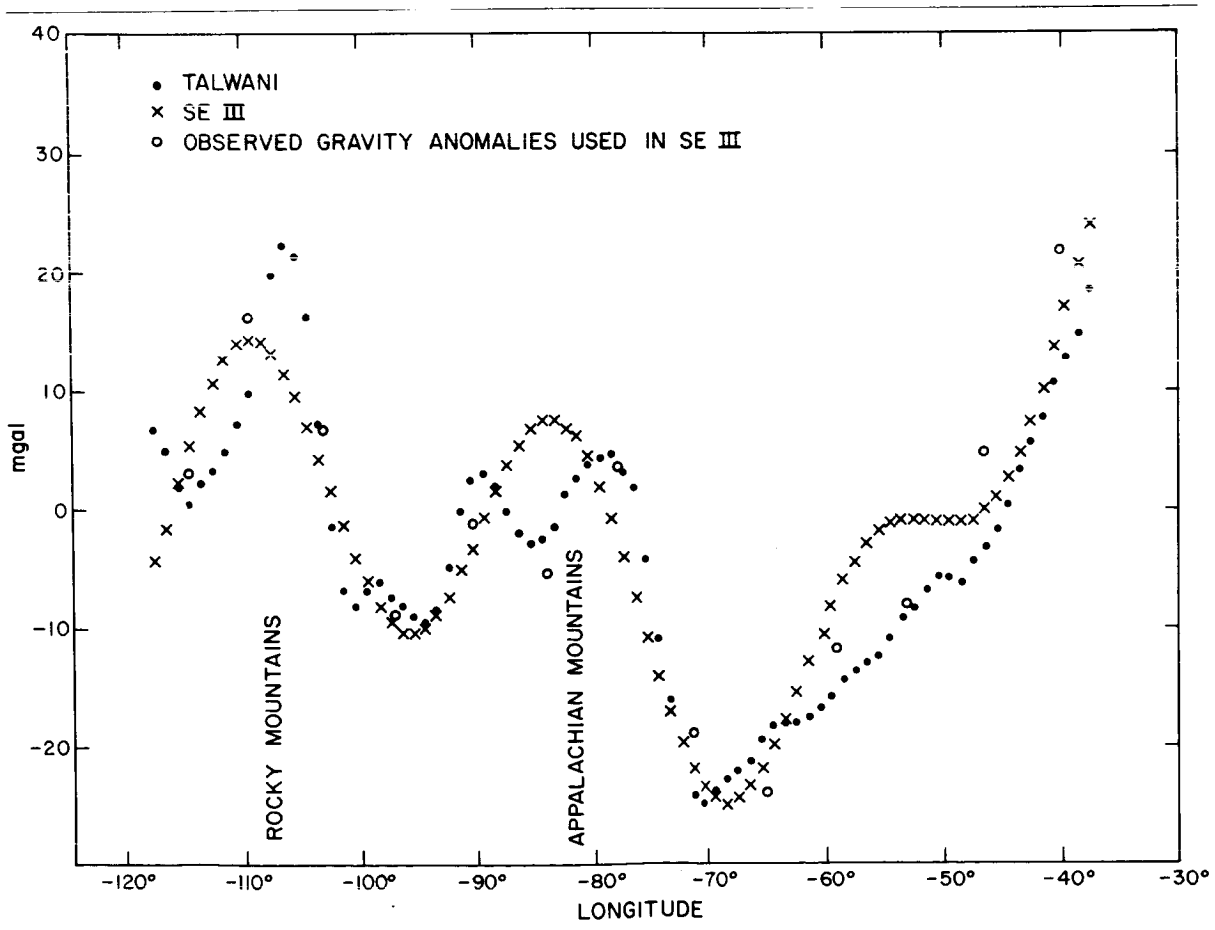

FIGURE 9.16.—Free-air mean gravity anomalies for North America at latitude 37°.5.

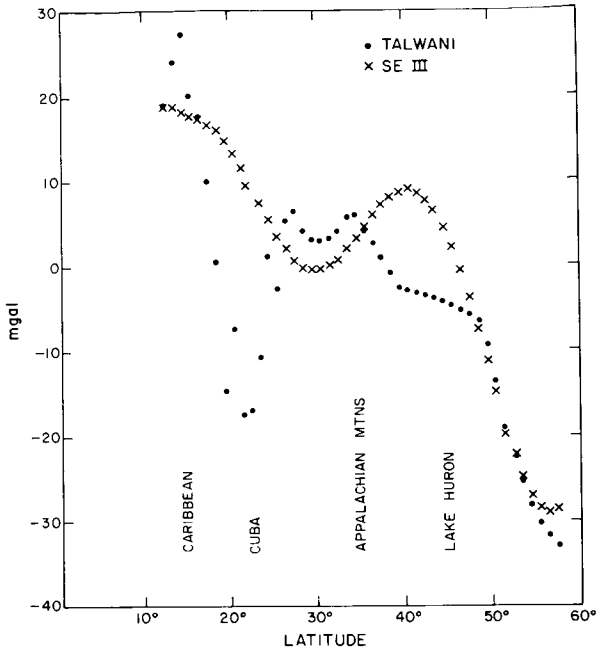

FIGURE 9.17.—Free-air mean gravity anomalies for North America at longitude −82°.5.

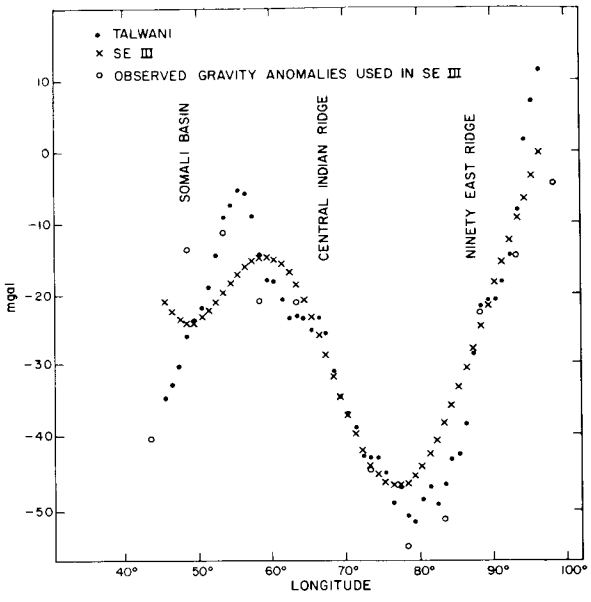

FIGURE 9.18.—Free-air mean gravity anomalies for the Indian Ocean at latitude −2°.5.

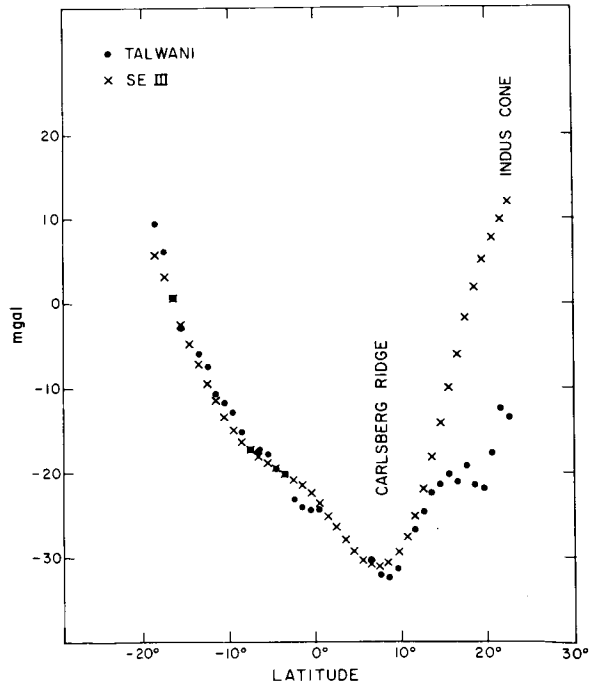

FIGURE 9.19.—Free-air mean gravity anomalies for the Indian Ocean at longitude 64°.5.

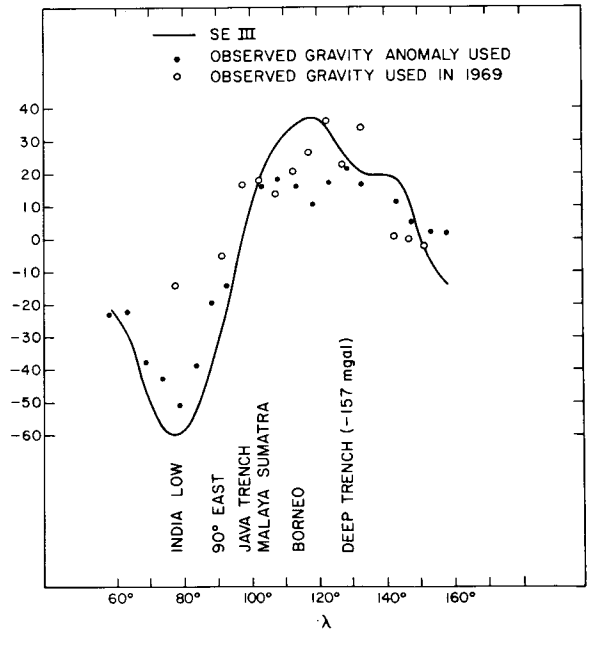

FIGURE 9.20.—Free-air mean anomalies; profile at $\phi = 2°.5$.

Figure 9.20 was selected because of the large change in the values at the India low from those given in SE II. However, the terrestrial gravity and the combination solution are in good agreement there. A further point is the disagreement, east of Borneo, between the observed gravity from the ACIC compilation and the anomalies used in 1969.

The results described above, the procedures, the tests and comparisons, and the experience of carrying out the work have led to the following conclusions about the use of artificial satellites for the determination of the geopotential:

(1) Satellite-tracking data from 25 satellites have been combined with terrestrial gravity data to determine the spherical-harmonic representation of the potential complete through degree and order 18, plus several higher harmonics to which satellite orbits are sensitive.

(2) The zonal harmonics are successfully determined from analysis of long-period and secular perturbations; the tesseral and sectorial harmonics are obtained from short-periodic satellite perturbations and terrestrial gravimetry. Low-degree and low-order $l,m \leq 8$ are primarily determined from satellite perturbations, and the short-wavelength $l,m \geq 8$, primarily from terrestrial gravity data.

(3) The principal improvements over Gaposchkin and Lambeck (1970) are due to the addition of two low-inclination satellites for the determination of the zonal harmonics, the use of a sizable number of precise laser observations, and the use of an improved set of terrestrial gravity anomalies.

(4) In the combination of satellite and surface-gravity measurements, some attention must be given to the unobserved areas.

(5) The unobserved areas were treated by using anomalies computed from a satellite-determined reference field and by taking the expected value of this residual field as zero, with a large variance.

(6) The accuracy of the solution is established by comparison with satellite orbits and with terrestrial gravity data not used in the solution.

(7) The lower harmonics have been improved such that the total orbit-computing system has an rms error of between 5 and 10 m for 4-day arcs.

(8) The accuracy of the generalized geoid is ≈ 64 mGal[2], or 3 m.

(9) The geoid is very similar to that found by Gaposchkin and Lambeck (1970); no new features have been found, and none has disappeared. Therefore, geophysical analyses from these results remain valid (see, e.g., Kaula, 1970, 1972; Gaposchkin *et al.*, 1970, unpublished).

9.5.3 The Geoid

Figure 9.21 shows the geoid computed from the $\{C_{lm}, S_{lm}\}$ given in section 9.5.2. The geoid in figure 9.21 is with respect to a best fitting ellipsoid of flattening 1/298.256; the geoid in fig. 9.21b is with respect to a hydrostatic ellipsoid of flattening 1/299.67; and the geoid in figure 9.21c is with respect to a surface computed from only those coefficients (found for the potential) which have l,m less than or equal to 5. In figure 9.22 are plotted the "gravity anomalies" calculated from the potential and with respect to the same ellipsoids as in figure 9.21.

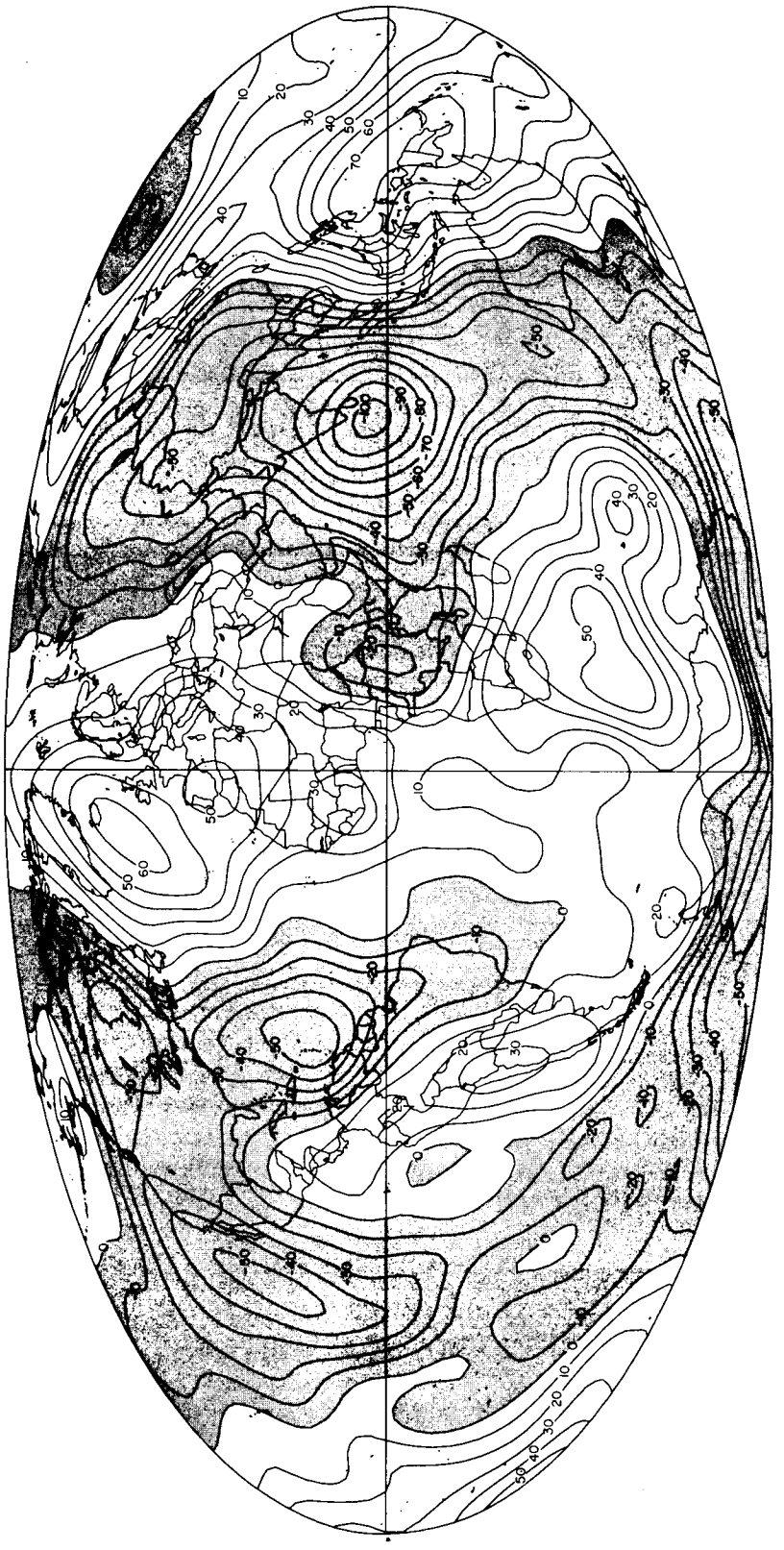

FIGURE 9.21a.—Standard Earth III, geoid heights in meters with respect to the best fitting ellipsoid, $f=1/298.256$.

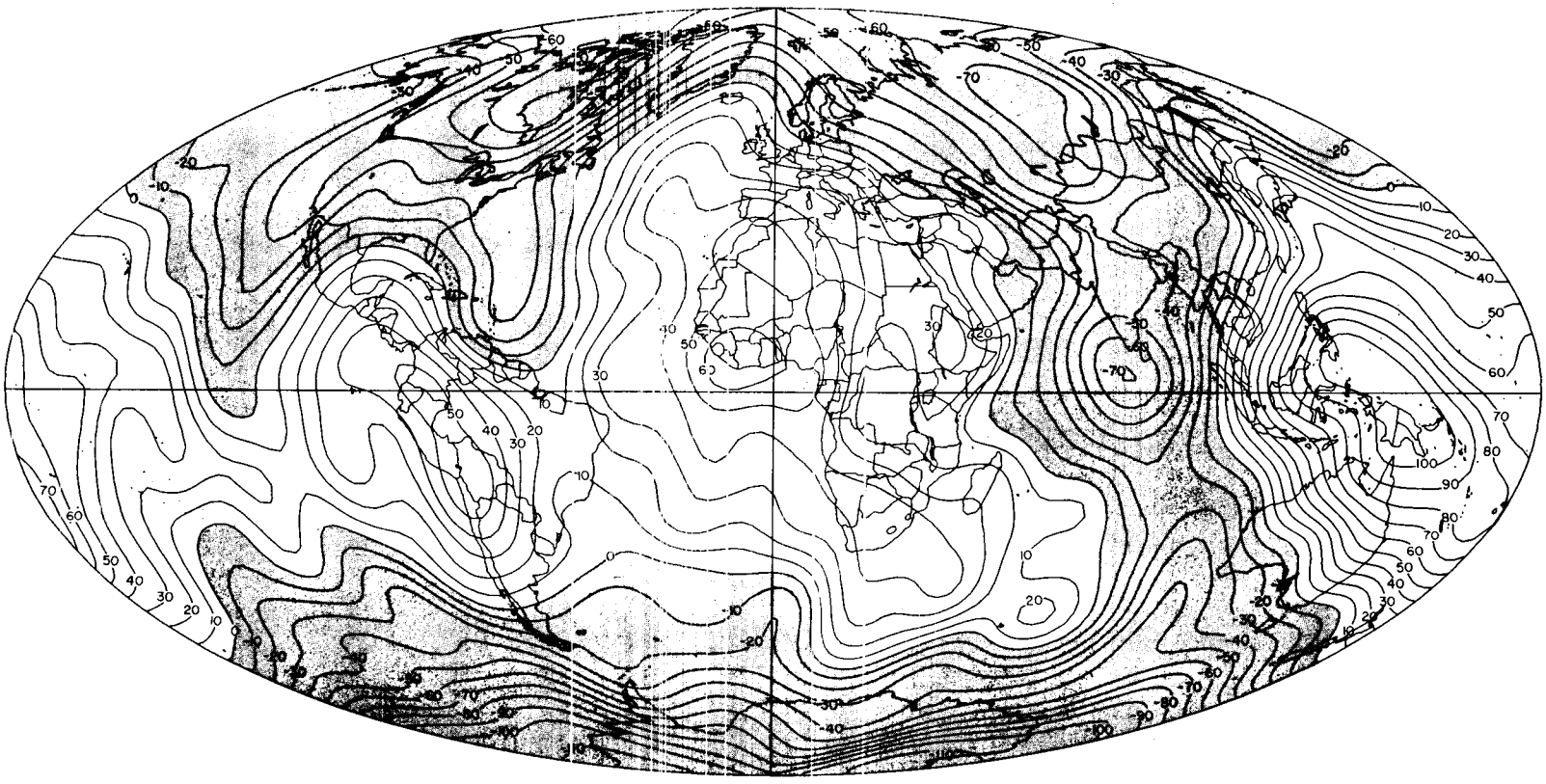

FIGURE 9.21b.—Standard Earth III, geoid heights in meters with respect to the hydrostatic ellipsoid, $f=1/299.67$.

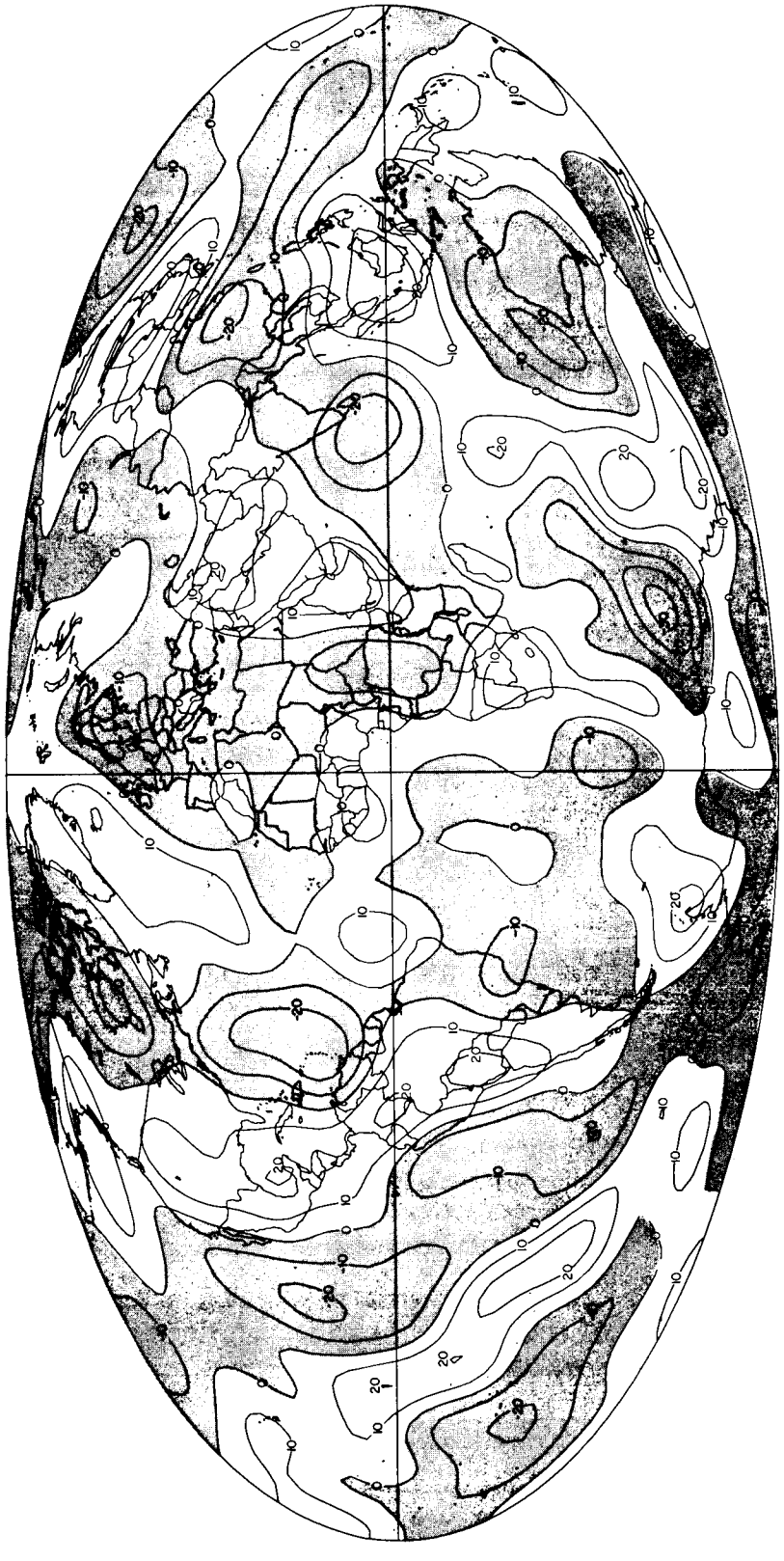

FIGURE 9.21c.—Standard Earth III, geoid heights in meters with respect to the fifth degree and order reference surface, $C_{lm}=S_{lm}=0$; $l,m\leq 5$.

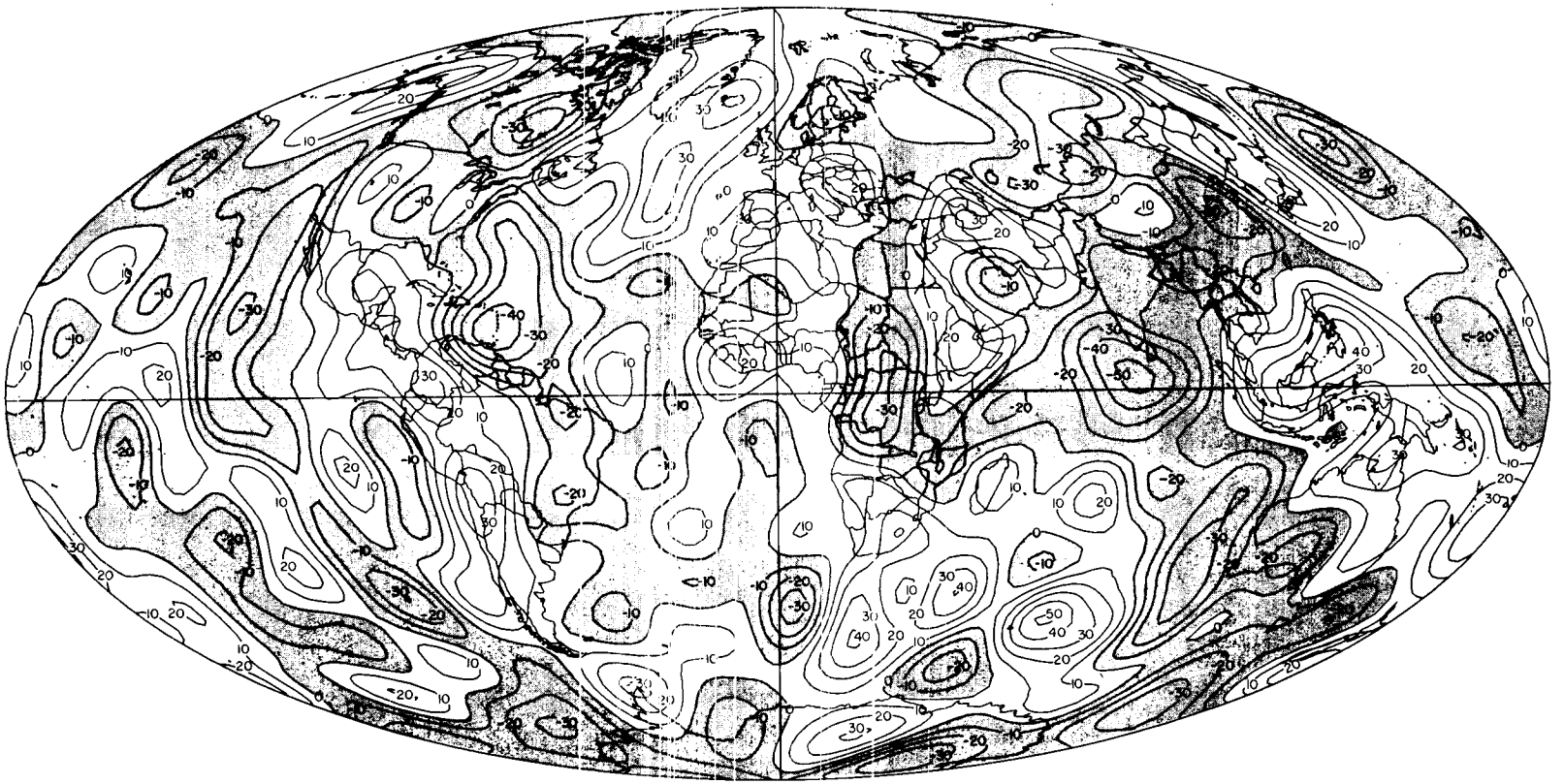

FIGURE 9.22a.—Standard Earth III, gravity anomalies in milligals with respect to the best fitting ellipsoid, $f=1/298.256$.

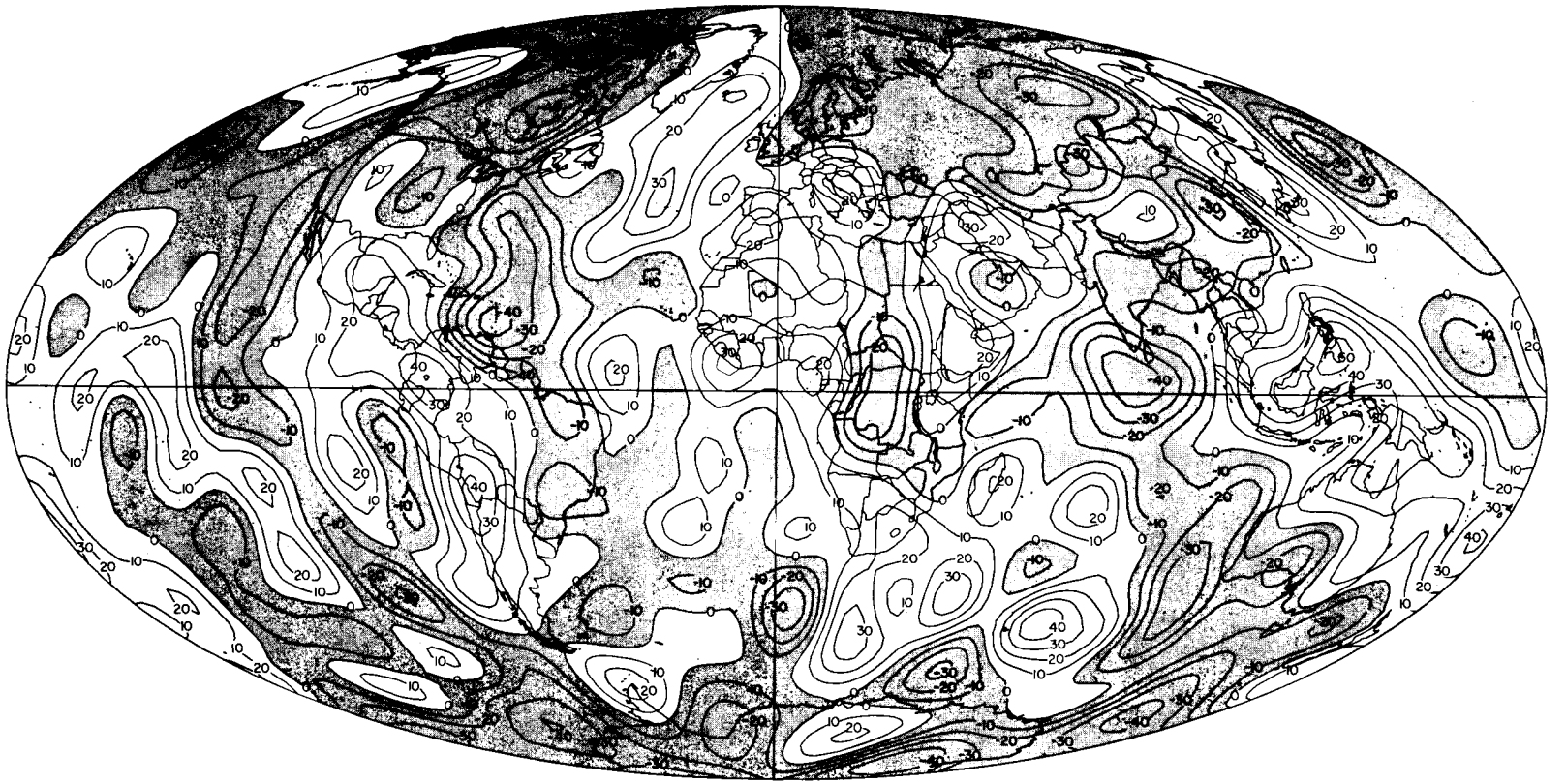

FIGURE 9.22b.—Standard Earth III, gravity anomalies in milligals with respect to the hydrostatic ellipsoid, $f=1/299.67$.

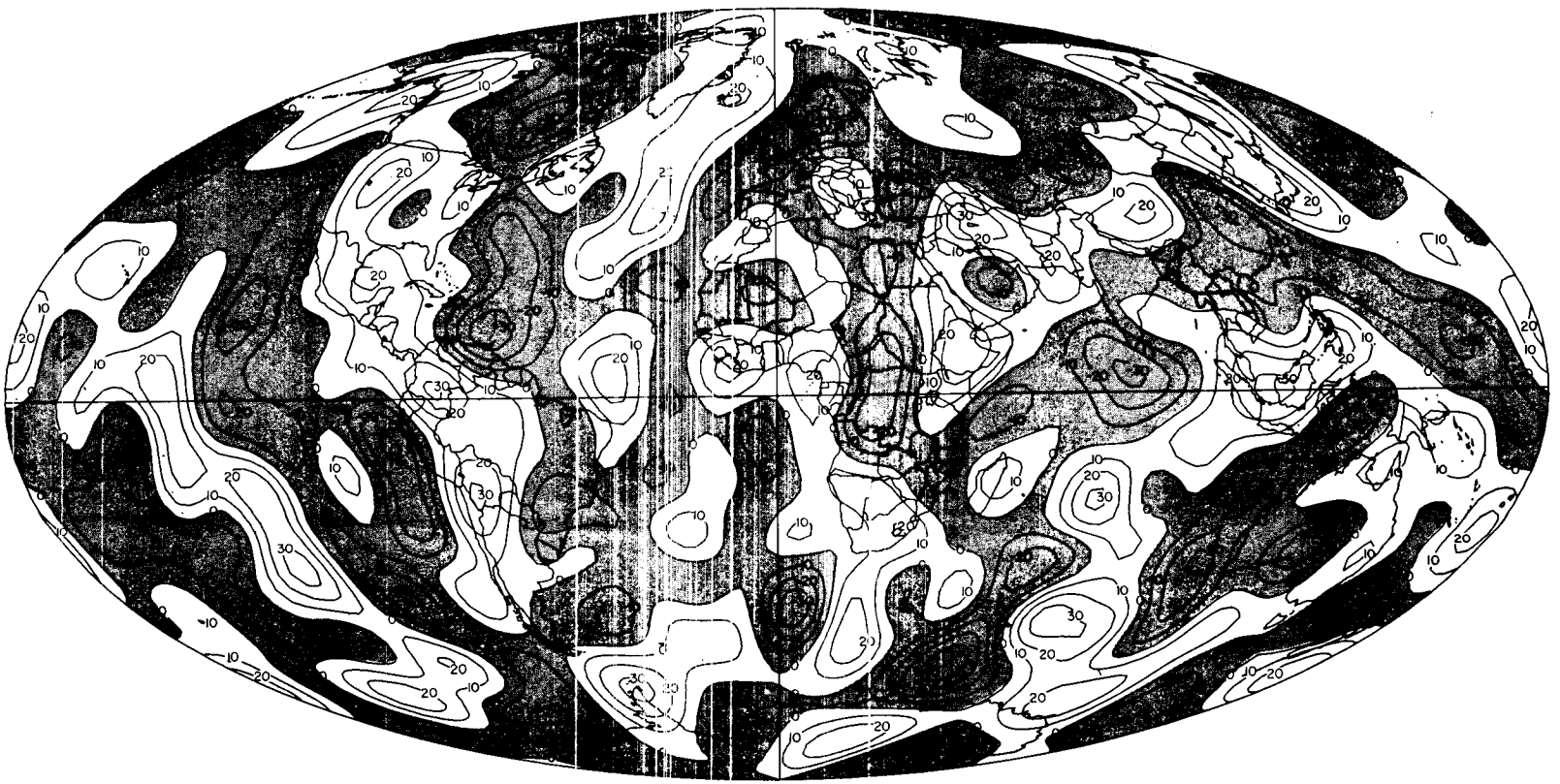

FIGURE 9.22c.—Standard Earth III, gravity anomalies in milligals with respect to the fifth degree and order reference surface, $\bar{C}_{lm}=\bar{S}_{lm}=0$; $l,m\leq 5$.

APPENDIX

TABLE 9.1.—*History of the SAO*

Satellite camera number	COSPAR number and station location	First successful observation	Last successful observation	Transferred to number and station
SC–1	9001 Organ Pass, New Mexico	November 26, 1957	March 18, 1968	9021 Mt. Hopkins, Arizona
SC–2	9002 Olifantsfontein, South Africa	March 18, 1958	December 17, 1970	9022 Olifantsfontein, South Africa (new building)
SC–3	9003 Woomera, Australia	March 11, 1968	June 1964	9023 Island Lagoon, Australia
SC–4	9004 San Fernando, Spain	March 18, 1958	----------	----------
SC–5	9005 Tokyo, Japan	April 5, 1958	May 24, 1968	9025 Dodaira, Japan
SC–6	9006 Naini Tal, India	August 29, 1958	----------	----------
SC–7	9007 Arequipa, Peru	July 4, 1958	May 30, 1970	9027 Arequipa, Peru (new building)
SC–8	9008 Shiraz, Iran	May 20, 1958	July 15, 1966	9088 Addis Ababa, Ethiopia
SC–9	9009 Curaçao, Netherlands Antilles	June 22, 1958	July 10, 1966	9029 Natal, Brazil
SC–10	9010 Jupiter, Florida	June 10, 1958	October 12, 1967	9091 Dionysos, Greece
SC–11	9011 Villa Dolores, Argentina	July 10, 1958	October 28, 1966	9031 Comodoro Rivadavia, Argentina
SC–11a[a]	9040 Dakar, Senegal	December 1970	September 1971	9040 Ouagadougou, Upper Volta
SC–12	9012 Maui, Hawaii	July 4, 1958	----------	----------

[a] On loan to CNES.

Baker-Nunn Satellite-Tracking Cameras

First successful observation	Last successful observation	Transferred to number and station	First successful observation	Last successful observation
March 31, 1968	----------	----------	----------	----------
January 5, 1971	----------	----------	----------	----------
July 1964	April 13, 1973	9043 Orroral Valley, Australia	January 1974 (est)	----------
----------	----------	----------	----------	----------
May 24, 1968	----------	----------	----------	----------
----------	----------	----------	----------	----------
June 1, 1970	----------	----------	----------	----------
August 15, 1966	----------	----------	----------	----------
September 27, 1966	May 5, 1970	9039 Natal, Brazil (new building)	May 7, 1970	----------
December 7, 1967	June 25, 1969	9030 Dionysos, Greece (new building)	July 3, 1969	----------
November 14, 1966	January 1970	See SC 11a	----------	----------
May 1972	----------	----------	----------	----------
----------	----------	----------	----------	----------

TABLE 9.2.—*Laser Sites*

Station number NGSP	SAO	Station location	Period of operation
9901	7901	Organ Pass, New Mexico	March 1966 to July 1967
9912	7912	Maui, Hawaii	May 24, 1968 to March 27, 1969
9902	7902	Olifantsfontein, South Africa	February 1971 to present
9907	7907	Arequipa, Peru	December 1970 to present
9921	7921	Mt. Hopkins, Arizona (prototype)	December 1967 to June 20, 1972
9921	7921	Mt. Hopkins, Arizona (rebuilt system)	November 1972 to present
9929	7929	Natal, Brazil	November 1970 to present
9991	7991	Athens, Greece	September 1968 to June 1969
9930	7930	Dionysos, Greece	July 1969 to present
9925	7925	Tokyo, Japan	November 1972 to present

TABLE 9.3.—*Air Force Baker-Nunn Sites*

Station number NGSP	SAO	Station location	Period of operation
9425	9113	Edwards AFB, California (Rosamund)	December 1960 to present
9424	9114	Cold Lake, Canada (I)	January 1963 to June 1971
9426	9115	Harestua, Norway	December 1959 to July 1967
	9116	Santiago, Chile	September 1960 to May 1964
9427	9117	Sand Island (Johnston Island), Pacific	September 1963 to present
	9118	Kwajalein Island	Not operational for satellite photography
9119	9119	Mt. John, New Zealand	October 1969 to present
9120	9120	San Vito, Italy	March 1971 to present
	9124	Cold Lake, Canada (II)	July 1971 to present
	9010[a]	Jupiter, Florida (AF)	June 1968 to July 1971

[a] Site previously occupied by SAO Baker-Nunn camera (see figure 9.10).

TABLE 9.4.—*Sources of Data Used in the Orbit-Generation Program*

Agency	Instrument
SAO	Baker-Nunn cameras
	Lasers
	MOONWATCH
NASA/GSFC	PRIME MINITRACK
	Lasers
U.S. Air Force	Baker-Nunn cameras
CNES	CNES cameras
	Lasers

TABLE 9.5.—*Number of Observations*

Line	n	Line	n
8015–8019	29	9006–9091	10
8015–9004	122	9006–9426	19
8015–8010	133	9007–9009	263
8015–9431	25	9007–9010	86
8015–8011	67	9007–9011	437
8015–9091	30	9007–9029	74
8019–9004	301	9007–9031	32
8019–9091	61	9008–9028	25
9001–9009	183	9008–8011	8
9001–9010	154	9008–9426	38
9001–9012	187	9009–9010	248
9001–9425	20	9009–9011	201
9001–9424	74	9009–9424	13
9001–9427	16	9010–9029	6
9002–9008	7	9010–9424	38
9002–9028	25	9011–9029	7
9004–9006	14	9011–9031	9
9004–9008	139	9012–9021	29
9004–9009	43	9012–9425	14
9004–9010	41	9012–9424	24
9004–9028	35	9012–9427	216
9004–9029	42	9021–9425	57
9004–8010	192	9021–9427	8
9004–9431	65	9028–9091	37
9004–8011	164	9029–9031	26
9008–9091	442	8010–9431	13
9004–9426	60	8010–8011	27
9005–9006	61	9431–9432	42
9005–9012	25	9431–9091	43
9005–9427	16	9432–9091	30
9006–9008	172	8425–9424	30

TABLE 9.6.—*Stations Whose Coordinates Were Determined by Orbital Theory*

Orbital theory alone		Orbital plus geometric theory		
				9021
8818	9003	1021	9001	9028
	9020	1030	9002	9029
	9023	1042	9004	9031
			9006	9050
		7050	9007	9091
		8815	9009	
		8816	9010	9113
			9011	9114
		8015	9012	9115
		8019		9117

TABLE 9.7.—*Dynamical Data Used in SE III*

Satellite										
Number	Name	Inclination	Eccentricity	a (km)	Perigee (km)	Laser observations	Station coordinates	Zonal harmonics	Tesseral harmonics	Number of files
7001701	DIAL	5°	0.088	7344	301			x		
7010901	PEOLE	15	0.017	7070	635	x		x	x	4
6001301	COURIER 1B 1970ν1	28	0.016	7465	965		x	x	x	7
5900101	VANGUARD 2 1959 α1	33	0.165	8300	557		x	x	x	7
5900701	1959 η1	33	0.188	8483	515		x			18
6100401	1961 δ1	39	0.119	7960	700				x	4
6701401	D1D	39	0.053	7337	569	x	x		x	10
6701101	D1C	40	0.052	7336	579	x	x		x	9
6503201	Explorer 24 BE-C	41	0.026	7311	941	x	x		x	13
6202901	TELSTAR 1 1962 $\alpha\epsilon$1	44	0.241	9672	962			x		4
6000902	1960 ι2	47	0.011	7971	1512		x	x	x	10
6206001	ANNA-1B 1962 $\beta\mu$1	50	0.007	7508	1077		x	x	x	12
6302601	Geophysical Research	50	0.062	7237	424			x		6
6508901	Explorer 29 GEOS-1	59	0.073	8074	1121	x	x	x	x	56
6101501	TRANSIT 4A 6101	67	0.008	7318	885			x	x	10
6101502	INJUN-1 6102	67	0.008	7316	896				x	9
6506301	SECOR-5	69	0.079	8159	1137		x		x	2
6400101		70	0.002	7301	921			x	x	4
6406401	Explorer 22 BE-B	80	0.012	7362	912	x	x	x	x	6
6508101	OGO-2	87	0.075	7344	420			x	x	5
6600501	OSCAR-07	89	0.023	7417	868		x		x	1
6304902	5BN-2	90	0.005	7473	1070		x		x	5
6102801	MIDAS-4 1961 $\alpha\delta$1	96	0.013	10005	3503		x	x	x	6
6800201	Explorer 36 GEOS-2	106	0.031	7709	1101	x	x		x	13
6507801	OV1-2	144	0.182	8306	416		x		x	4

TABLE 9.8.—*Assumed Accuracy for Data Used in SE III*

Data	Weight	Remarks
Baker-Nunn	4″	
Smoothed Baker-Nunn	2″	
SAO laser	5 m	Observed before 1970
CNES laser	10 m	Observed before 1970
GSFC laser	5 m	Observed before 1970
ISAGEX laser	5 m	1971 International Campaign

TABLE 9.9.—*Satellite Center of Mass*[a]

BE–B and BE–C	$\Delta = 0.3493 - 1.09183 \times 10^{-3} \times \phi + 2.9222 \times 10^{-6} \times \phi^2 - 1.5338 \times 10^{-7} \times \phi^3$ ($\Delta = 0$ for $\phi > 120°$)
D1C and D1D	$\Delta = 0.164612 - 2.824 \times 10^{-3} \times \phi + 2.0639 \times 10^{-5} \times \phi^2 + 8.1214 \times 10^{-7} \times \phi^3 - 5.81302 \times 10^{-9} \times \phi^4$ ($\Delta = 0$ for $\phi > 120°$)
GEOS–1	$\Delta = 0.3972 \cos \phi$
GEOS–2	$\Delta = 0.4298 \cos \phi$
PEOLE	$\Delta = 0.48 - 1.108 \times 10^{-2} \times \phi + 4.19267 \times 10^{-4} \times \phi^2 - 3.619 \times 10^{-6} \times \phi^3 + 8.12555 \times 10^{-9} \times \phi^4$ ($\Delta = 0.768$ for $\phi > 96°$)

[a] From D. Arnold and J. Latimer.

TABLE 9.10.—*Number of Observations Used in the Dynamical Solution*

Station no.	No. of observations
Pre-ISAGEX Data (15 satellites, 140 arcs)	
7050	274
8818	1223
8015	612
8815	1970
9001	4357
9002	2120
9003	349
9023	2630
9004	3343
9005	945
9006	3170
9007	1646
9008	2301
9009	1825
9010	2424
9011	1637
9012	3088
9028	525
9029	261
9031	467
9021	81
9066	809
9025	9
9080	47
9091	143
9921	9
8816	2382
8804	200
9901	761
ISAGEX Data (3 satellites, 15 arcs)	
7050	1425
7060	1514
8804	625
8809	1178
8820	296
9902	1484
9907	746
9921	225
9929	213
9930	89
9030	172
9021	29

TABLE 9.11.—*Adopted Constants*

$GM = 3.986\,013 \times 10^{20}$ cm^3 sec^{-2}	
$c = 2.997\,925 \times 10^{10}$ cm sec^{-1}	(velocity of light)
$k_2 = 0.30$	(Love number)

TABLE 9.12.—*DSN Data Used in LS 37*

Flight	Tracking time period	δ (deg)
Mariner 4 encounter	July 10–21, 1965	−3
Mariner 5 cruise	July 28–September 16, 1967	−8 to +8
Mariner 5 encounter	October 14–25, 1967	6
Mariner 5 post encounter	October 28–November 21, 1967	+2 to −2
Mariner 6	July 26–31, 1969	−24

TABLE 9.13.—*LS 37 Coordinates, From Mottinger (1973)*

Station	r (Mm)	λ	X (Mm)	Y (Mm)
DSS 11	5.206 340 9	243°15059	−2.351 428 8	−4.645 080 0
DSS 12	5.212 052 5	243°19452	−2.350 442 4	−4.651 979 4
DSS 14	5.203 997 8	243°11047	−2.353 621 1	−4.641 342 5
DSS 41	5.450 201 9	136°88749	−3.978 718 6	3.724 848 8
DSS 42	5.205 349 4	148°98126	−4.460 978 2	2.682 412 4
DSS 51	5.742 939 9	27°68542	5.085 441 5	2.668 265 9
DSS 61	4.862 608 3	355°75097	4.849 243 1	−0.360 278 5
DSS 62	4.860 818 1	355°63217	4.846 700 7	−0.370 196 0

TABLE 9.14.—*The Stations Related by the Survey*

Location	Station pairs	$1/\sigma^2$ (m^{-2})
Maryland	7050–6002	1.0
Hawaii	9012–6011	1.0
Argentina	9011–6019	1.0
Japan	9005–6013	0.1
Spain	DSS 61–DSS 62	5.0
	9004–DSS 61	0.20
Central Europe	9066–8015	0.25
	9066–6065	0.0025
	8816–9030	0.01
Brazil	9029–6067	1.0
California	DSS 14–DSS 12	5.0
	DSS 14–DSS 11	5.0
	9113–DSS 14	0.7
	9113–6111	2.0
	6111–6134	5.0
Ethiopia	9028–6042	2.0
Australia	6060–DSS 41	1.0
	9003–DSS 41	1.0
	9003–9023	1.0
	DSS 41–DSS 42	0.04
South Africa	9002–6068	1.0
	9002–DSS 51	0.1

TABLE 9.15.—*Geodetic Coordinates Used in SE–III*

Agency	Sta. no.	Latitude	Longitude	H_{msl} (m)	H_{ell} (m)	Datum	GH (m)	Name	X	Y (megameters)	Z
									a = 6 378 388.0 m		$1/f$ = 297.0000
JPL	DSS61	+40 25 47.717	355 45 06.178	788.4	766.4	EU50	−22.0	MADRI1	4.849 332 01	−.360 171 92	4.115 005 79
JPL	DSS62	+40 27 15.273	355 38 00.572	738.3	716.3	EU50	−22.0	MADRI2	4.846 789 68	−.370 090 30	4.117 028 98
NOAA	6006	+69 39 44.2698	018 56 31.9076	106.0	119.0	EU50	+13.0	TROMSO	2.103 040 80	.721 762 62	5.958 301 35
NOAA	6012	+19 17 23.227	166 36 39.780	3.5	3.5	ASTR	0.	WAKEIS	−5.858 825 61	1.394 575 85	2.093 679 89
NOAA	6015	+36 14 29.527	059 37 42.729	991.0	959.0	EU50	−32.0	MASMAD	2.604 467 55	4.444 277 33	3.750 465 44
NOAA	6016	+37 26 42.628	015 02 47.308	9.24	−6.8	EU50	−16.0	SICILY	4.896 494 12	1.316 269 43	3.856 792 86
NOAA	6020	−27 10 39.213	250 34 37.495	230.8	230.8	EI67	0.0	EASTER	−1.888 796 16	−5.355 031 80	−2.895 877 21
NOAA	6031	−46 25 03.491	168 19 31.155	0.9	.	NZ49	.	INVERC	−4.313 886 56	.891 374 93	−4.597 458 23
NOAA	6039	−25 04 07.146	229 53 11.882	339.4	339.4	PITC	0.0	PITCAN	−3.724 932 90	−4.421 406 20	−2.686 144 64
NOAA	6043	−52 46 52.468	290 46 29.573	80.7	.	CH63	.	SOMBRO	1.371 375 97	−3.614 945 94	−5.056 020 37
NOAA	6044	−53 01 12.031	073 23 27.415	3.8	3.8	HR69	0.0	HERDIS	1.099 079 48	3.684 662 62	−5.071 987 40
NOAA	6050	−64 46 33.98	295 56 37.04	16.44	.	PLMR	.	PALMER	1.192 460 38	−2.451 024 27	−5.747 260 40
NOAA	6053	−77 50 46.2487	166 38 07.5845	19.0	.	CA62	.	MCMURD	−1.310 740 80	.311 405 86	−6.213 514 12
NOAA	6055	−07 58 16.634	345 35 32.764	70.94	.	AS58	.	ASCENS	6.118 561 51	−1.571 840 78	−.878 654 81
NOAA	6065	+47 48 07.011	011 01 29.378	943.2	942.4	EU50	−0.8	PEISEN	4.213 664 69	.820 948 44	4.702 898 97
NOAA	6069	−37 03 26.2572	347 40 53.5548	24.8	24.8	TR68	0.0	DACUNA	4.979 075 44	−1.087 294 30	−3.822 545 43
NOAA	6073	−07 20 58.5270	072 28 32.1556	3.9	.	GRAC	.	CHAGOS	1.904 935 20	6.032 722 80	−.810 502 73
NOAA	6078	−17 41 46.956	168 17 57.921	15.2	.	EFAT	.	NWHBRD	−5.952 163 90	1.232 696 45	−1.926 425 29
CNES	8804	+36 27 50.1191	353 47 41.2862	25.40	−9.6	EU50	−35.0	SFRLAS	5.105 702 63	−.555 125 50	3.769 769 71
CNES	8809	+43 56 00.190	005 42 48.788	657.82	649.4	EU50	−8.4	HTPRVL	4.578 434 82	.458 082 30	4.403 291 78
CNES	8809	+43 56 00.190	005 42 48.788	657.82	647.8	EU50	−10.0	HTPRVL	4.578 435 96	.458 082 42	4.403 292 89
CNES	8815	+43 55 59.183	005 42 48.382	657.83	649.4	EU50	−8.4	HTPRVL	4.578 458 32	.458 075 55	4.403 270 50
CNES	8816	+37 45 17.043	022 49 43.313	803.11	788.7	EU50	−14.4	STPHNL	4.654 421 39	1.959 282 40	3.884 501 87
CNES	8818	+31 43 19.25	357 34 54.06	855.65	813.7	EU50	−42.0	BECHRL	5.426 419 14	−.229 172 16	3.334 728 56
SAO	9930	+38 04 46.147	023 55 59.991	473.02	466.62	EU50	−6.4	DIOSLS	4.595 303 76	2.039 557 34	3.912 743 97
CNES	8015	+43 56 01.142	005 42 49.277	658.85	650.4	EU50	−8.4	HTPROV	4.578 415 31	.458 091 32	4.403 314 74
CNES	8019	+43 43 36.496	007 18 03.309	377.42	369.4	EU50	−8.	NICEFR	4.579 557 55	.586 729 53	4.386 538 88
SAO	9004	+36 27 51.3666	353 47 42.0891	26.00	−9.0	EU50	−35.0	S.FERN	5.105 682 54	−.555 103 20	3.769 801 00
SAO	9006	+29 21 38.97	079 27 25.51	1927.	1827.	EU50	−100.	NA.TAL	1.018 269 70	5.471 218 80	3.109 759 10
SAO	9008	+29 38 18.112	052 31 11.445	1597.4	1549.4	EU50	−48.0	SHIRAZ	3.376 963 53	4.404 102 29	3.136 405 45
SAO	9028	+08 44 56.39	038 57 33.61	1923.2	1820.2	EU50	−105.	ETHIOP	4.903 855 04	3.965 304 21	.964 021 18
SAO	9030	+38 04 46.564	023 56 00.130	472.64	466.24	EU50	−6.4	DIOSBN	4.595 294 86	2.039 557 10	3.912 753 85
SAO	9051	+37 58 40.31	023 46 42.89	187.9	180.9	EU50	−7.0	ATHENG	4.606 949 19	2.029 849 75	3.903 882 23
INT.	8010	+46 52 40.318	007 27 58.238	903.44	900.3	EU50	−3.1	ZIMMWL	4.331 391 50	.567 637 49	4.633 236 85
INT.	9431	+56 56 54.98	024 03 37.81	8.0	2.4	EU50	−5.6	RIGALT	3.183 998 49	1.421 638 06	5.322 893 86
INT.	9432	+48 38 04.56	022 17 57.88	189.0	187.5	EU50	−1.5	UZGROD	3.907 492 64	1.602 532 61	4.764 032 96
INT.	8011	+52 08 39.116	358 01 59.492	113.19	108.6	EU50	−4.6	MALVRN	3.920 249 42	−.134 624 34	5.012 850 24
SAO	9091	+38 04 48.215	023 56 01.587	466.25	460.85	EU50	−6.4	DIONBN	4.595 247 88	2.039 575 10	3.912 790 60
AF	9426	+60 12 40.38	010 45 08.74	575.92	581.7	EU50	+5.8	HAREST	3.121 368 36	.592 747 33	5.512 829 59
AF	9427	+16 44 45.39	190 29 05.59	5.0	5.0	JI61	0.0	JOHNST	−6.007 589 42	−1.111 801 81	1.825 951 15

TABLE 9.15.—*(Cont'd)*

Agency	Sta. no.	Latitude	Longitude	H_{msl} (m)	H_{ell} (m)	Datum	GH (m)	Name	X	Y (megameters)	Z
									a = 6 377 397.2 m		$1/f$ = 299.1528
NOAA	6013	+31 23 30.1397	130 52 24.8595	65.9	46.9	TKYO	−19.	KANOYA	−3.565 710 19	4.120 207 06	3.302 741 97
SAO	9005	+35 40 11.078	139 32 28.222	59.77	59.8	TKYO	+0.0	TOKYOJ	−3.946 555 04	3.365 774 71	3.698 152 01
SAO	9025	+36 00 08.606	139 11 43.159	855.89	855.4	TKYO	−0.5	DODRAJ	−3.910 298 61	3.375 836 40	3.728 538 81
									a = 6 378 206.4 m		$1/f$ = 294.9787
GSFC	1021	+38 25 49.628	282 54 48.225	5.76	6.7	NA27	+0.9	IBPOIN	1.118 061 22	−4.876 472 15	3.942 793 54
JPL	DSS11	+35 23 22.346	243 09 05.262	1036.3	1014.3	NA27	−22.0	GOLDS1	−2.351 415 01	−4.645 228 10	3.673 582 42
JPL	DSS12	+35 17 59.854	243 11 43.414	988.9	966.9	NA27	−22.0	GOLDS2	−2.350 428 27	−4.652 127 55	3.665 447 06
JPL	DSS14	+35 25 33.340	243 06 40.850	1031.8	1009.8	NA27	−22.0	GOLDS4	−2.353 607 04	−4.641 490 95	3.676 870 68
NOAA	6001	+76 30 03.4106	291 27 51.8867	206.0	238.	NA27	+32.	THULEG	.546 580 65	−1.390 107 20	6.180 059 57
NOAA	6002	+39 01 39.003	283 10 26.942	44.3	43.9	NA27	−0.4	BELTVL	1.130 798 67	−4.830 987 41	3.994 520 58
NOAA	6003	+47 11 07.132	240 39 48.118	368.74	356.2	NA27	−12.5	MOSELK	−2.127 796 49	−3.786 014 63	4.655 848 03
NOAA	6004	+52 42 54.89	174 07 37.87	36.8	−9.2	NA27	−46.0	SHEMYA	−3.851 745 00	.396 192 09	5.051 199 36
NOAA	6011	+20 42 38.561	203 44 28.529	3049.27	3041.3	OHAW	−8.	HAVAII	−5.466 062 54	−2.404 129 70	2.242 407 61
NOAA	6022	−14 20 12.216	189 17 13.242	5.34	5.3	AS62	0.0	PAGOGO	−6.099 842 41	−.997 467 71	−1.569 008 83
NOAA	6038	+18 43 44.93	249 02 39.28	23.2	23.2	ISOC	0.0	GIGEDO	−2.161 114 55	−5.642 916 48	2.034 864 29
NOAA	6047	+06 55 26.132	122 04 04.838	9.39	10.1	LZ11	+0.7	ZAMBOA	−3.361 826 92	5.365 864 13	.763 735 96
NOAA	6111	+34 22 54.537	242 19 09.484	2284.41	2258.11	NA27	−26.3	WRWDBA	−2.448 815 18	−4.688 125 78	3.582 568 64
NOAA	6123	+71 18 49.882	203 21 20.720	8.3	−6.	NA27	+1.3	PTBRRW	−1.881 756 24	−.812 583 99	6.019 403 56
NOAA	6134	+34 22 44.444	242 19 09.259	2198.37	2172.07	NA27	−26.3	WRWDBB	−2.448 868 89	−4.668 215 79	3.582 263 30
GSFC	7050	+39 01 13.676	283 10 18.035	54.812	56.1	NA27	+1.2	GODLAS	1.130 704 28	−4.831 524 29	3.993 921 50
GSFC	7060	+13 18 28.6136	144 44 05.3744	85.873	85.9	GUAM	0.	GUAMLS	−5.068 867 06	3.584 334 33	1.458 509 59
SAO	9901	+32 25 24.56	253 26 51.17	1651.33	1648.93	NA27	−2.4	ORGN L	−1.535 725 37	−5.167 146 55	3.400 867 41
SAO	9912	+20 42 37.23	203 44 24.03	3034.14	3026.1	OHAW	−8.	MAUIHL	−5.466 115 22	−2.404 010 58	2.242 363 93
SAO	9921	+31 41 02.87	249 07 21.35	2383.14	2370.4	NA27	−12.7	MHSAOL	−1.936 750 26	−5.077 855 96	3.331 744 02
SAO	9001	+32 25 25.56	253 26 51.17	1651.3	1648.9	NA27	2.4	ORGN P	−1.535 725 37	−5.167 146 55	3.400 867 41
SAO	9010	+27 01 12.882	279 53 13.008	15.13	26.5	NA27	+11.4	JUPITE	.976 312 16	−5.601 550 92	2.880 064 23
SAO	9012	+20 42 37.50	203 44 24.08	3034.14	3026.1	OHAW	−8.	MAUI,H	−5.466 111 95	−2.404 010 72	2.242 371 70
SAO	9021	+31 41 02.67	249 07 21.35	2383.12	2370.4	NA27	−12.7	MTHPBN	−1.936 751 41	−5.077 858 98	3.331 738 78
AF	9425	+34 57 50.742	242 05 11.584	784.231	760.4	NA27	−23.8	ROSMND	−2.449 975 02	−4.624 572 36	3.634 851 19
AF	9424	+54 44 33.858	249 57 26.389	704.6	701.7	NA27	−2.9	CLALBC	−1.264 825 81	−3.467 044 42	5.185 275 10

TABLE 9.15.—*(Cont'd)*

Agency	Sta. no.	Latitude	Longitude	H_{msl} (m)	H_{ell} (m)	Datum	GH (m)	Name	X	Y (megameters)	Z
									a = 6 378 249.145 m		$1/f$ = 293.465
JPL	DSS51	−25 53 21.15	027 41 08.53	1391.0	1399.0	ARCC	+8.	JOHANG	5.085 580 65	2.668 370 93	−2.768 408 99
NOAA	6042	+08 46 08.501	038 34 49.164	1886.46	1857.5	ADDN	−29.0	ADDABA	4.900 912 36	3.968 254 30	.966 118 39
NOAA	6063	+14 44 44.228	342 30 55.594	26.3	26.3	YO67	0.	SENGAL	5.884 522 66	−1.853 639 29	1.612 760 05
NOAA	6064	+12 07 51.750	015 02 06.151	295.4	316.4	ADDN	+21.0	FTLAMY	6.023 554 50	1.617 955 70	1.331 525 26
NOAA	6068	−25 52 56.98	027 42 25.17	1523.8	1531.8	ARCC	+8.	JOHANS	5.084 982 16	2.670 466 91	−2.767 797 68
NOAA	6075	−04 40 07.23	035 28 50.38	588.98	.	SEIL	.	MAHEIS	3.602 875 32	5.238 427 44	−.515 676 27
CNES	8820	+14 46 04.878	342 35 22.462	28.48	28.5	YO67	0.0	DAKARL	5.886 315 60	−1.845 836 00	1.615 157 50
SAO	9902	−25 57 33.851	028 14 53.909	1543.88	1551.9	ARCC	+8.	OLIFTL	5.056 260 03	2.716 634 10	−2.775 471 14
SAO	9002	−25 57 33.85	028 14 53.91	1544.1	1552.1	ARCC	+8.	OLFSFT	5.056 260 19	2.716 634 22	−2.775 471 20
CNES	9020	+14 46 05.975	342 35 22.936	24.59	24.6	YO67	0.0	DAKARS	5.886 308 05	−1.845 818 78	1.615 189 11
SAO	9022	−25 57 33.815	028 14 54.351	1543.34	1551.3	ARCC	+8.	OLIFTS	5.056 254 16	2.716 644 91	−2.775 469 88
SAO	9028	+08 44 47.23	038 57 30.48	1925.2	1896.2	ADDN	−29.	ETHIOP	4.903 904 76	3.965 221 35	.963 656 06
									a = 6 378 160.0 m		$1/f$ = 298.25
JPL	DSS41	−31 22 59.4305	136 53 10.1244	148.28	147.3	AUGD	−1.0	WOOMAU	−3.978 581 94	3.724 896 03	−3.302 323 84
JPL	DSS42	−35 24 08.0381	148 58 48.2057	656.08	664.5	AUGD	+8.4	TIDBIN	−4.460 848 00	2.682 461 57	−3.674 729 47
NOAA	6008	+05 26 55.325	304 47 42.832	18.38	+8.7	SA69	−9.7	SURNAM	3.623 335 39	−5.214 222 41	.601 599 57
NOAA	6009	−00 05 50.468	281 34 49.212	2682.1	2706.7	SA69	+24.6	ECUADR	1.280 904 38	−6.250 970 09	−.010 769 28
NOAA	6019	−31 56 33.9540	294 53 41.3415	608.18	621.2	SA69	+13.0	DLORES	2.280 712 97	−4.914 539 50	−3.355 387 84
NOAA	6023	−10 35 08.0374	142 12 35.4955	60.5	61.7	AUGD	+1.2	THURIS	−4.955 236 08	3.842 309 46	−1.163 990 61
NOAA	6032	−31 50 28.992	115 58 26.618	26.30	32.5	AUGD	+6.2	PERTHA	−2.375 257 20	4.875 599 99	−3.345 531 90
NOAA	6060	−30 18 39.4182	149 33 36.8921	211.08	211.8	AUGD	+0.7	CULGOR	−4.751 500 46	2.792 121 93	−3.200 296 97
NOAA	6067	−05 55 37.414	324 50 06.200	40.63	66.7	SA69	+26.1	BRAZIL	5.186 494 84	−3.653 919 32	−.654 244 53
SAO	9907	−16 27 55.085	288 30 26.814	2452.274	2486.5	SA69	+34.2	ARQUPL	1.942 859 44	−5.804 087 19	−1.796 876 89
SAO	9929	−05 55 38.616	324 50 08.660	45.6	71.7	SA69	+26.1	NATALL	5.186 539 40	−3.653 858 15	−.654 281 78
SAO	9003	−31 06 07.2608	136 46 58.6988	159.21	158.1	AUGD	−1.1	WOOMER	−3.983 657 92	3.743 132 37	−3.275 676 47
SAO	9007	−16 27 55.085	288 30 26.814	2451.86	2486.1	SA69	+34.2	AREQUI	1.942 859 32	−5.804 086 83	−1.796 876 77
SAO	9009	+12 05 25.912	291 09 46.078	7.44	−3.4	SA69	−10.8	CURACA	2.251 890 08	−5.816 918 37	1.327 200 69
SAO	9011	−31 56 33.228	294 53 38.949	608.	621.0	SA69	+13.0	V.DLOR	2.280 660 87	−4.914 576 54	−3.355 368 76
SAO	9023	−31 23 30.8163	136 52 39.0156	137.91	136.9	AUGD	−1.0	LAGOON	−3.977 646 16	3.725 145 80	−3.303 143 65
SAO	9027	−16 27 54.365	288 30 26.578	2450.23	2484.4	SA69	+34.2	AREQU2	1.942 854 16	−5.804 093 46	−1.796 855 06
SAO	9029	−05 55 38.616	324 50 08.660	45.34	71.4	SA69	+26.1	NATLBR	5.186 539 16	−3.653 857 98	−.654 281 74
SAO	9031	−45 53 11.028	292 23 12.215	186.54	172.5	SA69	−14.0	CHDRVD	1.693 869 60	−4.112 339 51	−4.556 606 80
SAO	9039	−05 55 38.616	324 50 09.401	41.6	67.7	SA69	+26.1	NATAL2	5.186 549 28	−3.653 837 23	−.654 281 36

Agency	Sta. no.	Latitude	Longitude	H_{msl} (m)	H_{ell} (m)	Datum	GH (m)	Name	X	Y (megameters)	Z
									a = 6 378 140.0 m		$1/f$ = 298.258
NOAA	6007	+38 45 36.725	332 54 21.064	53.3	53.3	GRAC	0.0	AZORES	4.433 563 44	−2.268 197 74	3.971 629 06
NOAA	6040	−12 11 57.91	096 49 47.08	4.4	4.4	ASTR	0.0	COCOIS	−.741 462 10	6.190 800 89	−1.338 974 41
NOAA	6045	−20 13 50.	057 25 15.	149.4	.	NSPC	.	MAURIT	3.223 895 00	5.045 104 82	−2.191 716 44
NOAA	6051	−67 36 03.08	062 52 24.41	11.3	11.3	ASTR	0.0	MAWSON	1.111 359 85	2.169 307 95	−5.874 285 99
NOAA	6052	−66 16 45.12	110 32 04.61	18.0	18.0	ASTR	0.0	WILKES	−.902 551 77	2.409 545 73	−5.816 560 60
NOAA	6059	+02 00 35.622	202 35 21.962	2.75	.	XM67	.	XMASIS	−5.885 219 81	−2.448 507 30	.222 198 23
NOAA	6061	−54 16 39.515	323 30 42.531	4.2	.	SGRG	.	SOGEOR	3.000 591 10	−2.219 363 27	−5.154 853 86
NOAA	6072	+18 46 10.	098 58 15.	319.3	.	NSPC	.	TILAND	−.942 038 16	5.967 454 08	2.039 306 54

TABLE 9.16.—*Orbital Elements of Adopted Satellites*

Satellite	n (rev day^{-1})	i	e
7001701	13.800	5°.410	0.0880
7010901	14.811	15°.040	0.0165
6001301	13.454	28°.330	0.0166
5900101	11.460	32°.880	0.1650
6202901	9.126	44°.800	0.2428
6000902	12.197	47°.230	0.0114
6302601	14.108	49°.740	0.0600
6206001	13.345	50°.140	0.0070
6508901	11.968	59°.380	0.0717
6101501	13.870	66°.820	0.0080
6400101	13.920	69°.910	0.0015
6406401	13.746	79°.700	0.0129
6508101	13.805	87°.370	0.0743
6102801	8.677	95°.850	0.0121

TABLE 9.17.—*Coefficients of C_n Based on Kozai's (1964) Values*[a]

$C_2 = -1082.639$	$C_3 = 2.546$
$C_4 = 1.649$	$C_5 = 0.210$
$C_6 = 0.646$	$C_7 = 0.333$
$C_8 = 0.270$	$C_9 = 0.053$
$C_{10} = 0.054$	$C_{11} = -0.302$
$C_{12} = 0.357$	$C_{13} = 0.114$
$C_{14} = -0.179$	

[a] Given in units of 10^{-6}.

TABLE 9.18.—(O-C) *for Secular Motion and Their Differences*[a]

Satellite		(O-C)		I	II	1969	1962	1961	1959
7001701	$\dot{\omega}$ -----	−18060	±90	−57	271	29090	9540	18250	18840
	$\dot{\Omega}$ -----	10120	±70	−51	258	−17400	−5390	−9950	−10240
7010910	$\dot{\omega}$ -----	−2200	±800	−1530	−857	−4700	100	6200	6900
	$\dot{\Omega}$ -----	5160	±100	−83	99	−2160	−1450	−5560	−5900
6001301	$\dot{\omega}$ -----	170	±100	43	61	40	−300	−670	−90
	$\dot{\Omega}$ -----	−125	±5	−4	−10	−1	59	−611	−928
5900101	$\dot{\omega}$ -----	32	±3	1	3	1	18	−129	278
	$\dot{\Omega}$ -----	−9	±3	2	7	0	10	−248	−488
6202901	$\dot{\omega}$ -----	40	±6	11	10	2	300	827	1013
	$\dot{\Omega}$ -----	7	±3	5	8	2	−39	−247	−395
6000902	$\dot{\omega}$ -----	170	±50	0	21	47	−287	770	1070
	$\dot{\Omega}$ -----	−1	±3	1	5	4	−43	−342	−594
6302601	$\dot{\omega}$ -----	920	±10	−1	−6	−52	2650	4900	5290
	$\dot{\Omega}$ -----	1	±3	0	−2	19	261	−2	−352
6206001	$\dot{\omega}$ -----	600	±60	16	84	60	2230	4180	4500
	$\dot{\Omega}$ -----	−42	±3	1	2	8	−56	−437	−740
6508901	$\dot{\omega}$ -----	−110	±10	−1	−29	−26	1460	3180	3285
	$\dot{\Omega}$ -----	−70	±3	0	−6	−7	−670	−1465	−1670
6101501	$\dot{\omega}$ -----	−300	±80	14	97	65	−81	1900	2500
	$\dot{\Omega}$ -----	22	±3	−1	−1	3	−1252	−2815	−3057
6400101	$\dot{\omega}$ -----	600	±800	729	718	620	−600	580	−500
	$\dot{\Omega}$ -----	56	±8	10	6	9	−1073	−2703	−2921
6406401	$\dot{\omega}$ -----	−400	±100	−95	−231	−110	−2000	−4000	−4300
	$\dot{\Omega}$ -----	90	±10	9	9	15	−220	−1351	−1467
6508101	$\dot{\omega}$ -----	620	±30	15	100	−8	300	−3290	−3630
	$\dot{\Omega}$ -----	50	±3	−2	−9	−27	35	−306	−337
6102801	$\dot{\omega}$ -----	−35	±50	−47	−47	−47	−340	−915	−1008
	$\dot{\Omega}$ -----	−2.9	±0.5	0.6	0.7	0.6	62.7	192.3	212.6

[a] Given in units of 10^{-6} degrees per day.

TABLE 9.19.—(O-C) *for Amplitudes of* $\left.\begin{matrix}cos\\sin\end{matrix}\right\}$ 2ω *Terms and Their Differences*[a]

Satellite		(O-C)	I	II	1969	1962	1961	1959
5900101	ω	0.3 ± 0.5	−0.2	−0.2	−0.3	−0.6	1.5	1.4
	Ω	−2 ± 2	−1	−2	−2	−1	−4	−4
	i	−3 ± 6	−4	−4	−5	−4	3	3
	e	0 ± 1	1	1	1	1	−4	−4
6202901	ω	−0.1 ± 0.3	−0.2	−0.2	−0.2	−0.8	−2.5	−2.7
	Ω	−1 ± 1	1	1	1	−8	−14	−14
	i	4 ± 4	5	4	4	−3	−14	−15
	e	0 ± 1	0	0	0	5	12	12
6000902	ω	−3 ± 4	−2	−2	−2	−6	−10	−10
	e	0 ± 1	0	0	0	0	1	1
6302601	ω	−6 ± 2	−1	0	0	−14	−23	−23
	Ω	2 ± 2	3	3	3	−2	−3	−3
	i	−1 ± 3	1	1	1	−4	−6	−6
	e	3 ± 2	−3	−3	−3	12	20	20
6205001	ω	3 ± 6	7	6	6	−5	−13	−13
	e	1 ± 1	1	1	0	2	3	3
6508901	ω	6 ± 2	1	2	2	−22	−49	−50
	Ω	4 ± 2	2	2	0	9	10	10
	i	5 ± 5	4	4	4	−3	−11	−11
	e	−4 ± 1	2	1	1	30	62	63
6101501	ω[b]	−1 ± 2	−1	0	0	−3	0	0
	e	1 ± 2	0	0	−1	3	−1	−1
6406401	ω[b]	0 ± 2	0	0	0	−1	−1	−1
	e	4 ± 4	3	4	3	5	7	7
6508101	ω	7 ± 3	3	4	3	12	0	0
	Ω	1 ± 1	1	0	0	2	2	2
	i	−2 ± 8	−2	−2	−2	−2	−2	−2
	e	6 ± 2	1	−2	−1	−11	3	3

[a] Given in units of 10^3 degrees for ω, 10^4 degrees for Ω, 10^5 degrees for i, and 10^6 degrees for e per day.

[b] For these satellites, ω is in units of 10^2 degrees.

TABLE 9.20.—(O-C) *for Amplitudes of* $\left.\begin{matrix}cos\\sin\end{matrix}\right\}\omega$ *Terms and Their Differences*[a]

Satellite		(O-C)	I	II	1969	1962	1961	1959
7001701	ω	70 ± 5	−2	0	−126	−104	−85	−87
	Ω	−190 ± 30	0	−28	−248	−570	−168	−237
	i	430 ± 30	−34	−31	740	900	480	550
	e	−91 ± 6	−5	−5	−149	−179	−99	−112
7010901	ω	45 ± 30	9	41	160	−411	232	112
	Ω	−18 ± 45	−44	−48	0	10	9	7
	i	−170 ± 300	−166	−170	−181	−120	−190	−177
	e	28 ± 20	18	27	61	−102	83	49
6001301	ω	4 ± 1	0	0	0	46	314	241
	Ω	0 ± 3	2	2	0	3	−10	−7
	i	0 ± 30	0	0	0	−2	−16	−12
	e	1.6 ± 1.0	0.5	0.5	0.6	13.5	90.7	69.8
5900101	ω	−1.7 ± 0.3	0.0	0.3	0.0	4.8	22.4	17.2
	Ω	−2 ± 2	2	1	2	−7	−87	−58
	i	1 ± 5	−3	−3	−4	−8	−64	−57
	e	−3.1 ± 0.5	−0.3	−0.7	−0.1	3.2	40.0	35.6
6202901	ω	−0.1 ± 0.2	0.0	0.0	−0.1	−1.2	−4.0	6.1
	Ω	2 ± 3	2	3	3	16	5	31
	i	−2 ± 3	−5	−4	−4	−11	−26	−78
	e	± 0.8	0.2	0.0	0.2	4.2	15.2	49.7
6000902	ω	−19 ± 3	−4	−4	−10	42	1	315
	Ω	1 ± 1	1	1	0	3	4	6
	i	−2 ± 6	−2	−2	−6	−3	−2	−6
	e	−2.0 ± 0.6	1.0	1.0	0.3	10.5	2.4	64.8
6302601	ω	−17 ± 2	0	−4	−1	9	−17	86
	Ω	−6 ± 1	0	0	1	20	52	60
	i	14 ± 15	10	11	10	6	12	−19
	e	−12 ± 1	0	−1	2	16	−6	99
6206001	ω	−59 ± 4	0	5	0	187	122	931
	Ω	−2 ± 2	−2	−2	−2	0	3	4
	i	0 ± 10	0	0	0	−1	0	−4
	e	−8 ± 1	−1	0	−1	22	14	113
6508901	ω	3 ± 4	7	7	0	119	264	486
	Ω	10 ± 2	3	3	2	−10	8	−29
	i	−8 ± 8	−9	−9	−7	−40	−80	−144
	e	−4 ± 1	0	0	−2	127	292	555

TABLE 9.20.—*(Cont'd)*

Satellite		(O-C)	I	II	1969	1962	1961	1959
6101501	ω^b	−19 ± 5	−11	−11	−8	−46	−265	−413
	Ω	−3 ± 4	2	2	0	7	17	29
	i	0 ± 5	0	0	0	1	7	11
	e	−11 ± 1	0	0	4	−48	−354	−560
6400101	ω^b	−200 ± 10	6	3	1	−72	−445	−593
	e	−58 ± 3	−4	−5	−9	−24	−122	−161
6406401	ω	−110 ± 20	23	36	30	23	510	930
	Ω	6 ± 3	1	1	1	5	11	16
	i	0 ± 8	0	0	0	0	−2	−3
	e	−34 ± 5	−4	−2	−2	−4	106	199
6508101	ω	60 ± 2	1	−1	3	64	197	296
	Ω	20 ± 1	0	2	2	16	26	32
	i	−10 ± 10	−9	−9	−10	−10	−13	−16
	e	60 ± 3	−4	−5	−2	67	231	354
6102801	ω	−30 ± 50	−48	−47	−40	15	390	663
	Ω	−2 ± 2	−2	−2	−2	−2	−3	−4
	i	−6 ± 7	−6	−6	−6	−6	−6	−5
	e	3.0 ± 1.5	−0.7	−0.6	0.0	12.5	91.8	149.2

[a] Given in units of 10^3 degrees for ω, 10^4 degrees for Ω, 10^5 degrees for i, and 10^6 degrees for e per day.

[b] For these satellites, ω is in units of 10^2 degrees.

TABLE 9.21.—*Assumed Accuracy for SE III*

Data	Weight	Remarks
Baker-Nunn	4″	
Smoothed Baker-Nunn	2″	
SAO laser	5 m	Taken before 1970, observed before 1970
CNES laser	10 m	Taken before 1970, observed before 1970
GSFC laser	5 m	Taken before 1970, observed before 1970
ISAGEX laser	2 m	1971 International Campaign
Gravity anomalies	$\langle A \rangle \frac{13.5}{nA}$ mGal	n is the number of 1° × 1° squares in each 5° × 5° mean
Model (zero) anomalies	$\langle A \rangle \frac{27}{A}$ mGal	A is the area

TABLE 9.22.—*Smithsonian Atomic Time Defined With Respect to WWV and UTC (USNO)*[a,b]

Interval			A (sec)	B (sec/day)	T_0 (mod. J.d.)
$(A.S - WWV) = A + B\,(T - T_0)$ before September 20, 1967					
1961 Jan.	01.0—1961 Jul.	01.0	1.458 858	+ 0.001 296 000	$(T - 37\,300.0)$
1961 Jul.	01.0—1961 Jul.	13.0	1.693 434	+ 0.001 292 000	$(T - 37\,480.0)$
1961 Jul.	13.0—1961 Aug.	01.0	1.694 215	+ 0.001 245 000	$(T - 37\,480.0)$
1961 Aug.	01.0—1961 Sep.	21.0	1.643 160	+ 0.001 280 000	$(T - 37\,480.0)$
1961 Sep.	21.0—1961 Oct.	01.0	1.641 500	+ 0.001 300 000	$(T - 37\,480.0)$
1961 Oct.	01.0—1961 Nov.	01.0	1.642 184	+ 0.001 290 764	$(T - 37\,480.0)$
1961 Nov.	01.0—1962 Jan.	01.0	1.643 272	+ 0.001 289 444	$(T - 37\,480.0)$
1962 Jan.	01.0—1962 Apr.	01.0	1.865 000	+ 0.001 123 200	$(T - 37\,650.0)$
1962 Apr.	01.0—1962 Jul.	01.0	1.864 620	+ 0.001 126 800	$(T - 37\,650.0)$
1962 Jul.	01.0—1963 Jan.	01.0	1.864 704	+ 0.001 126 370	$(T - 37\,650.0)$
1963 Jan.	01.0—1963 Nov.	01.0	2.292 725	+ 0.001 118 458	$(T - 38\,030.0)$
1963 Nov.	01.0—1964 Jan.	01.0	2.392 725	+ 0.001 118 458	$(T - 38\,030.0)$
1964 Jan.	01.0—1964 Apr.	01.0	2.800 962	+ 0.001 293 560	$(T - 38\,395.0)$
1964 Apr.	01.0—1964 Jul.	01.0	2.900 766	+ 0.001 295 716	$(T - 38\,395.0)$
1964 Jul.	01.0—1964 Sep.	01.0	2.901 518	+ 0.001 292 659	$(T - 38\,395.0)$
1964 Sep.	01.0—1964 Oct.	01.0	3.001 518	+ 0.001 292 659	$(T - 38\,395.0)$
1964 Oct.	01.0—1965 Jan.	01.0	3.001 589	+ 0.001 296 048	$(T - 38\,395.0)$
1965 Jan.	01.0—1965 Mar.	01.0	3.575 732	+ 0.001 296 000	$(T - 38\,761.0)$
1965 Mar.	01.0—1965 Jul.	01.0	3.675 732	+ 0.001 296 000	$(T - 38\,761.0)$
1965 Jul.	01.0—1965 Sep.	01.0	3.775 732	+ 0.001 296 000	$(T - 38\,761.0)$
1965 Sep.	01.0—1966 Jan.	01.0	3.875 732	+ 0.001 296 000	$(T - 38\,761.0)$
1966 Jan.	01.0—1967 Jan.	01.0	3.348 772	+ 0.002 592 000	$(T - 39\,126.0)$
1967 Jan.	01.0—1967 Sep.	20.0	5.294 852	+ 0.002 592 000	$(T - 39\,491.0)$
$[A.S - UTC\,(USNO) = A + B\,(T - T_0)]$ after September 27, 1967					
1967 Sep.	20.0—1968 Jan.	01.0	5.294 688	+ 0.002 592 000	$(T - 39\,491.0)$
1968 Jan.	01.0—1968 Feb.	01.0	6.240 768	+ 0.002 592 000	$(T - 39\,856.0)$
1968 Feb.	01.0—1969 Jan.	01.0	6.140 768	+ 0.002 592 000	$(T - 39\,856.0)$
1969 Jan.	01.0—1970 Jan.	01.0	7.089 440	+ 0.002 592 000	$(T - 40\,222.0)$
1970 Jan.	01.0—1971 Jan.	01.0	8.035 520	+ 0.002 592 000	$(T - 40\,587.0)$
1971 Jan.	01.0—1972 Jan.	01.0	8.981 600	+ 0.002 592 000	$(T - 40\,952.0)$
1972 Jan.	01.0—1972 Jul.	01.0	10.035 280	+ 0.000 000 000	$(T - 41\,317.0)$

[a] From M. R. Pearlman, J. M. Thorp., C. R. H. Tsiang, D. A. Arnold, C. G. Lehr, and J. Wohn.

[b] Since September 20, 1967, SAO's satellite observations have been referred to UTC(USNO). Before that date, observations were referred to time of emission of WWV signals (WWV-emitted). Both timing systems are readily available for use in the field, yet both have occasional discontinuities which make them inappropriate for analysis.

When the satellite-tracking program began in the late 1950's, uniform time standards such as A1 and their differences from WWV emitted (and later UTC) were not available in a timely fashion. However, the intended relations between WWV (and later UTC) and the uniform time standard A1 were published regularly. SAO has used these intended relations to generate a facsimile of A1 from WWV and UTC data.

TABLE 9.23.—*Accuracy of an Observation as a Function of Topocentric Angular Velocity*

Cycle rate (sec)	Associated topocentric velocity of object (arc-sec sec^{-1})	With VLF and portable clocks		With VHF	
		Along track	Across track	Along track	Across track
32	0– 250	1".8	1".8	1".8	1".8
16	250– 500	1".8	1".8	2".1	1".8
8	500–1000	1".9	1".8	2".3	1".8
4	1000–2000	1".9	1".8	2".7	1".8
2	>2000	2".0	1".8	3".7	1".8

TABLE 9.24.—*Sensitivity Coefficients for Satellite 6701401*[a]

e = 0.084 313 0 A = 7614 km
I = 39°.454 59 perigee = 594 km
n = 13.064 356 apogee = 1878 km

m \ ℓ	11	12	13	14	15	16	17	18	19	20
1	154	229	121	75	139	160	66	69	118	67
2	113	43	61	94	58	35	59	46	0	33
3	52	78	65	25	54	43	12	18	39	26
4	66	34	19	39	38	14	10	27	0	0
5	38	28	51	29	0	23	10	0	0	18
6	65	48	42	14	27	19	0	17	0	0
7	68	62	61	45	10	0	18	16	0	0
8	46	62	45	37	18	12	0	0	18	0
9	21	30	46	64	55	53	23	0	0	0
10	0	0	29	44	43	58	37	32	0	0
11	0	0	8	16	27	48	47	57	48	44
12		0	0	21	44	64	89	101	75	99
13			425	1203	2987	4758	8014	9531	12277	11613
14				0	0	20	47	77	111	145
15					0	0	0	0	16	20
16						0	0	0	0	0
17							0	0	0	0
18								0	0	0
19									0	0
20										0

[a] Given in units of meters, with $|\mathfrak{C}_{\ell m}| \times 10^6$.

TABLE 9.25.—*Results of Complete Network Adjustment*

Interstation direction	Direction cosines			σ_ψ^2 (μrad)	σ_μ^2 (μrad)	$\sigma_{\psi\mu}$ (μrad)	No. obs.
	x	y	z				
			SAO Network				
8015-8019	0.008 826 76	0.991 566 88	−0.129 295 09	4378.25	3682.33	409.04	29
8015-9004	0.403 688 17	−0.775 736 75	−0.485 044 69	29.21	17.80	7.03	122
8015-9066	−0.696 237 98	0.308 764 57	0.648 010 12	552.99	204.51	−61.20	133
8015-9074	−0.723 132 48	0.499 652 76	0.476 892 59	54.68	21.55	−18.85	25
8015-9080	−0.612 142 61	−0.551 268 92	0.566 907 41	90.07	42.32	18.81	67
8015-9091	0.010 166 06	0.955 062 10	−0.296 231 40	24.96	25.68	0.97	30
8019-9004	0.375 702 50	−0.815 399 14	−0.440 422 38	8.99	5.46	2.27	301
8019-9091	0.010 266 10	0.950 679 22	−0.310 005 84	23.46	12.23	−1.87	61
9001-9007	0.553 303 12	−0.101 336 83	−0.826 792 90	7.19	4.91	−1.16	35
9001-9009	0.867 353 66	−0.148 829 84	−0.474 918 21	5.08	6.60	−3.13	183
9001-9010	0.965 435 98	−0.166 946 59	−0.200 155 43	12.00	14.31	−7.74	154
9001-9012	−0.795 296 06	0.559 031 40	−0.234 495 37	9.01	9.63	6.26	187
9001-9113	−0.839 865 57	0.498 415 57	0.214 959 85	119.75	227.49	110.69	20
9001-9114	0.109 263 14	0.685 666 26	0.719 668 92	41.57	18.51	−0.64	74
9001-9117	−0.716 762 03	0.649 994 62	−0.252 505 81	8.64	19.81	7.90	16
9002-9008	−0.263 480 98	0.264 768 12	0.927 618 25	23.08	145.74	−37.94	7
9002-9028	−0.038 627 03	0.316 476 94	0.947 813 43	52.37	119.71	21.28	25
9004-9006	−0.559 029 19	0.824 219 14	−0.090 272 72	8.87	8.85	−3.97	14
9004-9008	−0.326 789 15	0.937 481 22	−0.119 740 60	13.50	8.84	−6.96	139
9004-9009	−0.441 426 33	−0.813 880 96	−0.377 810 25	25.76	27.96	20.26	43
9004-9010	−0.627 485 32	−0.766 807 91	−0.135 158 44	26.73	28.14	18.57	41
9004-9028	−0.037 913 83	0.849 029 88	−0.526 982 74	18.85	15.61	−1.99	35
9004-9029	0.014 976 95	−0.573 627 21	−0.818 979 56	68.03	29.79	21.05	42
9004-9051	−0.189 212 79	0.980 621 32	0.050 797 07	2160.68	2169.11	−1375.13	47
9004-9066	−0.479 672 65	0.695 552 78	0.534 902 31	22.93	10.64	−5.24	192
9004-9074	−0.607 317 21	0.624 696 01	0.490 836 73	18.11	7.63	−4.83	65
9004-9080	−0.670 338 78	0.237 785 34	0.702 925 36	29.78	9.92	0.41	164
9004-9091	−0.192 739 02	0.979 763 41	0.053 993 83	3.29	3.55	−1.53	442
9004-9115	−0.689 044 82	0.398 593 75	0.605 260 49	74.58	28.34	−8.14	60
9005-9006	0.915 236 02	0.388 002 15	−0.108 615 64	44.80	34.23	32.36	61
9005-9012	−0.247 353 66	−0.939 455 40	−0.237 149 14	106.27	176.50	−114.45	25
9005-9117	−0.390 770 14	−0.849 194 96	−0.355 199 42	182.41	189.44	−154.07	16
9006-9008	0.911 043 75	−0.412 181 49	0.010 281 02	37.46	20.76	16.35	172
9006-9028	0.828 975 55	−0.321 287 02	−0.457 792 73	22.65	23.59	10.19	28

TABLE 9.25.—*(Cont'd)*

Interstation direction	Direction cosines			σ_ψ^2 (μrad)	σ_μ^2 (μrad)	$\sigma_{\psi\mu}$ (μrad)	
	x	y	z				
9006–9091	0.712 325 15	−0.683 388 19	0.159 917 01	20.83	36.31	14.13	10
9006–9115	0.360 690 12	−0.836 686 48	0.412 138 77	16.89	16.71	7.12	19
9007–9009	0.098 443 23	−0.004 084 91	0.995 134 28	4.04	9.65	2.17	263
9007–9010	−0.202 184 39	0.042 403 31	0.978 429 06	4.88	5.94	1.92	86
9007–9011	0.185 005 71	0.487 139 75	−0.853 503 22	17.65	9.35	5.14	437
9007–9029	0.799 740 13	0.530 146 21	0.281 710 37	14.15	32.67	2.56	74
9007–9031	−0.076 686 54	0.521 089 04	−0.850 050 22	31.70	22.18	1.86	32
9008–9028	0.567 329 00	−0.163 038 12	−0.807 190 42	69.25	59.45	15.59	25
9008–9051	0.442 138 26	−0.853 475 28	0.275 850 87	7168.06	6510.27	6102.56	13
9008–9080	0.109 946 43	−0.918 531 30	0.379 752 59	38.24	25.92	−8.53	8
9008–9115	−0.056 819 15	−0.847 191 43	0.528 240 73	30.33	16.42	8.31	38
9009–9010	−0.631 057 97	0.106 627 28	0.768 372 60	10.73	18.06	6.43	248
9009–9011	0.006 033 03	0.189 216 50	−0.981 916 86	7.28	2.47	0.50	201
9009–9029	0.707 260 24	0.521 304 13	−0.477 519 59	39.98	35.77	2.00	12
9009–9114	−0.614 261 56	0.410 481 04	0.673 934 76	8.47	10.52	3.09	13
9010–9029	0.721 923 97	0.333 948 56	−0.606 056 22	22.19	20.40	2.74	6
9010–9114	−0.580 737 58	0.553 105 20	0.597 342 87	19.62	15.65	5.54	38
9011–9029	0.698 052 66	0.302 858 53	0.648 844 50	52.36	41.72	−13.65	7
9011–9031	−0.376 336 08	0.514 540 22	−0.770 467 07	198.44	140.41	27.09	9
9012–9021	0.774 021 22	−0.586 319 09	0.239 000 17	75.78	18.83	−12.52	29
9012–9113	0.754 823 45	−0.555 631 45	0.348 590 37	23.64	21.19	14.81	14
9012–9114	0.801 985 13	−0.202 846 07	0.561 848 14	22.01	17.31	−0.17	24
9012–9117	−0.370 330 01	0.884 135 37	−0.284 886 53	49.17	46.84	27.96	216
9021–9113	−0.685 370 68	0.605 320 01	0.404 789 73	175.96	211.14	9.22	57
9021–9117	−0.692 362 28	0.674 539 06	−0.256 186 51	50.43	26.94	19.65	8
9028–9091	−0.087 279 58	−0.544 704 02	0.834 074 22	105.67	28.64	−3.90	37
9029–9031	−0.664 370 01	−0.087 213 96	−0.742 297 93	23.64	25.10	−2.78	26
9066–9074	−0.722 593 68	0.537 777 49	0.434 342 89	94.27	33.43	−29.12	13
9066–9080	−0.457 869 96	−0.782 066 08	0.422 762 05	120.67	109.92	26.05	27
9074–9077	0.776 325 65	0.194 165 54	−0.599 681 77	453.01	147.30	−165.47	42
9074–9091	0.675 716 06	0.295 891 28	−0.675 171 21	45.42	22.62	6.25	43
9077–9091	0.583 629 63	0.370 871 86	−0.722 378 38	187.65	121.07	−53.33	30
9113–9114	0.522 340 01	0.510 153 75	0.683 303 79	126.10	106.70	38.12	30
9113–9117	−0.669 105 98	0.660 671 02	−0.340 310 14	16.21	29.22	10.95	16

TABLE 9.25.—*(Cont'd)*

Interstation direction	Direction cosines			σ_ψ^2 (μrad)	σ_μ^2 (μrad)	$\sigma_{\psi\mu}$ (μrad)
	x	y	z			
6001-6002	0.141 867 57	−0.835 578 65	−0.530 737 14	4.88	2.13	0.12
6001-6003	−0.685 613 65	−0.614 208 86	−0.390 744 68	5.55	2.03	0.41
6001-6004	−0.901 363 80	0.366 090 55	−0.231 346 07	7.88	2.47	1.52
6001-6006	0.591 183 24	0.802 114 53	−0.084 348 41	10.68	2.69	−1.90
6001-6007	0.853 151 78	−0.192 741 70	−0.484 750 12	6.83	2.27	−0.37
6001-6016	0.773 269 54	0.481 076 40	−0.413 061 40	2.81	0.81	−0.44
6001-6065	0.809 558 20	0.488 080 94	−0.326 178 66	3.99	1.22	−1.02
6001-6123	−0.970 854 20	0.230 905 62	−0.064 223 96	19.08	6.47	−1.12
6002-6003	−0.934 936 56	0.299 816 54	0.189 746 36	3.10	2.95	1.48
6002-6007	0.790 059 49	0.613 005 38	−0.005 513 94	7.15	6.25	−1.91
6002-6008	0.589 564 10	−0.090 689 02	−0.802 614 27	4.37	3.76	−2.32
6002-6009	0.035 287 76	−0.333 951 82	−0.941 929 38	9.39	4.10	0.51
6002-6038	−0.840 626 18	−0.207 333 06	−0.500 360 51	4.85	4.12	1.11
6002-6111	−0.992 430 15	0.045 147 65	−0.114 210 70	6.70	6.52	2.33
6002-6134	−0.992 422 07	0.045 119 01	−0.114 292 19	6.19	5.00	1.27
6003-6004	−0.379 650 63	0.921 024 95	0.087 054 20	10.44	3.59	0.62
6003-6011	−0.768 297 61	0.317 940 94	−0.555 546 88	4.80	3.85	2.16
6003-6012	−0.542 340 66	0.753 078 57	−0.372 477 21	3.33	1.88	0.59
6003-6038	−0.010 322 05	−0.578 100 31	−0.815 900 41	5.50	2.64	−0.78
6003-6111	−0.225 140 91	−0.618 652 34	−0.752 715 65	34.64	18.77	12.08
6003-6123	0.075 002 12	0.906 419 74	0.415 665 66	11.48	8.39	0.56
6003-6134	−0.225 131 46	−0.618 590 94	−0.752 768 94	31.12	17.64	−4.62
6004-6012	−0.540 783 78	0.268 965 14	−0.797 001 04	18.71	5.13	−2.83
6004-6013	0.069 330 48	0.903 078 62	−0.423 842 30	9.58	8.25	3.02
6004-6123	0.786 132 00	−0.482 393 72	0.386 384 23	35.88	8.81	−4.98
6006-6007	0.544 571 14	−0.698 573 02	−0.464 153 00	7.50	3.40	−0.04
6006-6015	0.115 085 63	0.854 379 21	−0.506 745 95	5.03	3.21	0.14
6006-6016	0.787 806 62	0.167 660 50	−0.592 664 06	4.78	1.88	0.10
6006-6065	0.858 757 69	0.040 345 30	−0.510 791 05	7.60	3.14	0.19
6007-6016	0.127 976 51	0.991 267 29	−0.031 798 92	5.87	4.76	−1.86
6007-6055	0.325 134 21	0.134 399 75	−0.936 068 62	2.37	2.18	−0.80
6007-6063	0.518 127 69	0.148 082 01	−0.842 386 74	7.86	3.39	−2.96
6007-6064	0.320 536 02	0.783 539 87	−0.532 279 94	2.68	2.70	−0.75
6007-6065	−0.069 163 60	0.970 784 14	0.229 770 66	13.69	6.15	−0.88
6007-6067	0.154 021 10	−0.283 547 61	−0.946 508 46	3.36	2.86	1.14
6008-6009	−0.889 382 39	−0.393 627 48	−0.232 500 28	10.72	17.99	8.22
6008-6019	−0.320 491 21	0.071 535 74	−0.944 546 46	3.83	3.77	−1.25
6008-6067	0.615 252 90	0.614 120 14	−0.494 287 69	15.83	20.35	1.79
6009-6019	0.267 472 01	0.357 525 69	−0.894 781 60	6.28	5.31	3.34
6009-6020	−0.723 867 36	0.204 650 56	−0.658 888 60	10.08	11.65	−1.01
6009-6038	−0.849 821 14	0.150 178 73	0.505 223 10	7.40	9.49	3.01
6009-6043	0.015 902 71	0.463 052 32	−0.886 188 27	4.27	1.63	0.70
6011-6012	−0.102 697 51	0.993 954 29	−0.038 834 06	7.10	6.36	2.10
6011-6022	−0.154 186 69	0.342 233 00	−0.926 878 11	2.36	4.39	0.66

TABLE 9.25.—*(Cont'd)*

Interstation direction	Direction cosines			σ_ψ^2 (μrad)	σ_μ^2 (μrad)	$\sigma_{\psi\mu}$ (μrad)
	x	y	z			
6011–6038	0.713 571 02	−0.699 157 90	−0.044 661 29	4.93	4.11	−1.83
6011–6059	−0.203 146 66	−0.021 289 30	−0.978 916 85	12.93	3.89	1.67
6011–6111	0.753 727 27	−0.565 465 17	0.334 879 59	8.14	8.17	−2.05
6011–6134	0.753 729 93	−0.565 502 25	0.334 810 98	5.65	5.50	−2.71
6012–6013	0.609 450 15	0.724 692 18	0.321 545 90	13.41	8.85	4.80
6012–6022	−0.055 106 45	−0.545 974 12	−0.835 987 76	2.57	4.53	0.36
6012–6023	0.216 399 64	0.586 471 64	−0.780 526 88	4.01	7.30	0.90
6012–6059	−0.006 268 11	−0.898 976 36	−0.437 952 29	2.41	3.97	−1.42
6013–6015	0.996 026 91	0.052 213 03	0.072 140 17	3.28	3.62	0.01
6013–6040	0.485 672 28	0.356 024 41	−0.798 353 97	2.08	3.88	0.87
6013–6047	0.071 906 80	0.439 043 73	−0.895 583 62	8.33	7.00	4.50
6013–6072	0.760 880 82	0.535 459 13	−0.366 529 53	4.36	8.55	1.81
6013–6078	−0.370 956 05	−0.449 044 19	−0.812 865 87	0.94	12.01	−3.04
6015–6016	0.590 837 46	−0.806 324 68	0.027 415 57	2.95	2.82	1.04
6015–6040	−0.528 142 99	0.275 666 07	−0.803 164 49	1.65	2.08	−0.07
6015–6042	0.630 855 74	−0.130 742 05	−0.764 805 57	2.44	2.82	0.60
6015–6045	0.103 102 95	0.100 120 56	−0.989 618 94	1.27	0.81	0.32
6015–6064	0.676 713 19	−0.559 380 10	−0.478 699 44	1.74	1.85	0.53
6015–6065	0.394 666 49	−0.888 635 25	0.233 593 13	5.57	2.35	−0.21
6015–6072	−0.839 965 71	0.360 824 97	−0.405 293 67	2.98	4.19	−1.46
6015–6073	0.143 282 86	0.325 434 15	−0.934 645 73	2.72	1.85	−0.69
6015–6075	0.224 226 76	0.178 325 99	−0.958 082 57	2.84	1.86	0.81
6016–6042	0.001 109 29	0.676 082 54	−0.736 825 06	4.38	3.04	−0.43
6016–6063	0.246 574 17	−0.790 990 05	−0.559 942 79	3.84	2.99	1.33
6016–6064	0.405 181 93	0.108 489 72	−0.907 776 18	5.65	3.07	0.89
6016–6065	−0.571 507 16	−0.414 589 06	0.708 163 45	25.62	8.62	1.65
6019–6020	−0.988 544 61	−0.104 406 02	0.108 990 57	8.63	9.11	−4.07
6019–6043	0.390 990 19	0.558 928 98	−0.731 248 97	6.16	2.42	−0.23
6019–6061	0.216 670 72	0.811 860 39	−0.542 159 11	7.88	3.46	0.54
6019–6067	0.698 038 94	0.302 827 21	0.648 873 89	3.70	6.55	2.34
6019–6069	0.573 249 08	0.813 330 71	−0.099 391 40	14.67	10.84	5.58
6020–6038	−0.055 058 66	−0.058 182 22	0.996 786 52	9.75	3.90	−1.14
6020–6039	−0.886 798 99	0.450 925 46	0.101 261 01	46.24	84.34	−48.70
6020–6043	0.761 603 48	0.406 532 67	−0.504 669 51	12.13	7.22	2.77
6022–6023	0.229 398 44	0.969 946 65	0.081 116 30	3.97	4.22	0.22
6022–6031	0.447 512 00	0.473 203 10	−0.758 822 66	6.38	3.96	−1.71
6022–6039	0.550 539 48	−0.793 608 11	−0.259 022 11	9.48	15.45	6.00
6022–6059	0.092 732 48	−0.626 945 87	0.773 524 12	3.29	6.17	−0.26
6022–6060	0.310 640 87	0.873 041 83	−0.375 899 20	4.53	5.01	−0.95
6022–6078	0.065 258 85	0.985 289 47	−0.157 942 84	70.31	78.59	53.19
6023–6031	0.140 307 20	−0.645 359 19	−0.750 883 09	1.84	1.15	0.56
6023–6032	0.730 220 42	0.292 459 45	−0.617 450 90	4.71	2.62	−0.99
6023–6040	0.872 900 05	0.486 554 80	−0.036 192 95	3.22	4.69	−0.30
6023–6047	0.544 131 75	0.520 276 13	0.658 204 67	7.08	11.72	1.73
6023–6060	0.088 571 50	−0.456 559 81	−0.885 272 97	2.49	2.26	1.09
6023–6072	0.722 203 86	0.382 400 25	0.576 360 68	2.75	3.73	1.36

TABLE 9.25.—*(Cont'd)*

Interstation direction	Direction cosines			σ_v^2 (μrad)	σ_μ^2 (μrad)	$\sigma_{v\mu}$ (μrad)
	x	y	z			
6023-6078	−0.344 213 95	−0.901 266 78	−0.263 125 35	38.04	54.65	−32.36
6031-6032	0.421 012 31	0.865 343 95	0.271 897 94	2.21	2.25	−0.79
6031-6039	0.103 770 02	−0.935 883 55	0.336 680 52	7.68	9.08	3.79
6031-6051	0.948 773 86	0.223 489 34	−0.223 339 85	3.13	1.18	−0.29
6031-6052	0.868 470 44	0.386 519 64	−0.310 421 76	5.11	2.65	−1.05
6031-6053	0.868 120 23	−0.167 691 87	−0.467 168 82	6.20	2.29	0.62
6031-6060	−0.182 484 01	0.792 220 53	0.582 311 10	5.04	2.87	1.64
6031-6078	0.519 787 53	0.108 042 39	0.847 436 00	16.60	7.33	1.37
6032-6040	0.562 738 04	0.453 120 81	0.691 380 81	14.56	10.49	−4.02
6032-6044	0.856 098 02	−0.293 452 46	−0.425 419 60	11.72	9.87	−1.56
6032-6045	0.978 994 41	0.029 690 27	0.201 713 74	2.66	3.32	−0.96
6032-6047	−0.231 903 26	0.115 244 64	0.965 887 96	2.44	5.19	1.81
6032-6052	0.388 697 91	−0.650 824 51	−0.652 182 02	7.61	2.97	0.06
6032-6060	−0.751 113 54	−0.658 575 02	0.045 906 50	3.72	3.86	1.59
6038-6039	−0.305 337 11	0.238 502 97	−0.921 892 39	3.38	10.38	−1.16
6038-6059	−0.711 967 36	0.610 648 24	−0.346 714 88	3.44	3.33	1.84
6038-6134	−0.155 550 27	0.526 537 55	0.835 800 41	7.65	3.15	1.93
6039-6059	−0.523 780 88	0.478 273 00	0.704 917 39	7.29	16.49	−6.47
6040-6045	0.940 828 58	−0.271 770 48	−0.202 441 09	2.41	3.92	−1.07
6040-6047	−0.757 459 32	−0.238 511 17	0.607 756 37	6.92	9.42	−0.49
6040-6060	−0.719 063 73	−0.609 502 87	−0.333 846 68	2.87	3.23	0.49
6040-6072	−0.058 895 96	−0.065 862 14	0.996 089 08	8.00	9.57	0.10
6040-6073	0.979 007 93	−0.058 625 46	0.195 208 96	8.03	11.93	−2.38
6040-6075	0.960 512 05	−0.210 583 46	0.181 854 89	3.21	4.45	−1.29
6042-6045	−0.449 127 82	0.288 406 76	−0.845 639 25	2.23	2.36	0.15
6042-6064	0.426 834 35	−0.893 595 14	0.138 925 02	7.17	8.16	−0.92
6042-6068	0.046 510 08	−0.327 935 56	−0.943 554 49	2.02	3.55	−0.14
6042-6073	−0.739 897 12	0.509 802 26	−0.438 923 58	2.79	3.51	−0.32
6042-6075	−0.553 708 69	0.541 789 04	−0.632 353 80	5.24	9.84	1.47
6043-6050	−0.130 891 08	0.852 415 41	−0.506 216 84	39.52	14.49	−6.23
6043-6061	0.758 559 97	0.649 959 05	−0.046 260 24	21.33	11.80	1.07

TABLE 9.25.—*(Cont'd)*

Interstation direction	Direction cosines			σ_ψ^2 (μrad)	σ_μ^2 (μrad)	$\sigma_{\psi\mu}$ (μrad)	No. obs.
	x	y	z				
6044–6045	0.554 878 31	0.355 385 18	0.752 204 38	14.61	15.53	−2.69	
6044–6051	0.007 253 12	−0.883 713 18	−0.467 972 66	67.30	23.18	−2.08	
6045–6051	−0.411 896 51	−0.560 884 05	−0.718 157 61	4.08	2.14	−0.29	
6045–6068	0.605 912 70	−0.773 097 59	−0.187 589 76	4.79	5.03	−1.35	
6045–6073	−0.613 372 05	0.459 201 80	0.642 579 51	7.17	7.74	2.24	
6045–6075	0.219 418 94	0.111 565 29	0.969 230 89	13.52	7.81	−2.45	
6047–6072	0.863 993 41	0.214 776 50	0.455 397 01	8.25	9.11	3.04	
6050–6053	−0.666 360 22	0.735 231 19	−0.124 093 36	26.19	5.54	3.75	
6050–6061	0.943 372 93	0.120 914 00	0.308 913 11	44.80	21.02	−11.51	
6051–6052	−0.992 556 05	0.118 412 41	0.028 477 98	20.63	11.42	4.14	
6051–6053	−0.788 602 68	−0.604 920 10	−0.110 351 64	7.70	3.72	0.10	
6051–6061	0.390 885 48	−0.908 327 49	0.148 827 80	12.32	4.36	−0.77	
6051–6068	0.783 976 60	0.098 864 04	0.612 867 51	3.95	1.37	−0.67	
6052–6053	−0.187 775 83	−0.965 112 61	−0.182 477 11	12.18	5.73	1.01	
6052–6060	−0.824 242 87	0.081 916 08	0.560 279 80	4.14	1.63	0.39	
6053–6060	−0.661 296 78	0.476 791 55	0.579 099 64	2.98	1.20	−0.48	
6055–6063	−0.092 868 60	−0.111 882 65	0.989 372 37	6.33	6.52	1.12	
6055–6064	−0.024 459 13	0.821 692 72	0.569 405 67	2.34	4.58	0.72	
6055–6067	−0.406 559 49	−0.908 368 02	0.097 861 77	7.36	8.80	0.44	
6055–6069	−0.356 833 86	0.151 782 89	−0.921 754 60	32.27	18.85	3.97	
6061–6067	0.420 033 59	−0.275 587 72	0.864 652 07	5.97	4.53	1.70	
6061–6068	0.357 797 96	0.839 136 75	0.409 670 76	7.54	3.33	0.91	
6061–6069	0.749 334 62	0.428 916 57	0.504 507 89	53.39	28.14	16.96	
6063–6064	0.039 855 27	0.995 945 04	−0.080 653 84	3.07	3.81	−1.04	
6063–6067	−0.234 403 11	−0.604 571 06	−0.761 281 16	4.17	7.76	−0.64	
6064–6068	−0.216 482 33	0.242 737 19	−0.945 628 92	2.77	4.03	1.71	
6068–6069	−0.027 253 14	−0.962 401 53	−0.270 260 18	26.89	19.09	−9.25	
6068–6075	−0.398 041 64	0.689 693 01	0.604 885 45	5.43	5.59	0.88	
6072–6073	0.706 617 35	0.016 091 77	−0.707 412 87	4.53	6.29	1.63	
6072–6075	0.863 257 60	−0.138 517 63	−0.485 385 60	2.94	3.89	0.66	
6073–6075	0.894 816 33	−0.418 523 78	0.155 375 66	14.38	17.76	−0.98	

TABLE 9.26a.—*Accuracy Estimates for BC-4 Geometrical Network Station-Station Vectors*[a]

Line	σ_1^2 (μrad)	σ_2^2 (μrad)	δ^2 (μrad)	k^2
6002–6003	3.0	36.73	26.52	1.34
6002–6007	14.8	6.70	51.48	4.79
6002–6008	3.8	4.07	4.03	1.02
6002–6009	15.4	6.74	7.65	0.69
6002–6038	12.0	4.48	10.71	1.30
6002–6111	13.0	6.61	7.63	0.78
6003–6004	15.1	7.01	112.06	10.14
6003–6011	6.9	4.33	6.83	1.22
6003–6012	298.0	2.61	62.48	0.42
6003–6038	5.3	4.07	7.99	1.71
6003–6111	17.1	26.70	1.38	0.06
6003–6123	10.0	9.94	0.45	0.05
6003–6134	195.7	24.38	232.13	2.11
6004–6012	31.0	11.92	104.81	4.88
6004–6013	8.8	8.92	15.37	1.73
6004–6123	37.9	22.34	88.76	2.95
6006–6007	27.9	5.45	41.13	2.47
6006–6015	13.7	4.12	15.36	1.72
6006–6016	6.4	3.33	52.79	10.85
6006–6065	4.5	5.37	4.49	0.91
6007–6016	14.4	5.32	24.89	2.52
6007–6055	77.9	2.27	21.76	0.54
6007–6063	5.2	5.62	4.86	0.90
6007–6064	38.5	2.69	178.65	8.67
6007–6065	33.2	9.92	31.07	1.44
6007–6067	17.7	3.11	61.90	5.95
6008–6009	16.5	14.36	12.03	0.78
6008–6019	2.7	3.80	4.78	1.47
6008–6067	21.0	18.09	0.82	0.04
6009–6019	10.3	5.79	2.96	0.37
6009–6020	17.3	10.87	32.65	2.32
6009–6038	16.0	8.45	20.84	1.70
6009–6043	20.6	2.95	28.89	2.45
6011–6012	12.5	6.73	54.35	5.66
6011–6022	165.6	3.38	2.70	0.03
6011–6038	20.5	4.52	22.72	1.82
6011–6059	6.0	8.41	1.17	0.16
6011–6111	86.6	8.16	8.05	0.17
6011–6134	9.3	5.57	0.83	0.11
6012–6013	23.3	5.09	4.10	0.29
6012–6022	7.1	3.55	9.71	1.82
6012–6023	8.0	5.66	9.95	1.46
6012–6059	4.0	3.19	10.43	2.90
6013–6015	195.8	3.45	174.15	1.75
6013–6040	17.3	2.98	53.68	5.29
6013–6047	7.3	7.66	7.18	0.96
6013–6072	8.0	6.46	2.09	0.29
6013–6078	25.1	6.48	46.25	2.93
6015–6016	5.3	2.88	9.40	2.30
6015–6040	9.8	1.87	3.89	0.67
6015–6042	2.7	2.63	3.56	1.34
6015–6045	11.1	1.04	2.47	0.41
6015–6064	8.9	1.79	49.22	9.21
6015–6065	6.6	3.96	34.65	6.56
6015–6072	3.3	3.59	8.29	2.41
6015–6073	4.3	2.28	2.00	0.61
6015–6075	7.0	2.35	32.89	7.04
6016–6042	84.3	3.71	247.16	5.62
6016–6063	17.2	3.42	90.14	8.74
6016–6064	3.9	4.36	1.47	0.36
6016–6065	14.8	17.12	30.86	1.93
6019–6020	31.4	8.87	159.21	7.91
6019–6043	2.8	4.29	3.84	1.08
6019–6061	5.3	5.67	6.77	1.23
6019–6067	6.8	5.12	13.95	2.34
6019–6069	82.0	12.76	6.34	0.13
6020–6038	11.0	6.82	30.71	3.45
6020–6039	113.8	65.29	11.62	0.13
6020–6043	11.9	9.68	1.02	0.09
6022–6023	17.5	4.09	83.06	7.69
6022–6031	12.5	5.17	18.19	2.06
6022–6039	29.0	12.46	15.01	0.72
6022–6059	3.1	4.73	0.72	0.18
6022–6060	16.3	4.77	36.84	3.50
6022–6078	808.0	74.45	2970.60	6.73
6023–6031	11.1	1.49	11.13	1.77
6023–6032	4.9	3.66	52.75	12.32
6023–6040	30.2	3.96	65.25	3.76
6023–6047	17.8	9.40	63.17	4.64
6023–6060	1.6	2.38	2.09	1.05
6023–6072	94.9	3.24	268.78	5.48
6023–6078	663.6	46.34	1521.11	4.29
6031–6032	4.2	2.23	4.71	1.47
6031–6039	122.9	8.38	153.07	2.33
6031–6051	139.4	2.16	136.70	1.93
6031–6052	8.9	3.88	4.46	0.70
6031–6053	4.6	4.25	3.86	0.87
6031–6060	3.3	3.96	2.36	0.65
6031–6078	13.3	11.97	0.10	0.01
6032–6040	31.0	12.53	20.85	0.96
6032–6044	10.1	10.79	0.52	0.05
6032–6045	41.3	2.99	233.71	10.55
6032–6047	7.1	3.81	3.72	0.68
6032–6052	21.4	5.29	191.15	14.32
6032–6060	5.6	3.79	9.99	2.13
6038–6039	9.2	6.88	2.18	0.27
6038–6059	19.6	3.38	205.25	17.86
6038–6134	3.6	5.40	0.82	0.18
6039–6059	26.4	11.89	4.27	0.22
6040–6045	3.8	3.16	1.67	0.48
6040–6047	18.2	8.17	21.08	1.60
6040–6060	73.6	3.05	12.64	0.33
6040–6072	21.3	8.79	25.05	1.67
6040–6073	22.5	9.98	37.66	2.32
6040–6075	17.6	3.83	31.92	2.98
6042–6045	2.7	2.30	0.53	0.21

TABLE 9.26a.—*(Cont'd)*

Line	σ_1^2 (μrad)	σ_2^2 (μrad)	δ^2 (μrad)	k^2
6042–6064	9.6	7.67	8.74	1.01
6042–6068	2.8	2.78	1.55	0.56
6042–6073	162.0	3.15	720.92	8.73
6042–6075	15.5	7.54	23.07	2.00
6043–6050	19.1	27.00	58.35	2.53
6043–6061	29.9	16.57	78.65	3.38
6044–6045	74.5	15.07	19.43	0.43
6044–6051	38.3	45.24	0.16	0.00
6045–6051	8.2	3.11	1.14	0.20
6045–6068	5.0	4.91	0.50	0.10
6045–6073	6.5	7.46	0.53	0.08
6045–6075	7.6	10.67	6.83	0.75
6047–6072	8.2	8.68	13.27	1.57
6050–6053	51.3	15.86	512.41	15.26
6050–6061	32.7	32.91	174.32	5.31
6051–6052	22.2	16.02	11.87	0.62
6051–6053	4.8	5.71	6.28	1.20
6051–6061	20.4	8.34	32.94	2.29
6051–6068	2.5	2.66	8.36	3.24
6052–6053	7.1	8.96	1.59	0.20
6052–6060	6.2	2.88	3.66	0.81
6053–6060	27.8	2.09	6.33	0.42
6055–6063	6.0	6.42	2.28	0.37
6055–6064	4.6	3.46	11.38	2.82
6055–6067	5.9	8.08	0.71	0.10
6055–6069	23.5	25.56	4.41	0.18
6061–6067	238.0	5.25	1099.08	9.04
6061–6068	29.9	5.44	51.15	2.89
6061–6069	53.0	40.76	40.50	0.86
6063–6064	3.3	3.44	1.29	0.38
6063–6067	10.8	5.97	0.86	0.10
6064–6068	18.8	3.40	35.10	3.16
6068–6069	297.5	22.99	27.68	0.17
6068–6075	128.7	5.51	339.50	5.06
6072–6073	27.8	5.41	61.70	3.72
6072–6075	240.5	3.41	397.15	3.26
6073–6075	31.7	16.07	16.28	0.68
			k^2 ave =	2.60

[a] σ_1^2 and σ_2^2 are accuracy estimates before and after network adjustment, δ^2 is the square of the difference between the estimates, and k^2 is the scaling factor.

TABLE 9.26b.—*Accuracy Estimates for SAO Geometrical Network Station-Station Vectors*[a]

Line	n	σ_1^2 (μrad)	σ_2^2 (μrad)	δ^2 (μrad)	k^2	Line	n	σ_1^2 (μrad)	σ_2^2 (μrad)	δ^2 (μrad)	k^2
8015-8019	29	1514.4	4031.7	3114.8	1.12	9006-9091	10	30.0	28.6	38.6	1.32
8015-9004	122	7.2	23.4	44.9	2.93	9006-9115	19	5.9	16.8	201.5	17.75
8015-9066	133	79.2	378.5	258.9	1.13	9007-9009	263	1.1	6.9	1.5	0.38
8015-9074	25	37.2	38.1	487.9	12.96	9007-9010	86	2.3	5.5	0.6	0.15
8015-9080	67	20.8	66.2	217.4	5.00	9007-9011	437	1.7	13.5	0.1	0.01
8015-9091	30	10.6	25.3	0.01	0.00	9007-9029	74	1.2	24.1	10.6	0.84
8019-9004	301	0.9	7.2	0.6	0.15	9007-9031	32	3.5	27.0	0.4	0.03
8019-9091	61	4.0	17.9	2.3	0.21	9008-9028	25	16.7	64.3	6.4	0.16
9001-9009	183	1.0	5.8	1.3	0.38	9008-9080	8	233.1	32.1	453.1	3.42
9001-9010	154	2.1	13.1	6.8	0.89	9008-9115	38	6.4	23.3	33.4	2.25
9001-9012	187	1.6	9.4	0.8	0.15	9009-9010	248	2.2	14.4	0.1	0.01
9001-9113	20	32.3	174.1	195.2	1.89	9009-9011	201	1.3	4.9	0.2	0.06
9001-9114	74	5.8	30.0	11.7	0.65	9009-9114	13	21.5	9.5	13.8	0.89
9001-9117	16	11.7	14.4	85.3	6.54	9010-9029	6	59.6	24.9	79.9	1.89
9002-9008	7	19.3	84.3	369.4	7.13	9010-9114	38	7.4	17.6	146.4	11.71
9002-9028	25	11.0	86.0	40.6	0.84	9011-9029	7	734.0	47.9	6252.8	15.99
9004-9006	14	43.2	8.9	44.9	1.72	9011-9031	9	141.1	169.9	78.5	0.50
9004-9008	139	2.8	11.2	20.8	2.97	9012-9021	29	12.5	47.4	10.6	0.35
9004-9009	43	8.0	27.0	0.6	0.03	9012-9113	14	8.2	22.6	8.0	0.52
9004-9010	41	6.9	27.5	1.8	0.10	9012-9114	24	9.8	19.7	31.8	2.16
9004-9028	35	8.2	17.2	83.5	6.57	9012-9117	216	5.8	48.2	3.3	0.12
9004-9029	42	18.0	49.7	0.7	0.02	9021-9113	57	23.1	193.3	4.9	0.05
9004-9066	192	3.3	16.8	24.2	2.41	9021-9117	8	126.0	39.1	800.1	9.69
9004-9074	65	7.3	12.8	90.0	8.96	9028-9091	37	13.3	67.1	290.4	7.22
9004-9080	164	3.4	19.8	7.2	0.62	9029-9031	26	12.6	24.6	2.6	0.14
9004-9091	442	0.6	3.4	0.7	0.35	9066-9074	13	89.9	63.9	461.7	6.00
9004-9115	60	7.7	51.4	21.0	0.71	9066-9080	27	34.1	115.3	68.3	0.91
9005-9006	61	4.8	89.5	0.01	0.00	9074-9077	42	41.0	299.8	15.6	0.09
9005-9012	25	35.0	141.6	98.0	1.11	9074-9091	43	11.7	34.0	204.3	8.94
9005-9117	16	45.5	186.4	108.2	0.93	9077-9091	30	22.6	154.1	11.9	0.13
9006-9008	172	4.2	29.1	0.9	0.05	9113-9114	30	45.0	116.7	424.6	5.25

k^2 ave = 2.65

[a] n is the number of observations, σ_1^2 and σ_2^2 are accuracy estimates before and after network adjustment, δ^2 is the square of the angular difference between the two estimates, and k^2 is the scaling factor (σ_1, σ_2, and δ are in microradians).

TABLE 9.27.—*Coefficients of Zonal-Harmonic Coefficients in Equations for $\dot{\omega}$ and $\dot{\Omega}$*

Satellite		J_2	J_4	J_6	J_8	J_{10}	J_{12}	J_{14}	J_{16}	J_{18}	J_{20}	J_{22}	J_{24}	J_{26}	J_{28}	J_{30}	J_{32}	J_{34}	J_{36}
7001701	$\dot{\omega}$	11 306	−21 362	28 183	−31 767	32 678	−31 593	29 139	−25 835	22 092	−18 218	14 437	−10 903	7 717	−4 936	2 585	−665	−842	1 968
	$\dot{\Omega}$	−5 691	10 807	−14 617	16 932	−18 043	18 215	−17 685	16 649	−15 268	13 667	−11 950	10 197	−8 473	6 828	−5 299	3 913	−2 688	1 632
7010901	$\dot{\omega}$	12 165	−20 770	21 325	−14 509	3 882	6 305	−12 812	14 276	−11 222	5 463	756	−5 539	7 823	−7 500	5 223	−2 046	−967	3 043
	$\dot{\Omega}$	−6 414	11 751	−13 867	12 620	−8 995	4 414	−194	−2 781	4 171	−4 117	3 065	−1 574	144	891	−1 393	1 397	−1 052	547
6001301	$\dot{\omega}$	7 625	−5 479	−2 224	6 043	−3 260	−1 675	3 731	−2 045	−744	1 979	−1 213	−223	952	−671	−17	424	−348	38
	$\dot{\Omega}$	−4 671	5 169	−2 137	−945	1 924	−1 071	−157	703	−487	17	249	−211	37	84	−88	26	27	−36
5900101	$\dot{\omega}$	4 868	−1 560	−2 711	2 473	409	−1 902	926	665	−1 045	244	535	−517	−14	357	−230	−87	214	−85
	$\dot{\Omega}$	−3 236	2 540	−200	−1 095	787	106	−522	274	141	−264	85	114	−131	13	78	−61	−11	48
6202901	$\dot{\omega}$	1 836	1 040	−823	−645	400	342	−204	−179	107	94	−57	−50	31	27	−17	−14	9	8
	$\dot{\Omega}$	−1 717	301	512	−127	−208	60	97	−31	−48	16	24	−9	−13	5	7	−3	−4	1
6000902	$\dot{\omega}$	2 753	2 685	−1 224	−2 302	317	1 425	39	−763	−121	373	106	−171	−71	73	42	−30	−23	11
	$\dot{\Omega}$	−2 864	261	1 168	−16	−480	−37	194	34	−76	−21	29	12	−11	−6	4	3	−1	−1
6302601	$\dot{\omega}$	3 245	5 104	−765	−6 141	−1 782	4 990	3 273	−3 127	−3 678	1 374	3 334	−72	−2 612	−717	1 794	1 073	−1 055	−1 122
	$\dot{\Omega}$	−3 855	−145	2 333	645	−1 331	−761	677	685	−272	−540	41	385	77	−250	−124	144	128	−68
6206001	$\dot{\omega}$	2 741	4 130	−334	−4 065	−1 359	2 597	1 845	−1 190	−1 593	289	1 095	139	−632	−264	305	243	−112	−173
	$\dot{\Omega}$	−3 334	−187	1 667	489	−747	−441	278	301	−69	−174	−9	89	27	−39	−24	14	16	−3
6508901	$\dot{\omega}$	605	2 454	2 144	39	−1 392	−1 096	−10	604	438	−12	−240	−161	12	92	57	−7	−34	−20
	$\dot{\Omega}$	−2 076	−976	260	562	239	−92	−163	−64	32	50	18	−12	−16	−5	4	3	2	−2
6101501	$\dot{\omega}$	−641	1 893	4 419	4 327	1 628	−1 619	−3 300	−2 743	−816	1 016	1 750	1 305	295	−544	−809	−548	−82	264
	$\dot{\Omega}$	−2 240	−2 037	−809	331	811	657	219	−150	−284	−211	−57	62	98	67	14	−25	−34	−21
6400101	$\dot{\omega}$	−1 176	774	3 506	4 737	3 659	1 074	−1 486	−2 816	−2 596	−1 330	132	1 095	1 294	884	237	−292	−518	−449
	$\dot{\Omega}$	−1 971	−2 044	−1 205	−210	457	653	495	196	−60	−184	−179	−102	−14	43	58	43	16	−6
6406401	$\dot{\omega}$	−2 341	−2 483	−1 458	12	1 376	2 310	2 708	2 622	2 189	1 576	931	363	−68	−342	−471	−487	−427	−326
	$\dot{\Omega}$	−996	−1 298	−1 252	−1 026	−735	−455	−224	−59	44	96	110	101	79	55	33	15	2	−5
6508101	$\dot{\omega}$	−2 814	−3 984	−4 371	−4 299	−3 969	−3 508	−2 998	−2 491	−2 016	−1 588	−1 213	−893	−626	−406	−229	−90	18	−99
	$\dot{\Omega}$	−261	−375	−422	−431	−417	−392	−360	−327	−293	−260	−230	−201	−175	−152	−131	−112	−96	−81
6102801	$\dot{\omega}$	−903	−637	−331	−144	−53	−15	−2	2	2	1	1	0	0	0	0	0	0	0
	$\dot{\Omega}$	194.2	144.5	82.4	41.7	19.6	8.7	3.7	1.5	0.6	0.2	0.1	0.0	0.0	0.0	0.0	0.0	0.0	0.0

TABLE 9.28.—*Coefficients of Zonal-Harmonic Coefficients in Equations for ω, Ω, I, and e*

Satellite		J_3	J_5	J_7	J_9	J_{11}	J_{13}	J_{15}	J_{17}	J_{19}	J_{21}	J_{23}	J_{25}	J_{27}	J_{29}	J_{31}	J_{33}	J_{35}	J_{37}
7001701	ω	−5	12	−23	36	−50	63	−75	84	−90	93	−93	90	−85	77	−69	60	−50	40
	Ω	−211	381	−471	484	−436	347	−235	116	−1	−103	190	−258	307	−337	350	−348	334	−310
	I	203	−384	507	−573	592	−576	537	−484	423	−360	299	−241	190	−144	105	−72	45	−24
	e	−38	72	−95	107	−110	107	−100	90	−79	67	−56	45	−35	27	−20	13	−8	4
7010901	ω	−378	668	−753	644	−410	141	87	−229	275	−241	157	−59	−25	79	−97	86	−57	22
	Ω	−12	12	5	−31	54	−66	60	−40	12	16	−35	43	−38	25	−8	−7	18	−21
	I	38	−68	76	−64	41	−13	−9	23	−27	23	−15	5	3	−8	9	−8	5	−2
	e	−109	192	−216	183	−115	38	26	−66	77	−67	42	−15	−8	22	−26	23	−15	5
6001301	ω	−647	569	−67	−290	286	−76	−97	122	−47	−29	49	−25	−7	19	−12	−1	7	−5
	Ω	−2	−12	22	−12	−6	16	−11	−1	9	−7	1	4	−4	1	2	−2	1	1
	I	33	−29	3	15	−14	4	5	−6	2	1	−2	1	0	−1	1	0	0	0
	e	−187	164	−19	−84	82	−21	−28	35	−13	−8	14	−7	−2	5	−3	0	2	−1
5900101	ω	−77	53	14	−47	24	15	−26	8	12	−14	1	9	−7	−1	6	−3	−2	3
	Ω	9	−128	122	13	−103	65	25	−62	25	24	−34	7	18	−17	−1	12	−8	−3
	I	290	−143	−71	114	−33	−38	39	−4	−19	14	2	−9	5	2	−4	1	2	−2
	e	−193	95	48	−76	22	25	−26	3	12	−9	−1	6	−3	−2	3	−1	−1	1
6202901	ω	−74	−15	45	6	−25	−3	13	1	−7	−1	4	0	−2	0	1	0	−1	0
	Ω	103	−150	−66	96	33	−52	−16	28	8	−15	−4	8	2	−4	−1	2	1	−1
	I	319	98	−124	−31	45	11	−18	−4	8	2	−3	−1	2	0	−1	0	0	0
	e	−215	−66	83	21	−30	−7	12	3	−5	−1	2	1	−1	0	0	0	0	0
6000902	ω	−1365	−828	698	451	−269	−221	94	103	−29	−46	8	20	−1	−8	0	4	0	−1
	Ω	7	−9	−9	7	7	−4	−4	2	2	−1	−1	0	1	0	0	0	0	0
	I	16	10	−8	−5	3	3	−1	−1	0	1	0	0	0	0	0	0	0	0
	e	−271	−165	138	89	−53	−44	18	20	−6	−9	2	4	0	−2	0	1	0	0
6302601	ω	−305	−325	189	293	−61	−227	−17	159	55	−100	−68	55	66	−22	−55	1	42	11
	Ω	52	−57	−109	40	126	−1	−112	−32	84	50	−52	−54	25	49	−5	−39	−7	28
	I	91	97	−52	−82	14	58	6	−37	−14	21	15	−10	−12	3	9	0	−6	−2
	e	−311	−332	179	282	−49	−200	−20	126	47	−71	−50	34	42	−11	−31	−1	21	6

TABLE 9.28.—*(Cont'd)*

Satellite		J_3	J_5	J_7	J_9	J_{11}	J_{13}	J_{15}	J_{17}	J_{19}	J_{21}	J_{23}	J_{25}	J_{27}	J_{29}	J_{31}	J_{33}	J_{35}	J_{37}
6206001	ω	−2466	−2550	1113	1803	−168	−1033	−175	509	224	−213	−174	68	109	−8	−59	−11	28	13
	Ω	6	−6	−11	3	10	1	−7	−3	4	3	−2	−2	0	2	0	−1	0	0
	I	10	10	−5	−7	1	4	1	−2	−1	1	1	0	0	0	0	0	0	0
	e	−301	−311	136	220	−20	−126	−21	62	27	−26	−21	8	13	−1	−7	−1	3	2
6508901	ω	−268	−862	−417	160	309	126	−66	−106	−39	26	37	12	−10	−13	−4	4	5	1
	Ω	213	80	−186	−212	−32	108	97	8	−47	−37	−1	19	14	0	−7	−5	0	3
	I	77	249	119	−40	−78	−32	14	23	8	−5	−7	−2	2	2	1	−1	−1	0
	e	−314	−1019	−489	164	320	130	−57	−93	−34	19	27	9	−6	−8	−2	2	2	1
6101501	ω^a	−265	744	1046	652	48	−345	−396	−215	6	134	137	67	−10	−50	−46	−20	6	18
	Ω	−30	−40	−9	34	52	36	2	−26	−32	−18	1	14	15	7	−2	−7	−7	−3
	I	7	−20	−29	−18	−1	9	11	6	0	−4	−4	−2	0	1	1	1	0	0
	e	−370	1037	1459	909	68	−480	−551	−299	9	185	190	92	−14	−68	−64	−27	8	25
6400101	ω^a	−1447	1211	2666	2438	1244	−17	−771	−899	−598	−170	154	280	238	114	−6	−74	−83	−54
	Ω	−3	−5	−3	1	4	5	3	1	−2	−3	−2	−1	0	1	1	1	0	0
	I	1	−1	−2	−2	−1	0	1	1	0	0	0	0	0	0	0	0	0	0
	e	−378	317	698	638	326	−4	−202	−235	−157	−45	40	73	62	30	−2	−19	−22	−14
6406401	ω	−1750	−1123	−378	169	477	585	557	454	323	197	94	20	−26	−48	−54	−48	−38	−26
	Ω	−7	−15	−20	−21	−17	−12	−6	0	4	6	7	6	5	3	2	1	0	−1
	I	5	3	1	−1	−1	−2	−2	−1	−1	−1	0	0	0	0	0	0	0	0
	e	−394	−252	−85	38	107	130	124	101	71	43	21	4	−6	−10	−12	−10	−8	−6
6508101	ω	−318	−307	−261	−214	−173	−138	−109	−85	−65	−49	−36	−26	−17	−11	−5	−1	2	4
	Ω	−9	−22	−35	−45	−53	−57	−59	−59	−57	−54	−50	−46	−42	−37	−33	−29	−25	−22
	I	8	7	6	5	4	3	2	1	1	1	1	0	0	0	0	0	0	0
	e	−401	−377	−309	−242	−185	−139	−104	−76	−55	−39	−27	−18	−11	−7	−3	−1	1	2
6102801	ω	−1388	−638	−242	−81	−23	−5	0	1	1	0	0	0	0	0	0	0	0	0
	Ω	2	3	3	2	1	0	0	0	0	0	0	0	0	0	0	0	0	0
	I	−2	−1	0	0	0	0	0	0	0	0	0	0	0	0	0	0	0	0
	e	−293	−135	−51	−17	−5	−1	0	0	0	0	0	0	0	0	0	0	0	0

[a] For these satellites, ω is in units of 10^2 degrees.

TABLE 9.29.—*Coefficients of Zonal-Harmonic Coefficients in Equations for ω, Ω, I, and e*

Satellites		J_2	J_4	J_6	J_8	J_{10}	J_{12}	J_{14}	J_{16}	J_{18}	J_{20}	J_{22}	J_{24}	J_{26}	J_{28}	J_{30}	J_{32}	J_{34}	J_{36}
7001701	ω	0	0	0	0	1	−2	3	−4	6	−7	9	−11	12	−13	14	−15	15	−15
	Ω	0	−1	6	−15	25	−37	46	−54	57	−57	53	−46	36	−24	12	1	−13	23
	I	0	−1	6	−15	26	−39	52	−64	74	−81	85	−87	86	−82	77	−70	63	−55
	e	0	0	−1	3	−5	7	−10	12	−14	15	−16	16	−16	15	−14	13	−12	10
7010901	ω	0	−1	6	−13	20	−23	22	−15	6	4	−12	16	−15	11	−5	−1	6	−8
	Ω	0	0	0	0	0	0	−1	1	−2	2	−1	1	0	−1	2	−2	1	−1
	I	0	0	1	−1	2	−2	2	−2	1	0	−1	2	−2	1	0	0	1	−1
	e	0	0	−2	4	−6	7	−6	4	−2	−1	3	−4	4	−3	1	0	−2	2
6001301	ω	0	−4	10	−9	0	9	−9	2	4	−6	2	2	−3	2	1	−1	1	0
	Ω	0	0	0	0	0	0	0	0	0	0	0	0	0	0	0	0	0	0
	I	0	0	1	0	0	0	0	0	0	0	0	0	0	0	0	0	0	0
	e	0	1	−3	3	0	−3	3	−1	−1	2	−1	0	1	0	0	0	0	0
5900101	ω	0	−5	9	−4	−6	9	−2	−5	6	0	−4	3	1	−3	1	1	−2	1
	Ω	0	−2	−5	15	−11	−7	17	−8	−8	12	−3	−7	7	0	−5	4	1	−3
	I	0	−20	33	−9	−21	24	−2	−14	11	1	−8	4	2	−4	1	2	−2	0
	e	0	13	−22	6	14	−16	2	9	−7	−1	5	−3	−1	3	−1	−1	1	0
6202901	ω	0	−8	2	8	−3	−5	2	3	−2	−2	1	1	−1	−1	0	0	0	0
	Ω	0	2	−18	3	18	−4	−12	3	8	−2	−4	1	2	−1	−1	0	1	0
	I	0	−40	5	34	−6	−18	4	8	−2	−4	1	2	−1	−1	0	0	0	0
	e	0	27	−4	−23	4	12	−3	−6	1	3	−1	−1	0	1	0	0	0	0
6000902	ω	0	−10	−2	13	2	−9	−2	5	2	−3	−1	1	1	−1	0	0	0	0
	Ω	0	0	0	0	0	0	0	0	0	0	0	0	0	0	0	0	0	0
	I	0	0	0	0	0	0	0	0	0	0	0	0	0	0	0	0	0	0
	e	0	2	0	−3	0	2	0	−1	0	1	0	0	0	0	0	0	0	0
6302601	ω	0	−14	−9	27	19	−25	−26	16	27	−6	−25	−2	20	7	−14	−10	8	10
	Ω	0	1	−3	−3	6	7	−6	−10	4	11	0	−11	−3	9	5	−6	−6	3
	I	0	−4	−3	8	6	−7	−7	4	8	−1	−6	−1	5	2	−3	−2	2	2
	e	0	14	9	−27	−19	24	25	−14	−26	5	22	3	−17	−7	11	8	−6	−8

TABLE 9.29.—*(Cont'd)*

Satellites		J_2	J_4	J_6	J_8	J_{10}	J_{12}	J_{14}	J_{16}	J_{18}	J_{20}	J_{22}	J_{24}	J_{26}	J_{28}	J_{30}	J_{32}	J_{34}	J_{36}
6206001	ω	0	−13	−9	20	15	−14	−16	6	13	−1	−9	−2	5	3	−2	−2	1	2
	Ω	0	0	0	0	0	0	0	0	0	0	0	0	0	0	0	0	0	0
	I	0	0	0	0	0	0	0	0	0	0	0	0	0	0	0	0	0	0
	e	0	2	1	−2	−2	2	2	−1	−2	0	1	0	−1	0	0	0	0	0
6508901	ω	0	−22	−53	−16	35	38	5	−20	−18	−1	9	7	0	−4	−3	0	2	1
	Ω	0	4	−1	−12	−10	4	12	7	−3	−7	−3	2	4	1	−1	−2	−1	1
	I	0	−6	−16	−5	10	11	2	−5	−5	0	2	2	0	−1	−1	0	0	0
	e	0	26	65	19	−41	−44	−7	22	19	1	−9	−7	0	3	2	0	−1	−1
6101501	ω	0	4	78	114	62	−33	−97	−92	−34	29	59	47	13	−18	−29	−21	−4	9
	Ω	0	0	0	0	0	0	0	0	0	0	0	0	0	0	0	0	0	0
	I	0	0	0	0	0	0	0	0	0	0	0	0	0	0	0	0	0	0
	e	0	−1	−11	−16	−9	5	14	13	5	−4	−8	−7	−2	2	4	3	1	−1
6400101	ω	0	−5	30	62	60	24	−19	−47	−47	−27	0	20	25	18	5	−5	−10	−9
	Ω	0	0	0	0	0	0	0	0	0	0	0	0	0	0	0	0	0	0
	I	0	0	0	0	0	0	0	0	0	0	0	0	0	0	0	0	0	0
	e	0	0	−1	−2	−2	−1	1	1	1	1	0	−1	−1	0	0	0	0	0
6406401	ω	0	−11	−11	−2	8	17	22	23	20	15	9	4	0	−3	−5	−5	−4	−3
	Ω	0	0	0	0	0	0	0	0	0	0	0	0	0	0	0	0	0	0
	I	0	0	0	0	0	0	0	0	0	0	0	0	0	0	0	0	0	0
	e	0	2	2	1	−2	−4	−5	−5	−4	−3	−2	−1	0	1	1	1	1	1
6508101	ω	0	−13	−21	−25	−26	−25	−23	−20	−17	−14	−11	−8	−6	−4	−2	−1	0	1
	Ω	0	0	−1	−2	−4	−5	−6	−7	−8	−9	−9	−9	−9	−8	−8	−7	−7	−6
	I	0	0	−1	−1	−1	−1	−1	0	0	0	0	0	0	0	0	0	0	0
	e	0	16	26	31	31	29	26	22	18	14	11	8	6	4	2	1	0	−1
6102801	ω	0	−7	−5	−3	−1	0	0	0	0	0	0	0	0	0	0	0	0	0
	Ω	0	0	0	0	0	0	0	0	0	0	0	0	0	0	0	0	0	0
	I	0	0	0	0	0	0	0	0	0	0	0	0	0	0	0	0	0	0
	e	0	1	1	1	0	0	0	0	0	0	0	0	0	0	0	0	0	0

TABLE 9.30.—*Resonant Periods*

Resonant with order (m)	Satellite	Inclination (deg)	Period (days)
9	6102801	95	2.90
12	6100401	39	15.0
12	6000902	47	15.5
12	6508901	59	7.2
12	6506301	69	3.3
12	6507801	144	2.3
13	6701401	39	9.4, 10.9, 13.1, . . .
13	6503201	41	5.6
13	6701101	40	1.6
13	6206001	50	5.3
13	6800201	105	6.3
13	6600501	89	1.8
13	6304901	90	2.5
14	6701101	40	2.6
14	6302601	50	12.2
14	6101501	67	3.84
14	6101502	67	3.76
14	6400101	70	4.9
14	6406401	80	2.9
14	6408101	87	3.8
14	6600501	89	2.2

TABLE 9.31.—*Additional Parameters Determined*

Relation to the dynamical system	Translation parameters (m)	Rotation parameters about the axis (μrad)	Scale parameter
SAO geometrical	$X = -6.66$	$\epsilon_X = 0.70 \pm 1.56$	
	$Y = -14.88$	$\epsilon_Y = 0.84 \pm 1.24$	
	$Z = -9.90$	$\epsilon_Z = -0.40 \pm 1.43$	
BC–4 geometrical	$X = -11.25 \pm 9.60$	$\epsilon_X = 1.76 \pm 0.96$	
	$Y = -16.63 \pm 9.58$	$\epsilon_Y = -0.65 \pm 0.65$	
	$Z = -6.79 \pm 13.74$	$\epsilon_Z = -2.20 \pm 0.82$	
JPL		$\epsilon_Z = -3.43 \pm 1.02$	$0.18 \times 10^{-6} \pm 0.55 \times 10^{-6}$

TABLE 9.32.—*Geocentric Coordinates*

Station	*X* (Mm)	*Y* (Mm)	*Z* (Mm)	σ (m)	Location
7050	1.130 673 9	−4.831 373 5	3.994 101 0	1.81	Greenbelt, USA
1021	1.118 030 8	−4.876 321 3	3.942 973 0	1.81	Blossom Point, USA
7060	−5.068 964 1	3.584 106 1	1.458 744 3	2.88	Guam, USA
8816	4.654 336 9	1.959 179 0	3.884 358 5	2.26	Stephanion, Greece
8818	5.426 328 1	−0.229 326 6	3.334 606 4	6.07	Colomb-Bechar, Algeria
8015	4.578 327 7	0.457 974 8	4.403 179 7	2.07	Haute Provence, France
8815	4.578 370 7	0.457 959 1	4.403 135 5	2.07	Haute Provence, France
8809	4.578 348 4	0.457 965 9	4.403 157 9	2.07	Haute Provence, France
9001	−1.535 768 6	−5.166 989 0	3.401 042 5	2.44	Organ Pass, USA
9901	−1.535 768 8	−5.166 989 0	3.401 042 5	2.44	Organ Pass, USA
9002	5.056 126 7	2.716 513 6	−2.775 788 3	1.79	Olifantsfontein, Rep. S. Afr.
9902	5.056 126 5	2.716 513 5	−2.775 788 3	1.79	Olifantsfontein, Rep. S. Afr.
9022	5.056 120 7	2.716 524 3	−2.775 787 0	1.79	Olifantsfontein, Rep. S. Afr.
9003	−3.983 778 3	3.743 093 9	−3.275 561 0	2.49	Woomera, Australia
9023	−3.977 766 8	3.725 106 1	−3.303 028 3	2.16	Island Lagoon, Australia
9004	5.105 591 9	−0.555 230 0	3.769 662 5	3.06	San Fernando, Spain
8804	5.015 612 0	−0.555 252 3	3.769 631 2	3.06	San Fernando, Spain
9005	−3.946 690 6	3.366 295 7	3.698 833 4	6.26	Tokyo, Japan
9025	−3.910 434 2	3.376 357 4	3.729 220 2	6.26	Dodaira, Japan
9006	1.018 204 4	5.471 104 5	3.109 621 9	2.77	Naini Tal, India
9007	1.942 776 9	−5.804 089 4	−1.796 931 1	2.11	Arequipa, Peru
9907	1.942 777 0	−5.804 089 8	−1.796 931 2	2.11	Arequipa, Peru
9027	1.942 771 8	−5.804 096 1	−1.796 909 4	2.11	Arequipa, Peru
9008	3.376 892 9	4.403 982 3	3.136 257 8	5.08	Shiraz, Iran
9009	2.251 823 7	−5.816 915 7	1.327 163 5	4.42	Curacao, Antilles
9010	0.976 287 0	−5.601 394 7	2.880 234 7	2.86	Jupiter, USA
9011	2.280 591 3	−4.914 573 5	−3.355 423 0	3.19	Villa Dolores, Argentina
9012	−5.466 059 8	−2.404 278 8	2.242 180 5	2.72	Maui, USA
9912	−5.466 063 0	−2.404 278 7	2.242 172 7	2.72	Maui, USA
9021	−1.936 773 8	−5.077 708 3	3.331 902 4	3.16	Mt. Hopkins, USA
9921	−1.936 772 7	−5.077 705 3	3.331 907 6	3.16	Mt. Hopkins, USA
9028	4.903 765 2	3.965 216 0	0.963 868 0	4.85	Addis Ababa, Ethiopia
9029	5.186 459 7	−3.653 866 0	−0.654 334 7	3.86	Natal, Brazil
9929	5.186 459 9	−3.653 866 2	−0.654 334 8	3.86	Natal, Brazil
9039	5.186 469 8	−3.653 845 2	−0.654 334 4	3.86	Natal, Brazil
9031	1.693 805 4	−4.112 332 6	−4.556 653 1	5.24	Comodoro Rivadavia, Arg.
9091	4.595 167 5	2.039 466 0	3.912 658 7	4.11	Dionysos, Greece
9930	4.595 223 4	2.039 448 2	3.912 612 1	4.11	Dionysos, Greece
9030	4.595 214 5	2.039 448 0	3.912 622 0	4.11	Dionysos, Greece
8019	4.579 476 7	0.586 618 8	4.386 412 7	10.40	Nice, France
8010	4.331 304 7	0.567 521 8	4.633 101 2	3.67	Zimmerwald, Switzerland
9431	3.183 884 5	1.421 475 3	5.322 802 1	20.57	Riga, Latvia
9432	3.907 436 6	1.602 441 7	4.763 886 4	83.31	Uzhgorod, USSR
8011	3.920 168 9	−0.134 732 3	5.012 714 3	13.26	Malvern, U.K.
9425	−2.450 008 9	−4.624 414 9	3.635 028 8	3.70	Rosman, USA
9424	−1.264 845 1	−3.466 879 7	5.185 454 1	10.87	Cold Lake, Canada
9426	3.121 276 0	0.592 642 3	5.512 710 9	12.63	Harestua, Norway
9427	−6.007 407 9	−1.111 859 1	1.825 736 9	7.25	Johnston Is., USA
DSS11	−2.351 447 1	−4.645 070 6	3.673 760 0	3.80	California, USA
DSS12	−2.350 460 6	−4.651 969 9	3.665 624 7	3.80	California, USA
DSS14	−2.353 639 3	−4.641 333 2	3.677 048 3	3.77	California, USA
DSS41	−3.978 702 1	3.724 858 7	−3.302 208 1	2.78	Australia

TABLE 9.32.—*(Cont'd)*

Station	X (Mm)	Y (Mm)	Z (Mm)	σ (m)	Location
DSS42	−4.460 966 9	2.682 428 4	−3.674 613 8	6.05	Australia
DSS51	5.085 447 5	2.668 250 2	−2.768 726 1	4.73	So. Africa
DSS61	4.849 241 1	−0.360 297 2	4.114 867 3	3.64	Spain
DSS62	4.846 698 7	−0.370 214 9	4.116 890 5	3.66	Spain
6001	0.546 586 2	−1.389 973 0	6.180 232 9	11.15	Thule, Greenland
6002	1.130 768 8	−4.830 836 0	3.994 700 2	2.38	Beltsville, USA
6003	−2.127 825 1	−3.785 847 4	4.656 027 9	7.52	Moses Lake, USA
6004	−3.851 769 9	0.396 430 5	5.051 335 4	19.38	Shemya, USA
6006	2.102 948 2	0.721 679 1	5.958 176 5	13.56	Tromsø, Norway
6007	4.433 654 6	−2.268 140 7	3.971 641 0	12.86	Azores, Portugal
6008	3.623 253 6	−5.214 231 1	0.601 517 4	12.95	Paramaribo, Netherlands
6009	1.280 845 5	−6.250 943 5	−0.010 827 7	15.17	Quito, Ecuador
6011	−5.446 010 4	−2.404 397 9	2.242 216 3	3.12	Maui, USA
6012	−5.858 525 1	1.394 529 5	2.093 790 2	13.96	Wake Is., USA
6013	−3.565 847 0	4.120 728 3	3.303 421 8	7.56	Kanoyá, Japan
6015	2.604 378 6	4.444 166 7	3.750 317 1	10.37	Mashhad, Iran
6016	4.896 413 6	1.316 178 8	3.856 666 2	10.87	Catania, Italy
6019	2.280 642 9	−4.914 536 6	−3.355 441 9	3.54	Villa Dolores, Argentina
6020	−1.888 600 6	−5.354 864 7	−2.895 771 6	19.81	Easter Is., Chile
6022	−6.099 943 6	−0.997 320 8	−1.568 598 2	12.65	Tutuila, Am. Samoa
6023	−4.955 351 8	3.842 266 6	−1.163 859 8	8.96	Thursday Is., Australia
6031	−4.313 801 0	0.891 364 6	−4.597 282 7	9.29	Invercargill, New Zealand
6032	−2.375 370 7	4.875 567 2	−3.345 405 6	10.59	Caversham, Australia
6038	−2.160 977 9	−5.642 694 7	2.035 352 3	8.65	Revilla Gigedo, Mexico
6039	−3.724 752 5	−4.421 198 5	−2.686 105 0	22.12	Pitcairn Is., U.K.
6040	−0.741 936 4	6.190 810 5	−1.338 557 8	13.24	Cocos Is., Australia
6042	4.900 772 8	3.968 249 0	0.966 330 3	4.93	Addis Ababa, Ethiopia
6043	1.371 393 5	−3.614 735 8	−5.055 969 1	12.76	Cerro Sombrero, Chile
6044	1.098 926 5	3.684 646 5	−5.071 883 5	23.43	Heard Is., Australia
6045	3.223 459 4	5.045 345 3	−2.191 811 9	9.30	Mauritius, U.K.
6047	−3.361 922 1	5.365 826 1	0.763 621 4	12.76	Zamboanga, Philippines
6050	1.192 697 6	−2.450 987 7	−5.747 074 4	19.81	Palmer Sta., Antarctic
6051	1.111 361 9	2.169 282 1	−5.874 353 0	13.95	Mawson Sta., Antarctic
6052	−0.902 571 8	2.409 550 0	−5.816 569 5	13.80	Wilkes Sta., Antarctic
6053	−1.310 821 8	0.311 286 0	−6.213 299 2	13.45	McMurdo Sta., Antarctic
6055	6.118 349 5	−1.571 738 4	−0.878 618 1	11.14	Ascension Is., U.K.
6059	−5.885 323 7	−2.448 337 7	0.221 658 4	10.63	Christmas Is., U.K.
6060	−4.751 620 6	2.792 084 7	−3.200 181 2	3.19	Culgoora, Australia
6061	2.999 939 6	−2.219 352 6	−5.155 279 4	15.33	So. Georgia, U.K.
6063	5.884 483 9	−1.853 489 1	1.612 843 2	11.17	Dakar, Senegal
6064	6.023 411 3	1.617 937 3	1.331 725 4	9.89	Fort Lamy, Chad
6065	3.213 585 2	0.820 835 9	4.702 766 2	12.59	Hohenpeissenberg, W. Ger.
6067	5.186 415 4	−3.653 927 5	−0.654 297 7	4.13	Natal, Brazil
6068	5.084 848 9	2.670 346 3	−2.768 114 4	2.38	Johannesburg, Rep. S. Afr.
6069	4.978 443 0	−1.086 860 7	−3.823 181 6	26.56	Tristan Da Cunha, U.K.
6072	−0.941 663 5	5.967 461 5	2.039 307 2	13.65	Chiang Mai, Thailand
6073	1.905 165 3	6.032 287 8	−0.810 736 5	12.02	Chagos, Archipelg
6075	3.602 847 1	5.238 244 8	−0.515 950 7	11.39	Seychelles, U.K.
6078	−5.952 304 1	1.231 941 2	−1.925 939 0	22.93	New Hebrides, U.K.
6111	−2.448 849 2	−4.667 968 5	3.582 746 1	3.83	Wrightwood, USA
6123	−1.881 781 5	−0.812 422 7	6.019 588 6	17.73	Point Barrow, USA
6134	−2.448 902 9	−4.668 058 6	3.582 440 8	3.89	Wrightwood, USA

TABLE 9.33.—*Comparison of BC-4 Geometrical Solution With the Combination Solution*[a]

Station	Weight	Differences					
		ΔX	ΔY	ΔZ	North	East	Height
6001	12.22	−0	− 0	4	0	− 0	4
6002	5.54	12	−13	9	1	−15	13
6003	9.03	0	− 4	− 0	− 2	2	2
6004	20.01	2	− 9	1	3	9	− 0
6006	14.45	−6	−12	4	11	−10	0
6007	13.80	−6	− 5	− 1	1	− 7	− 3
6008	13.88	2	− 4	− 4	− 5	0	4
6009	15.97	5	− 5	− 1	− 1	4	6
6011	5.89	15	4	4	9	2	−13
6012	14.83	7	− 2	1	4	0	− 6
6013	9.06	−1	− 8	12	13	6	1
6015	11.51	−5	− 9	7	12	0	− 4
6016	11.96	−5	−11	3	8	−10	− 4
6019	6.13	13	3	− 5	− 3	13	5
6020	20.43	3	5	− 6	− 8	1	− 2
6022	13.60	7	6	− 1	− 3	− 4	− 8
6023	10.26	−2	3	0	1	− 1	4
6031	10.55	−2	4	− 9	− 4	− 4	9
6032	11.71	1	7	− 4	− 0	− 4	6
6038	9.99	4	5	− 1	0	2	− 6
6039	22.68	4	7	− 4	− 7	− 2	− 5
6040	14.15	−1	− 0	− 0	− 0	1	− 0
6042	7.02	−3	− 7	5	6	− 3	− 6
6043	13.70	11	8	− 8	− 8	13	4
6044	23.96	4	7	− 5	3	− 2	10
6045	10.56	−5	− 1	− 7	− 8	3	− 1
6047	13.70	−0	− 0	5	5	0	1
6050	20.43	10	2	− 6	− 0	10	6

TABLE 9.33.—*(Cont'd)*

Station	Weight	Differences ΔX	ΔY	ΔZ	North	East	Height
6051	14.82	5	4	−10	1	− 2	12
6052	14.68	4	5	− 9	− 0	− 5	10
6053	14.35	3	5	−12	− 5	− 5	11
6055	12.21	−9	0	11	10	− 1	−11
6059	11.75	9	5	− 2	− 2	− 1	−11
6060	5.93	−3	3	− 8	− 5	− 1	8
6061	16.12	8	3	− 4	1	8	6
6063	12.24	−8	− 2	0	2	− 4	− 7
6064	11.08	−6	−12	5	7	−10	− 7
6065	13.55	−6	−12	4	9	−11	− 2
6067	6.49	−5	13	10	9	7	−13
6068	5.54	−4	− 3	−24	−24	− 0	5
6069	27.03	−8	2	5	− 0	0	−10
6072	14.54	−3	− 1	9	9	4	1
6073	13.02	−7	− 2	0	0	6	− 4
6075	12.44	−4	− 2	1	1	1	− 4
6078	23.47	−8	3	9	12	− 1	5
6111	6.30	3	2	7	8	2	1
6123	18.42	1	−13	2	− 3	12	3
6134	6.33	4	12	6	12	− 1	− 7
					rms: 7.35	6.33	7.10
					Total rms: 12.02		

	Parameters determined		
	X	*Y*	*Z*
Translation (m)	16.32 ± 1.22	23.21 ± 1.22	−4.68 ± 1.22
Rotation (arc-sec)	−0.101 ± 0.050	0.086 ± 0.050	0.368 ± 0.046
		Scale (ppm) = 1.17 ± 0.19	

[a] Given in units of meters. The standard error of unit weight, σ_0, is 0.823.

TABLE 9.34.—*JPL–SAO Differences*

Rotation: -3.43 ± 1.02 μrad
Scale: $1.8 \times 10^{-7} \pm 5.5 \times 10^{-7}$

Station	R (m)	λ (m)
DSS 11	−0.81	2.69
DSS 12	−0.66	2.63
DSS 14	−0.86	2.57
DSS 41	4.31	−0.21
DSS 42	0.51	1.66
DSS 51	0.96	−3.03
DSS 61	−0.26	2.10
DSS 62	−0.31	2.31

TABLE 9.35.—*Translation, Rotation, and Scale Parameters for the Four Major Datums*

Datum	Number of stations	Translation (m)			Rotation (arc-sec)			Scale correction (ppm)	σ_0	σ (m)
		X	Y	Z	Azimuth	E–W	N–S			
NA27	10	−31.4	154.0	176.3	0.09	−0.62	−0.23	1.78	0.67	8
		±1.9	±2.2	±1.9	±0.24	±0.69	±0.24	±1.13		
EU50	17	−85.4	−111.1	−131.9	0.56	−0.51	−0.22	2.60	0.59	16
		±2.0	±1.9	±2.0	±0.21	±0.35	±0.22	±0.92		
SA69	8	−75.3	−3.3	−52.2	−0.33	−0.13	−0.33	−1.39	0.61	14
		±2.5	±2.6	±2.5	±0.21	±0.27	±0.33	±0.99		
AGD	7	−118.2	−38.6	+119.6	0.23	0.82	−0.22	2.33	0.35	5
		±1.5	±1.4	±1.4	±0.26	±0.41	±0.31	±1.22		

TABLE 9.36.—*Standard Deviations of Datum-Height Comparisons*

Datum	σ (m)
NAD27	3.07
SAD69	2.69
AGD	1.25
EU50	8.90
Average	3.98

TABLE 9.37.—*Comparison of Coordinates Determined in Both SE II and SE III*[a]

Station	Weight	Difference					
		X	*Y*	*Z*	North	East	Height
7050	7.23	1	− 6	− 9	−12	0	− 0
8015	5.41	−0	7	0	0	7	0
9001	5.58	−8	4	0	1	− 9	− 1
9002	7.23	1	− 0	− 3	− 2	− 1	2
9003	6.50	0	0	4	3	− 0	− 1
9004	5.86	3	− 3	− 4	− 5	− 3	0
9005	11.80	3	− 8	− 1	3	4	− 7
9006	9.42	0	− 2	− 2	− 1	− 1	− 3
9007	7.31	5	−10	3	6	1	10
9008	10.33	−1	2	6	5	2	4
9009	8.28	−2	1	4	5	− 1	− 1
9010	5.76	−1	1	− 4	− 3	− 1	− 3
9011	9.55	5	− 2	5	7	3	1
9012	7.51	−3	− 1	8	6	− 0	6
9021	15.33	11	− 6	−13	−13	12	− 5
9023	6.38	1	− 2	5	3	0	− 5
9028	12.94	14	11	− 4	− 6	0	17
9029	12.61	0	−11	− 7	− 7	− 9	7
9031	15.89	5	− 7	− 1	5	2	7
8010	7.90	−5	8	7	8	9	2
8011	16.03	−9	4	5	11	3	− 1
9425	7.92	4	3	− 6	− 2	2	− 8
9424	16.19	−5	2	−13	− 7	− 5	−11
9426	21.18	−4	− 2	8	8	− 1	5
9427	16.66	−2	− 4	5	4	4	4
				rms:	6.62	5.02	6.37
				Total rms:	10.47		

	Parameters determined		
	X	*Y*	*Z*
Translation (m)	−1.69 ± 1.19	3.76 ± 1.18	0.04 ± 1.18
Rotation (arc-sec)	−0.039 ± 0.047	−0.043 ± 0.049	−0.059 ± 0.044
	Scale (ppm) ≡ −0.26 ± 0.18		

[a] The systematic translation, rotation, and scale differences were removed before the differences were computed (in units of meters). The standard error of unit weight σ_0, is 0.662.

TABLE 9.38.—*Comparison of Spin-Axis Distances*

Using SAO station 9001 and geodetic tie	5 492 412.489 m
Using McDonald lunar laser	5 492 416.0 ± 3 m
Difference	−3.51 m

TABLE 9.39.—*Solutions for Even-Order Harmonics*[a]

J_2	J_4	J_6	J_8	J_{10}	J_{12}	J_{14}	J_{16}	J_{18}	J_{20}	J_{22}	J_n	n	$\sum$(residuals)^2
−3	30	−94	66	−178	161	−78	43	−77	−108	75			
±1	±2	±3	±4	±4	±3	±8	±7	±9	±9	±13			114
−3	31	−97	68	−178	155	−74	30	−75	−104	72	31		
±1	±2	±3	±4	±4	±5	±7	±10	±6	±9	±12	±17	24	106
−3	30	−94	67	−177	161	−76	43	−74	−108	73	−9		
±1	±2	±3	±4	±4	±3	±8	±7	±9	±9	±13	±20	26	113
−2	30	−89	61	−181	162	−80	35	−83	−132	80	94		
±1	±2	±3	±3	±3	±2	±6	±6	±5	±8	±9	±17	28	67
−3	28	−92	61	−178	167	−80	44	−75	−104	97	−61		
±1	±2	±3	±4	±4	±4	±7	±7	±6	±9	±15	±28	30	103
−3	29	−94	67	−176	159	−82	41	−76	−111	75	33		
±1	±2	±3	±4	±4	±3	±8	±7	±6	±9	±12	±25	32	110
−3	30	−94	66	−178	162	−78	40	−78	−107	74	14		
±1	±2	±3	±4	±4	±3	±7	±9	±7	±9	±12	±33	34	113
−2	31	−94	65	−183	165	−74	34	−102	−119	92	199		
±1	±1	±2	±2	±2	±2	±4	±4	±5	±5	±7	±22	36	39

[a] In units of 10^{-9}. Corrections are given for $n < 14$. Note that $J_n = -C_n$.

TABLE 9.40.—*Solutions for Odd-Order Harmonics*[a]

J_3	J_5	J_7	J_9	J_{11}	J_{13}	J_{15}	J_{17}	J_{19}	J_{21}	J_{23}	J_n	n	$\sum$(residuals)^2
6	−20	−12	−109	15	−222	104	−227	83	−70	111			
±3	±5	±7	±8	±7	±7	±11	±11	±12	±14	±21			53.7
8	−23	−8	−106	10	−210	88	−210	78	−83	137	−41		
±3	±4	±7	±7	±7	±10	±13	±13	±11	±13	±18	±20	25	49.4
3	−15	−18	−98	19	−226	121	−237	101	−78	101	−58		
±3	±4	±7	±8	±6	±7	±11	±11	±12	±11	±13	±20	27	44.7
5	−19	−12	−107	17	−222	107	−227	84	−64	103	−16		
±3	±5	±7	±8	±7	±7	±11	±11	±12	±14	±17	±23	29	53.0
6	−20	−11	−109	15	−220	106	−227	87	−72	115	−23		
±3	±4	±7	±8	±7	±8	±10	±11	±12	±12	±14	±28	31	52.8
7	−22	−11	−109	13	−219	102	−218	78	−69	124	−47		
±3	±4	±7	±8	±7	±8	±10	±12	±12	±12	±16	±32	33	51.1
5	−18	−19	−101	10	−225	105	−220	99	−83	145	−134		
±3	±4	±7	±7	±6	±7	±9	±10	±11	±11	±15	±36	35	40.6
6	−21	−11	−109	15	−222	102	−225	86	−66	110	−30		
±3	±4	±7	±8	±7	±7	±11	±11	±13	±13	±13	±44	37	53.1

[a] In units of 10^{-9}. Corrections are given for $n \leq 13$. Note that $J_n = -C_n$.

TABLE 9.41.—(O-C) *for Secular Motion and Their Differences*[a]

Satellite		(O-C)		I	II	1969	1963	1961	1959
7001701	$\dot{\omega}$	−18 060	± 90	−57	271	29 090	9 540	18 250	18 840
	$\dot{\Omega}$	10 120	± 70	−51	258	−17 400	−5 390	−9 950	−10 240
7010901	$\dot{\omega}$	−2 200	± 800	−1 530	−857	−4 700	100	6 200	6 900
	$\dot{\Omega}$	5 160	± 100	−83	99	−2 160	−1 450	−5 560	−5 900
6001301	$\dot{\omega}$	170	± 100	43	61	40	−300	−670	−90
	$\dot{\Omega}$	−125	± 5	−4	−10	−1	59	−611	−928
5900101	$\dot{\omega}$	32	± 3	1	3	1	18	−129	278
	$\dot{\Omega}$	−9	± 3	2	7	0	10	−248	−488
6202901	$\dot{\omega}$	40	± 6	11	10	2	300	827	1 013
	$\dot{\Omega}$	7	± 3	5	8	2	−39	−247	−395
6000902	$\dot{\omega}$	170	± 50	0	21	47	−287	770	1 070
	$\dot{\Omega}$	−1	±3	1	5	4	−43	−342	−594
6302601	$\dot{\omega}$	920	± 10	−1	−6	−52	2 650	4 900	5 290
	$\dot{\Omega}$	1	± 3	0	−2	19	261	−2	−352
6206001	$\dot{\omega}$	600	± 60	16	84	60	2 230	4 180	4 500
	$\dot{\Omega}$	−42	± 3	1	2	8	−56	−437	−740
6508901	$\dot{\omega}$	−110	± 10	−1	−29	−26	1 460	3 180	3 285
	$\dot{\Omega}$	−70	± 3	0	−6	−7	−670	−1 465	−1 670
6101501	$\dot{\omega}$	−300	± 80	14	97	65	−81	1 900	2 500
	$\dot{\Omega}$	22	± 3	−1	−1	3	−1 252	−2 815	−3 057
6400101	$\dot{\omega}$	600	± 800	729	718	620	−600	580	−500
	$\dot{\Omega}$	56	± 8	10	6	9	−1 073	−2 703	−2 921
6406401	$\dot{\omega}$	−400	± 100	−95	−231	−110	−2 000	−4 000	−4 300
	$\dot{\Omega}$	90	± 10	9	9	15	−220	−1 351	−1 467
6508101	$\dot{\omega}$	620	± 30	15	100	−8	300	−3 290	−3 630
	$\dot{\Omega}$	50	± 3	−2	−9	−27	35	−306	−337
6102801	$\dot{\omega}$	−35	± 50	−47	−47	−47	−340	−915	−1 008
	$\dot{\Omega}$	−2.9	± 0.5	0.6	0.7	0.6	62.7	192.3	212.6

[a] Given in units of 10^{-6} per day.

TABLE 9.42.—(O-C) *for Amplitudes of* $\left.\begin{matrix}cos\\sin\end{matrix}\right\}$ 2ω *Terms and Their Differences*[a]

Satellite		(O-C)	I	II	1969	1963	1961	1959
5900101	ω	0.3 ± 0.5	−0.2	−0.2	−0.3	−0.6	1.5	1.4
	Ω	−2 ± 2	−1	−2	−2	−1	−4	−4
	I	−3 ± 6	−4	−4	−5	−4	3	3
	e	0 ± 1	1	1	1	1	−4	−4
6202901	ω	−0.1 ± 0.3	−0.2	−0.2	−0.2	−0.8	−2.5	−2.7
	Ω	−1 ± 1	1	1	1	−8	−14	−14
	I	4 ± 4	5	4	4	−3	−14	−15
	e	0 ± 1	0	0	0	5	12	12
6000902	ω	−3 ± 4	−2	−2	−2	−6	−10	−10
	e	0 ± 1	0	0	0	0	1	1
6302601	ω	−6 ± 2	−1	0	0	−14	−23	−23
	Ω	2 ± 2	3	3	3	−2	−3	−3
	I	−1 ± 3	1	1	1	−4	−6	−6
	e	3 ± 2	−3	−3	−3	12	20	20
6206001	ω	3 ± 6	7	6	6	−5	−13	−13
	e	1 ± 1	1	1	0	2	3	3
6508901	ω	6 ± 2	1	2	2	−22	−49	−50
	Ω	4 ± 2	2	2	0	9	10	10
	I	5 ± 5	4	4	4	−3	−11	−11
	e	−4 ± 1	2	1	1	30	62	63
6101501	[b]ω	−1 ± 2	−1	0	0	−3	0	0
	e	1 ± 2	0	0	−1	3	−1	−1
6406401	[b]ω	0 ± 2	0	0	0	−1	−1	−1
	e	4 ± 4	3	4	3	5	7	7
6508101	ω	7 ± 3	3	4	3	12	0	0
	Ω	1 ± 1	1	0	0	2	2	2
	I	−2 ± 8	−2	−2	−2	−2	−2	−2
	e	−6 ± 2	−1	−2	−1	−11	3	3

[a] Given in units of 10^3 degrees for ω, 10^4 degrees for Ω, 10^5 degrees for I, and 10^6 for e, per day.
[b] For these satellites, ω is in units of 10^7 degrees.

TABLE 9.43.—(O-C) *for Amplitudes of* $\left.\begin{matrix}cos\\sin\end{matrix}\right\}$ *ω Terms and Their Differences*[a]

Satellite		(O-C)	I	II	1969	1963	1961	1959
7001701	ω	−70 ± 5	−2	0	−126	−104	−85	−87
	Ω	−190 ± 30	0	−28	−248	−570	−168	−237
	I	430 ± 30	−34	−31	740	900	480	550
	e	−91 ± 6	−5	−5	−149	−179	−99	−112
7010901	ω	45 ± 30	9	41	160	−411	232	112
	Ω	−18 ± 45	−44	−48	0	10	9	7
	I	−170 ± 300	−166	−170	−181	−120	−190	−177
	e	28 ± 20	18	27	61	−102	83	49
6001301	ω	4 ± 1	0	0	0	46	314	241
	Ω	0 ± 3	2	2	0	3	−10	−7
	I	0 ± 30	0	0	0	−2	−16	−12
	e	1.6 ± 1.0	0.5	0.5	0.6	13.5	90.7	69.8
5900101	ω	−1.7 ± 0.3	0.0	0.3	0.0	4.8	22.4	17.2
	Ω	−2 ± 2	2	1	2	−7	−87	−58
	I	1 ± 5	−3	−3	−4	−8	−64	−57
	e	−3.1 ± 0.5	−0.3	−0.7	−0.1	3.2	40.0	35.6
6202901	ω	−0.1 ± 0.2	0.0	0.0	−0.1	−1.2	−4.0	6.1
	Ω	2 ± 3	2	3	3	16	5	31
	I	−2 ± 3	−5	−4	−4	−11	−26	−78
	e	1.5 ± 0.8	0.2	0.0	0.2	4.2	15.2	49.7
6000902	ω	−19 ± 3	−4	−4	−10	42	1	315
	Ω	1 ± 1	1	1	0	3	4	6
	I	−2 ± 6	−2	−2	−6	−3	−2	−6
	e	−2.0 ± 0.6	1.0	1.0	0.3	10.5	2.4	64.8
6302601	ω	−17 ± 2	0	−4	−1	9	−17	86
	Ω	−6 ± 1	0	0	1	20	52	60
	I	14 ± 15	10	11	10	6	12	−19
	e	−12 ± 1	0	−1	2	16	−6	99
6206001	ω	−59 ± 4	0	5	0	187	122	931
	Ω	−2 ± 2	−2	−2	−2	0	3	4
	I	0 ± 10	0	0	0	−1	0	−4
	e	−8 ± 1	−1	0	−1	22	14	113
6508901	ω	3 ± 4	7	7	0	119	264	486
	Ω	10 ± 2	3	3	2	−10	8	−29
	I	−8 ± 8	−9	−9	−7	−40	−80	−144
	e	−4 ± 1	0	0	−2	127	292	555
6101501	[b]ω	−19 ± 5	−11	−11	−8	−46	−265	−413
	Ω	−3 ± 4	2	2	0	7	17	29
	I	0 ± 5	0	0	0	1	7	11
	e	−11 ± 1	0	0	4	−48	−354	−560
6400101	[b]ω	−200 ± 10	6	3	1	−72	−445	−593
	e	−58 ± 3	−4	−5	−9	−24	−122	−161
6406401	ω	−110 ± 20	23	36	30	23	510	930
	Ω	6 ± 3	1	1	1	5	11	16
	I	0 ± 8	0	0	0	0	−2	−3
	e	−34 ± 5	−4	−2	−2	−4	106	199
6508101	ω	60 ± 2	1	−1	3	64	197	296
	Ω	20 ± 1	0	2	2	16	26	32
	I	−10 ± 10	−9	−9	−10	−10	−13	−16
	e	60 ± 3	−4	−5	−2	67	231	354
6102801	ω	−30 ± 50	−48	−47	−40	15	390	663
	Ω	−2 ± 2	−2	−2	−2	−2	−3	−4
	I	−6 ± 7	−6	−6	−6	−6	−6	−5
	e	3.0 ± 1.5	−0.7	−0.6	0.0	12.5	91.8	149.2

[a] Given in units of 10^3 degrees for ω, 10^4 degrees for Ω, 10^5 degrees for *I*, and 10^6 for *e*, per day.
[b] For these satellites, ω is in units of 10^2 degrees.

TABLE 9.44.—*Comparison of Results*[a]

Solution	J_2	J_4	J_6	J_8	J_{10}	J_{12}	J_{14}	J_{16}	J_{18}	J_{20}	J_{22}	J_{36}
1959	1082.1	−2.15										
1961	1082.19	−2.13										
	±3	±5										
1963	1082.48	−1.84	0.39	−0.02								
	±4	±9	±9	±7								
1964	1082.639	−1.649	0.646	−0.270	−0.054	−0.357	0.179					
	±6	±16	±30	±50	±50	±44	±63					
1969	1082.628	−1.593	0.502	−0.118	−0.354	−0.042	−0.073	0.187	−0.231	−0.005		
	±2	±7	±14	±20	±25	±27	±28	±26	±22	±22		
1973 I	1082.637	−1.618	0.552	−0.205	−0.237	−0.192	0.105	0.034	−0.102	−0.119	0.092	0.199
	±1	±1	±2	±2	±2	±2	±4	±4	±5	±5	±7	±22
1973 II	1082.636	−1.619	0.552	−0.204	−0.232	−0.196	0.101	0.043	−0.077	−0.108	0.075	
	±1	±2	±3	±4	±4	±3	±8	±7	±9	±9	±13	
Cazenave *et al.* (1971)	1082.637	−1.619	0.558	−0.209	−0.233	−0.188	0.085	0.048	−0.137	−0.087		
	±4	±10	±17	±24	±26	±27	±34	±43	±44	±52		

Solution	J_3	J_5	J_7	J_9	J_{11}	J_{13}	J_{15}	J_{17}	J_{19}	J_{21}	J_{23}	J_{35}
1959	−2.20											
	±8											
1961	−2.29	−0.23										
	±2	±2										
1963	−2.562	−0.064	−0.470	0.117								
	±7	±7	±10	±11								
1964	−2.546	−0.210	−0.333	−0.053	0.302	−0.114						
	±20	±25	±39	±60	±35	±84						
1969	−2.538	−0.230	−0.361	−0.100	0.202	−0.123	−0.174	0.085	−0.216	0.145		
	±4	±7	±15	±23	±35	±49	±61	±65	±53	±29		
1973 I	−2.541	−0.228	−0.352	−0.154	0.312	−0.339	0.105	−0.220	0.099	−0.083	0.145	−0.134
	±3	±4	±7	±7	±6	±7	±9	±10	±11	±11	±15	±36
1973 II	−2.540	−0.230	−0.345	−0.162	0.317	−0.336	0.104	−0.227	0.083	−0.070	0.111	
	±3	±3	±7	±8	±7	±7	±11	±11	±12	±17	±21	
Cazenave *et al.* (1971)	−2.543	−0.226	−0.365	−0.118	0.236	−0.202	−0.081	−0.027	−0.112	0.106		
	±5	±7	±12	±13	±12	±14	±21	±23	±23	±15		

[a] Given in units of 10^{-6}.

TABLE 9.45.—*Fully Normalized Tesseral-Harmonic Coefficients for the Potential*[a]

Harmonic	Value	Harmonic	Value	Harmonic	Value	Harmonic	Value
$\overline{C}_{2,2}$	2.3799 −06	$\overline{S}_{2,2}$	−1.3656 −06	$\overline{C}_{3,1}$	1.9977 −06	$\overline{S}_{3,1}$	2.2337 −07
$\overline{C}_{3,2}$	7.7830 −07	$\overline{S}_{3,2}$	−7.5519 −07	$\overline{C}_{3,3}$	4.9011 −07	$\overline{S}_{3,3}$	1.5283 −06
$\overline{C}_{4,1}$	−5.1748 −07	$\overline{S}_{4,1}$	−4.8140 −07	$\overline{C}_{4,2}$	3.4296 −07	$\overline{S}_{4,2}$	6.7174 −07
$\overline{C}_{4,3}$	1.0390 −06	$\overline{S}_{4,3}$	−1.1923 −07	$\overline{C}_{4,4}$	−1.0512 −07	$\overline{S}_{4,4}$	3.5661 −07
$\overline{C}_{5,1}$	−5.3667 −08	$\overline{S}_{5,1}$	−7.9973 −08	$\overline{C}_{5,2}$	5.9869 −07	$\overline{S}_{5,2}$	−3.9910 −07
$\overline{C}_{5,3}$	−5.8429 −07	$\overline{S}_{5,3}$	−1.6338 −07	$\overline{C}_{5,4}$	−1.1583 −07	$\overline{S}_{5,4}$	−4.5393 −08
$\overline{C}_{5,5}$	1.3956 −07	$\overline{S}_{5,5}$	−8.6841 −07	$\overline{C}_{6,1}$	−7.2166 −08	$\overline{S}_{6,1}$	1.7756 −08
$\overline{C}_{6,2}$	2.4670 −08	$\overline{S}_{6,2}$	−4.0654 −07	$\overline{C}_{6,3}$	4.4139 −09	$\overline{S}_{6,3}$	2.9055 −08
$\overline{C}_{6,4}$	−1.0003 −07	$\overline{S}_{6,4}$	−3 .0297 −07	$\overline{C}_{6,5}$	−1.3504 −07	$\overline{S}_{6,5}$	−6.0964 −07
$\overline{C}_{6,6}$	−2.9136 −08	$\overline{S}_{6,6}$	−2.6327 −07	$\overline{C}_{7,1}$	2.3532 −07	$\overline{S}_{7,1}$	5.5634 −08
$\overline{C}_{7,2}$	2.0425 −07	$\overline{S}_{7,2}$	1.7321 −07	$\overline{C}_{7,3}$	2.1994 −07	$\overline{S}_{7,3}$	−3.4644 −07
$\overline{C}_{7,4}$	−2.8617 −07	$\overline{S}_{7,4}$	−2.7738 −07	$\overline{C}_{7,5}$	3.4727 −08	$\overline{S}_{7,5}$	8.7014 −08
$\overline{C}_{7,6}$	−2.7496 −07	$\overline{S}_{7,6}$	8.5865 −08	$\overline{C}_{7,7}$	−2.4856 −08	$\overline{S}_{7,7}$	−8.8968 −09
$\overline{C}_{8,1}$	1.0946 −08	$\overline{S}_{8,1}$	4.8429 −08	$\overline{C}_{8,2}$	1.1084 −07	$\overline{S}_{8,2}$	1.0359 −07
$\overline{C}_{8,3}$	−8.8578 −08	$\overline{S}_{8,3}$	−5.0715 −08	$\overline{C}_{8,4}$	−2.2315 −07	$\overline{S}_{8,4}$	2.6511 −07
$\overline{C}_{8,5}$	1.5318 −07	$\overline{S}_{8,5}$	8.1158 −08	$\overline{C}_{8,6}$	−9.7542 −08	$\overline{S}_{8,6}$	2.8082 −07
$\overline{C}_{8,7}$	2.0498 −07	$\overline{S}_{8,7}$	2.4592 −07	$\overline{C}_{8,8}$	1.6967 −07	$\overline{S}_{8,8}$	9.3261 −08
$\overline{C}_{9,1}$	1.8099 −07	$\overline{S}_{9,1}$	4.1091 −08	$\overline{C}_{9,2}$	−2.2013 −08	$\overline{S}_{9,2}$	2.4215 −09
$\overline{C}_{9,3}$	−9.9252 −08	$\overline{S}_{9,3}$	−2.3085 −08	$\overline{C}_{9,4}$	−4.0867 −08	$\overline{S}_{9,4}$	−3.8525 −08
$\overline{C}_{9,5}$	−5.8957 −08	$\overline{S}_{9,5}$	3.6834 −09	$\overline{C}_{9,6}$	4.8812 −08	$\overline{S}_{9,6}$	1.1115 −07
$\overline{C}_{9,7}$	−1.9880 −07	$\overline{S}_{9,7}$	−1.4978 −07	$\overline{C}_{9,8}$	2.3523 −07	$\overline{S}_{9,8}$	9.6355 −09
$\overline{C}_{9,9}$	−3.4533 −08	$\overline{S}_{9,9}$	5.9502 −08	$\overline{C}_{10,1}$	8.9008 −08	$\overline{S}_{10,1}$	−6.0157 −08
$\overline{C}_{10,2}$	−3.7256 −08	$\overline{S}_{10,2}$	−6.3676 −08	$\overline{C}_{10,3}$	−1.3307 −07	$\overline{S}_{10,3}$	−7.2728 −08
$\overline{C}_{10,4}$	−2.1887 −08	$\overline{S}_{10,4}$	−7.8408 −08	$\overline{C}_{10,5}$	−6.1509 −09	$\overline{S}_{10,5}$	−1.1904 −07
$\overline{C}_{10,6}$	−9.4142 −08	$\overline{S}_{10,6}$	−1.1728 −08	$\overline{C}_{10,7}$	1.8525 −07	$\overline{S}_{10,7}$	2.1656 −08
$\overline{C}_{10,8}$	1.0887 −09	$\overline{S}_{10,8}$	7.0781 −09	$\overline{C}_{10,9}$	7.8473 −08	$\overline{S}_{10,9}$	5.6381 −09
$\overline{C}_{10,10}$	1.3321 −07	$\overline{S}_{10,10}$	9.8839 −08	$\overline{C}_{11,1}$	−1.2194 −08	$\overline{S}_{11,1}$	7.5463 −08
$\overline{C}_{11,2}$	−2.0255 −08	$\overline{S}_{11,2}$	−6.2998 −08	$\overline{C}_{11,3}$	−1.0988 −09	$\overline{S}_{11,3}$	−3.8098 −08
$\overline{C}_{11,4}$	1.5676 −08	$\overline{S}_{11,4}$	−1.9551 −07	$\overline{C}_{11,5}$	−1.8591 −09	$\overline{S}_{11,5}$	6.1113 −08
$\overline{C}_{11,6}$	6.3601 −08	$\overline{S}_{11,6}$	−2.6457 −08	$\overline{C}_{11,7}$	−3.3761 −08	$\overline{S}_{11,7}$	−1.2825 −07
$\overline{C}_{11,8}$	−1.3634 −08	$\overline{S}_{11,8}$	4.5229 −08	$\overline{C}_{11,9}$	2.1256 −08	$\overline{S}_{11,9}$	6.6721 −08
$\overline{C}_{11,10}$	5.2555 −08	$\overline{S}_{11,10}$	−7.7401 −08	$\overline{C}_{11,11}$	8.6996 −08	$\overline{S}_{11,11}$	−2.5691 −08
$\overline{C}_{12,1}$	−5.6935 −08	$\overline{S}_{12,1}$	−6.6159 −08	$\overline{C}_{12,2}$	−9.7424 −08	$\overline{S}_{12,2}$	4.6341 −08
$\overline{C}_{12,3}$	1.5555 −07	$\overline{S}_{12,3}$	−4.8666 −08	$\overline{C}_{12,4}$	−5.0379 −08	$\overline{S}_{12,4}$	5.3568 −08
$\overline{C}_{12,5}$	8.1834 −08	$\overline{S}_{12,5}$	2.7932 −08	$\overline{C}_{12,6}$	−2.1177 −08	$\overline{S}_{12,6}$	3.5034 −08
$\overline{C}_{12,7}$	2.9751 −08	$\overline{S}_{12,7}$	3.1783 −08	$\overline{C}_{12,8}$	4.0190 −08	$\overline{S}_{12,8}$	5.6877 −08
$\overline{C}_{12,9}$	−1.1503 −07	$\overline{S}_{12,9}$	1.4508 −08	$\overline{C}_{12,10}$	−4.5921 −08	$\overline{S}_{12,10}$	−4.3264 −08
$\overline{C}_{12,11}$	−7.8443 −09	$\overline{S}_{12,11}$	−4.7858 −08	$\overline{C}_{12,12}$	−2.7617 −08	$\overline{S}_{12,12}$	−1.6808 −08
$\overline{C}_{13,1}$	8.6136 −09	$\overline{S}_{13,1}$	−3.2401 −08	$\overline{C}_{13,2}$	−1.0679 −08	$\overline{S}_{13,2}$	−9.0670 −08
$\overline{C}_{13,3}$	−3.2361 −08	$\overline{S}_{13,3}$	4.9286 −08	$\overline{C}_{13,4}$	3.9852 −08	$\overline{S}_{13,4}$	−1.0608 −07
$\overline{C}_{13,5}$	4.0047 −08	$\overline{S}_{13,5}$	3.8114 −08	$\overline{C}_{13,6}$	−2.1906 −08	$\overline{S}_{13,6}$	−1.1321 −08
$\overline{C}_{13,7}$	−7.6933 −08	$\overline{S}_{13,7}$	1.1140 −08	$\overline{C}_{13,8}$	−2.7448 −09	$\overline{S}_{13,8}$	1.4309 −08
$\overline{C}_{13,9}$	−1.1588 −08	$\overline{S}_{13,9}$	7.2989 −08	$\overline{C}_{13,10}$	4.1979 −09	$\overline{S}_{13,10}$	7.6769 −09
$\overline{C}_{13,11}$	−5.4381 −08	$\overline{S}_{13,11}$	1.3450 −08	$\overline{C}_{13,12}$	−4.6633 −08	$\overline{S}_{13,12}$	7.9963 −08
$\overline{C}_{13,13}$	−6.8944 −08	$\overline{S}_{13,13}$	7.1891 −08	$\overline{C}_{14,1}$	−1.4359 −08	$\overline{S}_{14,1}$	5.2390 −08

[a] Values given as coefficient and exponent of 10.

TABLE 9.45.—*(Cont'd)*

Harmonic	Value	Harmonic	Value	Harmonic	Value	Harmonic	Value
$\overline{C}_{14,2}$	−1.5908 −08	$\overline{S}_{14,2}$	−2.7374 −09	$\overline{C}_{14,3}$	9.6915 −08	$\overline{S}_{14,3}$	−2.5631 −08
$\overline{C}_{14,4}$	−2.9864 −08	$\overline{S}_{14,4}$	−3.8189 −09	$\overline{C}_{14,5}$	−1.3828 −09	$\overline{S}_{14,5}$	−5.8680 −08
$\overline{C}_{14,6}$	−1.3872 −08	$\overline{S}_{14,6}$	−2.7976 −08	$\overline{C}_{14,7}$	7.1056 −08	$\overline{S}_{14,7}$	2.4043 −09
$\overline{C}_{14,8}$	−1.8779 −08	$\overline{S}_{14,8}$	−5.8750 −08	$\overline{C}_{14,9}$	−2.4322 −08	$\overline{S}_{14,9}$	6.0461 −08
$\overline{C}_{14,10}$	2.8985 −08	$\overline{S}_{14,10}$	−3.4224 −08	$\overline{C}_{14,11}$	8.2611 −08	$\overline{S}_{14,11}$	−1.9627 −09
$\overline{C}_{14,12}$	1.1751 −09	$\overline{S}_{14,12}$	−3.0967 −08	$\overline{C}_{14,13}$	3.0793 −08	$\overline{S}_{14,13}$	4.7620 −08
$\overline{C}_{14,14}$	−6.5969 −08	$\overline{S}_{14,14}$	3.3030 −09	$\overline{C}_{15,1}$	2.9358 −08	$\overline{S}_{15,1}$	−1.6691 −08
$\overline{C}_{15,2}$	−1.2291 −08	$\overline{S}_{15,2}$	−6.8963 −08	$\overline{C}_{15,3}$	−5.8921 −08	$\overline{S}_{15,3}$	4.477 2 −08
$\overline{C}_{15,4}$	1.4876 −08	$\overline{S}_{15,4}$	7.0359 −09	$\overline{C}_{15,5}$	3.6806 −08	$\overline{S}_{15,5}$	−8.4051 −09
$\overline{C}_{15,6}$	1.0081 −08	$\overline{S}_{15,6}$	−3.0473 −08	$\overline{C}_{15,7}$	3.0439 −08	$\overline{S}_{15,7}$	1.5775 −08
$\overline{C}_{15,8}$	−6.8884 −08	$\overline{S}_{15,8}$	6.0808 −08	$\overline{C}_{15,9}$	−4.5169 −08	$\overline{S}_{15,9}$	5.5556 −08
$\overline{C}_{15,10}$	6.2126 −08	$\overline{S}_{15,10}$	−7.1799 −09	$\overline{C}_{15,11}$	−4.4724 −08	$\overline{S}_{15,11}$	−3.4391 −09
$\overline{C}_{15,12}$	−4.2025 −08	$\overline{S}_{15,12}$	5.9072 −09	$\overline{C}_{15,13}$	−4.1654 −08	$\overline{S}_{15,13}$	−5.5892 −09
$\overline{C}_{15,14}$	9.5654 −09	$\overline{S}_{15,14}$	−2.7145 −08	$\overline{C}_{15,15}$	−5.6358 −08	$\overline{S}_{15,15}$	3.4895 −08
$\overline{C}_{16,1}$	−9.9588 −09	$\overline{S}_{16,1}$	5.4160 −08	$\overline{C}_{16,2}$	5.5086 −09	$\overline{S}_{16,2}$	4.9455 −08
$\overline{C}_{16,3}$	5.4189 −08	$\overline{S}_{16,3}$	5.4887 −09	$\overline{C}_{16,4}$	4.6176 −08	$\overline{S}_{16,4}$	3.6270 −08
$\overline{C}_{16,5}$	−2.4432 −08	$\overline{S}_{16,5}$	2.9671 −08	$\overline{C}_{16,6}$	−3.7203 −09	$\overline{S}_{16,6}$	−2.0786 −08
$\overline{C}_{16,7}$	−2.2794 −09	$\overline{S}_{16,7}$	3.0609 −09	$\overline{C}_{16,8}$	−1.0459 −07	$\overline{S}_{16,8}$	−4.4731 −08
$\overline{C}_{16,9}$	2.4845 −08	$\overline{S}_{16,9}$	−8.6262 −08	$\overline{C}_{16,10}$	−3.9928 −08	$\overline{S}_{16,10}$	−4.5058 −09
$\overline{C}_{16,11}$	−2.0848 −08	$\overline{S}_{16,11}$	2.9738 −08	$\overline{C}_{16,12}$	1.5930 −08	$\overline{S}_{16,12}$	−1.2703 −08
$\overline{C}_{16,13}$	2.5280 −08	$\overline{S}_{16,13}$	6.6240 −09	$\overline{C}_{16,14}$	−1.4852 −08	$\overline{S}_{16,14}$	−8.1713 −09
$\overline{C}_{16,15}$	−7.7425 −08	$\overline{S}_{16,15}$	−2.6491 −08	$\overline{C}_{16,16}$	−1.8538 −08	$\overline{S}_{16,16}$	−2.2310 −08
$\overline{C}_{17,1}$	8.6593 −09	$\overline{S}_{17,1}$	−4.1093 −08	$\overline{C}_{17,2}$	−9.0769 −09	$\overline{S}_{17,2}$	−2.7205 −08
$\overline{C}_{17,3}$	−7.7864 −09	$\overline{S}_{17,3}$	−1.7913 −08	$\overline{C}_{17,4}$	−4.3231 −08	$\overline{S}_{17,4}$	6.8203 −08
$\overline{C}_{17,5}$	4.1513 −08	$\overline{S}_{17,5}$	−2.5453 −08	$\overline{C}_{17,6}$	−4.5453 −08	$\overline{S}_{17,6}$	−1.7273 −08
$\overline{C}_{17,7}$	1.6938 −08	$\overline{S}_{17,7}$	−3.3752 −08	$\overline{C}_{17,8}$	4.1231 −08	$\overline{S}_{17,8}$	5.8792 −09
$\overline{C}_{17,9}$	−4.3119 −08	$\overline{S}_{17,9}$	−1.5974 −08	$\overline{C}_{17,10}$	−1.0844 −08	$\overline{S}_{17,10}$	5.5628 −08
$\overline{C}_{17,11}$	−4.4136 −08	$\overline{S}_{17,11}$	−4.3123 −09	$\overline{C}_{17,12}$	3.1661 −08	$\overline{S}_{17,12}$	6.2982 −09
$\overline{C}_{17,13}$	2.5147 −08	$\overline{S}_{17,13}$	9.7728 −09	$\overline{C}_{17,14}$	−5.5945 −09	$\overline{S}_{17,14}$	7.2604 −09
$\overline{C}_{17,15}$	4.9113 −08	$\overline{S}_{17,15}$	3.1958 −08	$\overline{C}_{17,16}$	−2.3540 −08	$\overline{S}_{17,16}$	−1.5882 −08
$\overline{C}_{17,17}$	−9.0191 08	$\overline{S}_{17,17}$	−9.4775 −09	$\overline{C}_{18,1}$	−2.3557 −08	$\overline{S}_{18,1}$	−7.4536 −08
$\overline{C}_{18,2}$	−9.4249 −09	$\overline{S}_{18,2}$	3.0353 −08	$\overline{C}_{18,3}$	−3.5003 −08	$\overline{S}_{18,3}$	−2.0464 −08
$\overline{C}_{18,4}$	2.9433 −08	$\overline{S}_{18,4}$	−4.4672 −08	$\overline{C}_{18,5}$	1.7511 −09	$\overline{S}_{18,5}$	−6.0367 −09
$\overline{C}_{18,6}$	2.3931 −08	$\overline{S}_{18,6}$	−4.4966 −09	$\overline{C}_{18,7}$	−7.8040 −10	$\overline{S}_{18,7}$	−8.2010 −09
$\overline{C}_{18,8}$	5.3819 −08	$\overline{S}_{18,8}$	−2.2106 −08	$\overline{C}_{18,9}$	−3.6120 −10	$\overline{S}_{18,9}$	−5.0562 −09
$\overline{C}_{18,10}$	4.2146 −08	$\overline{S}_{18,10}$	7.8924 −09	$\overline{C}_{18,11}$	2.4981 −08	$\overline{S}_{18,11}$	2.3183 −08
$\overline{C}_{18,12}$	−6.2242 −09	$\overline{S}_{18,12}$	6.6025 −09	$\overline{C}_{18,13}$	−2.6685 −08	$\overline{S}_{18,13}$	−4.2500 −08
$\overline{C}_{18,14}$	9.1191 −09	$\overline{S}_{18,14}$	−3.3129 −08	$\overline{C}_{18,15}$	−4.1521 −08	$\overline{S}_{18,15}$	−1.7610 −08
$\overline{C}_{18,16}$	2.4850 −08	$\overline{S}_{18,16}$	−4.8182 −09	$\overline{C}_{18,17}$	3.5357 −08	$\overline{S}_{18,17}$	−4.7166 −08
$\overline{C}_{18,18}$	−3.4701 −10	$\overline{S}_{18,18}$	5.0554 −08	$\overline{C}_{19,12}$	3.6058 −08	$\overline{S}_{19,12}$	−3.4421 −09
$\overline{C}_{19,13}$	9.6876 −09	$\overline{S}_{19,13}$	−6.6095 −08	$\overline{C}_{19,14}$	7.6389 −09	$\overline{S}_{19,14}$	−2.7649 −08
$\overline{C}_{20,13}$	2.7630 −08	$\overline{S}_{20,13}$	3.2389 −08	$\overline{C}_{20,14}$	3.3687 −08	$\overline{S}_{20,14}$	−6.5741 −08
$\overline{C}_{21,13}$	−1.9799 −08	$\overline{S}_{21,13}$	−3.0711 −08	$\overline{C}_{21,14}$	1.6623 −08	$\overline{S}_{21,14}$	8.7215 −09
$\overline{C}_{22,13}$	−7.9435 −09	$\overline{S}_{22,13}$	4.1452 −09	$\overline{C}_{22,14}$	2.8516 −09	$\overline{S}_{22,14}$	−4.2148 −08
$\overline{C}_{23,13}$	−1.3236 −08	$\overline{S}_{23,13}$	−4.8892 −09	$\overline{C}_{23,14}$	−2.1148 −08	$\overline{S}_{23,14}$	2.2010 −08
$\overline{C}_{24,14}$	3.4668 −09	$\overline{S}_{24,14}$	2.2983 −08				

TABLE 9.46.—*Comparison of SE III With Satellite Observations*[a]

Epoch (MJD)	σ(m)	n	Epoch (MJD)	σ(m)	n
	6508901 (GEOS-A) A/m = 0.05				
41 000	4.1	289	41 010	7.7	523
41 002	5.5	367	41 012	9.8	577
41 004	3.2	314	41 014	9.2	715
41 006	8.9	601	14 016	4.1	425
41 008	10.6	696	41 018	3.6	221
	6800201 (GEOS-B) A/m = 0.05				
41 038	2.4	249	41 048	3.8	304
41 040	6.5	533			
41 042	7.8	681	41 052	2.8	388
41 044	6.3	651	41 054	6.6	602
41 046	2.7	441			
	6701401 (DID) A/m = 0.1				
41 072	10.3	467	41 080	7.4	621
41 074	9.9	332	41 082	6.9	764
41 076	16.3	341	41 084	4.9	427
41 078	17.0	254	41 086	3.6	519

[a] n is number of observations used.

TABLE 9.47.—*Comparison of SE III Combination Solution With Surface Gravity*[a]

Solution	ℓ,m	$\langle(g_t - g_s)^2\rangle$	$\langle g_t g_s\rangle$	$\langle g_s^2\rangle$	D	$\langle g_t^2\rangle$	$E\ (e_s^2)$	$E\ (e_t^2)$	$E\ (\delta g^2)$	n
SE II[b]	16	75	184	186	163	253	2	11	63	≥20
SE II	16	187	177	229	203	311	52	13	122	(306 anomalies)[c]
SE III	18	105	221	236	237	311	15	13	77	----------
SE III	10	195	150	192	163	302	42	24	129	≥ 1
	14	174	174	220	198	302	47	24	103	(1183 anomalies)
	18	156	202	258	237	302	56	24	75	----------
SE III	10	184	183	205	163	345	22	19	143	≥10
	14	151	215	236	198	345	20	19	111	(659 anomalies)
	18	117	255	281	237	345	26	19	63	----------
SE III	10	186	151	176	163	311	25 (24)	13	148	≥20
	14	146	182	200	198	311	17 (21)	13	116	(306 anomalies)
	18	105	221	236	237	311	15 (18)	13	77	----------

[a] Given in mGal^2.
[b] From the available data, there were 935, 369, and 136 gravity anomalies with $n \geq 1$,10, and 20 1° × 1° anomalies.
[c] Here, n is the number of 1° × 1° mean gravity anomalies used to obtain 5° × 5° mean gravity anomalies.

TABLE 9.48.—*Surface-Gravity Residuals for an $\ell = m = 36$ Potential From Numerical Quadrature*[a]

Degree of reference field	$\langle(g_t - g_s)^2\rangle$ $n = 1$	$n = 20$	$\langle(g_s - g_{ref})^2\rangle$ $n = 0$	$E\,(e_s^2)$
0	28	29	12	-----
6	38	39	12	10
8	53	54	20	25
10	56	53	21	24
14	61	50	19	21
18	70	48	16	18
Anomalies used	1183	306	471	-----

[a] Given in mGal^2.

TABLE 9.49.—*Comparison With Independent Surface-Gravity Data*[a]

Comparison field, g_c	Maximum ℓ, m	n	$\langle(g_t - g_s)^2\rangle$	$\langle g_t g_s\rangle$	$\langle g_t^2\rangle$	D	$\langle g_c^2\rangle$	$E\,(e_s^2)$	$E\,(e_t^2)$	$E\,(\delta_n^2)$	Region
SE III	18	3726	147	209	284	237	282	75	13	59	North Atlantic
SE III	18	1794	145	188	232	237	290	44	13	88	Indian Ocean
Averages								64 ≈ 3 m		68	

[a] Given in mGal^2.

10

UNIVERSITY OF CALIFORNIA, LOS ANGELES

W. M. Kaula

10.1 INTRODUCTION [1]

At the initiation of these analyses in 1960, it seemed convincing that (1) a purely analytic orbit calculation would be worth trying, for reasons of insight and economy; (2) to obtain the geophysically interesting tesseral harmonics, the sparseness of the data required formulation of partial derivatives with respect to the observations, rather than analysis of variations in the Kepler elements; (3) effects of tracking station location error, drag, radiation pressure, and luni-solar attraction would be comparable to tesseral harmonic effects; and (4) the optimum solution would combine satellite and terrestrial data. These ideas were the main themes of all the work described here. Most of the techniques are fully described in Kaula (1966b); more details on some other aspects are given in Kaula (1965) and Kaula (1971a).

The satellite orbit analyses described herein can be divided into four phases, which coincide with different data blocks, but which also entailed some differences of technique: (I) MINITRACK interferometry, 1960–1961; (II) early Baker-Nunn camera directions (i.e., rather active Sun, 1959–1961), 1961–1963; (III) late Baker-Nunn camera directions (i.e., quiet Sun, 1962–1963), 1963–1966; (IV) combined Baker-Nunn camera and TRANET Doppler data, 1966–1967.

[1] This work was originally undertaken in the Theoretical Division at NASA/GSFC in response to exhortations from R. D. Jastrow and J. A. O'Keefe to conduct work in parallel with SAO. Lloyd Carpenter helped greatly in learning how to use the computer. The setting up of the programs used in phases II–IV was done mainly in the summer of 1961 at SAO, where the advice of Imre G. Izsak was much appreciated. Later work at GSFC was assisted by Ed Monasterski, Susan Werner, and W. D. Putney. Subsequent to 1963, work at UCLA was done under NASA grant NSR 05–007–060, with the help of E. J. Bryan; much work was also done at Aerospace Corporation, El Segundo, California, assisted by D. H. Adams, and at USAF Aero Chart and Information Center, St. Louis, assisted by C. F. Martin and H. White.

10.2 ORBITAL DYNAMICS

In accord with premise 1 of the introduction, the theory of Brouwer (1959) was used throughout for the oblateness to order J_2^2 in long-period and secular effects. Linear analytic theories were developed for the effects of gravitational field spherical harmonics (Kaula, 1961a) and the Sun and Moon (Kaula, 1962). These theories were completely general as to harmonic degree and order and enabled considerably more compact computer programming than earlier developments. The analytic spirit was extended as far as possible by using numerical harmonic analysis for radiation pressure (Kaula, 1962, 1963a) and drag (Kaula, 1963a). The atmospheric models used for the drag effects were by Jacchia (1960) and Harris and Priester (1962).

Occasional examination was made of possible errors introduced by inadequacies in the Brouwer (1959) theory, using the higher-order theory of Kozai (1962b). However, the effects were always found to be less than 10 meters, and programming of a more accurate replacement never rose to high priority. If the effort had been continued, a more accurate and efficient theory, such as that of Aksnes (1970), would have to be programmed.

The physics of orbits will always make spherical harmonic coefficients the most effective means of representing the Earth's gravitational field in their analysis (Kaula, 1971b). For expansion of the inclination functions, the half-angle formulas (Izsak, 1964; Jeffreys, 1965) would probably be more efficient than the formulas of Kaula (1961a), but not so much so as to warrant a reprogramming.

The drag models were found to significantly improve the fit to orbital arcs which were of more than 10 days' duration, pre-1962, and at perigee below 1000 km. However, for orbits more suitable to satellite geodesy, the improvement over arbitrary ac-

celerations for the mean anomaly and partial derivatives with respect thereto for the other elements was negligible, and hence the drag routines lapsed into desuetude.

A formulation of tidal effects on orbits similar in form to the luni-solar perturbation theory was developed (Kaula, 1969), but never applied extensively in data analysis.

10.3 SATELLITE DATA ANALYSES

The phase I analyses of MINITRACK (Kaula, 1961b,c) data were rather crude. The phase II analyses of early Baker-Nunn camera data (Kaula, 1963a,b) involved an awesome variety of modeling and statistical complications in an attempt to overcome the inadequate distribution of orbital specifications and tracking stations and the excessive drag effects. The phase III analyses (Kaula, 1966c) were somewhat simpler because of the much better data. There were also significant improvements through adoption of the technique of partitioned normals (Anderle and Smith, 1967; Guier and Newton, 1965; Kaula, 1966b, pp. 104–106) and correction of a programming error which had caused previous solutions for coefficients S_{lm}, l-m odd, to have the wrong sign.

Since phase I–III analyses are fully described in Kaula (1961b,c, 1963a,b, 1966c), the discussion here concentrates on the phase IV analyses of Baker-Nunn directions combined with TRANET (Doppler) range rate, previously described only in a report of limited distribution (Kaula, 1968).

Tracking by the U.S. Navy TRANET network was received in the form of Doppler frequencies, scaled to a reference frequency of about 107 MHz, at intervals of 16 seconds. To utilize these data and the camera data in the same computer programs and to economize computer time, the following conversion and compression were applied to the Doppler data: (1) The form was converted to range rate in "canonical" units: Earth radii/(806.8137 sec.); (2) the time was converted from WWV emitted to Al; (3) observations within 15 degrees of the horizon were omitted, and tropospheric refraction corrections were applied; (4) three or four observations at equal intervals over each pass were selected; (5) for one day at a time, an orbit was fitted to these observations by iterated least squares, taking into account variations of the gravitational field up to l, $m=4,4$; (6) from this orbit, the range rate was calculated for each of the original 16-second interval observations; (7) for each pass, a combination of a polynomial in time and a station position shift was fitted to the residuals of the observed with respect to the computed range rates; (8) at three times within each pass, a range rate was calculated as the sum of the range rate from the orbit fitted for the day plus the polynomial and station shift fitted to the pass. The final information written on a binary tape for use in the subsequent analysis included as one record for each pass: a type number identifying the data as range rate, the tracking station number, the number of observations in the pass, the GST and A1 time (in modified Julian days) of the start of the pass, the three aggregated range rates formed by the process described above, and the time after pass-start for each of these range rates.

The zonal harmonics were held fixed at the values given in table 2 of Kaula (1966c). The tesseral harmonics selected for solution were all those for which a normalized coefficient of magnitude $8\times10^{-6}/l^2$ caused a perturbation of at least 10-meter amplitude in one satellite or at least 5-meter amplitude in two satellites, as listed in table 3 of Kaula (1966c)—all coefficients through 6,6; 7,1 through 7,5; 8,1 through 8,6; 9,1 and 9,2; 10,1 and 10,2; 11,1; and 12,1; plus the small-divisor, or near-resonant, harmonics: 9,9; 12,12; 13,12; 14,12; 15,12 through 15,14; and 17,14.

Thus there were a total of 88 unknowns common to all orbits. With seven unknowns represented by the Keplerian elements plus an acceleration parameter for each arc, the computer storage capacity for the normal equations as dimensioned was equalled. An increase of capacity to at least 145 unknowns could have been accomplished with very little difficulty. In the solutions described herein,

the positions of 16 Baker-Nunn camera and 33 TRANET Doppler tracking stations were held fixed at the values obtained by Gaposchkin (1966c) and Anderle and Smith (1967), respectively. It was intended to modify the programs to increase the capacity for unknowns and to solve for station position shifts when warranted by the accuracy of the solution for gravitational coefficients, but this stage was not reached.

The satellites used are summarized in table 10.1. For the five satellites which also were used in the Kaula (1966c) solution, the data are essentially the same (except for 5 more months of TRANSIT 4A), because 1963 was the year of minimum disturbances of atmospheric density by solar activity. There are minor modifications in the arcs actually used; however, because of changes in acceptance criteria for arcs, as well as number of iterations and number of observations (32 for TRANSIT 4A, 40 for Vanguard 2, 60 for the others), a chi-square test was applied.

The significant additions to the data are the tracking of Courier 1B (28.2 degrees), GEOS–1 (59.5 degrees), and Beacon Explorer B (79.7 degrees). It was found that adding a satellite of different orbital inclination made much more difference in the solution than did adding Doppler tracking. Considerable testing was done using different weights of the Doppler tracking, relative to the camera tracking of GEOS–1, in particular, with very little variation in the results. While this situation added to our confidence that the Doppler portions of the program were correct and accurate, it meant that the major benefit of adding the capability to analyze Doppler data would not come until it enabled analysis of orbits of appreciably different inclination than the set in table 10.1: in particular, a polar orbiter.

In addition to Doppler tracking of a polar satellite, it would have been desirable that the amount of tracking of Beacon Explorer B be increased appreciably and that tracking of all satellites from more overseas stations be added in order to give a better distribution of observations than that indicated by table 10.2. The poor distribution apparently arose in part from the unavailability, for administrative reasons, of tracking from some overseas stations. This maldistribution was more severe than that tested by Anderle (1966).

Because the station positions were held fixed, of the three types of supplemental equations used in the earlier analyses only the 24-hour orbit accelerations were applied (see table 4 of Kaula (1966c)). If these equations are carried at unit weight, they have a mild influence on the solutions for the 2,2; 3,1; and 3,3 coefficients.

The method of partitioned normals was utilized, so that there was no limit on the number of orbital arcs which could be analyzed. In addition, one reference-frequency correction per pass was included as an additional, optional unknown to be separated out of the normals in the same manner as the orbital elements. Exercise of this option, however, appeared to make little difference in the results for the gravitational coefficients.

The normal-equation blocks generated from the Doppler data were kept separate from the blocks generated from the camera data, in order to facilitate the testing of different relative weights of Doppler versus camera tracking. However, as was mentioned previously, variety of tracking type seems to make much less difference than variety of orbital specifications.

The best solution (by the criterion of minimum discrepancy from terrestrial gravimetry (Kaula, 1966a)) is given in table 10.3. This solution utilized a priori standard deviations of $\pm 10^{-5}/l^2$ for nonresonating coefficients of degree $l \geq 7$. This limitation was disappointing; the variety of inclinations was such that more than a threefold ambiguity in periodicity of perturbations by tesseral harmonics should have been resolvable.

10.4 USE OF TERRESTRIAL DATA

In phases I–II the relative positions of tracking stations connected to the same triangulation systems were held fixed, and the

stations were assumed to translate together in the solution. For the 12 Baker-Nunn cameras, six geodetic datums were required. Starting with phase III, station coordinates found from previous satellite orbit analyses were used as starting values, sometimes with a priori sigmas.

Terrestrial gravimetry was also used to give a priori sigmas for tesseral harmonic coefficients, to help overcome ill-conditioning. In phase II, these a priori values were based on the auto-covariance analysis of Kaula (1959b) and were extremely close to what later became familiar as the "$10^{-5}/l^2$ rule of thumb" (note the "preassigned σ" column in table 2 of Kaula (1963a)).

In 1966 a comprehensive comparison of satellite solutions with terrestrial gravimetry was undertaken (Kaula, 1966a). The principal conclusions were that the satellite analyses were indeed determining the real gravitational field, and that for the better solutions the errors of commission in the harmonic coefficients were very small in comparison with the errors of omission arising from the necessary truncation of the set of harmonics. A weighted combined solution was also made.

10.5 CONCLUSION

The four premises stated in the introduction still appear to stand. It would, though, be satisfying to see a good analytic theory used more extensively in geodetic orbit analysis. The work at UCLA was terminated in 1967 mainly because there was a shift to other interests, but also because the analyses had attained a complexity requiring attention from full-time professionals more appropriate to a government facility than a university. It was felt that our ideas of analyzing orbital data and their combination with terrestrial data were not sufficiently different from those of Gaposchkin and Lambeck (1971) to warrant continuation.

APPENDIX

TABLE 10.1.—*Satellite Specifications*

Satellite	*a* Earth radii	*e*	*I* Deg.	Days/ Arc	No. arcs	Total obs.	Starting date	Ending date	Type tracking
COURIER 1B	1.171	0.02	28.2	17	3	193	'65 Jun 11	'65 Oct 9	Camera
Vanguard 2	1.302	0.16	32.9	18	12	696	'62 Dec 31	'63 Dec 25	Camera
TRANSIT 4B	1.163	0.01	32.4	9	2	1350	'62 Apr 21	'62 Jun 23	Doppler
ECHO 1 ROCKET	1.250	0.01	47.2	18	14	1380	'63 Jan 1	'63 Dec 26	Camera
ANNA 2	1.177	0.01	50.1	18	15	1322	'62 Dec 31	'63 Oct 22	Camera
				9	2	3930	'63 May 16	'63 Jun 4	Doppler
GEOS–1	1.266	0.07	59.5	18	7	1126	'65 Nov 4	'66 Jun 10	Camera
				10	6	4768	'66 Jul 1	'67 Feb 9	Doppler
TRANSIT 4A	1.147	0.01	66.8	18	14	536	'62 Apr 6	'63 Dec 26	Camera
				9	2	2556	'62 Jul 19	'62 Aug 7	Doppler
Beacon Expl. B	1.154	0.01	79.7	9	2	2496	'65 Jan 30	'65 May 9	Doppler
MIDAS 4	1.568	0.01	95.9	30	12	3021	'62 Aug 3	'63 Dec 25	Camera

TABLE 10.2.—*Geographic Distribution of Doppler Tracking: Number of Passes Observed From Stations Within Each Octant*

Longitude E:	25	115	205	295	25
Latitude N 90					
	0	1109	3724	651	
0					
	333	352	0	315	
−90					

TABLE 10.3.—*Potential Fully Normalized Spherical Harmonic Coefficients* $\times 10^8$

Degree l	Order m	$\overline{C}_{lm}$	$\overline{S}_{lm}$
2	2	2.45	−1.37
3	1	1.99	0.13
3	2	0.80	−0.71
3	3	0.47	1.27
4	1	−0.58	−0.39
4	2	0.40	0.68
4	3	1.02	0.08
4	4	−0.36	−0.32
5	1	−0.09	0.02
5	2	0.84	−0.14
5	3	−0.50	−0.06
5	4	0.36	0.28
5	5	−0.22	−0.14
6	1	−0.13	0.05
6	2	0.10	−0.40
6	3	0.14	0.23
6	4	−0.16	−0.84
6	5	−0.24	−0.54
6	6	−0.30	−0.80
7	1	0.17	0.05
7	2	0.34	0.04
7	3	−0.01	−0.09
7	4	−0.11	0.06
7	5	0.05	−0.03
8	1	−0.02	0.12
8	2	0.10	−0.10
8	3	0.08	0.11
8	4	−0.05	0.02
8	5	−0.02	−0.01
8	6	−0.03	0.02
9	1	0.07	−0.06
9	2	0.01	0.02
9	9	−0.18	−0.14
10	1	0.00	0.00
10	2	−0.03	0.05
11	1	−0.03	−0.04
12	1	−0.05	−0.03
12	12	−0.11	−0.01
13	12	−0.08	0.08
14	12	−0.05	−0.04
15	12	−0.08	0.01
15	13	−0.03	−0.07
15	14	−0.00	0.02
17	14	−0.05	0.12

11

EVALUATION

S. W. Henriksen

11.1 INTRODUCTION

The *general* objectives of the National Geodetic Satellite Program (NGSP) were, first, to get sufficiently improved positions for satellite-tracking stations that errors in connections between major datums could be materially reduced, and, second, to get a better determination of the Earth's gravitational field out to the 15th degree and order in the expansion in spherical harmonics. An evaluation of the requirements for such positions and for orbital prediction led to quantification of these objectives and to the setting of *specific,* numerical objectives. It was decided that global geodetic projects would require accuracies better than ±10m (standard deviation) in each coordinate in an Earth-center-of-mass, North-oriented system and better than ±3 mGal in the average value of gravity over 12° × 12° regions. It was found that these two objectives made a third necessary—the quality of the data provided by the various tracking stations participating in the program would have to be determined. Preceding chapters have described how the NGSP set about achieving these objectives, and have given in detail the results of the program as they were determined separately by the participants.

An inspection of the results of the program shows that the *general* objectives have been met. The positions of enough stations on North American, European, South American, Tokyo, and Australian Geodetic datums have been determined to reduce the errors in ties between these datums by at least 50 percent. The number of terms in the series-expansion of the gravitational field has almost doubled. But instead of there being one set of coordinates and one gravity field, there are at least seven different major sets of coordinates and five different fields. Of course, if the various sets agree with one another to within the tolerances set by the specific objectives of the program, then the differences will be irrelevant from a practical standpoint (although they may be interesting from a scientific standpoint). But if the various sets do not so agree, then either the specific objectives of the NGSP have not been attained or a suitable set will have to be found to meet each of the objectives.

Unfortunately, the answers demanded by this assessment are not easy to obtain. In fact, a close examination not only of the various results, but also of the methods used in getting them, leads to the conclusion that the specific objectives of the NGSP were either too generally stated to allow one to tell whether they were met or were unobtainable. The existence of different results may indicate merely that the participants have gotten answers to different questions, all of which are contained within the original statement of the purposes of the program.

In this chapter, therefore, the results cited in chapters 2 through 9 [1] will be examined to see if the objectives of the program, as set forth in the first paragraph, have actually been met. As will be seen, the answer is "yes" as far as the general objectives are concerned, and "almost" as far as the specific objectives are concerned. But it is not possible to select from the various sets one that probably meets the specific objectives, and it is not within the scope of the chapter to create a compromise that does. Analysis of methods and results shows that the standard deviations assigned to the results are indications of precision, not accuracy, and cannot be used to rank the various sets in order of accuracy. There is enough information available that at least a guess can be made about why the solutions differ, and the main thrust of this section will be toward exploring the extent and reasons for the

[1] Only the results of chapters 3, 5, 7, 8, and 9 will be examined in detail, since only these were produced specifically to satisfy the program's objectives.

discrepancies. The order of discussion will be the same as that of the objectives set by the NGSP: coordinates (sec. 11.3), gravitation (sec. 11.4), and evaluation of observational data (sec. 11.5). Because the validity of the results depends so much on the statistical methods used in getting them, section 11.2 reviews briefly the *statistical theory* involved.

11.2 THEORY

11.2.1 General

For many years the results of geodetic computations consisted only of angles, distances, and coordinates without any information on the reliabilities of these data. Although Gauss introduced the method of least squares in the 19th century, applied it to the adjustment of geodetic data, and explained its probabilistic implications, even today there still exist many large geodetic networks in which the coordinates of the control points are known but not their standard deviations. In such situations the reliability of the data is a matter of one's confidence in the organization or individual who produced them. There is no reliable quantitative evaluation possible, and one cannot make satisfactory numerical estimates of the accuracy of results computed with the use of such data.

The situation for the NGSP data is fortunately much better since standard deviations were calculated for most of the geodetic quantities. Furthermore, almost all the results given in the report have been evaluated by their authors by using two or three different methods rather than only one. The first and universal basis for evaluation is of course the standard deviation or the covariance. All results were obtained by means of the method of least squares, and the standard deviation and covariances of the results are contained in the matrix $\underline{\underline{\Sigma}}_X$, where the corrections $\underline{X}$ to the unknowns and the residuals $\underline{Y}$ are connected by the equation

$$\underline{X} = [\underline{\underline{A}}^T \underline{\underline{\Sigma}}_Y^{-1} \underline{\underline{A}}]^{-1} \underline{\underline{\Sigma}}_Y^{-1} \underline{\underline{A}}^T \underline{Y}$$

and

$$\underline{\underline{\Sigma}}_Y = \underline{\underline{A}} \underline{\underline{\Sigma}}_X \underline{\underline{A}}^T$$

connects the covariances of $\underline{X}$ with the covariances of $\underline{Y}$ through the matrix $\underline{\underline{A}}$ of coefficients. (See ch. 1 for more complete discussion, or see, e.g., Anderson, 1958.)

The covariances are useful principally in comparisons between results and as indicators of accuracy. As indicators of internal consistency the correlation coefficients are more suitable. Denoting the elements of $\underline{\underline{\Sigma}}_X$ by σ_{ij} and the correlation coefficients by ρ_{ij}, we have

$$\rho_{ij} \equiv \frac{\sqrt{\sigma_{ij}}}{\sqrt{\sigma_{ii}\,\sigma_{jj}}}$$

As a first approximation, the quantities $\sqrt{\sigma_{ii}} \equiv \sigma_i$ can be interpreted as the bounds between which there is a 67 percent probability that the true value of x_i lies. The ρ_{ij} indicates roughly the extent to which x_i and x_j vary together, a value of 0 indicating that they are independent and a value of 1 that x_i and x_j are functions of each other. But, almost without exception, interpretations of σ_{ij} and ρ_{ij} as anything more than the roughest indicators of where the truth lies can lead to great trouble. There are many reasons for this; the most important is the fact that the observation equations themselves are only guesses and, often enough, only rough guesses. Almost always there are present in the observations systematic effects that are not accounted for in the observation equations. So it is not at all unusual for two scientists working independently to come up with values of x_i which differ by three to four times the amounts of the σ_i's that they find. (Such anomalies are particularly noticeable when star catalogs are being compared, but can also be found in tables of coefficients C_n^m, S_n^m, λ, ϕ, h, and so on.) Perhaps the most common, dangerous, and unwarranted error found in scientific and engineering reports is the assumption that σ_{ii} is a correct estimate of error with respect to the true value of x_i, rather than being only a first, and often poor, approximation to the error.

The second basis for evaluation is comparison with the results given by other organizations. Such results are usually derived from different types of measurements or from different sets of the same type or just from more measurements. The closeness of agreement is considered a good, if not quantitative, indication of how good the results are. An outstanding example of this kind of evaluation is that used by the National Geodetic Survey (NGS) (ch. 7), in which NGS's results obtained by geometric means are compared with the Naval Weapons Laboratory (NWL) by analyzing orbital perturbations. This is a valid comparison because the results were obtained using completely different methods and using completely different sets of observations. On the other hand, to evaluate the results of the Smithsonian Astrophysical Observatory (SAO) (ch. 9) and of NASA/Goddard Space Flight Center (GSFC) (ch. 5) by intercomparison does not help much, since SAO and NASA used many of the same observations and used similar theories. Again, comparison of the results of Ohio State University (OSU) and of NGS does not help in their evaluation because NGS's data are a subset of OSU's.

Even when the values derived by different scientists agree, there is no guarantee that the values are correct. The agreement merely means that the scientists were working with similar sets of data and with similar theories. And conversely, the fact that the values disagree does not mean that only one can be correct. For example, one cannot compare NGS's values for points' locations directly with SAO's values or those of NASA/GSFC because the values are given in different coordinate systems, and the radius of the earth derived by NGS is not directly comparable with that derived by the Jet Propulsion Laboratory (JPL) from *GM* because the radii found by the two organizations refer to totally different concepts.

The third basis for evaluation is comparison of results with values whose accuracies are known. For instance, one can compare gravity computed from observations on satellites with gravity measured on the surface of the Earth; or one can compare coordinates and/or distances derived by satellite geodesy with corresponding values derived by surveying on the surface. Unfortunately, very few useful referents of this kind are available. For evaluating the accuracies of the NGSP's coordinates, we have the coordinates of stations as determined by conventional, first-order surveys. But the accuracies of such coordinates are, when known at all, known satisfactorily only within local datums and not with respect to a global system as is desirable for evaluations of NGSP's accuracies. A similar situation exists in evaluating NGSP's gravitational fields. Values of suitable accuracy are known for less than 25 percent of the Earth's surface. The regions in which accuracies are well enough known are fortunately globally distributed and connected by gravimetry. Nevertheless, lack of suitable data on the other 75 percent of the surface introduces undesirable uncertainties in evaluation of NGSP's gravitational field.

Some interesting tests of the ability to determine precision and accuracy were made at NWL by R. Anderle in 1972. The data from the Department of Defense (DOD) frequency-measuring equipment (ch. 3) were used. Precision was tested by using different sets of data in various combinations with different sets of gravitational constants. The accuracy was tested by comparing station locations found from satellite data with station locations given by the NGS geodimeter traverse in the United States.

11.2.2 Effects of Discarding Data

One interesting and important characteristic common to the reduction procedures of all participants has been to throw out data that differ from their expected values by more than a certain amount. This discarding is known by various names: filtering, preprocessing, data improvement, and so on. It is, of course, contrary to sound statistical principles if applied rigorously to data from

a Gaussian distribution. All participants have assumed that the errors in the data have a Gaussian distribution. NGS's investigations have shown, at least, that this distribution applies approximately to its data (ch. 7).

The proper application of the rule for discarding data is to use it for identifying those values which differ greatly from the expected values. The background of a suspect value is investigated, and an explanation for its deviation is sought. If a valid reason can be found, the value is discarded. Such explanations as an error in copying or the known existence of a fault in the equipment provide adequate reasons. But if a valid reason cannot be found, the value should be retained regardless of how far it may be from the expected value. The assumption of a Gaussian distribution implies that values far from the expected values must be anticipated. Absence of such values would be as much of a reason for suspecting the data as their presence would be. So the discarding of values farther than a certain amount from the expected value is a direct violation of the assumption that a Gaussian distribution is present. The result of such discarding is to distort the distribution of values and to lower the root-mean-square error (rmse). If the distribution were Gaussian, the rmse would be a standard deviation and would have a probabilistic interpretation. Since, after the discarding, the set of values is no longer Gaussian, the rmse is no longer the same as the standard deviation. Nor is the weighted average any longer the best value. The problem of how to find the standard deviation from these processed data is not particularly difficult but has not been extensively studied. Grubbs (1950) and Remmer (1969) are good references for this matter.

It is easy to show that the true s.d., σ_t, of the truncated distribution is related to the putative σ by the relation

$$\sigma_t^2 = \sigma^2(1-k)$$

where

$$k \equiv \frac{2u_0 e^{-u_0^2/2}}{1-2\Phi(-u_0)} \cdot \frac{1}{\sqrt{2\pi}}$$

$$\Phi(-u_0) \equiv \frac{1}{\sqrt{2\pi}} \int_{-\infty}^{-u_0} e - u^2/2_{du}$$

and u_0 is the point of truncation. (The assumption is that the distribution is truncated at $u = \pm u_0$.)

If the rejection point is set at around 3σ, the rmse of the truncated set of data must be increased by 3 percent to get the standard deviation. If the cutoff is lower, the increase is greater. But all values used in the NGSP were so close to 3 that the increase is still less than 5 percent in all cases. Since the standard deviations themselves cannot be trusted to better than ± 10 percent at best, the effect of truncation would therefore seem to be negligible. In general, this may seem to be true. Unfortunately, some participants have discarded data in several cycles of processing. Expected values were compared with those found, data discarded, and new "expected" values computed on the basis of the abridged set. The new values applied again for still further discarding, and so on. Since the second set did not follow a Gaussian distribution, the effect on it is much more difficult to analyze. If the cycling is not continued too far (say, three times), we can assume that the effect of treating the distribution as if it were normal is insignificant. Then two discardings increase the σ by 6 percent and three cyclings increase it by about 10 percent. One difficulty with applying these numbers to the results cited in this volume is that those data finally used in getting the results have been put through such an involved process of sifting, checking, correcting, and discarding that keeping accurate track of the number of data discarded, their places in the distribution scheme, etc., is almost impossible. A safe rule would be to increase all standard deviations given in this book by at least 10 percent. This will be unfair to those organizations like OSU which discarded almost no data except those probably invalid. There are, however, so many other ways in which "improve-

ments" are, often unintentionally, introduced into the reduction process that the 10 percent increase is much more likely to be conservative than radical.

Among the many complicating factors that made the computation of σ's unrealistic is the non-Gaussian character of almost all data gathered during the NGSP. For example, if the errors in the α and δ of a satellite had a Gaussian distribution, all values should be possible. But since the camera has a limited field of view and since the Earth in any case is not transparent, errors of more than 180 degrees are physically unlikely. The limits can, of course, be cut down to within a few minutes in most cases. The resolution of the equipment is another factor acting in the opposite direction. Many geodesists and mathematicians have looked into these problems. (See, e.g., Henriksen, 1967, for consideration of mathematical limitations and Stearn, 1964, and Boyarsky, 1965, for experimental considerations.) For these and other reasons, the σ's in this book are best considered as expressions of precision rather than accuracy.

11.2.3 Inner Constraints

The statistical procedures applied by OSU to obtain results cannot in all cases be considered mathematically identical to those used by the other participants. In particular, OSU has applied the method of "inner constraints" (ch. 8) in obtaining the origin of its coordinate system (but not in obtaining its orientation). Since the location of an origin is usually dictated by practical considerations rather than mathematical ones, the advantage gained by selecting an origin that leads to smaller σ's is debatable. But, because the method does produce lower standard deviations, its validity can be challenged. A careful analysis of the mathematics (Blaha, 1971) shows that the method is valid. It also shows, however, that the improvement in σ's is not obtained with respect to an arbitrary reference system but with respect to one defined by the data themselves. A geodetically useful frame of reference must be established with respect to physical objects (see discussion of datums in ch. 1). A system established by inner constraints is determined by the data themselves and has presumably less utility than a local datum or a datum with origin at the Earth's center of mass.

11.3 COORDINATES

The coordinates resulting from the NGSP are presented in chapters 3 and 5 through 9. Table 11.1 gives, for each point involved, the location of the tables containing the initial (local) coordinates and tables giving their final computed coordinates. (The stations themselves are listed, in order of increasing longitude, in ch. 1, table 1.27.) These coordinates should, if the mathematics is correct, be independent of the values initially assumed for them. Of course, the utility of the final computed values will depend, in very many applications, on the coordinates of each point as given originally in its local datum. This information is given for most of the points in chapters 3, 7, 8, and 9.

11.3.1 Evaluation Based on Data and Method

The coordinates given in this volume have been derived by one of two methods: either by using pure (or nearly pure) geometry or by using the theory of dynamics with or without geometry. Since the two methods are quite different, one would expect to get identical answers only if the data were the same and the theories were mathematically equivalent. Neither requirement has been met. The first requirement can be gotten around to some extent. Through the work done by NASA (ch. 5) on the third objective, and through internal evidence on the performance of the various instruments, different kinds of data from the same locations (including locations tied together by local survey) can be weighted to give an approximate equivalence. Enough positions have been occupied in common by different kinds of instrumentation that one may ex-

pect the lack of complete correspondence of sets of tracking stations to be a minor factor. These are, of course, guesses, and a rigorous investigation of the extent to which changes in data affect results has not been made. That a substantial part of the differences noted in results (fig. 11.1) is attributable to differences in data is certain; the extent is not certain. That an additional substantial part is caused by differences in method is probable. Locations determined by geometry must give the shape of the Earth. This is by definition. Locations determined by dynamics depend for their location on the orbits of the satellites used. These orbits do not depend on the shape of the Earth but are related to its figure, which depends on the gravitational field. The resulting locations should therefore also relate to the figure of the Earth. That is, if the gravitational field were known perfectly (along with the minor perturbing forces), then the orbits could be determined perfectly. The location would be determined to the accuracy allowed by the observations and would be in the same system of coordinates as the orbit. This system is, unfortunately, at present not absolute (i.e., geometrically related). One can therefore expect that the locations determined by dynamics will be related to the figure of the Earth because it is customary in this method to determine locations and figure simultaneously. The extent to which the locations are affected by the figure of the Earth will depend on (1) the accuracy of the observations, (2) the equations used for the orbit, and (3) the number and kinds of constants used for approximating the gravitational field.

The geometric theories used by the National Ocean Survey (NOS), NASA/GSFC, OSU, and SAO are mathematically equivalent except for OSU's use of inner constraints (ch. 8). Since the effect of using inner constraints is simply to translate the origin, all results should be the same if they are put into the same coordinate system and if the data are the same. The results of NASA/GSFC (ch. 5) and SAO (ch. 9) were obtained by using dynamics as well as geom-

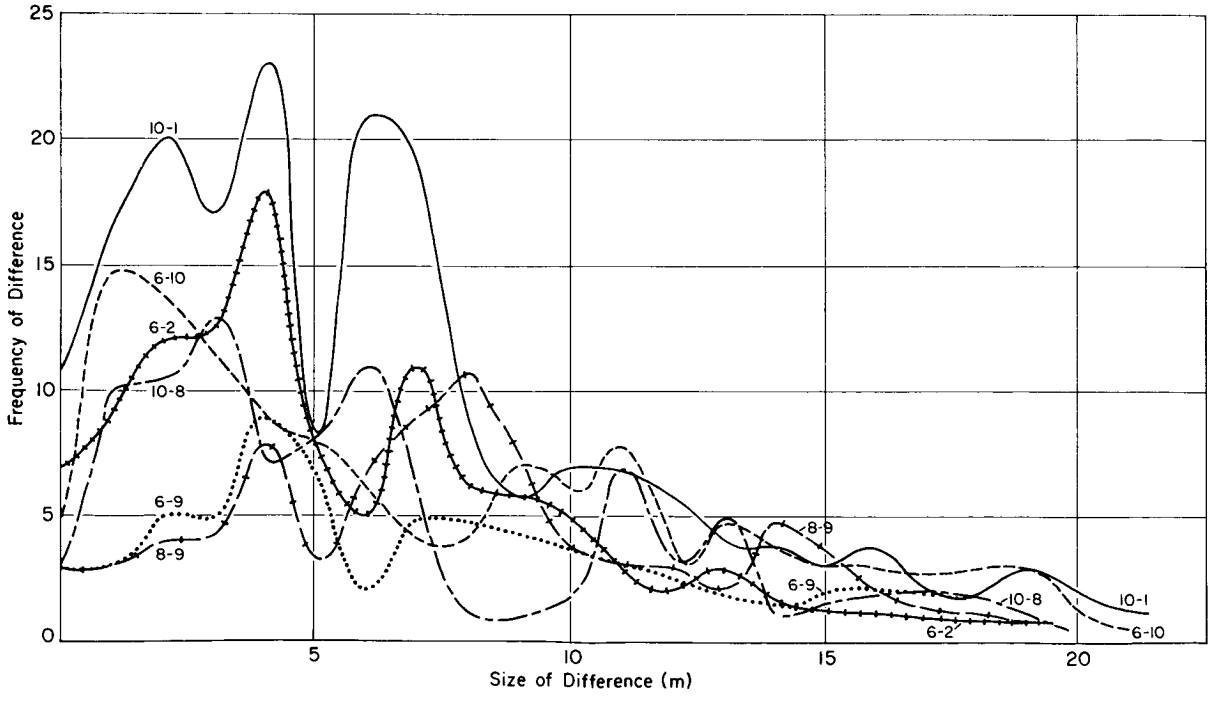

FIGURE 11.1.—Frequency of differences in coefficients.

etry, so only the results of NGS and OSU can be compared as geometric models. Comparison shows that the coordinates do not agree. This means that the differences, which are considerable (see fig. 11.1), must arise because the data are different and/or the applications of the theories are different. The former of these causes is certainly present. NGS used observations by one kind of camera (BC–4) on one satellite (PAGEOS), together with seven interstation distances determined by conventional survey (ch. 7). OSU used observations by more than four different kinds of cameras (BC–4, MOTS–40, PC–100, Baker-Nunn, and a few special types) and two kinds of radar (5-cm and SECOR). OSU used the same baselines as NGS but considerably different weights were used.

Furthermore, NGS used a slightly different set of BC–4 camera stations than did OSU, and OSU used observations on many different satellites. Therefore the differences between results are caused in large part by the considerably different data used. Theoretically, the results (WN14) of OSU should therefore be superior to those (WGN) of NGS. This is true, however, only if the additional observations used by OSU are properly weighted. But the only extensive series of experiments made to determine these weights—those made by NASA/GSFC (ch. 5) and Wallops Flight Center (WFC) (ch. 6)—were not completed in time to affect the reductions of OSU. The early, provisional results of these experiments are also, in some ways, difficult to interpret (sec. 11.4), and their use would therefore not have been advisable. The weights that were applied to the data were therefore derived from analyses of the data alone. Assignment of correct weights is not guaranteed, and the likelihood of erroneous weighting exists.

This is not the place for a detailed discussion of the weights to be assigned to the observations. Such a discussion is given by J. Berbert in chapter 5, and a discussion on Berbert's results is presented in section 11.4. The most detailed and extensive study of the errors present in a particular set of data is that of NGS on the errors in data from BC–4 cameras (ch. 7).

SAO's figure 9.13 in chapter 9 shows that, in the examples given, the axes of the error ellipses have the same orientation whether geometry or dynamics is used to find the direction. The ratios of the axes differ, however, and the centers are from 1σ to 3σ apart. The conclusion would be, if these figures are typical, that there are real differences between results obtained by geometry and results obtained by dynamics.

Anderle's use of a comparison between "dynamic geoid" and "geometric geoid" as a means of finding out how close NWL's coordinate system is to the Earth's center of mass is ingenious but inconclusive at present. The geometric geoid to which he refers is based on dynamics just as much as is the dynamic geoid, which is based on SAO's coefficients C_n^m and S_n^m, and the comparison is between geops both derived by dynamics. A further complication in this case is that the geoid based on SAO's coefficients is itself of unknown accuracy, as can be seen by comparing it with other geops.

As Anderle points out (ch. 3), the fact that station positions derived from Doppler data in tests in the United States agree with positions derived by conventional survey on the ground to within 1 to 3 meters does not mean that coordinates outside the United States are good to this accuracy. There is also the fact that the conventional survey itself is good only to 2 to 5 m overall. The accuracy of the global set of positions therefore may be better than 6 meters, but not, probably, as good as 1 to 3 meters.

11.3.2 Evaluation by Comparison of Results

Results cannot be evaluated on the basis of the results themselves. What is needed is an external set of standards with which comparison can be made. No such standard of unimpeachable accuracy exists. The closest we have to this is the set of seven baselines in North America, Europe, Australia, and Africa, which were used to insert lengths in to the WGN of NGS. Unfortunately (see

next section), there is disagreement about the accuracies of these baselines to an extent that makes it unwise to depend on them for evaluation.

Since the σ's of the baselines cannot at present be relied on, the σ's attached to those coordinates which were derived by using the baselines cannot be relied on either. They must be considered measures of precision rather than accuracy. This view is supported by a study of the differences between corresponding coordinates in different models. Whatever inferences are drawn, the results about their accuracies must come from comparison between results. Since no one set of results can be chosen from the evidence as "best," the inferences can only be indicative, not final or absolute.

Figure 11.1 shows the frequency with which differences of 0 to 20 m (the largest) between corresponding sets in GEM 6 (1), NWL–9D (2), WGN (6), GSFC '73 (8), and SAO SE III (9) occur. Six curves, corresponding to differences (6) – (9), (6) – (2), (6) – (10), (10) – (1), (10) – (8), and (9) – (8), are shown. (Only five of these curves are independent, of course.) The coordinates were rotated, translated, and scaled into a common system before differences were taken. The transformations were not based on full sets of stations common to all participants, but enough common stations were used so that the difference between this system and that obtained with a full system is small. The differences given are probably within 2 m of the correct values.

Note that in general the differences vary from 0 to 21 m, the most frequent difference being 4 m. A closer look at the figure shows that WGN and NWL–9D show remarkably few large differences, whereas WGN and SAO SE III also agree more closely in this respect than do WGN and OSU's set. The average difference between WGN and NWL–DOD is 4.5 m, between WGN and OSU's set, 7.0 m, and between SAO's SE III and GSFC '73, 9.2 m. Other interesting deductions could be made, but it is obvious that even if we add to those differences the σ's for corresponding sets, the results will still be close to the ± 10–m limits, although they will not always be within those limits. But there are enough differences greater than 10 m present to make it doubtful that acceptance on the basis of average differences would be permissible—i.e., would ensure that whatever set was chosen met the requirements.

It must in any case be remembered that the differences are for coordinates in the same systems. As indicators of error, the differences in the systems themselves, as well as the differences in coordinates, should be considered. This consideration is taken up in section 11.3.2.5.

11.3.2.1 Comparison With External Standards: Baselines

It is interesting to compare the lengths of the baselines established for use in NGS's WGN with lengths computed by OSU and NWL from their results. Table 11.2 gives the identifying numbers of the stations terminating the lines, the datums governing the lines, the approximate lengths of the lines, their standard deviations as estimated from the survey, and the differences of values from these lengths. The discrepancies for all the baselines except those in North America and the baseline from Hohenpeissenberg to Catania are much greater in OSU's case than the originally estimated σ's should allow. The line from Tromsø to Hohenpeissenberg is also suspect in NWL's analysis. Only if we accept OSU's estimates of the σ's of the surveyed length, do all the differences fall below 3σ. Since the results obtained by NWL are quite independent of the lengths from traverse, the line from Tromsø to Hohenpeissenberg is suspect even though it has the lowest value of σ^2 of all the baselines.

The σ's quoted for the original surveys (column 3) are smaller (in absolute value) than the nature of the survey would lead one to expect. This is particularly true for the European baseline out of Tromsø and for the two Australian baselines. The line from Hohenpeissenberg to Catania has a relative error of 1.2×10^6, which is not unreasonable for a line going through the Alps. OSU's

estimates (column 5) seem reasonable and make the results of both OSU and NWL reasonable. But, as was noted earlier, this apparent reasonableness of values is not evidence.

11.3.2.2 Comparison With External Standards: Distances Computed by Triangulation or Traverse

One useful, if not decisive, way of evaluating the coordinates given in this book is to compute from them the distances between various pairs of stations and to compare these distances with distances computed by using results of surveys carried out on the surface. Unfortunately, this method has been adopted only for one set of coordinates, that designated as GSFC '73 (ch. 5). The values given for GSFC '73 would indicate an agreement between satellite-derived and conventionally derived distances of, on the average, 5 m or so. But there are two reasons for being hesitant about accepting the 5–m value. First of all, the rms error in the distances computed from conventional survey is probably between 3 and 5 meters or more. A realistic estimate of the rms error in the satellite-derived distances would have to take this into account. But the second reason makes such an accounting difficult. The distances were apparently derived independently, but a glance at the geometry shows that they are not actually all independent. (The bar graphs shown are therefore misleading.) A number of different sets could be selected, each containing independent distances. The associated differences will differ from set to set; from the information now available there is no way of telling which set is the correct one. If, as seems reasonable from the evidence, the rms error of the distances calculated from the GSFC '73 data is assumed to be less than 10 m but greater than 5 m, the error in each coordinate would be between 3 m and 6 m. To these errors would, of course, have to be added the errors caused by errors in the coordinate system itself.

11.3.2.3 Comparison With External Standards: Miscellaneous

There exist a number of stations, not participants in the NGSP, whose distances from each other or from the Earth's axis of rotation have been computed by methods quite different from those used by the NGSP's participants. These distances have been used by NASA/GSFC and others for comparison with distances computed from NGSP's stations. The comparisons are given in chapters 4, 5, and 9. The comparisons are, unfortunately, not accompanied by an adequate error analysis. Although comparisons show agreement to within 5 m on the average, with excursions up to over 15 m in some cases, the lack of supporting information makes it impossible to infer from the comparisons anything about accuracy or precision. This is unfortunate, since results obtained by quite different methods are involved. One can say that the results do not contradict each other, but neither do they contradict an estimate that the NGSP's coordinates contain errors of over 10 m on the average.

11.3.2.4 Influence of the Reference System Used

Table 11.4 summarizes the differences between the coordinate systems (WGS's) used in this volume for satellite geodesy and the datums controlling the large horizontal networks. Table 11.5 summarizes the differences between the WGS's themselves. The data in table 11.4 are most useful from a geodetic and practical standpoint. They not only provide the necessary data for going from one datum or coordinate system to another, but also show clearly that the relationships are not well known, or at least not known to the degree of accuracy required by the NGSP. Of course, the systems of NGS and OSU are not strictly comparable either with each other or with the systems derived by dynamics. However, we can expect that the differences between local datums should be the same in either system. But the distances between origins of the Australian and

European datums are, e.g., 273 m in the system (WGN) of NGS and 289 m in the systems of WN14 (SU), or a difference of about 9 m in each component. These are purely geometric systems. SAO SE III gives a distance of about 360 m. The corresponding difference between EU50's and NAD 1927's origins in these systems is 49 m, and between EU50 and SAD 1969 is 37 m. On the other hand, the difference is only 8 m going from NAD 1927 to SAD 1969. These numbers lead to interesting speculations, but since no definite conclusions can be drawn, we will not go further.

The differences between local datums and global datums derived by using dynamics should be comparable, since the global systems not only have the same orientation but also, presumably, have the same origin, the Earth's center of mass. A glance at table 11.5 shows that coordinates of the origins are close together, but not as close together as the requirement for ± 10 m (sec. 11.1) would require. Coordinates of the center of the Australian Geodetic Datum 1965 differ by up to 18 m in X, 31 m in Y, and 35 m in Z. Even for NAD 1927, in which a large block of stations occurs, we have differences of 33 m, 41 m, and 14 m in the individual coordinates. One of the reasons for these differences is of course the very different number of stations used by the investigators in determining the constants involved. But it is not a major factor, as a comparison of the DOD/NWL column with the other will show. (NWL had the smallest number of stations per datum.)

The parameters in tables 11.4 and 11.5 are arranged as

X (m)	rotation about the X axis ($''\times 10^2$)	
Y (m)	rotation about the Y axis ($''\times 10^2$)	scale difference $\times 10^6$
Z (m)	rotation about the Z axis ($''\times 10^2$)	

The comparison in table 11.5 is skimpy because lack of time made it impossible to compute the many relationships involved. Those interested and able can extend the comparisons by using table 11.4, taking the geodetic datums as intermediaries.

The outstanding characteristic of the values in table 11.5 is, first of all, the large values for X, Y, Z and, second, the large size of the rotation about the Z axis. The close agreement between GSFC '73 and SAO SE III undoubtedly results from commonality of data. The closeness of GEM 6 to GSFC '73 (except in longitude) is not explainable on this basis. In assessing the effect of rotations, note that the linear equivalent of angle x is approximately one-third the number given, multiplied by the cosine of the angular distance from the angle of rotation.

11.3.2.5 Discussion of Particular Sets

11.3.2.5.1 SECOR EQUATORIAL NETWORK

The Defense Mapping Agency/Topographic Command (DMA/TC) estimates (ch. 3) that the coordinates in the SECOR Equatorial Network (SEN) have standard deviations (in accuracy) of the order of ± 20 m. This is a large value and is not in accord either with the assessment from NASA's evaluations of SECOR (ch. 5 and sec. 11.5) or with OSU's results using data from SECOR (table 11.3). It results from comparisons of interstation distances computed from DMA/TC's results with distances obtained by conventional survey. It does accord with DMA/TC's own estimate of SECOR's accuracy. This indicates, if all tests are valid, that the data from SECOR can provide standard deviations better than ± 20 m if properly handled.

The reasons for SEN's failure to reach its potential strength are difficult to assess from the information available. An obvious partial explanation lies in the combination of weak geometry intrinsic to SECOR with the less than optimal geometry enforced on SEN by the distribution of occupiable sites. Although Blaha (1971) has pointed out that the configuration involved in determining, by geometric means alone, the location of a

fourth point from three known points is such that small errors in distance measurements result in large errors in the coordinates of the fourth point if the four points are nearly coplanar, this conclusion does not apply to SEN. It holds only if more than 3 of the 12 coordinates are unknown. This consideration does affect OSU's procedure and results. (OSU—ch. 8—also used the data from the SEN.) However, it does not apply to the results from DMA/TC. DMA/TC used geometry only to obtain preliminary values for the coordinates; for the final coordinates, they used the short-arc method (ch. 1, ch. 3), in which a simple orbit is fitted to the observational data. The geometry could still be poor (DMA/TC gives no information on this point), but it is reasonable to suppose that a sufficient number of passes was observed at each station to give a good geometry. Certainly, the satellites GEOS–1 and GEOS–2, with their inclinations 59° and 106°, would provide good geometry for an "equatorial" network like SEN, and the SECOR series of satellites (ch. 3) had a good selection of inclinations and heights.

It is possible that the theory used by DMA/TC contains an error or was inadequate. No error is apparent in the theory given in chapter 3, although investigation of finer details might uncover one. The possibility of inadequacy is more likely. The original specifications on SECOR called for an rms error (in range) of ±1 m. GSFC's and OSU's evaluations of SECOR indicate that SECOR can give distances to better than ±5 m.

OSU, by requiring that the distances measured by SECOR agree with estimated distances to within a reasonable value (ch. 8), was able to keep the resulting rms error in SECOR-measured distances to well within GSFC's estimate. Since DMA/TC's results indicate that the standard deviations are 3 to 4 times larger than instrumental evaluation and OSU's results would show they should be, the conclusion is reached that the theory is inadequate rather than erroneous.

Errors too subtle to be evident from the theory may exist without being uncovered by OSU's analysis, particularly if they cause systematic errors of the same size as the deviation of OSU's results from, say, GEM 6 (ch. 5) or SE III (ch. 9). The refractive theory would be particularly suspect in this case.

Table 11.3 compares the coordinates in SEN and WN14. SEN has, according to chapter 3, the same origin and orientation as WGN. It is obvious that the heights are systematically off. Even when the difference in ellipsoids (about 12 m) is added, the difference still amounts to about 6 m on the average. This difference is almost certainly caused by the failure of DMA/TC to apply that method of correction used by OSU whereby the allowable error in SECOR's ranges was bracketed between assigned limits.

11.3.2.5.2 THE "COMBINED" SOLUTION OF NGS

A purely geometric solution has no relationship with the figure of the Earth that can be found from the data themselves. A full discussion of this point is presented in chapter 8, and OSU did not attempt to relate its system (WN14) to the figure of the Earth. For certain reasons connected with its intended use of WGN, however, NGS obtained a further set of coordinates, the "combined solution" (designated here as WGN–C) which *is* related to the figure of the Earth. This relationship was found by enforcing a certain amount of agreement between the coordinates in WGN–C and those in NWL–9D after appropriate transformations for scale, etc. (see ch. 7). The WGN–C therefore lies close to NWL–9D where the stations were colocated. Because of the way WGN–C was produced, it is not a purely geometric solution. Furthermore, its evaluation as an entity distinct from WGN and NWL–9D is easily subject to misinterpretation. WGN–C is therefore considered here as a compromise between WGN and NWL–9D. This does not imply that it is better or worse than either of the others, and present evidence is insufficient

to prove from the characteristics of either of the others what its own accuracy may be.

11.3.2.5.3 COORDINATES OF STATIONS OF DMA/AC AND AFCRL

The coordinates given by DOD/AC for positions in South America (ch. 3) are tied to the NGS's WGN 1973 (ch. 7). The accuracy of these positions therefore depends strongly on the accuracy of WGN 1973. Separate evaluation does not seem warranted. The stations serve very well to strengthen the results for NAD 1927 and could be included, where σ's permit, in adjustment of triangulation in North and South America. The coordinates of the stations on Johnston Island and Bermuda are of course not connected to the others and should be judged individually. (See ch. 3.)

11.3.3 Summary

From the preceding evaluation, it appears that the general (geometric) objective of the NGSP has been attained, and handsomely. But if one adopts a no-compromise attitude towards the relation of the various results to each other and to the NGSP, one must conclude that the specific (numerically stated) objectives of the NGSP have not been conclusively attained. There are six major sets (NWL–9D, SEN, GEM 6, WGN, WN14 and SE III) of coordinates resulting from responsibilities assumed at the start of the NGSP and several sets (GSFC '73, DMA/AC, etc.) resulting from later involvement in the NGSP. The σ's found for the coordinates in any one set are for the most part better than ± 6 m or are less than 10 m in absolute value for the total error in location of a station. If we look at the differences between systems (tables 11.4 and 11.5) and between the coordinates themselves when they are transferred to a common system (fig. 11.1), we find that these differences are, when combined, larger for most stations than the tolerances allowed by the objectives. To adopt *one particular* set not only would result in losing a few or many stations, depending on the set selected, but also could not in any case be justified on the basis of objective evidence now available. The selection would have to include subjective judgments.

To adopt *average* values for the coordinates cannot be justified on any basis that is theoretically sound. Some major systems have in the past been defined in this way, but the justification lay not in the scientific evidence but in the political situation. There is no reason to believe that the differences between sets are random; there is even less reason to believe that they have a Gaussian distribution. This is strongly shown by OSU's plotting of the rotational relationships between systems (ch. 8). To arbitrarily select one particular system would make, in the present circumstances, much more sense than to compute a scientifically meaningless compromise. Such a set would have to be derived by weighting the individual values. The only nonsubjective weights available are those intrinsic ones calculated by the participants, and an analysis of the differences shows that at best one of the six sets of standard deviations can be correct.

The most reasonable recommendation is that a user adopt that set which (1) contains a set of stations suitable for his work (i.e., as regards number of points, proximity to user's areas of interest, etc.) and (2) was derived by geometric methods (NGS or OSU), if the user is concerned only with geometry, or by dynamics (NWL, NASA/GSFC, or SAO), if the gravitational field is also involved. The closer the user's situation is geodetically to that of one of the NGSP's participants, the better will be the user's results employing that participant's model.

In one sense, fortunately, we can say that the ± 10–m objective has been partially met as far as some individual stations are concerned. Our reason for claiming that we have fallen short of the goal is the existence of differences larger than the ± 10 m. But such differences do not exist for all the stations. There is a reasonable number of stations for which the differences in the coordinates lie well within the ± 10–m limits.

For such stations, we can certainly claim that the objective has been met. Of course, there is still the fact that coordinate systems themselves differ by considerable amounts. In the absence of more information, we cannot rigorously compute correct σ's for the transformations. We assume, therefore, that the transformation between systems (i.e., rotation of one system to the true system) contributes half the total error, the errors within a system contributing the other half. At the risk of oversimplifying the situation, we then assume that the objectives are met by those stations whose coordinates agree to within ± 7 m and whose intrinsic σ's (those calculated by the participant) also lie close to ± 7 m. This results in the list of stations presented in table 11.6, which can be considered a list of fundamental stations.

In discussing the reasons for the observed differences in results, mention was made of the differences that must be caused by use of dynamics rather than geometry. The participants have not analyzed the statistical implications of the theories in sufficient depth that numerical values for these differences can be calculated. A very rough guess at what the difference should be is 1 to 2 m. This is considerably less than the differences calculated for the two sets most closely associated, NGS's WGN and NWL's NWL–9D (ch. 3). The differences between the coordinates in WGN and NWL–9D are for the most part considerably larger than would be expected from the σ's computed for either set. The same holds true for differences between OSU's WN14 and NWL–9D. But the differences between OSU's and NGS's values are also too large. At present we can say only that the geophysically significant difference between results using geometry and results using dynamics is not separable from differences arising from other causes.

The estimate that the coordinates of the majority of the stations have standard deviations of the order of over ± 10 m when the uncertainties in the reference system are included is supported by the results of a computation by Marsh, Douglas, and Kloska (unpublished paper, 1973) of the coordinates of over 50 satellite tracking stations which participated in the tracking project ISAGEX in 1970–1971. Some of the data from this project were used in deriving GSFC '73 (ch. 5). Computation using a larger set of data from ISAGEX alone showed that the new set of coordinates differed from the previous set by a representative amount of 20 m.

The one definite and important conclusion we can draw is that the data accumulated in the NGSP have not been exploited to the extent either possible or desirable. The existence of σ's generally well below ± 10 m in each coordinate and the existence of unexplained discrepancies considerably larger than this shows this definitely. It shows, furthermore, that one of the reasons for insufficient exploitation is that the theories, detailed as they are, are still inadequate.

11.4 EVALUATION OF REPRESENTATIONS OF THE GRAVITATIONAL POTENTIAL

The three major specific objectives of the NGSP were stated in section 11.1, and the first of these, determination of the locations of tracking stations to ± 10 m in a center-of-mass system, was discussed in section 11.3. The second objective, determination of the average gravitational field to ± 3 mGal over 12×12 degree regions, will be discussed in this section. Because many users of the results are interested in actual values rather than average values, the results will be considered from several different aspects.

11.4.1 Evaluation by Comparison Between Models

As a result of the NGSP, two major determinations were made of the coefficients $\{C_n^m, S_n^m\}$ in the representation of the gravitational potential as a series of associated Legendre polynomials (ch. 1). These two resulting representations (or models) are those of GSFC (GEM-6) and SAO (SE III). They are discussed in chapters 5 and 9 and extend the representation to beyond $n=16$, $m=16$. These chapters give some

indications of how good the representations are, and this information is used here in evaluating the models. (The models of Applied Physics Laboratory (APL), Koch and Wilet, and Rapp are also discussed in order to give a perspective to the two major representations.) An interesting and valuable approach is, however, to compare the representations with each other and with derivatives of the true potential. The latter comparison has also been made by Decker (1972) and is discussed later. The former comparison, while not as definitive, since it gives only relative values, does give an immediate indication of the variability.

Table 11. 7 gives the differences (and the percent differences) between the coefficients $\{C_n^m, S_n^m\}$ of SAO's SE III, of APL 5.0, of GEM 5 and GEM 6, and of Koch and Witte (1971), with respect to the corresponding coefficients of Rapp (ch. 3). The coefficients of Koch and Witte, APL 5.0, and GEM 5 are derived from tracking data alone. The coefficients of SAO SE III and GEM 6 are derived by using both mean gravity anomalies and tracking data. The set of coefficients used as referrent is that of Rapp (ch. 3), which is also based on mean gravity anomalies and on tracking data. Since Rapp's set used the coefficients in GEM 3 (ch. 5), one would expect GEM 5 and GEM 6 (which are descendants of GEM 3) to agree more closely with Rapp's set than any of the others do.

A perusal of table 11.7 shows that this expectation is indeed true. Similarly, as one would expect, SAO's set comes in third, and APL 5.0 and the set of Koch and Witte (1971) come in last—i.e., have the largest differences from Rapp's. If the contributions of the gravity anomalies were of major importance, one would also expect to find SE III agreeing more with GEM 6 than GEM 5 does. But this is not the case. GEM 5 and GEM 6 are in fact much closer together than are SE III and GEM 6. So we can conclude that the differences between sets depend so overridingly on the tracking data that the inclusion or omission of data on gravitation at the surface is unimportant.

But a glance at table 3.37 (ch. 3) shows that Rapp's set, GEM 3, GEM 4, and SE III gave essentially the same rms error in the orbit. Obviously, since the variation in coefficients is 600 percent from the reference set even for $n<8$, the sets determined by tracking data, with or without gravity data, must be considered as being representative more of the orbits used than of the Earth's gravitational field.

The percentage deviations [2] increase as n increases; there are values of over 3000 percent. Also interesting is the fact that the standard deviations for the zonal coefficients show differences an order of magnitude or more greater than the standard deviations given by SAO (ch. 9). The same pattern is almost certainly followed also by the tesseral coefficients.

One could take the data in the table and compute average deviations, rms deviations, and so on. But the usefulness of such numbers is uncertain because there is no evidence, external or internal, indicating how close any one of the five sets is to being correct. The sizes of the deviations cannot be trusted. R. L. Decker (1972) evaluated APL 5.0 against DMA/AC's accumulation of some 24 000 means of gravity anomalies over 1×1 degree "squares." The evaluation showed that APL 5.0 deviated more from DMA/AC's values than did any of the other models investigated. This agrees with the indications of the table that APL 5.0 and the models of Koch and Witte (1971) are least representative of the field. It also showed that the models of Lerch *et al.* (1972a,b,c), Gasposchkin and Lambeck (1970), and Rapp (1972a) agreed reasonably well with the mean values (to within ±13 mGal at worst and to within ±8 mGal at best). This again one would expect from the table. The sets used by Decker are of course not the same as those given in the table, with the exception of APL 5.0. But there is no evidence that the present sets are more than a moderate improvement over

[2] Care must be taken in considering these percentages, since for $n >$ about 12, the C_n^m, S_n^m are frequently very small.

Decker's sets. Trial computations indicate an agreement to within ±4–5 mGal, and this is supported by, e.g., figure 9.11 (ch. 9) and figures 5.47 and 5.48 (ch. 5). Consequently, one would not expect the relative standings (with respect to rms deviations or error) to be changed significantly.

The lack of agreement among sets and also between sets and the real Earth (as we know it) would seem to lie at least partly with the phase information in the coefficients. This is what the frequent serious imbalance in differences between C_n^m and S_n^m would indicate.

An obvious conclusion from the table is that representation of the gravitational potential by series of associated Legendre function is not a good idea for practical use, and is only of limited scientific value. This harsh judgment is supported not only by the variation in values shown in table 11.7, but by the following consideration. First, contributions from a particular term

$$\frac{k^2M}{a_0}P_n^m(\sin\psi)\ (C_n^m\cos m\lambda+S_n^m\sin m\lambda)$$

do not represent the contribution from a single region but from regions all over the Earth; i.e., the effect of a region is smeared out. Except in the case of harmonics of low degree, physical interpretation is therefore not rewarding. Second, to give average values of potential over regions of area A km^2 requires about $5.03\times10^6/A$ numbers. But to ensure that these are completely represented by spherical harmonics requires about as many coefficients to be specified. Thirdly, it is obvious that the gravitational field is not overly sensitive (as measured by allowed error) to large changes in the $\{C_n^m, S_n^m\}$. Almost the only advantage of using spherical harmonies is the ease with which algebra is carried out.

Rapp (1973) has compared the gravitational constants in GEM 6, SE III, and his own solution. He gives the comparisons of the rms averages when only those for the same $\{n,m\}$ are considered and also when all coefficients are considered. Table 11.8 is abstracted from Rapp's paper.

11.4.2 Evaluation by Comparison with Gravimetric Data

11.4.2.1 Evaluation on the Basis of NGSP's Stated Geodetic Objective

If we adhere strictly to the stated numerical terms of the NGSP's objective (sec. 11.1), we are concerned not with how well the various representations (models) can reproduce the gravitational field, but with how well they can reproduce averages over areas of a given size. There is a considerable difference between the two considerations. If we use as a measure of reproducibility the rms difference, then we want

$$E[(\bar{g}_{sn}-\bar{g}_{Tn})^2]$$

not

$$E[(g_{sn}-g_{Tn})^2]$$

We have, to work with,

$$(\bar{g}_{sn}),\ g_{Tnmi}$$

which are, respectively, the average value of g_{sn} over area n, and the measured values of gravity in the same area. Ideally,

$$\bar{g}_{nm}=\frac{1}{A_n}\int_{A_n} g_{Tno}\,dA_n$$

where $g_{Tno}(\lambda,\phi)$ is the true value of gravity at (λ,ϕ) in area n. g_{Tno} differs from the corresponding measured g_{Tnmi} (λ,ϕ) because of errors in measurement, reduction to the surface, etc. Let ϵ_{Tnmi} be the error in measurement. But $\bar{g}_{Tn}$ will differ from the average computed from g_{Tnmi} not only because of the ϵ_{Tnmi}, but because only a sample $\{g_{Tnmi}\}$ of g_{Tn} is taken. The error introduced into $\bar{g}_{Tn}$ because of improper sampling is denoted by $\bar{\epsilon}_{Tnr}$ and is called the error of representation. Then

$$\bar{g}_{Tn}=\frac{\sum_i (g_{Tnmi}-\epsilon_{Tnmi})}{I}-\epsilon_{Tnr}$$

$$\equiv\bar{g}_{Tnm}-\bar{\epsilon}_{Tnm}-\bar{\epsilon}_{Tnr}$$

If we define ϵ_{Tnri} by

$$\epsilon_{Tnri} \equiv g_{Tnmi} - \epsilon_{Tnmi} - \bar{g}_{Tn} \qquad (11.1)$$

we have quantities which indicate the variation of g_{Tno} over area n. The variation is not random. They and the average $\bar{\epsilon}_{Tnr}$ depend on how the sample is chosen. As I increases, $\bar{\epsilon}_{Tnr}$ will approach zero, but this does not guarantee that for a given I, the average of $\bar{\epsilon}_{Tnr}$ over many n will approach zero.

The behavior of ϵ_{Tnmi} and ϵ_{Tnm} is quite different. In general, ϵ_{Tnm} will not be zero, but will be small if care has been taken to calibrate the measuring equipment frequently. The $\{\epsilon_{Tnmi}\}$ are then, hopefully, random. $E[(\epsilon_{Tnmi})^2]$ will vary little within regions of considerable extent but can vary considerably from region to region. Typical values in oceanic areas are 70 to 20 mGal where measurements were made 10 years or more ago, and ± 2 to 5 mGal where recent measurements have been made. On land, the rms error is characteristically better than ± 0.1 mGal except in regions where heights are not well known. Now, using ν instead of n to prevent confusion with the degree n of spherical harmonics,

$$\begin{aligned} E[(\bar{g}_{s\nu} - \bar{g}_{T\nu})^2] = {} & E[(\bar{g}_{s\nu})^2] + E[(\bar{g}_{T\nu m})^2] \\ & + E[(\bar{\epsilon}_{T\nu r})^2] - 2E[\bar{g}_{s\nu}\bar{g}_{r\nu}] \\ & - 2E[\bar{g}_{s\nu}\,\bar{\epsilon}_{T\nu r}] \\ & - 2E[\bar{g}_{T\nu m}\,\bar{\epsilon}_{T\nu r}] \qquad (11.2)^3 \end{aligned}$$

Note that $E[(\bar{g}_{s\nu} - \bar{g}_{T\nu})^2]$ is not a measure of the agreement between two differently derived gravity fields, but a measure of agreement between averages. As the size of A increases, $\bar{g}_{s\nu}$ and $\bar{g}_{T\nu}$ become less representative of the field but agree more with each other. From equations (11.1) and (11.2),

$$\begin{aligned} & E[(\bar{g}_{s\nu} - \bar{g}_{T\nu})^2 - (\bar{g}_{s\nu} - \bar{g}_{T\nu m})^2] \\ & = E(\epsilon_{T\nu i})^2 - 2E[(\bar{g}_{s\nu} - g_{T\nu m})\,\epsilon_{T\nu r}] \end{aligned}$$

From the results of either SAO (SE III) or NASA (GEM 6), it is obvious that $E(\bar{\epsilon}_{T\nu 1})^2$ (which is roughly equivalent to $E(\epsilon_T)^2$ in their tables) is small in comparison with $E[(\bar{g}_{s\nu} - \bar{g}_{T\nu})^2]$ and $E[(\bar{g}_{s\nu} - \bar{g}_{T\nu m})^2]$. If it is also assumed that $E[(\bar{g}_{s\nu} - \bar{g}_{T\nu m})\bar{\epsilon}_{T\nu r}] \approx E(\bar{\epsilon}_{T\nu r})^2$, the tabulated quantity $E[(\bar{g}_{s\nu} - \bar{g}_{T\nu})^2]$ can be used as an estimate of difference between the two average gravitational fields.

Assume again that $E[(\bar{g}_{s\nu} - \bar{g}_{T\nu})^2]$ varies inversely as ν, and use the best estimates given. (For SE III this is given for n and m equal to 18 and for 5×5 degree regions containing 20 or more 1×1 degree regions for which average values are available.) For GEM 6 this is given for n and m equal to 16 and for the same kind of 5×5 degree regions. The value of $\sqrt{E[(\bar{g}_{s\nu} - \bar{g}_{s\nu})^2]}$ for 12×12 degree regions is then approximately ± 5 mGal for GEM 6 and ± 4 mGal for SE III. In view of the many assumptions made to arrive at these values, one must conclude that the values are decidedly on the optimistic side. But since optimism is, under the circumstances, at least as justifiable as pessimism, the easy corollary is that the results are close to what they should be. It is obvious, however, that we could have considerably more confidence in the results being within the desired limits if they were less than ± 3 mGal rather than greater.

This conclusion is deliberately made weak because of the many still unresolved problems involved. The information that relates to accuracy of the models presented by GSFC and SAO is contained in table 9.43 (ch. 9) and tables 5.60 and 5.61 (ch. 5). Both SAO and GSFC give values for all the quantities defined in Kaula (1966a) and repeated in chapter 9, although most of the quantities are significant only for—and defined for—the case where the representation of the

---

[3] Kaula (1966a) broke the quantity $\bar{g}_{sn}$ (actually $\overline{\Delta g}_{sn}$, but, as was remarked earlier, the distinction can be ignored in this discussion) into several components: $\bar{g}_{sno}$, the value of $\bar{g}_{sn}$ that would result if a complete and correct representation in terms of associated Legendre functions were available; ϵ_{gn1}, the error caused by errors in those coefficients $\{C_n^m, S_n^m\}$ explicitly present; and $\bar{\epsilon}_{gn2}$, the error caused by defining certain C_n^m, S_n^m to be zero, i.e., omitting certain terms. Such a breakup has no importance for the present evaluation, since only $\bar{g}_{sn}$ is relevant to the program's objectives. The values given by SAO and NASA for Kaula's components therefore need not be considered.

gravitational field is derived from observations only on satellites. The values given for the mean square error in average gravity anomaly are not worldwide in distribution—that is, do not cover the complete globe—but are restricted regions for which at least one average value over a $1°\times1°$ figure is known in each $5°\times5°$ figure for SAO and 10 values in each $5°\times5°$ figure for GSFC. The result of such selection is to concentrate on regions in which gravity has been measured accurately. The greatest s.d. used is 5 mGal and is for $5°\times5°$ figures in which at least $1°\times1°$ figure has an average gravity anomaly associated with it. The values given are therefore much too low if we wish to evaluate the representation globally, and a global basis is, of course, the one that makes most sense geodetically and orbitally. The average values computed from the representations are the values of gravity computed at the center of each figure. This introduces another error, although a small one. Also, it must be kept clearly in mind that quantities in the tables are all given to 1 in the units place, implying that the various gravity and gravitational quantities are good to 0.5 mGal at least. This implication is simply not true. The most thorough analysis of the errors in average gravity anomalies is probably that of DMA/AC (Decker, 1972), and that analysis indicates that except in regions with a high density of recent gravimetric data (and such regions are not numerous), 1-mGal errors are exceptional.

11.4.2.2 Evaluation by Comparison With the Gravitational Field

In section 11.4.2.1, the quantities considered were average values over regions $12°\times12°$ in area. For many applications, the value g_{Tn} (λ,ϕ) of gravity at locations $(\lambda,\phi;H\equiv0)$ is more important than $\bar{g}_{Tn}$. But comparison of g_{sn} with g_{Tn} would serve no useful purpose, since $\bar{g}_{sn}$ is calculated from a series that has been truncated long before even the contributions of the gravimetric data to it can be reproduced. So it makes more sense to compare g_{sn} with averages of g_{Tn} over regions of 1×1 degrees, since the $\{C_n^m, S_n^m\}$ were derived from such averages. But if we do this, we find immediately that only in small regions can $E(g_{sm}-\bar{g}_{Tn})^2$ be expected to be small. SAO (ch. 9) compared g_{sn} with $\bar{g}_{Tn}$ along fixed latitudes and longitudes in North America and in the Indian Ocean. The rms difference was about ±4 mGal. If R. L. Decker's (1972) evaluation of gravimetric data is anywhere near accurate, there are only limited regions in North America, Europe, and Africa where one can expect to find $[E(\bar{g}_{Tn})^2]^{1/2}$ to better than ±5 mGal. The value is between ±5 and ±15 mGal for most of the land area and greater than ±15 mGal for most of the oceanic areas where g has been measured at all. Part of each of these values results from measurement error and part from error of representation. It is not necessary to make the breakdown, however. It is enough to conclude that a representative value of $[E(\bar{g}_{sn}-\bar{g}_{Tn})^2]^{1/2}$ is at best ±15 mGal globally and ±4 to ±5 mGal in regions where accurate data have been used.

The values computed by using orbital theory can be compared with an independent set derived by Hajela (1973) using gravimetric data. Hajela's values range up to 8 mGal. In the northern hemisphere, 3 mGal is representative of the rms differences; in the southern hemisphere, 6 mGal. The range of 3 to 4 mGal for the rms difference in average gravity anomaly from orbital theory plus gravimetric data is therefore reasonable on a global basis.

11.4.2.3 The Model of Rapp

In the previous discussion, R. Rapp's model (ch. 3) was not included because the model is based on an earlier version of GEM 3 and on gravimetric data which do not differ greatly from those used in GEM 6. The major differences, if there are any, between Rapp's model and GEM 6 must result from the different procedures used in adjusting the data. An analysis of the procedures shows

that they cannot lead to results that differ by more than the uncertainties that already exist in the results. The evaluation of GEM 6 can therefore be taken as applicable to Rapp's model as far as attainment of NGSP's objective is concerned. The question of reliability of the $\{C_n^m, S_n^m\}$ is of course another question. This was covered previously.

Rapp has, using H. Moritz's "collocation method," combined the coefficients $\{C_n^m, S_n^m\}$ of GSFC's GEM 3 with the average gravity anomalies compiled by DMA/AC (ACIC). The results are close enough to those obtained by means of the usual method of least squares that any advantage in using a collocation method rather than the usual one is completely obscured by the uncertainties in the results.

Rapp's solutions are valuable, nevertheless, for their independence of method. Of course, since they use much the same data as the various GEM's, one would expect the various models to be close to each other. In the sense that they differ less from each other than they do from APL's and SAO's models, this expectation is true. To the extent that GEM 6 is based on more data than Rapp's coefficients are, one would expect GEM 6 to be superior to Rapp's coefficients. This expectation cannot be either proved or disproved on the basis of analyses made so far.

11.4.3 Evaluation by Comparison of Computed Orbits With Observations

The NGSP was intended to provide *geodetic* information. For this reason, the specification on gravitational errors was written in terms of a geodetically meaningful concept—the average value of gravity over an area of given size. This average, if known, together with a few other data, can be converted into approximations to the height of the geoid above a selected spheroid. The primary basis for evaluation of the gravitational part of the NGSP's results must therefore be in agreement with gravity.

As a secondary basis for evaluation of the gravitational part of the NGSP's results, *any* observable effect of the gravitational field may be used. The drawback to using such an effect is that it is contaminated by the presence of factors other than the gravitational field, so that these factors must be accounted for. The most readily available and observable effect of the gravitational field, as far as participants in the NGSP were concerned, was the orbital motion of spacecraft, with the observables being the directions or distances to the satellite at known times. The rate of change of distance between station and satellite can be computed from measurements of the Doppler shift in radio waves emitted by the satellite (ch. 2 and ch. 5). Since the relation between Doppler shift and component of velocity is simple, the component can be treated, to the accuracy we are concerned with, as if it were an observable. Hence there are three "observables" available for checking the accuracy of the gravitational field. They were used by NASA/GSFC and by SAO (which used only direction). The results are summarized in Table 11.9.

SAO has computed orbits for GEOS–A, GEOS–B, and D1D using SE III. The orbits gave residuals, over 2-day periods, whose rms values varied from 2 to 17 m, with almost 50 percent between 5 and 10 m. Since the satellites used were the same ones used in deriving the $\{C_n^m, S_n^m\}$, the results must be considered an *indication* of the accuracy of the gravitational field computed from the $\{C_n^m, S_n^m\}$. They do not, as shown earlier, tell anything about the accuracy of the coefficients, and, as SAO carefully points out, they result from errors in many quantities other than the coefficients.

SAO, in chapter 9, explains the difficulties that prevent satisfactory evaluation by orbital analysis. A very important difficulty not mentioned is that of obtaining independent data. It should be remembered that the orbits on which GSFC's and SAO's results depended were obtained by the adjustment of values of over 600 independent constants exclusive of the orbital elements, that many

disagreeable observations were discarded, and the weighting of equations was not entirely objective. With this amount of freedom available for computing orbits, any residuals computed on the basis of observations already used in the adjustment cannot be expected to tell much about the accuracy of the constants. Even residuals from observations not so used must be suspect if they refer to the same satellites. For these reasons, the rms variations in residuals quoted by GSFC and SAO are unsatisfactory. GSFC, in chapter 5, gives an rms variation of 2".74 for orbits computed using GEM 6 and 2".37 for orbits computed using GEM 5. GSFC also used distances measured by laser systems. The rms variation when using GEM 5 was 1.54 m; when using GEM 6 it was 1.64 m. These variations were for periods of 5^h rather than the 168^h within which camera data were used by GSFC and the 48^h used by SAO. The accumulation of errors in the orbits should not follow a three-dimensional, random walk, so the effects of discrepancies in periods cannot be reliably accounted for. Because of the short period covered by the arcs in GSFC's computations of residuals in range, the errors in the gravitational field cannot have much effect on the orbit or at least could be expected to be swamped by effects of errors in location of instrument, inadequacies in theory, etc.

For these reasons—those given by SAO and those given above—we must conclude that the evidence so far available for evaluating the models on the basis of orbits' accuracies is inadequate. Not only must we have completely independent data available, but there must be enough of these data that the errors in the gravitational field can be reliably separated from those in other constants. The tables provided in chapter 5 do show, however, in their comparison of variations, anomalous behavior from model to model, and further investigation to explain this behavior is urgently needed. (The tables give results using SE II. Variations have also been computed using SE III. The rms variations are slightly larger than those for SE II. However, because of the anomalous behavior mentioned, the increase may not be significant.)

11.4.4 Evaluation by Reference to the Geoid

The geoid is in theory derivable if gravity is known over it and if a connection between it and a suitable spheroid (center of mass at origin, etc.) can be established at one spot. The differences between a geoid calculated from one of NGSP's gravitational models and one calculated from astrogeodetic and/or gravimetric data could therefore be used as an indication of how good NGSP's representation is. But unless the geoid used as reference is considerably more accurate than the one to be evaluated, the comparison is not going to tell very much. There are unfortunately no geoids of this kind available. There are detailed representations over limited areas, such as North America (Fischer *et al.*, 1967), Europe (G. Bomford, 1972), and Australia (A. G. Bomford, 1971). But these are representations of geops (equipotential surfaces) which are either not part of the geoid or are connected to it by satellite-connected data. The differences therefore contain systematic errors which cannot themselves be computed.

Global gravimetric geoids are available—e.g., Uotila's geoid (1964). Unfortunately, these geoids are based on data which are a subset of the data used in producing GEM 6 and SE III. This makes their use as referents undesirable because the differences found could not be interpreted unambiguously.

The best standard of comparison, as far as independence of method of derivation is concerned, is an astrogeodetic geop, since it is least influenced by the *values* of gravity. There are objections to using such a geop—e.g., difficulty of connection to other geops, rapid rise of rms error with distance from datum point under certain conditions, and so on. However, Rapp (1973) has compared geoids computed from his own, GEM 6's, and SE III's sets of $\{C_n^m, S_n^m\}$ with astrogeodetic geops for North America and Australia. His comparison shows rms differences of

± 2.0 m, ± 2.2 m, and ± 2.6 m between the astrogeodetic geoid in Australia and his revised model, GEM 6, and SE III. It shows corresponding values of ± 4.4 m, ± 3.9 m, and ± 6.1 m with respect to the astrogeodetic geoid in North America. As remarked previously, geoid (or geop) is not at present a satisfactory concept for comparison because it is difficult to get definitive connections which are also completely independent of data from satellites but still accurate enough for the purpose. (Rapp's revised model uses GEM 5 rather than GEM 3 as support for the gravimetric data.)

11.4.5 Summary of Evaluation of Gravitational Field

The NGSP has produced two major representations of the gravitational field—GEM 6 and SE III—three, if GEM 5 is considered an independent representation rather than only a minor variant of GEM 6. These two models have been evaluated (or, more correctly, considered) in relation to each other and to models of lesser importance, in relation to areal averages of gravimetric measurements, and in relation to their effects on orbits calculated from them. The first and most important conclusion from these evaluations is that the models produced are considerable improvements over those available at the start of the NGSP and that the general objectives of the NGSP have, in this respect, been more than satisfactorily met.

But if the specific objective of the NGSP requiring a certain accuracy of the models is considered, we cannot say with certainty that the results are satisfactory. We do know that the individual coefficients differ from model to model by amounts which are much too large. These differences indicate that the results are less representative of the gravitational field than they are of the gravitational field plus the combination of observations and orbits involved. Part of the reason for the discrepancies must also be attributed to the fact that the procedures used in reduction are such that harmonic analysis does not correctly separate the effects. Consequently, the different models involved different numbers of terms; the effects of the residuals were distributed differently among the corresponding coefficients. This is a clear indication that the present method of representation is inefficient and inadequate.

We also know that while the average gravity anomalies computed from the models are close to those obtained from gravimetric data, the rms error is not sufficiently below the 3 mGal required for us to be certain that the objective has been met. In fact, the estimates available would indicate that the rms error is closer to 4 mGal than to 3 mGal, over a 12×12 degree square. (Note that most of the values given in tables 5.60 and 9.43 are not relevant to the basic objectives.)

Finally, we must conclude from a study of the residuals from observations on the satellites that the gravitational fields provide orbits which may be satisfactory considering the rms errors in the observations themselves, but that the data presented to support this conclusion are insufficient and inconsistent and have not been adequately analyzed. NASA/GSFC has, it must be said, been extremely conscientious in comparing computed distances, angles, velocities, etc., with observed quantities. But these comparisons have not been completely consistent as far as periods of time covered are concerned, and the information available for separating the contribution of the model from the contributions of other factors is inadequate. Much more work must be done to provide information for evaluating the models, and in any event the same criteria and methods of evaluation should be used by all participants, in particular by GSFC and SAO. No such common bases were used in the NGSP.

11.5 THE GEOID

Approximations to the geoid have been determined by four participants: APL (ch. 2), OSU (ch.3), NASA (ch. 5), and SAO (ch. 9). APL's geoid, being derived without reference to gravity on the surface, is useful primarily for evaluating the APL 5.0 poten-

tial. It cannot be considered a useful representation of the geoid, since it is not tied to surface measurements. As APL points out, its geoid does agree with Gaposchkin and Lambeck (1970) to within 10 m. This is a good approximation for a geoid derived entirely from one kind of tracking data. The agreement with SAO SE III is approximately the same.

There are many ways of comparing geoids. None in use at present is particularly convincing. The most common method is to take differences at equal intervals of longitude and latitude. Unfortunately, this will indicate that differences exist even though these differences may be caused only by one representation's being out of phase with the other. If the differencing is carried out at closely spaced intervals, contours of equal intervals can be drawn.

The diagram (fig. 5.38, ch. 5) comparing heights in GSFC '73 with heights from the geoid of Vincent and Marsh (ch. 5) shows that the surface determined from GSFC '73 is systematically lower than that of Vincent and Marsh.

11.6 EVALUATION OF THE PERFORMANCE OF SATELLITE-TRACKING SYSTEMS

One does not have to know how good a piece of equipment is in order to use the equipment and get useful service from it. This is especially true if, like satellite-tracking systems, the equipment is unique and known to represent merely one stage in the development of a rapidly advancing art. But one must have an estimate of the suitability of the equipment if one wants to make sure that the equipment develops and does not remain technologically retarded. Evaluation is therefore an essential part of the total knowledge about an instrument, as important as the manual of operation or the set of calibration constants.

Just what constitutes an evaluation depends partly on what one wants it for. There may be one evaluation of the performance of a tracking system if the data of the system are to be used only for orbit determination, another if the data are to be used to determine station coordinates, and a third if one is not sure of what the data will be used for. But what goes into an evaluation depends also on what one has available for making the evaluation. This is particularly true of satellite-tracking systems, where the system often includes not only the tracking station, but also the satellite, and where it is hard to find a standard against which to judge the system. For this reason, those evaluations that have appeared so far and which are reported in chapters 5 and 6 do not provide simple answers to the question of how "good" any system is, but say, "This system, if used for this purpose and compared with that system under these conditions, shows such-and-such differences."

It was pointed out earlier (sec. 11.1.3.1) that the characteristics of a tracking station are to some extent determined by the characteristics of the satellites with which they are used, or, what is almost the same thing, the characteristics of a tracking station determine what kind of satellite it can be used with. A fair comparison of the performance of one station with the performance of another therefore requires not only collocation of the stations, but also their use on the same satellite at nearly the same time. This is always difficult; it is often impossible. Even where near identity of measuring conditions could be found, there would be the fundamental difficulty that some of the stations measure angles, some distances, and some velocities. One cannot compare these data directly with each other; it is an apples-and-oranges situation. Any common standard of reference that is found may be so far removed from the basic data put out by the station, that the validity of the final comparison is hard to prove. For instance, laser DME can be compared with 6–GHz (5–cm) radar DME by locating the stations next to each other and then measuring distances to the same satellite at nearly the same time. Since the true satellite distances are not known and since refraction effects, and so on, are different for the two instruments, these factors must be accounted for in the com-

parison. But if one instrument measures distance and the other angle or velocity, it may be necessary to compare the ability of the instruments to give the correct satellite coordinates, which means bringing into the problem the orbit of the satellite. Then the comparison depends not only on the performance of the system *per se*, but also on the particular mathematics used in describing the orbit.

Since direct comparison of all tracking systems is impossible, comparison between systems of like natures must be considered the best that can be done. To go further, a common and valid standard or reference must be found. Only two standards need be considered: (1) the location of the satellite and (2) the location of the tracking instrument. Consider the several ways of getting a comparison on the basis of satellite locations.

(1) The data from each system are used to determine satellite locations in the manner best suited to that particular system: by simultaneous observations, by empirical curve fitting, or through orbital theory. Satellite locations for the same times are then compared. Insofar as a system is intended to be able to produce satellite locations, this is a fair method of comparison. It is not a valid method unless each system is used in its best geometric arrangement (for example, as a group of three SECOR stations arranged to form, with the satellite, a tetrahedron, or a set of two camera-type AME arranged to form, with the satellite, an equilateral triangle, and so on) and with suitable satellites. Assuming that this can be arranged, we then compare the systems on the basis of the standard deviations of those satellite locations determined by the data.

While this procedure is optimal in many respects, it is unsatisfactory in many others. It gives no answers to questions about the accuracies of the systems when used on satellites in general or about what the accuracies will be when the systems are forced to operate in geometries other than the best ones. Furthermore, there is no way of separating the effects of the theory on the performance from the effects of instrumental errors.

(2) The data from each system are all used in the same way to produce satellite locations—that is, by insertion of the data into the equations of the orbit, with the same orbital theory being used for all tracking. This method ensures that the systems alone are being compared so that any differences found do not arise from differences in theory. But now the hosts of error are attacking on the other flank. Every system has a best way of being used, and we are denigrating the performance of a system by forcing its data to conform to the same treatment as those of the others.

(3) The data from one particular system may be used in computing the orbit, and the values of the observables for each other system may then be computed by using that orbit. The "accuracy" of a system is then determined from formula (11.3), where y_{oi} are the computed values. This method is the one used by NASA/GSFC and NASA/Wallops Flight Center (WFC). It is excellent if the system used as standard is considerably more accurate than the other system involved and if performance under less than optimal conditions is wanted. For some of the equipment (such as FME) the conditions may indeed be much less than optimal. (For example, an insufficient number of stations may be used to determine the orbit, or the passes available may have poor geometry.) This method, therefore, can lead to misleading results.

The most important characteristic of a tracking system is its error—or at least its actual error σ_m compared with the error σ_r allowed for it. If the system measures values y_{oi} ($i=1$ to I) of an observable whose actual (true) values were y_{ti}, the measurement error of the system is defined to be

$$\sigma_m = \sqrt{\frac{\sum_i (y_{oi}-y_{ti})^2}{I}} \qquad (11.3)$$

The error performance or quality index of the system is the ratio

$$\rho = |\sigma_m/\sigma_r| \qquad (11.4)$$

where σ_r is the error allowed in or specified for the system.

A tracking system (ch. 1) measures one or more of the following quantities: phase angle, travel time of a pulse, frequency, or Cartesian coordinates of a point in a photographic image. Measuring these quantities can be considered equivalent to measuring the distance or direction of a satellite from the observer, or measuring that component of its velocity which is in the direction of the observer. But there is no way known at present of finding out the true values y_{ti} of these quantities. Equation (11.3) therefore cannot be used for evaluating the performance of a tracking system.

No completely satisfactory alternative has yet been found, or at least none has been used. The best alternative is to consider, as the most important characteristic, not the accuracy of the measurements of the system but the accuracy of the final results. With this criterion, the formulas for σ and ρ remain the same, but the definition of y_{oi} becomes different. Now y_{oi} is the value of a quantity for which accurate values are usually available.

The quantities $\{y_{oi}\}$ are now available, whereas they were not available if one used the first criterion. Furthermore, σ_r is now related directly to the user's needs rather than to the distance, direction, or velocity of the satellite, which are for most people only of minor interest.

One group has been engaged since the start of the NGSP in evaluating performance of the tracking systems used in the program. This group, under the direction of J. Berbert of NASA/GSFC, actually had two objectives: to evaluate the performance of the tracking systems and to calibrate those systems which were NASA's. Since the principal criterion used by the group for evaluation was the accuracies and precision of the systems, the procedures used in evaluating performance were in many cases the same as those used for calibration (except where calibration was done without satellites), and the results naturally also overlapped. But the objectives were not identical, and the results, while related, were not directly usable in either context. Berbert's group was more concerned with the problem of calibrating the instruments than with the problems of evaluating (comparing) them. As a consequence, the group's results, given principally for the calibration objective, do not convert readily into numbers that can be interpreted for evaluation (comparison). Table 11.10 gives values taken, with occasional slight changes, from the group's reports and intepreted as precision.

Note that the NASA group adopted the second approach discussed earlier. Instead of comparing measurements directly, the group assumed that the systems were intended to provide data for computation of orbits and compared measurements against quantities computed from the orbit. (The collocation tests did approximate direct comparison.) In the terminology of the group, the calibrations constants for a system are named: "zero-set bias coefficient" (symbol B_0) and "time bias coefficient" (symbol B_T), or "zero-set bias" and "timing bias." These constants appear in the linear equation

$$(y^i_{\text{obs}} - y^i_{\text{comp}}) = B_0 + \left(\frac{dy^i_{\text{comp}}}{dt}\right) B_T + \epsilon$$

where y^i_{obs} (y^i_{comp}) is the i^{th} measured (computed) value of the observable and ϵ is the measurement error. From the way in which B_0 and ϵ enter into the equation, the two quantities obviously cannot be separated unless some assumptions are made about the nature of B_0 and ϵ. The group assumed that B_0 was constant over long periods (one pass or longer), while ϵ varied randomly from measurement to measurement.

With respect to the data provided by the GEOCEIVERS (ch. 3), we should note that the stations involved in the test were located on or close to first-order control points. Many were on the precise traverse. If we accept the values derived for their coordinates, then the distances between stations are good to about 1 part in 10^6 (B. K. Meade, private conversation, 1973). The data from the stations will therefore be important in the new

adjustment of the North American triangulation.

Conclusions on the Evaluation of the Tracking Instruments.—The work done by NASA/GSFC and NASA/WFC has provided a very large amount of potentially useful information on the errors associated with some instruments. The potential has not, unfortunately, been fully realized during the lifetime of the NGSP, and the natural process of evolution in instruments is fast rendering most of the information obsolescent. The work did make evident the capability of 5–cm radar for greater precision than was generally thought, and it did provide reasonable starting values for the σ's of observations with the instruments. It is obvious from the results that the σ of 5–cm radar data can be reduced still further. It is also obvious that a large systematic error must still be present in data from SECOR, although the error cannot be considered serious since (1) SECOR is no longer being used and (2) the data can be corrected by using OSU's method (ch. 8).

The evaluation done by NASA/GSFC is particularly valuable in showing how future work of this kind can be improved. The methods that were used extracted only part of the information present. Because of this and because the statistical methods used sometimes gave ambiguous results, there was—and still is—some disagreement over the interpretations of these results. The work done by Berbert *et al.* is therefore an excellent basis on which to build more powerful methods in future evolution of the performance of an instrument.

11.7 SUMMARY OF EVALUATION

The broad purposes of the NGSP, to get substantially improved coordinates for tracking stations, to get an improved model of the gravitation field, and to compare the performance of the tracking systems involved, can be said to have been well satisfied. There is no doubt that the six major datums on which most of the tracking stations were located (NAD 1927, SAD 1969, EU50, Adindan, and AGD 1965) have been related to one another to within ± 20 m. Solutions for individual sets of tracking stations (those contained in NWL-9D, GEM 6, WGN, WN14, and SE III) give standard deviations for the coordinates of important stations that are well below ± 5 m. For a selected number of stations, the rms error in the coordinates is probably less than ± 10 m regardless of the set from which they are taken.

As for the gravitational field, the coefficients for which values have been determined have been extended to beyond a full $n=16$, $m=16$, and in land areas at least, the average value of gravity over a 12×12 degree region can be computed to about ± 4 to ± 5 mGal.

In an extensive series of tests, comparisons have been made of the performance of BC–4, Baker-Nunn, and MOTS cameras, of MINITRACK, of SECOR, 5–cm radar, GRARR, and laser systems, and of the TRANET Doppler systems. By comparing observations against values computed from "standard" orbits, instead of against each other, the participants avoided the "apples-versus-oranges" difficulty.

The values derived for instruments' differences are probably better than $\pm 1''$ for the cameras, ± 1 m for the ranging instruments, and ± 1 cm/sec for the instruments measuring range rate. The values derived for biases in the data must be even better, since they are themselves averages and would be approximately as good as the standard deviations of the observations, divided by the square root of the number of observations.

As regards the *specific* objectives of the NGSP, the situation is less satisfactory. The first specific objective was to get the positions of enough stations on the major datums to ± 10 m (in each coordinate) in a geocentric system to enable these datums to be tied together to approximately the same accuracy and to get coordinates of other stations also to ± 10 m. It was implicit in the statement of the objective that positions of other points on these datums would then be fixed to the geocentric system either directly or, in most cases, through conventional survey on the local datums. The requirement

may have been met, as was stated previously, for a selected set of stations and for six datums. It has not been met for all stations or for all the major datums. Furthermore, the assumption that it has been met for the six is a shaky one, since the assumption is first made that agreement of the participants on the values involved (to within the allowed uncertainty) is sufficient.

The discrepancies between coordinates of these and other tracking stations as determined by the various participants are so great, for the most part, that acceptance of one participant's set of coordinates will result in rejection of the coordinates of many stations determined by others. Every bit of evidence points to the conclusion that all the sets except perhaps one contain systematic and unexplained errors. The evidence seems to indicate that some of these errors lie in the definitions of the coordinate systems used, but that other error sources are also present. There is no doubt whatever that many of the sources could have been tracked down and the errors eliminated had the preliminary computations of results been more freely circulated and had the error analyses been carried out further. Certainly before a final set of coordinates is selected, the error analyses required to identify the sources of the errors will have to be made. Such analyses should be made in any case because so many geodetic and geophysical projects are being carried out using the methods developed by the NGSP. If nothing is done to clean up the work already done, these will carry within them the same errors that caused difficulties to the NGSP.

The second specific objective of the NGSP concerns the Earth's gravitational field. The evidence produced by the participants indicates that the NGSP has come close to achieving its objective of 3 mGal for $12° \times 12°$ quadrangles. Unfortunately, neither of the two major participants concerned with the gravitational field presented data relating directly to the NGSP's stated objective, and the data which were produced were, at best, inconclusive. The difficulties of evaluation were aggravated by lack of commonality between SAO and GSFC in test objects, at least as far as their use by SAO was concerned. GSFC did carry out parallel computations, using GSFC's and SAO's models, and these computations show a slight superiority of the GSFC model for computing orbits. But GSFC's data adduced for evaluation contain some anomalies that require explanation anyway, so nothing definite can be concluded.

As in the case of the conclusions about the geometric results, the gravitational results can be said to be capable of considerable improvement. Most of this improvement should come about by a definitive analysis of the errors. Considering the number of important and unanswered questions still existing in regard to the validity of the accuracies of the results, such an error analysis must be considered essential.

An inspection of the values of the coefficients $\{C_n^m, S_n^m\}$ shows, first, that the individual values for most of them have relative uncertainties of well over 50 percent, even as low as degree 6, while many of them have relative uncertainties of several thousand percent (based on differences from Rapp's model.) Representations of the gravitational field by series of spherical harmonics must therefore be considered completely unreliable. Since the various models are, however, well able to predict average gravity anomalies, as was mentioned previously, and to provide orbits that fit well to observed data, it must be concluded that much of the fault lies with the method of representation. Considered as a predictor of gravity anomalies, the various models are of course less successful than they are as predictors of average values, and an rms error of ± 15 mGal or poorer must be expected in all but a few land areas.

Evolution of the instrument performance, as contrasted to comparison of performance, was not an objective, but should be possible from the data accumulated and results obtained. There is not agreement among participants, or between participants and the editor, on the relation of these results to the precision and accuracy of the instruments. Since the objectives of the program have been

met in a broad sense, if not in a narrow one, since many of the participants are satisfied with their own solutions, and since much of the equipment is by now obsolescent with no thought of future use, final evaluation of the instruments has no immediate importance. Final evaluation is important to the extent that without it we cannot claim that the results of the NGSP are either complete or completely understood.

Although this evaluation shows that only the general objectives of the NGSP have been reached, such a statement is of little value without a further statement of why the program did not reach its objectives and of what (if anything) should be done.

First, it is obvious that the specific objectives, although not reached, are yet within sight from the NGSP's terminus. The accuracy of coordinates is surely within 10 meters of where it should be, and the accuracy of the average anomalies within 2 to 3 mGal. Had the NGSP continued another two years, and had appropriate steps been taken, the accuracies could probably have been brought to the deserved values.

There seem to be only three important reasons why accuracies were not attained during the NGSP. One arises from a fundamental rule laid down at the very start of the program—that in order to ensure that the results should be independent and hence usable as checks against each other, the participants should work along independent lines. This rule, excellent in purpose and concept, was unfortunately adhered to with a fixity that preserved independence but prevented full cooperation in the tracking down of sources of disagreement. The second reason is that the error analyses carried out by the individual participants have not been of the depth and sophistication needed to completely support the results. The need for such depth and sophistication was of course not apparent until too late, because cooperation was not close enough to show that significant discrepancies were going to occur. And the third reason was, of course, that the discrepancies and the need for their explanation became obvious too late for the participants to take steps to do much about it. The NGSP ended at that point where the participants had just discovered the magnitudes of the discrepancies and realized the need for reducing them.

To what extent independence of operation prevented the discrepancies from being anticipated can only be guessed at. In any case, we know that the discrepancies exist, that they are larger than we would like, and that their causes are still uncertain. We also know that the methods that were used in analyzing the data can be further refined to allow deeper analyses of the data. Until such an analysis is carried out and the present discrepancies explained to everyone's satisfaction, processing of more data by present methods is not merely unnecessary, but is undesirable. Since present results of the NGSP are open to objections that prevent their being considered as meeting the program's objectives, since these same objections will affect acceptance of future results obtained by techniques similar to those used during the program, and since eliminating the objections will also provide the specific objectives for which the NGSP was designed, we must consider a deeper analysis of the data as necessary for satisfactory completion of the NGSP.

A final word as to the results of the NGSP: The judgment that the objectives of the NGSP have been only partly satisfied is true only with respect to the most stringent requirements that were imposed by NASA. If the more liberal and general requirements that were also put down by NASA—that the program lead to substantial improvement in the number and accuracy of geodetic locations and in the knowledge of the Earth's gravitational field—are considered, then the NGSP has more than adequately met these requirements. The number of control points that can serve for international connections has increased from approximately 20 to over 200, and the rms error has dropped from an estimated ± 50 to ± 100 m to an estimated ± 10 to ± 20 m.

APPENDIX

TABLE 11.1.—*Solutions for Coordinates of Stations*

No.	Model	Reference[a] Original coordinates	Reference[a] Final coordinates
1	GEM 5, GEM 6	8.3, 11.5	5.6
2	NWL–9D	3.3	3.5
3	DMA/AC	8.3, 11.5	3.5
4	NASA/WFC	8.3, 11.5	6.5
5	SEN (SECOR)	8.3	3.5
6	WGN (NGS)	7.3	7.5
7	AFCRL	7.3, 11.5	3.5
8	GSFC '73	8.3, 9.3, 9.5	5.6
9	SE III (SAO)	9.3	9.5
10	WN14 (OSU)	8.3	8.5
J	JPL	11.5	4.5

[a] References are to chapter and section.

TABLE 11.2.—*Comparison of Lengths of Chords as Determined by NGS, NWL, and OSU*

Stations at chords' ends	Datum	Length (m) of chord (original survey) Value	S.D.[a] Original[b]	NWL	OSU	NGS[b]	Difference from original survey (m) NGS	NWL	OSU
North America	NAD1927								
6002–6003		3 486 363.232	±3.53	---	3.49	1.75	−0.06	+ 2	2.7 ± 2.3
6003–6111		1 425 876.452	±1.59	---	1.59	0.72	+1.50	---	2.3 ± 1.4
Europe[a]	EU50								
6006–6065		2 457 765.810	±0.80	---	3.5	1.23	+0.10	+ 3	6.1 ± 2.0
6065–6016		1 194 793.601	±1.43	---	1.41	0.60	+0.42	− 1	−2.9 ± 1.3
Australia	AGD								
6023–6060		2 300 209.803	±0.88	---	4.60	1.15	−0.98	−11	5.9 ± 3.0
6060–6032		3 163 623.866	±0.98	---	∞	1.58	−2.76	−10	−4.5 ± 3.6
North Africa	Adindan								
6063–6064		3 485 550.755	±2.10	---	4.11	1.75	+2.60	− 1	10.6 ± 2.3

[a] The lengths and standard deviations given by R. Kube and K. Schnädelbach in an unpublished paper presented in 1973 at Athens are as follows:

6006–6065	2 457 765.44 ± 1.2 m
6065–6016	1 194 793.601 ± 0.9 m

For the second of these, the chord from Hohenpeissenberg to Catania, J. C. Gergen and B. K. Meade of the National Geodetic Survey, in an unpublished memorandum of 15 May 1973, give the same length but a standard deviation of ± 1.428 m.

[b] Taken from table 7.3, chapter 7.

TABLE 11.3.—*Comparison of Positions Computed by OSU and by DMA/TC*

Station	$\Delta\phi$	$\Delta\lambda$	Δh	Δh_{com}	Datum
5001	51	61	−8	7	NAD 1927
5648	52	8	−3	14	NAD 1927
5712	−7	−44	−8	9	SAD
5713	−38	53	−26	−9	Azores
5715	−92	3	−27	−10	Adindan
5717	−208	18	−29	−12	Adindan
5720	−261	33	−23	−6	Adindan
5721	−252	58	−35	−18	EU50
5722	+231	17	−16	1	Indian
5723	−164	−20	−19	−2	China
5726	−136	13	−18	−1	Luzon
5730	22	−14	−11	6	--------
5732	−55	29	34	−17	--------
5733	35	32	31	−14	Pac. Mid
5734	48	−91	−22	−5	NAD 1927
5736	122	−66	−12	5	Atl. Mid
5739	−38	53	−25	−8	Azores
5744	−120	89	−46	−29	EU50

Spheroids used:

	a	*b*	*f*
DMA	6378155 m	6356770.1 m	1/298.255
OSU	6378155 m	6356769.7 m	1/298.249

TABLE 11.4.—*Relationship Between Major Geodetic Datums and Systems Used for NGSP*

	Model[a]						
	DOD/NWL (2)	NGS/WGN (6)	GSFC '73 (8)	GEM 6 (1)	CNES	SAO/SE III (9)	OSU (10)
Adindan	−150 ____ − 31 ____ ____ +199 ____	−163 ____ − 34 ____ ____ +207 ____	_____ _____ _____ _____ ____ _____ _____	−147 _____ − 3 _____ ____ 211 _____	_____ ____ _____ ____ ____ _____ ____	_____ ____ _____ ____ ____ _____ ____	−184 ± 19 _____ − 21 ± 11 _____ ____ +200 ± 6 _____
ARC (Cape)	−120 ____ −128 ____ ____ −296 ____	_____ ____ _____ ____ ____ _____ ____	_____ _____ _____ _____ ____ _____ _____	−126 _____ −110 _____ ____ −296 _____	_____ ____ _____ ____ ____ _____ ____	_____ ____ _____ ____ ____ _____ ____	−152 ± 7 _____ −126 ± 7 _____ ____ −298 ± 10 _____
Australian Geodetic (1965)	−125 ____ − 30 ____ ____ +148 ____	−124 ____ − 61 ____ ____ +145 ____	−137 34 − 50 18 1.9 155 38	−135 −100 − 39 −120 2.4 133 40	_____ ____ _____ ____ ____ _____ ____	−117 ____ − 39 ____ 2.44 +120 ____	−118 −103 − 41 − 99 1.2 +121 + 25
EU50	−729 ____ −105 ____ ____ −121 ____	− 96 ____ − 79 ____ ____ −126 ____	−149 60 −103 190 5.0 − 93 65	− 83 60 −116 40 −0.3 −120 −60	− 61 ____ −128 ____ ____ −150 ____	− 87 ____ −111 ____ ____ −134 ____	−134 41 −153 − 27 7.2 −145 51
Indian	+253 ____ +291 ____ ____ +359 ____	_____ ____ _____ ____ ____ _____ ____	_____ _____ _____ _____ ____ _____ _____	_____ _____ _____ _____ ____ _____ _____	_____ ____ _____ ____ ____ _____ ____	_____ ____ _____ ____ ____ _____ ____	+165 ± 17 _____ +711 ± 10 _____ ____ +228 ± 11 _____
NAD 1927	− 29 ____ +161 ____ ____ +183 ____	− 32 ____ +121 ____ ____ +173 ____	− 43 −100 162 − 20 0.9 179 − 5	− 24 − 20 +151 10 14 +187 − 80	_____ ____ _____ ____ ____ _____ ____	− 31 ____ +155 ____ 2.4 +179 ____	− 57 − 86 +148 − 23 −0.8 +186 − 33
SAD 1969	− 77 ____ 0 ____ ____ − 43 ____	− 44 ____ 2 ____ ____ − 44 ____	− 44 74 8 25 1.8 − 46 28	− 63 60 0 20 ____ − 32 0	..... _____ ____ ____ _____ ____	− 73 ____ − 2 ____ .98 − 50 ____	− 54 + 63 − 30 17 −6.7 − 43 + 12
Tokyo	−135 ____ +528 ____ ____ +670 ____	_____ ____ _____ ____ ____ _____ ____	_____ _____ _____ _____ ____ _____ _____	−147 _____ 509 _____ ____ 686 _____	_____ ____ _____ ____ ____ _____ ____	_____ ____ _____ ____ ____ _____ ____	−183 ± 10 _____ +506 ± 9 _____ ____ +686 ± 9 _____

[a] ΔX (m) | Rx (in $'' \times 10^3$) |
ΔY (m) | Ry (in $'' \times 10^2$) | scale difference $\times 10^6$
ΔZ (m) | Rz (in $'' \times 10^2$) |

TABLE 11.5.—*Comparison of Systems Used for Satellite Geodesy in NGSP Systems*

	Model[a]											
	WGN[b] (6)			GSFC '73 (8)			GEM 6 (1)			WN14 (10)		
NWL-9D	21	−11		----------			−6			16	29	
(2)	19	− 5	2.5	----------			3	− 3	−0.3	10	71	−0.14
	−16	64		----------			8	−59		−3	−15	
WGN	----------			----------			----------			[b]− 1	− 8	
(6)	----------			----------			----------			7	− 5	−2.3
	----------			----------			----------			12	11	
GSFC '73	----------			----------			0.5	0		14	96	
(8)	----------			----------			0.6	4	0.4	13	−30	0.24
	----------			----------			2.1	35		− 2	19	
GEM 6	----------			----------			----------			21	7	
(1)	----------			----------			----------			11	11	0.4
	----------			----------			----------			2	12	
SE III	18	−12		−1	−4		----------			14	−17	
(9)	26	30	1.3	2	−3	−0.6	----------			14	37	0.1
	−21	49		−9	8		----------			−10	15	
GEM 4	----------			----------			0.5	0	0	15	93	
	----------			----------			−0.4	− 2		12	− 2	0.2
	----------			----------			−0.2	4		2	12	

[a] ΔX (m) | Rx (in $'' \times 10^3$) | scale difference $\times 10^6$
ΔY (m) | Ry (in $'' \times 10^2$)
ΔZ (m) | Rz (in $'' \times 10^2$)

[b] Values specially computed by Computer Sciences Corporation.

TABLE 11.6.—*List of Stations With Acceptable Differences in Coordinates*

Geographic region	Models[a]
European Datum 1950	
St. Michael	8, 9, 10
Nice	8, 9, 10
Dionysos	8, 9, 10
San Fernando	8, 9, 10
North American Datum 1927	
Blossom Point	1, 8, 10
Ft. Myers	1, 8, 10
Beltsville	1, 6, 10
Columbia	1, 8, 10
San Juan	1, 8, 10
Denver	1, 8, 10
Jupiter	1, 8, 10
Mt. Hopkins	1, 8, 10
South American Datum 1960	
Paramaribo	1, 2, 6, 9, 10
ARC (Capc) Datum	
Johannesburg	
Australian Geodetic Datum 1965	
Thursday Island	1, 6, 9, 10
Culgoora	1, 2, 6, 9, 10
Caversham	1, 6, 9, 10
New Zealand Datum	
Invercargill	1, 2, 6, 9, 10
Miscellaneous (Minor) Datum	
Mahe	1, 2, 6, 10
Mauritius	1, 6, 10
Heard	1, 6, 10
Wilkes	1, 6, 10
Zamboango	1, 6, 9, 10
Christmas	1, 2, 6, 9, 10

[a] 1—GEM 6
2—NWL-9D
6—NGS/WGN
8—GSFC '73
9—SAO SE III
10—OSU's WN14

[a] The 7-m requirement is relaxed when only one coordinate is involved and the excess is less than 10 m.

TABLE 11.7.—*Summary of Differences in Coefficients Using Rapp's Model (Chapter 3) as Referent*

Type of comparison		Representation				
		GEM 5	GEM 6	SE III	APL 5.0	Kock and Witte
Terms included		12 × 12	16 × 16	16 × 16	12 × 12	4 × 4
				Differences[a]		
$n = 1 \sim 4$	$m = 0$	11/6	11/6	8/6	171/90	33/16
	$m = 1 \sim N$	90/22	22/10	229/80	171/41	435/190
$n = 5 \sim 8$	$m = 0$	18/13	19/13	12/8	320/203	---
	$m = 1 \sim N$	92/19	66/26	305/121	250/100	---
$n = 9 \sim 12$	$m = 0$	---	266/133	16/7	231/129	---
	$m = 1 \sim N$	---	97/30	297/80	268/99	---
$n = 13 \sim 16$	$m = 0$	---	29/6	24/16	---	---
	$m = 1 \sim N$	---	71/26	151/39	---	---
Percent differences, number						
Between 0–20		56	48	38	30	---
20–40		13	14	9	15	---
40–60		4	4	6	8	---
60–100		3	3	2	7	---
>100		--	3	17	17	---
Largest percent up to (8,8)						
$m = 0$		29 ($n = 8$)	29 ($n = 8$)	19 ($n = 8$)	516 ($n = 8$)	---
$m = 1 \sim N$		83 ($n = 7, m = 7$)	671 ($n = 7, m = 5$)	920 ($n = 8, m = 1$)	816 ($n = 8, m = 1$)	---
Differences × 10^8						

[a] Maximum difference/rms difference.

TABLE 11.8.—*Comparison of Gravitational Fields*

	Set						
	Rapp		GEM 6		SE III[a]		
	A	B	A	B	A	B	([b])
Rapp	--------	---	26 (49%)	---	58 (72%)	----	$\Delta\begin{Bmatrix} C_n^m \\ S_n^m \end{Bmatrix} \times 10^9$
	--------	---	3	3.7	7.2	7.4	[b]ΔN (m)
	--------	---	5.3	7.7	10.0	11.1	[c]Δg (mGal)
GEM 6	26 (49%)	---	--------	---	56 (80%)	---	$\Delta\begin{Bmatrix} C_n^m \\ S_n^m \end{Bmatrix} \times 10^9$
	3	3.7	--------	---	6.4	6.6	ΔN (m)
	5.3	7.7	--------	---	8.6	9.6	Δg (mGal)

[a] SE III, set B is taken only up to $n = 23$.
[b] $\Delta N \equiv$ difference in geoidal heights, rms value.
[c] Δg = difference in anomalies, rms value.

TABLE 11.9.—*Observational Errors Induced by Gravitational Representations (Average Value of RMS Error)*

Model	Distance	RMS error in direction, (7-day period)	Radial velocity (1-day period)
SAO SE III	4.9[a] (2[d])	----------	----------
GEM 5	1.54 m (0[d]2)	±2″4	±5.9 cm/sec
GEM 6	1.65 m (0[d]2)	±2″7	±5.5 cm/sec

[a] SAO (ch. 9) estimates that 2 to 3 m are contributed by errors in coordinates. This would still not make SAO's values for the contribution of the gravitational field consistent with GSFC's, which must also contain errors resulting from erroneous coordinates.

TABLE 11.10.—*Precision of Instruments Used for Satellite Tracking*

Instrument evaluated	Precision[a]			Instrument used as standard	Reference[c]
	Distance[b] (m)	Angle (″)	Velocity[b] (cm/sec)		
Camera	----------	±2 BC-4, BN ±1 MOTS, PC-1000	----------	----------	1967 (7)
		±2.8	----------	Camera	1968 (3)
		±3	----------	----------	1966
PRIME MINITRACK	----------	±50 m track ±100 m along track	----------	MINITRACK Camera	1966
	----------	±165 m	----------		1970 (5)
		±20″	----------		1967 (7)
GRARR	7 (1.p.) 12 (s.p.)	----------	----------	GRARR SECOR	1966 (8)
	±10.3 1.p. 7 s.p.	----------	----------	Camera	1969 (3)
	−2 to +2 (1.p.) ±3 to ±5 (s.p.)	----------	----------	Camera	1968 (4)
	±2.5 (1.p.)	----------	----------	Laser DME	1967 (1)
SECOR	1.2 − 6 (s.p.)	----------	----------	Camera	1966
	3.4 (1.p.) 1.7 (s.p.)	----------	----------	Laser DME	1968 (2)
	(−3 to +43) 1.p. ±1 to ±6 s.p.	----------	----------	Camera	1968 (4)
	±10	----------	----------		1967 (7)
FPQ-6	5 (1.p.) 1 (s.p.)	----------	----------	Laser DME	1968 (2)
	5	----------	----------	Laser DME	1969 (9)
FPS-16	3 (1.p.) (s.p.)	----------	----------	Laser DME	1968 (2)
Doppler DME TRANET	----------	----------	4.5/3 cm/sec (1.p.) 5.4/4 cm/sec (s.p.)	Laser DME	1968 (2)
GRARR	----------	----------	5 cm/sec		1967 (7)

[a] At lower frequency/higher frequency.
[b] 1.p. = long-period random error, s.p. = short-period random error.
[c] References:
(1) NASA Document X-514-67-447, 1967.
(2) J. Berbert and H. Parker, NASA Document X-514-68-458, 1968.
(3) J. Lerch *et al.*, NASA Technical Note TN-D-5036, 1969.
(4) J. Lerch *et al.*, NASA Document X-552-68-101, 1968.
(5) J. Marsh and C. Doll, NASA Technical Note TN-D-5337, 1970.
(6) R. Agreen and J. Marsh, NASA Document X-552-69-539, 1969.
(7) J. Berbert, NASA Document X-514-67-315, 1967.
(8) NASA Document X-514-66-513, 1966.
(9) Leital and Brocks, *C-Band Radar Range Measurements: An Assessment of Accuracy*, 1969.

Notation

The symbols in this list are the ones most frequently used by the contributors to this volume. Some deviations from this symbolism do occur. The symbolism of chapter 9 is so different from that of convention and the rest of the volume that it cannot conveniently be covered in this list.

a	Semi-major axis of orbit; semi-major axis of spheroid
a_z	Pseudo-azimuth (APL)
A_z	Azimuth
a,b,c	Constants
A	Area
A,B,C,D	Constants
b	Semi-minor axis of orbit; semi-minor axis of spheroid
c	Velocity of light
c_x,c_y	Scale factors (NGS)
C	Constant of annual aberration
C_D	Drag coefficient
C_n^m,C_{nm}	Coefficient of cosine term of nth degree, mth order, associated Legendre polynomial
d	Distance
D	Constant of annual aberration
e	Eccentricity of orbit or Earth; base of natural logarithms; charge on electron; humidity, partial pressure
e (subscript)	Earth
e_z	Pseudo-elevation (APL)
E	Eccentric anomaly
E_l	Elevation
f	Frequency; focal length; true anomaly; function; flattening
g	Gravity
G	Gravitational constant
GM	Gravitational constant times mass (of Earth)
h	Height above spheroid; local hour angle (ACIC)
H	Height above geoid; height above mean sea level
$\hat{H},\hat{L},\hat{Z}$	Coordinate system (APL)
i	$\sqrt{-1}$; inclination of plane of orbit
i,j,k,l,m,n	Indices
I	Inclination of orbital plane (SAO)

J	Joules; solar radiation constant (JPL) $=1.3525\times10^{3}\ W/m^{2}$
J_n	Bessel function of degree n; $-C_n$ (SAO, ch. 4)
k	Constant (APL); aberration constant $=2''.496$
l_x,l_y	Measured values of x and y (NGS)
l,m,n	Constants; indices; direction cosines
m	Mass of electron; mass of satellite
M	Mean anomaly; mass of Earth
n	Index of refraction
N_d	Refractivity of "dry" atmosphere
N_e	Number of electrons per unit volume
N_n^m	Normalization factor $\sqrt{\frac{(n-m)\,!\,(2n+1)\,!\,(\delta-2)}{(n+m)\,!}}$
N_g	Noise term for gth signal
N_w	Refractivity of "wet" atmosphere
$o(\ )$	Is of a smaller order of magnitude than ( )
$O(\ )$	Of the same order of magnitude as ( )
$P_\odot$	Solar radiation pressure in vicinity of Earth $=4.5\times10^{-6}$ kg-m/sec^2/m^2
P_s	Pressure at surface (APL)
P	Matrix of probabilities (NGS)
P_n^m	nth degree, mth order associated Legendre polynomial
q	Index of satellite signal (APL)
r_{ij}	Elements of rotation matrix (NGS)
r_s	Refraction of light from satellite (NGS)
r_∞	Atmospheric refraction (NGS)
R	Radius of Earth; refraction; perturbation; rotation matrix; gas constant 8.3143 J °K^{-1} mol^{-1}
s	RT_0/r (NGS); distance; surface
$\hat{S},\hat{L},\hat{C}$	Coordinate system (APL)
S_n^m, S_{nm}	Coefficient of sine term of nth degree, mth order associated Legendre polynomial
t	Time; temperature
T	Time; temperature (absolute or Kelvin)
v	Residual; velocity
$\mathbf{v}$	Vector of residuals
V	Radial velocity of star (NGS); gravitational potential
W	P/T_0; geodetic parameter $\equiv\sqrt{1-e^2\ \sin^{-2}\phi}$; geopotential; weight matrix
W	Weight matrix
$\mathbf{x}_{oo}$	Heliocentric coordinate of star at epoch o, equinox o (NGS)
x,y,z	Coordinates in rectangular, Cartesian coordinate system
α	Lapse-rate (APL; Hopfield); right ascension
α,β,γ	Angles

δ	Declination, increment
δ	Kronecker delta: $\delta_{ij}=1$ if $i=j$; $\delta_{ij}=0$ if $i\neq j$
ΔR	Radial distortion (NGS)
ΔT_o	Decentering distortion (NGS)
ϵ	Obliquity of the ecliptic; skew error in comparator (NGS)
ζ	Deflection of the vertical; (total) zenith distance
ζ,θ,Z	Newcombe's angles of rotation for precession and nutation
λ	Longitude on Earth; wavelength
Λ_G	Right ascension of Greenwich
μ	Subscript (APL); $\frac{g}{R\alpha}-1$
μ^x	Proper motion (NGS)
μ_α,μ_δ	Proper motion in right ascension (declination) (NGS)
ν	True anomaly
ν,ω,κ	Inner-orientation angles (NGS)
ξ,η	Deflection of vertical components; reduced coordinates of photographic image
π	Stellar parallax (NGS)
ρ	Density; distance ratio; range (APL)
σ	Standard deviation; surface
Σ	Covariance matrix
τ	Time
ϕ	Geodetic latitude
ϕ'	Geocentric latitude
ψ	Geocentric latitude
χ,μ,ν	Direction cosines (ACIC)
ω	Argument of perigee; rotation rate; Earth's rotation rate
$\odot$ (subscript)	Sun; solar
$\leftmoon$ (subscript)	Moon; lunar
$\oplus$ (subscript)	Earth; terrestrial
Ω	Longitude of the node
Υ	First point of Aries
$\approx$	Is approximately
$\equiv$	Is defined to be; is identical with
$=$	Is equal to
$<$	Is less than
$\leq$	Is less than or equal to
$>$	Is greater than
$\geq$	Is greater than or equal to
$\{\ \}$	The set of all elements (within the braces)
$\langle\ \rangle$	Average or expected value

References

AARDOOM, L., Some transformation properties for the coefficients in a spherical harmonic expansion of the Earth's external gravitational potential, *Tellus*, **21** (4), 572–584, 1969.

AARDOOM, L., A. GIRNIUS, AND G. VEIS, *Determination of the Absolute Space Directions Between Baker-Nunn Camera Stations*, Spec. Rep. 186, 29 pp., Smithsonian Astrophysical Observatory, Cambridge, Mass., 1965.

AARDOOM, L., A. GIRNIUS, AND G. VEIS, *Geometric Methods, Geodetic Parameters for a 1966 Smithsonian Standard Earth*, Spec. Rep. 200, edited by C. A. Lundquist and G. Veis, Vol. I, pp. 63–75, Smithsonian Astrophysical Observatory, Cambridge, Mass., 1966.

ABBY, D. G., AND M. S. TAVENNER, Definition of the refraction and shimmer problem affecting geodetic observations of satellites, *Österr. Z. Vermess.*, **25**, 269–281, 1967.

ABELE, M. K., A three-axis automatic photographic camera for satellite tracking, in *SAO Publ.*, edited by S. W. Kellogg, pp. 65–73, Smithsonian Astrophysical Observatory, Cambridge, Mass., 1962.

ABRAMOWITZ, M., AND I. STEGUN (EDS.), *Handbook of Mathematical Functions*, 9th printing, pp. 7–8, Government Printing Office, Washington, D.C., 1971.

ADAMS, L. H., Geodesy, *Eos Trans. Am. Geophys. Union*, **41** (2), 133, 1960.

AERONAUTICAL CHART AND INFORMATION CENTER, *1°×1° Mean Free-air Gravity Anomalies*, ACIC Ref. Publ. 29, 324 pp., August 1971.

AIRY, G. V., On the computation of the effect of the attraction of mountain masses as disturbing the apparent astronomical latitudue of stations in geodetic surveys, *Phil. Trans.*, **145**, 101–104, 1855.

AITCHISON, G., AND K. WEEKS, Some deductions of ionospheric information from the observations of emissions from satellite 1957 α2, *J. Atmos. Terrest. Phys.*, **14**, 236–243, 1959.

AKIM, E. L., ET AL., Refinements of the masses of the Earth and the Moon from observations of the motion of the automatic interplanetary stations Venera 4, Venera 5, Venera 6, and Venera 7 as they departed from Earth, *Soviet Phys. Doklady*, **16**, 1972.

AKSNES, K., A second-order artificial satellite theory based on an intermediate orbit, *Astron. J.*, **75**, 1066–1076, 1970.

AKSNES, L., A note on the relationship and agreement between two satellite theories, in *SAO ISAGEX Experience*, 1, Data Acquisition, E. M. Gaposchkin, ed., pp. 139–143, Smithsonian Astrophysical Observatory, Cambridge, Mass., 1972.

ALLAN, R. R., On the drift of SYNCOM 2 and the value of $J_{2,2}$, *Planet. Space Sci.*, **12**, 283–285, 1964.

ALLAN, R. R., On the motion of nearly synchronous satellites, *Proc. Roy. Soc.* (London), Sect. A, **288**, 60–68, 1965.

ALLAN, R. R., Satellite resonance with longitude-dependent gravity effects involving the eccentricity, *Planet. Space Sci.*, **15**, 1825, 1967.

ALTMAN, J. H., AND R. C. BALL, On the spatial stability of photographic plates, *Phot. Sci. Eng.*, **15** (5), 1961.

American Ephemeris and Nautical Almanac, U.S. Government Printing Office, Washington, D. C.

ANDERLE, R. J., Accuracy of the determination of gravity parameters and geocentric station coordinates on the basis of observations of artificial satellites, in *Use of Artificial Satellites for Geodesy*, edited by G. Veis, pp. 242–254, North Holland, Amsterdam, 1963.

ANDERLE, R. J., Observations of resonance effects on satellite orbits arising from the thirteenth- and fourteenth-order tesseral gravitational coefficients, *J. Geophys. Res.*, **70** (19), 2453 2458, 1965a.

ANDERLE, R. J., Use of Doppler observations on satellites, in *Record of the 1965 International Space Electronics Symposium*, IEEE, New York, 1965b.

ANDERLE, R. J., Computational methods employed with Doppler observations and derivations of geodetic results, in *Trajectories of Artificial Celestial Bodies as Determined by Observations*, edited by J. Kovalevsky, Springer-Verlag, New York, 1965c.

ANDERLE, R. J., Determination of the Earth's geoid by satellite observations, in *Mantles of the Earth and Terrestrial Planets*, edited by S. K. Runcorn, John Wiley, New York, 1967a.

ANDERLE, R. J., Geodetic parameter set NWL–SE–6 based on Doppler satellite observations, in *Use of Artificial Satellites for Geodesy*, edited by G. Veis, pp. 179–220, National Technical University, Athens, 1967b.

ANDERLE, R. J., Determination of polar motion from satellite observations, *Geophys. Surv.*, **1** (2), 147–161, 1973.

ANDERLE, R. J., Transformation of terrestrial survey data to Doppler satellite datum, *J. Geophys. Res.*, **79**(35), 5319–5331, 1974.

ANDERLE, R., AND L. BEUGLASS, Doppler satellite observations of polar motion, *Bull. Geod.*, **96**, 126–142, 1970.

ANDERLE, R. J., AND S. V. SMITH, Observations of twenty-seventh and twenty-eighth order gravity coefficients based on Doppler observations, *J. Astronaut. Sci.*, **15**(1), 1–4, 1968.

ANDERLE, R. J., C. A. MALYEVAC, AND H. L. GREEN, JR., Effect of neglected gravity coefficients on computed satellite orbits and geodetic parameters, *J. Spacecraft Rockets*, **6**(8), 951–954, 1969.

ANDERSON, J. D., AND D. E. HILT, Improvement of astronomical constants and ephemerides from Pioneer radio tracking data, *AIAA J.*, **7**, 1048–1054, 1969.

ANDERSON, P. H., C. G. LEHR, L. A. MAESTRE, H. W. HALSEY, AND G. L. SNYDER, Two-way transmission of a ruby-laser beam between Earth and a refracting satellite, *Proc. IEEE*, **54**, 426–427, 1966.

ANDERSON, T. W., *Introduction to Multivariate Analysis*, 172 pp., John Wiley, New York, 1958.

ANDOYER, H., Contribution à la théorie des petites planètes dout le moyen mouvement est sensiblement double de celiu de Jupiter, *Bull. Astron.*, **20**, 321–356, 1903.

ANON., Notations internationales relatives aux nivellements, *Bull. Geod.*, **18**, 474–477, 1950.

ANON., Resolutions internationales relatives aux nivellements de precision, *Bull. Geod.*, **18**, 479–492, 1950.

ANON., Basic regulations for the state geodetic network of the KNR, *Tsekhubey Tunbao* **1959** (15), 1959.

ANON., Geodetic operations, *Eos Trans. Am. Geophys. Union*, **44**(2), 307–325, 1963.

ANON., Comparative characteristics of atomic frequency standards, *Varian Frequency Control Bull.*, **3**, 1–4, 1966.

ANON., Geodetic operations, *Eos Trans. Am. Geophys. Union*, **48**(2), 366–387, 1967.

ANON., *NASA Directory of Observation-Station Locations* (2nd edition), Goddard Space Flight Center, Greenbelt, Md., 1971 (2 vols. with supplements, 1972/1973).

APPLETON, E. V., Influence of the Earth's magnetic field on wireless transmission, *URSI Proc.*, 1927.

ARD, E., Das Satellitenbeobachtungnetz der östlichen Hemisphäre, *Weltraumfahrt*, **14**, 18, 1963.

ARLEY, N., AND K. R. BUCH, *Introduction to the Theory of Probability and Statistics*, 236 pp., John Wiley, New York, 1950.

ARNOLD, K., Die Bewegung der Knotenlinie einer Satellitenbahnebene auf Grund der Schwereanomalien, *Gerlands Beitr. Geophys.*, **68**, 193–203, 1959.

ARNOLD, K., Die Präzessionabewegung der Erde und der Bahn der künstlichen Erdsatelliten, die Abplattung der Erde und die Dichtverteilung im Erdinnern, *Gerlands Beitr. Geophys.*, **69**, 191–199, 1960.

ARNOLD, K., *Die Freiluftanomalien im Europäischen Bereich*, Akademie-Verlag, Berlin, 1964.

ARNOLD, K., Die Bahnen der künstlichen Erdsatellitan in ihrer Arhängigkeit von der Schwereanomalien, *Veröff 27*, Geod. Inst., Potsdam, Germany, 1965.

ARNOLD, K., Eine Zusatzbedingung bei der Bestimmung des Potentialfelder der Erde aus Satellitenbeobachtungen, *Gerlands Beitr. Geophys.*, **76**, 18–20, 1967.

ARNOLD, K., Attempt to determine the unknown parts of the Earth's gravity field by successive satellite passages, *Bull. Geod.*, **87**, 97–102, 1968.

ARNOLD, K., AND D. SCHOEPS, Zur Genauigkeit von Verfahren der Satellitengeodesie, *Gerlands Beitr. Geophys.*, **73**(4), 193–198, 1964.

ARUR, M. G., *Analysis of Latitude Observations for Crustal Movements*, Rep. 139, Department of Geodetic Science, Ohio State University, Columbus, Ohio, 1970.

AUDOIN, C., State of the art in the field of very stable frequency generators, *Onde Elec.*, **53**(2), 39–45, 1973.

BAARDA, W., *Precision, Accuracy and Reliability of Observations*, 61 pp., Delft Geodetic Institute, Delft, 1960.

BAARDA, W., *Statistical Concepts in Geodesy*, Delft Geodetic Institute, Delft, 1967.

BAARDA, W., AND J. ALBERDA, Connection of geodetic adjustment procedures with methods of mathematical statistics, *Bull. Geod.*, **66**, 325–345, 1962.

BAILIE, A., AND R. BRYANT, Osculating elements derived from the modified Hansen theory for the motion of an artificial satellite, *Astron. J.*, **65**, 451–453, 1960.

BAKER, R. M. L., JR., Radiation on a satellite in the presence of partly diffuse and partly specular reflecting body, in *Trajectories of Artificial Celestial Bodies*, edited by J. Kovalevsky, pp. 85–150, Springer-Verlag, New York, 1966.

BALMINO, G., K. LAMBECK, AND W. KAULA, Spherical harmonic analysis of the Earth's topography, *J. Geophys. Res.*, **78**(2), 478–481, 1973.

BANACHIEWICZ, TH., Die polnische Sonnenfinsternisexpedition 1927, *Compt. Rendus Commun. Geod. Baltique* **1928**, 161–164, 1928.

BARLIER, F., Determination des elements instantanes d'un satellite artificiel à partir de l'observation d'un passage, *Space Res.*, **2**, 83–90, 1961.

BARRAR, R. B., Convergence of the von Zeipel procedure, *Celestial Mech.*, **2**, 494–504, 1970.

BARRELL, H., AND J. E. SEARS, Refraction and dispersion of air for the visible spectrum, *Phil. Trans. Roy. Soc. London*, Sec. A, **238**, 1–19, 1939.

BART, C., ET AL., Interferometer experiments with independent local oscillators, *Science*, **151**, 189–191, 1967.

BARTON, D. L., *Radar System Analysis*, 608 pp., Prentice-Hall, Englewood Cliffs, N.J., 1964.

BAŻAŃSKI, S., The problem of motion, in *Recent Developments in General Relativity*, pp. 13–29, Pergamon, New York, 1962.

BEAN, B. R., Atmospheric bending of radio waves, in *Electromagnetic Wave Propagation*, edited by M. Desirant and J. Michiels, Academic Press, New York, 1960.

BEAN, B. R., AND E. J. DUTTON, CRPL, *Exponential Reference Atmosphere*, U.S. Nat. Bureau Stand. Monogr. 4, Superintendent of Documents, Washington, D.C., 1959.

BEAN, B. R., AND G. D. THAYER, Models of the atmospheric radio-refractive index, *Proc. IRE*, **47** (5), 740–755, 1959.

BEEHLER, R. E., Historical review of atomic frequency standards, *Proc. IRE*, **55**(6), 792–805, 1967.

BELROSE, J., AND R. BURKE, Study of the lower ionosphere using partial reflection, 1, Experimental technique and method of analysis, *J. Geophys. Res.*, **69**(13), 2799–2818, 1964.

BELROSE, J. S., AND L. W. HEWITT, Study of the lower ionosphere using partial reflections, 2, The normal *D*-region, *Nature*, **202**(4929), 267, 1964.

BEN-MENAHEM, A., AND M. ISRAEL, Effects of major seismic events on the rotation of the Earth, *Geophys. J. Roy. Astron. Soc.*, **19**, 367–393, 1970.

BENNETT, J. M., Method for determining comparator screw errors with precision, *J. Opt. Soc. Am.*, **51** (10), 1133–1138, 1961.

BERBERT, J. H., Effect of tracking accuracy requirements on design of MINITRACK satellite tracking systems, *IRE Trans. Instrum.*, **I-9**, 84–88, 1961.

BERBERT, J. H., J. D. OOSTERHOUT, P. D. ENGELS, AND E. J. HABIB, MINITRACK calibration system, *Phot. Sci. Eng.*, **7**(7), 78–83, 1963.

BERGER, X., AND Y. BOUDON, Theorie analytique programmee de l'influence gravitationelle de la lune et du soleil dans le mouvement des satellites artificiels, *Bull. Groupe Rech. Geod. Spatiale*, **5**, 1–28, 1972.

BERKOWITZ, R. S., *Modern Radar*, John Wiley, New York, 1965.

BERMAN, A. L., A new tropospheric range refraction model, *Space Programs Summary 37–65*, Vol. II, Jet Propulsion Laboratory, Pasadena, Calif., September 1970.

BESSEL, F. W., *Tabulae Regiomontonae Reductionem*, 538 pp., Black and Young, London, 1830.

BEUGLASS, L. R., AND R. J. ANDERLE, Refined Doppler satellite determinations of the Earth's polar motion, in *Use of Artificial Satellites for Geodesy*, Geophysics Monograph 15, edited by S. Henriksen, A. Mancini, and B. Chovitz, pp. 181–187, American Geophysical Union, Washington, D.C., 1972.

BIALAS, V., Ausgleichung der Satellitenspur, in *Münchner Beiträge zur Satellitengeodesie*, edited by M. Kneissl, pp. 1–12, Bayerischen Akademie der Wissenschaften, München, 1967.

BJERHAMMAR, A., Rectangular reciprocal matrices with special reference to geodetic calculations, *Bull. Geod.*, **20**, 188–220, 1951.

BJERHAMMAR, A., General method for explicit determination of the shape of the Earth from gravimetric data, *Bull. Geod.*, **65**, 215–220, 1962.

BJERHAMMAR, A., *Theory of Errors With Generalized Matrix Inverses*, 420 pp., Elsevier, New York, 1973.

BLACKWELL, W. H., Adjustment of the Blue Nile geodetic control project, *J. Geophys. Res.*, **67**(11), 4421–4425, 1962.

BLAHA, G., *Inner Adjustment Constraints With Emphasis on Range Observations*, Rep. 148, 85 pp., Department of Geodesy, Ohio State University, Columbus, 1971a.

BLAHA, G., *Investigations of Critical Configurations for Fundamental Range Networks*, Rep. 150, Department of Geodetic Science, Ohio State University, Columbus, 1971b.

BLANK, S. J., AND L. H. SACKS, Phasing-grids solve polarization problems, *Microwaves*, **1965** (Oct.), 26–30, 1965.

BLISS, G. A., *Lectures in the Calculus of Variations*, 283 pp., University of Chicago Press, Chicago, Ill., 1946.

BLITZER, J., Lunar-solar perturbations of an Earth satellite, *Am. J. Phys.*, **27**, 634–645, 1959.

BLITZER, L., Equilibrium position and stability of 24-hour satellite orbits, *J. Geophys. Res.*, **70**(16), 3987–3992, 1965.

BLITZER, L., E. M. BOUGHTON, G. KANG, AND R. M. PAGE, Effect of the ellipicity of the equator on 24-hour nearly circular orbits, *J. Geophys. Res.*, **67** (1), 329–335, 1962.

BODEMULLER, H., Measurement and geodetic evaluation of vertical gradients of gravity, *Bull. Geod.*, **69**, 261–279, 1963.

BOHLER, W., Systematic errors in BC-4 observations, *Mitt. Geod. Inst. Tech. Hochsch. Graz*, **11**(1), 239–241, 1972.

BOMFORD, G., *Readjustment of the Indian Triangulation*, Prof. Pap. 28, Survey of India, 1938.

BOMFORD, G., Determination of the European geoid by means of deviations of the vertical, *Bull. Geod.*, **42**, 44–50, 1956.

BOMFORD, G., The junction of the Indian and European triangulation systems, *Bull. Geod.*, **56**, 177–190, 1960.

BOMFORD, G., *Geodesy*, 2nd ed., 561 pp., Clarendon Press, Oxford, England, 1962.

BOMFORD, G., *Geodesy*, Oxford University Press, London, 1971a.

BOMFORD, G., *The Australian Astrogeodetic Geoid*, Department of Natural Development, Canberra, 1971b.

BOMFORD, G., The astrogeodetic geoid in Europe and connected areas 1971, *Trav. Ass. Internat. Geod.* (Moscow), **24**, 357–372, 1972.

BOSS, B., *General Catalog of 33,342 Stars for the Epoch 1950*, Carnegie Institute, Wash., D.C., 1936.

BOSSLER, J. D., *The SAO Star Catalog—Its Qualitative and Quantitative Value to the C & GS Satellite Triangulation Program*, U.S. Coast and Geodetic Survey, Rockville, Md., 1966.

BOWEN, I. S., Schmidt cameras, in *Telescopes*, edited by G. Kuiper and B. Middlehurst, pp. 43–61, University of Chicago Press, Chicago, Ill., 1960.

BOWKER, D. E., *PAGEOS Project*, NASA TM–X–1344, 98 pp., National Technical Information Service, Springfield, Va., 1967.

BOYARSKI, E. A., Treatment of observations having non-normal error distribution (the best linear estimates for triangulation), *Can. Surv.* **24**(2), 207–214, 1970.

BOYKO, YE. G., B. M. KLENITSKY, I. M. LANDIS, AND G. A. USTINOV, *Plotting, Adjustments, and Estimation of the Accuracy of Space Geodetic Networks*, translated from the Russian, 309 pp., National Technical Information Service, Springfield, Va., 1973.

BRAATEN, N. F., Orthometric, dynamics, and barometric heights, in *Contemporary Geodesy*, Geophys. Monogr. 4, edited by C. Whitten and K. Drummond, pp. 36–39, American Geophysical Union, Washington, D. C., 1959.

BRAATEN, N. F., P. DORE, T. KUKKUMAKI, G. A. RUNE, AND J. VIGNAL, Note sur l'evaluation de la precision d'un nivellement, in French and English, *Bull. Geod.*, **18**, 493–548, 1950.

BRANDENBERGER, J., The use of Baker-Nunn cameras for tracking of artificial Earth satellites, *Photogramm. Eng.*, **28**, 727–735, 1962.

BRANDSTATTER, G., Accuracy of astronomical star-coordinates, *Oesterr. Z. Vermess.*, **56**(4), 153–154, 1968.

BRANDSTATTER, G., Theorie und Praktische durch Führung eines Programmes zur auswertung photographischer Satellitenbeobacktungen, *Mitt. Geod. Tech. Inst. Hochsch. Graz*, **1971**(9), 97–121, 1971.

BRANS, C., AND R. H. DICKE, Mach's principle and a relativistic theory of gravitation, *Phys. Rev.*, **124**, 925–935, 1961.

BRIXNER, B., Automatic lens design illustrated by a 600-mm f/2, 24°-field lens, *J. Soc. Motion Pict. Telev. Engrs.*, **73**(8), 654–658, 1964.

BROUCKE, R., Construction of rational and negative powers of a formal series, *Commun. Ass. Comput. Mach.*, **14**(1), 32–35, 1971.

BROUWER, D., The motion of a particle with negligible mass under the gravitational attraction of a spheroid, *Astron. J.*, **51**, 223–231, 1946.

BROUWER, D., Outline of general theories of the Hill-Brown and Delauney types for orbits of artificial satellites, *Astron. J.*, **63**, 433–438, 1958.

BROUWER, D., Solution of the problem of artificial satellite theory without drag, *Astron. J.*, **64**, 378–397, 1959.

BROUWER, D., Analytic study of resonance caused by solar radiation pressure, in *Dynamics of Satellite Orbits*, edited by M. Roy, pp. 34–39, Springer-Verlag, Berlin, 1963.

BROUWER, D., AND G. M. CLEMENCE, *Methods of Celestial Mechanics*, Academic, New York, 1961.

BROUWER, D., AND G. I. HORI, Theoretical evaluation of atmospheric drag effects in the motion of an artificial satellite, *Astron. J.*, **66**, 193–225, 1961.

BROWN, D. C., Notes on the reduction of stellar plates for determination of directions of flashing light beacons, in *The Use of Artificial Satellites for Geodesy*, edited by G. Veis, pp. 163–186, North Holland, Amsterdam, 1963.

BROWN, D. C., Decentering distortion of lenses, *Photogram. Eng.*, **32**(3), 444–462, 1966.

BROWN, R. H., AND R. Q. TWISS, A new type of interferometer for use in radio astronomy, *Phil. Mag.*, **45**, 663–682, 1954.

BROWN, R. H., AND R. Q. TWISS, Correlation between photons in two coherent beams of light, *Nature*, **177**(4497), 27–29, 1956.

BROWN, R. H., AND R. Q. TWISS, Interferometry of the intensity fluctuations in light, *Proc. Roy. Soc.* (London), Sect. A, **242**, 300, 1957.

BRUNS, H., *Die Figur der Erde-Ein Beitrag zur Europäischen Gradmessung*, Veröff. Preuss. Geod. Inst. Berlin, 1878.

BRYANT, R., Comparison of theory and observation of the ECHO–1 satellite, *J. Geophys. Res.*, **66**, 3066–3069, 1961.

BRYANT, R. W., The effect of solar radiation pressure on the motion of an artificial satellite, *Astron. J.*, **66**(8), 1961.

BUCHAR, E., Motion of the nodal line of the second Russian Earth satellite and the flattening of the Earth, *Nature*, **182**, 198–199, 1958.

BUCHAR, E., Determination of some parameters of the gravity field of the Earth from the rotation of the nodal line of artificial satellites, *Bull. Geod.*, **65**, 269–271, 1962.

BUCK, R., AND J. TANNER, Storage and retrieval of gravity data, *Bull. Geod.*, **103**, 63–84, 1972.

BUCKINGHAM, R. A., *Numerical Methods*, 605 pp., Pitman, London, 1966.

BULLARD, E. C., The figure of the Earth, *Mon. Notic. Roy. Astron. Soc., Geophys. Suppl.* **5**, 186–192, 1948.

BURSA, M., Determination des parameteres de l'ellipsoide de reference covenant aux reseaux geodesiques europeans d'apres les donnees astrogeodesiques du catalogue de l'A.I.G., *Bull. Geod.*, **68**, 139–143, 1963.

BURSA, M., Fundamentals of the theory of geometric satellite geodesy, *Geofys. Sbornik*, **1966** (241), 25–50, 1966.

BURSA, M., Zur derzeitigen Stand der Satellitengeodäsie, *Allg. Vermess.*, **1970**(4), 134–142, 1970.

BUTLER, C., AND H. RICHTER, JR., *Amateur Microlock Handbook*, 62 pp., San Gabriel Valley Radio Club, San Gabriel, Calif., 1959.

CAIN, B. J., Determination of mean elements for Brouwer's satellite theory, *Astron. J.*, **67**, 391–392, 1962.

CAPUTO, M., Gravity in space and the dimensions and mass of the Earth, *J. Geophys. Res.*, **68**(15), 4595–4600, 1963.

CAPUTO, M., Minimum strength of the Earth, *J. Geophys. Res.*, **70**, 955–963, 1965.

CARLTON, A. G., *Linear Estimation in Stochastic Processes*, Bumblebee Ser. Rep. 34, Applied Physics Laboratory, Johns Hopkins University, Silver Spring, Md., 1962.

CARLYLE, R., AND B. GILLETT, Romberg integration, *Oil Gas J.*, **68**(41), 81–84, 1970.

CARRU, H., R. GENDRIN, AND M. REYSSAY, La refraction ionospherique pour les frequences de 20, 40, 108 MHz et son application a l'effect Doppler des satellites, *Space Res.*, **1**, 286–303, 1960.

CARTWRIGHT, D. E., AND J. CREASE, Comparison of the geodetic reference levels of England and France by means of the sea surface, *Proc. Roy. Soc.* (London), Sect. A, **273**, 558–580, 1963.

CAYLEY, A., Tables of the developments of functions in the theory of elliptic motion, *Mem. Roy. Astron. Soc.*, **29**, 191–306, 1961.

CAZENAVE, A., O. DARGNIES, G. BALMINO, AND M. LEFEBVRE, Geometrical adjustment with simultaneous laser and photographic observations for the European datum, in *Use of Artificial Satellites for Geodesy*, Geophys. Monogr. 15, edited by S. Henriksen, A. Mancini, and B. Chovitz, pp. 43–48, American Geophysical Union, Washington, D.C., 1972a.

CAZENAVE, A., F. FORESTIER, F. NOVEL, AND J. PIEPLU, Improvement of zonal harmonics using observations of low-inclination satellites Dial, SAS, and Peole, in *Use of Artificial Satellites for Geodesy*, Geophys. Monogr. 15, edited by S. Henriksen, A. Mancini, and B. Chovitz, pp. 145–150, American Geophysical Union, Washington, D.C., 1972b.

CEBEY, L. G., Tracking in space by Doploc, IRE *Trans. Mil. Electron.*, **MIL**(4), 332–335, 1960.

CECCHINI, G., Le variazioni di latitudini e il movimento del polo di rotazione terrestre . . . 1949–1950, *Bull. Geod.*, **21**, 275–297, 1951.

CECCHINI, G., Sulla eventuale riorganizzavione del servizio internationale delle latitudini, *Bull. Geod.*, **59**, 23–25, 1961.

CHALLE, A., AND J. LACLAVERIE, Fonction perturbatrice et representation analytique du mouvement d'un satellite, *Astron. Astrophys.*, **3**, 15, 1969.

CHANDLER, K. N., On the effects of small errors in the angles of corner-cube reflectors, *J. Opt. Soc. Amer.*, **50**(3), 203–206, 1960.

CHANG, R. F., ET AL., Far-field diffraction pattern for corner reflectors with complete reflection coefficients, *J. Opt. Soc. Am.*, **61**(4), 431–438, 1971.

CHAO, C. C., *New Tropospheric Range Corrections With Signal Adjustment*, TR–32–1526, Vol. VI, Jet Propulsion Laboratory, Pasadena, Calif., December 15, 1971.

CHAPRONT-TOUZE, M., Determination locale des anomalies de gravité et hauteur du geoide a l'aide d'observations de satellites artificielle, *Bull. Geod.*, **103**, 47–62, 1972.

CHASSAING, J. P., Campagne Diademe resultats obtenus en geodesie semidynamique a l'aide de mesures Doppler, *Bull. Geod.*, **94**, 403–413, 1969.

CHEADLE, E. C., AND R. M. JEPPERSON, Time registration in cameras, *Phot. Sci. Eng.*, **7**, 137, 1963.

CHERNIACK, J. R., *Computation of Hansen Coefficients*, Spec. Rep. 346, 25 pp., Smithsonian Astrophysical Observatory, Cambridge, Mass., 1972.

CHERNIACK, J. R., A more general system for Poisson series manipulation, *Celestial Mech.*, **7**, 107–121, 1973.

CHERNIACK, J. R., AND E. M. GAPOSCHKIN, *Smithsonian Astrophysical Observatory Program Write-up (SCROGE)*, Spec. Rep. 121, 18 pp., Smithsonian Astrophysical Observatory, Cambridge, Mass., 1963.

CHI, A. R., AND H. S. FOSQUE, *A Step in Time: Changes in Standard-Frequency and Time-Signal Broadcasts* Jan. 1, 1972, NASA TN–D–7065, 1973.

CHIN, P. B., *Attitude Motion and Stabilization of Spinning Satellites Under the Influence of the Earth's Gravitational Gradient Force*, Ph.D. dissertation, 131 pp., Ohio State University, Columbus, 1962.

CICHOWICZ, L., Quelques aspects du services d'observation des satellites artificiels et recherches scientifiques sur leur utilisation en geodesy en pologne, in *The Use of Artificial Satellites for Geodesy*, edited by G. Veis, pp. 145–157, North Holland, Amsterdam, 1963.

CLARKE, A. R., Note on Archdeacon Pratt's paper on the effect of local attractions in the English arc, *Phil. Trans. Roy. Soc. London*, **148**, 787–789, 1858.

CLEMENCE, G. M., Standards of time and frequency, *Science*, **123**, 567–573, 1956.

CLEMENCE, G. M., Astronomical reference systems, in *Basic Astronomical Data*, edited by K. A. Strand, chap. 1, University of Chicago Press, Chicago, Ill., 1963.

CLEMENCE, G. M., Inertial frames of reference, *Quart. J. Roy. Astron. Soc.*, **7**, 10–21, 1966.

COESA, U.S. COMMITTEE ON EXTENSIONS TO THE STANDARD ATMOSPHERE, *The U.S. Standard Atmosphere, 1962*, Superintendent of Documents, Washington, D.C., 1962.

COESA, U.S. COMMITTEE ON EXTENSIONS TO THE STANDARD ATMOSPHERE, *The U.S. Standard Atmosphere Supplements, 1966*, 285 pp., Superintendent of Documents, Washington, D.C., 1966.

COHEN, A. C., Estimating the mean and variance of normal populations from singly truncated and doubly truncated samples, *Ann. Math. Statist.*, **21**, 557–569, 1969.

COHEN, C. J., AND R. J. ANDERLE, Verification of Earth's pear-shaped gravitational harmonic, *Science*, **132**, 807–808, 1960.

COHEN, C. J., AND K. C. HUBBARD, A nonsingular set of orbit elements, *Astron. J.*, **67**, 10–15, 1962.

COHEN, M. H., ET AL., Radio interferometry of one-thousandth second of arc, *Science*, **162**, 91–92, 1966.

COLE, A. E., A. COURT, AND A. KANTOR, Model atmospheres, in *Handbook of Geophysics and Space Environment*, edited by S. Valley, McGraw-Hill, New York, 1965.

COLLATZ, L., *Numerical Treatment of Differential Equations*, 3rd ed., Springer-Verlag, Berlin, 1966.

CONRADY, A., Decentered lens systems, *Mon. Notic. Roy. Astron. Soc.*, **79**, 384–390, 1919.

CONTE, S. D., Computation of satellite orbit trajectories, *Advan. Comput.*, **3**, 1–76, 1962.

COOK, A. H., Calibration of gravity meters by comparison with pendulums, *Geophys. J. Roy. Astron. Soc.*, **1**(1), 1958.

COOK, A. H., External gravity field of a rotating spheroid to the order of e^3, *Geophys. J. Roy. Astron. Soc.*, **2**, 199–214, 1959.

COOK, A. H., Resonant orbits of artificial satellites, *Space Res.*, **1**, 476–480, 1960.

COOK, A. H., Resonant orbits of artificial satellites and longitude terms in the Earth's external gravitational potential, *Geophys. J. Roy. Astron. Soc.*, **4**, 53–72, 1961a.

COOK, A. H., Report on absolute measurements of gravity, *Bull. Geod.*, **60**, 131–140, 1961b.

COOK, A. H., Sources of harmonics of low order in the external gravity field of the Earth, *Nature*, **198**(4886), 1186, 1963.

COOK, A. H., *Motion of Artificial Satellites in the Gravitational Field of the Earth*, Mem. 18 (3rd ser.), 138 pp., Commissione Geodetica Italiana, Bologna, Italy, 1967.

COOK, G. E., Luni-solar perturbations of the orbit of an Earth satellite, *Geophys. J. Roy. Astron. Soc.*, **6**(3), 271–291, 1962.

COOK, G. E., Use of simplified orbital theory for satellites of large area-to-mass ratio, *Planet. Space Sci.*, **11**, 1289–1295, 1963a.

COOK, G. E., Perturbations of satellite orbits by tesseral harmonics in the Earth's gravitational potential, *Planet. Space Sci.*, **11**, 797–815, 1963b.

COOK, G. E., Satellite drag coefficients, *Planet. Space Sci.*, **13**, 929, 1965.

COOK, G. E., AND R. N. A. PLIMMER, The effect of atmospheric rotation on the orbital plane of a near-Earth satellite, *Proc. Roy. Soc.* (London), Sec. A, **258**, 516–528, 1960.

CRAMÉR, H., *Mathematical Methods of Statistics*, Princeton University Press, Princeton, New Jersey, 1946.

CSC, 1971–1973 (see ANON., 1971).

CUNNINGHAM, L. E., The motion of a nearby satellite with highly inclined orbit, *Astron. J.*, **62**, 12–13, 1957.

DAVIS, D. D., Frequency-standard hides in every color TV set, *Electronics*, **1971** (10 May), 96–98, 1971.

DAVIS, D. D., ET AL., Use of television signals for time- and frequency-dissemination, *Proc. IEEE*, **58**(6), 931–933, 1970.

DAVIS, R. J., W. A. DEUTSCHMAN, AND K. L. HARAMUNDANIS, *Celoscope Catalog of Ultraviolet Stellar Observations*, Smithsonian Institute Press, Cambridge, Mass., 1973.

DECKER, B. L., Present day accuracy of the Earth's gravity field (abstract), *Eos Trans. Am. Geophys. Union*, **53**(10), 891, 1972.

DE GRAAFF HUNTER, J., Use of Stokes's formula in geodesy, *Bull. Geod.*, **32**, 147–153, **1954.**

DE GRAAFF HUNTER, J., The shape of the Earth's surface expressed in terms of gravity at ground level, *Bull. Geod.*, **56**, 191–200, 1960.

DE JAGER, C., Satellite photography by means of small Schmidt cameras, *Space Res.*, **2**, 47–49, 1961.

DEKER, H., *Die Anwendung der Photogrammetrie in der Satellitengeodesie (Satellitenphotogrammetrie)*, Heft III, ser. C, Deutsches Geodätisches Kommission, München, 1967.

DEMARIA, A., D. STETSER, AND W. GLENN, JR., Ultrashort light pulses, *Science*, **156**(3782), 1557–1568, 1967.

DEMARIA, A., W. GLENN, JR., AND M. MACK, Ultrafast light pulses, *Phys. Today*, **1971**(7), 19–26, 1971.

DE MCRAES, A., Effects of the Earth's oblateness on the orbit of an artificial Earth satellite, *Ann. Acad. Sci. Brazil*, **30**, 465–510, 1958.

DE MENDOÇA, F., AND O. K. GARRIOFF, Effect of the Earth's magnetic field on measurements of the Doppler shift of satellite radio transmission, *J. Geophys. Res.*, **67**(5), 2062–2065, 1962.

DE MUNCK, J. G., Some information about accurate satellite tracking at Delft, in *Use of Artificial Satellites for Geodesy*, edited by G. Veis, pp. 21–28, Technical University, Athens, 1964.

DE SITTER, W., On the system of astronomical constants, *Bull. Astron. Inst. Neth.* **8**, 213–229, 1938.

DICKE, R. H., W. F. HOFFMAN, AND R. KROTKOV, Tracking and orbit requirements for experiment to detect variations in the gravitational constant, *Space Res.*, **2**, 287–291, 1961.

DIECKVOSS, W., Photographic proper motions, in *Basic Astronomical Data*, edited by K. A. Strand, chap. 4, University of Chicago Press, Chicago, Ill., 1963.

DIMITRIJEVICH, V., Equal-area subdivision of the Earth's surface suitable for developing a gravitational potential function to the 50th degree and order, paper presented at Fall Annual Meeting, American Geophysical Union, San Francisco, Calif., 1972.

DOBACZEWSKA, W., Compte rendu de la reunion de la sous-commission de la geodesie satellitaire pour l'Europe de l'Est, *Bull. Geod.*, **89**, 309–314, 1968.

DOBACZEWSKA, W., Geodetic uses of artificial satellites: East European Sub-Commission. *Trav. Ass. Internat. Geod.* (Moscow), **24**, 173–180, 1972.

DOD COORDINATING COMMITTEE FOR THE GEOCEIVER TEST PROGRAM, *Report of the DOD GEOCEIVER Test Program*, DMA Rep. 001, Defense Documentation Center, Alexandria, Va., 1972.

DOUGLAS, B. C., J. G. MARSH, AND N. E. MULLINS, Mean elements of GEOS–1 and GEOS–2, *Celestial Mech.*, **7**, 195–204, 1973.

DUBYAGO, A. D., *The Determination of Orbits* (translation), Macmillan, New York, 1961.

DUFOUR, H. M., Extension de la methode des moindre carres—Modification des resultats compenses par adjunction d'observations nouvelles—Etude des observations correlees, *Bull. Geod.*, **33**, 229–282, 1954.

DUFOUR, H. M., Etude de la compensation du reseau European dan l'optique de la geodesie tridimensionelle, *Bull. Geod.*, **68**, 171–199, 1963.

DUFOUR, H., Resolution des systems lineares par la methods des residues conjugues, *Bull. Geod.*, **71**, 65–88, 1964a.

DUFOUR, H., Choix de formule de la refraction atmospherique pour les observations par chambre ballistique, *Bull. Geod.*, **73**, 217–230, 1964b.

DUFOUR, H. M., Generation et applications des tableaux de variances des systeme de moindres carres, *Bull. Geod.*, **98**, 309–340, 1970.

DUPUY, M., La determination des dimensions de la terre pour le travaux geodesiques un URSS, *Bull. Geod.*, **31**, 55–66, 1953.

DYSON, J., Correction for atmospheric refraction in surveying and alignment, *Nature*, **216**, 782, 1967.

EASTON, R. L., The Mark II MINITRACK system, *Ann. IGY*, **6**, 384–410, 1958.

ECKER, E., *Sphärische integral formeln in der geodäsie*, Heft 142, ser. C, 54 pp., Deutsches Geodätische Kommission, München, 1969.

ECKERT, W. J., AND D. BROUWER, The use of rectangular coordinates in the differential correction of orbits, *Astron. J.*, **46**, 125–132, 1937.

EDLEN, B., The dispersion of standard air, *J. Opt. Soc. Am.*, **43**, 339–344, 1953.

EDLEN, B., Refractive index of air, *Metrologia*, **2**(2), 71, 1966.

EGYED, L., The satellite geoid and the structure of the earth, *Nature*, **203**(4940), 67–69, 1964.

EICHHORN, H., AND C. A. WILLIAMS, On the systematic accuracy of photographic astrometric data, *Astron. J.*, **68**(4), 221–231, 1963.

EICHHORN, H., ET AL., Accurate positions of 502 stars in the region of the Pleiades, *Mon. Notic. Roy. Astron. Soc.*, **73**, 125–156, 1970.

ESCALANGON, F., Sur l'avance du perigee dans l'orbit des satellites artificiels de la terre, *Bull. Soc. Belg. Astron.*, **226**, 23–25, 1959.

ESCOBAL, P. R., *Methods of Orbit Determination*, John Wiley, New York, 1965.

ESPOSITO, P. B., AND S. K. WONG, Geocentric gravitational model determined from Mariner 9 radio tracking data (abstract), *Eos Trans. Am. Geophys. Union*, **53**(10), 891, 1972.

ESSEN, L., Frequency and time standards, *Proc. IRE*, **50**(5), 1158–1164, 1962.

ESTES, R. H., *On the Analytic Lunar and Solar Perturbations of a Near-Earth Satellite*, NASA X–645–72–297, 32 pp., 1972.

EULER, I. A., Versuch die Figur der Erden durch Beobachtungen des Mondes zu Bestimmen, *Abh. Churfurst. Akad. Wiss.*, **5**, 198, 1768.

EWART, D. G., The effect of atmospheric drag on the orbit of a spherical Earth satellite, *J. Brit. Interplanet. Soc.*, **18**(7), 1962.

EWING, M., J. L. WORZEL, AND M. TALWANI, Some aspects of physical geodesy, in *Contemporary Geodesy*, Geophys. Monogr. 4., edited by C. Whitten and K. Drummond, 7–18, American Geophysical Union, Washington, D.C., 1959.

FADDEEV, D. K., AND V. N. FADDEEVA, *Computational Methods of Linear Algebra*, W. H. Freeman, San Francisco, Calif., 1963.

FALLER, J. E., Precision measurement of the acceleration of gravity, *Science*, **158**, 60–67, 1967.

FALLON, F., Star catalogue requirements for satellite geodesy, *Astron. J.*, **72**(5), 588–596, 1967.

FEDOROV, YE. D., *Nutation and Forced Motion of the Earth's Pole*, Macmillan, New York, 1963.

FEHLBERG, E., *New One-Step Integration Methods of High-Order Accuracy . . .*, NASA TR–R–240, 46 pp., Superintendent of Documents, Washington, D.C., 1966a.

FEHLBERG, E., New high-order Runge-Kutta formulas with an arbitrarily small truncation error, *Z. Angew. Math. Mech.*, **46**, 1–12, 1966b.

FEHLBERG, E., *Low-Order Classical Runge-Kutta Formulas With Step-Size Control . . .*, 43 pp., NASA TR-R-315, Superintendent of Documents, Washington, D.C., 1969.

FELSENTREGER, T. L., *On the Second-Order Solution of Artificial Satellite Theory Without Drag*, NASA TN-D-1752, Superintendent of Documents, Washington, D.C., 1964.

FELSENTREGER, T. L., Classification of lunar satellite orbits, *Planet. Space Sci.*, **16**, 285–295, 1966.

FELSENTREGER, T. L., *On the Perturbation of Small Eccentricity Satellites*, NASA TN-D-4521, Superintendent of Documents, Washington, D.C., 1968.

FISCHER, I., Deflection of the vertical in the western and central European area, *Bull. Geod.*, **34**, 343–354, 1954.

FISCHER, I., The rough ellipsoid or the figure of the Earth from geoidal heights, *Bull. Geod.*, **54**, 45–52, 1959.

FISCHER, I., Map of geoidal contours of North America, *Bull. Geod.*, **57**, 321–324, 1960.

FISCHER, I., Present extent of the astrogeodetic geoid and the geodetic world datum derived from it, *Bull. Geod.*, **61**, 245–264, 1961.

FISCHER, I., Parallax of the Moon in terms of a world geodetic system, *Astron. J.*, **67**, 373–378, 1962.

FISCHER, I., *Geoid Charts of North and Central America*, TR-62, Army Map Service, Washington, D.C., 1967.

FISCHER, I., Development of the South American Datum 1969, *Surv. Rev.*, **158**, 354–365, 1970.

FISCHER, I., AND M. SLUTSKY, Preliminary geoid chart of Australia, *Aust. Surv.*, **2**(8), 327–333, 1967.

FISCHER, I., ET AL., New pieces in the picture puzzle of an astrogeodetic geoid map of the world, *Bull. Geod.*, **88**, 199–222, 1968.

FLEIG, A. J., *On the Libration of a Gravity-Gradient-Stabilized Spacecraft in an Eccentric Orbit*, 125 pp., Superintendent of Documents, Washington, D.C., 1970.

FLIEGEL, H. F., A world wide organization to secure Earth-related parameters for deep space missions, TR-32-1526, Vol. V, pp. 66–73, Jet Propulsion Laboratory, Pasadena, Calif., October 15, 1971.

FRAZER, R., W. DUNCAN, AND A. COLLAR, *Elementary Matrices*, University Press, London, 1938.

FRICKE, W., AND A. KOPFF, *Introductory Remarks, in Fourth Fundamental Catalog (FK4)*, Publ. 10, Astronomische Rechens Institut, Heidelberg, 1963.

FRICKE, W., ET AL., Report to the executive committee of "Working Group on the System of Astronomical Constants," *Bull. Geod.*, **75**, 59–68, 1965.

FROST, A., AND H. PATINES, Long-base-line interferometer at Joddrell Bank, *Sky Telesc.*, **25**(7), 21–24, 1966.

GABBARD, T. P., Ephemeris time, *J. Astronaut. Sci.*, **7**, 33–38, 1960.

GAPOSCHKIN, E. M., *Differential Orbit Improvement (DOI-3)*, Spec. Rep. 161, 70 pp., Smithsonian Astrophysical Observatory, Cambridge, Mass., 1964.

GAPOSCHKIN, E. M., Orbit determination, in *Geodetic Parameters for a 1966 Smithsonian Institution Standard Earth*, Vol. I, edited by C. Lundquist and G. Veis, pp. 77–184, Smithsonian Astrophysical Observatory, Cambridge, Mass., 1966a.

GAPOSCHKIN, E. M., Review of the rotation of the Earth, in *Scientific Horizon from Satellite Tracking*, Spec. Rep. 236, edited by C. Lundquist and H. Friedman, pp. 145–192, Smithsonian Astrophysical Observatory, Cambridge, Mass., 1966b.

GAPOSCHKIN, E. M., Tesseral harmonic coefficients and station coordinates from the dynamic method, in *Geodetic Parameters for a 1966 Smithsonian Institution Standard Earth*, Vol. II, edited by C. Lundquist and G. Veis, pp. 105–259, Smithsonian Astrophysical Observatory, Cambridge, Mass., 1966c.

GAPOSCHKIN, E. M., A dynamical solution for the tesseral harmonics of the geopotential and station coordinates using Baker-Nunn data, *Space Res.*, **7**, 683–693, 1967.

GAPOSCHKIN, E. M., Improved values for the tesseral harmonics of the geopotential and station coordinates, in *Dynamics of Satellites 1969*, edited by B. Morando, pp. 109–118, Springer-Verlag, Berlin, 1970.

GAPOSCHKIN, E. M., *Empirical Data and the Variance-Covariance Matrix for the 1969 Smithsonian Standard Earth (II)*, Spec. Rep. 342, 60 pp., Smithsonian Astrophysical Observatory, Cambridge, Mass., 1972.

GAPOSCHKIN, E. M., *Satellite Dynamics, 1973 Smithsonian Standard Earth (III)*, edited by E. M. Gaposchkin, Spec. Rep. 353, part 3, Smithsonian Astrophysical Observatory, Cambridge, Mass., 1973.

GAPOSCHKIN, E. M., AND K. LAMBECK, *1969 Smithsonian Standard Earth (II)*, Rep. SR-315, Smithsonian Astrophysical Observatory, Cambridge, Mass., May 1970.

GAPOSCHKIN, E. M., AND K. LAMBECK, Earth's gravity field to the sixteenth degree and station coordinates from satellite and terrestrial data, *J. Geophys. Res.*, **76**, 4855–4883, 1971.

GAPOSCHKIN, E. M., Earth's gravity field to the eighteenth degree and geocentric coordinates for 104 stations from terrestrial and satellite data, *J. Geophys. Res.*, **79**(35), 5377–5411.

GARFINKEL, B., An investigation in the theory of astronomical refraction, *Astron. J.*, **50**, 169–174, 1944.

GARFINKEL, B., On the motion of a satellite of an oblate planet, *Astron. J.*, **63**, 88–96, 1958.

GARFINKEL, B., The orbit of a satellite of an oblate planet, *Astron. J.*, **64**, 353–367, 1959.

GARFINKEL, B., On the critical inclination for satellite orbits of any eccentricity (abstract), in *The Use of Artificial Satellites for Geodesy*, edited by G. Veis, p. 41, North Holland, Amsterdam, 1963.

GARFINKEL, B., Formal solution in the problem of small divisors, *Astron. J.*, **71**, 657–699, 1966.

GARFINKEL, B., Astronomic refraction in a polytropic atmosphere, *Astron. J.*, **72**(2), 235–254, 1967.

GEBEL, G., AND B. MATTHEWS, Navigation at the prime meridian, *Navigation*, **18**(2), 141–146, 1971.

GEDEON, G. S., B. C. DOUGLAS, AND M. T. PALMITER, Resonance effects on eccentric satellite orbits, *J. Astronaut. Sci.*, **14**(4), 147–157, 1967.

GEODETIC REPORTS FOR 1957 TO UGGI/IAG, Survey of India, Delhi, 1957.

GEYLING, F. T., Satellite perturbations from extraterrestrial gravitation and radiation pressure, *J. Franklin Inst.*, **269**, 375–407, 1960.

GIACAGLIA, G. E. O., *Lunar Perturbations on Artificial Satellites of the Earth*, Spec. Rep. 352, 59 pp., Smithsonian Astrophysical Observatory, Cambridge, Mass., 1973. (Also *J. Celestial Mech.*, in press, 1974.)

GIACAGLIA, G. E. O., ET AL., Semianalytic theory for the motion of a lunar satellite, *J. Celestial Mech.*, **3**, 3–66, 1970.

GILVARRY, J., Verification of general relativity by means of artificial planets, *Nature*, **183**(4662), 666–667, 1959.

GIRNIUS, A., AND W. L. JOUGHIN, *Optical Simultaneous Observations*, Spec. Rep. 266, Smithsonian Astrophysical Observatory, Cambridge, Mass., 1968.

GLIESE, W., *Right-Ascension System of the FK4*, Pbl. 12, Astronomisches Rechen-Institut, Heidelberg, 1963.

GOLDSTEIN, H., *Classical Mechanics*, 399 pp., Addison-Wesley, Cambridge, Mass., 1950.

GOLDSTEIN, S., Influence of the Earth's magnetic field on electric transmission in the upper atmosphere, *Proc. Roy. Soc.* (London), **121**(787), 260–285, 1928.

GORDON, H. J., ET AL., *The Mariner VI and VII Flight Paths and Their Determination From Tracking Data*, TM-33-469, p. 2–204, Jet Propulsion Laboratory, Pasadena, Calif., December 1970.

GREEN, C. M., AND M. LOMASK, *Vanguard—A History*, 308 pp., National Technical Information Service, Springfield, Va., 1970.

GRÖBNER, W., *Die Lie-Riehen und Ihre Anwendungen*, Deutscher Verlag d. Wissenschaft, Berlin, 1960.

GRONBERG, F. T., Design considerations for a satellite-borne flashing light, *Photo. Sci. Eng.*, **7**, 137, 1963.

GROSS, J. E., III, *Preprocessing Electronic Satellite Observations*, 188 pp., National Technical Information Service, Springfield, Va., 1970.

GROTEN, E., Uber die Genaugkeiten der Bestimmung des zonalen Anteils des Schwerepotentials aus Satellitenmessungen, *Allg. Vermess. Nachr.*, **1967**(8), 325–329, 1967.

GROTEN, E., Ein Vergleich von Gravimetermessungen mit Satellitenbeobachtungen, *Z. Geophys.*, **34**, 169–174, 1968.

GRUBBS, F. E., Sample criteria for testing outlying observations, *Ann. Math. Statis.*, **21**, 27–58, 1950.

GUIER, W. H., The tracking of satellites by Doppler methods, *Space Res.*, **1**, 481–491, 1960.

GUIER, W. H., Ionospheric contribution to the Doppler shift at VHF from near-Earth satellites, *Proc. IRE*, **49**(11), 1680–1681, 1961.

GUIER, W. H., Determination of the nonzonal harmonics of the geopotential from satellite Doppler data, *Nature*, **200**(4902), 124–125, 1963a.

GUIER, W. H., *Studies on Doppler Residuals, 1*, Rep. TG-503, 70 pp., Applied Physics Laboratory, Johns Hopkins University, Silver Spring, Md., 1963b.

GUIER, W. H., Geodetic problems and satellite orbits, in *Lectures in Applied Mathematics*, Vol. 6, *Space Mathematics II*, edited by J. B. Rossen, pp. 170–211, American Mathematical Society, Providence, R. I., 1966a.

GUIER, W. H., Satellite navigation using integral Doppler data: The AN/SRN-9 equipment, *J. Geophys. Res.*, **71**(24), 5903–5910, 1966b.

GUIER, W. H., Data and orbit analysis in support of the U.S. Navy satellite Doppler system, *Phil. Trans. Roy. Soc. London*, Ser. A, **262**(1124), 89–99, 1967.

GUIER, W. H., AND R. R. NEWTON, Earth's gravity field as deduced from the Doppler tracking of five satellites, *J. Geophys. Res.*, **70**(18), 4613–4626, 1965.

GUIER, W. H., AND G. C. WEIFFENBACH, Theoretical analysis of Doppler radio signals from Earth satellites, *Nature*, **181**, 1525–1526, 1958.

GUIER, W. H., AND G. C. WEIFFENBACH, A satellite Doppler navigation system, *Proc. IRE*, **48**(4), 507–516, 1960.

GUINOT, B., *Independent Local Atomic Time Scales AT(i)*, Circ. D-73, Bureau International de l'Heure, Paris, 1972.

GUINOT, B., AND N. FEISEL, *Annual Report 1968*, Bureau International de l'Heure, Paris, 1969.

HABIB, T., ET AL., *Development of a Range and Range-Rate Tracking System*, NASA TN-D-2093, Superintendent of Documents, Washington, D.C., 1964.

HAEFNER, R. R., Precise reduction of Baker-Nunn films at the Smithsonian Astrophysical Observatory, in *Use of Artificial Satellites for Geodesy*, edited by G. Veis, pp. 81–94, National Technical University, Athens, 1967.

HAEFNER, R., AND R. MARTIN, Data reduction, in *Geodetic Parameters for a 1966 Smithsonian Institution Standard Earth*, Vol. XVII, edited by C. A. Lundquist and G. Veis, pp. 43–62, Smithsonian Astrophysical Observatory, Cambridge, Mass., 1966.

HAGIHARA, Y., Libration of an Earth satellite with critical inclination, *Smithson. Contrib. Astrophys.*, **5**(5), 39–51, 1961a.

HAGIHARA, Y., Recommendations on notation of the Earth potential, *Astron. J.*, **67**, 108, 1961b.

HAGIHARA, Y., The stability of the solar system, in *Planets and Satellites*, edited by G. P. Kuiper and B. M. Middlehurst, Vol. 3, *The Solar System III*, pp. 95–158, University of Chicago Press, Chicago, Ill., 1961c.

HAGIHARA, Y., *Celestial Mechanics*, Vol. II, *Perturbation Theory*, part 1, 504 pp., part 2, 414 pp., MIT Press, Cambridge, Mass., 1972.

HALD, A., Maximum likelihood estimation of the parameters of a normal distribution which is truncated at a known point, *Skand. Aktuarietids*, **1949**, 119–134, 1949.

HALL, N. M., AND J. R. CHERNIACK, *Smithsonian Package for Algebra and Symbolic Mathematics*, Spec. Rep. 291, 49 pp., Smithsonian Astrophysical Observatory, Cambridge, Mass., 1969.

HALLERT, B. P., Test measurements in comparators and tolerances for such instruments, *Photogram. Eng.*, **29**, 301–314, 1963.

HALLERT, B., Fundamental concepts and terminology for the quality of measurement, *Bull. Geod.*, **77**, 263–274, 1965.

HALMOS, F., Scaling a satellite triangulation net, *Bull. Geod.*, **95**, 87–90, 1970.

HAMBLEN, J., AND J. OAKES, Instrumentation and telemetry of TRANSIT navigational satellites, *Electronics*, **34**, 148–153, August 11, 1961.

HAMILTON, T. W., AND W. G. MELBOURNE, Information content of a single pass of Doppler data from a distant spacecraft, *Space Program Summary 37–39*, Vol. III, pp. 18–23, Jet Propulsion Laboratory, Pasadena, Calif., 1966.

HAMILTON, T. W., ET AL., *The Ranger 4 Flight Path and Its Determination From Tracking Data*, TR-32–245, p. 33, Jet Propulsion Laboratory, Pasadena, Calif., September 1962.

HAMILTON, W. C., *Statistics in Physical Science*, Ronald, New York, 1964.

HARAMUNDANIS, K., Experience of the Smithsonian Astrophysical Observatory in the construction and use of star catalogs, *Astron. J.*, **72**(5), 588–596, 1967.

HARKINK, K. F., Les conditions du cameras (essai d'un exposé rigouereaux), *Bull. Geod.*, **17**, 245–266, 1950.

HARRIS, I., AND W. PRIESTER, *Theoretical Models for the Solar-Cycle Variation of the Upper Atmosphere*, NASA TN-D-1444, 261 pp., Superintendent of Documents, Washington, D.C., 1962.

HARRIS, D. W., J. H. BERBERT, E. J. HABIB, AND B. W. MCKENDREE, MOTS—The MINITRACK optical tracking system, *Photo. Sci. Eng.*, **7**, 137, 1963.

HARTREE, D. R., Propagation of electromagnetic waves in a stratified medium, *Proc. Cambridge Phil. Soc.*, **25**(97), 97–120, 1929.

HAURWITZ, B., *Dynamic Meteorology*, p. 11 ff., McGraw-Hill, New York, 1946.

HAYES, E. N., *Trackers of the Skies*, 169 pp., Howard A. Dole, Cambridge, Mass., 1968.

HAYES, H. C., Method and apparatus for determining the force of gravity, U.S. Patent 1,995,305 (1935).

HEISKANEN, W., The Columbus geoid, *Eos Trans. Am. Geophys. Union*, **38**(6), 841–847, 1957.

HEISKANEN, W., The Finnish 864 m long Nummela standard baseline measured with Vaisala light interference comparator, *Bull. Geod.*, **17**, 294–298, 1960.

HEISKANEN, W. A., Is the Earth a triaxial ellipsoid? *J. Geophys. Res.*, **67**(1), 321–329, 1962.

HEISKANEN, W., AND H. MORITZ, *Physical Geodesy*, W. H. Freeman, San Francisco, Calif., 1967.

HELMERT, F. R., Die Schwerkraft und de Massenerteilung der Erde, *Encycl. Math. Wiss.*, 6.1b(2), Leipzig, 1910.

HELMERT, F. R., *Theorien der Höheren Geodesie*, 2nd ed., Vol. I, 632 pp., Vol. II, 610 pp., B. Teubner, Leipzig, 1962.

HENDERSHOTT, M. C., The effects of solid Earth deformation on global ocean tides, *Geophys. J. Roy. Astron. Soc.*, **29**, 389–403, 1972.

HENDERSHOTT, M. C., Ocean tides, *Eos Trans. Am. Geophys. Union*, **54**, 76–86, 1973.

HENIZE, K. G., The Baker-Nunn satellite-tracking camera, *Sky Telesc.*, **16**(3), 107–111, 1957.

HENRICI, P., *Discrete Variable Methods in Ordinary Differential Equations*, 407 pp., John Wiley, New York, 1962.

HENRIKSEN, S., Hydrostatic flattening of the Earth, *Ann. Internat. Geophys. Yr.*, **12**, 197–198, 1960.

HENRIKSEN, S., Calibration of measuring devices, *Can. Surv.*, **19**(5), 439–444, 1965.

HENRIKSEN, S., Application of probability limit theorems to measurements, *Photogrammetria*, **22**, 5–11, 1967.

HERRICK, S., *Astrodynamics*, Van Nostrand-Reinhold, New York, 1971.

HERRICK, S., R. M. L. BAKER, JR., AND C. G. HILTON, Gravitational and related constants for accurate space navigation, in *Proceedings of Eighth Astronautical Congress, Barcelona*, Springer-Verlag, Vienna, 1958.

HEWITT, J., A camera for recording satellite positions with high accuracy, *Space Res.*, **1**, 425–433, 1960.

HEWITT, J., An f/1 field-flattened Schmidt system for precision measurement of satellite position, *Photo. Sci. Eng.*, **9**(1), 11–19, 1965.

HIROSE, H., Note on simultaneous observation of artificial satellites for geodetic purposes, *Space Res.*, **2**, 34–37, 1961.

HIROSE, H., Researches on the geodetic uses of artificial satellites, 1, Methods of simultaneous observations, *J. Geod. Soc. Jap.*, **8**, 102–105, 1962.

HIRSCH, O., Die Satellitenbeobachtungen der Technischen Universität Berlin, *Allg. Vermess. Nachr.*, **1970**(4), 143, 1970.

HIRVONEN, R. A., *The Continental Undulations of the Geoid*, Publ. 19, Finnish Geodetic Institute, Helsinki, 1934.

HIRVONEN, R. A., The reformation of geodesy, *Bull. Geod.*, **65**, 197–214, 1962.

HOBSON, E. W., *Theory of Spherical and Ellipsoidal Harmonics*, 2nd ed., 410 pp., Chelsea, N.Y., 1955.

HÖHN, D., Effects of atmospheric turbulence on the transmission of a laser beam at 6328 Å, 1, Distribution of intensity; 2, Frequency spectra, *Appl. Opt.*, **5**(9), 1427–1436, 1966.

HOLLAND, A. C., The effects of atmospheric refraction on angles measured from a satellite, *J. Geophys. Res.*, **66**, 4171–4175, 1961.

HOPFIELD, H., The effect of tropospheric refraction on the Doppler shift of a satellite signal, *J. Geophys. Res.*, **68**(18), 5157–5168, 1963.

HOPFIELD, H., Two-quartic tropospheric refraction profile for correcting satellite data, *J. Geophys. Res.*, **74**(18), 4487–4499, 1969.

HOPFIELD, H. S., Tropospheric effect on electromagnetically measured range: Prediction from surface weather data, *Radio Sci.*, **6**, 357–367, 1971.

HOPFIELD, H., Tropospheric range error at the zenith, *Space Res.*, **12**, 581–594, 1972.

HÖPKE, W., Zum heutigen Stand der elektronischen Streckenmessungen, *Z. Vermess. Wiss.*, **1959**(10), 361–379, 1959.

HOPMANN AND LOHMANN, *Ballistische Photogrammetrie*, Hillersleben, 1943.

HORI, G. I., The motion of an artificial satellite in the vicinity of the critical inclination, *Astron. J.*, **65**, 291–300, 1960.

HORI, G., Theory of general perturbations with unspecified canonical variables, *Publ. Astron. Soc. Jap.*, **18**, 287–296, 1966.

HORNBARGER, D. H., *Comparison of Astrometric and Photogrammetric Plate Reduction Techniques for a Wild BC-4 Camera*, Rep. 106, 106 pp., Department of Geodetic Science, Ohio State University, Columbus, 1968.

HOTINE, M., *Mathematical Geodesy*, ESSA Monogr. 2, Superintendent of Documents, Wash., D.C. 1969.

HOTTER, F. D., *Preprocessing Optical Satellite Observations*, Rep. 82, 80 pp., Department of Geodetic Science, Ohio State University, Columbus, 1967.

HRISTOW, V. (CHAIRMAN), *Proposal by the Bulgarian National Committee on Geodesy and Geophysics for a Specification of the Geodetic Reference System 1967*, 29 pp., Bulgarian Academy of Sciences, Sofia, 1968.

HUBER, D. N., Densification of the world satellite triangulation network in South America with the PC-1000 camera (abstract), *Mitt. Geod. Inst. Tech. Hochsch. Graz*, **11**(2), 85, 1972.

HUDSON, G. E., Some characteristics of commonly used time scales, *Proc. IEEE*, **55**(6), 815–821, 1967.

HUTCHESON, J. H., *Basic Approach to the Use of Cannonical Variables and vonZeipel's Method in Perturbation Theory*, Rep. RM-4074-PR, 42 pp., The RAND Corporation, Santa Monica, Calif., 1964.

HYNEK, J. A., Satellites, in *Contemporary Geodesy*, Geophys. Monogr. 4, edited by C. Whitten and K. Drummond, pp. 58–66, American Geophysical Union, Washington, D.C., 1959.

HYNEK, J. A., *On the Effects of Image Motion on the Accuracy of Measurement of a Flashing Satellite*, Res. Space Sci. Spec. Rep. 33, Smithsonian Astrophysical Observatory, Cambridge, Mass., February 1960.

ILIFF, R. L., Photographing satellite-reflected laser pulses for geodetic stereo triangulation, *J. Geophys. Res.*, **70**(14), 3505–3508, 1965.

ISNER, J., *Determination of Surface Densities From A Combination of Gravimetry and Satellite Altimetry*, Rep. 186, 61 pp., Department of Geodetic Science, Ohio State University, Columbus, 1972.

ISOTOV, A. A., Reference ellipsoid and the standard geodetic datum adopted in the USSR, *Bull. Geod.*, **53**, 1–6, 1959.

ISOTOV, A. A., On establishment of the system of coordinates related to the Earth's axis of rotation, *Bull. Geod.*, **88**, 147–150, 1968.

IZSAK, I. G., *Orbit Determination From Simultaneous Doppler Shift Measurements*, Rep. 38, pp. 1–21, Smithsonian Astrophysical Observatory, Cambridge, Mass., 1960a.

IZSAK, I. G., Periodic drag perturbations of artificial satellites, *Astron. J.*, **65**(6), 355–357, 1960b.

IZSAK, I. G., On satellite orbits with very small eccentricities, *Astron. J.*, **66**(3), 129–131, 1961a.

IZSAK, I. G., *A Determination of the Ellipticity of the Earth's Equator From the Motion of Two Satellites*, Spec. Rep. 56, pp. 11–24, Smithsonian Astrophysical Observatory, Cambridge, Mass., 1961b.

IZSAK, I. G., *Differential Orbit Improvement With the Use of Rotated Residuals*, Spec. Rep. 73, Smithsonian Astrophysical Observatory, Cambridge, Mass., 1961c.

IZSAK, I. G., Differential orbit improvement with the use of rotated residuals, in *Space Age Astronomy*, edited by A. J. Deutsch and W. B. Klemperer, Academic, New York, 1962.

IZSAK, I. G., Tesseral harmonics in the geopotential, *Nature*, **199**, 137–139, 1963a.

IZSAK, I. G., A second order solution of Vinti's dynamical problem, *Smithsonian Contrib. Astrophys.*, **6**, 81–107, 1963b.

IZSAK, I. G., On the critical inclination in satellite theory, in *The Use of Artificial Satellites for Geodesy*, edited by G. Veis, pp. 17–40, North Holland, Amsterdam, 1963c.

IZSAK, I. G., A note on perturbation theory, *Astron. J.*, **68**, 559–561, 1963d.

IZSAK, I. G., Tesseral harmonics of the geopotential and corrections to station coordinates, *J. Geophys. Res.*, **69**(12), 2621–2631, 1964.

IZSAK, I. G., New determinations of non-zonal harmonics by satellites, in *Trajectories of Artificial Celestial Bodies*, edited by J. Kovalevsky, pp. 195–200, Springer-Verlag, Berlin, 1966.

IZSAK, I. G., J. M. GERARD, R. EFIMBA, AND M. P. BARNETT, *Construction of Newcomb Operators on a Digital Computer*, Spec. Rep. 140, 103 pp., Smithsonian Astrophysical Observatory, Cambridge, Mass., 1964.

JACCHIA, L. G., A variable atmospheric-density model from satellite accelerations, *J. Geophys. Res.*, **65**, 2775–2782, 1960.

JACCHIA, L. G., Satellite drag during the events of November 1960, *Space Res.*, **2**, 747–750, 1961.

JACCHIA, L. G., *Static Diffusion Models of the Upper Atmosphere With Empirical Temperature Profiles*, Spec. Rep. 170, 53 pp., Smithsonian Astrophysical Observatory, Cambridge, Mass., 1964.

JACCHIA, L. G., *Revised Static Models of the Themosphere and Exosphere With Empirical Temperature Profiles*, Spec. Rep. 332, Smithsonian Astrophysical Observatory, Cambridge, Mass., 1971.

JACCHIA, L. G., AND J. SLOWLEY, *Accurate Drag Determination for Eight Artificial Satellites—Atmospheric Densities and Temperatures*, Spec. Rep. 100, Smithsonian Astrophysical Observatory, Cambridge, Mass., 1962.

JAERNEFELT, G., On the satellite observation work done in Finland, *Ann. Acad. Sci. Fennicae*, Ser. A111, **61**, 87–96, 1961.

JAFFE, R., AND E. RECHTIN, Phase-lock circuits capable of near-optical performance, *Inst. Radio Eng. Trans.*, **IT**(1), 66–76, 1955.

JAKES, W. C., JR., Project Echo, *Bell Lab Record*, **39**(9), 306–311, 1961.

JASTROW, R., AND R. BRYANTS, Variations in the orbit of the ECHO satellite, *J. Geophys. Res.*, **66**, 3512–3513, 1960.

JAZUNSKIJ, I. M., Determination of illumination conditions and periods of an artificial satellite in shadows and in sunlight, *Planet. Space Sci.*, **8**, 159–164, 1961.

JEFFREYS, B. S., Transformation of tesseral harmonics under rotation, *Geophys. J. Roy. Astron. Soc.*, **10**, 141–145, 1965.

JEFFREYS, H., Determination of the Earth's gravitational field, *Mon. Notic. Roy. Astron. Soc.*, Geophys. Suppl., **5**, 55–66, 1942.

JEFFREYS, H., *The Earth*, 4th ed., 420 pp., Cambridge University Press, Cambridge, England, 1959.

JEFFREYS, H., On the hydrostatic theory of the figure of the Earth, *Geophys. J. Roy. Astron. Soc.*, **8**, 196–202, 1963.

JEFFREYS, H., *The Earth*, 5th ed., Cambridge University Press, London, 1970.

JEFFREYS, H., AND B. S. JEFFREYS, *Methods of Mathematical Physics*, 3rd ed., Cambridge University Press, Cambridge, England, 1956.

JENKINS, L. F., *General Catalogue of Trigonometric Stellar Parallaxes*, Yale University Observatory, New Haven, Conn., 1952.

JENKINS, R. E., Satellite observation of the relativistic Doppler shift, *Astron. J.*, **74**(7), 960–963, 1969.

JENKINS, R. E., Significant satellite relativity experiment without an atomic oscillator, *Astronaut. Acta*, **16**, 137–142, 1971.

JET PROPULSION LABORATORY, Range-gated lunar radar experiment, *Space Programs Summary* 37–25, Vol. III, pp. 38–47, Pasadena, Calif., 1964.

JOHNSON, T., H. PLOTKIN, AND P. SPADEN, Laser satellite ranging system, *IEEE J. Quantum Elec.*, **OE–3**(11), 435–439, 1967.

JONES, B. L., Photogrammetric refraction angle—satellite viewed from earth, *J. Geophys. Res.*, **66**, 1135–1138, 1961.

JORDAN/EGGBERT, *Handbuch der Vermessungskunde*, Vol. III, Part 1, p. 476, Metzlersche, Stuttgart, 1939.

KAARIAINEN, E., Adjustment of the northern bloc in U.E.I.N. and of the geopotential differences in it, *Bull. Geod.*, **57**, 299–310, 1960.

KABALEČ, J., Determination of astronomical equatorial coordinates of spatial network side direction by astrophotographic method, *Bull. Geod.*, **93**, 255–262, 1969.

KAHLE, H. G., AND M. TALWANI, Gravimetric Indian Ocean geoid, *Z. Geophys.*, **39**, 167–187, 1973.

KAHN, W. D., Calibration of MINITRACK Mark II, *Astron. J.*, **62**, 396–399, 1957.

KAISER, B. E., Anschluss von Digitalrechnern an Doppler-Radargeraete, *Electronics*, **32**(21), 46, 1959.

KAKKURI, J., *Errors in the Reduction of Photographic Plates*, Publ. 66, 14 pp., Finnish Geodetic Institute, Helsinki, 1969.

KAKKURI, J., Stellar triangulation net with balloons intermediating between satellite nets and classical triangulations, *Mitt. Geod. Inst. Tech. Hochsch. Graz*, **11.2**, 193–199, 1972.

KANE, M. F., Rotational inertia of continents: A proposed link between polar wandering and plate tectonics, *Science*, **175**, 1355–1357, 1972.

KARUBE, N., Optimum incident-ray direction into a cube-corner prism, *J. Opt. Soc. Am.*, **57**(10), 1272–1273, 1967.

KAULA, W. M., Accuracy of gravimetrically computed deflections of the vertical, *Eos Trans. Am. Geophys. Union*, **39**, 1027–1033, 1957.

KAULA, W. M., Reconciliation of Stokes' function and astrogeodetic geoid determination, *J. Geophys. Res.*, **64**(1), 61, 1959a.

KAULA, W. M., Statistical and harmonic analysis of gravity, *J. Geophys. Res.*, **64**(12), 2401–2421, 1959b.

KAULA, W. M., Analysis of gravitational and geometric aspects of geodetic utilization of satellites, *Geophys. J. Roy. Astron. Soc.*, **5**(2), 104–133, 1961a.

KAULA, W. M., Estimation of longitudinal variations in the Earth's gravitational field from MINITRACK observations, *J. Astronaut. Sci.*, **8**, 83–88, 1961b.

KAULA, W. M., Analysis of satellite observations for longitudinal variations of the gravitational field, *Space Res.*, **11**, 360–372, 1961c.

KAULA, W. M., Development of the lunar and solar disturbing functions for a close satellite, *Astron. J.*, **67**, 300–303, 1962.

KAULA, W. M., Tesseral harmonics of the gravitational field and geodetic datum shifts derived from camera observations of satellites, *J. Geophys. Res.*, **68**(2), 473–485, 1963a.

KAULA, W. M., Improved geodetic results from camera observations of satellites, *J. Geophys. Res.*, **68**(18), 5183–5191, 1963b.

KAULA, W. M., Gravitational and other perturbations of a satellite orbit, in *Dynamics of Rockets and Satellites*, edited by G. V. Groves, pp. 179–216, North-Holland, Dordrecht, 1965.

KAULA, W. M., Tests and combinations of satellite determinations of the gravity field with gravimetry, *J. Geophys. Res.*, **71**, 5303–5314, 1966a.

KAULA, W. M., *Theory of Satellite Geodesy*, 124 pp., Blaisdell, Waltham, Mass., 1966b.

KAULA, W. M., Tesseral harmonics of the Earth's gravitational field from camera tracking of satellites, *J. Geophys. Res.*, **71**, 4377–4388, 1966c.

KAULA, W. M., Geodetic satellites: Evaluation of results relative to those obtained by other means, *Eos Trans. Am. Geophys. Union*, **48**(2), 343–345, 1967a.

KAULA, W. M., Comparison and combination of satellite with results for geodetic parameters, in *Use of Artificial Satellites for Geodesy*, edited by G. Veis, pp. 423–442, National Technical University, Athens, 1967b.

KAULA, W. M., Theory of statistical analysis of data distributed over a sphere, *Rev. Geophys. Space Phys.*, **5**, 38–107, 1967c.

KAULA, W. M., Analysis of geodetic satellite tracking data to determine tesseral harmonics of the Earth's gravitational field, in *Proceedings of NASA Program Review Meeting*, Vol. XI, Geometric and gravimetric investigations with GEOS-1, 1–10, 1968.

KAULA, W. M., Tidal friction with latitude-dependent amplitude and phase lag, *Astron. J.*, **74**, 1108–1114, 1969.

KAULA, W. M., Earth's gravity field: Relation to global tectonics, *Science*, **169**, 982–985, 1970.

KAULA, W. M., Geopotential and geodetic models, AIAA Reprint Ser., 12, in *Astrodynamics and Celestial Mechanics*, edited by V. Szebehely, pp. 40–60, Am. Inst. of Aeronautics and Astronautics, New York, 1971a.

KAULA, W. M., The appropriate representation of the gravity field for satellite geodesy, *Proc. IAG Symp. Math. Geod.* (Bologna), **4**, 57–65, 1971b.

KAULA, W. M., Global gravity and tectonics, in *The Nature of the Solid Earth*, edited by E. C. Robinson, J. F. Hays, and L. Knopoff, pp. 385–405, McGraw-Hill, New York, 1972.

KAULA, W. M., AND W. LEE, A spherical harmonic analysis of the Earth's topography, *J. Geophys. Res.*, **72**, 753–758, 1967.

KELSO, J. M., Doppler shifts and Faraday rotation of radio signals in a time-varying, inhomogeneous ionosphere, 1, Single signal case, *J. Geophys. Res.*, **65**, 3909–3914, 1960.

KELSO, J. M., *Radio Ray Propagation in the Ionosphere*, 408 pp., McGraw-Hill, New York, 1964.

KERSHNER, R. B., The TRANSIT Program, *Astronautics*, **5**(6), 30–31, 104–105, 106–114, 1960.

KERSHNER, R. B., The GEOS satellite and its use in geodesy, in *The Use of Artificial Satellites for Geodesy*, edited by G. Veis, National Technical University, Athens, 1965.

KHAN, M. A., Some parameters of a hydrostatic Earth, *Eos Trans. Am. Geophys. Union*, **48**(1), 56, 1967.

KHAN, M. A., *On the Equilibrium Figure of the Earth*, Rep. HIG–68–10, Hawaiian Institute of Geophysics, University of Hawaii, Honolulu, 1968.

KHAN, M. A., General solution of the problem of hydrostatic equilibrium, *Geophys. J. Roy. Astron. Soc.*, **18**, 177–188, 1969.

KHAN, M. A., Nature of the satellite-determined gravity anomalies, in *Use of Artificial Satellites for Geodesy*, Geophys. Monogr. 15, edited by S. Henriksen, B. Chovitz, and A. Mancini, pp. 99–106, American Geophysical Union, Washington, D.C., 1972.

KHAN, M. A., AND G. P. WOOLARD, *Review of the Perturbation Theory as Applied to the Determination of Geopotential*, Rep. HIG–68–1, Hawaiian Institute of Geophysics, University of Hawaii, Honolulu, 1968.

KING-HELE, D. G., Density of the atmosphere at heights between 200 km and 400 km from analysis of artificial satellite orbits, *Nature*, **193**, 638–639, 1959.

KING-HELE, D. G., Variations in air density at a height of 480 km from the orbit of MIDAS-2, *Planet. Space Sci.*, **16**, 937–949, 1968.

KING-HELE, D. G., AND R. MERSON, The use of artificial satellites to explore the Earth's gravitational field—Results on Sputnik 2 (1958β), *Nature*, **182**, 640, 1958.

KING-HELE, D. G., AND R. H. MERSON, New value for the Earth's flattening derived from satellite orbits, *Nature*, **183**, 881–882, 1959.

KING-HELE, D. G., A. H. COOK, AND A. H. WATSON, Even zonal harmonics in the Earth's gravitational potential, *Nature*, **202**(4936), 996, 1964.

KING-HELE, D. G., G. E. COOK, AND D. W. SCOTT, Even zonal harmonics in the Earth's gravitational potential: A comparison of recent determinations, *Planet. Space Sci.*, **14**(1), 49–52, 1966.

KING-HELE, D. G., G. E. COOK, AND D. W. SCOTT, Evaluation of odd zonal harmonics in the geopotential, of degree less than 33, from the analysis of 22 satellite orbits, *Planet. Space Sci.*, **17**, 629–664, 1969.

KING-HELE, P. G., ET AL., *Table of Earth Satellites*, 2 vols., Royal Aircraft Establishment Technical Reports 70020 and 70111, Ministry of Technology, Farnborough Hanks, England.

KITCHEN, F., AND W. JOY, Some effects of fine structure of the ionosphere on transmission from the Russian Earth satellite 1958 δ, *Nature*, **181**, 1759–1761, 1958.

KNEISSL, M., Das europäischen Gravimetereichsystem, *Bull. Geod.*, **60**, 111–124, 1961.

KNEISSL, M., The geodetic integration of Europe, *Bull. Geod.*, **67**, 75–88, 1963.

KNEISSL, M., *Report for the Years 1963 to 1967 Presented to the XIVth General Assembly of the International Union of Geodesy and Geophysics*, Publ. 5, Association Internationale de Geodesie, Deutsche Geodetische Kommission, Munich, 1967.

KNEISSL, M., AND K. MARZAHN, Adjustment 1962 of the European calibration system, *Bull. Geod.*, **69**, 217–229, 1963.

KOCH, K. R., AND F. MORRISON, A simple layer model of the geopotential from a combination of satellite and gravity data, *J. Geophys. Res.*, **75**(8), 1483–1492, 1970.

KOCH, K. R., AND H. SCHMIDT, Error study for the determination of the center of mass of the Earth from PAGEOS observations, *Bull. Geod.*, **97**, 233–244, 1970.

KOCH, K. R., AND B. WITTE, Earth's gravity field represented by a simple layer potential from Doppler tracking of satellites, *J. Geophys. Res.*, **76** (35), 8471–8479, 1971.

KÖHNLEIN, W. J., Corrections to station coordinates and to nonzonal harmonics from Baker-Nunn observations, *Space Res.*, **7**, 694–707, 1967.

KÖNIG, A., Astrometry and astrographs, in *Astronomical Techniques*, edited by W. A. Hiltner, pp. 461–485, University of Chicago Press, Chicago, Ill., 1962.

KOPFF, A., Vergleich des FK3 mit dem General Catalogue von B. Boss, *Astron. Nachr.*, **269**, 160, 1939.

KOPFF, A., ET AL., *Individual Corrections to the FK3 and the Declination System of the FK4*, Publ. 14, Astron. Rechen-Institute, Heidelberg, 1964.

KORDYLEWSKI, K., Die polnische Sonnenfinsternisexpedition nach Schwedischlappland zur totalen Finstërnis 1927 Juni 29, *Acta Astron.*, **6**(1), 133–200, 1932.

KORN, G., AND T. KORN, *Mathematical Handbook for Scientists and Engineers*, 943 pp., McGraw-Hill, New York, 1961.

KOTELNIKOV, V. A., ET AL., Using the Doppler effect to determine the orbital parameters of Earth satellites, *Ann. Internat. Geophys. Yr.*, **12**, 880–891, 1961.

KOVALEVSKY, J., Valeur des elements moyens d'un satellite deduits de l'observation d'un passage, *Space Res.*, **2**, 91–101, 1961.

KOVALEVSKY, J., F. BARLIER, AND I. STELLMACHER, Les experiences geodesiques sur les satellites D1 —Description et premiers resultats, *Bull. Geod.*, **88**, 175–178, 1968.

KOZAI, Y., *Earth's Gravitational Potential Derived From the Motion of Satellite 1958 β2*, Spec. Rep. 22, 1–6, Smithsonian Astrophysical Observatory, Cambridge, Mass., 1959a.

KOZAI, Y., *On the Effect of the Sun and the Moon Upon the Motion of a Close Earth satellite*, Rep. 22, pp. 7–10, Smithsonian Astrophysical Observatory, Cambridge, Mass., 1959b.

KOZAI, Y., The motion of a close Earth satellite, *Astron. J.*, **64**, 367–377, 1959c.

KOZAI, Y., Effect of precession and nutation on the orbital elements of a close Earth satellite, *Astron. J.*, **65**, 621–623, 1960.

KOZAI, Y., Gravitational field of the Earth derived from three satellites, *Astron. J.*, **66**(1), 8–10, 1961a.

KOZAI, Y., Note on the motion of a close Earth satellite with a small eccentricity, *Astron. J.*, **66**(3), 132–134, 1961b.

KOZAI, Y., *Numerical Results From Orbits*, Spec. Rep. 101, Smithsonian Astrophysical Observatory, Cambridge, Mass., 1962a.

KOZAI, Y., Second-order solution of artificial satellite theory without air drag, *Astron. J.*, **67**(7), 446–461, 1962b.

KOZAI, Y., Numerical results on the gravitational potential of the Earth, in *Use of Artificial Satellites for Geodesy*, edited by G. Veis, pp. 305–316, North Holland, Amsterdam, 1963a.

KOZAI, Y., The potential of the Earth derived from satellite motions, in *Dynamics of Satellites*, M. Roy, ed., pp. 65–73, Springer-Verlag, Berlin, 1963b.

KOZAI, Y., Effects of solar radiation pressure on the motion of an artificial satellite, *Smithsonian Contrib. Astrophys.*, **6**, 109–112, 1963c.

KOZAI, Y., *New Determination of Zonal Harmonic Coefficients of the Earth's Gravitational Potential*, Spec. Rep. 165, 38 pp., Smithsonian Astrophysical Observatory, Cambridge, Mass., 1964. (Also *Publ. Astron. Soc. Jap.*, **16**, 263–284, 1964.)

KOZAI, Y., Effects of the tidal deformation of the Earth on the motion of close Earth satellites, *Publ. Astron. Soc. Jap.*, **17**(4), 395, 1965.

KOZAI, Y., The Earth gravitational potential derived from satellite motion, *Space Sci. Rev.*, **5**, 818–879, 1966a.

KOZAI, Y., *Lunisolar Perturbations With Short Periods*, Spec. Rep. 235, Smithsonian Astrophysical Observatory, Cambridge, Mass., 1966b.

KOZAI, Y., *Note on Expressions for Second-Order Short-Periodic Perturbations*, Spec. Rep. 234, 8 pp., Smithsonian Astrophysical Observatory, Cambridge, Mass., 1966c.

KOZAI, Y., Determination of Love's number from satellite observations, *Phil. Trans. Roy. Soc. London*, **262**(1124), 135–136, 1967a.

KOZAI, Y., Long-range analysis of satellite observations, in *Use of Artificial Satellites for Geodesy*, edited by G. Veis, pp. 169–178, National Technical University, Athens, 1967b.

KOZAI, Y., Love's number of the Earth derived from satellite observations, *Bull. Geod.*, **89**, 355–8, 1968a.

KOZAI, Y., Love's number of the Earth derived from satellite observations, *Publ. Astron. Soc. Jap.*, **20** (1), 24–26, 1968b.

KOZAI, Y., *Revised Values for Coefficients of Zonal Spherical Harmonics in the Geopotential*, Spec. Rep. 295, 16 pp., Smithsonian Astrophysical Observatory, Cambridge, Mass., February 1969.

KOZAI, Y., *A New Method To Compute Lunisolar Perturbations in Satellite Motions*, Spec. Rep. 349, 27 pp., Smithsonian Astrophysical Observatory, Cambridge, Mass., 1973.

KOZAI, Y., AND H. KINOSHITA, Effects of motion of the equatorial plane on the orbital elements of an Earth satellite, *Celestial Mech.*, **7**, 356–366, 1973.

KRAKIWSKY, E. J., Sequential least squares adjustment of satellite triangulation and trilateration in combination with terrestrial day, *Reports of the Department of Geodetic Science*, No. 114, The Ohio State University, Columbus, 1968.

KRAKIWSKY, E. J., AND A. J. POPE, *Least Squares Adjustment of Satellite Observations for Simultaneous Directions or Ranges, Part 1: Formulation of Equations*, Rep. 86, Department of Geodetic Science, Ohio State University, Columbus, 1967.

KRAKIWSKY, E. J., G. BLAHA, AND J. M. FERRIER, Least squares adjustment of satellite observations for simultaneous directions or ranges, part 2 of 3: computer programs, *Reports of the Department of Geodetic Science*, No. 87, The Ohio State University, Columbus, 1968.

KRAKIWSKY, E. J., J. FERRIER, AND J. P. REILLY, Least squares adjustment of satellite observations for simultaneous directions or ranges, part 3 of 3: subroutines, *Reports of the Department of Geodetic Science*, No. 88, The Ohio State University, Columbus, 1967.

KRAKIWSKY, E. J., D. E. WELLS, AND P. KIRKHAM, Geodetic control from Doppler shift observations, *Can. Surv.*, **26**(2), 146–162, 1972.

KRAUSE, H. G. L., *Astrorelativity*, NASA TR–188, 59 pp., Superintendent of Documents, Washington, D.C., 1964.

KUKKUMAKI, T. J., Results obtained by the Finnish solar eclipse expeditions, 1947, *Eos Trans. Am. Geophys. Union*, **35**, 99–102, 1954.

KUKKUMAKI, T. J., Stellar triangulation, *Bull. Geod.*, **54**, 53–69, 1959.

KUKKUMAKI, T., AND T. HONKASALO, Measurement of the standard baseline of Buenos Aires with Vaisala comparator, *Bull. Geod.*, **34**, 355–362, 1954.

KULIKOV, K. A., *Fundamental Constants of Astronomy*, translation, Office of Technical Services, U. S. Department of Commerce, Washington, D.C., 1964.

KUMAR, M., *Coordinate Transformation by Minimizing Correlations Between Parameters*, Rep. 88, Department of Geodetic Science, Ohio State University, Columbus, 1972.

KUNTZ, E., Beziehungen zwischen Sternkoordinaten und gemessenen Bildkoordinaten in Satellitenaufnahmen, *Z. Vermess.*, **1965**, 399–403, 1965.

KUNTZ, E., AND J. ARNOLD, On the identity and condition of different methods of plate reduction, *Mitt. Geod. Inst. Tech. Hochsch. Graz*, **11**(1), 209–221, 1972.

KURHONEN, J., Outlines the adjustment of the Finnish triangulation and the separate adjustment of the southernmost part of net, *Bull. Geod.*, **61**, 265–282, 1961.

KUTTA, W., Beitrag zur nährungsweisen integration totaler Differentialgleichungen, *Z. Math. Phys.*, **46**, 435–453, 1899.

LABRUM, R. G., ET AL., *The Surveyor 5, 6, and 7 Flight Paths and Their Determination From Tracking Data*, TR–32–1302, pp. 43, 95, 146, Jet Propulsion Laboratory, Pasadena, Calif., December 1968.

LACMAN, O., *Die Photogrammetrie in ihrer Anwendung auf nicht-topographischen Gebieten*, S. Hirzel Verlag, Leipzig, 1950.

LÁLA, P., Short-periodic perturbations of the satellite orbits caused by solar radiation pressure, *Bull. Astron. Czech.*, **19**, 233–239, 1968.

LÁLA, P., Semi-analytical theory of solar pressure perturbations of satellite orbits during short-time intervals, *Bull. Astron. Inst. Czech.*, **22**(2), 63–72, 1971.

LÁLA, P., AND L. SEHNAL, The Earth's shadowing effects in the short-periodic perturbations of satellite orbits, *Bull. Astron. Czech.*, **20**, 327, 1969.

LAMBECK, K., *Effect of Random Atmospheric Refraction on Optical Satellite Observations*, Spec. Rep. 269, 27 pp., Smithsonian Astrophysical Observatory, Cambridge, Mass., 1968.

LAMBECK, K., Position determination from simultaneous observations of artificial satellites: An optimization of parameters, *Bull. Geod.*, **92**, 155–169, 1969.

LAMBECK, K., Comparisons and combinations of geodetic parameters estimated from dynamic and geometric satellite solutions and from Mariner flights, in *Dynamics of Satellites 1969*, edited by B. Morando, pp. 170–179, Springer-Verlag, Berlin, 1970.

LAMBECK, K., Comparison of surface gravity data with satellite data, *Bull. Geod.*, **100**, 208–220, 1971a.

LAMBECK, K., Determination of the Earth's pole of rotation from laser range observations to satellites, *Bull. Geod.*, **101**, 263–282, 1971b.

LAMBECK, K., Relation of some geodetic datums to a global geocentric reference system, *Bull. Geod.*, **99**, 37–54, 1971c.

LAMBECK, K., AND A. CAZENAVE, *Fluid Tidal Effects on Satellite Orbit and Other Temporal Variations in the Geopotential*, Bull. no. 7, Groupe Recherches de Geodesie Spatiale, C.N.E.S., Bretigny-sur-Orge, France, January 1973.

LAMBERT, B. P., Geodetic survey and topographic mapping in Australia, *Aust. Surv.*, **1969**, 515–528, 1969.

LAMBERT, W. D., Geodetic applications of eclipses and occultations, *Bull. Geod.*, **13**, 274–293, 1949.

LAMBERT, W. D., *The Gravity Field of an Ellipsoid of Revolution as a Level Surface*, Rep. 14, Institute of Geodesy, Photogrammetry, and Cartography, Ohio State University, Columbus, 1961.

LAPUSHKA, K., AFU–75 photographic camera, *Trans. Ass. Internat. Geod.*, **24**, 194–209, 1972.

LASS, H., AND G. SOLLOWAY, *Doppler Shift for Accelerating Transmitters, Reflectors, and Receivers*, TR–32–95, 12 pp., Jet Propulsion Laboratory, Pasadena, Calif., 1961.

LASSOVSZKY, K., *On the Accuracy of Measurements Made Upon Films Photographed by Baker-Nunn Satellite Tracking Cameras*, Spec. Rep. 74, Smithsonian Astrophysical Observatory, Cambridge, Mass., 1961.

LAURILA, S. H., Statistical analysis of refractive index through the troposphere and stratosphere, *Bull. Geod.*, **92**, 139–153, 1969.

LEARY, F., Instruments: Key to missile programs, *Electronics*, **32**(2), 47–51, 1959.

LEDERSTEGER, K., Die absolute Lotabweichung in Potsdam und die geodätischen Ausgangswerte des gesamteuropäischen Netzes auf dem hayfordschen Ellipsoid, *Bull. Geod.*, **23**, 101–104, 1951.

LEE, W. H., AND W. M. KAULA, Spherical harmonic analysis of the Earth's topography, *J. Geophys. Res.*, **72**(2), 753–758, 1967.

LEFEBVRE, M., Etude comparative des differents resultats obtenus en geodesie spatiale sur la reseau Europeen, *Bull. Geod.*, **94**, 415–425, 1969.

LEHR, C., Atmospheric reduction of laser data, *SAO ISAGEX Experience, 1, Data Acquisition*, edited by E. M. Gaposchkin, p. 31, Smithsonian Astrophysical Observatory, Cambridge, Mass., May 1972.

LEHR, C. G., L. A. MAESTRE, AND R. R. DOWNER, *Geodetic Satellite Results during 1967*, Spec. Rep. 264, 344 pp., Smithsonian Astrophysical Observatory, Cambridge, Mass., 1967.

LEHR, C. G., L. A. MAESTRE, AND R. R. DOWNER, Laser ranging to satellites: The Smithsonian system on Mt. Hopkins, in *Proceedings of the Conference on Refractive Effects in Geodesy and Electronic Distance Measurement*, pp. 123–144, University of New South Wales, Kensington, Australia, 1968.

LE MENESTREL, J., Compensation du reseau geodesique Français du premier ordre, *Bull. Geod.*, **94**, 347–363, 1969.

LERCH, F., AND A. WAGNER, Preliminary Standard Earth (abstract), *Eos Trans. Am. Geophys. Union*, **53**(10), 892, 1972.

LERCH, F., J. MARSH, AND B. O'NEIL, *Evaluation of the Goddard Range and Range Rate System at Rosman by Intercomparison With GEOS–1 Long-Arc Orbital Solutions*, NASA TN–D–5036, 48 pp., 1969.

LERCH, F., ET AL., Gravitational field models of the Earth, paper presented at International Symposium on Earth Gravity Models and Related Problems, St. Louis, Mo., August 16–18, American Geophysical Union, Washington, D.C. 1972a.

LERCH, F., ET AL., *Gravitational Field Models for the Earth (GEM–1 and –2)*, NASA TM–X65970, National Technical Information Service, Springfield, Va., 1972b.

LERCH, F., ET AL., *Gravitational Field Models GEM–3 and –4*, NASA TM–X66207, National Technical Information Service, Springfield, Va., 1972c.

LEVALLOIS, J. J., Commentaires sur un cliché spatial, *Bull. Geod.*, **88**, 179–182, 1968.

LEVALLOIS, J. J., AND J. KOVALEVSKY, *Geodesie Generale*, Vol. IV, *Geodesie Spatiale*, 268 pp., Editions Eyrolles, Paris, 1970.

LEVY, J., Sur les trajectoires des satellites proches, *Bull. Geod.*, **53**, 7–20, 1959.

LIEBERMAN, H., Investigation of the geoid in Europe, *Bull. Geod.*, **37**, 1–11, 1955.

LIIGANT, M., AND Y. EINASTO, The theory of automatic satellite tracking telescopes, *Astron. Zh.*, **37**(6), 1023–1031, 1960.

LINNIK, Y. V., *Methods of Least Squares and Principles of the Theory of Observations*, translated from the Russian by R. C. Elandt, edited by N. P. Johnson, 360 pp., Pergamon, New York, 1961.

LIU, A., Range and angle corrections due to the ionosphere, Deep Space Network, *Space Programs Summary 37–41*, Vol. III, pp. 38–41, Jet Propulsion Laboratory, Pasadena, Calif., 1966.

LIU, A., Recent changes to the tropospheric refraction model used in the reduction of radio tracking data from deep space probes, Deep Space Network, *Space Programs Summary 37–50*, Vol. II, pp. 93–97, Pasadena, Calif., 1968.

LOMAX, H., *Operational Unification of Finite Difference Methods for the Numerical Integration of Ordinary Differential Equations*, 112 pp., Superintendent of Documents, Washington, D.C., 1967.

LORENS, C. S., *The Doppler Method of Satellite Tracking*, Rep. 30–2, 26 pp., Jet Propulsion Laboratory, Pasadena, Calif., 1959.

LOZINSKY, A., AND G. LEIKIN, New automatic camera for satellite tracking, *Space Res.*, **9**, 4–5, 1969.

LUBOWE, A. G., How critical is the critical inclination?, *Celestial Mech.*, **1**, 6–10, 1969.

LUBOWE, A. G., AND R. E. JENKINS, Numerical verification of analytical expressions for the perturbation due to an arbitrary zonal harmonic of the geopotential, *Celestial Mech.*, **2**, 21–40, 1970.

LUKAC, C., Use of overlap conditions in astrometric plate reductions, *Astron. J.*, **72**(5), 620–623, 1967.

LUNDQUIST, C. A. (ED.), *Geodetic Satellite Results During 1967*, Rep. 264, 344 pp., Smithsonian Astrophysical Observatory, Cambridge, Mass., 1967.

LUNDQUIST, C. A., AND G. E. O. GIACAGLIA, *Possible Improvement From Satellite Actimetry*, Spec. Rep. 294, Smithsonian Astrophysical Observatory, Cambridge, Mass., 1969.

LUNDQUIST, C., AND G. GIACAGLIA, A geopotential representation with sampling functions, in *Use of Artificial Satellites for Geodesy*, Geophys. Monogr. 15, edited by S. Henriksen, B. Chovitz, and A. Mancini, pp. 125–132, American Geophysical Union, Washington, D.C., 1972.

LUNDQUIST, C. A., AND G. VEIS (EDS.), *Geodetic Parameters for a 1966 Smithsonian Standard Earth*, Spec. Rep. 200, 3 vols., 683 pp., Smithsonian Astrophysical Observatory, Cambridge, Mass., 1966.

LYDDANE, R. H., Small eccentricities or inclinations in the Brouwer theory of artificial satellites, *Astron. J.*, **68**(8), 555–559, 1963.

LYDDANE, R. H., AND C. J. COHEN, Numerical comparison between Brouwer's theory and solution by Cowell's method for the orbit of an artificial satellite, *Astron. J.*, **67**, 176–177, 1962.

MACMILLAN, W. D., *Theory of the Potential*, 465 pp., McGraw-Hill, New York, 1930.

MACOMBER, M. M., Project ANNA, in *The Use of Artificial Satellites for Geodesy*, edited by G. Veis, North Holland, Amsterdam, 1963.

MAHAN, A. J., Astronomical refraction—Some history and theories, *Appl. Opt.*, **1**(4), 497–571, 1962.

MAINBERGER, W. A., Primary frequency-standard using resonant cesium, *Electronics*, **1958**, 80–85, 1958.

MANCINI, A., Space orientation and geodetic azimuths of long lines from observations of the ANNA satellite, *Bull. Geod.*, **76**, 97–113, 1965.

MANCINI, A., AND L. A. GAMBINO, Results of space triangulation adjustments from satellite data, in *The Use of Artificial Satellites for Geodesy*, edited by G. Veis, pp. 381–399, National Technical University, Athens, 1967.

MARCH, A., *Quantum Mechanics of Waves and Particle Fields*, John Wiley, New York, 1951.

MARCKWARDT, W., Beitrag zur Untersuchung der Genaugkeit von Koordinatenmessungeräten, *Vermessungstechnik*, **19**(3), 89–93, 1971.

MARGENAU, H., AND G. M. MURPHY, *Mathematics of Physics and Chemistry*, Vol. I, D. van Nostrand, New York, 1956.

MARKOWITZ, W., Photographic determination of the Moon's position—Applications to the measure of time, rotation of the Earth, and geodesy, *Astron. J.*, **59**, 69–73, 1954.

MARKOWITZ, W., The dual-rate satellite camera, *J. Geophys. Res.*, **64**, 1115, 1959.

MARKOWITZ, W., *Accurate Timing of Artificial Satellite Observations on a World-Wide Scale*, Rep. 15, Institute of Geodesy, Photogrammetry, and Cartography, Ohio State University, Columbus, 1961.

MARQUIS, D. C., Optical tracking—A brief survey of the field, *Appl. Opt.*, **5**(4), 481, 1966.

MARSH, J. G., ET AL., *Intercomparison of the MINITRACK and Optical Tracking Networks Using GEOS–1 Long-Arc Orbital Solutions*, NASA TN–D–5337, Superintendent of Documents, Washington, D.C., 1970.

MARSH, J. G., B. C. DOUGLAS, AND S. M. KLOSKO, *Unified Set of Tracking Station Coordinates Derived From Geodetic Satellite Tracking Data*, NASA TM–X65707, National Technical Information Service, Springfield, Va., 1971.

MARSH, J. G., F. J. LERCH, AND S. F. VINCENT, *Geoid and Free-Air Gravity Anomalies Corresponding to the GEM–4 Earth Gravitational Model*, NASA TM–X66240, National Technical Information Service, Springfield, Va., 1973.

MARTIN, C. F., AND T. C. VAN FLANDERN, Secular changes in the lunar ephemeris, *Science*, **168**, 246–247, 1970.

MARTIN, C. F., T. V. MARTIN, AND D. E. SMITH, Satellite-satellite tracking for estimating potential coefficients, in *Use of Artificial Satellites for Geodesy*, Geophys. Monogr. 15, edited by S. Henriksen, B. Chovitz, and A. Mancini, pp. 139–144, American Geophysical Union, Wash., D.C. 1972.

MARTIN, H. A., ET AL., Model of the upper atmosphere from 130 through 16000 km, derived from satellite orbits, *Space Res.*, **2**, 902–917, 1961.

MARZAHN, K., Vorbereitung der gemeinsamen Ausbeichung der Pendel und Gravimetermessungen des europäischen Gravimeter-Eichsystems, *Bull. Geod.*, **60**, 125–130, 1961.

MASSEVICH, A. G., Some results of international cooperation on visual and photographic simultaneous tracking of satellites at USSR and East European tracking stations in 1963, *Space Res.*, **5**, 839–848, 1965.

MASSEVICH, A. G., AND A. M. LOZINSKY, Norge Sovetskye kamery dlya fotonablyudenly iskusstrennykh nebesnyky bel, *Vestnik Acad. Nauk SSSR*, 1970.

MASSEVICH, A., S. TATEMAN, AND N. KOVALENKA, Simultaneous tracking of the PAGEOS satellite with small cameras placed at large distances, *Space Res.*, **5**, 6–14, 1969.

MATHER, R. S., *The Australian Geodetic Datum in Earth Space*, Rep. 19, University of New South Wales, Kensington, Australia, 1970.

MATHER, R. S., B. C. BARLOW, AND J. G. FRYER, *A Study of the Earth's Gravitational Field in the Australian Region*, Rep. 22, University of New South Wales, Kensington, Australia, 1971.

MCCLURE, F. T., Method of navigation, U.S. Patent 3,172,108, March 1965.

MCVITTIE, G. C., The general relativity "force" on a satellite, in *Dynamics of Satellite Orbits*, edited by M. Roy, pp. 197–201, Springer-Verlag, Berlin, 1963.

MEADE, B. K., High-precision, transcontinental, traverse surveys, *Surv. Mapping*, **27**, 41–46, 1967.

MEADE, B. K., High-precision geodimeter traverse surveys in the United States, *Bull. Geod.*, **90**, 371–386, 1968.

MELBOURNE, W. G., The determination of planetary masses from radio tracking of space probes and planetary radar, in *Dynamics of Satellites*, edited by B. Morando, Springer, New York, 1970.

MELBOURNE, W. G., ET AL., *Constants and Related Information for Astrodynamic Calculations*, 1968, TR–32–1306, Jet Propulsion Laboratory, Pasadena, Calif., July 1968.

MELCHIOR, P., R. DEJAIFFE, AND R. VERBEIREN, General considerations about the revision of all the calculations of the International Latitude Service, *IAU Symposium No. 48*, Int. Astron. Union, Paris, 1972.

MENGEL, J. T., Tracking the Earth satellite and data transmission by radio, *Proc. IRE*, **44**, 755–760, 1956.

MERSMAN, W. A., *Theory of the Secular Variations in the Orbit of a Satellite of an Oblate Planet*, NASA TR–R–99, 1961.

MERSON, R. H., D. G. KING-HELE, AND R. N. A. PLIMMER, Changes in the inclination of satellite orbits to the equator, *Nature*, **183**, 239–240, 1959.

MERTENS, L. E., AND R. H. TABELING, Tracking instrumentation and accuracy on the Eastern Test Range, *IEEE Trans. Space Electron. Telem.*, **11** (3), 14, 1965.

MESSAGE, P. J., On Mr. King-Hele's theory of the effect of the Earth's oblateness on the orbit of a close satellite, *Mon. Notic. Roy. Astron. Soc.*, **121**, 1–4, 1960.

MIKHAILOV, A. A., The astronomical unit of length, *Space Res.*, **3**, 857–871, 1962.

MILLER, J. C., *Quadrature in Terms of Equally Spaced Function Values*, Summary Rep. 167, Mathematical Research Center, University of Wisconsin, Madison, 1968.

MILLER, L. F., V. J. ONDRASIK, AND C. C. CHAO, *A Cursory Examination of the Sensitivity of the Tropospheric Range and Doppler Effects to the Shape and Refractivity Profile*, TR–32–1526, Vol. I, pp. 22–31, Jet Propulsion Laboratory, Pasadena, California, February 15, 1971.

MILLMAN, G. E., Atmosphere effects on VHF and UHF propagation, *Proc. IRE*, **46**(8), 1492–1501, 1958.

MILNE, W. E., *Numerical Calculus*, Princeton University Press, Princeton, N.J., 1949.

MITCHELL, H. C., *Definitions of Terms Used in Geodetic and Other Surveys*, Spec. Publ. 242, 87 pp., Superintendent of Documents, Washington, D.C., 1948.

MITTERMAYER, E., Generalization of the least-squares method for the adjustment of free networks, *Bull. Geod.*, **104**, 139–158, 1972.

MOLODENSKIJ, M., Lösung der intergralgleichung zur ermittlung der Erdfigur, *Bull. Geod.*, **64**, 181–187, 1962.

MOLODENSKY, M. S., V. F. EREMEEV, AND M. L. YURKINA, *Methods for the Study of the External Gravitational Field and Figure of the Earth*, Izdat. Geo-codez. Literati., Moscow, 1960.

MOLODENSKY, M., V. YEREMEYEV, AND M. YURKINA, Evaluation of accuracy of Stokes's series and of some attempts to improve his theory, *Bull. Geod.*, **63**, 19–38, 1962.

MORANDO, M. B., Orbites de resonance des satellites de 24 H., *Bull. Astron.* **24**, 47–67, 1963.

MORGAN, H. R., *Catalog of 5268 Standard Stars, 1950*, Astron. Pap. 12, part 3, Superintendent of Documents, Washington, D.C., 1952.

MORITZ, H., *Least-squares Estimation in Physical Geodesy*, Rep. 130, Department of Geodetic Science, Ohio State University, Columbus, 1970.

MORRISON, F., Density layer models for the geopotential, *Amer. Sci.*, **60**(2), 229–236, 1972.

MORSE, P. M., AND H. FESHBACH, *Methods of Mathematical Physics*, 2 vols., 1978 pp., McGraw-Hill, New York, 1953.

MOTSCH, R., AND D. W. CURKENDALL, PI 6 high frequency data noise analysis, *Space Programs Summary 37–43*, Vol. III, pp. 37–39, Jet Propulsion Laboratory, Pasadena, Calif., January 31, 1967.

MOTTINGER, N., Status of D.S.F. location solutions for deep space probe missions, Deep Space Network, *Space Programs Summary 37–60*, Vol. II, pp. 77–89, Jet Propulsion Laboratory, Pasadena, Calif., 1969.

MOTTINGER, N. A., AND W. L. SJOGREN, Consistency of Lunar Orbiter II ranging and Doppler data, *Space Programs Summary 37–46*, Vol. III, Jet Propulsion Laboratory, Pasadena, Calif., 1967.

MOURAD, A. G., Techniques used and some results obtained in two marine geodetic experiments, *Mar. Tech. Soc. J.*, **4**(6), November/December, 1970.

MOURAD, G., ET AL., *C-band Radar Marine Geodesy Experiment Using Vanguard—Acoustic Techniques and Results*, Rep. NAS6–1733, Battelle Memorial Institute, Columbus, Ohio, 1970a.

MOURAD, G., ET AL., Preliminary results of the establishment of a marine geodetic control point in the Pacific Ocean, *Bull. Geod.*, **96**, 107–124, 1970b.

MOURAD, G., D. M. FUBARA, A. T. HOPPER, AND G. T. RUCK, Geodetic location of acoustic ocean bottom transponders from surface positions, *Eos Trans. Am. Geophys. Union*, **53**(6), 644–649, 1972.

MOYER, T. D., *Mathematical Formulation of the Double-Precision Orbit Determination Program (DPOP)*, TR–32–1527, 160 pp., Jet Propulsion Laboratory, Pasadena, Calif., 1971.

MUELLER, I. I., *Introduction to Satellite Geodesy*, 415 pp., F. Ungar, New York, 1964.

MUELLER, I. I., *Proposed Optical Network for the National Geodetic Satellite Program*, Rep. 71, 50 pp., Department of Geodetic Science, Ohio State University, Columbus, 1966.

MUELLER, I. I., *Data Analysis in Connection With the National Geodetic Satellite Program*, Rep. 93, Department of Geodetic Science, Ohio State University, Columbus, 1967.

MUELLER, I. I., Global satellite triangulation and trilateration, *Bull. Geod.*, **87**, 53–71, 1968.

MUELLER, I. I., *Spherical and Practical Astronomy as Applied to Geodesy*, F. Ungar, New York, 1969.

MUELLER, I. I., AND M. KUMAR, *Geometric Adjustment of the South American Satellite Densification (PC–1000) Network*, Rep. 196, Department of Geodetic Science, Ohio State University, Columbus, 1973.

MUELLER, I. I., AND J. D. ROCKIE, *Gravimetric and Celestial Geodesy: A Glossary of Terms*, F. Ungar, New York, 1967.

MUELLER, I. I., AND M. C. WHITING, Free adjustment of a geometric global satellite network (solution MPS7), *Mitt. Geod. Inst. Tech. Hochsch. Graz*, **11**(2), 39–47, 1972.

MUELLER, I. I., J. P. REILLY, AND C. R. SCHWARZ, *The North American Datum in View of GEOS–1 Observations*, Rep. 125, Department of Geodetic Science, Ohio State University, Columbus, 1969.

MUELLER, I., C. SCHWARZ, AND J. REILLY, Analysis of geodetic satellite (GEOS–1) observations in North America, *Bull. Geod.* **96**, 143–163, 1970a.

MUELLER, I. I., J. P. REILLY, C. R. SCHWARZ, AND G. BLAHA, *SECOR Observations in the Pacific*, Rep. 140, Department of Geodetic Science, Ohio State University, Columbus, 1970b.

MUELLER, I. I., J. P. REILLY, AND T. SOLER, *Geodetic Satellite Observations in North America (Solution NA–9)*, Rep. 187, Department of Geodetic Science, Ohio State University, Columbus, 1972.

MUELLER, I. I., M. KUMAR, J. REILLY, AND N. SAXENA, *Free Geometric Adjustment of the DOC/DOD Cooperative Worldwide Geodetic Satellite (BC–4) Network*, Rep. 193, Department of Geodetic Science, Ohio State University, 1973a.

MUELLER, I. I., M. KUMAR, AND T. SOLER, *Free Geometric Adjustment of the SECOR Equatorial Network*, Rep. 195, Department of Geodetic Science, Ohio State University, Columbus, 1973b.

MUELLER, I. I., M. KUMAR, J. P. REILLY, N. SAXENA, AND T. SOLER, *Global Satellite Triangulation and Trilateration for the National Geodetic Satellite Program*, Rep. 199, Department of Geodetic Science, Ohio State University, Columbus, 1973c.

MULHALL, B. D., ET AL., *Tracking System Analytic Calibration Activities for the Mariner Mars 1969 Mission*, TR–32–1499, Jet Propulsion Laboratory, Pasadena, Calif., November 1970.

MULLER, P., Reperage des temps et reduction des cliches selon les methodes employees à l'observatoire de Meudon, *Space Res.*, **2**, 33, 1961.

MUNK, W., AND G. J. F. MACDONALD, *The Rotation of the Earth*, Cambridge University Press, London, 1960.

MUNK, W. H., AND G. J. F. MACDONALD, Continentality and the gravitational field of the Earth, *J. Geophys. Res.*, **65**, 2169–2172, 1960.

MURPHY, J., AND T. FELSENTREGER, *Analysis of Lunar and Solar Effects on the Motion of Close Earth Satellites*, NASA TN–D–494, 1966.

MURPHY, J. P., AND J. W. SIRY, Lunar mascon evidence from Apollo orbits, *Planet. Space Sci.*, **18**, 1137–1141, 1970.

MURPHY, J. P., AND E. L. VICTOR, Determination of second and fourth order sectorial harmonics in the geopotential from the motion of twelve-hour satellites, *Planet. Space Sci.*, **16**, 195–204, 1968.

MUSEN, P., Special perturbations of the vectorial elements, *Astron. J.*, **59**, 262–267, 1954.

MUSEN, P., The influence of solar radiation pressure on the motion of an artificial satellite, *J. Geophys. Res.*, **65**(5), 1391–1400, 1960.

MUSEN, P., On the long-period effects in the motion of an artificial satellite caused by the ellipticity of the equator, *J. Geophys. Res.*, **67**(1), 313–321, 1963a.

MUSEN, P., On determining the secular and critical effects in the motion of satellites by means of a nonsingular set of vectorial elements, *J. Geophys. Res.*, **68**(23), 6255–6261, 1963b.

MUSEN, P., AND D. ESTES, On the tidal effects in the motion of artificial satellites, *Celestial Mech.*, **6**, 4–21, 1972.

MUSEN, P., AND T. L. FELSENTREGER, On the determination of the long-period tidal perturbations in the elements of artificial Earth satellites, *Celestial Mech.*, **7**(2), 256, 1973.

NÄBAUER, M., Ein Verfahren zur strengen Ausgleichung von Satellitentriangulationen unter Berücksichtigung gewissen Korrelationen, in *Münchner Beiträge zur Satellitengeodesie*, edited by M. Kneissl, pp. 33–40, Bayerischen Akademy der Wissenschaft, München, 1967.

NANJO, M., Y. IZAWA, AND C. YAMANAKA, Multicoincidence method of photon counting for optical tracking, *Space Res.*, **9**, 15–22, 1969.

NASA DIRECTORY OF OBSERVATION STATION LOCATIONS, 2 vols., NASA Doc. NAS CR-130071, CR-130072, 1971.

NETTELBLAD, F., Studies of astronomical scintillation, *Lund Obs. Publ.*, Ser. II, no. 130, Sweden, 1953.

NEWCOMBE, S., *A Compendium of Spherical Astronomy*, 444 pp., Dover, New York, 1906.

NEWELL, H. F., AND L. N. CORNIER, Atmospheric density inferred from drag accelerations, *Ann. Internat. Geophys. Yr.*, **12**, 207–319, 1960.

NEWTON, R. R., Geodetic measurements by analysis of the Doppler frequency received from a satellite, *Space Res.*, **1**, 532–539, 1960.

NEWTON, R. R., Variables that are determinate for any orbit, *Amer. Rocket Soc. J.*, **31**(3), 364–366, 1961.

NEWTON, R. R., Ellipticity of the equator deduced from the motion of TRANSIT 4A, *J. Geophys. Res.*, **67**, 415–416, 1962.

NEWTON, R. R., Observation of the satellite perturbation produced by the solar tide, *J. Geophys. Res.*, **70**(24), 5983–5990, 1965.

NEWTON, R. R., The U.S. Navy Doppler geodetic system and its observational accuracy, *Phil. Trans. Roy. Soc. London*, Sect. A, **262**, 50–66, 1967.

NEWTON, R. R., A satellite determination of tidal parameters and Earth decelerations, *Geophys. J. Roy. Astron. Soc.*, **14**, 505, 1968.

NEWTON, R. R., AND R. B. KERSHNER, The TRANSIT system, *J. Inst. Navigat.*, **15**, 129–144, 1962.

NEWTON, R. R., H. S. HOPFIELD, AND B. C. KLINE, Odd harmonics of the Earth's gravitational field, *Nature*, **190**, 617–618, 1961.

NEY, C. H., Contours of the geoid for southeastern Canada, *Bull. Geod.*, **23**, 73–100, 1951.

NICHOLSON, W., AND D. SADLER, Atomic standards of frequency and the second of ephemeris time, *Nature*, **210**, 187, 1966.

NICOLAIDES, J. D., Project TRANSIT, *Aerosp. Eng.*, **20**(2), 20–21, 60–65, 1961.

NIETHAMMER, TH., *Die genauer Methoden der astronomisch-geographische Ortsbestimmung*, Verlag Birkhäuser, Basel, 1947.

NORTON, R. H., AND R. L. WILDEY, Fundamental limitations to optical Doppler measurements for space navigation, *Proc. IRE*, **49**, 1655–1659, 1961.

NOTTARP, K., *Untersuchung der Zeitsysteme der Satellitenkameras IGN Nr. 2A, IGN Nr. 25 und BC-4-BE2 Nr. 308 Einschlieslich der Langwellenzeitzeichenempfänger T75A und E390*, Institute für Angewandts Geodesie, Frankfurt am Main, 1969.

NULL, G. W., Recent determinations of the Earth-Moon mass ratio using radio tracking data from Mariner and Pioneer spacecraft, *Bull. Am. Astron. Soc.*, **2**, 1970.

NULL, G. W., ET AL., *The Mariner IV Flight Path and Its Determination From Tracking Data*, TR-32-1108, p. 38, Jet Propulsion Laboratory, Pasadena, Calif., August 1967.

O'HANDLEY, D. A., ET AL., *JPL Development Ephemeris Number 69*, TR-32-1465, Jet Propulsion Laboratory, Pasadena, Calif., December 1969.

O'KEEFE, J. A., Occultation method of long-line measurements, *Bull. Geod.*, **49**, 64–65, 1958.

O'KEEFE, J. A., Determination of the Earth's gravitational field, *Space Res.*, **1**, 448–457, 1960.

O'KEEFE, J. A., AND P. ANDERSON, The Earth's equatorial radius and the distance to the Moon, *Astron. J.*, **57**(4), 108–121, 1952.

O'KEEFE, J. A., ET AL., *Oblateness of the Earth by Artificial Satellites*, Harvard Announcement Card 1408, Harvard Astronomical Observatory, Cambridge, Mass., 1958.

O'KEEFE, J. A., A. ECKELS, AND R. SQUIRES, Gravitational field of the Earth, *Astron. J.*, **64**(7), 245–253, 1959a.

O'KEEFE, J. A., N. ROMAN, B. YAPLEE, AND A. ECKELS, Ellipsoid parameters from satellite data, in *Contemporary Geodesy*, Geophys. Monogr. 4, edited by C. Whitten and K. H. Drummond, pp. 45–51, American Geophysical Union, Washington, D.C., 1959b.

ONDRASIK, V. J., AND B. D. MULHALL, Estimation of the ionospheric effect on the apparent location of a tracking station, Deep Space Network, *Space Programs Summary 37-57*, Vol. II, pp. 29–42, Jet Propulsion Laboratory, Pasadena, Calif., May 31, 1969.

ONDRASIK, V. J., B. D. MULHALL, AND N. A. MOTTINGER, A cursory examination of the effect of space plasma on Mariner 5 and Pioneer 9 navigation with implications for Mariner Mars 1971 TSAC, Deep Space Network, *Space Programs Summary 37–60*, Vol. II, pp. 89–94, Jet Propulsion Laboratory, Pasadena, Calif., November 30, 1969.

O'NEIL, W. J., ET AL., *The Surveyor 3 and Surveyor 4 Flight Paths and Their Determination From Tracking Data*, TR–32–1292, pp. 45, 87, Jet Propulsion Laboratory, Pasadena, California, August 1968.

ORLIN, H., The three components of the external anomalous gravity field, *J. Geophys. Res.*, **64**(12), 2393–2401, 1959.

ORZAG, A. La station de telemetric laser de l'observatoire du Pic du Midi, *Bull. Groupe Rech. Geod. Spatiale* **1**, 85–93, 1971.

OSTACH, A. M., AND L. P. PELLINEN, *Effects of the Earth's Ellipticity on Its Stokes' Constants* (translation), Trans. Central Sci. Res. Inst. Geod., Aerial Surv. Control 171, 1960.

OTERMA, L., *Computing the Refraction for the Vaisala Astronomical Method of Triangulation*, Information 20, Astronomia-Optika Institute, University of Turku, Finland, 1960.

OWEN, S. D., Evaluation of HIRAN networks, *J. Geophys. Res.*, **65**(2), 467–471, 1960.

OWENS, J. C., Optical refractive index of air dependence on pressure, temperature, and composition, *Appl. Opt.*, **6**(1), 51–58, 1967.

PAGE, C. H., ET AL., IEEE recommended practice for units in published scientific and technical work, *Spectrum*, **3**(3), 169–174, 1966.

PALMAN, I., Ein Verfahren zur Komparatorprütung, in *München Beiträge zur Satellitenggeodesie*, edited by M. Kneissl, pp. 61–71, Bayerischen Akademy der Wissenschaft, München, 1967.

PARKYN, D. G., Satellite orbits in an oblate atmosphere, *J. Geophys. Res.*, **65**(1), 9–17, 1960.

PATTON, R. B., JR., AND V. W. RICHARD, Determination of orbital elements and refraction effects from single pass Doppler observations, *Space Res.*, **2**, 218–244, 1961.

PEARSON, F. F., TM–K67/65, Naval Weapons Laboratory, Washington, D.C., 1965.

PEASE, G., ET AL., *The Mariner 5 Flight Path and Its Determination From Tracking Data*, TR–32–1363, p. 7, Jet Propulsion Laboratory, Pasadena, Calif., July 1969.

PECK, E. R., AND K. REEDER, Dispersion of air, *J. Opt. Soc. Amer.*, **62**(8), 958–962, 1972.

PEKERIS, C. L., AND Y. ACCAD, Solution of Laplace's equations for the M2 tide in the world's oceans, *Phil. Trans. Roy. Soc. London*, Sect. A, **265**, 413–436, 1969.

PELLINEN, L. P., Accounting for topography in the calculation of quasigeoidal heights and plumb-line deflections from gravity anomalies, *Bull. Geod.*, **63**, 57–65, 1962.

PELLINEN, L. P., Computation of triangulation by the projection method and the corresponding accuracy required of the heights above the reference ellipsoid, *Bull. Geod.*, **68**, 121–126, 1963.

PELLINEN, L. P., Proper ways of joint reduction of ground and space triangulation, *Bull, Stantsii Opt. Nahl. Isz.*, **55**, 23–30, 1968.

PLAMONDON, J. A., The Mariner Mars 1969 temperature control flux monitor, Supporting Research and Advanced Development, *Space Programs Summary 37–59*, Vol. III, pp. 162–168, Jet Propulsion Laboratory, Pasadena, Calif., 1969.

PLOTKIN, G. G., Comparison of the interferometry and Doppler methods of satellite tracking, *Ond. Elec.*, **43**, 1227–1234, 1963.

PLOTKIN, H. H., The S–66 laser satellite tracking experiment, in *Quantum Electronics III*, Vol. II, edited by P. Grivet and N. Bloembergen, pp. 1319–1332, Columbia University Press, New York, 1964.

PLUMMER, H. C., *An Introductory Treatise on Dynamical Astronomy*, Cambridge University Press, Cambridge, 1918.

PODOBED, V. V., AND A. N. VYSSOTSKY (EDS.), *Fundamental Astrometry*, University of Chicago Press, Chicago, Ill., 1965.

POINCARÉ, H., *Les Methodes Nouvelles de la Mechanique Celeste*, Vol. II, 479 pp., Gauthier-Villars, Paris, 1893.

PORITSKY, H., Motion of a satellite around an oblate Earth, *Astron. J.*, **63**, 212–216, 1962.

PORTER, J. G., A comparative study of perturbation methods, *Astron. J.*, **63**, 405–406, 1958.

POTTER, K. D., On the use of observations of the Moon for geodetic purposes, *Astron. Zh.*, **35**, 618–622, 1958.

PRATT, J. H., On the attraction of the Himalaya Mountains, and of the elevated regions beyond them, upon the plumb-line in India, *Phil. Trans.*, **145**, 53–100, 1855.

PRATT, J. H., On the influence of the ocean on the plumb-line in India, *Phil. Trans.*, **149**, 779–796, 1859a.

PRATT, J. H., On the deflection of a plumb-line in India, caused by the attraction of the Himalaya Mountains and of the elevated regions beyond; and the modification by the compensating effect of a deficiency of matter below the mountain mass, *Phil. Trans.*, **149**, 745–778, 1859b.

PRATT, J. H., On the Indian arc of meridian, *Phil. Trans.*, **151**, 579–594, 1861.

PREUSS, H. D., *Determination and Distribution of Precise Time*, Rep. 70, 164 pp., Research Foundation, Ohio State University, Columbus, Ohio 1966.

PREY, A., Darstellung der Höhen- und Tiefenverhältnisse der Erde, *Abh. Gesell. Wiss. Göttingen*, **9**, 1, 1922.

PRIESTER, W., W. ROEMER, AND H. VOLLAND, *Physical Behavior of the Upper Atmosphere Deduced From Satellite Drag Data, Space Sci. Rev.*, **6**, 707–780, 1967.

PRIOR, E. J., Earth albedo effects on the orbital variations of ECHO–1 and PAGEOS–1, in *Proceedings of Dynamics of Satellites Symposium, Prague, Czechoslovakia, May 20–24, 1969*, pp. 303–312, Springer-Verlag, Berlin, 1970.

PRIOR, E. J., Observed effects of Earth-reflected radiation and hydrogen drag on the orbital accelerations of balloon satellites in *The Use of Artificial Satellites for Geodesy*, Geophys. Monogr. 15, edited by S. Henriksen, B. Chovitz, and A. Mancini, pp. 197–207, American Geophysical Union, Washington, D.C., 1972.

Proceedings of the 11th General Assembly, Berkeley, 1961 (Translation), Intern. Astron. Union, Vol. XI B, Academic, New York, 1962.

RADAU, R., *Compt. Rendus Acad. Sci. Paris*, **100**, 972–974, 1885.

RADER, F., P. BROWN, G. WINKLER, AND C. BICKERT, Results of a long-range clock synchronization experiment, *Proceedings IRE*, **49**(6), 1028–1032, 1961.

RAMSAYER, K., Beitrage zur Fehlertheorie der schwere Reduktion von Nivellements, *Deut. Z. Vermess.*, sonderhefte **1**, 1954.

RAPP, R. H., Geopotential to (14, 14) from a combination of satellite and gravimetry data, *Bull. Geod.*, **91**, 47–80, 1965.

RAPP, R. H., Comparison of mean gravity anomalies at elevation with corresponding ground anomalies, *Bull. Geod.*, **83**, 55–66, 1967.

RAPP, R. H., Gravitational potential of the Earth determined from a combination of satellite, observed, and model anomalies, *J. Geophys. Res.*, **73** (20), 6555–6563, 1968.

RAPP, R. H., Gravitational potential coefficients from gravity data alone, *Allg. Vermess. Nachr.*, **1969** (6), 228–233, 1969.

RAPP, R. H., Equal-area blocks, *Bull. Geod.*, **99**, 113–125, 1971a.

RAPP, R. H., Methods for the computation of geoid undulations from potential coefficients, *Bull. Geod.*, **101**, 283–298, 1971b.

RAPP, R. H., *Formation and Analysis of a 5° Equal-Area-Block Terrestrial Gravity Field*, Rep. 178, Research Foundation, Ohio State University, Columbus, 1972a.

RAPP, R. H., Geopotential coefficients behavior to high degree (abstract), *Eos Trans. Am. Geophys. Union*, **53**(10), 891, 1972b.

RAPP, R. H., *Comparison of Least Squares and Collocation Estimated Potential Coefficients*, Rep. 200, Department of Geodetic Science, Ohio State University, Columbus, Ohio, 1973a.

RAPP, R. H., The Earth's gravitational field from the combination of satellite and terrestrial data, in *Proceedings of Symposium on Earth's Gravitational Field and Secular Variations in Position*, edited by R. Mather and P. Angus-Leppan, Australian Acad. of Sci., Sydney, pp. 51–75, 1973b.

RAPP, R. H., AND K. LAMBECK, Comparison of surface gravity data with satellite data, *Bull. Geod.*, **105**, 343–350, 351–358, 1972.

RATYNSKIY, M. V., Problem of determination of the index of refraction of air during distance measurement with electro-optical and pulsed-wave range finders, *Geod. Aerophot.*, **1964**(2), 1964.

RAWER, K., Radio propagation between a space vehicle and the Earth in the presence of the ionosphere, *Space Res.*, **1**, 245–271, 1960.

REECE, J. S., AND J. G. MARSH, *Simultaneous Observation Solutions for NASA–MOTS and SPEOPTS Station Position on the North American Datum*, NASA TM–X–66297, National Technical Information Service, Springfield, Va., June 1973.

Refraction Tables of Polkora Observatory, 4th ed., Ist. Akad. Nauk SSSR, Moscow, 1956.

REILLY, J. P., C. R. SCHWARZ, AND M. C. WHITING, *The Ohio State University Geometric and Orbital (Adjustment) Program (OSUGOP) for Satellite Observations*, Rep. 190, Department of Geodetic Science, Ohio State University, Columbus, 1972.

REMMER, O., A statistical filter for geodetic observations, *Bull. Geod.*, **92**, 99–122, 1969.

RIBLET, R. B., A broad-band spherical satellite antenna, *Proc. Inst. Radio Eng.*, **48**(4), 631–635, 1960.

RICE, D. A., Ephemeris time and universal time, *Surv. Mapping*, **19**, 367–370, 1959.

RICE, D. A., Geoidal section of the United States, *Bull. Geod.*, **65**, 243–251, 1962.

RICHTER, H. L., JR., The microlock radio tracking system, *Ann. Internat. Geophys. Yr.*, **6**, 410–417, 1958.

RICHTER, H. L., JR., W. F. SAMPSON, AND R. STEVENS, Microlock: A minimum-weight radio instrumentation system for a satellite, in *Vistas in Astronautics*, edited by M. Alperin and M. Sterov, Pergamon Press, New York, 1958.

RIDENOUR, L. N. (ED.), *Radar System Engineering*, McGraw-Hill, New York, 1947.

RIKHLOVA, L. V., Oscillations du pole de la terre pour 119 ANS, *Diss. Obs. Astron. Englehardt*, 1969.

RINNER, K., *Systematic Investigations of Geodetic Networks in Space*, Contract 91–591–EUC 3584, Ann. TR, European Research Office, Graz, Austria, 1966.

RINNER, K., ET AL., *Beiträge zur Theorie der Geodätischen Netze im Raum*, Deutsche Geodätische Kommission, Reihe A, Heft 61, Munich, 1967.

ROLFF, J., *The PAGEOS Satellite*, Bull. 2, 6 pp., Smithsonian Astrophysical Observatory, Cambridge, Mass., 1966.

ROSEN, V. S., *Multi-Step Runge-Kutta Methods*, NASA TN-D-4408, 21 pp., Superintendent of Documents, Washington, D.C., 1965.

ROSENBERG, J., Objectives of the NGSP, in GEOS-1 Operations and Plans for GEOS-B, Vol. I of *Proceedings of the GEOS-1 Review Meeting*, edited by Communications and Systems, Inc., NASA, Washington, D.C., 1968.

ROSENFIELD, G. H., Present and future capability of optical systems with emphasis on the ballistic camera operation, *Photogram. Eng.*, **27**(1), 51–55, 1961.

ROSENFIELD, G. H., Calibration of a precision coordinate comparator, *Photogram. Eng.*, **29**(1), 161–173, 1963.

ROSSITER, J. R., An analysis of annual sea level variations in European waters, *Geophys. J. Roy. Astron. Soc.*, **12**, 259–299, 1967.

ROUTH, E. J., *Dynamics of a System of Rigid Bodies*, Vol. II, Dover, New York, 1960.

RUNGE, C., Über die numerishe Auflösung von Differentialgleichungen, *Math. Ann.*, **46**, 167–178, 1895.

RYAN, C. (ED.), *Across the Space Frontier*, Viking, New York, 1952.

SAASTAMOINEN, J., Some meteorological aspects in the measurement of long lines by electromagnetic means, *Bull. Geod.*, **88**, 159–162, 1968.

SAASTAMOINEN, J., Contribution to the theory of atmospheric refraction, *Bull. Geod.*, **105**, 279–298, 1972.

SAGITOV, M. U., Current status of determination of the gravitational constant and the mass of the Earth, *Sov. Astron. AJ*, **13**(4), 712–718, 1970.

SAKUMA, A., Etat actual de la nouvelle determination absolue de la pesanteur au Bureau International des Poids et Mesures, *Bull. Geod.*, **69**, 249–260, 1963.

SAXENA, N. K., *Improvement of a Geodetic Triangulation Through Control Points Established by Means of Satellite or Precision Traversing*, Rep. 177, Department of Geodetic Science, Ohio State University, Columbus, 1972.

SCARBOROUGH, J. B., *Numerical Mathematical Analysis*, 6th ed., Johns Hopkins University Press, Baltimore, Md., 1966.

SCHAUB, W., *Vorlesung über Spärische Astromie*, Akademische Verlagsges, Geest & Portig A.G., Leipzig, 1950.

SCHAUER, P. C., *The Determination of Geodetic Positions and Distances by Means of a Solar Eclipse*, Monogr. 2, Georgetown College Observatory, Washington, D.C., 1952.

SCHMID, E., *Phase Correction for Sun-Reflecting Spherical Satellites*, NOAA TR-NOS-43, 8 pp., Superintendent of Documents, Wash., D.C., 1971.

SCHMID, E., AND H. SCHMID, Curve and surface fitting with potential functions, *Z. Vermess.*, **1971** (11), 488–497, 1971.

SCHMID, H., Eine allgemein analytische Lösung für die Aufgabe der Photogrammetrie, *Bildmess. Luftbildwess.*, **1958**(4), 103–113, 1958.

SCHMID, H., Eine allgemein analytische Lösung für die Aufgabe der Photogrammetrie, *Bildmess. Luftbildwess.*, **1959**(1), 1–12, 1959.

SCHMID, H., Some problems connected with the execution of photogrammetric multi-station triangulations, in *The Use of Artificial Satellites for Geodesy*, edited by G. Veis, pp. 56–65, North Holland, Amsterdam, 1961.

SCHMID, H., Ein allgemeiner Ausgleichungs-Algorithmus zur Auswertung von hybriden Me Anordnungen, *Bildmess. Luftbildwess.*, **33**(3/4), 93–102, 173–176, 1965a.

SCHMID, H., Accuracy aspect of a worldwide passive satellite triangulation system, *Photogram. Eng.*, **21**(1), January 1965b.

SCHMID, H., Reformatory and revolutionary changes in geodesy, *Bull. Geod.*, **80**, 141–147, 1966a.

SCHMID, H., *The Status of Geometric Satellite Triangulation at the Coast and Geodetic Survey*, Environmental Science Services Administration, U.S. Dept. of Commerce, Washington, D.C., 1966b.

SCHMID, H., Satellite triangulation, in *The Use of Artificial Satellites for Geodesy*, edited by G. Veis, National Technical University, Athens, 1967a.

SCHMID, H., Geodetic satellites: Reduction of geometric data, *Eos Trans. Am. Geophys. Union*, **48** (2), 333–337, 1967b.

SCHMID, H., Application of photogrammetry to three-dimensional geodesy, *Eos Trans. Am. Geophys. Union*, **50**(1), 4–12, 1969.

SCHMID, H., Satellitengeodäsie—*Das Mittel zur Erstellung eines globalen geodätischen Bezugssystems*, Wild-Heerbrugg 50-Jahr-Festschrift, Heerbrugg, 1971.

SCHMID, H., AND E. SCHMID, Generalized least-squares solution for hybrid measuring systems, *Can. Surv.*, **9**(1), 27–41, 1965.

SCHMIDT, A., *Tafeln der normierten Kugelfunktionen*, Engelhard-Reyher Verlog, Gotha, 1935.

SCHMIDT, B., Ein lichstärkes komafries Spiegelsysteme, *Mitt. Hamburger Sternwarte*, **7**, 15, 1932.

SCHNELZER, G. A., *Comparison of Atmospheric Refractive Index Adjustments for Laser Satellite-Ranging*, Rep. HIG-72-14, 80 pp., Hawaii Institute of Geophysics, University of Hawaii, Honolulu, 1972.

SCHORR, R., AND A. KOHLSCHUTTER, *Zweiter Katalog der astronomischen Gesellschaft fur des Aquinoktium 1950*, vols. 1–10, Hamburg Sternwarte, Verladd. Sternwarte, Hamburg-Bergedorf, 1951–1953.

SCHRANK, H. E., AND R. D. GROVE, The helisphere passive beacon, *Microwaves*, **1968**, 59–64, August 1968.

SCHREIBER, M., AND T. WYATT, Evolution and testing of a navigational satellite, *Elec. Eng.*, **79**, 1033–1040, 1960.

SCHROEDER, C. A., C. H. LOONEY, JR., AND H. E. CARPENTER, JR., Tracking orbits of man-made moons, *Electronics*, **32**(1), 33–37, 1959.

SCHULKIN, M., Average radio-ray refraction in the lower atmosphere, *Proc. IRE*, **40**, 5, 1952.

SCHULZ, G., Reduktion photographischer Satellitenaufrahman der station Karlsruhe, *Allg. Vermess.*, **1970**(4), 148–155, 1970.

SCHWARZ, C. R., *The Use of Short Arc Orbital Constraints in the Adjustment of Geodetic Satellite Data*, Rep. 118, Department of Geodetic Science, Ohio State University, Columbus, Ohio, 1968.

SCHWARZ, C. R., *Gravity Field Refinement by Satellite to Satellite Doppler Tracking*, Rep. 147, Department of Geodetic Science, Ohio State University, Columbus, Ohio, 1970.

SCHWARZ, C. R., Refinement of the gravity field by satellite-to-satellite tracking, in *The Use of Artificial Satellites for Geodesy*, Geophys. Monogr. 15, edited by S. Henriksen, B. Chovitz, and A. Mancini, pp. 133–138, American Geophysical Union, Washington, D.C., 1972.

SCHWEBEL, R., Das ballistiche Messkammersystem BMK 46/18/1:2, *Bildmess. Luftbildwiss.*, **1970**, 135, 1970.

SCHWIDERSKI, E. W., Mantle convection and crustal tectonics inferred from a satellite orbit: A different view of sea-floor spreading, *J. Geophys. Res.*, **73**(8), 2828–2832, 1968.

SCOTT, F. P., Fundamental work at Washington, in *Transactions of International Astronomical Union IX*, pp. 713–716, Cambridge University Press, Cambridge, England, 1957.

SCOTT, F. P., The system of fundamental motions, in *Basic Astronomical Data*, edited by K. A. Strand, chap. 2, University of Chicago Press, Chicago, Ill., 1963.

SCOTT, F. P., A method of evaluating the elliptic *E* terms of the aberration, *Astron. J.*, **69**, 372–373, 1964.

SCOTT, F. P., AND J. A. HUGHES, Computation of apparent places for the southern reference star program, *Astron. J.*, **69**(5), 368–370, 1964.

SEARLE, R. C., AND B. W. DARRACOTT, *Catalogue of Gravity Data From Kenya, to January 1971*, Department of Geophysics and Planetary Physics, University of Newcastle Upon Tyne, England, 1971.

SEEBER, G., AND J. CAMPBELL, Note on the accuracy of the Zeiss BMK 46/18/1:45 satellite camera system, *Mitt. Geod. Inst. Tech. Hochsch. Graz*, **11**(1), 245–249, 1972.

SEHNAL, L., AND S. B. MILLS, *The Short-period Drag Perturbations of the Orbits of Artificial Satellites*, Spec. Rep. 233, 30 pp., Smithsonian Astrophysical Observatory, Cambridge, Massachusetts, 1966.

SHCHEGOLEV, D. E., A. G. MASSEVICH, AND B. G. AFAMASYEV, Simultaneous tracking of the balloon satellite ECHO–1 for geodetic purposes, *Vest. Akad. Nauk USSR*, (7), 74–77, 1964.

SIEGEL, C. L., *Vorlesungen über Himmelsmechanik*, 212 pp., Springer-Verlag, Berlin, 1956.

SIMONSEN, O., Preliminary report on the triangulation between Denmark and Norway carried out in 1945 by means of parachute flares, *Bull. Geod.*, **11**, 33–52, 1949.

SJOGREN, W. L., ET AL., *The Ranger 5 Flight Path and Its Determination From Tracking Data*, TR–32–562, p. 29, Jet Propulsion Laboratory, Pasadena, Calif., December 1963.

SJOGREN, W. L., ET AL., *The Ranger 6 Flight Path and Its Determination From Tracking Data*, TR–32–605, 193 pp., Jet Propulsion Laboratory, Pasadena, Calif., 1964.

SJOGREN, W. L., ET AL., *Physical Constants as Determined From Radio Tracking of the Ranger Lunar Probes*, TR–32–1957, Jet Propulsion Laboratory, Pasadena, Calif., 1966.

SKOLNIK, M. I., *Introduction to Radar Systems*, 648 pp., McGraw-Hill, New York, 1962.

SKOLNIK, M. I., *Radar Handbook*, McGraw-Hill, New York, 1970.

SLACK, F. F., AND A. A. SANDBERG, Tracking and display of Earth satellites, *Proc. IRE*, **48**, 655–662, 1960.

SLAMA, C. A., *Mathematical Model for the Simulation of a Photogrammetric Camera Using Stellar Control*, NOAA TR–NOS–55, 1972.

SLOWLEY, J. W., Earth radiation pressure and the determination of density from atmospheric drag, *Space Res.*, **14**, in press, 1974.

SLUDSKII, F. A., The general theory of the figure of the Earth, *Mat. Sbornik*, **13**(4), 633–706, 1888.

SMART, W. M., *Text-Book on Spherical Astronomy*, 430 pp., Cambridge University Press, Cambridge, England, 1962.

SMITH, D. E., Determination of the Earth's gravitational potential from satellite orbits, *Planet. Space Sci.*, **8**, 45–48, 1961.

SMITH, D. E., Determination of the even harmonics in the Earth's gravitational function, *Planet. Space Sci.*, **13**(11), 1151–1159, 1965.

SMITH, D. E., The western European satellite triangulation programme using ECHO satellite predictions and reports of observations, *Bull. Geod.*, **82**, 359–374, 1966.

SMITH, D. E., Earth-reflected radiation pressure, *Space Res.*, **10**, 284–294, 1969.

SMITH, D. E., ET AL., Polar motion from laser tracking of artificial satellites, *Science*, **178**, 404–406, 1972a.

SMITH, D. E., R. KOLENKIEWICZ, AND P. DUNN, Geodetic studies by laser ranging to satellites, in *The Use of Artificial Satellites for Geodesy*, Geophys. Monogr. 15, edited by S. Henriksen, B. Chovitz, and A. Mancini, pp. 187–196, American Geophysical Union, Washington, D.C., 1972b.

SMITH, D. E., R. KOLENKIEWICZ, AND P. J. DUNN, A determination of the Earth tidal amplitude and phase from orbital perturbations of the Beacon Explorer C spacecraft, *Nature*, **244**, 1498, August 24, 1973a.

SMITH, D. E., F. J. LERCH, AND C. A. WAGNER, A gravitational field model for the Earth, *Space Res.*, **13**, 10–20, 1973b.

SMITH, E., AND S. WEINTRAUB, Constants in the equations for atmospheric refraction index at radio frequencies, *Proc. IRE*, **41**, 1035–1037, 1953.

SOLANI, L., AND G. INGHILLERI, Some considerations on the measurements and calculations relating to the European calibration line, *Bull. Geod.*, **69**, 235–238, 1963.

SOWERBUTTS, W. T. C., *Catalogue of Tanzanian Gravity Data to August 1968*, Department of Geophysics and Planetary Physics, University of Newcastle Upon Tyne, England, 1968.

SPENCER, C. R., *Optical Theory of the Corner Reflector*, Rep. 433, Radiation Laboratory, Massachusetts Institute of Technology, Cambridge, 1944.

STAFF OF SMITHSONIAN ASTROPHYSICAL OBSERVATORY, Notes on the design and operation of satellite tracking stations for geodetic purposes, Spec. Rep. 124, Cambridge, Mass., 1963.

STAFF OF SMITHSONIAN ASTROPHYSICAL OBSERVATORY, *SAO Star Catalogue*, 4 vols., 2600 pp., Superintendent of Documents, Washington, D.C., 1966.

STEARNS, J. L., Tests of departure from the normal distribution for theodolite errors of observation, *Can. Surv.*, **18**, 1964.

STEARNS, J., AND H. RICHARDSON, Adjustment of conditions with parameters and error analysis, *Bull. Geod.*, **64**, 117–136, 1962.

STEINBACH, M., Some optical systems for the observation of artificial Earth satellites, *Jena Rundsch.*, **6**, 254–258, 1963.

STEINBACH, M., Satellite tracking SBG 420/500/760, in *The Use of Artificial Satellites for Geodesy*, edited by G. Veis, pp. 39–56, National Technical University, Athens, 1967.

STERNE, T. E., The gravitational orbit of a satellite of an oblate planet, *Astron. J.*, **63**, 28–40, 1958.

STERNE, T. E., Effect of the rotation of a planetary atmosphere upon the orbit of a close satellite, *Amer. Rocket Soc. J.*, **29**, 777–782, 1959.

STERNE, T. E., *An Introduction to Celestial Mechanics*, Interscience, New York, 1960.

STOKES, G. G., On the variation of gravity at the surface of the Earth, *Trans. Cambridge Phil. Soc. (Math. Phys.)*, **2**, 131–171, 1849.

STOYKO, N., Sur la determination de temps universal dans les services horaires d'apres les decisions de l'assemblee generale de l'UAI, *Bull. Horaire*, Ser. **4**(4), 77–96, 1955.

STRANGE, W. E., AND G. P. WOOLARD, *Prediction of Gravity in the United States, Utilizing Geologic and Geophysical Parameters*, Rep. HIG–64–18, Hawaii Institute of Geophysics, University of Hawaii, Honolulu, 1964.

STRUVE, O., *Tabulae Refractionum in usum Speculae Pulcovensis Congestae*, Typis Acad. Imp. Sci. Petropolitanae, Petropoli, Russia, 1870.

STUMPFF, K., *Himmelsmechaniks*, Vols. I and II, Deutsche Verlag d. Wissenschaft, Berlin, 1959 and 1965.

STURMS, F. M., JR., *Polynominal Expressions for Planetary Equators and Orbit Elements With Respect to the Mean 1950.0 Coordinate System*, TR–32–1508, Jet Propulsion Laboratory, Pasadena, Calif., January 15, 1971.

TALWANI, M., H. R. POPPE, AND P. D. RABINOWITZ, Gravimetrically determined geoid in the western North Atlantic, in *Sea Surface Topography from Space*, Vol. II, edited by J. Apel, NOAA TR–ERL 228–AOML 7–2, Superintendent of Documents, Washington, D.C., pp. 23–1 to 23–33, 1972.

TEICHMANN, L. A., *Fabrication and Testing of PAGEOS–1*, NASA TN–D–4596, 1968.

TENGSTRÖM, E., A comparison between the methods of Stokes, Molodenskii, and Hirvonen in physical geodesy, *Inst. Geod. Photogram. Cartogr.* **15**, 148–151, Ohio State University, Columbus, Ohio, 1961.

TENGSTRÖM, E., Simplified Rudzki reduction as a convenient method of reducing gravity data for geodetic and geophysical purposes, *Bull. Geod.*, **63**, 43–47, 1962.

THAYER, G. D., *Atmospheric Effects on Multiple-Frequency Range Measurements*, ESSA TR–IER 56–ITSA 53, Superintendent of Documents, Washington, D.C., 123 pp., 1967a.

THAYER, G. D., Rapid and accurate ray-tracing algorithm for a horizontally stratified atmosphere, *Radio Sci.*, **2**(2), 249–253, 1967b.

THOMAS, P. D., Geodetic positioning of the Hawaiian Islands, *Surv. Mapping*, **22**, 89–95, 1962.

THORTON, T. H., JR., ET AL., *The Surveyor 1 and Surveyor 2 Flight Paths and Their Determination From Tracking Data*, TR–32–1285, p. 48, Jet Propulsion Laboratory, Pasadena, Calif., August 1968.

THRONE, D. H., Rubidium-vapor frequency standard for systems requiring superior frequency stability, *Hewlett-Packard J.*, **19**(11), 8–14, 1968.

TISSERAND, F., *Traite de Mechanique Celeste*, Vol. I, Gauthier-Villars, Paris, 1960.

TOMLINSON, W. J., Spectrum of the flash-tube to be used on the Project ANNA satellite, *J. Opt. Soc. Am.*, **52**(3), 339–341, 1962.

TRASK, D. W., Tracking data and inherent accuracy analysis: Quality of two-way Doppler tracking data obtained during the Mariner 4 mission, *Space Programs Summary 37–38*, Vol. III, pp. 13–20, Jet Propulsion Laboratory, Pasadena, Calif., March 31, 1966.

TRASK, D. W,. AND L. EFRON, DSIF two-way Doppler inherent accuracy limitation, 3, Charged particles, The Deep Space Network, *Space Programs Summary 37–41*, Vol. III, pp. 3–12, Jet Propulsion Laboratory, Pasadena, Calif., September 30, 1966.

TRASK, D. W., AND T. W. HAMILTON, Tracking data and inherent accuracy analysis: DSIF two-way Doppler inherent accuracy limitations, *Space Programs Summary 37–38*, Vol. III, pp. 8–13, Jet Propulsion Laboratory, Pasadena, Calif., March 31, 1966.

TRASK, D. W., AND C. J. VEGOS, Intercontinental longitudinal differences of tracking stations as determined from radio tracking data, in *Continental Drift, Secular Motion of the Pole, and Rotation of the Earth*, edited by W. Markowitz and B. Guinot, pp. 91–94, D. Reidel, Dordrecht, 1968.

TSIMIS, E., *On the Geometric Analysis and Adjustment of Optical Satellite Observations*, Rep. 185, Department of Geodetic Science, Ohio State University, Columbus, Ohio, 1972.

TSIMIS, E., *Critical Configurations (Determinantal Loci) for Range and Range-Difference Satellite Networks*, Rep. 191, Department of Geodetic Science, Ohio State University, Columbus, Ohio, 1973.

TSUBOKAWA, I., A precise satellite tracking camera with a photoelectric timing device, *Space Res.*, **2**, 39–42, 1961.

TURNBULL, H. W., AND A. C. AITKEN, *Theory of Canonical Matrices*, Blackie, London, 1956.

TURNER, H. H., Preliminary note on the reduction of measures of photographic plates, *Mon. Notic. Roy. Astron. Soc.*, **54**, 11, 1895.

UNGUENDOLI, M., Division de la surface terrestre en blocs d'aire égale, *Bull. Geod.*, **104**, 221–230, 1972.

UOTILA, U., *Investigations on the Gravity Field and Shape of the Earth*, 92 pp., Institute of Geodesy, Photogrammetry, and Cartography, Ohio State University, Columbus, Ohio, 1960.

UOTILA, U., Harmonic analysis of world-wide gravity material, *Ann. Acad. Sci. Fenn.*, Ser. A, **3**(67), 18 pp., 1962.

UOTILA, U., *Gravity Anomalies for a Mathematical Model of the Earth*, Publ. 43, Isostatic Institute, IUG, Helsinki, Finland, 1964.

UOTILA, U., Existing surface gravity material, in *Gravity Anomalies: Unsurveyed Areas*, Geophys. Monogr. 9, edited by H. Orlin, pp. 4–5, American Geophysical Union, Washington, D.C., 1965.

U.S. DEPARTMENT OF COMMERCE: *Satellite Triangulation in the Coast and Geodetic Survey*, ESSA Tech. Bull. 24, February 1965.

VÄISÄLÄ, Y., An astronomical method of triangulation, *Sitzungsb. Finnischen Akad. Wiss., 1947*, 99–107, 1947.

VÄISÄLÄ, Y., AND L. OTERMA, Anwengdung der astronomischen Triangulations-methode, *Verhoff 55*, Finnish Geodetic Institute, Helsinski, 1960.

VAN HEES, G. L. S., *Gravity Anomalies on the Atlantic Ocean*, Laboratory Geodesie Technische Hoogeschool, Delft, 1970

VARIOUS, *Explanatory Supplement to the Astronomical Ephemeris . . .*, Her Majesty's Stationery Office, London, 1961.

VARIOUS, *International Symposium: Satellite and Terrestrial Triangulation*, Vol. I, 264 pp., Vol. II, 399 pp., Technische Hochschule, Graz, 1972.

VARIOUS, PANEL—The ballistic camera, accuracy review report, *Photogram. Eng.*, **30**(2), 307–311, 1964.

VASILEVSKIS, S., Reference system of bright stars, intermediate and faint stars and of galaxies, in *Basic Astronomical Data*, edited by K. A. Strand, chap. 3, University of Chicago Press, Chicago, Ill., 1963.

VEACH, J. P., *Investigations into the Utilization of Passive Satellite Observational Data*, Rep. 110, Department of Geodetic Science, Ohio State University, Columbus, Ohio, 1968.

VEGOS, C. J., AND D. W. TRASK, Ranger combined analysis, part 2, Determination of the masses of the Earth and Moon from radio tracking data, *Space Programs Summary 37–46*, Vol. III, pp. 11–28, Jet Propulsion Laboratory, Pasadena, Calif., July 1967.

VEGOS, C. J., ET AL., *The Ranger 9 Flight Path and the Determination from Tracking Data*, TR-32–1057, p. 49, Jet Propulsion Laboratory, Pasadena, Calif., November 1968.

VEIS, G., Geodetic uses of artificial satellites, *Smithsonian Contrib. Astrophys.*, **3**(9), 95–161, 1960.

VEIS, G., *The Positions of the Baker-Nunn Camera Stations*, Spec. Rep. 59, 5 pp., Smithsonian Astrophysical Observatory, Cambridge, Mass., 1961.

VEIS, G., *Precise Aspects of Terrestrial and Celestial Reference Systems*, Spec. Rep. 133, Smithsonian Astrophysical Observatory, Cambridge, Mass., 1963a.

VEIS, G., Optical tracking of artificial satellites, *Space Sci. Rev.*, **2**, 250–296, 1963b.

VEIS, G., Determination of absolute directions in space with artificial satellites, *Bull. Geod.*, **72**, 147–166, 1964a.

VEIS, G., On the optimum use of satellites for geodesy, *Bull. Geod.*, **74**, 283–290, 1964b.

VEIS, G., Deflection of the vertical of major geodetic datums and the semimajor axis of the Earth's ellipsoid as obtained from satellite observations, *Bull. Geod.*, **75**, 13–46, 1965a.

VEIS, G., Deflection of the vertical of major geodetic datums and the semimajor axis of the Earth's ellipsoid as obtained from satellite observation, *Bull. Geod.*, **78**, 367–368, 1965b.

VEIS, G., The deflection of the vertical of major geodetic datums and the semimajor axis of the Earth's ellipsoid as obtained from satellite observation, *Space Res.*, **5**, 849–875, 1965c.

VEIS, G., *Relation With DSIF Stations, Geodetic Parameters for a 1966 Smithsonian Institution Standard Earth*, Spec. Rep. 200, edited by C. A. Lundquist and G. Veis, Vol. III, pp. 115–125, Smithsonian Astrophysical Observatory, Cambridge, Mass., 1966a.

VEIS, G., The motion of the spin axis and the rotation of the Earth, *Scientific Horizons From Satellite Tracking*, Spec. Rep. 236, edited by C. A. Lundquist and H. D. Friedman, pp. 123–142, Smithsonian Astrophysical Observatory, Cambridge, Mass., 1966b.

VEIS, G., Differential orbit improvement program for lunar orbiters, *Scientific Horizons From Satellite Tracking*, Spec. Rep. 236, edited by C. A. Lundquist and H. D. Friedman, pp. 215–220, Smithsonian Astrophysical Observatory, Cambridge, Mass., 1966c.

VEIS, G., Geodetic interpretation of the results, *Space Res.*, **7**, 776–777, 1967a.

VEIS, G., Results from geometric methods, *Space Res.*, **7**, 778–782, 1967b.

VEIS, G., Determination of the radius of the Earth and other geodetic parameters as derived from optical satellite data, *Bull. Geod.*, **89**, 253–277, 1968.

VEIS, G., AND C. H. MOORE, Smithsonian Astrophysical Observatory differential orbit improvement program, in *JPL Seminar Proceedings on Tracking, Programs, and Orbit Determination*, pp. 165–184, Jet Propulsion Laboratory, Pasadena, Calif., 1960.

VERET, C., Laser goniometry on satellites, *Bull. Rech. Geod. Spatiale*, **1**, 7–23, 1971.

VINCENT, S., ET AL., *Detailed Gravimetric Geoid of North America, the North Atlantic, Eurasia, and Australia*, NASA TM–X66238, National Technical Information Service, Springfield, Va., 1972a.

VINCENT, S., ET AL., A detailed gravimetric geoid of North America, North Atlantic, Eurasia, and Australia (abstract), *Eos Trans. Am. Geophys. Union*, **53**(10), 897, 1972b.

VINTI, J. P., New method of solution for unretarded satellite orbits, *J. Nat. Bur. Stand.*, **63B**, 105–116, 1959.

VINTI, J. P., Theory of an accurate intermediary orbit for satellite astronomy, *J. Res. Nat. Bur. Stand.*, **65B**(3), 169–201, 1961.

VOGEL, A., Secular variations in the lower harmonics of the Earth's gravity field due to convection currents in the Earth's core, *Medd. Geod. Inst. Uppsala*, **7**, 1963.

VON ARX, W. S., Level-surface profiles across the Puerto Rico Trench, *Science*, December 30, 1966.

VONDRAK, J., Trajectory of a light ray through the atmosphere as a solution of a system of differential equations, *Studia Geophys. Geod.*, **13**(3) 231–238, 1969.

VON PUTTKAMER, J., *Survey and Comparative Analysis of Current Geophysical Models*, NASA TN D–5163, 60 pp., 1969.

VON ZEIPEL, H., Recherches sur le mouvement des petites planetes, *Ark. Astron. Mat. Fys.*, **11**, 1–58, 1916.

WAGNER, C. A., Longitudinal variations of the Earth's gravity field as sensed by the drift of three synchronous satellites, *J. Geophys. Res.*, **71**(6), 1703–1711, 1966.

WAGNER, C. A., Determination of low-order resonant gravity harmonics from the drift of two Russian 12-hour satellites, *J. Geophys. Res.*, **73**(14), 4661–4674, 1968a.

WAGNER, C. A., Combined solution for low-degree longitude harmonics of gravity from 12- and 24-hour satellites, *J. Geophys. Res.*, **73**, 7651–7660, 1968b.

WAGNER, C. A., *Earth Zonal Harmonics From Rapid Numerical Analysis of Long Satellite Arcs*, NASA TM–X66039, National Technical Information Service, Springfield, Va., 1972.

WAGNER, C. A., AND B. C. DOUGLAS, Resonant satellite geodesy by high-speed analysis of mean Keplerian elements, in *Dynamics of Satellites*, Springer-Verlag, Berlin, 1970.

WALLENHAUPT, W. R., ET AL., *Ranger 7 Flight Path and Its Determination From Tracking Data*, TR–32–694, p. 47, Jet Propulsion Laboratory, Pasadena, Calif., December 1964.

WALTERS, L., P. KOSKELA, AND I. ARSENAULT, Solar radiation pressure perturbations, in *Handbook of Astronautical Engineering*, edited by H. Koelle, pp. 8–33, to 8–34, McGraw-Hill, New York, 1961.

WARNER, M. R., M. W. MEAD, AND R. H. HUDSON, *The Orbit Determination Program of the Jet Propulsion Laboratory*, TM–33–168, Jet Propulsion Laboratory, Pasadena, Calif., March 18, 1968.

WATKINS, E. R., JR., *Preprocessing of MINITRACK Data*, NASA TN–D–5042, 21 pp., Superintendent of Documents, Washington, D.C., 1969.

WATTS, C. B., The marginal zone of the moon, in *Astron. Pap. Am. Ephemeris*, **17**, Superintendent of Documents, Washington, D.C., 1963.

WAYMAN, P. A., Determination of the inertial frame of reference, *Quart. J. Roy. Astron. Soc.*, **7**, 138–156, 1966.

WEEKES, K., On the interpretation of the Doppler effect from senders in an artificial satellite, *J. Atmos. Terrest. Phys.*, **12**(7), 335–338, 1958.

WEIGHTMAN, J., Gravity, geodesy, and artificial satellites: A unified analytical approach, in *The Use of Artificial Satellites for Geodesy*, edited by G. Veis, pp. 467–486, National Technical University, Athens, 1967.

WEIGHTMAN, J., AND C. MUNFORD, *First Experimental Computation of the West European Satellite Triangulation*, United Kingdom Computing Center, Feltham, 1970.

WEILER, A. R., Probleme de l'implantation d'une grille sur une sphére, 1, *Bull. Geod.*, **79**, 3–22, 1966a.

WEILER, A., Probleme de l'implantation d'une grille sur une sphére, 2, *Bull. Geod.*, **80**, 99–112, 1966b.

WEIMER, TH., Occultations d'etoiles et profils lunaires, *Bull. Geod.*, **31**, 37–46, 1953.

WHIPPLE, F., *Sky Telesc.*, **8**, 90, 1949.

WHIPPLE, F. L., Tracking by the Smithsonian Astrophysical Observatory, *Phil. Trans. Roy. Soc. London*, Ser. A, **262**, 14–25, 1967a.

WHIPPLE, F. L., On the satellite geodesy program at the Smithsonian Astrophysical Observatory, *Space Res.*, **7**, 675–683, 1967b.

WHIPPLE, F. L., AND J. A. HYNEK, A research program based on the optical tracking of artificial Earth satellites, *Proc. Inst. Radio Eng.*, **44**(6) 760–764, 1956.

WHIPPLE, F. L., AND J. A. HYNEK, Optical and visual tracking of artificial satellites, in *Proceedings of Eighth International Astronautical Congress*, pp. 429–435, Springer-Verlag, Vienna, 1958a.

WHIPPLE, F. L., AND J. A. HYNEK, The IGY satellite tracking program as a source of geodetic information, *Ann. Geophys.*, **14**(3), 326–328, 1958b.

WHIPPLE, F. L., AND C. A. LUNDQUIST, Tracking by the Smithsonian Astrophysical Observatory, *Phil. Trans. Roy. Soc. London*, Ser. A, **262**, 14–25, 1967.

WHISNANT, J. M., P. R. WASZKIEWICZ, AND V. L. PISCANE, Attitude performance of the GEOS–2 gravity-gradient spacecraft, *J. Spacecraft Rockets*, **6**(12), 1379–1384, 1969.

WHITTEN, C. A., Review of the adjustment of the Central European triangulation, *Bull. Geod.*, **7**, 45–46, 1948.

WHITTEN, C. A., Adjustment of European triangulation, 1, Southwestern bloc; 2, Northern bloc, *Bull. Geod.*, **24**, 187–206, 1951.

WHITTEN, C. A., Adjustment of European triangulation, *Bull. Geod.*, **24**, 187–206, 1952.

WIENER, N., *Extrapolation, Interpolation, and Smoothing of Stationary Time Series with Engineering Applications*, MIT Press, Cambridge, Mass., 1966.

WIGNER, E. P., The three-dimensional pure rotation group, in *Group Theory*, pp. 153–170, Academic Press, New York, 1959.

WILCOX, L. E., Development and projective methods of geodesy and their effect on large triangulation and trilateration networks, *Bull. Geod.*, **68**, 127–138, 1963.

WILKINS, G. A., The system of astronomical constants, 1, *Quart. J. Roy. Astron. Soc.*, **5**(1), 23–30, 1964.

WILKINS, G. A., The system of astronomical constants, 2, *Quart. J. Roy. Astron. Soc.*, **6**(1), 70–73, 1965.

WILLIAMS, J. G., J. D. MULHOLLAND, AND P. L. BENDER, Spin-axis distance of the McDonald Observatory (abstract), *Eos Trans. Am. Geophys. Union*, **53**, 968, 1972.

WILLIAMS, O. W., PC–1000 cameras, in *The Use of Artificial Satellites for Geodesy*, edited by G. Veis, p. 193, North Holland, Amsterdam, 1963.

WILSON, R. A., Optical and electronic tracking in *Contemporary Geodesy*, Geophys. Monogr. 4, edited by C. Whitten and K. H. Drummond, pp. 67–78, American Geophysical Union, Washington, D.C., 1959.

WINTER, A., *Analytical Foundations of Celestial Mechanics*, 448 pp., Princeton University Press, Princeton, N.J., 1941.

WOLF, E., Satellitenbeobachtungungen Aussmessung der Platten und Plattenreduktion beim Deutschen Geodätischen Foschungsinstitut in München, in *Münchener Beiträge zur Satellitengeodesie*, edited by M. Kneissl, pp. 73–90, Bayerischen Akademie der Wissenschaften, München, 1967.

WOLF, H., On the absolute deflection of the vertical at Potsdam, *Bull. Geod.*, **31**, 47–51, 1953.

WOLF, H., Die heutigen numersche Grundlagen zur Reduktion von Triangulationsmessungen auf das Ellipsoid, *Bull. Geod.*, **68**, 149–163, 1963.

WOLF, H., Rigorous computation of the European traverse, including the acompanying strip of triangulation, in *Die Europäische Basis Traverse Tromsø-Catania für eine geodätisches Satellitenweltnetze*, edited by M. Kneissl, German Geodetic Commission, Munich, 1967.

WOLF, H., *Ausgleichung nach der Methode der kleinsten Quadrate*, Dümmlers Verlag, Bonn, Germany, 1968.

WOLLENHAUPT, W. R., ET AL., *Ranger 7 Flight Path and Its Determination From Tracking Data*, TR–32–694, 188 pp., Jet Propulsion Laboratory, Pasadena, Calif., 1964.

WOLLARD, E. W., Theory of the rotation of the Earth around its center of mass, in *Astron. Pap. Am. Ephemeris Nautical Almanac*, **15**, part 1, 165 pp., Superintendent of Documents, Washington, D.C., 1953.

WOLLARD, E. W., AND G. M. CLEMENCE, *Spherical Astronomy*, Academic, New York, 1966.

WONG, S. K., Deep space station locations and physical constants solutions of Surveyor missions, *Space Programs Summary 37–52*, Jet Propulsion Laboratory, Pasadena, Calif., 1968.

WONG, S. K., Earth-Moon mass ratio from Mariner radio tracking data, *Nature*, **241**, 1973.

WYATT, S. P., Effect of terrestrial radiation pressure on satellite orbits, in *Dynamics of Satellite Orbits*, edited by M. Roy, pp. 180–196, Springer-Verlag, Berlin, 1963.

YAPLEE, B. S., ET AL., Mean distance of the Moon as determined by radar, in *Proceedings of the International Astronomical Union Symposium 21: Astronomical Constants*, edited by J. Kovalevsky, Gauthier-Villars, Paris, 1965.

YEREMEYEV, V. F., AND M. J. YURKINA, On orientation of the reference geodetic ellipsoid, *Bull. Geod.*, **91**, 13–16, 1969.

YIONOULIS, S. M., Study of the resonance effects due to the Earth's potential function, *J. Geophys. Res.*, **70**(24), 5991–5996, 1965.

YIONOULIS, S. M., Study of the resonance effects due to the Earth's potential function, *J. Geophys. Res.*, **71**(4), 1289–1291, 1966a.

YIONOULIS, S. M., Determination of coefficients associated with geopotential harmonics of order thirteen, *J. Geophys. Res.*, **71**(6), 1768, 1966b.

YIONOULIS, S. M., Algorithm to compute tropospheric-refraction effects on range measurements, *J. Geophys. Res.*, **75**(36), 7636–7637, 1970.

YIONOULIS, S. M., F. T. HEURING, AND W. H. GUIER, Geopotential model (APL 5.0–1967) determined from satellite Doppler data at seven inclinations, *J. Geophys. Res.*, **77**(20) 3671–3677, 1972.

YODER, P. R., Study of light deviation errors in triple mirrors and tetrahedral prisms, *J. Opt. Soc. Am.*, **48**(7), 496–499, 1958.

ZADUNAISKY, P., *Shutter Corrections in Time for Baker-Nunn Camera*, Spec. Rep. 41, pp. 21–37, Smithsonian Astrophysical Observatory, Cambridge, Mass., 1960.

ZHONGOLOVICH, I. D., The outer gravitational field of the Earth and the fundamental constants related to it, *Trudy Inst. Teor. Astron.*, **3**, 1952.

ZHONGOLOVITCH, I. D., Determination of the dimensions of the general Earth ellipsoid, *Trudy Inst. Teor. Astron.*, **6**, 5–66, 1956.

ZHONGOLOVICH, I. D., Gravitational potential of the Earth, *Bull. Inst. Theor. Astron.*, **6**, 505–523, 1957.

ZHONGOLOVICH, I. D., *Review of Results of Determining Parameters of the Earth's Gravitational Field From Satellite Tracking Data*, SAO Publ., pp. 23–37, Smithsonian Astrophysical Observatory, Cambridge, Mass., 1962.

ZIRKER, J., F. L. WHIPPLE, AND R. DAVIS, Time available for the optical observation of an Earth satellite, in *Scientific Uses of Earth Satellites*, edited by J. A. Van Allen, pp. 23–28, University of Michigan Press, Ann Arbor, Mich., 1956.

ZURMÜHL, R., *Matrizen*, 4th ed., Springer-Verlag, Berlin, 1965.

Author Index

Subject Index

☆ U.S. GOVERNMENT PRINTING OFFICE: 1977 0—588–174